

Kenneth S. Suslick

William H. & Janet Lycan Professor of Chemistry

and Professor of Materials Science and Engineering

Professor Suslick received his B.S. from Cal Tech in 1974 and his Ph. D. from Stanford in 1978, and came to the University of Illinois immediately thereafter. He is the recipient of the ACS Senior Cope Scholar Award, the ACS Nobel Laureate Signature Award for Graduate Education, the Materials Research Society Medal, an NIH Research Career Development Award, a Sloan Foundation Research Fellowship, and the Silver Medal of the Royal Society for Arts, Manufactures, and Commerce; he is a Fellow of the AAAS and the Acoustical Society of America.

Contact Information:

Kenneth S. Suslick
 Department of Chemistry
 University of Illinois
 at Urbana–Champaign
 600 S. Mathews Av.
 Urbana, Illinois 61801
 Office: (217) 333-2794
 Lab: (217) 333-1532
 Fax: (217) 333-2685
 Email: ksuslick@uiuc.edu



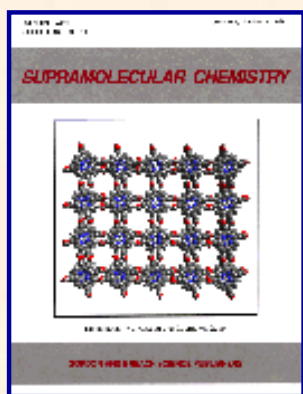
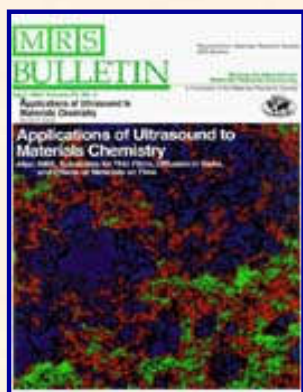
The Suslick Research Group at the University of Illinois at Urbana–Champaign is multi-disciplinary: our research projects involves individuals with interests not only in inorganic, but also in organometallic, bio-organic, materials (both inorganic and biomaterials), surface, and physical chemistry.

Our two major research areas ([click for outline](#)) are the [chemical effects of ultrasound](#) and the bioinorganic and materials chemistry of [metalloporphyrins and heme proteins](#). Our recent interest in [artificial olfaction and molecular recognition](#) is an exciting spinoff of the latter. As part of this diversity, we often collaborate with other researchers both at UIUC and at other universities across the world. Several of the [students in this group](#) are joint members in other research groups in the School of Chemical Sciences.

Note for potential postdoctoral applicants: Due to the very large volume of email applications for postdoctoral positions (~500 per year), I no longer will respond to individual applications sent by email. If you are seriously interested in postdoctoral research in my group, please send me your CV together with reprints of three papers, and arrange for three letters of recommendation to be sent separately.

SELECTED RECENT AND INTRODUCTORY PUBLICATIONS

Click on any highlighted reference below to download it in PDF format.
(To get the free Adobe PDF reader, click here.)



The Chemical Effects of Ultrasound

1. Suslick, K. S.; Choe, S. B.; Cichowlas, A. A.; Grinstaff, M. W. "Sonochemical Synthesis of Amorphous Iron," *Nature* **1991**, *353*, 414-416.
2. Suslick, K. S.; Fang, M.; Hyeon, T. "Sonochemical Synthesis of Iron Colloids" *J. Am. Chem. Soc.*, **1996**, *118*, 11960-11961.
3. Mdleleni, M. M.; Hyeon, T.; Suslick, K. S. "Sonochemical Synthesis of Nanostructured Molybdenum Sulfide" *J. Am. Chem. Soc.*, **1998**, *120*, 6189-6190.
4. McNamara III, W. B.; Didenko, Y.; Suslick, K. S. "Sonoluminescence Temperatures During Multibubble Cavitation" *Nature*, **1999**, *401*, 772-775.
5. Dantsin, G.; Suslick, K.S. "Sonochemical Preparation of a Nanostructured Bifunctional Catalyst" *J. Am. Chem. Soc.*, **2000**, *122*, 5214-5215.
6. Didenko, Y.; McNamara III, W. B.; Suslick, K. S. "Molecular Emission from Single Bubble Sonoluminescence" *Nature*, **2000**, *406*, 877-879.
7. Didenko, Y.; Suslick, K. S. "The Energy Efficiency of Formation of Photons, Radicals, and Ions During Single Bubble Cavitation" *Nature* **2002**, *418*, 394-397.
8. McNamara III, W. B.; Didenko, Y.; Suslick, K. S. "Pressure during Acoustic Cavitation" *J. Phys. Chem.* **2003**, *107*, 7303-7306 (Henglein Festschrift).
9. Lee, T. M.; Oldenburg, A. L.; Sitafalwalla, S.; Marks, D. L.; Luo, W.; Toublan, F. J.-J.; Suslick, K. S.; Boppart, S. A. "Engineered Microsphere Contrast Agents for Optical Coherence Tomography" *Optics Lett.* **2003**, *28*, 1546-1548.
10. Prozorov, T.; Prozorov, R.; Snezhko, A.; Suslick, K. S. "Sonochemical Modification of the Superconducting Properties of MgB₂" *Appl. Phys. Lett.* **2003**, *83*, 2019-2021

Metalloporphyrins and Bio-Inorganic Chemistry

1. Bhyrappa, P.; Wilson, S. R.; Suslick, K. S. "Hydrogen Bonded Porphyrinic Solids: Supramolecular Networks of Octahydroxy Porphyrins," *J. Am. Chem. Soc.*, **1997**, *119*, 8492-8502.
2. Huffman, D. L.; Rosenblatt, M. M.; Suslick, K. S. "Synthetic Heme-Peptide Complexes," *J. Am. Chem. Soc.*, **1998**, *120*, 6183-6184.
3. Patel, B. R.; Suslick, K. S. "Discotic Liquid Crystals from a Bis-Pocketed Porphyrin" *J. Am. Chem. Soc.*, **1998**, *120*, 11802-11803.
4. Sen, A.; Suslick, K. S. "Shape-Selective Discrimination of Small Organic Molecules" *J. Am. Chem. Soc.*, **2000**, *122*, 11565-11566.
5. Rakow, N. A.; Suslick, K. S. "A Colorimetric Sensor Array for Odour Visualization" *Nature*, **2000**, *406*, 710-714.
6. Zimmerman, S. C.; Wendland, M. S.; Rakow, N. A.; Zharov, I.; Suslick, K. S. "Synthetic Hosts by Monomolecular Imprinting Inside Dendrimers" *Nature* **2002**, *418*, 399-403.

7. Kosal, M. E.; Chou, J.-H.; Wilson, S. R.; Suslick, K. S. "A Functional Zeolite Analogue Assembled From Metalloporphyrins" *Nature Materials*, **2002**, *1*, 118-121.
8. Wang, J.; Luthey-Schulten, Z.; Suslick, K. S. "Is the Olfactory Receptor A Metalloprotein?" *Proc. Natl. Acad. Sci. U.S.A.*, **2003**, *100*, 3035-3039.
9. Zimmerman, S. C.; Zharov, I.; Wendland, M. S.; Rakow, N. A.; Suslick, K. S. "Molecular Imprinting Inside Dendrimers" *J. Am. Chem. Soc.* **2003**, *125*, 13504 - 13518.
10. Rosenblatt, M.M.; Wang, J.; Suslick, K. S. "De Novo Designed Cyclic-Peptide Heme Complexes" *Proc. Natl. Acad. Sci. U.S.A.*, **2003**, *100*, 13140-13145.

Some Introductory Reviews

1. Suslick, K. S. "The Chemical Effects of Ultrasound" *Scientific American*, **1989** (**2**), *260*, 80-86. (color figures, but reduced in size; large file, 1MB)
2. Suslick, K. S. "The Chemistry of Ultrasound," in *Encyclopaedia Britannica Yearbook of Science and the Future 1994*, Britannica: Chicago; 1994; pp. 138-155.
3. Suslick, K. S. "Sonochemistry," in *Kirk-Othmer Encyclopedia of Chemical Technology*; 4th Ed., J. Wiley & Sons: New York, 1998, vol. 26, 517-541.
4. Suslick, K. S.; Didenko, Y.; Fang, M. M.; Hyeon, T.; Kolbeck, K. J.; McNamara, W. B. III; Mdleleni, M. M.; Wong, M. "Acoustic Cavitation and Its Chemical Consequences" *Phil. Trans. Roy. Soc. A*, **1999**, *357*, 335-353.
5. Suslick, K. S.; Price, G. "Applications of Ultrasound to Materials Chemistry" *Annu. Rev. Matl. Sci.*, **1999**, *29*, 295-326.
6. Crum, L. A.; Mason, T. J.; Reisse, J.; Suslick, K. S., eds. *Sonochemistry and Sonoluminescence*, Kluwer Publishers: Dordrecht, Netherlands, 1999; NATO ASI Series C, v. 524.
7. Kosal, M. E.; Suslick, K. S. "Microporous Porphyrin and Metalloporphyrin Materials," *J. Sol. St. Chem.*, **2000**, *152*, 87-98 (invited review).
8. Suslick, K. S. "Shape Selective Oxidation by Metalloporphyrins," in *The Porphyrin Handbook*, Kadish, K.; Smith, K.; Guillard, R., ed.; Academic Press: New York, 2000; vol. 4, ch. 28, pp. 41-63.
9. Chou, J.-H.; Kosal, M. E.; Nalwa, H.S.; Rakow, N.A.; Suslick, K. S. "Applications of Porphyrins and Metalloporphyrins to Materials Chemistry" in *The Porphyrin Handbook*, Kadish, K.; Smith, K.; Guillard, R., ed.; Academic Press: New York, 2000; vol. 6, ch. 41, pp. 43-131. (This PDF file is without figures; for figures in html format, [click here](#))
10. Suslick, K. S. "Sonochemistry and Sonoluminescence" in *Encyclopedia of Physical Science and Technology*, 3rd ed. Academic Press: San Diego, 2001, vol. 17, pp. 363-376.

***For Press Clippings on various of the articles above,
click here.***

For a brochure describing the Suslick Research Group, click here.

For a complete list of Professor Suslick's publications, click here.

For Professor Suslick's curriculum vitae, click here.

SUSLICK GROUP WEBSITE:

THE SCIENCE	THE GROUP	THE MAÎTRE D'	LAGNIAPPE: A LITTLE EXTRA
Overview	Current Group Members	CV: Abbreviated, Full	Art and Science
Outline of Projects	Group Meetings	Suslick Group Brochure	Chymistes: The Distillers of Waters
Synopses: Sonochemistry Metalloporph.	Group Responsibilities	Complete Publication List	A Chemist Meets Hollywood
Executive Summary: Smell-Seeing	Web Based Resources	Academic Genealogy	A Chemist In Court
Introduction to Sonochemistry	Safety Resources	Press Clippings	Words of Humor and Wisdom
Proposal Excerpts	Group Equipment	How To Give A Seminar	Laws of the Universe
Funding	Past Group Members	Ch315 Inorganic Chemistry	Cartoons of Humor and Wisdom

**Information
for Visitors**

**Group
Photogallery**

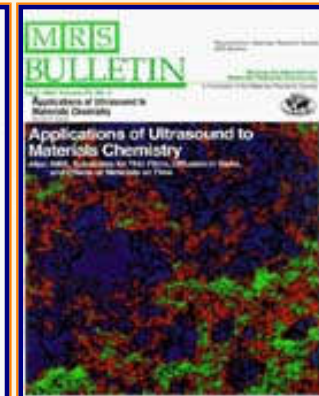
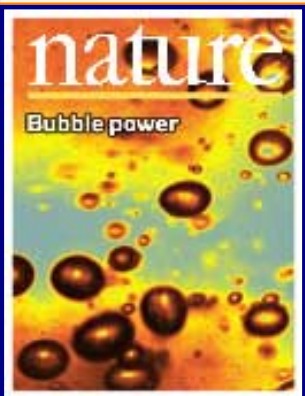
**Construction of the
CLS Lab**

**Sculpture
&
Masks**

©2003, K.S. Suslick; all rights reserved.

Comments and suggestions: ksuslick@uiuc.edu

The Suslick Research Group



CURRENT GROUP MEMBERS

Porphyrin Projects

[Overview](#)

[Outline of Research Projects](#)

[Introduction to Sonochemistry](#)

[Exec. Summary: Sonochemistry](#)

[Exec. Summary: Porphyrin Research](#)

[Exec. Summary: Smell-Seeing](#)

[Complete Publication List](#)

[Abbreviated Curriculum Vitae](#)

[Academic Genealogy](#)

[Press Clippings](#)



Jie Bai

B.S., Beijing University, 2002.

jiebai@uiuc.edu

217-333-1532



Ming Fang

B.S., Jilin University, 1998.

M.S., Jilin University, 2001.

mingfang@uiuc.edu

217-333-1532



Shirley Nakagaki

B.S., University of São Paulo, 1985; M.S., 1993.

Professor, Univ. Fed. do Paraná, Curitiba, 1992-.

Visiting Scholar, UIUC, 2002-2003.

shirley@s.scs.uiuc.edu

217-333-1532

[Current Research
Funding](#)

[Excerpts from
Funded Research](#)

[Inventory of
Group Equipment](#)

[Information
for Visiting](#)

[Current Research Group
Members](#)

[Group
Meetings](#)

[Group
Chores](#)

[Past Research
Group Members](#)

[Group
Photogallery](#)

[Web Resources](#)

[Laboratory Safety
Resources](#)

[Art and Science:
Journal Covers](#)

[Sculpture &
Masks](#)

[A Chemist
Meets Hollywood](#)

[Chymistes: The Distillers
of Waters](#)

[A Chemist
In Court](#)



Dennis Smithenry

B.S., University of Illinois, 1989.

smithnry@uiuc.edu

217-333-1532



Jiangyun Wang

B.S., University of Science and Technology of China, 1998.

jwang8@uiuc.edu

217-333-1532



Jennifer Wilson Ponder

B.S., Ball State University, 2000.

JBWilson@s.scs.uiuc.edu

217-333-1532



Chen Zhang

B.S., Peking University, 1999.

czhang5@uiuc.edu

217-333-1532

Sonochemistry Projects

[Humor and
Wisdom](#)

[Laws of the Universe](#)

[Cartoons of Humor and
Wisdom](#)

[Chem 115: Chemistry of
Everyday Phenomena](#)

[Chem 315: Inorganic
Chemistry](#)

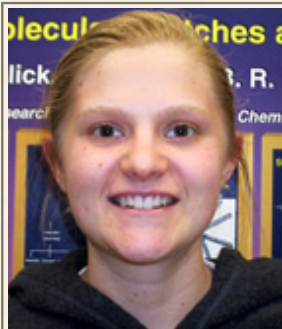


David Flannigan

B.S., University of Minnesota, 2001.

flanniga@uiuc.edu

217-333-1532



Elizabeth Dibbern

B.S., Univ. of Nebraska, 2002.

edibbern@scs.uiuc.edu

217-333-1532



Yury Didenko

B.S., M.S., Moscow State University, 1970-75.

Ph.D., Moscow State University, 1985.

Head of Laboratory, Pacific Oceanological Institute,
Vladivostok, Russia.

didenko@s.scs.uiuc.edu

217-333-1532



Steve Hopkins

B.S., Washington and Lee University, 2000.

shopkins@uiuc.edu

217-333-1532



Dong-Kyu Lee

Professor, Department of Industrial Chemical Engineering,
Chungbuk National University, South Korea

Visiting Scholar, UIUC, 2003.

dklee540@uiuc.edu

217-333-1532



Farah Jean-Jacques Toublan

B.S., M.S., SUNY-Stony Brook, 2000.

jeanjacq@uiuc.edu

217-333-1532



James D. Oxley

B.S., Texas Christian University, 1998.

joxley@s.scs.uiuc.edu

217-333-1532



Tanya Prozorov

M.S., Bar-Ilan University, 1998.

tprozoro@uiuc.edu

217-333-1532



Annabeth Ryder

B.S., Indiana University, 2002.

aryder@uiuc.edu

217-333-1532



Sara Skrabalak

B.A., Washington Univ., 2002.

skrabalk@uiuc.edu

217-333-1532



Won Hyuk Suh

B.S., M.S., Seoul National Univ., 2002.

wonsuh@uiuc.edu

217-333-1532

Group Executive Assistant



Ron Shen

M.S., Medicinal Chemistry, Univ. Toledo, 1996.

ronshen@scs.uiuc.edu

217-333-6852

Recent Group Event Photos

SUSLICK GROUP WEBSITE:

**THE
SCIENCE**

**THE
GROUP**

**THE
MAÎTRE D'**

**LAGNIAPPE:
A LITTLE EXTRA**

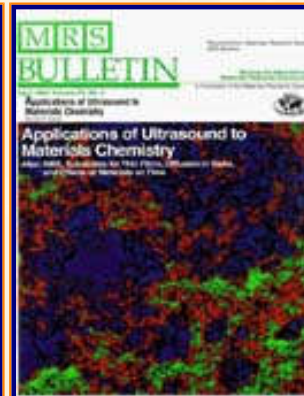
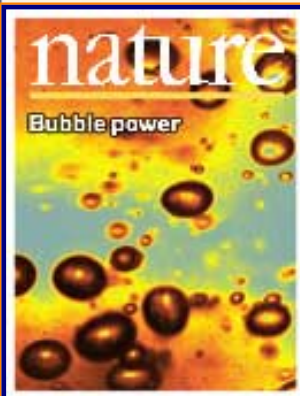
<u>Overview</u>	<u>Current Group Members</u>	<u>CV: Abbreviated, Full</u>	<u>Art and Science</u>
<u>Outline of Projects</u>	<u>Group Meetings</u>	<u>Suslick Group Brochure</u>	<u>Chymistes: The Distillers of Waters</u>
<u>Synopses: Sonochemistry</u>	<u>Group Responsibilities</u>	<u>Complete Publication List</u>	<u>A Chemist Meets Hollywood</u>
<u>Metalloporph.</u>			
<u>Executive Summary: Smell-Seeing</u>	<u>Web Based Resources</u>	<u>Academic Genealogy</u>	<u>A Chemist In Court</u>
<u>Introduction to Sonochemistry</u>	<u>Safety Resources</u>	<u>Press Clippings</u>	<u>Words of Humor and Wisdom</u>
<u>Proposal Excerpts</u>	<u>Group Equipment</u>	<u>How To Give A Seminar</u>	<u>Laws of the Universe</u>
<u>Funding</u>	<u>Past Group Members</u>	<u>Ch315 Inorganic Chemistry</u>	<u>Cartoons of Humor and Wisdom</u>
<u>Information for Visitors</u>	<u>Group Photogallery</u>	<u>Construction of the CLS Lab</u>	<u>Sculpture & Masks</u>

©2003, K.S. Suslick; all rights reserved.

Comments and suggestions: ksuslick@uiuc.edu



The Suslick Research Group



ART AND SCIENCE: COVER ART FROM THE SUSLICK GROUP

NATURE: 25 July 2002



[Overview](#)

[Outline of
Research Projects](#)

[Introduction to
Sonochemistry](#)

[Exec. Summary:
Sonochemistry](#)

[Exec. Summary:
Porphyrin Research](#)

[Exec. Summary: Smell-
Seeing](#)

[Complete
Publication List](#)

[Abbreviated Curriculum
Vitae](#)

[Academic
Genealogy](#)

[Press
Clippings](#)



[Current Research
Funding](#)

[Excerpts from
Funded Research](#)

[Inventory of
Group Equipment](#)

[Information
for Visiting](#)

[Current Research Group
Members](#)

[Group
Meetings](#)

[Group
Chores](#)

[Past Research
Group Members](#)

[Group
Photogallery](#)

[Web Resources](#)

[Laboratory Safety
Resources](#)

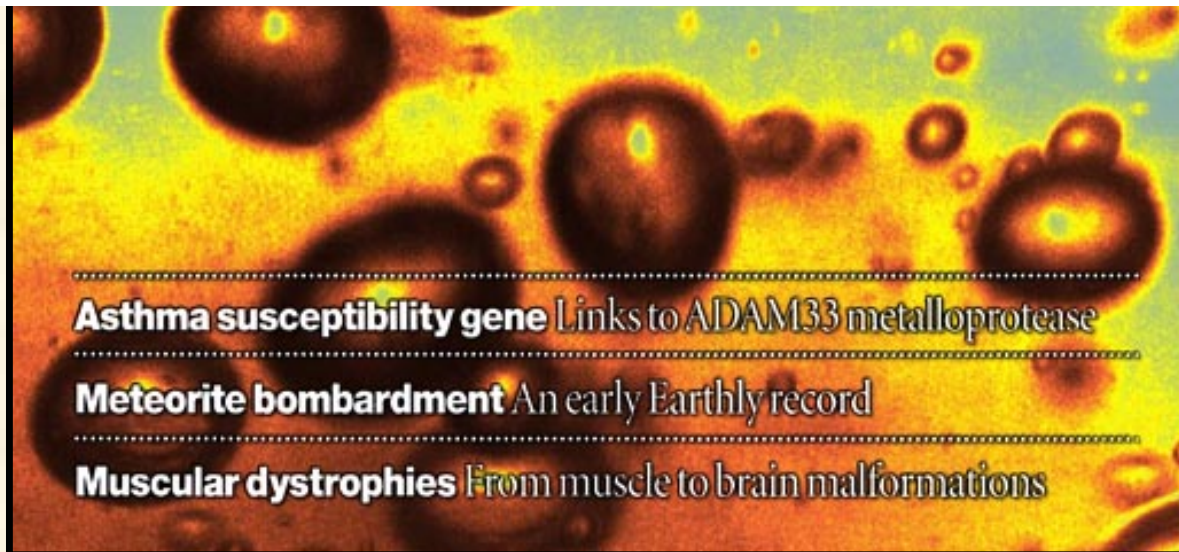
[Art and Science:
Journal Covers](#)

[Sculpture &
Masks](#)

[A Chemist
Meets Hollywood](#)

[Chymistes: The Distillers
of Waters](#)

[A Chemist
In Court](#)



When a gas bubble in a liquid is excited by ultrasonic acoustic waves, it can emit short flashes of light suggestive of extreme temperatures inside the bubble. These flashes of light, known as 'sonoluminescence', occur as the bubble implodes, or cavitates. Now Didenko and Suslick show that chemical reactions occur during cavitation of a single, isolated bubble, and they go on to determine the yield of photons, radicals, and ions formed. (Photo credit: Kenneth S. Suslick and Kenneth J. Kolbeck)

SCIENCE:
March 1990

SCIENCE:
September 1991

MRS BULLETIN:
April 1995

SUPRAMOLECULAR CHEMISTRY:
September 1998

NATURE:
25 July 2002

[Humor and
Wisdom](#)

[Laws of the Universe](#)

[Cartoons of Humor and
Wisdom](#)

[Chem 115: Chemistry of
Everyday Phenomena](#)

[Chem 315: Inorganic
Chemistry](#)

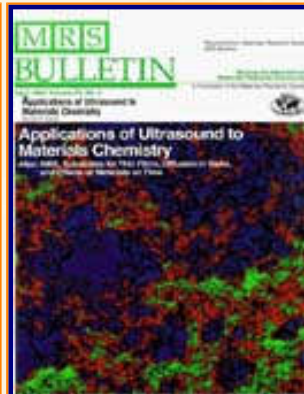
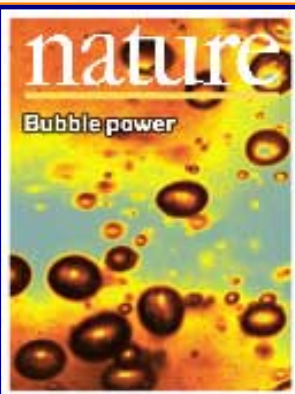
SUSLICK GROUP WEBSITE:

THE SCIENCE	THE GROUP	THE MAÎTRE D'	LAGNIAPPE: A LITTLE EXTRA
Overview	Current Group Members	CV: Abbreviated, Full	Art and Science
Outline of Projects	Group Meetings	Suslick Group Brochure	Chymistes: The Distillers of Waters
Synopses: Sonochemistry Metalloporph.	Group Responsibilities	Complete Publication List	A Chemist Meets Hollywood
Executive Summary: Smell-Seeing	Web Based Resources	Academic Genealogy	A Chemist In Court
Introduction to Sonochemistry	Safety Resources	Press Clippings	Words of Humor and Wisdom
Proposal Excerpts	Group Equipment	How To Give A Seminar	Laws of the Universe
Funding	Past Group Members	Ch315 Inorganic Chemistry	Cartoons of Humor and Wisdom
Information for Visitors	Group Photogallery	Construction of the CLS Lab	Sculpture & Masks

©2003, K.S. Suslick; all rights reserved.

Comments and suggestions: ksuslick@uiuc.edu

The Suslick Research Group



OUTLINE OF CURRENT RESEARCH PROJECTS

Click on highlighted topics below to see excerpts from the relevant funded proposal.

[Overview](#)

[Outline of
Research Projects](#)

[Introduction to
Sonochemistry](#)

[Exec. Summary:
Sonochemistry](#)

[Exec. Summary:
Porphyrin Research](#)

[Exec. Summary: Smell-
Seeing](#)

[Complete
Publication List](#)

[Abbreviated Curriculum
Vitae](#)

[Academic
Genealogy](#)

[Press
Clippings](#)

I. Porphyrins, Metalloporphyrins, and the Bio-Inorganic Chemistry of Heme Proteins

Molecular Recognition: "Smell-Seeing" and Molecular Sensors

Artificial Olfaction and an Electronic Nose

Shape Selective Molecular Sensors

Shape and Polarity Selectivity with Bis-Pocket Porphyrins

Molecular Recognition: Oxidation Catalysis

Molecular Recognition with Super-Structured Porphyrins

Dendrimer Porphyrins as Oxidation Catalysts

Metalloporphyrin Photochemistry

Oxygen Atom Transfers; Cytochrome P450 Intermediates

Actinide & Early Transition Metal Porphyrin Complexes

Sandwich Complexes as Photosynthetic Reaction Center Analogs

Photophysics of pi-pi Interactions

Porphyrinic Materials Chemistry

Non-Linear Optical Materials and Langmuir-Blodgett Films

Coordination Polymers

Network Solids; Hydrogen Bonded Porphyrinic Networks

Nanoporous Solids & Shape Selective Heterogeneous Catalysts

Totally Synthetic Heme Proteins: Peptides as Ligands

Oligopeptide Binding to Metalloporphyrins;

Electron Transfer with Heme-Peptides

[Current Research Funding](#)

[Excerpts from Funded Research](#)

[Inventory of Group Equipment](#)

[Information for Visiting](#)

[Current Research Group Members](#)

[Group Meetings](#)

[Group Chores](#)

[Past Research Group Members](#)

[Group Photogallery](#)

[Web Resources](#)

[Laboratory Safety Resources](#)

[Art and Science: Journal Covers](#)

[Sculpture & Masks](#)

[A Chemist Meets Hollywood](#)

[Chymistes: The Distillers of Waters](#)

[A Chemist In Court](#)

Synthetic Blood Substitutes: Heme Protein Microspheres
Synthesis, Characterization, and Animal Studies

II. The Chemical Effects of Ultrasound

Physical and Mechanistic Sonochemistry

Mechanisms of Sonochemistry
Tribochemical & Mechanochemical Reactions
Surface-Surface Reactivity

Sonoluminescence

Spectroscopic Probes of Cavitation Conditions
Multi-Bubble and Single-Bubble Cavitation

Synthetic, Materials, and Catalytic Applications of Sonochemistry

Nanostructured and Amorphous Metals, Carbides, Sulfides
Heterogeneous Catalysis
Organometallic Sonochemistry
Heterogeneous Sonochemistry; Liquid-Solid Reactions
Organic Sonochemistry
Environmental Remediation, Aqueous Sonochemistry;

Biomedical Applications of Sonochemistry

Protein Microspheres and Microencapsulation
Drug Delivery Systems
Medical Imaging Contrast Agents (MRI, sonographic, x-ray)

SUSLICK GROUP WEBSITE:

THE SCIENCE	THE GROUP	THE MAÎTRE D'	LAGNIAPPE: A LITTLE EXTRA
Overview	Current Group Members	CV: Abbreviated, Full	Art and Science
Outline of Projects	Group Meetings	Suslick Group Brochure	Chymistes: The Distillers of Waters

[Humor and
Wisdom](#)

[Laws of the Universe](#)

[Cartoons of Humor and
Wisdom](#)

[Chem 115: Chemistry of
Everyday Phenomena](#)

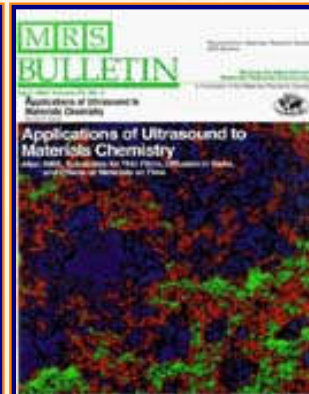
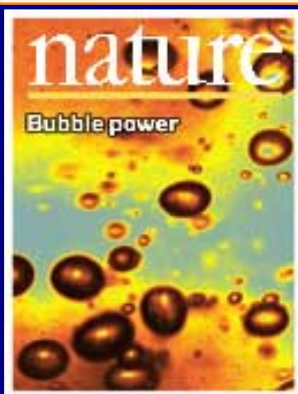
[Chem 315: Inorganic
Chemistry](#)

Synopses: Sonochemistry	Group Responsibilities	Complete Publication List	A Chemist Meets Hollywood
Metalloporph.			
Executive Summary: Smell-Seeing	Web Based Resources	Academic Genealogy	A Chemist In Court
Introduction to Sonochemistry	Safety Resources	Press Clippings	Words of Humor and Wisdom
Proposal Excerpts	Group Equipment	How To Give A Seminar	Laws of the Universe
Funding	Past Group Members	Ch315 Inorganic Chemistry	Cartoons of Humor and Wisdom
Information for Visitors	Group Photogallery	Construction of the CLS Lab	Sculpture & Masks

©2003, K.S. Suslick; all rights reserved.

Comments and suggestions: ksuslick@uiuc.edu

The Suslick Research Group



EXECUTIVE SUMMARY:

THE CHEMICAL AND PHYSICAL EFFECTS OF ULTRASOUND

Kenneth S. Suslick

The research team led by Professor Suslick has pioneered the exploration of ultrasound as a tool for chemists. He has developed new applications of sonochemistry in organometallic, inorganic, materials, and biological chemistry. His research at the UIUC has developed new approaches to amorphous and nanostructured materials, has shown great promise for the activation of heterogeneous catalysts, and has created a whole new class of medically important biomaterials.

[For a listing of commercially available sonochemical equipment, click here.](#)

Background — The chemical effects of ultrasound do not come from a direct interaction with molecular species. Instead, sonochemistry and sonoluminescence arises from acoustic cavitation: the formation, growth, and implosive collapse of bubbles in a liquid. Cavitation collapse produces *intense* local heating (~5000 K), high pressures (~1000 atm), and enormous heating and cooling rates ($>10^9$ K/sec). Acoustic cavitation provides a unique interaction of energy and matter, and ultrasonic irradiation of liquids causes high energy chemical reactions to occur, often accompanied by the emission of light [1].

[Overview](#)

[Outline of
Research Projects](#)

[Introduction to
Sonochemistry](#)

[Exec. Summary:
Sonochemistry](#)

[Exec. Summary:
Porphyrin Research](#)

[Exec. Summary: Smell-
Seeing](#)

[Complete
Publication List](#)

[Abbreviated Curriculum
Vitae](#)

[Academic
Genealogy](#)

[Press
Clippings](#)

[Current Research
Funding](#)

[Excerpts from
Funded Research](#)

[Inventory of
Group Equipment](#)

[Information
for Visiting](#)

[Current Research Group
Members](#)

[Group
Meetings](#)

[Group
Chores](#)

[Past Research
Group Members](#)

[Group
Photogallery](#)

[Web Resources](#)

[Laboratory Safety
Resources](#)

[Art and Science:
Journal Covers](#)

[Sculpture &
Masks](#)

[A Chemist
Meets Hollywood](#)

[Chymistes: The Distillers
of Waters](#)

[A Chemist
In Court](#)

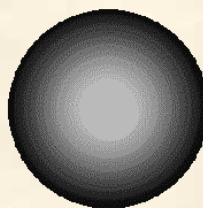


Fig. 1. Acoustic Cavitation: the formation, growth, and implosive collapse of bubbles in a liquid irradiated with high intensity ultrasound.

[For a 1MB download of an MPEG film of stroboscopic images of single collapsing bubble, click here.](#)
[Courtesy of Tom Matula, Applied Physics Lab, University of Washington.](#)

The field of sonochemistry has undergone a renaissance during the past few years, but still remains in its infancy. As our understanding of the nature of the chemical effects of ultrasound has grown, so too has the impact of sonochemistry on the chemical community and on a wide range of the physical sciences.

The collapse of bubbles caused by cavitation produces intense local heating and high pressures, with very short lifetimes. Sonoluminescence (Fig. 2) has provided us with a spectroscopic probe of cavitation and permitted determination of the effective temperatures and pressures inside the collapsing bubbles. In clouds of cavitating bubbles, these hot-spots [2] have equivalent temperatures of roughly 5000 K, pressures of about 1000 atmospheres, and heating and cooling rates above 10^{10} K/s. Thus, cavitation can create extraordinary physical and chemical conditions in otherwise cold liquids. Fig. 3 places sonochemistry in relationship to other forms of chemistry.

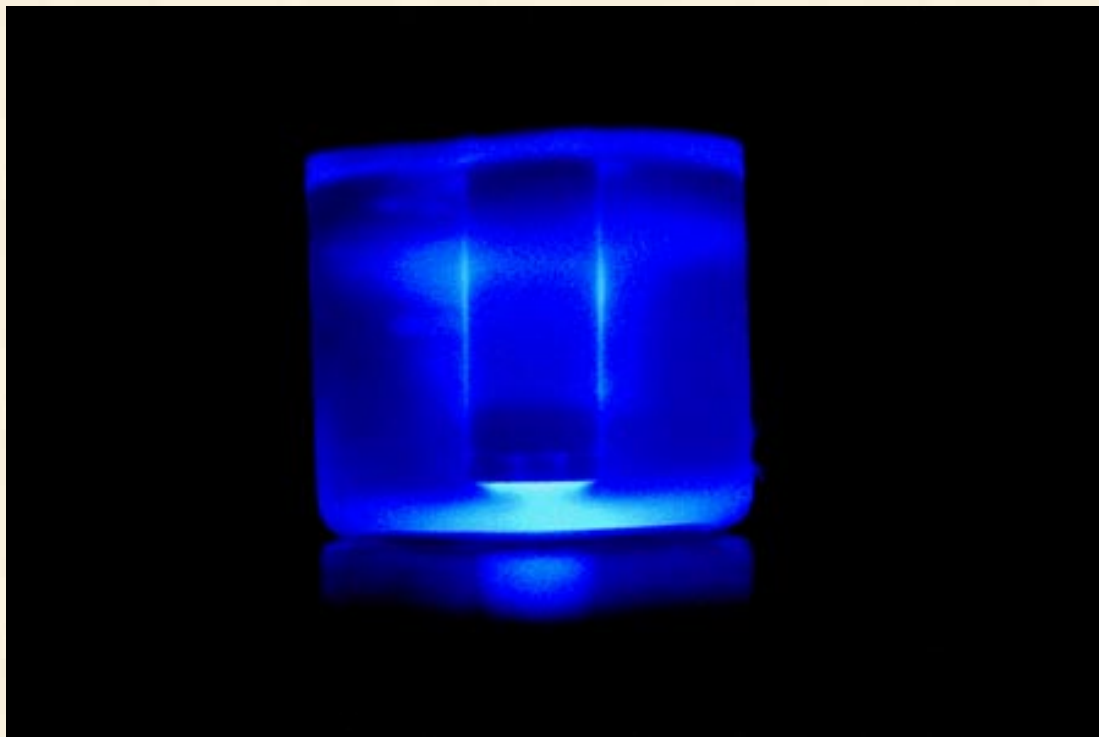


Fig. 2. Sonoluminescence from a high intensity ultrasonic horn.

[Humor and
Wisdom](#)

[Laws of the Universe](#)

[Cartoons of Humor and
Wisdom](#)

[Chem 115: Chemistry of
Everyday Phenomena](#)

[Chem 315: Inorganic
Chemistry](#)

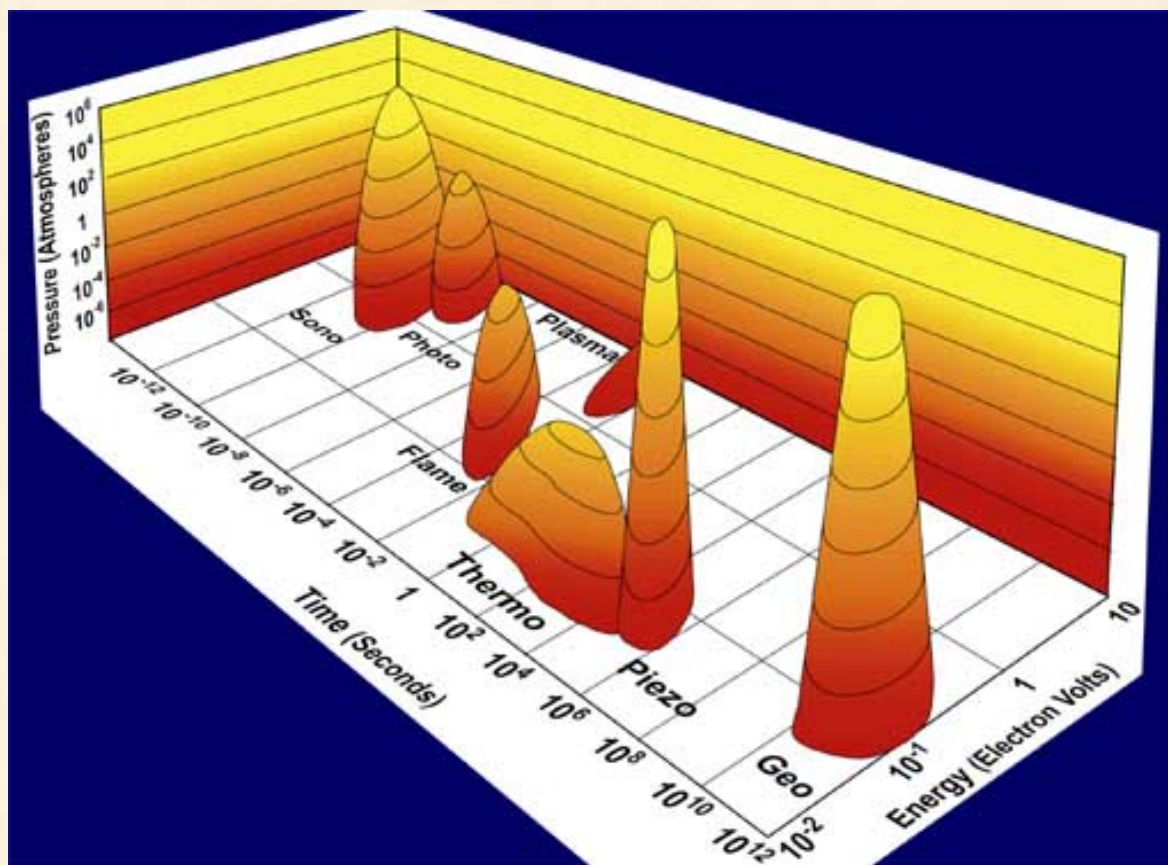


Fig. 3. Chemistry: the interaction of energy and matter.

Recent Accomplishments — Ultrasound has proved extremely useful in the synthesis of a wide range of nanostructured materials, including high surface area transition metals, alloys, carbides, oxides and colloids [1]. Sonochemical decomposition of volatile organometallic precursors in high boiling solvents produces nanostructured materials in various forms with high catalytic activities. Fig. 4 shows a typical laboratory apparatus for carrying out sonochemical reactions. Nanometer colloids, nanoporous high surface area aggregates, and nanostructured oxide supported catalysts can all be prepared by this general route. As one example, the recent discovery of a simple sonochemical synthesis of amorphous iron (Fig. 5) helped settle the longstanding controversy over its magnetic properties.

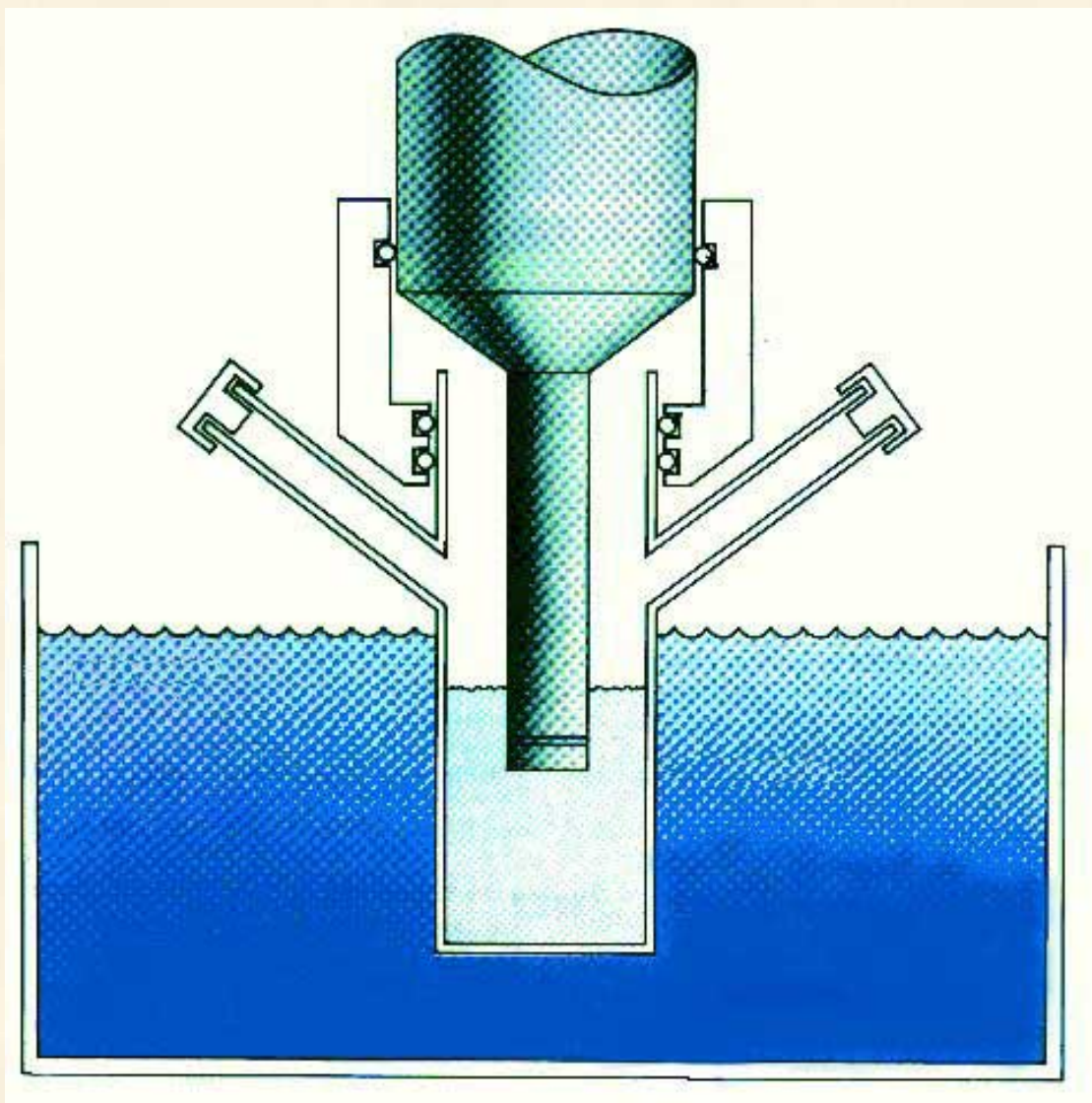


Fig. 4. Typical laboratory apparatus for carrying out sonochemistry.



Fig. 5. Scanning electron micrograph of amorphous nanostructured iron powder produced from the ultrasonic irradiation of $\text{Fe}(\text{CO})_5$. Particles making up this porous agglomerate are 10 to 20 nm in diameter.

Another important application has been the sonochemical preparation of biomaterials, most notably protein microspheres [3]. Using high intensity ultrasound and simple protein solutions, a remarkably easy method to make both air-filled microbubbles and nonaqueous liquid-filled microcapsules has been developed. Fig. 6 shows an electron micrograph of sonochemically prepared microspheres. These microspheres are stable for months, and being slightly smaller than erythrocytes, can be intravenously injected to pass unimpeded through the circulatory system. These protein microspheres, have a wide range of biomedical applications, including their use as echo contrast agents for sonography, magnetic resonance imaging contrast enhancement, drug delivery, among others.

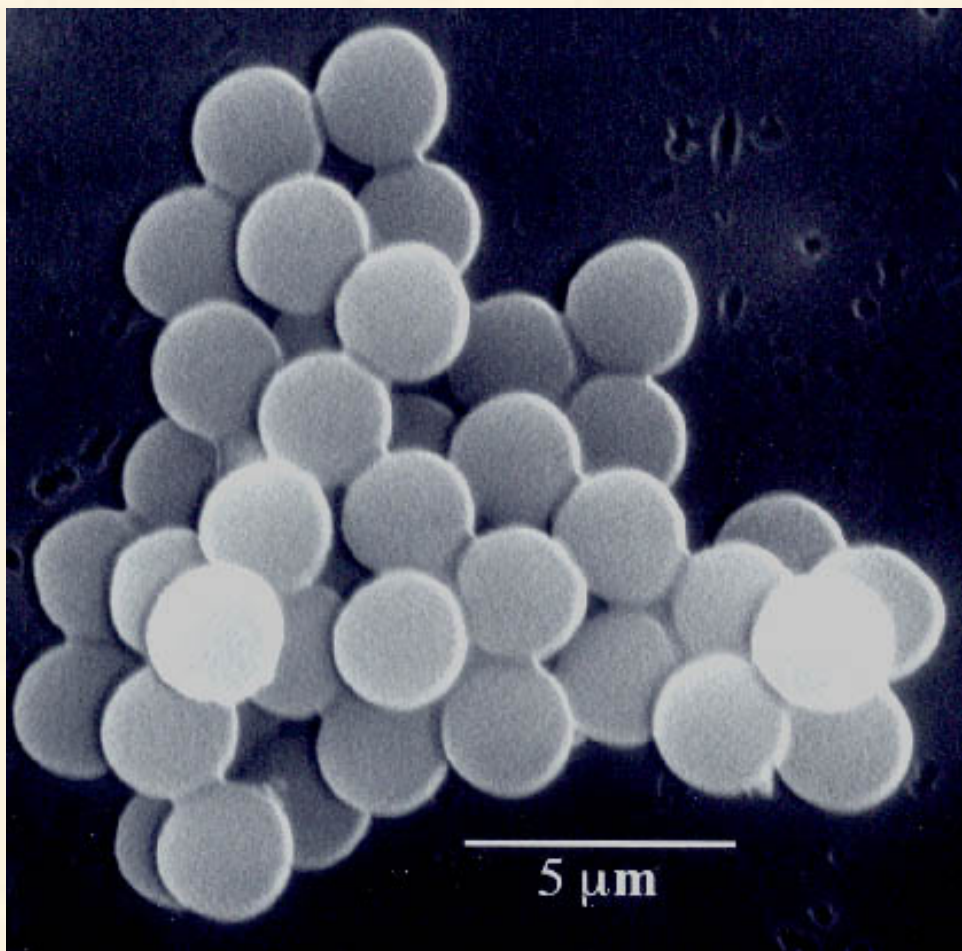


Fig. 6. Scanning electron micrograph of sonochemically synthesized hemoglobin microspheres.

When liquids that contains solids are irradiated with ultrasound, related phenomena can occur [1]. When cavitation occurs near an extended solid surface, cavity collapse is non-spherical and drives high-speed jets of liquid into the surface. These jets and associated shock waves can cause substantial surface damage and expose fresh, highly heated surfaces (Fig. 7).

Cavitation Collapse Near a Surface

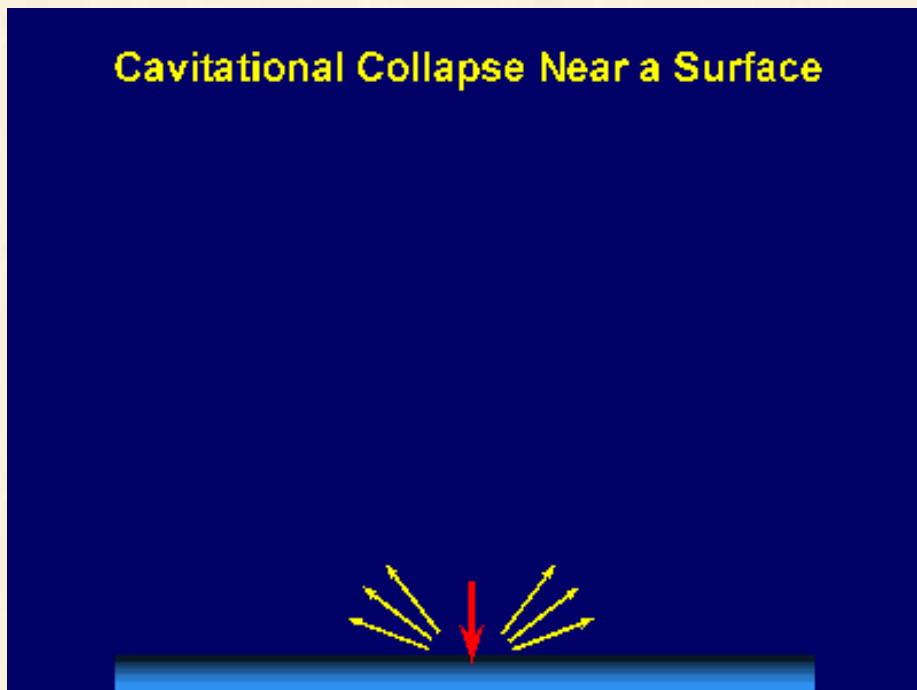


Fig. 7. Bubble collapse near an extended surface is distorted and leads to a shaped-charge effect with liquid jet impacts at $>100\text{m/s}$.

Ultrasonic irradiation of liquid-powder suspensions produces another effect: high velocity inter-particle collisions [4]. Cavitation and the shockwaves it creates in a slurry can accelerate solid particles to high velocities (Fig. 8). The resultant collisions are capable of inducing dramatic changes in surface morphology, composition, and reactivity. Heterogeneous catalysts often require rare and expensive metals. The use of ultrasound offers some hope of activating less reactive, but also less costly, metals. For example, the effects of ultrasound on Ni powder is shown in Fig. 9, with the chemical consequence of enormously increasing the catalytic rates of hydrogenation by Ni powder ($>10^5$ -fold) [5].

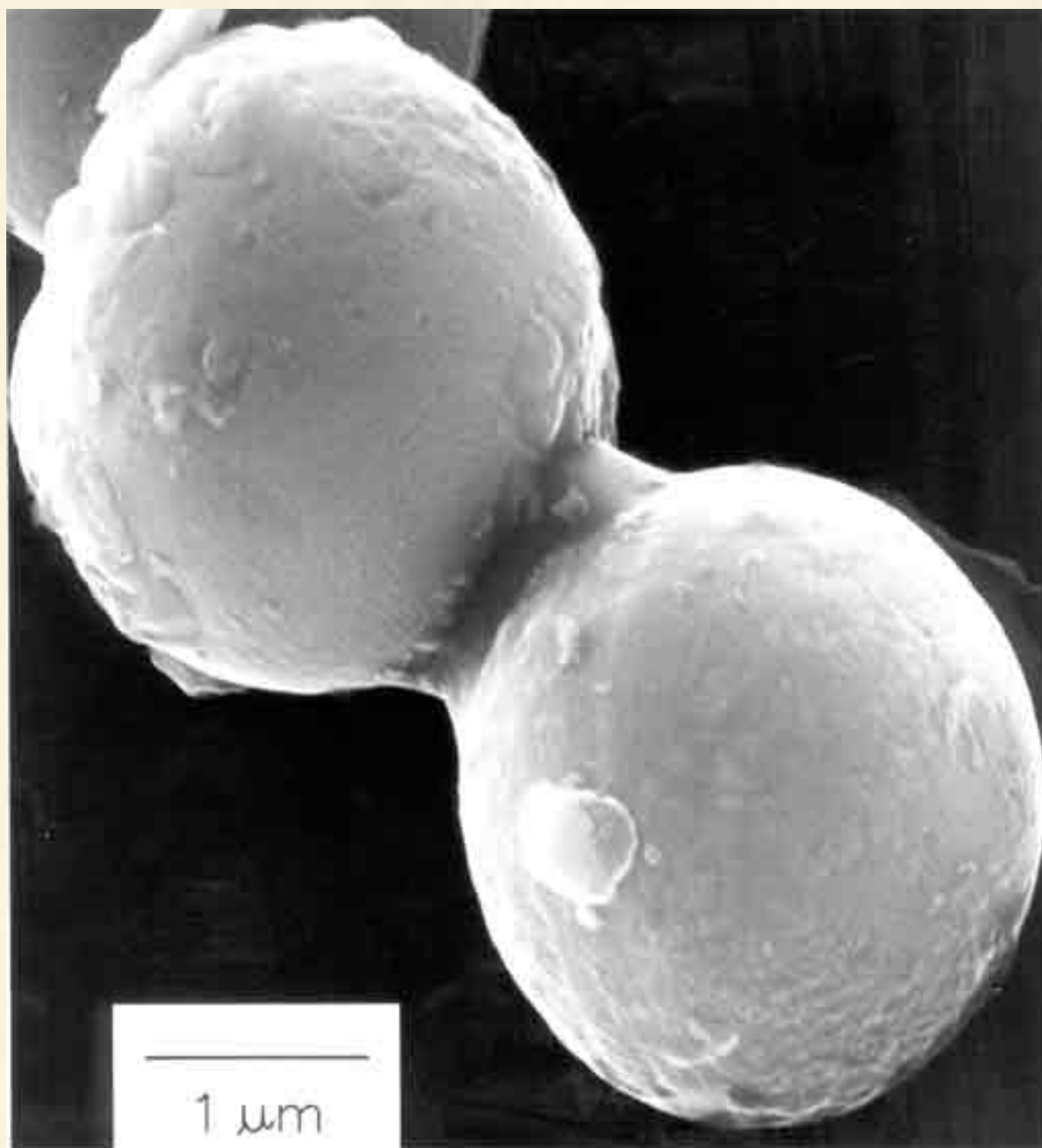


Fig. 8. Scanning electron micrograph of 5 μ m diameter Zn powder. Neck formation from localized melting is caused by high-velocity interparticle collisions.

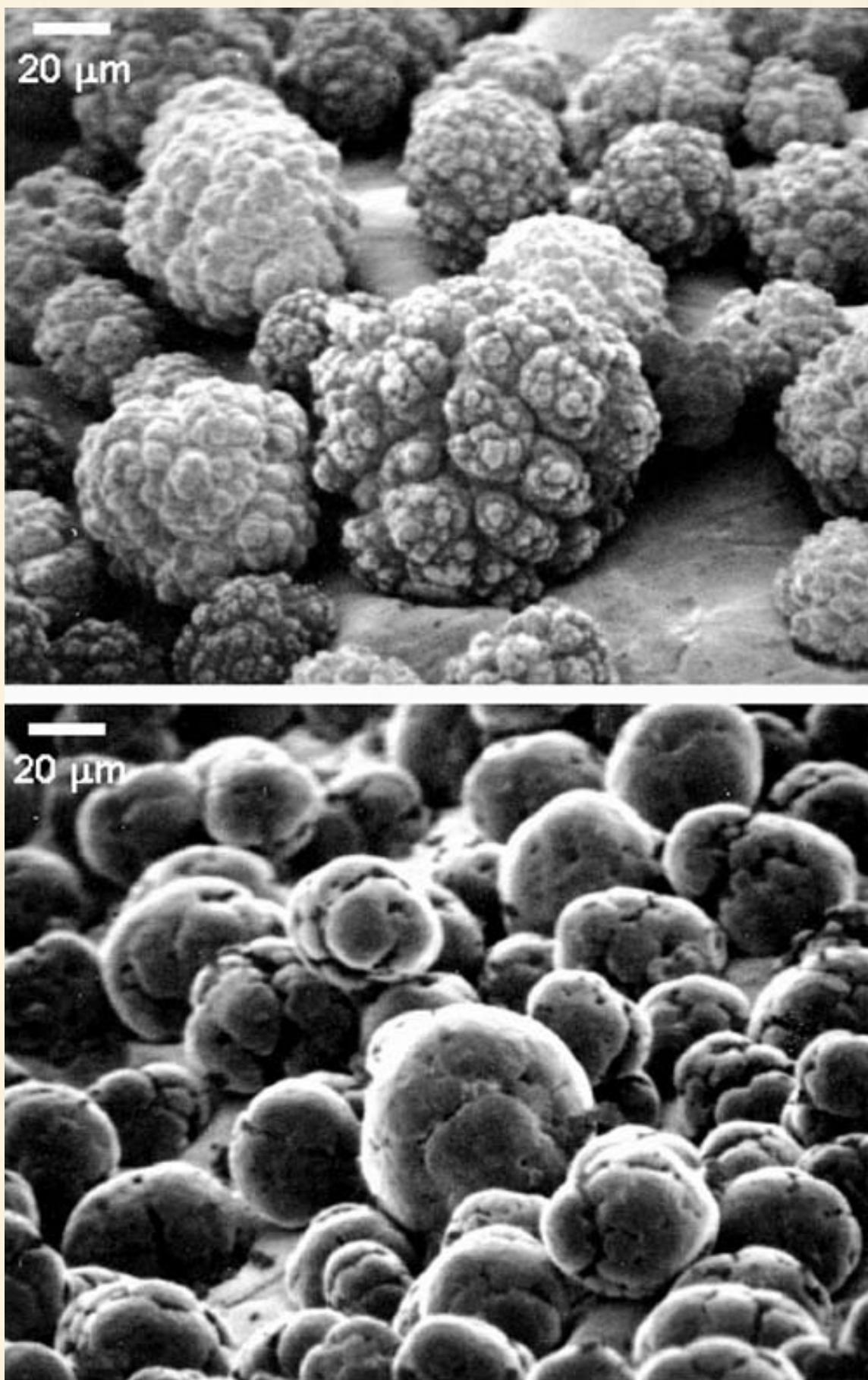


Fig. 9. The effect of ultrasonic irradiation on the surface morphology and particle size of Ni powder. Upper image is before ultrasound and lower is after irradiation of a slurry in decane. High-velocity interparticle collisions caused by ultrasonic irradiation of slurries are responsible for the smoothing and removal of

passivating oxide coating.

[Highlighted articles are downloadable in PDF format.](#)
[To get the free Adobe PDF reader, click on this text.](#)

[1] K.S. Suslick in *Kirk-Othmer Encyclopedia of Chemical Technology*; 4th Ed. J. Wiley & Sons: New York, 1998, vol. 26, 517-541.

[2] Suslick, K. S.; Didenko, Y.; Fang, M. M.; Hyeon, T.; Kolbeck, K. J.; McNamara, W. B. III; Mdleleni, M. M.; Wong, M. "Acoustic Cavitation and Its Chemical Consequences" *Phil. Trans. Roy. Soc. London A*, **1999**, *357*, 335-353.

[3] K.S. Suslick, M.W. Grinstaff, *J. Am. Chem. Soc.* **112**, 7807 (1990)

[4] S.J. Doktycz, K.S. Suslick *Science*, **247**, 1067 (1990).

[5] K.S. Suslick in *Handbook of Heterogeneous Catalysis*; Ertl, G.; Knozinger, H.; Weitkamp, J.; eds.; Wiley-VCH: Weinheim, 1997; vol. 3, ch. 8.6.

[Excerpts from Funded Proposals](#)

[Other Recent Publications](#)



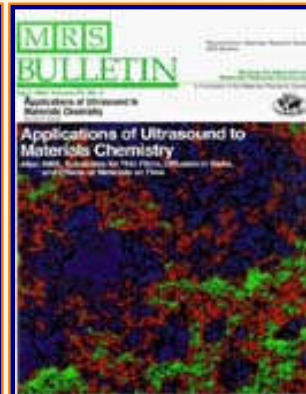
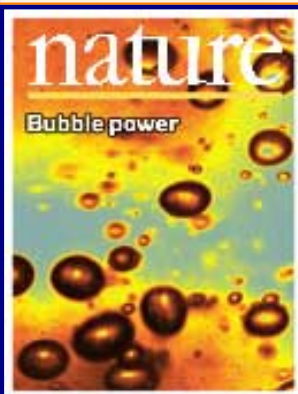
SUSLICK GROUP WEBSITE:

THE SCIENCE	THE GROUP	THE MAÎTRE D'	LAGNIAPPE: A LITTLE EXTRA
<u>Overview</u>	<u>Current Group Members</u>	<u>CV: Abbreviated, Full</u>	<u>Art and Science</u>
<u>Outline of Projects</u>	<u>Group Meetings</u>	<u>Suslick Group Brochure</u>	<u>Chymistes: The Distillers of Waters</u>
<u>Synopses: Sonochemistry</u> <u>Metalloporph.</u>	<u>Group Responsibilities</u>	<u>Complete Publication List</u>	<u>A Chemist Meets Hollywood</u>
<u>Executive Summary: Smell-Seeing</u>	<u>Web Based Resources</u>	<u>Academic Genealogy</u>	<u>A Chemist In Court</u>
<u>Introduction to Sonochemistry</u>	<u>Safety Resources</u>	<u>Press Clippings</u>	<u>Words of Humor and Wisdom</u>
<u>Proposal Excerpts</u>	<u>Group Equipment</u>	<u>How To Give A Seminar</u>	<u>Laws of the Universe</u>
<u>Funding</u>	<u>Past Group Members</u>	<u>Ch315 Inorganic Chemistry</u>	<u>Cartoons of Humor and Wisdom</u>
<u>Information for Visitors</u>	<u>Group Photogallery</u>	<u>Construction of the CLS Lab</u>	<u>Sculpture & Masks</u>

©2003, K.S. Suslick; all rights reserved.

Comments and suggestions: ksuslick@uiuc.edu

The Suslick Research Group



EXECUTIVE SUMMARY:

PORPHYRIN AND METALLOPORPHYRIN CHEMISTRY

Kenneth S. Suslick

[Overview](#)

[Outline of
Research Projects](#)

[Introduction to
Sonochemistry](#)

[Exec. Summary:
Sonochemistry](#)

[Exec. Summary:
Porphyrin Research](#)

[Exec. Summary: Smell-
Seeing](#)

[Complete
Publication List](#)

[Abbreviated Curriculum
Vitae](#)

[Academic
Genealogy](#)

[Press
Clippings](#)

The research team led by Professor Suslick has been at the leading edge of research on synthetic metalloporphyrins for applications as synthetic analogs of heme proteins, shape selective oxidations, , and diverse materials chemistry applications including nanoporous network solids, non-linear optical materials, and selective sensors.

Background —Porphyrins (which comes from the Greek for "purple") are based on 16-atom rings containing four nitrogen atoms (Fig. 1); they are of perfect size to bind nearly all metal ions. Heme proteins (which contain iron porphyrins) are ubiquitous in nature and serve many roles, including O₂ storage and transport (myoglobin and hemoglobin), electron transport (cytochromes b and c), and O₂ activation and utilization (cytochrome P450 and cytochrome oxidase). Related macrocycles include the chlorophylls (which have a central magnesium ion) and pheophytins (which are metal free) in the photosynthetic apparatus of plants and bacteria and vitamin B-12 (which has cobalt) found in bacteria and animals.

[Current Research
Funding](#)

[Excerpts from
Funded Research](#)

[Inventory of
Group Equipment](#)

[Information
for Visiting](#)

[Current Research Group
Members](#)

[Group
Meetings](#)

[Group
Chores](#)

[Past Research
Group Members](#)

[Group
Photogallery](#)

[Web Resources](#)

[Laboratory Safety
Resources](#)

[Art and Science:
Journal Covers](#)

[Sculpture &
Masks](#)

[A Chemist
Meets Hollywood](#)

[Chymistes: The Distillers
of Waters](#)

[A Chemist
In Court](#)

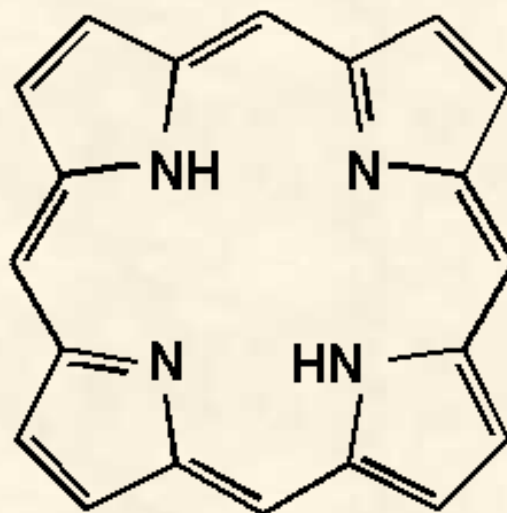


Fig. 1. Porphine, the simplest porphyrin.

In order to gain new insights into the structure and function of metalloproteins, we are involved in the design, synthesis, and physical characterization of complex molecules that look and behave like heme protein active sites. Here we are concerned with issues of oxidation chemistry, catalysis, and molecular recognition [1].

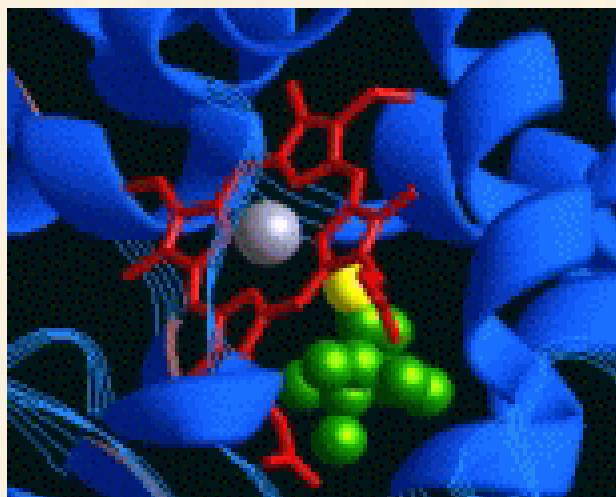


Fig. 2. The active site of cytochrome P450, the heme protein responsible for making water soluble molecules out of hydrophobic ones.

Metalloporphyrins and related macrocycles also provide an extremely versatile synthetic base on which to design physical and chemical properties. Another goal of our research effort has been the exploration of metalloporphyrin assemblies as field responsive materials, particularly for photoresponsive applications. Porphyrins can be molecularly engineered to provide erect desirable molecular and materials properties, including very large dipole moments, polarizabilities, and hyperpolarizabilities. The non-linear optical properties of these materials are of special interest. These molecules can be built for energy transfer with molecular control, giving them potential applications in optical communications, data storage, and electrooptical signal processing, as well as in modeling of the photosynthetic reaction center [2].

Recent Accomplishments — To probe the origins of molecular recognition, we have used

[Humor and
Wisdom](#)

[Laws of the Universe](#)

[Cartoons of Humor and
Wisdom](#)

[Chem 115: Chemistry of
Everyday Phenomena](#)

[Chem 315: Inorganic
Chemistry](#)

sterically hindered, "bis-pocket" porphyrins to *reverse* the normal reactivity of hydrocarbons, enabling us to oxidize selectively primary C-H bonds or the least substituted double bonds. In this work with synthetic metalloporphyrins and with dendrimer-porphyrins, we have synthesized superstructured macrocycles as shape, size, and polarity selective oxidation catalysts for both hydroxylation and epoxidation [1, 3].

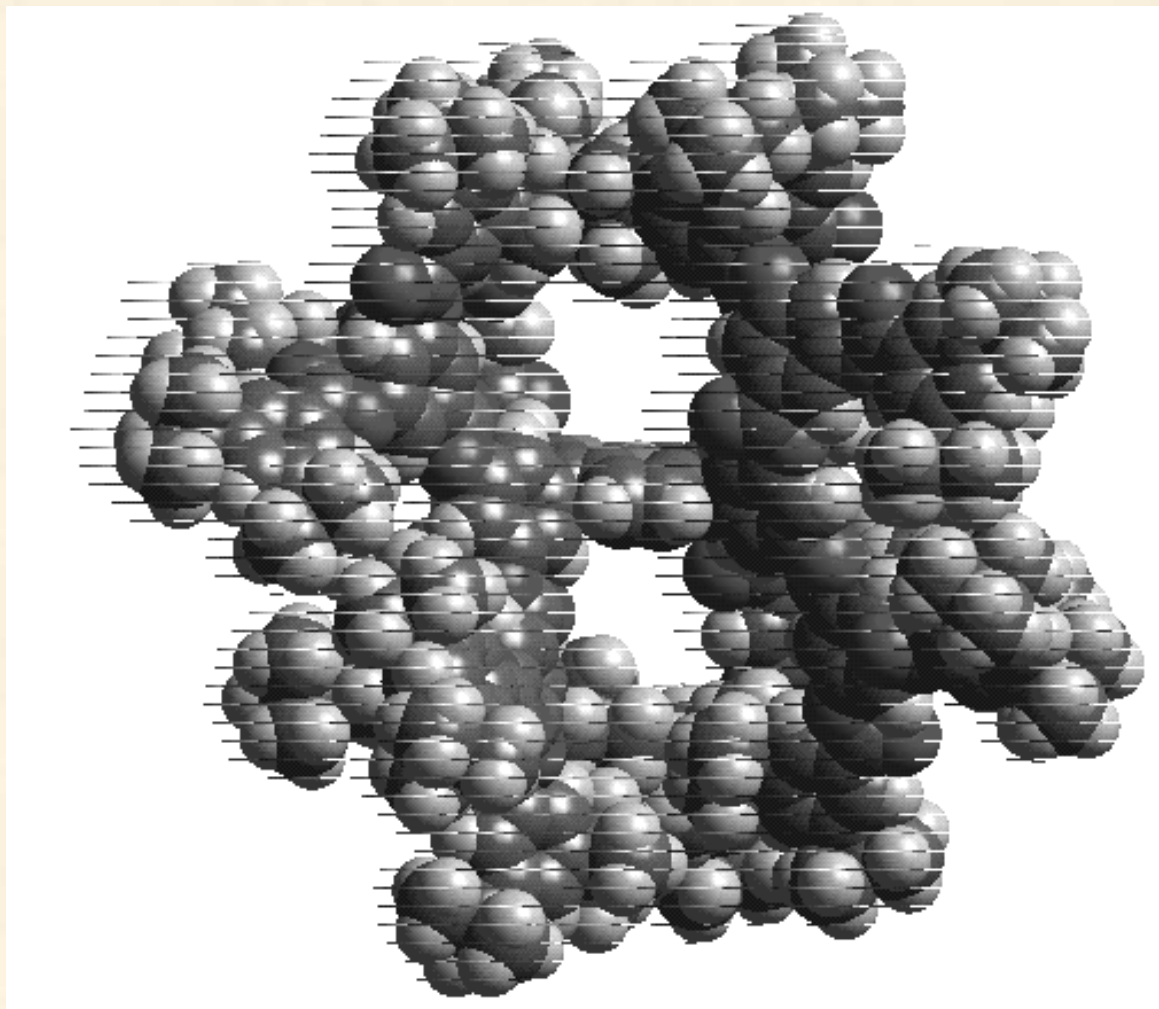


Fig. 3. A bis-pocketed dendrimer porphyrin. The protecting pockets on both sides of the porphyrin provides for molecular recognition of incoming substrates and for shape selective catalytic oxidation of alkanes and alkenes.

In other work, we are interested in the interaction of metalloporphyrins with peptides [4]. For example, we have designed synthetic heme-peptide complexes by the coordination of amphiphilic peptides to heme and have been examined to determine the influence of the peptide on the properties of the heme and vice versa. The presence of hydrophobic residues flanking a coordinated histidine dramatically increases peptide binding to the heme by a factor of nearly 6000 relative to histidine. Hydrophobic interactions between the porphyrin face and the non-polar side chains of the amino acid residues make a major contribution to the stability of the heme-peptide complexes. Circular dichroism spectra demonstrate that heme binding induces substantial helix formation, presumably to maximize the hydrophobic stabilization. The complexes with the most hydrophobic peptides are the most difficult to reduce, as expected from relative ligand binding to Fe^{II} vs. Fe^{III} .

Other projects are more materials and biomaterials oriented. For example, we are developing

the use of porphyrins as non-linear optical materials and as nanoporous catalytic materials.

As one example, we have recently created a new class of bis-pocketed discotic liquid crystals of porphyrins, metalloporphyrins and ligated metalloporphyrins to provide nanostructured assemblies of photoresponsive materials [5].

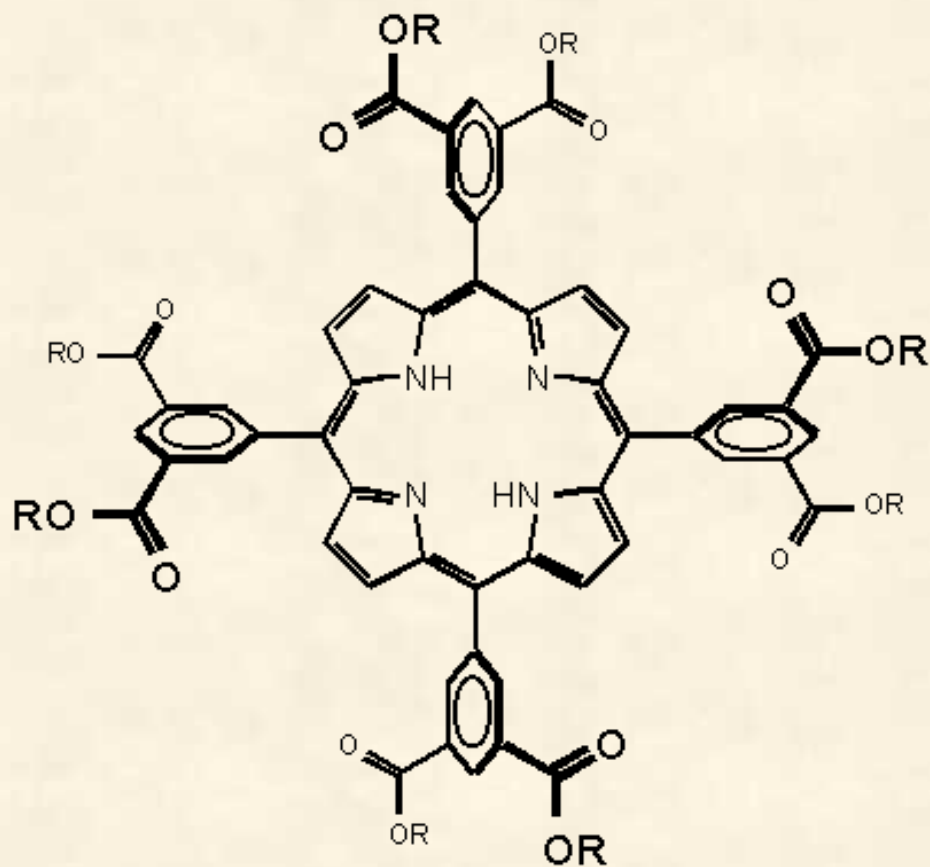


Fig. 4 Bis-pocketed columnar hexagonal liquid crystal porphyrins: *n*-alkyl esters of 5,10,15,20-(3,5-dicarboxyphenyl)porphyrin, H₂DCarPP, R = *n*-C_nH_{2n+1}, n = 8, 10, 12, 14, 16, 18, 20, 22.

We are also developing new nanoporous network solids of highly functionalized porphyrins to provide controlled porphyrin orientation in the solid state and to produce molecularly-designed molecular sieves [6]. We intend to explore the use of these solids as heterogeneous shape-selective oxidation catalysts. An example of one such structure is shown below:

Octahydroxy Porphyrins

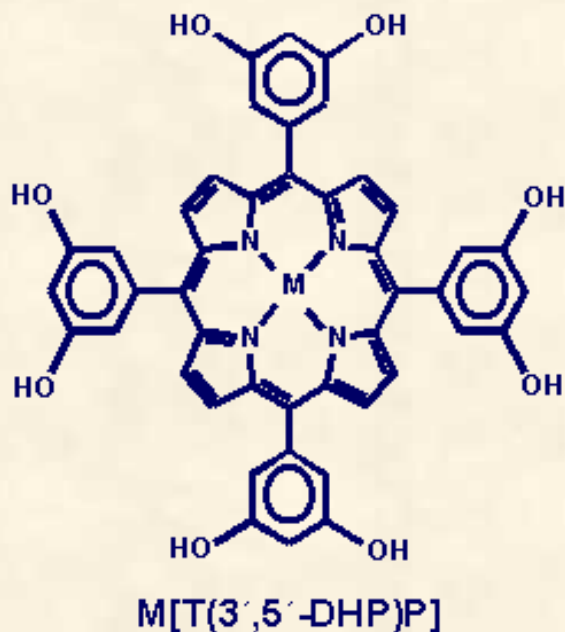


Fig. 5. A pair of octahydroxy substituted porphyrins. Hydrogen bonding networks of these porphyrins are easily prepared in a wide variety of crystal morphologies depending on metal, solvates, and axial ligation.(3,5-dihydroxyphenyl)porphyrin.

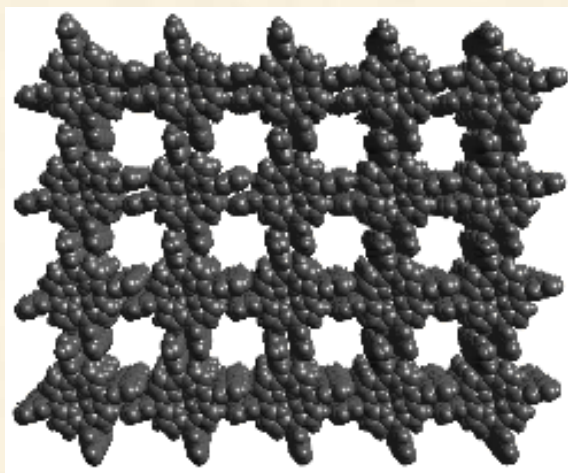


Fig. 6. A porphyrin nanoporous solid. Eight hydrogen bonds per porphyrin produce a columnar stacking in this molecular packing diagram of the x-ray structure of tetrakis(3,5-dihydroxyphenyl)porphyrin.

Our most recent success has involved the use of metalloporphyrin arrays as sensors for a new concept in artificial olfaction. This electronic nose is based on visualizing the color changes associated with the interaction of vapors with metalloporphyrin dyes. We call this technique "Smell-Seeing" [7].

[Highlighted articles are downloadable in PDF format.](#)
[To get the free Adobe PDF reader, click on this text.](#)

- [1] Suslick, K. S.; van Duesen-Jeffries, S. "Shape Selective Oxidation Catalysis" *Comprehensive Supramolecular Chemistry*, vol. 5; ed. Suslick, K.S.; Elsevier Publishers: Oxford, 1996, pp. 141-170.
- [2] Girolami, G. S.; Hein, C. L.; Suslick, K. S. "Bis(porphyrin) Sandwich Complex with an Appended Quinone," *Angew. Chem. Intl. Ed.* **1996**, *35*, 1223-1225.
- [3] Bhyrappa, P.; Young, J. K.; Moore, J. S.; Suslick, K. S. "Dendrimer-Metalloporphyrins: Synthesis and Characterization," *J. Am. Chem. Soc.*, **1996**, *118*, 5708-5711.
- [4] Huffman, D. L.; Rosenblatt, M. M.; Suslick, K. S. "Synthetic Heme-Peptide Complexes," *J. Am. Chem. Soc.*, **1998**, *120*, 6183-6184.
- [5] Patel, B. R.; Suslick, K. S. "Discotic Liquid Crystals from a Bis-Pocketed Porphyrin" *J. Am. Chem. Soc.*, **1998**, *120*, 11802-11803.
- [6] Bhyrappa, P.; Wilson, S. R.; Suslick, K. S. "Hydrogen Bonded Porphyrinic Solids: Surpramolecular Networks of Octahydroxy Porphyrins," *J. Am. Chem. Soc.*, **1997**, *119*, 8492-8502.
- [7] Rakow, N. A.; Suslick, K. S. "A Colorimetric Sensor Array for Odour Visualization" *Nature*, **2000**, *406*, 710-714.

[Excerpts from Funded Proposals](#)

[Other Recent Publications](#)

SUSLICK GROUP WEBSITE:

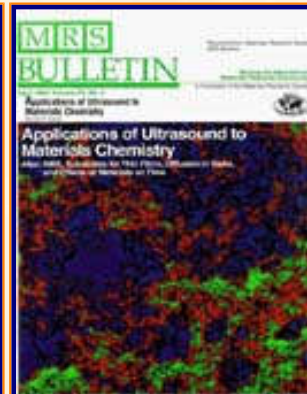
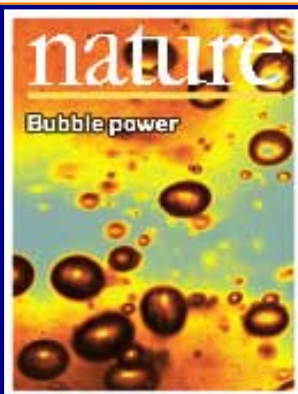
THE SCIENCE	THE GROUP	THE MAÎTRE D'	LAGNIAPPE: A LITTLE EXTRA
<u>Overview</u>	<u>Current Group Members</u>	<u>CV: Abbreviated, Full</u>	<u>Art and Science</u>

<u>Outline of Projects</u>	<u>Group Meetings</u>	<u>Suslick Group Brochure</u>	<u>Chymistes: The Distillers of Waters</u>
<u>Synopses: Sonochemistry</u>	<u>Group Responsibilities</u>	<u>Complete Publication List</u>	<u>A Chemist Meets Hollywood</u>
<u>Metalloporph.</u>			
<u>Executive Summary: Smell-Seeing</u>	<u>Web Based Resources</u>	<u>Academic Genealogy</u>	<u>A Chemist In Court</u>
<u>Introduction to Sonochemistry</u>	<u>Safety Resources</u>	<u>Press Clippings</u>	<u>Words of Humor and Wisdom</u>
<u>Proposal Excerpts</u>	<u>Group Equipment</u>	<u>How To Give A Seminar</u>	<u>Laws of the Universe</u>
<u>Funding</u>	<u>Past Group Members</u>	<u>Ch315 Inorganic Chemistry</u>	<u>Cartoons of Humor and Wisdom</u>
<u>Information for Visitors</u>	<u>Group Photogallery</u>	<u>Construction of the CLS Lab</u>	<u>Sculpture & Masks</u>

©2003, K.S. Suslick; all rights reserved.

Comments and suggestions: ksuslick@uiuc.edu

The Suslick Research Group



SMELL-SEEING

[Click here for information about *ChemSensing, Inc.*, which we've recently established for the commercialization of this technology.](#)

[Overview](#)

[Outline of
Research Projects](#)

[Introduction to
Sonochemistry](#)

[Exec. Summary:
Sonochemistry](#)

[Exec. Summary:
Porphyrin Research](#)

[Exec. Summary: Smell-
Seeing](#)

[Complete
Publication List](#)

[Abbreviated Curriculum
Vitae](#)

[Academic
Genealogy](#)

[Press
Clippings](#)

Array based vapor sensing has emerged as a powerful approach toward the detection of chemically diverse analytes. Based on cross-responsive sensor elements, these systems aim to produce composite responses unique to each odorant, in a fashion similar to the mammalian olfactory system. We have recently discovered [Rakow, N. A.; Suslick, K. S. "A Colorimetric Sensor Array for Odour Visualization" *Nature*, **2000**, *406*, 710-714.; Suslick, K. S.; Rakow, N. A. "Colorimetric Artificial Nose Having an Array of Dyes and Method for Artificial Olfaction" *U.S. Patent 6,368,558*; April 9, 2002. Suslick, K. S.; Rakow, N. A.; Sen, A. "Colorimetric Artificial Nose Having an Array of Dyes and Method for Artificial Olfaction: Shape Selective Sensors" *U.S. Patent 6,495,102 B1*; Dec. 17, 2002.] a new and simple approach to array detection of odorants using the colorimetric response from a library of immobilized vapor-sensing dyes. We call this technique "smell-seeing".

[Current Research
Funding](#)

[Excerpts from
Funded Research](#)

[Inventory of
Group Equipment](#)

[Information
for Visiting](#)

[Current Research Group
Members](#)

[Group
Meetings](#)

[Group
Chores](#)

[Past Research
Group Members](#)

[Group
Photogallery](#)

[Web Resources](#)

[Laboratory Safety
Resources](#)

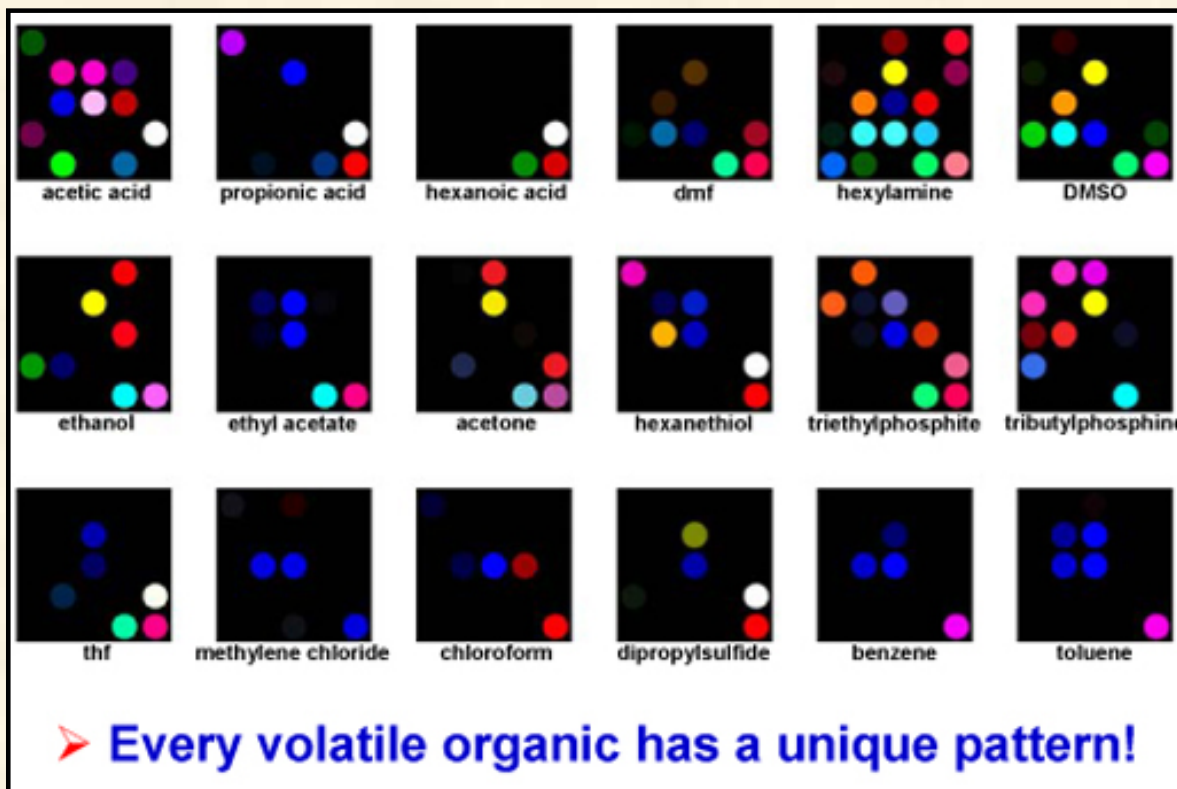
[Art and Science:
Journal Covers](#)

[Sculpture &
Masks](#)

[A Chemist
Meets Hollywood](#)

[Chymistes: The Distillers
of Waters](#)

[A Chemist
In Court](#)



"Smell-Seeing"

As inorganic chemists have long realized, compounds that bind to metal ions are nearly always highly odiferous. For this reason, metal-containing dyes, such as metalloporphyrins, provide a way of reporting the presence of odors by changes in color. We use a two-dimensional display of metalloporphyrins as sensor elements for the visual identification of a wide range of olfactants (including alcohols, amines, ethers, phosphines, phosphites, thioethers, and thiols) and even weakly-ligating solvent vapors (arenes, halocarbons, and ketones). The solid-state color changes are similar to those known for metal ligation in solution. The array shows good linear response to single analytes and interpretable responses to analyte mixtures. Water vapor does not interfere with other analytes. Unique color fingerprints can be obtained below 1 ppm, and responses to analyte concentrations below 100 ppb have been observed. Applications for this sensing array include general-purpose vapor dosimeters and analyte-specific detectors (e.g., for insecticides, drugs, or neurotoxins).

Metalloporphyrins provide a versatile synthetic base on which to design desired properties: i.e., molecular engineering. To tailor our molecular recognition of olfactants, we have used sterically hindered, "bis-pocket" porphyrins to control the response of our array sensors. In this work with synthetic metalloporphyrins and with dendrimer-porphyrins, we are developing superstructured macrocycles as shape, size, and polarity selective oxidation catalysts and as selective molecular sensors.

In other recent work, we have made the connection complete by finding a conserved metal ion binding site in the mammalian olfactory receptors. Wang, J.; Luthey-Schulten, Z.; Suslick, K. S. "Is the Olfactory Receptor A Metalloprotein?" *Proc. Natl. Acad. Sci. U.S.A.*, **2003**, *100*, 3035-3039.

[Humor and
Wisdom](#)

[Laws of the Universe](#)

[Cartoons of Humor and
Wisdom](#)

[Chem 115: Chemistry of
Everyday Phenomena](#)

[Chem 315: Inorganic
Chemistry](#)

Our Papers on Smell-Seeing, Olfaction, and Some Related Topics:

To download the full paper in PDF format, click on the reference below.

Wang, J.; Luthey-Schulten, Z.; Suslick, K. S. "Is the Olfactory Receptor A Metalloprotein?" [*Proc. Natl. Acad. Sci. U.S.A.*, 2003, 100, 3035-3039.](#)

Rakow, N. A.; Suslick, K. S. "A Colorimetric Sensor Array for Odour Visualization" [*Nature*, 2000, 406, 710-714.](#)

*The following won the Wolfgang Göpel Award for Best Paper;
ISOEN-8, The Electrochemical Society, 2001:*

Suslick, K. S.; Rakow, N. A. "[A Colorimetric Nose: 'Smell-Seeing'](#)" *Artificial Chemical Sensing: Olfaction and the Electronic Nose*, Stetter, J.R.; Pensrose, W. R., eds. Electrochem. Soc.: Pennington, NJ, 2001, pp. 8-14.

; Suslick, K. S.; Rakow, N. A. "Colorimetric Artificial Nose Having an Array of Dyes and Method for Artificial Olfaction" [*U.S. Patent 6,368,558; April 9, 2002.*](#)

Suslick, K. S.; Rakow, N. A.; Sen, A. "Colorimetric Artificial Nose Having an Array of Dyes and Method for Artificial Olfaction: Shape Selective Sensors" [*U. S. Patent 6,495,102 B1; Dec. 17, 2002.*](#)

Suslick, K.S.; Kosal, M.E.; Rakow, N. A.; Sen, A. "['Smell-Seeing: A New Approach to Artificial Olfaction'](#)" *Proc. EURODEUR, Paris, 2001, in press.*

Sen, A; Suslick, K. S. "Shape-Selective Discrimination of Small Organic Molecules" [*J. Am. Chem. Soc.*, 2000, 122, 11565-11566.](#)

Suslick, K. S. "[Shape Selective Oxidation by Metallo-porphyrins,](#)" in *The Porphyrin Handbook*, Kadish, K.; Smith, K.; Guilard, R., ed.; Academic Press: New York, 2000; vol. 4, ch. 28, pp. 41-63.

Bhyrappa, P.; Vijayanthimala, G.; Suslick, K. S. "Shape-Selective Ligation to Dendrimer-Metalloporphyrins," [*J. Am. Chem. Soc.*, 1999, 121, 262-263.](#)

Press Clippings on Smell-Seeing:

[News & Views Commentary, 17 Aug 00,](#)
["Picture the Smell", Nature 2000, 406, 682-683](#)

[CBS Evening News \(WCIA, Champaign, IL\), 8/16/00;](#)
[3 min. video clip in RealPlayer format \(3.7 MB\).](#)

[To download the free RealPlayer Basic viewer, click here.](#)

[CNBC, 8/17/00:](#)
["What's That Smell? Get a Good Look."](#)

[ABC News in Science 21/08/00:](#)
["Artificial nose sees smell"](#)

[CBC News \(Canadian Broadcasting Corp.\), 8/21/00:](#)
["Fake nose actually smells"](#)

[Chemical & Engineering News, 08/21/00:](#)
["NEWS OF THE WEEK - A 'Nose' That Shows Scents In Color"](#)

[Business Week, 09/04/00:](#)
["Developments To Watch"](#)

[New Scientist, 08/17/00:](#)
["Sniffing out fakes"](#)

[The News-Gazette, 8/17/00, p. 1 \(!\):](#)
["UI scientists say smells are really quite a sight to see."](#)

[Chicago Tribune, 8/17/00, sect. 1, p. 5:](#)
["U. OF I. Researcher Provides Whiff of Brand-New Technology"](#)

[Reuters/Yahoo News; 8/17/00:](#)
["Artificial Nose 'Sees'" Smells](#)

[Inside Illinois, 8/17/00:](#)
["Artificial Nose Knows"](#)

[NewsDay, 9/19/00:](#)
["The Artificial Sniffer" p. C8-C9.](#)

[The Scientist 14\[17\]:19, Sep. 4, 2000:](#)
["Does The Nose Always Know?"](#)

[Nature Science Update, 8/17/00:](#)
["Seeing scents."](#)

[Discovery.com, 8/16/00:](#)

"Paper Nose Detects Toxics."

Chemistry and Industry, 08/21/2000

"Artificial nose sniffs out colour of odours."

Photonics Spectra, Nov. 2000

"Color-Changing Array Identifies Odors"

Biophotonics International, Nov. 2000

"What the nose knows can also be seen"

Environmental Health Perspectives (NIH), March 2001

"Smelling in Color: A Rainbow of Possibilities"

Scientific American, March 2001

"Plenty to Sniff At"

Wang, J.; Luthey-Schulten, Z.; Suslick, K. S. "Is the Olfactory Receptor A Metalloprotein?" *Proc. Natl. Acad. Sci. U.S.A.*, **2003**, *100*, 3035-3039.

Chemical & Engineering News, Mar. 3, 2003.

"The Right Snuff," *St. Louis Post-Dispatch*, (Front Page!) Feb. 25, 2003.

Champaign News Gazette, p. 2, Mar. 2, 2003.

"Heavy Metals Play Crucial Role in the Ability to Smell" *Orlando Sentinel*, Mar. 2, 2003.

"Metals Attract Strong, Bad Odors" *Baltimore Sun*, Mar. 3, 2003.

"Raising A Stink" *San Diego Union Tribune*, Mar. 12, 2003.

"Metals Ions May Play Big Role In How We Sense Smells" *Science Daily*, Mar. 3, 2003.

"The Nose of the Matter" *Food Navigator*, Mar. 2, 2003.

"The Right Snuff," *STL Today* Feb. 24, 2003.

"Dead Nose," *Die Zeit Wissen* Mar. 1, 2003. /b>

EXCERPTS FROM FUNDED RESEARCH PROPOSALS:

[The Chemical Effects of High Intensity Ultrasound](#)

[Heme Proteins, Microspheres, and their Synthetic Analogs](#)

[Metalloporphyrins as Field Responsive Materials](#)

[Dendrimer-Porphyrins as Sensor Materials](#)

[Smell-Seeing and Molecular Recognition](#)

SUSLICK GROUP WEBSITE:

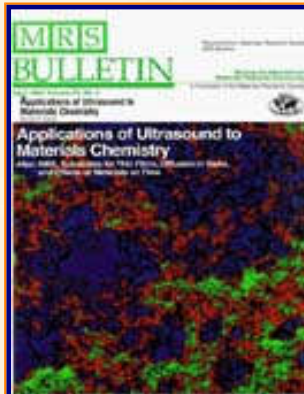
THE SCIENCE	THE GROUP	THE MAÎTRE D'	LAGNIAPPE: A LITTLE EXTRA
<u>Overview</u>	<u>Current Group Members</u>	<u>CV: Abbreviated, Full</u>	<u>Art and Science</u>
<u>Outline of Projects</u>	<u>Group Meetings</u>	<u>Suslick Group Brochure</u>	<u>Chymistes: The Distillers of Waters</u>
<u>Synopses: Sonochemistry</u>	<u>Group Responsibilities</u>	<u>Complete Publication List</u>	<u>A Chemist Meets Hollywood</u>
<u>Metalloporph.</u>			
<u>Executive Summary: Smell-Seeing</u>	<u>Web Based Resources</u>	<u>Academic Genealogy</u>	<u>A Chemist In Court</u>
<u>Introduction to Sonochemistry</u>	<u>Safety Resources</u>	<u>Press Clippings</u>	<u>Words of Humor and Wisdom</u>

<u>Proposal Excerpts</u>	<u>Group Equipment</u>	<u>How To Give A Seminar</u>	<u>Laws of the Universe</u>
<u>Funding</u>	<u>Past Group Members</u>	<u>Ch315 Inorganic Chemistry</u>	<u>Cartoons of Humor and Wisdom</u>
<u>Information for Visitors</u>	<u>Group Photogallery</u>	<u>Construction of the CLS Lab</u>	<u>Sculpture & Masks</u>

©2003, K.S. Suslick; all rights reserved.

Comments and suggestions: ksuslick@uiuc.edu

The Suslick Research Group



ART AND SCIENCE: COVER ART FROM THE SUSLICK GROUP

SCIENCE: March 1990



[Overview](#)

[Outline of
Research Projects](#)

[Introduction to
Sonochemistry](#)

[Exec. Summary:
Sonochemistry](#)

[Exec. Summary:
Porphyrin Research](#)

[Exec. Summary: Smell-
Seeing](#)

[Complete
Publication List](#)

[Abbreviated Curriculum
Vitae](#)

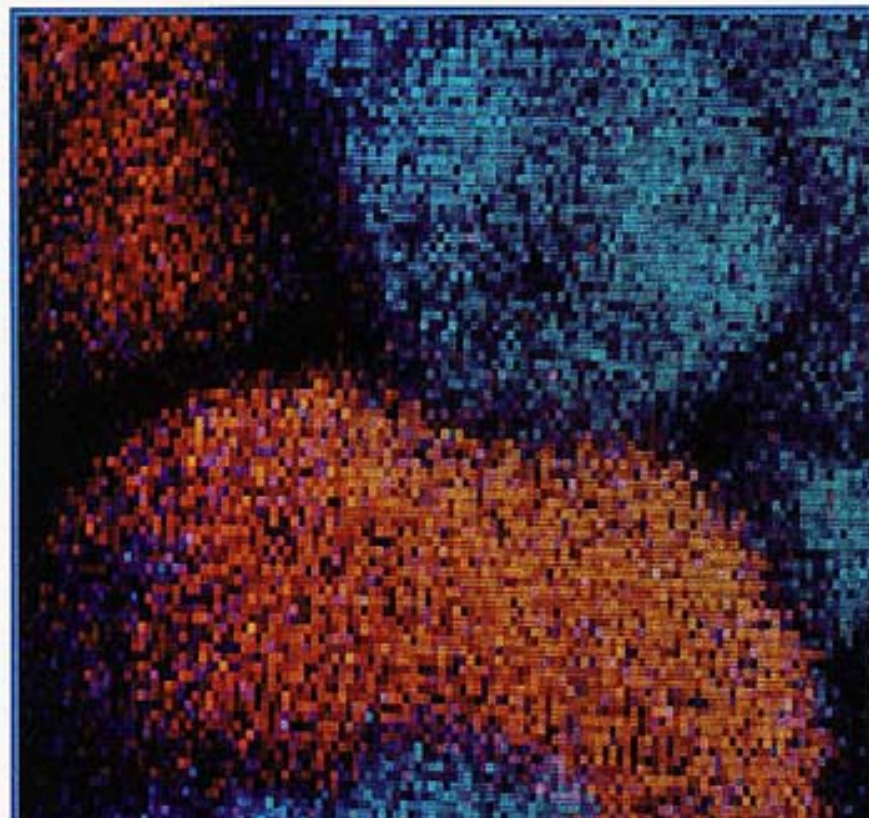
[Academic
Genealogy](#)

[Press
Clippings](#)

AMERICAN
ASSOCIATION FOR THE
ADVANCEMENT OF
SCIENCE

SCIENCE

23 MARCH 1990 \$3.50
VOL. 247 ■ PAGES 1373-1520
PART I



[Current Research](#)

[Funding](#)

[Excerpts from
Funded Research](#)

[Inventory of
Group Equipment](#)

[Information
for Visiting](#)

[Current Research Group
Members](#)

[Group
Meetings](#)

[Group
Chores](#)

[Past Research
Group Members](#)

[Group
Photogallery](#)

[Web Resources](#)

[Laboratory Safety
Resources](#)

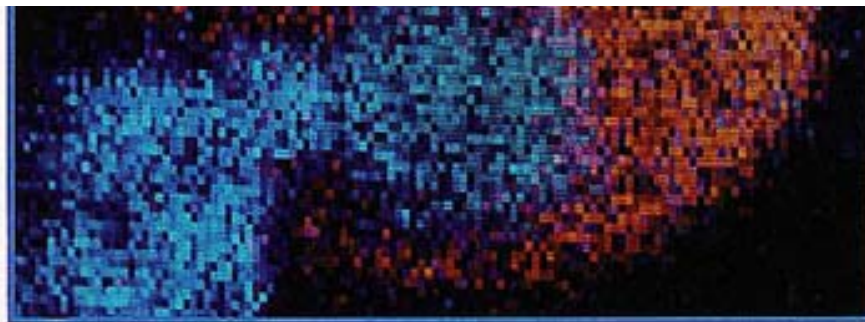
[Art and Science:
Journal Covers](#)

[Sculpture &
Masks](#)

[A Chemist
Meets Hollywood](#)

[Chymistes: The Distillers
of Waters](#)

[A Chemist
In Court](#)



This micrograph shows interparticle collisions induced by ultrasound between tin and iron particles about 20 microns in size. The velocity of such collisions can be as high as 500 m/s (1100 mph). The elemental composition dot map was produced by scanning Auger electron spectroscopy and show tin in orange and iron in blue. [Courtesy of Kenneth S. Suslick and Stephen J. Doktycz, University of Illinois at Urbana-Champaign, on instrumentation in the Center for Microanalysis of Materials, from work funded by the National Science Foundation]

SCIENCE:
March 1990

SCIENCE:
September 1991

MRS BULLETIN:
April 1995

SUPRAMOLECULAR CHEMISTRY:
September 1998

NATURE:
25 July 2002

SUSLICK GROUP WEBSITE:

**Humor and
Wisdom**

Laws of the Universe

**Cartoons of Humor and
Wisdom**

**Chem 115: Chemistry of
Everyday Phenomena**

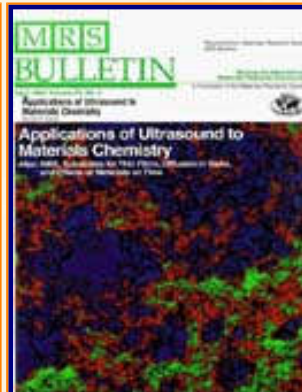
**Chem 315: Inorganic
Chemistry**

THE SCIENCE	THE GROUP	THE MAÎTRE D'	LAGNIAPPE: A LITTLE EXTRA
<u>Overview</u>	<u>Current Group Members</u>	<u>CV: Abbreviated, Full</u>	<u>Art and Science</u>
<u>Outline of Projects</u>	<u>Group Meetings</u>	<u>Suslick Group Brochure</u>	<u>Chymistes: The Distillers of Waters</u>
<u>Synopses: Sonochemistry</u> <u>Metalloporph.</u>	<u>Group Responsibilities</u>	<u>Complete Publication List</u>	<u>A Chemist Meets Hollywood</u>
<u>Executive Summary: Smell-Seeing</u>	<u>Web Based Resources</u>	<u>Academic Genealogy</u>	<u>A Chemist In Court</u>
<u>Introduction to Sonochemistry</u>	<u>Safety Resources</u>	<u>Press Clippings</u>	<u>Words of Humor and Wisdom</u>
<u>Proposal Excerpts</u>	<u>Group Equipment</u>	<u>How To Give A Seminar</u>	<u>Laws of the Universe</u>
<u>Funding</u>	<u>Past Group Members</u>	<u>Ch315 Inorganic Chemistry</u>	<u>Cartoons of Humor and Wisdom</u>
<u>Information for Visitors</u>	<u>Group Photogallery</u>	<u>Construction of the CLS Lab</u>	<u>Sculpture & Masks</u>

©2003, K.S. Suslick; all rights reserved.

Comments and suggestions: ksuslick@uiuc.edu

The Suslick Research Group



ART AND SCIENCE: COVER ART FROM THE SUSLICK GROUP

SCIENCE: September 1991



[Overview](#)

[Outline of
Research Projects](#)

[Introduction to
Sonochemistry](#)

[Exec. Summary:
Sonochemistry](#)

[Exec. Summary:
Porphyrin Research](#)

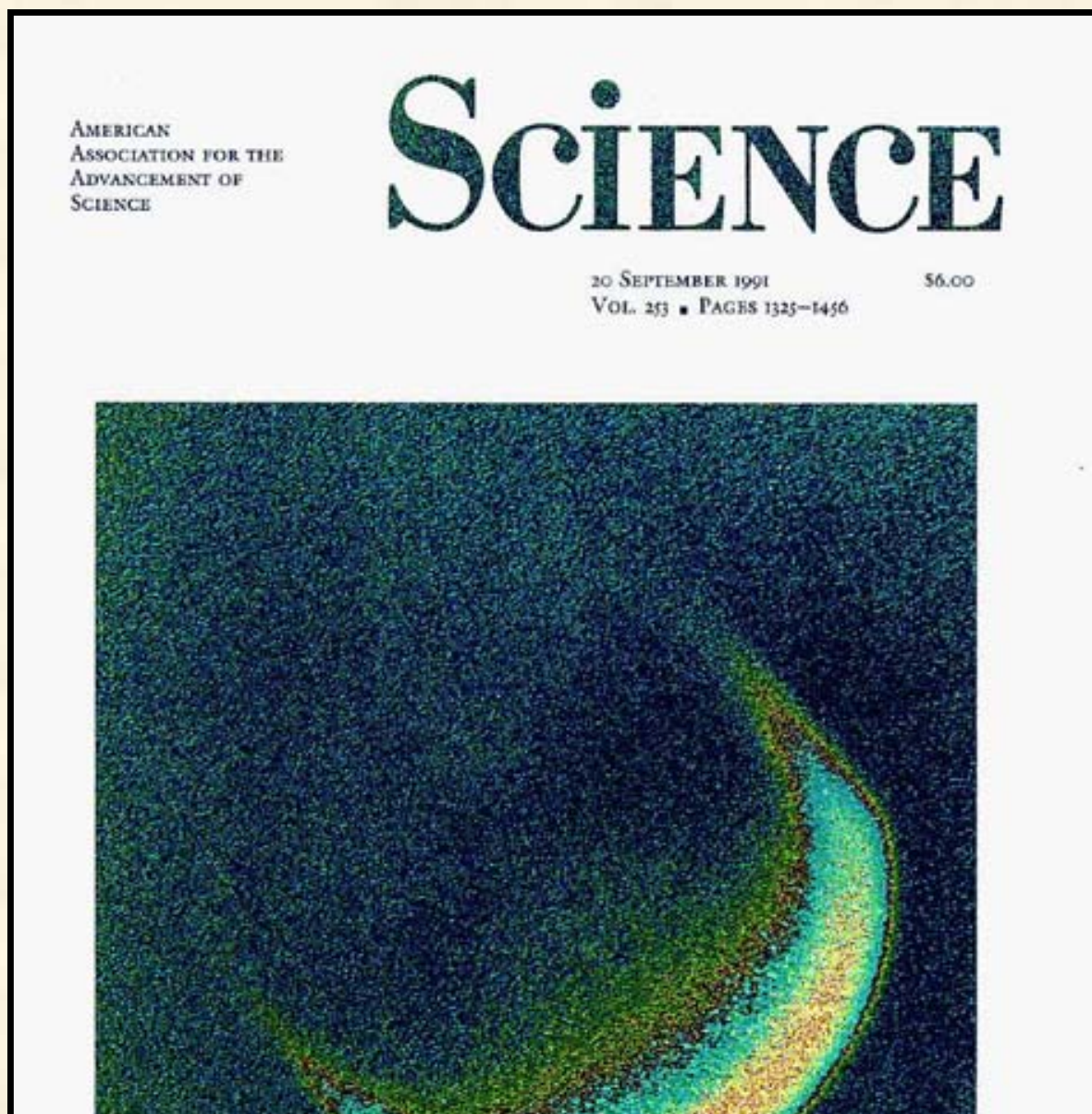
[Exec. Summary: Smell-
Seeing](#)

[Complete
Publication List](#)

[Abbreviated Curriculum
Vitae](#)

[Academic
Genealogy](#)

[Press
Clippings](#)



[Current Research
Funding](#)

[Excerpts from
Funded Research](#)

[Inventory of
Group Equipment](#)

[Information
for Visiting](#)

[Current Research Group
Members](#)

[Group
Meetings](#)

[Group
Chores](#)

[Past Research
Group Members](#)

[Group
Photogallery](#)

[Web Resources](#)

[Laboratory Safety
Resources](#)

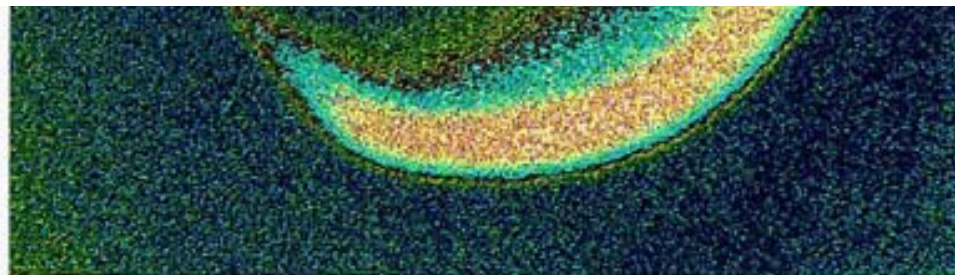
[Art and Science:
Journal Covers](#)

[Sculpture &
Masks](#)

[A Chemist
Meets Hollywood](#)

[Chymistes: The Distillers
of Waters](#)

[A Chemist
In Court](#)



High intensity ultrasound creates localized hot-spots in liquids through the process of cavitation: the formation, growth, and implosive collapse of bubbles. Local heating produces excited states of diatomic carbon (C_2) from hydrocarbons; these states emit light just as they do in a flame. The image of such sonoluminescence from a vibrating titanium rod (1 cm diameter) is shown in false-color. The temperature created in cavitation hot-spots, determined from the spectrum of this emission, is ~ 5000 K. [Photograph by J. A. Gray, K. A. Kemper, and K. S. Suslick in the Department of Chemistry of the University of Illinois at Urbana-Champaign; from work funded by the National Science Foundation.]

SCIENCE:
March 1990

SCIENCE:
September 1991

MRS BULLETIN:
April 1995

SUPRAMOLECULAR CHEMISTRY:
September 1998

NATURE:
25 July 2002

[Humor and
Wisdom](#)

[Laws of the Universe](#)

[Cartoons of Humor and
Wisdom](#)

[Chem 115: Chemistry of
Everyday Phenomena](#)

[Chem 315: Inorganic
Chemistry](#)

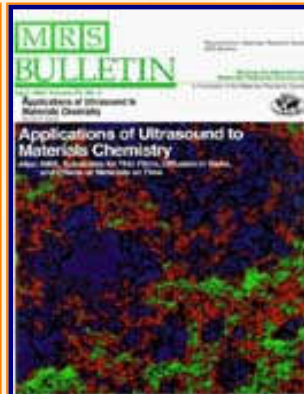
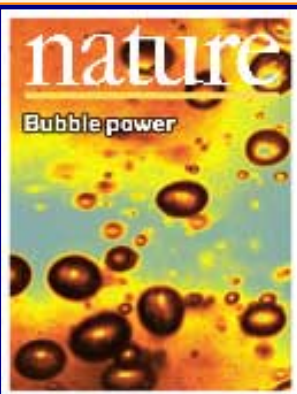
SUSLICK GROUP WEBSITE:

THE SCIENCE	THE GROUP	THE MAÎTRE D'	LAGNIAPPE: A LITTLE EXTRA
Overview	Current Group Members	CV: Abbreviated, Full	Art and Science
Outline of Projects	Group Meetings	Suslick Group Brochure	Chymistes: The Distillers of Waters
Synopsis: Sonochemistry <hr/> Metalloporph.	Group Responsibilities	Complete Publication List	A Chemist Meets Hollywood
Executive Summary: Smell-Seeing	Web Based Resources	Academic Genealogy	A Chemist In Court
Introduction to Sonochemistry	Safety Resources	Press Clippings	Words of Humor and Wisdom
Proposal Excerpts	Group Equipment	How To Give A Seminar	Laws of the Universe
Funding	Past Group Members	Ch315 Inorganic Chemistry	Cartoons of Humor and Wisdom
Information for Visitors	Group Photogallery	Construction of the CLS Lab	Sculpture & Masks

©2003, K.S. Suslick; all rights reserved.

Comments and suggestions: ksuslick@uiuc.edu

The Suslick Research Group



ART AND SCIENCE: COVER ART FROM THE SUSLICK GROUP

[Overview](#)

[Outline of Research Projects](#)

[Introduction to Sonochemistry](#)

[Exec. Summary: Sonochemistry](#)

[Exec. Summary: Porphyrin Research](#)

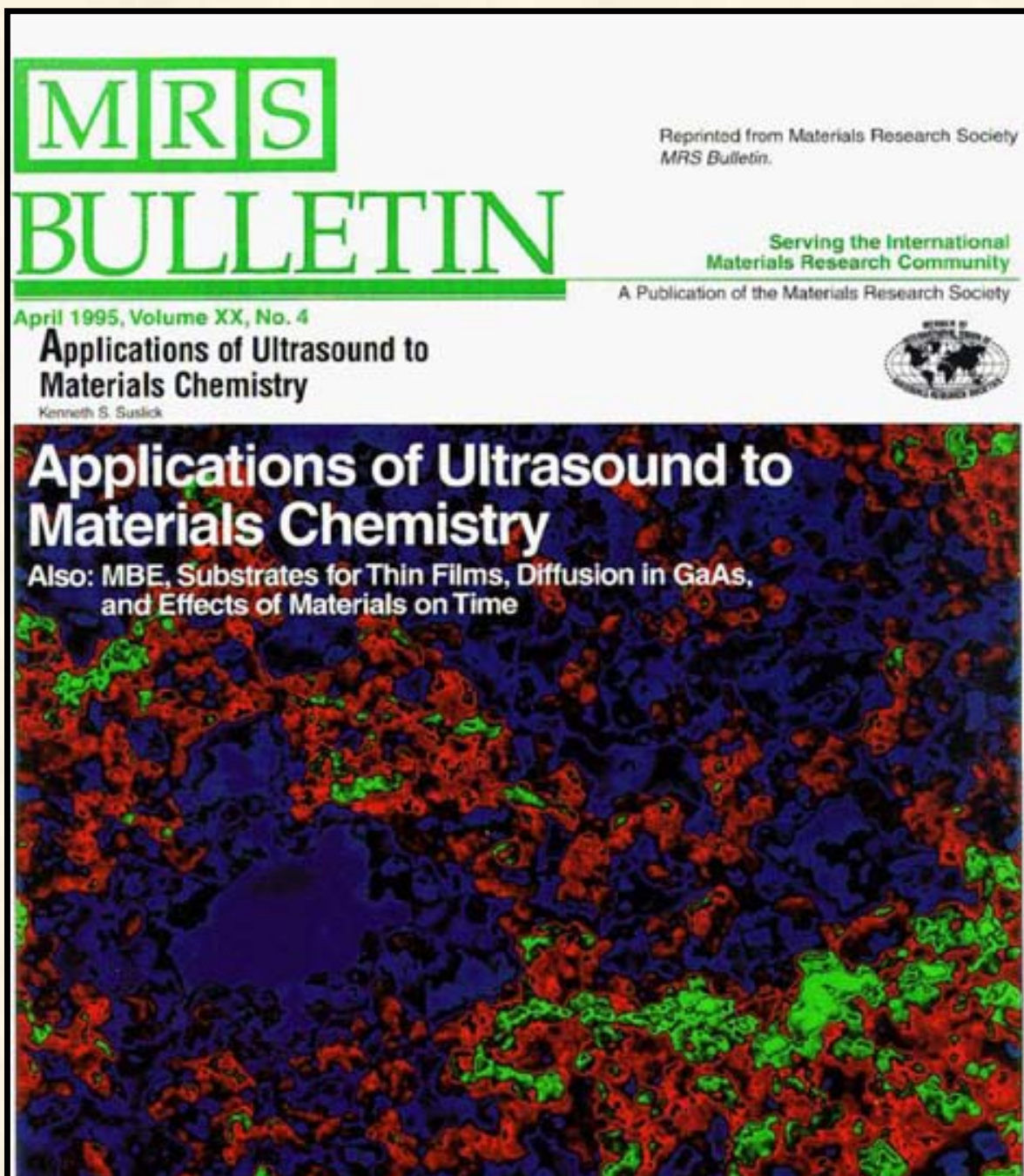
[Exec. Summary: Smell-Seeing](#)

[Complete Publication List](#)

[Abbreviated Curriculum Vitae](#)

[Academic Genealogy](#)

[Press Clippings](#)



[Current Research
Funding](#)

[Excerpts from
Funded Research](#)

[Inventory of
Group Equipment](#)

[Information
for Visiting](#)

[Current Research Group
Members](#)

[Group
Meetings](#)

[Group
Chores](#)

[Past Research
Group Members](#)

[Group
Photogallery](#)

[Web Resources](#)

[Laboratory Safety
Resources](#)

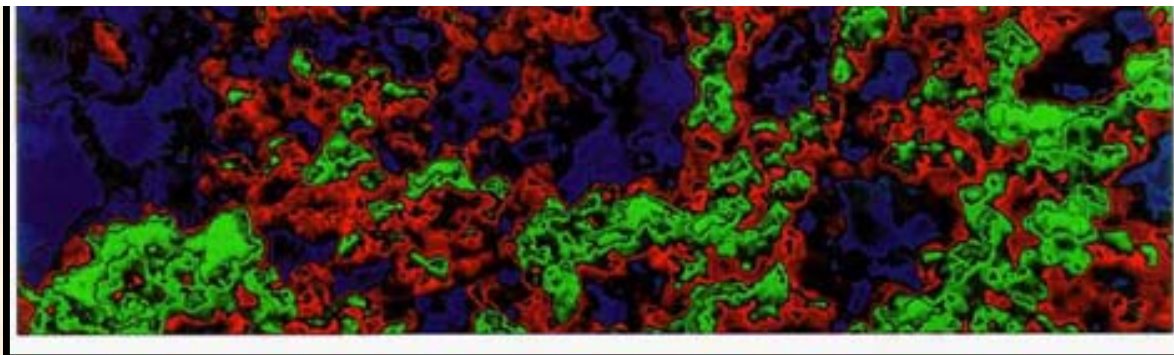
[Art and Science:
Journal Covers](#)

[Sculpture &
Masks](#)

[A Chemist
Meets Hollywood](#)

[Chymistes: The Distillers
of Waters](#)

[A Chemist
In Court](#)



False-color image of the scanning electron micrograph of nanophase, amorphous iron prepared by the ultrasonic irradiation of iron pentacarbonyl solutions. The micrograph shows the porous, coral-like structure formed from nanometer-sized clusters created during acoustic cavitation. The amorphous iron is an extremely soft ferromagnetic material with high catalytic activity. Magnification of the cover image is approximately 100,000. The micrograph was obtained on a Hitachi S800 SEM in the UIUC Center for Microanalysis of Materials, which is supported by the US Department of Energy. Courtesy of Kenneth S. Suslick, Mark W. Grinstaff, and James A. Gray, School of Chemical Sciences, Univ. of Illinois at Urbana-Champaign.

SCIENCE:
March 1990

SCIENCE:
September 1991

MRS BULLETIN:
April 1995

SUPRAMOLECULAR CHEMISTRY:
September 1998

NATURE:
25 July 2002

SUSLICK GROUP WEBSITE:

THE SCIENCE	THE GROUP	THE MAÎTRE D'	LAGNIAPPE: A LITTLE EXTRA
------------------------	----------------------	--------------------------	--------------------------------------

[Humor and
Wisdom](#)

[Laws of the Universe](#)

[Cartoons of Humor and
Wisdom](#)

[Chem 115: Chemistry of
Everyday Phenomena](#)

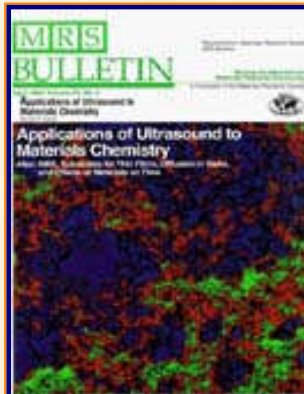
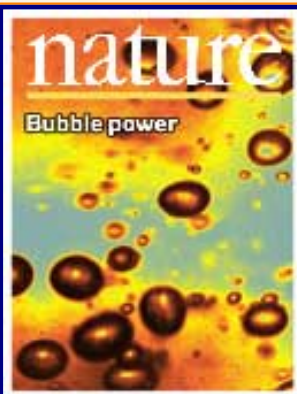
[Chem 315: Inorganic
Chemistry](#)

Overview	Current Group Members	CV: Abbreviated, Full	Art and Science
Outline of Projects	Group Meetings	Suslick Group Brochure	Chymistes: The Distillers of Waters
Synopsis: Sonochemistry	Group Responsibilities	Complete Publication List	A Chemist Meets Hollywood
Metalloporph.			
Executive Summary: Smell-Seeing	Web Based Resources	Academic Genealogy	A Chemist In Court
Introduction to Sonochemistry	Safety Resources	Press Clippings	Words of Humor and Wisdom
Proposal Excerpts	Group Equipment	How To Give A Seminar	Laws of the Universe
Funding	Past Group Members	Ch315 Inorganic Chemistry	Cartoons of Humor and Wisdom
Information for Visitors	Group Photogallery	Construction of the CLS Lab	Sculpture & Masks

©2003, K.S. Suslick; all rights reserved.

Comments and suggestions: ksuslick@uiuc.edu

The Suslick Research Group



ART AND SCIENCE: COVER ART FROM THE SUSLICK GROUP

SUPRAMOLECULAR CHEMISTRY: September 1998



[Overview](#)

[Outline of
Research Projects](#)

[Introduction to
Sonochemistry](#)

[Exec. Summary:
Sonochemistry](#)

[Exec. Summary:
Porphyrin Research](#)

[Exec. Summary: Smell-
Seeing](#)

[Complete
Publication List](#)

[Abbreviated Curriculum
Vitae](#)

[Academic
Genealogy](#)

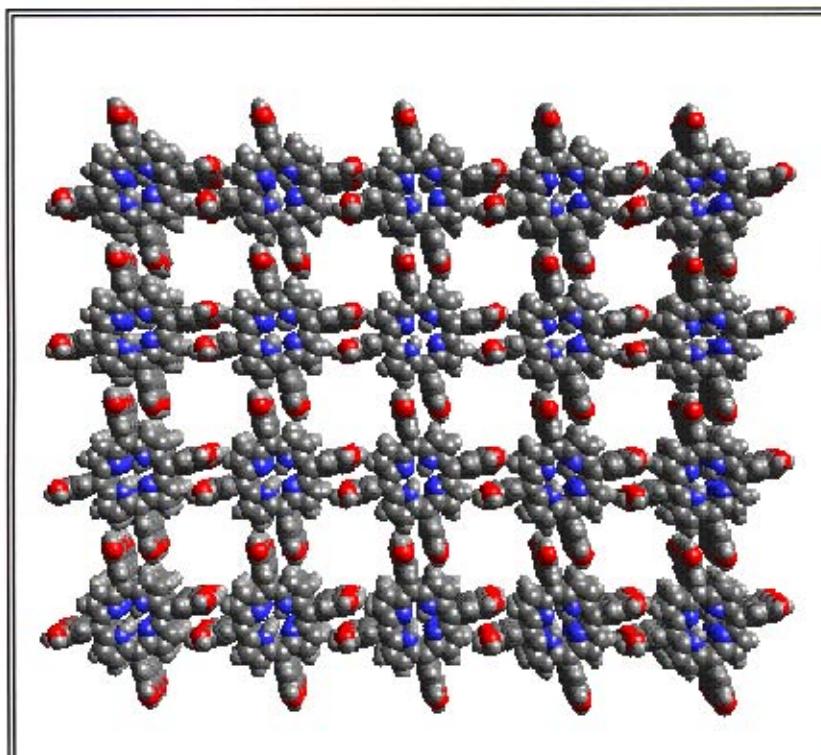
[Press
Clippings](#)

ISSN 1061-0278

SCHCCR 9(3) 159-244

Volume 9, Number 3 (1998)

SUPRAMOLECULAR CHEMISTRY



[Current Research
Funding](#)

[Excerpts from
Funded Research](#)

[Inventory of
Group Equipment](#)

[Information
for Visiting](#)

[Current Research Group
Members](#)

[Group
Meetings](#)

[Group
Chores](#)

[Past Research
Group Members](#)

[Group
Photogallery](#)

[Web Resources](#)

[Laboratory Safety
Resources](#)

[Art and Science:
Journal Covers](#)

[Sculpture &
Masks](#)

[A Chemist
Meets Hollywood](#)

[Chymistes: The Distillers
of Waters](#)

[A Chemist
In Court](#)



Edited by Jerry L. Atwood and George W. Gokel

GORDON AND BREACH SCIENCE PUBLISHERS

X-ray crystal structure of a supramolecular network of an octahydroxyporphyrin: 5,10,15,20-tetrakis(3',5'-dihydroxy-phenyl)porphine. Symmetrically substituted octa-hydroxy porphyrins have been developed as solid-state building blocks for nanoporous materials. The position of the peripheral hydroxyl groups, the choice of metallo- or free base porphyrin, and the nature of the solvate (i.e., guest) dramatically influence structural features. The channels are 0.65 x 0.65 nm between the columns, and the pore volume is exceptionally large at 56% of the unit cell. Courtesy of Kenneth S. Suslick, P. Bhyrappa, and Scott R. Wilson, University of Illinois at Urbana-Champaign.

SCIENCE:
March 1990

SCIENCE:
September 1991

MRS BULLETIN:
April 1995

SUPRAMOLECULAR CHEMISTRY:
September 1998

NATURE:
25 July 2002

SUSLICK GROUP WEBSITE:

**Humor and
Wisdom****Laws of the Universe****Cartoons of Humor and
Wisdom****Chem 115: Chemistry of
Everyday Phenomena****Chem 315: Inorganic
Chemistry**

THE SCIENCE	THE GROUP	THE MAÎTRE D'	LAGNIAPPE: A LITTLE EXTRA
<u>Overview</u>	<u>Current Group Members</u>	<u>CV: Abbreviated, Full</u>	<u>Art and Science</u>
<u>Outline of Projects</u>	<u>Group Meetings</u>	<u>Suslick Group Brochure</u>	<u>Chymistes: The Distillers of Waters</u>
<u>Synopses: Sonochemistry</u> <u>Metalloporph.</u>	<u>Group Responsibilities</u>	<u>Complete Publication List</u>	<u>A Chemist Meets Hollywood</u>
<u>Executive Summary: Smell-Seeing</u>	<u>Web Based Resources</u>	<u>Academic Genealogy</u>	<u>A Chemist In Court</u>
<u>Introduction to Sonochemistry</u>	<u>Safety Resources</u>	<u>Press Clippings</u>	<u>Words of Humor and Wisdom</u>
<u>Proposal Excerpts</u>	<u>Group Equipment</u>	<u>How To Give A Seminar</u>	<u>Laws of the Universe</u>
<u>Funding</u>	<u>Past Group Members</u>	<u>Ch315 Inorganic Chemistry</u>	<u>Cartoons of Humor and Wisdom</u>
<u>Information for Visitors</u>	<u>Group Photogallery</u>	<u>Construction of the CLS Lab</u>	<u>Sculpture & Masks</u>

©2003, K.S. Suslick; all rights reserved.

Comments and suggestions: ksuslick@uiuc.edu

Sonochemical synthesis of amorphous iron

Kenneth S. Suslick*§, Seok-Burm Choe†, Andrzej A. Cichowlas‡ & Mark W. Grinstaff*

* School of Chemical Sciences, University of Illinois at Urbana-Champaign, 505 S. Mathews Avenue, Urbana, Illinois 61801, USA

† College of Engineering, Kei-Mgung University, Taegu, Korea

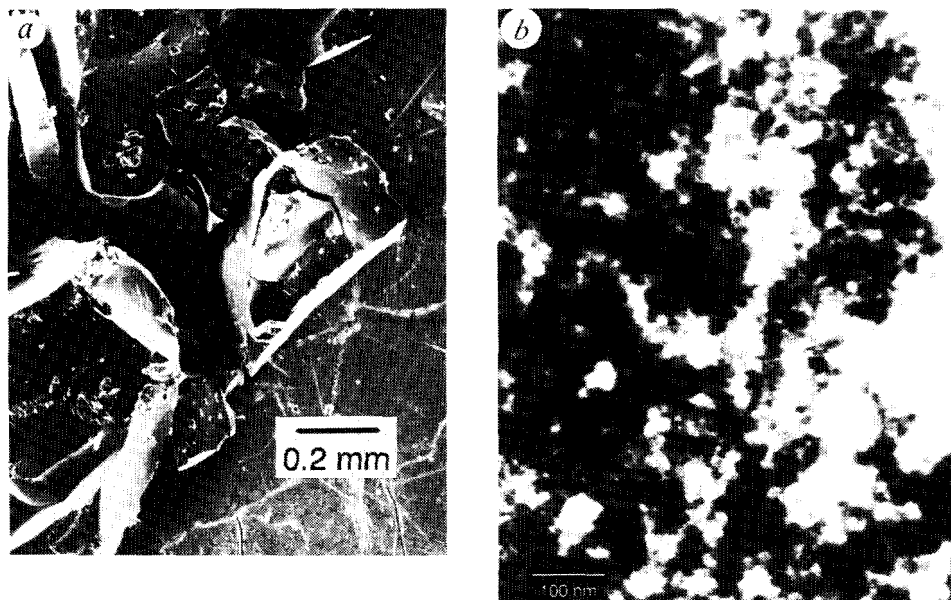
‡ Institute of Organic Chemistry, Polish Academy of Sciences, Warsaw, Poland

AMORPHOUS metallic alloys ('metallic glasses') lack long-range crystalline order and have unique electronic, magnetic and corrosion-resistant properties¹⁻³. Their applications include use in power-transformer cores, magnetic storage media, cryothermometry and corrosion-resistant coatings. The production of metallic glasses is made difficult, however, by the extremely rapid cooling from the melt that is necessary to prevent crystallization. Cooling rates of about 10^5 to 10^7 K s⁻¹ are generally required; for comparison, plunging red-hot steel into water produces cooling rates of only about 2,500 K s⁻¹. Metallic glasses can be formed by splattering molten metal on a cold surface using techniques such as gun, roller or splat quenching^{4,5}. Acoustic cavitation is known to induce extreme local heating in otherwise cold liquids, and to provide very rapid cooling rates^{6,7}. Here we describe the synthesis of metallic-glass powders using the microscopically extreme (yet macroscopically mild) conditions induced by high-intensity ultrasound. The sonolysis of iron pentacarbonyl, a volatile organometallic compound, produces nearly pure amorphous iron. This amorphous iron powder is a highly active catalyst for the Fischer-Tropsch hydrogenation of carbon monoxide and for hydrogenolysis and dehydrogenation of saturated hydrocarbons.

The chemical effects of ultrasound derive primarily from hot spots formed during acoustic cavitation (that is, the formation, growth and collapse of bubbles in a liquid)^{6,7}. This process serves to concentrate dramatically the low energy density of a sound field. Our previous experiments have established^{2,4} that the effective temperature reached during bubble collapse is ~5,200 K, with a calculated hot-spot lifetime of <2 ns. More recent sonoluminescence experiments suggest⁸ possible lifetimes of <1 ns. Thus, we expect that heating and cooling rates during cavitation collapse are greater than 2×10^9 K s⁻¹ and may be as large as 10^{13} K s⁻¹.

§ To whom correspondence should be addressed

FIG. 1 a, Scanning electron micrograph of amorphous iron powder, obtained on a Hitachi S800 electron microscope. b, Transmission electron micrograph of amorphous iron powder, obtained on a Phillips EM 400T electron microscope.



Ultrasonic irradiation of iron pentacarbonyl, $\text{Fe}(\text{CO})_5$, yields a dull black powder. A scanning electron micrograph of the powder is shown in Fig. 1a. Pure $\text{Fe}(\text{CO})_5$ or 4.0 M solutions in decane were irradiated at 0°C with a high-intensity ultrasonic probe (Sonics and Materials, model VC-600, 0.5 in. Ti horn, 20 kHz, 100 W cm^{-2}) for 3 h under argon. After irradiation, the iron powder produced was filtered and washed with dry pentane in an inert atmosphere box (Vacuum Atmospheres, $<1\text{ p.p.m. O}_2$). Gram quantities of material were isolated. Elemental analysis of the amorphous iron powder shows it to be $>96\%$ iron by weight, with trace amounts of carbon (3%) and oxygen (1%), presumably from the decomposition of alkane solvent or carbon monoxide during ultrasonic irradiation¹⁶⁻¹⁸. The applications of ultrasound to chemical synthesis^{11,19-21} and useful experimental apparatus²² are described in detail elsewhere.

The amorphous nature of these powders has been confirmed by several different techniques, including scanning and transmission electron microscopy, differential scanning calorimetry, X-ray powder diffraction and electron-beam microdiffraction. Scanning electron micrographs of iron powder from ultrasonic irradiation of $\text{Fe}(\text{CO})_5$ show conchoidal fractures, typical of a non-crystalline material (Fig. 1 a). Transmission electron microscopy show no evidence for crystallite formation to a resolution of below 4 nm (Fig. 1 b). Differential scanning calorimetry shows one large exothermic transition at 308°C corresponding to a disorder-order transition (crystallization) of the amorphous iron (Fig. 2).

Initial X-ray powder diffraction shows no diffraction peaks; after heat treatment under N_2 at 350°C (sufficient to induce crystallization), the lines characteristic of α -iron metal (d spacings of 2.03, 1.43, 1.17 and 1.04 \AA) are observed (Fig. 3). After crystallization, the X-ray powder diffraction pattern contains no peaks attributable to iron carbide or other iron-based phases, thus confirming the formation of essentially pure iron glass from ultrasonic irradiation of $\text{Fe}(\text{CO})_5$. This is especially noteworthy because all iron-containing metallic glasses prepared previously contain large amounts of other alloying elements (typically $>20\%$)^{1-3,23,24}. Electron microdiffraction with a transmission electron microscope confirms these observations and shows only a diffuse ring characteristic of an amorphous material. After continued sample exposure to the electron beam and its consequent heating, the iron powder crystallizes *in situ* and the diffraction rings from α -Fe are observed.

Transmission electron micrographs reveal the microstructure of the powder (Fig. 16). The large particles shown in the scan-

ning electron micrograph are composites of very small particles ($\sim 10\text{ nm}$) with significant void volume. Surface areas, determined by Brunauer-Emmett-Teller gas adsorption isotherms, were found to be $120\text{ m}^2\text{ g}^{-1}$, which is about 150 times greater than the $5\text{-}\mu\text{m}$ -diameter iron powder commercially available (Aldrich Chemicals). The sonochemically produced amorphous iron powder sinters at unusually low temperatures. At 350°C , the amorphous powder acquires a metallic lustre and the transmission electron micrographs show loss of porosity and growth of $\sim 50\text{-nm}$ crystallites. After heating, the surface area decreases by roughly one hundredfold and becomes comparable to that of the commercial crystalline powder.

We probed the catalytic activity of the amorphous iron powder for two commercially important reactions: the Fischer-Tropsch process (hydrogenation of CO) and the hydrogenolysis and dehydrogenation of saturated hydrocarbons. Catalytic studies were carried out in a continuous flow microreactor. The iron catalyst was loaded in the reaction chamber under an inert atmosphere and placed on the flow microreactor without exposure to air. The reaction products were monitored using

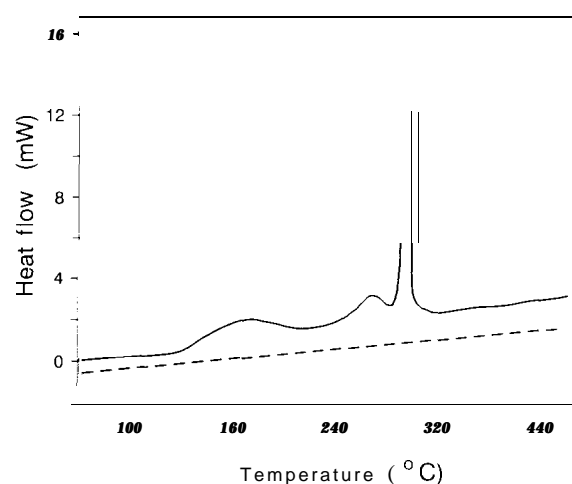


FIG. 2 Differential scanning calorimetry of amorphous (solid line) and crystalline (dashed line) iron powders, obtained at $10^\circ\text{C min}^{-1}$ on a DuPont 1090 calorimeter.

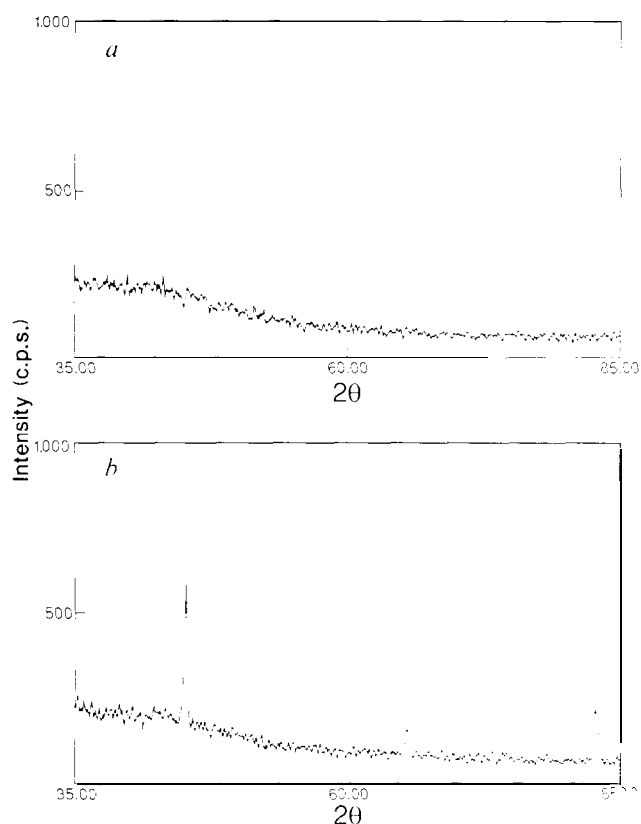


FIG. 3 X-ray diffracton powder patterns of amorphous iron powder (a) before heat treatment and (b) after crystallization at 350 °C for 6 h. Data collected on a Rigaku D-max diffractometer.

gas chromatography. The Fischer-Tropsch conversion of carbon monoxide and hydrogen to low-molecular-weight alkanes occurred at very low reaction temperatures (200 °C). The amorphous powder was roughly ten times more reactive per gram than 5- μm -diameter crystalline iron powder. At 250 °C, the overall activity for cyclohexane dehydrogenation (to benzene) and hydrogenolysis (predominantly to methane) was >30 times greater for the sonochemically produced amorphous iron relative to crystalline iron (Fig. 4). We believe that the high surface area of the amorphous iron accounts for much of the increase in chemical reactivity. As expected, sintering and crystallization of the metallic glass powder at >300 °C significantly decreased its catalytic activity. The ratio of cyclohexane dehydrogenation to hydrogenolysis depended on temperature and ranged from 0.3 to 1.0.

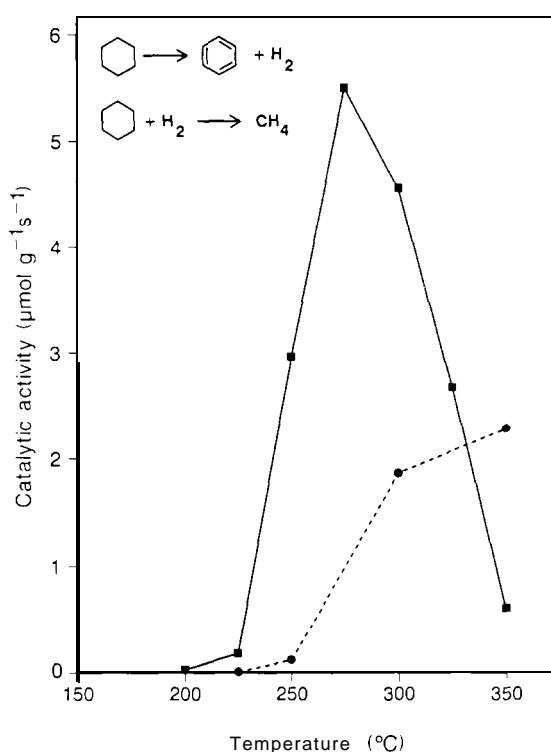


FIG. 4 The catalytic activity of amorphous and crystalline iron powder as a function of temperature for the cyclohexane dehydrogenation and hydrogenolysis reaction. Solid line, amorphous iron powder, prepared sonochemically from $\text{Fe}(\text{CO})_5$; dashed line, crystalline iron powder (5- μm diameter, Aldrich Chemicals).

The production of metal powder is not the only possible sonochemical reaction of $\text{Fe}(\text{CO})_5$. We have previously reported²⁵⁻²⁷ on sonochemical ligand substitution, cluster formation and catalytic alkene isomerization. The extent of CO loss can be controlled by the experimental parameters that affect cavitation collapse, including solvent vapour pressure, thermal conductivity of dissolved gas, and the ratio of heat capacities C_p/C_v of the dissolved gas. Complete ligand dissociation leading to formation of metallic glass powders occurs when the cavitation collapse is most extreme (for example, at low vapour pressure and with low gas thermal conductivity). Under such conditions, we have recently observed iron atomic emission lines in the sonoluminescence spectra (K.S.S., E. B. Flint, M.W.G. and K. A. Kemper, manuscript in preparation), confirming that iron atoms are formed during ultrasonic irradiation of $\text{Fe}(\text{CO})_5$. c

Received 29 April; accepted 31 July 1991

- 1 Anatharam: T R *Metal/Glasses*, Trans Tech Aedermannsorf Switzerland 1984
- 2 Haasen P & Jaffee, R I *Amorphous Metals and Semiconductors* -Pergamon London 1986
- 3 Steed H & Warlimont, H (eds): *Rapidly Quenched Metals* (Elsevier Amsterdam 1985)
- 4 Foes F W & Savage S J (eds): *Processing of Structural Metals by Rapid Solidification* (American Society for Metals Metals Park, Ohio 1987)
- 5 Takayama, S J *Mar Sci* 11, 164-185 U976,
- 6 Acheley A A & Crum L A in *Ultrasonic Its Chemical Physical and Biological Effects* ted Suslick, K S (ed) ICH New York 1988
- 7 Apfel R E (ed) *Methods in Experimental Physics* Vol 19 (ed Edmonds P D, 356-413, Academic, New York, 1981)
- 8 Neppiras E A *Phys Rep* 61, 159-251 (1980)
- 9 Suslick K S *Science* 247, 1439-1445 (1990),
- 10 Suslick K S *Scient Am* 260, 80-86 (1989)
- 11 Suslick K S (ed) *Ultrasonic Its Chemical, Physical and Biological Effects* WC, 1988,
- 12 Suslick K S Clone Jr, R E & Hammeron, D A *J Am Chem Soc* 106, 5641-5642 (1986)
- 13 Suslick, K S Clone Jr, R E & Hammeron, D A *IEEE Ultrason Symp Proc* 4, 1116-1121 (1985)
- 14 Suslick K S & Hammeron D A *IEEE Inters Ultrason Ferroelec Freq Conf* 33, 143-147 (1986)
- 15 Barber B P & Putterman S J *Nature* 352, 3X-320 (1991)
- 16 Cl, T E B & Suslick K S, *Am Chem Soc* 111, 6987-6992 (1989)

- 17 Suslick K S & Flint, E B *Nature* 330, 553-555 (1987)
- 18 Suslick K S Gawienowski J W, Schubert P F & Wane, H H *Jews Chem* 87, 2299-2301 (1983)
- 19 Einhorn C Einhorn J & Lxhe J L *Synthes* 11, 787-813 (1989)
- 20 Lindler J & Mason, T J *Chem Soc Rev* 16, 275-311 (1987);
- 21 Boudouk P *J Chem Ed* 65, 427-429 (1986)
- 22 Suslick K S & Flint E B in *Experimental Organometallic Chemistry A Practicum in Synthesis and Characterization* ted Wayda, A & Darenbourg M Y (195-198 (American Chemical Society Washington DC 1987)
- 23 Takashi S *Mat Sci, Lett* 6, 844-846 (1987)
- 24 Luborsky F E (ed) *Amorphous Metallic Alloys* (Butterworths London, 1983)
- 25 Suslick, K S Schubert P F & Goodale, J W *J Am Chem Soc* 103, 7324-7344 (1981)
- 26 Suslick K S, Goodale, J W, Wang H H & Schubert P F *J Am Chem Soc* 105, 5781-5785 (1983)
- 27 Suslick K S & Schubert P F *J Am Chem Soc* 105, 6042-6044 (1983)

ACKNOWLEDGEMENTS This work was supported by the NSF loan of ultrasonic equipment from Sonics and Materials. We gratefully acknowledge receipt of the American Chemical Society Fellowship in Colloid and Surface Chemistry sponsored by Procter and Gamble Co. (M.W.G.) We thank Peggy Mochel and the UIUC Center for Microanalysis of Materials supported by the US Department of Energy for their assistance in the characterization studies.

Sonochemical Synthesis of Iron Colloids

Kenneth S. Suslick,* Mingming Fang, and Taeghwan Hyeon
 School of Chemical Sciences
 University of Illinois at Urbana–Champaign
 505 South Mathews Avenue, Urbana, Illinois 61801
 Received May 29, 1996

Nanostructured materials have been intensively studied in recent years particularly because the physical properties of these materials are quite different from those of the bulk.^{1–3} A variety of chemical and physical preparative methods have been developed to produce materials with nanometer domain size, including metal evaporation,^{4,5} reduction of metal salts by borohydride derivatives,^{6,7} laser pyrolysis,⁸ and thermal decomposition.⁹ Colloids of ferromagnetic materials are of special interest due to their many important technological applications as ferrofluids.^{10,11} Such magnetic fluids find uses in information storage media, magnetic refrigeration, audio reproduction, and magnetic sealing.^{12,13} Commercial magnetic fluids are generally produced by exhaustive grinding of magnetite (Fe₃O₄) in ball or vibratory mills for several weeks in the presence of surfactants, which produces a very broad particle size distribution.¹⁰ Chemical methods such as thermolysis of organometallic compounds and metal evaporation have also been applied to produce colloids of ferromagnetic materials.^{14,15} We present here a new method for the preparation of stable ferromagnetic colloids of iron using high-intensity ultrasound to sonochemically decompose volatile organometallic compounds. These colloids have narrow size distributions centered at a few nanometers and are found to be superparamagnetic.

Sonochemistry arises from acoustic cavitation, the formation, growth, and implosive collapse of bubbles in a liquid.¹⁶ The collapse of bubbles generates localized hot spots with transient temperatures of ~5000 K and cooling rates in excess of 10¹⁰ K/s.^{17,18} Volatile organometallic compounds inside the cavitating bubble are decomposed to yield individual metal atoms as shown by the observed sonoluminescence from electronic excited states of metal atoms, including Fe.¹⁹ In alkanes, in the

- (1) Schmid, G., Ed. *Clusters and Colloids*; VCH Press: New York, 1994.
- (2) Weller, H. *Adv. Mater.* **1993**, *5*, 88.
- (3) Gleiter, H. *Adv. Mater.* **1992**, *4*, 474.
- (4) Hahn, H.; Averbach, R. S. *J. Appl. Phys.* **1990**, *67*, 1113.
- (5) Klambunde, K. J.; Zhang, D.; Glavee, G. N.; Sorensen, C. M. *Chem. Mater.* **1994**, *6*, 784.
- (6) Bönnemann, H.; Brijoux, W.; Brinkmann, R.; Jousen, T. *Angew. Chem., Int. Ed. Engl.* **1990**, *29*, 273.
- (7) Tsai, K.-L.; Dye, J. L. *J. Am. Chem. Soc.* **1991**, *113*, 1650.
- (8) Rice, G. W. In *Laser Chemistry of Organometallics*; Chaiken, J., Ed.; American Chemical Society: Washington, DC, 1993; p 273.
- (9) Bradley, J. S.; Hill, E. W.; Klein, C.; Chaudret, B.; Duteil, A. *Chem. Mater.* **1993**, *5*, 254.
- (10) Fertman, V. E. *Magnetic Fluids Guidebook: Properties and Applications*; Hemisphere Publishing Co.: New York, 1990.
- (11) Berkovsky, B. M.; Medvedev, V. F.; Krakov, M. S. *Magnetic Fluids: Engineering Applications*; Oxford University Press: Oxford, 1993.
- (12) Raj, K.; Moskowitz, R. *J. Magn. Magn. Mater.* **1990**, *85*, 233.
- (13) Charles, S. W.; Popplewell, J. *IEEE Trans. Magn.* **1980**, *Mag-16*, 172.
- (14) Smith, T. W.; Wychick, D. *J. Phys. Chem.* **1980**, *84*, 1621.
- (15) Hoon, S. R.; Kilner, M.; Russell, G. J.; Tanner, B. K. *J. Magn. Magn. Mater.* **1983**, *39*, 107.
- (16) Suslick, K. S., Ed. *Ultrasound: Its Chemical, Physical, and Biological Effects*; VCH Press: New York, 1988.
- (17) Suslick, K. S. *Science* **1990**, *247*, 1439.
- (18) Flint, E. B.; Suslick, K. S. *Science* **1991**, *253*, 1397.
- (19) (a) Suslick, K. S.; Flint, E. B.; Grinstaff, M. W.; Kemper, K. A. *J. Phys. Chem.* **1993**, *97*, 3098. (b) Suslick, K. S.; Choe, S. B.; Cichowlas, A. A.; Grinstaff, M. W. *Nature* **1991**, *353*, 414.
- (20) Suslick, K. S.; Hyeon, T.; Fang, M.; Cichowlas, A. A. *Mater. Sci. Eng. A* **1995**, *204*, 186.
- (21) (a) Grinstaff, M. W.; Salamon, M. B.; Suslick, K. S. *Phys. Rev. B* **1993**, *48*, 269. (b) Bellissent, R.; Galli, G.; Grinstaff, M. W.; Migliardo, P.; Suslick, K. S. *Phys. Rev. B* **1993**, *48*, 15797. (c) Rozenfeld, O.; Koltypin, Y.; Bammolker, H.; Margel, S.; Gedanken, A. *Langmuir* **1994**, *11*, 3919.
- (22) Suslick, K. S. *MRS Bull.* **1995**, *20*, 29.
- (23) Hyeon, T.; Fang, M.; Suslick, K. S. *J. Am. Chem. Soc.* **1996**, *118*, 5492.

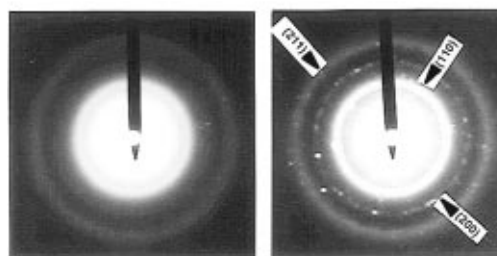
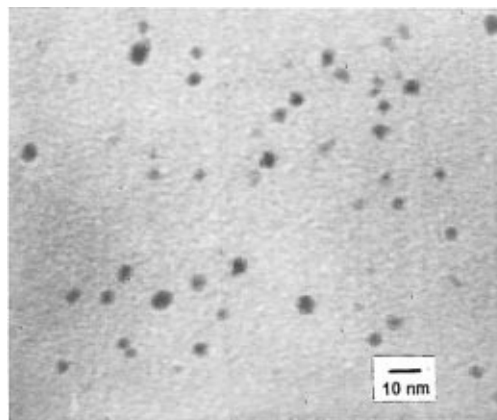


Figure 1. (Top) Transmission electron micrograph of sonochemically prepared nanometer iron colloid particles dispersed in a polyvinylpyrrolidone matrix. (Bottom left) Electron microdiffraction pattern before crystallization. (Bottom right) Electron microdiffraction pattern after *in situ* crystallization. Obtained on a Phillips EM400T electron microscope.

absence of any trapping agent, these atoms agglomerate to produce various highly porous nanostructured materials including amorphous metals, alloys, and carbides.^{19–23} We have now found it possible to stabilize the nanometer-sized cluster produced during cavitation, preventing their agglomeration and permitting the isolation of stable nanocolloids.

In this work, a volatile organometallic precursor, Fe(CO)₅, was sonochemically decomposed in the presence of a stabilizer to create a nanosized iron colloid. Ultrasonic irradiation of 0.2 mL of Fe(CO)₅ in 20 mL of octanol with 1 g of polyvinylpyrrolidone (PVP, average molecular weight of 40 000, Sigma Chemicals) at 20 °C under a rigorously oxygen free argon atmosphere produced a black colloidal solution. The TEM (transmission electron microscopy) image in Figure 1 shows that iron particles in the polymer matrix range in size from 3 to 8 nm. Electron microdiffraction shows that these iron clusters are amorphous as initially formed (Figure 1, bottom left). By irradiating the particles with a high-intensity electron beam in the TEM chamber, crystallization was induced presumably from local heating in the electron beam. Electron microdiffraction following the *in situ* crystallization revealed dense ring patterns with d spacings of 2.0, 1.4, and 1.2 Å, which match the standard body centered cubic iron lines (Figure 1, bottom right). Electron microdiffraction also shows a very weak ring pattern with d spacing of 2.5 Å, which corresponds to a slight contamination from the (111) line of cubic iron oxide FeO.

Oleic acid (octadec-9-ene-1-carboxylic acid) can also serve as a colloid stabilizer.¹⁰ The tail of oleic acid is kinked at the double bond, which is critical to its effectiveness: stearic acid, for example, does not stabilize the colloid. A hexadecane solution of 2 M Fe(CO)₅ and 0.3 M oleic acid was sonicated at 30 °C for 1 h, during which time the initially yellow solution turned black. The resulting black solution was evacuated at 50 °C for 1 h to remove unreacted iron pentacarbonyl and isolated an inert atmosphere box for further characterization. Transmission electron micrograph revealed that the oleic acid

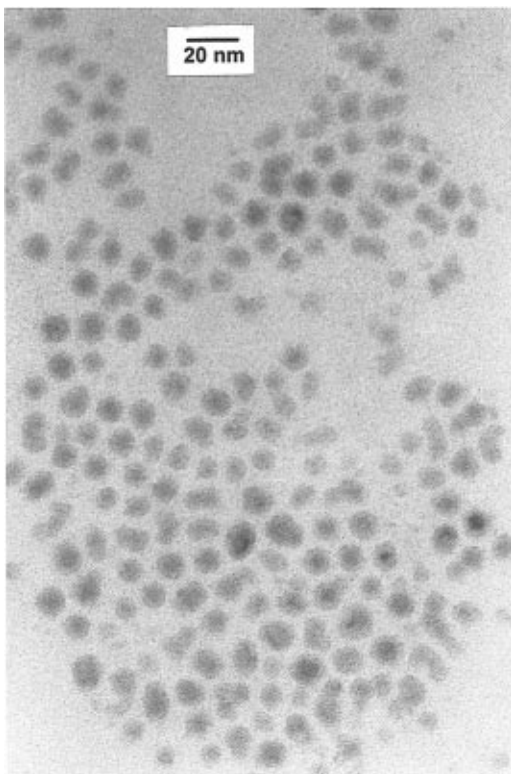


Figure 2. Transmission electron micrograph of sonochemically prepared iron colloid particles (with average particle size of 8 nm) stabilized by oleic acid.

colloid particles were slightly larger than the PVP colloid but much more uniform, with average particle size of 8 nm (Figure 2). The electron microdiffraction after *in situ* crystallization showed that oleic acid particles are a mixture of Fe and FeO.

When the particles of ferro- or ferrimagnetic materials are smaller than the dimensions of a single domain (which for Fe and Co is ≈ 20 nm), thermal fluctuations will supersede the Weiss anisotropy above the blocking temperature. Such particles are called superparamagnetic.²⁴ An operational definition of a superparamagnetism has two requirements. First, the plot of magnetization (M) vs applied magnetic field (H) must show no hysteresis. Second, the magnetization of an isotropic sample at different temperatures must superimpose when plotted against H/T , after correction for the temperature dependence of the spontaneous magnetization. Sonochemically synthesized nanosized iron particles show no hysteresis in their magnetization data at 290 K (Figure 3).²⁵ Furthermore plots of magnetization vs (magnetic field)/(temperature) for the Fe/PVP sample at 290, 250, and 200 K (Figure 4) superimpose after correction for the temperature dependence of the spontaneous magnetization. Thus, sonochemically prepared nanometer Fe colloids are superparamagnetic.

High saturation magnetization is desirable for magnetic fluid application and is highly sensitive to the method of preparation. The saturated magnetization (M_s) of the initially prepared PVP colloidal nanometer Fe particles is a respectable 101 emu/g (Fe) at 290 K. M_s is determined by extrapolating the experimental plot of M vs $1/H$ using data at high magnetic fields. Standard crystalline bcc Fe has a saturated magnetization of 222 emu/g (Fe) at 298 K,²⁶ whereas bulk amorphous Fe saturates at 156

(24) Jacobs, I. S.; Bean, C. P. In *Magnetism III*; Rado, G. T., Suhl, H., Eds.; Academic Press: New York, 1963; pp 271–351.

(25) Magnetic studies were conducted with a Quantum Design MPMS, 7 T, SQUID magnetometer. Colloidal iron samples were loaded into gelatin capsules inside an inert atmosphere box, carried to the magnetometer under inert atmosphere, and rapidly transferred to the sample chamber. All magnetic data have been corrected for the diamagnetism of the gelatin capsules, solvents, and colloid stabilizers.

(26) Cullity, B. D. *Introduction to Magnetic Materials*; Addison-Wiley: New York, 1972; pp 171–190.

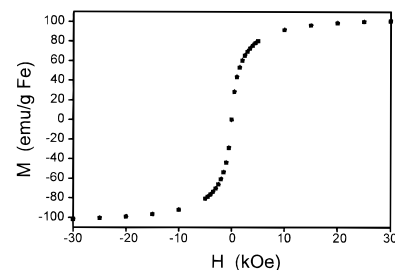


Figure 3. Magnetization hysteresis loops for the nanometer iron particles dispersed in a PVP matrix at 250 K: (+) magnetization data points; (■) demagnetization points. No hysteresis is observed and consequently the magnetization data points are overlapped by the demagnetization data.

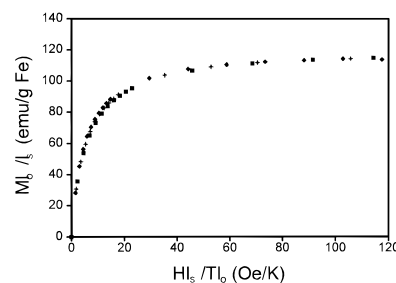


Figure 4. Magnetization (M) versus magnetic field/temperature (H/T) at (■) 200 K, (+) 250 K, and (◇) 290 K, after correcting for the temperature dependence of spontaneous magnetization (I_s/I_0) for the nanometer iron colloid particles dispersed in a polyvinylpyrrolidone matrix.

emu/g (Fe).²¹ The saturation magnetization of our sonochemically prepared iron colloid is greater than that of solvated nanometer-scale iron particles produced by metal vapor deposition (55 emu/g (Fe) at 55 kOe)²⁷ or ion-exchange resin stabilized nanocrystalline γ -Fe₂O₃ (99 emu/g at 10 kOe),²⁸ but smaller than those of copoly(styrene-butadiene)-stabilized iron colloids (120–170 emu/g (Fe) at 10 kOe).¹⁴ For a comparison, the saturation magnetization of a commercial magnetite-based magnetic fluid is 123 emu/g (Fe).²⁹

In conclusion, a simple synthetic method has been discovered to produce nanosized iron colloid using high-intensity ultrasound. Nanometer iron particles dispersed in polyvinylpyrrolidone (PVP) matrix or stabilized by adsorption of oleic acid have been synthesized by sonochemical decomposition of Fe(CO)₅. Transmission electron micrographs show that the iron particles have a relatively narrow range in size from 3 to 8 nm for polyvinylpyrrolidone, while oleic acid gives an even more uniform distribution at 8 nm. Magnetic measurements revealed that these nanometer iron particles are superparamagnetic with a saturation magnetization of 101 emu/g (Fe) at 290 K. This work is easily extended to colloids of other metals and to alloys of two or more metals, simply by using multiple volatile precursors. For example, we have recently made nanostructured Fe/Co alloys sonochemically.²⁰ Controlled reaction with O₂ or other oxidants will also permit the formation of transition metal oxide colloids.

Acknowledgment. We gratefully acknowledge Professor Myron B. Salamon for many helpful discussions. This work was supported by the NSF (DMR-8920538 and CHE-9420758). For electron microscopy, we thank the assistance of the UIUC Center for Microanalysis of Materials, supported by the DOE.

JA961807N

(27) Kernizan, C. F.; Klabunde, K. J.; Sorensen, C. M.; Hadjipanayis, G. C. *Chem. Mater.* **1990**, *2*, 70.

(28) Ziolo, R. F.; Giannelis, E. P.; Weinstein, B. A.; O'Horo, M. P.; Ganguly, B. N.; Mehrotra, V.; Russell, M. W.; Huffman, D. R. *Science* **1992**, *257*, 219.

(29) Ferrofluids Corporation, catalog no. APG 047. Magnetite (Fe₃O₄) is dispersed in hydrocarbon with an aromatic amine as stabilizer (12.3 wt % of Fe).

Sonochemical Synthesis of Nanostructured Molybdenum Sulfide

Millan M. Mdleleni, Taeghwan Hyeon, and
Kenneth S. Suslick*

School of Chemical Sciences
University of Illinois at Urbana-Champaign
601 South Goodwin Avenue, Urbana, Illinois 61801

Received January 5, 1998

There is growing interest in nanostructured inorganic materials, in large part because they often exhibit properties distinct from those of the bulk that can prove useful in various applications, including heterogeneous catalysis.^{1–4} The established methods for the preparation of nanostructured inorganic materials include metal evaporation,⁵ reduction of metal salts,^{6,7} and thermal decomposition and laser pyrolysis of organometallic compounds.^{8,9} In addition, the sonochemical reaction of volatile organometallics is a recent and general synthetic approach to nanophase transition metal powders, alloys, carbides, and colloids.^{10–13} We report here a simple sonochemical synthesis of nanophase, high-surface-area molybdenum sulfide and the examination of its catalytic activity for thiophene hydrodesulfurization (HDS).

MoS₂ was prepared by irradiating a slurry of molybdenum hexacarbonyl and sulfur in 1,2,3,5-tetramethylbenzene (isodurene) with high-intensity ultrasound (20 kHz) under Ar.^{14a} Elemental analysis of the purified powder indicates a stoichiometric molybdenum sulfide (S/Mo atomic ratio of 2.0) with a trace amount (<2 wt %) of carbon contamination. For comparison, a conventional molybdenum sulfide sample was also prepared by

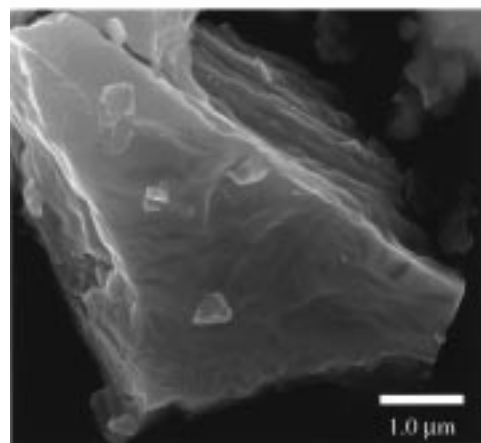
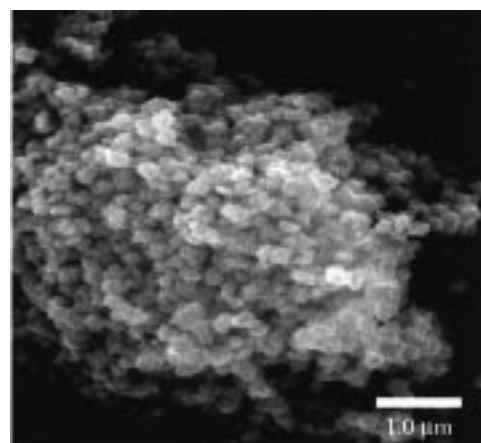


Figure 1. SEM micrographs of (a, top) sonochemical and (b, bottom) conventional preparations of MoS₂.

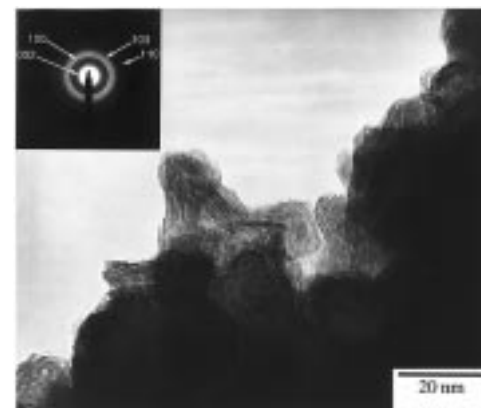


Figure 2. TEM micrographs of sonochemically prepared MoS₂. Basal planes are seen as dark fringes with interlayer spacings of 0.62 ± 0.01 nm, the same as those for conventional MoS₂.

- (1) Ozin, G. A. *Adv. Mater.* **1992**, *4*, 612.
- (2) Weller, H. *Adv. Mater.* **1993**, *54*, 88.
- (3) Moser, W. R., Ed. *Advanced Catalysts and Nanostructured Materials*; Academic Press: New York, 1996.
- (4) Lewis, L. N. *Chem. Rev.* **1993**, *93*, 2693.
- (5) Klabunde, K. J. *Free Atoms, Clusters, and Nanoscale Particles*; Academic Press: New York, 1994.
- (6) Boennenmann, H.; Brijoux, W.; Brinkmann, R.; Jousen, T. *Angew. Chem., Int. Ed. Engl.* **1990**, *129*, 273.
- (7) Tsai, K.-L.; Dye, J. L. *J. Am. Chem. Soc.* **1991**, *113*, 1650. (b) Tsai, K.-L.; Dye, J. L. *Chem. Mater.* **1993**, *5*, 540.
- (8) Lisitsyn, A. S.; Golovin, A. V.; Chuvilin, A. L.; Kuznetsov, V. L.; Romanenko, A., V.; Danilyuk, A. F.; Yermankov, Y. I. *Appl. Catal.* **1989**, *55*, 235.
- (9) Chaiken, J. *Chem. Ind.* **1993**, 751.
- (10) Suslick, K. S.; Choe, S.-B.; Cichowlas, A. A.; Grinstaff, M. W. *Nature* **1991**, *353*, 414. (b) Grinstaff, M. W.; Salamon, M. B.; Suslick, K. S. *Phys. Rev. B* **1993**, *48*, 269. (c) Bellissent, R.; Galli, G.; Grinstaff, M. W.; Migliardo, P.; Suslick, K. S. *Phys. Rev. B* **1993**, *48*, 15797. (d) Bellissent, R.; Galli, G.; Hyeon, T.; Magazu, S.; Majolino, D.; Migliardo, P.; Suslick, K. S. *Phys. Scr.* **1995**, *40*, 67. (e) Bellissent, R.; Galli, G.; Hyeon, T.; Migliardo, P.; Parette, G.; Suslick, K. S. *J. Non-Cryst. Solids* **1996**, *205–207*, 656.
- (11) Suslick, K. S.; Hyeon, T.; Fang, M.; Cichowlas, A. A. *Mater. Sci. Eng. A* **1995**, *204*, 186. (b) Hyeon, T.; Fang, M.; Suslick, K. S. *J. Am. Chem. Soc.* **1996**, *118*, 5492. (c) Suslick, K. S.; Hyeon, T.; Fang, M. *Chem. Mater.* **1996**, *8*, 2172.
- (12) Suslick, K. S.; Fang, M.; Hyeon, T. *J. Am. Chem. Soc.* **1996**, *118*, 11960.
- (13) Cao, X.; Prozorov, R.; Koltypin, Y.; Kataby, G.; Felner, I.; Gedanken, A. *J. Mater. Res.* **1997**, *12*, 402. (b) Shafi, K. V. P. M.; Gedanken, A.; Goldfarb, R. B.; Felner, I. *J. Appl. Phys.* **1997**, *81*, 6901.
- (14) In a typical preparation, a slurry of molybdenum hexacarbonyl (2.5 g, 9.5 mmol) and sulfur (0.75 g, 23 mmol) in 35 mL of 1,2,3,5-tetramethylbenzene was irradiated with high-intensity ultrasound (20 kHz, ≈ 80 W/cm², 1 cm² titanium horn; Sonics & Materials VCX600) for 1.5 h at 80 °C under Ar. The resulting black powder (yield: 0.6 g, 40% theoretical; longer sonication increases yield but also C contamination) was filtered and washed several times with degassed, distilled pentane inside an Ar-filled glovebox (Vacuum Atmospheres, <0.5 ppm O₂). The washed powder was then heated at 80 °C for 3 h under vacuum to remove any unreacted molybdenum hexacarbonyl. Any excess sulfur was removed by heating the amorphous product at 450 °C for 10 h under He flow (30 cm³/min), which also leads to crystallization of the initially amorphous MoS₂. (b) Prasad, T. P.; Diemann, E.; Müller, A. *J. Inorg. Nucl. Chem.* **1973**, *35*, 1895.

thermally decomposing ammonium tetrathiomolybdate (Aldrich) under helium.^{14b} Surface areas of the thermally treated sonochemical and conventional MoS₂ were 55 and 32 m²/g, respectively, as determined by Brunauer–Emmett–Teller (BET) N₂ adsorption isotherms.

The X-ray diffraction (XRD)¹⁵ pattern of the initial amorphous powder sonochemically prepared shows ill-defined, extremely

(15) XRD: Rigaku D-max diffractometer using Cu K α radiation. SEM: Hitachi S800. TEM: Philips CM-12. PES: Phi-540 spectrometer using Mg K α radiation.

broad peaks. After thermal treatment under He, however, the MoS₂ exhibits sharper peaks with corresponding *d* spacings of 6.30, 2.68, 1.57, and 1.22 Å corresponding to the {002}, {100}, {103}, and {110} reflections of hexagonal MoS₂ (6.16, 2.67, 1.58, and 1.22 Å), respectively.¹⁶ An average crystallite size of ~1.6 nm was estimated from the {002} peak width.¹⁷

Scanning electron micrographs of sonochemically and conventionally prepared MoS₂ are shown in Figure 1. The sonochemical MoS₂ exists as a porous agglomeration of clusters of spherical particles with an average diameter of 15 nm, which are themselves aggregates of smaller particles. Energy dispersive X-ray (EDX) analysis performed on these particles gave a S/Mo atomic ratio of 2.06, identical within experimental error to that from bulk chemical analysis. In contrast, the conventional MoS₂ shows a platelike morphology typical for such layered materials. Despite the morphological difference between the sonochemical and conventional MoS₂, the transmission electron microscopy (TEM) images (Figure 2) of these sulfides both show lattice fringes with interlayer spacings of 0.62 ± 0.01 nm, the same as those for conventional MoS₂.¹⁸ The sonochemically prepared MoS₂, however, shows much greater edge and defect content, as the layers must bend, break, or otherwise distort to fit the outer surface of the 15-nm particle size (Figure 2).

The electronic states of Mo and S in the sonochemically prepared MoS₂ were determined by X-ray photoelectron spectroscopy (XPS), which showed well-defined spin-coupled Mo(3d_{5/2}, 3d_{3/2}) and S(2p_{3/2}, 2p_{1/2}) doublets at binding energies¹⁹ the same as that for conventional MoS₂.²⁰ Analysis of the Mo(3d) and S(2p) peak intensities (corrected with sensitivity factors based on Scofield cross sections)²¹ gave a S/Mo atomic ratio of 2.03, in agreement with the EDX and chemical analysis results.

Molybdenum sulfide is an excellent high-temperature lubricant, but more importantly, it is also the predominant HDS catalyst.²² It is well established that the activity of MoS₂ is localized at the edges and not on the flat basal planes.²² Given the inherently higher edge concentrations in nanostructured materials, the catalytic properties of our sonochemically prepared MoS₂ become especially interesting. To this end, the catalytic activity and selectivity for thiophene HDS by sonochemically prepared MoS₂ was examined in a single-pass microreactor.²³ Conventional MoS₂, sonochemical Mo₂C, commercial ReS₂ (Gallard-Schlesinger Ind., Carle Place, NY), and RuS₂ (Gallard-Schlesinger) were also investigated under the same conditions for comparison. For conventionally prepared sulfides, ReS₂ and RuS₂ are inherently more reactive than MoS₂²⁴ but are too expensive to be generally used. Given the difference in edge versus basal surface activity, catalytic activity does not correlate with total surface area²⁴ and therefore comparisons must be made on a catalyst mass basis.

The observed turnover frequencies as a function of temperature for these catalysts are shown in Figure 3. The principal products detected by GC were the C₄ hydrocarbons butadiene, 1-butene,

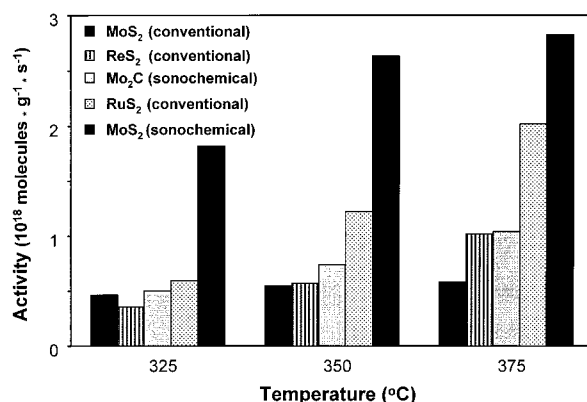


Figure 3. Catalytic activities of various catalysts in thiophene HDS as a function of temperature.

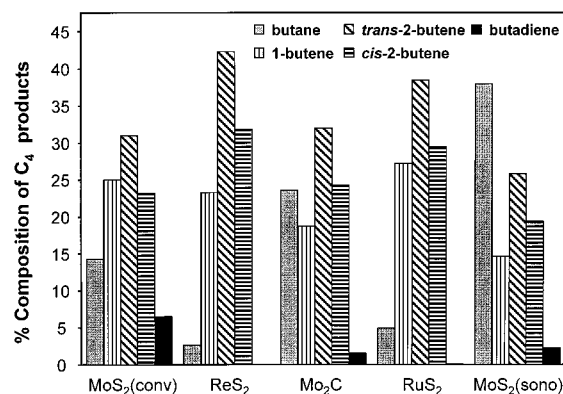


Figure 4. Distribution of C₄ hydrocarbon products observed during thiophene HDS with various catalysts at 375 °C.

trans-2-butene, *cis*-2-butene, and butane. No partially hydrogenated thiophenes were detected, and lighter (C₁–C₃) hydrocarbons accounted for less than 1% of the reaction products. The observed HDS activity order is MoS₂ (sonochemical) > RuS₂ (conventional) > ReS₂ (conventional) ~ Mo₂C (sonochemical¹¹) > MoS₂ (conventional). Catalytic activity of the sonochemically prepared samples decreased initially somewhat (<50% over 20 h), so the activities reported here were measured *after* 20 h of use. The product selectivities, expressed as percent of total C₄ hydrocarbons, observed at 375 °C are shown in Figure 4. All of the catalyst studied show high selectivity for butenes with the exception of the sonochemical MoS₂, which gives more butane due to its higher activity. The accepted mechanism for thiophene HDS involves initial hydrogenolysis of the C–S bonds to give butadiene, followed by rapid hydrogenation to 1-butene, which is subsequently hydrogenated to butane or isomerized to a thermodynamic mixture of *cis*- and *trans*-2-butenes.^{22,25}

In summary, high-surface-area nanostructured MoS₂ can be generated sonochemically from molybdenum hexacarbonyl and sulfur. It is morphologically distinct from its conventional counterpart and catalyzes thiophene HDS with higher activities than those of the most active materials. Further studies on the use of the sonochemically prepared MoS₂ as supported and Co- or Ni-promoted heterogeneous catalysts are underway.

Acknowledgment. These studies were supported by the NSF (CHE942078) and in part by the DOE (96ER14730). Microscopic analyses were carried out in the UIUC Center for Microanalysis of Materials, supported by the DOE. The assistance of Drs. Rick Haash, Vania Petrova, and Peggy Mochel is appreciated.

JA9800333

(25) Luo, S.; Rauchfuss, T. B.; Gan, Z. *J. Am. Chem. Soc.* **1993**, *115*, 4943. (b) Benson, J. W.; Schrader, G. L.; Angelici, R. J. *J. Mol. Catal. A: Chemical* **1995**, *96*, 283.

(16) JCPDS Card No. 37-1492.

(17) Klug, H. P.; Alexander, L. E. *X-ray Diffraction Procedures for Polycrystalline and Amorphous Materials*; John Wiley and Sons: New York, 1974; p 687.

(18) Inamura, K.; Prins, R. *J. Catal.* **1994**, *147*, 515.

(19) For sonochemically prepared MoS₂: Mo(3d_{5/2}) and Mo(3d_{3/2}) at 228.5 and 232.16 eV, respectively; S(2s) at 226.16 eV, characteristic of S²⁺; S(2p_{3/2}) and S(2p_{1/2}) at 161.65 and 162.82 eV, respectively.

(20) Göbölös, S.; Wu, Q.; Ladriere, J.; Delannay, F.; Delmon, B. *Bull. Soc. Chim. Belg.* **1984**, *93*, 687. (b) Chin, R. L.; Hercules, D. M. *J. Phys. Chem.* **1982**, *86*, 3079.

(21) Scofield, J. H. *Electron Spectrosc. Relat. Phenom.* **1976**, *8*, 129.

(22) Gates, B. C. *Catalytic Chemistry*; Wiley & Sons: New York, 1992; pp 406–422.

(23) Catalytic studies were performed at 1 atm in a single-pass quartz microreactor. The substrate vapors were carried at a constant partial pressure of 75 mbar by a flow of hydrogen (27.5 cm³(STP)/min). The reaction products were analyzed with an on-line quadrupole mass spectrometer (Spectra Instruments) and a 5730A Hewlett-Packard gas chromatograph fitted with a 3-m *n*-octane/Porasil C column and FID.

(24) Pecoraro, T. A.; Chianelli, R. R. *J. Catal.* **1981**, *67*, 430.

somewhat slower) mixing for spatially periodic forcing; (4) for temporally non-periodic forcing, there are no recurrences.

The one-dimensional spatial power spectrum $E(k)$ computed in the standard way¹⁰ provides a useful diagnostic for the development of fine structure in the concentration field. An example is shown in Fig. 4a for time-periodic forcing using the spatially disordered magnet array (as in Fig. 2), at several different times. For $l < t < 10$, the high frequency tail of $E(k)$ rises, as stretching and folding produce fine structure. Later, the entire spectrum declines at all frequencies with little further change of shape. The decline at high k is due to diffusion, and the decline at low k is due to the continuing transport of spectral variance to high k by stretching. The spectrum does not follow a well-defined power law (nor is one expected⁶ for transient mixing); it is steeper at higher k . The behaviour of the second spectral moment (k^2), shown in Fig. 4b, increases rapidly at first and then essentially saturates, consistent with the asymptotic structure noted earlier.

The fine structure of the dye pattern may also be investigated by studying the PDF of the magnitude of the concentration gradient. An example is shown in Fig. 5 for the same conditions as in Fig. 2. Gradients have been expressed in units of the standard deviation of the concentration field to compensate for the gradual homogenization. It is striking to see that the gradient PDF reaches an invariant form that is essentially identical at $t = 20$ and 50 periods. The distribution at high gradients is accurately exponential. Such exponential tails for distributions of concentration gradients have been noted in several theoretical studies¹³. When the same experiment is done for the weakly turbulent flow at lower viscosity, the resulting distribution is similar to that of Fig. 5 for $t = 10$, but the shape continues to evolve, approaching a maxwellian distribution (characteristic of independent gaussian components) at longer times. Therefore, the large gradients are attenuated more rapidly than are small gradients for the turbulent flow. Diffusion broadens the striations in two-dimensional turbulence, but not in chaotic mixing.

We find that chaotic mixing, produced by time-periodic cellular flows, leads to a remarkable persistent spatial structure, a complex pattern that recurs periodically while its contrast decays slowly with time. The recurrence is surprising (when first encountered) since additional striations are created during each cycle. The corresponding spatial power spectrum retains its shape as it declines simultaneously at all wavenumbers owing to a delicate balance of two

distinct processes: stretching and diffusion. The probability distribution of the magnitude of the concentration gradient reaches an invariant form (when suitably normalized) with a peak at non-zero gradient and exponential tails. All of these properties show that the recurrent mixing pattern represents a dynamical non-equilibrium state rather than a static condition. Finally, we note that identically forced but weakly turbulent flows at lower viscosity become homogeneous and transport material much more rapidly than the time-periodic flows manifesting chaotic advection. However, turbulence is generally unavailable when mixing in small scale devices is required. □

Received 3 June; accepted 18 August 1999.

1. Aref, H. Stirring by chaotic advection. *J. Fluid Mech.* **143**, 1–21 (1984).
2. Ottino, J. M. Mixing, chaotic advection, and turbulence. *Annu. Rev. Fluid Mech.* **22**, 207–253 (1990).
3. Fountain, G. O., Khakhar, D. V. & Ottino, J. M. Visualization of three-dimensional chaos. *Science* **281**, 683–686 (1998).
4. Pierrehumbert, R. T. Tracer microstructure in the large-eddy dominated regime. *Chaos Solitons Fractals* **4**, 1091–1110 (1994).
5. Antonsen, T. M., Fan, Z., Ott, E. & Garcia-Lopez, E. The role of chaotic orbits in the determination of power spectra of passive scalars. *Phys. Fluids* **8**, 3094–3104 (1996).
6. Antonsen, T. M. & Ott, E. Multifractal power spectra of passive scalars convected by chaotic fluid flows. *Phys. Rev. A* **44**, 851–857 (1991).
7. Muzzio, F. J., Meneveau, C., Swanson, P. D. & Ottino, J. M. Scaling and multifractal properties of mixing in chaotic flows. *Phys. Fluids A* **4**, 1439–1456 (1992).
8. Alvarez, M. M., Muzzio, F. J., Cerbelli, S., Adrover, A. & Giona, M. Self-similar spatiotemporal structure of intermaterial boundaries in chaotic flows. *Phys. Rev. Lett.* **81**, 3395–3398 (1998).
9. Paret, J., Marteau, D., Paireau, O. & Tabeling, P. Are flows electromagnetically forced in thin stratified layers two-dimensional? *Phys. Fluids* **9**, 3102–3104 (1997).
10. Williams, B. S., Marteau, D. & Gollub, J. P. Mixing of a passive scalar in two-dimensional turbulence. *Phys. Fluids* **9**, 2061–2080 (1997).
11. Paret, J. & Tabeling, P. Experimental observation of the two-dimensional inverse energy cascade. *Phys. Rev. Lett.* **79**, 4162–4165 (1997).
12. Miller, P. L. & Dimotakis, P. E. Reynolds number dependence of scalar fluctuations in a high Schmidt number turbulent jet. *Phys. Fluids A* **3**, 1156–1163 (1991).
13. Shraiman, B. I. & Siggia, E. D. Lagrangian path integrals and fluctuations in random flow. *Phys. Rev. E* **49**, 2912–2927 (1994).

Acknowledgements

We thank J. Andersen, J.-C. Geminard, A. Kudrolli, and W. Losert for experimental contributions, and E. Ott and B. Shraiman for discussions. This work was supported by the Condensed Matter Physics Program of the US NSF.

Correspondence and requests for materials should be addressed to J.P.G. (e-mail: jgollub@haverford.edu).

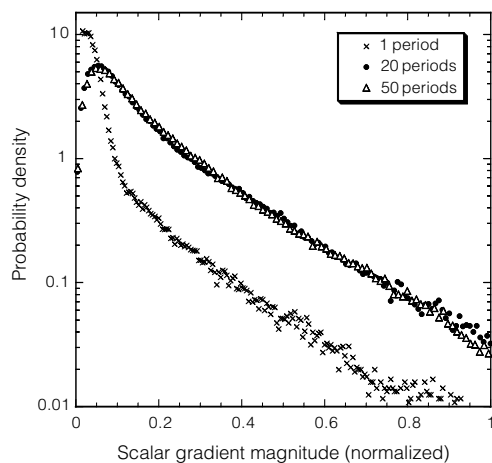


Figure 5 Probability distribution of the magnitude of the concentration gradient for chaotic mixing (Fig. 2). The distribution, here normalized by the standard deviation of the intensity field to compensate for the gradual loss of contrast, reaches an invariant form after about 20 periods, with a peak at finite gradient and an exponential tail.

Sonoluminescence temperatures during multi-bubble cavitation

William B. McNamara III*, Yuri T. Didenko*‡ & Kenneth S. Suslick*

* Department of Chemistry, University of Illinois at Urbana-Champaign, 600 S. Mathews Avenue, Urbana, Illinois 61801, USA

Acoustic cavitation—the formation and implosive collapse of bubbles—occurs when a liquid is exposed to intense sound. Cavitation can produce white noise, sonochemical reactions, erosion of hard materials, rupture of living cells and the emission of light, or sonoluminescence^{1,2}. The concentration of energy during the collapse is enormous: the energy of an emitted photon can exceed the energy density of the sound field by about twelve orders of magnitude³, and it has long been predicted that the interior bubble temperature reaches thousands of degrees Kelvin during collapse. But experimental measurements^{4,5} of

‡ Permanent address: Pacific Oceanological Institute, Vladivostok 690061, Russia.

conditions inside cavitating bubbles are scarce, and there have been no studies of interior temperature as a function of experimental parameters. Here we use multi-bubble sonoluminescence from excited states of metal atoms as a spectroscopic probe of temperatures inside cavitating bubbles. The intense atomic emission allows us to change the properties of the gas–vapour mixture within the bubble, and thus vary the effective emission temperature for multi-bubble sonoluminescence from 5,100 to 2,300 K. We observe emission temperatures that are in accord with those expected from compressional heating during cavitation.

We previously discovered that sonication of solutions of $\text{Fe}(\text{CO})_5$, $\text{Cr}(\text{CO})_6$ and $\text{Mo}(\text{CO})_6$ produced multi-bubble sonoluminescence (MBSL) spectra from excited states of iron, chromium, and molybdenum atoms⁶. Improved spectral resolution now enables us to use these emissions to determine effective temperatures for the emitting excited states. As an example, calculated and observed spectra for Cr under Ar at 20 kHz are given in Fig. 1; the synthetic spectra are generated using the theory of atomic emission⁷. Analogous spectra were also collected for Mo and Fe in order to test the validity of this method. The relative integrated intensities (I_1/I_2) of two atomic lines emitted from the different excited states of the same metal atom are given by equation (1):

$$\frac{I_1}{I_2} = \frac{g_1 A_1 \lambda_2}{g_2 A_2 \lambda_1} \exp[(E_1 - E_2)/kT_e] \quad (1)$$

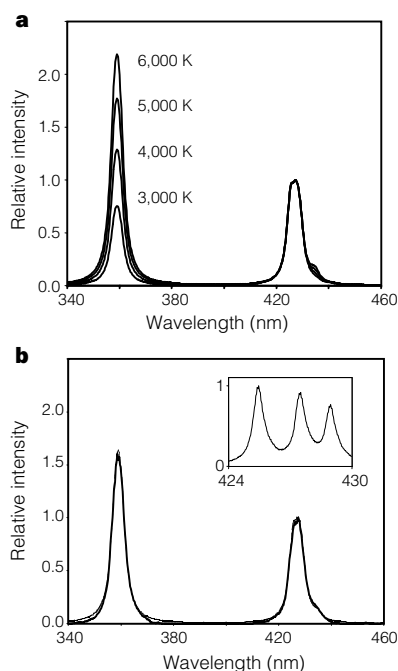


Figure 1 Multi-bubble sonoluminescence (MBSL) emission from excited states of Cr atoms. **a**, Calculated spectra as a function of temperature. **b**, The observed emission spectrum compared to the best-fit calculated spectrum (4,700 K). Inset, observed spectrum at higher resolution, which resolves the individual atomic emission lines. Sonoluminescence was generated from 2.5 mM solutions of metal carbonyls (0.25 mM for $\text{Mo}(\text{CO})_6$ due to solution absorbance) in poly(dimethylsiloxane) (Dow 200 silicone oil, 100 centistokes viscosity) irradiated at $\sim 90 \text{ W cm}^{-2}$ at 20 kHz (Heat Systems Mysonix 375, with 0.5 inch Ti horn), and spectra collected with an 0.5 m spectrograph (Acton Research 505F with a Princeton Instruments IRY 512N diode array). The solutions were continuously sparged with the appropriate gas during sonication, and each spectrum is the average of at least 15 10-second collections. All spectra were corrected for absorbance by the solution and for the response of the optical system. Imaging of the MBSL shows that the emission comes from a dense cloud of emitting bubbles rather than from a few exceptional ones.

where g is the degeneracy of the electronic state, A is the Einstein transition probability for the electronic transition, λ is the wavelength of the emitted line, E is the energy of the electronic state, and T_e is the electronic temperature. The transition probabilities, degeneracies, wavelengths, and excited-state energies were taken from the literature^{8–10}. This technique has been well established for flame and plasma diagnostics^{11,12}, and is proving to be a versatile method of determining the effective temperature of cavitational bubble collapse under a variety of experimental conditions.

The temperatures from three different metal atomic line emissions yielded very consistent results. High-resolution spectra of the MBSL emission from Cr and Mo atoms were collected from solutions of the hexacarbonyl complexes of these metals (Fig. 1 inset). The relative intensity of each line within a given multiplet was measured from these spectra, and the relative intensity of each multiplet was then determined from lower-resolution spectra. This process allowed for a line by line comparison of relative intensities for these two metals across the entire spectral window. The temperatures were then determined by the use of atomic Boltzmann plots¹³: Cr and Mo atom emission temperatures were respectively $4,700 \pm 300 \text{ K}$ and $4,800 \pm 400 \text{ K}$, under Ar at 20 kHz. The linearity of these plots also indicated that the emission is thermally equilibrated. The high resolution MBSL spectra of Fe emission are too complex to allow for the determination of individual line intensities, and the experimental spectra were therefore compared to synthetic spectra generated using equation (1), with an excellent fit to data found for a temperature of $5,100 \pm 300 \text{ K}$.

We previously used two different techniques to measure the temperature of cavitation in Ar-saturated liquids. The first made use of sonochemical kinetics for a comparative rate thermometry analysis of the dissociation of CO from various metal carbonyls⁵. This technique is independent of sonoluminescence, and yielded an effective reaction temperature of $5,200 \pm 500 \text{ K}$ for the gas phase of cavitation under Ar. The second technique applied spectral analysis to C_2 emission bands in the MBSL from the sonication of silicone oil under Ar, giving an effective emission temperature of $5,075 \pm 150 \text{ K}$ (ref. 4). The temperatures reported here are in good agreement with these previously determined values. We note that the previous MBSL emission spectra of C_2 under similar conditions also appeared to be thermally equilibrated^{4,14}.

These metal-atom emissions are the most intense sonoluminescence yet observed. This allows us to study MBSL under conditions previously experimentally inaccessible. Multi-bubble sonoluminescence is generally believed to arise from compressional heating of the bubble contents during the final stage of bubble collapse. The intrabubble temperature should therefore depend on the properties

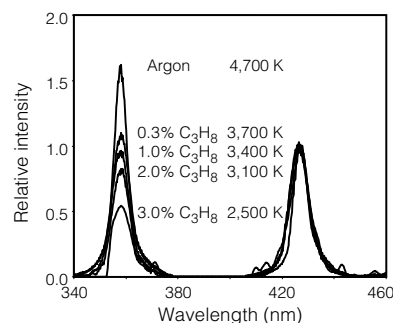


Figure 2 Effect of polyatomic gases on the observed emission temperatures from MBSL. The MBSL spectra are from solutions of $\text{Cr}(\text{CO})_6$ in silicone oil, obtained as in Fig. 1. From top to bottom, the sparge gas was Ar mixed with 0.0, 0.3, 1.0, 2.0, and 3.0 vol % propane, yielding respective emission temperatures of 4,700 K, 3,700 K, 3,400 K, 3,100 K and 2,500 K.

of the gas and vapour mixture within the bubble, particularly the polytropic ratio ($\gamma = C_p/C_v$, ratio of heat capacities) and the thermal conductivity. The effect of each of these parameters was examined by collecting MBSL spectra from several liquids containing a variety of dissolved gases.

If emission results from compressional heating, the effective temperature and pressure reached during cavitation will drop as γ decreases (for a given compression ratio). This prediction was tested by collecting MBSL spectra from $\text{Cr}(\text{CO})_6$ solutions that were saturated with Ar doped with low concentrations of various gaseous hydrocarbons (methane, ethane, ethylene and propane). These polyatomic molecules have much higher heat capacities than does Ar, particularly at temperatures sufficient to populate their excited-state vibrational modes. Note that the thermal conductivities of these mixtures vary by less than a factor of two relative to argon.

The observed emission temperature does indeed decrease substantially as the polyatomic gas content is increased. For example, as Ar is doped with increasing amounts (up to 3%) of propane (Fig. 2), the emission temperature progressively decreases from 4,700 K to 2,500 K. The low resolution of the Cr spectra was necessitated by the decreasing intensity of emission at the higher concentrations of hydrocarbons. The measured emission temperatures for Ar mixtures with various hydrocarbons (methane, ethane, ethylene and propane) are given in Fig. 3. In all instances, the temperature of MBSL decreases as the percentage of a given hydrocarbon is increased (that is, as the polytropic ratio of the gas within the bubble is decreased). Similar results were observed for Fe with methane.

The very simplest model for cavitation assumes adiabatic compression during bubble collapse^{2,15}: a gas with a polytropic ratio γ , compressed from an initial radius R_i to a final radius R_f , with an initial temperature T_i , has a final temperature T_f according to equation (2):

$$T_f = T_i \left(\frac{R_i}{R_f} \right)^{3(\gamma-1)} \quad (2)$$

This equation includes no dynamics of bubble motion, and neglects all effects from thermal transport, solvent vapour pressure, and chemical reactions within the bubble. Furthermore, equation (2) assumes a temperature-independent γ ; however, γ decreases substantially as excited vibrational states become fully populated and it decreases even more if chemical reactions occur. Nonetheless, as shown in Fig. 3, the data are fitted reasonably well by equation (2) for a compression ratio of 3.65. We calculated the temperatures and

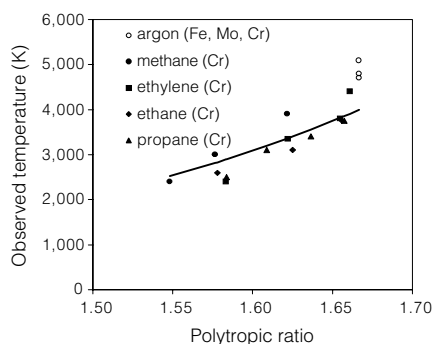


Figure 3 Observed emission temperatures versus gas-mixture polytropic ratios at 298 K. The polytropic ratio of heat capacities, γ , is given by C_p/C_v . The solid line is the best fit to simple adiabatic compression of a bubble with a radius ratio of 3.65, from equation (2); as γ is not temperature independent, equation (2) provides only an approximate model. The open circles give the observed emission temperatures from Fe, Mo, and Cr atom MBSL under argon; all other data are from Cr atom emission under given gases.

pressures during bubble collapse by finite difference using a temperature dependent γ , and can fit our data to within experimental error. Given the lack of dynamics and the failure to incorporate chemical reactions (whose endothermicity is not negligible compared to the compressional heating), more detailed modelling¹⁶ will be required to give meaningful results.

The polytropic ratio of the bubble interior can also be varied by changing the identity and vapour pressure of the solvent. The solvent vapours behave in the same manner as the gaseous hydrocarbons described above: an increase in the solvent vapour pressure is equivalent to increasing the percentage of hydrocarbon gas and leads to similar drops in temperature. Both MBSL intensities¹⁷⁻¹⁹ and sonochemical rates^{20,21} decrease dramatically with solvent vapour pressure increases. We collected MBSL spectra at different bulk solution temperatures from solutions of $\text{Cr}(\text{CO})_6$ under Ar in octanol, a low volatility liquid whose vapour pressure as a function of temperature is well documented²². The results in Fig. 4 are consistent with compressional heating of the bubble contents: the temperature of MBSL decreases as the vapour pressure increases. Similar results were observed using other long-chain alcohols and alkanes, and using helium instead of argon.

Several reports have shown that the total intensity of MBSL from solutions saturated with noble gases decreases as the thermal conductivity of the noble gas increases. This has generally been attributed to thermal transport during cavitation: compressional heating combined with limited thermal transport in a “quasi-adiabatic”

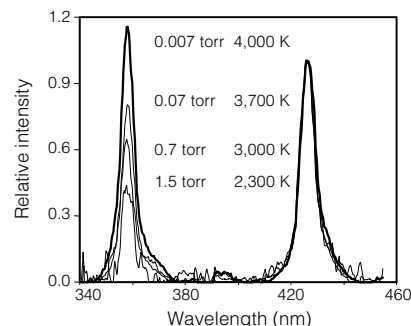


Figure 4 Effect of solvent vapour pressure on the observed emission temperatures from MBSL. The MBSL spectra are from solutions of $\text{Cr}(\text{CO})_6$ in octanol, obtained as in Fig. 1. From top to bottom, the vapour pressure was 0.007, 0.07 and 1.5 torr, yielding emission temperatures of 4,000 K, 3,700 K, 3,000 K and 2,300 K, respectively.

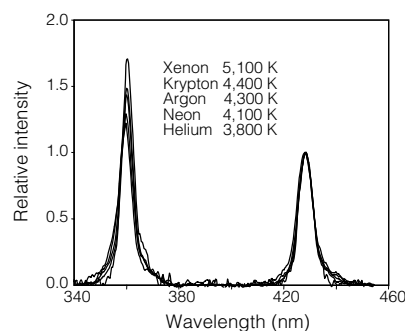


Figure 5 Effect of dissolved noble gases on the observed emission temperatures from MBSL. The MBSL spectra are from solutions of $\text{Cr}(\text{CO})_6$ in octanol, obtained as in Fig. 1. From top to bottom, the dissolved gas was Xe, Kr, Ar, Ne and He, with respective emission temperatures of 5,100 K, 4,400 K, 4,300 K, 4,100 K and 3,800 K.

collapse^{16,23–25}. The rate at which energy is transferred out of the bubble is expected to increase as the thermal conductivity of the gas within the bubble increases. Bubbles containing helium, therefore, should be cooler than bubbles containing argon or xenon, although the predicted extent of this effect is debatable²⁴. In order to examine the importance of thermal conduction, MBSL spectra were obtained from solutions of Cr(CO)₆ in octanol saturated with different noble gases. The results in Fig. 5 show that the temperature of MBSL decreases as the thermal conductivity of the gas within the bubble increases. Similar results were observed using dodecane.

We note that the thermal conductivities of the noble gases used here span a factor of thirty, while the thermal conductivities of the argon and hydrocarbon mixtures differ by only a factor of two, therefore, the temperature changes observed upon the addition of hydrocarbons to argon are not due to changes in thermal conductivity.

We have shown that the observed emission temperature within imploding cavitation bubbles depends on both the polytropic ratio and the thermal conductivity of the bubble contents. The processes occurring within the bubble, however, are more complex than can be described by the simple physics of compressional heating. A cavitation bubble functions as a small chemical reactor, and so the identity of the bubble contents will change during bubble collapse. The sonolysis of organic liquids generates H₂ and C₂H₂ as well as other small hydrocarbons²⁰, and similar processes will occur during the sonolysis of silicone oil. Evidence for this is seen in the MBSL spectra: the spectra of all the systems described here contain features attributable to excited states of C₂ and CH (refs 4, 18, 26), and we also find that sonication of silicone oil leads to intense emission from excited Si atoms. These chemical processes can absorb large amounts of energy during the compression. Furthermore, if sufficient dissociation occurs, the sonolysis products (mostly diatomics and polyatomics) will substantially lower the polytropic ratio and increase the pressure inside the bubble. This makes it increasingly difficult to further compress and heat the bubble²⁷. These factors will limit the temperatures achievable by compressional heating within cavitation bubbles. □

Received 4 May; accepted 23 August 1999.

1. Suslick, K. S. & Crum, L. A. in *Handbook of Acoustics* (ed. Crocker, M. J.) 243–253 (Wiley-Interscience, New York, 1998).
2. Knapp, R. T., Daily, J. W. & Hammit, F. G. *Cavitation* (McGraw-Hill, New York, 1970).
3. Barber, B. P. & Putterman, S. J. Observation of synchronous picosecond sonoluminescence. *Nature* **352**, 318–320 (1991).
4. Flint, E. B. & Suslick, K. S. The temperature of cavitation. *Science* **253**, 1325–1326 (1991).
5. Suslick, K. S., Hammerton, D. A. & Cline, R. E. Jr Sonochemical hot spot. *J. Am. Chem. Soc.* **108**, 5641–5642 (1986).
6. Suslick, K. S., Flint, E. B., Grinstaff, M. W. & Kemper, K. A. Sonoluminescence from metal carbonyls. *J. Phys. Chem.* **97**, 3098–3099 (1993).
7. Alkemande, C. T. J., Hollander, T., Snelleman, W. & Zeegers, P. J. T. *Metal Vapours in Flames* (Pergamon, New York, 1982).
8. Wiese, W. L., Fuhr, J. R. & Martin, G. A. Atomic transition probabilities: scandium through manganese. *J. Phys. Chem. Ref. Data* **17**, 311–327 (1988).
9. Wiese, W. L., Fuhr, J. R. & Martin, G. A. Atomic transition probabilities: iron through nickel. *J. Phys. Chem. Ref. Data* **14**, 13–67 (1988).
10. Whaling, W. & Brault, J. W. Comprehensive transition probabilities in molybdenum I. *Phys. Scr.* **38**, 707–715 (1988).
11. Gaydon, A. G. *The Spectroscopy of Flames* 2nd edn (Wiley, New York, 1974).
12. Cabannes, F. & Chapelle, J. in *Reactions Under Plasma Conditions* 1st edn Vol. 1 (ed. Venugopalan, M.) 367–470 (Wiley-Interscience, New York, 1971).
13. Reif, I., Fassel, V. A. & Kniseley, R. N. Spectroscopic flame measurements and their physical significance I: theoretical concepts. *Spectrochim. Acta B* **28**, 105–123 (1973).
14. Jeffries, J. B., Copeland, R. A., Suslick, K. S. & Flint, E. B. Thermal equilibration during cavitation. *Science* **256**, 248 (1992).
15. Noltingk, B. E. & Neppiras, E. Cavitation produced by ultrasonics. *Proc. Phys. Soc. B* **63**, 674–685 (1950).
16. Kamath, V., Prosperetti, A. & Egolfopoulos, F. N. A theoretical study of sonoluminescence. *J. Acoust. Soc. Am.* **94**, 248–260 (1993).
17. Jarman, P. Measurements of sonoluminescence from pure liquids and some aqueous solutions. *Proc. Phys. Soc.* **73**, 628–640 (1959).
18. Flint, E. B. & Suslick, K. S. Sonoluminescence from nonaqueous liquids: emissions from small molecules. *J. Am. Chem. Soc.* **111**, 6987–6992 (1989).
19. Suslick, K. S. & Flint, E. B. Sonoluminescence of alkali metal salts. *J. Phys. Chem.* **95**, 1484–1488 (1991).

20. Suslick, K. S., Gawienowski, J. J., Schubert, P. F. & Wang, H. H. Alkane sonochemistry. *J. Phys. Chem.* **87**, 2299–2301 (1983).
21. Suslick, K. S., Gawienowski, J. W., Schubert, P. F. & Wang, H. H. Sonochemistry in non-aqueous liquids. *Ultrasonics* **22**, 33–36 (1984).
22. Yaws, C. L. *Handbook of Vapor Pressures* Vol. 3, 383 (Gulf, Houston, 1994).
23. Hickling, R. Effects of thermal conduction in sonoluminescence. *J. Acoust. Soc. Am.* **35**, 967–974 (1963).
24. Young, F. R. Sonoluminescence from water containing dissolved gases. *J. Acoust. Soc. Am.* **60**, 100–104 (1976).
25. Yasui, K. *J. Phys. Soc. Jpn* **65**, 2830–2840 (1996).
26. Suslick, K. S. & Flint, E. B. Sonoluminescence of non-aqueous liquids. *Nature* **330**, 553–555 (1987).
27. Zel'dovich, Y. D. & Raizer, Y. P. *Physics of Shock Waves and High Temperature Hydrodynamic Phenomenon* 2nd edn (Academic, New York, 1966).

Acknowledgements

This work was supported by the US National Science Foundation, the US Department of Energy, and in part by the US Defence Advanced Research Projects Agency.

Correspondence and requests for materials should be addressed to K.S.S. (e-mail: ksuslick@uiuc.edu).

Carbon cycling and chronology of climate warming during the Palaeocene/Eocene transition

Richard D Norris* & Ursula Röhl†

* MS-23, Woods Hole Oceanographic Institution, Woods Hole, Massachusetts 02540-1541, USA

† Fachbereich Geowissenschaften, Universität Bremen, Postfach 330 440, 28334 Bremen, Germany

Current models of the global carbon cycle lack natural mechanisms to explain known large, transient shifts in past records of the stable carbon-isotope ratio ($\delta^{13}\text{C}$) of carbon reservoirs^{1,2}. The injection into the atmosphere of ~1,200–2,000 gigatons of carbon, as methane from the decomposition of sedimentary methane hydrates, has been proposed to explain a $\delta^{13}\text{C}$ anomaly^{3,4} associated with high-latitude warming¹ and changes in marine^{5–7} and terrestrial⁸ biota near the Palaeocene–Eocene boundary, about 55 million years ago. These events may thus be considered as a natural ‘experiment’ on the effects of transient greenhouse warming. Here we use physical, chemical and spectral analyses of a sediment core from the western North Atlantic Ocean to show that two-thirds of the carbon-isotope anomaly occurred within no more than a few thousand years, indicating that carbon was catastrophically released into the ocean and atmosphere. Both the $\delta^{13}\text{C}$ anomaly and biotic changes began between 54.93 and 54.98 million years ago, and are synchronous in oceans and on land. The longevity of the $\delta^{13}\text{C}$ anomaly suggests that the residence time of carbon in the Palaeocene global carbon cycle was ~120 thousand years, which is similar to the modelled response after a massive input of methane^{3,4}. Our results suggest that large natural perturbations to the global carbon cycle have occurred in the past—probably by abrupt failure of sedimentary carbon reservoirs—at rates that are similar to those induced today by human activity.

The carbon isotope record of marine carbonates is interrupted by a transient negative $\delta^{13}\text{C}$ anomaly of –3‰ over an interval of ~100–200 kyr near the end of the Palaeocene^{1,9–13}. In the oceans, the $\delta^{13}\text{C}$ anomaly is associated with the extinction of 35–50% of cosmopolitan benthic foraminifera^{7,10}, the appearance of three short-ranging planktic foraminifera⁵, a widespread increase in

Sonochemical Preparation of a Nanostructured Bifunctional Catalyst

Gennady Dantsin and Kenneth S. Suslick*

School of Chemical Sciences
University of Illinois at Urbana-Champaign
600 S. Mathews Avenue, Urbana, Illinois 61801

Received December 8, 1999

The catalytic conversion of methane to higher hydrocarbons, in particular aromatics such as benzene, is extremely important for the effective utilization of natural gas. This transformation has been performed with bifunctional catalysts, most notably metal-impregnated zeolite ZSM-5.^{1–7} Lunsford and co-workers⁸ have carefully studied the kinetics of Mo on ZSM-5, which becomes an active catalyst for dehydroaromatization, and concluded that the active phase is actually Mo₂C. Various methods of preparation such as incipient wetness and ion exchange, however, produce nonuniform materials that have varying catalytic activity and selectivity. We have previously developed a sonochemical preparation of nanostructured, high surface area Mo₂C.⁹ While this form of Mo₂C is a very active dehydrogenation catalyst for cyclohexane,⁹ it shows no activity for methane aromatization. We report here a simple sonochemical preparation of a bifunctional “eggshell” catalyst for the conversion of methane to benzene. Because the Mo₂C clusters are formed during acoustic cavitation inside a collapsing bubble, their deposition on the ZSM-5 occurs only on the outer surface of the zeolite, and thus does not obstruct the channels of the ZSM-5 support.

Sonochemical preparation of nanophase materials arises from acoustic cavitation: the formation, growth, and implosive collapse of bubbles in a liquid irradiated with high-intensity ultrasound.¹⁰ During the collapse of such bubbles, local hot spots are created with controllable temperatures as high as ~5000 K,¹¹ which provides an unusual method for the decomposition of volatile organometallic precursors. Of particular relevance for supported catalysts, the event responsible for the formation of metal clusters is the gas phase of the collapsing bubble, which is therefore separate from the oxide support onto which the clusters attach.¹² This *inherently* generates “eggshell catalysts” where the outer surface of the support holds the nanometer sized catalyst particles. Given the surface accessibility of such catalysts, they often exhibit

enhanced activity compared to conventionally prepared analogs.¹⁰

In the preparation of Mo₂C/ZSM-5, Mo(CO)₆ and HZSM-5 were irradiated as a slurry in hexadecane with ultrasound at 20 kHz for 3 h at 85 °C under Ar flow.¹³ Scanning transmission electron microscopy (STEM)¹⁴ shows that the channel structure in the zeolite corresponding to the (200) and (020) faces was maintained for both the control of sonicated HZSM-5 and the sonochemically prepared Mo₂C/ZSM-5. These lattice fringes separated by 10 Å (quantified by Fourier diffractography) are shown in Figure 1a. The dark field image of the Mo₂C/ZSM-5 shows uniform particles of about 2 nm in diameter dispersed uniformly on the outer surface of the ZSM-5 support (Figure 1b). EDX detection was used to quantify local elemental concentrations of the Mo₂C/ZSM-5 by high-resolution spot analysis using a 1 nm beam width (which is on the order of the Mo₂C particle size). Multiple Mo₂C particles (shown as lighter areas in Figure 1b) were analyzed and compared to particle-free areas on the ZSM-5 support. Spot EDX analyses of adsorbed Mo₂C particles gave a high Mo/Si molar ratio (as high as 0.8), whereas analyses of regions without Mo₂C particles showed essentially no detectable Mo (Mo/Si ratios are 0.04 ± 0.02). For comparison to our sonochemically prepared catalyst, we synthesized Mo₂C/ZSM-5 by the conventional incipient wetness method,⁸ impregnating ZSM-5 with (NH₄)₆Mo₇O₂₄, and examined its microstructure by STEM-EDX. The distribution of Mo₂C particles onto ZSM-5 was *much* more uniform in the sonochemically prepared samples.¹⁵

X-ray photoelectron spectroscopy (XPS) analysis,¹⁶ which has a depth penetration of ~50 Å, confirms that the Mo₂C is concentrated on the surface of the ZSM-5 support. The electronic states of the Mo, C, and support were also analyzed by XPS. The Mo₂C is characterized by a spin-coupled doublet for the Mo(3d_{5/2}) and Mo(3d_{3/2}) peaks and the C(1s) peak at characteristic binding energies.^{16b} Analysis of the Mo(3d) and Si(2p) peak intensities gave a Mo/Si mole ratio of 0.15, while the bulk elemental analysis gave a Mo/Si mole ratio of 0.01. This comparison means that there is more than a 15-fold enhancement of surface Mo versus the bulk material.

(13) Mo(CO)₆ (0.053 g) and HZSM-5 (1.0 g, Si/Al = 50, H_{1.88}(Al_{1.88}Si_{94.18}O₁₉₂)) (Zeolyst Intl., Kansas City, KS) were added to dry hexadecane (35 mL) in an Ar-filled glovebox (Vacuum Atmospheres, <0.5 ppm O₂). The reaction slurry was irradiated with high-intensity ultrasound at 20 kHz and ~80 W/cm² with a 1 cm² titanium horn (Sonics & Materials VCX600) for 3 h at 85 °C under Ar flow. After sonication, the reaction vessel was brought into the glovebox and the mixture was filtered, washed with degassed, dry pentane (60 mL), and then heated for 5 h under vacuum at 80 °C to remove any unreacted Mo(CO)₆. Excess carbon contamination was mostly removed by treating the catalyst at 450 °C for 10 h under 1:1 CH₄/H₂ (30 cm³/min) flow; typical samples were prepared at 2 wt % Mo. As a control, another HZSM-5 sample was sonicated as described without the addition of Mo(CO)₆ and given identical posttreatment and compared to the above material.

(14) Scanning transmission electron microscopy (STEM) utilized a VG HB501 microscope with EDX detection (Oxford Instruments). Long exposure to the electron beam must be avoided for zeolite samples to avoid sample degradation during STEM. (b) Reimer, L. *Transmission Electron Microscopy*, 2nd ed.; Springer-Verlag: Berlin, 1989; pp 452–457.

(15) The conventionally made sample had a wide distribution of Mo₂C particle sizes on the ZSM-5 support, ranging from greater than ~20 nm down to ~2 nm. In addition, not all ZSM-5 particles had uniform amounts of Mo₂C on their surfaces. Furthermore, there were also substantial numbers of free Mo₂C particles not in contact with ZSM-5 particles. In comparison, the sonochemically synthesized material has a homogeneous distribution of Mo₂C particles (~2 nm) all supported on uniformly coated particles of ZSM-5.

(16) (a) X-ray photoelectron spectroscopy was recorded on a Phi-540 Perkin-Elmer spectrometer using Mg Kα radiation. The XPS was internally calibrated to the known Si (2p) peak at 102.9 eV in ZSM-5; Briggs, D. *Practical Surface Analysis*, 2nd ed.; John Wiley & Sons: Chichester, 1990; Vol. 1, pp 407–413. (b) For sonochemically prepared Mo₂C, the Mo(3d_{5/2}) and Mo(3d_{3/2}) peaks are at 228.6 and 231.7 eV, internally calibrated to the background C(1s) peak at 283.5 eV; Moulder J. F.; Stickle, W. F.; Sobol, P. E.; Bomben, K. D. *Handbook of X-ray Photoelectron Spectroscopy*; Chastain J., Ed.; Perkin-Elmer: Eden Prairie, MN, 1992. (c) XPS analysis of both the O(1s) and Si(2p) in the HZSM-5 and the HZSM-5 control sample gave an O/Si atomic ratio of 2.1, as expected.

(1) (a) Wang, L.; Tao, L.; Xie, M.; Xu, G.; Huang, J.; Xu, Y. *Catal. Lett.* **1993**, *21*, 35–41. (b) Xu, Y.; Lin, L. *Appl. Catal. A* **1999**, *188*, 53–67.

(2) (a) Weckhuysen, B. M.; Wang, D.; Rosynek, M. P.; Lunsford, J. H. *J. Catal.* **1998**, *175*, 338–346. (b) Weckhuysen, B. M.; Wang, D.; Rosynek, M. P.; Lunsford, J. H. *J. Catal.* **1998**, *175*, 347–351.

(3) Lunsford, J. H.; Rosynek, M. P.; Wang, D. *Stud. Surf. Sci. Catal.* **1997**, *107*, 257–261.

(4) Solymosi, F.; Cserenyi, J.; Szoke, A.; Bansagi, T.; Oszko, A. *J. Catal.* **1997**, *165*, 150–161.

(5) Solymosi, F.; Szoke, A.; Cserenyi, J. *Catal. Lett.* **1996**, *39*, 157–161.

(6) Wong, S.-T.; Xu, Y.; Liu, W.; Wang, L.; Guo, X. *Appl. Catal., A* **1996**, *136*, 7–17.

(7) Choudhary, V. R.; Kinage, A. K.; Choudhary, T. V. *Science* **1997**, *275*, 1286–1288.

(8) Wang, D.; Lunsford, J. H.; Rosynek, M. P. *J. Catal.* **1997**, *169*, 347–358.

(9) Hyeon, T.; Fang, M.; Suslick, K. S. *J. Am. Chem. Soc.* **1996**, *118*, 5492–5493.

(10) (a) Suslick, K. S. *Annu. Rev. Mater. Sci.* **1999**, *29*, 295–326. (b) Crum, L. A.; Mason, T. J.; Reisse, J. L.; Suslick, K. S., Eds. *Sonochemistry and Sonoluminescence*; Kluwer Academic Publishers: Dordrecht, 1999. (c) Suslick, K. S. In *Handbook of Heterogeneous Catalysis*; Ertl, G., Knozinger, H., Weitkamp, J., Eds.; Wiley-VCH: Weinheim, 1997; Vol. 3, Chapter 8.6, pp 1350–1357.

(11) (a) McNamara, W. B., III; Didenko, Y.; Suslick, K. S. *Nature* **1999**, *401*, 772–776. (b) Flint, E. B.; Suslick, K. S. *Science* **1991**, *253*, 1397–1399.

(12) At 20 kHz, the cavitation bubble will be on the order of 100 μm in size, and much too large to occur within the nm pores of a zeolite.

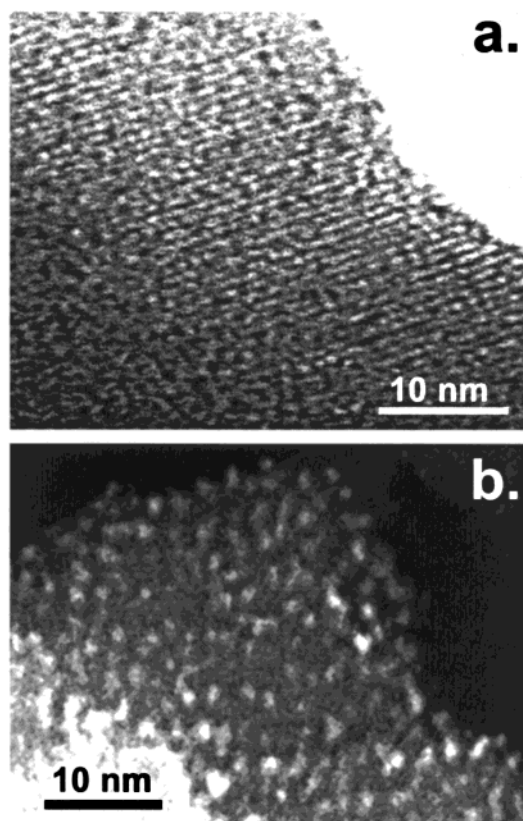


Figure 1. STEM micrographs of Mo₂C/ZSM-5 prepared sonochemically showing (a) the lattice fringes of the ZSM-5 and (b) a typical dark field image showing Mo₂C particles on the surface of the ZSM-5.

To assess the dispersion of Mo₂C on the ZSM-5 support (i.e., the fraction of surface atoms of Mo_(carbide)), chemisorption with CO was done at room temperature. The catalyst was pretreated by heating it to 400 °C for 3 h under high vacuum (10⁻⁵ Torr) to remove any adsorbed gases. The chemisorption isotherms gave a dispersion of 34% CO-binding surface metal sites per total metal in the sample. An approximation of particle size for the Mo₂C/ZSM-5 catalyst was modeled after that used for Pt/SiO₂ catalysts (eq 1).^{17,18}

$$d_{\text{particle}} = 1.105(d_{\text{atomic}})(N_t)^{1/3} \quad (1)$$

where N_t is the total number of Mo_(carbide) atoms per particle for a dispersion of 34%. This equation assumes the particles are cubooctahedral with $d_{\text{atomic}} = 0.29$ nm (the inter-Mo distance for Mo₂C) and a 1:1 binding stoichiometry for CO:Mo_(carbide).¹⁹ For 34% dispersion, $N_t \sim 1700$ and the particle diameter is ~ 3.8 nm. This value is somewhat larger than the 2 nm particle diameter directly observed by STEM, probably due both to the surface Mo atoms in direct contact with the zeolite (which are unavailable for CO chemisorption) and to partial carbon coating of the Mo₂C surfaces.

(17) van Harveld, R.; Hartog, F. *Surf. Sci.* **1969**, *15*, 189–230.

(18) Humblot, F.; Didillon, D.; Lepeltier, F.; Candy, J. P.; Corker, J.; Clause, O.; Bayard, F.; Basset, J. M. *J. Am. Chem. Soc.* **1998**, *120*, 137–146.

(19) Lee, J. S.; Lee, K. H.; Lee, J. Y. *J. Phys. Chem.* **1992**, *96*, 362–366.

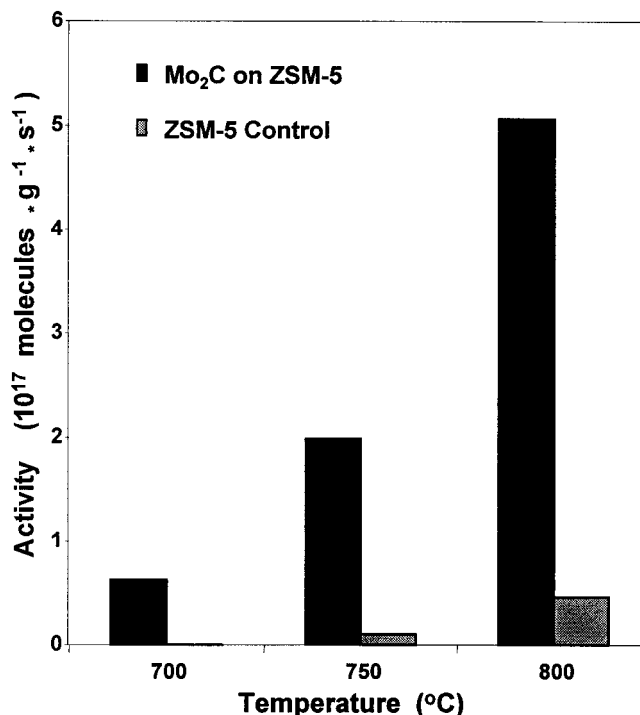


Figure 2. Catalytic activity for dehydroaromatization of methane by sonochemically prepared Mo₂C/ZSM-5 and sonicated ZSM-5 control.

Catalytic studies on the Mo₂C/ZSM-5 powder for the dehydroaromatization of methane to benzene were performed with a single-pass quartz microreactor²⁰ at 700 to 800 °C. The observed turnover frequencies based on CH₄ consumption are shown as a function of temperature in Figure 2 and compared to the sonicated ZSM-5 control. The product distribution is comprised of ethane and benzene, with selectivity for the latter of 60% at 700 °C. The sonicated HZSM-5 control sample treated in the same way does not show any significant activity. Literature values for other Mo₂C/ZSM-5 catalysts are reported as approximately 6 × 10¹⁷ molecules g⁻¹ s⁻¹ at 700 °C with a 70% selectivity for benzene,⁸ quite comparable to the sonochemically prepared samples.

In conclusion, the sonication of molybdenum hexacarbonyl in hexadecane with HZSM-5 has been shown to produce nanophase Mo₂C particles of about 2 nm decorating the outside of the ZSM-5 support. This eggshell catalyst has essentially all of the Mo₂C on the outer surface of the ZSM-5 support relative to the pores. The catalyst is both active and selective for the aromatization of methane to benzene.

Acknowledgment. We would like to thank Dr. Millan M. Mdlleleni for his initial ideas on the project. This work was supported by the National Science Foundation (CHE 9420758). For surface analysis, we would like to thank Dr. Rick Haasch and Dr. R. D. Twisten at the Center for Microanalysis of Materials, University of Illinois at Urbana-Champaign, supported by the U.S. Department of Energy (DEFG02-ER-45439).

JA994300W

(20) Ultrahigh purity (99.99%) CH₄ was used with a flow of 12 cm³/min. The reaction products were analyzed with a quadrupole mass spectrometer (Spectral Instruments) and gas chromatograph (Hewlett-Packard) with an *n*-octane/Porasil C column and FID.

Molecular emission from single-bubble sonoluminescence

Yuri T. Didenko, William B. McNamara III & Kenneth S. Suslick

Department of Chemistry, University of Illinois at Urbana-Champaign, 600 S. Mathews Avenue, Urbana, Illinois 61801, USA

Ultrasound can drive a single gas bubble in water into violent oscillation; as the bubble is compressed periodically, extremely short flashes of light (about 100 ps) are generated with clock-like regularity^{1–4}. This process, known as single-bubble sonoluminescence, gives rise to featureless continuum emission^{4,5} in water (from 200 to 800 nm, with increasing intensity into the ultraviolet). In contrast, the emission of light from clouds of cavitating bubbles at higher acoustic pressures (multi-bubble sonoluminescence¹) is dominated by atomic and molecular excited-state emission^{6–11} at much lower temperatures⁶. These observations have spurred intense effort to uncover the origin of sonoluminescence and to generalize the conditions necessary for its creation. Here we report a series of polar aprotic liquids that generate very strong single-bubble sonoluminescence, during which emission from molecular excited states is observed. Previously, single-bubble sonoluminescence from liquids other than water has proved extremely elusive^{12,13}. Our results give direct proof of the existence of chemical reactions and the formation of molecular excited states during single-bubble cavitation, and provide a spectroscopic link between single- and multi-bubble sonoluminescence.

The origin of the featureless emission of single-bubble sonoluminescence (SBSL) in water has become the subject of many theoretical speculations, and several mechanisms have been proposed, including black-body radiation⁵, bremsstrahlung^{14,15}, ion–electron recombination¹⁵, and confined electrons¹⁶. Regardless of the detailed mechanism, a consensus has emerged that SBSL involves extraordinary temperatures inside the bubble^{14–16}.

Whereas SBSL from water has been extensively studied, SBSL from other liquids in air has not¹². For a single cavitating bubble in water, Lohse and co-workers have argued convincingly that N₂ and O₂ are removed from the bubble's interior by reaction to form NO_x (which dissolves in and reacts with the bulk water), leaving primarily monatomic argon inside the bubble^{17,18}. In addition, sonolysis of water (to H atoms and OH radicals) is highly reversible. These properties make water a nearly perfect liquid for SBSL under air: cavitation-induced reactions do not yield gaseous polyatomic products that would hinder compressional heating of the bubble.

The only previous report¹³ of SBSL from liquids other than water found a weak emission from organic liquids (mostly alcohols), but only for unstable, moving xenon bubbles (*n*-butanol in air apparently also gives a very weak emission about 200 times less intense than water¹³). The spectra of these liquids under Xe again are featureless continua (we note, however, that emission from an excited state of C₂ was observed from a xenon bubble pulsating asymmetrically on a thermocouple wire in dodecane¹⁹). In contrast to water, sonolysis of other liquids produces small polyatomic gases⁸ during the entropy-driven, high-energy chemistry that occurs within the bubble. We believe that build-up of such gases inside a single cavitating bubble precludes the heating necessary to generate SBSL.

From this hypothesis, we predict that a liquid will support SBSL under air if it has (1) a low vapour pressure (necessary to minimize the amount of gas formed during sonolysis) and (2) a high content of heteroatoms such as O or N (to form species that dissolve in or react with the surrounding liquid, and thus are removed from the

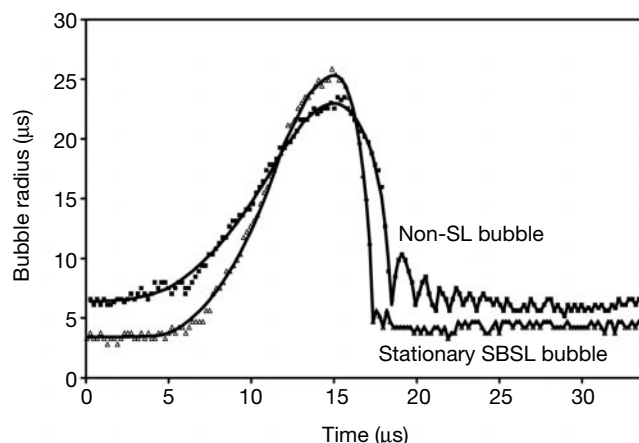


Figure 1 Radius versus time curves for single-bubble cavitation in methylformamide. Data are shown slightly below and slightly above the sonoluminescence (SL) threshold (acoustic pressure, ~ 1.1 bar). The radius data (shown as data points) were generated from stroboscopic imaging, so the time axis is relative and does not represent the phase of the bubble with respect to the acoustic field. The SBSL apparatus consisted of a spherical, quartz, 100-ml cell with a cylindrical piezoceramic transducer cemented to the bottom. The transducer was driven by a function generator and amplifier at a resonant frequency of about 30 kHz. A calibrated needle hydrophone (DAPCO) was used to measure the approximate pressure amplitude at the bubble location. The stroboscopic imaging system was similar to that used in ref. 21. The image of the bubble was recorded through a microscope by a Pulnix 9701 CCD camera. The bubble was illuminated by a light-emitting diode, which was driven by a pulse generator (HP 8116A). One of the outputs from HP 8904A signal synthesizer was used to trigger the pulse generator and the other sent to the power amplifier that drove the SBSL cell.

bubble). The kinetics of the reactions that form emissive excited states (of, for example, C₂ or CN) may also be important, given the short period of emission during SBSL. Using these criteria, we have discovered intense SBSL in air from numerous polar, aprotic liquids, including formamide (H₂NCHO), *N*-methylformamide ((H₃C)HNCHO), *N,N*-dimethylformamide ((H₃C)₂NCHO), *N*-methylacetamide ((H₃C)HNC(CH₃)O), 1,2-diaminoethane (H₂NCH₂CH₂NH₂), dimethylsulphoxide ((H₃C)₂SO) and adiponitrile (NC(CH₂)₄CN). In keeping with our prediction, the intensity of sonoluminescence in these liquids can be comparable to, or even higher than, that of water. We note that both constraints—that is, (1) and (2) above—on the liquid properties must be met: SBSL is not observed from silicone oil or long-chain aliphatic alcohols (which have very low volatility, but low heteroatom content) in air, nor from formic acid (which has a high heteroatom content, but high volatility).

Both the dynamics of bubble motion in these organic liquids and their SBSL spectra differ significantly from that seen in water. We will discuss the bubble behaviour of *N*-methylformamide in detail. A bubble can be trapped at low acoustic pressure ($P_A \approx 0.9$ bar for *N*-methylformamide) in the centre of the flask (see Fig. 1 legend for details), where it is spatially stationary and pulsates without emitting light. As P_A is increased, the bubble starts to move around the flask's centre and sonoluminescence is first observed (at $P_A \approx 1.3$ bar for *N*-methylformamide). The velocity of the bubble motion at this point is about 3 mm s⁻¹, and its trajectory is often circular or elliptical. The light intensity and the bubble movement both increase with increasing P_A . Microbubble shedding²⁰ or bubble-induced detuning may be responsible for such bubble motion, but additional work is required to explain this phenomenon.

We will refer to light emission from a non-stationary bubble as moving single-bubble sonoluminescence, M-SBSL. These M-SBSL bubbles can be maintained at maximum emission intensities for several minutes. The maximum emission intensities (relative to water at 1.0) are adiponitrile, 2.0; formamide, 1.2; methylforma-

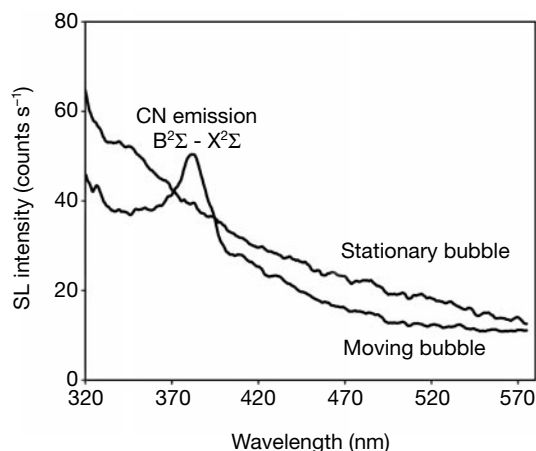


Figure 2 S-BSSL spectra of methylformamide at an acoustic pressure of ~ 1.1 bar for both a stationary and a moving single bubble. The excited-state CN comes from the liquid vapour rather than from the nitrogen gas initially present inside the bubble, because (1) M-SBSL spectra under a partial pressure of Ar (in the absence of N_2 or O_2) show greater CN emission; and (2) M-SBSL spectra from dimethylsulphoxide (which contains no nitrogen) in air do not exhibit CN emission. S-BSSL spectra of methylformamide were collected at 295 K under 10 torr of air, using a Jobin-Yvon Triax 320 monochromator with a Spectrum One CCD detector (Instrument SA, $1,024 \times 256$ array). Spectra were corrected for both the light absorption by the solutions and the response of the optical system against standard lamps (which could be traced back to NIST standards).

amide, 0.14; dimethylsulphoxide, 0.14; dimethylformamide, < 0.05 ; and 1,2-diaminoethane, < 0.05 ; intensities were measured in the same cell with the spectrograph in zeroth order. These liquids all absorb light much more strongly in the ultraviolet region than water does, so the relative intensities of emission can only be taken as an approximate measure of the efficiency of SBSL. Above about 1.5–1.6 bar in *N*-methylformamide, the bubble cannot be held at the centre of the flask and disappears; such behaviour is typical for all liquids reported here.

Hysteresis is observed for SBSL in these liquids. By decreasing the amplitude of ultrasound reaching a moving emitting bubble, it was possible to get light emission at lower P_A than the initial threshold of sonoluminescence inception for all of our non-aqueous liquids. In the cases of formamide and methylformamide, upon decreasing the acoustic amplitude to about 1.1 bar, the bubble becomes stationary and still emits; we will refer to this as stationary single-bubble sonoluminescence, S-SBSL. The intensity of sonoluminescence under the conditions of S-SBSL was approximately the same as, or a little higher than, the emission intensity during M-SBSL at the same acoustic pressure. S-SBSL can be obtained only by first establishing a bubble showing M-SBSL and then reducing P_A .

Stroboscopic imaging²¹ revealed that the stationary emitting bubble pulsates regularly with only a few, weak after-bounces. In contrast, a non-emitting stationary bubble is much larger in size and shows strong, multiple afterbounces (Fig. 1). This difference in dynamics between sonoluminescent and non-sonoluminescent bubbles has also been observed in water, and is consistent with gas removal from the bubble by chemical reactions during SBSL^{18,21}.

The emission spectra from these liquids are especially revealing. In contrast to the featureless spectrum of water SBSL, M-SBSL from adiponitrile, formamide and methylformamide all show relatively strong emission from excited-state CN ($B^2\Sigma^- - X^2\Sigma^+$). At or near the minimum P_A necessary for M-SBSL, this molecular emission is superimposed on an underlying continuum (Figs 2, 3). As the P_A increases, the continuum increases in intensity until the CN emission is no longer discernible (Figs 3, 4). The bubble hysteresis made it possible to collect spectra from *N*-methylformamide for both S-SBSL (which is featureless) and M-SBSL (which

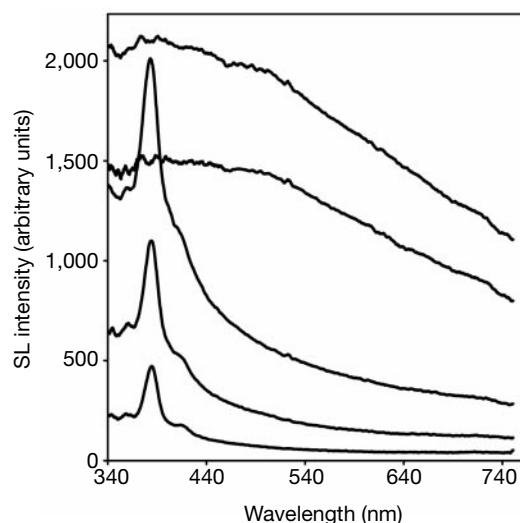


Figure 3 M-SBSL spectra of adiponitrile. Acoustic pressure increases from bottom to top, from 1.7 to 1.9 bar.

shows CN emission) under essentially identical acoustic conditions (Fig. 2).

We propose that the difference between S-SBSL and M-SBSL spectra at similar acoustic pressure lies in the sphericity and severity of the bubble collapse and the effect this has on the bubble contents. A moving bubble cannot collapse as symmetrically as a stationary bubble; it is therefore likely that the effective temperatures reached during S-SBSL are much higher than during M-SBSL. The observation of emission from CN excited states during M-SBSL shows that the temperature is below about 15,000 K under these conditions, for at least part of the emitting bubble; above this temperature the CN (whose dissociation energy is 7.8 eV) would not be stable long enough to emit²². In the case of S-SBSL (which is presumably at higher temperatures than M-SBSL), CN is either thermally dissociated or no longer is formed within the collapsing bubble, and CN emission is not observed.

Several experimental parameters are found to affect the intensity and stability of SBSL in these liquids. Vapour pressure (which plays an essential role in the intensity and temperature of MBSL⁶) appears to be important for SBSL: all of our successful non-aqueous liquids have very low volatilities. For example, adiponitrile (vapour pressure < 0.1 torr at 22 °C; ref. 23) gives intense SBSL, whereas acetonitrile (CH_3CN , vapour pressure 90 torr), a liquid very similar in chemical properties to adiponitrile, fails to give any SBSL. Similarly, the intensity of SBSL decreases more than 20 times from formamide (vapour pressure 0.05 torr at 22 °C) to methylformamide (0.2 torr at 22 °C), to dimethylformamide (3.2 torr at 22 °C). M-SBSL occurs in *N*-methylformamide equilibrated with air pressures from 10 to 150 torr; as the gas pressure increases, M-SBSL occurs at higher acoustic pressures and the bubble's spatial stability decreases.

The acoustic pressure during M-SBSL significantly affects the emission spectra (Fig. 3). As P_A is increased during M-SBSL, the intensity of bubble collapse will also increase, leading to higher temperatures and an initial increase in CN emission as more CN excited states are formed. As the P_A is further increased, however, CN is either thermally dissociated or no longer formed within the collapsing bubble, and a sharp decrease in the intensity of CN emission is observed. Subsequent experiments have shown that the transition between the absence and presence of CN emission occurs on a timescale of about 0.1 s. This is further evidence that CN emission comes from sonolysis of vapour of the liquid, rather than dissolved N_2 , because N_2 diffusion into the bubble requires several

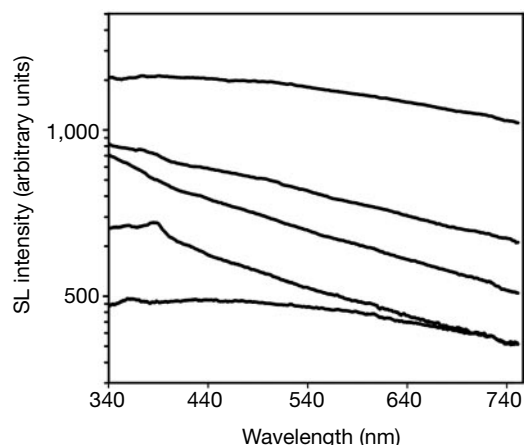


Figure 4 M-SBSL spectra of adiponitrile, formamide, water, methylformamide and dimethylsulphoxide (from the top to the bottom of the figure). The acoustic pressure was 1.4 bar for all liquids except adiponitrile, where it was ~ 1.9 bar. High-purity non-aqueous liquids ($> 99\%$ purity) were used as purchased. Water was purified by ion exchange (to $18\text{ M}\Omega\text{ cm}$) and filtration through $0.2\ \mu\text{m}$ pore filters.

seconds to replenish¹⁷. The observation of CN emission during SBSL also proves that chemical reactions are taking place during SBSL, as has been suggested from hydrodynamic modelling of single-bubble cavitation^{17,18}.

The M-SBSL spectra of dimethylsulphoxide and adiponitrile at high acoustic intensities are significantly different from those of other liquids (Fig. 4): their intensity is essentially flat above 380 nm and cannot be fitted to black-body emission at a single temperature. Because there is no nitrogen in dimethylsulphoxide, there is no CN emission observed. One might have hoped to see band emission from S_2 , SO, SO_2 or other species that should be produced from sonolysis of dimethylsulphoxide. None of these species, however, is as stable as CN at high temperatures. For reference, the dissociation energies for SO and CN are 5.4 and 7.8 eV, respectively²³.

The origin of the continuum in SBSL remains an open question. There are two likely contributors: (1) the sum of broadened emission from multiple molecular and atomic sources, and (2) bremsstrahlung emission from partial ionization of the heated gas within the bubble. The continuum in flames is generally assigned to the former mechanism²⁴. For example, broadened CO emission could be a significant ultraviolet component of SBSL spectra as it has a dissociation energy considerably higher than that of CN (11.1 eV; refs 24, 25). Emission from CO_2 , N_2O , NO and NO_2 (refs 24–26) may also be contributors to the continuum. Recent experiments on the timing of the SBSL flash from water²⁷ showed that the emission at long wavelengths can last slightly longer than that at short wavelengths; this difference could originate from the varying emissivities and lifetimes of multiple emitting species as a function of wavelength and internal temperature.

The other likely component of the continuum emission is bremsstrahlung radiation from electron–neutral and electron–ion interactions due to partial ionization of the heated gas within the bubble. Calculations show that lower-temperature bremsstrahlung (approximately 12,000 K) could give wavelength-independent intensities similar to those we observe in dimethylsulphoxide (Fig. 4; P.L. Hagelstein, personal communication). Under conditions of maximum collapse efficiency (that is, stationary single-bubble cavitation, minimum solvent vapour pressure, Xe gas within the bubble, and so on), the temperature within the cavity increases, and bremsstrahlung emission is expected to increase. From comparison of our experimental data to Hagelstein's calculations, the

wavelength dependence of S-SBSL from *N*-methylformamide is consistent with an effective bremsstrahlung emission temperature of approximately 30,000 K.

We believe that M-SBSL represents less extreme conditions ($< 15,000\text{ K}$) than those present during S-SBSL, due to the less-effective collapse of moving bubbles. M-SBSL therefore provides a long-sought spectroscopic link between the phenomena of single-bubble cavitation (which occurs at low acoustic pressures) and bubble-cloud cavitation (which occurs at high acoustic pressures). As the sphericity of bubble collapse increases (from MBSL to M-SBSL to S-SBSL), the efficacy of compression increases, the effective temperatures within the bubble increase, and the emission changes from spectra dominated by excited-state molecular emission to featureless (bremsstrahlung-like) spectra. □

Received 2 June; accepted 30 August 2000.

- Suslick, K. S. & Crum, L. A. in *Encyclopedia of Acoustics* (ed. Crocker, M. J.) 271–282 (Wiley-Interscience, New York, 1997).
- Gaitan, D. F., Crum, L. A., Church, C. C. & Roy, R. A. Sonoluminescence and bubble dynamics for a single, stable, cavitation bubble. *J. Acoust. Soc. Am.* **91**, 3166–3183 (1992).
- Gompf, B. *et al.* Resolving sonoluminescence pulse width with time-correlated single photon counting. *Phys. Rev. Lett.* **79**, 1405–1408 (1997).
- Hiller, R. A., Putterman, S. J. & Weninger, K. R. Time-resolved spectra of sonoluminescence. *Phys. Rev. Lett.* **80**, 1090–1093 (1998).
- Hiller, R., Putterman, S. J. & Barber, B. P. Spectrum of synchronous picosecond sonoluminescence. *Phys. Rev. Lett.* **69**, 1182–1184 (1992).
- McNamara, W. B. III, Didenko, Y. T. & Suslick, K. S. Sonoluminescence temperatures during multi-bubble cavitation. *Nature* **401**, 772–775 (1999).
- Suslick, K. S. & Flint, E. B. Sonoluminescence from non-aqueous liquids. *Nature* **330**, 553–555 (1987).
- Flint, E. B. & Suslick, K. S. Sonoluminescence from nonaqueous liquids: emission from small molecules. *J. Am. Chem. Soc.* **111**, 6987–6992 (1989).
- Flint, E. B. & Suslick, K. S. Sonoluminescence from alkali metal salt solutions. *J. Phys. Chem.* **95**, 1484–1488 (1991).
- Suslick, K. S., Flint, E. B., Grinstaff, M. W. & Kemper, K. Sonoluminescence from metal carbonyls. *J. Phys. Chem.* **97**, 3098–3099 (1993).
- Didenko, Y. T. & Pugach, S. P. Spectra of water sonoluminescence. *J. Phys. Chem.* **98**, 9742–9749 (1994).
- Gaitan, D. F. *et al.* Spectra of single-bubble sonoluminescence in water and glycerine-water mixtures. *Phys. Rev. E* **54**, 525–528 (1996).
- Weninger, K. *et al.* Sonoluminescence from single bubbles in nonaqueous liquids: new parameter space for sonochemistry. *J. Phys. Chem.* **99**, 14195–14197 (1995).
- Moss, W. C., Clarke, D. B. & Young, D. A. Calculated pulse widths and spectra of a single sonoluminescing bubble. *Science* **276**, 1398–1401 (1997).
- Hilgenfeldt, S., Grossmann, S. & Lohse, D. A simple explanation of light emission in sonoluminescence. *Nature* **398**, 402–405 (1999).
- Bernstein, L. S. & Zakin, M. R. Confined electron model for single-bubble sonoluminescence. *J. Phys. Chem.* **99**, 14619–14627 (1995).
- Lohse, D. *et al.* Sonoluminescing air bubbles rectify argon. *Phys. Rev. Lett.* **78**, 1359–1362 (1997).
- Lohse, D. & Hilgenfeldt, S. Inert gas accumulation in sonoluminescing bubbles. *J. Chem. Phys.* **107**, 6986–6997 (1997).
- Weninger, K. R. *et al.* Sonoluminescence from an isolated bubble on a solid surface. *Phys. Rev. E* **56**, 6745–6749 (1997).
- Matula, T. J. & Crum, L. A. Evidence for gas exchange in single-bubble sonoluminescence. *Phys. Rev. Lett.* **80**, 865–868 (1998).
- Ketterling, J. A. & Apfel, R. E. Experimental validation of the dissociation hypothesis for single bubble sonoluminescence. *Phys. Rev. Lett.* **81**, 4991–4994 (1998).
- Bernstein, L. S., Zakin, M. S., Flint, E. B. & Suslick, K. S. Cavitation thermometry using molecular and continuum sonoluminescence. *J. Phys. Chem.* **100**, 6612–6619 (1996).
- Lide, D. R. (ed.) *CRC Handbook of Chemistry and Physics* (CRC Press, Boca Raton, 1993–1994).
- Gaydon, A. G. *The Spectroscopy of Flames* 2nd edn (Chapman and Hall, London, 1974).
- Hertzberg, G. *Molecular Spectra and Molecular Structure: Electronic Spectra and Electronic Structure of Polyatomic Molecules* (Van Nostrand, New York, 1966).
- Zel'dovich, Y. B. & Raizer, Yu. P. *Physics of Shock Waves and High Temperature Hydrodynamic Phenomena* (Academic, New York, 1966).
- Moran, M. J. & Sweider, D. Measurements of sonoluminescence temporal pulse shape. *Phys. Rev. Lett.* **80**, 4987–4990 (1998).

Acknowledgements

We thank T. J. Matula for the loan of a calibrated needle hydrophone and many discussions, and S. Kulikov for assistance in constructing the imaging system. This work was supported by the US Defense Advanced Research Projects Agency and in part by the National Science Foundation.

Correspondence and requests for materials should be addressed to K.S.S. (e-mail: ksuslick@uiuc.edu).

reduction or an increase in coherence of illumination of the collectors took place. Therefore, time spectra with counting rates outside these limits were discarded.

To prove antibunching, a total of four spectra were accumulated for about 30 h each. The first spectrum was for incoherent illumination of the detectors; the next three spectra were, respectively, for partially coherent, totally coherent and then again for partially coherent illumination. The evaluation procedure of the experimental time spectra consisted of smoothing and normalizing the spectra, followed by visually superimposing the incoherent with the coherent and partially coherent spectra, respectively. The results are summarized in Fig. 3 and Table 1. The antibunching signal S , that is, the missing coincidences ΔN in the coherent and partially coherent spectra versus the incoherent spectrum, becomes visible as a flattening of the peak in Fig. 3 within the time resolution window of ± 13 ps. The measured relative reduction in coincidences amounts to $S_{\text{rel}} = 1.26 \times 10^{-3}$ with a signal-to-noise ratio of 3. This agrees with the theoretically expected value calculated from the characteristic features of our cold tungsten field emitter. As expected, the reduction in coincidence rate and the signal-to-noise ratio are smaller for partially coherent illumination.

Antibunching—in general, interference between two particles (second order coherence)—has now been observed for massive free particles. This experimental technique opens a gateway to new fundamental tests of quantum mechanics and statistics: for example, observation of quantum statistics on interference phenomena, and experimental tests of interaction of fields and potentials with charged two-fermion systems^{16–19}. □

Received 26 April; accepted 12 June 2002; doi:10.1038/nature00911.

- Hanbury Brown, R. & Twiss, R. Q. A new type of interferometer for use in radio astronomy. *Phil. Mag.* **45**, 663–682 (1954).
- Hanbury Brown, R. & Twiss, R. Q. Correlation between photons in two coherent beams of light. *Nature* **177**, 27–29 (1956).
- Hanbury Brown, R. & Twiss, R. Q. The question of correlation between photons in coherent light rays. *Nature* **178**, 1447–1448 (1956).
- Hanbury Brown, R. & Twiss, R. Q. Interferometry of the intensity fluctuation in light I. *Proc. R. Soc. Lond.* **242**, 300–324 (1957).
- Hanbury Brown, R. & Twiss, R. Q. Interferometry of the intensity fluctuation in light II. An experimental test of the theory for partially coherent light. *Proc. R. Soc. Lond.* **243**, 291–319 (1958).
- Purcell, E. M. The question of correlation between photons in coherent light rays. *Nature* **178**, 1449–1450 (1956).
- Brannen, E. & Ferguson, H. I. S. The question of correlation between photons in coherent light beams. *Nature* **178**, 481–482 (1956).
- Hanbury Brown, R. *The Intensity Interferometer* 7 (Taylor and Francis, New York, 1974).
- Hanbury Brown, R. & Twiss, R. Q. A test of a new type of stellar interferometer on Sirius. *Nature* **178**, 1046–1048 (1956).
- Silverman, M. P. On the feasibility of observing electron antibunching in a field-emission beam. *Phys. Lett. A* **120**, 442–446 (1987).
- Kodama, T. *et al.* Feasibility of observing two-electron interference. *Phys. Rev. A* **57**, 2781–2785 (1998).
- Henny, M. *et al.* The fermionic Hanbury Brown and Twiss experiment. *Science* **284**, 296–298 (1999).
- Oliver, W. D., Kim, J., Liu, R. C. & Yamamoto, Y. Hanbury Brown and Twiss-type experiment with electrons. *Science* **284**, 299–301 (1999).
- Twiss, R. Q. & Little, A. G. The detection of time-correlated photons by a coincidence counter. *Aust. J. Phys.* **12**, 77–93 (1959).
- Hasselbach, F. A ruggedized miniature UHV electron biprism interferometer for new fundamental experiments and applications. *Z. Phys. B* **71**, 443–449 (1988).
- Goldberger, M. L., Lewis, H. W. & Watson, K. M. Use of intensity correlations to determine the phase of a scattering amplitude. *Phys. Rev.* **132**, 2764–2787 (1963).
- Silverman, M. P. New quantum effects of confined magnetic flux on electrons. *Phys. Lett. A* **118**, 155–158 (1986).
- Silverman, M. P. in *OSA Proceedings on Photon Correlation Techniques and Applications* (eds Abbiss, J. B. & Smart, E. A.) Vol. 1 26–34 (OSA, Washington DC, 1988).
- Silverman, M. P. Distinctive quantum features of electron intensity correlation interferometry. *Il Nuovo Cimento* **97**, 200–219 (1987).

Acknowledgements

We thank M. Silverman, M. Lenc, T. Tyc, A. Oed and P. Sonnentag for discussions, and the Deutsche Forschungsgemeinschaft for financial support.

Competing interests statement

The authors declare that they have no competing financial interests.

Correspondence and requests for materials should be addressed to F.H. (e-mail: franz.hasselbach@uni-tuebingen.de).

The energy efficiency of formation of photons, radicals and ions during single-bubble cavitation

Yuri T. Didenko & Kenneth S. Suslick

Department of Chemistry, University of Illinois at Urbana-Champaign, Urbana, Illinois 61801, USA

It is extremely difficult to perform a quantitative analysis of the chemistry^{1,2} associated with multibubble cavitation: unknown parameters include the number of active bubbles, the acoustic pressure acting on each bubble and the bubble size distribution. Single-bubble sonoluminescence^{3–7} (characterized by the emission of picosecond flashes of light) results from nonlinear pulsations of an isolated vapour-gas bubble in an acoustic field. Although the latter offers a much simpler environment in which to study the chemical activity of cavitation, quantitative measurements have been hindered by the tiny amount of reacting gas within a single bubble (typically $<10^{-13}$ mol). Here we demonstrate the existence of chemical reactions within a single cavitating bubble, and quantify the sources of energy dissipation during bubble collapse. We measure the yields of nitrite ions, hydroxyl radicals and photons. The energy efficiency of hydroxyl radical formation is comparable to that in multibubble cavitation, but the energy efficiency of light emission is much higher. The observed rate of nitrite formation is in good agreement with the calculated diffusion rate of nitrogen into the bubble. We note that the temperatures attained in single-bubble cavitation in liquids with significant vapour pressures will be substantially limited by the endothermic chemical reactions of the polyatomic species inside the collapsing bubble.

Single-bubble sonoluminescence (SBSL)^{3,4} has attracted much attention owing to both the apparent simplicity of its creation and the complexity of processes occurring during bubble pulsation. A single bubble of gas can be trapped in partially degassed liquid by a standing acoustic wave and driven into highly nonlinear pulsations. At appropriate acoustic intensities, the bubble can emit short (~ 50 –

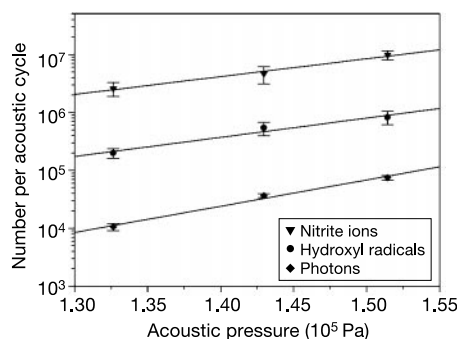


Figure 1 The yields of nitrite ions, hydroxyl radicals, and photons from a single cavitating bubble at 52 kHz in a 15-ml glass cell at 3 °C. The SBSL apparatus is described elsewhere²⁶. Solutions of 10^{-3} M disodium terephthalate in high-purity water were used to measure the yields of hydroxyl radicals. Liquid was degassed and equilibrated with an air pressure of 150 torr. The fluorescence of the product, 2-hydroxyterephthalate, was measured at 425 nm (excitation: 315 nm)²⁷. 2-hydroxyterephthalic acid was synthesized²⁸ and used as a standard after calibration for the OH[•] trapping efficiency²⁹. The yields of NO₂⁻ were measured from the fluorescence at 405 nm (excitation: 365 nm) of the product of reaction of NO₂⁻ with 2,3-diaminonaphthalene³⁰. The acoustic pressure at the position of the bubble was measured with a needle hydrophone (DAPCO), which was calibrated against a Bruel and Kjaer 8103 hydrophone³¹.

500 ps) flashes^{6,7} of light with clock-like regularity⁵. The featureless spectra of SBSL from 200 to 800 nm with the increasing intensity toward the ultraviolet^{6,8} suggested the existence of extraordinary temperatures inside the bubble, with black-body effective temperatures⁸ as high as $\sim 20,000$ K. Ionization of the bubble contents would also occur at these temperatures, so SBSL is now generally believed to be due, at least in part, to black-body radiation, bremsstrahlung and ion–electron recombination processes^{8–10}.

Before the discovery of SBSL, research on sonoluminescence and sonochemistry was limited to studies of clouds of cavitating bubbles formed in high-intensity ultrasound field^{1,2}. Using sensitive fluorescent analyses, we now report the yields of hydroxyl radicals (OH[•]) and nitrite ions (NO₂⁻) from a single cavitation bubble. This allowed us to determine energetic characteristics of sonochemical activity of acoustic cavitation. We also present quantitative comparisons between single-bubble sonochemical rates and sonoluminescence intensity.

A bubble pulsating in water containing dissolved air is thought to contain primarily argon, because the N₂, O₂ and H₂O that diffuse into the bubble during expansion should burn off to form soluble products during bubble compression: the “dissociation hypothesis”¹¹. The expected initial products of chemical reactions inside the bubble include OH[•] and nitrogen oxides (NO_x). OH[•] will react with organic compounds in the water or dimerize to H₂O₂, and NO_x will react with water giving nitrite and nitrate ions.

The formation of OH[•] in multibubble sonochemistry of water was predicted more than 50 years ago and measured quantitatively using EPR spin-trap methods¹². The formation of nitrite and nitrate ions in multibubble sonochemistry has also been measured, and the yield of NO₃⁻ is much lower than NO₂⁻ (ref. 13).

We have now measured the yields of OH[•] and NO₂⁻ from a single cavitating bubble in water at 28 and 52 kHz, and at 3 °C and 22 °C. Most experiments were conducted at 52 kHz, as the smaller cell volume gives a higher concentration of products. Spectra of SBSL were collected under identical conditions, and a direct correlation between the yields of photons and chemical products was observed. In order to quantify gas diffusion processes, we also measured the size of the cavitating bubble throughout its cycle by a direct stroboscopic method¹⁴. The yields of photons, OH[•], and NO₂⁻ increase with increasing acoustic intensity, and the yields of OH[•] and NO₂⁻ are substantially higher than the number of photons emitted (Fig. 1).

Our data allow a meaningful estimate of the yield of radicals and ions per joule of absorbed energy (that is, a *G* value) for acoustic cavitation. From Table 1, the *G* value for OH[•] formation during single bubble cavitation is $1 \times 10^{-10} \text{ mol J}^{-1}$ comparable to $3 \times 10^{-10} \text{ mol J}^{-1}$ for multibubble sonochemistry¹⁵, but much less than typical radiolysis *G* values of $3 \times 10^{-7} \text{ mol J}^{-1}$. Previous reports of *G* values for multibubble sonochemistry¹⁵ are difficult to interpret because the absorbed acoustic energy is distributed among all bubbles in the cloud to varying degrees, and not

exclusively to the few strongly cavitating bubbles that are chemically active at any one time.

The potential energy possessed by a single bubble¹⁶ at its maximum size, R_{max} , is the upper limit of the energy available for the formation of radicals and ions. During bubble compression, the potential energy of the bubble is converted into mechanical energy (both bubble/liquid wall motion and shock waves into the liquid), heat, chemical reactions and light emission. The data in Table 1 on the yields of photons, radicals and ions can be used to calculate the energy balance of a collapsing bubble. From the endothermicity of the sonochemical reactions, we estimate that $\sim 1 \times 10^{-4}$ of potential energy of the bubble goes to the formation of radicals and ions that escape the collapsing bubble, and that the energy of the photons is another factor of 100 less.

This represents, however, only the lower limit of chemical reactions within the bubble. Substantial recombination of radicals or ions must occur inside the collapsing bubble and will be converted to heat¹⁷. For a 30- μm -radius bubble containing 0.01 bar of water vapour, there are $\sim 2.6 \times 10^{10}$ water molecules present; to dissociate all of these to hydrogen and oxygen atoms would require $\sim 2.5 \times 10^{11}$ eV, that is, several times the total potential energy of the bubble. It is likely, therefore, that sonochemical reactions within the bubble are the primary limiter of the efficiency of the bubble collapse.

Spectra of SBSL were collected under identical conditions to those used for the chemical analyses. As shown in Figs 2 and 3, the spectral distribution of SBSL does not change with an increase in acoustic intensity or of frequency. However, the spectra of sonoluminescence are dependent on the water temperature. This effect has been previously reported for different gases dissolved in water^{4,18}. The ultraviolet component of SBSL is significantly less intense at 22 °C even though the overall SBSL intensity is the same or even higher at 22 °C compared to 3 °C (Figs 2 and 3). It is worth noting that our measured energy efficiency of photon production by SBSL is $\sim 10^4$ higher than that estimated grossly for multibubble sonoluminescence¹⁹. In SBSL, substantial emission of deep-ultraviolet photons that are absorbed by the liquid is likely to occur; this means that our estimate of the energy efficiency of photon production is only a lower limit.

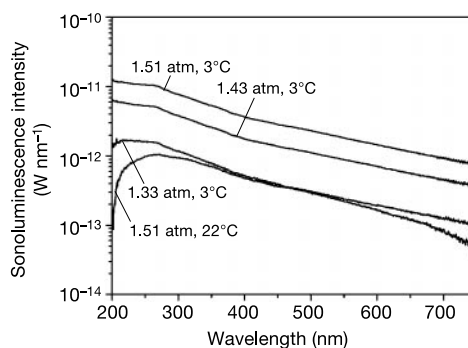


Figure 2 SBSL spectra of water collected at 52 kHz and 3 °C at acoustic intensities of 1.51, 1.43 and 1.33 atm, and at 22 °C and 1.51 atm. Quartz windows were attached to a 15-ml glass cell for better transmittance in the ultraviolet. Spectra were collected at the same acoustic intensities as chemical measurements, that is, at intensities where the bubble can be stable for a long time. Maximum SBSL intensities in the same cells can be ~ 2 to 3 times higher for brief periods of time. SBSL spectra were collected using a Jobin-Ivon Triax-320 monochromator with a spectrum one CCD detector (Instrument SA, 1,024 \times 256 array). Spectra were corrected for light absorbance by water, quartz and the response of the optical system against NIST traceable standard lamps (OLUV-40, Optronics Lab., Inc. and EH-132 Eppley Lab). A long-pass filter was used for the data collection at wavelengths above 400 nm in order to cut off the second-order light. For absolute measurements of SBSL intensity, an OLUV-40 lamp with a neutral density filter (Oriol Corp.) was used.

Table 1 Quantitative sonochemistry in a single cavitation bubble at 52 kHz

Conditions	22 °C	3 °C
R_{max} , μm^*	28.9	30.5
Number of OH [•] radicals per cycle	6.6×10^5	8.2×10^5
Number of photons per cycle	8.1×10^3	7.5×10^4
Number of NO ₂ ⁻ ions per cycle	3.7×10^6	9.9×10^6
Potential energy at R_{max} (eV)	6.4×10^{10}	7.5×10^{10}
Energy to form OH [•] radicals (eV per cycle)†	3.4×10^6	4.3×10^6
Energy to form NO ₂ ⁻ ions (eV per cycle)†	1.6×10^6	4.2×10^6
Energy of photons (200–750 nm) (eV per cycle)	2.7×10^4	2.6×10^5
Energy efficiency of sonoluminescence‡	4.3×10^{-7}	3.5×10^{-6}
Energy efficiency of sonochemistry§	7.8×10^{-5}	1.1×10^{-4}

*Experimentally observed (see text). Acoustic pressure: 1.5 atm.

†From the enthalpy of formation of H₂O \rightarrow OH[•] + H[•] and of 2H₂O + 2N₂ + O₂ \rightarrow 4HNO₂ in the gas phase at 273 K and 1 atm, respectively.

‡Energy of photons/potential energy of bubble.

§Endothermicity of reactions/potential energy of bubble.

Storey and Szeri conducted a detailed theoretical examination of the effect of water vapour on SBSL and sonochemistry¹⁷, and predicted that water vapour must significantly decrease the peak temperature inside the collapsing bubble by reducing compressional heating and through endothermic chemical reactions. They calculated that the temperature inside the bubble is $\sim 7,000$ K, insufficient to cause substantial ionization of molecules, and thus did not incorporate ionization in their model¹⁷. Thus, SBSL can be at least partially due to broadened emission from small molecules, similar to multibubble sonoluminescence². The calculated peak temperature inside the bubble does not change as the compression ratio (R_{\max}/R_{\min}) increases: more water is trapped inside the bubble at higher compression ratios, which counteracts the greater energy initially deposited in the larger bubble¹⁷. It has been found in a theoretical paper²⁰ that the excluded volume of the non-ideal gas results in significant suppression of the particle-producing endothermic chemical reactions within the bubble under sonoluminescence conditions. Thus, temperatures of up to 13,000 K can be achieved, which is sufficient for considerable bremsstrahlung emission.

Our data on the yield of nitrite ions during single-bubble cavitation allow us to estimate the diffusion rate of nitrogen inside the bubble and to compare it with theoretical predictions. N_2 , O_2 and Ar will diffuse into a pulsating bubble in water containing dissolved air during the expansion phase. When the bubble compresses, N_2 and O_2 react under the high-temperature conditions inside the bubble and the products of these reactions dissolve in the surrounding water. This selectively leaves Ar inside the bubble, and after many pulsations the bubble will contain primarily Ar (ref. 11). Small amounts of N_2 and O_2 diffuse into the bubble during each expansion. If each molecule of nitrogen gives two molecules of nitrite ions, we can estimate a theoretical yield of nitrite ions from expected diffusion rates. Using a standard diffusion model¹¹, we would expect $\sim 1.2 \times 10^6$ nitrite ions per cycle to be formed in the range 3 °C to 22 °C. This is somewhat low compared to experiment (by factors of 8 and 3 at 3 °C and 22 °C, respectively), probably owing to the neglect of convective flows around the cavitating bubble, which would increase calculated rates of diffusion into the bubble.

Observation of chemical activity from single-bubble cavitation has been claimed recently by LePoint and co-workers^{21,22}, but these authors assert that the chemical yields were uncorrelated with the observation of sonoluminescence. Chemical activity was reported from a single bubble in an aqueous solution of carbon tetrachloride containing a mixture of sodium iodide and starch²¹; however, we observe under similar conditions that such 'bubbles' are actually droplets of CCl_4 whose presence appears to enhance the already facile oxidation of aqueous iodide. The only other report of single-

bubble sonochemistry consists of the formation of solid particles (composition undetermined) during pulsation of a single bubble in an aqueous solution of carbon disulphide²².

The paper by Taleyarkhan *et al.*²³ announcing the observation of D–D nuclear fusion during neutron-induced acoustic cavitation has proved highly controversial²⁴. The authors claim the observation of neutrons and production of tritium after neutron-induced cavitation of perdeuterated acetone (C_3D_6O). Our results raise an important question. Acetone is considerably more volatile than water (30 kPa versus 3.2 kPa at 25 °C; 9.0 kPa versus 0.6 kPa at 0 °C), therefore cavitating bubbles in acetone will contain many more polyatomic molecules. The temperatures reached during cavitation will be substantially limited by the endothermic chemical reactions of the polyatomic molecules inside the collapsing bubble. We therefore expect that the extraordinary conditions necessary to initiate nuclear fusion will be exceedingly difficult to obtain in any liquid with a significant vapour pressure. However, the possibility of such events²⁵ in very low volatility liquids (for example, some polar organic liquids²⁶, molten salts or liquid metals) cannot be ruled out.

The present results show that endothermic sonochemical reactions within a collapsing bubble are a major limitation on the conditions produced during cavitation. □

Received 1 March; accepted 29 May 2002; doi:10.1038/nature00895.

- Suslick, K. S. (ed.) *Ultrasound: Its Chemical, Physical, and Biological Effects* (VCH, New York, 1988).
- Suslick, K. S. *Kirk-Othmer Encyclopedia of Chemical Technology*, 4th edn Vol. 26 517–541 (Wiley, New York, 1998).
- Brenner, M. P., Hilgenfeldt, S. & Lohse, D. Single-bubble sonoluminescence. *Rev. Mod. Phys.* **74**, 425–483 (2002).
- Putterman, S. J. & Weninger, K. R. Sonoluminescence: How bubbles turn sound into light. *Annu. Rev. Fluid Mech.* **32**, 445–476 (2000).
- Gaitan, D. F., Crum, L. A., Church, C. C. & Roy, R. A. Sonoluminescence and bubble dynamics for a single, stable, cavitation bubble. *J. Acoust. Soc. Am.* **91**, 3166–3183 (1992).
- Hiller, R. A., Putterman, S. J. & Weninger, K. R. Time-resolved spectra of sonoluminescence. *Phys. Rev. Lett.* **80**, 1090–1093 (1998).
- Gompf, B. *et al.* Resolving sonoluminescence pulse width with time-correlated single photon counting. *Phys. Rev. Lett.* **79**, 1405–1408 (1997).
- Vazquez, G., Camara, C., Putterman, S. & Weninger, K. Sonoluminescence: Nature's smallest blackbody. *Opt. Lett.* **26**, 575–577 (2001).
- Moss, W. C., Clarke, D. B. & Young, D. A. Calculated pulse widths and spectra of a single sonoluminescing bubble. *Science* **276**, 1398–1401 (1997).
- Hilgenfeldt, S., Grossmann, S. & Lohse, D. A simple explanation of light emission in sonoluminescence. *Nature* **398**, 402–405 (1999).
- Lohse, D. & Hilgenfeldt, S. Inert gas accumulation in sonoluminescing bubbles. *J. Chem. Phys.* **107**, 6986–6997 (1997).
- Makino, K., Mossoba, M. M. & Riesz, P. Chemical effects of ultrasound on aqueous solutions. Evidence for OH and H by spin trapping. *J. Am. Chem. Soc.* **104**, 3537–3539 (1982).
- Mead, E. L., Sutherland, R. G. & Verrall, R. E. The effect of ultrasound on water in the presence of dissolved gases. *J. Phys. Chem.* **54**, 1114–1120 (1976).
- Tian, Y., Ketterling, J. A. & Apfel, R. E. Direct observation of microbubble oscillations. *J. Acoust. Soc. Am.* **100**, 3976–3978 (1996).
- Mark, G. *et al.* OH radical formation by ultrasound in aqueous solutions. Part 2: Terephthalate and Fricke dosimetry and the influence of various conditions on the sonolytic yield. *Ultrason. Sonochem.* **5**, 41–52 (1998).
- Zel'dovich, Ya. B. & Raizer, Yu. P. *Physics of Shock Waves and High-Temperature Hydrodynamic Phenomena* (Academic, New York, 1966).
- Storey, B. D. & Szeri, A. J. Water vapour, sonoluminescence and sonochemistry. *Proc. R. Soc. Lond. A* **456**, 1685–1709 (2000).
- Barber, B. P. *et al.* Defining the unknowns of sonoluminescence. *Phys. Rep.* **281**, 65–143 (1997).
- Margulis, M. A. Modern views on the nature of acousto-chemical reactions. *Russ. J. Phys. Chem.* **50**, 1–18 (1976).
- Toegel, R., Hilgenfeldt, S. & Lohse, D. Suppressing dissociation in sonoluminescing bubbles: The effect of excluded volume. *Phys. Rev. Lett.* **88**, 34301–1–34301–4 (2002).
- Lepoint, T., Lepoint-Mullie, F. & Henglein, A. in *Sonochemistry and Sonoluminescence* (eds Crum, L. A., Mason, T. J., Reisse, J. L. & Suslick, K. S.) 285–290 (Kluwer Academic, Dordrecht, 1999).
- Verraes, T., Lepoint-Mullie, F., Lepoint, T. & Longuet-Higgins, M. S. Experimental study of the liquid flow near a single sonoluminescing bubble. *J. Acoust. Soc. Am.* **108**, 117–125 (2000).
- Taleyarkhan, R. P. *et al.* Evidence for nuclear emissions during acoustic cavitation. *Science* **295**, 1868–1873 (2002).
- Levi, B. G. Skepticism greets claim of bubble fusion. *Phys. Today* **55**(4), 16–18 (2002).
- Moss, W. C., Clarke, D. B., White, J. W. & Young, D. A. Sonoluminescence and the prospects for tabletop micro-thermonuclear fusion. *Phys. Lett. A* **211**, 69–74 (1996).
- Didenko, Y. T., McNamara, W. B. III & Suslick, K. S. Molecular emission from single-bubble sonoluminescence. *Nature* **407**, 877–879 (2000).
- McLean, J. R. & Mortimer, A. J. A cavitation and free radical dosimeter for ultrasound. *Ultrasound Med. Biol.* **14**, 59–64 (1988).

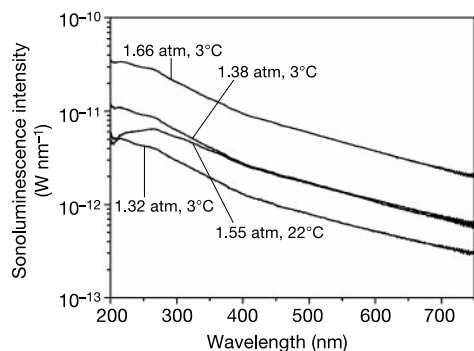


Figure 3 SBSL spectra of water collected at 28 kHz from a 100-ml quartz cell at 3 °C, 1.66 atm; 3 °C, 1.38 atm; 22 °C, 1.5 atm and 3 °C, 1.32 atm.

28. Field, L. & Engelhardt, P. R. Organic disulfides and related substances. XXX. Preparations and reactions of mercaptoterephthalic acids and derivatives. *J. Org. Chem.* **35**, 3647–3654 (1970).
29. Fang, X., Mark, G. & von Sonntag, C. OH radical formation by ultrasound in aqueous solutions. Part 1: the chemistry underlying the terephthalate dosimeter. *Ultrason. Sonochem.* **3**, 57–63 (1996).
30. Damiani, P. & Burini, G. Fluorometric determination of nitrite. *Talanta* **33**, 649–652 (1986).
31. Matula, T. J. *et al.* The acoustic emission from single-bubble sonoluminescence. *J. Acoust. Soc. Am.* **103**, 1377–1382 (1998).

Acknowledgements

We thank W.B. McNamara III for discussions. This work was supported by the US Defense Advanced Research Project Agency and in part by the National Science Foundation. We thank the UIUC Laboratory for Fluorescence Dynamics for use of their facilities.

Competing interests statement

The authors declare that they have no competing financial interests.

Correspondence and requests for materials should be addressed to K.S.S. (e-mail: ksuslick@uiuc.edu).

Equilibrium lithium transport between nanocrystalline phases in intercalated TiO₂ anatase

M. Wagemaker*, A. P. M. Kentgens† & F. M. Mulder*

* *Interfaculty Reactor Institute, Delft University of Technology, Mekelweg 15, 2629 JB Delft, The Netherlands*

† *NSR Center for Molecular Design, Synthesis and Structure, Department of Physical Chemistry/Solid-state NMR, University of Nijmegen, Toernooiveld 1, 6525 ED Nijmegen, The Netherlands*

Microcrystalline TiO₂ with an anatase crystal structure is used as an anode material for lithium rechargeable batteries^{1,2}, and also as a material for electrochromic^{3–6} and solar-cell devices^{7,8}. When intercalated with lithium, as required for battery applications, TiO₂ anatase undergoes spontaneous phase separation into lithium-poor (Li_{0.01}TiO₂) and lithium-rich (Li_{0.6}TiO₂) domains on a scale of several tens of nanometres⁹. During discharge, batteries need to maintain a constant electrical potential between their electrodes over a range of lithium concentrations. The two-phase equilibrium system in the electrodes provides such a plateau in potential, as only the relative phase fractions vary on charging (or discharging) of the lithium. Just as the equilibrium between a liquid and a vapour is maintained by a continuous exchange of particles between the two phases, a similar exchange is required to maintain equilibrium in the solid state. But the time and length scales over which this exchange takes place are unclear. Here we report the direct observation by solid-state nuclear magnetic resonance of the continuous lithium-ion exchange between the intermixed crystallographic phases of lithium-intercalated TiO₂. We find that, at room temperature, the continuous flux of lithium ions across the phase boundaries is as high as $1.2 \times 10^{20} \text{ s}^{-1} \text{ m}^{-2}$.

We used ⁷Li magic-angle-spinning (MAS) solid-state NMR, because this microscopic probe gives information on structure and dynamics^{10,11}. The anatase starting material had a particle size of ~10 μm (nitrogen BET specific surface area <0.5 m² g⁻¹). In Fig. 1, the central part of the ⁷Li MAS NMR spectrum of a lithium-intercalated sample, Li_{0.12}TiO₂, is shown. In this sample, two phases coexist: the lithium-poor phase Li_{0.01}TiO₂ with the anatase struc-

ture (space group *I41/amd*), and the lithium-rich phase indicated by lithium titanate (Li_{0.6}TiO₂; space group *Imma*). The Li in anatase gives a sharp line in addition to the broad Li in titanate signal.

The exchange of Li between the two phases is established by performing two-dimensional exchange measurements¹². This technique effectively measures the spectrum of the ⁷Li atoms at $t = 0$ s, then waits a ‘mixing time’ t_{mix} , and subsequently measures the spectrum of the same ⁷Li atoms again at $t = t_{\text{mix}}$. The results of such measurements are shown in Fig. 2. The signal occurring on the diagonal in the plots represents ⁷Li atoms that have the same spectrum before and after t_{mix} —that is, ⁷Li that remained in the same crystallographic phase. The spectral intensity produced by ⁷Li that is located in anatase at $t = 0$ and in titanate at $t = t_{\text{mix}}$ (or *vice versa*) is at the corresponding off-diagonal positions. The ridges in Fig. 2b are off-diagonal signals of this type; they are strong because of the large amount of Li that has exchanged between the two phases within the diffusion time of $t_{\text{mix}} = 50$ ms.

In Fig. 2a $t_{\text{mix}} = 50 \mu\text{s}$, which means virtually no diffusion time, and thus no exchange. Because about 40% of the intensity in the sharp peak in Fig. 2a is transferred to intensity in the ridges in Fig. 2b, about 40% of the initial amount of ⁷Li in anatase has exchanged with ⁷Li in the titanate phase after $t_{\text{mix}} = 50$ ms, as can be seen when comparing Fig. 2a and b. In Fig. 2c, a measurement is shown at 148 K using a t_{mix} of 50 ms. At this temperature the Li motion between anatase and titanate is frozen. But there still appears to be diffusion within the titanate phase; this will be due to the low activation energy for hopping between sites within this phase⁹. The measurement is shown here to prove that the cross-signal intensities in Fig. 2b cannot arise from spin diffusion due to the presence of dipolar couplings (these are suppressed by MAS).

Faster one-dimensional experiments were performed to quantify the exchange in terms of the magnetization of Li in anatase as a function of t_{mix} and temperature T . The technique is described in Fig. 3 legend. The experimental results in Fig. 3 are given as a function of t_{mix} , and for several temperatures. The data are analysed using the solution of Fick’s law of diffusion, $\partial m(\mathbf{r}, t) / \partial t = \nabla \cdot \{D(\mathbf{r})m(\mathbf{r}, t)\}$, where $m(\mathbf{r}, t)$ is the magnetization of Li at position \mathbf{r} and t , and D is the Li diffusivity. Best results were obtained with

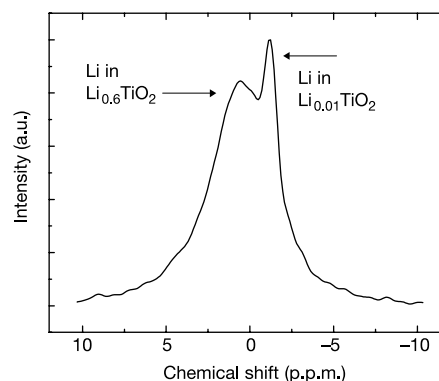


Figure 1 Central part of the ⁷Li magic-angle-spinning NMR spectrum of Li_{0.12}TiO₂ at 100 °C, showing the resonances of Li in the two coexisting phases. A spinning speed of $20,000 \pm 3$ Hz and a radio-frequency field strength corresponding to a ⁷Li spin nutation frequency of 192 kHz was used on a Chemagnetics 600 spectrometer. Two phases are coexisting in thermal equilibrium: a Li-poor anatase phase with a composition of Li_{0.01}TiO₂ (narrow peak) and a Li-rich titanate phase with composition Li_{0.6}TiO₂ (this peak is homogeneously broadened, with the transverse relaxation time T_2 giving its linewidth, indicating that the ⁷Li in this phase are all experiencing similar environments).

Pressure during Sonoluminescence[†]

William B. McNamara III, Yuri T. Didenko, and Kenneth S. Suslick*

School of Chemical Sciences, University of Illinois at Urbana–Champaign, 601 South Goodwin Avenue, Urbana, Illinois 61801

Received: January 29, 2003; In Final Form: May 27, 2003

Multibubble sonoluminescence (MBSL) spectra were collected from solutions containing volatile metal-containing compounds in silicone oil saturated with helium or argon. Ultrasonic irradiation of these solutions at 20 kHz and 90 W/cm² led to emission from excited states of the free metal atoms. The widths and peak positions of these lines varied as a function of the gas used to saturate the solution, indicating that the emission was from the gas phase of the bubble. High-resolution MBSL spectra showed that the pressure within the bubble at the point of emission was on the order of 300 bar in argon-saturated silicone oil, which is consistent with simple adiabatic compression during cavitation.

Introduction

The phenomenon of light emission arising from the ultrasonic irradiation of liquids (sonoluminescence) has been known for more than 60 years,¹ and the mechanism by which acoustic energy is converted to light by bubbles imploding in a multibubble cavitation field (multibubble sonoluminescence, MBSL) has been the subject of much research.² MBSL spectra are analogous to the spectra of hot flames and contain features that are characteristic of the volatiles found inside the collapsing bubble (e.g., solvent vapor, volatile solutes, and dissolved gases).^{3–5} These features have been used as cavitation thermometers, revealing that the temperature of cavitation under an argon atmosphere is ~5000 K and that this temperature systematically changes in a manner consistent with compressional heating during bubble collapse.^{6,7} Other facets of MBSL are less well understood. Although there have been several experimental determinations of temperature, the pressure that is attained inside the bubble has not been extensively or convincingly probed.^{8,9} On an even more fundamental level, there is still some debate as to whether the emission arises from the gas phase of the bubble or from the liquid shell surrounding the bubble.^{9–12} We report here the high-resolution MBSL spectra arising from the ultrasonic irradiation of metal carbonyls and other volatile metal-containing compounds dissolved in silicone oil saturated with helium or argon. These spectra feature emission from the free metal atoms.⁴ Both the linewidths and peak positions of the atomic emission lines vary as a function of the noble gas, indicating that the emission is from the gas phase and, for the argon-saturated systems, the metal atom is emitted from a noble gas atmosphere of at least 300 bar.

Experimental Section

The experimental setup has been described in detail elsewhere.⁶ Solutions (2.5 mM) of the metal carbonyls in silicone oil (poly(dimethylsiloxane), Dow Fluid 200, viscosity of 100 cSt) were held at 65 °C in the sonoluminescence cell while they were sparged with the appropriate noble gas for 90 min prior

to ultrasonic irradiation. Silicone oil was chosen for its extremely low vapor pressure and the very intense MBSL that this low volatility produces.^{3,13} This sparge continued throughout the course of ultrasonic irradiation. It was experimentally determined that the widths and positions of the metal-atom lines reach a constant value after 60 min of sparging, indicating that the noble gas has completely displaced the air within the silicone oil. The sparge was continued for an additional 30 min to ensure that this was the case. The silicone oil solutions were irradiated at 20 kHz using a 0.5-in. titanium immersion horn (Heat Systems model W-375). The total acoustic power, as measured calorimetrically, was 90 W. The bubble cloud filled the entire 1.2 cm gap between the acoustic horn and the optical window.

The sonoluminescence spectra were collected in 10-s increments. The sonicator was turned on, a spectrum was collected, and the sonicator was turned off. The solution was sparged for an additional 10 min and another spectrum was then collected in an identical manner. There is no change over this 10-s interval in the peak position or full width at half-maximum (fwhm), nor was there a difference between successive spectrum acquisitions, other than a slow decrease in intensity that was due to a gradual darkening of the solutions, which was monitored by UV–vis spectrophotometry.

The light was dispersed by a spectrograph (Acton Research model AM-505F, focal length of 0.5 m) that was equipped with a 1200 grooves/mm grating and various slit widths, and the light was detected with a diode array (Princeton Instruments model IRY 512N). The resolution of the spectrograph, as configured with a 10- μ m-wide entrance slit and a 1200/mm grating, is 0.028 nm in the first order at 435.8 nm (see operating instructions for the Acton Research spectrograph). High-resolution Cr line-shift measurements for pressure determination were collected in the second order of the 1200 groove/mm grating, using a 10- μ m-wide entrance slit.

Results and Discussion

These studies rely on the change in MBSL metal-atom emission line profiles as a function of gas density within the bubble (i.e., the fwhm and the peak position). The broadening and shifting of spectral lines have been extensively discussed in the literature and result from the perturbation of the atomic

[†] Part of the special issue “Arnim Henglein Festschrift”.

* Author to whom correspondence should be addressed. E-mail: ksuslick@uiuc.edu.

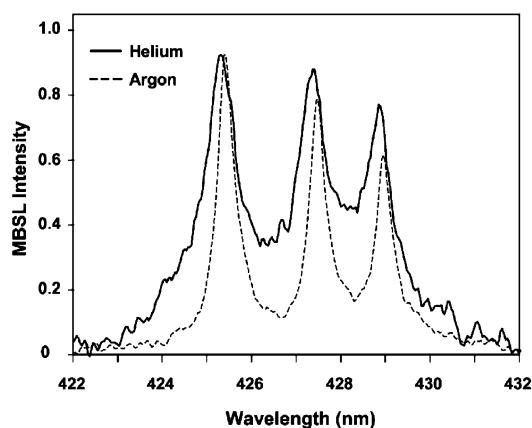


Figure 1. MBSL spectra of 2.5 mM $\text{Cr}(\text{CO})_6$ in silicone oil saturated with helium and argon. Background continuum has been subtracted from MBSL spectra for clarity. Both spectra were collected with a slit width of 20 μm .

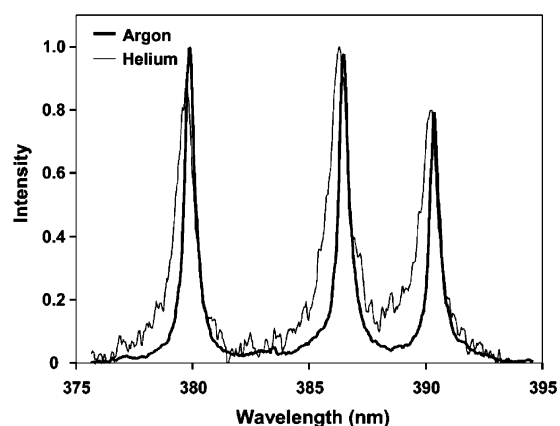


Figure 2. MBSL spectra of 2.5 mM $\text{Mo}(\text{CO})_6$ in silicone oil saturated with helium and argon. Background continuum has been subtracted from MBSL spectra for clarity. Both spectra were collected with a slit width of 20 μm .

electronic energy levels by the surrounding gas.¹⁴ Lines are typically red-shifted and broadened by polarizable atoms such as Ar, as well as being blue-shifted and more substantially broadened by hard, less-polarizable atoms such as He. For quantitative evaluations, we will make particular comparisons later to data collected from ballistic compressors, in which atomic emission occurs under high-temperature and pressure conditions that approximate those within a cavitation bubble.

The MBSL spectra of $\text{Cr}(\text{CO})_6$ in silicone oil saturated with helium and argon are shown in Figure 1. Both spectra were collected using a slit width of 20 μm . Each line under a helium atmosphere is broader (fwhm = 1.0 nm) and located at a higher energy than its counterpart under an argon atmosphere (fwhm = 0.5 nm). For comparison, the Cr hollow cathode lamp spectrum was characterized by a fwhm value of 0.1 nm. As discussed later, the lineshifts of Cr emission are consistent with literature reports on ballistic compressor studies.¹⁵ There are, however, no data in the literature describing the linewidth of Cr emission under conditions approximating those within a cavitation bubble. The emission under a helium atmosphere is clearly different than that observed under an argon atmosphere, which is also consistent with the behavior observed for other metals in ballistic compressors. The MBSL spectra of $\text{Mo}(\text{CO})_6$ in silicone oil saturated with helium and argon are shown in Figure 2. Again, each line under a helium atmosphere is both

broadened and blue-shifted, relative to its line profile under an argon atmosphere.

Similar results were observed in the MBSL spectra arising from the ultrasonic irradiation of $\text{Mn}(\text{C}_5\text{H}_4\text{CH}_3)(\text{CO})_3$ and $\text{Fe}(\text{CO})_5$ under argon and helium atmospheres: all metal-atom MBSL lines were substantially broader than those emitted by the corresponding hollow cathode lamp. Furthermore, the lines under a helium atmosphere were blue-shifted and further broadened, relative to their behavior under an argon atmosphere. This has been documented for both metals in ballistic compressor studies.^{16,17} MBSL spectra were also obtained from the sonication of TiCl_4 and $\text{W}(\text{CO})_6$ in argon-saturated silicon oil (the emission was too weak to obtain high-resolution spectra under a helium atmosphere). These spectra contained atomic emission lines from Ti and W, respectively, and, in both cases, the lines were broadened, relative to the corresponding lines from a hollow cathode lamp. All data are consistent with emission from a high-pressure noble gas environment: MBSL originates from the gas phase of the bubble.

These data refute the recent interpretation of MBSL as a "manifestation of the cooperative dynamical phase transition effect."¹⁰ Kuhn et al. attributed the asymmetry of the Na lines in the MBSL spectra arising from the ultrasonic irradiation of argon-saturated aqueous NaCl solutions to the Rayleigh wing effect in nonequilibrium light emission, and they viewed the surrounding liquid as a gain medium.¹⁰ The asymmetry they observed was, in fact, well documented in emission from high-pressure gas environments almost fifty years ago¹⁴ and reflects the density of that environment rather than any special cooperativity or nonequilibrium emission.

The bubble contains not only noble gas, but also solvent vapor, the metal-atom precursor, and the sonolysis products of both of these components.^{3,7,11,13,18} The MBSL spectrum from neat silicone oil, for example, contains molecular features attributable to C_2 , CH, and atomic emission from silicon.^{3,13} It also contains an underlying continuum that we believe is due to emission from multiple small hydrocarbons, as in flames. The production of these species from silicone oil will lead to an increase in pressure within the bubble, as will the generation of CO from the destruction of the metal carbonyls. Each of these species could hypothetically perturb the profiles of the metal-atom lines.

Further experiments were conducted over a range of metal carbonyl concentrations to determine if resonance broadening by other metal atoms were operative or if collisional broadening from species other than helium or argon were important. The resulting line profiles were invariant of the metal carbonyl (and, hence, the metal atom) concentration, indicating that this was not the case. It is furthermore unlikely that the emission is greatly perturbed by the products of silicone oil sonolysis, or by CO that dissociates from the metal carbonyls during the bubble collapse. The sonolysis products should be the same under helium and argon atmospheres, although there may be some differences in their concentrations. If the sonolysis products or the volatile precursors were the dominant collisional partners for the excited-state metal atoms, the resulting linewidths and lineshifts would be similar under helium and argon atmospheres, which is clearly not the case. We are of the opinion, therefore, that the major factor influencing the line profile of the metal-atom emission is the high-density noble gas atmosphere within the bubble.

The MBSL spectra reported here are compared to spectra from hollow cathode lamps that have been collected under identical spectrograph parameters, and the lineforms of these

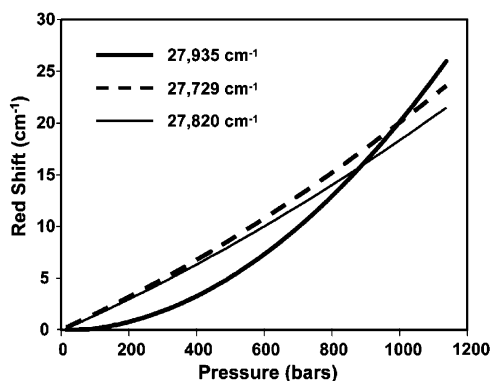


Figure 3. Frequency shift of Cr atom emission lines from ballistic compression data at 3300 K.¹⁵

metal-atom emission spectra are taken to represent the natural linewidth and peak positions of the respective atomic lines. This is not rigorously true, because the spectra recorded by the diode array detector will also be dependent on the slit function of the spectrograph. The slit function, however, can be treated as a minor perturbation, relative to the linewidths observed in MBSL. Scattering from the bubble cloud more seriously broadens the emitted MBSL lines. To measure the effect of light scattering by the cavitation field, a different cell design was used. A glass tube with a distance of 2 cm between the end of the tube and the horn was placed at an orientation of 90° in front of the slit of the spectrograph, such that the slit was aligned 1 cm from the horn surface. The extent of broadening due to scattering was then estimated by placing a hollow cathode lamp opposite the spectrograph slit, so that its light passed through a cavitation cloud in neat silicone before entering the spectrograph.

Apparent broadening from the slit function and light scattering was not negligible, although it accounted for less than half of the observed MBSL linewidths. Such apparent broadening is sufficient, however, to make detailed analysis of the MBSL linewidths problematic. This is particularly true, given the fact that MBSL occurs from within a volume rather than from a surface, and each photon will experience a different degree of scattering. As will be discussed below, the MBSL linewidths do indeed reflect the high-pressure environment within the cavitation bubble; they cannot, however, be used to determine the pressure within the bubble with much accuracy.

It has been well documented that the positions of lines emitted by metal atoms in a noble gas atmosphere are sensitive to the density of the gas. This behavior is well understood for the alkali metals, and theory has advanced to the point of being reasonably predictive for these systems at low pressures.¹⁷ Such is not the case for the transition metals, however, and the shift and width of a given line cannot yet be used to determine a priori the density of the surrounding noble gas. Rather, the pressure during emission is best determined by comparing MBSL spectra with spectra of the same metals collected under similar conditions: i.e., ballistic compressors. This mandates that (i) reliable high-pressure data for a given metal must exist in the literature, and (ii) this metal must emit gas-phase MBSL that is both intense and easily resolvable.

Chromium is the only metal that meets these criteria, and, as such, it was studied in further detail. The red shift of the lines constituting the Cr triplet at 27 800 cm⁻¹ lines, as a function of the relative density of argon, is shown in Figure 3 (similar data for the triplet at 23 300 cm⁻¹ are also available).¹⁵ These data represent ballistic pressure measurements conducted at 3300 K and serve as the reference data against which our MBSL spectra will be compared.

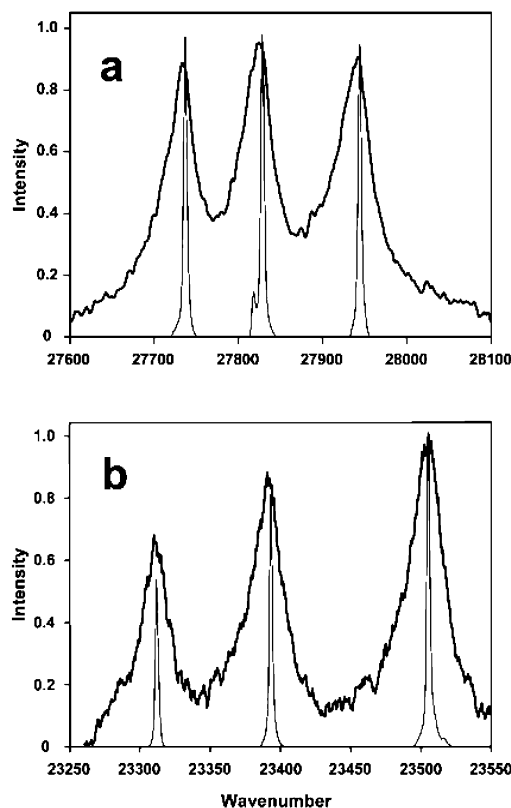


Figure 4. MBSL spectra of 2.5 mM Cr(CO)₆ in silicone oil saturated with argon. Spectra from hollow cathode lamp (thin lines) are shown for comparison. Background continuum has been subtracted from MBSL spectra for clarity. Resolution is ~1 cm⁻¹.

TABLE 1: Observed Peak Positions of Cr Atom Emission and Corresponding Pressure Estimates for Multibubble Cavitation in Silicone Oil Saturated with Argon

peak (cm ⁻¹)	lineshift (cm ⁻¹)	relative density	pressure (bar)
23 305	-1.6	18.5	290
23 386	-2.4	20.5	320
27 729	-3.7	15.0	240
27 820	-5.0	20.5	320
27 935	-1.9	19.5	310

The spectra of chromium MBSL collected in the second order of the 1200 groove/mm grating, along with those from a hollow cathode lamp collected using the same experimental configuration, are shown in Figure 4. The MBSL resulted from the ultrasonic irradiation of a 2.5 mM solution of Cr(CO)₆ in silicone oil saturated with argon (MBSL under a helium atmosphere was too weak to be observed in the second order of the grating; thus, no quantitative pressure estimates can be made under a helium atmosphere).

The lineshifts observed in Figure 4 were compared to the published ballistic compression data,¹⁵ which are reported in terms of argon density, relative to that at 298 K and 1 atm. The MBSL pressure was determined by scaling from ambient temperature using the ideal gas law to the known temperature of chromium MBSL in silicone oil saturated with argon (4700 K).⁷ Use of the ideal gas law could have been problematic if the cavitation pressures had proved to be extreme. As shown in Table 1, the experimentally observed MBSL lineshifts and the corresponding relative densities and pressures are not so high as to require a more sophisticated equation of state.

As shown in Figure 4, the frequency shifts are well defined for five of the six Cr emission lines. These yield a relative density of 19 (standard deviation of ±2) and a pressure of 300

± 30 bar. (The Cr line at $23\,499\text{ cm}^{-1}$ was less well defined; after fitting to a Lorentzian curve, the resulting peak position corresponded to a relative density of 20, which is consistent with the other data.) It should be noted, however, that the reference ballistic compressor data were collected at 3300 K, and the authors reported that the lineshift decreased as the temperature increased. The values reported here, therefore, should be taken as the minimum pressure of argon within the bubble, and the actual pressure is likely somewhat higher.

The experimentally measured pressure is comparable to that predicted from adiabatic compression. If the collapse of the bubble is purely adiabatic, a gas with a polytropic ratio γ ($\gamma = C_p/C_v$) that is compressed from an initial radius R_i to a final radius R_f will be heated from an initial temperature T_i and pressure P_i to a final temperature T_f and pressure P_f , according to eqs 1 and 2:

$$T_f = T_i \left(\frac{R_i}{R_f} \right)^{3(\gamma-1)} \quad (1)$$

$$P_f = P_i \left(\frac{R_i}{R_f} \right)^{3\gamma} \quad (2)$$

The Cr atom emission temperature during MBSL is 4700 K under an argon atmosphere,⁷ which has a constant polytropic ratio of $\gamma = 1.67$. If T_i and P_i are assumed to have values of 298 K and 1 atm, respectively, the corresponding compression ratio, R_f/R_i , is 3.95. This, in turn, implies a final pressure, according to eq 2, of ~ 1000 atm. As a bubble collapses, it is generally agreed that the transition from slow, isothermal compression to fast, adiabatic compression occurs relatively late in the cycle, at pressures below ambient (i.e., $P_i < 1$ atm), which would decrease the calculated final pressure. Equations 1 and 2 are obviously oversimplifications of the very complex events that occur during cavitation. Nonetheless, the experimental results are in reasonable agreement, even with the very simple model of adiabatic compression during bubble collapse.

Acknowledgment. This work was supported by the National Science Foundation and by ONR/DARPA.

References and Notes

- (1) (a) Frenzel, H.; Schultes, H. *Z. Phys. Chem.* **1934**, *27B*, 421. (b) Flynn, H. G. In *Physical Acoustics*; Mason, W. P., Ed.; Academic Press: New York, 1964; Vol. 1B, p 57.
- (2) (a) Suslick, K. S.; Crum, L. A. Sonochemistry and Sonoluminescence. In *Handbook of Acoustics*; Crocker, M. J., Ed.; Wiley-Interscience: New York, 1998; pp 243–253. (b) Suslick, K. S.; Didenko, Y.; Fang, M. M.; Hyeon, T.; Kolbeck, K. J.; McNamara, W. B., III; Mdeleleni, M. M.; Wong, M. *Philos. Trans. R. Soc. London A* **1999**, *357*, 335.
- (3) (a) Suslick, K. S.; Flint, E. B. *Nature* **1987**, *330*, 553–555. (b) Flint, E. B.; Suslick, K. S. *J. Am. Chem. Soc.* **1989**, *111*, 6987–6992.
- (4) Suslick, K. S.; Flint, E. B.; Grinstaff, M. W.; Kemper, K. A. *J. Phys. Chem.* **1993**, *97*, 3098.
- (5) Didenko, Y. T.; Pugach, S. P. *J. Phys. Chem.* **1994**, *98*, 9742.
- (6) Didenko, Y. T.; McNamara, W. B., III; Suslick, K. S. *Phys. Rev. Lett.* **2000**, *84*, 777.
- (7) McNamara, W. B., III; Didenko, Y. T.; Suslick, K. S. *Nature* **1999**, *401*, 772.
- (8) Suslick, K. S.; Kemper, K. A. In *Bubble Dynamics and Interface Phenomena*; Blake, J. R., Thomas, N., Eds.; Kluwer Publishers: Dordrecht, The Netherlands, 1994; pp 311–320.
- (9) (a) Sehgal, C.; Steer, R. P.; Sutherland, R. G.; Verrall, R. E. *J. Chem. Phys.* **1979**, *70*, 2242. (b) Flint, E. B.; Suslick, K. S. *J. Phys. Chem.* **1991**, *95*, 1484.
- (10) Kuhns, D. W.; Brodsky, A. M.; Burgess, L. W. *Phys. Rev. E* **1998**, *57*, 1702.
- (11) Henglein, A. *Adv. Sonochem.* **1993**, *3*, 17.
- (12) Prosperetti, A. *J. Acoust. Soc. Am.* **1997**, *101*, 2003.
- (13) Flint, E. B.; Suslick, K. S. *Science* **1991**, *253*, 1325.
- (14) (a) Ch'en, S. Y.; Takeo, M. *Rev. Mod. Phys.* **1957**, *29*, 20. (b) Allard, N.; Kielkopf, J. *Rev. Mod. Phys.* **1982**, *54*, 1103.
- (15) Holmes, Q. A.; Ch'en, S. Y.; Takeo, M. *J. Quant. Spectrosc. Radiat. Transfer* **1969**, *9*, 761.
- (16) (a) Holmes, Q. A.; Ch'en, S. Y.; Takeo, M. *J. Quant. Spectrosc. Radiat. Transfer* **1969**, *9*, 749. (b) Chen, S. Y.; Bennett, R. B. *Phys. Rev.* **1960**, *119*, 1029.
- (17) (a) Peach, G. *J. Phys. B: At. Mol. Phys.* **1984**, *17*, 2599. (b) Al-Saqabi, B. N. I.; Peach, G. *J. Phys. B: At. Mol. Phys.* **1987**, *20*, 1175.
- (18) (a) Didenko, Y. T.; McNamara, W. B., III; Suslick, K. S. *J. Phys. Chem. A* **1999**, *103*, 10783. (b) Suslick, K. S.; Gawienowski, J. W.; Schubert, P. F.; Wang, H. H. *J. Phys. Chem.* **1983**, *87*, 2299.

Engineered microsphere contrast agents for optical coherence tomography

Tin Man Lee, Amy L. Oldenburg, Shoeb Sitafalwalla, Daniel L. Marks, and Wei Luo

Beckman Institute for Advanced Science and Technology, University of Illinois at Urbana—Champaign, Urbana, Illinois 61801

Farah Jean-Jacques Toublan and Kenneth S. Suslick

Department of Chemistry, University of Illinois at Urbana—Champaign, Urbana, Illinois 61801

Stephen A. Boppart

Department of Electrical and Computer Engineering, Bioengineering Program, Beckman Institute for Advanced Science and Technology, College of Medicine, 405 North Mathews Avenue, University of Illinois at Urbana—Champaign, Urbana, Illinois 61801

Received February 10, 2003

Contrast agents are utilized in virtually every imaging modality to enhance diagnostic capabilities. We introduce a novel class of optical contrast agent, namely, encapsulating microspheres, that are based not on fluorescence but on scattering nanoparticles within the shell or core. The agents are suitable for reflection- or scattering-based techniques such as optical coherence tomography, light microscopy, and reflectance confocal microscopy. We characterize the optical properties of gold-, melanin-, and carbon-shelled contrast agents and demonstrate enhancement of optical coherence tomography imaging after intravenous injection of such an agent into a mouse. © 2003 Optical Society of America

OCIS codes: 170.4500, 160.4760, 170.4580.

When one is imaging biological tissues, it is often desirable to enhance the signals measured from specific structures. Contrast agents that produce specific image signatures have been utilized in virtually every imaging modality, including ultrasound,¹ computed tomography,² magnetic resonance imaging,³ and optical microscopy.⁴ Optical coherence tomography (OCT) is an emerging imaging technology that has found application in a wide range of biological and medical applications.⁵ In this Letter we characterize and demonstrate a new class of optical contrast agent suitable for reflection- or scattering-based optical imaging techniques, namely, OCT but that also includes light and reflectance confocal microscopy. These agents are biocompatible,⁶ are suitable for *in vivo* use, and produce enhanced backscatter that is detectable in highly scattering tissue. These agents may be tailored to adhere to specific molecules, cells, or tissue types, and thus provide additional selectivity that can enhance the utility of OCT as an emerging diagnostic technique.

OCT is capable of cellular-resolution imaging and may ultimately have a role in the early diagnosis of human malignancies.⁷ Although morphological differences between normal and neoplastic tissues can be obvious at later stages of tumor development, it is challenging to detect early-stage tumors or tumors that are morphologically (or optically) similar to surrounding normal tissue. Contrast agents have been known to increase the diagnostic and analytical capabilities of the modality by site-specifically labeling of tissues or cells of interest. This should also be true for OCT, which overcomes the limitation of relying on inherent optical properties of the

tissue to provide contrast to differentiate normal from pathological tissue. Inasmuch as OCT detects scattering changes, image contrast enhancement can be achieved by delivery of highly scattering contrast agents into the tissue and allowing the agents to attach to specific regions of interest. In ultrasound and OCT, air-filled microbubbles have been used as contrast agents,^{1,8} but they have not been designed to incorporate nanoparticles or materials that can enhance the optical signal. We have engineered optical contrast agents that are microspheres 0.2 to 15 μm in diameter with an approximately 50-nm-thick protein shell. The microspheres are designed to incorporate in their shells and encapsulate in their cores a wide range of nanoparticles and materials that alter the local optical properties of tissue. The protein shell may also be functionalized to target the agents to specific regions of interest.

Fabrication protocols have been developed to facilitate variation of microsphere size, shell or encapsulated materials, and surface protein features. We fabricated microspheres by sonicating with high-intensity ultrasound the interface between a 5% weight per volume solution of bovine serum albumin and a solution containing the material to be incorporated into the shell or encapsulated in the core. The high-intensity ultrasound necessary for the reaction was generated by a titanium horn with tip diameter of 1.25 cm, driven at 20 kHz. The solutions were sonicated for 3 min at an acoustic power of 76 W/cm². The diameter of the microspheres (0.2–15 μm) depended on the acoustic power and on the frequency of the ultrasound. Solutions of microspheres were washed with nanopure water and filtered to remove

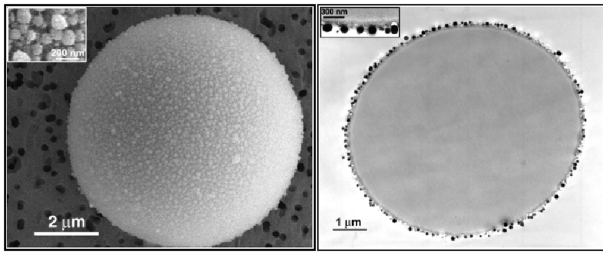


Fig. 1. Scanning- (left) and transmission- (right) electron micrographs of an oil-filled microsphere contrast agent, showing scattering silica nanoparticles in the shell.

fragments. A size range of 0.2–2 μm was selected to enable the microspheres to pass readily through the living microcirculation.

Microspheres were resuspended in nanopure water. To prevent settling during optical characterization, they were mixed and warmed liquid agarose and allowed to solidify. Average size, size distributions, and initial concentrations (average 1.1×10^{10} microspheres/mL) were determined by Coulter Multisizer II analysis of each sample. Scanning- and transmission-electron micrographs of a representative contrast agent with an oil-filled core and scattering silica nanoparticles embedded in the shell are shown in Fig. 1. The transmission-electron micrograph demonstrates that the shell comprises essentially a monolayer of scattering nanoparticles. For this study we investigated the optical properties of three types of contrast agent for OCT by incorporating melanin, gold, and carbon nanoparticles into the shells of oil-filled microspheres. These nanoparticles were chosen to provide a higher degree of optical scattering than does biological tissue. Comparisons are also made with oil-filled contrast agents without shell nanoparticles. The encapsulation of vegetable oil as a core material made the contrast agents more stable and robust than air-filled microbubbles, extending their lifetime in solution from 3 days to several months.

The refractive indices at 800 nm, the center wavelength of our OCT optical source, were obtained from the literature for bulk melanin, gold, and carbon (Table 1). The refractive indices of the encapsulated oil ($n = 1.47$), of the agarose gel ($n = 1.34$), and of the four types of sample were also measured by OCT. For

all contrast-agent samples, refractive indices were within experimental error (5%) of the index of pure agarose because of the small fractional volume of the microspheres.

The reduced scattering coefficients of the contrast agents (average concentration, 2.8×10^9 microspheres/mL) were determined by oblique-incidence reflectometry,¹¹ with an 800-nm laser diode. This method was chosen to characterize thick preparations and will allow for *in situ* measurement of reduced scattering coefficients simultaneously with OCT. The oil-filled agents that contained melanin, carbon, and gold nanoparticles in their shells exhibited higher reduced scattering coefficients than microspheres without scattering nanoparticles. Upper limits of the absorption coefficients were measured for the contrast agents (average concentrations, 3.1×10^7 microspheres/mL) by a spectrophotometer (Thermo Spectronic 20). All agents exhibited low absorption coefficients, as expected for these near-infrared wavelengths. We used microsphere concentrations obtained from Coulter Multisizer II measurements and an approximate anisotropy coefficient of 0.8, based on microsphere size, to calculate scattering and absorption cross sections.

To demonstrate the effects of these contrast agents on OCT images and in tissue we performed OCT following the intravenous injection of gold-shelled contrast agents into a mouse. Our fiber-based OCT system used a Nd:YVO₄-pumped titanium:sapphire laser (Lexel Laser, Inc.) as a broad-bandwidth optical source that produced 500-mW average power and approximately 90-fs pulses with an 80-MHz repetition rate at 800-nm center wavelength. Laser output was coupled into an ultrahigh-numerical-aperture fiber (UHNA4, Thorlabs, Inc.) to broaden the light spectrally from 20 to more than 100 nm, increasing the axial resolution of our system¹² from 14 to 3 μm . The ultrahigh-numerical-aperture fiber was spliced directly to the single-mode fiber of a broadband 50:50 fiber coupler (Gould Fiber Optics). The reference arm of the OCT interferometer contained a galvanometer-driven retroreflector delay line that was scanned a distance of 3 mm at a rate of 30 Hz. The sample arm beam was focused into the tissue by a 12.5-mm-diameter, 30-mm focal-length achromatic lens to a 10- μm -diameter spot size (transverse resolution). The 6-mW beam was scanned over the tissue with a

Table 1. Optical Properties of OCT Contrast Agents^a

Contrast Agent	Microsphere Diameter (μm)	Refractive Index	Reduced Scattering Coefficient (cm^{-1})	Absorption Coefficient (cm^{-1})	Scattering Cross Section per Sphere (cm^2)	Absorption Cross Section per Sphere (cm^2)
Oil	1.61 ± 0.72	1.47	10.8 ± 1.4	0.26 ± 0.01	2.22×10^{-8}	9.4×10^{-9}
Melanin	1.99 ± 0.99	1.66 ^b	18.3 ± 3.6	0.45 ± 0.02	2.33×10^{-8}	1.0×10^{-8}
Gold	1.85 ± 0.79	0.18 ^c	15.2 ± 4.1	0.69 ± 0.03	4.70×10^{-8}	3.8×10^{-8}
Carbon	1.66 ± 0.66	3.08 ^c	19.9 ± 4.3	0.51 ± 0.03	3.26×10^{-8}	1.5×10^{-8}

^aValues are mean \pm standard deviation for $N = 30$ measurements.

^bRef. 9.

^cRef. 10.

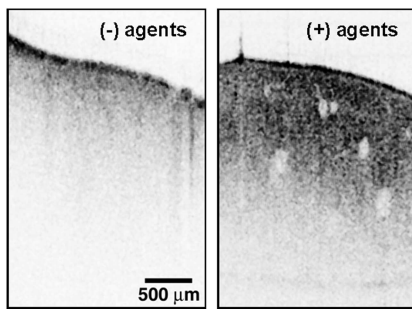


Fig. 2. OCT image enhancement with contrast agents. Images of mouse liver (left) without and (right) with gold-shelled oil-filled microsphere contrast agents.

galvanometer-controlled mirror. The envelope of the interference signal was digitized to 12-bit accuracy.

We performed OCT imaging on Swiss mice (6-week old, 27-g, males) with and without contrast agents. All animals used in this study were cared for under protocols approved by the Institutional Animal Care and Use Committee of the University of Illinois at Urbana—Champaign. Mice were anesthetized by inhalation from halothane-soaked gauze. We exposed the liver for OCT imaging by shaving the abdomen of the mouse, making a midline incision, and reflecting the abdominal skin and peritoneal wall. The liver was imaged because this is one end-organ site for collection of these contrast agents as they are broken down and cleared. A 1.3- μ L volume (6.5×10^9 microsphere/mL concentration) of gold-shelled oil-filled contrast agents was injected into a tail vein. OCT of surgically exposed liver was performed 20 min after injection and following euthanasia. OCT imaging was also performed on surgically exposed liver from control mice without contrast agents. Intravenous injection is one possible route for delivering these contrast agents to living tissue. Other routes include topical administration and direct injection into a tissue site. Figure 2 shows OCT images acquired from the exposed peritoneal surface of the liver. The left-hand OCT image, acquired from a control mouse, shows little subsurface structure. A change in scattering is readily apparent in the right-hand image of Fig. 2, which was acquired following the intravenous injection of the contrast agent. More structural detail, including liver sinusoids, is shown at greater depths in the contrast-agent-enhanced liver image. We conclude, based on transmission-electron micrograph observations, that the contrast agents in the microvascular network of the liver were being phagocytosed by Kupffer cells (macrophages) and broken down.

In summary, we have engineered, characterized, and demonstrated the use of a novel class of optical contrast agent. Although we have shown the suitability of these agents for OCT, they may be broadly applicable for other reflectance- and scattering-based techniques such as light and reflectance confocal microscopy. These contrast agents are encapsulating

microspheres with liquid-filled cores and various scattering particles incorporated into the protein shell, the core, or both. The flexible fabrication protocol for these agents allows for control of size, shell material, core material, and shell surface modifications. Further investigations will include modeling and optimizing the contrast agent's signal enhancement by varying microsphere size and by incorporating and encapsulating other combinations of scattering, absorbing, or light-modulating particles. A theoretical framework with which to predict the scattering properties of these contrast agents will need to account for the interaction between the host microsphere and the nanoparticles incorporated into its shell. Related research with multiple multipole expansions of the electromagnetic field suggests that one must also take into account the fractal nature of the distribution of nanoparticles.¹³ Shell surface modifications will be used to target agents to specific tissue types such as neoplastic tissue. Similarly to contrast agents in other imaging modalities, these agents have the potential to increase the diagnostic utility of OCT by site-specifically targeting cells and tissues, particularly when pathological tissue is morphologically or optically similar to normal tissue.

We thank John Fahrner for his technical contributions and acknowledge the support of this research by the Whitaker Foundation (for S. A. Boppart) and the National Institutes of Health (grant HL25934 to K. S. Suslick). Additional information can be found at <http://nb.beckman.uiuc.edu/biophotonics>. S. A. Boppart's e-mail address is boppart@uiuc.edu.

References

1. C. Christiansen, H. Kryvi, P. C. Sontum, and T. Skotland, *Biotechnol. Appl. Biochem.* **19**, 307 (1994).
2. G. S. Gazelle, G. L. Wolf, G. L. McIntire, E. R. Bacon, E. F. Halpern, E. R. Cooper, and J. L. Torner, *Acad. Radiol.* **1**, 373 (1994).
3. M. Y. Su, A. Muhler, X. Lao, and O. Nalcioglu, *Magn. Reson. Med.* **39**, 259 (1998).
4. J. E. Bugaj, S. Achilefu, R. B. Dorshow, and R. Rajagopalan, *J. Biomed. Opt.* **6**, 122 (2001).
5. B. E. Bouma and G. J. Tearney, eds., *Handbook of Optical Coherence Tomography* (Marcel Dekker, New York, 2001).
6. K. J. Liu, M. W. Grinstaff, J. Jiang, K. S. Suslick, H. M. Swartz, and W. Wang, *Biophys. J.* **67**, 896 (1994).
7. S. A. Boppart, B. E. Bouma, C. Pitris, J. F. Southern, M. E. Brezinski, and J. G. Fujimoto, *Nature Med.* **4**, 861 (1998).
8. J. K. Barton, J. B. Hoying, and C. J. Sullivan, *Acad. Radiol.* **9S**, 52 (2002).
9. A. Vitkin, J. Woolsey, B. C. Wilson, and R. R. Anderson, *Photochem. Photobiol.* **59**, 455 (1994).
10. S. K. Kurtz, S. D. Kozikowski, and L. J. Wolfram, in *Electro-Optics and Photorefractive Materials*, P. Gunther, ed. (Springer-Verlag, Berlin, 1986), p. 110.
11. L. Wang and S. L. Jacques, *Appl. Opt.* **34**, 2362 (1995).
12. D. L. Marks, A. L. Oldenburg, J. J. Reynolds, and S. A. Boppart, *Opt. Lett.* **27**, 2010 (2002).
13. K. A. Fuller, *J. Opt. Soc. Am. A* **12**, 881 (1995).

Sonochemical modification of the superconducting properties of MgB₂

Tanya Prozorov

Department of Physics and Astronomy and USC NanoCenter, University of South Carolina, Columbia, South Carolina 29208 and School of Chemical Sciences, University of Illinois at Urbana-Champaign, Urbana, Illinois 61801

Ruslan Prozorov^{a)} and Alexey Snezhko

Department of Physics and Astronomy and USC NanoCenter, University of South Carolina, Columbia, South Carolina 29208

Kenneth S. Suslick

School of Chemical Sciences, University of Illinois at Urbana-Champaign, Urbana, Illinois 61801

(Received 16 May 2003; accepted 10 July 2003)

Ultrasonic irradiation of magnesium diboride slurries in decalin produces material with significant intergrain fusion. Sonication in the presence of Fe(CO)₅ produces magnetic Fe₂O₃ nanoparticles embedded in the MgB₂ bulk. The resulting superconductor–ferromagnet composite exhibits considerable enhancement of its magnetic hysteresis, which implies an increase of vortex pinning strength due to embedded magnetic nanoparticles. © 2003 American Institute of Physics.

[DOI: 10.1063/1.1609248]

Controlled modification of the pinning properties of bulk granular superconductors is an active area of applied and fundamental research.^{1–8} Doping with different metals,^{9,10} variation of stoichiometry,¹¹ and nonsuperconducting phase precipitation¹² are recent examples of the chemical tuning of superconducting materials. Systematic modification of superconductor *morphology* provides another way to influence intergrain coupling and intragrain critical currents.^{1,6,13}

Various techniques to control pinning properties of MgB₂ have been suggested.¹⁴ Alternative synthetic routes^{13,15} and postsynthesis treatments,¹⁶ fabrication of dense wires,¹⁷ pellets,¹⁶ and tapes,¹⁸ annealing in Mg vapor,¹⁹ doping with Na,²⁰ Co, Fe,²¹ Cu, or Ag,¹⁰ introduction of SiC nanoparticles,²² Ag powder,²³ Ti precipitates,²⁴ synthesis of MgB₂/Mg nanocomposites,²⁵ intralayer carbon substitution^{11,26} have all been reported.

In this letter, we report the sonochemical modification of grain morphology and intergrain coupling of polycrystalline MgB₂. The method is further extended for the *in situ* synthesis and embedding of ferromagnetic nanoparticles, which are shown to act as efficient magnetic vortex pinning centers.

In ultrasonically irradiated slurries, turbulent flow, and shock waves are produced by acoustic cavitation. The implosive collapse of bubbles during cavitation results in extremely high local temperatures (~ 5000 K)^{27,28} and also creates high-velocity collisions between suspended particles with effective temperatures at the point of impact of ~ 3000 K.²⁹ These high velocity collisions cause localized interparticle melting and “neck” formation.^{27–29} The estimated speed of colliding particles approaches half of the speed of sound in the liquid. MgB₂ polycrystalline powder (325 mesh, Alfa Aesar) was ultrasonically irradiated for 60 min at -5 °C in 15 ml of decalin (0.13%, 0.26%, 0.5%, and 2% wt, respectively, at 20 kHz and ~ 50 W/cm²) under am-

bient atmosphere using direct-immersion ultrasonic horn (Sonics VCX-750). A similar set of slurries was sonicated with the addition of 1.8 mmol of Fe(CO)₅. The resulting material was filtered, washed repeatedly with pentane, and air-dried overnight.

Magnetic measurements were conducted using a *Quantum Design* Superconducting Quantum Interference Device (SQUID) MPMS magnetometer. For magnetic measurements, the powder was sintered at room temperature at a pressure of 2 GPa for 24 h. (Study of high-temperature annealing is in progress.) The average sample mass was 10 mg. The magnetic moment was normalized using the initial slope, dM/dH , measured at 5 K after zero-field cooling. The slope is proportional to the fraction of the superconducting phase. For materials without magnetic nanoparticles, such normalization gives the volume magnetization. For composites containing Fe₂O₃ nanoparticles, the normalization was done after subtraction of the paramagnetic contribution.

Scanning electron micrographs (SEM) were taken on a Hitachi S-4700 instrument. Samples were additionally characterized by powder x-ray diffraction and differential thermal analysis. All reported results were reproduced on more than 25 samples. We use the following sample designations: original MgB₂ powder (A) and sintered pellet (AP); MgB₂ sonicated in decalin with various loadings of the slurry (pellets: S1, 0.13% wt; S2, 0.26% wt; S3, 0.5% wt; S4, 2% wt); MgB₂ sonicated in decalin with 1.8 mmol of Fe(CO)₅ (pellets SF1, SF2, and SF3 with the same loading of MgB₂ as S1, S2, and S3). SEM images of the original (A and AP) as well as the sonicated samples (S1 and SF1) are shown in Fig. 1. Samples A and AP (a sintered pellet made from sample A) are shown in Figs. 1(a) and 1(b), respectively; no particular structural modification was observed upon making the sintered pellet. In contrast, the sonicated powder used for sample S1 [Fig. 1(c)] and sonicated with Fe(CO)₅ for sample SF1 [Fig. 1(d)] have distinctively modified morphologies. Even though the decomposition temperature of MgB₂

^{a)}Author to whom correspondence should be addressed; electronic mail: prozorov@mailaps.org

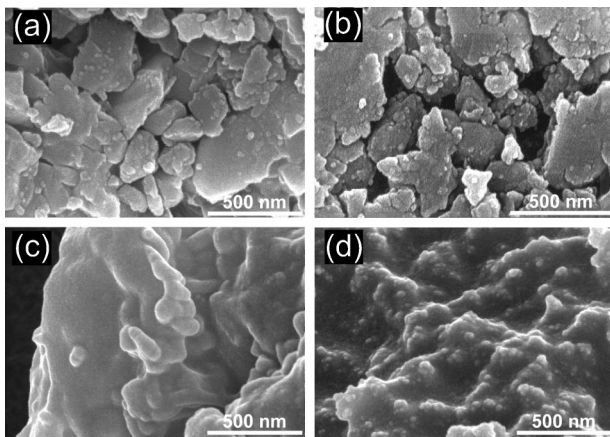


FIG. 1. Scanning electron images of (a) original MgB_2 powder, sample A; (b) MgB_2 pellet, sample AP; (c) MgB_2 sonicated in decalin, sample S1; and (d) MgB_2 sonicated in decalin with $\text{Fe}(\text{CO})_5$, sample SF1.

(~ 1100 K)¹⁴ is lower than the effective local temperatures achieved during transient cavitation, the initial material apparently undergoes surface melting, as implied by Fig. 1(d). This can be attributed to extremely high cooling rates ($>10^9$ K/s)^{29,30} leading to formation of smooth welded grains in sonochemical process. In the case of a superconductor, such morphological changes produce better intergrain coupling and annealing of the intragrain defects, consistent with our observations. Sonication of MgB_2 powder in decalin with $\text{Fe}(\text{CO})_5$ is accompanied by the *in situ* sonochemical formation of iron oxide nanoparticles³¹ directly on MgB_2 grain surfaces, while concurrent ultrasound-driven melting results in embedding of Fe_2O_3 nanoparticles into the MgB_2 matrix, Fig. 1(d). The embedded particles act as efficient pinning centers where magnetic interaction with Abrikosov vortices provides extra force in addition to the core pinning. Similar enhancement was reported in 1966 for Hg–In alloys with mechanically dispersed Fe nanoparticles.^{32,33} Related recent work has also examined the effect of magnetic particles placed on the surface of low- T_c superconducting films.^{34–36} Our method is to embed ferromagnetic nanoparticles into high- T_c superconductors.

Figure 2 shows $M(T)$ curves measured in magnetic field of 10 Oe after zero-field cooling (ZFC). The superconducting transition temperature remains unchanged, $T_c \approx 38.5$ K.

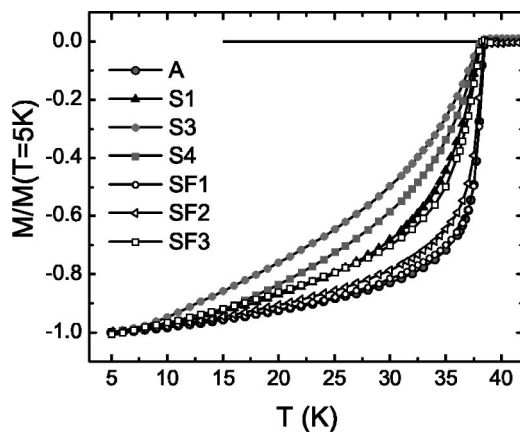


FIG. 2. Zero-field cooled magnetization measured in $H=10$ Oe, normalized to its value at 5 K. The paramagnetic contribution for SF samples was subtracted using Curie–Weiss law measured up to 150 K.

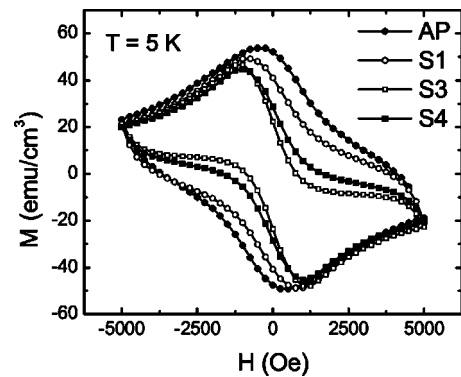


FIG. 3. Magnetization loops at $T=5$ K for sonicated samples S1, S2, and S3 compared to the original sample AP. Width of the hysteresis loops is reduced, but the Meissner expulsion is not.

Curves in Fig. 2 were normalized by the magnetization value at 5 K, and the paramagnetic contribution for the SF samples was subtracted. Figure 3 shows the effect of sonication on the magnetization loops measured at 5 K for samples with different initial loading of MgB_2 slurries. The loops become less hysteretic and more asymmetric for loading up to 1% wt, after which the effect diminishes. This is as expected for the material, where intragrain defects are annealed during sonication and most of the grains are fused together. This also provides the evidence that Meissner expulsion in granular superconductors is mostly due to intragrain shielding and not to weak intergrain coupling.

As shown in Fig. 4, the situation is different for the samples sonicated with $\text{Fe}(\text{CO})_5$. The magnetization loops are more hysteretic compared to sample A. However, the hysteresis decreases with increasing MgB_2 loading. This is in agreement with the results of Fig. 3 where the optimum effect of sonication was achieved for 0.5% wt of MgB_2 slurry. Figure 5 shows magnetization loops measured in sample SF3 at 30 and 42 K. The curve at 42 K is well described by the Langevin function, indicative of a superparamagnetic behavior. The hysteresis at $T=42$ K is due to some magnetic anisotropy and dipole–dipole interactions³⁷ of the dispersed Fe_2O_3 nanoparticles, and it is much smaller than the hysteresis due to pinning. We verified this conclusion by measuring remnant magnetization as a function of temperature.

The irreversibility practically disappears at T_c . The difference, $\Delta M = M(30 \text{ K}) - M(42 \text{ K})$, shown by solid squares

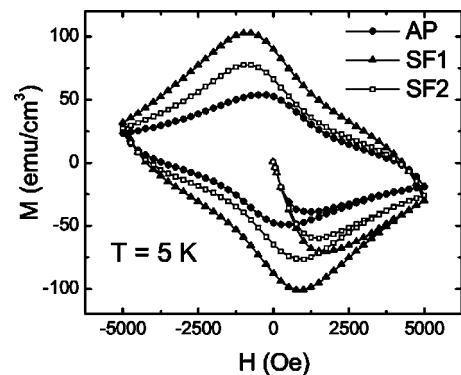


FIG. 4. Magnetization loops measured at $T=5$ K in MgB_2 sonicated in decalin with $\text{Fe}(\text{CO})_5$. The hysteresis is largest for the lowest loading of MgB_2 .

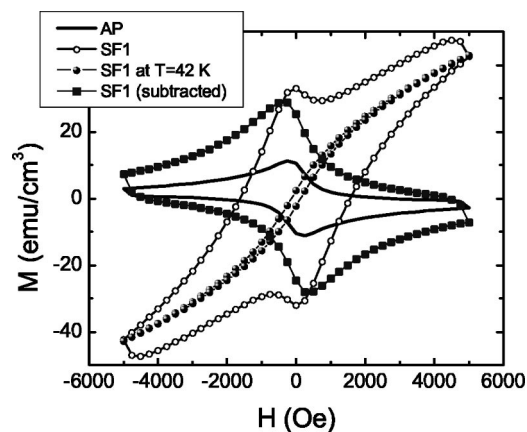


FIG. 5. Open symbols—measured magnetization loops for sample SF1; filled squares—same curve with paramagnetic contribution subtracted; filled circles— $M(H)$ curve measured at $T=42$ K. The solid line is the $M(H)$ curve of the unmodified MgB_2 , sample AP measured at 30 K.

in Fig. 5 is typical for a superconductor with significant pinning. The solid line shows magnetization curve of the original sample AP. The comparison indicates more than twofold enhancement of pinning.

In conclusion, a method of a controlled modification of the superconducting properties of magnesium diboride is described. Ultrasonic cavitation leads to a significant change in morphology without affecting chemical composition. Sonication in decalin results in a granular superconducting material with significant intergrain fusion and a much less defective structure compared to the original MgB_2 powder. Sonication in decalin with the addition of $\text{Fe}(\text{CO})_5$ produces a superconductor–ferromagnet composite in which ferromagnetic nanoparticles are embedded into the MgB_2 matrix. These particles act as efficient pinning centers. Our continuing research indicates that the described experimental technique and conclusions are applicable to other granular superconductors, such as $\text{YBa}_2\text{Cu}_3\text{O}_7$.

Discussions with V. Geshkenbein, B. Ivlev, E. Sonin, and A. Koshelev are greatly appreciated. This work is supported by the NSF (EPSCoR Grant No. EPS-0296165 and CHE-0079124), a Grant from the University of South Carolina Research and Productive Scholarship Fund, and the donors of the American Chemical Society Petroleum Research Fund. The SEM study was carried out in the Center for Microanalysis of Materials (UIUC), which is partially supported by the DOE under Grant No. DEFGO2-91-ER45439.

¹D. C. Larbalestler, L. D. Cooley, M. O. Rikel, A. A. Polyanskii, J. Jiang, S. Patnalk, X. Y. Cal, D. M. Feldmann, A. Gurevich, A. A. Squitieri, M. T. Naus, C. B. Eom, E. E. Hellstrom, R. J. Cava, K. A. Regan, N. Rogado,

M. A. Hayward, T. He, J. S. Slusky, P. Khalifah, K. Inumaru, and M. Haas, *Nature (London)* **410**, 186 (2001).
²V. N. Vieira, J. P. de Silva, and J. Schaf, *Phys. Rev. B* **64**, 094516 (2001).
³L. Burlachkov, E. Mogilko, Y. Schlesinger, Y. M. Strel'niker, and S. Havlin, *Phys. Rev. B* **67**, 104509 (2003).
⁴M. Schechter, J. V. Delft, Y. Imry, and Y. Levinson, *Phys. Rev. B* **67**, 064506 (2003).
⁵A. Frydman, O. Naaman, and R. C. Dynes, *Phys. Rev. B* **66**, 052509 (2002).
⁶J. L. Cardoso and P. Pereyra, *Phys. Rev. B* **61**, 6360 (2000).
⁷H. Hilgenkamp and J. Mannhart, *Rev. Mod. Phys.* **74**, 485 (2002).
⁸M. Sigrist and T. M. Rice, *Rev. Mod. Phys.* **67**, 503 (1995).
⁹A. Yamamoto, K. Minami, W.-Z. Hu, A. Miyakita, M. Izumi, and S. Tajima, *Phys. Rev. B* **65**, 104505 (2002).
¹⁰S. Soltanian, X. L. Wang, J. Horvat, A. H. Li, H. K. Liu, and S. X. Dou, *Physica C* **382**, 187 (2002).
¹¹T. Takenobu, T. Ito, D. H. Chi, K. Prassides, and Y. Iwasa, *Phys. Rev. B* **64**, 134513 (2001).
¹²M. Muralidhar, N. Sakai, N. Chikumoto, M. Jirsa, T. Machi, M. Nishiyama, Y. Wu, and M. Murakami, *Phys. Rev. Lett.* **89**, 237001 (2002).
¹³D. G. Hinks, J. D. Jorgensen, H. Zheng, and S. Short, *Physica C* **382**, 166 (2002).
¹⁴Review, *Physica C* **385**, 1 (2003).
¹⁵H. Fujii, K. Togano, and H. Kumakura, *Supercond. Sci. Technol.* **15**, 1571 (2002).
¹⁶R. A. Ribeiro, S. L. Bud'ko, C. Petrovic, and P. C. Canfield, *Physica C* **382**, 194 (2002).
¹⁷P. C. Canfield, D. K. Finnemore, S. L. Bud'ko, J. E. Ostenson, G. Laperot, C. E. Cunningham, and C. Petrovic, *Phys. Rev. Lett.* **86**, 2423 (2001).
¹⁸O. Suzuki, N. Enomoto, M. Aodai, Y. Yamada, and K. Tachikawa, *J. Adv. Sci.* **14**, 17 (2002).
¹⁹V. Braccini, L. D. Cooley, S. Patnaik, D. C. Larbalestier, P. Manfrinetti, A. Palenzona, and A. S. Siri, *Appl. Phys. Lett.* **81**, 4577 (2002).
²⁰Y.-S. Wang, Z.-Y. Zheng, and W. Yu, *Rengong Jingti Xuebao* **31**, 494 (2002).
²¹E. Kuzmann, Z. Homonnay, Z. Klencsar, M. Kuhberger, A. Vertes, and G. Gritzner, *Supercond. Sci. Technol.* **15**, 1479 (2002).
²²S. X. Dou, S. Soltanian, J. Horvat, X. L. Wang, S. H. Zhou, M. Ionescu, H. K. Liu, P. Munroe, and M. Tomsic, *Appl. Phys. Lett.* **81**, 3419 (2002).
²³M. Zouaoui, A. M'Chirgui, F. Ben Azzouz, B. Yangui, and M. Ben Salem, *Physica C* **382**, 217 (2002).
²⁴M. J. Kramer, S. L. Bud'ko, P. C. Canfield, R. D. Wilke, D. K. Finnemore, and R. J. Suplinskas, *cond-mat/0302443* (2003).
²⁵Q. Li, G. D. Gu, and Y. Zhu, *Appl. Phys. Lett.* **82**, 2103 (2003).
²⁶Y. Yan and M. M. Al-Jassim, *J. Appl. Phys.* **92**, 7687 (2002).
²⁷K. S. Suslick and G. J. Price, *J. Ann. Rev. Mater. Sci.* **29**, 295 (1999).
²⁸K. S. Suslick, D. A. Hammerton, and R. E. Cline, Jr., *J. Am. Chem. Soc.* **108**, 5641 (1986).
²⁹K. S. Suslick and S. J. Doctycz, *Science* **247**, 1067 (1990).
³⁰T. Prozorov, K. S. Suslick, and R. Prozorov (unpublished).
³¹X. Cao, R. Prozorov, Y. Kolytyn, G. Kataby, I. Felner, and A. Gedanken, *J. Mater. Res.* **12**, 402 (1997).
³²T. H. Alden and J. D. Livingston, *Appl. Phys. Lett.* **8**, 6 (1966).
³³T. H. Alden and J. D. Livingston, *J. Appl. Phys.* **37**, 3551 (1966).
³⁴Y. Nozaki, Y. Otani, K. Runge, H. Miyajima, and B. Pannetier, *J. Appl. Phys.* **79**, 8571 (1996).
³⁵Y. Nozaki, Y. Otani, K. Runge, H. Miyajima, and B. Pannetier, *J. Appl. Phys.* **79**, 6599 (1996).
³⁶M. J. V. Bael, K. Temst, V. V. Moshchalkov, and Y. Bruynseraede, *Phys. Rev. B* **59**, 14674 (1999).
³⁷R. Prozorov, Y. Yeshurun, T. Prozorov, and A. Gedanken, *Phys. Rev. B* **59**, 6956 (1999).

Hydrogen-Bonded Porphyrinic Solids: Supramolecular Networks of Octahydroxy Porphyrins

P. Bhyrappa, Scott R. Wilson, and Kenneth S. Suslick*

Contribution from the Department of Chemistry, University of Illinois at Urbana–Champaign, 601 South Goodwin Avenue, Urbana, Illinois 61801

Received April 7, 1997[⊗]

Abstract: Symmetrically substituted octahydroxy porphyrins, tetrakis(3',5'-dihydroxyphenyl)porphyrin, H₂T(3',5'-DHP)P, tetrakis(2',6'-dihydroxyphenyl)porphyrin, H₂T(2',6'-DHP)P, and their Zn(II) and Mn(III) derivatives have been developed as building blocks for supramolecular hydrogen-bonded networks. The crystal structures of a series of these porphyrins exhibit unique structural features through assembly of porphyrin networks by means of directional hydrogen bonding. The position of the peripheral hydroxyl groups, the choice of metallo- or free base porphyrin, and the nature of the solvate (i.e., guest) dramatically influence structural features. A one-dimensional, columnar structure is found for H₂T(3',5'-DHP)P·5EtOAc. With benzonitrile as solvate, the structure of H₂T(3',5'-DHP)P·7C₆H₅-CN changes substantially to a three-dimensional corrugated-sheet structure in order to accommodate a larger pore size. When the hydroxyl substituents are simply changed from the *m*- to the *o*-phenyl positions, an essentially two-dimensional layered structure is formed for H₂T(2',6'-DHP)P·4EtOAc. Zn[T(2',6'-DHP)P](EtOAc)₂·2EtOAc has a two-dimensional layered structure, similar to that of its free base H₂T(2',6'-DHP)P interaction between the aryl rings of the adjacent layers. The crystal structures of both Zn[T(3',5'-DHP)P] and Mn[T(3',5'-DHP)P](Cl) exhibited three-dimensional hydrogen-bonding features. Zn[T(3',5'-DHP)P](THF)₂·2THF·3CH₂Cl₂ has a three-dimensional interconnected layered structure with metalloporphyrins arranged in a slipped stack orientation within the layers. In the structure of Mn[T(3',5'-DHP)P](THF)₂·Cl·2THF·5C₆H₅CH₃, a chloride anion dictates the three-dimensional packing by bridging four metalloporphyrin molecules through Cl···HO bonding interactions. In all of these structures, large solvate-filled channels are present with cross-sections as large as 42 Å². The pore volumes of these channels are exceptionally large: as much as 67% of the unit cell volume.

Introduction

In recent years there has been an increasing interest in nanoporous molecular crystalline solids and their various applications.¹ Of special importance is the development of molecular building blocks for the design and crystal engineering of such materials. A wide variety of organic molecules have been engineered for generating nanoporous crystalline materials.¹ Porphyrins and metalloporphyrins provide a relatively unexplored class of such building blocks because of their large size, ease of synthesis, excellent thermal stability, and diversity of their coordination and catalytic chemistry. Furthermore, porphyrins provide an extremely versatile platform on which to build desired peripheral functionality with designed orientations. Such functionality can provide the intermolecular interactions that control self-assembly both in solution and in the solid state. There have been a few recent reports on the supramolecular architectures of porphyrin solids with hydrogen-bonded² and metal–organic coordination³ networks. In addition, the extensive structural work that exists for porphyrins and metalloporphyrins⁴ provides a database for the systematic examination of intermolecular interactions in the solid state. Notably, Strouse

and co-workers⁵ have reported a wide range of clathrate-like host/guest solid state structures of H₂TPP and its metal derivatives. *meso*-Tetraphenylporphyrins are the most widely used systems due to their ease of synthesis and facile functionalization.

In order to more rationally control the structure of porphyrinic solids, we prepared a family of symmetric octahydroxy-substituted porphyrins and their metal complexes, wherein the three-dimensional structure is determined by the directional hydrogen bonding of hydroxyl groups. We report here the synthesis of two octahydroxy porphyrins,⁶ H₂T(3',5'-DHP)P and H₂T(2',6'-DHP)P, and their Zn(II) and Mn(III) derivatives (Figure 1) as building blocks for the synthesis of hydrogen-bonded crystalline solids, together with six X-ray structures derived from these porphyrins; this paper is an extension of our preliminary communication of the free base porphyrin structures.^{6b} Several structural architectures in the packing of these porphyrins have been observed and are discussed below in some detail. The use of hydroxy substitution, combined with the rigidity and high symmetry of the porphyrinic building blocks, leads to the formation of highly open structures with large void volumes.

[⊗] Abstract published in *Advance ACS Abstracts*, August 15, 1997.

(1) Bein, T., Ed.; *Supramolecular Architecture*; ACS Symposium Series; American Chemical Society: Washington, DC, 1992; Vol. 499, pp 88–253. (b) Komarneni, S.; Smith, D. M.; Beck, J. S. Ed.; *Advances in Porous Materials*; Materials Research Society: Pittsburgh, PA, 1995. (c) Yaghi, O. M.; Li, G.; Li, H. *Nature* **1995**, 378, 703. (d) Yaghi, O. M.; Hailian, L.; Groy, T. L. *J. Am. Chem. Soc.* **1996**, 118, 9096 and references cited therein. (e) Venkataraman, D.; Garner, G. B.; Lee, S.; Moore, J. S. *J. Am. Chem. Soc.* **1996**, 118, 9096.

(2) Goldberg, I.; Krupitsky, H.; Stein, Z.; Hsiou, Y.; Strouse, C. E. *Supramol. Chem.* **1995**, 4, 203 and references cited therein.

(3) (a) Abrahams, B. F.; Hoskins, B. F.; Michall, D. M.; Robson, R. *Nature* **1994**, 369, 727. (b) Abrahams, B. F.; Hoskins, B. F.; Michall, D. M.; Robson, R. *J. Am. Chem. Soc.* **1991**, 113, 3606.

(4) Scheidt, W. R.; Lee, Y. *J. Struct. Bond. (Berlin)* **1987**, 64, 1.

(5) Byrn, M. P.; Curtis, C. J.; Hsiou, Y.; Khan, S. I.; Sawin, P. I.; Tendick, S. K.; Terzis, A.; Strouse, C. E. *J. Am. Chem. Soc.* **1993**, 115, 9480 and references cited therein. (b) Krupitsky, H.; Stein, S.; Goldberg, I. *J. Inclusion Phenom. Mol. Recognit. Chem.* **1995**, 20, 211. (c) Krupitsky, H.; Stein, S.; Goldberg, I.; Strouse, C. E. *J. Inclusion Phenom. Mol. Recognit. Chem.* **1994**, 18, 177.

(6) (a) Abbreviations: T(2',6'-DMP)P, 5,10,15,20-tetrakis(2',6'-dimethoxyphenyl)porphyrinate(−2); T(2',6'-DHP)P, 5,10,15,20-tetrakis(2',6'-dihydroxyphenyl)porphyrinate(−2); T(3',5'-DMP)P, 5,10,15,20-tetrakis(3',5'-dimethoxyphenyl)porphyrinate(−2); T(3',5'-DHP)P, 5,10,15,20-tetrakis(3',5'-dihydroxyphenyl)porphyrinate(−2); EtOAc, ethyl acetate; THF, tetrahydrofuran. (b) Bhyrappa, P.; Wilson, S. R.; Suslick, K. S. *Supramol. Chem.* In press.

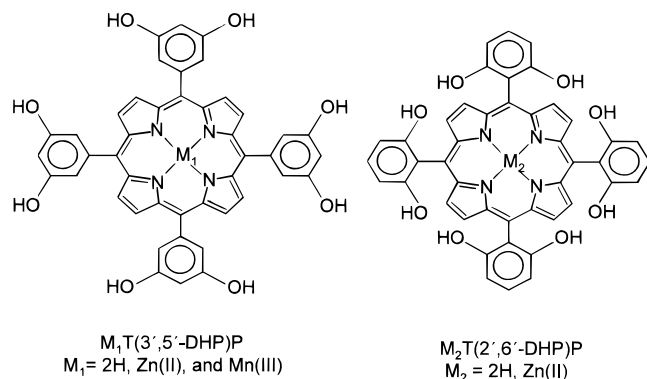


Figure 1. Chemical structures of octahydroxy porphyrins, $H_2T(3',5'-DHP)P$ and $H_2T(2',6'-DHP)P$, and their metal derivatives.

Experimental Section

Materials. Octamethoxy porphyrins, 5,10,15,20-tetrakis(2',6'-dimethoxyphenyl)porphyrin,^{7a} $H_2T(2',6'-DMP)P$, and 5,10,15,20-tetrakis(3',5'-dimethoxyphenyl)porphyrin,^{7b} $H_2T(3',5'-DMP)P$, were synthesized using reported procedures. 5,10,15,20-Tetrakis(3',5'-dihydroxyphenyl)porphyrin, $H_2T(3',5'-DHP)P$, was prepared using literature method.⁷ Demethylation of $H_2T(2',6'-DMP)P$ was unsuccessful with BBr_3 and was carried out using pyridinium hydrochloride at 220 °C under N_2 .⁸ Zinc complexes, $Zn[T(2',6'-DHP)P]$ and $Zn[T(3',5'-DHP)P]$, were prepared by metallation in the usual fashion.⁹ Dichloromethane, purchased from Fisher was distilled over CaH_2 under nitrogen before use. Ethyl acetate was purchased from Fisher and used as received. Toluene obtained from Fisher was distilled over sodium under nitrogen before use. Tetrahydrofuran was predried from 4 Å molecular sieves and distilled from sodium/benzophenone under nitrogen before use. *n*-Heptane and benzonitrile, C_6H_5CN , obtained from Aldrich were used as received.

Synthesis of 5,10,15,20-tetrakis(2',6'-dihydroxyphenyl)porphyrin, $H_2T(2',6'-DHP)P$. Demethylation of $H_2T(2',6'-DMP)P$ was carried out using reported procedures⁸ with slight modifications. To a Schlenk flask containing $H_2T(2',6'-DMP)P$ (0.38 g, 0.5 mmol) was added pyridinium hydrochloride (20.0 g, 0.17 mol). The reaction mixture was stirred and refluxed (200–220 °C) under Ar for 2 h. At the end of this period, the mixture was cooled to room temperature and poured into water (500 mL). The porphyrin was extracted with ethyl acetate. The organic layer was washed twice with hydrochloric acid (0.1 M) followed by saturated aqueous $NaHCO_3$ solution and dried over anhydrous Na_2SO_4 . The resulting solution was concentrated and chromatographed on a silica gel column using 20% THF in ethyl acetate as the eluent. The yield of the product was 0.25 g (75%). Anal. Calcd for $C_{44}H_{30}N_4O_8 \cdot H_2O$: C, 69.47; H, 4.24; N, 7.36. Found: C, 69.70; H, 4.25; N, 7.18. ¹H NMR in CD_3CN : -2.75 (s, 2H, imino-H), 7.2–7.8 (12H, m, phenyl-H), and 8.85 (8H, s, pyrrole-H) ppm.

Synthesis of 5,10,15,20-Tetrakis(3',5'-dihydroxyphenyl)porphyrinotomanganese(III) Chloride, $Mn[T(3',5'-DHP)P](Cl)$. This complex was prepared using variant of reported procedure.¹⁰ To a DMF (30 mL) solution containing (0.2 g, 0.25 mmol) $H_2T(3',5'-DHP)P$ was added anhydrous $MnCl_2$ (0.5 g, 3.9 mmol), and the solution was refluxed for a period of 6 h. At the end of this period, DMF was removed under reduced pressure. The residue thus obtained was redissolved in ethyl acetate and washed with distilled water to remove excess $MnCl_2$. The product was recrystallized from 1:1 mixture of THF/ CH_2Cl_2 and dried under vacuum at 100 °C for 12 h. The yield of the product was found to be 0.12 g (65%). Anal. Calcd. for $C_{44}H_{28}N_4O_8MnCl$: C, 63.61; H, 3.40; N, 6.75; Mn, 6.62; Cl, 4.21%. Found: C, 63.10; H, 3.30; N, 6.65; Mn, 6.40; Cl, 4.30. UV–vis absorption spectrum in THF, λ_{max} : 375, 395, 479, 523, 584, and 623

(7) (a) Tsuchida, E.; Komatsu, T.; Hasegawa, E.; Nishide, H. *J. Chem. Soc., Dalton Trans.* **1990**, 2713. (b) Jin, R.-H.; Aida, T.; Inoue, S. *J. Chem. Soc., Chem. Commun.* **1993**, 1260.

(8) Momenteau, M.; Mispelter, J.; Loock, B.; Bisagni, E. *J. Chem. Soc., Perkin Trans. 1* **1983**, 189.

(9) Dorough, G. D.; Miller, J. R.; Huennekens, F. M. *J. Am. Chem. Soc.* **1948**, *70*, 1808.

(10) Jones, R. D.; Summerville, D. A.; Basolo, F. *J. Am. Chem. Soc.* **1978**, *100*, 4416.

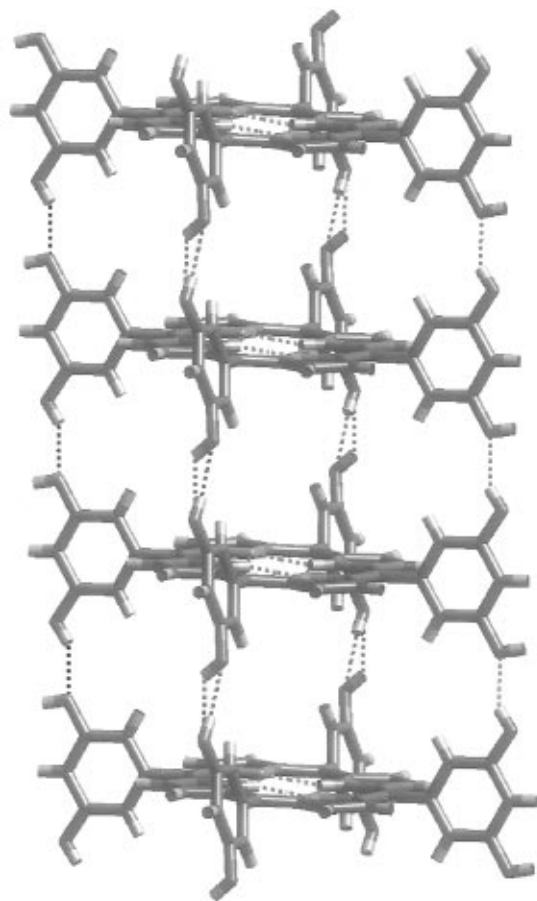


Figure 2. Molecular packing diagram of $H_2T(3',5'-DHP)P \cdot 6EtOAc$ showing one-dimensional columnar structure. Hydrogen-bonding interactions between the hydroxyl groups are shown with dotted lines.

nm. Negative ion electrospray mass spectrum: calcd (m/e) for $[M - Cl]^+$, 795.67; found, 794.90.

Crystallization. Porphyrin crystals were grown by liquid diffusion of a second solvent into a porphyrin solution. For $H_2T(3',5'-DHP)P \cdot 5EtOAc$, $H_2T(3',5'-DHP)P \cdot 7C_6H_5CN$, $H_2T(2',6'-DHP)P \cdot 4EtOAc$, and $Zn[T(2',6'-DHP)P](EtOAc)_2 \cdot 2EtOAc$, crystals were grown by direct diffusion of *n*-heptane into a $EtOAc$ (or benzonitrile) porphyrin solution. For $Mn[T(3',5'-DHP)P](THF)_2 \cdot Cl \cdot 2THF \cdot 5C_6H_5CH_3$, toluene was allowed to diffuse slowly over a period of roughly 3 days into a saturated solution of $Mn[T(3',5'-DHP)P](Cl)$ in THF. Crystals of $Zn[(T(3',5'-DHP)P)(THF)_2 \cdot 2THF \cdot 3CH_2Cl_2]$ were grown by direct diffusion of CH_2Cl_2 into a saturated solution of $Zn[T(3',5'-DHP)P]$ in THF. All crystallization procedures were carried out at room temperature. The crystals employed in this study were found to lose solvates upon removal from the mother liquor, and subsequent loss of crystallinity occurred. Attempts to replace solvate into dried solids by vapor diffusion resulted in partial resolution (based on thermogravimetric data) in some but not all cases.

X-ray Data Collection. The X-ray diffraction data were collected on an automated Enraf-Nonius CAD-4 diffractometer. Single crystals were covered with oil (Paratone-N, Exxon), mounted on to a thin glass fiber, and then cooled to 198 K to prevent solvate loss. Porphyrin crystals tend to lose crystallinity upon removal from mother liquor at room temperature. Intensity data was collected by $\omega-2\theta$ mode in the range of 1.0–23° at 198 K. Three standard intensities were monitored for every 90 min and showed 1.6, 0.8, 0.54, and 0.5% decay for $H_2T(3',5'-DHP)P \cdot 5EtOAc$, $H_2T(3',5'-DHP)P \cdot 7C_6H_5CN$, $Zn[T(3',5'-DHP)P](THF)_2 \cdot 2THF \cdot 3CH_2Cl_2$, and $Mn[T(3',5'-DHP)P](THF)_2 \cdot Cl \cdot 2THF \cdot 5C_6H_5CH_3$ crystals, respectively. No intensity decay was observed for $H_2T(2',6'-DHP)P \cdot 4EtOAc$ and $Zn[T(2',6'-DHP)P](EtOAc)_2 \cdot 2EtOAc$ crystals. No decay corrections were applied.

Crystal structure data for $H_2T(3',5'-DHP)P \cdot 5EtOAc$: red prismatic crystals; $C_{64}H_{70}N_4O_{18}$, $M = 1183.24$, triclinic, $P\bar{1}$, $a = 7.245(2)$ Å, $b = 14.727(3)$ Å, $c = 14.835(4)$ Å, $\alpha = 90.18(2)^\circ$, $\beta = 92.90(2)^\circ$, $\gamma = 90.02(2)^\circ$, $V = 1580.8(7)$ Å³, $Z = 1$. The structure was refined

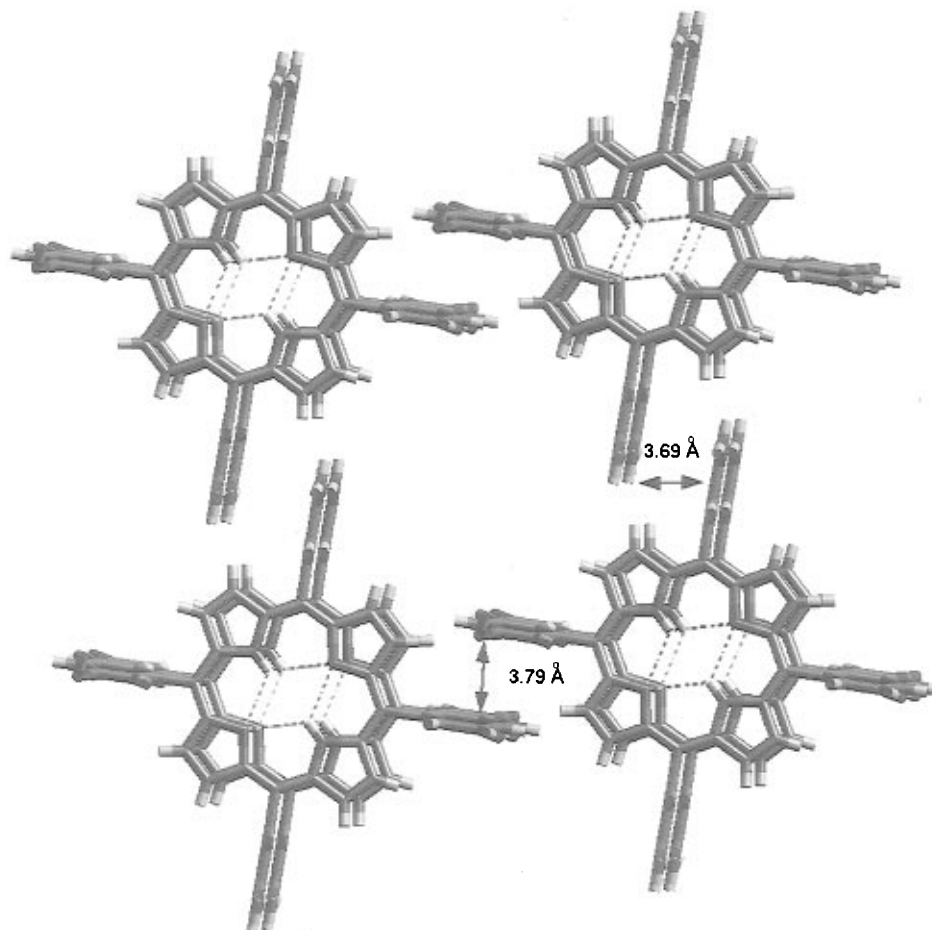


Figure 3. Crystal packing modes showing close contact and a channel for $\text{H}_2\text{T}(3',5'\text{-DHP})\text{P}\cdot 5\text{EtOAc}$. Solvent molecules are not shown for clarity.

using full-matrix least-squares on F_o^2 (data/restraints/parameters 4369:336:391), converging to $R_1 = 0.1138$, $wR2 = 0.2801$ (on 2588, $I > 2\sigma(I)$ observed data). The solvate molecules were highly disordered.

Crystal structure data for $\text{H}_2\text{T}(3',5'\text{-DHP})\text{P}\cdot 7\text{C}_7\text{H}_5\text{N}$: purple plate-like crystals; $\text{C}_{93}\text{H}_{65}\text{N}_{11}\text{O}_8$, $M = 1464.56$, monoclinic, $P2_1/m$, $a = 11.105(4)$ Å, $b = 25.744(7)$ Å, $c = 14.022(3)$ Å, $\beta = 108.09(2)^\circ$, $V = 3811(2)$ Å³, $Z = 2$. The structure was refined using full-matrix least-squares on F_o^2 (data/restraints/parameters 6106:0:548), converging to $R_1 = 0.0622$, $wR2 = 0.1305$ (on 2588, $I > 2\sigma(I)$ observed data).

Crystal structure data for $\text{H}_2\text{T}(2',6'\text{-DHP})\text{P}\cdot 4\text{EtOAc}$: purple prismatic crystals; $\text{C}_{60}\text{H}_{62}\text{N}_4\text{O}_{16}$, $M = 1095.14$, triclinic, $P\bar{1}$, $a = 13.736(3)$ Å, $b = 14.032(3)$ Å, $c = 17.029(3)$ Å, $\alpha = 93.77(3)^\circ$, $\beta = 110.92(3)^\circ$, $\gamma = 111.81(3)^\circ$, $V = 2770.9(10)$ Å³, $Z = 2$. The structure was refined using full-matrix least-squares on F_o^2 (data/restraints/parameters 8624:64:846), converging to $R_1 = 0.0457$, $wR2 = 0.1129$ (on 6260, $I > 2\sigma(I)$ observed data).

Crystal structure data for $\text{Zn}[\text{T}(2',6'\text{-DHP})\text{P}](\text{EtOAc})_2\cdot 2\text{EtOAc}$: red prismatic crystals; $\text{C}_{60}\text{H}_{60}\text{N}_4\text{O}_{16}\text{Zn}$, $M = 1158.49$, triclinic, $P\bar{1}$, $a = 10.599(3)$ Å, $b = 11.301(4)$ Å, $c = 12.535(6)$ Å, $\alpha = 85.70(4)^\circ$, $\beta = 70.19(4)^\circ$, $\gamma = 79.15(3)^\circ$, $V = 1387.2(9)$ Å³, $Z = 1$. The structure was refined using full-matrix least-squares on F_o^2 (data/restraints/parameters 3850:20:371), converging to $R_1 = 0.0984$, $wR2 = 0.2527$ (on 2610, $I > 2\sigma(I)$ observed data).

Crystal structure data for $\text{Zn}[\text{T}(3',5'\text{-DHP})\text{P}](\text{THF})_2\cdot 2\text{THF}\cdot 3\text{CH}_2\text{Cl}_2$: purple, plate-like crystals; $\text{C}_{63}\text{H}_{66}\text{N}_4\text{Cl}_6\text{O}_{12}\text{Zn}$, $M = 1349.27$, triclinic, $P\bar{1}$, $a = 10.212(3)$ Å, $b = 12.365(3)$ Å, $c = 14.628(3)$ Å, $\alpha = 99.71(2)^\circ$, $\beta = 108.52(2)^\circ$, $\gamma = 107.49(2)^\circ$, $V = 1597.6(7)$ Å³, $Z = 1$. The structure was refined using full-matrix least-squares on F_o^2 (data/restraints/parameters 5585:255:528), converging to $R_1 = 0.0679$, $wR2 = 0.1889$ (on 4121, $I > 2\sigma(I)$ observed data).

Crystal structure data for $\text{Mn}[\text{T}(3',5'\text{-DHP})\text{P}](\text{THF})_2\cdot \text{Cl}\cdot 2\text{THF}\cdot 5\text{C}_6\text{H}_5\text{CH}_3$: purple, tabular crystals; $\text{C}_{95}\text{H}_{100}\text{N}_4\text{Cl MnO}_{12}$, $M = 1580.18$, monoclinic, $P2_1/n$, $a = 13.937(4)$ Å, $b = 16.443(5)$ Å, $c = 19.541(6)$ Å, $\alpha = 90^\circ$, $\beta = 106.71(2)^\circ$, $\gamma = 90^\circ$, $V = 4289(2)$ Å³, $Z = 2$. The structure was refined using full-matrix least-squares on F_o^2 (data/

restraints/parameters 5942:226:567), converging to $R_1 = 0.0797$, $wR2 = 0.1742$ (on 2568, $I > 2\sigma(I)$ observed data).

Structure Analysis and Refinement. Structures were solved by direct methods (SHELXS).^{11a} In all cases, porphyrin macrocycle non-H-atoms were deduced from an E-map. For all structures, one cycle of isotropic least-squares refinement followed by an unweighted difference Fourier synthesis revealed positions for ordered atoms. H atoms and disordered solvate molecules were idealized. Successful convergence of the full-matrix least-squares refinement on F^2 (SHELXL)^{11b} was indicated by the maximum shift/error for the cycle. Final difference electron density maps for $\text{Zn}[\text{T}(3',5'\text{-DHP})\text{P}](\text{THF})_2\cdot 2\text{THF}\cdot 3\text{CH}_2\text{Cl}_2$ and $\text{Zn}[\text{T}(2',6'\text{-DHP})\text{P}](\text{EtOAc})_2\cdot 2\text{EtOAc}$ structures showed a residual density of 1.05 and 1.43 e Å⁻³ in the vicinity of disordered solvate molecules, respectively. Final difference electron-density maps were featureless. Molecular modeling of porphyrins and solvent molecules were performed on a Silicon Graphics Indigo² Extreme workstation using Cerius,² Quanta 4.0, and CHARMM software package.

Results and Discussion

In order to more rationally control the structure of porphyrinic solids, we have examined a pair of symmetric polysubstituted porphyrins, wherein the three-dimensional structure is determined by the directional hydrogen bonding of eight hydroxyl groups per porphyrin. To this end, we have examined two *meso*-tetraaryl porphyrins, with four dihydroxyphenyl groups either *m*- or *o*-substituted: $\text{H}_2\text{T}(3',5'\text{-DHP})\text{P}$ and $\text{H}_2\text{T}(2',6'\text{-DHP})\text{P}$, and their Zn(II) and Mn(III) derivatives with several different solvates (Figure 1). The characteristic solid state structural features of these octahydroxy porphyrins are dictated by

(11) (a) Sheldrick, G. M. SHELXS-86. *Acta Crystallogr.* **1990**, *A46*, 467. (b) Sheldrick, G. M. SHELXL-93. *Program for the Refinement of Crystal Structures from Diffraction Data*; University of Goettingen, Germany, 1993.

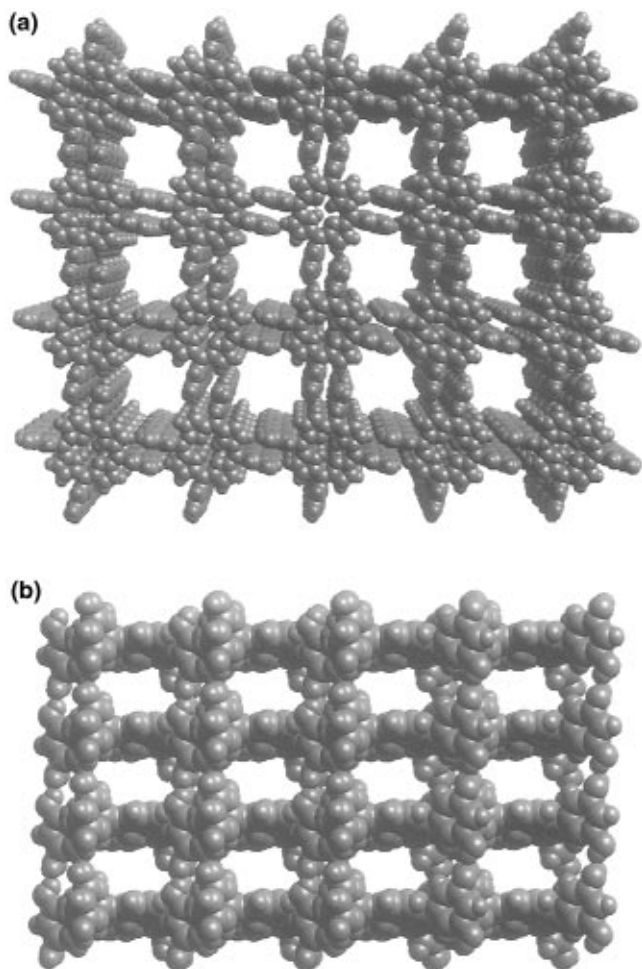


Figure 4. Molecular packing diagrams of $\text{H}_2\text{T}(3',5'\text{-DHP})\text{P}\cdot 5\text{EtOAc}$ (van der Waals spheres shown at 0.7 of atomic radii): (a) showing channels of 6.5 Å by 6.5 Å, between the columns; (b) showing channels of 3.4 Å \times 3.4 Å running perpendicular to the columns. Solvent molecules are not shown for clarity. Distances shown for the channels exclude van der Waals radii of 3.6 Å.

directional hydrogen bonding. This can lead to one-dimensional columnar structures, two-dimensional sheet structures, and three-dimensional networks. The order of discussion below follows the increasing dimensionality of these solid state structures. As a consequence of the constraints that the hydrogen-bonding networks impose, the solids of these complexes have very large amounts of solvate molecules in the lattice relative to previously known porphyrin crystals:^{2,5} in some cases, as many as seven solvates per porphyrin, with lattice solvate volume occupying as much as two-thirds of the total.

(A) Free Base Porphyrin Structures. To delineate the effect of substituent position on the crystal packing and porosity of the structure, diffraction quality crystals of $\text{H}_2\text{T}(3',5'\text{-DHP})\text{P}$ and $\text{H}_2\text{T}(2',6'\text{-DHP})\text{P}$ were obtained with the same lattice guest, ethyl acetate. The observed bond lengths and bond angles for the porphyrin macrocycle are not significantly different from that of the *meso*-tetraphenylporphyrin.²⁰

$\text{H}_2\text{T}(3',5'\text{-DHP})\text{P}\cdot 5\text{EtOAc}$. As shown in Figure 2, $\text{H}_2\text{T}(3',5'\text{-DHP})\text{P}\cdot 5\text{EtOAc}$ shows an essentially one-dimensional columnar structure and the unit cell has one porphyrin with five EtOAc molecules. The structure is controlled by the presence of strong, directional hydrogen bonding between the *meso*-(phenylhydroxyl) groups. The phenyl rings are roughly perpendicular to the porphyrin plane with angles of 70–85°. To optimize hydrogen-bonding interactions, the porphyrin macrocycles are almost planar and are nearly eclipsed with respect to one another within each of the columns. Hydrogen bonding exists only

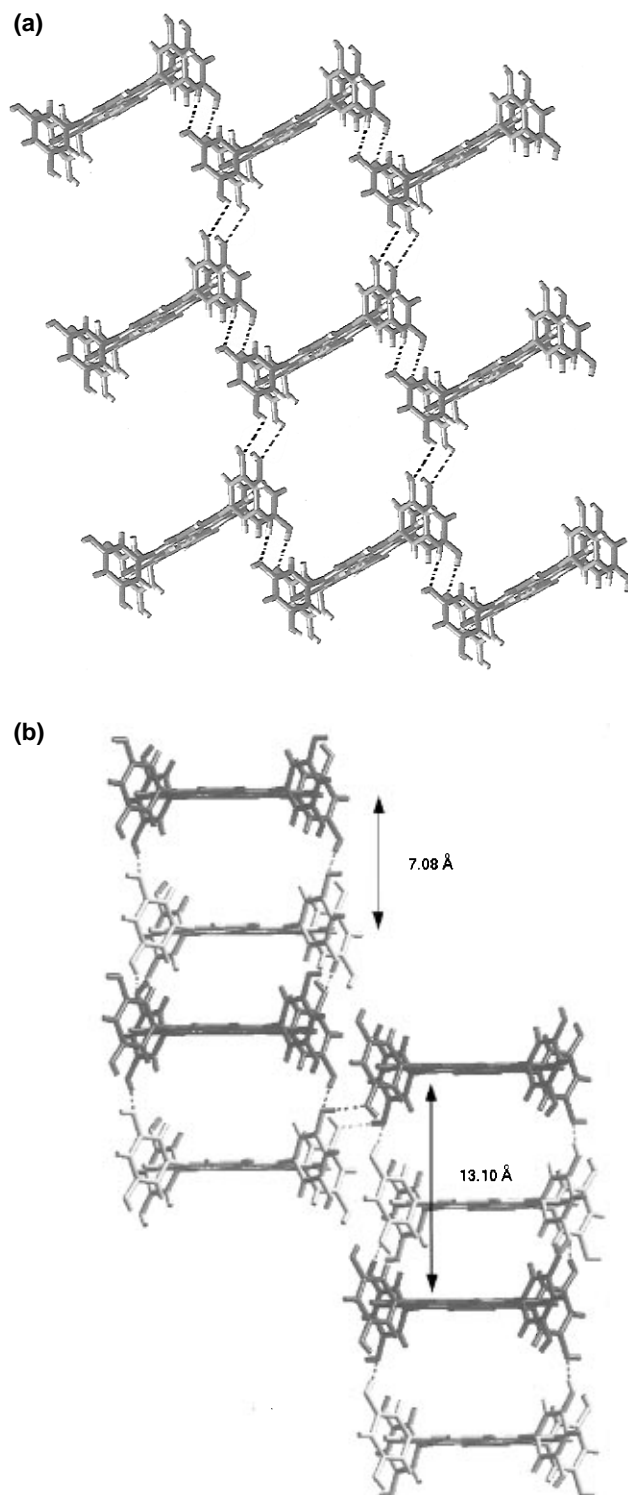


Figure 5. Depicts the molecular packing of $\text{H}_2\text{T}(3',5'\text{-DHP})\text{P}\cdot 7\text{C}_6\text{H}_5\text{CN}$ complex. Hydrogen bonds are shown in dotted lines. (a) Corrugated two-dimensional layer of hydrogen-bonded porphyrins. (b) Interconnections by hydrogen bonding between layers. The porphyrins in dark and light shades indicate front and back, respectively.

between each porphyrin and its nearest neighbor above and below within the column, with an interporphyrin plane separation of 7.0 Å and negligible π - π interactions between the macrocycles. The average O...O separation between hydrogen-bonded OH groups was found to be 2.68 Å, indicative of strong directional hydrogen bonding and comparable to previously reported structures.²

As shown in Figure 3, the columns stack parallel to one another, forming a porous network in $\text{H}_2\text{T}(3',5'\text{-DHP})\text{P}\cdot 5\text{EtOAc}$. There is no hydrogen bonding between columns, instead the

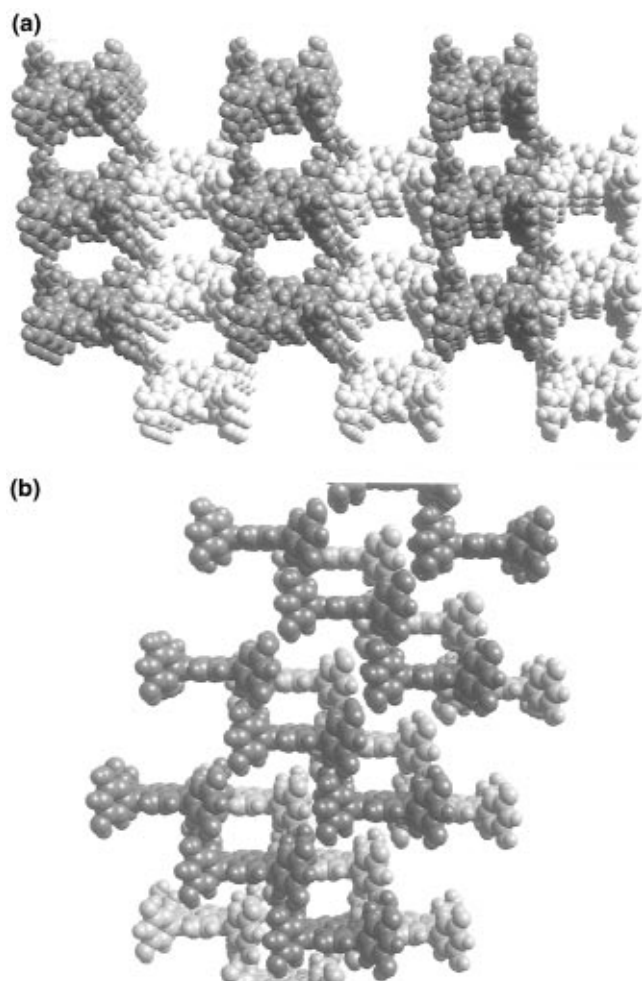


Figure 6. Molecular packing diagrams of $\text{H}_2\text{T}(3',5'\text{-DHP})\text{P}\cdot 7\text{C}_6\text{H}_5\text{CN}$: (a) showing channels of $5.5 \text{ \AA} \times 6.0 \text{ \AA}$ (molecules shown in light and dark shades indicates different one-dimensional corrugated sheets); (b) showing $4.0 \text{ \AA} \times 5.0 \text{ \AA}$ wide channels running approximately perpendicular to the channels shown in Figure 6a (molecules shown in dark and light shades indicate front and farther away, respectively). Atoms are drawn at 70% of their VDW atomic radii. Solvate molecules are not shown for clarity.

columns are held together by weak van der Waals forces. The closest intercolumnar phenyl–phenyl ring separations are at 3.79 and 3.69 Å, which indicate only limited π – π interaction between them. The center-to-center distance between the adjacent porphyrins of the neighboring columns is 14.83 Å. Four columns form a large solvate-filled channel of $6.5 \text{ \AA} \times 6.5 \text{ \AA}$ (van der Waals surface to van der Waals surface), i.e., a cross-sectional area of 42 \AA^2 (Figure 4a). There are two smaller channels ($3.4 \text{ \AA} \times 3.4 \text{ \AA}$) running perpendicular to each other and perpendicular to the columns, as shown in Figure 4b. The solvent molecules show some disorder and are free of any hydrogen-bonding interactions.

$\text{H}_2\text{T}(3',5'\text{-DHP})\text{P}\cdot 7\text{C}_6\text{H}_5\text{CN}$. For examination of the effect of the solvate on the molecular packing in these systems, crystals of $\text{H}_2\text{T}(3',5'\text{-DHP})\text{P}$ were grown from benzonitrile, a much larger solvate molecule. The solid state structure of $\text{H}_2\text{T}(3',5'\text{-DHP})\text{P}\cdot 7\text{C}_6\text{H}_5\text{CN}$ is dramatically altered by the benzonitrile (Figure 5). The structure has changed from a one-dimensional columnar structure (for ethyl acetate) to a three-dimensional corrugated slipped-stack structure, with a pore size matched to the benzonitrile. Two corrugated sheets (Figure 5a) are interconnected by a third, which forms the observed three-dimensional structure. The unit cell contains 2 planar porphyrin molecules and 14 benzonitrile solvate molecules. Molecular packing diagrams (Figure 6) show two solvate-filled channels

perpendicular to each other with sizes of $5.5 \text{ \AA} \times 6.0 \text{ \AA}$ (i.e., cross-sectional area 33 \AA^2) and $4.0 \text{ \AA} \times 5.0 \text{ \AA}$, respectively. Porphyrin molecules are arranged in an offset fashion to favor hydrogen-bonding interactions at the expense of π – π interactions.

In the structure of $\text{H}_2\text{T}(3',5'\text{-DHP})\text{P}\cdot 7\text{C}_6\text{H}_5\text{CN}$, each porphyrin is hydrogen bonded to three closest neighbor porphyrins. The center-to-center distance between the adjacent layers is about 12.6 Å, and the vertical distance between nearest hydrogen-bonded porphyrins is 7.4 Å. Porphyrins are arranged in an offset fashion within the sheet to maximize hydrogen bonding between the OH groups, with a mean porphyrin–porphyrin vertical separation of 7.08 Å. Within the layer, the average $\text{O}\cdots\text{O}$ distance between the hydrogen-bonded OH groups is 2.85 Å. The largest vertical separation between the two nearest neighbors in a given sheet is 13.10 Å. The two corrugated layers are held together by means of hydrogen bonding ($\text{OH}\cdots\text{OH}$) with a mean $\text{O}\cdots\text{O}$ distance of 2.73 Å. Hydrogen bonding between the porphyrins is partially disrupted by the benzonitrile due to hydrogen bonding from the porphyrin hydroxyl groups to nitriles of the solvates with an average $\text{O}\cdots\text{N}$ distance of 2.85 Å. Two benzonitrile molecules are located above the porphyrin plane with a mean plane separation of 3.60 Å. The closest separation between the neighboring porphyrin phenyl rings is 3.44 Å.

$\text{H}_2\text{T}(2',6'\text{-DHP})\text{P}\cdot 4\text{EtOAc}$. When the position of the hydroxyl substituents is changed from the *m*- to the *o*- positions of the phenyl rings, a substantial change in the structure occurs: $\text{H}_2\text{T}(2',6'\text{-DHP})\text{P}\cdot 4\text{EtOAc}$ has a two-dimensional layered structure, as shown in the molecular packing diagram in Figure 7. The unit cell has two porphyrins, each with four ethyl acetate molecules. The porphyrin rings are slightly ruffled and show strong directional hydrogen bonding induced by the peripheral hydroxyl groups. Each porphyrin has four hydrogen-bonded nearest neighbors in an offset orientation. The average hydrogen-bonding distance ($\text{O}\cdots\text{O}$) is 2.79 Å. In a given layer, the vertical distance between the offset porphyrins is 7.0 Å. The center-to-center distance between the adjacent layers is 11.8 Å, and no hydrogen bonding occurs between the porphyrinic layers. This suggests a minimal interaction between the layers which are held together by van der Waals forces.

There exists an interesting interaction between the layers in $\text{H}_2\text{T}(2',6'\text{-DHP})\text{P}\cdot 4\text{EtOAc}$. *meso*-Aryl rings of the adjacent layers are at a mismatched orientation with one aryl C–H pointing into the middle of another aryl ring on a porphyrin in the adjacent layer. The slightly short distance of 3.33 Å from the aryl C–H to the adjacent porphyrin aryl-carbon indicates there is weak $\text{C}\text{--}\text{H}\cdots\pi$ interactions between the layers.¹² A channel of about $3.0 \text{ \AA} \times 3.6 \text{ \AA}$ (van der Waals surface to van der Waals surface) runs along the layers and is filled with ethyl acetate molecules (Figure 8). Ethyl acetate molecules in the lattice are hydrogen bonded through their carbonyl groups to the hydroxyl groups of the porphyrins with an $\text{O}\cdots\text{O}$ average distance of 2.65 Å.

(B) Metalloporphyrin Structures. For examination of the effects of metallation on the structures and porosity of these octahydroxy porphyrins, Zn(II) and Mn(III) complexes were prepared and crystallized. These both form axially ligated complexes under crystallization conditions, which increases the steric demands of the porphyrin building block. For Zn(II)

(12) (a) Steiner, T. *J. Chem. Soc., Chem. Commun.* **1995**, 95. (b) Hunter, R.; Hauelsen, R. H.; Irving, A. *Angew. Chem., Int. Ed. Engl.* **1994**, 33, 566. (c) Desiraju, G. R. *Acc. Chem. Res.* **1996**, 29, 441.

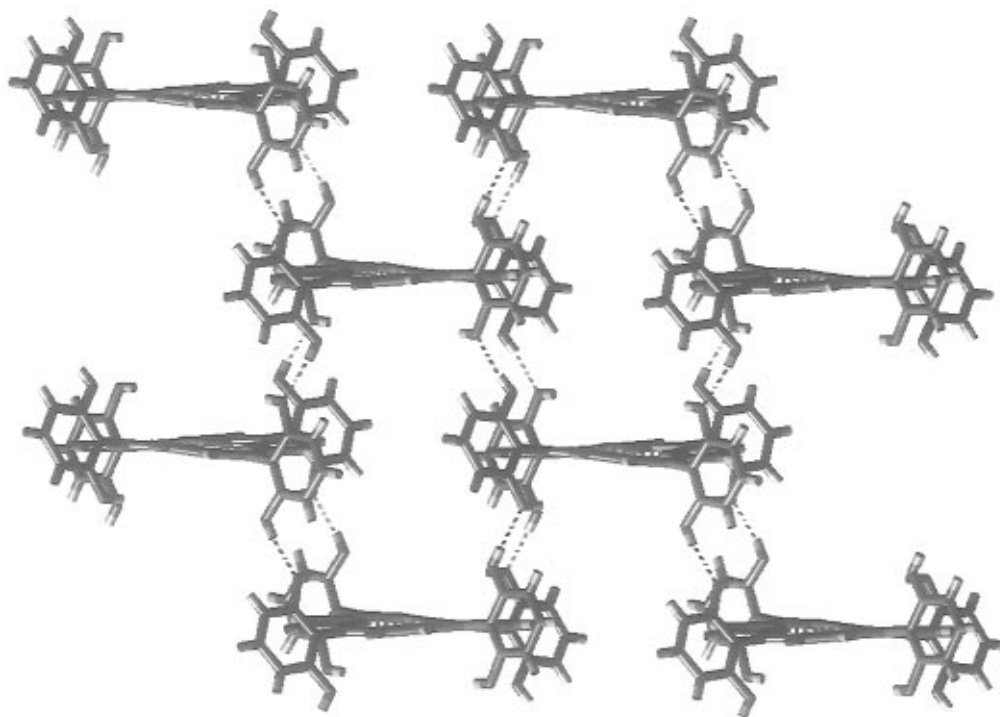


Figure 7. Molecular packing diagram of $H_2T(2',6'\text{-DHP})P \cdot 4EtOAc$ showing a two-dimensional layered structure. Hydrogen-bonding interactions between the hydroxyl groups are shown with dotted lines. Solvent molecules are not shown for clarity.

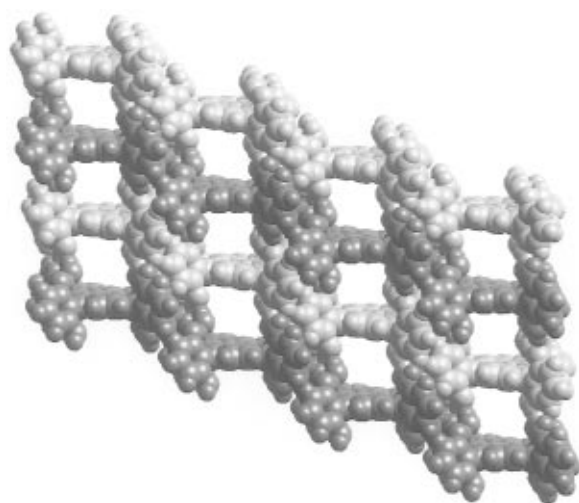


Figure 8. Molecular packing diagram of $H_2T(2',6'\text{-DHP})P \cdot 4EtOAc$ showing $3.0 \text{ \AA} \times 3.6 \text{ \AA}$ wide channels along the layers. Space filling is shown at 0.7 of VDW atomic radii, and solvent molecules are not shown for clarity. Distances shown for the channels exclude van der Waals radii of 3.6 \AA . The porphyrins in dark and light shades indicate that they are closer and further away, respectively.

metalloporphyrins, six-coordinate¹³ complexes are less common than five-coordinate^{4,14} ones. Mn(III) on the other hand generally forms six-coordinate complexes in the presence of excess ligands; in addition, the Mn(III) have a counteranion to place in the lattice as well. The observed bond lengths and bond angles for the metalloporphyrin macrocycles are not significantly different from those of similar metal complexes of the *meso*-tetraphenylporphyrin.

Zn[T(2',6'-DHP)P](EtOAc)₂·2EtOAc. Crystals of $H_2T(2',6'\text{-DHP})P$ and $Zn[T(2',6'\text{-DHP})P](EtOAc)_2$ were prepared with the same solvate (i.e., guest) to delineate the effect of axial ligation on the crystal packing and structural porosity. As shown

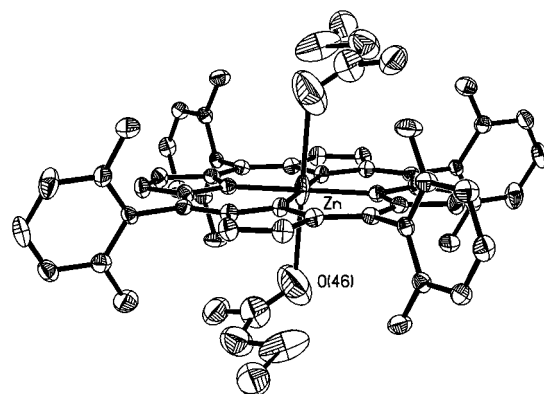


Figure 9. ORTEP diagram of the metalloporphyrin unit in the crystal structure of $Zn[T(2',6'\text{-DHP})P](EtOAc)_2 \cdot 2EtOAc$

in Figure 9, the porphyrin ring is nearly planar in $Zn[T(2',6'\text{-DHP})P]$ while it is slightly ruffled in $H_2T(2',6'\text{-DHP})P$. It can be seen that both crystals have four ethyl acetates per porphyrin. The ethyl acetate molecules are hydrogen bonded to hydroxyl groups in $H_2T(2',6'\text{-DHP})P$, whereas for the Zn(II) complex, two ethyl acetate molecules are bonded to the metal center (Figure 9), while the other two are hydrogen bonded to the OH groups of the porphyrin. Axially ligated ethyl acetate molecules are in a *trans*-orientation and are bonded through the carbonyl oxygen of the ester with an average Zn–O distance of $2.532\text{--}(3) \text{ \AA}$. This rather long bond length may represent a crystallographic average of twin disordered five-coordinate complexes with the Zn atom out of the porphyrin plane closer to one ethyl acetate and with the second (*trans*) ethyl acetate only very loosely interacting. The large thermal parameters in the axial direction of the Zn and of the coordinated carbonyl oxygen make this a plausible explanation. Unfortunately, the Zn atom is at a center of inversion in this structure, so it is not possible to be more definitive. The average equatorial Zn–N distance is an unexceptional $2.043(2) \text{ \AA}$.

The molecular packing structure of $Zn[T(2',6'\text{-DHP})P](EtOAc)_2 \cdot 2EtOAc$ exhibits a two-dimensional layered structure (Figure 10) remarkably similar to that found in $H_2T(2',6'\text{-$

(13) (a) Schauer, G. C.; Anderson, O. P.; Eaton, S. S.; Eaton, G. R. *Inorg. Chem.* **1985**, *24*, 4082. (b) Bhyrappa, P.; Krishnan, V.; Nethaji, M. *J. Chem. Soc., Dalton Trans.* **1993**, 1901.

(14) Collins, D. M.; Hoard, J. L. *J. Am. Chem. Soc.* **1970**, *92*, 3761.

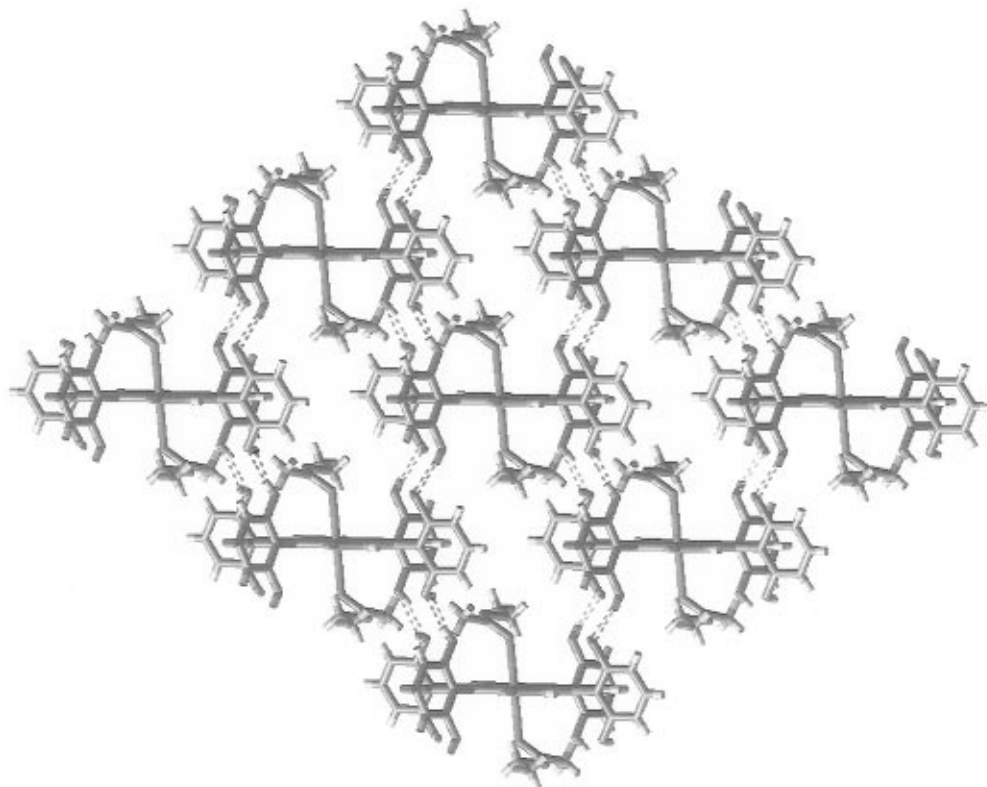


Figure 10. Molecular packing diagram of two-dimensional layered structure of $\text{Zn}[\text{T}(2',6'\text{-DHP})\text{P}](\text{EtOAc})_2 \cdot 2\text{EtOAc}$; a single plane of hydrogen-bonded porphyrin complexes is shown. The solvate (noncoordinated) molecules are not shown for clarity.

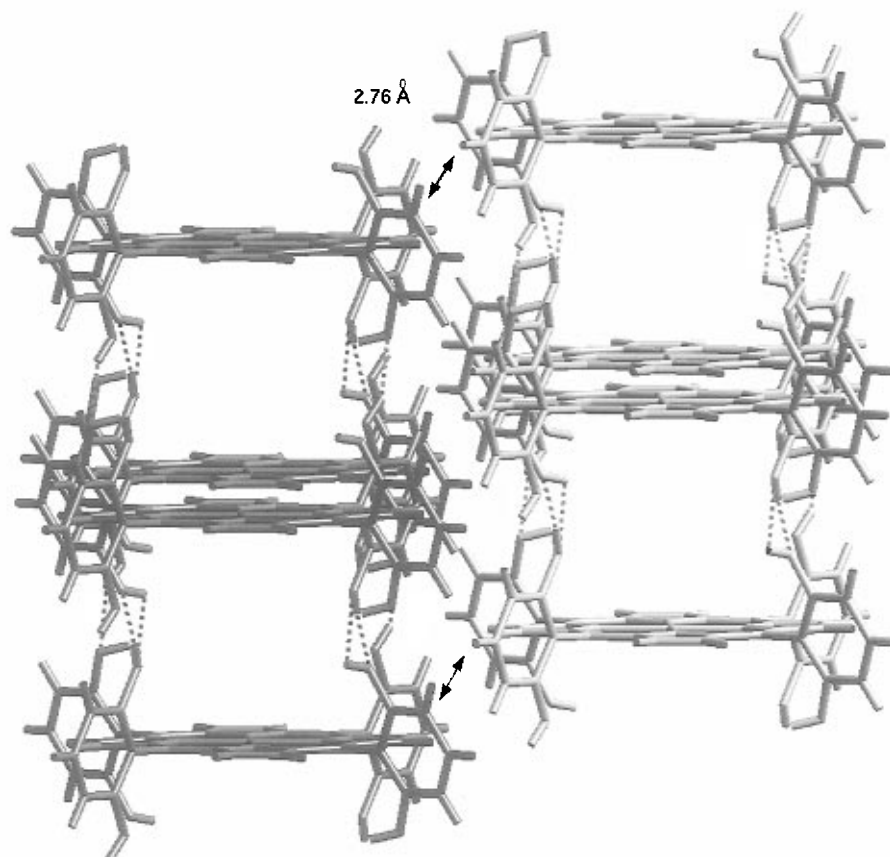


Figure 11. A perspective view of the $\text{Zn}[\text{T}(2',6'\text{-DHP})\text{P}](\text{EtOAc})_2 \cdot 2\text{EtOAc}$ showing interlayer ($\text{C}-\text{H} \cdots \pi$) interaction between layers. Coordinated ethyl acetate molecules are not shown for clarity. Hydrogen-bonding interactions are shown with dotted lines. Molecules shown in dark and light shades indicate front and farther away, respectively.

$\text{DHP})\text{P} \cdot 4\text{EtOAc}$. The two noncoordinated EtOAc molecules are hydrogen bonded to the hydroxyl groups with an $\text{O} \cdots \text{O}$ distance of 2.620 Å. The weakly coordinated ethyl acetate molecules help fill the solvated channel space. The porphyrins

interact through peripheral hydroxyl groups via strong directional hydrogen bonding and are arranged in an offset fashion with an interporphyrin vertical separation of 6.91 Å. The average hydrogen-bonding distance for $\text{O} \cdots \text{O}$ ($\text{HO} \cdots \text{HO}$) is 2.75

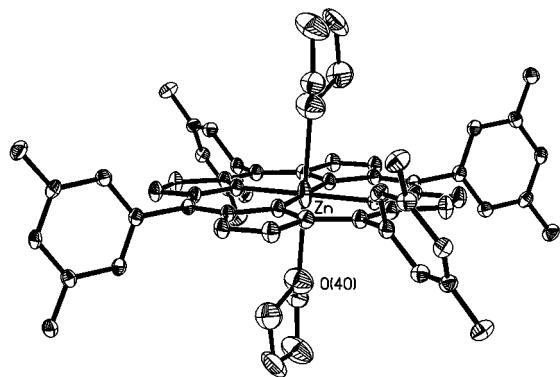
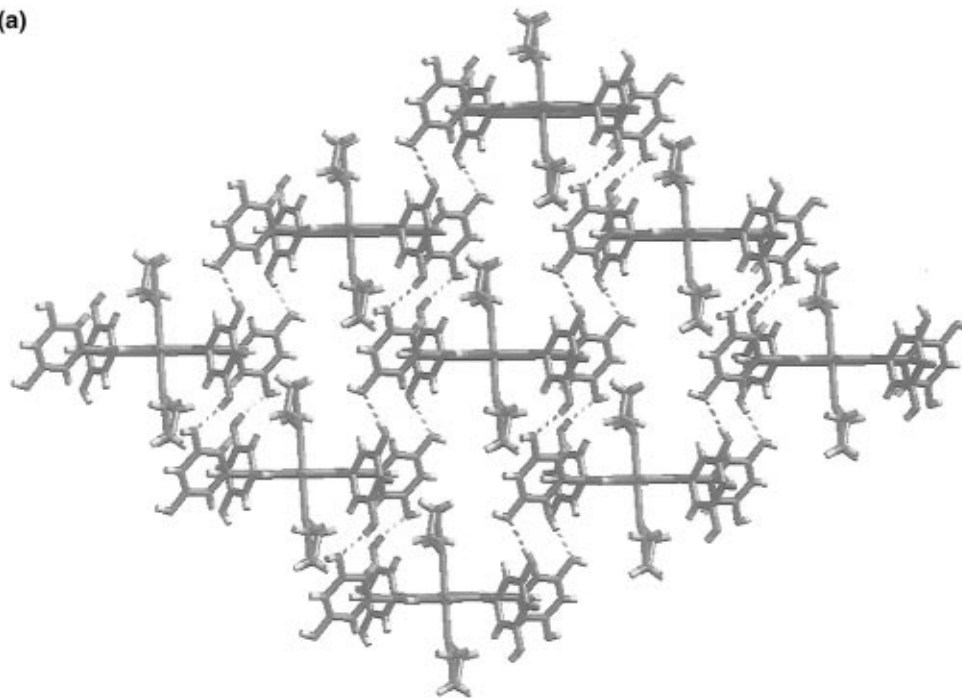


Figure 12. ORTEP diagram of the metalloporphyrin unit in the crystal structure of $\text{Zn}[\text{T}(3',5'\text{-DHP})\text{P}](\text{THF})_2 \cdot 2\text{THF} \cdot 3\text{CH}_2\text{Cl}_2$.

(a)



(b)

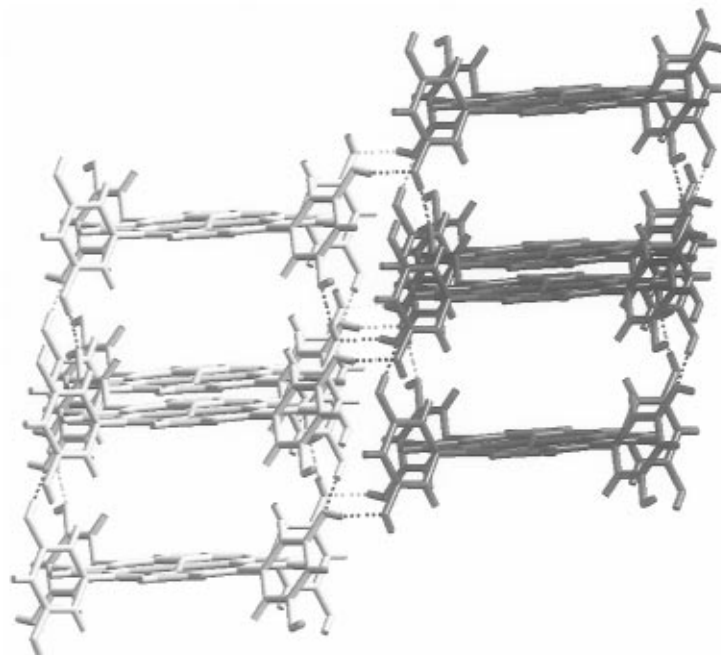


Figure 13. (a) Two-dimensional layer from the crystal structure of $\text{Zn}[\text{T}(3',5'\text{-DHP})\text{P}](\text{THF})_2 \cdot 2\text{THF} \cdot 3\text{CH}_2\text{Cl}_2$. Noncoordinated solvates are not shown for clarity. (b) Molecular packing diagram of $\text{Zn}[\text{T}(3',5'\text{-DHP})\text{P}](\text{THF})_2 \cdot 2\text{THF} \cdot 3\text{CH}_2\text{Cl}_2$ showing interconnected layers. Porphyrins in dark and light shades indicate two different layers. Hydrogen-bonding interactions are shown with dotted lines. Noncoordinated solvates are not shown for clarity.

Å. Each layer is separated by a center-to-center distance of 11.00 Å. No hydrogen bonding was observed between the layers.

As seen with $\text{H}_2\text{T}(2',6'\text{-DHP})\text{P} \cdot 4\text{EtOAc}$, there exists an unusual interaction between the hydrogen-bonded porphyrin layers in $\text{Zn}[\text{T}(2',6'\text{-DHP})\text{P}](\text{EtOAc})_2 \cdot 2\text{EtOAc}$. *meso*-aryl rings of the adjacent layers are at a mismatched orientation with one aryl C–H pointing into the middle of another aryl ring on a porphyrin in the adjacent layer (Figure 11). The short distance of 2.71 Å from the aryl C–H to the adjacent porphyrin aryl-carbon indicates there is some C–H $\cdots\pi$ interactions between the layers.¹²

$\text{Zn}[\text{T}(3',5'\text{-DHP})\text{P}](\text{THF})_2 \cdot 2\text{THF} \cdot 3\text{CH}_2\text{Cl}_2$. Crystals were not forthcoming from $\text{Zn}[\text{T}(3',5'\text{-DHP})\text{P}]$ in ethyl acetate, but

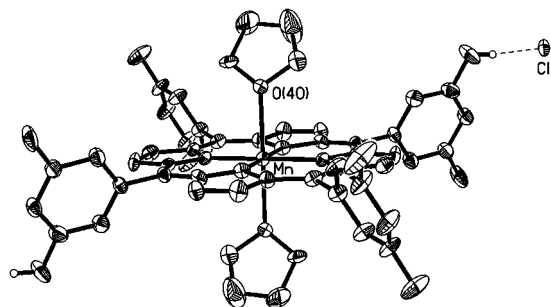


Figure 14. ORTEP diagram of the metalloporphyrin unit in the crystal structure of $\text{Mn}[\text{T}(3',5'\text{-DHP})\text{P}](\text{THF})_2 \cdot \text{Cl} \cdot 2\text{THF} \cdot 5\text{C}_6\text{H}_5\text{CH}_3$.

were formed upon crystallization from THF. The porphyrin ring is planar with a six-coordinate geometry at the Zn(II) center. Two oxygen atoms of axial THF molecules are bonded to Zn(II) center with a Zn–O distance of 2.44(2) Å (Figure 12). The average Zn–N distance in the equatorial plane is 2.045(3) Å.

A dramatic change in the crystal packing of $\text{H}_2\text{T}(3',5'\text{-DHP})\text{P}$ arises with the inclusion of Zn(II) ion. The unit cell of Zn-

$[\text{T}(3',5'\text{-DHP})\text{P}](\text{THF})_2 \cdot 2\text{THF} \cdot 3\text{CH}_2\text{Cl}_2$ has one porphyrin and seven solvate molecules (including the ligated THF). A molecular packing diagram showing a two-dimensional layered structure is shown in Figure 13a. Each porphyrin has four nearest hydrogen-bonded porphyrin neighbors. The interplanar separation between the hydrogen-bonded neighbors in a given layer is 6.81 Å. Within each layer the overlapping porphyrins are separated by 13.32 Å. The porphyrins are arranged in a slipped-stack orientation within the layer to maximize hydrogen-bonding interactions, with a mean O···O separation of 2.72 Å.

The two noncoordinated THF molecules are hydrogen bonded to the porphyrin OH groups. The (O···O) separation is 2.62 Å within the layers and 2.71 Å between the layers. Two layers are interconnected to give a three-dimensional structure, as shown in Figure 13b. The planes of the phenyl rings are offset between the adjacent layer, separated by a distance of 5.0 Å, and show negligible π – π interaction. The nearest neighbor in the adjacent layer is offset by a vertical distance of 4.98 Å from the porphyrin plane. In this complex, the adjacent layers are held together by means of hydrogen-bonding interactions, while

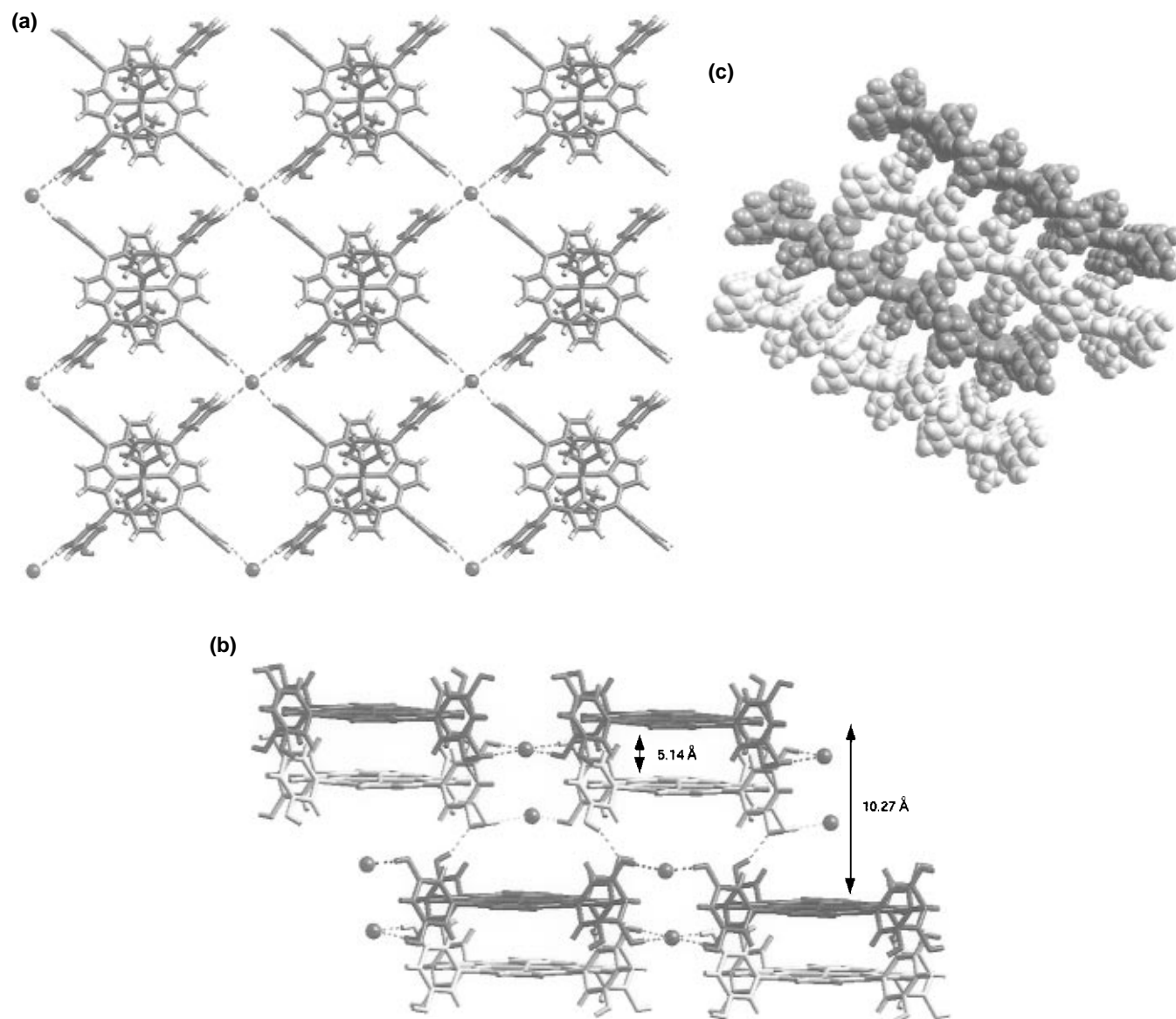


Figure 15. Molecular packing diagrams of $\text{Mn}[\text{T}(3',5'\text{-DHP})\text{P}](\text{THF})_2 \cdot \text{Cl} \cdot 2\text{THF} \cdot 5\text{C}_6\text{H}_5\text{CH}_3$. The porphyrins in light and dark shades indicate farther away and front, respectively. (a) Two-dimensional sheets of porphyrins (001 plane) linked by unusual square-planar Cl^- anions hydrogen bonding to four metalloporphyrins. Spheres indicate bridging chloride ions. Solvate molecules and coordinated THF ligands are not shown for clarity. (b) A perpendicular view of the (100) plane showing interporphyrin hydrogen-bonding interactions. Spheres indicate bridging chloride ions. Solvate molecules and coordinated THF ligands are not shown for clarity. (c) Space-filled diagram showing channels of $4.6 \text{ \AA} \times 3.4 \text{ \AA}$ (0.7 of their VDW atomic radii), viewed along the 100 plane (i.e., down the *b* axis). Noncoordinated solvates are not shown for clarity.

Table 1. Calculation of Channel Volumes for Various Porphyrin Complexes

porphyrin complex	Z	unit cell vol. (Å ³)	porphyrin vol./unit cell ^a (Å ³)	solvate vol./unit cell ^a (Å ³)	void vol./unit cell ^a (Å ³)	total channel vol./unit cell ^b (Å ³)
H ₂ TPP ^c	1	801.9	590.8	0	211	211 [26.3%]
H ₂ T(3',5'-DHP)P•5EtOAc	1	1581	620.8	412.5	547.7	960.2 [60.7%]
H ₂ T(2',6'-DHP)P•4EtOAc	2	2770.9	1233.0	660	877.9	1537.9 [55.5%]
H ₂ T(3',5'-DHP)P•7C ₆ H ₅ CN	2	3811	1241.6	1547	1022	2569.4 [67.4%]
Zn[T(2',6'-DHP)P](EtOAc) ₂ •2EtOAc	1	1387.2	804.1	168	415.2	583.2 [42.0%]
Zn[T(3',5'-DHP)P](THF) ₂ •3CH ₂ Cl ₂ •2THF	1	1597.6	755.8	326.9	514.8	841.7 [52.7%]
Mn[T(3',5'-DHP)P](THF) ₂ •Cl•2THF•5C ₆ H ₅ CH ₃	2	4289	1612.2	1355	1321.8	2676.7 [62.4%]

^a Porphyrin and solvate van der Waals volumes were calculated using Quanta for each unit cell. Void volume is defined as the unit cell volume minus the sum of the porphyrin volume and the solvate volume. For the metalloporphyrins, the volumes of the coordinated ligands were counted as part of the porphyrin volume. ^b Total channel volume is defined as the sum of void and solvate volume, in Å³. Values in brackets refer to the percentage of total channel volume in the unit cell. ^c Crystallographic data is taken from ref 20.

the porphyrin layers in the H₂T(2',6'-DHP)P•4EtOAc crystal lattice interact only with weaker van der Waals and C–H⋯π interactions.

Mn[T(3',5'-DHP)P](THF)₂•Cl•2THF•5C₆H₅CH₃. Generally, Mn(III) porphyrin chloride derivatives retain Cl⁻ as the axial ligand, regardless of the solvent employed. They tend to show both five- and six-coordination geometry in the solid state depending on the crystallization solvent.^{4,15–19} For example, even crystallization of MnTPP(Cl) from 1:1 benzene/pyridine solution does not displace the coordinated Cl⁻, instead producing a six-coordinate complex with pyridine occupying the sixth coordination site.¹⁶

Surprisingly, for Mn[T(3',5'-DHP)P]Cl, the Mn(III) porphyrin is six-coordinate with *two* axially ligated THF molecules (Figure 14). The average equatorial Mn–N distance is 2.004(2) Å, and the average axial Mn–O distance is 2.320(2) Å. A few six-coordinate complexes derived from MnTPP(ClO₄) have been reported in the literature, including [MnTPP(CH₃OH)₂](ClO₄),¹⁷ [MnTPP(DMF)₂](ClO₄),¹⁸ and [MnTPP(2,6-lutidine *N*-oxide)₂](ClO₄).¹⁹

A chloride ion bridges four hydroxyl groups from four different porphyrins in a square planar arrangement with an average Cl⋯O distance of 3.01 Å, as shown in Figure 15a,b. This unusual mode of anion coordination in Mn[T(3',5'-DHP)P](THF)₂•Cl•2THF•5C₆H₅CH₃ is probably due to lattice stabilization by the hydrogen bonding between the Cl⁻ and HO groups.

Packing diagrams of Mn[T(3',5'-DHP)P](THF)₂•Cl•2THF•5C₆H₅CH₃ are shown in Figure 15. In Figure 15a, one can see the two-dimensional porphyrin layers held together by the unusual square-planar Cl⁻ anions, each hydrogen bonding to four metalloporphyrin molecules. Figure 15b show that these layers are themselves interconnected through hydrogen bonding between metalloporphyrins of different layers, resulting in the three-dimensional network structure. The largest distance between the adjacent porphyrins within a layer is 10.27 Å, while a shortest distance between the offset porphyrins is 5.14 Å. The molecules are arranged alternatively in an offset fashion to give interconnected layers. The distance between the aryl rings of the adjacent porphyrins is greater than 4.69 Å, showing no π–π interaction between the porphyrins. Within a given layer, the

distance between Mn(III) centers is 16.44 Å, while a 13.13 Å separation is observed between two adjacent Mn(III) centers in different planes.

A space-filled molecular packing diagram shown in Figure 15c reveals 4.6 Å × 3.4 Å channels. There is a very large amount of solvate in the lattice. The five toluene molecules show some disorder, whereas the two unligated THF solvates are well ordered. The axially coordinated THF ligands partially fill the remaining void volume.

Molecular Modeling. To rationalize the crystal packing and the void space in these lattices, molecular modeling studies were performed on these structures. Molecular van der Waals radii of the solvate and the porphyrin or metalloporphyrin complex were calculated from energy-minimized structures. The total void volume of the unit cell was calculated by subtracting total solvate and porphyrin volumes from crystallographic unit cell volume and are summarized in Table 1. The porosity of these structures is striking. Even though porphyrin structures have been noted for high porosity, very few free base porphyrin structures show more than three solvates per porphyrin:^{2,5} triclinic H₂TPP, for example, has *no* solvate.²⁰ As noted in Table 1, for these hydrogen-bonding porphyrins, the total channel volume is typically one-half to two-thirds of the total unit cell.

There is no systematic difference in void space for H₂T(2',6'-DHP)P versus H₂T(3',5'-DHP)P or their derivatives. Metal ions do not appear to influence void volume significantly, and the total channel volumes are comparable to the free base structures, if one counts the coordinated solvate ligands.

Conclusions

A series of two tetrakis(dihydroxyphenyl)porphyrins and their metal complexes have been explored as nanoporous supramolecular hydrogen-bonded network solids. The crystal structures for six such compounds have been determined. The self-assembly of these porphyrin networks is dominated by directional hydrogen bonding and is largely independent of π–π interactions. Profound structural differences arise by simple permutation of phenyl substitution, solvate, and metal ion. Examples of one-dimensional columnar, two-dimensional layered, and three-dimensional network structures have all been found. In these structures, solvate-filled channels are observed with cross-sectional areas as large as 42 Å². The pore volumes

(15) (a) Cheng, H.; Scheidt, W. R. *Acta. Crystallogr.* **1996**, C52, 361.

(b) Tulinsky, A.; Chen, B. M. L. *J. Am. Chem. Soc.* **1977**, 99, 3647.

(16) Kirner, J. F.; Scheidt, W. R. *Inorg. Chem.* **1975**, 14, 2081.

(17) Hatano, K.; Anzai, K.; Itaka, Y. *Bull. Chem. Soc. Jpn.* **1983**, 56, 422.

(18) Hill, C. L.; Williamson, M. M. *Inorg. Chem.* **1985**, 24, 2836.

(19) Hill, C. L.; Williamson, M. M. *Inorg. Chem.* **1985**, 24, 3024.

(20) Silvers, S. J.; Tulinsky, A. *J. Am. Chem. Soc.* **1967**, 89, 3331.

of these channels are exceptionally large and can be as much as two-thirds of the total unit cell volume.

The present study demonstrates the effect of the directionality of the porphyrin substituents and size of the solvate on the supramolecular architectures of these molecules. We are currently exploring the possibility of using these supramolecular architectures in conjunction with the established reactivity of

(21) (a) Suslick, K. S. In *Comprehensive Supramolecular Chemistry*; Bioinorganic Systems; Lehn, J. M., Ed.; Elsevier: London, 1996; Vol. 5, p 141. (b) Suslick, K. S.; Cook, B. R.; Fox, M. M. *J. Chem. Soc., Chem. Commun.* **1985**, 580. (c) Cook, B. R.; Reinert, T. J.; Suslick, K. S. *J. Am. Chem. Soc.* **1986**, 108, 7281. (d) Suslick, K.; Cook, B. *J. Chem. Soc., Chem. Commun.* **1987**, 200. (e) Suslick, K. S.; Cook, B. R. Shape Selective Oxidation as a Mechanistic Probe. In *Inclusion Phenomena and Molecular Recognition*; Atwood, J. L., Ed.; Plenum Press: London, 1990; pp 209–215.

metalloporphyrins to create heterogeneous catalysts for shape selective oxidations.²¹

Acknowledgment. We thank Teresa Prussak for technical assistance in solving the crystal structures. This work was supported by the National Institute of Health (HL 5R01-25934) and in part by the DOE (DEFG0291ER45439).

Supporting Information Available: Tables of crystallographic data including atomic positional, thermal parameters, bond lengths, and bond angles for all the six crystal structures (46 pages). See any current masthead page for ordering and Internet access instructions.

JA971093W

Synthetic Heme–Peptide Complexes

David L. Huffman, Michael M. Rosenblatt, and Kenneth S. Suslick*

School of Chemical Sciences
University of Illinois at Urbana–Champaign
Urbana, Illinois 61801

Received February 1, 1997

Revised Manuscript Received May 9, 1998

The “mesomolecular” regime (i.e., from roughly 1000 to 10 000 amu) represents an emerging field that has only recently become synthetically and analytically accessible. We report here the synthesis and characterization of mesomolecular synthetic analogues of heme proteins. While small-molecule studies have provided extremely useful insights into structure–function relationships in heme proteins,¹ there often remain significant differences between the properties of the synthetic analogs and the heme proteins themselves. There has been considerable recent interest in peptides that bind metalloporphyrins and the de novo design of artificial heme proteins. Three general classes of complexes have emerged: heme-bound helical bundle peptides;² peptides covalently attached to the heme periphery;³ and disulfide–dimer peptides coordinated to exchange-inert metalloporphyrins.⁴ Relatively little is yet known, however, about the factors that influence peptide binding to metalloporphyrins. We have prepared a series of peptides that form 1:2 metalloporphyrin–peptide complexes and examined the effect of their sequence on binding constants, secondary structure, and electrochemical behavior.

The utilization of peptides as ligands for metalloporphyrins poses several challenges: viz., control of conformational demands to favor metal coordination, enhancement of water solubility, and optimization of intramolecular interactions. To simplify characterization and interpretation, we have limited our peptides to amphiphilic 15-mers with a restricted repertoire of amino acid residues. We chose this size because this is roughly the minimum necessary to form good α -helices (~4 turns).⁵ For comparison, a metalloporphyrin is about 1.0 nm across, i.e., about two helix turns (0.54 nm per turn). The peptides also possess a palindromic sequence symmetry about the central ligating residue (in these cases, the imidazole of a histidine). To delineate the factors that stabilize heme–peptide complexes, we have systematically altered key peptide residues in contact with the heme. The remaining residues of the sequences were chosen to encourage helix formation and good solubility. For strong intrinsic helix-forming ability,⁶ Aib,⁷ Ala, Leu, Lys, and Nva were used. To probe hydrophobic interactions, Phe, Leu, Nva, Ala, and Ser were

(1) Collman, J. P. *Inorg. Chem.* **1997**, *36*, 5145. (b) Traylor, T. G. *Pure Appl. Chem.* **1991**, *63*, 265. (c) Van Deusen-Jeffries, S.; Suslick, K. S. *Comprehensive Supramolecular Chemistry*; Lehn, J. M., Ed.; Elsevier Publishers: Oxford, 1996; Vol. 5, pp 141–170.

(2) Bryson, J. W.; Betz, S. F.; Lu, H. S.; Suich, D. J.; Zhou, H. X.; O’Neil, K. T.; DeGrado, W. F. *Science* **1995**, *270*, 935 and references therein.

(3) Arnold, P. A.; Benson, D. R.; Brink, D. J.; Hendrich, M. P.; Jas, G. S.; Kennedy, M. L.; Petasis, D. T.; Wang, M. *Inorg. Chem.* **1997**, *36*, 5306 and references therein. (b) Nastri, F.; Lombardi, A.; Morelli, G.; Maglio, O.; D’Auria, C. P.; Pavone, V. *Chem. Eur. J.* **1997**, *3*, 340. (c) Karpishin, T. B.; Vannelli, T. A.; Glover, K. J. *J. Am. Chem. Soc.* **1997**, *119*, 9063.

(4) Arnold, P. A.; Shelton, W. R.; Benson, D. R. *J. Am. Chem. Soc.* **1997**, *119*, 3181. (b) Sakamoto, S.; Sakurai, S.; Ueno, A.; Mihara, H. *Chem. Commun.* **1997**, 1221.

(5) Padmanabhan, S.; Marqusee, S.; Ridgeway, T.; Laue, T. M.; Baldwin, R. L. *Nature* **1990**, *344*, 268.

(6) Shoemaker, K. R.; Kim, P. S.; York, E. J.; Stewart, J. M.; Baldwin, R. L. *Nature* **1987**, *326*, 563. (b) O’Neil, K. T.; DeGrado, W. F. *Science* **1990**, *250*, 646. (c) Pingchiang, C. L.; Sherman, J. C.; Chen, A.; Kallenbach, N. R. *Proc. Natl. Acad. Sci. U.S.A.* **1991**, *88*, 5317.

(7) Basu, G.; Baghi, K.; Kuki, A. *Biopolymers* **1991**, *31*, 1763.

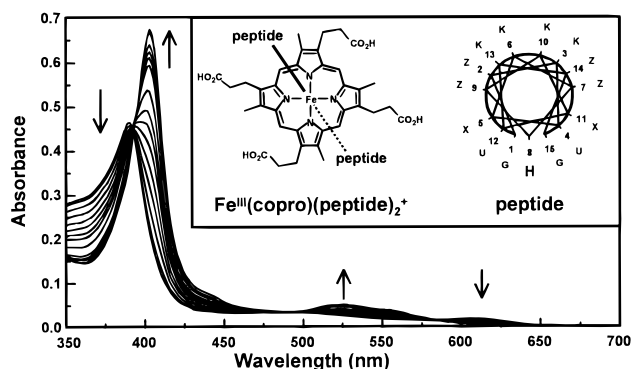


Figure 1. Spectrophotometric titration of coproporphyrin-I-ato iron(III) with peptide AA-A.

Table 1. Properties of Fe^{III} Coproporphyrin–Peptide Complexes

ligand ^a	hydrophobicity (kcal/mol)	K (mM ⁻²) ^b	$K/K_{\text{His-OMe}}$	$E_{1/2}$ (mV) ^c	θ_{ub} (deg cm ² /dmol) ^d	θ_{b} (deg cm ² /dmol) ^e
His		0.0081	0.32	-214		
His-OCH ₃		0.025	1.0			
AA-A	1.74	0.23	9.0	-223	-1530	-10 200
LL-A	9.87	1.62	65	-252	-3910	-11 600
NvNv-A	7.64	3.1	120	-238	-2420	-10 800
SS-Aib	-3.38	0.25	10	-218	-1940	-2 840
AA-Aib	1.74	2.6	100	-253	-2810	-11 300
FA-Aib	5.97	15.4	620	-300	-2910	-12 800
LL-Aib	9.87	22.7	910	-288	-6760	-13 800
NvNv-Aib	7.64	24.1	1000	-268	-3030	-12 200
FF-Aib	10.20	47	1880	-304	-2210	-7 670

^a Abbreviations: UX-Z, 15-mer peptide, Ac-GZKUXKZHKKX-UKZG-NH₂; copro, coproporphyrin-I-ate(2-); His-OCH₃, methyl ester of His. ^b Binding constants in 500 mM MOPS, pH 7 at 25 °C; errors less than $\pm 5\%$. ^c Relative to NHE with a glassy carbon electrode in 100 mM PO₄³⁻, pH 7; error ± 1 mV. For Fe^{III}(copro)⁺, $E_{1/2} = -186$ mV in the absence of peptide. ^d Mean residue ellipticity at 222 nm in the absence of Fe^{III}(copro), error less than $\pm 3\%$. ^e Mean residue ellipticity of peptide bound to complex; $\theta_{\text{obs}} = \theta_{\text{ub}}(F_{\text{ub}}) + \theta_{\text{b}}(F_{\text{b}})$, where θ_{obs} is the observed ellipticity, F_{ub} is the fraction of unbound peptide, and F_{b} is the fraction of bound peptide in the complex. The concentration of the complex was determined from the cubic solution of the equilibrium expression. With caveats, the percentage of helicity of peptides bound to the metal in the complex may be calculated⁹ roughly: % Helicity = $\theta_{\text{b}}/33\ 333 = \theta_{\text{b}}/[40\ 000(1 - 2.5/n)]$, where $n = \text{number of residues} = 15$. The porphyrin itself does not contribute significantly to θ , as shown by near-zero θ for heme–His complexes.

examined. Peptide solubility was provided by Lys residues in every third or fourth position. The sequence termini were capped to enhance helix dipole formation.⁸ A list of the peptide sequences is shown in Table 1. It should be noted that the location of His in the middle tends to destabilize helix formation by the free peptide, since His is a helix breaker. Coproporphyrin-I-atoiron(III) chloride, Fe^{III}(copro)(Cl), (Figure 1) was chosen as the metalloporphyrin for its excellent aqueous solubility, nonaggregation, and high symmetry. Binding constants (Table 1) of the peptides with Fe^{III}(copro) were determined by spectrophotometric analysis of titration data using standard methods.¹⁰ Surprisingly, the heme–peptide binding constants span a range

(8) Hol, W. G. J.; vanDuijnen, P. T.; Berendsen, H. J. C. *Nature* **1978**, *273*, 443.

(9) Chen, Y. H.; Yang, J. T.; Chau, K. H. *Biochemistry* **1974**, *13*, 3350.

(10) Isosbestic behavior (Figure 1) showed that there were only two absorbing species in solution, and spectrophotometric data analysis confirmed 2:1 peptide–metalloporphyrin complex formation for all cases. Visible spectra confirmed bis-imidazole complexation, and EPR spectra were consistent with the expected low spin ($S = 1/2$) iron(III) center.^{10b} (b) Huffman, D. L. Ph.D. Thesis, University of Illinois at Urbana–Champaign, 1994. Also see the Supporting Information.

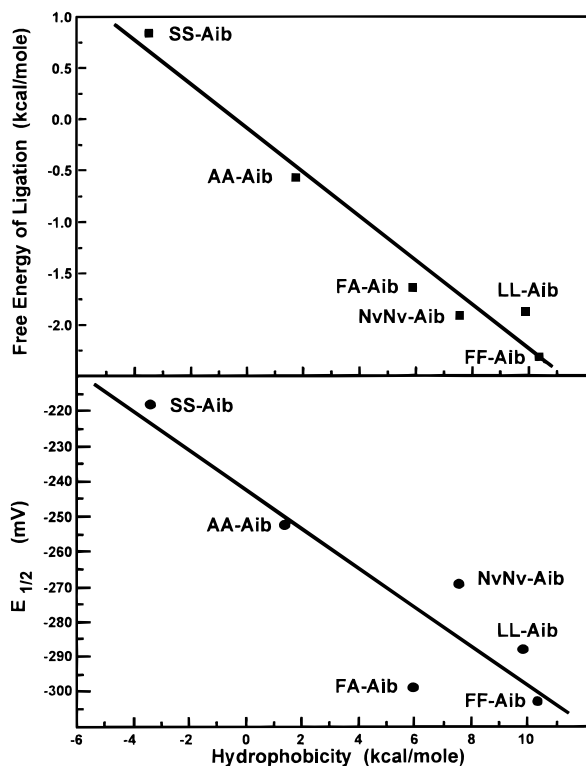


Figure 2. (a) Free energy of ligation for formation of 2:1 peptide–heme complexes versus the hydrophobicity of the peptide residues in contact with the porphyrin face. (b) Reduction potentials of Fe^{III} porphyrin–peptide complexes versus strength of peptide binding. The iron(III) coproporphyrin-I-ate concentration was $\sim 100 \mu\text{M}$, and the peptides' concentrations were sufficient to ensure $>99\%$ complexation.

of almost 6000-fold relative to His. Hydrophobic interactions between the amphiphilic α -helices with the hydrophobic heme surface provide an explanation for this large variation in binding. The magnitude of the hydrophobic effect has been estimated to be 2.4 kcal/nm^2 of accessible surface area.¹¹ The surface area of a porphyrin is approximately 1.0 nm^2 per side; counting the matching surface of the peptide, a maximum of $\sim 4 \text{ nm}^2$ could be hidden in the formation of a 2:1 complex. The strongest binding peptide, **FF-Aib**, has phenylalanine residues in contact with the heme¹² and Aib residues to enhance helicity; the binding of this peptide is 1880 times stronger than that of His-OCH₃ alone, i.e., 4.5 kcal/mol in ΔG° .¹² This corresponds to $\sim 1.9 \text{ nm}^2$ of buried hydrophobic contact, or roughly half of the total excluded surface possible. The importance of the hydrophobic effect in metalloporphyrin–peptide complex stability is further illustrated in Figure 2a. We demonstrate a strong correlation between side chain hydrophobicity and free energy of ligation for the Aib-containing peptides; similar correlations were obtained with the non-Aib peptides.^{10b} Quantitative side chain hydrophobicities determined by the fragment method¹⁴ were used. Only the hydrophobicities of side chains in contact with the heme face were used and assumed to be additive (Table 1).

(11) Chothia, C. *Nature* **1974**, *248*, 338.

(12) The T_1 relaxation times of the free and complexed **FF-Aib** peptide provide further evidence for contact of the hydrophobic residues with the heme: the aromatic protons of the phenyl alanine residue in the free peptide show an average $T_1 \approx 1.8 \text{ s}$, whereas in the complexed peptide, the T_1 decreases to 0.43 s . This 4-fold decrease in T_1 arises from the close proximity of the Phe residues to paramagnetic heme. By comparison, T_1 values for backbone, lysine, and Aib protons are unaffected by complexation. (b) Comparison is made to the His methyl ester to avoid zwitterionic effects, which are not present in the capped 15-mers. (c) Edge to face π – π interactions¹³ may also contribute to complex stability in ligands **FA-Aib** and **FF-Aib**.

(13) Jorgensen, W. L.; Severance, D. L. *J. Am. Chem. Soc.* **1990**, *112*, 4768.

(14) Abraham, D. J.; Leo, A. J. *Proteins: Struct., Funct., Genet.* **1987**, *130*.

The reduction potentials of the heme–peptide complexes (Table 1, Figure 2b) also correlate with peptide hydrophobicity. As side chain hydrophobicity of the contact amino acids increases, the reduction potential drops over a 90 mV range. This reflects the difference in ligand binding in the Fe^{III} vs Fe^{II} complexes: Fe^{III} binds imidazoles and basic pyridines more tightly than Fe^{II}; as the binding constant of these bases increases, the reduction potential of the complexes decreases.¹⁵ Increased binding constants for our peptides should scale with more negative reduction potentials, as is observed (Figure 2b). Multiple factors may contribute to the observed redox potentials of these complexes; for example, the increase in peptide hydrophobicity may also tend to stabilize the neutral complex of Fe^{II}, lessening the magnitude of the observed trend.

These heme–peptide complexes have the same ligand environment as *b* type cytochromes, yet the measured reduction potentials are approximately 200–300 mV more negative, as with other water-soluble hemes with (nonprotein) bis-imidazole ligation.¹⁶ This apparent anomaly is likely explained by differences in electrostatic environments and shielding of the heme by the low dielectric protein interior.¹⁷ In our complexes, the heme is more exposed to the aqueous environment, and therefore the reduction potentials remain more negative than in the *b* cytochromes.

Metal coordination can induce structural changes in peptides,¹⁸ so we have used circular dichroism to assess changes in peptide structure upon metalloporphyrin ligation. A large increase in helicity, as defined by the ellipticity at 222 nm (Table 1), is seen for all of the peptides upon ligation. This proves that peptide ligation to the metalloporphyrin is coupled to concomitant structural changes in the helicity of the peptide. The qualitative results of the circular dichroism experiments nicely corroborate the binding constant and NMR T_1 data.¹² This further underscores the importance of the hydrophobic effect in these complexes: the hydrophobic interaction can be maintained between the metalloporphyrin surface and the peptides' nonpolar residues *only* in the presence of substantial helix formation in the peptide.¹⁹

We have examined both the influence of the peptide on the properties of the heme (e.g., reduction potential, binding constant) and the influence of the heme on the properties of the peptide (e.g., degree of helicity). These peptide complexes provide a quantitative insight into a major and previously little recognized contribution to the stability of heme proteins: heme–peptide hydrophobic interactions.

Acknowledgment. We thank N. Chang for assistance with peptide synthesis and hydrolysis. Dr. Xiaotang Wang is gratefully acknowledged for invaluable assistance with the NMR measurements and useful discussions. This work was supported by the NIH (HL25934).

Supporting Information Available: UV titration data; titration analysis; EPR spectra; and NMR T_1 data (17 pages, print/PDF). See any current masthead page for ordering information and Web access instructions.

JA9704545

(15) Kadish, K. M. In *Iron Porphyrins*; Lever, A. B. P., Gray, H. B., Eds.; Addison-Wesley: Reading, MA, 1984; Vol. 2, pp 161–251. (b) Safo, M. K.; Nasset, M. J. M.; Walker, F. A.; Debrunner, P. G.; Scheidt, W. *J. Am. Chem. Soc.* **1997**, *119*, 9438 and references therein.

(16) Henderson, R. W.; Mortin, T. C. *CRC Handbook of Biochemistry and Molecular Biology*; Fasman, G. D., Ed.; CRC Press: Cleveland, OH, 1976; Vol. 1, p 131.

(17) Sharp, K. A.; Honig, B. *Annu. Rev. Biophys. Chem.* **1990**, *19*, 301. (b) Rogers, K. K.; Sliagar, S. G. *J. Am. Chem. Soc.* **1991**, *113*, 9419.

(18) Ghadiri, M. R.; Fernholz, A. *J. Am. Chem. Soc.* **1990**, *112*, 9633.

(19) Despite these striking results, we hesitate to assess *quantitatively* the structural content of the peptides for the following reasons: (1) for these peptides, significant end-fraying is likely; (2) for Aib-containing peptides, quantitative structure prediction by CD is not well-established; (3) for peptides with aromatic residues (i.e., **FA-Aib** and **FF-Aib**), far-UV CD bands can be induced, causing significant underestimation of the helical content. Nonetheless, the data are consistent with two turns (~ 7 residues) of an idealized α -helix in contact with the heme.

Discotic Liquid Crystals from a Bis-Pocketed Porphyrin

Bimal R. Patel and Kenneth S. Suslick*

Department of Chemistry
University of Illinois at Urbana-Champaign
600 S. Mathews Avenue, Urbana, Illinois 61801

Received June 15, 1998

Porphyrin,¹ phthalocyanine,² and tetraazaporphyrin³ liquid crystals⁴ are of interest for optoelectronic, NLO, and other device applications due to their synthetic versatility, thermal stability, large π -electron systems, and photochemical properties.⁵ With few exceptions,⁶ nearly all of the previously reported macrocyclic mesogens share one feature in common; they are flat molecules with alkyl chains coplanar with the macrocycle core. Porphyrins and phthalocyanines with dipole moments perpendicular to the macrocycle plane are very rare;⁷ facile dimerization with cancellation of net dipoles presents a serious problem for further applications. We report here the synthesis and characterization of a homologous series of liquid crystalline octa-meta-substituted tetraphenylporphyrins (Figure 1) with protecting pockets on both faces of the macrocycle. Because the phenyl groups of *meso*-tetraarylporphyrins are rotated with respect to the porphyrin core, the alkyl substituents that provide the mesophase properties of these porphyrins project out and away from the porphyrin core in three dimensions. This provides pocketed sites which permit axial ligation to the metalloporphyrin without loss of the liquid crystal phase. Five-coordinate metalloporphyrin mesogens of this type will have a permanent dipole moment which may prove useful for control of orientation or of other field responsive properties of the liquid crystal phase. Only a very few metallomesogens have been reported with oriented dipoles.⁸

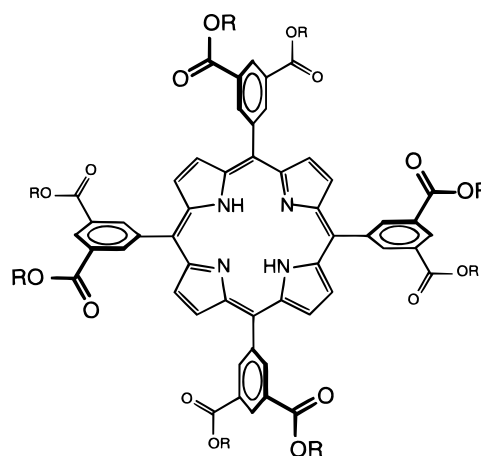


Figure 1. Bis-pocketed columnar hexagonal liquid crystal porphyrins: *n*-alkyl esters of 5,10,15,20-(3,5-dicarboxyphenyl)porphyrin (H₂DCarPP), R = *n*-C_nH_{2n+1}, *n* = 8, 10, 12, 14, 16, 18, 20, 22.

The parent porphyrin for our mesogenic derivatives is 5,10,15,20-tetrakis(3,5-dicarboxyphenyl)porphyrin (H₂DCarPP), and the liquid crystalline derivatives are its octa-*n*-alkyl esters (Figure 1). We prepared the octa-ethyl ester of H₂DCarPP by the reaction of diethyl 5-formylisophthalate with pyrrole in refluxing acetic acid for 8 h. After the solvent was removed with the use of a rotary evaporator, the porphyrin was washed extensively with methanol and then purified by column chromatography on silica gel. The desired fraction was concentrated, and the porphyrin was precipitated with petroleum ether, isolated by filtration, and then dried in vacuo at 100 °C.⁹ The ethyl esters were hydrolyzed in biphasic refluxing THF/KOH (aqueous), and the octacarboxylic acid was precipitated with 50% HCl (aqueous). After the solid was isolated and washed, the porphyrin was recrystallized from pyridine/ethyl acetate, resulting in a red-brown powder which was dried in vacuo at 150 °C.¹⁰

A homologous series (*n*-alkyl chain: C_nH_{2n+1}, *n* = 8, 10, 12, 14, 16, 18, 20, and 22) of octa-alkyl esters of H₂DCarPP esters were then prepared using the following general method: H₂DCarPP (20 mg), *p*-toluenesulfonic acid (10 mg), and the appropriate alcohol (1 mL) were stirred and heated at 80 °C for 72 h under argon. The acid was then neutralized with NH₄OH (aqueous), and ethanol was added to the reaction solution to dissolve excess alcohol and precipitate the porphyrin. The product was isolated by filtration, washed with hot ethanol, and then redissolved in chloroform and filtered. The filtrate was concentrated and then chromatographed on silica gel with chloroform.¹¹

The liquid crystalline phase was characterized by differential scanning calorimetry (DSC) and the characterization was confirmed by viewing the birefringence of the samples between

(1) (a) Gregg, B. A.; Fox, M. A.; Bard, A. J. *J. Chem. Soc., Chem. Commun.* **1987**, 1134–1135. (b) Gregg, B. A.; Fox, M. A.; Bard, A. J. *J. Am. Chem. Soc.* **1989**, *111*, 3024–3029. (c) Kugimiya, S.; Takemura, M. *Tetrahedron Lett.* **1990**, *31*, 3157–3160. (d) Ramasseul, R.; Maldivi, P.; Marchon, J.-C.; Taylor, M.; Guillon, D. *Liq. Cryst.* **1993**, *13*, 729–733. (e) Shimizu, Y.; Miya, M.; Nagata, A.; Ohta, K.; Yamamoto, I.; Kusabayashi, S. *Liq. Cryst.* **1993**, *14*, 795–805.

(2) (a) Guillon, D.; Weber, P.; Skoulios, A.; Piechocki, C.; Simon, J. *Mol. Cryst. Liq. Cryst.* **1985**, *130*, 223–229. (b) van der Pol, J. F.; Neeleman, E.; Zwikker, J. W.; Nolte, R. J. M.; Drenth, W.; Aerts, J.; Visser, R.; Picken, S. J. *Liq. Cryst.* **1989**, *6*, 577–592. (c) Cook, M. J.; Cracknell, S. J.; Harrison, K. J. *J. Mater. Chem.* **1991**, *1*, 703–704. (d) van Nostrum, C. F.; Bosman, A. W.; Gelinck, G. H.; Picken, S. J.; Schouten, P. G.; Warman, J. M.; Schouten, A.-J.; Nolte, R. J. M. *J. Chem. Soc., Chem. Commun.* **1993**, 1120–1122. (e) Ford, W. T.; Sumner, L.; Zhu, W.; Chang, Y. H.; Um, P.-J.; Choi, K. H.; Heiney, P. A.; Maliszewskyj, N. C. *New J. Chem.* **1994**, *18*, 495–505. (f) Mohr, B.; Wegner, G.; Ohta, K. *J. Chem. Soc., Chem. Commun.* **1995**, 995–996.

(3) (a) Doppelt, P.; Huille, S. *New J. Chem.* **1990**, *14*, 607–609. (b) Lelj, F.; Morelli, G.; Ricciardi, G.; Roviello, A.; Sirigu, A. *Liq. Cryst.* **1992**, *12*, 941–960.

(4) (a) Chandrasekhar, S. *Liq. Cryst.* **1993**, *14*, 3–14. (b) Destrade, C.; Foucher, P.; Gasparoux, H.; Tinh, N. H.; Levelut, A. M.; Malthete, J. *Mol. Cryst. Liq. Cryst.* **1984**, *106*, 121–146. (c) Destrade, C.; Tinh, N. H.; Gasparoux, H.; Malthete, J.; Levelut, A. M. *Mol. Cryst. Liq. Cryst.* **1981**, *71*, 111–135.

(5) Liu, C.-Y.; Pan, H.-L.; Fox, M. A.; Bard, A. J. *Science* **1993**, *261*, 897–899.

(6) (a) Xu, B.; Swager, T. M. *J. Am. Chem. Soc.* **1995**, *117*, 5011–12. (b) Milgrom, L. R.; Yahsioglu, G.; Bruce, D. W.; Morrone, S.; Henari, F. Z.; Blau, W. J. *Adv. Mater.* **1997**, *9*, 313–316. (c) Wang, Q. M.; Bruce, D. W. *Angew. Chem. Int. Ed. Engl.* **1997**, *36*, 150–152.

(7) (a) Shimizu, Y.; Matsuno, J.-Y.; Miya, M.; Nagata, A. *J. Chem. Soc., Chem. Commun.* **1994**, 2411–2412. (b) Weber, P.; Guillon, D.; Skoulios, A. *J. Phys. Chem.* **1987**, *91*, 2242–2243. (c) Piechocki, C.; Boulou, J.-C.; Simon, J. *Mol. Cryst. Liq. Cryst.* **1987**, *149*, 115–120.

(8) (a) Weber, P.; Guillon, D.; Skoulios, A. *J. Phys. Chem.* **1987**, *91*, 2242–2243. (b) Hanack, M.; Beck, A.; Lehmann, H. *Synthesis* **1987**, 703–705. (c) Hanack, M.; Lang, M. *Adv. Mater.* **1994**, *6*, 819–833. (d) Zheng, H. X.; Lai, C. K.; Swager, T. M. *Chem. Mater.* **1995**, *7*, 2067–2077.

(9) Yield: 25%. Characterization: Anal. Calcd (C₆₈H₆₂N₄O₁₆) C, 68.56; H, 5.26; N, 4.70. Found C, 68.51; H, 5.51; N, 4.82. ¹H NMR (300 MHz, CDCl₃): δ 9.17 (4H, *p*-phenyl H), 9.08 (8H, *o*-phenyl H), 8.80 (8H, β-pyrrole H), 4.53 (16H, ArCOOCH₂CH₃), 1.44 (24H, ArCOOCH₂CH₃), -2.80 (s, 2H, inner pyrrole H). ES⁺MS (chloroform/formic acid, *m/z*) Theory 1191.4 (MH⁺), 959.4 (MH⁺ - 8CH₂CH₃). Found 1191.4 (MH⁺), 959.4 (MH⁺ - 8CH₂CH₃). Found parent peak isotope distribution matched theoretical isotope distribution. Electronic absorption λ_{max} (dichloromethane, 25 °C): 421 Soret, 515, 550, 590, 646 nm.

(10) Yield: quantitative. Characterization: Anal. Calcd (C₅₂H₃₀N₄O₁₆) C, 64.60; H, 3.13; N, 5.80. Found C, 64.23; H, 3.36; N, 5.65. ¹H NMR (300 MHz, DMSO-*d*₆) δ 13.55 (s, 8H, -COOH), 8.92 (8H, β-pyrrole H), 8.90 (4H, *p*-phenyl H), 8.85 (8H, *o*-phenyl H), -2.96 (s, 2H, inner pyrrole H). ES⁺MS (DMSO/formic acid, *m/z*) Theory 967 (MH⁺), Found 967 (MH⁺). Found parent peak isotope distribution matched theoretical isotope distribution. Electronic absorption λ_{max} (ε × 10³ M⁻¹ cm⁻¹, pyridine, 25 °C) 423 Soret (441), 516 (20.0), 561 (7.6), 591 (6.1), 647 (3.5) nm. IR (KBr) 3432, 3107, 2872, 2612, 2555, 2367, 1701 (C=O), 1602, 1443, 1402, 1385, 1279, 1243, 1209, 1114, 979, 916, 801, 761, 720, 670, 603, 532 cm⁻¹.

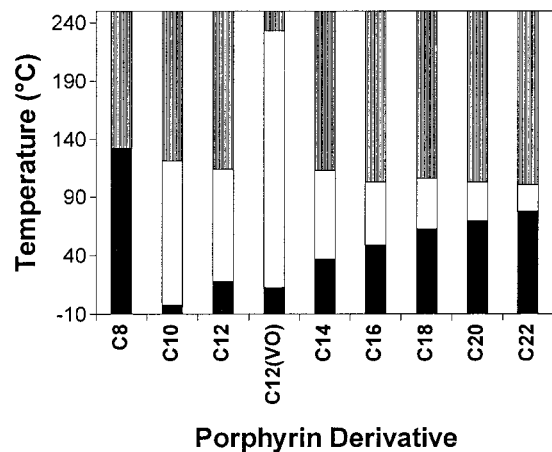


Figure 2. Differential scanning calorimetry of the octa-*n*-alkyl esters of H₂DCarPP; black = solid phase, white = mesophase, gray = isotropic. The DSC peak maxima for the heating cycle (3 °C/s) are as follows: [temperature (ΔH), M = melting transition (solid to mesophase), C = clearing transition (mesophase to isotropic)]. C₈ [132 °C (143 kJ/mol) M]; C₁₀ [-3 °C (17 kJ/mol) M , 121 °C (35 kJ/mol) C]; C₁₂ [17 °C (38 kJ/mol) M , 114 °C (28 kJ/mol) C]; C₁₂VO [13 °C M , 233 °C C]; C₁₄ [36 °C (66 kJ/mol) M , 113 °C (23 kJ/mol) C]; C₁₆ [49 °C (119 kJ/mol) M , 103 °C (21 kJ/mol) C]; C₁₈ [63 °C (188 kJ/mol) M , 106 °C (25 kJ/mol) C]; C₂₀ [70 °C (214 kJ/mol) M , 103 °C (22 kJ/mol) C]; C₂₂ [78 °C (266 kJ/mol) M , 101 °C (21 kJ/mol) C].

crossed polarizers in a polarizing microscope. The DSC results are summarized in Figure 2. Rate-dependent hysteresis upon cooling the samples is due to supercooling. The peak corresponding to the melting of the solid to the liquid crystal phase was large and sharpened as the alkyl chain length increased. The clearing transition (from liquid crystal to isotropic liquid phase) was somewhat broad in all samples. The enthalpy of melting increased with increasing alkyl chain length (from 38 kJ/mol for R = C₁₂H₂₅ to 266 kJ/mol for R = C₂₂H₄₅ for the heating cycle) although the clearing enthalpy stayed relatively constant (from 28 kJ/mol for R = C₁₂H₂₅ to 21 kJ/mol for R = C₂₂H₄₅ for the heating cycle). The C₈ derivative is *not* mesogenic; the C₁₀ and C₁₂ derivatives are liquid crystals at room temperature.

We grew single liquid crystalline domains on the order of 25–50 μm for all of the mesogenic samples by annealing them at their clearing temperature. Figure 3 shows an example of the birefringence texture for C₂₀ H₂DCarPP. Due to alignment of the molecules with the polarizer and the analyzer, a classic Maltese cross extinction pattern¹² was observed in the polarizer direction (vertical in the figure) and analyzer direction (horizontal in the figure).

(11) Yields of isolated octaesters averaged ca. 25%. The octa-alkyl esters of H₂DCarPP were characterized by ES⁺MS (chloroform/formic acid) and elemental analysis. Found parent peak isotope distribution matched theoretical isotope distribution for all compounds. For R = *n*-C₈H₁₇: Anal. Calcd (C₁₁₆H₁₅₈N₄O₁₆) C, 74.72; H, 8.54; N, 3.00. Found C, 74.37; H, 8.34; N, 2.62. ES⁺MS (m/z) Theory 1865.2 (MH⁺). Found 1864.8 (MH⁺). For R = *n*-C₁₀H₂₁: Anal. Calcd (C₁₃₂H₁₉₀N₄O₁₆): C, 75.90; H, 9.17; N, 2.68. Found: C, 75.70; H, 8.50; N, 2.78. ES⁺MS (m/z) Theory 2089.4 (MH⁺). Found 2089.4 (MH⁺). For R = *n*-C₁₂H₂₅: Anal. Calcd (C₁₄₈H₂₂₂N₄O₁₆) C, 76.83; H, 9.69; N, 2.42. Found C, 76.68; H, 9.73; N, 2.44. ES⁺MS (m/z) Theory 2313.7 (MH⁺). Found 2313.7 (MH⁺). For R = *n*-C₁₄H₂₉: Anal. Calcd (C₁₆₄H₂₅₄N₄O₁₆) C, 77.62; H, 10.09; N, 2.21. Found C, 77.55; H, 10.18; N, 2.45. ES⁺MS (m/z) Theory 2537.9 (MH⁺). Found 2537.5 (MH⁺). For R = *n*-C₁₆H₃₃: Anal. Calcd (C₁₈₀H₂₈₆N₄O₁₆) C, 78.27; H, 10.44; N, 2.03. Found C, 78.48; H, 10.48; N, 2.12. ES⁺MS (m/z) Theory 2763.2 (MH⁺). Found 2762.6 (MH⁺). For R = *n*-C₁₈H₃₇: Anal. Calcd (C₁₉₆H₃₁₈N₄O₁₆) C, 78.82; H, 10.75; N, 1.88. Found C, 79.07; H, 10.78; N, 1.91. ES⁺MS (m/z) Theory 2987.4 (MH⁺). Found 2987.6 (MH⁺). For R = *n*-C₂₀H₄₁: Anal. Calcd (C₂₁₂H₃₅₀N₄O₁₆) C, 79.30; H, 10.99; N, 1.74. Found C, 79.98; H, 11.19; N, 1.72. ES⁺MS (m/z) Theory 3211.7 (MH⁺). Found 3211.1 (MH⁺). For R = *n*-C₂₂H₄₅: Anal. Calcd (C₂₂₈H₃₈₂N₄O₁₆) C, 79.71; H, 11.21; N, 1.63. Found C, 80.08; H, 11.51; N, 1.76. ES⁺MS (m/z) Theory 3635.9 (MH⁺). Found 3635.4 (MH⁺).

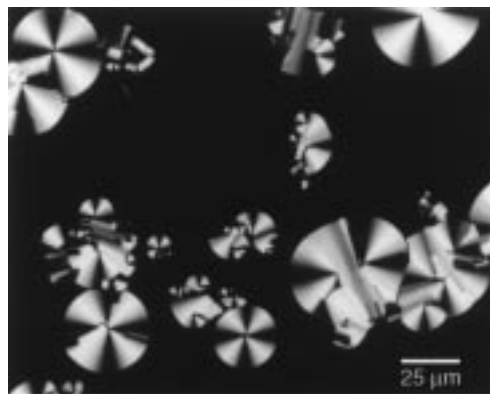


Figure 3. Birefringence texture micrograph of the octa-*n*-alkyl ester, C₂₀ H₂DCarPP, viewed between crossed polarizers. The domains were grown from the isotropic phase as the sample was being annealed.

Small-angle X-ray scattering (SAXS) of C₁₈ H₂DCarPP at 75 °C shows reflections with d -spacing of 32.7 and 19.2 Å, which corresponds to the first two reflections of a hexagonal columnar structure (reciprocal d -spacings of $1:\sqrt{3}$).¹³ The corresponding inter-columnar spacing is 37 Å, which compares well to expected porphyrin dimensions. We conclude that the mesophase structure is probably a hexagonal columnar discotic columnar, Col_h (previously designated D_h).¹⁴ Wide-angle X-ray diffraction¹⁵ gave two broad, overlapping peaks. One of the peaks is centered at ~ 4.5 Å and the other at ~ 4.2 Å. One of these peaks is due to the commonly seen liquid-like packing of alkyl chains in the mesophase; the other (probably the 4.2 Å peak) is likely due to intra-columnar spacing of the porphyrins. Further studies are required to specifically assign the wide-angle peaks.

We are currently exploiting the unusual pockets of these discotic mesogens to prepare five-coordinate metalloporphyrins that have a perpendicular dipole moment and yet retain their mesogenic behavior. For example, the vanadyl derivatives of the C₁₂ bis-pocketed mesogen, C₁₂ DCarPP(VO),¹⁶ not only retains its liquid crystallinity (Figure 2) but in fact also has a greatly expanded mesophase temperature range with a span of 246 K! Further work is required to characterize the field-responsive properties of these materials.

In conclusion, a new class of meta-substituted bis-pocket porphyrins and metalloporphyrins have been prepared. We have demonstrated that these materials are mesogenic even in the presence of axial ligation.

Acknowledgment. We gratefully thank Professor J. S. Moore for the use of his polarizing microscope and Dr. T. Rieker (U. New Mexico) and Professor M. Caffrey (Ohio State U.) for collection of SAXS data. Wide-angle X-ray data was collected at the UIUC Center for Microanalysis of Materials, supported by the DOE. Mass spectral data was obtained on a Quattro MS purchased in part with a grant from the NIH (RR 07141). This work was supported by the NIH (HL 5R01-25934) and in part by DOE (DEFG0291ER45439).

JA9820689

(12) Haudin, J. M. In *Optical Properties of Polymers*; Meeten, G. H., Ed.; Elsevier: New York, 1986; pp 167–264.

(13) SAXS data were collected on a Rigaku RU300 diffractometer with rotating anode using Cu K α radiation ($\lambda = 1.5418$ Å).

(14) In some cases, disorder within the columns may produce a discotic lamellar phase instead. The reciprocal d -spacings would then be 1:2.

(15) Wide-angle X-ray data were collected using a Rigaku D-Max diffractometer in the 6–26° 2θ range using Cu K α radiation ($\lambda = 1.5418$ Å).

(16) Metalation with VO(SO₄) refluxed in glacial acetic acid 18 h; purification by silica gel chromatography. Yield: 83%. UV/Vis λ_{max} (dichloromethane, 25 °C) 425 Soret, 547 nm; addition of acid confirmed the absence of nonmetalated porphyrin. MALDI m/z 2378.2 [M⁺].

Shape-Selective Discrimination of Small Organic Molecules

Avijit Sen and Kenneth S. Suslick*

School of Chemical Sciences
University of Illinois at Urbana-Champaign
601 South Goodwin Avenue, Urbana, Illinois 61801

Received January 3, 2000
Revised Manuscript Received October 3, 2000

Over the past few decades there has been remarkable progress in the synthesis of molecular scaffolds based on superstructured porphyrins.¹ A number of these modified porphyrins have been synthesized to mimic various aspects of the enzymatic functions of heme proteins, especially oxygen binding (myoglobin and hemoglobin), and substrate oxidation (cytochrome P-450).^{1,2} The notable property of many heme proteins is their remarkable substrate selectivity; the development of highly regioselective synthetic catalysts, however, is still at an early stage. Discrimination of one site on a molecule from another and distinguishing among many similar molecules presents a difficult and important challenge to both industrial and biological chemistry.³ Although the axial ligation properties of simple synthetic metalloporphyrins are well documented in literature,⁴ size and shape control of ligation to peripherally modified metalloporphyrins has been largely unexplored, with few notable exceptions, where only limited selectivities have been observed.⁵

We report here the synthesis, characterization, and remarkable shape-selective ligation of silyl ether–metalloporphyrin scaffolds derived from the reaction of 5,10,15,20-tetrakis(2',6'-dihydroxyphenyl)porphyrinatozinc(II) with *tert*-butyldimethylsilyl chloride, whereby the two faces of the Zn(II) porphyrin were protected with six, seven, or eight siloxyl groups. This results in a set of three porphyrins of nearly similar electronics but with different steric encumbrance around the central metal atom present in the porphyrin. Ligation to Zn by classes of different sized ligands reveals shape selectivities as large as 10⁷.

A family of siloxyl-substituted bis-pocket porphyrins were prepared according to the process in Scheme 1.⁶ Zn[(OH)₆PP] and Zn[(OH)₈PP] were obtained^{5a} from demethylation⁷ of corresponding free base methoxy compounds followed by zinc(II) insertion. The methoxy porphyrins were synthesized by acid catalyzed condensation of pyrrole with respective benzaldehydes following Lindsey procedures.⁸ Metalation was done in methanol with Zn(O₂CCH₃)₂. The *tert*-butyldimethylsilyl groups were incorporated into the metalloporphyrin by stirring a DMF solution of hydroxyporphyrin complex with TBDMSiCl in the presence of imidazole.⁹ The octa (Zn(Si₈PP)), hepta (Zn(Si₇OHPP)), and hexa (Zn(Si₆PP)) silyl ether porphyrins were obtained from Zn-[(OH)₈PP] and Zn[(OH)₆PP], respectively. The compounds were purified by silica gel column chromatography and fully characterized by UV–visible, ¹H NMR, HPLC, and MALDI-TOF MS.

(1) (a) Suslick, K. S.; Reinert, T. J. *J. Chem. Ed.* **1985**, 62, 974. (b) Collman, J. P.; Zhang, X.; Lee, V. J.; Uffelman, E. S.; Brauman, J. I. *Science* **1993**, 261, 1404.

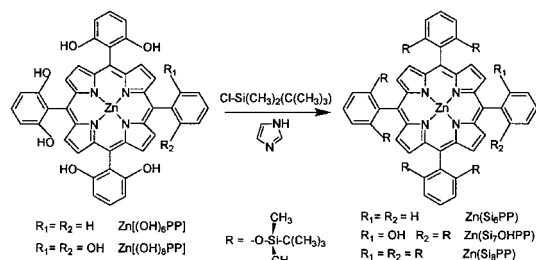
(2) (a) Collman, J. P.; Zhang, X. In *Comprehensive Supramolecular Chemistry*; Atwood, J. L., Davies, J. E. D., MacNicol, D. D., Vogtel, F., Eds.; Pergamon: New York, 1996; Vol. 5, pp 1–32. (b) Suslick, K. S.; van Deusen-Jeffries, S. In *Comprehensive Supramolecular Chemistry*; Atwood, J. L., Davies, J. E. D., MacNicol, D. D., Vogtel, F., Eds.; Pergamon: New York, 1996; Vol. 5, pp 141–170. (c) Suslick, K. S. In *Activation and Functionalization of Alkanes*; Hill, C. L., Ed.; Wiley & Sons: New York, 1989; pp 219–241.

(3) *Metalloporphyrins in Catalytic Oxidations*; Sheldon, R. A., Ed.; Marcel Dekker: New York, 1994.

(4) (a) Bampos, N.; Marvaud, V.; Sanders, J. K. M. *Chem. Eur. J.* **1998**, 4, 325. (b) Stibrany, R. T.; Vasudevan, J.; Knapp, S.; Potenza, J. A.; Emge, T.; Schugar, H. J. *J. Am. Chem. Soc.* **1996**, 118, 3980.

(5) (a) Bhyrappa, P.; Vaijayanthimala, G.; Suslick, K. S. *J. Am. Chem. Soc.* **1999**, 121, 262. (b) Imai, H.; Nakagawa, S.; Kyuno, E. *J. Am. Chem. Soc.* **1992**, 114, 6719.

Scheme 1



The size and shape selectivities of the binding sites of these bis-pocket Zn silyl ether porphyrins were probed using the axial ligation of various nitrogenous bases of different shapes and sizes in toluene at 25 °C. Zn(II) porphyrins were chosen for this study because, in solution, they generally bind only a single axial ligand. Successive addition of ligand to the porphyrin solutions caused a red-shift of the Soret band typical of coordination to zinc porphyrin complexes. There is no evidence from the electronic spectra of these porphyrins for significant distortions of the electronic structure of the porphyrin. The binding constants (K_{eq}) and binding composition (always 1:1) were evaluated using standard procedures.¹⁰ The K_{eq} values of the silyl ether porphyrins with nitrogenous bases of different classes are compared with the sterically undemanding Zn(TPP) in Figure 1. It is worth noting the parallel between shape selectivity in these equilibrium measurements and prior kinetically controlled epoxidation and hydroxylation.^{2,11} While direct comparisons are not yet available, the selectivity for equilibrated ligation appears to be substantially larger than that for irreversible oxidations of similarly shaped substrates.

The binding constants of silyl ether porphyrins are remarkably sensitive to the shape and size of the substrates relative to Zn(TPP) (Figure 1). The binding constants of different amines could be controlled over a range of 10¹ to 10⁷ relative to Zn(TPP). We believe that these selectivities originate from strong steric repulsions created by the methyl groups of the *tert*-butyldimethylsilyloxy substituents. The steric congestion caused by these bulky silyl ether groups is pronounced *even* for linear amines and small cyclic amines (e.g., azetidine and pyrrolidine).

There are very large differences in K_{eq} for porphyrins having three versus four silyl ether groups on each face (e.g., hexa- vs

(6) (a) Abbreviations: Zn(TPP), 5,10,15,20-tetraphenylporphyrinatozinc(II); Zn[(OH)₆PP], 5-phenyl-10,15,20-tris(2',6'-dihydroxyphenyl)porphyrinatozinc(II); Zn[(OH)₈PP], 5,10,15,20-tetrakis(2',6'-dihydroxyphenyl)porphyrinatozinc(II); Zn(Si₆PP), 5-phenyl-10,15,20-tris(2',6'-disilyloxyphenyl)porphyrinatozinc(II); Zn(Si₇OHPP), 5,10,15-tris(2',6'-disilyloxyphenyl)-20-(2'-hydroxy-6'-silyloxyphenyl)porphyrinatozinc(II); Zn(Si₈PP), 5,10,15,20-tetrakis(2',6'-disilyloxyphenyl)porphyrinatozinc(II); TBDMSiCl, *tert*-butyldimethylsilyl chloride. (b) Characterization details provided as Supporting Information. (c) X-ray structure of Zn(Si₈PP) determined at 173(2) K from single crystals grown from a mixture of CHCl₃ and C₆H₆Cl (3:1, v/v). X-ray data collected with a Bruker SMART system with a CCD detector; λ (Mo K α) = 0.7107 Å. Structure solved by direct methods (G. M. Sheldrick, 1998, SHELX-97-2; Institute for Anorg. Chemie, Göttingen, Germany) and refined by full-matrix least squares against all F^2 data. Crystal data for Zn(Si₈PP): crystal dimension 0.20 × 0.22 × 0.24 mm, triclinic, space group $P1$, $a = 13.114(3)$ Å, $b = 13.577(3)$ Å, $c = 28.590(6)$ Å, $\alpha = 78.703(8)^\circ$, $\beta = 83.449(8)^\circ$, $\gamma = 89.214(8)^\circ$, $V = 4959(2)$ Å³, $Z = 2$, $2\theta_{max} = 50^\circ$, $R_1 = 0.0793$, $wR_2 = 0.1944$ (due to some disorder of one of the *t*-Bu groups), GOF = 1.018, residual electron density $-0.417(0.671)$ eÅ⁻³. Details provided as Supporting Information.

(7) Momenteau, M.; Mispelter, J.; Loock, B.; Bisagni, E. *J. Chem. Soc., Perkin Trans. 1* **1983**, 189.

(8) Lindsey, J. S.; Wagner, R. W. *J. Org. Chem.* **1989**, 54, 828.

(9) Corey, E. J.; Venkateswarlu, A. *J. Am. Chem. Soc.* **1972**, 94, 6190.

(10) (a) Collman, J. P.; Brauman, J. I.; Doxsee, K. M.; Halbert, T. R.; Hayes, S. E.; Suslick, K. S. *J. Am. Chem. Soc.* **1978**, 100, 2761. (b) Suslick, K. S.; Fox, M. M.; Reinert, T. *J. Am. Chem. Soc.* **1984**, 106, 4522.

(11) (a) Bhyrappa, P.; Young, J. K.; Moore, J. S.; Suslick, K. S. *J. Am. Chem. Soc.* **1996**, 118, 5708–5711. (b) Suslick, K. S.; Cook, B. R. *J. Chem. Soc., Chem. Commun.* **1987**, 200–202. (c) Cook, B. R.; Reinert, T. J.; Suslick, K. S. *J. Am. Chem. Soc.* **1986**, 108, 7281–7286. (d) Suslick, K. S.; Cook, B. R.; Fox, M. M. *J. Chem. Soc., Chem. Commun.* **1985**, 580–582.

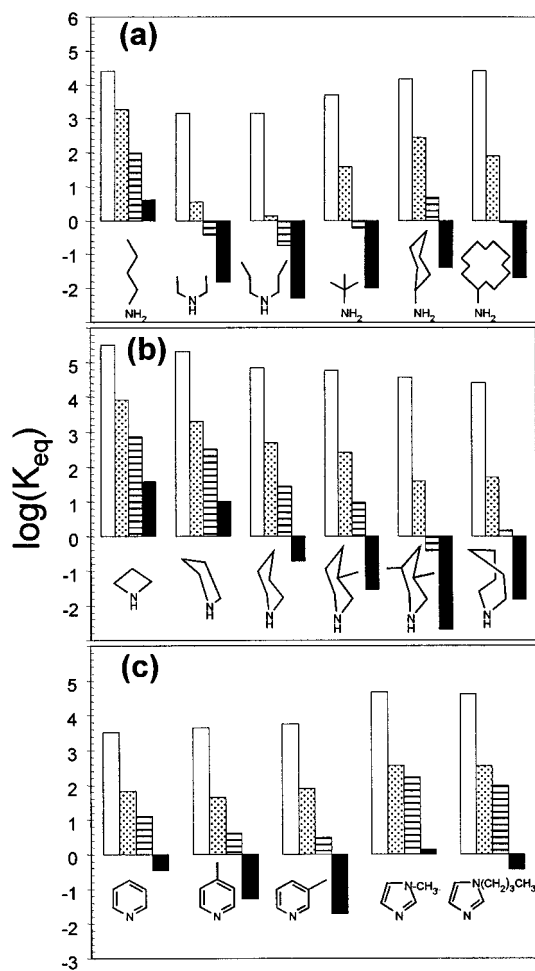


Figure 1. Ligand binding constants for siloxyl porphyrins compared to Zn(TPP): (a) aliphatic primary and secondary amines; (b) alicyclic secondary amines, and (c) aromatic amines. Errors in K_{eq} were typically $\pm 10\%$ (i.e., ± 0.05 log units): open bar, Zn(TPP); dotted bar, Zn(Si₆-PP); horizontally ruled bar, Zn(Si₇-OHPP); and solid bar, Zn(Si₈-PP).

octasilyl ether porphyrins), as expected based on obvious steric arguments (Figure 1). Even between the hexa- over heptasilyl ether porphyrins, however, there are still substantial differences in binding behavior. We suggest that this is probably due to doming of the macrocycle in the hexa- and heptasilyl ether porphyrins, which lessens the steric constraint relative to the octasilyl ether porphyrin. Such doming will be especially important in porphyrins whose two faces are not identical. The free hydroxy functionality of the heptasilyl ether may play a role in binding of bifunctionalized ligands (e.g., free amino acids); for the simple amines presented here, however, we have no evidence of any special effects.

These silyl ether porphyrins showed remarkable selectivities for *normal*, linear amines over their cyclic analogues. For a series of linear amines (*n*-propylamine through *n*-decylamine), K_{eq} values were very similar for each of the silyl ether porphyrins. In comparison, the relative K_{eq} for linear versus cyclic primary amines (Figure 1a, *n*-butylamine vs cyclohexylamine) were significantly different: $K_{eq}^{linear}/K_{eq}^{cyclic}$ ranges from 1 to 23 to 115 to >200 for Zn(TPP), Zn(Si₆-PP), Zn(Si₇-OHPP), and Zn(Si₈-PP), respectively. The ability to discriminate between linear and cyclic compounds is thus established.

A series of cyclic secondary amines (Figure 1b) demonstrate the remarkable size and shape selectivities of this family of bis-pocket porphyrins, whereas the binding constants to Zn(TPP) with those amines are virtually similar. In contrast, the K_{eq} values for silyl ether porphyrins strongly depend on the ring size and its peripheral substituents. The effect of these shape-selective binding

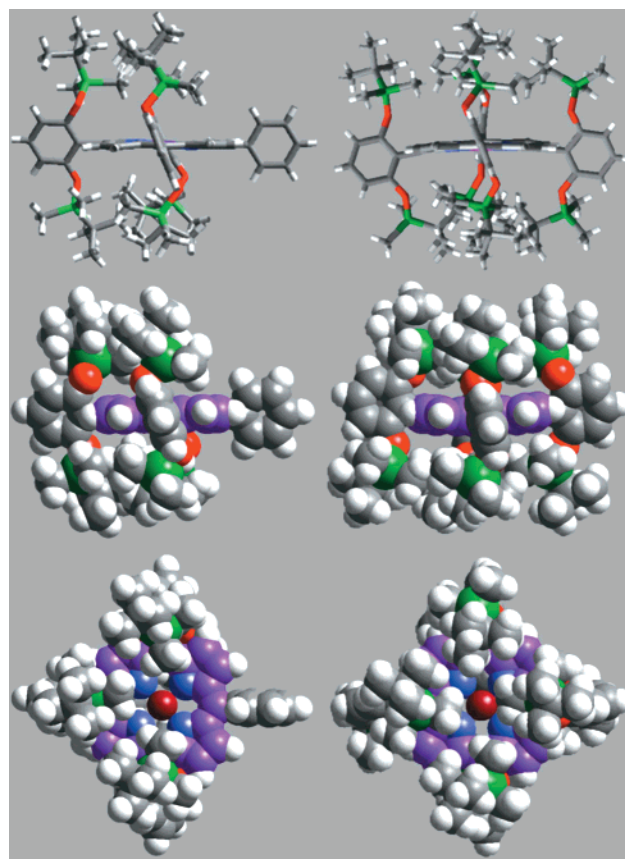


Figure 2. Molecular models of Zn(Si₆-PP) (left column) and Zn(Si₈-PP) (right column). Pairs of images (top to bottom) are cylinder side-views, side-views, and top-views, respectively; space filling shown at 70% van der Waals radii, with porphyrin carbon atoms (purple), oxygen atoms (red), silicon atoms (green), and Zn (dark red). The X-ray single-crystal structure of Zn(Si₈-PP) determined at 173(2) K is shown;^{6c} for Zn(Si₆-PP), an energy-minimized structure was obtained using Cerius 2 from MSI.

sites is clear, even for compact aromatic ligands with non-*ortho*-methyl substituents (Figure 1c).

The molecular structures of these silyl ether porphyrins explain their ligation selectivity. We have solved the X-ray single-crystal structure of Zn(Si₈-PP) in the triclinic *P*1 space group.^{6c} As shown in Figure 2, Zn(Si₆-PP) (energy minimized molecular model) and Zn(Si₈-PP) (single crystal X-ray structure) have dramatically different binding pockets. In the octasilyl ether porphyrin, the top access on both faces of the porphyrin is very tightly controlled by the siloxyl pocket. In contrast, the metal center of the hexasilyl ether porphyrin is considerably more exposed for ligation.

In summary, a series of bis-pocket siloxylmetalloporphyrin complexes were prepared with sterically restrictive binding pockets on both faces of the macrocycle. Ligation to Zn by various nitrogenous bases of different sizes and shapes was investigated. Shape selectivities as large as 10^7 were found, compared to unhindered metalloporphyrins. Fine-tuning of ligation properties of these porphyrins was also possible using pockets of varying steric demands. The shape selectivities shown here rival or surpass those of any biological system.

Acknowledgment. We thank Dr. Richard Milberg (UIUC, Mass Spectroscopy Lab) for MALDI-TOF spectral measurements and Drs. J. H. Chou and S. R. Wilson for assistance in solving the crystal structure. This work was supported by the National Institute of Health (HL 5R01-25934) and in part by the U.S. Army Research Office (DAAG55-97-0126).

Supporting Information Available: Synthesis, characterization, and X-ray crystallographic details (PDF). This material is available free of charge via the Internet at <http://pubs.acs.org>.

JA000002J

geometrical correlation length), and consequently a purely diffusive large-scale behaviour for the force. Therefore, we conclude that our results are certainly applicable to disordered packings such as cohesionless soils or sand piles. In contrast, for the particular case of non-random, textured packings, biased and long-range correlated q -series along the force transmission tree are likely to be encountered, thus altering the previous purely diffusive behaviour. □

Received 4 October 1999; accepted 15 June 2000.

- Ennis, B. J. in *Powders and Grains 97* (eds Behringer, R. P. & Jenkins, T. J.) 13–23 (A. A. Balkema, Rotterdam, 1997)
- Gray, J. M. & Hutter, K. Physik granularer Lawinen. *Phys. Bl.* **54**, 37–43 (1998).
- Terzaghi, K. *Theoretical Soil Mechanics* (Wiley, New York, 1943)
- Bouchaud, J. P., Cates, M. E. & Claudin, P. Stress distribution in granular media and nonlinear wave equation. *J. Phys. I (Fr.)* **5**, 639–656 (1995)
- Cates, M. E., Wittmer, J., Bouchaud, J. P. & Claudin, P. Development of stresses in cohesionless poured sand. *Phil. Trans. R. Soc. Lond. A* **356**, 2535–2560 (1998).
- Sokolovski, V. V. *Statics of Granular Media* (Pergamon, New York, 1965).
- Timoshenko, S. & Goodier, J. N. *Theory of Elasticity* (McGraw Hill, New York, 1951)
- Landau, L. D. & Lifschitz, E. M. *Theory of Elasticity* (Pergamon, New York, 1980).
- Boussinesq, J. *Application des Potentiels à l'Étude de l'Équilibre et des Mouvements des Solides Élastiques* (Gauthier-Villars, Paris, 1885).
- Coppersmith, S. N., Liu, C. H., Majumdar, S., Narayan, O. & Witten, T. A. Model for force fluctuations in bead packs. *Phys. Rev. E* **53**, 4673–4685 (1996).
- Liu, C. H. *et al.* Force fluctuations in bead packs. *Science* **269**, 513–515 (1995).
- Miller, B., O'Hern, C. & Behringer, R. P. Stress fluctuations for continuous sheared granular packing. *Phys. Rev. Lett.* **77**, 3110–3113 (1996).
- Mueth, D. M., Jaeger, H. M. & Nagel, S. R. Force distribution in granular packing. *Phys. Rev. E* **57**, 3164–3169 (1998).
- Ngadi, A. & Rajchenbach, J. Intermittencies in the compression process of a model granular medium. *Phys. Rev. Lett.* **80**, 273–276 (1998).
- Radjai, F., Jean, M., Moreau, J. J. & Roux, S. Force distribution in dense two dimensional granular systems. *Phys. Rev. Lett.* **77**, 274–277 (1996).
- Peralta-Fabi, R., Malaga, C., Reichtman, R. in *Powders and Grains 97* (eds Behringer, R. P. & Jenkins, T. J.) 227–230 (A. A. Balkema, Rotterdam, 1997).
- Moukarzel, C. Isostatic phase transition and instability in stiff granular materials. *Phys. Rev. Lett.* **81**, 1634–1637 (1998).

Acknowledgements

We thank E. Bringuier for a critical reading of the manuscript.

Correspondence and requests for materials should be addressed to J.R. (e-mail: jer@ccr.jussieu.fr).

A colorimetric sensor array for odour visualization

Neal A. Rakow & Kenneth S. Suslick

Department of Chemistry, University of Illinois at Urbana-Champaign, 600 S. Mathews Avenue, Urbana, Illinois 61801, USA

Array-based vapour-sensing devices are used to detect and differentiate between chemically diverse analytes. These systems—based on cross-responsive sensor elements—aim to mimic the mammalian olfactory system^{1–3} by producing composite responses unique to each odorant. Previous work has concentrated on a variety of non-specific chemical interactions^{4–11} to detect non-coordinating organic vapours. But the most odiferous, toxic compounds often bind readily to metal ions. Here we report a simple optical chemical sensing method that utilizes the colour change induced in an array of metalloporphyrin dyes upon ligand binding while minimizing the need for extensive signal transduction hardware. The chemoselective response of a library of immobilized vapour-sensing metalloporphyrin dyes permits the visual identification of a wide range of ligating (alcohols, amines, ethers, phosphines, phosphites, thioethers and thiols) and even weakly ligating (arenes, halocarbons and ketones) vapours. Water

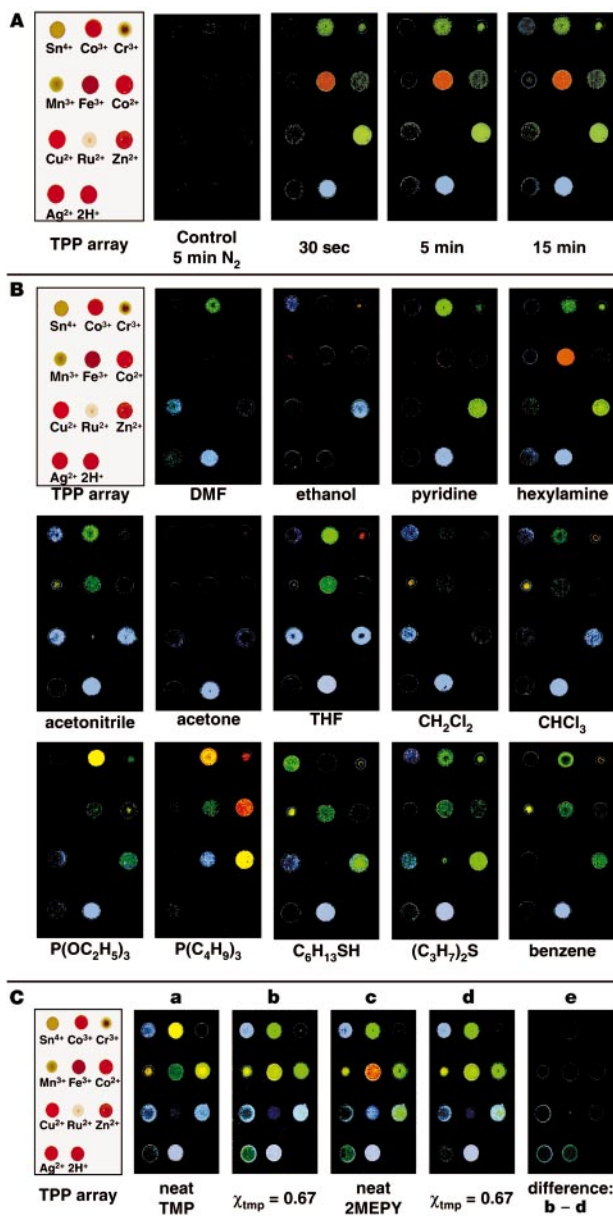


Figure 1 Colour change profiles of a metalloporphyrin sensor array. **A**, Colour change profiles of the metalloporphyrin sensor array as a function of exposure time to *n*-butylamine vapour. Metalloporphyrins were immobilized on reverse phase silica gel plates. Colour images were obtained with a flatbed scanner (HP Scanjet 3c) at 200 d.p.i. resolution. Subtraction of the initial scan from a scan after 5 min of N₂ exposure was used as a control, giving a black response, as shown. 9.3% *n*-butylamine in N₂ was then passed over the array and scans made after exposure for 30 s, 5 min and 15 min. The RGB mode images were subtracted (absolute value) using Adobe Photoshop software, with contrast enhancement by expanding the pixel range (a 32-value range was expanded to 256 each for the R, G and B values). **B**, Colour change profiles for a series of vapours; the degree of ligand softness (roughly their polarizability) increases from left to right, top to bottom. Each analyte was delivered to the array as a nitrogen stream saturated with the analyte vapour at 20 °C (to ensure complete saturation, vapour exposures of 15 min or greater were used). DMF, dimethylformamide; THF, tetrahydrofuran. **C**, Two component analysis; saturation responses to mixtures of 2-methylpyridine and trimethylphosphite. Vapour mixtures were obtained by mixing the analyte-saturated N₂ streams at variable flow ratios. A single plate was first exposed to pure trimethylphosphite vapour in N₂ (**a**), followed by increasing mole fractions of 2-methylpyridine up to pure 2-methylpyridine vapour (**c**), followed by decreasing mole fractions of 2-methylpyridine back to pure trimethylphosphite vapour. In both directions, scans were taken at the same mole fraction of trimethylphosphite (χ_{tmp}) and showed excellent reversibility; scans are shown at $\chi_{tmp} = 0.67$ (**b** and **d**), and their difference map is also shown (**e**).

vapour does not affect the performance of the device, which shows a good linear response to single analytes, and interpretable responses to analyte mixtures. Unique colour fingerprints can be obtained at analyte concentrations below 2 parts per million, and responses to below 100 parts per billion have been observed. We expect that this type of sensing array will be of practical importance for general-purpose vapour dosimeters and analyte-specific detectors (for insecticides, drugs or neurotoxins, for example).

Previous arrays have employed a variety of chemical interaction strategies, including the use of conductive polymers⁴, conductive polymer/carbon-black composites⁵, fluorescent dye/polymer systems^{6,7}, tin oxide sensors^{8,9} and polymer-coated surface acoustic wave devices^{10,11}. Although these systems have demonstrated success in chemical vapour detection and differentiation, their primary aim has been the detection of non-coordinating organic vapours. Many of the most toxic and certainly the most odiferous compounds, however, are excellent ligands for metal ions. Array detection of metal-binding species, such as amines, phosphines and thiols, has been much less explored. (We note that there are two obvious exceptions to the correlation between metal binding and olfactory sensitivity: NO and CO, both of which are produced endogenously as intercellular messenger molecules, and therefore should be olfactorily undetectable¹².) Although very little is known about the structures of the olfactory receptor proteins¹³, we speculate that many of the sensors are likely to contain metal ions at their active site.

Metalloporphyrins are a natural choice for the detection of metal-ligating vapours because of their open coordination sites for axial ligation, their large spectral shifts upon ligand binding, and their intense coloration. Metalloporphyrins have been previously employed for optical detection of gases such as oxygen^{13,14} and ammonia¹⁵, and for vapour detection as chemically interactive layers on quartz crystal microbalances^{16,17}. Here we have taken advantage of the large colour changes induced in metalloporphyrins upon ligand binding, and developed an easy colorimetric technique that minimizes the need for extensive signal transduction hardware. This represents, to our knowledge, the first example of a colorimetric array detector for vapour-phase ligands. Simply by taking the difference before and after exposure of scanned images of the array, we are able to obtain unique colour-change signatures for analytes; these signatures can be used for both qualitative recognition and quantitative analysis.

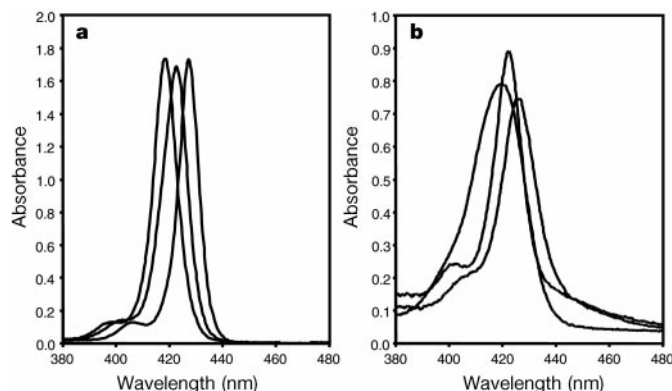


Figure 2 Comparison of Zn(TPP) spectral shifts upon exposure to ethanol and pyridine (py). **a**, In methylene chloride solution; **b**, on the reverse phase support. In both **a** and **b**, the bands correspond, from left to right, to Zn(TPP), Zn(TPP)(C₂H₅OH) and Zn(TPP)(py), respectively. Solution spectra (**a**) were collected using a Hitachi U-3300 spectrophotometer; Zn(TPP), C₂H₅OH and py concentrations were approximately 2 μM, 170 mM and 200 μM, respectively. Diffuse reflectance spectra (**b**) were obtained *in situ* with an integrating sphere attachment before exposure to analytes, after exposure to ethanol (5.8% in N₂), and after exposure to pyridine (2.1% in N₂) for 30 min.

Previous studies have elucidated the large spectral changes (and readily observable colour changes) that occur in solution during ligand binding to metalloporphyrins¹⁸. Solution studies have indicated that the magnitude of spectral shift correlates with the polarizability of the ligand¹⁹; hence, there exists an electronic basis for analyte distinction. Using metal centres that span a range of chemical ‘hardness’ and ligand-binding affinity, a wide range of volatile analytes should be differentiable. Because porphyrins show significant solvatochromic effects, even weakly interacting vapours (for example, arenes, halocarbons or ketones) show distinguishable colorimetric effects.

Solutions of various metalated tetraphenylporphyrins in either methylene chloride or chlorobenzene were spotted onto reverse phase silica thin-layer-chromatography plates to produce the sensor array shown in Fig. 1. The chosen metalloporphyrins have excellent chemical stability on the solid support, and most have well-studied solution ligation chemistry. A stainless-steel flow cell equipped with a quartz window held the plate in a fixed position on an inexpensive flatbed scanner, and permitted exposure of the plate to nitrogen carrying the vapour analyte of interest. Scanning after analyte exposure and subtracting new images from the original scan produces a colour change profile, such as that shown for *n*-butylamine in Fig. 1A. (Details of the image processing are given in Fig. 1 legend.) Virtually all porphyrins are saturated after 30 seconds of exposure, yielding a unique colour fingerprint.

In order to demonstrate the generality of this sensing technique, the vapours were chosen to represent a wide range of chemical functionalities. A comparison of colour changes at saturation for a wide range of analytes is shown in Fig. 1B. Each analyte is easily distinguished from the others, and there are family resemblances among chemically similar species (for example, pyridine and *n*-hexylamine). Analyte distinction originates both in the metal-specific ligation affinities and in their specific, unique colour changes upon ligation.

The metalloporphyrin array can also be used to quantify single analytes and to identify vapour mixtures. Because the images’ colour-channel data (that is, RGB values) vary monotonically with porphyrin concentration, we were able to quantify single porphyrin responses to different analytes. Colour-channel data were collected for individual spots and plotted as the quantity $(R_{\text{plt}} - R_{\text{spt}})/R_{\text{plt}}$, where R_{plt} was the red-channel value for the initial silica surface and R_{spt} the average value for the spot. A good linear response is observed until saturation for each porphyrin spot. For example, Zn(TPP), where TPP is 5,10,15,20-tetraphenylporphyrinate(-2), responded linearly to *n*-octylamine between 0 and 0.5 parts per million (p.p.m.). Other porphyrins showed linear response ranges that varied with ligand affinity. Quantifiable, reversible responses are observed even for analyte mixtures of strong ligands, such as pyridines and phosphites (Fig. 1C). Colour change patterns for the mixtures are distinct from either of the neat vapours. Good reversibility was demonstrated for this analyte pair as the vapour mixtures were cycled between the

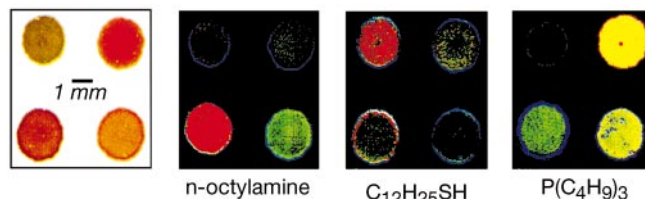


Figure 3 Colour fingerprints at low levels of analyte. The response of a minimized array of four metalloporphyrins (Sn(TPP)(Cl)₂, Co(TPP)(Cl), Zn(TPP) and Fe(TFP)(Cl)), clockwise from the upper left) is shown for *n*-octylamine, dodecanethiol and tri-*n*-butylphosphine at 1.8 p.p.m.

neat analyte extremes, as shown in Fig. 1C. Response curves of individual porphyrins with varying analyte composition provide a multicomponent analysis of mixtures. For example, for the trimethylphosphite/2-methylpyridine system, Co(TPP) responded linearly in this range to the mole fraction of trimethylphosphite, enabling quantification of an unknown blend of the two vapours.

In an effort to understand the origin of the colour changes upon vapour exposure, diffuse reflectance spectra were obtained for single porphyrin spots before and after exposure to analyte vapours. Porphyrin solutions were spotted in 50- μl aliquots onto a plate and allowed to dry under vacuum at 50 °C. Spectral shifts on the plate upon analyte exposure correlated well with those seen from solution ligation. For example, exposure of Zn(TPP) to ethanol and pyridine gave shifts very similar to those resulting from ligation in methylene chloride solutions (Fig. 2).

Reverse phase silica was initially chosen as a non-interacting dispersion medium for the metalloporphyrin array, as well as a suitable surface for diffuse reflectance spectral measurements. The hydrophobic nature of the support also greatly reduces interference from water vapour. For instance, a colour fingerprint generated from exposure of the array to *n*-hexylamine vapour (0.86% in N_2) was identical to that for *n*-hexylamine spiked heavily with water vapour (0.43% *n*-hexylamine plus 1.2% H_2O in N_2); see Supplementary Information for further details. The ability to easily detect species in the presence of a large water background represents a substantial advantage over mass-sensing techniques or methodologies that employ polar polymers as part of the sensor array.

Our array's responses come from selective and specific interactions between the analytes and the metalloporphyrin library. This is in marked contrast to the use of a single indicating fluorophore doped in a variety of matrices, where weak matrix-analyte interactions are required to provide selectivity^{6,7}. An advantage of utilizing chemoselective sensors in an array is that unique patterns can be identified at low vapour concentrations. As shown in Fig. 3, an array of four metalloporphyrins can very easily distinguish *n*-octylamine, dodecanethiol and tri-*n*-butylphosphine at 1.8 p.p.m. in N_2 . Colour changes of metalloporphyrins on reverse phase silica are slow at analyte exposures below 1 p.p.m. owing primarily to the time necessary to equilibrate the high surface area of the silica surface. As shown in Fig. 4, deposition of the metalloporphyrin library as films on Teflon provides an easy route to miniaturization and gives greatly improved response times. Deposition of spots of approximately 500- μm on a side present no difficulty; at this size a 20 \times 20 array can be interfaced to an inexpensive CCD (charge-coupled device) detector for device fabrication. Deposition by ink-jet

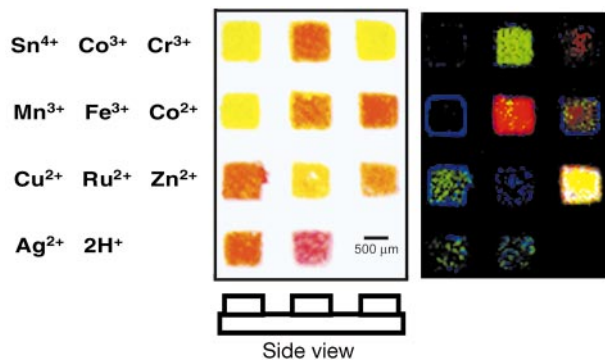


Figure 4 Miniaturized array. The metalloporphyrins were dissolved in a polymer film (dibutylphthalate in polystyrene) and deposited on Teflon; the miniaturization greatly reduces response times. On the left is the array before vapour exposure; on the right is the colour change profile after exposure to *n*-butylamine (1 min, 9.3% in N_2).

printing of these films should permit ready, and reproducible, production of chemoselective sensor arrays.

An important goal is the shape-selective distinction of analytes (for example, *n*-hexylamine versus cyclohexylamine). Functionalized metalloporphyrins that limit steric access to the metal ion^{20–22} are candidates for such differentiation. For instance, we have been able^{23,24} to control ligation of various inorganic ligands to dendrimer-metalloporphyrins and siloxyl-metalloporphyrins, and induce selectivities over a range of up to 10^7 . The initial results from a small library of siloxyl-metalloporphyrins reveal striking differences between analytes as similar as *n*-octylamine, cyclohexylamine and dipropylamine. Such shape-selective analyte discrimination should add a second tier of molecular recognition to the metal-based array.

The technique that we report here can differentiate between a wide range of species. Such 'smell-seeing' could have a number of different applications, including disposable general-purpose vapour dosimeters as well as analyte-specific detectors. The ability to target metal-binding species provides a complementary technique to currently developing methodologies for non-ligating organic vapours. We are at present working to optimize the array components, complete device fabrication, extend such analysis to liquids, and automate the pattern recognition. □

Methods

Porphyrin preparation

5,10,15,20-Tetraphenylporphyrin, H_2TPP , and its metal complexes were prepared using published methods^{25–28}, and fully characterized by fast-atom-bombardment mass spectrometry, elemental analysis, and ultraviolet-visible and NMR spectroscopies. 5,10,15,20-Tetrakis(pentafluorophenyl)-porphyrinatoiron(III) chloride, Fe(TFPF)(Cl), (purchased from Aldrich and used as-received) was added to the porphyrin array because it shows higher ligand-binding constants.

Porphyrin immobilization

The porphyrin array was spotted onto C2 reverse phase silica gel thin-layer-chromatography plates (Whatman KC2, 200 μm thickness, 350 $\text{m}^2 \text{g}^{-1}$ surface area). Porphyrins were spotted from solutions (of a few mM) in chlorobenzene or methylene chloride using a 1- μl microcapillary tube or microlitre syringe. After spotting, sensor plates were dried under vacuum at 50 °C for 1 h before use.

Vapour exposure

Gas streams containing the vapour of interest were generated by flowing nitrogen at 0.5 min^{-1} through the neat liquid analyte in a water-jacketed, glass fritted bubbler. All liquid analytes were obtained from Aldrich or Fisher Scientific, and used as-received. Vapour pressures were controlled by regulating the bubbler temperature²⁹. Low p.p.m. levels of *n*-octylamine and tri-*n*-butylphosphine were generated from temperature-regulated analyte/dodecane solutions with the assumption of solution ideality.

Received 25 November 1999; accepted 25 May 2000.

- Dryer, L. & Berghard, A. Odorant receptors: a plethora of G-protein-coupled receptors. *Trends Pharmacol. Sci.* **20**, 413–417 (1999).
- Lancet, D. & Ben-Arie, N. Olfactory receptors. *Curr. Biol.* **3**, 668–674 (1993).
- Axel, R. The molecular logic of smell. *Sci. Am.* **273**, 154–159 (1995).
- Freund, M. S. & Lewis, N. S. A chemically diverse conducting polymer-based "electronic nose". *Proc. Natl Acad. Sci. USA* **92**, 2652–2656 (1995).
- Loneragan, M. C. *et al.* Array-based vapor sensing using chemically sensitive, carbon black-polymer resistors. *Chem. Mater.* **8**, 2298–2312 (1996).
- Walt, D. R. Fiber optic imaging sensors. *Acc. Chem. Res.* **31**, 267–278 (1998).
- Dickinson, T. A., White, J., Kauer, J. S. & Walt, D. R. A chemical-detecting system based on a cross-reactive optical sensor array. *Nature* **382**, 697–700 (1996).
- Heilig, A. *et al.* Gas identification by modulating temperatures of SnO_2 -based thick film resistors. *Sens. Actuators B* **43**, 45–51 (1997).
- Gardner, J. W., Shurmer, H. V. & Tan, T. T. Application of an electronic nose to the discrimination of coffees. *Sens. Actuators B* **6**, 71–75 (1992).
- Crooks, R. M. & Ricco, A. J. New organic materials suitable for use in chemical sensor arrays. *Acc. Chem. Res.* **31**, 219–227 (1998).
- Grate, J. W. & Abraham, M. H. Solubility interactions and the design of chemically selective sorbent coatings for chemical sensors and arrays. *Sens. Actuators B* **3**, 85–111 (1991).
- Gelperin, A., Flores, J. & Raccuia-Behling, F. Nitric oxide and carbon monoxide modulate oscillations of olfactory interneurons in a terrestrial mollusk. *J. Neurophysiol.* **83**, 116–127 (2000).
- Baron, A. E., Danielson, J. D. S., Gouterman, M., Wan, J. R. & Callis, J. B. Submillisecond response times of oxygen-quenched luminescent coatings. *Rev. Sci. Instrum.* **64**, 3394–3402 (1993).
- Lee, W. *et al.* Halogenated platinum porphyrins as sensing materials for luminescence-based oxygen sensors. *J. Mater. Chem.* **3**, 1031–1035 (1993).
- Vaughan, A. A., Baron, M. G. & Narayanaswamy, R. Optical ammonia sensing films based on an immobilized metalloporphyrin. *Anal. Commun.* **33**, 393–396 (1996).

16. Brunink, J. A. J. *et al.* The application of metalloporphyrins as coating material for quartz microbalance-based chemical sensors. *Anal. Chim. Acta* **325**, 53–64 (1996).
17. Di Natale, C. *et al.* The exploitation of metalloporphyrins as chemically interactive material in chemical sensors. *Mater. Sci. Eng. C* **5**, 209–215 (1998).
18. Blauer, G. & Sund, H. (eds) *Optical Properties and Structure of Tetrapyrroles* (de Gruyter, Berlin, 1985).
19. Nappa, M. & Valentine, J. S. The influence of axial ligands on metalloporphyrin visible absorption spectra. Complexes of tetraphenylporphinatozinc. *J. Am. Chem. Soc.* **100**, 5075–5080 (1978).
20. Suslick, K. S. & Van Deussen-Jeffries, S. in *Comprehensive Supramolecular Chemistry* (ed. Lehn, J. M.) 141–170 (Elsevier, Oxford, 1996).
21. Bhyrappa, P., Young, J. K., Moore, J. S. & Suslick, K. S. Dendrimer porphyrins: synthesis and catalysis. *J. Am. Chem. Soc.* **118**, 5708–5711 (1996).
22. Chou, J.-H., Nalwa, H. S., Kosal, M. E., Rakow, N. A. & Suslick, K. S. in *The Porphyrin Handbook* (eds Kadish, K., Smith, K. & Guillard, R.) 43–132 (Academic, New York, 2000).
23. Bhyrappa, P., Vijayanthimala, G. & Suslick, K. S. Shape-selective ligation to dendrimer-metalloporphyrins. *J. Am. Chem. Soc.* **121**, 262–263 (1999).
24. Sen, A. & Suslick, K. S. Shape selective discrimination of small organic molecules. *J. Am. Chem. Soc.* (in the press).
25. Adler, A. D. *et al.* A simplified synthesis for meso-tetraphenylporphyrin. *J. Org. Chem.* **32**, 476 (1967).
26. Adler, A. D., Longo, F. R., Kampas, F. & Kim, J. On the preparation of metalloporphyrins. *J. Inorg. Nucl. Chem.* **32**, 2443–2445 (1970).
27. Barley, M., Becker, J. Y., Domazetis, G., Dolphin, D. & James, B. R. Synthesis and redox chemistry of octaethylporphyrin complexes of ruthenium(II) and ruthenium(III). *Can. J. Chem.* **61**, 2389–2396 (1983).
28. Datta-Gupta, N. & Bardos, T. J. Synthetic porphyrins II: preparation and spectra of some metal chelates of para-substituted-meso-tetraphenylporphyrins. *J. Pharm. Sci.* **57**, 300–304 (1968).
29. Yaws, C. L. *Handbook of Vapor Pressure* (Gulf, Houston, 1994).

Supplementary Information is available on Nature's World-Wide Web site (<http://www.nature.com>) or as paper copy from the London editorial office of Nature.

Acknowledgements

This work was supported by the US NIH and in part by the US DOD and DOE.

Correspondence and requests for materials should be addressed to K.S.S. (e-mail: ksuslick@uiuc.edu).

Timing of the Last Glacial Maximum from observed sea-level minima

Yusuke Yokoyama*†, Kurt Lambeck*, Patrick De Deckker‡, Paul Johnston* & L. Keith Fifield§

* Research School of Earth Sciences, ‡ Department of Geology, § Department of Nuclear Physics, Research School of Physical Sciences and Engineering, The Australian National University, Canberra, ACT 0200, Australia

During the Last Glacial Maximum, ice sheets covered large areas in northern latitudes and global temperatures were significantly lower than today. But few direct estimates exist of the volume of the ice sheets, or the timing and rates of change during their advance and retreat^{1,2}. Here we analyse four distinct sediment facies in the shallow, tectonically stable Bonaparte Gulf, Australia—each of which is characteristic of a distinct range in sea level—to estimate the maximum volume of land-based ice during the last glaciation and the timing of the initial melting phase. We use faunal assemblages and preservation status of the sediments to distinguish open marine, shallow marine, marginal marine and brackish conditions, and estimate the timing and the mass of the ice sheets using radiocarbon dating and glacio-hydroisostatic modelling. Our results indicate that from at least 22,000 to 19,000 (calendar) years before present, land-based ice volume was at its maximum, exceeding today's grounded ice sheets by $52.5 \times 10^6 \text{ km}^3$. A rapid decrease in ice volume by about 10% within a few hundred years terminated the Last Glacial Maximum at $19,000 \pm 250$ years.

† Present address: Space Sciences Laboratory, University of California, Berkeley, California, USA, and Lawrence Livermore National Laboratory, 7000 East Avenue, PO Box 808, L-202 Livermore, California 94550, USA.

The broad and shallow continental margin of northern Australia includes several local bathymetric depressions, the largest of which is the Bonaparte Gulf. During times of sea-level lowstands much of the shelf was exposed, and the sediments deposited in the depressions were protected from wave action by the outer shelf edge. A total of 23 gravity cores, 10 vibrocores and 3 grab samples were collected from present-day water depths of 34 to 147 m along transects across the shelf margin and the Bonaparte depression (Fig. 1a). All cores were sedimentologically examined and a number were selected for micropalaeontological analysis and radiocarbon dating. Depending on faunal assemblages and preservation status (Fig. 1b, see also Methods section below) four distinct bio-sedimentary facies have been recognized: open marine, shallow marine, marginal marine, and brackish water, denoted by OM, SM, MM and BR, respectively, in Fig. 1b. We obtained 41 radiocarbon dates of foraminifera and bivalve molluscs using accelerator mass spectrometry (AMS) techniques and dated some of the larger bivalves using conventional liquid scintillation counting methods. All AMS-dated samples were severely etched (about 40% to 50%) to discard outer shell material that may have been contaminated by secondary carbonate precipitation. Figure 1b summarizes the results for 7 of the cores from water depths between 128 and 95 m. All carbonate ages have been corrected for reservoir effect (400 years; refs 3, 4) and calibrated to a calendar timescale^{5,6}. The cores indicate excellent preservation of faunal specimens, many without evidence for reworking, and the ¹⁴C dates indicate only rare instances of age inversions.

Last Glacial Maximum (LGM) sea-level indicators are preserved in a number of the cores. To reconstruct a sea-level curve based on micropalaeontological evidence, it is necessary to consider the palaeoenvironmental conditions as a sequence of events assuming that little or no break in sedimentation, and no erosion, has occurred. (If a hiatus does occur it results in missing bio-facies and in reworking of the faunas; and this is not observed.) Thus, through identification of a transition from shallow marginal marine to brackish conditions and then back to shallow marginal marine conditions, the timing of the brackish conditions records the interval of lowest sea level. Once this depth is identified in a single core, other cores with depths either side of the identified low sea-level stand are examined to substantiate the reconstruction. This has been done using core GC5 as the master core because it has the best preserved and dated record for brackish water conditions. No truly lacustrine phase has been recognised in any of the cores, indicating that throughout the LGM the Bonaparte depression remained in open contact with the Timor Sea⁷.

The transition from marginal marine to brackish facies occurs in core GC5 at 21,280 calendar years before present (cal. yr BP) at a depth of 340 cm below the sea floor (Fig. 1b). Sediments below this depth contain marine ostracods and planktonic foraminifers, whereas above this boundary dwarf specimens of the benthic foraminifer *Ammonia beccarii* occur along with other shallow to brackish water indicators such as the benthic foraminifer *Elphidium* spp. and the euryhaline ostracod *Cyprideis australiensis*^{8,9}. Marginal marine and brackish-water conditions existed for about 3,000 years, in agreement with results from cores GC4 and GC6 (Fig. 1b) as well as GB1. Sea level at GC5 was, therefore, a few metres below -121 m (Fig. 2a) in this time interval. Deeper cores, both within the depression (GC1, GC2 and GC3) and outside it, do not indicate any brackish facies and place a lower limit of -125 m on the position of relative sea-level at these locations. The microfossil assemblages of cores GC10 and GC11, at -103 and -101 m respectively, are indicative of a marginal beach or coastal lagoon environment between 17,650 and 17,450 cal. yr BP. In core GC7, undamaged littoral-dwelling bivalves occur at -107 m with an age of 17,610 cal. yr BP (Fig. 1b). Figure 2a illustrates the results for all samples free from post-depositional disturbance. They indicate that between 22,000 and 19,000 cal. yr BP a rapid rise of 10–15 m occurred.

motion of crystalline domains in an otherwise rigid solid-state system. □

Received 7 January; accepted 10 June 2002; doi:10.1038/nature00901.

- Huang, S. Y., Kavan, L., Exnar, I. & Grätzel, M. J. Rocking chair lithium battery based on nanocrystalline TiO₂ (anatase). *J. Electrochem. Soc.* **142**, L142–L144 (1995).
- Ohzuku, T., Kodama, T. & Hirai, T. Electrochemistry of anatase titanium dioxide in lithium non-aqueous cells. *J. Power Sources* **14**, 153–166 (1985).
- Ohzuku, T. & Hirai, T. An electrochromic display based on titanium dioxide. *Electrochim. Acta* **27**, 1263–1266 (1982).
- Ottaviani, M., Panero, S., Morzilli, S. & Scrosati, B. The electrochromic characteristics of titanium oxide thin film electrodes. *Solid State Ionics* **20**, 197–202 (1986).
- Cantao, M. P., Cisneros, J. I. & Torresi, R. M. Electrochromic behaviour of sputtered titanium-oxide thin-films. *Thin Solid Films* **259**, 70–74 (1995).
- Bechinger, C., Ferrere, S., Zaban, A., Sprague, J. & Gregg, B. A. Photoelectrochromic windows and displays. *Nature* **383**, 608–610 (1996).
- O'Regan, B. & Grätzel, M. A low-cost, high-efficiency solar-cell based on dye-sensitized colloidal TiO₂ films. *Nature* **353**, 737–740 (1991).
- Hagfeldt, A. & Grätzel, M. Light-induced redox reactions in nanocrystalline systems. *Chem. Rev.* **95**, 49–68 (1995).
- Wagemaker, M., van de Krol, R., Kentgens, A. P. M., van Well, A. A. & Mulder, F. M. Two phase morphology limits lithium diffusion in TiO₂ (anatase): A Li-7 MAS NMR study. *J. Am. Chem. Soc.* **123**, 11454–11461 (2001).
- Xu, Z. & Stebbins, J. F. Cation dynamics and diffusion in lithium orthosilicate — 2-dimensional Li-6 NMR. *Science* **270**, 1332–1334 (1995).
- Verhoeven, V. W. J. et al. Lithium dynamics in LiMn₂O₄ probed directly by two-dimensional Li-7 NMR. *Phys. Rev. Lett.* **86**, 4314–4317 (2001).
- Ernst, R. R., Bodenhausen, G. & Wokaun, A. *Principles of Nuclear Magnetic Resonance in One and Two Dimensions* (Clarendon, Oxford, 1994).
- Lunell, S., Stashans, A., Ojamae, L., Lindstrom, H. & Hagfeldt, A. Li and Na diffusion in TiO₂ from quantum chemical theory versus electrochemical experiment. *J. Am. Chem. Soc.* **119**, 7374–7380 (1997).
- Kavan, L., Grätzel, M., Gilbert, S. E., Klemenz, C. & Schell, H. J. Electrochemical and photoelectrochemical investigation of single-crystal anatase. *J. Am. Chem. Soc.* **118**, 6716–6723 (1996).
- Claus, J., Schmidt-Rohr, K. & Spiess, H. W. Determination of domain sizes in heterogeneous polymers by solid-state NMR. *Acta Polym.* **44**, 1–17 (1993).
- Schmidt-Rohr, K. & Spiess, H. W. *Multidimensional Solid-state NMR and Polymers* (Academic, London, 1994).
- Koudriachova, M. V., Harrison, N. M. & de Leeuw, S. W. Effect of diffusion on lithium intercalation in titanium dioxide. *Phys. Rev. Lett.* **86**, 1275–1278 (2001).

Acknowledgements

This work is a contribution from the Delft Institute for Sustainable Energy (DISE).

Competing interests statement

The authors declare that they have no competing financial interests.

Correspondence and requests for materials should be addressed to F.M.M. (e-mail: mulder@iri.tudelft.nl).

Synthetic hosts by monomolecular imprinting inside dendrimers

Steven C. Zimmerman*†, Michael S. Wendland*, Neal A. Rakow*, Ilya Zharov† & Kenneth S. Suslick*†

* Department of Chemistry; † Beckman Institute for Advanced Science and Technology, University of Illinois at Urbana-Champaign, 600 S. Mathews Avenue, Urbana, Illinois 61801, USA

Synthetic host systems capable of selectively binding guest molecules are of interest for applications ranging from separations and chemical or biological sensing to the development of biomedical materials. Such host systems can be efficiently prepared by 'imprinting' polymers or inorganic materials with template molecules, which, upon removal, leave behind spatially arranged functional groups that act as recognition sites^{1–4}. However, molecularly imprinted polymers have limitations, including incomplete template removal, broad guest affinities

and selectivities, and slow mass transfer^{5–8}. An alternative strategy for moulding desired recognition sites uses combinatorial libraries of assemblies that are made of a relatively small number of molecules, interconverting in dynamic equilibrium; upon addition of a target molecule, the library equilibrium shifts towards the best hosts^{9–11}. Here we describe the dynamic imprinting of dendritic macromolecules with porphyrin templates to yield synthetic host molecules containing one binding site each. The process is based on our general strategy to prepare cored dendrimers^{12,13}, and involves covalent attachment of dendrons to a porphyrin core, cross-linking of the end-groups of the dendrons, and removal of the porphyrin template by hydrolysis. In contrast to more traditional polymer imprinting, our approach ensures nearly homogeneous binding sites and quantitative template removal. Moreover, the hosts are soluble in common organic solvents and amenable to the incorporation of other functional groups, which should facilitate further development of this system for novel applications.

When developing our 'monomolecular imprinting' methodology, we selected dendrimers as macromolecular hosts because their molecular homogeneity and excellent solubility facilitate characterization¹⁴. The choice of a porphyrin as templating agent was motivated by the scarce availability of synthetic hosts for large molecule guests¹⁵ and the fact that porphyrins are excellent probes of binding, owing to the sensitivity of their intense colour to the local environment¹⁶. Porphyrins have been integrated into molecularly imprinted polymers¹⁷ and synthetic hosts¹⁸, but have to our knowledge not been used as templates. Moreover, the chemistry of porphyrin-core dendrimers is well established, given their role as well-studied synthetic models of haem proteins and related proteins^{19–22}.

The basic strategy for synthesizing dendrimer hosts follows our earlier work on cored dendrimers^{12,13}. The preparation of porphyrin-core dendrimer **1** is summarized in Fig. 1. The key structural features of this pre-cross-linked dendrimer are the tetrakis-meso(3,5-dihydroxyphenyl)-porphyrin (**3**)¹⁹ unit at the core, and hydrolysable ester-bond links to eight third-generation Fréchet-type dendrons²³ (**2**)¹², which give a total of 64 homoallyl end-groups (see Supplementary Information). In addition to **1**, a small amount (~5%) of dendrimers containing six or seven dendrons was formed (see below).

Porphyrin-core dendrimer **1** was cross-linked¹² using 4 mol% (per alkene) of Grubbs' catalyst **4**²⁴ at 10⁻⁶ M in benzene to produce cross-linked dendrimer **5** in 88% yield. Size exclusion chromatography (SEC) established that cross-linking occurs largely (≥95%) intramolecularly. The ¹H NMR spectrum of **5** confirmed the formation of internal, disubstituted alkene groups and gave the average number of cross-links as approximately 29. The matrix-assisted laser desorption/ionization–time of flight (MALDI–TOF) mass spectrum of **5** provided conclusive evidence for extensive intramolecular cross-linking: it contained peaks corresponding to individual isomers from 28 to 32 out of 32 possible cross-links (mass/charge ratios (*m/z*) 10,369, 10,341, 10,313, 10,285, 10,257), with the tallest peak at *m/z* 10,285 (31 cross-links, see Supplementary Information). The ability of catalyst **4** to produce from **1** a compact structure with a median of 30 out of 32 possible cross-links may be due to the reversibility of the ring closing metathesis (RCM) reaction²⁴. The precise details of the cross-linking process remain to be determined. But analogy with the quantitative RCM of polyolefins²⁵ suggests that it may be a dynamic process, thus ensuring that millions of kinetically favoured cross-link isomers may equilibrate into a small number of thermodynamically stable ones.

Treatment of the cross-linked dendrimer **5** with 2.5 M aqueous KOH solution in tetrahydrofuran (THF) quantitatively removed the porphyrin template (that is, **3**), forming **6** in a 43% yield. The ¹H NMR spectrum of **6** showed no signals originating from the porphyrin core, and the UV–vis. spectrum of **6** showed no detectable absorbance at 420 nm, the Soret band of the porphyrin. Elemental analysis of the hydrolysis product was consistent with a

dodecahydrate of **6** containing 30 cross-links. Elemental analysis for both nitrogen and ruthenium showed none present ($0.0 \pm 0.3\%$) and only a trace of potassium. Finally, comparison of the MALDI-TOF mass spectra of **5** and **6** showed the peaks in the latter shifted to lower m/z values by 597 (see Supplementary Information), corresponding to the loss of the porphyrin core ($C_{44}H_{14}N_4$; m/z 598.6).

The hydrolysis reaction that removes the template molecule $H_2T(3,5-OHPh)P$ (**3**) results in the addition of eight $-OH$ groups inside the dendrimer host, so **3** does not generate an ideal imprint for binding of itself (Fig. 2). In the limit of a well-formed imprint, the hydrolysis reaction creates a binding site that is too small to accommodate **3**, but might be suitable for the isomeric hydroxy compound, $H_2T(2,6-OHPh)P$ (**7**) or tetrapyrimidyl porphyrin ($H_2T(3,5\text{-pyrimidyl})P$) **8**. An extensive series of porphyrins, **7–16** (Fig. 3), was therefore prepared^{26,27}, and used to study the binding of imprinted dendrimer **6**.

To conduct the binding experiments, the solvent had to be sufficiently apolar to allow formation of hydrogen bonds, but polar enough to dissolve both **6** and the porphyrin. The complexation studies with octahydroxyporphyrins **3** and **7** were performed in 5% (v/v) ethyl acetate–toluene, whereas **8–16** were sufficiently soluble to study in toluene. Spectrophotometric titrations were performed by adding aliquots of a concentrated solution of imprinted dendrimer to a dilute solution of porphyrin and recording the Soret region after 10 minutes of equilibration.

Complexation of porphyrin **7** by imprinted dendrimer **6** was signalled by a significant bathochromic (red) shift in the λ_{max} of the Soret band of **7** ($3 \mu M$ solution in 5% ethyl acetate–toluene) upon addition of **6** (see Supplementary Information). Consistent with

hydrogen-bond complexation, the red shift could be fully reversed by increasing the ethyl acetate content from 5% (v/v) to >15% (v/v) in toluene. Furthermore, no red shift was observed when **6** was added to a solution of **7** in 50% (v/v) ethyl acetate–toluene. In 5% ethyl acetate–toluene no change in the Soret band of H_2TPP (**9**) or $H_2T(3,5-OHPh)P$ (**3**) occurred upon addition of **6**. The latter result argues for a relatively rigid imprint; that is, **6** is not a flexible octa-acid that can complex any guest with sufficient hydrogen bond donors or acceptors. The magnitude of the shift in the Soret band of **7** was directly dependent on the amount of **6** added and the time elapsed. Extensive studies to be published separately indicate a relatively homogeneous imprint that produces within two hours a complex with a 5 nm red shift and a diminished apparent extinction coefficient, which, in turn, undergoes a slow conformation change over 17 days producing a tighter complex (10-fold increase in apparent association constant K_{app}) with an additional 6 nm red shift and an increased apparent extinction coefficient. The results described below are for the fast binding process only.

Complexation of $H_2T(2,6-OHPh)P$ (**7**) by imprinted dendrimer **6** was also observed by SEC. Porphyrin **7** does not elute from the SEC matrix by itself, but in the presence of the imprinted dendrimer **6** it elutes with a measured retention time identical to that of the dendrimer. Thus, complexation within the dendrimer protects the polar porphyrin from adsorption during the course of its elution and decomplexation is slow on the timescale of the SEC experiment (minutes).

To determine the shape selectivity and number of binding contacts to the ligand, quantitative binding studies were carried out with porphyrins **7–16** (Fig. 3) using standard methods²⁸. The

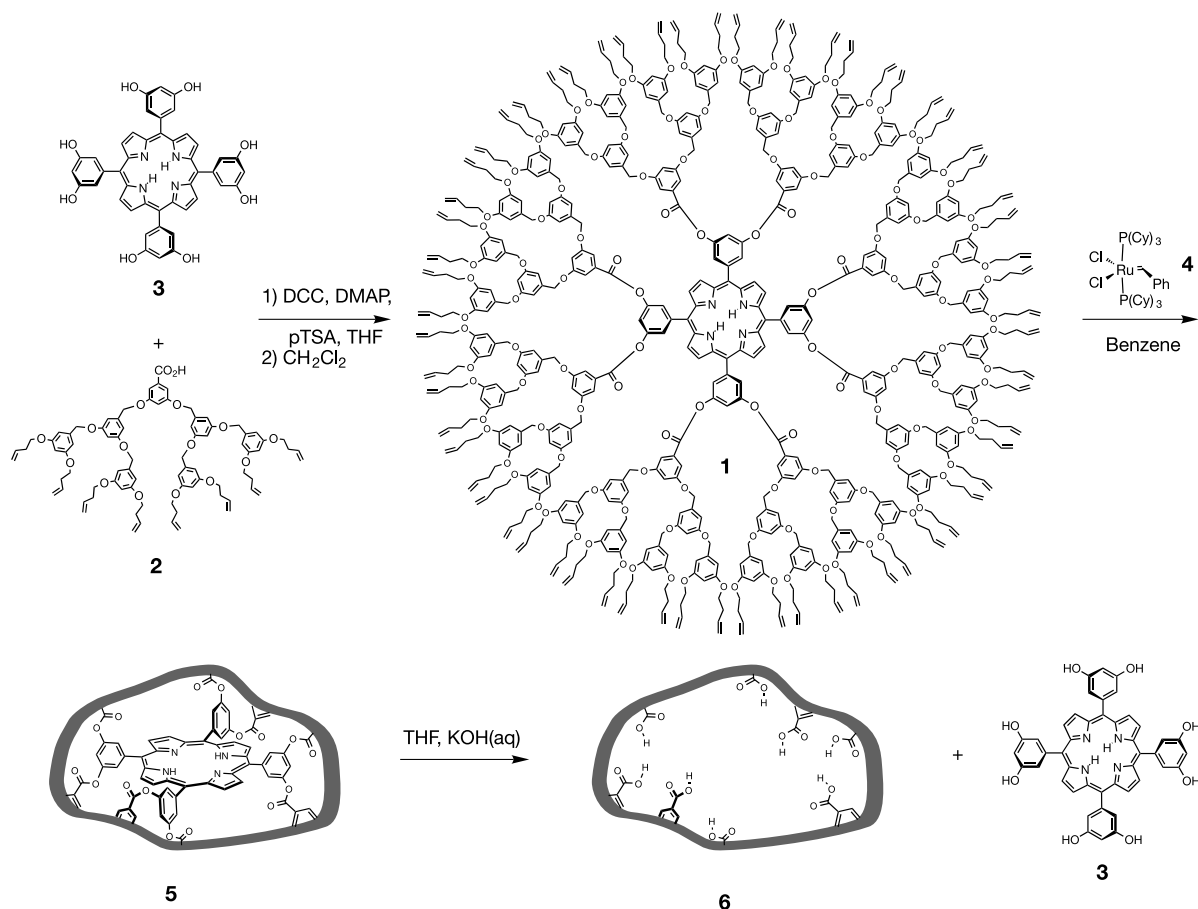


Figure 1 Scheme illustrating the preparation of imprinted dendrimer **6**. First, dendrons **2** are attached to the core porphyrin **3** to produce the dendrimer **1**, then **1** is cross-linked using Grubbs' catalyst **4** to give the dendrimer **5**, followed by the hydrolysis of **5** to remove

the porphyrin core **3** and produce **6**. DCC, dicyclohexylcarbodiimide; DMAP, 4-(dimethylamino)pyridine; pTSA, *p*-toluene sulphonic acid; THF, tetrahydrofuran.

association constants (Fig. 3) are denoted as K_{app} because of the likely heterogeneity in **6** and time dependence of the binding process. $H_2T(3,5\text{-pyrimidyl})P$ (**8**) is bound by **6** with a K_{app} ($5 \times 10^4 M^{-1}$) of the same magnitude as the **6-7** association. The pyridyl porphyrins $H_2T(2\text{-pyridyl})P$ (**10**), $H_2T(3\text{-pyridyl})P$ (**11**) and $H_2T(4\text{-pyridyl})P$ (**12**) bind equally well, despite their capacity to make only half as many hydrogen bonds as **8**. Although this may suggest that the full eight carboxylic acids are not simultaneously engaged in binding $H_2T(3,5\text{-pyrimidyl})P$ (**8**), the difference must partly originate in the 10^4 -fold higher basicity of pyridine relative to pyrimidine. Along the same lines, given that typical pyridine-carboxylic acid association constants in apolar organic solvents are $\sim 10^2 M^{-1}$, it might be expected that complexes containing at least four such interactions would exhibit absolute K_{app} values higher than 10^4 to $10^5 M^{-1}$. Factors that may lower the K_{app} values for **6** include the need to break any internal carboxylic acid dimers or otherwise conformationally reorganize the binding site, and remove water molecules bound to the carboxylic acid groups. Although infrared studies of **6** were inconclusive with respect to possible dimerization of its carboxylic groups, elemental analysis of **6** indicates the presence of water presumably solvating the polar core. The K_{app} for the **6-10** (2-pyridyl isomer) is approximately 2-fold lower than that for the 3- and 4-pyridyl isomers **11** and **12**, indicating a degree of shape selectivity in the imprint. No binding was detected for tetraphenyl mono, bis, and trispyridyl porphyrins **9**, **13**, **14**, **15** or **16**. Thus, a minimum of four binding contacts is necessary for complexation under the conditions used in this study.

To further support the importance of reversible complexation by hydrogen bonding and the direct involvement of the carboxylic acid groups, the octa-ethyl ester dendrimer **6**-(CO₂Et)₈ was prepared by ethanolysis of **5** (K₂CO₃, toluene, ethanol, reflux). The structure of **6**-(CO₂Et)₈ was verified by SEC, ¹H NMR spectroscopy, MALDI-TOF mass spectrometry, and UV-vis. spectroscopy. The addition of approximately 60 equivalents of **6**-(CO₂Et)₈ to $H_2T(3\text{-pyridyl})P$ (**11**) caused no red shift over the course of 4 days. Likewise addition of simple carboxylic acids did not cause a red shift of $H_2T(3\text{-pyridyl})P$ (**11**). Neither the addition of 640 equivalents of dendron carboxylic acid **2** to a $\sim 3 \mu M$ solution of $H_2T(2,6\text{-OHPh})P$ (**7**) in 5% ethyl acetate-toluene nor the addition of 2,000 equivalents of 4-*t*-butyl benzoic acid to a $\sim 3 \mu M$ solution of $H_2T(3\text{-pyridyl})P$ (**11**) in toluene led to any red shift. Finally, a smaller dendrimer with three acid groups, which was imprinted with 1,3,5-tri(hydroxymethyl)benzene¹², did not alter the position of the Soret band of a $\sim 3 \mu M$ solution of **11** in toluene even upon addition of 49 equivalents.

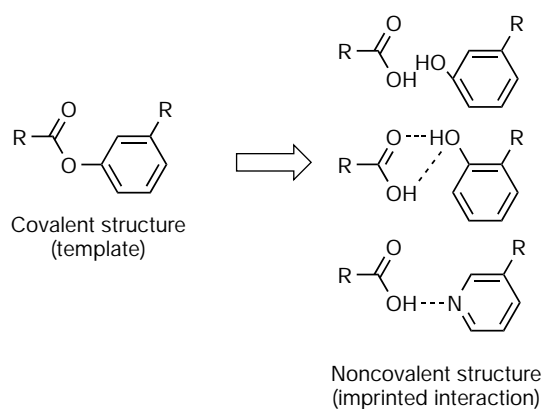


Figure 2 Structural drawing illustrating structural changes that occur upon hydrolysis of the cross-linked dendrimer **5**. The covalent structure contains eight phenyl benzoates formed by esterification of the phenolic porphyrin **3** with the carboxylic acid dendrons **2**. Note that two oxygen atoms would be left in the same space if both components of the covalent structure were held fixed. The isomeric phenol is better accommodated and phenyl benzoate appears to imprint well for a 3-pyridyl or 3,5-pyrimidyl porphyrin.

As indicated above, a known source of heterogeneity in the imprinted dendrimer arises from incomplete reaction of **2** with **3**. This imperfect material was shown not to play a role in binding by carefully removing it with repeated preparative SEC. A different type of heterogeneity may originate in the RCM reaction of dendrimer **1**, which can produce **5** containing a very large number of cross-link isomers. The broad peaks observed in the ¹H NMR of **5** and **6** might be attributed to the presence of a mixture of such isomers, although the heterogeneity does not manifest itself in the binding (see above).

To gain insight into the three-dimensional structure of **6** and how it changes with the extent and position of the cross-links, molecular modelling was performed using molecular mechanics and dynamics. A series of cross-linked dendrimers **5** were built and minimized. The porphyrin core was removed, providing a globular porous structure with eight carboxyl groups in its interior. The resulting models of **6** were subjected to 60 ps of molecular dynamics alone and with $H_2T(3,5\text{-pyrimidyl})P$ (**8**) within the binding site. In both cases the overall globular shape of **6** did not significantly change compared to that of **5**. The van der Waals surface of a modelled imprinted dendrimer with nine intra- and 20 inter-dendron cross-links (Fig. 4a) reveals a slightly porous structure with no obvious large channels to the binding site. Thus, complexation and decomplexation must involve a dynamic breathing process (in other models with a higher fraction of intra-dendron cross-

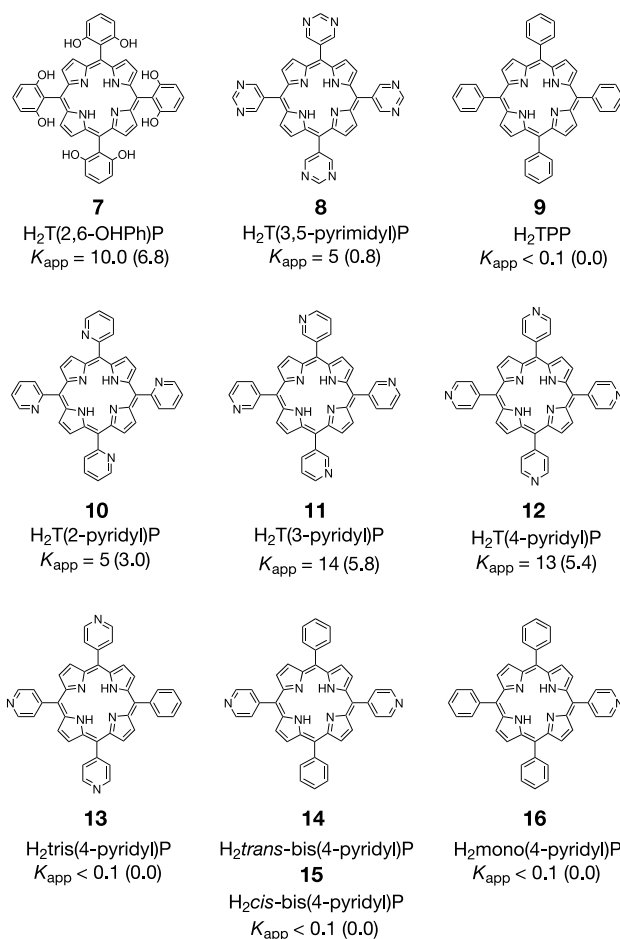


Figure 3 Porphyrins used to study binding properties of imprinted dendrimer **6**. Each structure is accompanied by the corresponding apparent association constant K_{app} ($\times 10^4 M^{-1}$), and the red shift value of the Soret band ($\Delta\lambda_{max}$, nm) for the complex formed between imprinted dendrimer **6** and the porphyrin. A value of $\Delta\lambda_{max} = 0.0$ indicates no observed change in the absorption spectrum. Upper limits on solubility prevented a more accurate upper limit of K_{app} from being obtained.

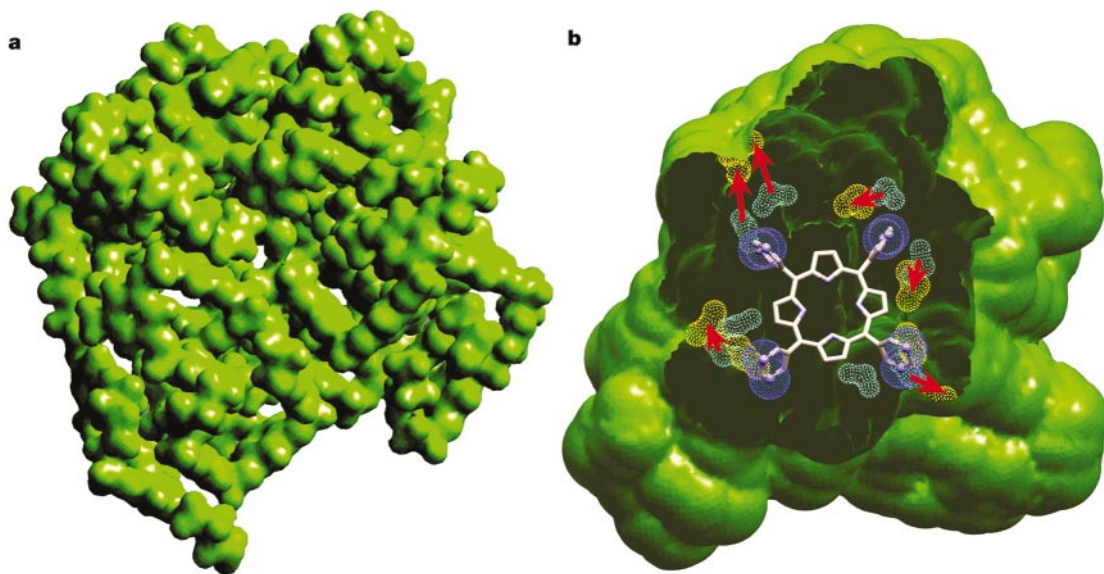


Figure 4 Calculated structure of imprinted dendrimer **6** built by iterative attachment of dendrons to the core porphyrin, minimization and cross-linking of neighbouring double bonds. **a**, van der Waals surface of a representative dendrimer structure produced by a 60 ps annealed dynamics simulation. **b**, Calculated binding pocket inside **6**; yellow clouds

represent positions of carboxyl groups when **6** is minimized without the host porphyrin **8**, cyan clouds represent positions of carboxyl groups when **6** is minimized in the presence of the host porphyrin **8**, red arrows show the movement of carboxylic groups.

links, the binding pocket appears more readily accessible). The carboxyl groups in **6** moved from their original positions in the ester links of **5**, but the binding pocket was mostly intact (Fig. 4b). The displacement of carboxyl groups was less significant when **8** was present in the interior of the cored dendrimer as seen in the overlaid structures in Fig. 4b.

As a demanding test of the monomolecular imprinting process, we chose a particularly large molecule guest, a polyfunctionalized porphyrin, as the template within an octa-dendron array. Extensive cross-linking using the RCM reaction followed by template removal produced an imprinted dendrimer that selectively and tightly ($K_{app} = (0.5-1.4) \times 10^5 M^{-1}$) bound porphyrins presenting an appropriate size and four or more hydrogen-bonding sites (for example, **7**, **8**, **10-12**). The binding is size selective on the basis of results with the octahydroxyl porphyrins **3** and **7**, and modestly shape-selective on the basis of the results with the isomeric pyridyl porphyrins (**10-12**).

The limitations of this approach are the need for multi-step synthesis of the dendrimers, and the high dilution conditions needed for the RCM reaction. (We note that it was recently shown that this high dilution is not necessary for a dendrimer where the alkene groups reside in the branching units¹³.) But even in its current implementation, the monomolecular imprinting approach has several characteristics not yet obtainable through traditional polymer imprinting. These include high-efficiency imprinting with nearly all templates producing functional binding sites, quantitative removal of the template, solubility of the imprinted material in common organic solvents, and separation of imperfectly assembled binding sites. By using resins covalently linked to the target ligand, it should be possible to fractionate heterogeneous material after imprinting. In this manner, selection of imprinted sites on the basis of affinity or binding kinetics should be possible. Finally, the single-step synthesis of hyperbranched or analogous macromolecules, combined with the ability to integrate reporter groups, makes the monomolecular imprinting approach a promising one for further development. □

Methods

The titration data were analysed by plotting $[ID]$ against $[ID]/\Delta A$, where $[ID]$ is the imprinted dendrimer concentration and ΔA is the change in absorbance upon addition of

6. This method allows association constants to be determined by finding the line intercept that gives $1/K_{app}$ and does not require knowledge of the concentration of the free or complexed porphyrin. The titrations were all completed within 1 h and all gave linear plots. As with other Scatchard-type plots, linearity indicates the formation of 1:1 complexes.

Molecular mechanics and dynamics were performed using Cerius², version 4.5 (Accelrys). For energy minimizations and simulated annealing (60 ps, 300–500 K), the Dreiding force field was used.

Preparation of 1

Compound **1** (5,10,15,20-tetrakis[3,5-bis[3,5-bis(3,5-bis(3-buten-1-oxy)benzyloxy)benzyloxy]benzyloxy]phenyl]porphyrin ([G-3]₈-T(3,5-OHPh)P) was synthesized as follows. [G-3]-CO₂H (**2**) (283 mg, 215 μmol), 13.2 mg (17.8 μmol) of **3** (5,10,15,20-tetrakis(3',5'-dihydroxyphenyl)porphyrin, referred to as H₂T(3,5-OHPh)P), 519 mg (2.5 mmol) of dicyclohexylcarbodiimide (DCC), 78.6 mg (643 μmol) of 4-(dimethylamino)pyridine (DMAP) and 118 mg (621 μmol) of *p*-toluene sulphonic acid (pTSA) were dissolved in 15 ml of THF. The reaction mixture was stirred overnight at room temperature and filtered to remove the dicyclohexylurea (DCU) formed. The filtrate was concentrated under reduced pressure and dissolved in 15 ml of CH₂Cl₂. To this solution, 510 mg (2.5 mmol) of DCC, 75.8 mg (620 μmol) of DMAP and 117 mg (615 μmol) of pTSA was added, and the mixture was stirred at room temperature. The reaction was complete after three days (by thin-layer chromatography and SEC). The reaction mixture was filtered to remove the DCU, and the resulting filtrate was concentrated under reduced pressure. The remaining residue was loaded onto a silica gel column (4 × 15 cm) and eluted with 30% EtOAc/PE. The product was further purified by loading it onto a SEC column and eluting it with toluene. The product was dried overnight under vacuum to afford 107 mg (54%) of **1** as a deep red oil: ¹H NMR (CD₂Cl₂) δ 9.22 (s, 8H), 8.15 (d, 8H), 7.75 (t, 4H), 7.54 (d, 16H), 6.81 (t, 8H), 6.64 (d, 32H), 6.48 (m, 80H), 6.31 (t, 32H), 5.81 (ddt, 64H), 5.07 (ddt, 64H), 5.01 (ddt, 64H), 4.98 (s, 32H), 4.87 (s, 64H), 3.88 (t, 128H), 2.42 (tddd, 128H), -2.86 (s, 2H); ¹³C NMR (CD₂Cl₂) 165.1, 160.7, 160.5, 160.4, 150.3, 144.2, 139.6, 139.3, 135.0, 131.6, 126.3, 118.9, 117.0, 109.3, 108.1, 106.7, 106.2, 101.9, 101.0, 70.5, 70.3, 67.6, 33.9; MS (MALDI-TOF) *m/z* 11,174.7 (M + Na⁺); SEC (toluene) calculated *M_w* = 8,155; UV-vis. (CH₂Cl₂) λ_{max} = 275.0, 420.5 (Soret). Analysis: calculated for C₆₉₂H₇₃₄N₄O₁₂₈: C, 74.51; H, 6.63; N, 0.50. Found: C, 74.56; H, 6.41; N, 0.48.

Cross-linked [G-3]₈-T(3,5-OHPh)P (**5**)

To a solution of 497 mg (44.6 μmol) of **1** in 4.4 litres of benzene was added 99.6 mg (120 μmol) of Grubbs' catalyst (**4**). The reaction mixture was stirred at room temperature for 22 h. The benzene was removed under reduced pressure. The crude product was loaded onto a silica gel plug (4 × 6 cm) and eluted with 400 ml of 50% petroleum ether/50% CH₂Cl₂ and 400 ml of 5% EtOAc/CH₂Cl₂. The EtOAc/CH₂Cl₂ solution was concentrated under reduced pressure. The product was dried overnight under vacuum to afford 409 mg (89%) of **5** as a dark red powder: ¹H NMR (*d*₈-toluene) δ 9.17 (bs, 8H), 8.15 (bs, 8H), 7.70 (bs, 20H), 6.59 (bs, 152H), 5.78 (bs, ~4H), 5.51 (bs, ~60H), 5.04 (bs, ~8H), 4.82 (bs, 96H), 3.70 (bs, 128H), 2.33 (bs, 128H); MS (MALDI-TOF) *m/z* 10,258.2 (M + H⁺ - 32C₂H₄), 10,286.3 (M + H⁺ - 31C₂H₄), 10,311.8 (M + H⁺ - 30C₂H₄); SEC (toluene) calculated *M_w* = 5509; UV-vis. (CH₂Cl₂) λ_{max} = 276.0, 421.0 (Soret).

Imprinted [G-3]₈-T(3,5-OH)P(6)

To a solution of 102 mg (9.88 μmol) of **5** dissolved in 15 ml of THF, was added 10 ml of 2.5 M aqueous KOH. The reaction mixture was stirred vigorously at reflux until the reaction was complete by TLC. The reaction was stopped by removing the THF under reduced pressure. The resulting aqueous layer was extracted with CHCl₃ (3 × 25 ml). The combined organic layers were washed with 1 M aqueous HCl and water, and concentrated under reduced pressure. The product was dried under vacuum to afford 41.5 mg (43%) of **6** as a beige powder: ¹H NMR δ 7.23 (bs, 16H), 6.51 (bs, 152H), 5.86 (bs, ~4H), 5.60 (bs, ~60H), 5.12 (bs, ~8H), 4.86 (bs, 96H), 3.92 (bs, 128H), 2.45 (bs, 128H); MS (MALDI-TOF) *m/z* 9,710.8 (M + Na⁺ - 31C₂H₄ - C₄₄H₁₄N₄), 9,756.0 (M + K⁺ - 30C₂H₄ - C₄₄H₁₄N₄), 9,779.8 (M + K⁺ - 29C₂H₄ - C₄₄H₁₄N₄), 9,810.7 (M + K⁺ - 28C₂H₄ - C₄₄H₁₄N₄). Analysis: calculated for C₅₈₈H₆₀₀O₁₂₈: C, 72.70; H, 6.22; N, 0.00; Ru, 0.00. Found: C, 70.83; H, 6.19; N, 0.00; Ru, 0.00.

Received 28 February; accepted 28 May 2002; doi:10.1038/nature00877.

1. Wulff, G. & Sarhan, A. The use of polymers with enzyme-analogous structures for the resolution of racemates. *Angew. Chem. Int. Edn Engl.* **11**, 341–343 (1972).
2. Shea, K. J. Molecular imprinting of synthetic network polymers: the de novo synthesis of macromolecular binding and catalytic sites. *Trends Polym. Sci.* **2**, 166–173 (1994).
3. Andersson, L., Sellergren, B. & Mosbach, K. Imprinting of amino acid derivatives in macroporous polymers. *Tetrahedr. Lett.* **25**, 5211–5214 (1984).
4. Katz, A. & Davis, M. E. Molecular imprinting of bulk, microporous silica. *Nature* **403**, 286–289 (2000).
5. Wulff, G. Molecular imprinting in cross-linked materials with the aid of molecular templates—a way towards artificial antibodies. *Angew. Chem. Int. Edn Engl.* **34**, 1812–1832 (1995).
6. Katz, A. & Davis, M. Investigations into the mechanisms of molecular recognition with imprinted polymers. *Macromolecules* **32**, 4113–4121 (1999).
7. Sellergren, B. & Shea, K. J. Influence of polymer morphology on the ability of imprinted network polymers to resolve enantiomers. *J. Chromatogr.* **635**, 39–41 (1993).
8. Vlatakis, G., Anderson, L. I., Müller, R. & Mosbach, K. Drug assay using antibody mimics made by molecular imprinting. *Nature* **361**, 645–647 (1993).
9. Lehn, J.-M. & Eliseev, A. V. Dynamic combinatorial chemistry. *Science* **291**, 2331–2332 (2001).
10. Cousins, G. R. L., Poulsen, S.-A. & Sanders, J. K. M. Molecular evolution: dynamic combinatorial libraries, autocatalytic networks and the quest for molecular function. *Curr. Opin. Chem. Biol.* **4**, 270–279 (2000).
11. Klekota, B. & Miller, B. L. Dynamic diversity and small-molecule evolution: a new paradigm for ligand identification. *Trends Biotechnol.* **17**, 205–209 (1999).
12. Wendland, M. S. & Zimmerman, S. C. Synthesis of cored dendrimers. *J. Am. Chem. Soc.* **121**, 1389–1390 (1999).
13. Schultz, L. G., Zhao, Y. & Zimmerman, S. C. Synthesis of cored dendrimers with internal cross-links. *Angew. Chem. Int. Edn Engl.* **40**, 1962–1966 (2001).
14. Newkome, G. R., Moorefield, C. N. & Vögtle, F. *Dendrimers and Dendrons: Concepts, Syntheses, Perspectives* (Wiley-VCH, Weinheim, 2001).
15. Sanders, J. K. M. Templated chemistry of porphyrin oligomers. *Compreh. Supramolec. Chem.* **9**, 131–164 (1996).
16. Rakon, N. A. & Suslick, K. S. A colorimetric sensor array for odour visualization. *Nature* **406**, 710–714 (2000).
17. Matsui, J., Higashi, M. & Takeuchi, T. Molecularly imprinted polymer as 9-ethyladenine receptor having a porphyrin-based recognition center. *J. Am. Chem. Soc.* **122**, 5218–5219 (2000).
18. Ogoshi, H. & Mizutani, T. Novel approaches to molecular recognition using porphyrins. *Curr. Opin. Chem. Biol.* **3**, 736–739 (1999).
19. Bhyrappa, P., Young, J. K., Moore, J. S. & Suslick, K. S. Dendrimer-metalloporphyrins: synthesis and catalysis. *J. Am. Chem. Soc.* **118**, 5708–5711 (1996).
20. Dandliker, P. J., Diederich, F., Gisselbrecht, J.-P., Louati, A. & Gross, M. Water-soluble dendritic iron porphyrins: synthetic models of globular heme proteins. *Angew. Chem. Int. Edn Engl.* **34**, 2725–2728 (1996).
21. Sadamoto, R., Tomioka, N. & Aida, T. Photoinduced electron transfer reactions through dendrimer architecture. *J. Am. Chem. Soc.* **118**, 3978–3979 (1996).
22. Balzani, V. *et al.* Dendrimers based on photoactive metal complexes. Recent advances. *Coord. Chem. Rev.* **219–221**, 545–572 (2001).
23. Hawker, C. J. & Frechet, J. M. J. A new convergent approach to monodisperse dendritic macromolecules. *J. Am. Chem. Soc.* **112**, 7638–7647 (1990).
24. Trnka, T. M. & Grubbs, R. H. The development of L₂X₂Ru = CHR olefin metathesis catalysts: an organometallic success story. *Acc. Chem. Res.* **34**, 18–29 (2001).
25. Coates, G. W. & Grubbs, R. H. Quantitative ring-closing metathesis of polyolefins. *J. Am. Chem. Soc.* **118**, 229–230 (1996).
26. Adler, A. D. *et al.* A simplified synthesis of meso-tetraphenylporphyrin. *J. Org. Chem.* **32**, 476 (1967).
27. Rho, T. & Abuh, F. One-pot synthesis of pyrimidine-5-carboxaldehyde and ethyl pyrimidine-5-carboxylate by utilizing pyrimidin-5-yl-lithium. *Synth. Commun.* **24**, 253–256 (1994).
28. Collman, J. P. *et al.* Oxygen binding to cobalt porphyrins. *J. Am. Chem. Soc.* **100**, 2761–2766 (1978).

Supplementary Information accompanies the paper on Nature's website (<http://www.nature.com/nature>).

Acknowledgements

We thank W.A. Goddard and T. Cagin for help with dendrimer modelling. This work was funded by the NIH and the US Army Research Office. I.Z. thanks the Arnold and Mabel Beckman Foundation for a Beckman fellowship.

Competing interests statement

The authors declare that they have no competing financial interests.

Correspondence and requests for materials should be addressed to S.C.Z. (e-mail: sczimmer@uiuc.edu).

Tungsten isotope evidence from ~3.8-Gyr metamorphosed sediments for early meteorite bombardment of the Earth

Ronny Schoenberg*, **Balz S. Kamber***, **Kenneth D. Collerson*** & **Stephen Moorbath†**

* *Advanced Centre for Queensland University Research Excellence (ACQUIRE), The University of Queensland, St Lucia, Queensland 4072, Australia*
 † *Department of Earth Sciences, University of Oxford, Parks Road, Oxford OX1 3PR, UK*

The 'Late Heavy Bombardment' was a phase in the impact history of the Moon that occurred 3.8–4.0 Gyr ago, when the lunar basins with known dates were formed^{1,2}. But no record of this event has yet been reported from the few surviving rocks of this age on the Earth. Here we report tungsten isotope anomalies, based on the ¹⁸²Hf–¹⁸²W system (half-life of 9 Myr), in metamorphosed sedimentary rocks from the 3.7–3.8-Gyr-old Isua greenstone belt of West Greenland and closely related rocks from northern Labrador, Canada. As it is difficult to conceive of a mechanism by which tungsten isotope heterogeneities could have been preserved in the Earth's dynamic crust–mantle environment from a time when short-lived ¹⁸²Hf was still present, we conclude that the metamorphosed sediments contain a component derived from meteorites.

It is widely conjectured that the Earth suffered contemporaneous Late Heavy Bombardment (LHB) with the Moon, scaled up proportionally to its much greater gravitational cross-section. Earth's estimated³ mass accretion rate during the LHB was of the order of (1–2) × 10¹⁵ g yr⁻¹, or (2–4) × 10⁻⁴ g cm⁻². Over a 100-Myr period of LHB, this accretion rate would have yielded (1–2) × 10²³ g of material. If added as a continuous veneer over the entire planet, this would correspond to 200 t m⁻². The distinct deuterium/hydrogen ratio of the terrestrial hydrosphere⁴ argues against significant cometary accretion, whereas compositions of projectiles in lunar impact melts⁵ indicate infall from asteroids of enstatite chondrite or iron meteorite parentage. Thus, unless the Earth's early crust was continually recycled into the mantle, it should be possible to detect chemical 'fingerprints' of the LHB in the oldest terrestrial sediments.

In a recent study⁶, the extinct radioactive decay scheme ⁵³Mn–⁵³Cr (half-life, 3.7 Myr) was used to detect meteoritic infall in Cretaceous/Tertiary (K/T) boundary sediments. As Cr isotopes in all classes of meteorites and terrestrial samples are distinct, discovery of a non-terrestrial Cr isotope composition⁶ confirmed extraterrestrial origin. A similar opportunity for detecting meteoritic infall is afforded by the ¹⁸²Hf–¹⁸²W system (half-life, 9 Myr). By analogy with the homogeneous terrestrial Cr isotope composition⁶, any variations in W isotope composition that may have existed in the first ~60 Myr of Earth's history would have been homogenized by convection in the early mantle. Therefore the terrestrial W isotope composition is constant^{7,8}. Indeed, all our terrestrial samples other than the early Archaean metamorphosed sediments (metasediments) yield a constant ¹⁸²W/¹⁸³W ratio (Fig. 1 and Table 1) of 0.10 ± 0.22 ε_W units (where ε_W is the deviation, in 0.1‰, from the terrestrial ¹⁸²W/¹⁸³W ratio), identical to our standard (ACQUIRE-W), which was reproduced at 0.00 ± 0.10 ε_W.

In contrast, a well-resolved W isotope variability exists among different classes of meteorites. Iron meteorites⁹ have much lower ¹⁸²W/¹⁸³W ratios (Fig. 1) of, on average, -3.7 ε_W, reflecting removal of metal-loving W from silicate into the core of planete-

Embedded Secure Document

The file <http://www.scs.uiuc.edu/~suslick/pdf/natmatl02118.pdf> is a secure document that has been embedded in this document. Double click the pushpin to view.



Is the olfactory receptor a metalloprotein?

Jiangyun Wang, Zaida A. Luthey-Schulten, and Kenneth S. Suslick*

Department of Chemistry, University of Illinois at Urbana-Champaign, 600 South Mathews Avenue, Urbana, IL 61801

Communicated by Peter G. Wolynes, University of California at San Diego, La Jolla, CA, December 26, 2002 (received for review December 11, 2002)

The sense of smell is arguably our most primal faculty and also the least understood. Even our own olfactorily impaired species is capable of detecting $\approx 10,000$ distinct scents [Buck, L. & Axel, R. (1991) *Cell* 65, 175–187]. To achieve that amazing diversity, mammals have $\approx 1,000$ olfactory genes, which accounts for $\approx 3\%$ of their entire genome [Mombaerts, P. (1999) *Science* 286, 707–711]. The olfactory receptors (ORs) are believed to be seven-helix transmembrane proteins, with an odorant-binding site on the periplasmic domain and a G protein-binding site on the cytoplasmic domain. Odorants first bind to an OR, which then undergoes some structural change that triggers the G protein activation and the following cascade of events leading to nerve cell activity. The structural details of ORs, however, remain to be determined. In this paper, we will describe a hypothesis in which metal ions play an important role for odorant recognition. We analyze the predicted structure and consensus sequence of the ORs and propose a metal-binding site in the loop between fourth and fifth helix (4–5 loop). We have prepared synthetically a pentapeptide that contains this putative binding site and find that it not only has high affinity for binding Cu(II) and Zn(II) ions, but that it also undergoes a dramatic transition to an α -helical structure upon metal ion binding. Based on these observations, we propose a “shuttlecock” mechanism for the possible structural change in ORs upon odorant binding. This mechanism involves membrane penetration of the 4–5 loop after residue charge neutralization by metal ion binding.

olfaction | G protein-coupled receptors | transmembrane protein

Inorganic chemists know as a rule of thumb that if a volatile compound is a good ligand for metal ion coordination complexes, it probably smells strongly; this observation has led to recent advances in artificial olfaction (1). The only notable exceptions to this rule are CO and NO, which are produced endogenously as neural messengers (2) and, therefore, elicit no olfactory response. In general, the human olfactory system is extremely sensitive to amines and thiols (good ligands for metal ions) but not to alcohols (which are only weak ligands; ref. 3), as shown in Fig. 1. For example, one can smell methylthiol at less than 1 ppb, methylamine at 18 ppb, but methanol only above 100 ppm, and methane is undetected even at 10^6 ppm.

Odorants need to bind to an olfactory receptor (OR) to trigger the cascade of events that finally enables us to smell: methylthiol is bound by some OR >1 million times stronger than the OR that responds to methanol, and methylamine is bound $>100,000$ times stronger than methanol. Differences in hydrogen bonding or van der Waals interactions are insufficient to account for this range, but differences in Lewis basicity to metal ions can. This range of affinities is critical to the pattern recognition processes proposed for neural computation (4).

Thus, the most natural explanation to account for this odorant affinity difference is coordination to a metal ion bound in an OR. Cu(II) or Zn(II) are particularly likely candidates, because they have strong amine- and thiol-binding property and are frequently found in metalloproteins. More than two decades ago, Crabtree (7) prophetically speculated that Cu(I) might be found in ORs, because of the high olfactory sensitivity to amines and thiols.

Consistent with the metalloprotein hypothesis, the ORs also show unusual differences in their shape selectivity for alcohols

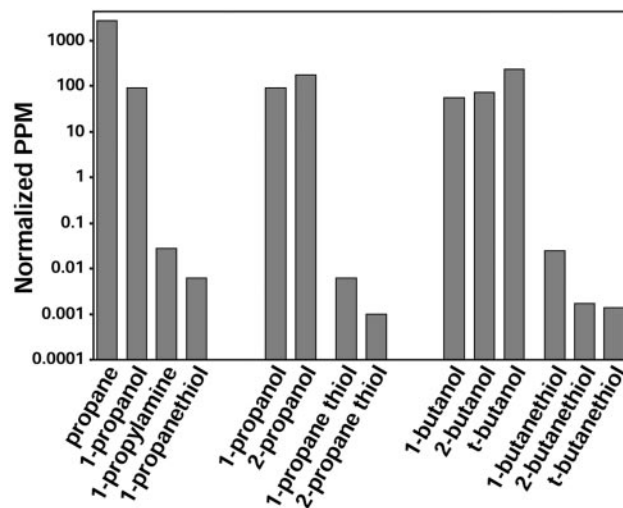


Fig. 1. Human olfactory thresholds. Shown are gas phase concentrations at threshold of detection (3); vapors of liquids have been normalized (5) by analyte vapor pressure at 298 K (6).

compared with thiols. Substitution at the α -carbon of alcohols increases the olfactory threshold for alcohols; i.e., greater steric bulk gives weaker binding, as expected for sterically restricted binding sites. In surprising contrast, however, α -substitution of thiols normally decreases the olfactory threshold for thiols. This observation can be explained by OR binding sites that contain a coordinately accessible metal ion, because α -substitution increases the Lewis basicity of the thiol and, hence, its strength of binding to metal ions, as long as the increased steric hindrance is not too great. In keeping with this trend, the human nose is often more sensitive to secondary amines than primary amines; comparisons among amines, however, are complicated by issues of protonation in the olfactory mucosa.

Materials and Methods

Peptide Synthesis. A five-residue peptide, with sequence HAKCE, was synthesized to study its metal-binding property. The C terminus was amide-capped and the N terminus was capped with an acetyl group to prevent terminus binding to metal ions. The peptide was synthesized by using solid-phase methods and the Fmoc/t-Bu strategy on a Multiple Symphony synthesizer (Protein Technologies, Woburn, MA). Amino acid coupling using *N*-hydroxybenzotriazole chemistry and Fmoc deprotection was performed by using 20% piperidine in dimethylformamide. The peptide was cleaved with a trifluoroacetic acid/thioanisole/ethanedithiol/anisole/water mixture (82.5/5/2.5/5/5; Reagent K) and purified by reversed-phase C18 HPLC with a linear gradient of acetonitrile and water. The identity and purity of the peptide were confirmed by HPLC and electrospray mass spectroscopy.

Abbreviations: OR, olfactory receptor; HMM, hidden Markov model; hOR, human OR.

*To whom correspondence should be addressed. E-mail: ksuslick@uiuc.edu.

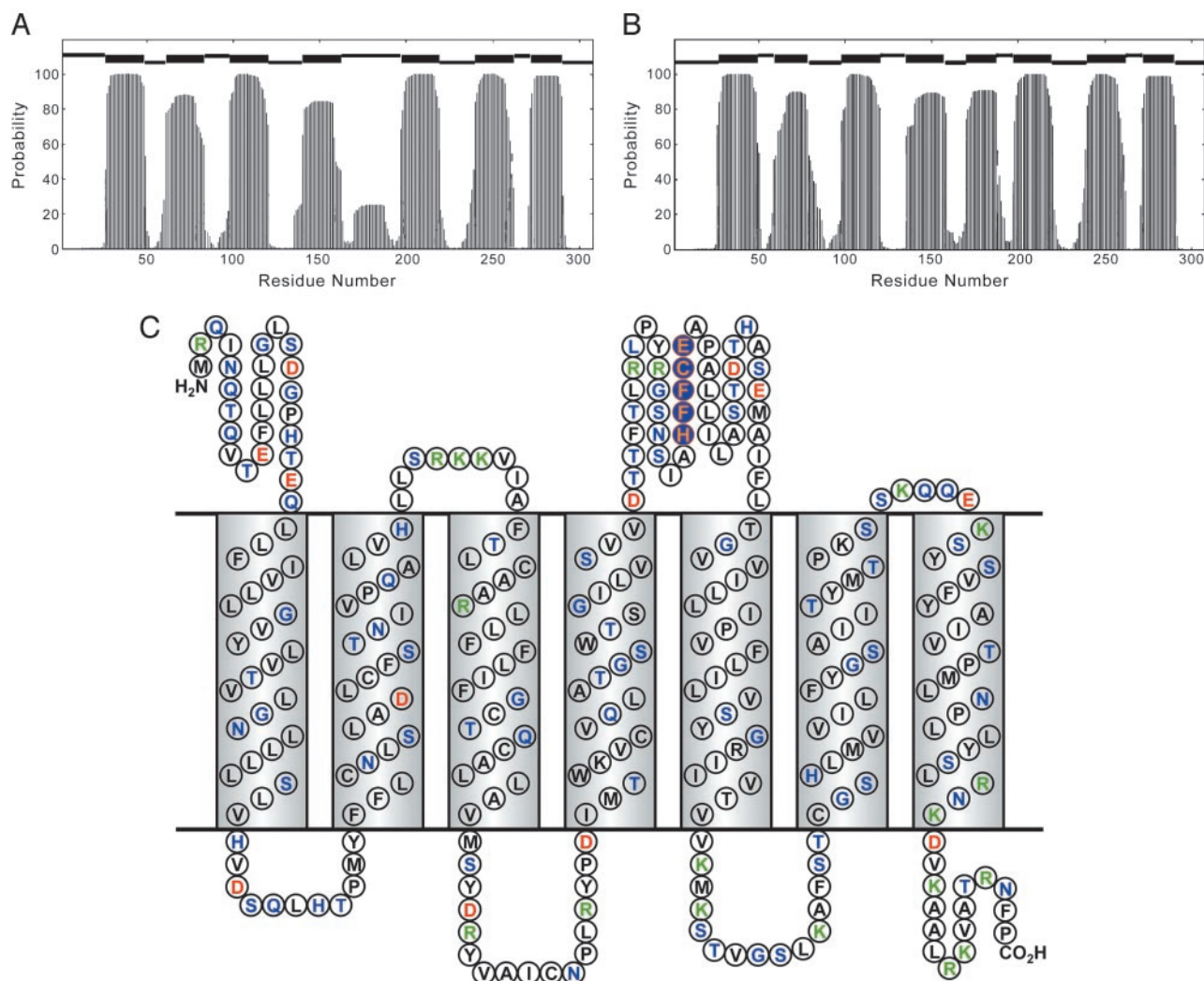


Fig. 2. (A) Secondary structure prediction of hOR o2d2 using the HMM for the native sequence. At the top, the thick bars indicate predicted TM helices and the higher and lower thin bars designate periplasmic and cytoplasmic loops, respectively. (B) Secondary structure prediction of hOR o2d2 using HMM for the charge-neutralized structure (as modeled by Glu-180→Val mutation). (C) Secondary structure prediction with amino acid aligned to the TM helix and loop regions. Coding: hydrophobic residues in black, polar residue in green, positively charged in blue, and negatively charged in red. The consensus metal ion-binding site (conserved in nearly three-quarters of known sequences) is highlighted in orange on blue.

CD Spectroscopy. All CD spectra were measured on a Jasco J-700 spectropolarimeter (Jasco, Easton, MD) at 20°C. All measurements were made on samples whose concentrations were 20 μM (20 mM potassium phosphate, pH 7.4). The binding constants were determined by standard techniques (8).

Molecular Modeling. Molecular modeling was performed on an Indigo2 Extreme running IRIX V.6.2 with the program MODELER and BIOPOLYMER in INSIGHT-II. (Accelrys, San Diego) Sequence analysis used public domain software: TMHMM V.2.0 (www.cbs.dtu.dk/services/TMHMM).

Results and Discussion

The hidden Markov model (HMM) has been used with high confidence to predict the secondary structure of membrane proteins (9), because residues buried in membrane are normally hydrophobic, and those exposed at loops are hydrophilic, which makes for very distinctive sequence patterns. The ORs are well fit as seven-helix membrane proteins by using this approach (Fig. 2). Structural models have also been calculated from homology modeling (10) by using the structure of bovine rhodopsin, which

is also a seven-helix membrane protein. Goddard and coworkers (10) observed in their model that a long narrow pocket is formed in the middle of the membrane helices that seem capable of binding linear alcohols. Their model is consistent with the observed shape selectivity for alcohols, but it does not provide an explanation for the reverse selectivity with substituted thiols.

In looking for possible metal ion-binding sites in the genome sequences of ORs, we first made the general observation that zinc and copper metalloproteins usually have clusters of the metal-coordinating amino acids His, Cys, Glu, or Asp: i.e., two or more metal-binding amino acids are generally found to be separated by no more than four amino acids. This proximity is likely a consequence of entropic requirements in the coordination of multiple residues to the metal ion. Keeping that in mind, we immediately find the consensus sequence HXXC[DE] in the 4–5 loop (Fig. 2C) of many OR sequences (11), where Xs generally are hydrophobic residues (especially phenylalanine). More specifically, of the 83 human olfactory receptor (hOR) sequences we extracted from the SWISS-PROT database, 70% (i.e., 58) are found to contain this motif. In a recent study, Zuzulya and coworkers (12) have identified some 347 putative

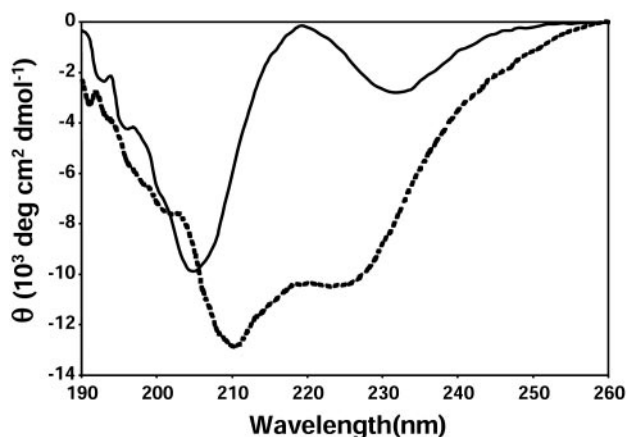


Fig. 3. Far-UV CD spectrum of HAKCE peptide, in the absence of metal ions (solid line) and in the presence of 1.0 equivalent of Cu(II) added (dotted line); 20 mM peptide, pH 7.4 potassium phosphate buffer, 298 K.

hOR genes; we find the HXXC[DE] consensus sequence in 74% (i.e., 257) of these sequences, as well.

To test this sequence as a possible metal ion-binding site, we synthesized a pentapeptide by standard solid-state techniques. To retain water solubility, it was necessary to set XX to alanine-lysine (AK). HAKCE thus was examined for its metal ion-binding capability. As expected for a short peptide, the CD spectrum of HAKCE shows that it is a random coil (Fig. 3).

Surprisingly, upon addition of 1.0 equivalents of Cu^{2+} , the far-UV CD spectrum changes dramatically to one characteristic of an α -helix. A careful titration with CD monitoring shows 1:1 binding with a dissociation constant between the peptide and Cu^{2+} of 500 nM. The formation of an α -helix normally requires a relatively lengthy peptide (≈ 15 residues) to provide sufficient hydrogen bonding to stabilize the helix (13). To the best of our knowledge, no helix-forming oligopeptide as short as five residues has been previously reported. In this special case, however, the chelation of the oligopeptide residues forces its conformation into a helix. Similar helix induction is observed for Zn^{2+} or Ni^{2+} (with somewhat larger dissociation constants), but not for Cu^+ . These observations provide significant evidence for the possible role of Cu(II), Zn(II), or Ni(II) in some ORs, but does not rule out Cu(I), because the real protein environment is much more complex. It is worth noting in passing that one of the distinctive symptoms of dietary zinc deficiency is anosmia (i.e., loss of the sense of smell; ref. 14).

If the active sites of some ORs indeed contain a metal ion, how might an odorant binding create a response mechanism? As a starting point, let us examine the possible structure of these membrane-bound proteins. ORs fall into the broad category of G protein-coupled receptors, which are predicted to be seven-helix membrane proteins and which include bovine rhodopsin, bacteriorhodopsin, halorhodopsin, and sensory rhodopsin. Among those, bacteriorhodopsin is the best understood, and its structure has been available since 1990 (15); high-resolution structures of bacteriorhodopsin (16), bovine rhodopsin (17), halorhodopsin (18), and sensory rhodopsin (19) are also now available. Bacteriorhodopsin is composed of seven-helix bundle protein scaffold covalently linked to *all-trans* retinal through Lys-216. Absorption of a photon by retinal causes its isomerization to a 13-*cis* configuration, inducing torsional strain in the chromophore as well as disrupting the Schiff base/Asp-85 ion pair. This isomerization increases the local energy and moves two helices relative to the other five (20), opening a pathway for proton transfer.

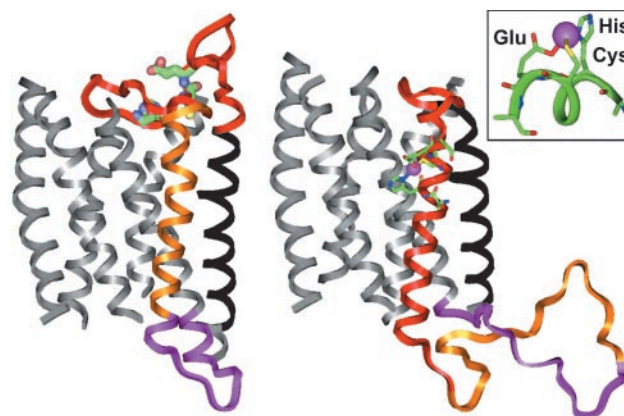


Fig. 4. The homology models of the hOR o2d2 are constructed by using the program MODELER and BIOPOLYMER in INSIGHT-II (Accelrys). (Left) A model of the nonmetallated apoprotein; the predicted hOR transmembrane helix is aligned to the transmembrane helix of bovine rhodopsin (PDB ID code 1F88). (Right) Proposed structure after binding a metal ion (e.g., Cu^{2+} or Zn^{2+}); the alignment shifts to reflect the speculated 4–5 loop insertion and ejection of the fourth helix. (Inset) Predicted coordination geometry to the metal ion from the glutamate, histidine, and cysteine residues of the consensus sequence HXXC[DE] in the 4–5 loop.

Similarly, for a metal ion containing OR, odorants that bind to the metal ion (e.g., thiols, amines, etc.) could disrupt the charge balance by replacing one of the metal-ligated amino acid residues (or a coordinated water or hydroxide ion), resulting in protein structural rearrangement. Alternatively, odorant ligation would also increase the local steric interactions in the active site with a similar effect on protein structure.

Such a mechanism of action for OR–odorant interactions explains the very high sensitivities for metal ion coordinating analytes (e.g., Fig. 1). Metal-ligand bonds range in their bond enthalpies from ≈ 40 to ≈ 200 kJ/mol. In contrast, the enthalpy of absorption (e.g., into polymers) relies on weak, van der Waals and dipolar interactions and is only ≈ 5 – 20 kJ/mol (i.e., roughly a tenth of a metal bond) for small molecules. Therefore, the equilibrium constant for absorption will typically only be about 5×10^{-5} as large as that for ligation to metal ions.

A more detailed examination of the OR structure leads to a provocative hypothesis concerning the structural change upon odorant binding (Fig. 4). The loop between the putative 4th and 5th transmembrane helices of ORs is uncommonly long and surprisingly hydrophobic. This loop is sufficiently long to be transmembrane helix, but the HMM algorithm does not designate it as such, because of the anionic residue (Asp or Glu) in the middle of the sequence, which would interact unfavorably with the hydrophobic membrane environment. After binding to a metal ion, however, the anionic charge is cancelled. For example, if we replace just that single anionic residue by Val, the HMM algorithm projects an entirely different structure for the specific sequence of hOR-o2d2 (21).

The structure resulting from metal ion binding would be consistent with a new helical region originating from the original 4–5 extramembrane loop; the metal binding site HXXC[DE] is located in the middle of this new helical region. In addition, a tetrahedrally ligating metal ion [e.g., Cu(II) or Zn(II)] can bind to the residues of this new α -helix (to one nitrogen atom from His, one sulfur from Cys, and one oxygen from Glu) without any significant unfavorable steric interaction (Figs. 4 and 5).

The possibility of two different stable conformations for the OR seven-helix bundle leads to an interesting “shuttlecock” hypothesis for metal ion-assisted odorant recognition, as shown in Fig. 5. Initially, the OR is a seven-helix bundle in the

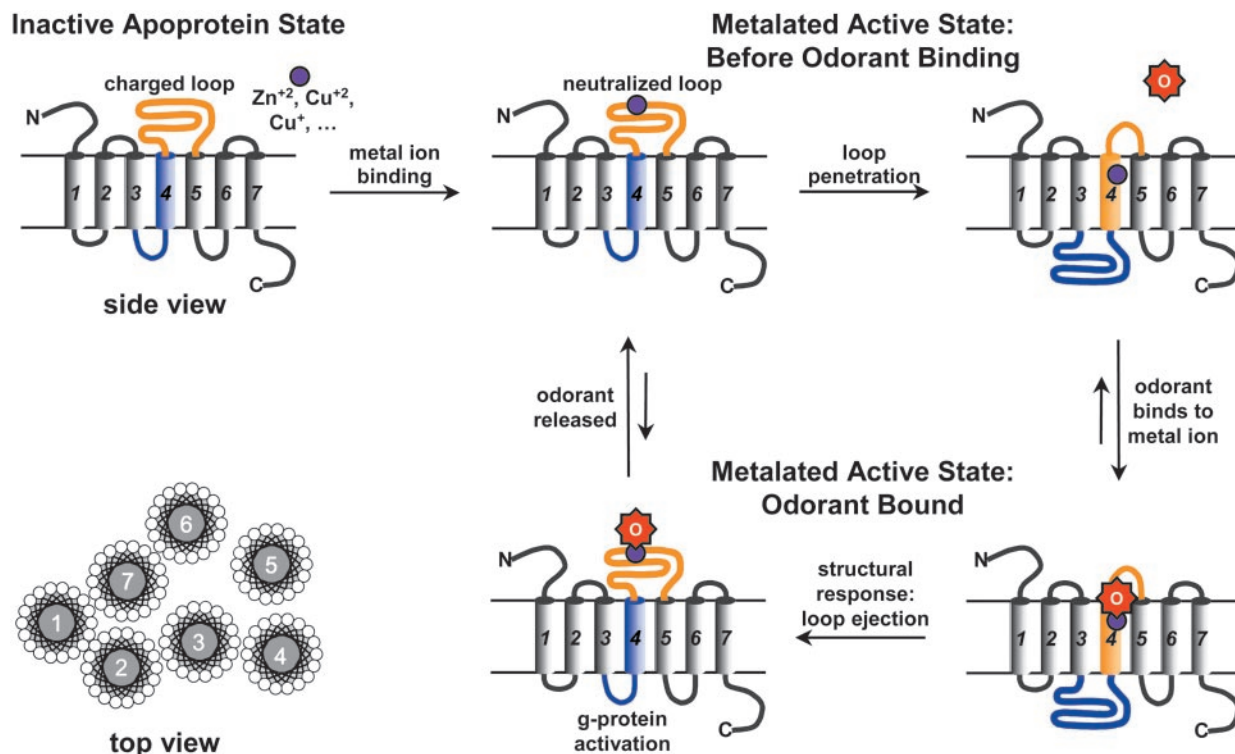


Fig. 5. The proposed mechanism of olfactory response via a transmembrane shuttlecock. In the absence of odorant binding, the stable state is the embedded loop conformation (*Upper Right*). Upon odorant binding, the primary structural response is loop ejection (*Lower Left*). The G protein activation is a kinetic phenomenon in this mechanism; full equilibration of the OR with odorant leads to no further G protein activation, which may, in part, account for the process of olfactory adaptation (i.e., loss of response after initial exposure to a constant odorant concentration).

conformation currently accepted. Upon metal binding, however, the anionic charge of the 4–5 loop is neutralized, permitting the loop to become helical and penetrate into the membrane, pushing the fourth helix out of the membrane. This configuration, we speculate, is the active form of metal ion-containing ORs.

When an odorant capable of metal ion ligation (e.g., amines, thiols, carboxylic acids, etc.) approaches the active form of the OR, it replaces one of the coordinated amino acids or a bound water or hydroxide, disrupts the local charge and steric balance, and causes the original 4–5 loop to eject from the membrane, permitting the original fourth helix to return into the membrane. This sequence of events causes large structural change in the cytoplasmic domain (Figs. 4 and 5) and activates the G protein. Meanwhile, the metal-binding site will then be exposed to the extracellular water, shifting the equilibrium of ligation and enhancing the departure of the bound odorant. When the odorant leaves the OR, the 4–5 loop again turns into a hydrophobic helix and pushes the fourth helix out of the membrane once again, returning the OR back to its active state.

This hypothesis is testable. Overexpression and purification of olfactory proteins is possible now that their genome has been identified. Identification of metal ion content by trace metal analysis [e.g., using inductively coupled plasma mass spectrometry (ICP-MS)] or, in the case of Cu(II), electron paramagnetic resonance is quite possible. In addition, identification of specific OR sequences that respond strongly to amines and thiols may be possible by using Ca^{2+} -imaging technique and single-cell RT-PCR (22).

There is a possible precedent for the conformational change we are suggesting. Hunt and coworkers (23) discovered that a 36-residue peptide can insert into lipid bilayers as a transmembrane helix after one of its Asp residues is neutralized by lowering the pH. This observation supports our hypothesis that

the OR 4–5 loop may turn into a TM helix after its charge is cancelled by ligation to a metal ion. It is also possible that some olfactory proteins are indeed eight-helix bundles after metal ion binding, as predicted by the HMM.

We can use a standard hydrophobicity scale, e.g., Kyte-Doolittle (24), to estimate which helix is likely to eject when the 4–5 loop inserts. For hOR o2d2 (19), the predicted fourth helix has a total hydrophobicity value of 21.9 for residues 140–162; the 4–5 loop has total hydrophobicity value of 21.1 for residues 170–192 (and a total hydrophobicity value of 24.3 after charge-neutralization by Val substitution of Glu); the fifth helix has a total hydrophobicity value of 39.9 for residues 197–219. Because the hydrophobicity of the 4–5 loop and fourth helix are so close, it is very likely that the 4–5 loop can replace the fourth helix when the metal binding cancels the charge on Glu-180 (E180) and decreases polarity on H176. The fifth helix, however, should be more difficult to eject, because it is much more hydrophobic than the 4–5 loop. More generally, the fifth helix is also much more hydrophobic than the fourth helix and the 4–5 loop in the consensus sequence of hOR.

A “shuttlecock” protein motion has not been previously suggested in other membrane bound proteins. Bacteriorhodopsin and bacterial chemotaxis receptors have only small sliding motions, perhaps because their membrane helices are tightly packed (24). Larger motions are observed for acetylcholine receptor and potassium channel (25), where a whole subunit moves to open or close the channel. It will prove interesting to apply atomic force microscopy to ORs and measure the forces necessary to pull helices out of their membrane environments, as has been done recently for bacteriorhodopsin (26).

In conclusion, we have assembled both computer modeling and experimental evidence for the binding of metal ions to a consensus sequence found in ORs. From HMM, we believe that

binding of a metal ion precipitates a major rearrangement of the transmembrane helices. Upon odorant binding to the metal ion, a shuttlecock motion that converts loop to helix provides a useful hypothesis for the mechanism of activation of the coupled cytoplasmic G protein. This rearrangement of transmembrane proteins may be generalized to charge-neutralization events other than metal ion coordination: large extramembrane loops

may become transmembrane helices upon protonation of anionic residues, deprotonation of cationic residues, or formation of internal salt bridges between oppositely charged residues.

We thank Dr. Avijit Sen, Dr. Neal A. Rakow, Prof. K. Schulten, and Prof. P. G. Wolynes for valuable suggestions. This work was supported by National Institutes of Health Grant HL25934.

1. Rakow, N. A. & Suslick, K. S. (2000) *Nature* **406**, 710–714.
2. Snyder, S. H., Jaffrey, S. R. & Zakhary, R. (1998) *Brain. Res. Rev.* **26**, 167–175.
3. Devos, M., Patte, F., Rouault, J., Laffort, P. & Van Gemert, L. J. (1990) *Standardized Human Olfactory Thresholds* (Oxford Univ. Press, New York).
4. Hopfield, J. J. (1999) *Proc. Natl. Acad. Sci. USA* **96**, 12506–12511.
5. Doleman, B. J., Severin, E. J. & Lewis, N. S. (1998) *Proc. Natl. Acad. Sci. USA* **95**, 5442–5447.
6. Yaws, C. L., Lin, X. & Bu, L. (1994) *Handbook of Vapor Pressure* (Gulf, London).
7. Crabtree, R. H. (1978) *J. Inorg. Nucl. Chem.* **40**, 1453.
8. Huffman, D. L., Rosenblatt, M. M. & Suslick, K. S. (1998) *J. Am. Chem. Soc.* **120**, 6183–6184.
9. Eddy, S. R. (1996) *Curr. Opin. Struct. Biol.* **6**, 361–365.
10. Floriano, W. B., Vaidehi, N., Goddard, W. A., III, Singer, M. S. & Shepherd, G. M. (2000) *Proc. Natl. Acad. Sci. USA* **97**, 10712–10716.
11. Buck, L. & Axel, R. (1991) *Cell* **65**, 175–187.
12. Zuzulya, S., Echeverri, F. & Nguyen, T. (2001) *Genome Biol.* **2**, 18.1–18.12.
13. Chakrabarty, A. & Baldwin, R. L. (1995) *Adv. Protein Chem.* **46**, 141–176.
14. Ackerman, B. H. & Kasbekar, N. (1997) *Pharmacotherapy* **17**, 482–496.
15. Henderson, R., Baldwin, J. M., Ceska, T. A., Zemlin, F., Beckmann, E. & Downing, K. H. (1990) *J. Mol. Biol.* **213**, 899–929.
16. Faham, S. & Bowie, J. U. (2002) *J. Mol. Biol.* **316**, 1–6.
17. Palczewski, K., Kumasaka, T., Hori, T., Behnke, C. A., Motoshima, H., Fox, B. A., Le Trong, I., Teller, D. C., Okada, T., Stenkamp, R. E., *et al.* (2000) *Science* **289**, 739–745.
18. Kolbe, M., Besir, H., Essen, L. O. & Oesterhelt, D. (2000) *Science* **288**, 1390–1396.
19. Luecke, H., Schobert, B., Lanyi, J. K., Spudich, E. N. & Spudich, J. L. (2001) *Science* **293**, 1499–1503.
20. Subramaniam, S. & Henderson, R. (2000) *Nature* **406**, 653–657.
21. Lane, R. P., Cutforth, T., Young, J., Athanasiou, M., Friedman, C., Rowen, L., Evans, G., Axel, R., Hood, L. & Trask, B. J. (2001) *Proc. Natl. Acad. Sci. USA* **98**, 7390–7395.
22. Malnic, B., Hirono, J., Sato, T. & Buck, L. B. (1999) *Cell* **96**, 713–723.
23. Hunt, J. F., Rath, P., Rothschild, K. J. & Engelman, D. M. (1997) *Biochemistry* **36**, 15177–15192.
24. Kyte, J. & Doolittle, R. F. (1982) *J. Mol. Biol.* **157**, 105–132.
25. Gerstein, M. & Chothia, C. (1999) *Science* **285**, 1682–1683.
26. Oesterhelt, F., Oesterhelt, D., Pfeiffer, M., Engel, A., Gaub, H. E. & Muller, D. J. (2000) *Science* **288**, 143–146.

Molecular Imprinting Inside Dendrimers

Steven C. Zimmerman,* Ilya Zharov, Michael S. Wendland, Neal A. Rakow, and Kenneth S. Suslick*

Contribution from the Department of Chemistry and Beckman Institute for Advanced Science and Technology, University of Illinois at Urbana-Champaign, Urbana, Illinois 61801

Received April 21, 2003; E-mail: sczimmer@uiuc.edu

Abstract: Synthetic hosts capable of binding porphyrins have been produced by a mixed-covalent-noncovalent imprinting process wherein a single binding site is created within cross-linked dendrimers. Two synthetic hosts were prepared, using as templates 5,10,15,20-tetrakis(4-hydroxyphenyl)porphyrin and 5,10,15,20-tetrakis(3,5-dihydroxyphenyl)porphyrin. These two templates were esterified with, respectively, fourth- and third-generation Fréchet-type dendrons containing homoallyl end-groups. The resulting tetra- and octadendron macromolecules underwent the ring-closing metathesis reaction using Grubbs' Type I catalyst, $\text{RuCl}_2(\text{P}(\text{C}_6\text{H}_5)_3)_2(\text{CHCH}_2\text{C}_6\text{H}_5)$, to give extensive interdendron cross-linking. Hydrolytic removal of the porphyrin cores afforded imprinted hosts whose ability to bind porphyrins with various peripheral substituents was investigated by UV-visible spectrophotometric titrations and size exclusion chromatography. The results indicate a high yield of imprinted sites that show high selectivity for binding of porphyrins capable of making at least four hydrogen bonds, but only a moderate degree of shape selectivity.

Introduction

Host-guest chemistry has emerged as a central paradigm within organic chemistry.¹ The design and synthesis of diverse host molecules that selectively and tightly complex many different classes of guest molecules have been notably successful. As effective as this approach has been, especially for small molecule hosts, the requirement to prepare hosts bond by bond through multistep synthetic routes has limited their widespread application. Furthermore, each new target guest typically requires an entirely new host design and development program.

Two strategies that have the potential to significantly extend the host-guest approach involve molding an organic receptor around the guest "template". The first, using molecularly imprinted polymers (MIP), was initially described in Wulff's seminal 1972 report,² in which a matrix was polymerized around the template molecules, followed by removal of the template; this leaves host cavities that, ideally, retain a shape and functional group complementarity to the guest-template. This early synthesis of a MIP is referred to as the covalent approach because the template is reversibly linked to the matrix by covalent bonds.³ A noncovalent approach, in which one or more monomers complex the template, was pioneered by Mosbach and co-workers and is now the most commonly used method of MIP synthesis.⁴ Subsequently, mixed covalent-noncovalent methods were developed⁵ as well as numerous related approaches.^{6,7} Indeed, molecularly imprinted polymers (MIPs)

have been among the most extensively studied host-guest systems. MIPs have several drawbacks, however, including incomplete template removal and slow mass transfer;^{6,7-9} their practical application is also severely limited by the heterogeneity of the binding sites for which a broad range of affinities are observed.^{6,10}

A second strategy for rapid host construction has emerged more recently. It uses a dynamic combinatorial library (DCL) of hosts, in which one or more members are bound to and stabilized by the guest molecule.¹¹⁻¹³ The molding process in the DCL approach is different in two ways. First, the molding uses reversible reactions so that ineffective hosts may be sacrificed in favor of superior ones. The DCL approach is further distinguished in that the molded receptors each contain a single binding site so that individual receptors or classes of receptors can be separated, characterized, and studied in solution.

We recently described a "monomolecular imprinting" approach, which contains elements of both the DCL and the mixed-covalent-noncovalent imprinting approaches and pro-

- (1) *Comprehensive Supramolecular Chemistry*; Lehn, J.-M., Series Ed.; Elsevier Science Ltd.: New York, 1996; Vols. 1-2. Lehn, J.-M. *Angew. Chem., Int. Ed. Engl.* **1988**, *27*, 89-112. Cram, D. J. *Angew. Chem., Int. Ed. Engl.* **1988**, *27*, 1009-1020.
- (2) Wulff, G.; Sarhan, A. *Angew. Chem., Int. Ed. Engl.* **1972**, *11*, 341.
- (3) Shea, K. J. *Trends Polym. Sci.* **1994**, *2*, 166-173.
- (4) Andersson, L.; Sellergren, B.; Mosbach, K. *Tetrahedron Lett.* **1984**, 5211-5214.

- (5) Whitcombe, M. J.; Rodriguez, M. E.; Villar, P.; Vulfson, E. N. *J. Am. Chem. Soc.* **1995**, *117*, 7105-7111.
- (6) For books and recent literature reviews of MIPs, see: Wulff, G. *Chem. Rev.* **2002**, *102*, 1-27. Ye, L.; Mosbach, K. *J. Inclusion Phenom. Macrocycl. Chem.* **2001**, *41*, 107-113. Haupt, K.; Mosbach, K. *Chem. Rev.* **2000**, *100*, 2495-2504. *Molecularly Imprinted Polymers.*; Sellergren, B., Ed.; Elsevier: Amsterdam, 2001. Bartsch, R. A.; Maeda, M., Eds. *Molecular and Ionic Recognition with Imprinted Polymers*; ACS Symposium Series 703; Oxford Press: New York, 1998.
- (7) Wulff, G. *Angew. Chem., Int. Ed. Engl.* **1995**, *34*, 1812-1832.
- (8) Katz, A.; Davis, M. E. *Macromolecules* **1999**, *32*, 4113-4121.
- (9) Sellergren, B.; Shea, K. J. *J. Chromatogr.* **1993**, *635*, 31-49.
- (10) Vlatakis, G.; Andersson, L. I.; Müller, R.; Mosbach, K. *Nature* **1993**, *361*, 645-647.
- (11) Cousins, G. R. L.; Poulsen, S.-A.; Sanders, J. K. M. *Curr. Opin. Chem. Biol.* **2000**, *270*, 270-279.
- (12) Lehn, J.-M.; Eliseev, A. V. *Science* **2001**, *291*, 2331-2332.
- (13) Klekota, B.; Miller, B. L. *Trends Biotechnol.* **1999**, *17*, 205-209.

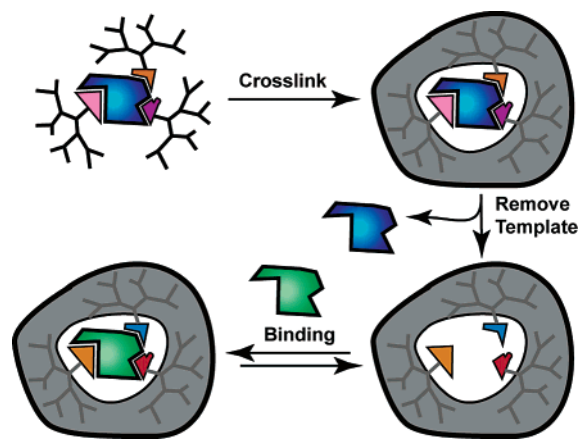


Figure 1. Schematic representation of the monomolecular imprinting process.

duces macromolecular hosts containing a single binding site.^{14,15} Herein, full details of those studies are described, including binding kinetics and imprinting experiments using a different but related template.

Design of a Monomolecular Imprinting System

To make a selective MIP, each template should produce an effective binding site, and each binding site must originate from template-mediated imprinting. The approach chosen to test the basic strategy involves three distinct steps (Figure 1): (1) covalent attachment of functional dendrons to the template with cleavable bonds, (2) cross-linking of the dendron end-groups, and (3) removal of the template. In principle, a single binding site could be imprinted into virtually any macromolecule. Even though they often require multistep synthesis, dendrimers were attractive candidates for these early studies both because their homogeneity assists in purification and characterization and because the large number of end-groups should allow a significant degree of cross-linking.¹⁶

With respect to the cross-linking reaction, a reversible chemical process was desirable as a way to effect a dynamic molding that might result in a “best-fit” imprint for the template. Recent advances in the development of novel catalysts for olefin metathesis have made reversible, but robust, alkene cross-links

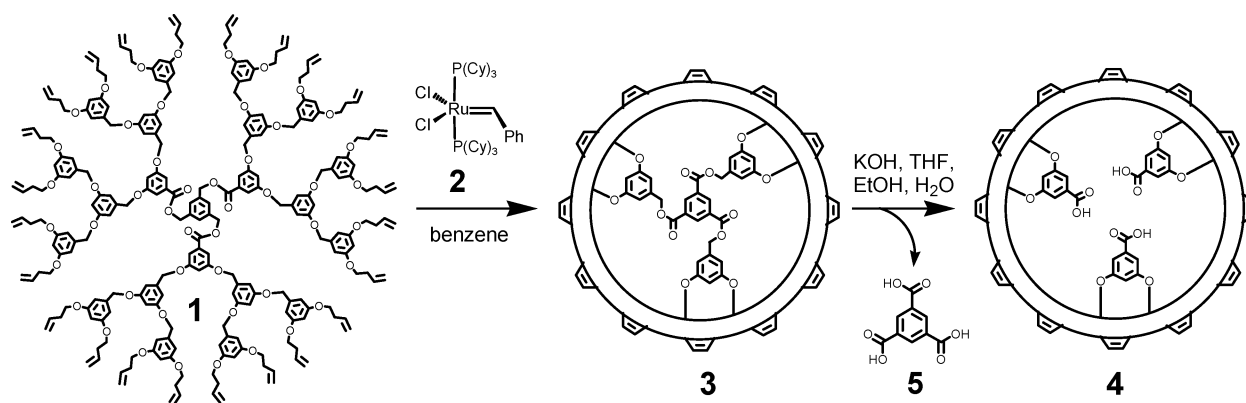
easily accessible.^{19,20} For example, the Grubbs’ ruthenium benzylidene catalysts exhibit broad functional group tolerance and are relatively insensitive to water, oxygen, or other impurities.²⁰ The commercially available Type I catalyst (**2**) is particularly well studied and known to produce medium and large ring systems,²¹ although the more recently reported Type II catalyst has certain advantages in this regard.²² The Type I catalyst has also been used to covalently capture supramolecular assemblies.²³ Most appealing from the perspective of dynamic molding was the finding that the pendant alkene groups in 1,2-polybutadiene underwent extensive ring-closing metathesis (RCM) reactions and that undesirable ring closings were reopened, ultimately allowing nearly all adjacent alkenes to couple.²⁴ To demonstrate this concept of monomolecular imprinting, we decided to imprint a porphyrin within a Fréchet-type dendrimer²⁵ for multiple reasons. First, the dendrimer shell must be relatively nonpolar to permit hydrogen bond-mediated recognition in the core.²⁶ The Fréchet-type phenyl-benzyl ether-based dendrimers fulfill this requirement, and a range of other recognition processes have been shown to occur readily within the interior of these dendrimers.¹⁷ Fréchet-type dendrimers are also chemically robust, which allows considerable latitude in the chemistry used to implement the imprinting process outlined in Figure 1. Furthermore, they possess an intermediate degree of flexibility in comparison to that of poly(propylene imine) or phenylacetylene based systems. Most importantly, we reported that, upon treatment with RCM catalyst **2**, dendrimer **1** underwent extensive cross-linking to give **3**, which subsequently afforded **4** upon core removal (Scheme 1).²⁷

To our knowledge, porphyrins have not been used as templates for the synthesis of MIPs, although their incorporation into MIPs for recognition and sensing was reported by Takeuchi,²⁸ and porphyrins have been used extensively in molecular recognition, shape selective oxidation, and self-assembly studies.²⁹ In the current work, polyhydroxylated tetraphenylporphyrins were considered excellent candidates as templates because the multiple hydroxyl groups provide sites for dendron attachment. These, in turn, would produce an imprinted structure capable of multipoint recognition. Furthermore, the visible

- (14) Zimmerman, S. C.; Wendland, M. S.; Rakow, N. A.; Zharov, I.; Suslick, K. S. *Nature* **2002**, *418*, 399–403.
- (15) Shinkai and co-workers have pioneered the imprinting of a single binding site on a single fullerene molecule: Ishi-i, T.; Shinkai, S. *Chem. Commun.* **1998**, *9*, 1047–1048. Ishi-i, T.; Iguchi, R.; Shinkai, S. *Tetrahedron* **1999**, *55*, 3883–3892.
- (16) Selected reviews focusing on the synthesis and properties of dendrimers: Fréchet, J. M. J.; Tomalia, D. A. *Dendrimers and Other Dendritic Polymers*; Wiley: New York, 2002. Newkome, G. R.; Moorefield, C. N.; Vögtle, F. *Dendrimer and Dendrons: Concepts Syntheses, Applications*; VCH: Weinheim, 2001. Grayson, S. M.; Fréchet, J. M. J. *Chem. Rev.* **2001**, *101*, 3819–3867. Crooks, R. M.; Lemon, B. L., III; Sun, L.; Yeung, L. K.; Zhao, M. *Top. Curr. Chem.* **2001**, *212*, 81–135. van Manen, H.-J.; van Veggel, F. C. J. M.; Reinhoudt, D. N. *Top. Curr. Chem.* **2001**, *217*, 121–162. Wiesler, U.-M.; Weil, T.; Müllen, K. *Top. Curr. Chem.* **2001**, *212*, 1–40. Balzani, V.; Ceroni, P.; Juris, A.; Venturi, M.; Campagna, S.; Puntoriero, F.; Serroni, S. *Coord. Chem. Rev.* **2001**, *219–221*, 545–572. Rockendorf, N.; Lindhorst, T. K. *Top. Curr. Chem.* **2001**, *217*, 201–238. Frey, H.; Schlenk, C. *Top. Curr. Chem.* **2000**, *210*, 69–129. Hawker, C. J.; Piotti, M. *ACS Symp. Ser.* **2000**, *755*, 107–118. Majoral, J.-P.; Caminade, A.-M. *Chem. Rev.* **1999**, *99*, 845–880. Janssen, H. M.; Meijer, E. W. *Mater. Sci. Technol.* **1999**, *20*, 403–458. Chow, H.-F.; Mong, T. K.-K.; Wan, C.-W.; Wang, Z.-Y. In *Adv. Dendritic Macromol.* **1971**, *4*, 107–133. Schluter, A.-D. *Top. Curr. Chem.* **1998**, *197*, 165–191. Seebach, D.; Rheiner, P. B.; Greiveldinger, G.; Butz, T.; Sellner, H. *Top. Curr. Chem.* **1998**, *197*, 125–164. Archut, A.; Vögtle, F. *Chem. Soc. Rev.* **1998**, *27*, 233–240. Moore, J. S. *Acc. Chem. Res.* **1997**, *30*, 402–413. Constable, E. C. *Chem. Commun.* **1997**, *12*, 1073–1080. Hawker, C. J.; Wooley, K. L. *Adv. Dendritic Macromol.* **1995**, *2*, 1–39.

- (17) Selected reviews on the supramolecular chemistry of dendrimers: Zeng, F.; Zimmerman, S. C. *Chem. Rev.* **1997**, *97*, 1681–1712. Newkome, G. R.; He, E.; Moorefield, C. N. *Chem. Rev.* **1999**, *99*, 1689–1746. Baars, M. W. P. L.; Meijer, E. W. *Top. Curr. Chem.* **2000**, *210*, 131–182. Smith, D. K.; Diederich, F. *Top. Curr. Chem.* **2000**, *210*, 183–227. Gorman, C. B.; Smith, J. C. *Acc. Chem. Res.* **2001**, *34*, 60–71. Zimmerman, S. C.; Lawless, L. J. *Top. Curr. Chem.* **2001**, *212*, 95–120.
- (18) Selected reviews focusing on functionalized dendrimers and their applications including in catalysis: Kreiter, R.; Kleij, A. W.; Klein Gebbink, R. J. M.; van Koten, G. *Top. Curr. Chem.* **2001**, *212*, 163–199. Bosman, A. W.; Janssen, H. M.; Meijer, E. W. *Chem. Rev.* **1999**, *99*, 1665–1688. Smith, D. K.; Diederich, F. *Chem.-Eur. J.* **1998**, *4*, 1353–1361.
- (19) Schrock, R. R. *Top. Organomet. Chem.* **1998**, *1*, 1–36. Hoveyda, A. H.; Schrock, R. R. *Chem.-Eur. J.* **2001**, *7*, 945–950. Randall, M. L.; Snapper, M. L. *J. Mol. Catal. A* **1998**, *133*, 29–40. Fürstner, A. *Top. Organomet. Chem.* **1998**, *1*, 37–72.
- (20) Grubbs, R. H.; Khosravi, E. *Mater. Sci. Technol.* **1999**, *20*, 65–104. Trnka, T. M.; Grubbs, R. H. *Acc. Chem. Res.* **2001**, *34*, 18–29.
- (21) Delgado, M.; Martin, J. D. *J. Org. Chem.* **1999**, *64*, 4798–4816.
- (22) Lee, C. W.; Grubbs, R. H. *J. Org. Chem.* **2001**, *66*, 7155–7158.
- (23) Clark, T. F.; Ghadiri, M. R. *J. Am. Chem. Soc.* **1995**, *117*, 12364–12365. Cardullo, F.; Calama, M. Crego; Snellink-Ruel, B. H. M.; Weidmann, J.-L.; Bielejewska, A.; Timmerman, P.; Reinhoudt, D. N.; Fokkens, R.; Nibbering, N. M. M. *Chem. Commun.* **2000**, *5*, 367–368.
- (24) Coates, G. W.; Grubbs, R. H. *J. Am. Chem. Soc.* **1996**, *118*, 229–230.
- (25) Hawker, C. J.; Fréchet, J. M. J. *J. Am. Chem. Soc.* **1990**, *112*, 7638–7647.
- (26) Zimmerman, S. C.; Wang, Y.; Bharathi, P.; Moore, J. S. *J. Am. Chem. Soc.* **1998**, *120*, 2172–2173.
- (27) Wendland, M. S.; Zimmerman, S. C. *J. Am. Chem. Soc.* **1999**, *121*, 1389–1390.
- (28) Matsui, J.; Higashi, M.; Takeuchi, T. *J. Am. Chem. Soc.* **2000**, *122*, 5218–5219.

Scheme 1



absorption bands of the porphyrin chromophore are intense and sensitive to the local environment. Porphyrin-core dendrimers have been studied as synthetic models of heme proteins, and porphyrins have been shown to be excellent reporter groups in studies of the photochemical and electrochemical properties of dendrimers.³⁰

Two synthetic hosts were prepared by imprinting 5,10,15,20-tetrakis(3,5-dihydroxyphenyl)porphyrin (**6**) and 5,10,15,20-tetrakis(4-hydroxyphenyl)porphyrin (**22**) into octa- and tetra-dendron macromolecules, respectively. Extensive complexation studies with several potential porphyrin guests probed the structural requirements for binding. The results suggest that this strategy, wherein a single molecular template imprints a single binding site within a single macromolecule, is a promising one that merits further development.

Results and Discussion

Imprinting 5,10,15,20-Tetrakis(3,5-dihydroxyphenyl)porphyrin (6**) Inside of a Dendrimer.** As shown in Scheme 2, porphyrin-core dendrimer **7** was synthesized by DCC-mediated esterification using dendron **8** and 5,10,15,20-tetrakis(3,5-dihydroxyphenyl)porphyrin (**6**). Large-scale (ca. 40 g) preparation of dendron **8** was accomplished in six steps in 48% overall yield from commercially available methyl 3,5-dihydroxybenzoate and homoallyl alcohol. Because of poor solubility, the reaction was initially carried out in THF, but after partial esterification the solvent was replaced with methylene chloride. Typically, the esterification was partially incomplete with ca. 5% of the product containing only six or seven dendrons, as discussed in greater detail below.

Porphyrin-core dendrimer **7** was cross-linked in benzene (10^{-6} M) with 4 mol % Grubbs' catalyst (**2**) per alkene to produce the cross-linked dendrimer **9** in 88% yield, with less than 5%

interhost cross-linking. The ^1H NMR spectrum of **9** showed the expected broadening of all of its signals, as well as the nearly complete loss of the alkene methine resonance at ca. 5.81 ppm and the appearance of a new alkene peak at 5.60 ppm corresponding to the disubstituted alkene group. Integration of these overlapping signals suggested that the average number of cross-links was about 29. Comparison of the MALDI-TOF mass spectra of **7** and **9** (Figure 2A and 2B, respectively) revealed a reduction in mass consistent with the formation of 28–32 cross-links, with the signal corresponding to 30 cross-links being the most intense (Table 1).

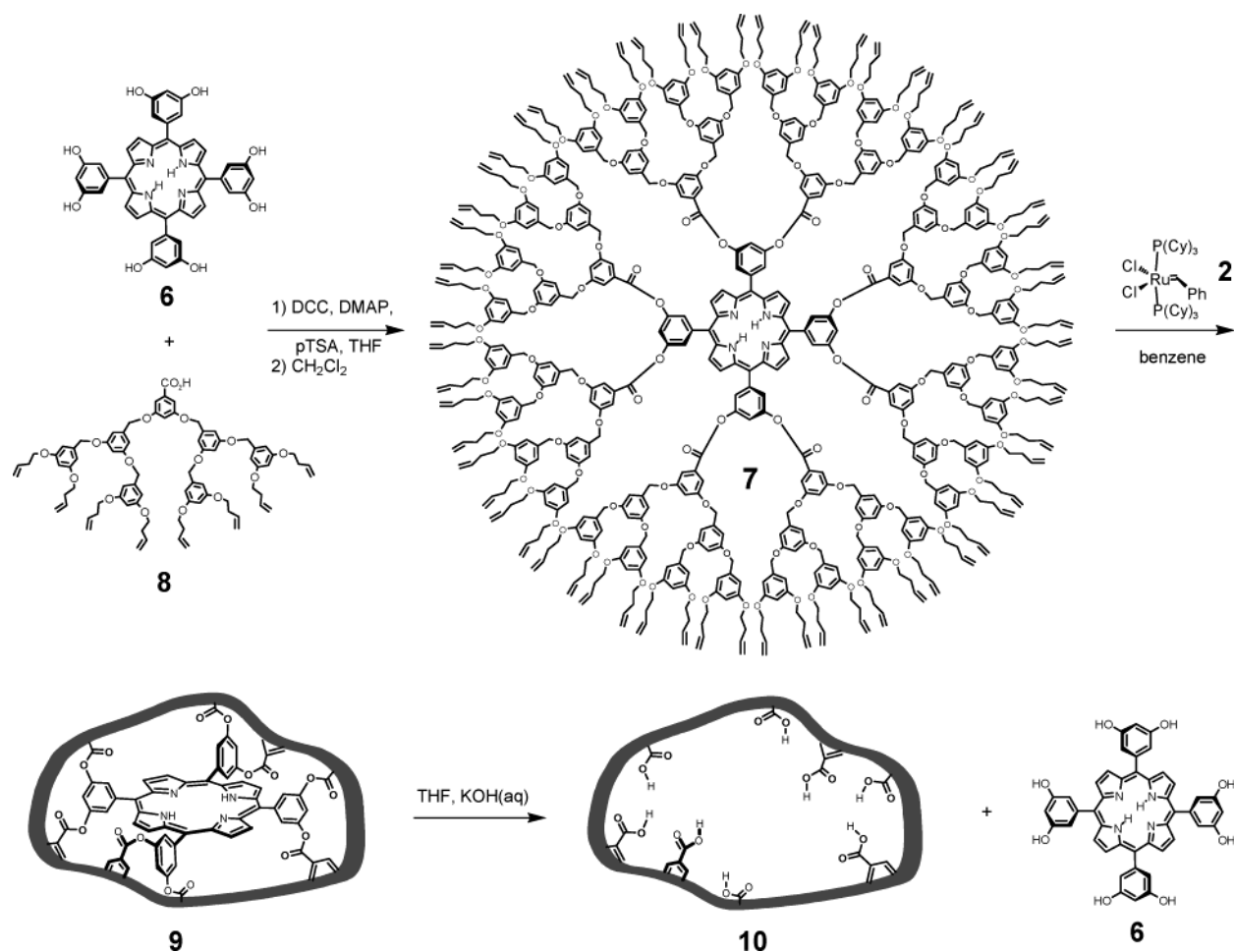
Dendrimers **7** and **9** were studied by size-exclusion chromatography (SEC). The apparent M_w of **7** as determined by SEC in toluene is 8200 Da, 26% below its actual M_w as measured by MALDI-TOF MS. This discrepancy is due to the globular shape of **7** being more compact than the linear polystyrene standards used for the M_w calibration. The SEC-determined apparent M_w of the cross-linked dendrimer **9** is 5500 Da, nearly 54% below its actual molecular weight observed by MALDI-TOF MS. This is consistent with the formation of an even more compact structure upon cross-linking.

Cross-linked dendrimer **9** was hydrolyzed using a 2.5 M aqueous KOH solution in THF to produce **10** in 43% yield. The ^1H NMR spectrum of the imprinted dendrimer **10** showed loss of the porphyrin signals at 9.21, 8.14, 7.74, and -2.86 ppm. Additionally, the aromatic protons ortho to the ester group and appearing at 7.53 ppm in **9** were replaced by a signal at 7.20 ppm, consistent with loss of the porphyrin core and ester to carboxylic acid conversion. Comparison of the MALDI-TOF mass spectra of **9** and **10** (Figure 2B and 2D, respectively) showed a difference of 605.4 Da corresponding to the loss of the porphyrin core ($\text{C}_{44}\text{H}_{22}\text{N}_4$: 606.7 Da).

The molecular weight of **10** could not be determined by SEC because this rather polar compound did not elute from the column. However, its octa-ethyl ester analogue **10-(CO₂Et)₈**, prepared by ethanolysis of **9**, had an apparent molecular weight of 4700 Da, 48% below its calculated molecular weight. In comparison to **9**, whose SEC-derived M_w was 5500, **10-(CO₂Et)₈** appears to be even more compact. This result suggests maintenance of a compact cross-linked dendrimer after the core removal with partial or full contraction of the carboxylic acid groups. It is not consistent with formation of a flexible, unfolded structure. Elemental analysis of **10** confirmed that no nitrogen was present, and, most significantly, the UV–visible spectrum of **10** showed no detectable absorbance (i.e., less than 0.01

- (29) Kosal, M. E.; Chou, J.-H.; Wilson, S. R.; Suslick, K. S. *Nat. Mater.* **2002**, *1*, 118–121. Sen, A.; Suslick, K. S. *J. Am. Chem. Soc.* **2000**, *122*, 11565–11566. Rakow, N. A.; Suslick, K. S. *Nature* **2000**, *406*, 710–714. Suslick, K. S. In *The Porphyrin Handbook*; Kadish, K., Smith, K., Guillard, R., Eds.; Academic Press: New York, 2000; Vol. 4, Chapter 28, pp 41–63. Ogoshi, H.; Mizutani, T. *Curr. Opin. Chem. Biol.* **1999**, *3*, 736–739. Sanders, J. K. M. *Compr. Supramol. Chem.* **1996**, *9*, 131–164. Suslick, K. S.; Van Deusen-Jeffries, S. In *Comprehensive Supramolecular Chemistry*; Lehn, J. M., Ed.; Elsevier Publishers: Oxford, 1996; Vol. 5, pp 141–170.
- (30) Selected references: Bhyrappa, P.; Young, J. K.; Moore, J. S.; Suslick, K. S. *J. Am. Chem. Soc.* **1996**, *118*, 5708–5711. Dandliker, P. J.; Diederich, F.; Gisselbrecht, J.-P.; Louati, A.; Gross, M. *Angew. Chem., Int. Ed. Engl.* **1996**, *34*, 2725–2728. Sadamoto, R.; Tomioka, N.; Aida, T. *J. Am. Chem. Soc.* **1996**, *118*, 3978–3979. Harth, E. M.; Hecht, S.; Helms, B.; Malmstrom, E. E.; Fréchet, J. M. J.; Hawker, C. J. *J. Am. Chem. Soc.* **2002**, *124*, 3926–3938.

Scheme 2



absorbance, which is less than 0.1% of retained porphyrin) at 420 nm (Soret band). Thus, despite extensive cross-linking, the porphyrin template can be quantitatively removed.

Several aspects of the cross-linking reaction warrant additional comment. First, cross-links may form within or between dendritic wedges. As seen in Figure 3, there are two types of intrawedge cross-links, a–b and a–c, and two types of interwedge cross-links, a–d and a–e. Proximity likely promotes intrawedge links, whereas interwedge connections are favored statistically. Although none of the methods of characterization used is capable of directly distinguishing the cross-link isomers, if all were of type a–b and b–c, then the hydrolysis reaction of **9** to **10** would lead to fragmentation with loss of one or more cross-linked wedges. Neither the MALDI-TOF MS nor the SEC traces of the crude reaction mixture or purified **10** showed significant evidence of fragmentation. Thus, the cross-linking reaction produces at least seven cross-links between the eight dendritic wedges, seven interwedge cross-links being the minimum needed to hold the cored dendrimer together.

In the RCM reaction of **1**, it was estimated that nearly 1.7 million isomers are possible with just six cross-links. This number, which was determined by enumeration, took into account formation of both cis and trans alkenes, but neglected topological isomers and the many isomers that would be structurally untenable. Many more cross-link isomers are possible for **9** in comparison to **3**, but in both cases it is likely that only a subset of isomers is formed.

At issue are whether these isomers are kinetically or thermodynamically favored and by what mechanism is **9** able to become nearly fully cross-linked (i.e., 29–30 of 32 possible cross-links)? Molecular modeling experiments to be published elsewhere suggest that kinetic products are formed with several alkenes left dangling sufficiently far from one another that they cannot undergo the RCM reaction. Thus, a model is favored in which the reversibility of the RCM reaction allows the cross-linked dendrimer to dynamically mold itself around the porphyrin template.

Complexation Studies. In the noncovalent approach to MIPs, the ligand that is the ultimate target for binding is also used as the template in the imprinting reaction. In contrast, the target ligand for covalently synthesized MIPs may not be an appropriate template. For example, in the hydrolytic removal of template **6** from cross-linked dendrimer **9**, eight additional hydroxyl groups are added to the cored dendrimer, reducing the size of the binding cavity. Thus, as seen by the very simple analysis shown in Figure 4, a rigidly imprinted **10** would have a binding cavity too small to complex **6**, although the isomeric porphyrin **11** (Chart 1) could fit and potentially form multiple CO₂H...OH hydrogen bonds. The same analysis indicates that the covalent phenyl ester linkage is, to a good approximation, isosteric with a pyridine-carboxylic acid hydrogen bond (Figure 4). As a result, a series of porphyrins (**11**–**20**, Chart 1) was prepared and used to study the binding selectivity of imprinted dendrimer **10**.

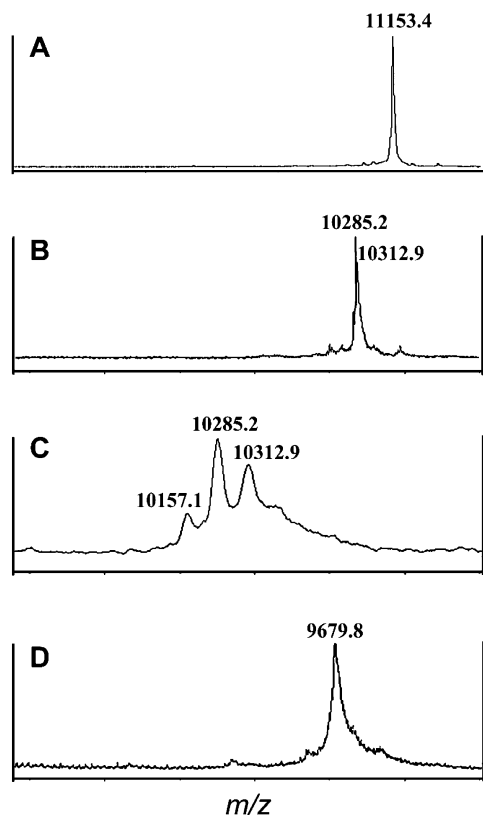


Figure 2. MALDI-TOF MS spectra of (A) porphyrin-core dendrimer **7**; (B) and (C) cross-linked dendrimer **9**; and (D) cored dendrimer **10**.

Table 1. A List of Observed Values, Peak Assignments, and Calculated Values for the Mass Spectra of **7**, **9**, and **10**

compound	observed value	peak assignment	calculated value
7	11 153	$M + H^+$	11 156.4
9	10 313	$M + H^+ - 30C_2H_4$	10 313.9
	10 285	$M + H^+ - 31C_2H_4$	10 285.9
	10 257	$M + H^+ - 32C_2H_4$	10 257.9
10	9680	$M + H^+ - 31C_2H_4 - C_{44}H_{22}N_4$	9679.2

A typical binding experiment consisted of titrating a dilute porphyrin solution with a concentrated imprinted dendrimer solution in toluene (5% EtOAc–toluene for **6** and **11**) by adding a 10^{-2} M solution of **10** to a 10^{-5} M solution of porphyrin and recording the absorbance of the Soret band region 10 min after each addition of imprinted dendrimer. Complexation of the porphyrin by the dendrimer host was signaled by a red shift of the λ_{max} of the Soret band. Factors that might produce such a red shift include a general polarity change in the environment, π – π stacking, hydrogen bonding between the pyrrole nitrogen atoms and the carboxylic acid groups, and a complexation-induced deplanarization of the porphyrin ring.³¹ Initial experiments using **11** indicated that the extent of the red shift was dependent both on the amount of **10** added and on the time elapsed. Similar observations were made for **12** and **14–16**, and in each case it appeared that the red shift occurred in two distinct phases, one fast (seconds/minutes) and one very slow (hours/days). The apparent biphasic binding kinetics is discussed in greater detail below, but the experiments described first focused on the fast binding component.

(31) Shelnut, J. A.; Song, X.-Z.; Ma, J.-G.; Jia, S.-L.; Jentzen, W.; Medforth, C. J. *Chem. Soc. Rev.* **1998**, *27*, 31–42.

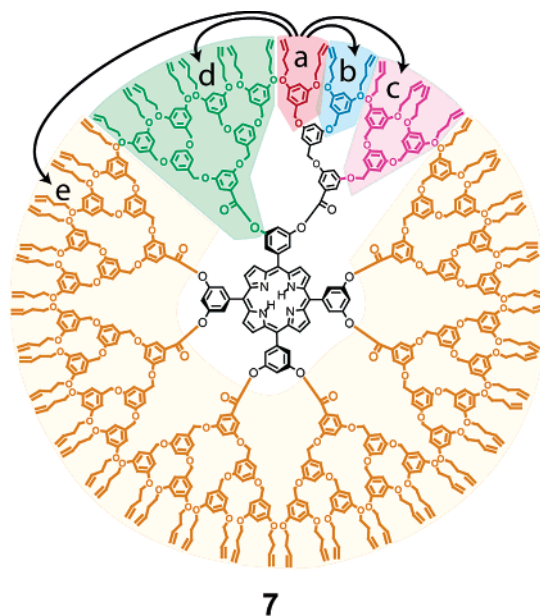


Figure 3. Dendrimer **7** with wedges and subwedges color-coded to show different types of cross-link isomers.

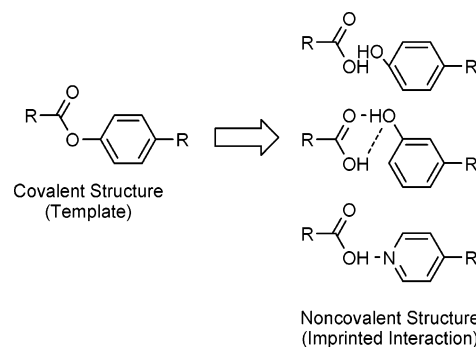
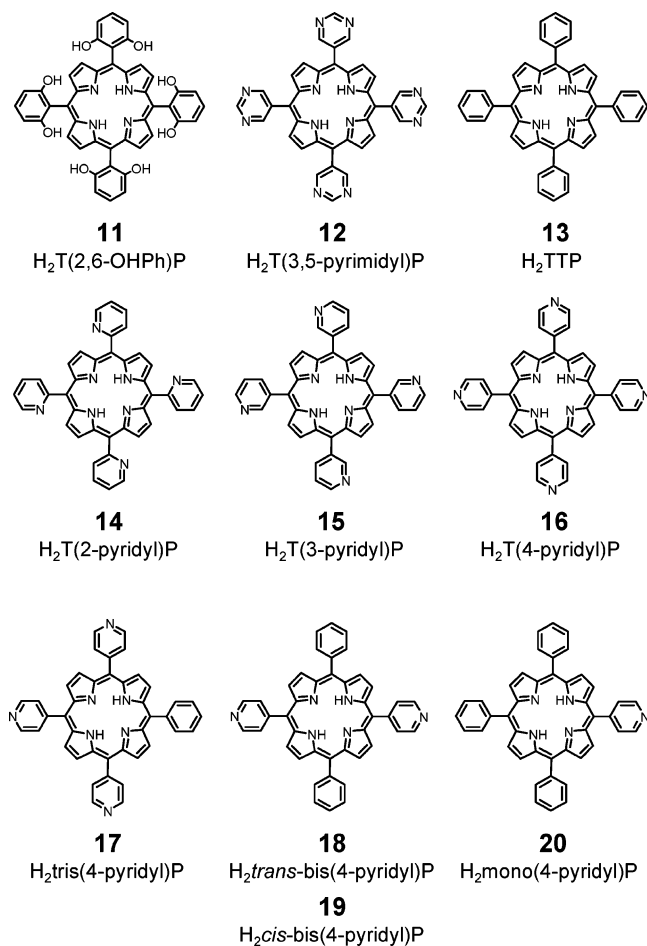


Figure 4. Schematic illustration of how covalent linkage between template and dendrimer scaffold impacts the ultimate binding interaction between imprinted dendrimer and ligand.

Several control experiments were performed that are consistent with reversible complexation of **11**, **12**, and **14–16** by hydrogen bonding. First, no red shift was observed with porphyrins lacking hydrogen bond donor–acceptor groups such as 5,10,15,20-tetraphenylporphyrin, **13**. The red shift observed upon addition of **10** to a solution of **11** could be fully reversed by increasing the EtOAc content from 5% to 15% (v/v) in toluene. Likewise, addition of **10** to a solution of **11** in 50% EtOAc did not produce a red shift. To demonstrate the importance of the carboxylic acid groups of **10** in the binding, the octa-ethyl ester dendrimer **10**-(CO₂Et)₈ was prepared by ethanolysis of **9** (K₂CO₃, toluene, ethanol, reflux). The structure of **10**-(CO₂Et)₈ was verified by SEC, ¹H NMR spectroscopy, MALDI-TOF MS, and UV–visible spectroscopy. The addition of approximately 60 equiv of **10**-(CO₂Et)₈ to H₂T(3-pyridyl)P (**15**) did not produce a red shift even over the course of 95 h. Likewise, addition of simple carboxylic acids did not cause a red shift of H₂T(3-pyridyl)P (**15**). Neither the addition of 640 equiv of dendron carboxylic acid **2** to a ca. 3 μ M solution of H₂T(2,6-OHPh)P (**11**) in 5% EtOAc–toluene nor the addition of 2000 equiv of 4-*tert*-butyl benzoic acid to a ca. 3 μ M solution of H₂T(3-pyridyl)P (**15**) in toluene led to any red shift. Finally, cored dendrimer **4** with three acid groups, which was imprinted

Chart 1



with 1,3,5-tris(hydroxymethyl)benzene, did not alter the position of the Soret band of a ca. 3 μM solution of **11** in toluene even upon addition of 49 equiv in 95 h.

The results of two additional experiments indicated that porphyrins **11**, **12**, and **14–16** were complexed within **10** and that its binding sites arose from an imprinting process. First, complexation of $\text{H}_2\text{T}(2,6\text{-OHPh})\text{P} (**11**) by imprinted dendrimer **10** was observed by SEC. A 5% EtOAc–toluene solution containing a 5:1 molar ratio of **10** to **11** was analyzed by analytical SEC using 5% EtOAc–toluene as the eluent. Whereas porphyrin **11** absorbs to the SEC matrix and does not elute by itself, it coelutes with imprinted dendrimer **10** (as detected at $\lambda_{\text{max}} = 417$ nm Soret band). Thus, complexation within the dendrimer protects the polar porphyrin from SEC matrix absorption during the course of its elution. A second, key experiment involved adding **10** to template **6** in 5% EtOAc–toluene. No change in the Soret band was observed upon titration of **6** with **10**. This finding supports the model presented in Figure 4 and is inconsistent with **10** being a flexible octa-acid able to complex any guest with sufficient hydrogen bond donor and acceptor groups.$

To determine more quantitatively the binding profile of **10**, the titration data for porphyrins **11–20** (Chart 1) were analyzed using a modified form of the Drago equation: $[\mathbf{10}]$ versus $[\mathbf{10}]/\Delta A$, where ΔA is the change in absorbance upon addition of **10**.³² The reciprocal of the intercept of this plot gives the association constant (K_{assoc}). One advantage of this approach is

Table 2. Apparent Association Constants (K_{app}) for Complexes Formed between Imprinted Dendrimer **10** and Porphyrins

porphyrin	$\Delta\lambda_{\text{max}}^a$	$K_{\text{app}} (\times 10^4 \text{ M}^{-1})^b$
$\text{H}_2\text{T}(3,5\text{-OHPh})\text{P} (6)$	0	<0.1
$\text{H}_2\text{T}(2,6\text{-OHPh})\text{P} (11)$	6.8	10
$\text{H}_2\text{T}(3,5\text{-pyrimidyl})\text{P} (12)$	0.8	5
$\text{H}_2\text{TTP} (13)$	0	<0.1
$\text{H}_2\text{T}(2\text{-pyridyl})\text{P} (14)$	3.0	5
$\text{H}_2\text{T}(3\text{-pyridyl})\text{P} (15)$	5.8	14
$\text{H}_2\text{T}(4\text{-pyridyl})\text{P} (16)$	5.4	13
$\text{H}_2\text{-tris}(4\text{-pyridyl})\text{P} (17)$	0	<0.1
$\text{H}_2\text{-trans-bis}(4\text{-pyridyl})\text{P} (18)$	0	<0.1
$\text{H}_2\text{-cis-bis}(4\text{-pyridyl})\text{P} (19)$	0	<0.1
$\text{H}_2\text{-mono}(4\text{-pyridyl})\text{P} (20)$	0	<0.1
$\text{CuT}(3\text{-pyridyl})\text{P} (15a)$	4.6	11

^a A value of $\Delta\lambda_{\text{max}} = 0$ indicates no observed change in the absorption spectrum. ^b Upper limits on solubility prevented a more accurate upper limit from being obtained.

that the K_{assoc} values can be determined without knowledge of the concentration of the free or complexed porphyrin. To examine the fast binding component, the titrations were completed within 1 h. All gave linear plots, which, by analogy to Scatchard-type plots, indicates formation of 1:1 complexes.

The association constants, which are listed in Table 2, are denoted as K_{app} because of the likely heterogeneity in **10** and time dependency of the binding. As predicted by Figure 4, $\text{H}_2\text{T}(3,5\text{-pyrimidyl})\text{P} (**12**) is bound by **10**, and its $K_{\text{app}} = 5 \times 10^4 \text{ M}^{-1}$ is of the same magnitude as the value determined for the **10**·**15** complex. The pyridyl porphyrins **14–16** bind equally well despite their capacity to make only half as many hydrogen bonds as **12**. This may indicate that all eight carboxylic acids are not involved in binding $\text{H}_2\text{T}(3,5\text{-pyrimidyl})\text{P} (**12**); however, the difference must at least partially originate in the 10^4 -fold higher basicity of pyridine relative to pyrimidine ($\text{p}K_{\text{a}} 5.23$ vs 1.2).³³ The K_{app} for the **10**·**14** complex (2-pyridyl isomer) is approximately 2-fold lower than that for the 3- and 4-pyridyl isomers **15** and **16**. Thus, there is a small degree of shape selectivity in the imprint. No binding was detected for pyridyl porphyrins **17–20**, showing that a minimum of four binding contacts are necessary for complexation under the conditions used in this study.$$

Although the K_{app} values for several of the porphyrin guests are large, one might have expected them to be even larger given that a typical benzoic acid–pyridine complex in apolar organic solvents has a $K_{\text{assoc}} \approx 10^2 \text{ M}^{-1}$.³⁴ Several factors may be responsible for lowering the absolute porphyrin affinity exhibited by **10**. Conformational reorganization may be necessary if the empty imprint relaxes into a lower energy structure; such a state might include partial collapse of the core site through internal carboxylic acid dimerization or the internal binding of multiple water molecules. The IR spectra of **10** were inconclusive with regard to the latter possibility, but the elemental analysis did reveal the presence of multiple water molecules, presumably solvating the polar carboxylic acid groups. In studies of adenine complexation by molecular tweezers with a single “active site” carboxylic acid group, we reported that added water in chloroform led to a measurable depression in the binding constant.³⁵

(32) Collman, J. P.; Brauman, J. I.; Doxsee, K. M.; Halbert, T. R.; Hayes, S. E.; Suslick, K. S. *J. Am. Chem. Soc.* **1978**, *100*, 2761–2766.

(33) Stewart R. *The Proton: Applications to Organic Chemistry*; Academic Press: Orlando, FL, 1985.

(34) Dega-Szafran, Z.; Szafran, M. *Heterocycles* **1994**, *37*, 627–659.

Dendrimer Fractionation. The observation of slow and fast binding processes may be consistent with two limiting populations of imprinted dendrimers, one that is tightly cross-linked with a somewhat inaccessible core and another that is more flexible and open. The latter properties are exactly those which would be expected for an impurity of **10** missing one or more dendron segments, and, thus, attention was focused on the ca. 5% impurity in **10** containing just six and seven dendrons (vide supra). To determine if this imperfect component was responsible for the observed two-phase binding, two series of experiments were conducted. In the first, dendrimer **10** was synthesized using a large excess of dendron **8**. The new sample of **10** obtained in this way contained significantly less hexa- and heptadendritic material. The titration of **15** with this new sample of **10**, however, was essentially identical to that with the original (Table 2).

In the second set of experiments, the hexa- and heptadendrons associated with impurities in **10** were isolated and examined directly. Thus, **6-Zn** was found to be significantly less reactive in the Mitsunobu esterification reaction. Thus, treatment of **6-Zn** with 8 equiv of **8** under the same conditions used with **6** afforded **7-Zn** containing a significant amount of hexa- and heptadendron product. Cross-linking of **7-Zn** under standard conditions gave **9-Zn** whose MALDI-TOF spectrum is shown in Figure 5A. The material containing predominantly six and seven dendrons was separated from the dendrimers containing mainly eight dendrons by selective absorption on a diethylenetriamine-modified polystyrene resin in benzene. The material left in solution contained mostly seven and eight dendrons (Figure 5B), while the material “trapped” on the resin and removed with 5% pyridine contained mostly six and seven dendrons (Figure 5C). The selectivity in the absorption was explained by a stronger amino group ligation to the more accessible Zn(II) center in the imperfect dendritic macromolecules. The dendrimers with six and seven dendrons were cored, resulting in “imperfect” imprinted material. When added to a toluene solution of **15**, this material, which was noticeably less soluble than previous preparations of **10**, did not induce a red shift. Therefore, it was concluded that hexa- and heptadendritic structures do not participate in porphyrin binding to a measurable extent and that the origin of biphasic binding kinetics lies elsewhere.

Binding Site Heterogeneity, Complexation Kinetics, and Cu-T(3-pyridyl)P. The incomplete reaction between **6** and **8** led to one type of heterogeneity in imprinted dendrimer **10**. A second type originates in the RCM reaction of dendrimer **7**, which can produce **9** containing a very large number of cross-link isomers (vide supra). It is possible that the slow and fast binding kinetics indicate two populations of cross-link isomers. For example, it is likely that isomers containing cross-links primarily between dendrons will be more compact and rigid with slower binding kinetics than those isomers where intradendron cross-links predominate. To examine more systematically the kinetics of binding, six 3 μ M solutions of H₂T(3-pyridyl)P (**15**) containing 0.0, 0.5, 1, 1.5, 2.0, and 5.0 equiv of **10** were monitored over a period of 408 h (17 days). Shown in

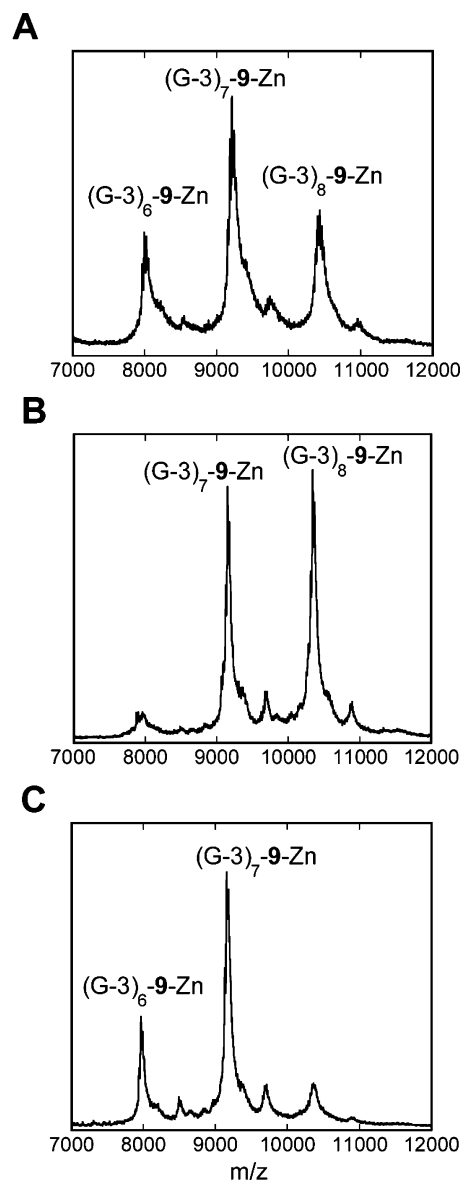


Figure 5. MALDI-TOF MS spectra of (A) a mixture of porphyrin-core dendrimer **9-Zn**; (B) dendrimers with mainly eight dendrons left in solution; and (C) dendrimers with mainly six and seven dendrons absorbed on the resin.

Figure 6A and B are overlaid spectra of the solutions taken at 1 and 408 h, respectively. The overlaid spectra at intermediate times similarly show an isosbestic point, whose position moves only slightly with time. These data indicate that (1) a single equivalent of **10** is able to complex most of H₂T(3-pyridyl)P, and (2) there are two classes of bound species. The former observation has important implications for the monomolecular imprinting approach in that it demonstrates that the chemistry shown schematically in Figure 1 and in detail in Scheme 2 produces **10** containing >95% effective imprinted binding sites.

To gain insight into the nature of the bound species, the 35 spectra described above (5 solutions at 0.17, 1, 3, 28, 116, 206, 408 h) were deconvoluted using model spectra for three species (Figure 6C): (1) free porphyrin ($\lambda_{\max} = 421$ nm), (2) the fast forming complex (Complex I), and (3) the slow forming complex (Complex II). The model spectrum for Complex I ($\lambda_{\max} = 426$ nm) was obtained 1 h after mixing 50 equiv of **10** and H₂T(3-pyridyl)P in toluene, conditions that led to >95% bound

(35) Zimmerman, S. C.; Wu, W.; Zeng, Z. *J. Am. Chem. Soc.* **1991**, *113*, 196–201. In a receptor using two carboxylic acid groups, Adrian and Wilcox reported an ca. 15% decrease in K_{assoc} and further showed a much larger, but compensating, effect on the complexation enthalpies and entropies of complexation: Adrian, J. C., Jr.; Wilcox, C. S. *J. Am. Chem. Soc.* **1991**, *113*, 678–680. It is possible with multiple carboxylic acids that the effect is cumulative.

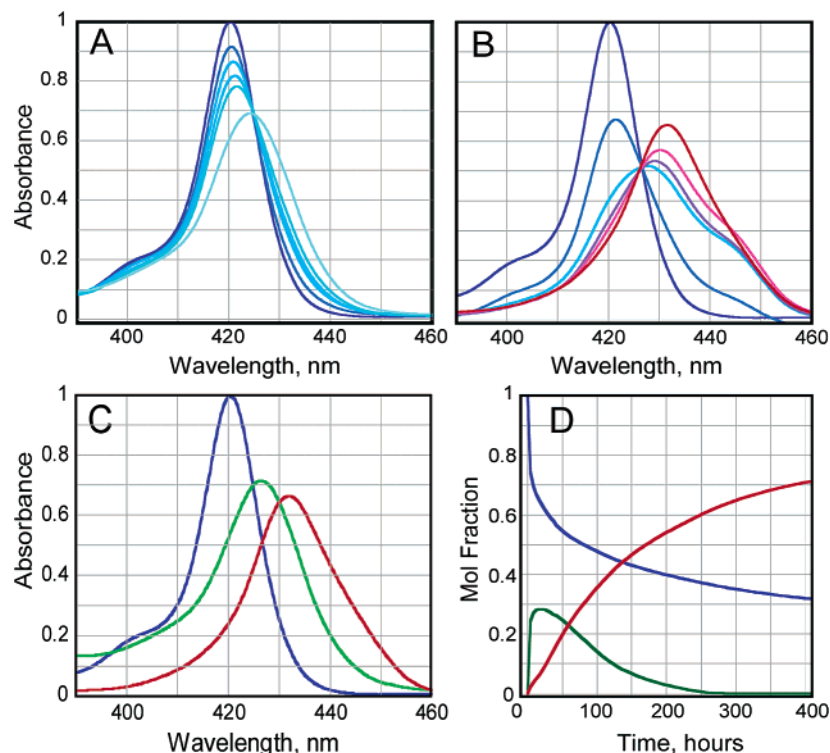


Figure 6. Overlaid spectra of the titration solutions taken at (A) 1 h and (B) 408 h; spectra of the model species (C) and the time course of the binding of the porphyrin **15** with 1 equiv of **10** (D); blue line, **15**; green line, Complex I; red line, Complex II.

porphyrin. The model spectrum for Complex II ($\lambda_{\max} = 432$ nm) was that generated after equilibrating 5 equiv of **10** and $\text{H}_2\text{T}(3\text{-pyridyl})\text{P}$ in toluene for 408 min. The model spectra of Complexes I and II are broader than that of the free porphyrin, suggesting that each is a class of complexes that are similar in their stability, formation kinetics, and UV–visible spectra. Using the three model spectra, we deconvoluted each titration spectrum with an average deviation of 0.019 au. The apparent molar absorption coefficients determined for Complexes I and II are 2.07×10^5 and $1.92 \times 10^5 \text{ mol}^{-1} \text{ cm}^{-1}$, respectively.

The time course of the binding as revealed by the spectral deconvolution is shown in Figure 6D. Taken together, all of the results are consistent with the free porphyrin rapidly forming Complex I with an approximately 5 nm red shift. The deconvolution indicates a maximum of 30% of $\text{H}_2\text{T}(3\text{-pyridyl})\text{P}$ (at 10^{-5} M concentration of the porphyrin) is bound by a single equivalent of **10**, consistent with the amount expected given the $K_{\text{app}} = 1.4 \times 10^5 \text{ M}^{-1}$. Over time, Complex I is replaced by Complex II whose K_{app} is about 10-fold higher, leading to 70% $\text{H}_2\text{T}(3\text{-pyridyl})\text{P}$ being bound. Although the two complexes may arise from heterogeneity in the imprint (i.e., separate isomers of **10**), the stronger binding, the additional 6 nm red shift observed for Complex II, and the evolution of the red shift seen in Figure 6D are particularly well explained by a slow conformational change to a tighter fitting complex.

Although there are several explanations for the observed fast and slow complex formation, a conformation change represents a likely candidate, and it is possible to speculate on its nature. Given that only four of the carboxylic acid groups of **10** are needed to complex $\text{H}_2\text{T}(3\text{-pyridyl})\text{P}$, a free carboxylic acid group might hydrogen bond to an inner pyrrole nitrogen atom of the porphyrin guest. Such a significant conformational reorganization might take considerable time. Furthermore, the increased

nonplanarity of the porphyrin nucleus required for the additional stabilizing hydrogen bond would explain the additional 6 nm red shift.³¹ Direct support for such a mechanism is not available, but the use of $\text{CuT}(3\text{-pyridyl})\text{P}$ (**15-Cu**) which lacks a free pyrrole nitrogen atom completely eliminates the slow complexation process. The dramatic change in the binding course is clearly seen in the side-by-side comparison of the spectrophotometric titrations of $\text{H}_2\text{T}(3\text{-pyridyl})\text{P}$ and $\text{CuT}(3\text{-pyridyl})\text{P}$ with **10** (Figure 7). Whereas the Soret band of **15** continues to shift to longer wavelength after the initial rapid red shift, $\text{CuT}(3\text{-pyridyl})\text{P}$ gives $\Delta\lambda_{\max} = 4.6 \text{ nm}$ in 10 min and then shows no additional shift. The K_{app} values determined for $\text{10} \cdot \text{H}_2\text{T}(3\text{-pyridyl})\text{P}$ and $\text{10} \cdot \text{CuT}(3\text{-pyridyl})\text{P}$ are quite similar (Table 2).

Imprinted Tetradendron Molecule. To examine whether a porphyrin template with only four attachment points could imprint an effective binding site containing four carboxylic acid groups, dendritic porphyrin **21** was synthesized from 5,10,15,20-tetrakis(4-hydroxyphenyl)porphyrin and **23** (Scheme 3). Thus, **8** was treated with oxalyl chloride in THF to produce **23** in 64% yield, which was reacted directly with 5,10,15,20-tetrakis(4-hydroxyphenyl)porphyrin and DMAP in THF, affording porphyrin core dendrimer **21** in 90% yield. The cross-linking of **21** was accomplished in 79% yield using Grubbs' catalyst **2** and the same conditions described for **7**. Analysis by MALDI-TOF MS indicated an average of 15 out of 16 possible cross-links. However, upon core removal (same conditions as for **10**), MALDI-TOF mass spectra showed clear evidence of fragmentation as peaks corresponding to cross-linked dendrimers with only two and three dendrons were observed. The results suggested that the dendrons in **21** were too far apart to promote extensive interdendron cross-linking.

To favor interdendron cross-linking, the larger, fourth-generation dendron **24** was employed (Scheme 4). Dendron **24**

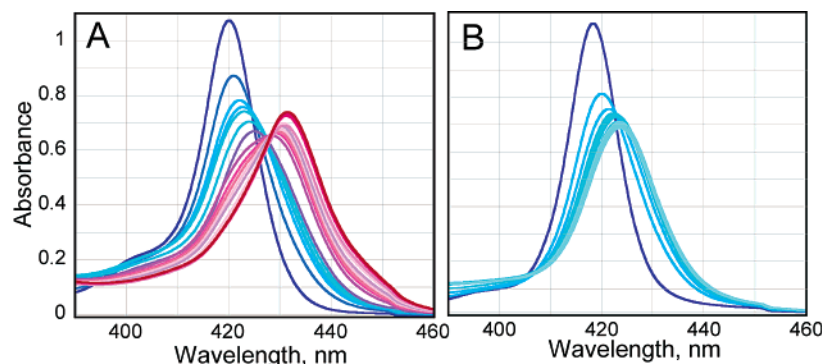
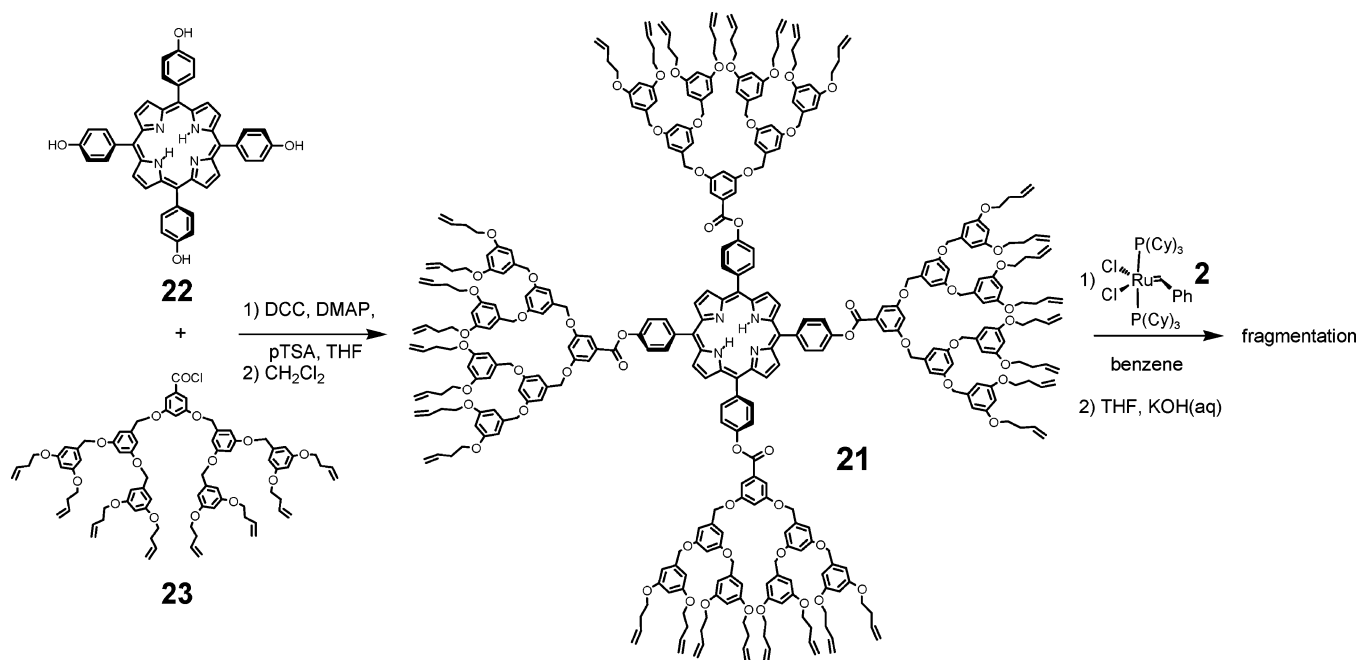


Figure 7. Overlaid spectra of the titration solutions for (A) $\text{H}_2\text{T}(3\text{-pyridyl})\text{P}$ and (B) $\text{Cu-T}(3\text{-pyridyl})\text{P}$ after 408 h; fast binding is shown in blue, and slow binding is shown in red.

Scheme 3



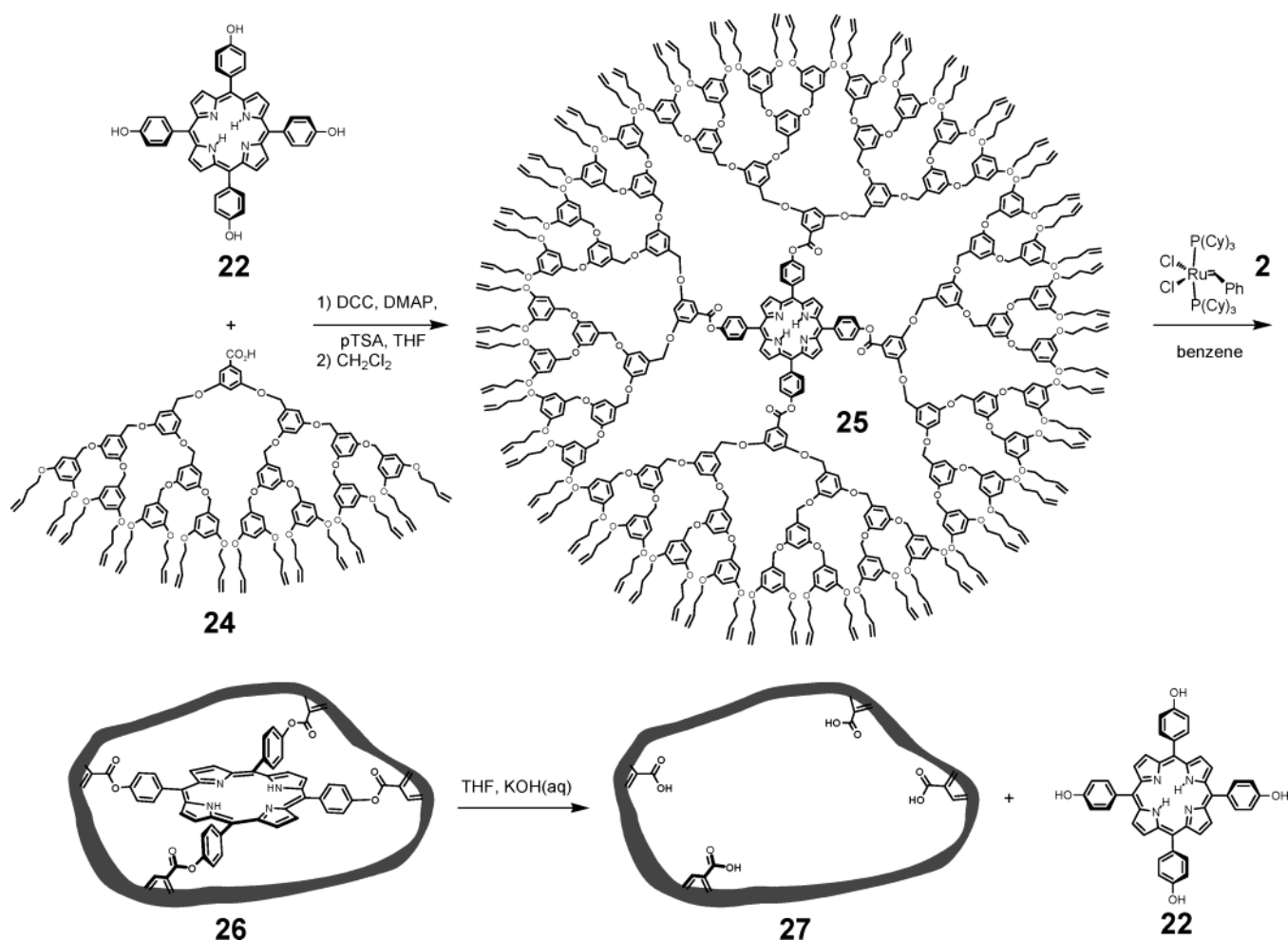
was prepared in 83% yield by basic hydrolysis of the corresponding methyl ester, which was prepared in 89% yield by reaction of methyl 3,5-dihydroxybenzoate with [G-3]-OH under Mitsunobu conditions. Porphyrin-core dendrimer **25** was synthesized in 46% yield by coupling **22** to **24** in THF with DPTS and DCC (same conditions as for **7**). Dendrimer **25** was cross-linked in benzene using 5 mol % Grubbs' catalyst per alkene to afford the cross-linked dendrimer **26** in 88% yield, which was hydrolyzed to produce the imprinted dendrimer **27** in 48% yield.

As in the **7** \rightarrow **9** \rightarrow **10** conversion, the MALDI-TOF mass spectra provide the most conclusive evidence for the success of the cross-linking and coring reactions. The observed and calculated values for the MALDI-TOF mass spectra peaks, as well as the corresponding peak assignments for **25**, **26**, and **27**, are listed in Table 3. The data indicate an average of 31 of 32 cross-links for **26**. Evidence of the removal of the porphyrin core was obtained by comparing the MALDI-TOF mass spectra of **26** and **27**. No peak corresponding to **26** was observed in the spectrum of **27**, but a new peak was present consistent with a loss of ca. 607 Da. The loss in mass was within experimental error of that expected for loss of the core ($\text{C}_{44}\text{H}_{28}\text{N}_4$, 614.7).

The mass spectrum of **27** also showed that, in contrast to the cross-linked and cored product from **21**, little if any of **26** fragmented upon coring.

The pyridyl porphyrins **14**–**16** were titrated with imprinted dendrimer **27** in toluene, and their binding constants were determined (Table 4). The decrease in binding constants in the series **14**–**16** may result from a combination of the shape-selective binding and decreasing basicity of the pyridyl groups. The plots used to calculate binding constants for the complexes formed between porphyrins **14**–**16** and **27** were linear, indicating the stoichiometry of these complexes was 1:1. A control study was performed by titrating tetraphenylporphyrin (**13**) with imprinted dendrimer **27**, and no change in the Soret band position of **13** was observed even upon the addition of 66 equiv of **27**, confirming that hydrogen-bonding to the imprinted dendrimer is the cause for the red shift observed for the pyridyl porphyrins. The titration solutions of **14** and **15** with **27** were injected onto an analytical SEC column and eluted with toluene. Porphyrins **14** and **15** coeluted with the imprinted dendrimer **27**. When toluene was removed from the solution of **15** and **27** and the mixture redissolved in THF was injected into the SEC

Scheme 4

**Table 3.** A List of Observed Values, Peak Assignments, and Calculated Values for the Mass Spectra of **25**, **26**, and **27**

compound	observed value	peak assignment	calculated value
25	11 526	M + H ⁺	11 525.0
26	10 624	M + H ⁺ - 32C ₂ H ₄	10 627.2
	10 653	M + H ⁺ - 31C ₂ H ₄	10 655.3
27	10 041	M + Na ⁺ - 32C ₂ H ₄ - C ₄₄ H ₂₈ N ₄	10 034.5
	10 069	M + Na ⁺ - 31C ₂ H ₄ - C ₄₄ H ₂₈ N ₄	10 062.6

Table 4. Apparent Association Constants (K_{app}) for Complexes Formed between Imprinted Dendrimer **27** and Porphyrins

porphyrin	$\Delta\lambda_{\text{max}}$	K_{app} ($\times 10^4$ M)
H ₂ T(2-pyridyl)P (14)	1.0	3.3
H ₂ T(3-pyridyl)P (15)	2.8	1.6
H ₂ T(4-pyridyl)P (16)	1.6	0.9

column, the porphyrin **15** eluted significantly later than the imprinted dendrimer **27**.

Conclusions

Described herein is a new strategy to make synthetic hosts that combines elements of the traditional polymer imprinting and dynamic combinatorial library approaches. There are several appealing features of this monomolecular imprinting strategy. The first is the use of the RCM reaction, which forms robust carbon-carbon double-bond cross-links but is nonetheless reversible. The ability to equilibrate cross-link isomers poten-

tially allows the dendritic framework to reach a lowest-energy "mold" around the template. Perhaps more importantly this strategy produces soluble and sizable macromolecular hosts ($M_w \approx 10$ kDa) but with a single imprinted site per molecule. Although there was no strong evidence of binding site heterogeneity in the present system, in cases where mixed imprints do arise, the potential exists for fractionation. In this regard, the ability to select hosts based on binding kinetics, selectivity, or affinity would be quite powerful.

In conventional polymer imprinting, removing the template remains a challenge. Retained template has been shown to be a serious obstacle to trace analysis applications³⁶ and to be involved in apparent chiral recognition exhibited by imprinted polymers.⁸ In the two cases described here, the template was quantitatively removed. Another significant finding is that 1 equiv of H₂T(3-pyridyl)P, **15**, was nearly fully complexed by a single equivalent of **10**, indicating that almost all of the imprints were effective. Improvements in affinity and shape selectivity are clearly needed but will come as the structure of the dendron is tuned to provide a greater degree of rigidity. In this respect, there are limitless variations possible, and one can even envision highly rigid imprints with entry and exit channels designed into the system.

(36) Venn, R. F.; Goody, R. J. In *Drug Development Assay Approaches Including Molecular Imprinting and Biomarkers*; Reid, E., Hill, H. M., Wilson, I. D., Eds.; Royal Society of Chemistry: Cambridge, U.K., 1998; pp 13–20.

The cross-linking of **7** and **25** was performed under high dilution conditions that favored intramolecular cross-linking but made it difficult to scale-up the preparations and obtain significant quantities of the imprinted hosts. It is possible to overcome this limitation given the recent finding that alkene groups within the branching units of a dendrimer can avoid intermolecular cross-linking at significantly higher concentrations.³⁷ One of the advantages of using dendrimers for imprinting is in their monodispersity, which facilitates characterization. For example, in the current work, this allowed the number of cross-links to be determined. Ultimately, more rapid dendrimer syntheses,³⁸ or even hyperbranched polymerizations³⁹ or single-step syntheses of related macromolecules, might be applied. Along with efforts in these areas, our current attention is focused on expanding the types of binding contacts used, developing new dendrons, and integrating reporter groups into the binding site.

Experimental Section

General. All of the reactions described below were run under a dry nitrogen atmosphere, and all temperatures reported as reaction or drying conditions were the temperatures of the heating medium. All solvents and reagents were of reagent quality, purchased commercially, and used without further purification, except as noted below. The following solvents were freshly distilled prior to use: diethyl ether (Et₂O) and tetrahydrofuran (THF) from sodium-benzophenone; ethyl acetate (EtOAc), methylene chloride (CH₂Cl₂), and toluene from calcium hydride; benzene from sodium; and methanol (MeOH) from calcium sulfate. Acetone and *N,N*-dimethylformamide (DMF) were stored over 4 Å molecular sieves. 3,5-Dihydroxybenzoic acid methyl ester,⁴⁰ 5-, 10, 15, 20-tetrakis(3',5'-dihydroxyphenyl)porphyrin (**6**),⁴¹ 5, 10, 15, 20-tetrakis(2',6'-dihydroxyphenyl) porphyrin (**11**),⁴² 5, 10, 15, 20-tetrakis(2'-pyridyl)porphyrin (**14**),⁴³ 5, 10, 15, 20-tetrakis(3'-pyridyl)porphyrin (**15**),⁴³ pyrimidine-5-carboxaldehyde,⁴⁴ and 5, 10, 15, 20-tetrakis(phenyl)porphyrin (**13**)⁴⁵ were synthesized according to published procedures.

Thin-layer chromatography was performed on 0.2 mm silica 60 coated plastic sheets (EM Science) with F₂₅₄ indicator. Flash chromatography was performed on Merck 40–63 μm silica gel. Solvent ratios for the purification of compounds by flash chromatography are reported as percent volume (v/v). Dimensions of the columns used for the flash chromatography are reported as (width × height).

All nuclear magnetic resonance (NMR) spectra were acquired in the Varian-Oxford Center for Excellence in NMR Spectroscopy (VOICE) laboratory at the University of Illinois, Urbana-Champaign. All ¹H and ¹³C NMR spectra were recorded on a Varian Unity 500 spectrometer (¹H, 500 MHz; ¹³C, 125.7 MHz). Heteronuclear multiple quantum coherence (HMQC) and heteronuclear multiple bond correlation (HMBC) NMR experiments were performed on a Varian Unity Inova 500NB spectrometer (¹H, 500 MHz; ¹³C, 125.7 MHz). ¹H NMR coupling constants are reported in hertz (Hz). The ¹H NMR chemical

shifts were referenced to the residual protio solvent peak at 7.26 ppm in chloroform-*d* (CDCl₃), 5.32 ppm in methylene chloride-*d*₂ (CD₂Cl₂), and 2.09 in toluene-*d*₈. The ¹³C NMR chemical shifts were referenced to the solvent peak at 77.0 ppm in CDCl₃ and 53.8 ppm in CD₂Cl₂. Unless stated otherwise, the ¹H and ¹³C NMR spectra were acquired in CDCl₃.

All mass spectra were obtained in the Mass Spectrometry Laboratory, School of Chemical Sciences, University of Illinois, Urbana-Champaign. Mass spectra were measured by the technique of field desorption (FD) and field ionization (FI) on a Finnigan-MAT 731 spectrometer, chemical ionization (CI) and electron impact (EI) on a VG 70-VSE spectrometer, and fast atom bombardment (FAB) on a VG ZAB-SE spectrometer. Mass spectra were measured by matrix-assisted laser desorption ionization time-of-flight (MALDI-TOF) on a PerSeptive Biosystems Voyager DE-STR spectrometer; 2-(4-hydroxyphenylazo)benzoic acid was used as the matrix to obtain the MALDI-TOF mass spectrum.

Infrared spectra were recorded on a Mattson Galaxy Series FTIR 5000 spectrometer and are reported in cm⁻¹. Ultraviolet/visible (UV/vis) absorbance spectra were recorded on a Hitachi U-3300 spectrophotometer using a tungsten lamp light source, and λ_{max} are reported in nanometers. Elemental analyses were performed at the Microanalysis Laboratory, School of Chemical Sciences, University of Illinois, Urbana-Champaign.

Analytical size-exclusion chromatography (SEC) was performed on a Waters Styragel HR3 column (molecular weight range 500–30 000) coupled with a Water 410 differential refractometer and PD2000 dual angle laser light scattering detectors or with an Hitachi L-4000H UV detector using an Hitachi L-6000 pump. Molecular weights (*M_w*) calculated from SEC were based on using polystyrene standards. Preparative SEC was carried out on Bio-Beads S-X1 Beads gel permeation gel 200–400 mesh (Bio-Rad Laboratories), which has exclusion limits from 400 to 14 000.

In addition to a compound name, dendrons and dendrimers are designated using the notation [G-*x*]-core, where [G-*x*] refers to the generation number (*x* = 1, 2, 3, or 4), and core refers to the functional group at the focal point of the dendron or the molecule used as the core to make the dendrimer. Because of the complexity of structure, the cross-linked and cored dendrimers are named with the word cross-linked or cored preceding the shorthand name for that compound. This shorthand notation is used throughout the text to refer to these compounds.

The titration data were analyzed by plotting [ID] versus [ID]/Δ*A*, where [ID] is the imprinted dendrimer concentration and Δ*A* is the change in absorbance upon addition of **10** or **27**. This method allows association constants to be determined by finding the line intercept that gives 1/*K_{app}* and does not require knowledge of the concentration of the free or complexed porphyrin. The titrations were all completed within 1 h and all gave linear plots. As with other Scatchard-type plots, linearity indicates the formation of 1:1 complexes.

3,5-Bis(3-buten-1-oxy)benzoic Acid Methyl Ester ([G-1]-CO₂Me). To a mixture of 75.0 g (1.04 mol) of 3-buten-1-ol, 79.4 g (472 mmol) of 3,5-dihydroxybenzoic acid methyl ester, and 310.0 g (1.18 mol) of triphenylphosphine (PPh₃) in 1.0 L of THF cooled to 0 °C with an ice/water bath was added dropwise a solution of 262.2 g (1.51 mol) of diethyl azodicarboxylate (DEAD) in 3.0 L of THF. The reaction was allowed to warm to room temperature and stirred until the reaction was complete as indicated by TLC. The reaction was stopped by adding 700 mL of water and removing the THF under reduced pressure. The resulting aqueous layer was extracted with Et₂O (3 × 2 L). The organic layers were combined and washed with an equal volume of 2.5 M aqueous potassium hydroxide (KOH) and an equal volume of water. The organic layers were dried over sodium sulfate and filtered. The filtrate was reduced to one-third of its volume and placed in the freezer (–17 °C) overnight. A white precipitate (triphenylphosphine oxide) was filtered off and washed with cold Et₂O. The resulting filtrate was concentrated under reduced pressure. Approximately 25–30 g of the

(37) Schultz, L. G.; Zhao, Y.; Zimmerman, S. C. *Angew. Chem., Int. Ed.* **2001**, *40*, 1962–1966.

(38) Cf.: Zeng, F.; Zimmerman, S. C. *J. Am. Chem. Soc.* **1996**, *118*, 5326–5327.

(39) Kim, Y. *J. Polym. Sci., Polym. Chem.* **1998**, *36*, 1685–1698. Sunder, A.; Heinemann, J.; Frey, H. *Chem.-Eur. J.* **2000**, *6*, 2499–2506. Jikei, M.; Kakimoto, M. *Prog. Polym. Sci.* **2001**, *26*, 1233–1285.

(40) Chakraborty, T. K.; Reddy, G. V. *J. Org. Chem.* **1992**, *57*, 5462–5469.

(41) Jin, R.; Aida, T.; Inoue, S. *J. Chem. Soc., Chem. Commun.* **1993**, 1260–1262.

(42) Bhyrappa, P.; Vajjayanthimala, G.; Suslick, K. S. *J. Am. Chem. Soc.* **1999**, *121*, 262–263. Mometeau, M.; Mispetter, J.; Looock, B.; Bisagni, E. *J. Chem. Soc., Perkin Trans. 1* **1983**, 189–196.

(43) Sugata, S.; Yamanouchi, S.; Matsushima, Y. *Chem. Pharm. Bull.* **1977**, *25*, 884–889.

(44) Rho, T.; Abuh, Y. *Synth. Commun.* **1994**, *24*, 253–256.

(45) Adler, A. D.; Longo, F. R.; Finarelli, J. D.; Goldmacher, J.; Assour, J.; Korsakoff, L. *J. Org. Chem.* **1967**, *32*, 476.

crude product was purified at a time by column chromatography. The crude product was loaded onto a silica gel plug (8 × 12 cm) and eluted with 1.5 L of petroleum ether (PE), 2.0 L of 5% EtOAc/95% PE, and 1.0 L of 10% EtOAc/90% PE. The product was dried under vacuum (0.1 mmHg, 45 °C) overnight to afford 109.9 g (84%) of [G-1]-CO₂-Me as a clear, colorless oil. ¹H NMR: δ 7.16 (d, 2H, *J* = 2.4), 6.64 (t, 1H, *J* = 2.4), 5.88 (ddt, 2H, *J* = 17.2, 10.3, 6.8), 5.16 (ddt, 2H, *J* = 17.2, *J* = 1.8, 1.5), 5.11 (ddt, 2H, *J* = 10.3, *J* = 1.8, 1.3), 4.01 (t, 4H, *J* = 6.6), 3.88 (s, 3H), 2.52 (dtdd, 4H, *J* = 6.8, 6.6, 1.5, 1.3). ¹³C NMR: 166.8, 159.9, 134.3, 131.9, 117.1, 107.8, 106.7, 67.4, 52.2, 33.5. IR (neat): 3070, 2980, 1724, 1642, 1597, 1169, 1057, 996, 918. MS (FAB): *m/z* 277.1 (M + H⁺). Anal. Calcd for C₁₆H₂₀O₄: C, 69.55; H, 7.30. Found: C, 69.41; H, 7.12.

3,5-Bis(3-buten-1-oxy)benzyl Alcohol ([G-1]-OH). To a suspension of 24.6 g (649 mmol) of lithium aluminum hydride (LAH) in 500 mL of THF cooled to 0 °C with an ice/water bath was added dropwise a solution of 109.8 g (397 mmol) of [G-1]-CO₂-Me in 1.5 L of THF. The suspension was allowed to warm to room temperature and stirred until no starting material remained by TLC. The reaction was stopped by quenching the excess hydride with 200 mL of water and neutralizing the pH with 200 mL of 3 M aqueous hydrochloric acid (HCl). The THF was removed under reduced pressure, and the resulting aqueous layer was extracted with Et₂O (4 × 750 mL). The combined organic layers were washed with water, dried over sodium sulfate, filtered, and concentrated under reduced pressure. The product was purified by vacuum distillation (140–150 °C, 0.2 mmHg) to afford 96.4 g (98%) of [G-1]-OH as a clear, colorless oil. ¹H NMR: δ 6.51 (d, 2H, *J* = 2.2), 6.38 (t, 1H, *J* = 2.2), 5.89 (ddt, 2H, *J* = 17.2, 10.3, 6.8), 5.17 (ddt, 2H, *J* = 17.2, 1.8, 1.5), 5.10 (ddt, 2H, *J* = 10.3, 1.8, 1.3), 4.60 (s, 2H), 3.99 (t, 4H, *J* = 6.6), 2.53 (dtdd, 4H, *J* = 6.8, 6.6, 1.5, 1.3), 1.87 (bs, 1H). ¹³C NMR: 160.3, 143.3, 134.4, 117.1, 105.3, 100.7, 67.2, 65.3, 33.6. IR (neat): 3370 (bs), 3077, 1642, 1597, 1167, 1057, 992, 917. MS (FAB): *m/z* 249.2 (M + H⁺). Anal. Calcd for C₁₅H₂₀O₃: C, 72.55; H, 8.12. Found: C, 72.27; H, 8.35.

3,5-Bis[3,5-bis(3-buten-1-oxy)benzyloxy]benzoic Acid Methyl Ester ([G-2]-CO₂Me). To a mixture of 96.0 g (387 mmol) of [G-1]-OH, 29.6 g (176 mmol) of 3,5-dihydroxybenzoic acid methyl ester, and 115.6 g (441 mmol) of PPh₃ in 500 mL of THF cooled to 0 °C with an ice/water bath was added dropwise a solution of 99.6 g (572 mmol) of DEAD in 1.5 L of THF. The reaction was allowed to warm to room temperature and stirred until the reaction was complete as indicated by TLC. The reaction was stopped by adding 500 mL of water and removing the THF under reduced pressure. The resulting aqueous layer was extracted with Et₂O (4 × 750 mL). The combined organic layers were washed with an equal volume of 2.5 M aqueous KOH and an equal volume of water. The organic layers were dried over sodium sulfate and filtered. The filtrate was reduced to one-third its volume and placed in the freezer (−17 °C) overnight. A white precipitate (triphenylphosphine oxide) was filtered off and washed with cold Et₂O. The resulting filtrate was concentrated under reduced pressure. Approximately 25–30 g of the crude product was purified at a time by column chromatography. The crude product was loaded onto a silica gel plug (8 × 12 cm) and eluted with 1.0 L of PE, 3.0 L of 5% EtOAc/95% PE, and 3.0 L of 10% EtOAc/90% PE. The product was dried under vacuum (0.15 mmHg, 68 °C) overnight to afford 94.0 g (85%) of [G-2]-CO₂-Me as a clear, colorless oil. ¹H NMR: δ 7.29 (d, 2H, *J* = 2.4), 6.79 (t, 1H, *J* = 2.4), 6.58 (d, 4H, *J* = 2.2), 6.43 (t, 2H, *J* = 2.2), 5.90 (ddt, 4H, *J* = 17.2, 10.3, 6.8), 5.18 (ddt, 4H, *J* = 17.2, 1.8, 1.5), 5.11 (ddt, 4H, *J* = 10.3, 1.8, 1.3), 4.99 (s, 4H), 4.01 (t, 8H, *J* = 6.6), 3.91 (s, 3H), 2.54 (dtdd, 8H, *J* = 6.8, 6.6, 1.5, 1.3). ¹³C NMR: 166.8, 160.3, 159.7, 138.7, 134.4, 132.0, 117.1, 108.4, 107.2, 105.9, 101.1, 70.2, 67.3, 52.3, 33.6. IR (neat): 3094, 2980, 1734, 1656, 1597, 1174, 1062, 997, 924. MS (FD): *m/z* 628.3 (M⁺). Anal. Calcd for C₃₈H₄₄O₈: C, 72.59; H, 7.05. Found: C, 72.64; H, 6.84.

3,5-Bis[3,5-bis(3-buten-1-oxy)benzyloxy]benzyl Alcohol ([G-2]-OH). To a suspension of 6.29 g (166 mmol) of LAH in 250 mL of

THF cooled to 0 °C with an ice/water bath was added dropwise a solution of 64.5 g (103 mmol) of [G-2]-CO₂-Me in 750 mL of THF. The suspension was allowed to warm to room temperature and stirred until no starting material remained by TLC. The reaction was stopped by quenching the excess hydride with 150 mL of water and neutralizing the pH with 130 mL of 1 M aqueous HCl. The THF was removed under reduced pressure, and the resulting aqueous layer was extracted with Et₂O (3 × 1.5 L). The combined organic layers were washed with water, dried over sodium sulfate, filtered, and concentrated under reduced pressure. Approximately 20 g of the crude product was purified at a time by column chromatography. The crude product was loaded onto a silica gel column (8 × 26 cm) and eluted with 20% EtOAc/80% PE. The product was dried under high vacuum (0.2 mmHg, 75 °C) overnight to afford 54.8 g (89%) of [G-2]-OH as a clear, colorless oil. ¹H NMR: δ 6.61 (d, 2H, *J* = 2.2), 6.57 (d, 4H, *J* = 2.2), 6.53 (t, 1H, *J* = 2.2), 6.41 (t, 2H, *J* = 2.2), 5.90 (ddt, 4H, *J* = 17.2, 10.3, 6.8), 5.17 (ddt, 4H, *J* = 17.2, 1.8, 1.5), 5.11 (ddt, 4H, *J* = 10.3, 1.8, 1.3), 4.96 (s, 4H), 4.63 (d, 2H, *J* = 6.2), 4.00 (t, 8H, *J* = 6.6), 2.53 (dtdd, 8H, *J* = 6.8, 6.6, 1.5, 1.3), 1.57 (t, 1H, *J* = 6.2). ¹³C NMR: 160.3, 160.1, 143.5, 139.1, 134.4, 117.1, 105.9, 105.7, 101.3, 101.0, 70.0, 67.3, 65.3, 33.6. IR (neat): 3425 (bs), 3077, 2979, 1641, 1599, 1166, 1054, 993, 918. MS (FD): *m/z* 600.3 (M⁺). Anal. Calcd for C₃₇H₄₄O₇: C, 73.98; H, 7.38. Found: C, 73.92; H, 7.18.

3,5-Bis{3,5-bis[3,5-bis(3-buten-1-oxy)benzyloxy]benzyloxy}-benzoic Acid Methyl Ester ([G-3]-CO₂Me). To a mixture of 49.3 g (82.1 mmol) of [G-2]-OH, 6.28 g (37.3 mmol) of 3,5-dihydroxybenzoic acid methyl ester, and 24.5 g (93.5 mmol) of PPh₃ in 200 mL of THF cooled to 0 °C with an ice/water bath was added dropwise a solution of 20.2 g (116 mmol) of DEAD in 300 mL of THF. The reaction was allowed to warm to room temperature and stirred until the reaction was complete as indicated by TLC. The reaction was stopped by adding 150 mL of water and removing the THF under reduced pressure. The resulting aqueous layer was extracted with Et₂O (3 × 500 mL). The combined organic layers were washed with an equal volume of 2.5 M aqueous KOH and an equal volume of water. The organic layers were dried over sodium sulfate and filtered. The filtrate was reduced to one-third its volume and placed in the freezer (−17 °C) overnight. A white precipitate (triphenylphosphine oxide) was filtered off and washed with cold Et₂O. The resulting filtrate was concentrated under reduced pressure. Approximately 40 g of the crude product was purified at a time by column chromatography. The crude product was loaded onto a silica gel column (10 × 25 cm) and eluted with 7.0 L of 20% EtOAc/80% PE and 3.0 L of 30% EtOAc/70% PE. The product was dried under vacuum (0.1 mmHg, 75 °C) overnight to afford 44.7 g (90%) of [G-3]-CO₂-Me as a clear, colorless oil. ¹H NMR: δ 7.29 (d, 2H, *J* = 2.4), 6.80 (t, 1H, *J* = 2.4), 6.68 (d, 4H, *J* = 2.20), 6.58 (d, 8H, *J* = 2.4), 6.57 (t, 2H, *J* = 2.2), 6.42 (t, 4H, *J* = 2.4), 5.90 (ddt, 8H, *J* = 17.2, 10.3, 6.6), 5.16 (ddt, 8H, *J* = 17.2, 1.8, 1.5), 5.10 (ddt, 8H, *J* = 10.3, 1.8, 1.3), 5.01 (s, 4H), 4.96 (s, 8H), 4.00 (t, 16H, *J* = 6.8), 3.91 (s, 3H), 2.53 (dtdd, 16H, *J* = 6.8, 6.6, 1.5, 1.3). ¹³C NMR: 166.8, 160.3, 160.2, 159.7, 139.0, 138.8, 134.4, 132.1, 117.1, 108.4, 107.2, 106.4, 105.9, 101.7, 101.0, 70.2, 70.1, 67.3, 52.3, 33.6. IR (neat): 3078, 2979, 1721, 1641, 1597, 1166, 1054, 994, 917. MS (MALDI-TOF): *m/z* 1355.0 (M + Na⁺). SEC (toluene) Calcd *M_w* = 1338. Anal. Calcd for C₈₂H₉₂O₁₆: C, 73.85; H, 6.95. Found: C, 74.16; H, 7.08.

3,5-Bis-{3,5-bis[3,5-bis(3-buten-1-oxy)benzyloxy]benzyloxy}-benzoic Acid ([G-3]-CO₂H) (8). A 40% (w/w) aqueous KOH solution was made by dissolving 2.48 g (38.0 mmol) of KOH in 4 mL of water. This solution was added to a solution of 4.85 g (3.64 mmol) of [G-3]-CO₂-Me dissolved in 25 mL of THF. Ethanol (20 mL) was added to make the reaction mixture homogeneous. The reaction was stirred at reflux until no starting material remained by TLC. The reaction was stopped by adding concentrated aqueous HCl to make the reaction mixture acidic (pH < 3). The solvents were removed under reduced pressure. The remaining residue was partitioned between 100 mL of water and 100 mL of CH₂Cl₂. The aqueous layer was extracted with

CH_2Cl_2 (3×100 mL). The combined organic layers were washed with water, dried over sodium sulfate, and filtered. The resulting filtrate was concentrated under reduced pressure. The product was loaded onto a silica gel column (10×12 cm) and eluted with 1% acetic acid/30% EtOAc/69% PE. The product was dried under vacuum (0.15 mmHg, 100°C) overnight to afford 4.08 g (85%) of **8** as a beige oil. ^1H NMR: δ 7.35 (d, 2H, $J = 2.4$), 6.84 (t, 1H, $J = 2.4$), 6.68 (d, 4H, $J = 2.2$), 6.57 (d, 8H, $J = 2.2$), 6.56 (t, 2H, $J = 2.2$), 6.42 (t, 4H, $J = 2.2$), 5.89 (ddt, 8H, $J = 17.2, 10.3, 6.6$), 5.16 (ddt, 8H, $J = 17.2, 1.8, 1.5$), 5.10 (ddt, 8H, $J = 10.3, 1.8, 1.3$), 5.01 (s, 4H), 4.96 (s, 8H), 4.00 (t, 16H, $J = 6.8$), 2.52 (tddd, 16H, $J = 6.8, 6.6, 1.5, 1.3$). ^{13}C NMR: 171.2, 160.3, 160.2, 159.8, 139.0, 138.7, 134.4, 131.1, 117.1, 108.9, 108.0, 106.5, 105.9, 101.8, 101.0, 70.2, 70.1, 67.3, 33.6. IR (neat): 3196, 3078, 2977, 1692, 1642, 1594, 1163, 1055, 993, 917. MS (MALDI-TOF): m/z 1342.7 ($\text{M} + \text{Na}^+$). Anal. Calcd for $\text{C}_{81}\text{H}_{90}\text{O}_{16}$: C, 73.73; H, 6.87. Found: C, 73.86; H, 6.80.

5,10,15,20-Tetrakis{3,5-bis[3,5-bis(3,5-bis(3,5-bis(3-buten-1-oxy)benzyloxy)benzyloxy]benzyloxy]phenyl}porphyrin ([G-3]₈-T(3,5-OHPh)P) (7**).** [G-3]-CO₂H (**8**) (283 mg, 215 μmol), 13.2 mg (17.8 μmol) of 5,10,15,20-tetrakis(3',5'-dihydroxyphenyl)porphyrin ($\text{H}_2\text{T}(3,5\text{-OHPh})\text{P}$) **6**, 519 mg (2.5 mmol) of DCC, 78.6 mg (643 μmol) of DMAP, and 118 mg (621 μmol) of *p*-toluenesulfonic acid were dissolved in 15 mL of THF. The reaction was stirred overnight at room temperature. The reaction mixture was vacuum filtered to remove the DCU formed. The filtrate was concentrated under reduced pressure and dissolved in 15 mL of CH_2Cl_2 . To this solution, 510 mg (2.5 mmol) of DCC, 75.8 mg (620 μmol) of DMAP, and 117 mg (615 μmol) of *p*-toluenesulfonic acid were added. This solution was stirred at room temperature and monitored by TLC and SEC. The reaction was determined to be complete after 3 days. The reaction mixture was vacuum filtered to remove the DCU, and the resulting filtrate was concentrated under reduced pressure. The remaining residue was loaded onto a silica gel column (4×15 cm) and eluted with 30% EtOAc/PE. The product was further purified by loading it onto a SEC column and eluting it with toluene. The product was dried overnight under vacuum (1.0 mmHg, 98°C) to afford 107 mg (54%) of **7** as a deep red oil. ^1H NMR (CD_2Cl_2): δ 9.22 (s, 8H), 8.15 (d, 8H, $J = 2.1$), 7.75 (t, 4H, $J = 2.1$), 7.54 (d, 16H, $J = 2.1$), 6.81 (t, 8H, $J = 2.1$), 6.64 (d, 32H, $J = 2.1$), 6.48 (m, 80H), 6.31 (t, 32H, $J = 2.1$), 5.81 (ddt, 64H, $J = 17.2, 10.2, 6.7$), 5.07 (ddt, 64H, $J = 17.2, 1.8, 1.5$), 5.01 (ddt, 64H, $J = 10.2, 1.8, 1.2$), 4.98 (s, 32H), 4.87 (s, 64H), 3.88 (t, 128H, $J = 6.7$), 2.42 (tddd, 128H, $J = 6.7, 6.7, 1.5, 1.2$), -2.86 (s, 2H). ^{13}C NMR (CD_2Cl_2): 165.1, 160.7, 160.5, 160.4, 150.3, 144.2, 139.6, 139.3, 135.0, 131.6, 126.3, 18.9, 17.0, 109.3, 108.1, 106.7, 106.2, 101.9, 101.0, 70.5, 70.3, 67.6, 33.9. MS (MALDI-TOF): m/z 1153.4 ($\text{M} + \text{H}^+$). SEC (toluene) Calcd $M_w = 8155$. UV/vis (CH_2Cl_2) $\lambda_{\text{max}} = 275.0, 420.5$ (Soret). Anal. Calcd for $\text{C}_{692}\text{H}_{734}\text{N}_4\text{O}_{128}$: C, 74.51; H, 6.63; N, 0.50. Found: C, 74.56; H, 6.41; N, 0.48.

Cross-linked [G-3]₈-T(3,5-OHPh)P (9**).** To a solution of 497 mg (44.6 μmol) of **7** in 4.4 L of benzene was added 99.6 mg (120 μmol) of the Grubbs' catalyst **2**. The reaction was stirred at room temperature for 22 h. The benzene was removed under reduced pressure. The crude product was loaded onto a silica gel plug (4×6 cm) and eluted with 400 mL of 50% PE/50% CH_2Cl_2 and 400 mL of 5% EtOAc/ CH_2Cl_2 . The EtOAc/ CH_2Cl_2 solution was concentrated under reduced pressure. The product was dried overnight under vacuum (2 mmHg, 85°C) to afford 409 mg (89%) of **9** as a dark red powder. ^1H NMR (d_8 -toluene): δ 9.17 (bs, 8H), 8.15 (bs, 8H), 7.70 (bs, 20H), 6.59 (bs, 152H), 5.78 (bs, ~4H), 5.51 (bs, ~60H), 5.04 (bs, ~8H), 4.82 (bs, 96H), 3.70 (bs, 128H), 2.33 (bs, 128H). MS (MALDI-TOF): m/z 10 257.1 ($\text{M} + \text{H}^+ - 32\text{C}_2\text{H}_4$), 10 285.2 ($\text{M} + \text{H}^+ - 31\text{C}_2\text{H}_4$), 10 312.3 ($\text{M} + \text{H}^+ - 30\text{C}_2\text{H}_4$). SEC (toluene) Calcd $M_w = 5509$. UV/vis (CH_2Cl_2) $\lambda_{\text{max}} = 276.0, 421.0$ (Soret).

Imprinted [G-3]₈-T(3,5-OHPh)P (10**).** To a solution of 102 mg (9.88 μmol) of **9** dissolved in 15 mL of THF was added 10 mL of 2.5 M aqueous KOH. The reaction was stirred vigorously at reflux until

the reaction was complete by TLC. The reaction was stopped by removing the THF under reduced pressure. The resulting aqueous layer was extracted with CHCl_3 (3×25 mL). The combined organic layers were washed with 1 M aqueous HCl, washed with water, and concentrated under reduced pressure. The product was dried under vacuum (0.2 mmHg, 70°C) to afford 41.5 mg (43%) of **10** as a beige powder. ^1H NMR: δ 7.23 (bs, 16H), 6.51 (bs, 152H), 5.86 (bs, ~4H), 5.60 (bs, ~60H), 5.12 (bs, ~8H), 4.86 (bs, 96H), 3.92 (bs, 128H), 2.45 (bs, 128H). MS (MALDI-TOF): m/z 9679.8 ($\text{M} + \text{H}^+ - 31\text{C}_2\text{H}_4 - \text{C}_{44}\text{H}_{22}\text{N}_4$). SEC (toluene) Calcd $M_w = 4656$. Anal. Calcd for $\text{C}_{588}\text{H}_{600}\text{O}_{128}$: C, 72.70; H, 6.22; N, 0.00; Ru, 0.00. Found: C, 70.83; H, 6.19; N, 0.00; Ru, 0.00.

5,10,15,20-Tetrakis(3',5'-pyrimidyl)porphyrin (12**).** Pyrimidine-5-carboxaldehyde (245 mg, 2.27 mmol) and 160 μL (2.31 mmol) of freshly distilled pyrrole were added to 12 mL of refluxing propionic acid. The solution quickly turned black and was maintained at reflux for 1 h. The reaction mixture was cooled, and the propionic acid was removed under reduced pressure to give a tarry residue. The resulting residue was partitioned between water and CHCl_3 . The aqueous layer was extracted with CHCl_3 . The organic layers were combined and concentrated under reduced pressure. The resulting residue was loaded onto a silica gel column and eluted with 50% CHCl_3 /50% acetone. The second, more intense band was collected and concentrated under reduced pressure. The product was dried under vacuum to afford 2.8 mg (1%) of **12** as a purple solid. ^1H NMR: δ 9.72 (s, 4H), 9.59 (s, 8H), 8.94 (s, 8H), -2.87 (s, 2H). MS (FAB): m/z 623.4 ($\text{M} + \text{H}^+$). UV/vis (chloroform) $\lambda_{\text{max}} = 420.0$ (Soret), 515.5, 549.5, 590.5, 646.0.

Mixed Porphyrin Condensation. Pyrrole (12.5 mL, 180 mmol) was added dropwise to a refluxing solution of benzaldehyde (14.0 mL, 138 mmol) and pyridine-4-carboxaldehyde (6.0 mL, 63.0 mmol) in propionic acid (500 mL). The solution quickly changed color from yellow to black. The solution was stirred at reflux for 1.5 h. The reaction flask was cooled in an ice/water bath. Diethylene glycol (350 mL) was added to the cooled reaction solution. The solution was refrigerated overnight. The purple precipitate that formed was isolated by vacuum filtration. The solid was washed with MeOH. The crude product mixture (1.25 g) was loaded on a silica gel column and eluted with CHCl_3 . The following compounds were isolated from the column in this order: 5,10,15,20-tetrakis(phenyl)porphyrin (**13**), 5-(4'-pyridyl)-10,15,20-tris(phenyl)porphyrin (**20**), *cis*-5,10-bis(4'-pyridyl)-15,20-bis(phenyl)porphyrin (**19**), *trans*-5,15-bis(4'-pyridyl)-10,20-bis(phenyl)porphyrin (**18**), and a mixture of 5,10,15-tris(4'-pyridyl)-20-(phenyl)porphyrin (**17**) and 5,10,15,20-tetrakis(4'-pyridyl)porphyrin (**16**). Porphyrins **16** and **17** were isolated by loading the mixture of the two from the first column onto a second silica gel column. The column was eluted with 2% MeOH/98% CHCl_3 with **17** eluting from the column first.

5,10,15-Tris(4'-pyridyl)-20-(phenyl)porphyrin (17**).** Compound **17** was isolated in 2.3% yield from the mixed porphyrin condensation reaction as a reddish-purple solid. ^1H NMR (CDCl_3): δ 9.08 (m, 6H), 8.94 (d, 2H, $J = 4.8$), 8.88 (s, 4H), 8.84 (d, 2H, $J = 4.8$), 8.23 (m, 2H), 8.18 (m, 6H), 7.81 (m, 3H), -2.86 (s, 2H). MS (high-resolution FAB): m/z 618.24 ($\text{M} + \text{H}^+$). UV/vis (CHCl_3) $\lambda_{\text{max}} = 417.5$ (Soret), 513.5, 548.0, 589.0, 645.0.

***trans*-5,15-Bis(4'-pyridyl)-10,20-bis(phenyl)porphyrin (**18**).** Compound **18** was isolated in 0.7% yield from the mixed porphyrin condensation reaction as a reddish-purple solid. ^1H NMR (CDCl_3): δ 9.04 (m, 4H), 8.91 (d, 4H, $J = 4.6$), 8.81 (d, 4H, $J = 4.6$), 8.22 (m, 4H), 8.17 (m, 4H), 7.78 (m, 6H), -2.85 (s, 2H). MS (high-resolution FAB): m/z 617.24 ($\text{M} + \text{H}^+$). UV/vis (CHCl_3) $\lambda_{\text{max}} = 418.0$ (Soret), 514.0, 548.5, 590.5, 645.0.

***cis*-5,10-Bis(4'-pyridyl)-15,20-bis(phenyl)porphyrin (**19**).** Compound **19** was isolated in 1.2% yield from the mixed porphyrin condensation reaction as a reddish-purple solid. ^1H NMR (CDCl_3): δ 9.05 (m, 4H), 8.91 (d, 2H, $J = 4.9$), 8.87 (s, 2H), 8.84 (s, 2H), 8.81 (d, 2H, $J = 4.9$), 8.22 (m, 4H), 8.17 (m, 4H), 7.77 (m, 6H), -2.85 (s,

2H). MS (high-resolution FAB); m/z 617.24 ($M + H^+$). UV/vis ($CHCl_3$) $\lambda_{max} = 418.0$ (Soret), 514.0, 549.0, 590.0, 645.0.

5-(4'-Pyridyl)-10,15,20-tris(phenyl)porphyrin (20). Compound **20** was isolated in 2.9% yield from the mixed porphyrin condensation reaction as a reddish-purple solid. 1H NMR ($CDCl_3$): δ 9.04 (m, 2H), 8.90 (d, 2H, $J = 4.9$), 8.87 (s, 4H), 8.80 (d, 2H, $J = 4.9$), 8.22 (m, 6H), 8.17 (m, 2H), 7.77 (m, 9H), -2.80 (s, 2H). MS (FAB): m/z 616.3 ($M + H^+$). UV/vis ($CHCl_3$) $\lambda_{max} = 418.0$ (Soret), 515.0, 549.0, 589.5, 645.0. Anal. Calcd for $C_{43}H_{29}N_5$: C, 83.88; H, 4.75; N, 11.37. Found: C, 83.13; H, 4.57; N, 11.13.

Imprinted Octakis(ethyl ester) [G-3]₈-T(3,5-OHPh)P (10-(CO₂Et)₈). To a solution of 409 mg (39.7 μ mol) of cross-linked [G-3]₈-T(3,5-OHPh)P dendrimer (**9**) in 10 mL of toluene were added 2.0 mL of EtOH and 88.0 mg (637 μ mol) of potassium carbonate. The suspension was stirred at reflux until the reaction was complete by TLC. The toluene and EtOH were removed under reduced pressure. The resulting residue was partitioned between 100 mL of EtOAc and 30 mL of water. The pH was brought to 7 by adding 1 M aqueous HCl. The aqueous layer was further extracted with EtOAc (3 \times 100 mL). The combined organic layers were washed with an equal volume of water, dried over sodium sulfate, and filtered. The filtrate was concentrated under reduced pressure. The crude product was loaded onto a silica gel plug (4 \times 6 cm) and eluted with 5% EtOAc/95% CH_2Cl_2 . The EtOAc/ CH_2Cl_2 solution was concentrated under reduced pressure. The product was dried overnight under vacuum (0.2 mmHg, 75 $^\circ$ C) to afford 116 mg (30%) of **10-(CO₂Et)₈** as a beige powder. 1H NMR (toluene- d_8): δ 7.47 (bs, 16H), 6.62 (bs, 152H), 5.75 (bs, \sim 4H), 5.48 (bs, \sim 60H), 5.03 (bs, \sim 8H), 4.78 (bs, 96H), 4.17 (bs, 16H), 3.67 (bs, 128H), 2.31 (bs, 128H), 1.12 (bs, 24H). MS (MALDI-TOF): m/z 9906.8 ($M + Na^+ - 32C_2H_4 - C_{28}H_{18}N_4$), 9934.6 ($M + Na^+ - 31C_2H_4 - C_{28}H_{18}N_4$), 9963.2 ($M + Na^+ - 30C_2H_4 - C_{28}H_{18}N_4$), 9990.1 ($M + Na^+ - 29C_2H_4 - C_{28}H_{18}N_4$). SEC (toluene) Calcd $M_w = 4656$.

3,5-Bis{3,5-bis[3,5-bis(3-buten-1-oxy)benzyloxy]benzyloxy}-benzoyl Chloride ([G-3]-COCl) (23). [G-3]-CO₂H (**8**) (351 mg, 266 μ mol) was dissolved in 10 mL of THF. To this solution were added 10 μ L (129 μ mol) of DMF and 50 μ L (537 μ mol) of oxalyl chloride. The reaction mixture was stirred at room temperature for 30 min. The reaction mixture was heated to 50 $^\circ$ C and stirred at this elevated temperature for 15 min. An aliquot of the reaction mixture was placed in dry MeOH (to form the methyl ester), and TLC of this solution showed that the starting material has disappeared. The reaction was stopped by removing the solvent (and the HCl formed) under reduced pressure. The crude material was loaded onto a silica gel column (2.5 \times 20 cm) and eluted with 30% EtOAc/70% PE. This afforded 227 mg (64%) of **23** as clear, colorless oil. It was discovered that the product partially hydrolyzed on silica gel as the remainder of the material was isolated as the starting material. Subsequent formation of acyl chloride dendrons followed this procedure with the modification that once the reaction was determined to be complete by TLC, the solvent was removed under reduced pressure, and the resulting material was dried gently with heat under vacuum until it was considered dry and the excess HCl was removed. 1H NMR: δ 7.34 (d, 2H, $J = 2.2$), 6.88 (t, 1H, $J = 2.2$), 6.67 (d, 4H, $J = 2.2$), 6.59 (t, 2H, $J = 2.2$), 6.58 (d, 8H, $J = 2.2$), 6.43 (t, 4H, $J = 2.2$), 5.90 (ddt, 8H, $J = 17.2$, 10.3, 6.6), 5.17 (ddt, 8H, $J = 17.2$, 1.8, 1.5), 5.11 (ddt, 8H, $J = 10.3$, 1.8, 1.3), 5.01 (s, 4H), 4.97 (s, 8H), 4.00 (t, 16H, $J = 6.8$), 2.54 (tddd, 16H, $J = 6.8$, 6.6, 1.5, 1.3). IR (neat): 3078, 2980, 1760, 1642, 1593, 1163, 1055, 992, 919.

5,10,15,20-Tetrakis{4-[3,5-bis(3,5-bis(3,5-bis(3-buten-1-oxy)benzyloxy)benzyloxy)benzyloxy]phenyl}porphyrin ([G-3]-T(4-OHPh)P) (21). [G-3]-COCl (**23**) (684 mg, 511 μ mol) was dissolved in 15 mL of THF and added to a flask containing 57.8 mg (85.2 μ mol) of H₂T(4-OHPh)P (**22**) and 251 mg (2.05 mmol) of DMAP in 10 mL of THF. The reaction was stirred at reflux for 17 h. TLC showed the reaction was progressing very slowly. Additional DMAP (252 mg, 2.07 mmol) was added to the reaction mixture. The reaction mixture was

stirred at reflux until complete as indicated by TLC. The reaction was stopped by removing the THF under reduced pressure. The resulting residue was loaded onto a silica gel column (3 \times 17 cm) and eluted with 1% acetic acid/30% EtOAc/69% PE. The product was further purified by loading it onto a series of preparatory SEC columns and eluting it with toluene. The product was dried overnight under vacuum (0.2 mmHg, 75 $^\circ$ C) to afford 450 mg (90%) of **21** as a dark red oil. 1H NMR (CD_2Cl_2): δ 8.97 (s, 8H), 8.31 (m, 8H), 7.69 (m, 8H), 7.62 (d, 8H, $J = 2.3$), 6.95 (t, 4H, $J = 2.3$), 6.76 (d, 16H, $J = 2.3$), 6.59 (t, 8H, $J = 2.3$), 6.58 (d, 32H, $J = 2.3$), 6.39 (t, 16H, $J = 2.3$), 5.88 (ddt, 32H, $J = 17.1$, 10.4, 6.7), 5.13 (m, 48H), 5.07 (ddt, 32H, $J = 10.4$, 1.8, 1.2), 5.01 (s, 32H), 3.99 (t, 64H, $J = 6.7$), 2.50 (tddd, 64H, $J = 6.7$, 6.7, 1.8, 1.2), -2.80 (s, 2H). MS (MALDI-TOF): m/z 5884.0 ($M + H^+$).

Cross-linking and Hydrolysis of [G-3]-T(4-OHPh)P. To a solution of 50.0 mg (8.49 μ mol) of **21** in 1.15 L of benzene was added 8.87 mg (10.8 μ mol) of the Grubbs' catalyst. The reaction was stirred at room temperature for 18 h. The benzene was removed under reduced pressure. The crude product was loaded onto a silica gel plug (4 \times 6 cm) and eluted with 250 mL of 50% PE/50% CH_2Cl_2 and 300 mL of 5% EtOAc/95% CH_2Cl_2 . The EtOAc/ CH_2Cl_2 solution was concentrated under reduced pressure. The product was dried overnight under vacuum (0.2 mmHg, 80 $^\circ$ C) to afford 36.5 mg (79%) of a dark red powder. 1H NMR (CD_2Cl_2): δ 8.98 (bs, 8H), 8.30 (bs, 8H), 7.60 (bs, 16H), 6.96 (bs, 4H), 6.45 (bs, 72H), 5.87 (bs, \sim 2H), 5.65 (bs, \sim 30H), 5.04 (bs, \sim 52H), 3.99 (bs, 64H), 2.45 (bs, 64H), -2.74 (bs, 2H). MS (MALDI-TOF): m/z 5440.9 ($M + H^+ - 16C_2H_4$), 5468.9 ($M + H^+ - 15C_2H_4$), 5498.2 ($M + H^+ - 14C_2H_4$).

A 25% (w/w) aqueous KOH solution was made by dissolving 48.3 mg (740 μ mol) of KOH in 145 μ L of water. This solution was added to a solution of 36.5 mg (6.68 μ mol) of cross-linked [G-3]-T(4-OHPh)P dissolved in 2.0 mL of THF. Ethanol (145 μ L) was added to make the reaction mixture homogeneous. The reaction was stirred at 85 $^\circ$ C until no starting material remained by TLC. The reaction mixture was allowed to settle such that two layers formed. The organic layer was decanted off, and the remaining aqueous layer was washed two more times with THF. The THF extracts were combined and concentrated under reduced pressure. The remaining residue was partitioned between 5.0 mL of 2.5 M aqueous KOH and 5.0 mL of CH_2Cl_2 . The aqueous layer was extracted with CH_2Cl_2 (3 \times 5 mL). The organic layers were combined and washed with 2.5 M aqueous KOH, 1 M aqueous HCl (twice), and water. The organic layer was dried over sodium sulfate and filtered. The filtrate was concentrated under reduced pressure and dried under vacuum (0.1 mmHg, 75 $^\circ$ C) overnight to afford 24.0 mg of a beige powder. 1H NMR (CD_2Cl_2): δ 7.23 (bs, 8H), 6.74 (bs, 4H), 6.45 (bs, 72H), 5.85 (bs, \sim 2H), 5.64 (bs, \sim 30H), 5.10 (bs, \sim 4H), 4.99 (bs, 48H), 3.99 (bs, 64H), 2.45 (bs, 64H). MS (MALDI-TOF): m/z 4855.9 ($M + Na^+ - 16C_2H_4 - C_{44}H_{22}N_4$), 4883.3 ($M + Na^+ - 15C_2H_4 - C_{44}H_{22}N_4$), 4911.3 ($M + Na^+ - 14C_2H_4 - C_{44}H_{22}N_4$), and peaks corresponding to the loss of one and two dendrons.

3,5-Bis{3,5-bis[3,5-bis(3-buten-1-oxy)benzyloxy]benzyloxy}-benzyl Alcohol ([G-3]-OH). To a suspension of 886 mg (23.4 mmol) of LAH in 50 mL of THF cooled to 0 $^\circ$ C with an ice/water bath was added dropwise a solution of 18.4 g (13.8 mmol) of [G-3]-CO₂Me in 150 mL of THF. The suspension was allowed to warm to room temperature and stirred until no starting material remained by TLC. The reaction was stopped by quenching the excess hydride with 100 mL of water and neutralizing the pH with 20 mL of 1 M aqueous HCl. The THF was removed under reduced pressure, and the resulting aqueous layer was extracted with Et₂O (3 \times 400 mL). The combined organic layers were washed with water, dried over sodium sulfate, filtered, and concentrated under reduced pressure. Half of the crude product was purified at a time by column chromatography. The crude product was loaded onto a silica gel column (10 \times 20 cm) and eluted with 30% EtOAc/70% PE. The product was dried under vacuum (0.02 mmHg, 75 $^\circ$ C) overnight to afford 16.3 g (90%) of [G-3]-OH as a

clear, colorless oil. $^1\text{H NMR}$: δ 6.66 (d, 4H, $J = 2.20$), 6.60 (d, 2H, $J = 2.2$), 6.56 (d, 8H, $J = 2.2$), 6.54 (t, 2H, $J = 2.2$), 6.52 (t, 1H, $J = 2.2$), 6.41 (t, 4H, $J = 2.2$), 5.89 (ddt, 8H, $J = 17.2, 10.3, 6.6$), 5.16 (ddt, 8H, $J = 17.2, 1.8, 1.5$), 5.10 (ddt, 8H, $J = 10.3, 1.8, 1.3$), 4.97 (s, 4H), 4.95 (s, 8H), 4.62 (d, 2H, $J = 6.0$), 3.93 (t, 16H, $J = 6.8$), 2.52 (tddd, 16H, $J = 6.8, 6.6, 1.5, 1.3$), 1.72 (t, 1H, $J = 6.0$). $^{13}\text{C NMR}$: 160.3, 160.1, 160.0, 143.5, 139.3, 139.1, 134.4, 117.1, 106.3, 105.9, 105.7, 101.6, 101.3, 101.0, 70.1, 70.0, 67.3, 65.3, 33.6. IR (neat): 3531 (bs), 3077, 2979, 1641, 1591, 1140, 1058, 994, 916. MS (MALDI-TOF): m/z 1328.3 ($\text{M} + \text{Na}^+$). SEC (toluene) Calcd $M_w = 1324$. Anal. Calcd for $\text{C}_{81}\text{H}_{92}\text{O}_{15}$: C, 74.52; H, 7.10. Found: C, 74.52; H, 7.05.

3,5-Bis[3,5-bis(3,5-bis(3,5-bis(3-buten-1-oxy)benzyloxy)benzyloxy]benzyloxy} Benzoic Acid Methyl Ester ([G-4]-CO₂Me). To a mixture of 1.13 g (862 μmol) of [G-3]-OH, 61.6 mg (366 μmol) of methyl-3,5-dihydroxybenzoate, and 241 mg (920 μmol) of PPh_3 in 10 mL of THF cooled to 0 °C with an ice/water bath was added dropwise a solution of 197 mg (1.13 mmol) of DEAD in 10 mL of THF. The reaction was allowed to warm to room temperature and stirred until the reaction was complete as indicated by TLC. The reaction was stopped by adding 20 mL of water and removing the THF under reduced pressure. The resulting aqueous layer was extracted with Et_2O (3×75 mL). The combined organic layers were washed water, dried over sodium sulfate, filtered, and concentrated under reduced pressure. The resulting residue was loaded onto a silica gel column (4×20 cm) and eluted with 30% $\text{EtOAc}/70\%$ PE. The product was dried under vacuum (0.05 mmHg, 80 °C) overnight to afford 889 mg (89%) of [G-4]-CO₂-Me as a clear, colorless oil. $^1\text{H NMR}$: δ 7.30 (d, 2H, $J_{2,4} = 2.0$), 6.81 (t, 1H, $J = 2.0$), 6.68 (m, 12H), 6.57 (d, 16H, $J = 2.0$), 6.56 (m, 6H), 6.42 (t, 8H, $J = 2.0$), 5.89 (ddt, 16H, $J = 17.2, 10.3, 6.6$), 5.16 (ddt, 16H, $J = 17.2, 1.8, 1.5$), 5.10 (ddt, 16H, $J = 10.3, 1.8, 1.3$), 5.01 (s, 4H), 4.97 (s, 8H), 4.95 (s, 16H), 3.99 (t, 32H, $J = 6.8$), 3.90 (s, 3H), 2.52 (tddd, 32H, $J = 6.8, 6.6, 1.5, 1.3$). $^{13}\text{C NMR}$: 166.7, 160.3, 160.1, 159.8, 139.2, 139.1, 138.9, 134.4, 132.1, 117.1, 108.5, 107.1, 106.4, 106.0, 101.7, 101.6, 101.0, 70.2, 70.1, 67.3, 52.3, 33.6. IR (neat): 3077, 2976, 1723, 1642, 1595, 1164, 1052, 992, 916. MS (MALDI-TOF): m/z 2766.7 ($\text{M} + \text{Na}^+$). SEC (toluene) Calcd $M_w = 2699$. Anal. Calcd for $\text{C}_{170}\text{H}_{188}\text{O}_{32}$: C, 74.43; H, 6.91. Found: C, 74.46; H, 6.82.

3,5-Bis[3,5-bis(3,5-bis(3,5-bis(3-buten-1-oxy)benzyloxy)benzyloxy]benzyloxy} Benzoic Acid ([G-4]-CO₂H) (24). A 40% (w/w) aqueous KOH solution was made by dissolving 1.20 g (18.4 mmol) of KOH in 1.8 mL of water. This solution was added to a solution of 4.81 g (1.75 mmol) of [G-4]-CO₂Me dissolved in 25 mL of THF. Ethanol (13 mL) was added to make the reaction mixture homogeneous. The reaction was stirred at reflux until no starting material remained by TLC. The reaction flask was removed from the heat and cooled to 0 °C in an ice/water bath. Water (5 mL) was added to the reaction mixture. The reaction was stopped by adding 1 M aqueous HCl until the reaction mixture was acidic ($\text{pH} < 3$). The solvents were removed under reduced pressure. The remaining residue was partitioned between 60 mL of water and 100 mL of CH_2Cl_2 . The aqueous layer was extracted with CH_2Cl_2 (3×100 mL). The combined organic layers were washed with water, dried over sodium sulfate, and filtered. The resulting filtrate was concentrated under reduced pressure. The remaining residue was loaded onto a silica gel column (8×30 cm) and eluted with 3.0 L of 5% $\text{EtOAc}/95\%$ CH_2Cl_2 and 2.0 L of 10% $\text{EtOAc}/90\%$ CH_2Cl_2 . The product was dried under vacuum (0.05 mmHg, 70 °C) overnight to afford 3.99 g (83%) of **24** as a beige oil. $^1\text{H NMR}$: δ 7.38 (d, 2H, $J = 2.4$), 6.87 (t, 1H, $J = 2.4$), 6.71 (d, 4H, $J = 2.1$), 6.70 (d, 8H, $J = 2.1$), 6.60 (t, 2H, $J = 2.1$), 6.59 (d, 16H, $J = 2.1$), 6.57 (t, 4H, $J = 2.1$), 6.43 (t, 8H, $J = 2.1$), 5.90 (ddt, 16H, $J = 17.2, 10.3, 6.7$), 5.18 (ddt, 16H, $J = 17.2, 1.7, 1.5$), 5.12 (ddt, 16H, $J = 10.3, 1.7, 1.3$), 5.03 (s, 4H), 4.99 (s, 8H), 4.96 (s, 16H), 4.00 (t, 32H, $J = 6.7$), 2.54 (tddd, 32H, $J = 6.7, 6.7, 1.5, 1.3$). $^{13}\text{C NMR}$: 171.4, 160.5, 160.4, 160.1, 139.4, 139.3, 139.1, 134.7, 131.4, 117.3, 109.2, 108.2, 106.8, 106.7, 106.2, 102.0, 101.9, 101.2, 70.5, 70.3, 67.5, 33.8. MS (MALDI-TOF): m/z 2753.6

($\text{M} + \text{Na}^+$). Anal. Calcd for $\text{C}_{169}\text{H}_{186}\text{O}_{32}$: C, 74.37; H, 6.87. Found: C, 74.45; H, 6.86.

5,10,15,20-Tetrakis[4-[3,5-bis(3,5-bis(3,5-bis(3-buten-1-oxy)benzyloxy)benzyloxy)benzyloxy]phenyl]porphyrin ([G-4]-T(4-OHPh)P) (25). [G-4]-CO₂H (**24**) (296 mg, 109 μmol), 11.8 mg (17.4 μmol) of $\text{H}_2\text{T}(4\text{-OHPh)P}$ (**22**), 13.4 mg (110 μmol) of DMAP, and 20.3 mg (107 μmol) of *p*-toluenesulfonic acid were dissolved in 10 mL of THF. In a separate flask, 86.5 mg (419 μmol) of DCC was dissolved in 5 mL of THF. This solution was added to the reaction mixture. The reaction was stirred overnight at room temperature. The reaction mixture was vacuum filtered to remove the DCU formed. The filtrate was concentrated under reduced pressure and redissolved in 10 mL of CH_2Cl_2 . To this solution were added 286 mg (105 μmol) of **24**, 13.2 mg (108 μmol) of DMAP, and 20.2 mg (106 μmol) of *p*-toluenesulfonic acid. In a separate flask, 85.5 mg (414 μmol) of DCC was dissolved in 5 mL of CH_2Cl_2 . This solution was added to the reaction mixture. The reaction mixture was stirred at room temperature until complete as indicated by both TLC and SEC. The reaction was stopped by vacuum filtering the mixture and condensing the filtrate under reduced pressure. The resulting residue was loaded onto a silica gel column (4×17 cm) and eluted with 5% $\text{EtOAc}/95\%$ CH_2Cl_2 . The crude product was further purified by loading it onto a large preparatory (7×120 cm) SEC column and eluting it with toluene. The product was dried under vacuum (0.2 mmHg, 75 °C) overnight to afford 92.1 mg (46%) of **25** as a deep red oil. $^1\text{H NMR}$ (CD_2Cl_2): δ 9.01 (s, 8H), 8.34 (m, 8H), 7.73 (m, 8H), 7.68 (d, 8H, $J = 2.1$), 7.02 (t, 4H, $J = 2.1$), 6.80 (d, 16H, $J = 2.1$), 6.73 (d, 32H, $J = 2.3$), 6.64 (t, 8H, $J = 2.1$), 6.58 (d, 64H, $J = 2.3$), 6.57 (t, 16H, $J = 2.3$), 6.41 (t, 32H, $J = 2.3$), 5.90 (ddt, 64H, $J = 17.2, 10.4, 6.7$), 5.16 (ddt, 64H, $J = 17.2, 1.8, 1.5$), 5.09 (ddt, 64H, $J = 10.4, 1.8, 1.2$), 5.05 (s, 32H), 4.99 (s, 16H), 4.98 (s, 64H), 3.98 (t, 128H, $J = 6.7$), 2.51 (tddd, 128H, $J = 6.7, 6.7, 1.5, 1.2$), -2.78 (s, 2H). MS (MALDI-TOF): m/z 11 546.3 ($\text{M} + \text{Na}^+$). SEC (toluene) Calcd $M_w = 10 793$.

Cross-linked [G-4]-T(4-OHPh)P (26). To a solution of 90.0 mg (7.81 μmol) of **81** in 2.0 L of benzene was added 20.5 mg (24.9 μmol) of the Grubbs' catalyst. The reaction was stirred at room temperature for 20 h. The benzene was removed under reduced pressure. The crude product was loaded onto a silica gel plug (4×5 cm) and eluted with 250 mL of 50% $\text{PE}/50\%$ CH_2Cl_2 and 250 mL of 5% $\text{EtOAc}/95\%$ CH_2Cl_2 . The $\text{EtOAc}/\text{CH}_2\text{Cl}_2$ solution was concentrated under reduced pressure. The product was dried under vacuum (0.05 mmHg, 65 °C) overnight to afford 73.2 mg (88%) of **26** as a dark red powder. MS (MALDI-TOF): m/z 10 624.4 ($\text{M} + \text{H}^+ - 32\text{C}_2\text{H}_4$), 10 652.7 ($\text{M} + \text{H}^+ - 31\text{C}_2\text{H}_4$).

Imprinted [G-4]-T(4-OHPh)P (27). To a solution of 73.2 mg (6.87 μmol) of cross-linked [G-4]-T(4-OHPh)P (**26**) dissolved in 100 mL of THF was added 25 mL of 2.5 M aqueous KOH. The reaction was stirred vigorously at reflux until the reaction was complete by TLC. The reaction was stopped by removing the THF under reduced pressure. The resulting aqueous layer was extracted with CH_2Cl_2 (3×25 mL). The organic layers were combined and washed with an equal volume of 2.5 M aqueous KOH and water. The organic layer was stirred vigorously with an equal volume of 1 M aqueous HCl for 3 h at room temperature. The organic layer was concentrated under reduced pressure. The product was dried under vacuum (0.2 mmHg, 75 °C) overnight to afford 33.2 mg (48%) of **27** as a beige powder. MS (MALDI-TOF): m/z 10 040.9 ($\text{M} + \text{Na}^+ - 32\text{C}_2\text{H}_4 - \text{C}_{44}\text{H}_{22}\text{N}_4$), 10 069.1 ($\text{M} + \text{Na}^+ - 31\text{C}_2\text{H}_4 - \text{C}_{44}\text{H}_{22}\text{N}_4$).

Acknowledgment. This work was funded by the NIH (GM61067 and HL 25934) and U.S. Army Research Office (DAAG55-97-0126). I.Z. is grateful to the Arnold and Mabel Beckman Foundation for a Beckman Fellowship.

JA0357240

De novo designed cyclic-peptide heme complexes

Michael M. Rosenblatt*, Jiangyun Wang*, and Kenneth S. Suslick†

Department of Chemistry, University of Illinois at Urbana-Champaign, 600 South Mathews Avenue, Urbana, IL 61801

Edited by Harry B. Gray, California Institute of Technology, Pasadena, CA, and approved September 2, 2003 (received for review March 4, 2002)

The structural characterization of *de novo* designed metalloproteins together with determination of chemical reactivity can provide a detailed understanding of the relationship between protein structure and functional properties. Toward this goal, we have prepared a series of cyclic peptides that bind to water-soluble metalloporphyrins (Fe^{III} and Co^{III}). Neutral and positively charged histidine-containing peptides bind with a high affinity, whereas anionic peptides bind only weakly to the negatively charged metalloporphyrin. Additionally, it was found that the peptide becomes helical only in the presence of the metalloporphyrin. CD experiments confirm that the metalloporphyrin binds specific cyclic peptides with high affinity and with isodichroic behavior. Thermal unfolding experiments show that the complex has “native-like” properties. Finally, NMR spectroscopy produced well dispersed spectra and experimental restraints that provide a high-resolution solution structure of the complexed peptide.

One approach to understanding the folding and function of proteins is to attempt their design from first principles (1–3). Such design, however, requires not only incorporation of nonpolar interactions, but also inclusion of specific hydrogen bonds, disulfide bridges, ion pairs, and metal chelation. Without these interactions, proteins form compact folding intermediates referred to as molten globules (4). Molten-globule structures are compact and possess a high degree of secondary structure, but they are also highly dynamic, with both internal and external side chains rapidly interconverting among a large family of rotamers. Analysis of protein structures, on the other hand, reveals that the interior hydrophobic core is well packed and rigid. Therefore, two challenges occur in the design of “native-like” proteins. By using positive design (3, 5–7), one can take into account issues such as hydrophobicity and the helix- or sheet-forming propensity of amino acids. By using negative design [a term developed to describe the selective introduction of unique stabilizing interactions (2, 3)], one can introduce features that stabilize one specific fold, while, at the same time, they destabilize alternative topologies. By using this dual strategy, one can increase the free-energy gap between the native and molten-globule states.

With the challenge of design making rapid progress, several groups have begun to look at the incorporation of functional cofactors in hopes of producing *de novo* catalytic proteins (8–14). Many enzymes require mono- and dinuclear metal ions (15), metal clusters (ferredoxin and nitrogenase) (16), heme (cytochromes and globins) (17), and organic cofactors (flavin- and quinone-based enzymes) (18). These cofactors are important, especially when processes such as oxidation/reduction or substrate binding and activation are required (15).

Studies of natural enzymes have led to considerable understanding of their structure and function. Reduction of these complicated systems to minimal models, however, will allow us to test our understanding of their functional properties and to explore environmental and therapeutic applications. The creation of new biocatalysts is a sizable challenge. The problem has been approached by a variety of methods, including *de novo* (“rational”) design (2, 3, 12, 14, 19), directed evolution of new catalytic processes (20–22), production of catalytic antibodies (23), and the use of phage display to identify proteins that bind to transition-state analogs (24–27). Rational design, which we

use here, allows us to start with a simplified initial model that can be characterized at each stage in detail and refined accordingly.

Another step toward the creation *de novo* of catalytic proteins is the acquisition of high-resolution structures of the synthetic proteins. Although several such structures exist (28–31), very few have a cofactor bound to the polypeptide (1). With the confirmation of these structures in hand, it should then be possible to design features that can bind and activate small substrate molecules, such as dioxygen and hydrocarbons.

We have described the design and characterization of 15-mer, tweezers, and cyclic heme-binding peptides (32–34). In this work, we present the solution structure of a metalloporphyrin–peptide complex, designed from first principles. This complex is a unique example of a high-resolution solution structure of a metalloporphyrin cofactor bound to a designed peptide. What is perhaps most interesting about this system is that the peptide is unfolded in the absence of the porphyrin. In the presence of the porphyrin, however, the peptide is folded and rigid, with only a single, well defined conformation in solution.

Materials and Methods

UV Spectroscopy. UV-binding studies were done on a Hitachi U-3300 UV spectrometer (Hitachi, Tokyo) in a thermostated cell holder. For studies comparing charge, all measurements were made in 50 mM KH₂PO₄ (pH 6.8–7.5). Binding constants were determined as reported earlier (32).

CD Spectroscopy. All CD spectra were measured on a Jasco J-700 spectropolarimeter (Jasco, Easton, MD) at 4°C. Unless otherwise specified, all measurements were made on samples whose concentration was 2–10 μM (pH 7.0, 2 mM potassium phosphate/5 mM potassium chloride). Analyses of thermal unfolding data were done with established methods (35). The chemical unfolding data were best-fit by using the nonlinear least-squares algorithms in SIGMA-PLOT to a two-state denaturation function (36).

NMR Spectroscopy. All NMR spectra were acquired at 4°C by using samples that were 3 mM in the peptide complexes of [Co^{III}(coproporphyrinate I)]³⁻ (pH 7.2, 50 mM potassium phosphate/10 mM potassium chloride). All spectra were acquired in 90% H₂O/10% D₂O to suppress the exchange of backbone amide protons with deuterons. Suppression of the water signal was accomplished by selective excitation of the water signal during the recycling delay. NOESY spectra were acquired by using standard methods (37–39). Spectra were acquired by using mixing times ranging from 10 to 250 ms. For total correlation spectroscopy experiments (40, 41), the spin-lock power was set to 49 and mixing times to 70 ms. All other parameters were identical with those in NOESY experiments. Double-quantum-filtered COSY experiments (42) were acquired at very high

This paper was submitted directly (Track II) to the PNAS office.

Abbreviation: NOE, nuclear Overhauser effect.

Data deposition: The atomic coordinates have been deposited in the Protein Data Bank, www.rcsb.org (PDB ID code 1PBZ).

*M.M.R. and J.W. contributed equally to this work.

†To whom correspondence should be addressed. E-mail: ksuslick@uiuc.edu.

© 2003 by The National Academy of Sciences of the USA

digital resolution, typically with 512–1,024 increments in the F1 dimension.

Structure Calculations. Interproton distance restraints were derived from NOESY experiments with 10-, 20-, 50-, 100-, and 250-ms mixing times acquired on a Varian Innova spectrometer operating at 600 MHz. It was found that, with a mixing time of 100 ms, the nuclear Overhauser effect (NOE) intensities were still in the linear region of the build-up curve, so a two-spin approximation was applied for the generation of distance constraints (31). Peaks involving nonexchanging protons were scaled to the largest H β –H β NOE cross-peak intensity, assuming a 1.8-Å separation. Peaks with exchangeable amide protons were scaled to the largest HN⁽ⁱ⁾–HN⁽ⁱ⁺¹⁾ cross-peak intensity, assuming a distance of 2.8 Å, as in an ideal α -helix. For those cross-peaks involving methyl groups, a pseudoatom approximation was used and the NOE distance was increased 0.5 Å. Finally, the upper-bound limit for each distance constraint was increased 10%. Backbone ϕ -angle restraints, derived from ³J_{NH-CH} coupling constants, were determined by using the method of Kim and Prestegard (43). Restraints were restricted to -60 ± 40 for coupling constants < 7 Hz and to -120 ± 50 for coupling constants > 8 Hz.

Three-dimensional structure calculations were done by using the program INSIGHT/DISCOVER (Accelrys, San Diego) with a modified consistent valence force field. An NOE-restrained, simulated annealing protocol developed by Nilges and coworkers (44–46) was used for structure calculations by starting with a randomized set of structures, heating the molecule to 2,000 K, and then slowly cooling the molecule over the course of 45 ps to 50 K. Force constants for bonds were set to 25 kcal/(mol·rad²), whereas the constants for angles were set to 100 kcal/(mol·rad²). Of the 50 structures, 75% converged to acceptable structures. Of the acceptable structures, 14 were deemed exceptional. All of these structures displayed no violations > 0.5 Å or $> 5^\circ$.

Results and Discussion

Design of the Cyclic (Cy) Peptides. The design of the primary sequence for Cy-AA-KK (Fig. 1; the sequences of Cy-AA-KK, Cy-AA-EE, and Cy-AA-EK are given in the legend) has been described (34). Our design approach is illustrated in Fig. 1*b*. Cy-AA-KK contains all lysines on its polar face (and hence is positively charged), whereas Cy-AA-EE has only glutamates on its polar face (and hence is negatively charged). The sequence of Cy-AA-EK is similar to Cy-AA-KK, except that the lysines in positions 4 and 14 were changed to glutamates with the intention of introducing salt-bridge contacts. Cysteines are at the termini of each of the monomeric peptides to permit cyclization. The oxidative cyclization of the peptide was carried out by using the orthogonal protecting groups described (34).

Starting from our earlier work with monomeric 15-mer peptides (32–34), we have iterated systematically toward a peptide that would display “native-like” properties. We have described the effect of disulfide addition on the binding affinity and secondary structure (34). We have now extended this work to the effect of charge and salt bridges on the 3D structure of the complex.

Solution Binding Studies. We have examined the effect of peptide charge on the binding affinity to M^{III}(coproporphyrinate) I³⁻. Coproporphyrin I has four carboxylates on the periphery of the macrocycle, so its M^{III} complex has a net charge of -3 at pH 7. A spectrophotometric titration, shown in Fig. 2*a*, displays the binding of the free peptide to the metalloporphyrin. The data indicate that the high-spin metalloporphyrin is converted into a low-spin complex, typical of bishistidine-ligated hemes (17). Isosbestic behavior confirms that the only species in solution are the free and complexed (six-coordinate) metalloporphyrin.

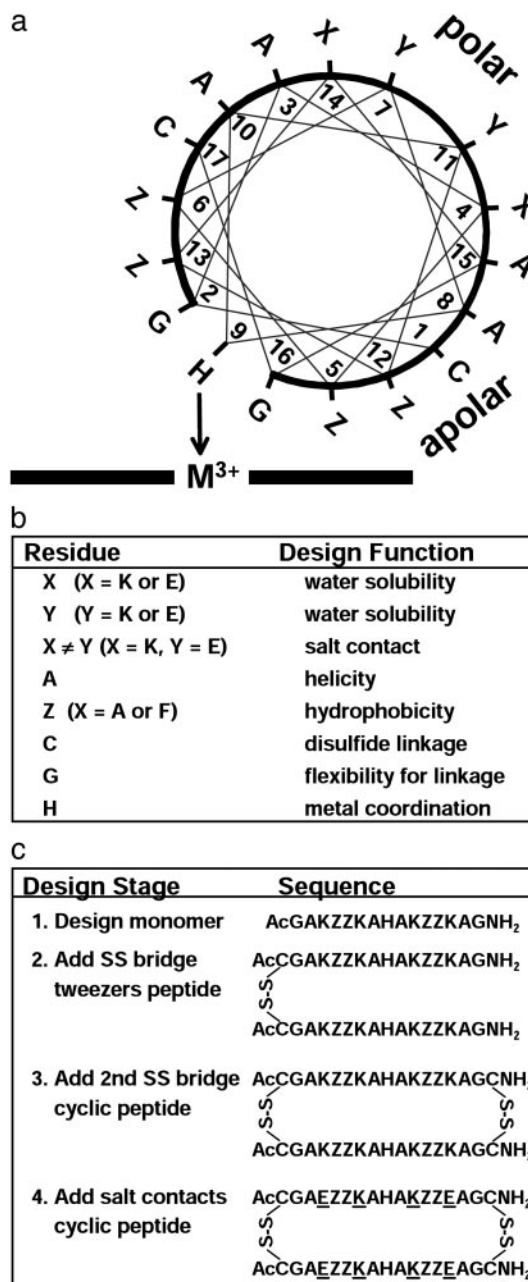


Fig. 1. (a) Helix-wheel representation depicting the designed peptide complexed with the metalloporphyrin on one face. The 60° tilt of the bound peptides (from NMR solution structure) shows that residues 5 and 12 are in contact with the porphyrin. The peptide abbreviations are Cy-ZZ-XY, where residues 4 and 14 are X, residues 7 and 11 are Y, and residues 5, 6, 12, and 13 are Z, as shown. (b) Design strategy and intended function of specific residues. (c) Sequence of design (32–34) resulting in the current cyclic peptides. Cy-AA-KK [$-\text{C}(\text{Ac})\text{GAKAAKAHAKAAKAGC}(\text{NH}_2)-$]₂ is design stage 3 with lysines (K) on the polar face. Cy-AA-EE [$-\text{C}(\text{Ac})\text{GAEAAEAHAEAAEAGC}(\text{NH}_2)-$]₂ also is at design stage 3 but with glutamates (E) on the polar face. Cy-AA-EK [$-\text{C}(\text{Ac})\text{GAEAAKAHAKAAEAGC}(\text{NH}_2)-$]₂ is at design stage 4 with X = glutamate and Y = lysine; it thus provides salt bridges between lysines and glutamates on the polar face. Cy-FF-KK [$-\text{C}(\text{Ac})\text{GAKFFKAHAKFFKAGC}(\text{NH}_2)-$]₂ is the same as Cy-AA-KK, except Z = phenylalanine (F) in place of alanine (A). SS, disulfide link.

Three peptides were synthesized: Cy-AA-KK (positively charged), Cy-AA-EE (negatively charged), and Cy-AA-EK (overall neutral). Fig. 2*b* shows a comparison of the binding of Fe–porphyrin complexes at pH 6.7 and 7.6.

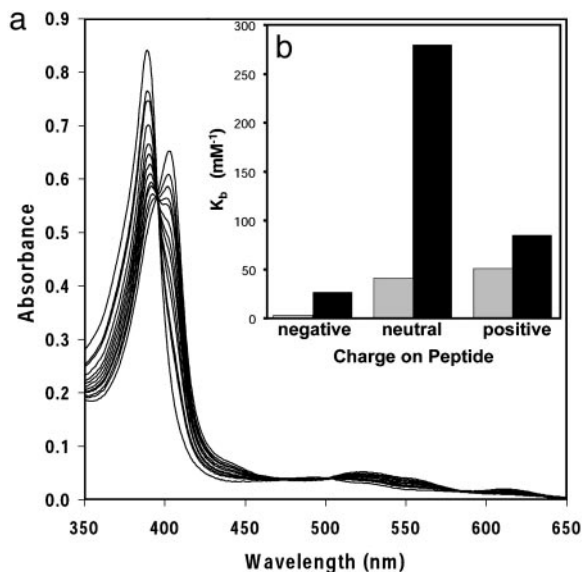


Fig. 2. (a) Spectrophotometric titration of $[\text{Fe}^{\text{III}}(\text{coproporphyrinate I})]^{3-}$ with Cy-AA-KK at 21°C. Clean isosbestic behavior was observed in all titrations, implying that only free porphyrin and the complex are present in solution. (b) Summary of binding affinities for the negatively charged (Cy-AA-EE), neutral (Cy-AA-EK), and positively charged (Cy-AA-KK) peptides to $[\text{Fe}^{\text{III}}(\text{coproporphyrinate I})]^{3-}$ at pH 6.7 (□) and 7.6 (■). The measured binding constants were ≈ 0.03 , 40, and 50 mM^{-1} at pH 6.7 and 25, 279, and 83 mM^{-1} at pH 7.6 for Cy-AA-EE, Cy-AA-EK, and Cy-AA-KK, respectively. Cy-FF-KK (data not shown) has $K_b = 390 \text{ mM}^{-1}$ at pH 7.6. For comparison, histidine has $K_b = 0.008 \text{ mM}^{-2}$. Estimated errors are less than $\pm 10\%$.

The preorganization provided by the cyclization of the peptides with disulfide bonds has a dramatic impact on heme binding compared with free histidine. Despite the different stoichiometries (2:1 histidine/metalloporphyrin vs. 1:1 cyclic peptides/metalloporphyrin, as determined from Hill plots of the titration data), it is still possible to roughly compare the binding properties. At pH 7.6, the ratio of free to bound $[\text{Fe}^{\text{III}}(\text{coproporphyrinate I})]^{3-}$ will be 1.0 for Cy-AA-EK (the cyclic peptide with the strongest binding; Fig. 2b) at a peptide concentration of $3.6 \mu\text{M}$. By way of comparison with histidine itself, a free-to-bound heme ratio of 1.0 requires a histidine concentration of 5.6 mM, a three order of magnitude difference.

Because the metalloporphyrin has a substantial overall negative charge (-3), electrostatic interactions play a major role in affecting the binding constants. At pH 6.7, the positively charged (Cy-AA-KK) and neutral (Cy-AA-EK) peptides bind to the metalloporphyrin with similar affinities and much more strongly than the negatively charged peptide (Fig. 2b). We expected Cy-AA-KK (positively charged) to bind most tightly; competition between the metal center and protons for binding to the imidazole, however, may affect the binding affinity at pH 6.7; alternatively, the weakening of the salt bridges in Cy-AA-EK at lower pH values might also be expected to affect the relative affinities. In comparison, the negatively charged peptide (Cy-AA-EE) is bound relatively weakly. As an aside, during prolonged periods (several hours) at pH < 6.7 only, the heme complex of this negatively charged peptide appears to precipitate (i.e., all heme absorption bands decrease).

Salt bridges and hydrophobic interactions are important positive design elements in the creation of metalloporphyrin-binding peptides. At pH 7.6, when all the lysines are still protonated and the glutamates are deprotonated, the neutral peptide has the highest affinity. This finding probably reflects the effects of the salt bridges of Cy-AA-EK that stabilize helix formation and hence increase binding to the metalloporphyrin.

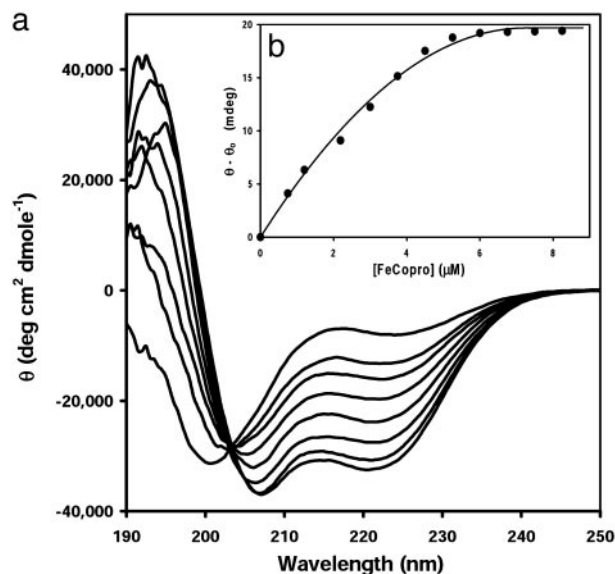


Fig. 3. (a) CD titration of Cy-AA-KK with $[\text{Fe}^{\text{III}}(\text{coproporphyrinate I})]^{3-}$ at 4°C. Aliquots of a metalloporphyrin solution (0.1 equivalent) were added until no change occurred in the negative signal at 222 nm. For clarity, only the spectra of the first seven aliquots are shown. Note that an isodichroic point occurs at $\approx 204 \text{ nm}$, again implying two-state solution behavior. (b) Binding isotherm showing saturation at 1 equivalent to bound porphyrin ($[\text{porphyrin}] = 7 \mu\text{M}$).

Salt bridges can stabilize proteins by up to 1 kcal/mol each (3). Hydrophobic contacts also affect the binding constants. The alanine residues shown by the NMR structure to be in contact with the heme face were replaced by phenylalanine (Cy-FF-KK). This replacement increases binding 5-fold compared with Cy-AA-KK, at pH 7.6, presumably because of increased hydrophobic interactions.

Studies of Secondary Structure and Stability. Both Cy-AA-KK and Cy-AA-EK bind the Fe and the Co system with good isodichroic behavior (Fig. 3a). This finding was not true for the tweezers or 15-mer peptides, as reported earlier (34). As expected, Cy-AA-EE does not assume any secondary structure. The observation of a random-coil to helix (Zimm–Bragg) type of transition in Cy-AA-KK and Cy-AA-EK is consistent with the metalloporphyrin binding to the unfolded peptide (Fig. 3), with the resulting complex assembling into one conformation.

One characteristic of small, single-domain globular proteins is that they show a single, cooperative, thermal unfolding transition (47). The thermal unfolding (Fig. 4) of Cy-AA-KK bound to the slow-exchanging $[\text{Co}^{\text{III}}(\text{coproporphyrinate I})]^{3-}$ is similar to that of small globular proteins, and similar data were obtained for Cy-AA-EK. In contrast, peptides containing phenylalanine residues at positions 4, 5, 11, and 12 gave a nonsigmoidal unfolding curve, possibly due to the high number of nonspecific interactions between the porphyrin and the peptide, which create a large ensemble of conformations. Table 1 lists the melting temperature and the van't Hoff enthalpies of the systems analyzed. Small, single-domain globular proteins typically have unfolding enthalpies (ΔH_m) on the order of $\approx 40 \text{ kcal/mol}$ (5, 6). The enthalpies that we have measured are somewhat lower than that ($\approx 10\text{--}15 \text{ kcal/mol}$), as expected, because our complexes have much less buried hydrophobic surface area. The T_m of the cyclic peptides varies from 47 to 55°C. The alanine-based peptides appear to be half-unfolded at 47°C, which is slightly smaller than many small globular proteins, emphasizing the importance of working

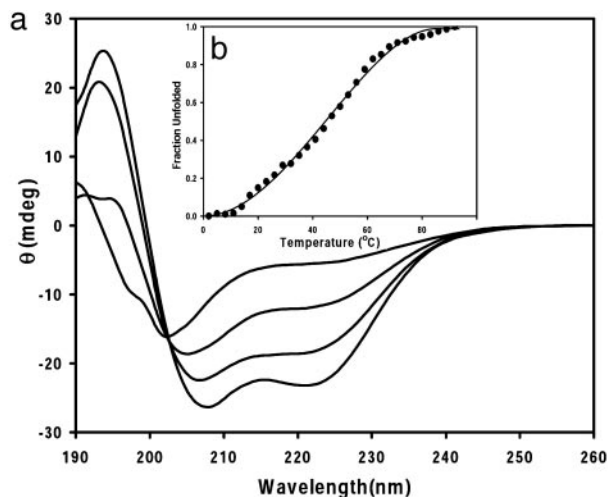


Fig. 4. (a) Thermal unfolding for the complex formed between $[\text{Co}^{\text{III}}(\text{coproporphyrinate I})]^{3-}$ and Cy-AA-KK (similar results were seen for the complex with Cy-AA-EK). Again, the isodichroic point confirms the two-state unfolding of the peptide. (b) Cooperative, two-state unfolding of the same complex monitored at 222 nm, with a melting temperature of 47°C.

with them at low temperatures. The phenylalanine-based derivatives have higher T_m values, which might be due to π - π interactions or hydrophobic stabilization.

Urea-induced unfolding of the alanine peptides was also investigated. The free energies (Table 1) are a bit lower than the average value of 4 kcal/mol seen for globular proteins. However, these systems are miniature proteins without the extensive hydrophobic core seen in globular proteins. The most stabilizing interactions seen in these systems are the Co-histidine bond, the hydrophobic interactions of the porphyrin face with the alanine residues, and electrostatic interactions (in Cy-AA-EK).

NMR Spectroscopy. Two-dimensional NMR spectra were well dispersed, consistent with conformational singularity (Fig. 5a). All the resonances for this molecule could be assigned by using standard methods after analysis of NOESY, total correlation spectroscopy, and double-quantum-filtered COSY data in 90% $\text{H}_2\text{O}/10\% \text{D}_2\text{O}$ (38). Analysis of the NOE cross-peak intensities reveals significant secondary structure in the molecule (Fig. 5b). Only one of the helices is shown for clarity because the other helix gives the same pattern. The data reveal a stronger intensity for the d_{NN} cross-peaks relative to the $d_{\alpha\text{N}}$ cross-peaks, which is a sign of helicity. Another strong pattern is the $d_{\alpha\beta}(i, i + 3)$

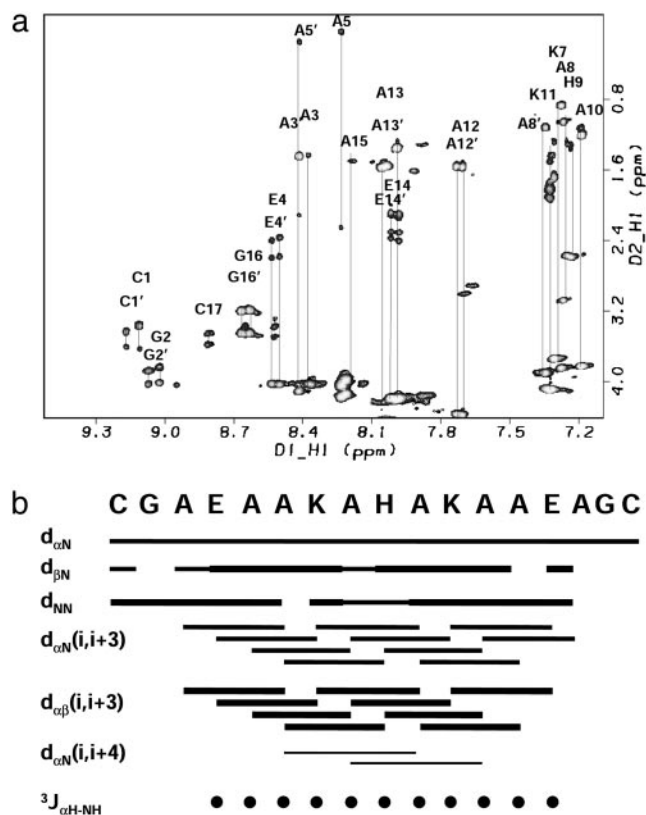


Fig. 5. (a) Two-dimensional ^1H - ^1H total correlation spectroscopy spectrum of the complex of $[\text{Co}^{\text{III}}(\text{coproporphyrinate I})]^{3-}$ and Cy-AA-EK. The spectra show nice dispersion, characteristic of a structured system. (b) Summary of the sequential NOEs for the complex of $[\text{Co}^{\text{III}}(\text{coproporphyrinate I})]^{3-}$ and Cy-AA-EK. The intensities were grouped into three sets: weak, medium, and strong. The size of the bars reflects these intensities. NOEs were taken from a NOESY spectrum recorded with a mixing time of 100 ms. The three-bond $2J_{\alpha\text{NH}}$ coupling constants were taken from a high-resolution double-quantum-filtered COSY experiment and converted to ϕ -angle restraints by using the standard methods (36, 37). Only one of the helices is shown for clarity because the other helix gives the same pattern. The data reveal a stronger intensity for the d_{NN} cross-peaks relative to the $d_{\alpha\text{N}}$ cross-peaks, which is a sign of helicity. Another strong pattern is the $d_{\alpha\beta}(i, i + 3)$ cross-peaks. Although it is difficult to distinguish between 3_{10} and α -helices from NMR data, the presence of the $d_{\alpha\beta}(i, i + 3)$ cross-peaks as the most intense in the spectra, the presence of $d_{\alpha\text{N}}(i, i + 4)$, and the absence of $d_{\alpha\text{N}}(i, i + 2)$ cross-peaks provide further support for the α -helical structure. Several unique NOEs also exist between the metalloporphyrin and the peptide and the imidazole of the histidine and other residue side chains.

cross-peaks. Although it is difficult to distinguish between 3_{10} and α -helices from NMR data, the presence of the $d_{\alpha\beta}(i, i + 3)$ cross-peaks as the most intense in the spectra, the presence of $d_{\alpha\text{N}}(i, i + 4)$, and the absence of $d_{\alpha\text{N}}(i, i + 2)$ cross-peaks provides further support for the α -helical structure. Several unique NOEs also exist between the metalloporphyrin and the peptide and the imidazole of the histidine and other residue side chains.

Structure Calculations. The quality of the NMR data permitted the use of NOE-restrained simulated annealing protocols for the calculation of the solution structure. By using the INSIGHTII/ DISCOVER package, and a modified form of the consistent valence force field, 50 random structures were calculated from a total of 224 distance restraints (including 22 hydrogen bond restraints) and 30 ϕ -angle restraints (Table 2). Rigorous analysis of NOE cross-peaks gave a total of 202 distance restraints determined from peak volume measurements. Torsion-angle

Table 1. Thermodynamic properties of cyclic peptide complexes of $[\text{Co}^{\text{III}}(\text{coproporphyrinate I})]^{3-}$

Parameter	Cy-AA-KK	Cy-AA-EK	Cy-FF-KK
$T_m, ^\circ\text{C}^*$	47 ± 3	47 ± 3	52 ± 3
$\Delta S_m, \text{cal}\cdot\text{mol}^{-1}\cdot\text{deg}^{-1}\dagger$	31 ± 5	47 ± 5	34 ± 5
$\Delta H_m, \text{kcal}\cdot\text{mol}^{-1}\ddagger$	9.9 ± 2	15.0 ± 2	11.1 ± 3
$\Delta G_{\text{unfolding}}^{\ddagger}, \text{kcal}\cdot\text{mol}^{-1}\S$	2.9 ± 0.24	3.3 ± 0.26	— [¶]
$m, \text{cal}\cdot\text{mol}^{-1}\cdot\text{M}^{-1}\ \$	598 ± 47	735 ± 54	— [¶]

*Melting temperature. This is the temperature when $\Delta G = 0$ and the molecule is half-unfolded.

[†]Entropy of unfolding (1 cal = 4.184 J).

[‡]van't Hoff enthalpy.

[§]Free energy of unfolding in urea.

[¶]Not measured because of the dynamic nature of the complex and limited sample quantities.

^{||}Molar cosolvation term.

Table 2. Structural statistics for a family of 14 calculated structures of the Cy-AA-EK complex of [Co^{III}(coproporphyrinate I)]³⁻

Experimental restraints	
Intraresidue ($ i-j = 0$)	64
Short to medium ($1 \leq i-j \leq 5$ residues)	131
Long range ($ i-j > 5$ residues)	8
Hydrogen bonds	22
ϕ -angles	30
Total	255
Deviations from experimental restraints	
Distance restraints	0.07
Dihedral angle	2.7
Deviations from ideal geometry	
Bonds, Å	0.02
Angles, °	1.87
Impropers	0.96
rms deviations from the mean structure, Å	
Backbone atoms (residues 1–34: N, C $^{\alpha}$, C)	0.6
Backbone atoms (residues 19–31: N, C $^{\alpha}$, C)	0.4
All nonhydrogen atoms (residues 1–34)	0.93

Of the 50 structures, 40 converged to acceptable structures. Of these, 14 structures were deemed exceptionally good (i.e., displayed no violations >0.5 Å or 5°). Distances were constrained in a square well potential by using force constants for bonds set to 25 kcal/(mol·rad²) and for angles set to 100 kcal/(mol·rad²). The structures were checked by using the NMRREFINE/PROSTAT module in the INSIGHT/DISCOVER package.

constraints were determined from analysis of double-quantum-filtered COSY spectral data. Displayed in Fig. 6 *Top* is a stereoview of the 14 best structures; topologically, the structure is similar to a leucine zipper. A representative low-energy structure is shown in Fig. 6 *Middle*. Strikingly, the structure shows that the two helices tilt to maximize close packing of the hydrophobic porphyrin π system and the hydrophobic residues of the peptide, so that the lysines are proximal to the carboxylates of the porphyrin. In this design, alanines were positioned on the side of the helix so that they could interact favorably with the hydrophobic porphyrin face. Of the 14 structures displayed, the overall backbone rms deviation is 0.9 Å for all nonhydrogen atoms (Table 2), 0.6 Å for the backbone atoms, and a very low 0.4 Å in the helical regions of the peptide. As expected, the turn regions, where the cysteine bridges have been placed, have more disorder and are presumably dynamic in solution.

Conclusions

The unifying theme in this work has shown that the metal-porphyrin plays a substantial role in the induction and stabilization of peptide structure. Furthermore, the described structures display native-like properties similar to small proteins. The broadening of the free energy gap between native and molten structures was possible only after incorporation of disulfide bridges and ionic contacts.

Stability studies reveal a cooperative denaturation of both the Cy-AA-KK and Cy-AA-EK complexes. Whereas the thermodynamic data show only a marginal increase in the stability of Cy-AA-EK over Cy-AA-KK, the NMR spectra of Cy-AA-EK were the best resolved. NMR, therefore, is a critical screen for native-like properties.

The use of the diamagnetic, slow-exchanging Co^{III} analogue of [Fe^{III}(coproporphyrinate I)]³⁻ in the characterization of the cyclic complexes permitted the solution of the high-resolution structure of the [Co^{III}(coproporphyrinate I)]³⁻ complex of Cy-AA-EK. Notably, the structure shows an $\approx 60^{\circ}$ helical tilt relative to the heme, which maximizes hydrophobic contacts and intramolecular ion pairing. Analysis of the structure suggested that

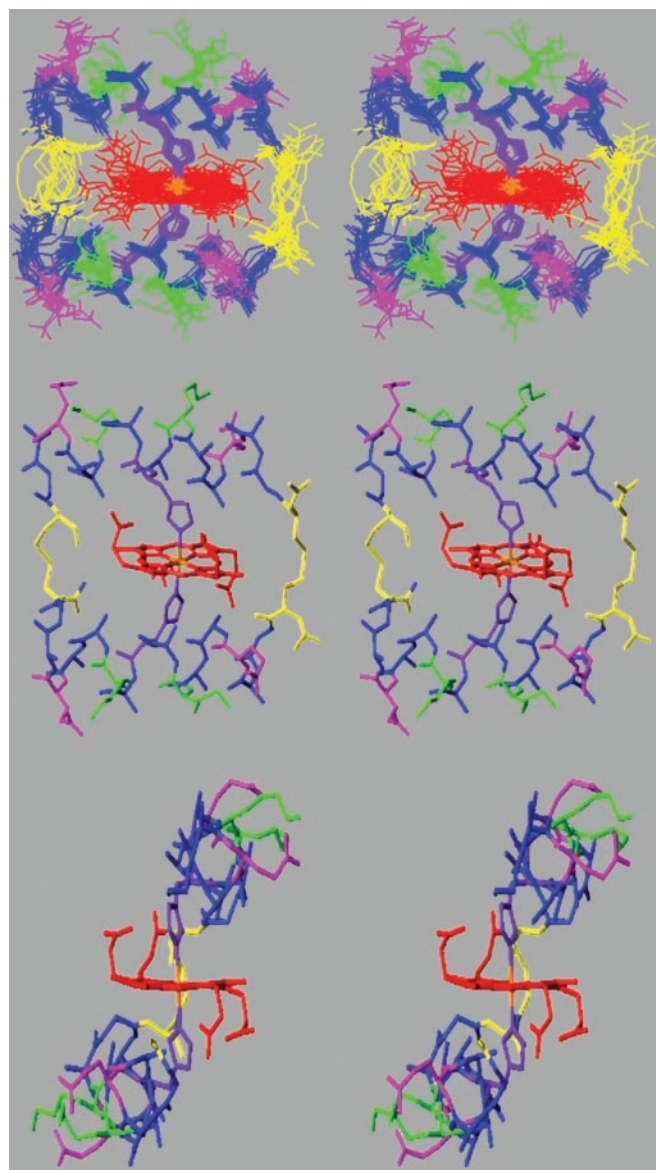


Fig. 6. (Top) Overlay of the 14 best structures for the complex of [Co^{III}(coproporphyrinate I)]³⁻ and Cy-AA-EK. Two stereo side views are shown for clarity. Structures were generated by using the INSIGHT/DISCOVER package. The color scheme is as follows: Ala and Gly, blue; Lys, green; Glu, pink; Cys, yellow; and His, purple. (Middle) Stereo view of the solution structure of [Co^{III}(coproporphyrinate I)]³⁻ and Cy-AA-EK. (Bottom) As in *b*, rotated 90°. Coordinates for these structures are available in the Protein Data Bank at www.rcsb.org/pdb with PDB ID code 1PBZ.

a four-helix bundle could easily be engineered by extension of these sequences.

Possible biomedical implications exist for these studies. It has been well established that intrinsically unstructured proteins (i.e., prions) (48, 49) are key elements in neurodegenerative diseases. We find it most interesting that porphyrins (50, 51) and other cofactors (52) have been shown to interact strongly with these unstructured proteins and may have important pharmaceutical applications. The ability of porphyrins and metal-porphyrins to stabilize α -helical structures in peptides may have important implications for remediation of peptide aggregates *in vivo*.

This work was supported by National Institutes of Health Grant HL 25934, with instrument support, in part, from the W. M. Keck Foundation.

- Lombardi, A., Summa, C. M., Geremia, S., Randaccio, L., Pavone, V. & DeGrado, W. F. (2000) *Proc. Natl. Acad. Sci. USA* **97**, 6298–6305.
- Hill, R. B., Raleigh, D. P., Lombardi, A. & DeGrado, W. F. (2000) *Acc. Chem. Res.* **33**, 745–754.
- Nastri, F., Lombardi, A. & Pavone, V. (2001) *Chem. Rev.* **101**, 3165–3189.
- Ptitsyn, O. B. (1995) *Trends Biochem. Sci.* **20**, 485.
- DeGrado, W. F., Raleigh, D. P. & Handel, T. (1991) *Curr. Opin. Struct. Biol.* **1**, 984–993.
- Betz, S. F., Raleigh, D. P. & DeGrado, W. F. (1993) *Curr. Opin. Struct. Biol.* **3**, 601–610.
- Bryson, J. W., Betz, S. F., Lu, H. S., Suich, D. J., Zhou, H. X., O’Neil, K. T. & DeGrado, W. F. (1995) *Science* **270**, 935–941.
- Gibney, B. R. & Dutton, P. L. (1999) *Protein Sci.* **8**, 1888–1898.
- Rojas, N. R. L., Kamtekar, S., Simons, C. T., McLean, J. E., Vogel, K. M., Spiro, T. G., Farid, R. S. & Hecht, M. H. (1997) *Protein Sci.* **6**, 2512–2524.
- Rau, H. K., Snigula, H., Struck, A., Robert, B., Scheer, H. & Haehnel, W. (2001) *Eur. J. Biochem.* **268**, 3284–3295.
- Mutz, M. W., Case, M. A., Wishart, J. F., Ghadiri, M. R. & McLendon, G. L. (1999) *J. Am. Chem. Soc.* **121**, 858–859.
- Moffet, D. A., Certain, L. K., Smith, A. J., Kessel, A. J., Beckwith, K. A. & Hecht, M. H. (2000) *J. Am. Chem. Soc.* **122**, 7612–7613.
- Hellinga, H. W. (1998) *Folding Des.* **3**, R1–R8.
- Benson, D. E., Wisz, M. S. & Hellinga, H. W. (2000) *Proc. Natl. Acad. Sci. USA* **97**, 6292–6297.
- Holm, R. H., Kennepohl, P. & Solomon, E. I. (1996) *Chem. Rev.* **96**, 2239–2314.
- Beinert, H., Holm, R. H. & Munck, E. (1997) *Science* **277**, 653–659.
- Lever, A. B. P. & Gray, H. B., eds. (1983) *Iron Porphyrins*, Physical Bioinorganic Chemistry Series 1 (Addison-Wesley, Reading, MA), Parts 1 and 2.
- Klinman, J. P. (1996) *J. Biol. Chem.* **271**, 27189–27192.
- Summa, C. M., Lombardi, A., Lewis, M. & DeGrado, W. F. (1999) *Curr. Opin. Struct. Biol.* **9**, 500–508.
- Kuchner, O. & Arnold, F. H. (1997) *Trends Biotechnol.* **15**, 523–530.
- Arnold, F. H. (2001) *Nature* **409**, 253–257.
- Arnold, F. H. (1998) *Acc. Chem. Res.* **31**, 125–131.
- Wade, H. & Scanlan, T. S. (1997) *Annu. Rev. Biophys. Biomol. Struct.* **26**, 461–493.
- Demartis, S., Huber, A., Viti, F., Lozzi, L., Giovannoni, L., Neri, P., Winter, G. & Neri, D. (1999) *J. Mol. Biol.* **286**, 617–633.
- Atwell, S. & Wells, J. A. (1999) *Proc. Natl. Acad. Sci. USA* **96**, 9497–9502.
- Smith, G. P. & Petrenko, V. A. (1997) *Chem. Rev.* **97**, 391–410.
- Forrer, P., Jung, S. & Pluckthun, A. (1999) *Curr. Opin. Struct. Biol.* **9**, 514–520.
- Hill, R. B. & DeGrado, W. F. (1998) *J. Am. Chem. Soc.* **120**, 1138–1145.
- Walsh, S. T. R., Cheng, H., Bryson, J. W., Roder, H. & DeGrado, W. F. (1999) *Proc. Natl. Acad. Sci. USA* **96**, 5486–5491.
- Struthers, M. D., Cheng, R. P. & Imperiali, B. (1996) *Science* **271**, 342–345.
- Skalicky, J. J., Gibney, B. R., Rabanal, F., Urbauer, R. J. B., Dutton, P. L. & Wand, A. J. (1999) *J. Am. Chem. Soc.* **121**, 4941–4951.
- Huffman, D. L., Rosenblatt, M. M. & Suslick, K. S. (1998) *J. Am. Chem. Soc.* **120**, 6183–6184.
- Huffman, D. L. & Suslick, K. S. (2000) *Inorg. Chem.* **39**, 5418–5419.
- Rosenblatt, M. M., Huffman, D. H., Wang, X., Remmer, H. & Suslick, K. S. (2002) *J. Am. Chem. Soc.* **124**, 12394–12395.
- Pace, C. N. & Scholtz, J. M. (1997) in *Protein Structure: A Practical Approach*, ed. Creighton, T. E. (Oxford Univ. Press, New York), 2nd Ed., pp. 299–321.
- Ghadiri, M. R., Soares, C. & Choi, C. (1992) *J. Am. Chem. Soc.* **114**, 825–831.
- Wüthrich, K. (1986) *NMR of Proteins and Nucleic Acids* (Wiley, New York).
- Cavanagh, J., Fairbrother, W. J., Palmer, A. G. & Skelton, N. J. (1996) *Protein NMR Spectroscopy: Principles and Applications* (Academic, San Diego).
- Bax, A. (1988) *J. Magn. Reson.* **77**, 134–147.
- Davis, D. G. & Bax, A. (1985) *J. Am. Chem. Soc.* **107**, 2820–2821.
- Bax, A. & Davis, D. G. (1985) *J. Magn. Reson.* **65**, 355–360.
- Griesinger, C., Sorensen, O. W. & Ernst, R. R. (1986) *J. Chem. Phys.* **85**, 6837–6852.
- Kim, Y. & Prestegard, J. H. (1990) *Proteins Struct. Funct. Genet.* **8**, 377–385.
- Nilges, M., Clore, G. M. & Gronenborn, A. M. (1987) *FEBS Lett.* **219**, 11–16.
- Nilges, M., Gronenborn, A. M., Bruenger, A. T. & Clore, G. M. (1988) *Protein Eng.* **2**, 27–38.
- Nilges, M., Clore, G. M. & Gronenborn, A. M. (1988) *FEBS Lett.* **239**, 129–136.
- Privalov, P. L. & Gill, S. J. (1988) *Adv. Protein Chem.* **39**, 191–234.
- Wright, P. E. & Dyson, H. J. (1999) *J. Mol. Biol.* **293**, 321–331.
- Dyson, H. J. & Wright, P. E. (1998) *Nat. Struct. Biol.* **5**, 499–503.
- Caughy, W. S., Raymond, L. D., Horiuchi, M. & Caughy, B. (1998) *Proc. Natl. Acad. Sci. USA* **95**, 12117–12122.
- Priola, S. A., Raines, A. & Caughy, W. S. (2000) *Science* **287**, 1503–1506.
- Viles, J. H., Cohen, F. E., Prusiner, S. B., Goodin, D. B., Wright, P. E. & Dyson, H. J. (1999) *Proc. Natl. Acad. Sci. USA* **96**, 2042–2047.

The Chemical Effects of Ultrasound

Intense ultrasonic waves traveling through liquids generate small cavities that enlarge and implode, creating tremendous heat. These extreme conditions provide an unusual chemical environment

by Kenneth S. Suslick

During the early tests of the first British destroyer in 1894, Sir John I. Thornycroft and Sydney W. Barnaby noticed a severe vibration from the destroyer's propeller. They suggested that large bubbles, or cavities, formed by the spinning propeller and imploded by water pressure, were the source of the vibrations. Thornycroft and Barnaby redesigned the propeller to reduce the vibrations from what came to be known as cavitation, but as the British navy built even faster propulsion systems the phenomenon became an increasingly significant problem. In 1917, therefore, the navy commissioned Lord Rayleigh to study the matter. He confirmed that the vibrations were due to the enormous turbulence, heat and pressure of imploding cavities. Although cavitation continues to be troublesome for nautical engineers, it has provided chemists with a unique environment for high-energy reactions.

Chemistry, after all, is the interaction of energy and matter. Specific energy sources limit the control chemists have over the reactivity of matter. Light interacts with matter on a short time scale at high energies, whereas

heat interacts on longer time scales at lower energies. The interaction of sound with matter through the process of cavitation makes available to chemists a range of energies on time scales that are not available from other sources.

Chemists usually induce cavitation not by applying mechanical pressure but rather by generating intense sound waves in a liquid. Such waves create alternating regions of compression and expansion that can form bubbles 100 microns in diameter. The bubbles implode violently in less than a microsecond, heating their contents to 5,500 degrees Celsius-about the temperature of the sun's surface.

The first chemist to recognize the unusual effects of intense sound waves traveling through a liquid, known as sonochemistry, was Alfred L. Loomis in 1927. In spite of his early results, the study of sonochemistry remained exceedingly modest. A renaissance in sonochemistry took place in the 1980's, soon after the advent of inexpensive and reliable generators of high-intensity ultrasound (sound pitched above human hearing at frequencies greater than 16 kilohertz, or 16,000 cycles per second).

Today ultrasound is applied in hospitals for medical imaging, in industry for welding plastics and cleaning materials and even in the home for burglar alarms and vaporizers. These applications, however, do not utilize the chemical effects of ultrasound. Ultrasound can increase the reactivity of metal powders by more than 100,000 times. Ultrasound can drive metal particles together at such high speeds that they melt at the point of collision, and ultrasound can generate microscopic flames in cold liquids.

These chemical effects of ultrasound arise from the physical processes that create, enlarge and implode gaseous and vaporous cavities in a liquid. Ultrasound waves, like all sound waves, consists of cycles of compression and expansion. Compression cycles exert a positive pressure on the liquid, pushing the molecules together; expansion cycles exert a negative pressure, pulling the molecules away from one another.

During the expansion cycle a sound wave of sufficient intensity can generate cavities. A liquid is held together by attractive forces, which determine the tensile strength of a liquid. In order for a cavity to form, a large negative pressure associated with the expansion cycle of the sound wave is needed to overcome the liquid's tensile strength.

The amount of negative pressure needed depends on the type and purity of the liquid. For truly pure liquids, tensile strengths are so great that available ultrasound generators cannot produce enough negative pressure to make cavities. In pure water, for instance, more than 1,000 atmospheres of negative pressure would be required, yet the most powerful ultrasound generators produce only about 50 atmospheres of negative pressure. The tensile strength of liquids is reduced, however, by gas trapped in the crevices of small solid particles. The effect is analogous to the reduction in strength that occurs from cracks in solid materials. When a gas-filled crevice is exposed to a negative-pressure cycle from a sound wave, the reduced pressure makes the gas in the crevice expand until a small bubble is released into solution. Most liquids are sufficiently contaminated by small particles to initiate cavitation. In tap

KENNETH S. SUSLICK is professor of chemistry at the University of Illinois at Urbana-Champaign. He received his B.S. at the California Institute of Technology in 1974 and his Ph.D. from Stanford University in 1978. He holds a Research Career Development Award from the National Institutes of Health and a Sloan Foundation Research Fellowship. In 1986 he was a visiting fellow of Balliol College at the University of Oxford. In addition to sonochemistry, he is interested in the role of metals in biological systems. Suslick also enjoys singing folk music and sculpting bronzes.

water, negative pressures of only a few atmospheres will form bubbles.

A bubble in a liquid is inherently unstable. If the bubble is large, it will float away and burst at a surface; if it is small, it will redissolve into the liquid. A bubble irradiated with ultrasound, however, continually absorbs energy from alternating compression and expansion cycles of the sound wave. These cause the bubbles to grow and contract, striking a dynamic balance between the vapor inside the bubble and the liquid outside. In some cases the ultrasonic waves will sustain a bubble that simply oscillates in size.

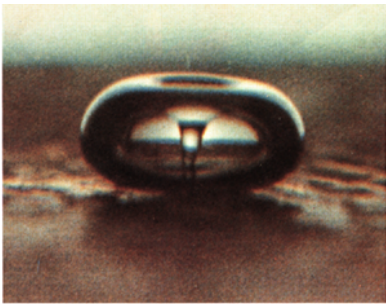
In other cases the average size of the bubble will increase.

Cavity growth depends on the intensity of sound. High-intensity ultrasound can expand the cavity so rapidly during the negative-pressure cycle that the cavity never has a chance to shrink during the positive-pressure cycle. In this process, therefore, cavities can grow rapidly in the course of a single cycle of sound.

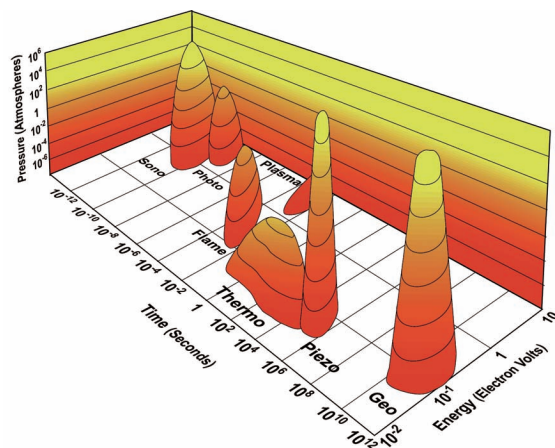
For low-intensity ultrasound the size of the cavity oscillates in phase with the expansion and compression cycles. The surface area of a cavity produced by low-intensity ultrasound

is slightly greater during expansion cycles than during compression cycles. Since the amount of gas that diffuses in or out of the cavity depends on the surface area, diffusion into the cavity during expansion cycles will be slightly greater than diffusion out during compression cycles. For each cycle of sound, then, the cavity expands a little more than it shrinks. Over many cycles the cavities will grow slowly.

The growing cavity can eventually reach a critical size where it will most efficiently absorb energy from the ultrasound. The critical size depends on



IMPLoding CAVITY in a liquid irradiated with ultrasound is captured in a high-speed flash photomicrograph (above). The implosion heats the gases inside the cavity to 5,500 degrees Celsius. Since this cavity formed near a solid surface, the implosion is asymmetric, expelling a jet of liquid at roughly 400 kilometers per hour. Both the heat and the jet contribute to a unique chemical environment in the liquid. The diameter of the cavity is about 150 microns. The drawing (left) shows the stages of cavity implosion and the formation of the jet. The cavity is spherical at first and then shrinks rapidly. The jet develops opposite the solid surface and moves toward it.



SONOCHEMISTRY makes available a range of energies as well as combinations of pressure and duration not available from any other source. The relations among energy, pressure and time are shown for sonochemistry and other chemistry fields.

the frequency of the ultrasound wave. At 20 kilohertz, for example, the critical size is a cavity roughly 170 microns in diameter. At this point the cavity can grow rapidly in the course of a single cycle of sound.

Once a cavity has experienced a very rapid growth caused by either low- or high-intensity ultrasound, it can no longer absorb energy as efficiently from the sound waves. Without this energy input the cavity can no longer sustain itself. The liquid rushes in and the cavity implodes.

The implosion of cavities establishes an unusual environment for chemical reactions. The gases and vapors inside the cavity are compressed, generating intense heat that raises the temperature of the liquid immediately surrounding the cavity and creates a local hot spot. Even though the temperature of this region is extraordinarily high, the region it-

self is so small that the heat dissipates quickly. My co-workers and I at the University of Illinois at Urbana-Champaign estimate that the heating and cooling rates during cavitation are more than a billion degrees C per second! This is similar to the cooling that occurs if molten metal is splattered onto a surface cooled near absolute zero. At any given time, therefore, the bulk of the liquid remains at the ambient temperature.

The exact temperatures and pressures generated during cavity implosion are difficult both to calculate theoretically and to determine experimentally. Yet these quantities are fundamental to describing the potential of sonochemistry. Theoretical models have been proposed that approximate the dynamics of cavity implosion at various levels of accuracy. All have difficulty accurately describing cavity dynamics during the last stages of implosion. The most sophis-

ticated models give temperatures of thousands of degrees Celsius, pressures of from hundreds to thousands of atmospheres and heating times of less than a microsecond.

The temperature of the imploding cavity cannot be measured with a physical thermometer because the heat is dissipated too quickly to be registered. Recently my collaborators and I found an alternative that enables one to check theoretical results experimentally. One way to gauge temperature is to observe the rate at which familiar chemical reactions take place. More precisely, the temperature is related to the negative inverse logarithm of the rate of the reaction. If the rates of several different reactions are measured in an ultrasound environment, the temperature from cavity implosion can be calculated.

In the process of determining the relative rates of a series of sonochemical reactions, David A. Hammerton in

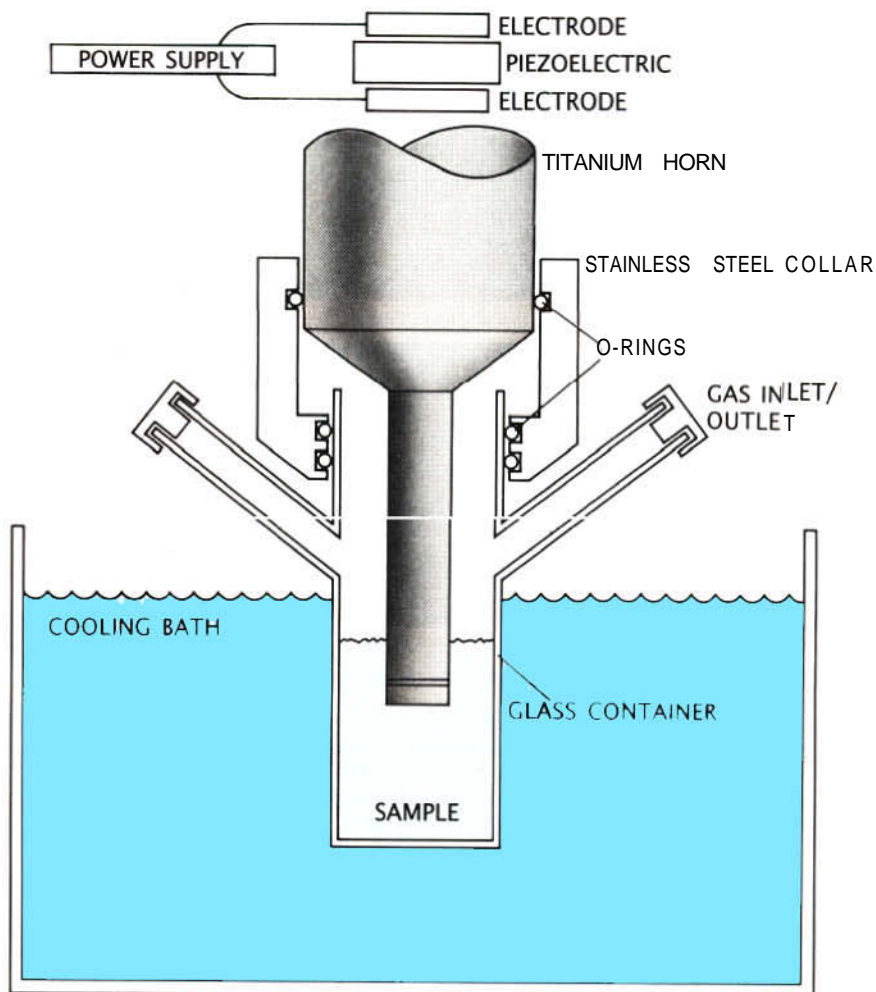
our laboratory discovered two distinct temperature regions associated with cavity implosion. The original gaseous contents of the cavity reached temperatures of about 5,500 degrees C, whereas the liquid immediately surrounding the cavity reached 2,100 degrees. The temperature of the flame from an acetylene torch, in comparison, is about 2,400 degrees.

Although the pressures attained during cavity implosion are harder to determine experimentally than temperature, the two quantities are correlated. One can therefore estimate the peak pressure to be 500 atmospheres, which is half the pressure at the deepest region of the ocean, the Mariana Trench.

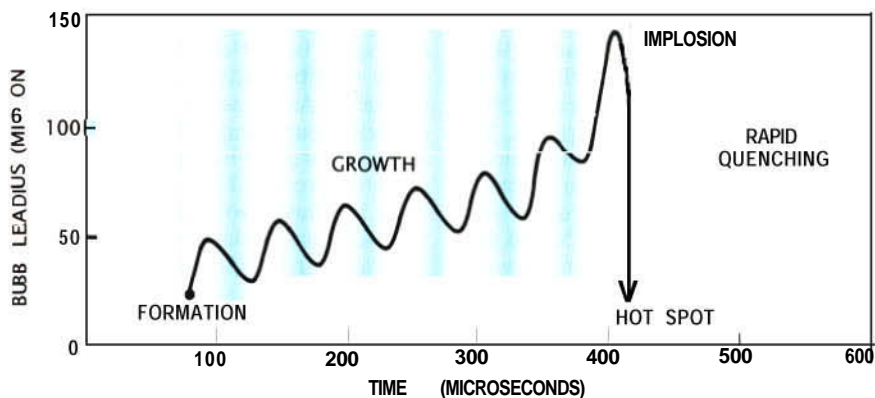
Even though the local temperature and pressure conditions created by cavity implosion are extreme, chemists have good control over sonochemical reactions. The intensity of cavity implosion, and hence the nature of the reaction, can easily be altered by such factors as acoustic frequency, acoustic intensity, ambient temperature, static pressure, choice of liquid and choice of ambient gas. The way these factors alter sonochemistry often defies basic intuitions about chemistry. Let me cite three examples.

First, unlike virtually all chemical reactions, most sonochemical reactions decrease in rate with increasing ambient temperature—that is, the temperature outside the cavity. The higher the ambient temperature is, the more vapor there will be inside the cavity. The extra vapor cushions the implosion of the cavity and lowers the temperature of implosion. Therefore sonochemical reactions proceed more slowly as ambient temperature increases. Second, unlike chemical events driven by light, sonochemical reactions do not depend greatly on frequency. The major effect of frequency is to change the critical size of a cavity before implosion, which does not change the cavitation process significantly. Third, unlike many chemical reactions in solution, the ambient gas that is dissolved in the liquid is quite important. If xenon fills a cavity, the peak temperature reached during cavity implosion will be high because xenon conducts heat poorly and retains the heat of the collapsing cavity. Helium, on the other hand, conducts heat so well that it can virtually shut down sonochemical reactions.

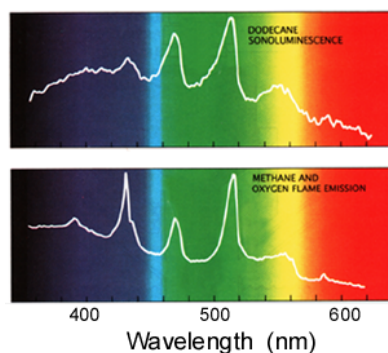
The dynamics of cavity growth and implosion are strongly dependent on local conditions, including the form of the materials: whether they are



An Ultrasonic Immersion Horn is the intensest generator of ultrasound in general use. Ultrasound is produced in liquids by means of piezoelectric or magnetostrictive materials: materials that expand or contract when they are placed in electromagnetic fields. Exposing such materials to a field alternating at an ultrasonic frequency produces ultrasound. In the ultrasonic horn there is a piezoelectric ceramic attached to a tapered titanium rod, which serves to amplify the sound. The horn vibrates at a fixed acoustic frequency, typically 20 kilohertz, but the intensity is variable. Since power outputs are quite high, the reaction solution must be cooled.



BUBBLE GROWTH AND IMPLOSION in a liquid irradiated with ultrasound is the physical phenomenon responsible for most sonochemistry. Intense ultrasound waves generate large alternating stresses within a liquid by creating regions of positive pressure (dark color) and negative pressure (light color). A cavity can form and grow during the episodes of negative pressure. When the cavity attains a critical size, the cavity implodes, generating intense heat and tremendous pressure.



LIGHT resembling that from a gas flame is generated when cold hydrocarbon liquids are exposed to ultrasound, the phenomenon is known as sonoluminescence. The graphs show the spectrum produced by the sonoluminescence of dodecane, $C_{12}H_{24}$ (top), and the combustion of methane, CH_4 (bottom). The similarities between the spectra are due to the formation and emissions of diatomic carbon in both cases.

liquids, extended solid surfaces in liquids or solid particles in liquids. In each case, because the dominant physical effects from cavity implosion differ, the chemistry changes as well.

The sonochemistry of liquids depends mainly on physical effects of the quick heating and cooling caused by cavity implosion. For instance, when Peter Riesz and his colleagues at the National Cancer Institute irradiated water with ultrasound, they proved that the heat from cavity implosion decomposes water (H_2O) into extremely reactive hydrogen atoms ($H\cdot$) and hydroxyl radicals ($OH\cdot$). During the quick cooling phase, hydrogen atoms and hydroxyl radicals recombine to form hydrogen peroxide (H_2O_2) and molecular hydrogen (H_2). If other compounds are added to water irradiated with ultrasound, a wide range of secondary reactions can occur. Organic compounds are highly degraded in this environment, and inorganic compounds can be oxidized or reduced.

Other organic liquids also yield interesting reactions when they are irradiated with ultrasound. For example, alkanes, major components of crude oil, can be "cracked" into smaller, desirable fragments, such as gasoline.

Crude oil is normally cracked by heating the entire mixture to temperatures above 500 degrees C. Irradiating alkanes with ultrasound, however, makes cracking possible at room temperature and produces acetylene, which cannot be produced through simple heating.

Perhaps the most unusual chemical phenomenon associated with ultrasound is its ability to produce microscopic flames in cold liquids by a process known as sonoluminescence. When an imploding cavity creates a hot spot in various liquids, molecules may be excited into high-energy states. As these molecules return to their ground state, they emit visible light. Edward B. Flint in our laboratory discovered in 1987 that hydrocarbons irradiated with ultrasound provide a most striking result: emitted light similar in color to a flame from a gas stove.

The effects of ultrasound on liquids have also been used to enhance the chemistry of compounds in solution. Compounds that contain metal-carbon bonds, called organometallics, are particularly illustrative. This diverse class of chemicals is important in the formation of plastics, in the production of microelectronics and in the synthesis of pharmaceuticals, herbi-

cides and pesticides. In 1981 Paul F. Schubert and I first investigated the effects of ultrasound on organometallics, in particular iron pentacarbonyl, or $Fe(CO)_5$. The results, when compared with the effects of light and heat on $Fe(CO)_5$, underscore the distinctive chemistry that ultrasound can induce [see illustration on opposite page]. When $Fe(CO)_5$ is exposed to heat, it decomposes into carbon monoxide (CO) and a fine iron powder, which ignites spontaneously in air. When $Fe(CO)_5$ is exposed to ultraviolet light, it first breaks down into $Fe(CO)_4$ and free CO fragments. $Fe(CO)_4$ can then recombine to form $Fe_2(CO)_9$. Cavity implosion creates different results. It delivers enough heat to dissociate several CO molecules but cools quickly enough to quench the reaction before decomposition is complete. Thus when $Fe(CO)_5$ is exposed to ultrasound, it yields the unusual cluster compound $Fe_3(CO)_{11}$.

The sonochemistry of two immiscible liquids (such as oil and water) stems from the ability of ultrasound to emulsify liquids so that microscopic droplets of one liquid are suspended in the other. Ultrasonic compression and expansion stress liquid surfaces, overcoming the cohesive forces that hold a large droplet together. The droplet bursts into smaller ones, and eventually the liquids are emulsified.

Emulsification can accelerate chemical reactions between immiscible liquids by greatly increasing their surface contact. A large contact area enhances crossover of molecules from one liquid to the other, an effect that can make some reactions proceed quickly. Emulsifying mercury with various liquids has particularly interesting chemistry as delineated by the investigations of Albert J. Fry of Wesleyan University. He developed the reactions of mercury with a variety of organobromide compounds as an intermediate in the formation of new carbon-carbon bonds. Such reactions are critical in the synthesis of complex organic compounds.

The sonochemistry of solid surfaces in liquids depends on a change in the dynamics of cavity implosion. When cavitation occurs in a liquid near an extended solid surface, the cavity implosion differs substantially from the symmetrical, spherical implosion observed in liquid-only systems. The presence of the surface distorts the pressure from the ultrasound field so that a cavity implosion near a surface is markedly asymmet-

ric. This generates a jet of liquid directed at the surface that moves at speeds of roughly 400 kilometers per hour. The jet, as well as the shock waves from cavity implosion, erode solid surfaces, remove nonreactive coatings and fragment brittle powders. Reactions are further facilitated by high temperatures and pressures associated with cavity implosion near surfaces. These processes all enhance the chemical reactivity of solid surfaces, which is important in the synthesis of drugs, specialty chemicals and polymers.

The sonochemistry of solid surfaces in liquids is best exemplified by reactions of active metals, such as lithium, magnesium, zinc and aluminum. Ultrasonic irradiation of reaction mixtures constituting these metals provides better control at lower temperatures and produces relatively higher yields. Pierre Renaud of the University of Paris first examined such reactions. More recently Jean-Louis Luche of the University of Grenoble and Philip

Boudjouk of North Dakota State University have popularized the use of an ultrasonic cleaning bath to accelerate the reactions of active metals.

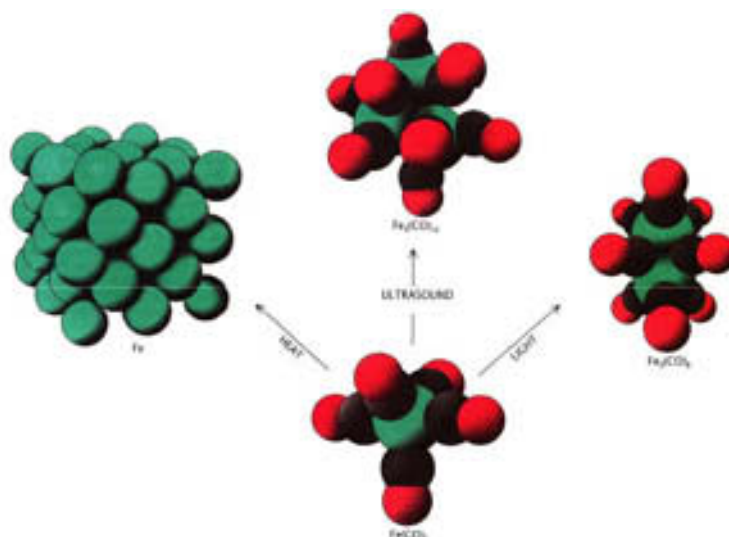
The chemistry of these metals is very difficult to control. Traces of water, oxygen or nitrogen can react at the surface to form protective coatings. Increasing the reactivity of the protected surface by direct heating, however, can result in undesirable explosions. Ultrasound can keep the surface clean and allows the reaction to proceed evenly at reduced ambient temperatures. Excellent yields and improved reliability can be achieved for many reactive metals in large-scale industrial applications.

The extreme conditions generated by cavitation near surfaces can also be utilized to induce reactivity in "unreactive" metals. Robert E. Johnson in our laboratory, for instance, examined reactions between carbon monoxide and molybdenum and tantalum, as well as other comparable metals. Conventional techniques require pres-

ures of from 100 to 300 atmospheres and temperatures of from 200 to 300 degrees C. to form metal carbonyls. Using ultrasound, however, formation of metal carbonyls can proceed at room temperature and pressure.

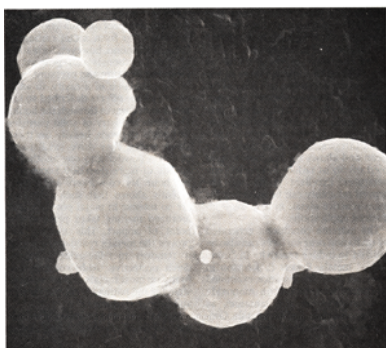
The implosion of a cavity, in addition to all the effects described so far, sends shock waves through the liquid. The sonochemistry of solid particles in liquids depends heavily on these shock waves; they drive small particles of a powder into one another at speeds of more than 500 kilometers per hour. My co-workers and I have recently shown that such collisions are so intense in metal powders that localized melting takes place at the point of impact. This melting improves the metal's reactivity, because it removes metallic-oxide coatings. (Such protective oxide coatings are found on most metals and are responsible for the patina on copper gutters and bronze sculpture.)

Since ultrasound improves the reactivity of metal powders, it also makes



CHEMISTRY OF ULTRASOUND can differ greatly from the chemistries of light and heat. The reactions of iron pentacarbonyl $\text{Fe}(\text{CO})_5$, an iron atom (green) bonded to five carbon monoxide units (gray and red), exemplify the differences. Heat decom-

poses iron pentacarbonyl into pure iron and carbon monoxide. Light yields two iron atoms bonded to nine carbon monoxide units. Ultrasound produces the cluster compound consisting of three iron atoms bonded to 12 carbon monoxide units.



INTERPARTICLE COLLISIONS driven by shock waves from cavity implosion cause particles to agglomerate. The collisions between particles of zinc (here magnified 13,000 diameters) were so violent that the zinc particles melted on impact.

them better catalysts. Many reactions require a catalyst in order to proceed at useful or even appreciable rates. Catalysts are not consumed by the reaction but instead speed the reaction of other substances.

The effects of ultrasound on particle morphology, surface composition and catalyst reactivity have been investigated by Dominick J. Casadonte and Stephen J. Doktycz in our laboratory. They have discovered that catalysts

such as nickel, copper and zinc powders irradiated with ultrasound show dramatic changes in surface morphology. Individual surfaces are smoothed and particles are consolidated into extended aggregates. An experiment to determine the surface composition of nickel revealed that its oxide coating was removed, greatly improving the reactivity of the nickel powder. Ultrasonic irradiation increased the effectiveness of nickel powder as a catalyst



METAL SURFACES can be physically altered by ultrasound. Before this sample of nickel powder was irradiated with ultrasound (left) it had an unreactive crystalline coating on its surface. After irradiation (right) the coating was gone, exposing the nickel and boosting its reactivity. Without the coating the nickel powder becomes an excellent catalyst for chemical reactions. The magnification is about 100 diameters.

more than 100,000 times. The nickel powder is as reactive as some special catalysts currently in use, yet it is nonflammable and less expensive.

Ultrasound is a useful tool in nearly every case where a liquid and a solid must react. Furthermore, since ultrasound can radiate through large volumes of liquid, it is well suited for industrial applications. For these reasons future applications of ultrasound in chemical reactions will be diverse. In the synthesis of pharmaceuticals, ultrasound will improve chemical yields over conventional methods.

The greatest advances in sonochemistry, however, may be in the production of new materials that have unusual properties. The extraordinary temperatures and pressures reached during cavitation, for example, may lead to the synthesis of refractory materials (such as carborundum, tungsten carbide and even diamond). Refractory solids have high temperature stability and enormous structural strength. They are important as industrial abrasives and hardened tool bits.

The extremely rapid cooling that follows cavity implosion may be employed to create metallic glasses. Such amorphous metals have outstanding corrosion resistance and unusually high strength.

Although chemical applications of ultrasound are still in the early stages of development, the next few years promise rapid progress in sonochemistry. The use of ultrasound in laboratory reactions is becoming commonplace, and the extension of the technology to industrial-scale reactions is likely to follow. Underlying these developing technologies are the recent advances in our understanding of the nature of cavitation and the chemical effects of ultrasound.

FURTHER READING

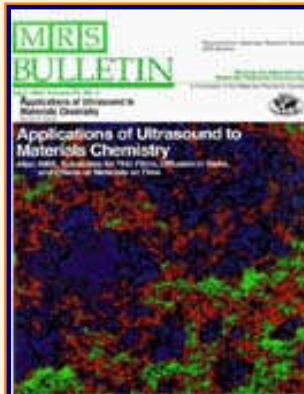
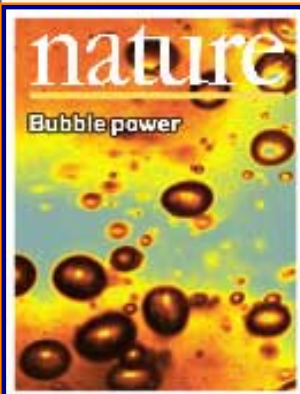
ULTRASOUND in Synthesis Kenneth S. Suslick in *Modem Synthetic Methods*, Vol. 4, pages 1-60; 1986.

SYNTHESIS WITH ULTRASONIC WAVES. Philip Boudjouk in *Journal of Chemical Education*, Vol. 63, No. 5, pages 427-429; May, 1986.

SONOLUMINESCENCE FROM NON-AQUEOUS Liquids. Kenneth S. Suslick and Edward B. Flint in *Nature*, Vol. 330, No. 6148, pages 553-555; December 10, 1987.

ULTRASOUND: ITS CHEMICAL, PHYSICAL AND BIOLOGICAL Effects. Edited by Kenneth S. Suslick VCH Publishers, 1988.

The Suslick Research Group



THE CHEMISTRY OF ULTRASOUND

by Kenneth S. Suslick

from *The Yearbook of Science & the Future* 1994;
Encyclopaedia Britannica: Chicago, 1994; pp 138-155.

[Overview](#)

[Outline of
Research Projects](#)

[Introduction to
Sonochemistry](#)

[Exec. Summary:
Sonochemistry](#)

[Exec. Summary:
Porphyrin Research](#)

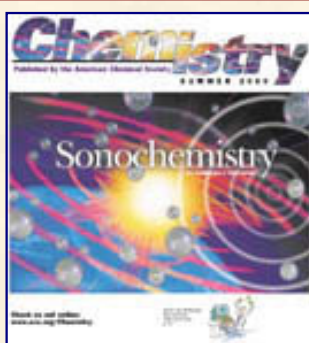
[Exec. Summary: Smell-
Seeing](#)

[Complete
Publication List](#)

[Abbreviated Curriculum
Vitae](#)

[Academic
Genealogy](#)

[Press
Clippings](#)



For a recent popular press account of our work, see "Sonochemistry" *Chemistry*, Summer 2000, pp. 3, 17-22.

Chemistry is a free quarterly magazine published by the American Chemical Society and distributed to its more than 160,000 members and student affiliates. [For other press clippings, click here.](#)

[For a listing of commercially available
sonochemical equipment, click here.](#)

Ultrasound can produce temperatures as high as those on the surface of the Sun and pressures as great as those at the bottom of the ocean. In some cases, it can also increase chemical reactivities by nearly a millionfold.

Ultrasound is simply sound pitched above human hearing. It has found many uses in many areas. At home, we use ultrasound for dog whistles, burglar alarms, and jewelry cleaners. In hospitals, doctors use ultrasound to remove kidney stones without surgery, to treat cartilage injuries (such as "tennis elbow"), and to image fetal development during pregnancy. In industry, ultrasound is important for emulsifying cosmetics and foods, welding plastics, cutting alloys, and large-scale cleaning. None of these applications, however, take advantage of the effects that ultrasound can have on chemical reactivity.

[Current Research
Funding](#)

[Excerpts from
Funded Research](#)

[Inventory of
Group Equipment](#)

[Information
for Visiting](#)

[Current Research Group
Members](#)

[Group
Meetings](#)

[Group
Chores](#)

[Past Research
Group Members](#)

[Group
Photogallery](#)

[Web Resources](#)

[Laboratory Safety
Resources](#)

[Art and Science:
Journal Covers](#)

[Sculpture &
Masks](#)

[A Chemist
Meets Hollywood](#)

[Chymistes: The Distillers
of Waters](#)

[A Chemist
In Court](#)

The chemical applications of ultrasound, "sonochemistry", has become an exciting new field of research during the past decade. The history of sonochemistry, however, begins in the late 1800s. During field tests of the first high-speed torpedo boats in 1894, Sir John I. Thornycroft and Sydney W. Barnaby discovered severe vibrations from and rapid erosion of the ship's propeller. They observed the formation of large bubbles (or cavities) formed on the spinning propeller and postulated that the formation and collapse of these bubbles were the source of their problems. By increasing the propeller size and reducing its rate of rotation, they could minimize this difficulty of "cavitation". As ship speeds increased, however, this became a serious concern and the Royal Navy commissioned Lord Rayleigh to investigate. He confirmed that the effects were due to the enormous turbulence, heat, and pressure produced when cavitation bubbles imploded on the propeller surface. In the same work, he explained that cavitation was also the origin of teakettle noise!

This phenomenon of cavitation occurs in liquids not only during turbulent flow but also under high-intensity ultrasonic irradiation. It is responsible for both propeller erosion and for the chemical consequences of ultrasound. Alfred L. Loomis noticed the first chemical effects of ultrasound in 1927, but the field of sonochemistry lay fallow for nearly 60 years. The renaissance of sonochemistry occurred in the 1980's, soon after the advent of inexpensive and reliable laboratory generators of high-intensity ultrasound.

Scientists now know that the chemical effects of ultrasound are diverse and include substantial improvements in both stoichiometric and catalytic chemical reactions. In some cases, ultrasonic irradiation can increase reactivities by nearly a millionfold. The chemical effects of ultrasound fall into three areas: homogeneous sonochemistry of liquids, heterogeneous sonochemistry of liquid-liquid or liquid-solid systems, and sonocatalysis (which overlaps the first two). Because cavitation can take place only in liquids, chemical reactions do not generally occur during the ultrasonic irradiation of solids or solid-gas systems.

[Humor and
Wisdom](#)

[Laws of the Universe](#)

[Cartoons of Humor and
Wisdom](#)

[Chem 115: Chemistry of
Everyday Phenomena](#)

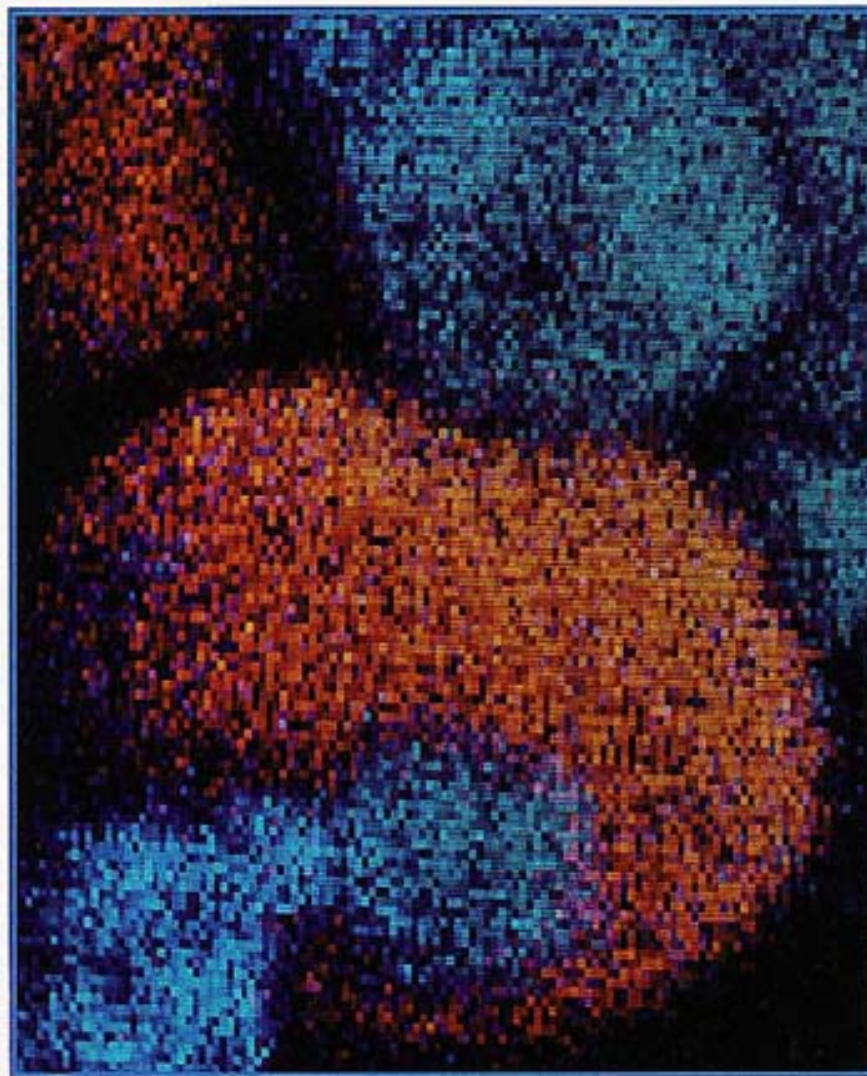
[Chem 315: Inorganic
Chemistry](#)

AMERICAN
ASSOCIATION FOR THE
ADVANCEMENT OF
SCIENCE

SCIENCE

23 MARCH 1990
VOL. 247 ■ PAGES 1373-1520
PART I

\$3.50



Frontpiece. This micrograph shows interparticle collisions induced by ultrasound between tin and iron particles about 20 microns in size. The velocity of such collisions can be as high as 500 m/s (1100 mph). The elemental composition dot map was produced by scanning Auger electron spectroscopy and show tin in orange and iron in blue.

Ultrasonic irradiation differs from traditional energy sources (such as heat, light, or ionizing radiation) in duration, pressure, and energy per molecule (Figure 1). Because of the immense temperatures and pressures and the extraordinary heating and cooling rates generated by cavitation bubble collapse, ultrasound provides an unusual mechanism for generating high-energy chemistry. As in photochemistry, very large amounts of energy

are introduced in a short period of time, but it is thermal rather than electronic excitation. High thermal temperatures are reached. Furthermore, sonochemistry has a high-pressure component, which suggests that it might be possible to produce on a microscopic scale the same large-scale conditions produced during explosions or by shock waves (a shock wave is a compressional wave formed whenever the speed of a body or fluid relative to a medium exceeds that at which the medium can transmit sound).

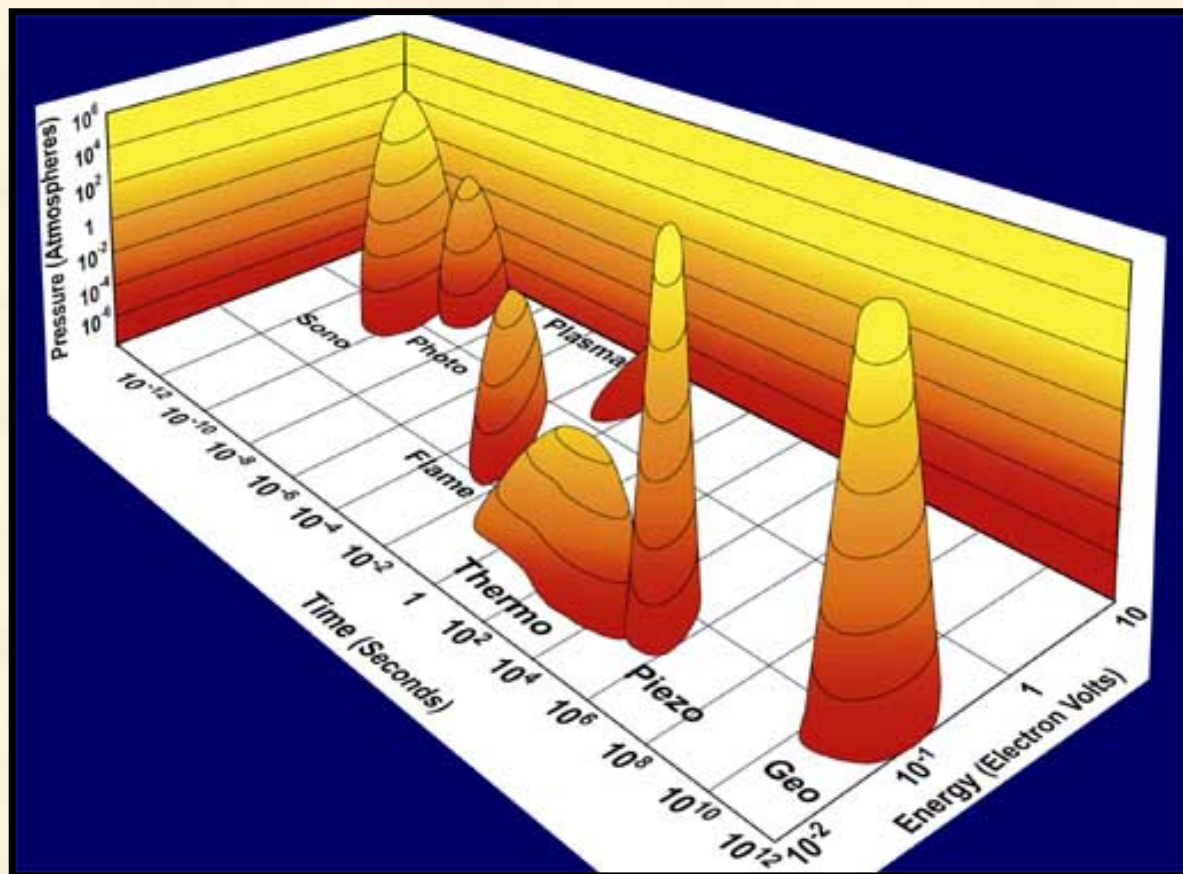


Figure 1. Chemistry: the interaction of energy and matter. The three axes represent duration of the interaction, pressure, and energy per molecule. The labeled islands represent the nature of the interaction of energy and matter in various different kinds of chemistry.

Sound, Ultrasound, and Cavitation

Sound is nothing more than waves of compression and expansion passing through gases, liquids or solids. We can sense these waves directly through our ears if they have frequencies from about Hertz to 16 kHz (the Hertz unit is cycles of compression or expansion per second; kiloHertz, abbreviated kHz, is thousands of cycles per second). These frequencies are similar to low frequency radio waves, but sound is intrinsically different from radio or other electromagnetic radiation. For example, electromagnetic radiation (radio waves, infrared, visible light, ultraviolet, x-rays, gamma rays) can pass through a vacuum without difficulty; on the other hand, sound cannot because the compression and expansion waves of sound must be contained in some form of matter.

High intensity sound and ultrasound are generally produced in a similar fashion: electric energy is used to cause the motion of a solid surface, such as a speaker coil or a piezoelectric ceramic. Piezoelectric materials expand and contract when an electric field is applied. For ultrasound a high frequency alternating electric current is applied to a piezoelectric attached to the wall of a metal container (as in an ultrasonic cleaning bath of the kind used, for example, by jewelers) (Figure 2).

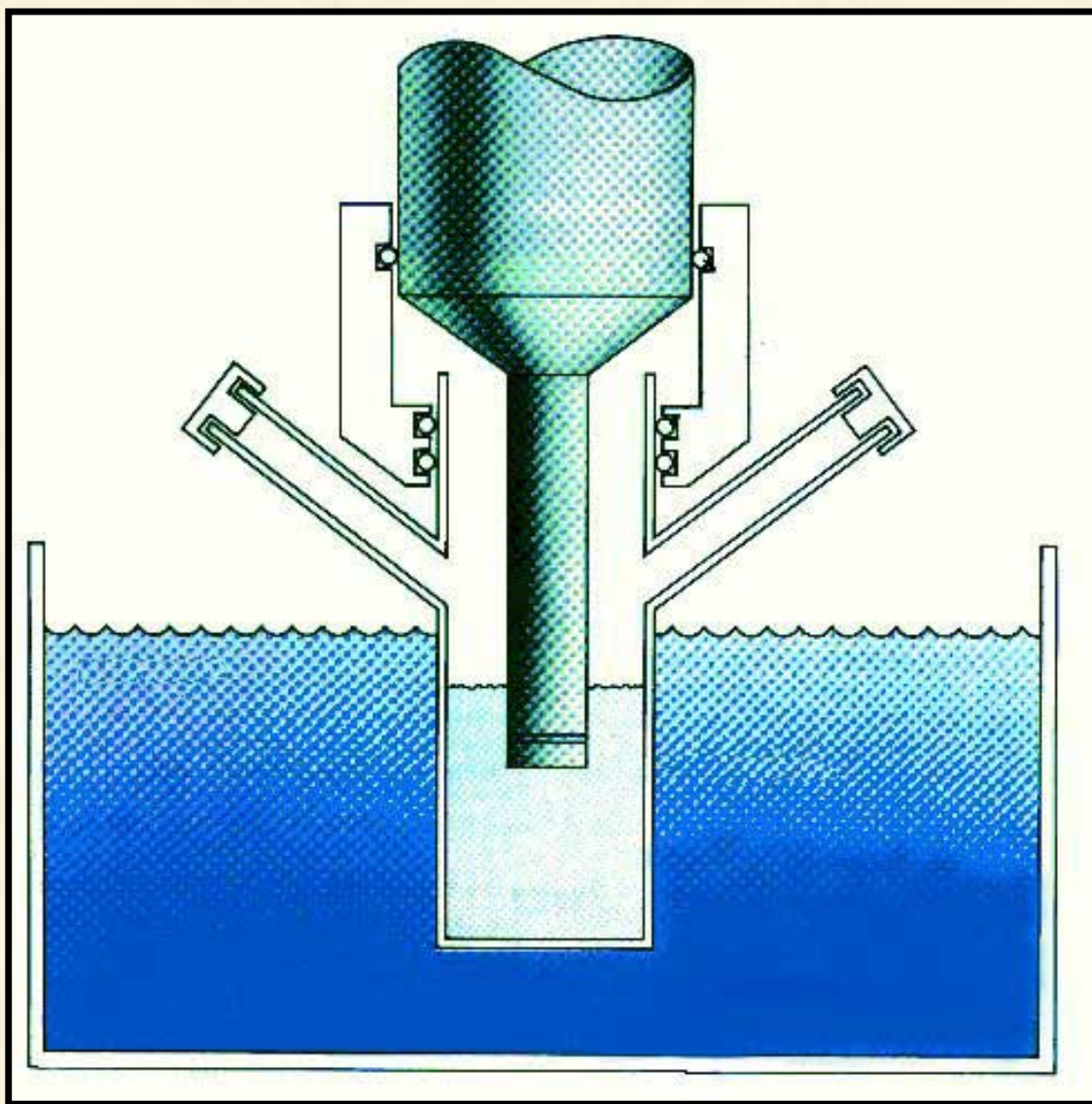


Figure 2. Diagram shows a typical sonochemical apparatus. Ultrasound can easily be introduced into a chemical reaction in which there is good control of temperature and ambient atmosphere. The titanium rod shown immersed in the reaction liquid is driven into vibration by a piezoelectric, which vibrates when subjected to an alternating current electric field. The usual piezoelectric ceramic is PZT, a lead zirconate titanate material.

Ultrasound has frequencies pitched above human hearing (above roughly 16 kHz). Scientists can make narrow beams of "silent" ultrasound far more intense than the roar of a jet engine, but completely unheard by our ears. Ultrasound has wavelengths between succession compression waves measuring roughly 10 cm to 10^{-3} centimeters. These are not comparable to molecular dimensions. Because of this mismatch, the chemical effects of ultrasound cannot result from a direct interaction of sound with molecular species.

Nonetheless, the ultrasonic irradiation of liquids does produce a plethora of high energy chemical reactions. This occurs because ultrasound causes other physical phenomena in liquids that create the conditions necessary to drive chemical reactions. The most important of these is cavitation: the formation, growth, and implosive collapse of bubbles in a liquid. The dynamics of cavity growth and collapse are strikingly dependent on the local environment. Cavity collapse in a homogeneous liquid is very different from cavitation near a liquid-solid interface, which will be considered later.

As ultrasound passes through a liquid, the expansion cycles exert negative pressure on the liquid, pulling the molecules away from one another. If the ultrasound is sufficiently intense, the expansion cycle can create cavities in the liquid. This will occur when the negative pressure exceeds the local tensile strength of the liquid, which varies according to the type and purity of liquid. (Tensile strength is the maximum stress that a material can withstand from a stretching load without tearing.) Normally, cavitation is a nucleated process; that is, it occurs at pre-existing weak points in the liquid, such as gas-filled crevices in suspended particulate matter or transient microbubbles from prior cavitation events. Most liquids are sufficiently contaminated by small particles that cavitation can be readily initiated at moderate negative pressures.

Once formed, small gas bubbles irradiated with ultrasound will absorb energy from the sound waves and grow. Cavity growth depends on the intensity of the sound. At high intensities, a small cavity may grow rapidly through inertial effects. If cavity expansion is sufficiently rapid during the expansion half of a single cycle, it will not have time to recompress during the compression half of the acoustic cycle.

At lower acoustic intensities cavity growth can also occur by a slower process called rectified diffusion (Figure 3). Under these conditions a cavity will oscillate in size over many expansion and compression cycles. During such oscillations the amount of gas or vapor that diffuses in or out of the cavity depends on the surface area, which is slightly larger during expansion than during compression. Cavity growth during each expansion is, therefore, slightly larger than shrinkage during the compression. Thus, over many acoustic cycles, the cavity will grow. The growing cavity can eventually reach a critical size where it can efficiently absorb energy from the ultrasonic irradiation. Called the resonant size, this critical size depends on the liquid and the frequency of sound; at 20 kHz, for example, it is roughly 170 micrometers. At this point the cavity can grow rapidly during a single cycle of sound.

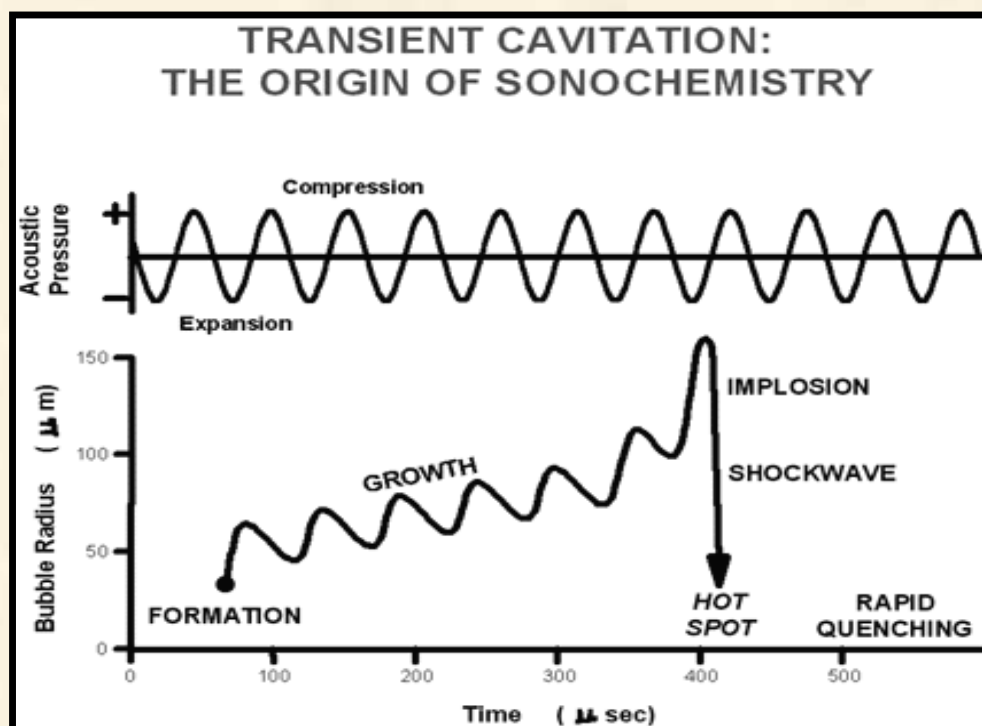
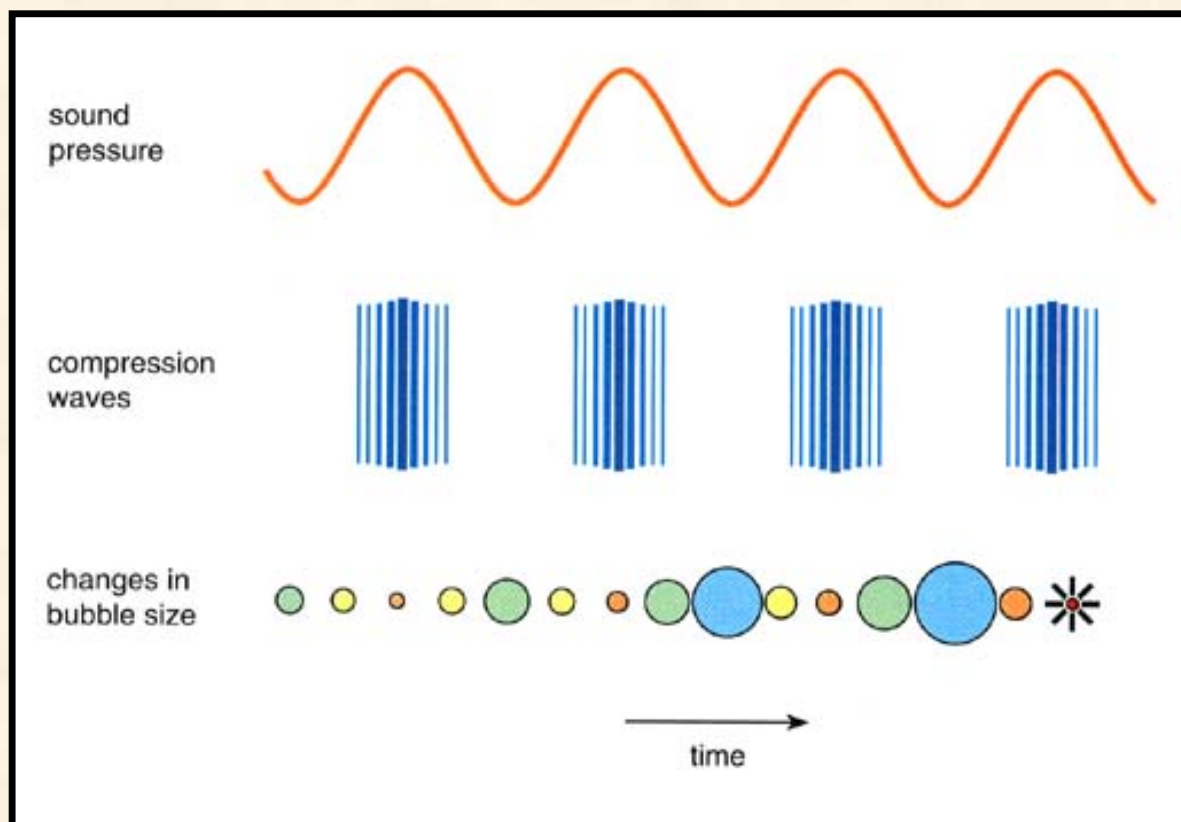


Figure 3. Liquids irradiated with ultrasound can produce bubbles. These bubbles oscillate, growing a little more during the expansion phase of the sound wave than they shrink during the compression phase. Under the proper conditions these bubbles can undergo a violent collapse, which generates very high pressures and temperatures. This process is called cavitation.

Once the cavity has overgrown, either at high or low sonic intensities, it can no longer absorb energy as efficiently. Without the energy input the cavity can no longer sustain itself. The surrounding liquid rushes in, and the cavity implodes. It is the implosion of the

cavity that creates an unusual environment for chemical reactions.

The Sonochemical Hot-Spot

Compression of a gas generates heat. On a macroscopic scale, one can feel this when pumping a bicycle tire; the mechanical energy of pumping is converted into heat as the tire is pressurized. The compression of cavities when they implode in irradiated liquids is so rapid that little heat can escape from the cavity during collapse. The surrounding liquid, however, is still cold and will quickly quench the heated cavity. Thus, one generates a short-lived, localized hot spot in an otherwise cold liquid. Such a hot spot is the source of homogeneous sonochemistry; it has a temperature of roughly 5000°C ($9,000^{\circ}\text{F}$), a pressure of about 1000 atmospheres, a lifetime considerably less than a microsecond, and heating and cooling rates above 10 billion $^{\circ}\text{C}$ per second. For a rough comparison, these are, respectively, the temperature of the surface of the sun, the pressure at the bottom of the ocean, the lifetime of a lightning strike, and a million times faster cooling than a red hot iron rod plunged into water! Thus, cavitation serves as a means of concentrating the diffuse energy of sound into a chemically useful form. Alternative mechanisms involving electrical microdischarge have been proposed (most recently by M.A. Margulis of the Russian Institute for Organic Synthesis), but they do not appear fully consistent with observed data.

Determination of the temperatures reached in a cavitating bubble has remained a difficult experimental problem. The transient nature of the cavitation event precludes direct measurement of the conditions generated during bubble collapse. Chemical reactions themselves, however, can be used to probe reaction conditions. The effective temperature of a system can be determined with the use of competing unimolecular reactions whose rate dependencies on temperature have already been measured. This technique of "comparative-rate chemical thermometry" was used by K.S. Suslick, D.A. Hammerton and R.E. Cline, Jr., at the University of Illinois to determine the effective temperature reached during cavity collapse. For a series of organometallic reactions, the relative sonochemical rates were measured. In combination with the known temperature behavior of these reactions, the conditions present during cavity collapse could then be determined. The effective temperature of these hot spots was 5,200 K. Of course, the comparative rate data represent only a composite temperature: during the collapse, the temperature has a highly dynamic profile, as well as a spatial gradient in the surrounding liquid.

When a liquid is subjected to ultrasound, not only does chemistry occur, but light is also produced (Figure 4). Such "sonoluminescence" provides an alternate measure of the temperature of the high-energy species produced during cavitation. High-resolution sonoluminescence spectra were recently reported and analyzed by E.B. Flint and Suslick. From a comparison of synthetic to observed spectra, the effective cavitation temperature of the emitting species is 5,100 K. The agreement between this spectroscopic determination of the cavitation temperature and that made by comparative rate thermometry of sonochemical reactions is surprisingly close.

AMERICAN
ASSOCIATION FOR THE
ADVANCEMENT OF
SCIENCE

SCIENCE

20 SEPTEMBER 1991
VOL. 253 ■ PAGES 1325-1456

\$6.00

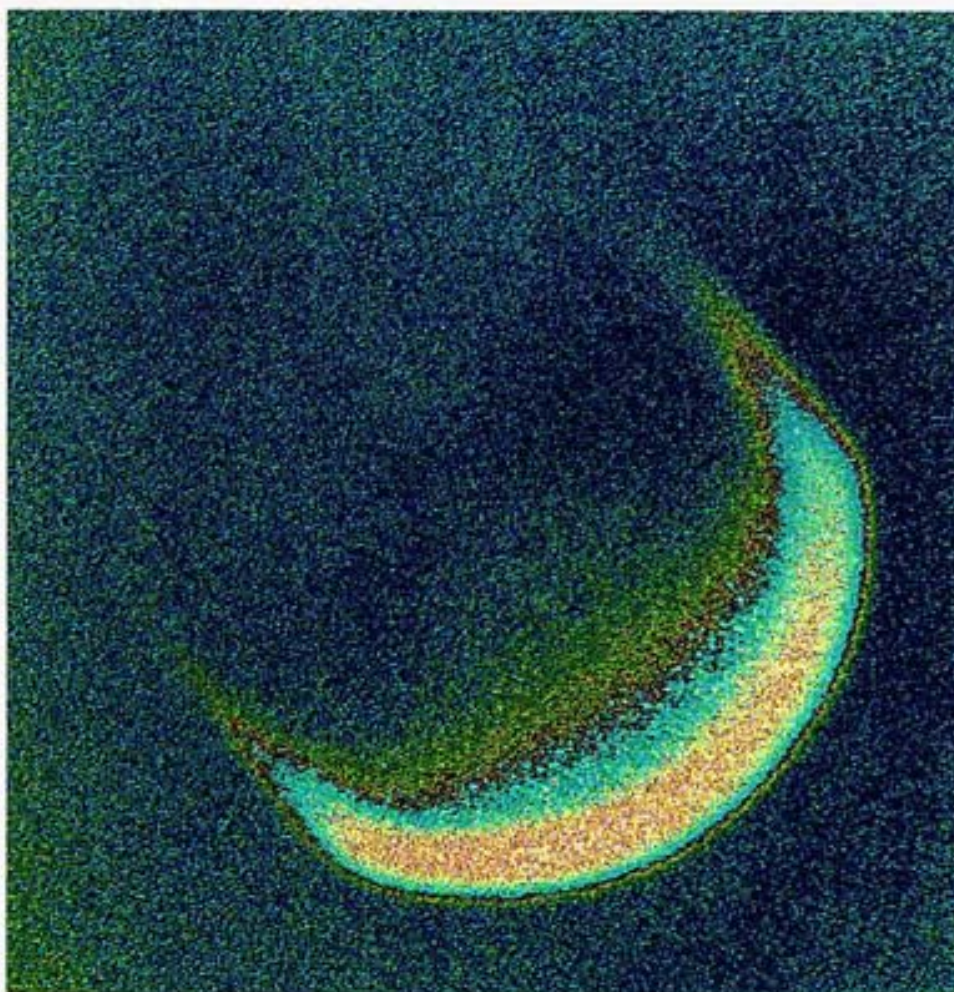


Figure 4. High intensity ultrasound creates localized hot spots in liquids through the process of cavitation. Local heating produces excited states of molecules that emit light, just as they do in a flame. The image shown is such sonoluminescence seen from a vibrating titanium rod (about 0.4 inch) in diameter. False color is used to enhance contrast. The temperature created in cavitation hot-spots, determined from the spectrum of this emission, is ~ 5000 K.

Cavitation in Liquid-Solid Systems

When cavitation occurs in a liquid near a solid surface, the dynamics of cavity collapse changes dramatically. In pure liquids, the cavity remains spherical during collapse because its surroundings are uniform. Close to a solid boundary, however, cavity collapse is very asymmetric and generates high-speed jets of liquid (Figure 5). The potential energy of the expanded bubble is converted into kinetic energy of a liquid jet that moves through the bubble's interior and penetrates the opposite bubble wall. Werner Lauterborn at the Technische Hochschule in Darmstadt, Germany, observed liquid jets driving into the surface with velocities of roughly 400 kilometers/hour (Figure 6). These jets hit the surface with tremendous force. This process can cause severe damage at the point of impact and can produce newly exposed, highly reactive surfaces; it has great importance for understanding the corrosion and erosion of metals observed in propellers, turbines, and pumps where cavitation is a continual technological problem.



Figure 5. A bubble in a liquid irradiated with ultrasound implodes near a solid surface. The presence of the solid causes the implosion to be asymmetrical, forming a high-speed jet of liquid that impacts the surface. The cavity is spherical at first, but as it collapses the

jet develops opposite the solid surface and moves towards it. (L.A. Crum)

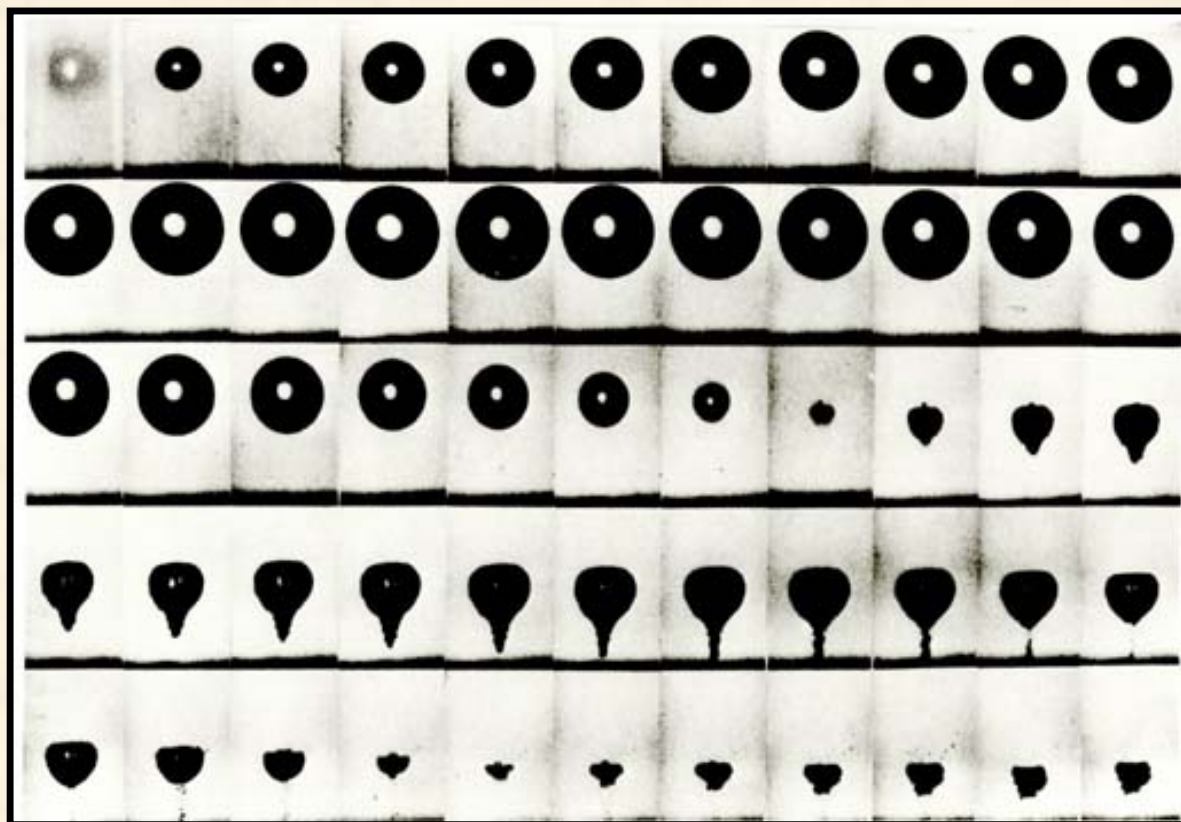


Figure 6. High-speed microcinematographic sequence of laser-induced cavitation near a solid surface shows the formation of a microjet impact with a velocity of approximately 400 kilometers (250 miles) per hour. (W. Lauterborn)

Distortions of bubble collapse depend on a surface several times larger than the resonant size of the bubble. The presence of fine powders, therefore, does not induce jet formation. In the case of liquid-powder slurries, the shock waves created by homogeneous cavitation can create high-velocity interparticle collisions. The turbulent flow and shock waves produced by intense ultrasound can drive metal particles together at sufficiently high speeds to cause effective melting at the point of collision (Figure 7). Such interparticle collisions are capable of inducing striking changes in surface texture, composition, and reactivity, as discussed later.

S. J. Doktycz and K. S. Suslick used metal powders to estimate the effective maximum temperatures and speeds reached during interparticle collisions (Figure 8). When chromium, molybdenum, and tungsten powders of a few micrometers in size are irradiated in decane at 20 kHz and 50 watts per square centimeter, one observes agglomeration and welding of particles for the first two metals but not for the third. On the basis of the melting points of these metals, the effective transient temperature reached at the point of impact during interparticle collisions is roughly 3000° C. On the basis of the volume of the melted region of impact, the amount of energy generated during collision was determined. From this, the velocity of impact is estimated to be roughly 1800 kilometers per hour, which is half the speed of sound in liquids. It should be noted that the

conditions reached during interparticle collisions are not directly related to the temperatures reached during cavitation collapse of bubbles.

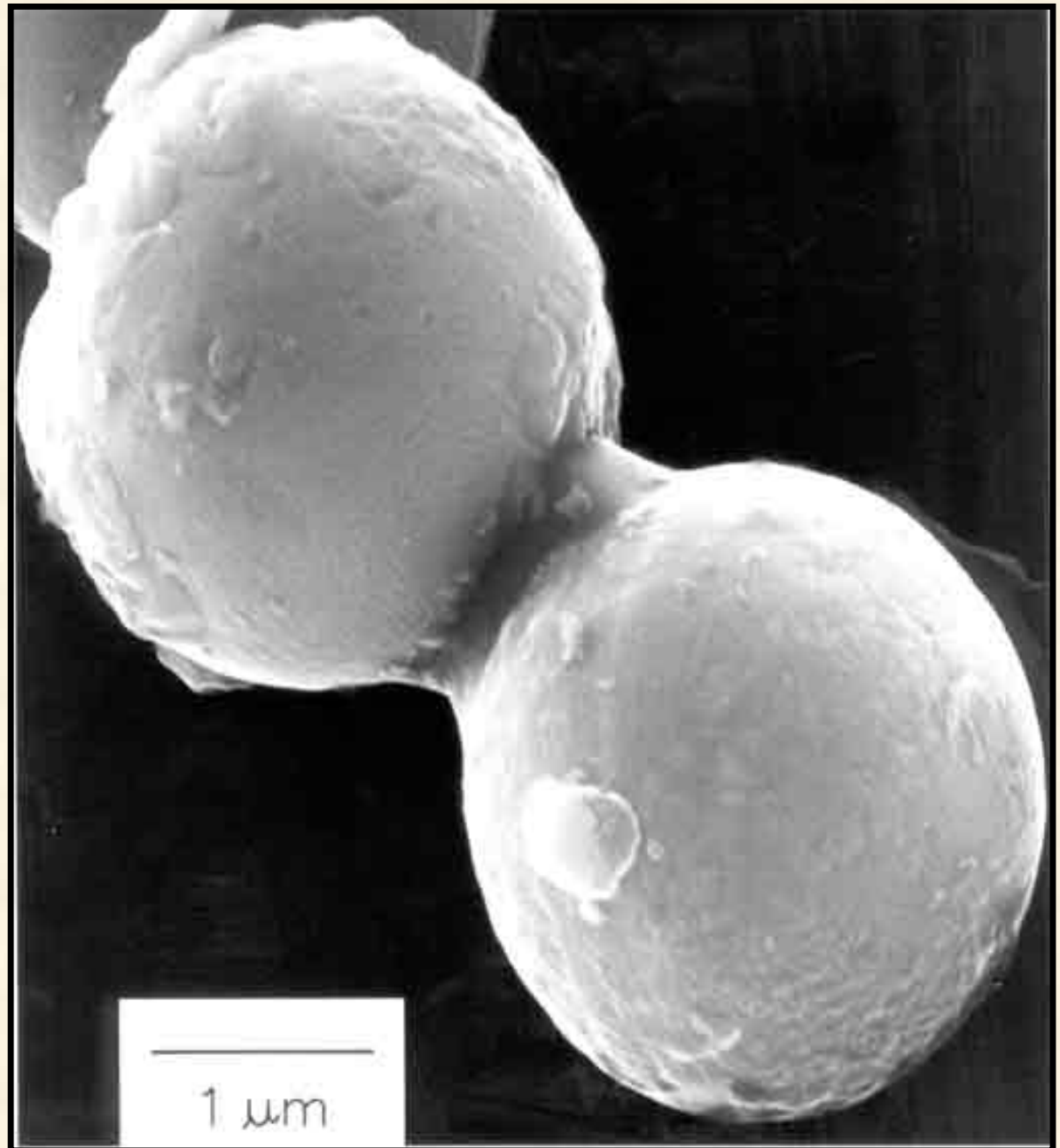


Figure 7. Scanning electron micrograph reveals zinc powder after ultrasonic irradiation. The neck formation from localized melting or plastic deformation was caused by high-velocity collisions of the zinc particles.

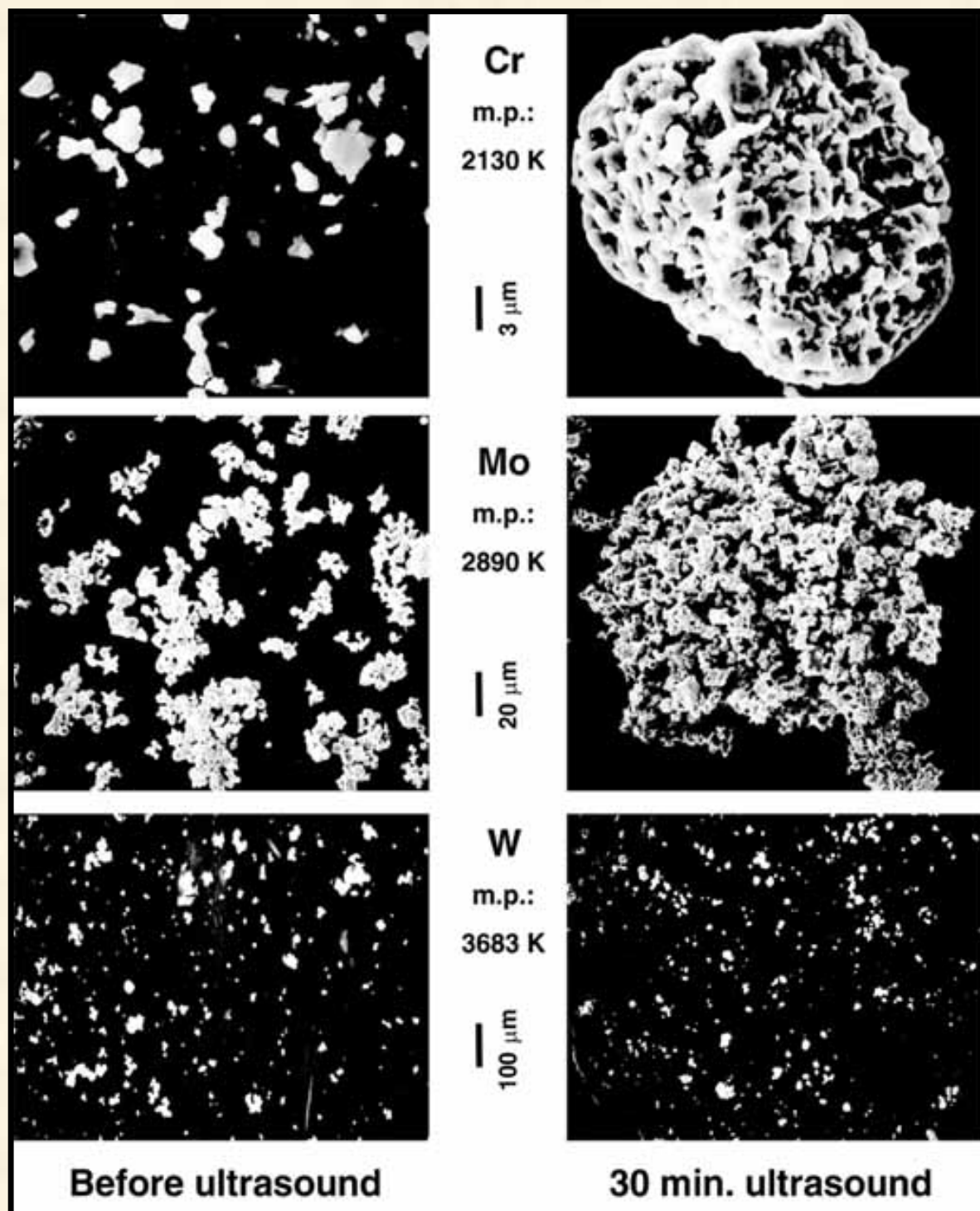


Figure 8. Scanning electron micrographs reveal slurries of metal powders both before and after ultrasonic irradiation. Chromium has a melting point of 1857° C (3,374.6° F), and its particles both agglomerate and are deformed; molybdenum melts at 2617° C (4,742.6° F), and its particles are slightly agglomerated but not smoothed or deformed; tungsten melts at 3410° C (6,170° F) and is unaffected.

Sonochemistry in Homogeneous Liquids

High-intensity ultrasonic probes (10 to 500 watts per square centimeter) are the most reliable and effective sources for laboratory-scale sonochemistry. A typical laboratory apparatus permits easy control over ambient temperature and atmosphere (Figure 2). Lower acoustic intensities can often be used in liquid-solid heterogeneous systems because of the reduced liquid tensile strength at the liquid-solid interface. For such reactions a common ultrasonic cleaning bath will often be adequate. The low intensity available in these devices (about one watt per square centimeter) can, however, prove to be a limitation. On the other hand, ultrasonic cleaning baths are easily accessible, comparatively inexpensive, and usable on moderately large scales. Finally, for large-scale irradiations, flow reactors with high ultrasonic intensities are commercially available in modular units as powerful as 20 kilowatts.

The chemical effect of ultrasound on aqueous solutions have been studied for many years. The primary products are molecular hydrogen (H_2) and hydrogen peroxide (H_2O_2). Other high-energy intermediates may include HO_2 (superoxide), $H\bullet$ (atomic hydrogen), $OH\bullet$ (hydroxyl), and $e^-_{(aq)}$ (solvated electrons). Peter Riesz and collaborators at the National Institutes of Health used electron paramagnetic resonance with chemical spin-traps to demonstrate definitively the generation of $H\bullet$ and $OH\bullet$. The extensive recent work in Arne Henglein's laboratory at the Hahn-Meitner Institute involving aqueous sonochemistry of dissolved gases has established analogies to combustion processes. As one would expect, the sonolysis of water, which produces both strong reductants and oxidants, is capable of causing secondary oxidation and reduction reactions, as often observed by Margulis and coworkers.

In contrast, the ultrasonic irradiation of organic liquids has been little studied. Suslick and co-workers established that, as long as the total vapor pressure is low enough to allow effective bubble collapse, almost all organic liquids will generate free radicals (uncharged, reactive intermediates possessing an unpaired electron) when they undergo ultrasonic irradiation. The sonolysis of simple hydrocarbons creates the same kinds of products associated with very high temperature pyrolysis. Most of these products - H_2 , CH_4 (methane), and the smaller 1-alkenes, derive from a well-understood radical chain mechanism. Relatively large amounts of acetylene (C_2H_2) are also produced, which is explained by the stability of this gas at very high temperatures.

The sonochemistry of solutes dissolved in organic liquids also remains largely unexplored, though that of metal carbonyl compounds is an exception. In 1981, P. F. Schubert, J. W. Goodale and Suslick reported the first sonochemistry of discrete organometallic complexes and demonstrated the effects of ultrasound on metal carbonyls. Detailed studies of these systems led to important understandings of the nature of sonochemistry. Unusual reactivity patterns have been observed during ultrasonic irradiation, including novel metal cluster formation and the initiation of homogeneous catalysis at low ambient temperature, with rate enhancements greater than 100,000-fold.

Polymers and Biomaterials: Bond Making and Breaking

The effects of ultrasound on polymers (giant molecules formed by the coupling of small molecules-monomers) have been thoroughly studied over the past 30 years. The controlled cleavage of polymers in solutions irradiated with ultrasound has been examined in detail. Polymer degradation produces chains of smaller lengths with relatively uniform molecular weight distributions, with cleavage occurring primarily in the center of the polymer chain. Several mechanisms have been proposed for this sonochemical cleavage, which is usually described as a mechanical breakage of the chains induced by shock

waves or solvent flow created by cavitation during the ultrasonic irradiation of liquids.

This polymer fragmentation has been used by G. J. Price at the University of Bath to synthesize block copolymers of various sorts. Block copolymers are long chain polymers with two different, but linked, parts. As an analogy, imagine a train made up in front by passenger cars and in back by freight cars. In this fashion, block copolymers can do double-duty in their properties. Peter Kruus at Carleton University, Ottawa, reported the use of ultrasound to initiate polymerization in solutions of various monomers.

Applications of ultrasound to the synthesis of biomaterials are under rapid development. While the chemical effects of ultrasound on aqueous solutions have been studied for many years, the development of aqueous sonochemistry for biomaterials synthesis is very recent. The area of protein microencapsulation has proved especially interesting. Microencapsulation, the enclosing of materials in capsules a few micrometers in size, has diverse important applications; these include uses with dyes, flavors and fragrances, as drug delivery systems, and as medical diagnostic agents.

One recent example is the use of high intensity ultrasound to make aqueous suspensions of long-lived proteinaceous microspheres filled with air or with water-insoluble liquids for medical applications (Figure 9). By itself, emulsification is insufficient to produce these long-lived microspheres; chemical reactions requiring oxygen are critical in forming them. Specifically, the sonolysis of water produces hydrogen atoms that react with oxygen to produce superoxide. Suslick and M. W. Grinstaff demonstrated that the proteinaceous microspheres are held together by disulfide bonds between protein cysteine residues and that superoxide is the cross-linking agent.

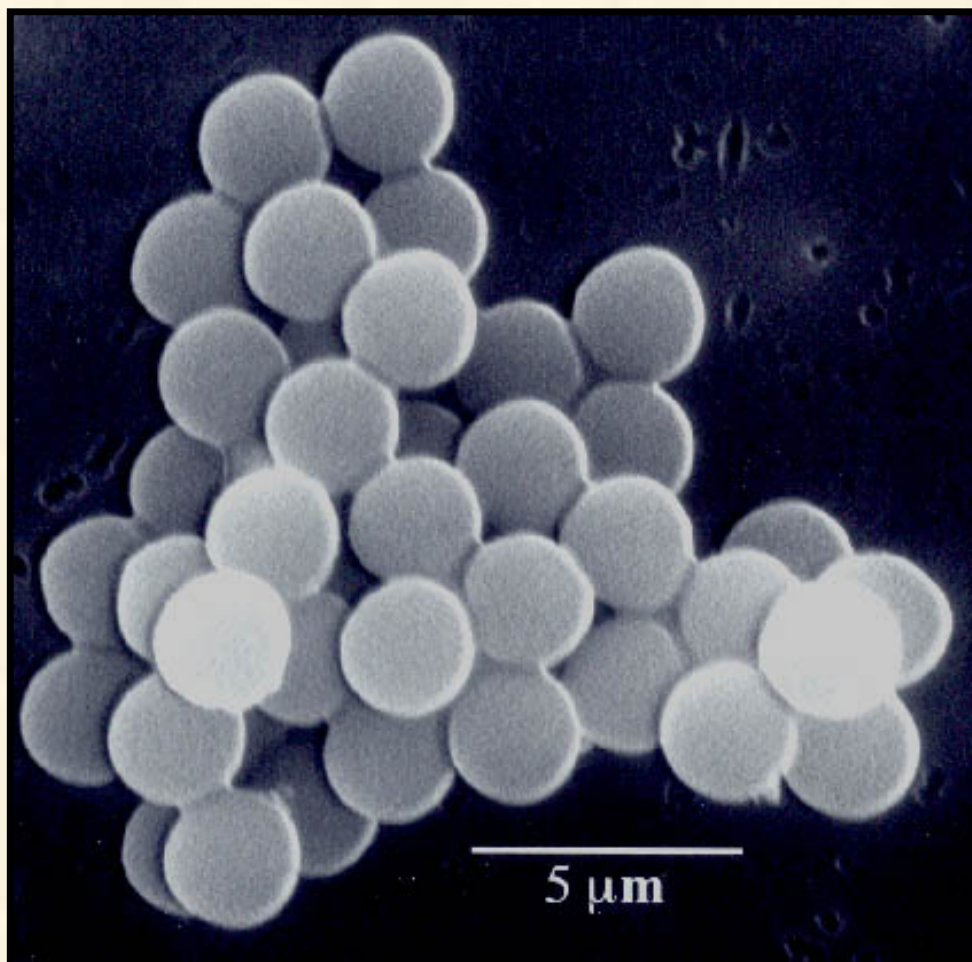


Figure 9. Protein microspheres filled with the oily hydrocarbon dodecane were formed by the ultrasonic irradiation of albumin solutions. Such microspheres may prove useful for drug delivery and medical diagnostic imaging.

Sonoluminescence: Microscopic Thunder and Lightning

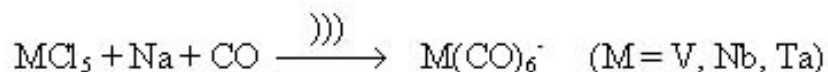
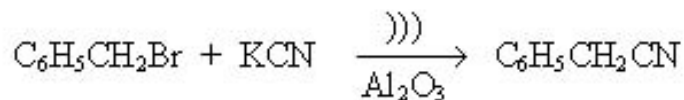
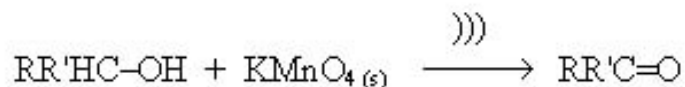
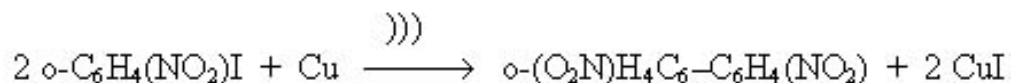
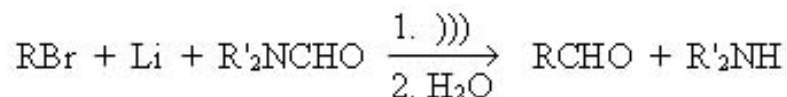
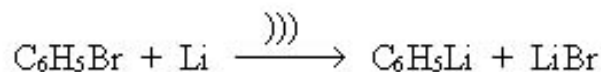
A few years after the discovery of sonochemical reactions, H. Frenzel and H. Schultes in 1934 first observed sonoluminescence from water. As with sonochemistry, sonoluminescence derives from acoustic cavitation. Although sonoluminescence from aqueous solutions has been studied in some detail, only recently has significant work been reported on sonoluminescence from non-aqueous liquids containing no water. In both cases, the emission of light comes from the high temperature formation of reactive chemical species in electronic excited states. The emitted light from these excited states provides a spectroscopic probe of the cavitation event.

High resolution sonoluminescence spectra from hydrocarbons and silicone oil were recently analyzed by Flint and Suslick. The observed emission comes from excited state diatomic carbon which are the same transitions responsible for the blue color of a hydrocarbon flame (from the kitchen stove, for example). The details of this emission depend on the temperature of the emitted C_2 and can be accurately modeled with synthetic spectra as a function of presumed temperature. From a comparison of synthetic to observed spectra, the average effective temperature of the excited state of C_2 is about 5,100 K, as mentioned above.

Recently, it was discovered that sonoluminescence can be observed, quite remarkably, in a single, oscillating gas bubble. In 1990 E. Gaitan and L. A. Crum at the University of Mississippi discovered conditions under which a single, stable gas bubble could produce sonoluminescent emission on each acoustic cycle, and continue this process essentially indefinitely. Seth J. Putterman at the University of California Los Angeles examined these bubbles with a time resolution in picoseconds. Gaitain, Crum, and Putterman were able to use sophisticated light scattering techniques to measure the radius-time curve of the luminescing bubble and to correlate the optical emissions with a particular phase of the sound field. As expected, the emissions occurred during cavity collapse. Quite surprisingly, the duration of the sonoluminescence emissions was less than a hundred picoseconds, roughly one millionth the duration of the acoustic cycle used. This very short emission appears to originate from the formation of shock waves within the collapsing bubble during the first stages of compression.

Heterogeneous Sonochemistry: Reactions of Solids with Liquids

The use of high-intensity ultrasound to enhance the reactivity of metals as stoichiometric reagents has become an important synthetic technique for many heterogeneous organic and organometallic reactions, especially those involving reactive metals, such as magnesium, lithium, and zinc. This development originated from the early work of Pierre Renaud in France in the 1950's and the more recent breakthroughs of J.-L. Luche at the University of Grenoble, France. This application of sonochemistry grew rapidly during the past decade in a large number of laboratories across the world. The effects are quite general and apply to reactive inorganic salts as well. Reactivity rate enhancements of more than 10-fold are common, yields are often substantially improved, and by-products avoided. A few simple examples of the sonochemistry of reactive reagents are shown below (where))) indicates ultrasonic irradiation), taken from the work of Takashi Ando, Philip Boudjouk, Luche, Timothy J. Mason, and Suslick, among others.



The mechanism of the rate enhancements in reactions of metals has been unveiled by monitoring the effect of ultrasonic irradiation on the kinetics of the chemical reactivity of the solids, examining the effects of irradiation on surface structure and size distributions of powders and solids, and, determining depth profiles of the surface elemental composition. The power of this three-pronged approach has been proved in studies of the sonochemistry of transition metal powders. Doktycz and Suslick found that ultrasonic irradiation of liquids nickel, zinc, and copper powders leads to dramatic changes in structure. The high-velocity interparticle collisions produced in such slurries cause smoothing of individual particles (Figure 10) and agglomeration of particles into extended aggregates (Figure 8). Surface composition was probed by Auger electron spectroscopy and mass spectrometry to generate depth profiles of these powders; they revealed that ultrasonic irradiation effectively removed the inactive surface oxide coating. The removal of such passivating coatings dramatically improves reaction rates.

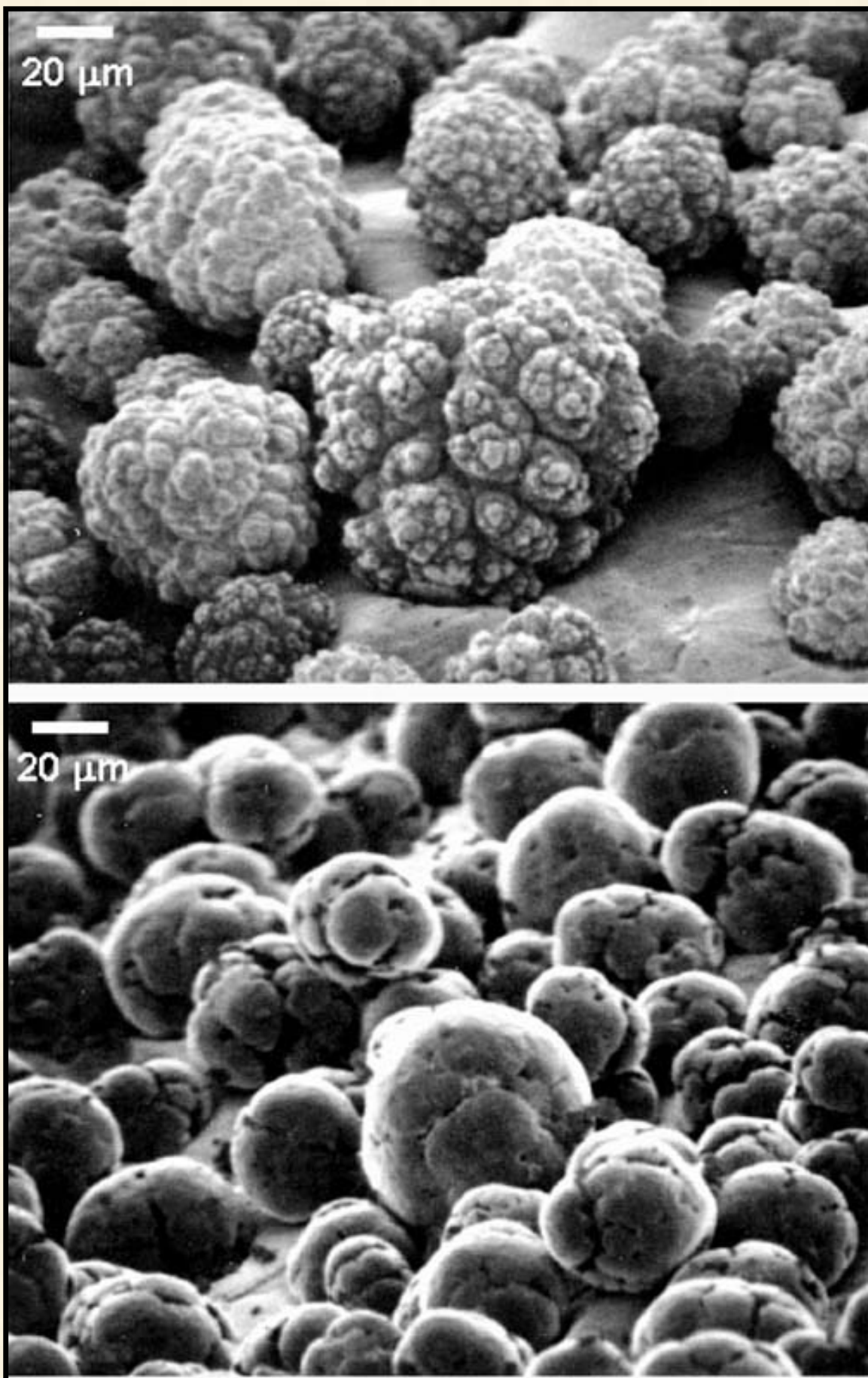


Figure 10. The effect of ultrasonic irradiation on the surface texture of nickel powder. High-velocity interparticle collisions caused by ultrasonic irradiation of slurries is responsible for these

effects.

Considerably less work has been done on the activation of less reactive metals. This goal continues to attract major efforts in both synthetic organometallic chemistry and heterogeneous catalysis. Ultrasound can be used at room temperature and pressure to promote heterogeneous reactions that normally occur only under extreme conditions of hundreds of atmospheres and hundreds of degrees. For example, R. E. Johnson and Suslick found good results with the use of ultrasound to drive some of the most difficult reactions known for transition metals: the attack of carbon monoxide on the very unreactive early transition metals such as vanadium, tantalum, molybdenum and tungsten.

Another application of ultrasound in materials chemistry involves the process of intercalation, which is the adsorption of organic or inorganic compounds as guest molecules between the atomic sheets of layered solid hosts, such as graphite or molybdenum sulfide. Intercalation permits the systematic change of optical, electronic, and catalytic properties. Such materials have many technological applications (for example, lithium batteries, hydrodesulfurization catalysts, and solid lubricants). The kinetics of intercalation, however, are generally extremely slow, and syntheses usually require high temperatures and very long reaction times. M.L.H. Green at University of Oxford, Suslick and their students discovered that high-intensity ultrasound dramatically increases the rates of intercalation of a wide range of compounds (including amines, metallocenes, and metal sulfur clusters) into various layered inorganic solids such as ZrS_2 , V_2O_5 , TaS_2 , MoS_2 , and MoO_3 . Scanning electron microscopy of the layered solids in conjunction with studies of chemical kinetics demonstrated that the origin of the observed rate enhancements comes from particle fragmentation (which dramatically increases surface areas), and to a lesser extent from surface damage. Because high-intensity ultrasound can rapidly form uniform dispersions of micrometer-sized powders of brittle materials, it is useful for a wide range of liquid-solid reactions.

Another application of heterogeneous sonochemistry involves the preparation of amorphous metals. If one can cool a molten metal alloy quickly enough, it can be frozen into a solid before it has a chance to crystallize. Such amorphous metallic alloys lack long range crystalline order and have unique electronic, magnetic, and corrosion resistant properties. The production of amorphous metals, however, is difficult because extremely rapid cooling of molten metals is necessary to prevent crystallization. Cooling rates of approximately 10^6 K per second are required; for comparison, plunging red hot steel into water produces cooling at only about 2500 K per second. Very recently, the use of ultrasound to synthesize amorphous metal powders by using the sonochemical decomposition of volatile organometallics was reported by Suslick, S.-B. Choe, A. A. Cichowlas, and M. W. Grinstaff. This exciting discovery opens new applications of ultrasound for the low temperature synthesis of unusual phases. For example, the sonolysis of iron pentacarbonyl produces nearly pure amorphous iron, which was characterized by a variety of techniques to prove its lack of long-range order. Scanning electron micrographs show conchoidal fractures (those with smoothly curved surfaces, which are typical of an amorphous material), and at higher magnification reveals a coral-like porosity coming from the agglomeration of small clusters of iron (Figures 11 and 12).

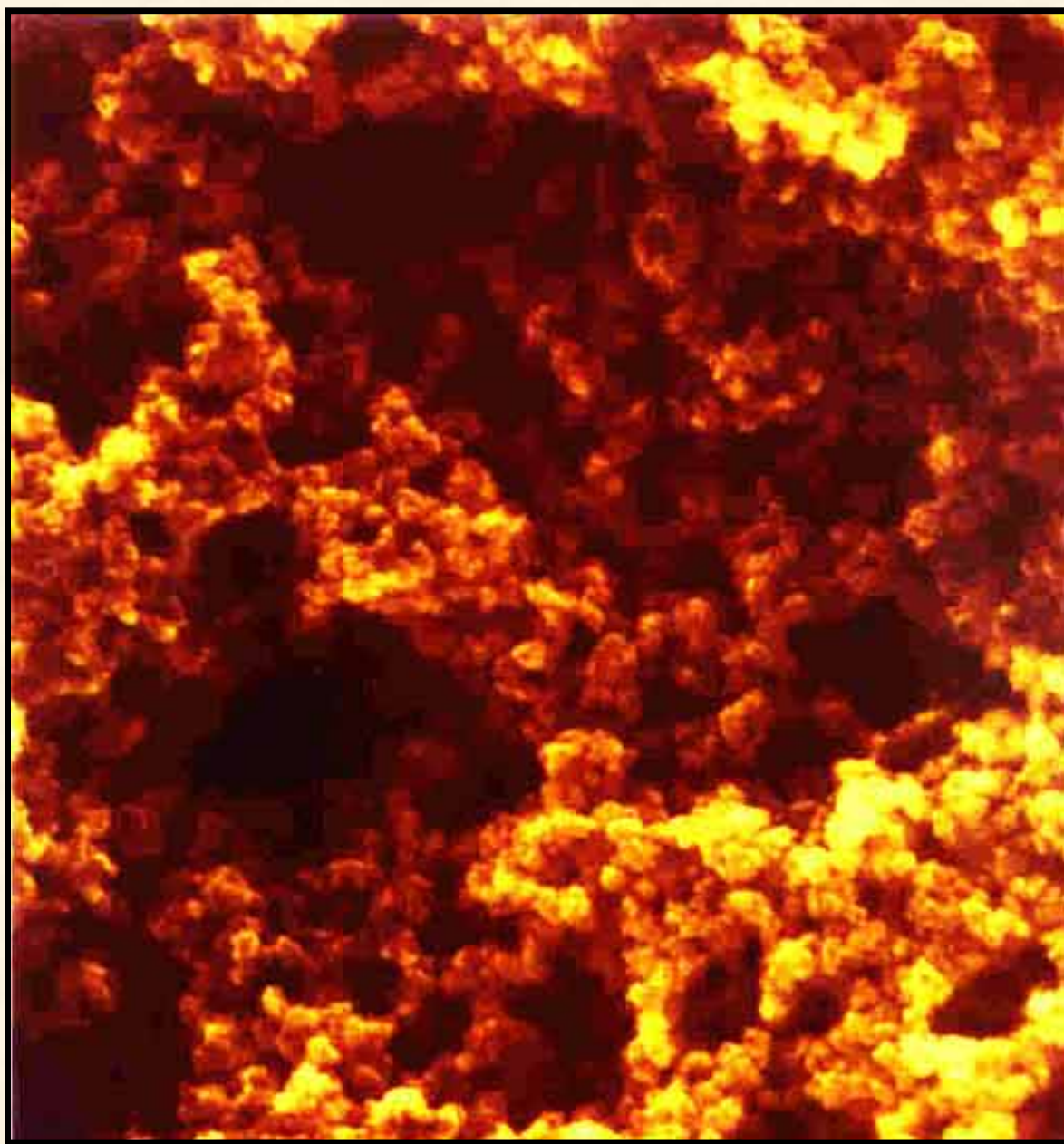


Figure 11. Amorphous iron powder is formed from the ultrasonic irradiation of iron carbonyl. The micrograph shows the porous, coral-like structure formed from nanometer-sized clusters created during acoustic cavitation. The amorphous iron is an extremely soft ferromagnetic material with high catalytic activity. The heating and cooling produced by cavitation are so rapid that the iron atoms cluster and solidify before they can form a well-ordered crystal.

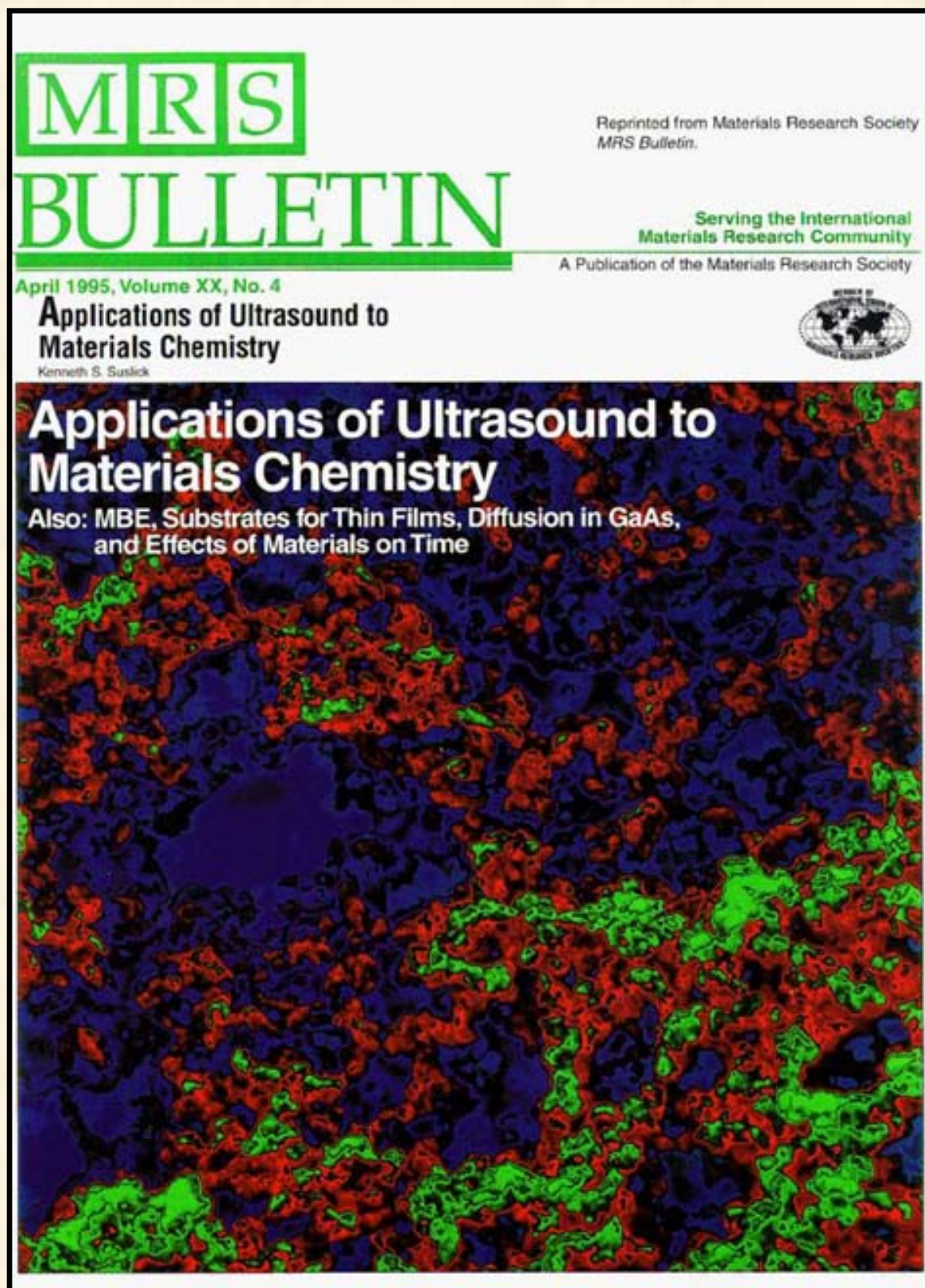


Figure 12. A transmission electron micrograph of amorphous iron powder, in false-color to enhance contrast. Because of their excellent magnetic properties, amorphous metals have important technological applications; these can include electrical transformer cores and magnetic tape recorder heads. Magnification of the cover image is approximately 100,000.

The sonochemically synthesized amorphous powders may have important technological applications. For example, the amorphous iron powder is an active catalyst for several important

reactions, including the synthesis of liquid fuels from CO and H₂ (which can be produced from coal). In addition, magnetic measurements reveal the amorphous iron to be a very soft ferromagnet, that is, a material that very quickly forgets its magnetization once an magnetic field has been turned off. While such materials would be very bad for making permanent magnets, they are very good for making magnetic shielding, electrical transformer cores, or magnetic media recording heads.

Sonocatalysis

Catalytic reactions are of enormous importance in both laboratory and industrial applications. Catalysts increase the rates of chemical reactions without being consumed themselves; they are generally divided into two types. If the catalyst is a molecular or ionic species dissolved in a liquid, then the system is "homogeneous"; if the catalyst is a solid, with the reactants either in a percolating liquid or gas, then it is "heterogeneous." In both cases, it is often a difficult problem either to activate the catalyst or to keep it active.

Ultrasound has potentially important applications in both homogeneous and heterogeneous catalytic systems. Heterogeneous catalysis is generally more industrially important than homogeneous systems. For example, virtually all of the petroleum industry is based on a series of catalytic transformations. Heterogeneous catalysts often require rare and expensive metals. The catalytic converters used on automobiles to lessen pollution, for example, use platinum or rhodium, which are enormously expensive; rhodium costs about \$1500 dollars per ounce!

Using ultrasound offers some hope of activating less reactive, but also less costly, metals. Some early investigations of the effects of ultrasound on heterogeneous catalysis can be found in the Soviet literature. In this early work, increases in turnover rates were usually observed upon ultrasonic irradiation, but were rarely more than 10-fold. In the case of modest rate increases, it appears likely that the cause is increased effective surface area; this is especially important in the case of catalysts supported on brittle solids.

More impressive accelerations, however, have been recently reported, including hydrogenations (catalytic reactions of hydrogen with unsaturated organic compounds) by nickel, palladium, or platinum. For example, D. J. Casadonte and Suslick discovered that hydrogenation of alkenes by nickel powder is enormously enhanced (about 100,000-fold) by ultrasonic irradiation. A very interesting effect on the surface morphology was observed (Figure 10). Ultrasonic irradiation smoothes, at a macroscopic scale, the initially crystalline surface and causes agglomeration of small particles. Both effects are probably due to interparticle collisions caused by cavitation-induced shock waves. Auger electron spectroscopy reveals that there is a considerable decrease in the thickness of the oxide coat after ultrasonic irradiation. The removal of this layer is probably responsible for the great increase observed in catalytic activity.

A Sound Future

Acoustic cavitation results in an enormous concentration of energy. If the energy density in an acoustic field that produces cavitation is compared with that in the collapsed cavitation bubble, there is an amplification of almost one trillion. The enormous local temperatures and pressures of cavitation result in sonochemistry and sonoluminescence. Cavitation produces an unusual method for fundamental studies of chemistry and physics under extreme conditions, and sonochemistry provides a unique interaction of energy and matter.

In addition, ultrasound is well suited to industrial applications. Since the reaction liquid itself carries the sound, there is no barrier to its use with large volumes. In fact, ultrasound is already heavily used industrially for the physical processing of liquids, such as emulsification, solvent degassing, solid dispersion, and sol formation. It is also extremely important in solids processing,

including cutting, welding, cleaning, and precipitation.

The extension of ultrasound to the chemical processing of liquids is underway. The future uses of ultrasound to drive chemical reactions will be diverse. It is becoming a common tool in nearly any case where a liquid and a solid must react. In the synthesis of pharmaceuticals, for example, ultrasound may permit improved yields and facilitate reactions run on larger scale. In the development and use of catalysts, ultrasound also has potential applications. Its ability to create highly reactive surfaces and thereby increase their catalytic activity has only just now been established. Ultrasound can produce materials with unusual properties. The extraordinary temperatures and pressures reached during cavitation collapse, combined with the exceptionally high rates of cooling, may allow researchers to synthesize novel solid phases difficult to prepare in other ways. One may be optimistic that the unusual reactivities caused by ultrasound will find important industrial application in the years to come.

SUSLICK GROUP WEBSITE:

THE SCIENCE	THE GROUP	THE MAÎTRE D'	LAGNIAPPE: A LITTLE EXTRA
<u>Overview</u>	<u>Current Group Members</u>	<u>CV: Abbreviated, Full</u>	<u>Art and Science</u>
<u>Outline of Projects</u>	<u>Group Meetings</u>	<u>Suslick Group Brochure</u>	<u>Chymistes: The Distillers of Waters</u>
<u>Synopses: Sonochemistry</u>	<u>Group Responsibilities</u>	<u>Complete Publication List</u>	<u>A Chemist Meets Hollywood</u>
<u>Metalloporph.</u>			
<u>Executive Summary: Smell-Seeing</u>	<u>Web Based Resources</u>	<u>Academic Genealogy</u>	<u>A Chemist In Court</u>
<u>Introduction to Sonochemistry</u>	<u>Safety Resources</u>	<u>Press Clippings</u>	<u>Words of Humor and Wisdom</u>
<u>Proposal Excerpts</u>	<u>Group Equipment</u>	<u>How To Give A Seminar</u>	<u>Laws of the Universe</u>

<u>Funding</u>	<u>Past Group Members</u>	<u>Ch315 Inorganic Chemistry</u>	<u>Cartoons of Humor and Wisdom</u>
<u>Information for Visitors</u>	<u>Group Photogallery</u>	<u>Construction of the CLS Lab</u>	<u>Sculpture & Masks</u>

©2003, K.S. Suslick; all rights reserved.

Comments and suggestions: ksuslick@uiuc.edu

"Sonochemistry"

Kenneth S. Suslick

University of Illinois at Urbana-Champaign

Kirk-Othmer Encyclopedia of Chemical Technology

Fourth Edition, vol. 26;

John Wiley & Sons, Inc.: New York, 1998,
pp. 516-541.

SONOCHEMISTRY

Ultrasonic irradiation of liquids causes high energy chemical reactions to occur, often with the emission of light (1-5). The origin of sonochemistry and sonoluminescence is acoustic cavitation: the formation, growth, and implosive collapse of bubbles in liquids irradiated with high intensity sound. The collapse of bubbles caused by cavitation produces intense local heating and high pressures, with very short lifetimes. In clouds of cavitating bubbles, these hot-spots (6,7) have equivalent temperatures of roughly 5000 K, pressures of about 1000 atmospheres, and

heating and cooling rates above 10^{10} K/s. In single-bubble cavitation, conditions may be even more extreme. Thus, cavitation can create extraordinary physical and chemical conditions in otherwise cold liquids.

When liquids that contains solids are irradiated with ultrasound, related phenomena can occur. When cavitation occurs near an extended solid surface, cavity collapse is nonspherical and drives high-speed jets of liquid into the surface (8,9). These jets and associated shock waves can cause substantial surface damage and expose fresh, highly heated surfaces. Ultrasonic irradiation of liquid-powder suspensions produces another effect: high velocity interparticle collisions. Cavitation and the shockwaves it creates in a slurry can accelerate solid particles to high velocities (10). The resultant collisions are capable of inducing dramatic changes in surface morphology, composition, and reactivity (11).

Sonochemistry can be roughly divided into categories based on the nature of the cavitation event: homogeneous sonochemistry of liquids, heterogeneous sonochemistry of liquid-liquid or liquid-solid systems, and sonocatalysis (which overlaps the first two) (12-15). In some cases, ultrasonic irradiation can increase reactivity by nearly a million-fold (16). Because cavitation can only occur in liquids, chemical reactions are not generally seen in the ultrasonic irradiation of solids or solid-gas systems.

Sonoluminescence in general may be considered a special case of homogeneous sonochemistry; however, recent discoveries in this field have heightened interest in the phenomenon in and by itself (17,18). Under conditions where an isolated, single bubble undergoes cavitation, recent studies on the duration of the sonoluminescence flash suggest that a shock wave may be created within the collapsing bubble, with the capacity to generate truly enormous temperatures and pressures within the gas.

Acoustic Cavitation

The chemical effects of ultrasound do not arise from a direct interaction with molecular species. Ultrasound spans the frequencies of roughly 15 kHz to 1 GHz. With sound velocities in liquids typically about 1500 m/s, acoustic wavelengths range from roughly 10 to 10^{-4} cm. These are not molecular dimensions. Consequently, no direct coupling of the acoustic field with chemical species on a molecular level can account for sonochemistry or sonoluminescence.

Instead, sonochemistry and sonoluminescence derive principally from acoustic cavitation (9), which serves as an effective means of concentrating the diffuse energy of sound. Compression of a gas generates heat. The compression of bubbles during cavitation is more rapid than thermal transport, which generates a short-lived, localized hot-spot. There is a general consensus that this hot-spot is the source of homogeneous sonochemistry. Rayleigh's early description of a mathematical model for the collapse of cavities in incompressible liquids predicted enormous local temperatures and pressures (19). Ten years later, Richards and Loomis reported the first chemical and biological effects of ultrasound (20). Alternative mechanisms involving electrical microdischarge have been occasionally proposed (21,22), but remain a minority viewpoint.

If the acoustic pressure amplitude of a propagating acoustic wave is relatively large (greater than ≈ 0.5 MPa), local inhomogeneities in the liquid (eg, gas-filled crevices in particulates) can give rise to the explosive growth of a nucleation site into a cavity of macroscopic dimensions, primarily filled with vapor. Such a bubble is inherently unstable, and its subsequent collapse can result in an enormous concentration of energy (Fig. 1). This violent cavitation event has been termed "transient cavitation" (23). A normal consequence of this unstable growth and subsequent collapse is that the cavitation bubble itself is destroyed. Gas-filled remnants from the collapse, however, may give rise to reinitiation of the process.

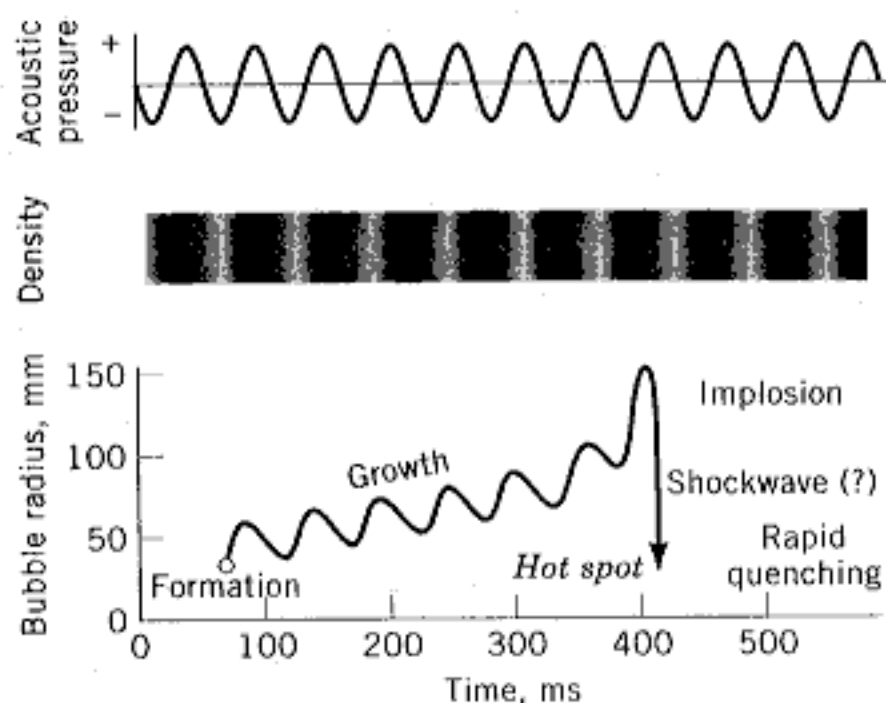


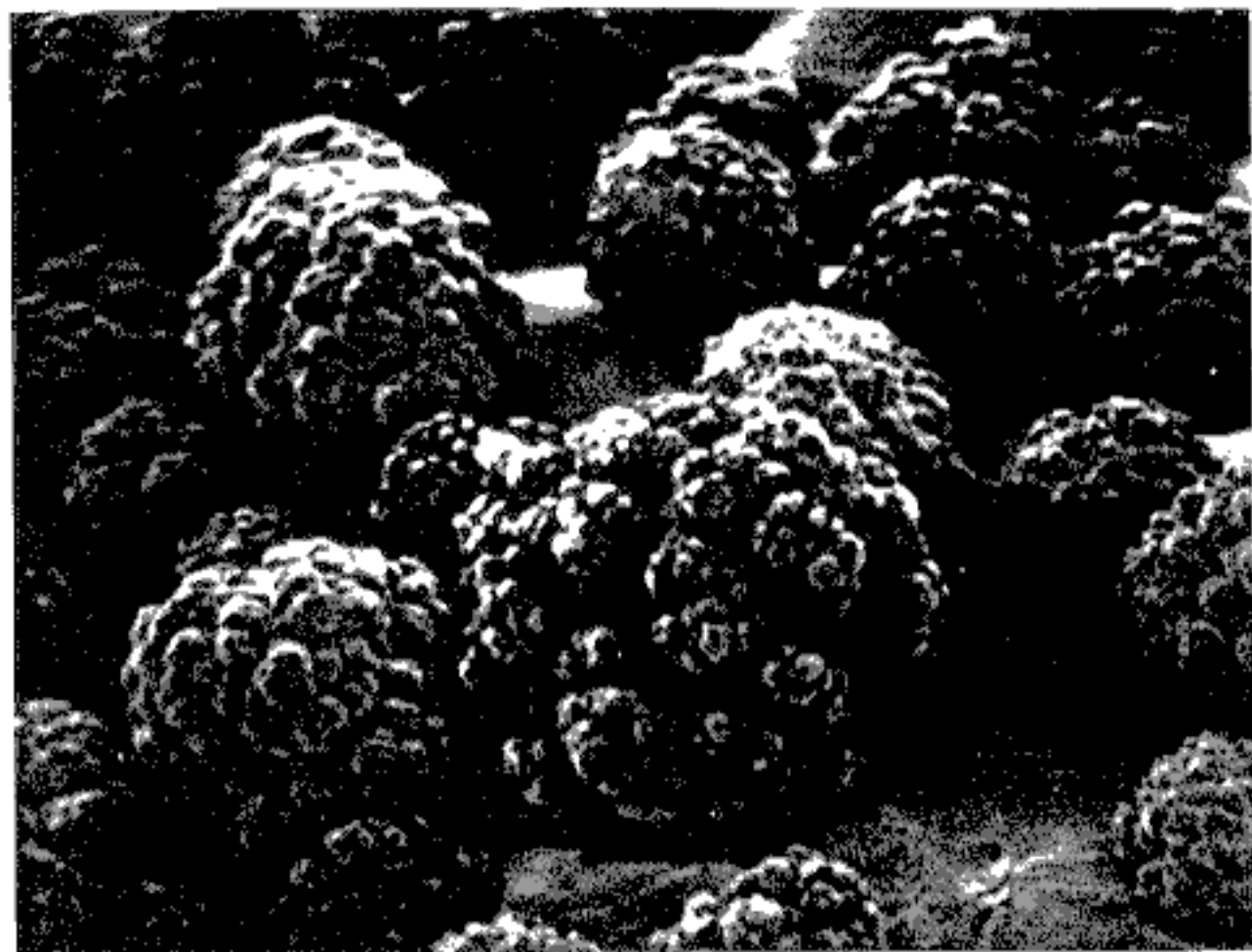
Fig. 1. Transient acoustic cavitation: the origin of sonochemistry and sonoluminescence.

The generally accepted explanation for the origin of sonochemistry and sonoluminescence is the hot-spot theory, in which the potential energy given the bubble as it expands to maximum size is concentrated into a heated gas core as the bubble implodes. The oscillations of a gas bubble driven by an acoustic field are generally described by Rayleigh-Plesset equation; one form of which, called the Gilmore equation (9,23), can be expressed a second-order nonlinear differential equation given as

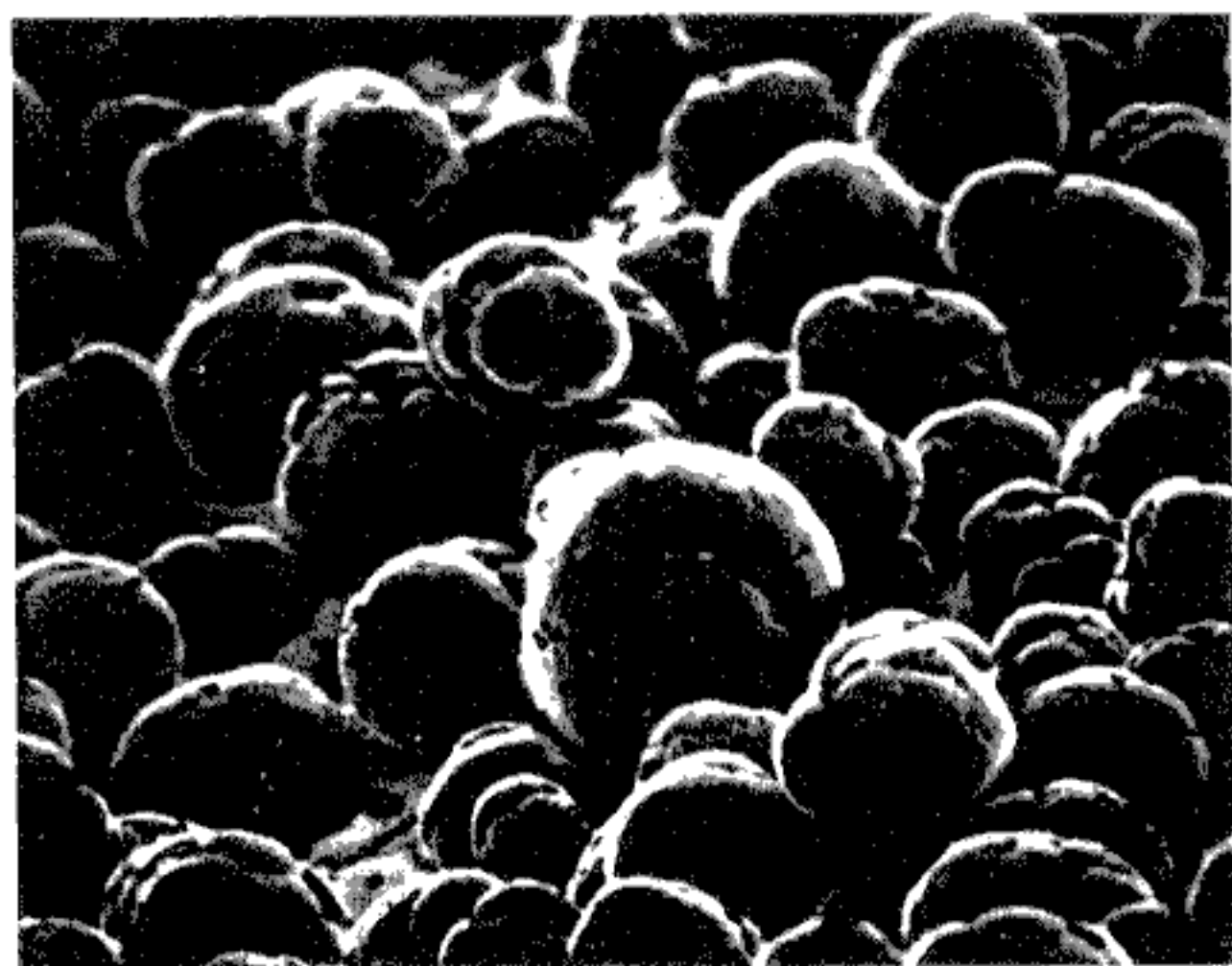
$$R\left(1 - \frac{U}{C}\right)\frac{d^2R}{dt^2} + \frac{3}{2}\left(1 - \frac{U}{3C}\right)\left(\frac{dR}{dt}\right)^2 - \left(1 + \frac{U}{C}\right)H - \frac{R}{C}\left(1 - \frac{U}{C}\right)\frac{dH}{dt} = 0 \quad (1)$$

The radius and velocity of the bubble wall are given by R and U respectively. The values for H , the enthalpy at the bubble wall, and C , the local sound speed, may be expressed as follows, using the Tait equation of state for the liquid.

$$H = \frac{n}{n-1} \frac{A^{1/n}}{\rho_0} \left[(P(R) + B)^{n-1/n} - (P_\infty(t) + B)^{n-1/n} \right] \quad (2)$$



(a)



(b)

Fig. 5. The effect of ultrasonic irradiation on the surface morphology and particle size of Ni powder. Initial particle diameters (a) before ultrasound were $\approx 160 \mu\text{m}$; (b) after ultrasound, $\approx 80 \mu\text{m}$. High velocity interparticle collisions caused by ultrasonic irradiation of slurries are responsible for the smoothing and removal of passivating oxide coating. Reproduced with permission (11).

and

$$C = [c_o^2 + (n - 1)H] \quad (3)$$

The linear speed of sound in the liquid is c_o . A , B , and n are constants that should be set to the appropriate values for water. Any acoustic forcing function is included in the pressure at infinity term, $P_\infty(t)$. The pressure at the bubble wall, $P(R)$, is given by

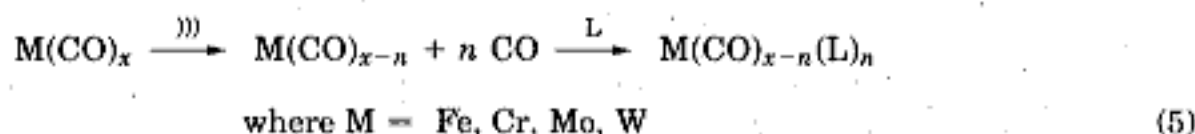
$$P(R) = \left(P_o + \frac{2\sigma}{R} \right) \left(\frac{R_o}{R} \right)^{3\gamma} - \frac{2\sigma}{R} - \frac{4\mu U}{R} \quad (4)$$

where the initial radius of the bubble at time zero is R_o . The ambient pressure of the liquid is P_o , the surface tension σ , the shear viscosity μ , and the polytropic exponent γ .

The validity of the Gilmore equation to compute the behavior of a single, isolated cavitating bubble has been experimentally confirmed. For example, using a light scattering technique, various researchers have obtained measurements of the radius-time curve for single collapsing bubbles, simultaneous with optical emission from sonoluminescence (see below). The single-bubble sonoluminescent emission is seen as a sharp spike, appearing at the final stages of bubble collapse, and the general shape of the theoretical radius-time curve is observed (24–26).

Two-Site Model of Sonochemical Reactivity

The transient nature of the cavitation event precludes conventional measurement of the conditions generated during bubble collapse. Chemical reactions themselves, however, can be used to probe reaction conditions. The effective temperature realized by the collapse of clouds of cavitating bubbles can be determined by the use of competing unimolecular reactions whose rate dependencies on temperature have already been measured. This technique of comparative-rate chemical thermometry was used by Suslick, Hammerton, and Cline to first determine the effective temperature reached during cavity collapse (6). The sonochemical ligand substitutions of volatile metal carbonyls were used as these comparative rate probes (eq. 5, where the symbol $\xrightarrow{\text{)))}}$ represents ultrasonic irradiation of a solution, and L represents a substituting ligand). These kinetic studies revealed that there were in fact



two sonochemical reaction sites: the first (and dominant site) is the bubble's interior gas-phase while the second is an *initially* liquid phase. The latter corresponds either to heating of a shell of liquid around the collapsing bubble or to droplets of liquid ejected into the hot-spot by surface wave distortions of the collapsing bubble, as shown schematically in Figure 2.

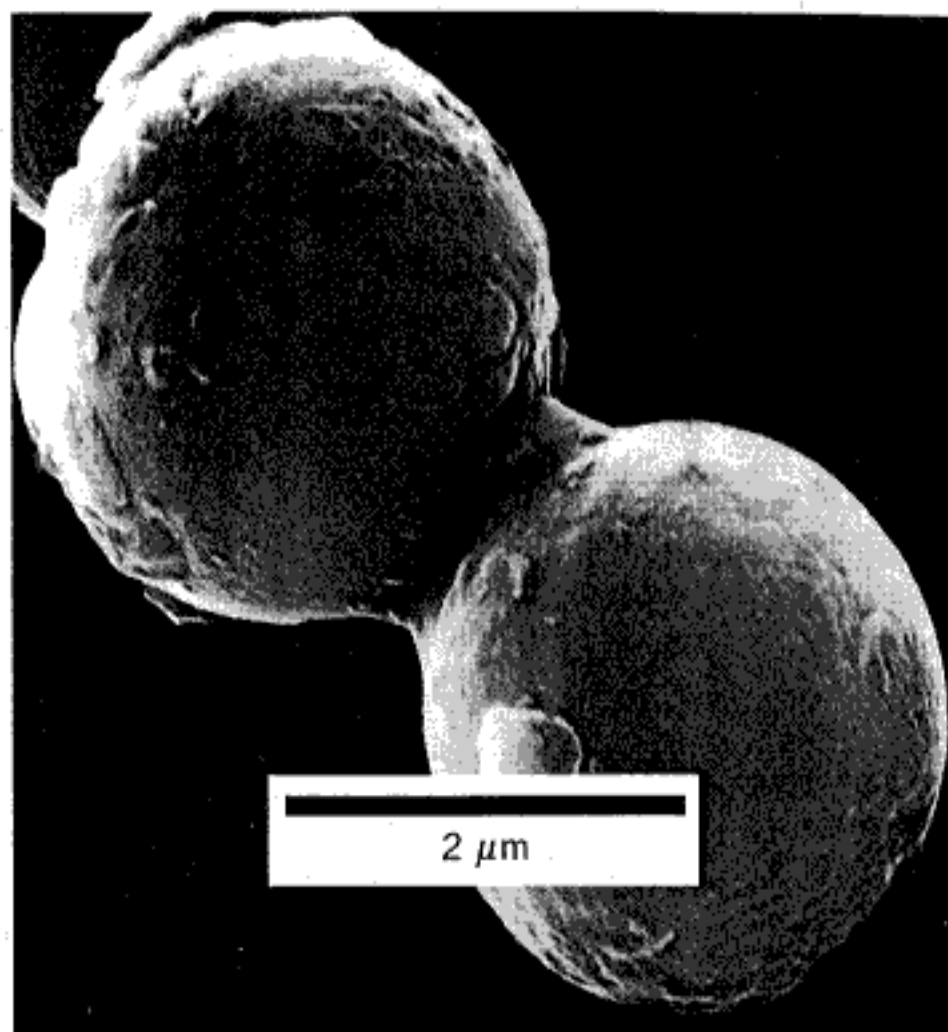


Fig. 4. Scanning electron micrograph of 5- μm diameter Zn powder. Neck formation from localized melting is caused by high-velocity interparticle collisions. Similar micrographs and elemental composition maps (by Auger electron spectroscopy) of mixed metal collisions have also been made. Reproduced with permission (10).

Sonoluminescence

Types of Sonoluminescence. In addition to driving chemical reactions, ultrasonic irradiation of liquids can also produce light. Sonoluminescence was first observed from water in 1934 by Frenzel and Schultes (29). As with sonochemistry, sonoluminescence derives from acoustic cavitation. It is now generally thought that there are two separate forms of sonoluminescence: multiple-bubble sonoluminescence (MBSL) and single-bubble sonoluminescence (SBSL) (17,24,30). Since cavitation is a nucleated process and liquids generally contain large numbers particulates that serve as nuclei, the cavitation field generated by propagating or standing acoustic wave typically consists of very large numbers of interacting bubbles, distributed over an extended region of the liquid. If this cavitation is sufficiently intense to produce sonoluminescence, then this phenomenon is called multiple-bubble sonoluminescence (MBSL) (2,17).

Under the appropriate conditions, the acoustic force on a bubble can be used to balance against its buoyancy, holding the single bubble isolated in the liquid by acoustic levitation. This permits examination of the dynamic characteristics of the bubble can in considerable detail, from both a theoretical and an experimental perspective. Such a bubble is typically quite small, compared to an acoustic wavelength (eg, at 20 kHz, the resonance size is approximately 150 μm). It was

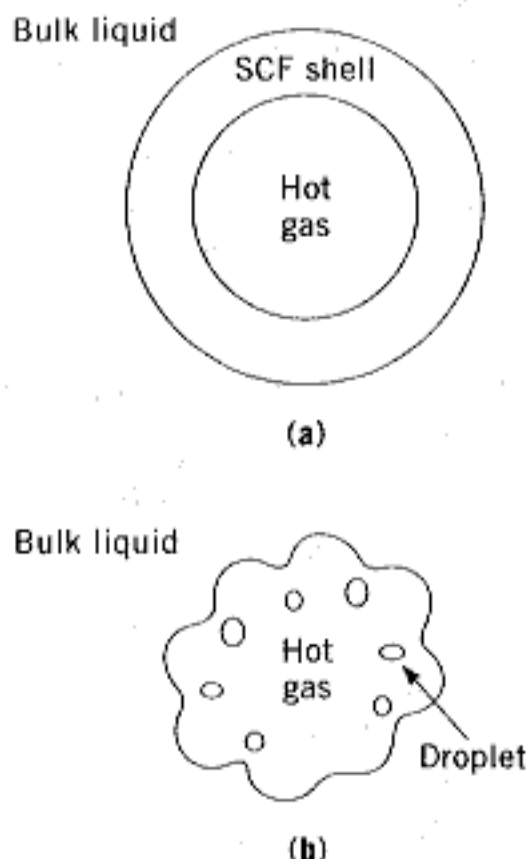


Fig. 2. Two-site models of the sonochemical reactions sites. (a) Thermal diffusion shell model; (b) surface wave droplet model.

The effective local temperatures in both sites were determined. By combining the relative sonochemical reaction rates for equation 5 with the known temperature behavior of these reactions, the conditions present during cavity collapse could then be calculated. The effective temperature of these hot-spots was measured at ≈ 5200 K in the gas-phase reaction zone and ≈ 1900 K in the initially liquid zone (6). Of course, the comparative rate data represent only a composite temperature: during the collapse, the temperature has a highly dynamic profile, as well as a spatial temperature gradient. This two-site model has been confirmed with other reactions (27,28) and alternative measurements of local temperatures by sonoluminescence are consistent (7), as discussed later.

Microjet Formation during Cavitation at Liquid–Solid Interfaces

A very different phenomenon arises when cavitation occurs near extended liquid–solid interfaces. There are two proposed mechanisms for the effects of cavitation near surfaces: microjet impact and shockwave damage. Whenever a cavitation bubble is produced near a boundary, the asymmetry of the liquid particle motion during cavity collapse can induce a strong deformation in the cavity (9). The potential energy of the expanded bubble is converted into kinetic energy of a liquid jet that extends through the bubble's interior and penetrates the opposite bubble wall. Because most of the available energy is transferred to the accelerating jet, rather than the bubble wall itself, this jet can reach velocities of hundreds of meters per second. Because of the induced asymmetry, the jet often impacts the solid boundary and can deposit enormous energy densities at

the site of impact. Such energy concentration can result in severe damage to the boundary surface. Figure 3 is a photograph of a jet developed in a collapsing cavity. The second mechanism of cavitation-induced surface damage invokes shockwaves created by cavity collapse in the liquid. The impingement of microjets and shockwaves on the surface creates the localized erosion responsible for much of ultrasonic cleaning and many of the sonochemical effects on heterogeneous reactions. In this process, the erosion of metals by cavitation generates newly exposed, highly heated surfaces that are highly reactive.

A solid surface several times larger than the resonance bubble size is necessary to induce distortions during bubble collapse. For ultrasound of ≈ 20 kHz, damage associated with jet formation cannot occur if the solid particles are smaller than ≈ 200 μm . In these cases, however, the shockwaves created by homogeneous cavitation can create high velocity interparticle collisions (10,11). Suslick and co-workers have found that the turbulent flow and shockwaves produced by intense ultrasound can drive metal particles together at sufficiently high speeds to induce effective melting in direct collisions (Fig. 4) and the abrasion of surface crystallites in glancing impacts (Fig. 5). A series of transition metal powders were used to probe the maximum temperatures and speeds reached during interparticle collisions. Using the irradiation of Cr, Mo, and W powders in decane at 20 kHz and 50 W/cm^2 , agglomeration and essentially a localized melting occurs for the first two metals, but not the third (Fig. 6). On the basis of the melting points of these metals, the effective transient temperature reached at the point of impact during interparticle collisions is roughly 3000°C (which is unrelated to the temperature inside the hot-spot of a collapsing bubble). From the volume of the melted region of impact, the amount of energy generated during collision was determined. From this, a lower estimate of the velocity of impact is roughly one half the speed of sound (10). These are precisely the effects expected on suspended particulates from cavitation-induced shockwaves in the liquid.



Fig. 3. Liquid jet produced during collapse of a cavitation bubble near a solid surface. The width of the bubble is about 1 mm. Reproduced with permission (8).

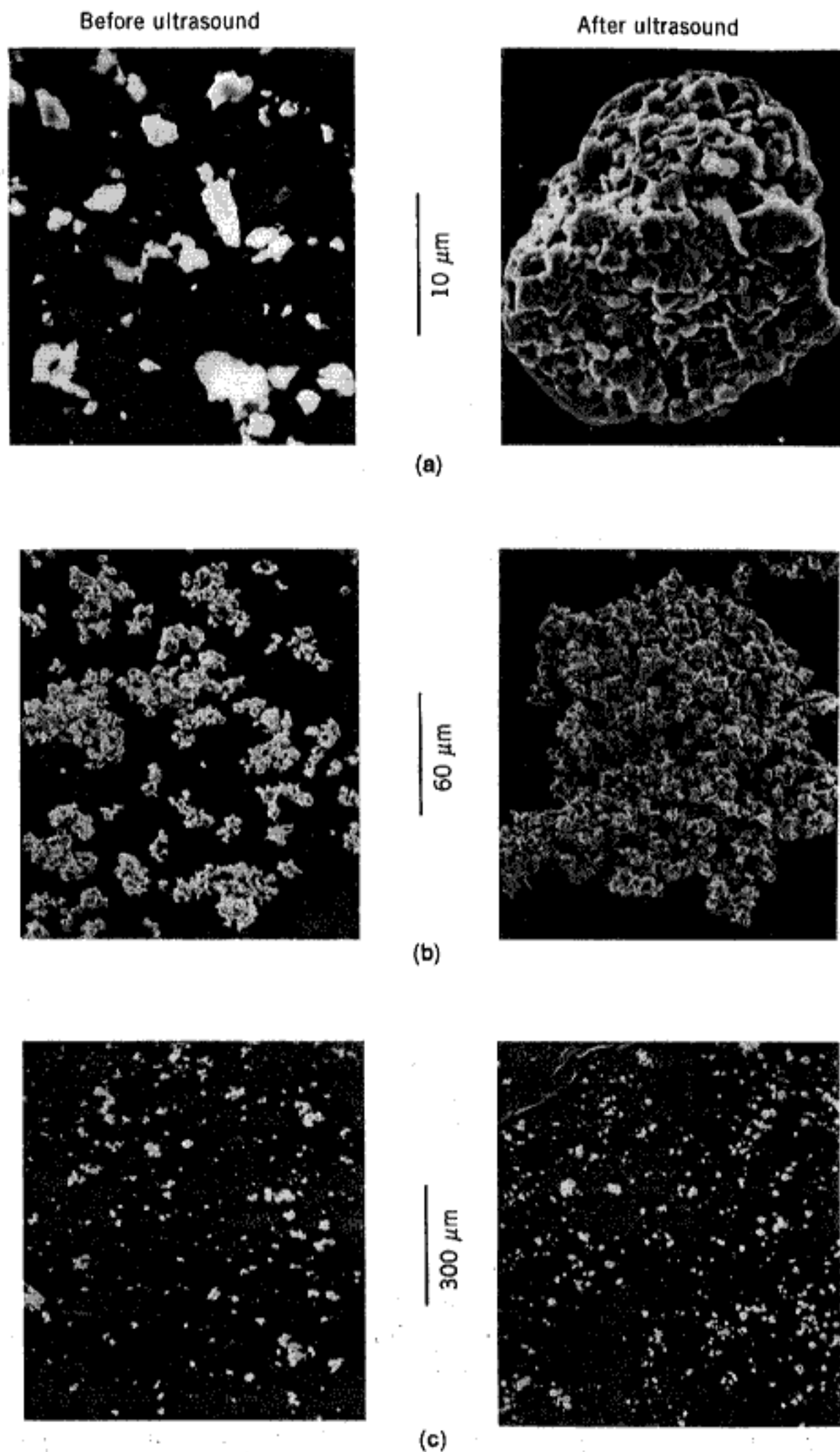


Fig. 6. The effect of ultrasound on particle agglomeration of (a) Cr (mp 1857°C), (b) Mo (mp 2617°C), and (c) W (mp 3410°C) after irradiation of decane slurries under Ar. Reproduced with permission (10).

recently discovered for rather specialized but easily obtainable conditions, that a single, stable, oscillating gas bubble can be forced into such large amplitude pulsations that it produces sonoluminescence emissions on each (and every) acoustic cycle (31,32). This phenomenon is called single-bubble sonoluminescence, and has received considerable recent attention (17,18,33,34).

Multiple-Bubble Sonoluminescence. The sonoluminescence of aqueous solutions has been often examined over the past thirty years. The spectrum of MBSL in water consists of a peak at 310 nm and a broad continuum throughout the visible region. An intensive study of aqueous MBSL was conducted by Verrall and Sehgal (35). The emission at 310 nm is from excited-state OH^* , but the continuum is difficult to interpret. MBSL from aqueous and alcohol solutions of many metal salts have been reported and are characterized by emission from metal atom excited states (36).

Sonoluminescence from nonaqueous liquids has only recently been examined. Flint and Suslick reported the first MBSL spectra of organic liquids (37). With various hydrocarbons, the observed emission is from excited states of C_2 ($d^3\Pi_g - a^3\Pi_u$, the Swan lines), the same emission seen in flames. Furthermore, the ultrasonic irradiation of alkanes in the presence of N_2 (or NH_3 or amines) gives emission from CN excited states, but not from N_2 excited states. Emission from N_2 excited states would have been expected if the MBSL originated from microdischarge, whereas CN emission is typically observed from thermal sources. When oxygen is present, emission from excited states of CO_2 , CH^* , and OH^* is observed, again similar to flame emission.

For both aqueous and nonaqueous liquids, MBSL is caused by chemical reactions of high-energy species formed during cavitation by bubble collapse, and its principal source is most probably not blackbody radiation or electrical discharge. MBSL is predominantly a form of chemiluminescence.

Single-Bubble Sonoluminescence. The spectra of MBSL and SBSL are dramatically different. MBSL is generally dominated by atomic and molecular emission lines, but SBSL is an essentially featureless emission that increases with decreasing wavelength. For example, an aqueous solution of NaCl shows evidence of excited states of both OH^* and Na in the MBSL spectrum; however, the SBSL spectrum of an identical solution shows no evidence of either of these peaks (30). Similarly, the MBSL spectrum falls off at low wavelengths, while the SBSL spectrum continues to rise, at least for bubbles containing most noble gases (38).

An intriguing aspect of SBSL is the extremely short duration of the sonoluminescence flash. The hydrodynamic models of adiabatic collapse of a single bubble suggest that the temperature of the gas within the bubble should remain at elevated temperatures for times on the order of tens of nanoseconds; however, there is strong evidence that the pulse duration of the SBSL flash is three orders of magnitude shorter. Putterman and his colleagues, using the fastest PMT available, reported that this duration is less than 50 ps, perhaps much less (39). The most plausible explanation for this short flash interval, and some of the observed spectra (see below), is that an imploding shock wave is created within the gas bubble during the final stages of collapse. If this shock wave does indeed exist, exciting possibilities can be inferred about the temperatures that could be attained within the bubble and the physics that might result. Indeed,

speculations on the possibilities of inertial confinement (*hot*) fusion have been made (40,41).

Spectroscopic Probes of Cavitation Conditions. Determination of the temperatures reached in a cavitating bubble has remained a difficult experimental problem. As a spectroscopic probe of the cavitation event, MBSL provides a solution. High resolution MBSL spectra from silicone oil under Ar have been reported and analyzed (7). The observed emission comes from excited state C_2 and has been modeled with synthetic spectra as a function of rotational and vibrational temperatures, as shown in Figure 7. From comparison of synthetic to observed spectra, the effective cavitation temperature is 5050 ± 150 K. The excellence of the match between the observed MBSL and the synthetic spectra provides definitive proof that the sonoluminescence event is a thermal, chemiluminescence process. The agreement between this spectroscopic determination of the cavitation temperature and that made by comparative rate thermometry of sonochemical reactions is surprisingly close (6).

The interpretation of the spectroscopy of SBSL is much less clear. At this writing, SBSL has been observed primarily in aqueous fluids, and the spectra obtained are surprisingly featureless. Some very interesting effects are observed when the gas contents of the bubble are changed (39,42). Furthermore, the spectra show practically no evidence of OH emissions, and when He and Ar bubbles are considered, continue to increase in intensity even into the deep ultraviolet. These spectra are reminiscent of black body emission with temperatures *considerably* in excess of 5000 K and lend some support to the concept of an imploding shock wave (41). Several other alternative explanations for SBSL have been presented, and there exists considerable theoretical activity in this particular aspect of SBSL.

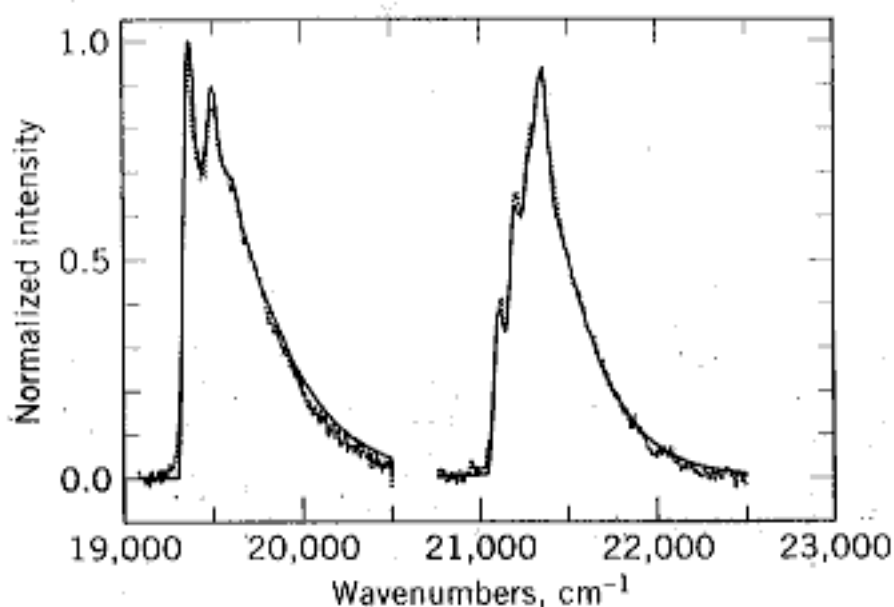


Fig. 7. Sonoluminescence of excited state C_2 . Emission from the $\Delta v = +1$ manifold of the $d^3\Pi_g - a^3\Pi_u$ transition (Swan band) of C_2 . Reproduced with permission (7). \cdots , Observed sonoluminescence from polydimethylsiloxane silicone oil under Ar at 0°C ; — , best fit synthetic spectrum, with $T_v = T_r = 4900$ K.

Sonochemistry

In a fundamental sense, chemistry is the interaction of energy and matter. Chemical reactions require energy in one form or another to proceed: chemistry stops as the temperature approaches absolute zero. One has only limited control, however, over the nature of this interaction. In large part, the properties of a specific energy source determines the course of a chemical reaction. Ultrasonic irradiation differs from traditional energy sources (such as heat, light, or ionizing radiation) in duration, pressure, and energy per molecule. The immense local temperatures and pressures and the extraordinary heating and cooling rates generated by cavitation bubble collapse mean that ultrasound provides an unusual mechanism for generating high energy chemistry. Like photochemistry, very large amounts of energy are introduced in a short period of time, but it is thermal, not electronic, excitation. As in flash pyrolysis, high thermal temperatures are reached, but the duration is very much shorter (by $>10^4$) and the temperatures are even higher (by five- to ten-fold). Similar to shock-tube chemistry or multiphoton infrared laser photolysis, cavitation heating is very short lived, but occurs within condensed phases. Furthermore, sonochemistry has a high-pressure component, which suggests that one might be able to produce on a microscopic scale the same macroscopic conditions of high temperature–pressure “bomb” reactions or explosive shockwave synthesis in solids. Figure 8 presents an interesting comparison of the parameters that control chemical reactivity (time, pressure, and energy) for various forms of chemistry.

Experimental Design. A variety of devices have been used for ultrasonic irradiation of solutions. There are three general designs in use presently: the ultrasonic cleaning bath, the direct immersion ultrasonic horn, and flow reactors.

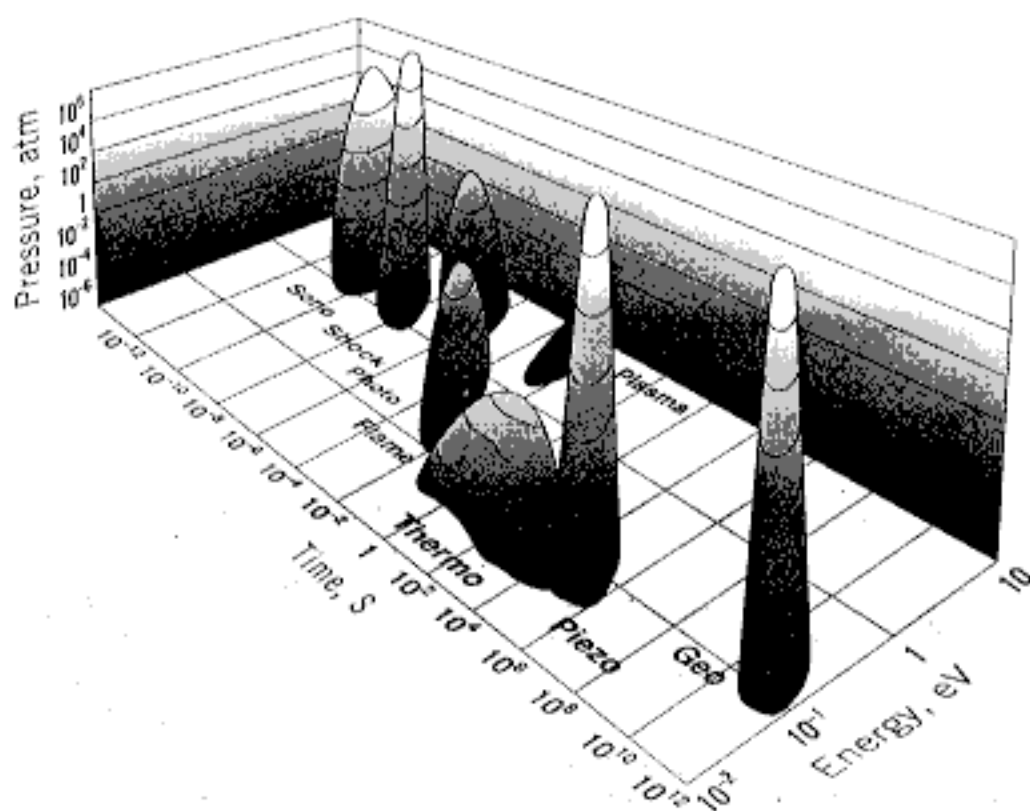


Fig. 8. Chemistry: the interaction of energy and matter. To convert atm to Pa, multiply by 1.013×10^5 .

The originating source of the ultrasound is generally a piezoelectric material, usually a lead zirconate titanate ceramic (PZT), which is subjected to a high a-c voltage with an ultrasonic frequency (typically 15 to 50 kHz). For industrial use, the more robust magnetostrictive metal alloys (usually of Ni) can be used as the core of a solenoid generating an alternating magnetic field with an ultrasonic frequency. The vibrating source is attached to the wall of a cleaning bath, to an amplifying horn, or to the outer surfaces of a flow-through tube or diaphragm.

The ultrasonic cleaning bath is clearly the most accessible source of laboratory ultrasound and has been used successfully for a variety of liquid–solid heterogeneous sonochemical studies. Lower acoustic intensities can often be used in liquid–solid heterogeneous systems, because of the reduced liquid tensile strength at the liquid–solid interface. For such reactions, a common ultrasonic cleaning bath will therefore often suffice. The low intensity available in these devices ($\approx 1 \text{ W/cm}^2$), however, can prove limiting. In addition, the standing wave patterns in ultrasonic cleaners require accurate positioning of the reaction vessel. On the other hand, ultrasonic cleaning baths are easily accessible, relatively inexpensive, and usable on moderately large scale. Even in the case of heterogeneous sonochemistry, however, the ultrasonic cleaning bath must be viewed as an apparatus of limited capability.

The most intense and reliable source of ultrasound generally used in the chemical laboratory is the direct immersion ultrasonic horn (50 to 500 W/cm^2), as shown in Figure 9, which can be used for work under either inert or reactive atmospheres or at moderate pressures (< 10 atmospheres). These devices are available from several manufacturers at modest cost and are often used by biochemists for cell disruption. A variety of sizes of power supplies and titanium horns are available, thus allowing flexibility in sample size. Commercially available flow-through reaction chambers which will attach to these horns allow the processing of multiliter volumes. The acoustic intensities are easily and reproducibly variable; the acoustic frequency is well controlled, albeit fixed (typically at 20 kHz). Since power levels are quite high, counter-cooling of the reaction solution is essential to provide temperature control. Erosion of the titanium tip is a potential disadvantage, especially in corrosive media. Such erosion is generally a very slow process without chemical consequences (given the high tensile strength and low reactivity of Ti metal) and can be avoided by using the horn to irradiate through a cooling solution into a reaction solution held in a glass container (a so-called cup-horn).

Large-scale ultrasonic generation in flow-through configurations is a well-established technology (43–46). Liquid processing rates as high as 200 L/min are routinely accessible from a variety of modular, in-line designs with acoustic power of $\approx 20 \text{ kW}$ per unit. The industrial uses of these units include (1) degassing of liquids, (2) dispersion of solids into liquids, (3) emulsification of immiscible liquids and (4) large-scale cell disruption (45,46).

Homogeneous sonochemistry typically is not a very energy efficient process (although it can be more efficient than photochemistry), whereas heterogeneous sonochemistry is several orders of magnitude better. Unlike photochemistry, whose energy inefficiency is inherent in the production of photons, ultrasound

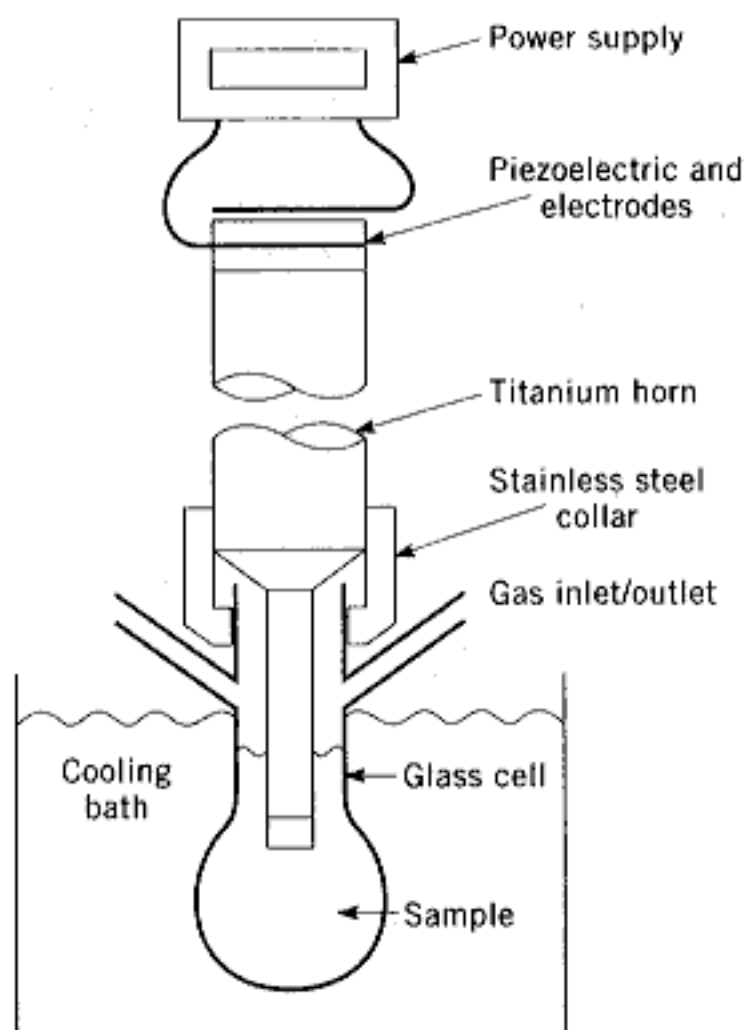


Fig. 9. A typical sonochemical apparatus with direct immersion ultrasonic horn. Ultrasound can be easily introduced into a chemical reaction with good control of temperature and ambient atmosphere. The usual piezoelectric ceramic is PZT, a lead zirconate titanate ceramic. Similar designs for sealed stainless steel cells can operate at pressures above 10 bar.

can be produced with nearly perfect efficiency from electric power. A primary limitation of sonochemistry remains the small fraction of the acoustic power actually involved in the cavitation events. This might be significantly improved, however, if a more efficient means of coupling the sound field to generate cavitation can be found.

Sonochemistry is strongly affected by a variety of external variables, including acoustic frequency, acoustic intensity, bulk temperature, static pressure, ambient gas, and solvent (47). These are the important parameters which need consideration in the effective application of ultrasound to chemical reactions. The origin of these influences is easily understood in terms of the hot-spot mechanism of sonochemistry.

The frequency of the sound field is not a commonly altered variable in most sonochemistry. Changing sonic frequency alters the resonant size of the cavitation event and to some extent, the lifetime of the bubble collapse, but the overall process remains unchanged. Sonochemistry is therefore less influenced over the range where cavitation can occur (from tens of Hz to a few MHz). The observed sonochemical rates may change, but well-controlled comparisons of efficiency are lacking at this time and will prove difficult. Subtle differences in product distributions from homogeneous reactions have been occasionally

reported (48). At very high frequencies (above a few MHz), cavitation ceases, and sonochemistry is generally not observed.

Acoustic intensity has a dramatic influence on the observed rates of sonochemical reactions. Below a threshold value, the amplitude of the sound field is too small to induce nucleation or bubble growth. Above the cavitation threshold, increased intensity of irradiation (from an immersion horn, for example) will increase the effective volume of the zone of liquid which will cavitate, and thus, increase the observed sonochemical rate. Furthermore, as the acoustic pressures increase, the range of bubble sizes which will undergo transient cavitation increases; this too will increase the observed sonochemical rate. It is often observed experimentally, however, that as one continues to increase acoustic amplitude, eventually rates begin to diminish. At high intensities, the cavitation of the liquid near the radiating surface becomes so intense as to produce a shroud of bubbles which will diminish the penetration of the sound into the liquid. In addition, bubble growth may become so rapid that the bubble grows beyond the size range of transient cavitation before implosive collapse can occur.

The effect of the bulk solution temperature lies primarily in its influence on the bubble content before collapse. With increasing temperature, in general, sonochemical reaction rates are *slower*! This reflects the dramatic influence which solvent vapor pressure has on the cavitation event: the greater the solvent vapor pressure found within a bubble prior to collapse, the less effective the collapse. There is generally a linear correlation of the log of the sonochemical rate and the total solvent vapor pressure (49). When secondary reactions are being monitored (as in chemical reactions occurring after initial acoustic erosion of a passivated surface), temperature will play its usual role in thermally activated chemical reactions. This explains the common observation that rates of heterogeneous sonochemistry often have an optimal reaction temperature: below this temperature, cavitation processes are improved, but secondary chemical reactions are slowed, and at higher temperatures, vice versa.

Increases in the applied static pressure increase the acoustic intensity necessary for cavitation, but if equal number of cavitation events occur, the collapse should be more intense. In contrast, as the ambient pressure is reduced, eventually the gas-filled crevices of particulate matter which serve as nucleation sites for the formation of cavitation in even "pure" liquids, will be deactivated, and therefore the observed sonochemistry will be diminished.

The choice of ambient gas will also have a major impact on sonochemical reactivity. The maximum temperature reached during cavitation is strongly dependent on the polytropic ratio ($\gamma = C_p/C_v$) of the ambient gas, which defines the amount of heat released during the adiabatic compression of that gas. Monatomic gases give much more heating than diatomic, which are much better than polyatomic gases (including solvent vapor). Sonochemical rates are also significantly influenced by the thermal conductivity of the ambient, so even the noble gases affect cavitation differently: He is generally much worse than Ar and Xe is the best; Ar is often the most cost-effective choice. In addition, sonochemical reactions will often involve the gases present in the cavitation event.

The choice of the solvent also has a profound influence on the observed sonochemistry. The effect of vapor pressure has already been mentioned. Other

liquid properties, such as surface tension and viscosity, will alter the threshold of cavitation, but this is generally a minor concern. The chemical reactivity of the solvent is often much more important. No solvent is inert under the high temperature conditions of cavitation (50). One may minimize this problem, however, by using robust solvents that have low vapor pressures so as to minimize their concentration in the vapor phase of the cavitation event. Alternatively, one may wish to take advantage of such secondary reactions, for example, by using halocarbons for sonochemical halogenations. With ultrasonic irradiations in water, the observed aqueous sonochemistry is dominated by secondary reactions of $\text{OH}\cdot$ and $\text{H}\cdot$ formed from the sonolysis of water vapor in the cavitation zone (51–53).

Control of sonochemical reactions is subject to the same limitation that any thermal process has: the Boltzmann energy distribution means that the energy per individual molecule will vary widely. One does have easy control, however, over the energetics of cavitation through the parameters of acoustic intensity, temperature, ambient gas, and solvent choice. The thermal conductivity of the ambient gas (eg, a variable He/Ar atmosphere) and the overall solvent vapor pressure provide easy methods for the experimental control of the peak temperatures generated during the cavitation collapse.

Homogeneous Sonochemistry: Bond Breaking and Radical Formation.

The chemical effect of ultrasound on aqueous solutions have been studied for many years. The primary products are H_2 and H_2O_2 ; there is strong evidence for various high-energy intermediates, including HO_2 , $\text{H}\cdot$, $\text{OH}\cdot$, and perhaps $e_{(\text{aq})}^-$. The elegant work of Riesz and collaborators used electron paramagnetic resonance with chemical spin-traps to demonstrate definitively the generation of $\text{H}\cdot$ and $\text{OH}\cdot$ during ultrasonic irradiation, even with clinical sources of ultrasound (51–53). The extensive work in Henglein's laboratory involving aqueous sonochemistry of dissolved gases has established clear analogies to combustion processes (27,28). As one would expect, the sonolysis of water, which produces both strong reductants and oxidants, is capable of causing secondary oxidation and reduction reactions, as often observed by Margulis and co-workers (54). Most recently there has been strong interest shown in the use of ultrasound for remediation of low levels of organic contamination of water (47,55,56). The $\text{OH}\cdot$ radicals produced from the sonolysis of water are able to attack essentially all organic compounds (including halocarbons, pesticides, and nitroaromatics) and through a series of reactions oxidize them fully. The desirability of sonolysis for such remediation lies in its low maintenance requirements and the low energy efficiency of alternative methods (eg, ozonolysis, uv photolysis).

In contrast, the ultrasonic irradiation of organic liquids has been less studied. Suslick and co-workers established that virtually all organic liquids will generate free radicals upon ultrasonic irradiation, as long as the total vapor pressure is low enough to allow effective bubble collapse (49). The sonolysis of simple hydrocarbons (for example, *n*-alkanes) creates the same kinds of products associated with very high temperature pyrolysis (50). Most of these products (H_2 , CH_4 , and the smaller 1-alkenes) derive from a well-understood radical chain mechanism.

The sonochemistry of solutes dissolved in organic liquids also remains largely unexplored. The sonochemistry of metal carbonyl compounds is an

exception (57). Detailed studies of these systems led to important mechanistic understandings of the nature of sonochemistry. A variety of unusual reactivity patterns have been observed during ultrasonic irradiation, including multiple ligand dissociation, novel metal cluster formation, and the initiation of homogeneous catalysis at low ambient temperature (57).

Applications of Sonochemistry to Materials Synthesis. Of special interest is the recent development of sonochemistry as a synthetic tool for the creation of unusual inorganic materials (58,59). As one example, the recent discovery of a simple sonochemical synthesis of amorphous iron (Fig. 10) helped settle the longstanding controversy over its magnetic properties (60,61). More generally, ultrasound has proved extremely useful in the synthesis of a

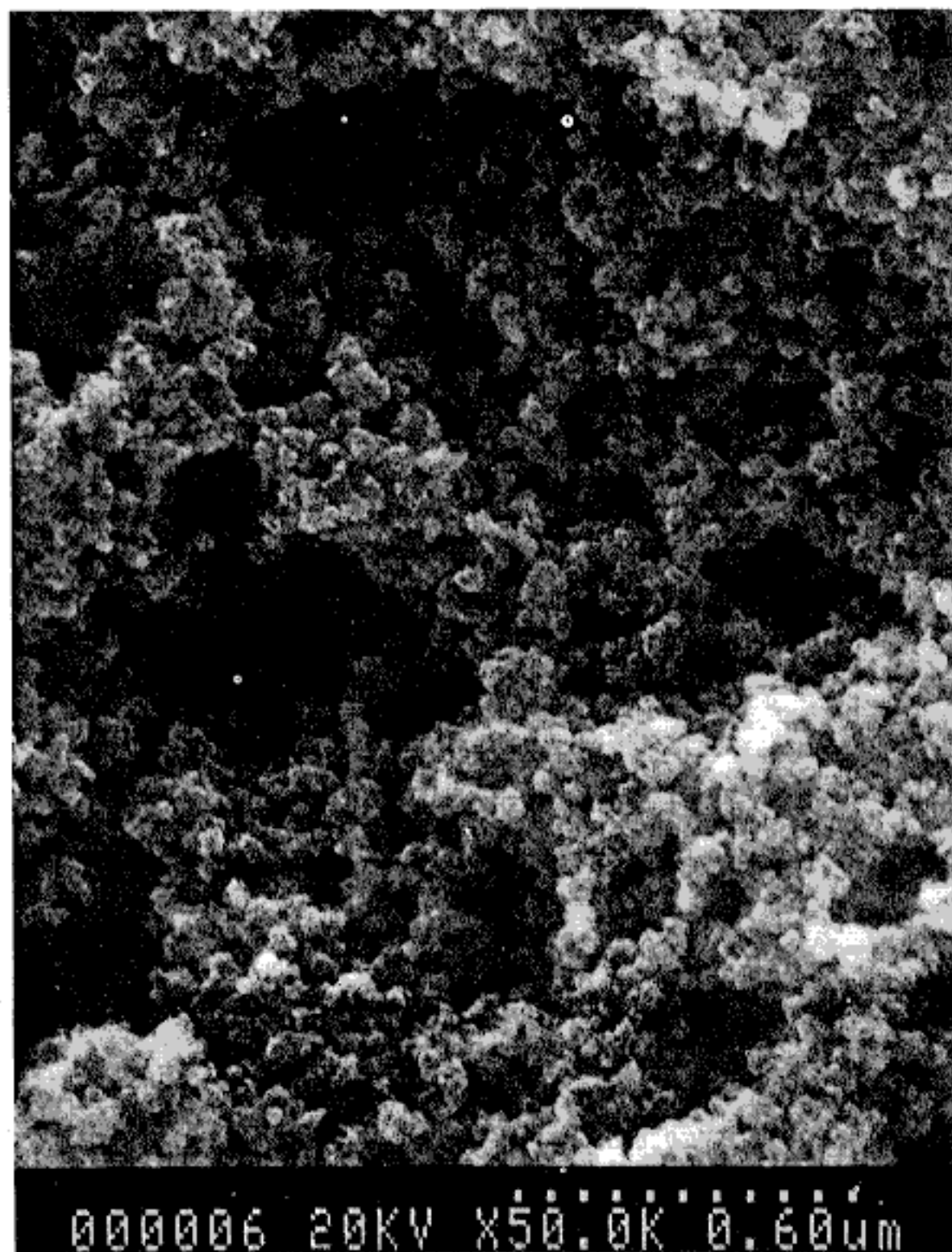


Fig. 10. Scanning electron micrograph of amorphous nanostructured iron powder produced from the ultrasonic irradiation of $\text{Fe}(\text{CO})_5$. Reproduced with permission (60).

wide range of nanostructured materials, including high surface area transition metals, alloys, carbides, oxides and colloids (62,64). Sonochemical decomposition of volatile organometallic precursors in high boiling solvents produces nanostructured materials in various forms with high catalytic activities. Nanometer colloids, nanoporous high surface area aggregates, and nanostructured oxide supported catalysts can all be prepared by this general route, as shown schematically in Figure 11. For example, sonication of iron pentacarbonyl with silica generated an amorphous nanostructured Fe-SiO₂ supported catalyst. This catalyst showed higher catalytic activity for the Fischer-Tropsch synthesis compared to the conventional Fe-silica catalyst prepared by the traditional incipient wetness method. Sonochemical synthesis of high surface area alloys can be accomplished by the sonolysis of Fe(CO)₅ and Co(CO)₃(NO). As another example, ultrasonic irradiation of Mo(CO)₆ produces aggregates of nanometer-sized clusters of face centered cubic molybdenum carbide. The extremely porous material had a high surface area and consisted of aggregates of ≈2-nm sized particles. The catalytic properties showed that the molybdenum carbide generated by ultrasound is an active and highly selective dehydrogenation catalyst comparable to commercial ultrafine platinum powder.

Sonochemistry is also proving to have important applications with polymeric materials. Substantial work has been accomplished in the sonochemical initiation of polymerization and in the modification of polymers after synthesis (3,5). The use of sonolysis to create radicals which function as radical initiators has been well explored. Similarly the use of sonochemically prepared radicals and other reactive species to modify the surface properties of polymers is being developed, particularly by G. Price. Other effects of ultrasound on long chain polymers tend to be mechanical cleavage, which produces relatively uniform size distributions of shorter chain lengths.

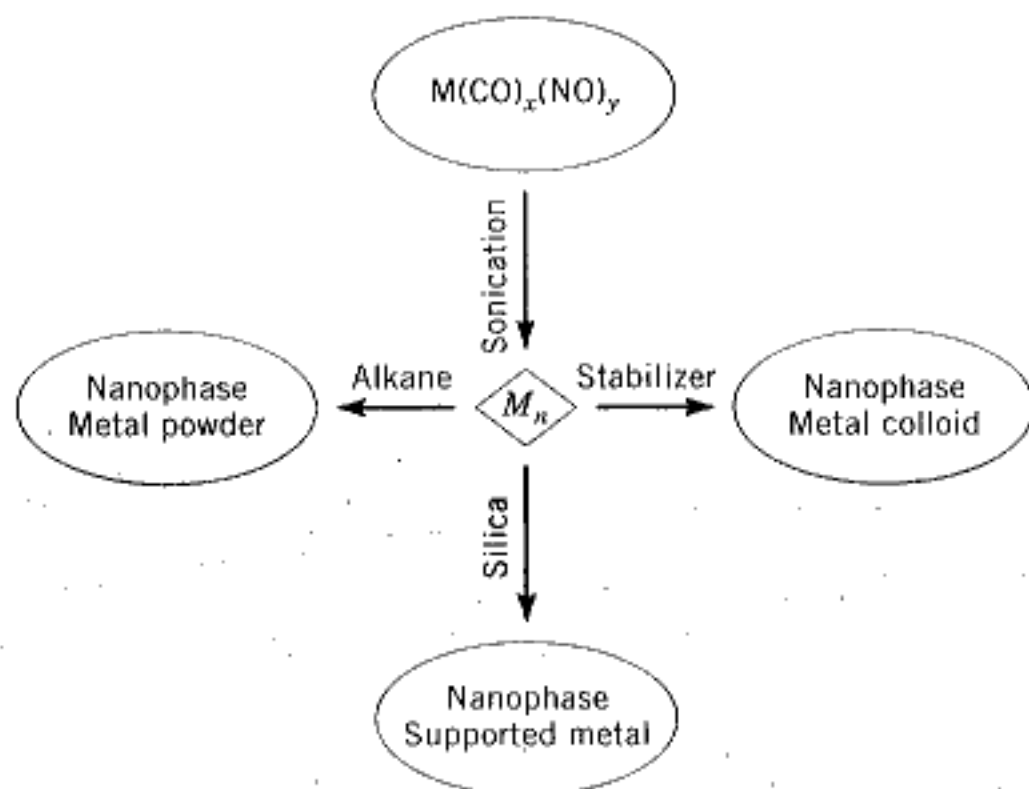


Fig. 11. Sonochemical synthesis of various forms of nanostructured materials. $n = 100-1000$.

Another important application has been the sonochemical preparation of biomaterials, most notably protein microspheres (65–68). Using high intensity ultrasound and simple protein solutions, a remarkably easy method to make both air-filled microbubbles and nonaqueous liquid-filled microcapsules has been developed. Figure 12 shows an electron micrograph of sonochemically prepared microspheres. These microspheres are stable for months, and being slightly smaller than erythrocytes, can be intravenously injected to pass unimpeded through the circulatory system. The mechanism responsible for microsphere formation is a combination of *two* acoustic phenomena: emulsification and cavitation. Ultrasonic emulsification creates the microscopic dispersion of the protein solution necessary to form the proteinaceous microspheres. Alone, however, emulsification is insufficient to produce long-lived microspheres. The long life of these microspheres comes from a sonochemical cross-linking of the protein shell. Protein cysteine residues are oxidized during microsphere formation by sonochemically produced superoxide. These protein microspheres, have a wide range of biomedical applications, including their use as echo contrast agents for sonography, magnetic-resonance-imaging contrast enhancement, drug delivery, among others.

Heterogeneous Sonochemistry: Reactions of Solids with Liquids. The use of ultrasound to accelerate chemical reactions in heterogeneous systems has

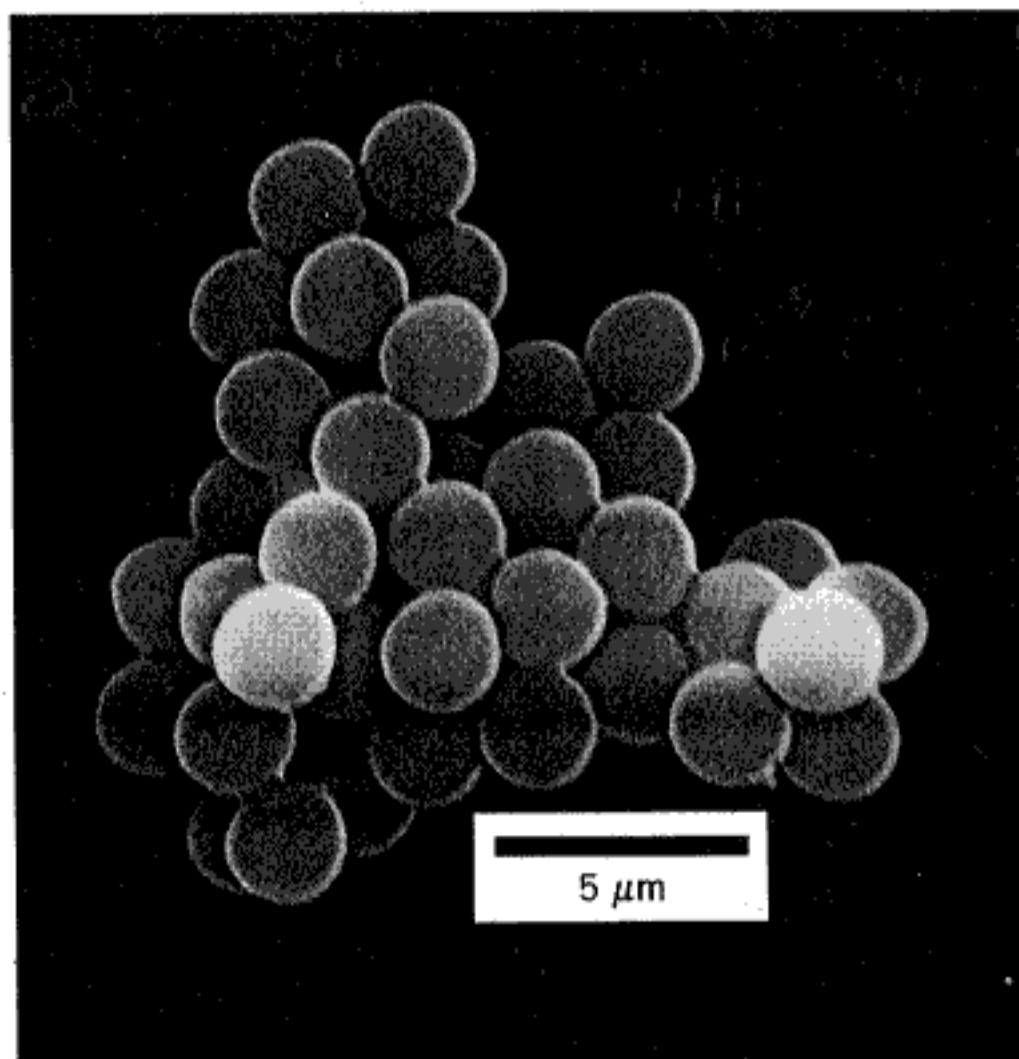


Fig. 12. Scanning electron micrograph of sonochemically synthesized hemoglobin microspheres.

become increasingly widespread. The physical phenomena which are responsible include the creation of emulsions at liquid-liquid interfaces, the generation of cavitation erosion and cleaning at liquid-solid interfaces, the production of shock wave damage and deformation of solid surfaces, the enhancement in surface area from fragmentation of friable solids, and the improvement of mass transport from turbulent mixing and acoustic streaming.

The use of high-intensity ultrasound to enhance the reactivity of reactive metals as stoichiometric reagents has become an especially routine synthetic technique for many heterogeneous organic and organometallic reactions (11-15), particularly those involving reactive metals, such as Mg, Li or Zn. This development originated from the early work of Renaud and the more recent breakthroughs of Luche (12,13). The effects are quite general and apply to reactive inorganic salts and to main group reagents as well (69). Less work has been done with unreactive metals (eg, V, Nb, Mo, W), but results here are promising as well (11). Rate enhancements of more than tenfold are common, yields are often substantially improved, and by-products avoided. A wide range of synthetically useful heterogeneous sonochemical reactions have been listed in Table 1. The applications of sonochemistry to organic synthesis have been reviewed recently in great detail (13).

The mechanism of the sonochemical rate enhancements in both stoichiometric and catalytic reactions of metals is associated with dramatic changes in morphology of both large extended surfaces and of powders. As discussed earlier, these changes originate from microjet impact on large surfaces and high-velocity interparticle collisions in slurries. Surface composition studies by Auger electron spectroscopy and sputtered neutral mass spectrometry reveal that ultrasonic irradiation effectively removes surface oxide and other contaminating coatings (11). The removal of such passivating coatings can dramatically improve reaction rates. The reactivity of clean metal surfaces also appears to be responsible for the greater tendency for heterogeneous sonochemical reactions to involve single electron transfer rather than acid-base chemistry (70).

Applications of ultrasound to electrochemistry have also seen substantial recent progress. Beneficial effects of ultrasound on electroplating and on organic synthetic applications of organic electrochemistry (71) have been known for quite some time. More recent studies have focused on the underlying physical theory of enhanced mass transport near electrode surfaces (72,73). Another important application for sonoelectrochemistry has been developed by J. Reisse and co-workers for the electroreductive synthesis of sub-micrometer powders of transition metals (74).

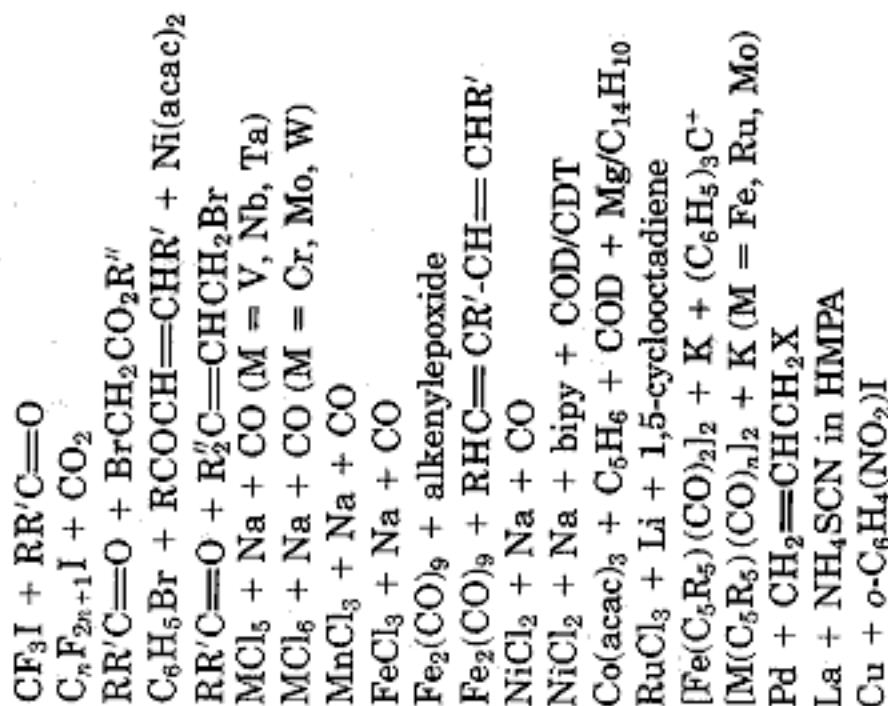
Sonocatalysis. Ultrasound has potentially important applications in both homogeneous and heterogeneous catalytic systems. The inherent advantages of sonocatalysis include (1) the use of low ambient temperatures to preserve thermally sensitive substrates and to enhance selectivity; (2) the ability to generate high energy species difficult to obtain from photolysis or simple pyrolysis; and (3) the mimicry of high temperature and pressure conditions on a microscopic scale.

Homogeneous catalysis of various reactions often uses organometallic compounds. The starting organometallic compound, however, is often catalytically inactive until loss of metal-bonded ligands (such as carbon monoxide) from the

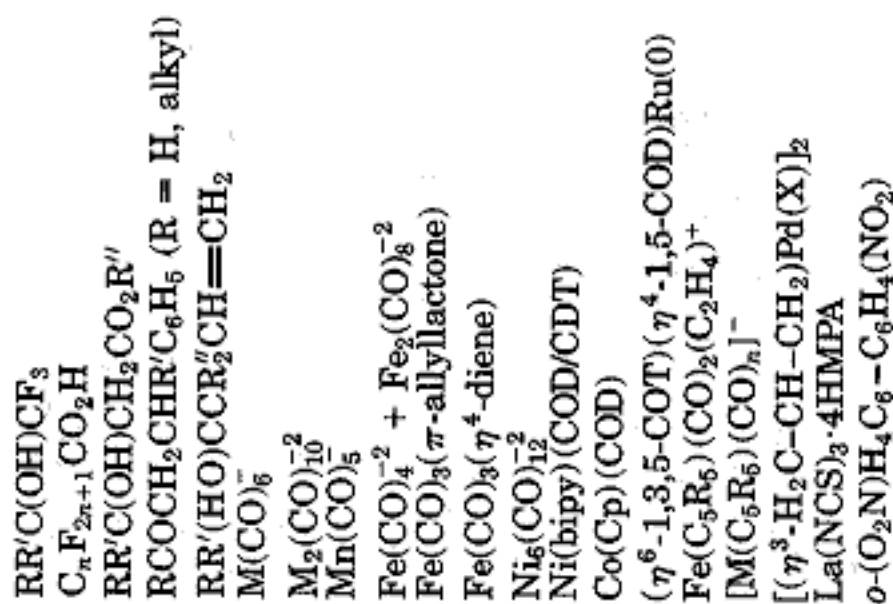
Table 1. Some Representative Examples of Heterogeneous Sonochemistry

Heterogeneous reagent	Reactant	Products
Compounds of metals		
LiAlH ₄	Ar-X	ArH
LiAlH ₄	R ₃ M-X (X = Cl, NR ₂ , OR)	R ₃ M-H (M = Si, Ge, Sn)
Al ₂ O ₃	C ₆ H ₅ CH ₂ Br + KCN	C ₆ H ₅ CH ₂ CN
KMnO ₄	RR'HCOH	RR'CO
CrO ₂ Cl ₂	RR'HCOH	RR'CO
HBR ₂	R' ₂ C=CR' ₂	HR' ₂ C-CR' ₂ (BR ₂)
MS ₂ , M = Mo, Ta, Zr	NR ₃ , py, Cp ₂ Co	intercalates
Hg	(HR ₂ BrC) ₂ CO + R'CO ₂ H	(HR ₂ C)CO(C(O ₂ CR')R ₂)
	(HR ₂ BrC) ₂ CO + R'OH	(HR ₂ C)CO(C(OR')R ₂)
Mg	R-Br	R-MgBr
	R ₂ C=CHCH ₂ Cl + Mg/C ₁₄ H ₁₄	R ₂ C=CHCH ₂ MgCl
Li	R-Br (R = C ₃ H ₆ , <i>m</i> -C ₄ H ₉ , C ₆ H ₅)	R-Li
	R-Br + R'R''CO	RR'R''COH
	R-Br + (H ₃ C) ₂ NCHO	RCHO
	R ₃ M-Cl (M = C, Si, Sn)	R ₃ MMR ₃
	R ₂ SiCl ₂ (R = arenes)	cyclo-(R ₂ Si) ₃
	R ₂ MCl ₂ + Na + Se (M = Si, Sn)	(R ₂ MSe) ₃

Zn



Transition metals



metal. Having demonstrated that ultrasound can induce ligand dissociation, the initiation of homogeneous catalysis by ultrasound becomes practical. A variety of metal carbonyls upon sonication will catalyze the isomerization of 1-alkenes to the internal alkenes (57), through reversible hydrogen atom abstraction, with rate enhancements of as much as 10^5 over thermal controls.

Heterogeneous catalysis is generally more industrially important than homogeneous systems, and the applications of ultrasound here have been reviewed recently (75). Heterogeneous catalysts often require rare and expensive metals. The use of ultrasound offers some hope of activating less reactive, but also less costly, metals. Such effects can occur in three distinct stages: (1) during the formation of supported catalysts, (2) activation of pre-formed catalysts, or (3) enhancement of catalytic behavior during a catalytic reaction. Some early investigations of the effects of ultrasound on heterogeneous catalysis can be found in the Soviet literature (76). In this early work, increases in turnover rates were usually observed upon ultrasonic irradiation, but were rarely more than tenfold. In the cases of modest rate increases, it appears likely that the cause is increased effective surface area; this is especially important in the case of catalysts supported on brittle solids (77). More impressive accelerations, however, include hydrogenations and hydrosilations by Ni powder, Raney Ni, and Pd or Pt on carbon. For example, as shown in Figure 13, the hydrogenation of alkenes

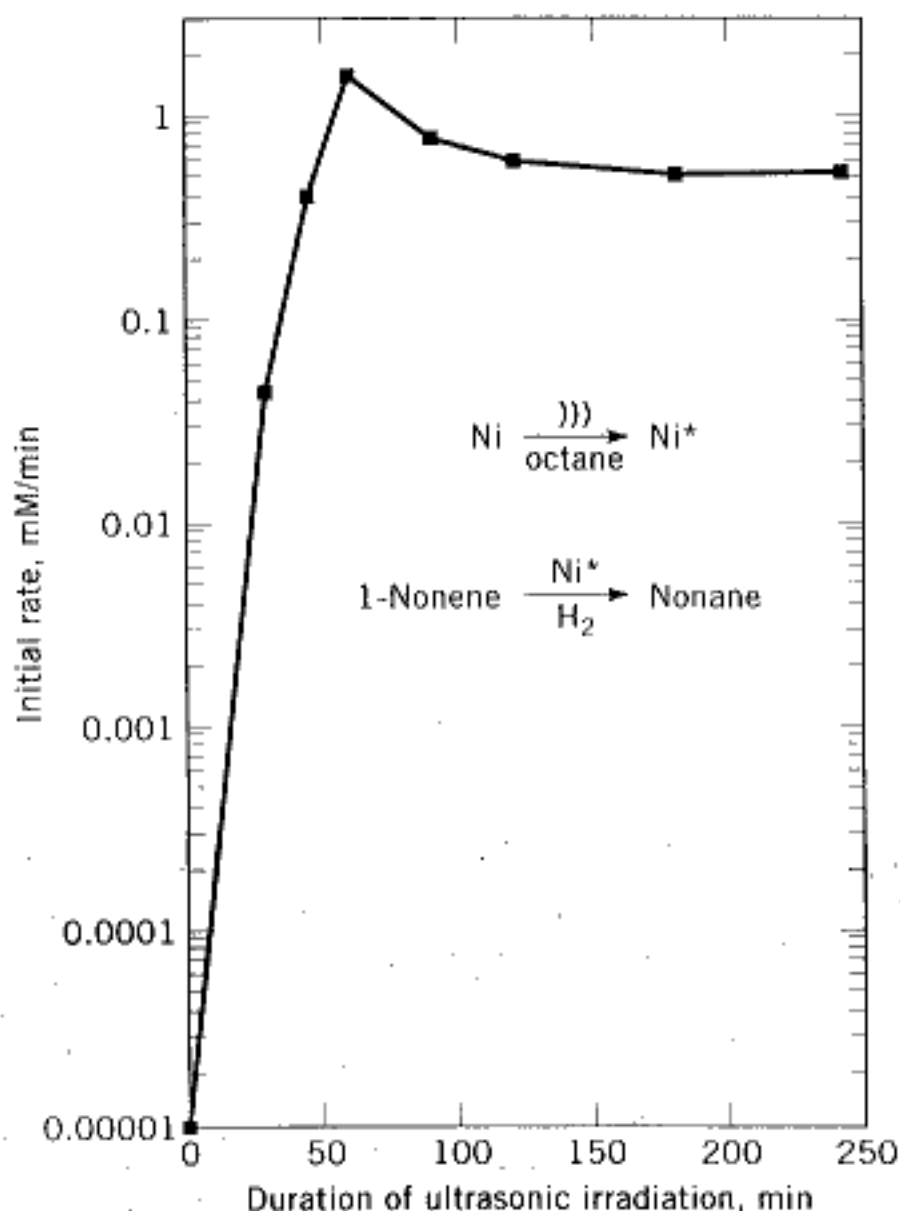


Fig. 13. The effect of ultrasonic irradiation on the catalytic hydrogenation activity of Ni powder. Reproduced with permission (16).

by Ni powder is enormously enhanced ($>10^5$ -fold) by ultrasonic irradiation (16). This dramatic increase in catalytic activity is due to the formation of uncontaminated metal surfaces from interparticle collisions caused by cavitation-induced shockwaves.

Summary

The phenomenon of acoustic cavitation results in an enormous concentration of energy. If one considers the energy density in an acoustic field that produces cavitation and that in the collapsed cavitation bubble, there is an amplification factor of over eleven orders of magnitude. The enormous local temperatures and pressures so created result in phenomena such as sonochemistry and sonoluminescence and provide a unique means for fundamental studies of chemistry and physics under extreme conditions. A diverse set of applications of ultrasound to enhancing chemical reactivity has been explored, with important applications in mixed-phase synthesis, materials chemistry, and biomedical uses.

BIBLIOGRAPHY

1. K. S. Suslick, ed., *Ultrasound: Its Chemical, Physical, and Biological Effects*, VCH Publishers, New York, 1988.
2. K. S. Suslick, *Science* **247**, 1439 (1990).
3. T. J. Mason, ed., *Advances in Sonochemistry*, vols. 1–4, JAI Press, New York, 1990, 1991, 1993, 1996.
4. T. J. Mason and J. P. Lorimer, *Sonochemistry: Theory, Applications and Uses of Ultrasound in Chemistry*, Ellis Horwood, Ltd., Chichester, U.K., 1988.
5. G. J. Price, ed., *Current Trends in Sonochemistry*, Royal Society of Chemistry, Cambridge, 1992.
6. K. S. Suslick, D. A. Hammerton, and R. E. Cline, Jr., *J. Am. Chem. Soc.* **108**, 5641 (1986).
7. E. B. Flint and K. S. Suslick, *Science* **253**, 1397 (1991).
8. L. A. Crum, *Proc. 1982 Ultrasonics Symp.* **1**, 1 (1982).
9. T. G. Leighton, *The Acoustic Bubble*, Academic Press, London, 1994, pp. 531–551.
10. S. J. Doktycz and K. S. Suslick, *Science* **247**, 1067 (1990).
11. K. S. Suslick and S. J. Doktycz, *Adv. Sonochem.* **1**, 197–230 (1990).
12. C. Einhorn, J. Einhorn, and J.-L. Luche, *Synthesis*, 787 (1989).
13. J. L. Luche, *Comptes Rendus Serie IIB* **323**, 203, 337 (1996).
14. J. M. Pestman, J. B. F. N. Engberts, and F. de Jong, *Recl. Trav. Chim. Pays-Bas* **113**, 533 (1994).
15. K. S. Suslick, "Sonochemistry of Transition Metal Compounds," in R. B. King, ed., *Encyclopedia of Inorganic Chemistry*, John Wiley & Sons, Inc., New York, vol. 7, pp. 3890–3905.
16. K. S. Suslick and D. J. Casadonte, *J. Am. Chem. Soc.* **109**, 3459 (1987).
17. L. A. Crum, *Physics Today* **47**, 22 (1994).
18. S. J. Putterman, *Scientific American*, 46 (Feb. 1995).
19. Lord Rayleigh, *Philos. Mag.* **34**, 94 (1917).
20. W. T. Richards and A. L. Loomis, *J. Am. Chem. Soc.* **49**, 3086 (1927).
21. M. A. Margulis, *Ultrasonics* **30**, 152 (1992).
22. T. Lepoint and F. Mullie, *Ultrasonics Sonochem.* **1**, S13 (1994).

23. H. G. Flynn, "Physics of Acoustic Cavitation in Liquids," in W. P. Mason, ed., *Physical Acoustics*, vol. 1B, Academic Press, New York, 1964, p. 157.
24. L. A. Crum, *J. Acoust. Soc. Am.* **95**, 559 (1994).
25. B. P. Barber and S. J. Putterman, *Phys. Rev. Lett.* **69**, 3839 (1992).
26. R. Lofstedt, B. P. Barber, and S. J. Putterman, *Phys. Fluids A* **5**, 2911 (1993).
27. A. Henglein, *Ultrasonics* **25**, 6 (1985).
28. A. Henglein, *Adv. Sonochem.* **3**, 17 (1993).
29. H. Frenzel and H. Schultes, *Z. Phys. Chem.* **27b**, 421 (1934).
30. T. J. Matula, R. A. Roy, P. D. Mourad, W. B. McNamara III, and K. S. Suslick, *Phys. Rev. Lett.* **75**, 2602 (1995).
31. D. F. Gaitan and L. A. Crum, in D. T. Blackstock, ed., *Frontiers of Nonlinear Acoustics*, 12th ISNA, Elsevier Applied Science, New York, 1990, pp. 459-463.
32. D. F. Gaitan, L. A. Crum, R. A. Roy, and C. C. Church, *J. Acoust. Soc. Am.* **91**, 3166 (1992).
33. B. P. Barber, R. A. Hiller, R. Lofstedt, S. J. Putterman, and K. R. Weninger, *Phys. Rev. Lett.* **72**, 1380 (1994).
34. L. A. Crum and R. A. Roy, *Science* **266**, 233 (1994).
35. R. E. Verrall and C. Sehgal in Ref. 1, pp. 227-287.
36. E. B. Flint and K. S. Suslick, *J. Phys. Chem.* **95**, 1484 (1991).
37. E. B. Flint and K. S. Suslick, *J. Amer. Chem. Soc.* **111**, 6987 (1989).
38. R. Hiller, K. Weninger, S. J. Putterman, and B. P. Barber, *Science* **266**, 248 (1994).
39. B. P. Barber, R. Hiller, K. Arisaka, H. Fetterman, and S. J. Putterman, *J. Acoust. Soc. Am.* **91**, 3061 (1992).
40. B. P. Barber, C. C. Wu, R. Lofstedt, P. H. Roberts, and S. J. Putterman, *Phys. Rev. Lett.* **72**, 1380 (1994).
41. W. C. Moss, D. B. Clarke, and D. A. Young, *Science* **276**, 1398 (1997).
42. D. Lohse and co-workers, *Phys. Rev. Lett.* **78**, 1359 (1997).
43. J. Berlan and T. J. Mason, *Ultrasonics* **30**, 203 (1992).
44. T. J. Mason and E. D. Cordemans, *Chem. Eng. Res. Des.* **74**, 511 (1996).
45. R. L. Hunicke, *Ultrasonics* **28**, 291 (1990).
46. A. Shoh in Ref. 1, pp. 97-122.
47. J. Reisse, T. Caulier, C. Deckerkheer, O. Fabre, J. Vandercammen, J. L. Delplancke, and R. Winand, *Ultrason. Sonochem.* **3**, S147 (1996).
48. C. Petrier and S. Laguian, *Chemosphere* **32**, 1709 (1996).
49. K. S. Suslick, J. W. Gawienowski, P. F. Schubert, and H. H. Wang, *Ultrasonics* **22**, 33 (1984).
50. K. S. Suslick, J. W. Gawienowski, P. F. Schubert, and H. H. Wang, *J. Phys. Chem.* **87**, 2229 (1983).
51. P. Riez, *Adv. Sonochem.* **2**, 23 (1991).
52. V. Misik and P. Riesz, *Ultrason. Sonochem.* **3**, S173 (1996).
53. P. Riesz, D. Berdahl, and C. L. Christman, *Environ. Health Perspect.* **64**, 233 (1985).
54. M. A. Margulis and N. A. Maximenko, *Adv. Sonochem.* **2**, 253 (1991).
55. M. R. Hoffmann, I. Hua, and R. Hochemer, *Ultrasonics Sonochemistry* **3**, S163 (1996).
56. I. Hua, R. H. Hochemer, and M. R. Hoffmann, *Env. Sci. Tech.* **29**, 2790 (1995).
57. K. S. Suslick, *Adv. Organomet. Chem.* **25**, 73 (1986).
58. K. S. Suslick, *MRS Bull.* **20**, 29 (1995).
59. O. V. Abramov, *Ultrasound in Liquid and Solid Metals*, CRC Press, Boca Raton, Fla., 1994.
60. K. S. Suslick, S. B. Choe, A. A. Cichowlas, and M. W. Grinstaff, *Nature* **353**, 414 (1991).
61. M. W. Grinstaff, M. B. Salamon, and K. S. Suslick, *Phys. Rev. B* **48**, 269 (1993).
62. K. S. Suslick, T. Hyeon, and M. Fang, *Chem. Mater.* **8**, 2172 (1996).

63. T. Hyeon, M. Fang, and K. S. Suslick, *J. Am. Chem. Soc.* **118**, 5492 (1996).
64. K. S. Suslick, M. Fang, and T. Hyeon, *J. Am. Chem. Soc.* **118**, 11960 (1996).
65. K. S. Suslick and M. W. Grinstaff, *J. Am. Chem. Soc.* **112**, 7807 (1990).
66. K. S. Suslick and M. W. Grinstaff, *Proc. Natl. Acad. Sci. USA* **88**, 7708 (1991).
67. K. J. Liu, M. W. Grinstaff, J. Jiang, K. S. Suslick, H. M. Swartz, and W. Wang, *Biophys. J.* **67**, 896 (1994).
68. A. G. Webb, M. Wong, K. J. Kolbeck, R. L. Magin, L. J. Wilmes, and K. S. Suslick, *J. Mag. Res. Imaging* **6**, 675 (1996).
69. T. Ando and T. Kimura, *Adv. Sonochem.* **2**, 211 (1991).
70. J.-L. Luche, *Ultrasonics Sonochem.* **1**, S111 (1994).
71. A. Durant, H. Francois, J. Reisse, and A. Kirschdemesmaeker, *Electrochim. Acta* **41**, 277 (1996).
72. R. G. Compton, J. C. Eklund, and F. Marken, *Electroanalysis*. **9**, 509 (1997).
73. N. A. Madigan and L. A. Coury, *Anal. Chem.* **69**, 5 (1997).
74. A. Durant, J. L. Delplancke, R. Winand, and J. Reisse, *Tetrahedron Lett.* **36**, 4257 (1995).
75. K. S. Suslick, "Sonocatalysis," in G. Ertl, H. Knozinger, and J. Weitkamp, eds., *Handbook of Heterogeneous Catalysis*, vol. 3, Wiley-VCH, Weinheim, 1997, Chapt. 8.6, pp. 1350-1357.
76. A. N. Mal'tsev, *Zh. Fiz. Khim.* **50**, 1641 (1976).
77. B. H. Han and P. Boudjouk, *Organometallics* **2**, 769 (1983).

KENNETH S. SUSLICK

University of Illinois at Urbana-Champaign

Acoustic cavitation and its chemical consequences

BY KENNETH S. SUSLICK, YURI DIDENKO, MING M. FANG,
TAEGHWAN HYEON, KENNETH J. KOLBECK,
WILLIAM B. MCNAMARA III, MILLAN M. MDLELENI AND MIKE WONG
*School of Chemical Sciences, University of Illinois at Urbana-Champaign,
600 S. Mathews Ave., Urbana, IL 61801, USA*

Acoustic cavitation is responsible for both sonochemistry and sonoluminescence. Bubble collapse in liquids results in an enormous concentration of energy from the conversion of the kinetic energy of liquid motion into heating of the contents of the bubble. The high local temperatures and pressures, combined with extraordinarily rapid cooling, provide a unique means for driving chemical reactions under extreme conditions. A diverse set of applications of ultrasound to enhance chemical reactivity has been explored, with important applications in mixed-phase synthesis, materials chemistry, and biomedical uses. For example, the sonochemical decomposition of volatile organometallic precursors in low-volatility solvents produces nanostructured materials in various forms with high catalytic activities. Nanostructured metals, alloys, carbides and sulphides, nanometre colloids, and nanostructured supported catalysts can all be prepared by this general route. Another important application of sonochemistry to materials chemistry has been the preparation of biomaterials, most notably protein microspheres. Such microspheres have a wide range of biomedical applications, including their use as echo contrast agents for sonography, magnetic resonance imaging contrast enhancement, and oxygen or drug delivery.

Keywords: sonochemistry; sonoluminescence; materials;
nanostructures; microspheres

1. Introduction

The chemical effects of ultrasound (Suslick 1988, 1998; Mason & Lorimer 1988) do not derive from a direct coupling of the acoustic field with chemical species on a molecular level. Instead, sonochemistry and sonoluminescence derive principally from acoustic cavitation: the formation, growth and implosive collapse of bubbles in liquids irradiated with high-intensity ultrasound (Leighton 1994). Bubble collapse during cavitation serves as an effective means of concentrating the diffuse energy of sound: compression of a gas generates heat. When the compression of bubbles occurs during cavitation, heating is more rapid than thermal transport, creating a short-lived localized hot spot. There is a nearly universal consensus that this hot spot is the source of homogeneous sonochemistry. Rayleigh's early descriptions of a mathematical model for the collapse of cavities in incompressible liquids predicted enormous local temperatures and pressures (Rayleigh 1917). Ten years later, Richards & Loomis (1927) reported the first chemical effects of ultrasound. Cavitation was heavily studied during the 1950s and 1960s, culminating in a relatively detailed

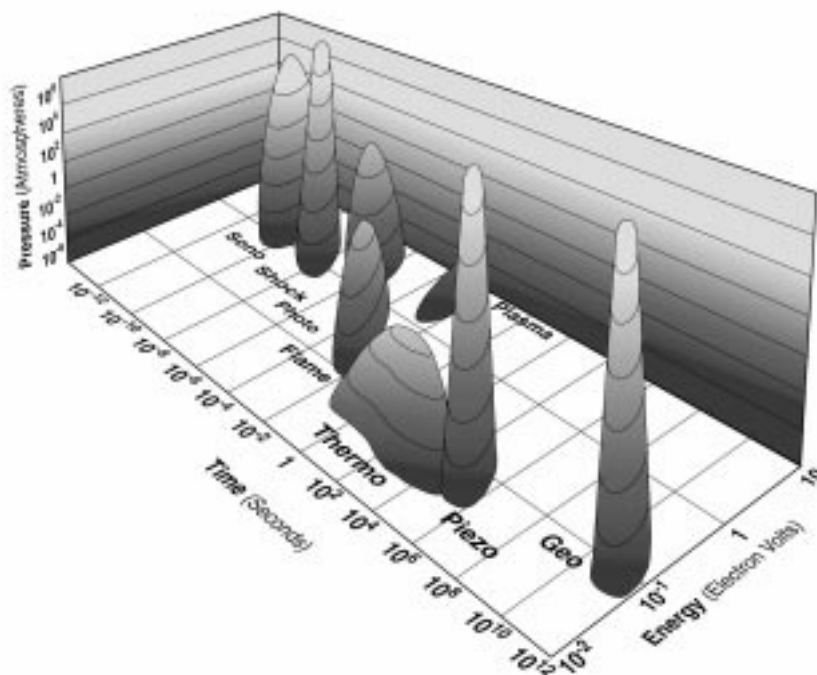


Figure 1. Chemistry: the interaction of energy and matter.

understanding (Neppiras 1980; Flynn 1964). From that time on, the chemical effects of ultrasound have been well explained as the consequence of localized hot spots created during bubble collapse.

Emission of light often accompanies sonochemistry. Such sonoluminescence provides an extremely useful spectroscopic probe of the conditions created during cavitation bubble collapse (Suslick 1990; Suslick & Crum 1997). As with sonochemistry, sonoluminescence is a consequence of acoustic cavitation. The collapse of bubbles caused by cavitation produces intense local heating and high pressures, with very short lifetimes. As we will show in this paper, the collapse of bubbles in a multi-bubble cavitation field produces hot spots with effective temperatures of *ca.* 5000 K, pressures of *ca.* 1000 atm, and heating and cooling rates above 10^{10} K s^{-1} . In single-bubble cavitation, conditions may be even more extreme (Crum 1994*a*; Putterman 1995). Thus, cavitation can create extraordinary physical and chemical conditions in otherwise cold liquids.

Chemistry is fundamentally the interaction of energy and matter. Chemical reactions require energy in one form or another to proceed: chemistry stops as the temperature approaches absolute zero. Chemists have only limited control, however, over the nature of this interaction. In large part, the properties of a specific energy source determine the course of a chemical reaction. Ultrasonic irradiation differs from traditional energy sources (such as heat, light or ionizing radiation) in duration, pressure and energy per molecule. The immense local temperatures and pressures together

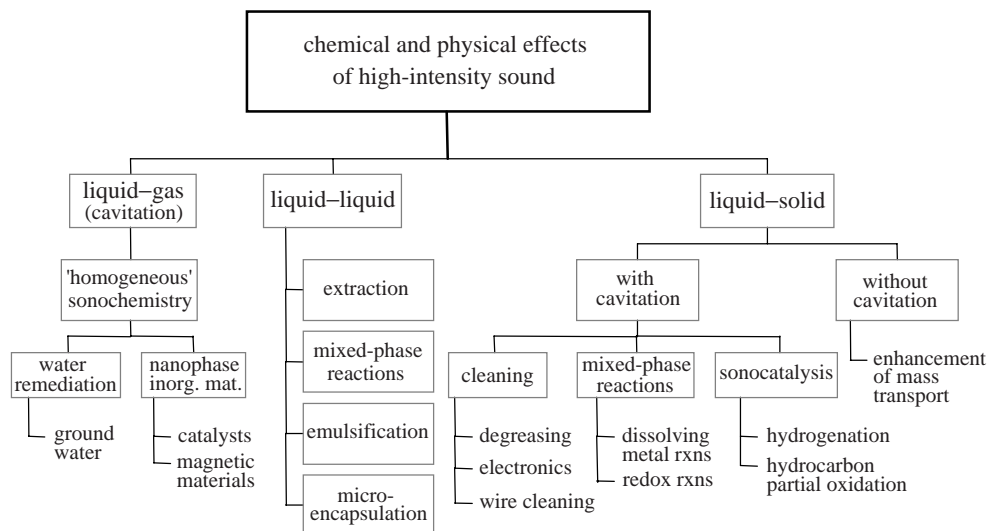


Figure 2. Classification of the chemical and physical effects of ultrasound.

with the extraordinary heating *and* cooling rates generated by cavitation bubble collapse mean that ultrasound provides a unique mechanism for generating high-energy chemistry. Figure 1 presents an interesting comparison of the parameters that control chemical reactivity (time, pressure and energy) for various forms of chemistry.

There is a wide range of chemical and physical consequences that high intensity can induce, as shown schematically in figure 2. The chemical effects of ultrasound can be divided into three general types: neat liquids; heterogeneous liquid-liquid; and heterogeneous liquid-solid systems. Sonocatalysis, i.e. the use of ultrasound to initiate or modify catalytic reactions, overlaps these classes. Over the past few years, the synthesis of inorganic and bio-materials has developed as one of the most important applications of sonochemistry (Suslick 1995, 1997). Cavitation provides a unique set of conditions to produce unusual materials from precursors dissolved in solution. In order to illustrate the utility of ultrasound in the synthesis of new and unusual materials, we will examine several recent examples discovered at the University of Illinois. Specifically, the sonochemical synthesis of nanostructured amorphous metals and alloys, nanocolloids of Fe, and nanostructured MoS₂ will be described.

Although length limitations prevent a detailed discussion here, the role of ultrasound in increasing reactivity in liquid-solid systems has proved extremely important in chemical synthesis (Suslick 1994; Mason & Luche 1996). Cavitation has dramatic effects on the reactivities of solutions containing either extended solid surfaces or fine powders. Cavity collapse near an extended solid surface becomes non-spherical, drives high-speed jets of liquid into the surface, and creates shockwave damage to the surface (Leighton 1994). This process can produce newly exposed highly heated surfaces and is responsible for the erosion/corrosion problems associated with hydrodynamic cavitation (Preece & Hansson 1981). Furthermore, cavitation and the shockwaves produced during ultrasonic irradiation of liquid-powder slurries can accelerate solid particles to high velocities (Suslick & Doktycz 1990; Doktycz & Suslick 1990). The interparticle collisions that result are capable of inducing striking changes in surface morphology, composition and reactivity. Thus, microjet and shockwave impact (on

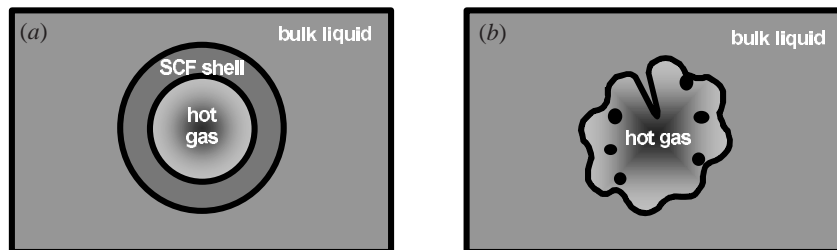


Figure 3. Two-site models of sonochemical reactions. (a) Thermal diffusion shell model; (b) surface wave droplet and jet model.

large surfaces) and interparticle collisions (with powders) have substantial effects on the chemical composition and physical morphology of solids that can dramatically enhance chemical reactivity.

2. Two-site model of sonochemical reactivity

The transient nature of cavitation, especially in bubble clouds, precludes conventional measurement of the conditions generated during bubble collapse. Chemical reactions themselves, however, can be used to probe reaction conditions. The effective temperature realized by the collapse of bubbles in cavitation clouds can be determined by the use of competing unimolecular reactions whose rate dependencies on temperature have already been measured. This technique of ‘comparative-rate chemical thermometry’ was used by Suslick *et al.* (1986) to make the first experimental determination of the effective temperature reached during cavity collapse. The sonochemical ligand substitutions of volatile metal carbonyls were used as the comparative rate probes. These kinetic studies revealed that there are in fact *two* sonochemical reaction sites: the first (and dominant site) is the bubble’s interior gas-phase, while the second is an *initially* liquid phase. The latter corresponds either to the heating of a shell of liquid around the collapsing bubble or to the injection of liquid droplets into the hot spot by surface-wave distortions or jets of the collapsing bubble, as shown schematically in figure 3.

The effective local temperatures in both sites were determined by combining the relative sonochemical reaction rates for ligand dissociation with the known temperature behaviour of these reactions. The effective temperatures of these hot spots were measured at *ca.* 5200 K in the gas-phase reaction zone and *ca.* 1900 K in the initially liquid zone (Suslick *et al.* 1986). Of course, the comparative rate data represent only a composite temperature: during the collapse, the temperature within the bubble has a rapidly changing temporal and spatial profile. This two-site model has been confirmed with other reactions (Henglein 1993). The study of sonoluminescence, which will now be discussed, has both confirmed and extended these temperature measurements of the cavitation hot spot.

3. Sonoluminescence

(a) Types of sonoluminescence

Sonoluminescence was first observed from water by Frenzel & Schultes (1934). As with sonochemistry, sonoluminescence derives from acoustic cavitation. There are

two classes of sonoluminescence (Crum 1994*a, b*; Matula *et al.* 1995): multiple-bubble sonoluminescence (MBSL) and single-bubble sonoluminescence (SBSL). Cavitation is a nucleated process and liquids generally contain large numbers of particulates that serve as nuclei. Consequently, the 'cavitation field' generated by a propagating or standing acoustic wave typically consists of very large numbers of interacting bubbles distributed over an extended region of the liquid. If this cavitation is sufficiently intense to produce sonoluminescence, then this phenomenon is called 'multiple-bubble sonoluminescence'.

Under appropriate conditions, the acoustic force on a bubble can balance against its buoyancy, holding the bubble stable in the liquid by acoustic levitation. This permits examination of the dynamic characteristics of the bubble in considerable detail, from both a theoretical and an experimental perspective. Such a bubble is typically quite small compared to an acoustic wavelength (e.g. at 20 kHz, the maximum radius observed during SBSL is *ca.* 50 μm). It was recently discovered, for rather specialized but easily obtainable conditions, that a single stable oscillating gas bubble can be forced into such large-amplitude pulsations that it produces sonoluminescence emissions during each (and every) acoustic cycle (Cheeke 1997; Barber *et al.* 1997). This phenomenon is called 'single-bubble sonoluminescence'.

(b) MBSL spectra

Over the last three decades, the sonoluminescence of aqueous solutions has been studied at length, most recently and carefully by Didenko and co-workers (Didenko *et al.* 1994; Didenko & Pugach 1994). The spectrum of MBSL in water consists of a peak at 310 nm and a broad continuum spanning the visible region. The emission at 310 nm is from excited-state OH^* , but the continuum is difficult to interpret. MBSL spectra from aqueous and alcohol solutions of many metal salts have been reported and are characterized by emission from metal-atom excited states (Flint & Suslick 1991*a*).

Sonoluminescence spectra have also been examined for non-aqueous liquids. Flint & Suslick (1989) reported the first MBSL spectra of organic liquids and found that the spectra were consistent with thermal excitation rather than electrical discharge. The observed emission during ultrasonic irradiation of various hydrocarbons comes from excited states of C_2 ($d^3\Pi_g - a^3\Pi_u$, the Swan lines), the same emission that is seen in flames. Furthermore, the ultrasonic irradiation of hydrocarbons in the presence of N_2 , NH_3 or amines gives emission from CN excited states, but not from N_2 excited states. Emission from N_2 excited states would have been expected if the MBSL originated from microdischarge, whereas CN emission is typically observed from thermal sources. When oxygen is present, emission from excited states of CO_2 , CH^* and OH^* is observed, again similar to flame emission.

Most recently, we have extended our spectral analysis approach to excited-metal-atom MBSL spectra. Ultrasonic irradiation of volatile organometallics ($\text{Fe}(\text{CO})_5$ or $\text{Cr}(\text{CO})_6$, for example) in a low-volatility organic liquid produces intense sonoluminescence that corresponds to the known atomic emission lines of the metals (Suslick *et al.* 1993), again analogous to flame emission. Hot-spot temperatures are sufficient not only to dissociate all the CO ligands from the metal complex, but also to produce excited-state metal atoms. Figure 4 shows a typical MBSL spectrum from a metal carbonyl solution ($\text{Cr}(\text{CO})_6$ in this example). Note the intense line emission from

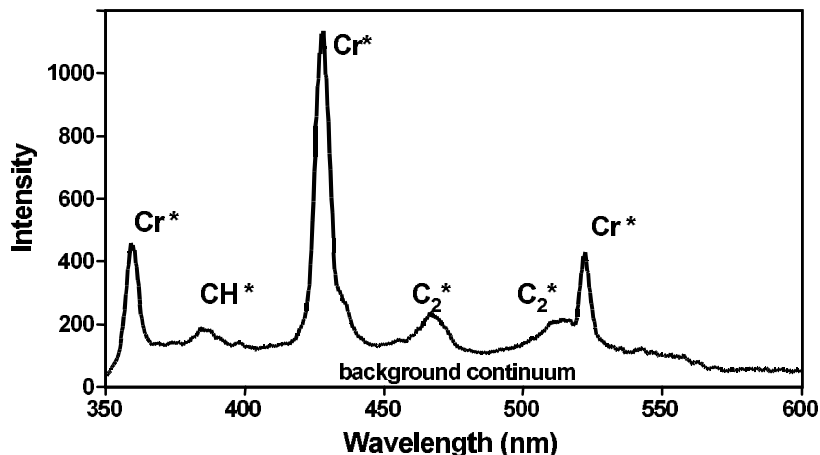


Figure 4. Typical MBSL spectrum from a metal carbonyl solution in silicone oil.

the metal-atom excited states as well as bands from excited states of the diatomics, C_2 and CH .

For both aqueous and non-aqueous liquids, MBSL is caused by chemical reactions of high-energy species formed during cavitation by bubble collapse. Its principal source is most probably not blackbody radiation or electrical discharge. MBSL is a form of chemiluminescence, not unlike flame emission.

(c) *The sonoluminescence spectrum as a probe cavitation condition*

Determination of the conditions reached in a cavitating bubble has remained a difficult experimental problem. Spectral analysis of MBSL provides a solution. We have used two very different spectroscopic reporters to provide such information:

- (i) resolved molecular emission from diatomics (notably C_2) produced during cavitation; and
- (ii) atomic line emission derived from the sonolysis of volatile organometallic compounds.

Flint & Suslick first reported high-resolution MBSL spectra from silicone oil under Ar (Flint & Suslick 1991*b*). The observed emission comes from excited-state C_2 and has been modelled with synthetic spectra as a function of rotational and vibrational temperatures (as shown in figure 5). From comparison of synthetic to observed spectra for several different emission bands, the effective rotational and vibrational emission temperature is 5050 ± 150 K. The excellence of the match between the observed MBSL and the synthetic spectra provides definitive proof that the sonoluminescence event is a thermal chemiluminescence process, although the issue of thermal equilibration in such systems is not without its complexities (Jeffries *et al.* 1992). The agreement between this spectroscopic determination of the cavitation temperature and that made by comparative-rate thermometry of sonochemical reactions (Suslick *et al.* 1986) is surprisingly good.

We have now analysed the relative intensities of atomic emission lines in the sonoluminescence spectra of excited-state metal atoms produced by sonolysis of volatile

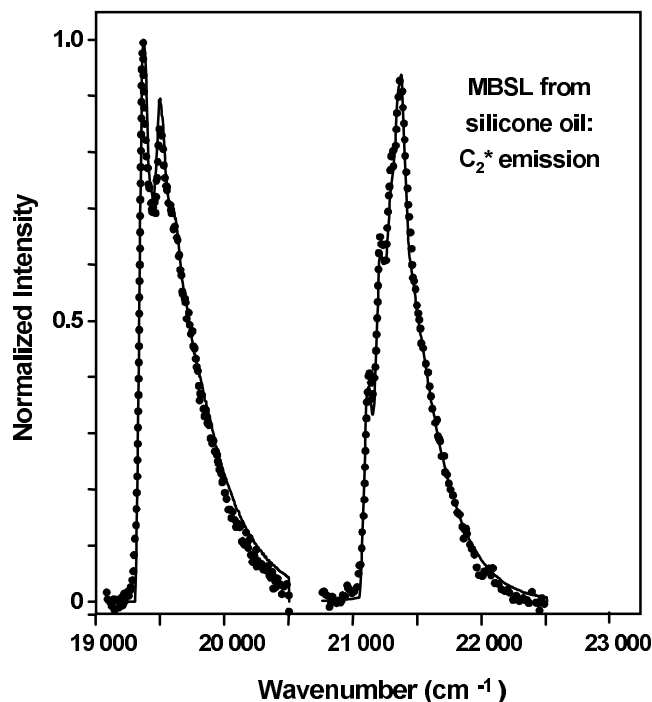


Figure 5. Excited-state C_2 MBSL spectrum from silicone oil under Ar. Emission from the $\Delta v = +1$ manifold of the $d^3\Pi_g - a^3\Pi_u$ transition (Swan band) of C_2 (Suslick *et al.* 1986). Observed MBSL spectrum from polydimethylsiloxane oil under Ar at 0°C (\cdots). Best-fit synthetic spectrum for these two bands, with $T_v = T_r = 4900\text{ K}$ (—).

Fe, Cr and Mo carbonyls dissolved in silicone oil under argon. Sufficient spectral information about emissivities of many metal-atom excited states are available to readily calculate emission spectra as functions of temperature. Because of this, the emission spectra of metal atoms are extensively used to monitor the surface temperature of stars. For example, the expected spectra for iron emission as functions of temperature are shown in figure 6.

From comparison of such calculated spectra and the observed MBSL spectra from metal carbonyls, another measurement of the cavitation temperature can be obtained. The effective emission temperature during cavitation under argon at 20 kHz is $4900 \pm 250\text{ K}$, with excellent agreement among the three systems tested ($5150 \pm 300\text{ K}$ for Fe, $4700 \pm 400\text{ K}$ for Cr and $4750 \pm 400\text{ K}$ for Mo), as shown in examples given in figures 7 and 8. Again, agreement with our prior comparative-rate thermometry and the MBSL emission temperature of C_2^* excited states is excellent.

We are also able to control the temperature within the cavitation bubble simply by changing the bubble contents. Upon addition of gaseous hydrocarbons (methane, ethylene or propane), the observed emission temperatures from Cr atom excited states systematically decrease: just 3% propane in Ar, for example, reduces the measured emission temperature to 2500 K. As polyatomic molecules are added to the bubble contents, the polytropic ratio of the gas in the bubble decreases, and so too does the expected temperature from adiabatic compression, as shown by equa-

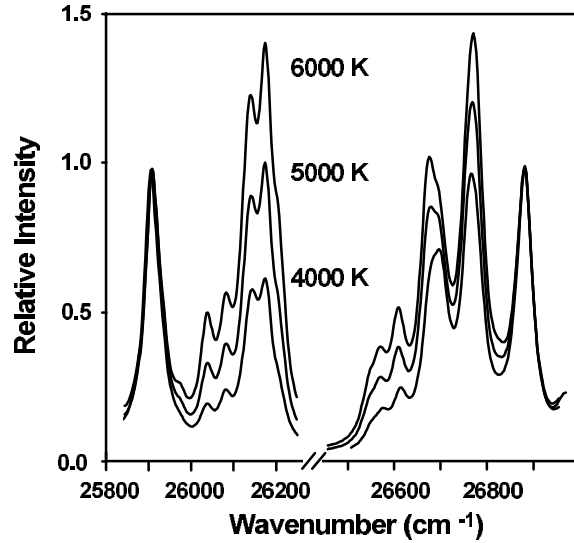


Figure 6. Calculated emission spectra of Fe atoms as functions of temperature.

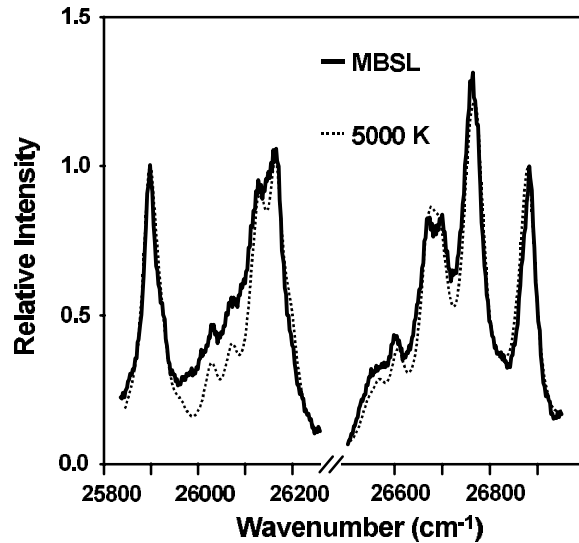


Figure 7. Sonoluminescence of excited-state Fe atoms produced during sonolysis of $\text{Fe}(\text{CO})_5$ dissolved in silicone oil under Ar. Effective emission temperature is 5150 ± 300 K.

tion (3.1):

$$T_{\max} = T_{\min} (R_{\max}/R_{\min})^{3(\gamma-1)}. \quad (3.1)$$

The presence of the polyatomic gas simply provides vibrational and rotational modes that will divert much of the kinetic energy of collapse away from a direct temperature increase. The effects of the addition of polyatomic gases on the observed cavitation emission temperature can be quantitatively modelled by simple adiabatic compression of a bubble during cavitation collapse. This simple model predicts

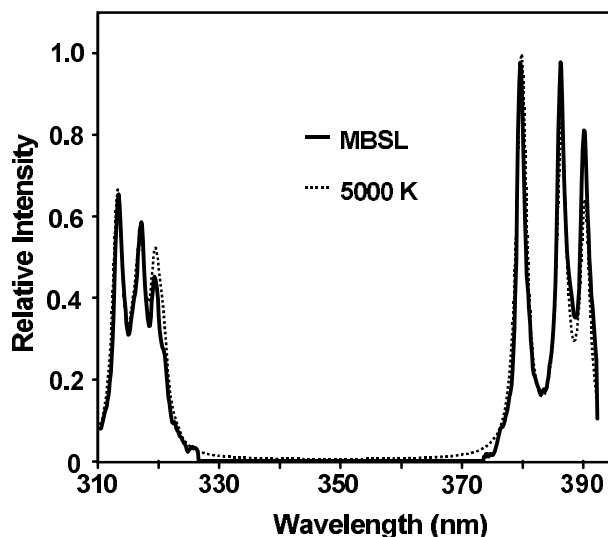


Figure 8. Sonoluminescence of excited-state Mo atoms produced during sonolysis of $\text{Mo}(\text{CO})_6$ dissolved in silicone oil under Ar. Effective emission temperature is 4750 ± 400 K.

pressures of the order of 10^3 bar, which is quantitatively consistent with the linewidth broadening and small peak-wavelength shifts observed in the metal-atom emission. The lifetime of the hot spot is less well determined. Certainly, it is under $1 \mu\text{s}$ and may be considerably less, given the 200 ps emission lifetimes seen in SBSL. The cooling rates, even at microsecond lifetimes, are enormous: above 10^{10} K s^{-1} .

(d) *SBSL spectra*

It has recently proved possible to trap a single stable bubble in a standing wave in a spherical or cylindrical transducer. Under certain conditions, a single bubble can be driven sufficiently hard so as to produce sonoluminescence. Study of this SBSL has provided much insight into the physics of cavitation. Unfortunately, single bubbles simply do not contain sufficient material to be useful for driving chemical reactions in any practical amount. In multibubble systems ('cavitation clouds'), on the other hand, the interactions between bubbles as they collapse will lead to both substantial asymmetry and the formation of jets during collapse (Leighton 1994), which one may well expect to limit the collapse efficiency. Thus, the conditions created during multibubble cavitation, which is used of necessity for all sonochemical reactions, will be less extreme than those created during SBSL.

The spectra of MBSL and SBSL are dramatically different (Matula *et al.* 1995), and the interpretation of SBSL spectra is much less clear. MBSL can be observed in essentially all liquids, whereas SBSL has been observed primarily in aqueous liquids. While MBSL is generally dominated by atomic and molecular emission lines (e.g. excited states of OH^* in water and of C_2 in hydrocarbons), SBSL is an essentially featureless emission that increases with decreasing wavelength. Unusual effects on the intensity of this featureless SBSL emission are observed when the gas contents of the bubble are changed (Barber *et al.* 1997; Cheeke 1997; Lohse *et al.* 1997; Barber *et al.* 1992). Furthermore, the SBSL spectra show no evidence of OH emission, and when He and Ar bubbles are considered, continue to increase in intensity even into the

deep ultraviolet. For example, the MBSL spectrum of an aqueous solution of NaCl is dominated by strong features from excited states of both OH[•] and Na; however, the SBSL spectrum of an identical solution shows no evidence of these peaks (Matula *et al.* 1995). Similarly, the MBSL spectrum falls off at low wavelengths, while the SBSL spectrum continues to rise, at least for most noble gases.

Early work on SBSL stirred intense interest due, primarily, to the exceptionally short duration of the sonoluminescence flash. The initial reports by Putterman placed the emission lifetimes well below 50 ps (Barber & Putterman 1992; Barber *et al.* 1997), but more recent studies by Gompf *et al.* (1997) have shown that the emission is generally longer, *ca.* 200 ps, and varies with dissolved-gas concentration and acoustic pressure. Hiller *et al.* (1998) have confirmed these results, but are still able to find lifetimes of *ca.* 50 ps under some conditions. The standard hydrodynamic models of adiabatic collapse of a single bubble could not have explained emission lifetimes much below 50 ps, which generated a wide range of quite speculative theories on the origin of SBSL. The consensus appears to be settling on intense adiabatic compression, leading to the reaction of O₂ and N₂ from air-filled bubbles with rectification into the water of NO_x products (Lohse *et al.* 1997). Partial ionization occurring in the last hottest stages of bubble collapse generate a featureless bremsstrahlung emission (Moss *et al.* 1997; Bernstein *et al.* 1996). There may also be a convergent shockwave within the single bubble (Barber *et al.* 1994), although this remains an open issue.

The difference between SBSL and MBSL spectra appears likely to be related to the severity of collapse. In SBSL, where bubble collapse is more spherical and the extent of compression greater, sufficient temperatures are reached (probably above *ca.* 20 000 K) to form a plasma and the primary emission becomes electron-ion or electron-atom bremsstrahlung (Moss *et al.* 1997; Bernstein *et al.* 1996). In such plasma, the temperatures will ensure dissociation of all molecules and will broaden, through Stark and pressure effects, any remaining molecular or atom emission beyond recognition (Moss *et al.* 1997). The issue of a spherically convergent shockwave and the possibility of extraordinarily high-energy conditions (Moss *et al.* 1997; Barber *et al.* 1994) remains an open question, since direct observation of core conditions will be shielded by the opacity of the surrounding plasma.

4. Synthesis of nanostructured inorganic materials

Solids made from nanometre-sized components often exhibit properties distinct from those of the bulk, in part because clusters that small have electronic structures with a high density of states, but not continuous bands (Weller 1993; Moser 1996). Such nanostructured materials are of intense current interest, and several preparative methods have been developed for their synthesis. Nanostructured-material syntheses include both gas-phase techniques (e.g. molten-metal evaporation, flash-vacuum-thermal and laser-pyrolysis decomposition of volatile organometallics); liquid-phase methods (e.g. reduction of metal halides with various strong reductants, colloid techniques with controlled nucleation); and mixed-phase approaches (e.g. synthesis of conventional heterogeneous catalysts on oxide supports, metal-atom vapour deposition into cryogenic liquids, explosive shock synthesis). Over the past ten years we have added the sonochemical reactions of volatile organometallics to this range of techniques, as a general approach to the synthesis of nanophase materials (figure 9).

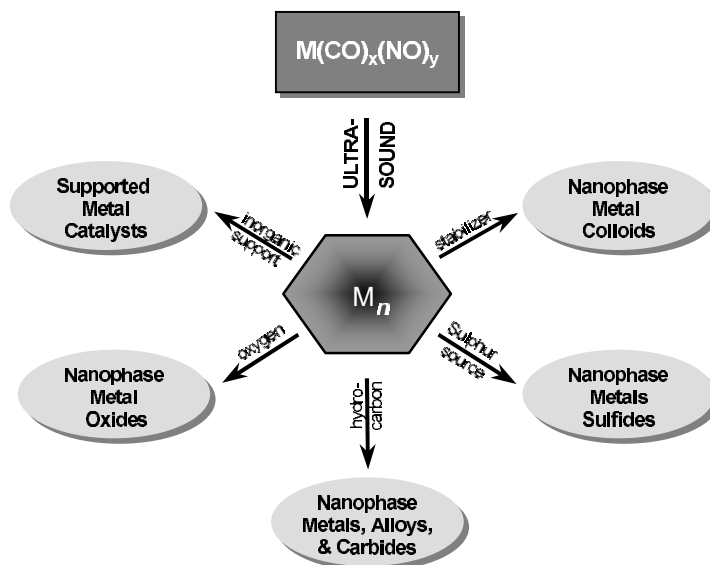


Figure 9. Sonochemical synthesis of nanostructured materials ($n \approx 100\text{--}1000$).

We have used the extreme conditions of cavitation to produce a variety of nanostructured and often amorphous metals, alloys and carbides, and have examined their catalytic activity (Suslick 1995, 1997; Suslick *et al.* 1996b; Hyeon *et al.* 1996). Volatile organometallic compounds decompose inside a collapsing bubble, and the resulting metal atoms agglomerate to form nanostructured materials. Our sonochemical synthesis of nanostructured materials is also extremely versatile: various forms of nanophase materials can be generated simply by changing the reaction medium (figure 9). When precursors are sonicated in low-volatility alkanes, nanostructured metal powders are formed. If sonication occurs in the presence of a bulky or polymeric surface ligand, stable nanophase metal colloids are created. Sonication of the precursor in the presence of an inorganic support (silica or alumina) provides an alternative means of trapping the nanometre clusters. The nanoparticles, once fixed on the surface of these supports, are very active supported heterogeneous catalysts.

(a) Amorphous metals

The ultrasonic irradiation of solutions containing volatile transition-metal carbonyls (e.g. $\text{Fe}(\text{CO})_5$, $\text{Co}(\text{CO})_3\text{NO}$) produces highly porous aggregates of nanometre-sized clusters of amorphous metals (Suslick *et al.* 1991; Grinstaff *et al.* 1993; Bellissent *et al.* 1993). For example, sonication of 1 M iron pentacarbonyl in decane at 0°C under a flow of argon yielded a dull black powder. Elemental analysis of the powder, after heating at 100°C under vacuum to remove residual solvent, showed it to be greater than 96% iron by weight, with trace amounts of carbon (less than 3%) and oxygen (1%, by difference), presumably from the decomposition of alkane solvent or carbon monoxide during ultrasonic irradiation. Scanning electron micrographs (SEMs) revealed that the powder is an agglomerate of 20 nm particles (figure 10). Transmission electron micrographs (TEMs) further indicated that these 20 nm particles consist of smaller 4–6 nm particles.

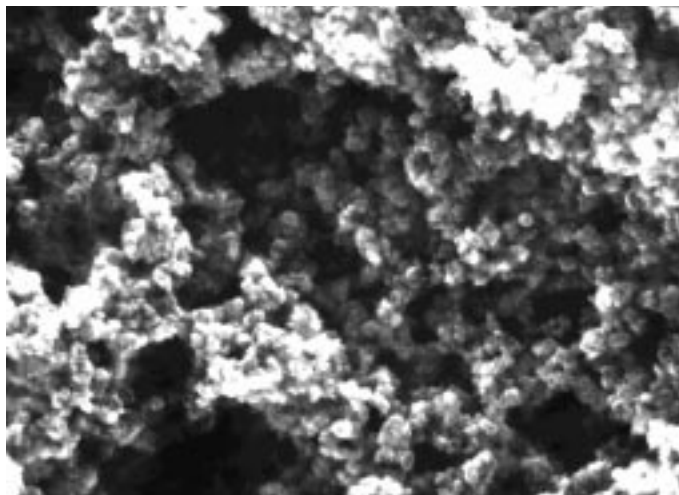


Figure 10. SEM of amorphous iron prepared by the sonochemical decomposition of $\text{Fe}(\text{CO})_5$ (Suslick *et al.* 1991). Image size is $1.20 \times 1.67 \mu\text{m}^2$.

The amorphous nature of the iron powder was confirmed by several different techniques, including SEM, differential scanning calorimetry (DSC), electron microdiffraction, X-ray powder diffraction and neutron diffraction. Initial X-ray powder diffraction showed no diffraction peak; after heat treatment under helium at 350°C the diffraction lines characteristic of BCC iron metal are observed. Electron microdiffraction revealed a diffuse ring pattern, characteristic of amorphous materials. DSC also shows one exothermic irreversible disorder–order transition temperature at 308°C . The amorphous metal formation appears to result from the extremely high cooling rate during acoustic cavitation.

There had been a long-standing controversy concerning the magnetic properties of amorphous iron, which had not been previously available without a substantial amount of added alloying elements (e.g. boron). Magnetic studies of the sonochemically prepared amorphous iron showed that amorphous iron is a very soft ferromagnetic with a saturation magnetization of *ca.* 173 emu g^{-1} and a Curie temperature in excess of 580 K . The effective magnetic moment is $1.7\mu_{\text{B}}$ with an effective exchange constant of only *ca.* 30% of crystalline Fe (Grinstaff *et al.* 1993; Bellissent *et al.* 1993; Long *et al.* 1998). The neutron-diffraction data confirmed these measurements and are consistent with a random packing model, as observed for many thin amorphous metal films. The magnetic properties fall close to those of liquid iron.

In passing, we note that sonochemical techniques can also be used to prepare nanostructured alloys. For example, Fe–Co alloys have been synthesized from the readily available $\text{Fe}(\text{CO})_5$ and $\text{Co}(\text{CO})_3(\text{NO})$ precursors. The composition of the Fe–Co alloys can be controlled simply by changing the ratio of solution concentrations of the precursors; alloy compositions ranging from pure Fe to pure Co are easily obtained (Hyeon *et al.* 1995).

(b) Transition-metal colloids

The existence of aggregates of nanometre clusters in our sonochemically prepared materials suggests the possibility of trapping these particles before they aggregate.

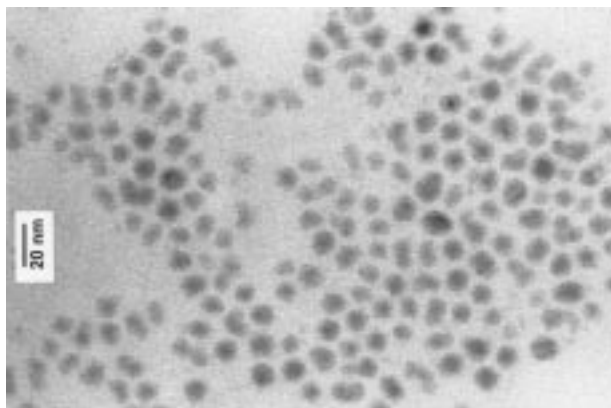


Figure 11. TEM of sonochemically prepared iron colloid stabilized by oleic acid (Suslick *et al.* 1996a).

Colloids of ferromagnetic materials are of special interest due to their many important technological applications as ferrofluids (Berkovsky *et al.* 1993). Such magnetic fluids find uses in information-storage media, magnetic refrigeration, audio reproduction and magnetic sealing. Commercial magnetic fluids are generally produced by exhaustive grinding of magnetite (Fe_3O_4) in ball or vibratory mills for several weeks in the presence of surfactants, which produces a very broad particle-size distribution.

We have developed a new method for the preparation of stable ferromagnetic colloids of iron. High-intensity ultrasound is used to sonochemically decompose volatile organometallic compounds in the presence of a colloid-stabilizing ligand (Suslick *et al.* 1996a). These colloids have narrow size distributions centred at a few nanometres and are found to be superparamagnetic. Sonochemical decomposition of iron pentacarbonyl in the presence of stabilizers such as polyvinylpyrrolidone or oleic acid produced a colloid of nanometre-sized iron particles. TEMs show that the iron particles have a relatively narrow range in size from 3 to 8 nm for polyvinylpyrrolidone, while oleic acid gives an even more uniform distribution at 8 nm (figure 11). Electron microdiffraction revealed that the particles are amorphous on the nanometre scale as formed and that during *in situ* electron-beam heating these particles crystallize to BCC iron.

Magnetic studies indicate that these colloidal iron particles are superparamagnetic with a respectable saturation magnetization of $101 \text{ emu g}^{-1} (\text{Fe})$ at 290 K. High-saturation magnetization is desirable for magnetic fluid applications and is highly sensitive to the method of preparation. Bulk amorphous Fe saturates at $156 \text{ emu g}^{-1} (\text{Fe})$ (Grinstaff *et al.* 1993; Bellissent *et al.* 1993). In comparison, the saturation magnetization of a commercial magnetite-based magnetic fluid is $123 \text{ emu g}^{-1} (\text{Fe})$ (Ferrofluids Corp. cat. no. APG-047).

(c) Nanostructured molybdenum sulphide

Very recently, we have reported the sonochemical synthesis of nanostructured molybdenum sulphide (Mdeleleni *et al.* 1998). MoS_2 is best known as a standard automotive lubricant; its lubricant properties are due to its layered structure. Planes

of molybdenum atoms are sandwiched on both faces by planes of sulphur atoms tightly bonded to the Mo. Interactions between the sulphur planes are weak, thus producing lubrication properties similar to graphite. Of greater interest here, however, MoS₂ is also the predominant hydrodesulphurization catalyst, heavily used by the petroleum industry to remove sulphur from fossil fuels before combustion (Gates 1992).

We prepared an unusual morphology of MoS₂ by irradiating solutions of molybdenum hexacarbonyl and sulphur in 1,2,3,5-tetramethylbenzene with high-intensity ultrasound (Mdleleni *et al.* 1998). The MoS₂ was amorphous as initially prepared, but subsequently crystallized upon heating at 725 K for 10 h under an atmosphere of flowing He. EDX analysis performed on these particles gave a S to Mo atomic ratio of 2.06, identical within experimental error to bulk chemical analysis. The morphologies of the sonochemical and conventional MoS₂, however, are dramatically different, as shown in figure 12. Conventional MoS₂ shows a plate-like morphology typical for such layered materials. The sonochemical MoS₂ exists as a porous agglomeration of clusters of spherical particles with an average diameter of 15 nm.

Despite the morphological difference between the sonochemical and conventional MoS₂, TEM images of both sulphides show lattice fringes with interlayer spacings of 0.62 ± 0.01 nm. The sonochemically prepared MoS₂, however, shows much greater edge and defect content, as the layers must bend, break or otherwise distort to form the outer surface of the 15 nm particle size.

It is well established that the activity of MoS₂ is localized at the edges and not on the flat basal planes (Gates 1992; Pecoraro & Chianelli 1981). Unfortunately, most synthetic techniques yield a structure whose surface area is dominated by the basal planes. Given the inherently higher edge concentrations in nanostructured materials, the catalytic properties of our sonochemically prepared MoS₂ become especially interesting. To this end, the catalytic activity and selectivity for thiophene hydrodesulphurization (HDS) by sonochemically prepared MoS₂ was examined in a single-pass microreactor. Conventional MoS₂, sonochemical Mo₂C, commercial ReS₂ (Gallard-Schlesinger Ind., Carle Place, NY) and RuS₂ (Gallard-Schlesinger) were also investigated under the same conditions for purposes of comparison. For conventionally prepared sulphides, ReS₂ and RuS₂ are inherently more reactive than MoS₂ (Pecoraro & Chianelli 1981), but are too expensive to be generally used. Given the difference in edge versus basal surface activity, catalytic activity does not correlate with total surface area and therefore comparisons must be made on a catalyst mass basis.

The observed turnover frequencies as a function of temperature were measured for these catalysts using a standard solid-gas catalytic flow microreactor (Mdleleni *et al.* 1998). The principal products detected by GC were the C₄ hydrocarbons: butadiene, 1-butene, *trans*-2-butene, *cis*-2-butene and butane. No partially hydrogenated thiophenes were detected, and lighter (C₁-C₃) hydrocarbons accounted for less than 1% of the reaction products. The observed HDS activity order is

MoS₂ (sonochemical) > RuS₂ (conventional)
> ReS₂ (conventional) ~ Mo₂C (sonochemical) > MoS₂ (conventional).

The sonochemically prepared MoS₂ catalyses the HDS of thiophene with activities roughly five-fold better than conventional MoS₂ and comparable to those observed with RuS₂, one of the best prior catalysts.

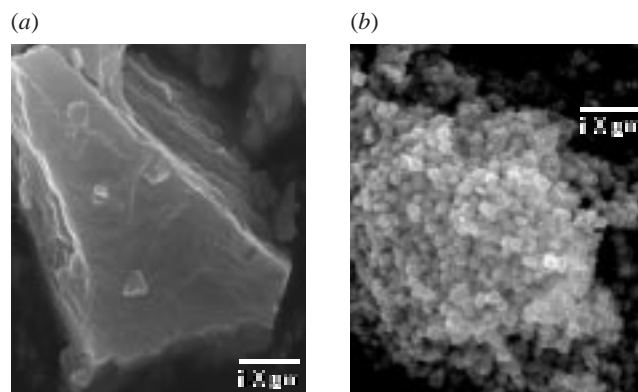


Figure 12. Morphology of (a) conventional and (b) sonochemically prepared MoS₂ (Mdleleni *et al.* 1998).

The product selectivities, expressed as percent of total C₄ hydrocarbons, observed at 375 °C were also examined. All catalysts showed high selectivity for formation of butenes, with the exception of the sonochemical MoS₂ that produced more butane. The accepted mechanism for thiophene HDS involves initial hydrogenolysis of the C–S bonds to give butadiene, followed by rapid hydrogenation to 1-butene, which is subsequently hydrogenated to butane or isomerized to a thermodynamic mixture of *cis*- and *trans*-2-butenes (Gates 1992). It is not surprising to see increased butane production from the sonochemical MoS₂, given its higher HDS activity.

There remains much to explore in the sonochemical synthesis of inorganic materials, and this technique has only begun to be exploited. The use of ultrasound in the synthesis of metal oxides, for example, has some promise as well (Shafi *et al.* 1997; Cao *et al.* 1997).

5. Sonochemical synthesis of biomaterials

Another important application of sonochemistry to materials chemistry has been in the preparation of biomaterials, most notably protein microspheres (Suslick & Grinstaff 1990; Liu *et al.* 1994; Wong & Suslick 1995; Eckburg *et al.* 1996; Webb *et al.* 1996). While the chemical effects of ultrasound on aqueous solutions have been studied for many years, the development of aqueous sonochemistry for biomaterials synthesis is very recent, particularly in the area of microencapsulation. It is beyond the scope of this article to review this area thoroughly, but a brief synopsis and bibliography will be provided.

Using high-intensity ultrasound and simple protein solutions, a remarkably easy method to make both air-filled microbubbles and non-aqueous liquid-filled microcapsules has been developed. Figure 13 shows an electron micrograph of sonochemically prepared microspheres. These microspheres are stable for months and, being slightly smaller than erythrocytes, can be intravenously injected to pass unimpeded through the circulatory system.

The mechanism responsible for microsphere formation is a combination of *two* acoustic phenomena: emulsification and cavitation. Ultrasonic emulsification creates the microscopic dispersion of the protein solution necessary to form the proteinaceous microspheres. Emulsification alone, however, is insufficient to produce long-

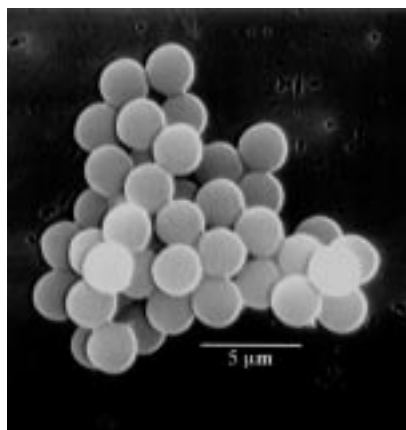


Figure 13. SEM of sonochemically prepared protein microspheres made from haemoglobin (Suslick 1998).

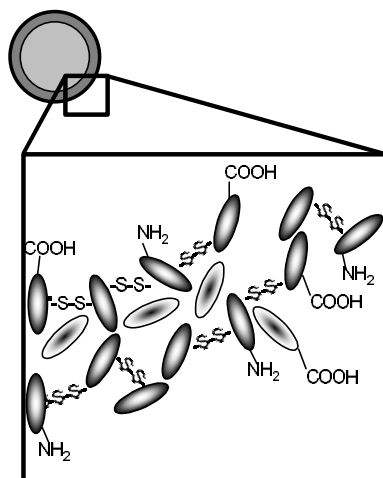


Figure 14. Disulphide cross-linking holds the protein microspheres together.

lived microspheres. The long life of these microspheres comes from a sonochemical cross-linking of the protein shell. Chemical reactions requiring O_2 are critical in forming the microspheres. It has been known for some time that the primary products from the sonolysis of water are H_2 and H_2O_2 coming H^\bullet and OH^\bullet ; in the presence of O_2 , HO_2 is also produced (Riesz *et al.* 1985). We have used chemical trapping experiments to establish that the proteinaceous microspheres are held together by disulphide bonds between protein cysteine residues and that superoxide is the cross-linking agent. This is shown schematically in figure 14. The cross-linked shell of the microspheres is only about ten protein molecules thick, as shown in figure 15.

These protein microspheres have a wide range of biomedical applications, including their use as echo contrast agents for sonography (Keller & Feinstein 1988), as magnetic resonance imaging contrast agents (Liu *et al.* 1994; Eckburg *et al.* 1996; Webb *et al.* 1996), and for oxygen or drug delivery (Liu *et al.* 1994; Wong & Suslick 1995), among others. An extensive patent literature now exists in this area.



Figure 15. TEM of protein-stained microtome section from sonochemically prepared protein microspheres (Wong & Suslick 1995).

6. Conclusions

The chemical consequences of acoustic cavitation are far reaching. Bubble collapse in liquids creates unique high-energy conditions to drive chemical reactions in otherwise cold liquids. The utility of sonochemistry has been explored, and important applications have been developed for synthesis of unusual inorganic and biomedical materials.

This work was supported by the National Science Foundation and in part by the Department of Energy. We also thank M. Marshall, P. Mochel, V. Petrova and the UIUC Center for Microanalysis of Materials, which is supported by the Department of Energy, for their assistance in surface characterizations.

References

- Barber, B. P. & Putterman, S. J. 1992 *Phys. Rev. Lett.* **69**, 3839.
- Barber, P., Hiller, R., Arisaka, K., Fetterman, H. & Putterman, S. J. 1992 *J. Acoust. Soc. Am.* **91**, 3061.
- Barber, P., Hiller, R. A., Lofstedt, R., Putterman, S. J. & Weninger, K. R. 1994 *Phys. Rev. Lett.* **72**, 1380.
- Barber, B. P., Hiller, R. A., Lofstedt, R., Putterman, S. J. & Weninger, K. R. 1997 *Phys. Rep.* **281**, 65–143.
- Bellissent, R., Galli, G., Grinstaff, M. W., Migliardo, P. & Suslick, K. S. 1993 *Phys. Rev. B* **48**, 15 797–15 800.
- Berkovsky, B. M., Medvedev, V. F. & Krakov, M. S. 1993 *Magnetic fluids: engineering applications*. Oxford University Press.
- Bernstein, L. S., Zakin, M. S., Flint, E. B. & Suslick, K. S. 1996 *J. Phys. Chem.* **100**, 6612–6619.
- Cao, X., Prozorov, R., Koltypin, Y., Kataby, G., Felner, I. & Gedanken, A. 1997 *J. Mater. Res.* **12**, 402.
- Cheeke, J. D. N. 1997 *Can. J. Phys.* **75**, 77–98.
- Crum, L. A. 1994a *Phys. Today* **47**, 22.
- Crum, L. A. 1994b *J. Acoust. Soc. Am.* **95**, 559.
- Didenko, Y. T. & Pugach, S. P. 1994 *Ultrasonics Sonochem.* **1**, s10–s12.

- Didenko, Y. T., Nastich, D. N., Pugach, S. P., Polovinka, Y. A. & Kvochka, V. I. 1994 *Ultrasonics* **32**, 71–76.
- Doktycz, S. J. & Suslick, K. S. 1990 *Science* **247**, 1067.
- Eckburg, J. J., Chato, J. C., Liu, K. J., Grinstaff, M. W., Swartz, H. M., Suslick, K. S. & Auteri, F. P. 1996 *J. Biomech. Engng* **118**, 193–200.
- Flint, E. B. & Suslick, K. S. 1989 *J. Am. Chem. Soc.* **111**, 6987.
- Flint, E. B. & Suslick, K. S. 1991a *J. Phys. Chem.* **95**, 1484.
- Flint, E. B. & Suslick, K. S. 1991b *Science* **253**, 1397.
- Flynn, H. G. 1964 Physics of acoustic cavitation in liquids. In *Physical acoustics* (ed. W. P. Mason), vol. IB, p. 157. New York: Academic.
- Frenzel, H. & Schultes, H. 1934 *Z. Phys. Chem.* **27b**, 421.
- Gates, B. C. 1992 *Catalytic chemistry*, pp. 387–392. New York: Wiley.
- Gompf, B., Günther, R., Nick, G., Pecha, R. & Eisenmenger, W. 1997 *Phys. Rev. Lett.* **79**, 1405.
- Grinstaff, M. W., Salamon, M. B. & Suslick, K. S. 1993 *Phys. Rev. B* **48**, 269.
- Henglein, A. 1993 *Adv. Sonochem.* **3**, 17.
- Hiller, R. A., Putterman, S. & Weninger, K. 1998 *Phys. Rev. Lett.* **80**, 1090.
- Hyeon, T., Fang, M., Cichowlas, A. A. & Suslick, K. S. 1995 *Mater. Sci. Engng A* **204**, 186–192.
- Hyeon, T., Fang, M. & Suslick, K. S. 1996 *J. Am. Chem. Soc.* **118**, 5492–5493.
- Jeffries, J. B., Copeland, R. A., Flint, E. B. & Suslick, K. S. 1992 *Science* **256**, 248.
- Keller, M. W. & Feinstein, S. B. 1988 In *Echocardiography in coronary artery disease* (ed. R. E. Kerber). New York: Future.
- Leighton, T. G. 1994 *The acoustic bubble*, pp. 531–551. London: Academic.
- Liu, K. J., Grinstaff, M. W., Jiang, J., Suslick, K. S., Swartz, H. M. & Wang, W. 1994 *Biophys. J.* **67**, 896–901.
- Lohse, D., Brenner, M. P., Dupont, T. F., Hilgenfeldt, S. & Johnston, B. 1997 *Phys. Rev. Lett.* **78**, 1359–1362.
- Long, G. J., Hautot, D., Pankhurst, Q. A., Vandormael, D., Grandjean, F., Gaspard, J. P., Briois V., Hyeon, T. & Suslick, K. S. 1998 *Phys. Rev. B* **57**, 10716–10722.
- Mason, T. J. & Lorimer, J. P. 1988 *Sonochemistry: theory, applications and uses of ultrasound in chemistry*. Chichester, UK: Ellis Horwood.
- Mason, T. J. & Luche, J.-L. 1996 Ultrasound as a new tool for synthetic chemists. In *Chemistry under extreme or non-classical conditions* (ed. R. Van Eldik & C. D. Hubbard), pp. 317–380. New York: John Wiley.
- Matula, T. J., Roy, R. A., Mourad, P. D., McNamara III, W. B. & Suslick, K. S. 1995 *Phys. Rev. Lett.* **75**, 2602.
- Mdleni, M. M., Hyeon, T. & Suslick, K. S. 1998 *J. Am. Chem. Soc.* **120**, 6189–6190.
- Moser, W. R. (ed.) 1996 *Advanced catalysts and nanostructured materials*. New York: Academic.
- Moss, W. C., Clarke, D. B. & Young, D. A. 1997 *Science* **276**, 1398–1401.
- Neppiras, E. A. 1980 *Phys. Rep.* **61**, 159–251.
- Pecoraro, T. A. & Chianelli, R. R. 1981 *J. Catal.* **67**, 430.
- Preece, C. M. & Hansson, I. L. 1981 *Adv. Mech. Phys. Surf.* **1**, 199.
- Putterman, S. J. 1995 *Scient. Am.* (February), p. 46.
- Rayleigh, Lord 1917 *Phil. Mag.* **34**, 94.
- Richards, W. T. & Loomis, A. L. 1927 *J. Am. Chem. Soc.* **49**, 3086.
- Riesz, P., Berdahl, D. & Christman, C. L. 1985 *Environ. Health Perspect.* **64**, 233.
- Shafi, K. V. P. M., Gedanken, A., Goldfarb, R. B. & Felner, I. 1997 *J. Appl. Phys.* **81**, 6901.
- Suslick, K. S. (ed.) 1988 *Ultrasound: its chemical, physical, and biological effects*. New York: VCH.
- Suslick, K. S. 1990 *Science* **247**, 1439.

- Suslick, K. S. 1994 Sonochemistry of transition metal compounds. In *Encyclopedia of inorganic chemistry* (ed. R. B. King), vol. 7, pp. 3890–3905. New York: John Wiley.
- Suslick, K. S. 1995 *MRS Bull.* **20**, 29.
- Suslick, K. S. 1997 Sonocatalysis. In *Handbook of heterogeneous catalysis* (ed. G. Ertl, H. Knozinger & J. Weitkamp), vol. 3, ch. 8.6, pp. 1350–1357. Weinheim: Wiley-VCH.
- Suslick, K. S. 1998 Sonochemistry. In *Kirk-Othmer encyclopedia of chemical technology*, 4th edn, vol. 26, 517–541. New York: John Wiley.
- Suslick, K. S. & Crum, L. A. 1997 Sonochemistry and sonoluminescence. In *Encyclopedia of acoustics* (ed. M. J. Crocker), vol. 1, ch. 26, pp. 271–282. New York: Wiley-Interscience.
- Suslick, K. S. & Doktycz, S. J. 1990 The effects of ultrasound on solids. In *Advances in sonochemistry* (ed. T. J. Mason), pp. 197–230. New York: JAI.
- Suslick, K. S. & Grinstaff, M. W. 1990 *J. Am. Chem. Soc.* **112**, 7807.
- Suslick, K. S., Hammerton, D. A. & Cline Jr, R. E. 1986 *J. Am. Chem. Soc.* **108**, 5641.
- Suslick, K. S., Choe, S. B., Cichowlas, A. A. & Grinstaff, M. W. 1991 *Nature* **353**, 414.
- Suslick, K. S., Flint, E. B., Grinstaff, M. W. & Kemper, K. A. 1993 *J. Phys. Chem.* **97**, 3098–3099.
- Suslick, K. S., Fang, M. & Hyeon, T. 1996a *J. Am. Chem. Soc.* **118**, 11960–11961.
- Suslick, K. S., Hyeon, T. & Fang, M. 1996b *Chem. Mater.* **8**, 2172–2179.
- Webb, A. G., Wong, M., Kolbeck, K. J., Magin, R. L., Wilmes, L. J. & Suslick, K. S. 1996 *J. Mag. Res. Imaging* **6**, 675–683.
- Weller, H. 1993 *Adv. Mater.* **5**, 88.
- Wong, M. & Suslick, K. S. 1995 Sonochemically produced hemoglobin microbubbles, hollow and solid spheres and microspheres. In *MRS Symp. Proc.* (ed. D. L. Wilcox, M. Berg, T. Bernat, D. Kellerman & J. K. Corchran), vol. 372, pp. 89–94. Pittsburgh, PA: Materials Research Society.

—

—

—

—

|

|

APPLICATIONS OF ULTRASOUND TO MATERIALS CHEMISTRY

Kenneth S. Suslick

Department of Chemistry, University of Illinois at Urbana-Champaign, Urbana,
Illinois 61801; e-mail: ksuslick@uiuc.edu

Gareth J. Price

Department of Chemistry, University of Bath, Claverton Down, Bath BA2 7AY,
United Kingdom; e-mail: chsgjp@bath.ac.uk

KEY WORDS: sonochemistry, cavitation, polymer chemistry, nanostructure, heterogeneous catalysis, biomaterials

ABSTRACT

The chemical effects of ultrasound derive primarily from acoustic cavitation. Bubble collapse in liquids results in an enormous concentration of energy from the conversion of the kinetic energy of the liquid motion into heating of the contents of the bubble. The high local temperatures and pressures, combined with extraordinarily rapid cooling, provide a unique means for driving chemical reactions under extreme conditions. A diverse set of applications of ultrasound to enhance chemical reactivity has been explored with important uses in synthetic materials chemistry. For example, the sonochemical decomposition of volatile organometallic precursors in low-volatility solvents produces nanostructured materials in various forms with high catalytic activities. Nanostructured metals, alloys, oxides, carbides and sulfides, nanometer colloids, and nanostructured supported catalysts can all be prepared by this general route. Another important application of sonochemistry in materials chemistry has been the preparation of biomaterials, most notably protein microspheres. Such microspheres have a wide range of biomedical applications, including their use in echo contrast agents for sonography, magnetic resonance imaging, contrast enhancement, and oxygen or drug delivery. Other applications include the modification of polymers and polymer surfaces.

INTRODUCTION: ACOUSTIC CAVITATION

The study of chemical effects of ultrasound is a rapidly growing research area (1–7). Some of the most important recent aspects of sonochemistry have been its applications in the synthesis and modification of both organic and inorganic materials (8–12). High-intensity ultrasound can induce a wide range of chemical and physical consequences. The chemical effects of ultrasound fall into three areas: homogeneous sonochemistry of liquids, heterogeneous sonochemistry of liquid-liquid or liquid-solid systems, and sonocatalysis (which overlaps the first two). Applications of ultrasound to materials chemistry are found in all of these categories. Physical effects of high-intensity ultrasound, which often have chemical consequences, include enhanced mass transport, emulsification, bulk thermal heating, and a variety of effects on solids.

The chemical consequences of high-intensity ultrasound do not arise from an interaction of acoustic waves and matter at a molecular or atomic level. Instead, in liquids irradiated with high-intensity ultrasound, acoustic cavitation (the formation, growth, and collapse of bubbles) (13) provides the primary mechanism for sonochemical effects. During cavitation, bubble collapse produces intense local heating, high pressures, and very short lifetimes; these transient, localized hot spots drive high-energy chemical reactions. As described in detail elsewhere (4, 14–16), these hot spots have temperatures of $\sim 5000^{\circ}\text{C}$, pressures of about 1000 atm, and heating and cooling rates above 10^{10} K/s. Thus, cavitation serves as a means of concentrating the diffuse energy of sound into a unique set of conditions to produce unusual materials from dissolved (and generally volatile) precursors. Chemical reactions are not generally seen in the ultrasonic irradiation of solids or solid-gas systems.

In addition, the interfacial region around cavitation bubbles has very large temperature, pressure, and (possibly) electric field gradients. Liquid motion in this vicinity also generates very large shear and strain gradients; these are caused by the very rapid streaming of solvent molecules around the cavitation bubble, as well as the intense shock waves emanated on collapse. These physical effects have special importance in polymer sonochemistry (described below).

Ultrasonic cavitation in liquid-solid systems also produces high-energy phenomena. The physical effects primarily responsible for such enhancements include (a) improvement of mass transport from turbulent mixing and acoustic streaming, (b) the generation of surface damage at liquid-solid interfaces by shock waves and microjets, (c) the generation of high-velocity interparticle collisions in slurries, and (d) the fragmentation of friable solids to increase surface area.

Cavitation near extended liquid-solid interfaces is very different from cavitation in pure liquids (13). Near a solid surface, bubble collapse becomes

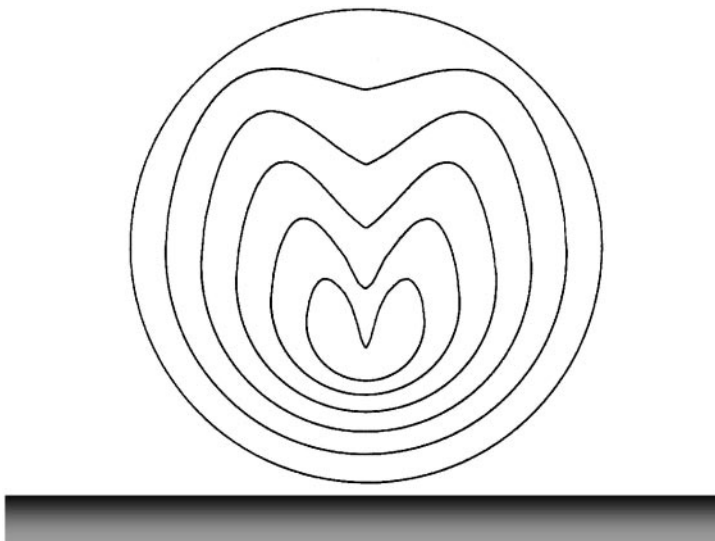


Figure 1 Formation of a liquid microjet during bubble collapse near an extended surface.

nonspherical, driving high-speed jets of liquid into the surface (Figure 1) and creating shockwave damage to the surface. Because most of the available energy is transferred to the accelerating jet, rather than the bubble wall itself, this jet can reach velocities of hundreds of meters per second. In addition, shockwaves created by cavity collapse in the liquid may also induce surface damage and the fragmentation of brittle materials. The impingement of microjets and shockwaves on the surface creates the localized erosion responsible for ultrasonic cleaning and many of the sonochemical effects on heterogeneous reactions. The importance of this process to corrosion and erosion phenomena of metals and machinery has been thoroughly reviewed elsewhere (17).

Finally, during ultrasonic irradiation of liquid-powder slurries, cavitation and the shockwaves it creates can accelerate solid particles to high velocities (18, 19). As discussed below, the interparticle collisions that result are capable of inducing striking changes in surface morphology, composition, and reactivity.

A wide range of commercial equipment is now readily available for sonochemical research. High-intensity ultrasonic probes (50 to 500 W/cm^2) of the type used for biological cell disruption are the most reliable and effective source for laboratory-scale sonochemistry and permit easy control over ambient temperature and atmosphere. Ultrasonic cleaning baths are less satisfactory, owing to their low intensities (≈ 1 W/cm^2). For larger-scale irradiations, flow reactors

with high ultrasonic intensities are commercially available in 20-kW modular units (20).

Sonochemical rates for homogeneous reactions depend on a variety of experimental parameters such as vapor pressure of precursors, solvent vapor pressure, and ambient gas. To achieve high sonochemical yields, the precursors should be relatively volatile, because the primary sonochemical reaction site is the vapor inside the cavitating bubbles (21). In addition, however, the solvent vapor pressure should be low at the sonication temperature, because significant solvent vapor inside the bubble reduces the bubble collapse efficiency.

SONOCHEMICAL MODIFICATION OF MATERIALS

Effects of Ultrasound on Polymers

Although the search for new polymers with improved properties continues to attract great research interest, the economic drivers in the polymer industry demand continual improvement of existing materials. This has led to a large effort aimed at modifying existing polymers. For example, the interaction of an article with its surroundings is largely determined by its surface properties. The ability to alter the surface properties of an inexpensive commodity polymer is therefore of great economic interest. In a similar manner, modification of a bulk polymer by the incorporation of small amounts of other compounds is an economical method of producing highly functional materials. In addition, the material properties shown by a particular polymer sample depend critically on its molecular weight and chain microstructure so these must be precisely controlled. Sonochemistry has a part to play in each of these areas.

The effects of ultrasound on polymers can be both physical and chemical. Irradiation of liquids with ultrasound can cause solely physical changes from acoustic streaming, such as rapid mixing and bulk heating. Although cavitation is not always necessary for these effects, they almost always accompany cavitation. Examples of physical changes induced by ultrasound in polymer systems include the dispersal of fillers and other components into base polymers (as in the formulation of paints), the encapsulation of inorganic particles with polymers, modification of particle size in polymer powders, and, perhaps most important, the welding and cutting of thermoplastics (11). In contrast, chemical changes can also be created during ultrasonic irradiation, invariably as a result of cavitation, and these effects have been used to benefit many areas of polymer chemistry.

CHARACTERISTICS OF ULTRASONIC DEGRADATION The degradation (meaning an irreversible lowering of the chain length caused by cleavage, and not necessarily any chemical change) of polymer chains in solution was one of the

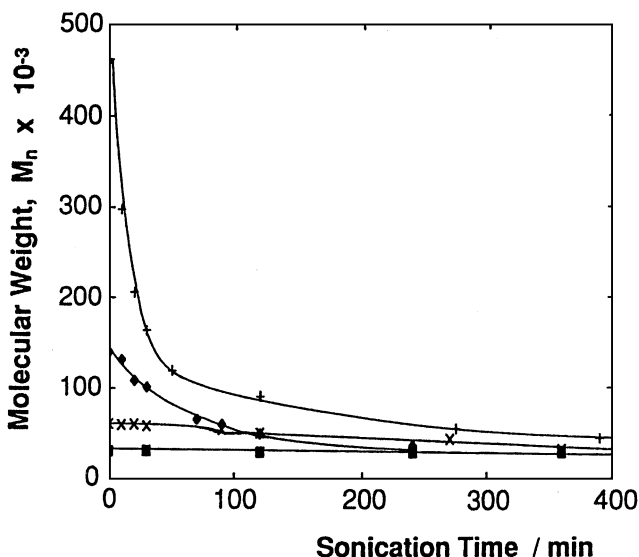


Figure 2 Ultrasonic degradation of 1% solutions of narrow polydispersity polystyrenes in toluene (11).

first reported effects of high-intensity ultrasound (22, 23). Although the precise origin is still open to debate, the process is now understood in sufficient detail to make it commercially applicable in a number of areas (24, 25). The basic effects (26) of irradiating a polymer solution with power ultrasound are shown in Figure 2, with polystyrene in toluene as an example.

The degradation proceeds more rapidly at higher molecular weights and approaches a limiting value, M_{lim} , below which no further degradation takes place (in this case $\sim 30,000$). Polymers with this value or lower values are unaffected by ultrasound under these conditions. These effects have been reported in all types of macromolecules in solution and include both organic (22, 23) and inorganic [e.g. poly(organosiloxanes) and polyorganosilanes (27)] polymers in organic solvents and various polymers in aqueous media [such as polyethylene oxide (28), cellulose (29), polypeptides, proteins (30), and DNA (31)]. This common behavior is a result of a physical process that is independent of the chemical nature of the polymer, but rather depends on the polymer chain dimensions in solution. A large number of studies have demonstrated that the rate of degradation and M_{lim} are insensitive to the nature of the polymer when sonicated under the same conditions. Encina et al (32) found that the rate of degradation of poly(vinyl pyrrolidone) increased tenfold when the polymer was prepared with a small number of peroxide linkages in the backbone, suggesting

that chain cleavage can occur preferentially at weak spots in the chain. It is clear, however, that there must be a substantial difference in the relative bond energies for this effect to be noticed.

Many studies have been performed to characterize the rate of degradation in order to develop quantitative models of the process. In summary, the degradation proceeds faster and to lower molecular weights at lower temperatures, in more dilute solutions, and in solvents with low volatility. This pattern follows the effect of the parameters on cavitation bubble collapse. Sonication at higher temperatures or in volatile solvents results in more vapor entering the bubble and so cushioning the collapse, making it less violent. In dilute solutions, the polymer chains are not entangled and so are free to move in the flow fields around the bubbles. As expected, the degradation is more efficient at high ultrasonic intensities, owing to the greater number of bubbles with larger radii. Many other factors have been quantified, including the nature of any dissolved gases and the conformation that the polymer adopts in solution. Hence, by suitable manipulation of the experimental conditions, one can exert a great deal of control over the degradation process.

Although there is still some debate about the precise origins of the degradation, it has been shown that under conditions that suppress cavitation, degradation does not occur. The polymer chains are subjected to extremely large forces in the rapid liquid flows near collapsing cavitation bubbles and in the shock waves generated after bubble implosion; these can result in the breakage of a bond in the chain. There is no evidence that the extreme conditions of temperature found in cavitation bubbles contribute to polymer degradation in nonaqueous liquids, because the polymer chains have negligible vapor pressure and are unlikely to be found at the bubble interface. In contrast, however, pyrolysis can occur in aqueous solutions in which hydrophobic polymers concentrate at the bubble-air interface.

The kinetics and regiospecificity of ultrasonic degradation are different from those of thermal processes. Thermal degradation produces cleavage at random points along the chain, whereas ultrasonic degradation is much more specific, with cleavage occurring preferentially near the middle of the chain (33). The most quantitative model for this comes from the work of Van der Hoff & Gall (34), who investigated the degradation of polystyrene in tetrahydrofuran. They found that the degradation could be best modeled when it was assumed that the probability of chain breakage was distributed in a Gaussian manner within $\sim 15\%$ of the center of the chain. This center cleavage model is also consistent with the stretching and breakage mechanism suggested above. Degradation in shear fields of capillary flow (35) or in high-shear stirrers (36) also results in preferential breakage at the chain centers. A comparison of the chain breakage caused by ultrasound and extensional flows was published recently (37).

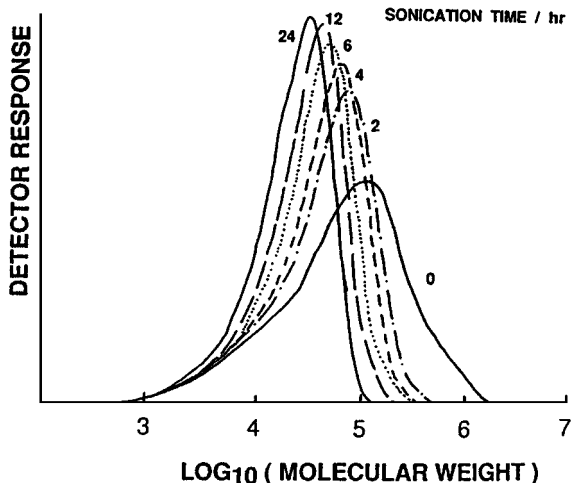


Figure 3 Gel permeation chromatography chromatograms of a 2% solution of a polyalkane sonicated in toluene (11); the numbers by each curve indicate the duration of sonication in hours.

APPLICATIONS OF ULTRASONIC DEGRADATION The molecular-weight dependence of the degradation means that longer chains are preferentially removed from a sample and the polydispersity of the polymer is changed. Thus, degradation can be used as an additional processing parameter to control the molecular-weight distribution. For example, Figure 3 shows gel permeation chromatography (GPC) chromatograms of a polymer solution undergoing sonication (GJ Price, unpublished data). The degradation of the higher-molecular-weight species narrows the distribution markedly, and after 24 h of sonication, no material with molecular weight $>100,000$ remains. A recent commercial process, in fact, uses a sonochemical treatment during the final processing stage to control the molecular-weight distribution to give the desired processing properties of the polymer (11).

In all the carbon backbone polymers studied to date, the primary products of the degradation are radical species arising from homolytic bond breakage along the chain. The evidence for macromolecular radicals arises from radical trapping experiments as well as from the use of electron spin resonance spectroscopy (39). A second application of the degradation uses these macromolecular radicals as initiating species in the preparation of copolymers. A number of workers have sonicated mixtures of two polymers dissolved in a common solvent. Combination of the two different macromolecule fragments leads to formation of a block copolymer. However, this can be difficult to separate from the starting materials, and there are problems in

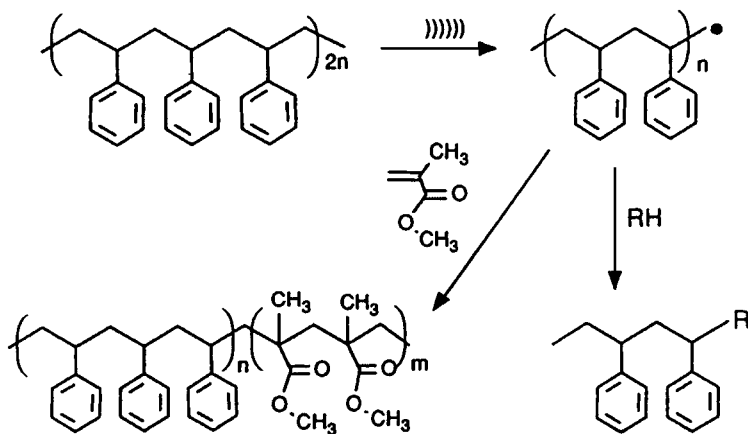


Figure 4 Sonochemical production of end-capped polymers and block copolymers (11).

controlling the block structure. An alternative approach (GJ Price, unpublished data) involves sonicating a polymer dissolved in a solution containing the second monomer. The macromolecular radical initiates polymerization of the second monomer, as illustrated in Figure 4 for polystyrene and methyl methacrylate.

By using the results of degradation studies, the structure and block length of the first polymer can be controlled quite precisely. By changing the concentration of monomer in solution, the block size of the second polymer can also be varied, allowing a large degree of control over the resulting material structure. A related approach is to sonicate the polymer in the presence of a species labile to radical attack, forming end-capped polymers. One may also use this approach to prepare, for example, polystyrene- and poly(alkane)-bearing fluorescent groups.

SONOCHEMICAL MODIFICATION OF POLYMER SURFACES As mentioned above, bubble collapse near a surface results in jets of liquid impinging at high velocity onto the surface. These are primarily responsible for the cleaning action of ultrasound but can also be used to effect chemical change at the surface.

One of the first reports of this technique was by Urban & Salazar-Rojas (40), who worked with poly(vinylidene difluoride), a piezoelectric material. This is normally an insulator, but after treatment with a strong base, dehydrofluorination will produce a surface with carbon-carbon double bonds, and ultrasound accelerates this process significantly. The enhanced contact between the solid surface and the solution promoted by ultrasound provided excellent wetting of the surface as well as better mass transport of reagents. The unsaturated sites

can be reacted further; for example, phthalocyanine dyes (41) can be grafted onto the fluorocarbon polymer surface.

Related work has involved poly(vinyl chloride), PVC, an inexpensive, commodity polymer. Functionalizing the surface would confer the surface properties of more expensive polymers in an inexpensive manner. A number of compounds including metal ions, dyes, and hydrophilic monomers have been grafted to the surface (GJ Price, AA Clifton, unpublished data). In this way, one can change the chemical nature of the surface so that it has greater functionality than the base polymer. A more difficult example is polyethylene, which is widely used but has an inert surface that makes adhesion or printing very difficult. Current methods involve activation with chromic acid or an oxygen plasma. Using ultrasound to enhance the reaction, it was possible to rapidly modify the surface character of polyethylene (43) with milder, more environmentally friendly oxidizing agents such as potassium persulfate or hydrogen peroxide. Contact angle and spectroscopic analysis indicated that a thin layer of polar groups such as hydroxyl and carbonyl had been formed on the surface, providing for greater adhesion of surface coatings.

Effects of Ultrasound on Inorganic Materials

The use of ultrasound to accelerate chemical reactions in liquid-solid heterogeneous systems has become increasingly widespread. Sonochemical enhancement of the reactivity of reactive metals as stoichiometric reagents has become an especially routine synthetic technique for many heterogeneous organic and organometallic reactions (1–7), particularly those involving reactive metals, such as Mg, Li, or Zn. Rate enhancements of more than tenfold are common, yields are often substantially improved, and byproducts are avoided. This development originated from the early work of Renaud and the more recent breakthroughs of Luche (5). The effects are quite general and apply to reactive inorganic salts and to main group reagents as well.

Distortions of bubble collapse depend on a surface several times larger than the resonance bubble size. Thus, for ultrasonic frequencies of ~ 20 kHz, damage associated with microjet formation cannot occur for solid particles smaller than ~ 200 μm . This takes on a special importance for sonochemistry, since fine powders are generally preferred for use as solid reagents or catalysts.

In liquid-solid slurries, cavitation still occurs, and the bubble collapse will still launch shock waves out into the liquid. When these shock waves pass over particles in close proximity to one another, high-velocity interparticle collisions can result. If the collision is at a direct angle, metal particles can be driven together at sufficiently high speeds to induce effective melting at the point of collision (18, 19), as seen in Figure 5. From the volume of the melted region of impact, the amount of energy generated during collision is determined. From

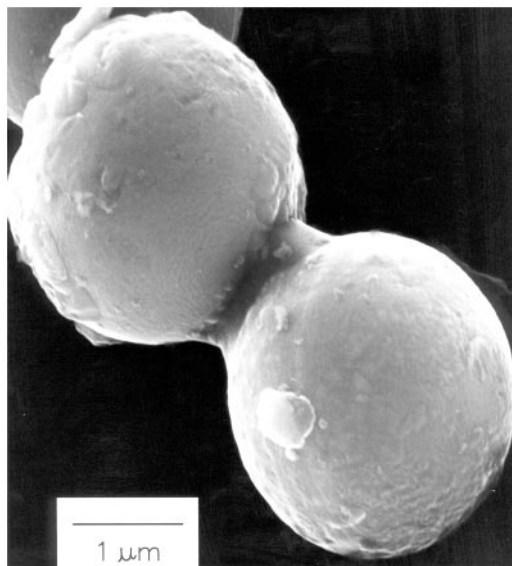


Figure 5 Scanning electron micrograph of Zn powder after ultrasonic irradiation as a slurry in decane (18).

this, a lower estimate of the velocity of impact was calculated, several hundred meters per second or roughly half the speed of sound!

If the particles collide at a glancing angle, a mechanical removal of surface material results in a macroscopic smoothing (and at the atomic level, a microscopic roughening) of the surface (as shown in Figure 6), in analogy to

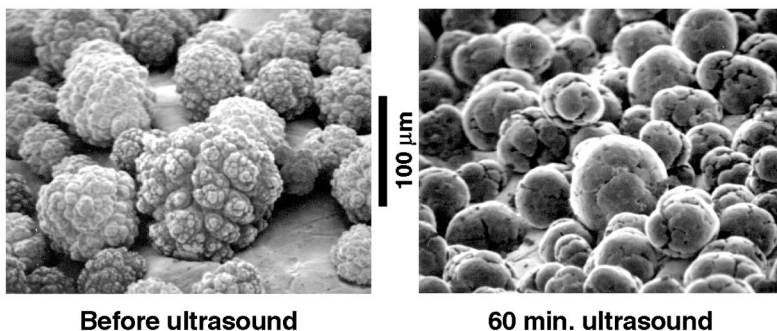


Figure 6 The effect of ultrasonic irradiation on the surface morphology of Ni powder. High-velocity interparticle collisions are created during ultrasonic irradiation of slurries (48).

lapidary ball milling. Especially for reactive metals that form oxide, nitride, or carbonaceous coatings, the consequences to the reactivity of metal particles can be quite substantial. Surface composition studies with depth profiling by Auger electron spectroscopy and by sputtered neutral mass spectrometry reveal that ultrasonic irradiation effectively removes surface oxide and other contaminating coatings (18, 44–48). The removal of such passivating coatings can dramatically improve chemical reaction rates.

To probe the conditions created during interparticle collisions in slurries irradiated with ultrasound, Doktycz & Suslick (18) examined a series of transition metal powders (Figure 7). Using the irradiation of Cr, Mo, and W powders in decane at 20 kHz and 50 W/cm², one observes agglomeration and what appears to be localized melting for Cr and Mo but not for W (18). A compilation of the effects of ultrasonic irradiation of slurries of different metal powders as a function of their melting points reveals a break point in aggregation and surface deformations: The effective transient temperature reached at the point of impact during interparticle collisions is roughly 3000°C. This effective local temperature has no direct connection with the temperatures inside the cavitating bubble, but they are another demonstration of the extreme conditions that ultrasound can create in an otherwise cold liquid.

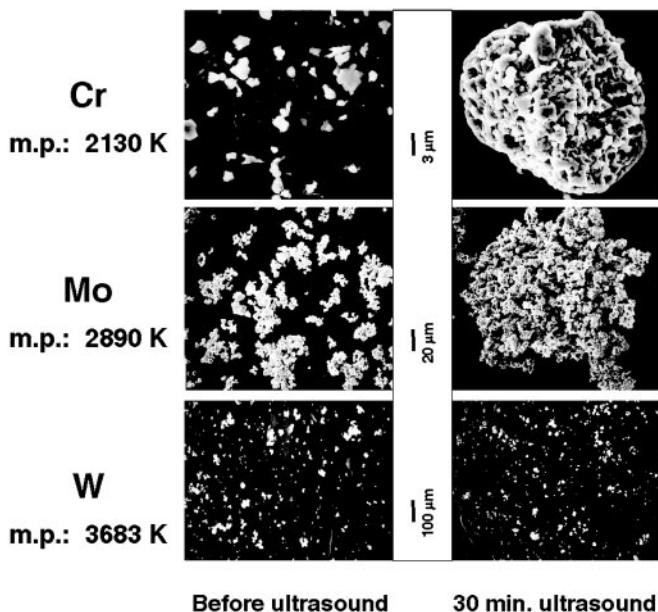


Figure 7 Scanning electron micrograph of Cr, Mo, and W powder after ultrasonic irradiation of decane slurries under Ar (18).

For brittle materials, most notably layered inorganic sulfides and oxides, interparticle collisions can also induce fragmentation. This can substantially increase the available surface area of the powders and thus enhance liquid-solid reaction rates. An example of this effect is found in the application of ultrasound to the process of molecular intercalation into layered inorganic solids (49, 50). The adsorption of organic or inorganic compounds between the atomic sheets of layered solids permits the systematic change of optical, electronic, and catalytic properties. Such materials have many technological applications (for example, lithium batteries, hydrodesulfurization catalysts, and solid lubricants). The kinetics of intercalation, however, are generally extremely slow, and syntheses usually require high temperatures and very long reaction times. High-intensity ultrasound dramatically increases the rates of intercalation (by as much as 200-fold) of a wide range of compounds (including amines, metallocenes, and metal sulfur clusters) into various layered inorganic solids (such as ZrS_2 , V_2O_5 , TaS_2 , MoS_2 , and MoO_3). Scanning electron microscopy of the layered solids coupled to chemical kinetics studies demonstrated that the origin of the observed rate enhancements comes from particle fragmentation (which dramatically increases surface areas) and to a lesser extent from surface damage.

Effects of Ultrasound on Heterogeneous Catalysis

Catalytic reactions are of enormous importance in both laboratory and industrial applications. Heterogeneous catalysts often require rare and expensive metals. The use of ultrasound offers some hope of activating less reactive, but also less costly, metals. Such effects can occur in three distinct stages: (a) during the formation of supported catalysts, (b) activation of preformed catalysts, or (c) enhancement of catalytic behavior during a catalytic reaction. As discussed below, the bulk of this research deals with the first stage, the preparation of catalysts. Some early investigations of the effects of ultrasound on heterogeneous catalysis itself can be found in the Soviet literature (12, 51). In this early work, increases in turnover rates were usually observed upon ultrasonic irradiation but were rarely more than tenfold. For modest rate increases, it appears likely that the cause is increased effective surface area; this is especially important for catalysts supported on brittle solids (e.g. noble metals supported on carbon).

More impressive effects, however, have been reported, especially for hydrogenations and hydrosilations with Ni or Raney Ni powder. For example, the hydrogenation of alkenes by Ni powder is enormously enhanced by ultrasonic irradiation (12, 44, 48). This is not caused by fragmentation of the solid; the surface area does not change significantly even after lengthy irradiation. There is, however, a very interesting effect on the surface morphology (Figure 6). Ultrasonic irradiation smoothes, at a macroscopic scale, the initially crystalline

surface and causes agglomeration of small particles. Both effects are caused by interparticle collisions owing to cavitation-induced shockwaves. Auger elemental depth profiling revealed that there is a striking decrease in the thickness of the oxide coat after ultrasonic irradiation. It is the physical removal of this passivating layer that is responsible for the $>10^5$ -fold increase observed in catalytic activity.

SONOCHEMICAL PREPARATION OF NOVEL MATERIALS

Sonochemical Synthesis of Polymers

INORGANIC-POLYMER SYSTEMS Although not nearly as commonly used as organic materials, polymers with backbones consisting of inorganic elements have some special properties that are making them commercially significant. For example, the polysiloxanes (silicones) and polyphosphazenes remain flexible to very low temperatures. Poly(organosilanes) have a conjugated silicon backbone that confers interesting photo- and electroactive properties.

It has been reported (27) that ultrasound produces a significant acceleration in the cationic polymerization of cyclic siloxanes to give the commercially very important silicone resins. Polymers produced under sonication had narrower polydispersities but higher molecular weights than those produced under normal conditions. The acceleration of the polymerization was caused by more efficient dispersion of the acid catalyst throughout the monomer, leading to a more homogeneous reaction and hence a lower distribution of chain lengths. There is also the issue of ultrasonic degradation of long chains, which must be considered during the late stages of such polymerizations.

A second example of an inorganic polymer is also taken from silicon-based chemistry. Normally, poly(organosilanes) are prepared by a Wurtz-type coupling of dichlorodiorganosilanes that uses molten sodium in refluxing toluene to remove the halogens (52). However, yields are normally low, the reactions are difficult to reproduce, and the resulting polymers often have a very wide molecular-weight distribution and often contain two or three distinct distributions. For routine commercial use, preparation under more environmentally acceptable conditions to produce polymers with a controlled structure and preferably monomodal distribution is desirable.

The usefulness of ultrasound in this reaction was suggested by the work of Han & Boudjouk, who used lithium to couple organochlorosilanes to give R_3SiR_3 (53). Extension of the reaction by using R_2SiCl_2 gives the polymeric materials. The first reports of sonochemical synthesis of these polymers were by Kim & Matyjaszewski (54) and Kim et al (55), who produced materials

with monomodal molecular-weight distributions, albeit in rather low yield (11–15%). In contrast, Miller et al (56) reported conflicting results because sonication did not yield polymers with a monomodal distribution unless diglyme or 15-crown-5 was added to the solvent. In more recent work, Price (57) and Price & Patel (58) have established that a number of polysilanes with diverse substituents can be prepared under a range of conditions, and all give higher yields and faster reactions under ultrasound. Significantly, the effect of ultrasonic intensity on polymer molecular weights and distributions under otherwise identical conditions clearly established that higher intensities lead to narrower distributions and smaller amounts of low-molar-mass material. A similar reaction was used by Weidman and coworkers (59) to prepare polysilynes, $(RSi)_n$ with sonochemical activation of Na-K alloy. Again the use of ultrasound removed the very high-molecular-weight fractions and hence allowed the synthesis of polymers with molecular weights in the 10,000–100,000 range and monomodal distributions.

ORGANIC-POLYMER SYSTEMS *Vinyl polymers* The majority of organic polymers are prepared from monomers containing a reactive double bond (e.g. α -olefins and vinyl monomers), which undergo chain growth or addition reactions. These polymerize by a variety of mechanisms and, with various degrees of interest, ultrasound has been applied to examples of each type. The most straightforward preparative method is that initiated by radicals. As already noted, cavitation can produce high concentrations of radicals. Hence, application of ultrasound to vinyl monomers provides an alternative, highly controllable method of initiation.

Water itself is susceptible to cavitation and, in early work, sonochemically generated $H\bullet$ and $OH\bullet$ radicals were used by Henglein (60) to prepare poly(acrylonitrile) in aqueous solution. It was long considered that the lower degree of radical formation in organic liquids would preclude polymerization (61); this was shown to be wrong, however, and a number of workers have since studied radical polymerization both of single monomers and their mixtures.

One of the most studied systems has been methyl methacrylate. Kruus (62) and Kruus & Patraboy (62, 63) described a detailed study of the mechanism of polymerization using sonochemically generated radicals. Under some conditions, pyrolysis of the monomer occurred inside cavitation bubbles, causing the formation of significant amounts of insoluble chars in addition to linear polymers. However, as long as the monomers were properly purified and deoxygenated, soluble, high-molecular-weight polymers of methyl methacrylate and styrene could be produced. It was found that reasonable rates of conversion could be achieved over a range of temperatures and, significantly, that the reaction ceased when sonication was stopped.

The mechanistic work of Price et al (64) illustrates some of the features of sonochemical polymerization. High-molecular-weight polymers are formed early in the reaction, but the average chain length shortens at longer times. This is caused by the onset of the degradation process discussed earlier, once sufficiently long chains are formed. A conversion of $\sim 2\text{--}3\% \text{ h}^{-1}$ was achieved with methyl methacrylate at 25°C . However, above a particular conversion, the viscosity increase suppresses both cavitation and the consequent radical formation, and no further conversion to polymer occurs.

The primary role of ultrasound in this type of reaction is to produce the radicals needed to initiate polymerization. This can take place by two routes. Sonication of pure monomers produces radicals through decomposition inside the bubble or at its interface; alternatively, the decomposition of added initiators such as peroxides or azo compounds could be accelerated (64, 65). Kinetic results at 25°C indicate that sonication increased the rate of decomposition of 2,2'-azobisisobutyronitrile (AIBN) over the conventional reaction by some three orders of magnitude. This may be related to thermal effects in the interfacial regions around cavitating bubbles. By suitable manipulation of conditions such as temperature, solvent vapor pressure, and ultrasonic intensity, one may predict and control the rate of initiation.

The kinetics of the other parts of the polymerization have been measured (62, 64). To summarize, the rate was found to be proportional to the monomer concentration and to depend on the square root of ultrasonic intensity. The final molecular weight varied inversely with the monomer concentration and scaled inversely with the square root of the ultrasonic intensity. By analogy with the usual treatment of radical polymerization kinetics, a detailed mechanism was proposed for the sonochemical process. Essentially, the rate of initiation is proportional to the number of cavitation sites available, which depends in turn on the ultrasound intensity. Using this mechanism, the time dependence of the rate of polymerization, the molecular weight, and the conversion to polymer were described and were in good agreement with the experimental observations.

In contrast to the initiation, higher temperatures led to an increase in the rate of polymerization. The termination steps, being bimolecular radical reactions, do not depend strongly on temperature, whereas addition of monomer to the growing chain is controlled by diffusion and thus would be expected to increase with temperature. The experimental results suggest that ultrasound has relatively little effect on the propagation or termination reactions, compared with the acceleration of initiation. This conclusion is also supported by the small amount of published work on copolymerization, in which two or more different monomers can be incorporated into the same polymer chain. If ultrasound were affecting the propagation, differences in the sequences of the two

monomers along the chain would be expected. No significant differences were found by Miyata & Nakashio (66) for styrene-acrylonitrile copolymerizations or by Price et al (67) for mixtures of styrene with methyl or butyl methacrylates.

An alternative route for vinyl polymerizations uses a latex dispersion as an emulsion or suspension in an aqueous medium. In addition to water and the monomer(s), a number of other components (such as stabilizers, dispersants, and initiators) are usually added. The large degree of motion induced by acoustic streaming and cavitation shockwaves creates very high shear forces, which act to break up droplets of liquid and maintain a small and even distribution of droplet sizes.

The first reports of applying ultrasound to this type of reaction date from the early 1950s when it was found that better dispersion of styrene was obtained under sonication (68), which also significantly accelerated the rate of polymerization. In the most recent example of this type, Cooper and coworkers (69) have used a horn system to produce latexes of polystyrene, poly(butyl acrylate) and poly(vinyl acetate) with low amounts of or even no surfactant and with smaller particle sizes than in conventional processes. The rates of reaction were also accelerated but, as expected, this depended on the vapor pressure of the monomer. In contrast to the bulk or solution polymerizations described earlier, conversions of $\sim 100\%$ were routinely achieved.

There has been only a small amount of work on polymerizations proceeding via an ionic mechanism. Schultz et al (70) described how sonication had little effect on the anionic polymerization of styrene itself but allowed the butyl lithium initiators to be prepared at faster rates than under conventional conditions. Additionally, successful initiators could be prepared even in undried solvents. These findings parallel much of the work in synthetic sonochemistry of organometallic compounds (5, 6, 9).

Other organic polymers Although vinyl polymers are an important class of materials, there are a wide variety of other compounds that are polymerized by other mechanisms. Perhaps the largest group of these is the condensation or step growth polymerizations. Given the large number of industrially important polymers and plastics (e.g. polyesters, polyurethanes, and nylons) prepared by condensation reactions, there have been surprisingly few reports of the application of ultrasound in this area.

Among the very few other published studies is the patent of Long (71), who described various reactors that incorporated ultrasonically vibrating walls. These could be used for the precise control of both when and where polymerization took place for several polyurethane systems and were especially useful for producing foams. Another commercially significant mechanism for producing polymers is the ring-opening mechanism of a cyclic monomer. A

range of polyesters can be produced from cyclic lactones, but probably the most commercially significant in terms of amount of polymer manufactured is the reaction of ϵ -caprolactam to give nylon-6. This normally is a two-stage process where the initial ring opening is catalyzed by a small amount of water, and this is followed by polymerization to high molecular weight under vacuum. Ragaini (72a) and Carli et al (72b) showed that application of ultrasound enhanced the ring-opening phase, allowing a single-step polymerization without the need to add water to start the reaction. High-molecular-weight materials with narrower distributions were formed in shorter reaction times and at lower temperatures than with the conventional process.

The examples described thus far have dealt with linear polymers. Many items, however, are manufactured from elastomeric, lightly cross-linked materials, e.g. tubes and tires made from natural or synthetic rubber. Cross-linking is often carried out by heating with sulfur, a process known as vulcanization. Long processing times and high temperatures must be used because rubber is a poor conductor of heat, so that it is a very energy-intensive process. In the sonochemical process (73), the heat is generated inside the article from acoustic attenuation, so the reaction is faster and less thermal degradation of the rubber occurs. In some cases, both the treatment time and the energy requirements were lowered 50%. The same ultrasonic heating method can be applied to other systems such as epoxy resins (74). In a new application (75) of sonochemical technology, the opposite effect can be used, in which a combination of heat, pressure, and ultrasound breaks the cross-links, permitting the recycling of waste rubber such as car tires.

Biomaterials Preparation: Protein Microspheres

Another important application of sonochemistry to materials chemistry has been the preparation of biomaterials, most notably protein microspheres (76–82). Although the chemical effects of ultrasound on aqueous solutions have been studied for many years, the development of aqueous sonochemistry for biomaterial synthesis is very recent, particularly in the area of microencapsulation. It is beyond the scope of this chapter to review this area thoroughly, but a brief synopsis and bibliography are provided.

With high-intensity ultrasound and simple protein solutions, a remarkably easy method to make both air-filled microbubbles and nonaqueous liquid-filled microcapsules has been developed. Figure 8 shows an electron micrograph of sonochemically prepared microspheres. These microspheres are stable for months and, being slightly smaller than erythrocytes, can be intravenously injected to pass unimpeded through the circulatory system.

The mechanism responsible for microsphere formation is a combination of two acoustic phenomena, emulsification and cavitation. Ultrasonic

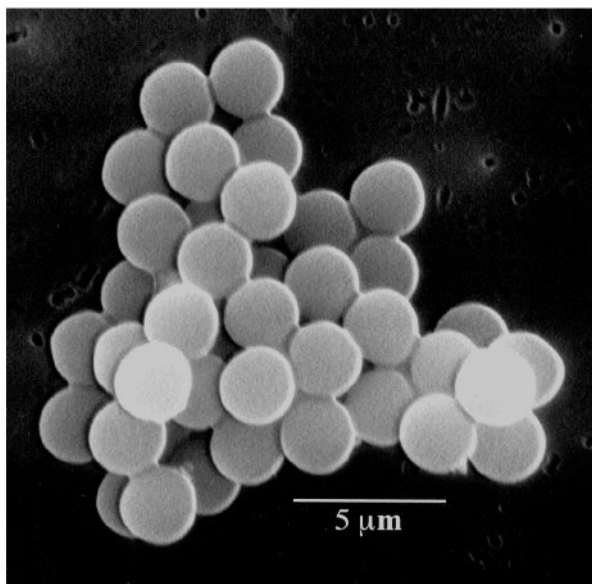


Figure 8 Scanning electron micrograph of sonochemically prepared protein microspheres from bovine serum albumin (6).

emulsification creates the microscopic dispersion of the protein solution necessary to form the proteinaceous microspheres. Alone, however, emulsification is insufficient to produce long-lived microspheres. The long life of these microspheres comes from a sonochemical cross-linking of the protein shell. Chemical reactions requiring O_2 are critical in forming the microspheres. It has been known for some time that the primary products from the sonolysis of water are H_2 and H_2O_2 , yielding $H\cdot$ and $OH\cdot$; in the presence of O_2 , the latter produces HO_2 (83). Based on chemical trapping experiments, Wong & Suslick (80) established that the proteinaceous microspheres are held together by disulfide bonds between protein cysteine residues and that superoxide is the cross-linking agent. The cross-linked shell of the microspheres is only ~ 10 protein molecules thick, as shown in transmission electron micrographs of protein-stained microtome sections from sonochemically prepared protein microspheres.

These protein microspheres have a wide range of biomedical applications, including their use as echo contrast agents for sonography (84), magnetic-resonance-imaging contrast enhancement (79, 81, 82), and oxygen or drug delivery (80), among others. An extensive body of patent literature now exists in this area (85–96).

Inorganic Nanostructured Materials Synthesis

Solids made from nanometer-sized components often exhibit properties distinct from those of the bulk, in part because clusters that small have electronic structures with a high density of states yet no continuous bands (97, 98). Such nanostructured materials have been a matter of intense current interest, and several preparative methods have been developed for their synthesis. Nanostructured materials syntheses include gas-phase techniques (e.g. molten-metal evaporation and flash vacuum thermal and laser pyrolysis decomposition of volatile organometallics), liquid-phase methods (e.g. reduction of metal halides with various strong reductants and colloid techniques with controlled nucleation), and mixed-phase approaches (e.g. synthesis of conventional heterogeneous catalysts on oxide supports, metal atom vapor deposition into cryogenic liquids, and explosive-shock synthesis). To this range of techniques, over the past 10 years the sonochemical reactions of volatile organometallics have been exploited as a general approach to the synthesis of nanophase materials, as shown in Figure 9.

Using the extreme conditions inside a cavitating bubble, Suslick and coworkers have produced a variety of nanostructured and often amorphous metals, alloys, and carbides and examined their catalytic activity (99–114). Volatile

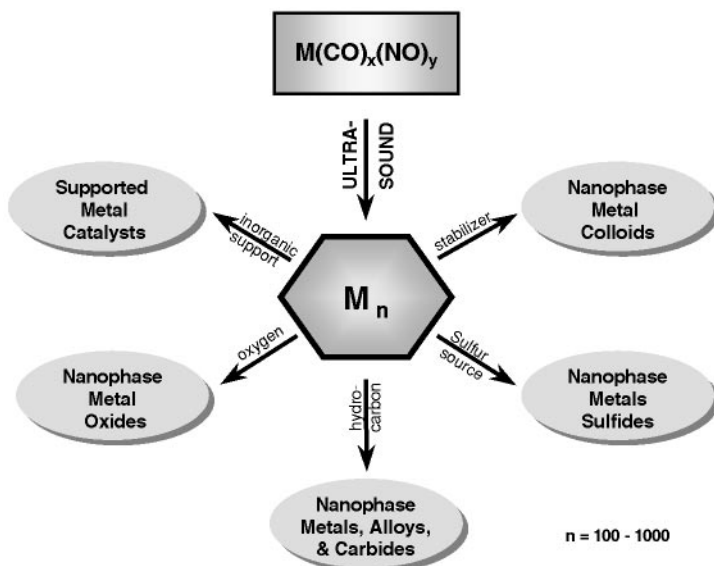


Figure 9 Sonochemical synthesis of nanostructured materials.

organometallic compounds decompose inside a collapsing bubble, and the resulting metal atoms agglomerate to form nanostructured materials. This sonochemical synthesis of nanostructured materials is extremely versatile; various forms of nanophase materials can be generated simply by changing the reaction medium. When precursors are sonicated in high-boiling-point alkanes, nanostructured metal powders are formed. If sonication occurs in the presence of a bulky or polymeric surface ligand, stable nanophase metal colloids are created. Sonication of the precursor in the presence of an inorganic support (silica or alumina) provides an alternative means of trapping the nanometer clusters. The nanoparticles trapped on these supports produce active supported heterogeneous catalysts.

AMORPHOUS METALS, ALLOYS, AND COLLOIDS The ultrasonic irradiation of solutions containing volatile transition metal organometallic compounds [e.g. $\text{Fe}(\text{CO})_5$, $\text{Ni}(\text{CO})_4$, and $\text{Co}(\text{CO})_3\text{NO}$] produces highly porous aggregates of nanometer-sized clusters of amorphous metals (99–102). For example, sonication of 1 M iron pentacarbonyl in decane at 0°C under argon yielded a dull black powder. Elemental analysis of the powder, after heating at 100°C under vacuum to remove residual solvent, showed it to be $>96\%$ iron by weight, with trace amounts of carbon ($<3\%$) and oxygen (1%, by difference), presumably from the decomposition of alkane solvent or carbon monoxide during ultrasonic irradiation. Scanning electron micrographs revealed that the powder is an agglomerate of 20-nm particles (Figure 10). Transmission electron micrographs further indicated that these 20-nm particles consist of smaller ~ 4 - to 6-nm particles.

The amorphous nature of the iron powder was confirmed by several different techniques, including scanning electron microscopy, differential scanning calorimetry, electron microdiffraction, powder x-ray diffraction (XRD), and neutron diffraction. Initial powder XRD showed no diffraction peak; after heat treatment under helium at 350°C , the diffraction lines characteristic of bcc iron metal are observed. Electron microdiffraction revealed a diffuse ring pattern, characteristic of amorphous materials. Differential scanning calorimetry also showed one exothermic irreversible disorder-order transition temperature at 308°C . The amorphous metal formation appeared to result from the extremely high cooling rate during acoustic cavitation.

There had been a long-standing controversy concerning the magnetic properties of amorphous iron, which had not been previously available without substantial amounts of added alloying elements (e.g. boron). Magnetic studies of the sonochemically prepared amorphous iron showed that amorphous iron is a very soft ferromagnetic material with a saturation magnetization density of ≈ 173 emu/g and a Curie temperature in excess of 580 K. The effective magnetic moment is $1.7 \mu_{\text{B}}$, with an effective exchange constant of only $\approx 30\%$ of

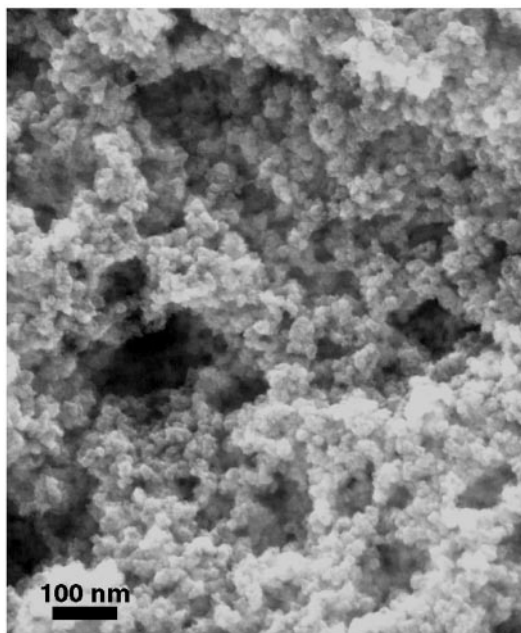


Figure 10 Amorphous iron prepared by the sonochemical decomposition of $\text{Fe}(\text{CO})_5$ (99).

crystalline Fe (101). The neutron diffraction data (102) confirmed these measurements and were consistent with a random packing model, as in many thin amorphous metal films. The magnetic properties fall close to those of liquid iron.

Sonochemical techniques can also be used to prepare nanostructured alloys. Suslick and coworkers (103–114) first demonstrated this for Fe-Co alloys, chosen because $\text{Fe}(\text{CO})_5$ and $\text{Co}(\text{CO})_3(\text{NO})$ were readily available as precursors that are thermally stable at the modest bulk solution temperatures necessary for high volatility. The composition of the Fe-Co alloys can be controlled simply by changing the ratio of solution concentrations of the precursors; alloy compositions ranging from pure Fe to pure Co are readily obtained and homogeneous on a nanometer scale (104–106). As with iron, the cobalt and Fe-Co alloys produced by ultrasound are initially amorphous, as determined by XRD and electron-beam microdiffraction. The catalytic properties of the sonochemically prepared Fe, Co, and Fe-Co alloys in the cyclohexane reaction exhibit an interesting effect: Fe-Co alloys generate much more dehydrogenation product (benzene) than pure Fe or Co owing to selective poisoning of the sites responsible for hydrogenolysis by small amounts of surface carbon. Significant recent work by Gedanken and his group have extended the sonochemical synthesis of

nanostructured alloys to Co-Ni and Fe-Ni systems (115, 116). Again the materials are amorphous as initially prepared with near uniform particles of ~ 6 to 10 nm. Magnetic measurements indicated that the Co-Ni alloy particles were superparamagnetic.

The existence of aggregates of nanometer clusters in our sonochemically prepared materials suggests the possibility of trapping these particles before they aggregate. Colloids of ferromagnetic materials are of special interest owing to their many important technological applications as ferrofluids (117). Such magnetic fluids find uses in information storage media, magnetic refrigeration, audio reproduction, and magnetic sealing. Commercial magnetic fluids are generally produced by exhaustive grinding of magnetite (Fe_3O_4) in ball or vibratory mills for several weeks in the presence of surfactants, which produces a very broad particle size distribution (117).

Suslick and coworkers developed a new method for the preparation of stable ferromagnetic colloids of iron using high-intensity ultrasound to sonochemically decompose volatile organometallic compounds (112). These colloids have narrow size distributions centered at a few nanometers and are found to be superparamagnetic. Sonochemical decomposition of iron pentacarbonyl in the presence of stabilizers such as poly(vinyl pyrrolidone) or oleic acid produced a colloid of nanometer-sized iron particles. Transmission electron micrographs showed that the iron particles have a relatively narrow range in size, from 3 to 8 nm for poly(vinyl pyrrolidone), whereas oleic acid gives an even more uniform distribution at 8 nm (Figure 11). Electron microdiffraction revealed that the particles are amorphous on the nanometer scale as formed and that, after *in situ* electron beam heating, these particles crystallize to bcc iron.

Magnetic studies indicate that these colloidal iron particles are superparamagnetic with a saturation magnetization density of a respectable 101 emu/g (Fe) at 290 K. High saturation magnetization is desirable for magnetic fluid application and is highly sensitive to the method of preparation. Bulk amorphous Fe saturates at 156 emu/g (Fe) (101, 102, 111). For a comparison, the saturation magnetization of a commercial magnetite-based magnetic fluid is 123 emu/g Fe (Ferrofluids Corp, Nashua, NH, catalog #APG-047). Kataby et al (118) found similar results with long-alkyl-chain alcohols on nanophase amorphous-Fe nanoparticles. The formation of chemical bonds between the substrate and the alcohols was demonstrated by Fourier transform infrared spectroscopy (FTIR) and x-ray photoelectron spectroscopy (XPS) measurements (118). This group has also sonochemically produced colloidal cobalt solutions in decalin stabilized by oleic acid and Fe_2O_3 colloidal solutions in hexadecane stabilized by oleic acid (119, 120).

A different approach to the sonochemical synthesis of nanostructured metals is by cavitation to produce strong reductants from aqueous or alcohol solutions, thereby reducing metal salts *in situ*. Several researchers have used this approach.

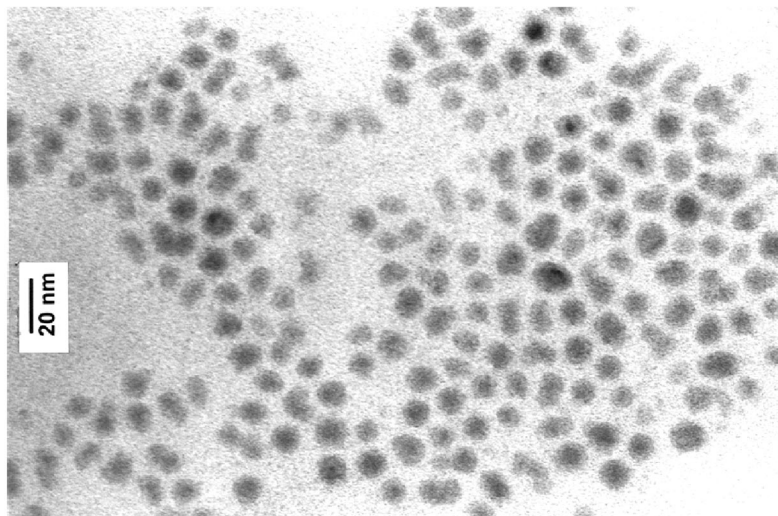


Figure 11 Transmission electron micrograph of sonochemically-prepared iron colloid stabilized by oleic acid (112).

For example, gold colloids can be produced by the sonochemical reduction of AuCl_4^- solutions under Ar (121). The colloid particle sizes had number averages of about 10 nm, with a fairly narrow size distribution, and could be stabilized for months by using the usual surfactants. Grieser and coworkers found that the addition of aliphatic alcohols significantly enhanced the rate of colloid formation and that the more hydrophobic the alcohol, the greater the effect (122). They concluded that radical reductants were being generated from the alcohols in the interfacial region surrounding the cavitation bubbles. Dhas et al recently reported (123) the synthesis of metallic copper nanoparticles (porous aggregates of 50–70 nm that contain an irregular network of small nanoparticles) from aqueous sonolysis of a copper(II) hydrazine complex.

NANOSTRUCTURED SUPPORTED CATALYSTS Most heterogeneous metal catalysts are supported, i.e. the metal is deposited on a high-surface-area solid, such as silica or alumina. In general, these materials are made by taking simple metal salts (usually the nitrates), soaking aqueous solutions of them into the porous support, and calcining under hydrogen at high temperatures to produce small metal particles throughout the support. Often the metal particles are not very uniform in size and are dispersed throughout the ill-defined pore structure of the support. The creation of “eggshell” catalysts in which uniform-sized nanoparticles of metals are deposited on the outer surface of supports has potential advantages for catalyst preparation (124).

Suslick and coworkers found that ultrasonic irradiation of decane solutions of iron pentacarbonyl, $\text{Fe}(\text{CO})_5$, in the presence of silica gel produces a silica-supported amorphous nanostructured iron in which the iron particles are all on the outer surface of the silica (104, 109). The iron particles are formed during cavitation events and then deposited on the silica suspended in solution. The iron loading on the SiO_2 can be easily varied by changing the initial concentration of the $\text{Fe}(\text{CO})_5$ solution. The amorphous nature of these supported iron particles as initially deposited has been confirmed by several different techniques, which also showed crystallization to α -Fe metal particles on heating above 300°C . Transmission electron microscopy showed that the iron particles produced by sonolysis of $\text{Fe}(\text{CO})_5$ were highly dispersed on the SiO_2 surface. The iron particles range in size from 3 to 8 nm. The particles are on the surface of the silica only, which gives a very different surface morphology to the silica compared with that of a conventionally prepared catalyst. In closely related studies, Ramesh et al prepared Fe and Fe_3O_4 particles on the surface of colloidal nonporous silica (125). In either system, high-temperature drying of the silica is necessary to prevent oxidation of the iron nanoparticles.

The catalytic activity of the silica-supported nanostructured iron was probed in the commercially important Fischer-Tropsch synthesis reaction (i.e. hydrogenation of CO) (104, 109). The major reaction products for both catalysts are short-chain C_1 to C_4 hydrocarbons and CO_2 . The catalytic activity of the sonochemically produced iron on silica catalyst is an order of magnitude higher than the conventional supported iron at similar loadings and dispersions. Moreover, the silica-supported nanostructured iron catalyst exhibits high activity at low temperatures ($<250^\circ\text{C}$), whereas the conventional catalyst has no activity. The dramatic difference in activity between the two samples below 300°C may be caused by the amorphous nature of iron and the inherently highly defective surface formed during sonolysis of $\text{Fe}(\text{CO})_5$, when the amorphous state of iron is preserved. At higher temperatures, the activity decreases owing to iron crystallization, surface annealing, or catalyst deactivation from surface carbon deposition.

NANOSTRUCTURED CARBIDES, NITRIDES, OXIDES, AND SULFIDES

Carbides and Nitrides

Molybdenum and tungsten carbides have been explored as heterogeneous catalysts because of the similar activity that these carbides share with platinum group metals (126–128). For catalytic applications, high-surface-area materials are generally needed, but the refractory nature of these carbides makes this very

difficult. Suslick and coworkers (106–110) have developed a simple sonochemical synthesis of nanophase molybdenum carbide from the ultrasonic irradiation of molybdenum hexacarbonyl (106–110). Sonochemical decomposition of molybdenum hexacarbonyl in hexadecane produced an amorphous molybdenum oxycarbide; the oxygen was removed by heating under 1:1 CH_4/H_2 . The elemental analytical results showed that the sample had a stoichiometry of $\text{Mo}_2\text{C}_{1.02}$ with <0.09 wt% oxygen (by difference) and <0.02 wt% hydrogen. Scanning electron microscopy showed that the surface is extremely porous, and transmission electron microscopy revealed that the material is a porous aggregate of 3-nm-diameter particles; gas adsorption showed a surface area of $130 \text{ m}^2/\text{g}$.

Catalytic dehydrogenation versus hydrogenolysis of cyclohexane served as a standard reaction with a flow catalytic microreactor. To compare the catalytic properties, commercial ultrafine powders of platinum and ruthenium were also used under identical conditions. At all reaction temperatures examined, benzene was the only product formed for both samples, and their activities were comparable; no hydrogenolysis products were detected. In contrast, only hydrogenolysis, mostly to methane, occurred with commercial ruthenium powder. The analogy has often been made that Mo_2C is similar to Ru, whereas W_2C behaves like Pt (129). These results demonstrate, however, that for dehydrogenation of alkanes, sonochemically prepared nanostructured molybdenum carbide has selectivity similar to Pt rather than to Ru.

There is only one report in the literature concerning the sonochemical preparation of nitrides (130). $\text{Fe}(\text{CO})_5$ was sonicated in a decane solution under a gaseous mixture of NH_3 and H_2 at $\sim 0^\circ\text{C}$. Alternatively, the sonochemically prepared amorphous iron was nitrated at $\sim 400^\circ\text{C}$ under a mixed stream of NH_3 and H_2 . Different products were obtained in the two cases. The product of the first preparation was an amorphous Fe_{2-3}N and a small quantity of iron oxide (presumably from adventitious air). In the second case, the XRD patterns showed FeN as a main product.

Nanostructured Oxides

Ultrasound for the preparation of both main-group and transition metal oxides has found some significant use. For example, the ultrasonic irradiation of $\text{Si}(\text{OC}_2\text{H}_5)_4$ in water with an acid catalyst produces a silica “sonogel” (131). In conventional preparation of silica gels from $\text{Si}(\text{OC}_2\text{H}_5)_4$, ethanol is typically used as a cosolvent, because $\text{Si}(\text{OC}_2\text{H}_5)_4$ is not soluble in water. Such solvents can become problematic because they may cause cracking during drying. These volatile cosolvents become unnecessary with sonication owing to enhanced mixing. The silica sonogel produced by the sonication of $\text{Si}(\text{OC}_2\text{H}_5)_4$ in the absence of ethanol has a higher density than the conventionally prepared gel.

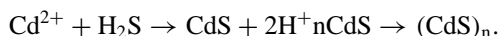
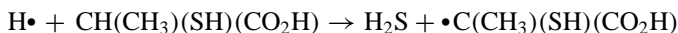
The particle size is also smaller than that of conventional gels (132). Small-angle x-ray-scattering experiments have been conducted on a silica sonogel and conventional silica aerogel. Conventional aerogels consist of a low-density matrix with large empty pores. The sonogels, in contrast, have finer porosity and the pores are approximately sphere-shaped, with a smooth surface (133). Monolithic silica glasses have been produced from silica sonogels prepared to 1150°C (134). Zirconium sonogels have also been produced from sonication of zirconium tetrapropoxide with acetic acid. Gelation time was reduced on sonication, and the sonogel had a much smaller particle size (135). Finally, this technique has been extended to trap large, organic dye molecules within the sonogel (136).

The synthesis of hydroxyapatite, $\text{Ca}_5(\text{PO}_4)_3\text{OH}$, from the hydrolysis of calcium oxyphosphates is also accelerated by ultrasound (137). Extensive research has been conducted on the synthesis of hydroxyapatite, owing to its potential application in medicine as artificial bone. The reaction time required to produce hydroxyapatite from a mixture of $\text{Ca}_4(\text{PO}_4)_2\text{O}$ and $\text{CaHPO}_4(\text{H}_2\text{O})$ (brushite) at 38°C was reduced from 3 h without sonication to 15 min with sonication. XRD showed that neither product was very crystalline. The morphologies of these two products were, however, quite different. The hydrolysis of $\alpha\text{-Ca}_3(\text{PO}_4)_2$ ($\alpha\text{-TCP}$) produced hydroxyapatite with better crystallinity. This reaction was also accelerated by ultrasonic irradiation.

In related work, Gasgnier and coworkers reported the acceleration formation of rare earth oxide formation via ultrasound (138), and Cao et al (139), Shafi et al (140), and Kataby et al (141) have extended the sonochemical synthesis of amorphous transition metals to the production of nanostructured metal oxides, simply by sonication in the presence of air (139–141).

Sulfides

Nanocrystalline CdS colloids have been produced by high-intensity ultrasound (142), as shown in the equations below. In situ-generated hydrogen sulfide from the sonication of 2-mercaptopropionic acid acted as the sulfiding agent. Spectroscopic studies revealed that sonication produces CdS particle sizes in the quantum dot range (Q-state) and the sonication time and the thiol type determine the particle size distribution. The colloid particles produced by the ultrasound process clearly show quantum size effects and are estimated to be <3 nm in diameter.



Very recently, Mdleleni et al reported the sonochemical synthesis of nanostructured molybdenum sulfide (114). MoS_2 is best known as the standard

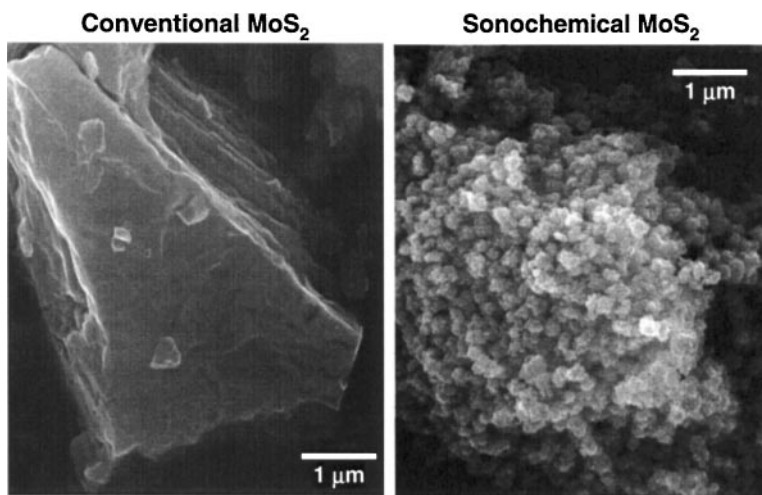


Figure 12 Morphology of conventional and sonochemically prepared MoS_2 ; scale bar is $1 \mu\text{m}$ (114).

automotive lubricant; its lubricant properties are caused by its layered structure. Planes of molybdenum atoms are sandwiched on both faces by planes of sulfur atoms tightly bonded to the Mo. Interactions between the sulfur planes are weak, thus producing lubrication properties similar to graphite. Of greater interest here, however, MoS_2 is also the predominant hydrodesulfurization catalyst heavily used by the petroleum industry to remove sulfur from fossil fuels before combustion (143).

An unusual morphology of MoS_2 was produced by the irradiation of solutions of molybdenum hexacarbonyl and sulfur in 1,2,3,5-tetramethylbenzene with high-intensity ultrasound (114). The morphologies of the sonochemical and conventional MoS_2 are dramatically different, as shown in Figure 12. Conventional MoS_2 shows a platelike morphology typical for such layered materials. The sonochemical MoS_2 exists as a porous agglomeration of clusters of spherical particles with an average diameter of 15 nm. Despite the morphological difference between the sonochemical and conventional MoS_2 , transmission electron microscopy images (Figure 13) show both to have the same interlayer spacing. The sonochemically prepared MoS_2 , however, shows much greater edge and defect content because the layers must bend, break, or otherwise distort to fit to the outer surface of the 15-nm particle size (Figure 13).

It is well established that the activity of MoS_2 is localized at the edges and not on the flat basal planes (143, 144). Unfortunately, the nature of this

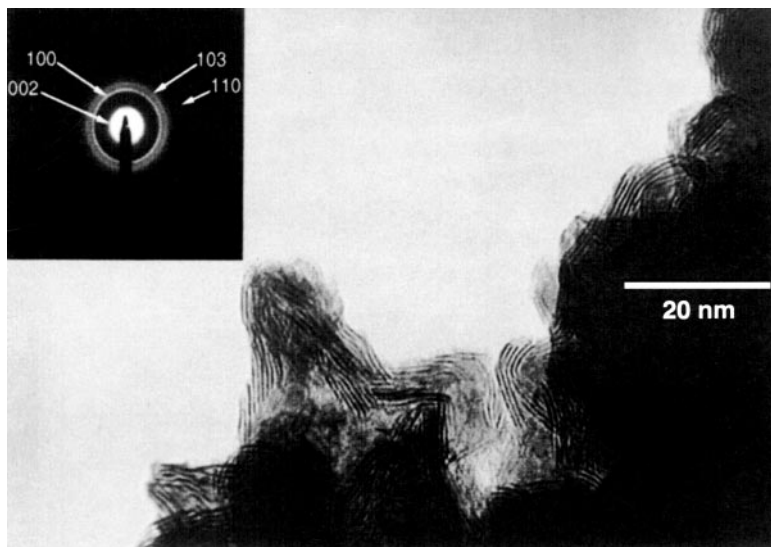


Figure 13 Transmission electron micrograph of sonochemically prepared MoS₂. Basal planes are seen as dark fringes with interlayer spacings of 0.62 ± 0.01 nm, the same as conventional MoS₂ (114).

layered material causes the basal planes to dominate the total surface area under most synthetic conditions. Given the inherently higher edge concentrations in nanostructured materials, the catalytic properties of our sonochemically prepared MoS₂ become especially interesting. The catalytic activity and selectivity for thiophene hydrodesulfurization by sonochemically prepared MoS₂ were examined in a single-pass microreactor (114). Conventional MoS₂, sonochemical Mo₂C, and commercial ReS₂ and RuS₂ were also investigated under the same conditions for comparison. For conventionally prepared sulfides, ReS₂ and RuS₂ are inherently more reactive than MoS₂ (144) but are too expensive to be generally used. The observed turnover frequencies for these catalysts were examined as a function of temperature. The principal products detected by gas chromatography were the C₄ hydrocarbons: butadiene, 1-butene, *trans*-2-butene, *cis*-2-butene, and butane. The observed order of hydrodesulfurization activity is MoS₂ (sonochemical) > RuS₂ (conventional) > ReS₂ (conventional) > Mo₂C (sonochemical) > MoS₂ (conventional). The sonochemically prepared MoS₂ catalyzes the hydrodesulfurization of thiophene with activities roughly fivefold better than conventional MoS₂ and comparable to those observed with RuS₂, one of the best commercial catalysts.

CONCLUSIONS

Bubble collapse in liquids results in an enormous concentration of energy from the conversion of the kinetic energy of liquid motion into heating of the contents of the bubble. The enormous local temperatures and pressures so created provide a unique means for fundamental studies of chemistry and physics under extreme conditions.

Cavitation in liquids can have dramatic effects on the reactivities of both extended solid surfaces and fine-powder slurries. Microjet and shockwave impact (on large surfaces) and interparticle collisions (with powders) have substantial effects on the chemical composition and physical morphology of solids that can dramatically enhance chemical reactivity of both organic polymers and inorganic solids.

The extreme conditions inside collapsing bubbles produce highly reactive species that can be used for various purposes, for instance, the initiation of polymerization without added initiators. As another example, the sonochemical decomposition of volatile organometallic precursors in high-boiling-point solvents produces nanostructured materials in various forms with high catalytic activities. Nanostructured metals, alloys, carbides and sulfides, nanometer colloids, and nanostructured supported catalysts can all be prepared by this general route.

We have seen a diverse and promising set of applications for ultrasound in materials chemistry. There still remains, however, much to explore in the sonochemical synthesis of organic, inorganic, and even biomaterials.

ACKNOWLEDGMENTS

This work was supported by the National Science Foundation. We acknowledge our coworkers listed in the cited references, without whose efforts none of this work would have been possible. We also thank M Marshall, P Mochel, V Petrova, and the UIUC Center for Microanalysis of Materials, which is supported by the Department of Energy, for their assistance in surface characterizations.

Visit the *Annual Reviews* home page at
<http://www.AnnualReviews.org>

Literature Cited

1. Suslick KS, ed. 1988. *Ultrasound: Its Chemical, Physical, and Biological Effects*. New York: VCH
2. Mason TJ, Lorimer JP. 1988. *Sonochemistry: Theory, Applications and Uses of Ultrasound in Chemistry*. Chichester, UK: Harword
3. van Eldik R, Hubbard CC, eds. 1997. *Chemistry Under Extreme or Non-Classical Conditions*. New York: Wiley & Sons
4. Suslick KS, Crum LA. 1997. In *Encyclopedia of Acoustics*, ed. MJ Crocker, 1: 271–82. New York: Wiley-Interscience

5. Luche J-L. 1998. *Synthetic Organic Sonochemistry*. New York: Plenum
6. Suslick KS. 1998. In *Kirk-Othmer Encyclopedia of Chemical Technology*, 26: 517-41. New York: Wiley & Sons, 4th ed.
7. Crum LA, Mason TJ, Reisse JL, Suslick KS, eds. 1999. *Sonochemistry and Sonoluminescence, Proc. NATO Adv. Study Inst. Ser. C Vol. 524*. Dordrecht, Netherlands: Kluwer
8. Suslick KS. 1993. In *Encyclopedia of Materials Science and Engineering*, ed. RW Cahn, pp. 2093-98. Oxford, UK: Pergamon. 3rd Suppl.
9. Suslick KS. 1994. In *Encyclopedia of Inorganic Chemistry*, ed. RB King, 7:3890-905. New York: Wiley & Sons
10. Suslick KS. 1995. *MRS Bull.* 20:29
11. Price GJ. 1996. In *Chemistry Under Extreme or Non-Classical Conditions*, ed. R van Eldik, CC Hubbard. New York: Wiley & Sons
12. Suslick KS. 1997. In *Handbook of Heterogeneous Catalysis*, ed. G Ertl, H Knozinger, J Weitkamp, 3:1350-57. Weinheim: Wiley-VCH
13. Leighton TG. 1994. *The Acoustic Bubble*. London: Academic
14. Flint EB, Suslick KS. 1991. *Science* 253: 1397
15. Suslick KS, Didenko Y, Fang MM, Hyeon T, Kolbeck KJ, et al. 1999. *Philos. Trans. R. Soc. London Ser. A*. In press
16. McNamara WB III, Didenko Y, Suslick KS. 1999. In *Sonochemistry and Sonoluminescence, Proc. NATO Adv. Study Inst. Ser. C Vol. 524*. Dordrecht, Netherlands: Kluwer
17. Preece CM, Hansson IL. 1981. *Adv. Mech. Phys. Surf.* 1:199
18. Doktycz SJ, Suslick KS. 1990. *Science* 247:1067
19. Suslick KS, Doktycz SJ. 1990. In *Advances in Sonochemistry*, ed. TJ Mason, 1:197-230. Greenwich, CT: JAI
20. Mason TJ, Cordemans ED. 1996. *Chem. Eng. Res. Des.* 74:511
21. Suslick KS, Cline RE Jr, Hammerton DA. 1986. *J. Am. Chem. Soc.* 106:5641
22. Flosdorf EW, Chambers LA. 1933. *J. Am. Chem. Soc.* 55:3051
23. Gyorgi AS. 1933. *Nature* 131:278
24. Basedow AM, Ebert K. 1977. *Adv. Polym. Sci.* 22:83
25. Price GJ. 1990. See Ref. 19, pp. 231-87
26. Price GJ, Smith PF. 1993. *Eur. Polym. J.* 29:419
27. Price GJ, Wallace EN, Patel AM. 1995. In *Silicon Containing Polymers*, ed. RG Jones, p. 147. Cambridge, UK: R. Soc. Chem.
28. Koda S, Mori H, Matsumoto K, Nomura H. 1994. *Polymer* 35:30
29. Sato T, Nalepa DE. 1977. *J. Coat. Technol.* 49:45
30. Bradbury JH, O'Shea J. 1973. *Aust. J. Biol. Sci.* 26:583
31. Davison PF, Freifelder D. 1962. *Biophys. J.* 2:235
32. Encina MV, Lissi E, Sarasusa M, Gargallo L, Radic D. 1980. *J. Polym. Sci. Polym. Lett.* 18:757
33. Van der Hoff BME, Glynn PAR. 1974. *J. Macromol. Sci. Macromol. Chem.* A8:429
34. Van der Hoff BME, Gall CE. 1977. *J. Macromol. Sci. Macromol. Chem.* A11: 1739
35. Muller AJ, Odell JA, Keller A. 1990. *Macromolecules* 23:3090
36. Watanabe O, Tabata M, Kuedo T, Sohma J, Ogiwara T. 1985. *Prog. Polym. Phys. Jpn.* 28:285
37. Nguyen TQ, Liang QZ, Kausch HH. 1997. *Polymer* 38:3783
38. Deleted in proof
39. Tabata M, Miyawaza T, Sohma J, Kobayashi O. 1980. *Chem. Phys. Lett.* 73:178
40. Urban MW, Salazar-Rojas EM. 1988. *Macromolecules* 21:372
41. Exsted BJ, Urban MW. 1994. *Polymer* 35: 5560
42. Deleted in proof
43. Price GJ, Keen F, Clifton AA. 1996. *Macromolecules* 29:5664
44. Suslick KS, Casadonte DJ. 1987. *J. Am. Chem. Soc.* 109:3459
45. Suslick KS, Johnson RE. 1984. *J. Am. Chem. Soc.* 106:6856-58
46. Suslick KS, Doktycz SJ. 1989. *Chem. Mater.* 1:6
47. Suslick KS, Doktycz SJ. 1989. *J. Am. Chem. Soc.* 111:2342
48. Suslick KS, Casadonte DJ, Doktycz SJ. 1989. *Solid State Ion.* 32/33:444-52
49. Chatakondou K, Green MLH, Thompson ME, Suslick KS. 1987. *J. Chem. Soc. Chem. Commun.* 1987:900
50. Suslick KS, Casadonte DJ, Green MLH, Thompson ME. 1987. *Ultrasonics* 25:56-59
51. Mal'tsev AN. 1976. *Z. Fiz. Khim.* 50:1641
52. Miller RD, Michl J. 1989. *Chem. Rev.* 89:1359
53. Han BH, Boudjouk P. 1981. *Tetrahedron Lett.* 22:3813
54. Kim HK, Matyjaszewski K. 1989. *J. Am. Chem. Soc.* 110:3321
55. Kim HK, Uchida H, Matyjaszewski K. 1995. *Macromolecules* 28:59

56. Miller RD, Thompson D, Sooriyakumaran R, Fickes GN. 1991. *J. Polym. Sci. Polym. Chem.* 29:813
57. Price GJ. 1992. *J. Chem. Soc. Chem. Commun.* 1992:1209
58. Price GJ, Patel AM. 1997. *Eur. Polym. J.* 33:599
59. Weidman TW, Bianconi PA, Kwock EW. 1990. *Ultrasonics* 28:310
60. Henglein A. 1954. *Makromol. Chem.* 14: 15
61. El'Piner IE. 1964. *Ultrasound: Physical, Chemical and Biological Effects*. New York: Consultants Bureau
62. Kruus P, Patraboy TJ. 1985. *J. Phys. Chem.* 89:3379
63. Kruus P. 1991. *Adv. Sonochem.* 2:1
64. Price GJ, Norris DJ, West PJ. 1992. *Macromolecules* 25:6447
65. Lorimer JP, Mason TJ, Kershaw D. 1991. *J. Chem. Soc. Chem. Commun.* 1991: 1217
66. Miyata T, Nakashio F. 1975. *J. Chem. Eng. Jpn.* 8:469
67. Price GJ, Daw MR, Newcombe NJ, Smith PF. 1990. *Br. Polym. J.* 23:63
68. Ostroski AS, Stanbaugh RB. 1950. *J. Appl. Phys.* 21:478
69. Cooper G, Greiser F, Biggs S. 1994. *J. Coll. Interface Sci.* 184:52
70. Schultz DN, Sissano JA, Costello CA. 1994. *Polym. Prep.* 35:514
71. Long GB. 1967. *U.S. Patent No. 3346472*
- 72a. Ragaini V. *Italian Patent Appl. 20478-A/90*.
- 72b. Carli R, Bianchi CL, Gariboldi P, Ragaini V. 1993. *Proc. Europ. Sonochem. Soc., 3rd, Coimbra, Portugal*. Eur. Sonochem. Soc.
73. Senapati N, Mangaraj D. 1985. *U.S. Patent No. 45489771*
74. Salensa TK, Babbar NK. 1971. *Ultrasonics* 13:21
75. Isayev I, Yushanov SP, Chen J. 1996. *J. Appl. Polym. Sci.* 59:803, 815
76. Suslick KS, Grinstaff MW. 1990. *J. Am. Chem. Soc.* 112:7807
77. Suslick KS, Grinstaff MW. 1991. *Proc. Natl. Acad. Sci. USA* 88:7708-10
78. Suslick KS, Grinstaff MW, Kolbeck KJ, Wong M. 1994. *Ultrason. Sonochem.* 1: S65-68
79. Liu KJ, Grinstaff MW, Jiang J, Suslick KS, Swartz HM, Wang W. 1994. *Biophys. J.* 67:896-901
80. Wong M, Suslick KS. 1995. *Hollow and Solid Spheres and Microspheres, MRS Symp. Proc.*, ed. DL Wilcox, M Berg, T Bernat, D Kellerman, JK Corchran, 372: 89-94. Pittsburgh: Mater. Res. Soc.
81. Eckburg JJ, Chato JC, Liu KJ, Grinstaff MW, Swartz HM, et al. 1996. *J. Biomech. Eng.* 118:193-200
82. Webb AG, Wong M, Kolbeck KJ, Magin RL, Wilmes LJ, Suslick KS. 1996. *J. Magn. Reson. Imaging* 6:675-83
83. Riesz P, Berdahl D, Christman CL. 1985. *Environ. Health Perspect.* 64:233
84. Keller MW, Feinstein SB. 1988. In *Echocardiography in Coronary Artery Disease*, ed. RE Kerber. New York: Future
85. Desai NP, Soon-Shiong P, Sandford PA, Grinstaff MW, Suslick KS. 1994. *U.S. Patent No. 5362478*
86. Desai NP, Soon-Shiong P, Sandford PA, Grinstaff MW, Suslick KS. 1995. *U.S. Patent No. 543686*
87. Grinstaff MW, Soon-Shiong P, Wong M, Sandford PA, Suslick KS, Desai NP. 1996. *U.S. Patent No. 5498421*
88. Grinstaff MW, Desai NP, Suslick KS, Soon-Shiong P, Sandford PA, Merideth NR. 1996. *U.S. Patent 5505932*
89. Grinstaff MW, Desai NP, Suslick KS, Soon-Shiong P, Sandford PA, Merideth NR. 1996. *U.S. Patent No. 5508021*
90. Grinstaff MW, Desai NP, Suslick KS, Soon-Shiong P, Sandford PA, Merideth NR. 1996. *U.S. Patent No. 5512268*
91. Desai NP, Soon-Shiong P, Sandford PA, Grinstaff MW, Suslick KS. 1996. *U.S. Patent No. 5560933*
92. Grinstaff MW, Soon-Shiong P, Wong M, Sandford PA, Suslick KS, Desai NP. 1997. *U.S. Patent No. 5635207*
93. Grinstaff MW, Soon-Shiong P, Wong M, Sandford PA, Suslick KS, Desai NP. 1997. *U.S. Patent No. 5639473*
94. Grinstaff MW, Soon-Shiong P, Wong M, Sandford PA, Suslick KS, Desai NP. 1997. *U.S. Patent No. 5650156*
95. Grinstaff MW, Soon-Shiong P, Wong M, Sandford PA, Suslick KS, Desai NP. 1997. *U.S. Patent No. 5665382*
96. Grinstaff MW, Soon-Shiong P, Wong M, Sandford PA, Suslick KS, Desai NP. 1997. *U.S. Patent No. 5665383*
97. Weller H. 1993. *Adv. Mater.* 5:88
98. Moser WR, ed. 1996. *Advanced Catalysts and Nanostructured Materials*. New York: Academic
99. Suslick KS, Choe SB, Cichowlas AA, Grinstaff MW. 1991. *Nature* 353:414
100. Grinstaff MW, Cichowlas AA, Choe SB, Suslick KS. 1992. *Ultrasonics* 30: 168
101. Grinstaff MW, Salamon MB, Suslick KS. 1993. *Phys. Rev. B* 48:269
102. Bellissent R, Galli G, Grinstaff MW, Migliardo P, Suslick KS. 1993. *Phys. Rev. B* 48:15797-800

103. Suslick KS, Hyeon T, Fang M, Cichowlas AA. 1994. *Molecularly Designed Nanostructured Materials*, MRS Symp. Proc., ed. KE Gonsalves, GM Chow, TO Xiao, RC Cammarata, 351:201–06. Pittsburgh: Mater. Res. Soc.
104. Suslick KS, Fang M, Hyeon T, Cichowlas AA. 1994. *Molecularly Designed Nanostructured Materials*, MRS Symp. Proc., ed. KE Gonsalves, GM Chow, TO Xiao, RC Cammarata, 351:443–48. Pittsburgh: Mater. Res. Soc.
105. Bellissent R, Galli G, Hyeon T, Magazu S, Majolino D, et al. 1995. *Phys. Scripta* T57:79–83
106. Hyeon T, Fang M, Cichowlas AA, Suslick KS. 1995. *Mater. Sci. Eng. A* 204:186–92
107. Suslick KS, Hyeon T, Fang M, Ries JT, Cichowlas AA. 1996. *Mater. Sci. Forum* 225–27:903–12
108. Hyeon T, Fang M, Suslick KS. 1996. *J. Am. Chem. Soc.* 118:5492–93
109. Suslick KS, Hyeon T, Fang M, Cichowlas AA. 1996. In *Advanced Catalysts and Nanostructured Materials*, ed. WR Moser, pp. 197–211. New York: Academic
110. Suslick KS, Hyeon T, Fang M. 1996. *Chem. Mater.* 8:2172–79
111. Bellissent R, Galli G, Hyeon T, Migliardo P, Parette P, Suslick KS. 1996. *J. Non-Cryst. Solids* 205:656–59
112. Suslick KS, Fang M, Hyeon T. 1996. *J. Am. Chem. Soc.* 118:11960–61
113. Long GJ, Hautot D, Pankhurst QA, Vandormael D, Grandjean F, et al. 1998. *Phys. Rev. B* 57:10716–22
114. Mdleleni MM, Hyeon T, Suslick KS. 1998. *J. Am. Chem. Soc.* 120:6189–90
115. Shafi KVPM, Gedanken A, Prozorov R. 1998. *J. Mater. Chem.* 83:769–73
116. Shafi KVPM, Gedanken A, Goldfarb RB, Felner I. 1997. *J. Appl. Phys.* 81:6901–5
117. Berkovsky BM, Medvedev VF, Krakov MS. 1993. *Magnetic Fluids: Engineering Applications*. London/New York: Oxford Univ. Press
118. Kataby G, Ulman A, Prozorov R, Gedanken A. 1998. *Langmuir* 147:1512–15
119. Shafi KVPM, Wizer S, Prozorov T, Gedanken A. 1998. *Thin Solid Films* 31:38–41
120. Shafi KVPM, Gedanken A, Prozorov R. 1998. *Adv. Mater.* 10:590–91
121. Nagata Y, Mizukoshi Y, Okitsu K, Maeda Y. 1996. *Radiat. Res.* 146:333–38
122. Grieser F, Hobson R, Sostaric J, Mulvaney P. 1996. *Ultrasonics* 34:547–50
123. Dhas NA, Raj CP, Gedanken A. 1998. *Chem. Mater.* 10:1446–52
124. Klabunde KJ, Li Y-X. 1993. *Selectivity in Catalysis*, ed. ME Davis, SL Suib, pp. 88–108. Washington, DC: Am. Chem. Soc.
125. Ramesh S, Prozorov R, Gedanken A. 1997. *Chem. Mater.* 9:2996–3004
126. Ranhotra GS, Haddix GW, Bell AT, Reimer JA. 1987. *J. Catal.* 108:40
127. Lee JS, Oyama ST, Boudart M. 1990. *J. Catal.* 125:157
128. Ledoux MJ, Pham-Huu C, Guille J, Dunlop H. 1992. *J. Catal.* 134:383
129. Volpe L, Boudart M. 1985. *J. Solid State Chem.* 59:332
130. Koltypin Y, Cao X, Prozorov R, Balogh J, Kaptas D, Gedanken A. 1997. *J. Mater. Chem.* 7:2453–56
131. Esquivias L, Zarzycki J. 1986. In *Current Topics on Non-Crystalline Solids*, ed. M Baro, DN Clavaguera, p. 409. Singapore: World Sci.
132. Esquivias L, Zarzycki J. 1988. In *Ultrastructure Processing of Advanced Ceramics*, ed. JD Mackenzie, DR Ulrich, p. 255. New York: Wiley & Sons
133. De la Rosa-Fox N, Esquivias L, Craievich AF, Zarzycki J. 1990. *J. Non-Cryst. Solids* 121:211
134. Blanco E, Ramirezdelosolar M, De la Rosa-Fox N, Esquivias L. 1995. *Mater. Lett.* 225–226:265–70
135. Chaumont D, Craievich A, Zarzycki J. 1992. *J. Non-Cryst. Solids* 147–148: 41
136. Litran R, Blanco E, Ramirezdelosolar M, Esquivias L. 1997. *J. Sol-Gel Sci. Technol.* 8:985–90
137. Fang Y, Agrawal DK, Roy DM, Roy R, Brown PW. 1992. *J. Mater. Res.* 7:2294
138. Gasgnier M, Albert L, Derouet J, Beaury L. 1995. *J. Solid State Chem.* 115:532
139. Cao X, Prozorov R, Koltypin Y, Kataby G, Felner I, Gedanken A. 1997. *J. Mater. Res.* 12:402–6
140. Shafi KVPM, Koltypin Y, Gedanken A, Prozorov R, Balogh J, et al. 1997. *J. Phys. Chem. B.* 101:6409–14
141. Kataby G, Prozorov T, Koltypin Y, Cohen H, Sukenik CN, et al. 1997. *Langmuir* 13:6151–58
142. Sostaric JZ, Carusohobson RA, Mulvaney P, Grieser F. 1997. *J. Chem. Soc. Faraday Trans. pp.* 1791–95
143. Gates BC. 1992. *Catalytic Chemistry*, pp. 387–92. New York: Wiley & Sons
144. Pecoraro TA, Chianelli RR. 1981. *J. Catal.* 67:430

Embedded Secure Document

The file <http://www.scs.uiuc.edu/~suslick/pdf/jssc0087.pdf> is a secure document that has been embedded in this document. Double click the pushpin to view.



Shape-Selective Oxidation by Metalloporphyrins

KENNETH S. SUSLICK

*School of Chemical Sciences
University of Illinois at Urbana-Champaign
600 S. Goodwin Av.
Urbana, IL 61801
tel: 217-333-2794 fax: 217-333-2685 email: ksuslick@uiuc.edu*

I. Introduction

II. Hydrocarbon Oxidation by Metalloporphyrins

A. Cytochrome P450

1. Overview
2. Regioselectivity

B. Synthetic Metalloporphyrins

1. Mechanisms of Oxidation
2. Metalloporphyrin Catalyzed Oxidations

III. Shape Selective Oxidation of Hydrocarbons

A. Homogeneous Catalysts

1. Hydroxylation
2. Epoxidation
3. Comparisons to Enzymatic Selectivities

B. Heterogeneous and Micro-Heterogeneous Catalysts

C. Shape Selectivity as a Mechanistic Probe

D. Regioselectivity Based on Polarity

IV. Enantioselective Oxidations

V. Conclusions

VI. Acknowledgments

VII. References

VIII. Tables

IX. Figure Captions

X. Figures

I. Introduction

Discriminating one site on a molecule from another and distinguishing among many similar molecules presents a difficult challenge to both industrial and biological chemistry. Shape selective catalysis of hydrocarbon reforming and other reductive processes have been extremely successful (most notably with zeolites and related microporous solids) and has formed the basis for important industrial processes.^{1,2} Oxidative processes with organic substrates also has an important place in both biological and industrial processes.³⁻⁷ The uniqueness of enzymes in such reactions is their ability to direct the oxidation to *specific* substrates and at specific sites on these substrates.⁸ Regioselectivity often originates from discrimination based on the size and shape of substrate molecules, i.e., shape selectivity arises from both steric repulsions and van der Waals attractions. Dipole-dipole, hydrogen bonding, ion pairing, and other weak forms of bonding provide other sorts of interactions to induce selective binding, specific substrate orientation, and regioselectivity. Nonetheless, the creation of shape selective *oxidation* catalysts is still in an early stage of development.

While there has been a huge effort to develop the field of supramolecular chemistry,⁹ the vast majority of this work has concentrated on molecular recognition, *i.e.*, the design of host-guest systems that exhibit specificity in binding substrates. Few such systems, however, have been designed to actually *do* something to the substrate once it has been bound. Thus, molecular recognition is not enough. There must be *two* goals for researchers interested in mimicking the specificity typical of enzymatic reactions: not only the design and synthesis of chemical species capable of molecular recognition, but also the inclusion in such hosts of a reactive center that can produce a regioselective or enantioselective chemical transformation on the guest substrate.

In the absence of steric restraints, regioselectivity in oxidations generally is heavily influenced by thermodynamics. For example, in the hydroxylation of alkanes by metalloporphyrins, product distribution analyses are consistent with a radical intermediate formed by hydrogen atom abstraction.^{10,11} Hydroxylation selectivities are therefore dominated by C-H bond strengths¹² (Table 1), and the rates of oxidation are tertiary C-H bonds much faster than secondary, which are much faster than primary (i.e., $3^\circ \gg 2^\circ \gg 1^\circ$). In epoxidations, the active oxidant is extremely electrophilic and therefore preferentially attacks the most electron rich (i.e., most substituted) double bond.¹³

In principle, however, regioselectivities can be controlled by kinetic access to reactive sites by specificity in substrate binding. In this fashion, various metalloproteins can yield products dramatically different than those expected from simple bond strengths. The most important enzyme used for catalytic oxidation of organic compounds is cytochrome P450, and intense efforts have been made to generate similar catalytic behavior with transition metal macrocycle or chelate complexes. The synthetic versatility of the porphyrins makes them especially attractive for the construction of enzyme analogues through the elaboration of the superstructure of the macrocycle.¹⁴⁻¹⁷ In terms of the enzyme specificity, some of the isozymes of cytochrome P450 and the non-heme, iron-containing proteins known as ω -hydroxylases, are especially impressive.

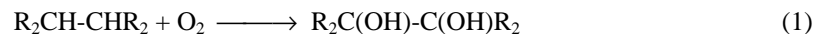
This Chapter begins with an overview of oxidation catalysis by heme proteins and by synthetic porphyrins. This is followed by an examination of the regioselectivity of enzymatic oxidation of hydrocarbons, especially those enzymes responsible for primary alcohol synthesis from the terminal hydroxylation of alkyl chains (e.g., cholesterol, fatty acids, and n-alkanes) (Section II.A.2). The bulk of the Chapter is a description of the development of synthetic oxidation catalysts based on metalloporphyrins whose superstructure takes on the enzymatic role of substrate discrimination.

II. Hydrocarbon Oxidation by Metalloporphyrins

A. Cytochrome P450

1. Overview

Oxidations in biological systems are catalyzed by various classes of enzymes, including dehydrogenases, dioxygenases, peroxidases, and monooxygenases.⁵ Of these, the dehydrogenases do not directly involve redox chemistry of dioxygen or its products. Instead, they catalyze the removal of two hydrogen atoms from a substrate to form either a ketone or a carboxylic acid. The large majority of biological oxidations involve dioxygen. The dioxygenases utilize O₂ and insert both oxygen atoms into substrate, as shown in eq 1.



A large fraction of enzymes responsible for oxygen utilization are heme proteins. The hydroperoxidases (Figure 1) consist of the subclasses of peroxidases, catalases, and the monooxygenase cytochrome P450. The peroxidases catalyze the one-electron oxidation of a large variety of substrates, including cytochrome *c*, halide anions, and various organic substrates, as generalized in eqs 2 and 3. Two intermediate oxidation states of the enzyme are seen during this process, compound I, which is two oxidation equivalents above the Fe(III) resting state, and compound II, which is one oxidation equivalent above Fe(III). Catalase converts H₂O₂ to O₂ and H₂O, through a compound I type intermediate.



[FIGURE 1 HERE]

Monooxygenases catalyze the insertion of one oxygen atom, derived from the reductive activation of dioxygen, into a substrate as shown for example in eq 4. Not all monooxygenases are heme proteins, or even metalloproteins. Nonetheless, cytochrome P450, the best studied of this general class of oxidation enzymes, is a heme protein closely related to the peroxidases. It is the diverse and highly regioselective reactions of various forms of cytochrome P450 that has motivated most of the effort to produce the bioinorganic analogues that are the primary focus of this Chapter.



2. Regioselectivity

Cytochromes P450 are a class of heme-containing monooxygenases that transfer an oxygen atom from dioxygen to various organic substrates.¹⁴ In mammalian systems, these include cholesterol and other steroids, prostaglandins, and a variety of xenobiotics. P450 is also responsible for the carcinogenesis of otherwise unreactive molecules such as benzene. The types of reactions catalyzed by cytochromes P450 are extremely diverse, as shown in Figure 2, and include aliphatic and arene hydroxylations, alkene epoxidation, N-oxidation, S-oxidation, and N-, O-, and S-dealkylation.¹⁹ Cytochrome P450 is found in prokaryotes, and both higher and lower eukaryotes. These enzymes contain an iron protoporphyrin IX prosthetic group, with unusual axial ligation of the thiolate of a proximal cysteine.

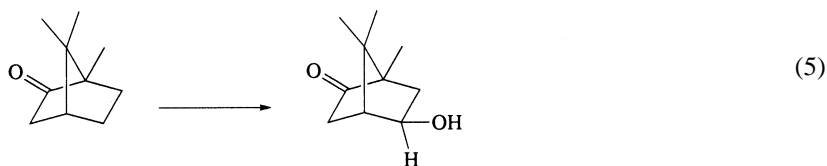
[FIGURE 2 HERE]

The catalytic cycle of cytochrome P450 involves several discrete steps¹⁸ and is shown in Figure 3. The resting state of the heme is a water-bound six-coordinate low-spin iron(III) complex. Substrate binding results in loss of water coordination leaving a high-spin five-coordinate iron(III) complex. One electron reduction (usually from an Fe-S protein) gives the five-coordinate iron(II) heme which can bind O₂ to give the superoxo-bound iron(III) complex. A second one electron reduction results in cleavage of the O-O bond and presumed formation of a short-lived iron-oxo intermediate. The iron-oxo species is proposed to be an Fe^{IV}=O porphyrin π-radical cation similar to the Compound I of peroxidase or catalase. For hydroxylations, the iron-oxo species is thought to abstract a hydrogen from the substrate generating a hydroxo-bound iron complex. Rapid recombination of the substrate radical with the hydroxo-complex generates the product.²⁰ This step also regenerates the water-bound six-coordinate complex after the product leaves the active site.

[FIGURE 3 HERE]

There are often distinct substrate specificities associated with different forms of cytochrome P450 and other monooxygenases, varying both from species to species and from isozyme to isozyme. This diversity of specificity requires tailored interactions between the protein's binding site and substrate. Examples include cytochrome P450_{cam},²¹ cytochrome P450_{ω-2},^{21,22} ω-hydroxylases,²³⁻²⁶ the liver microsomal enzymes involved in cholesterol and prostaglandin biosynthesis,²⁷ and fatty acid metabolism.²⁸

The best studied of these is a bacterial cytochrome P450 from *Pseudomonas putida*, P450_{cam}, which oxidizes camphor to 5-exo-hydroxycamphor exclusively, both *in vivo* and in reconstituted enzyme systems (eq 5).²¹



The extreme regioselectivity of this reaction is due in part to the match in shape between the substrate and the enzyme binding site and in part to a hydrogen bond between tyrosine-96 and the camphor carbonyl (Figure 4).²⁹ Mutant cytochromes P450, unable to form this hydrogen bond with camphor, show less selectivity with a wider range of products,³⁰ as does the native enzyme with camphane and thioamphor, neither of which can form the important hydrogen bond.

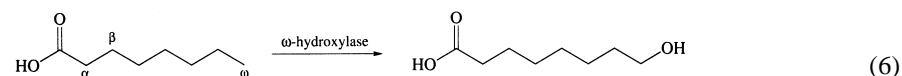
[FIGURE 4 HERE]

In order to probe the effect of steric interactions on the specificity of hydroxylation, Atkins and Sligar altered two of the residues in P450_{cam} that have interactions with the substrate, valine-247 and valine-295.³⁰ Site specific mutagenesis of valine-247 to alanine (which has less steric bulk) results in lower selectivity of hydroxylation and greater product distributions. Valine-295 was mutated to isoleucine, which resulted in increased selectivity of hydroxylation for both 1-methylnorcamphor and norcamphor and no change for camphor versus the native enzyme. Thus, the increased steric bulk of isoleucine versus valine holds the smaller molecules more tightly in the pocket than the native enzyme.

Fowler et al. have produced a single site mutant of P450_{cam} (tyrosine 96 to alanine) that is able to bind diphenylmethane.³¹ While the rate of hydroxylation was diminished eight-fold compared to native P450_{cam}, it was highly regioselective for the aromatic hydroxylation of diphenylmethane to produce *p*-hydroxydiphenylmethane.

Another bacterial enzyme, cytochrome P450_{ω-2} from *Bacillus megaterium*, catalyzes the hydroxylation of the ω-1, ω-2 and ω-3 carbons of fatty acids (i.e., the methylenes at the end of the alkyl tail). P450_{ω-2} also hydroxylates the ω-1, ω-2 and ω-3 positions of alcohols and amides but not the terminal methyl groups of any substrate.^{22,32,33} Miura and Fulco suggested that the substrate is held in place by strong interactions with the protein at the ends of the molecule but has more freedom in the central portion.³³ This binding model would account for the enzyme's inability to hydroxylate the terminal carbon, given the substantial difference in bond dissociation energies for 1° and 2° C-H bonds (Table 1). Unlike the non-heme and heme containing ω-hydroxylases, this enzyme will not hydroxylate alkanes. The reason cytochrome P450_{ω-2} is unable to hydroxylate alkanes is unknown, but is likely due to poor binding.

In higher organisms, the enzymes involved in fatty acid metabolism also often exhibit high regioselectivity. The initial hydroxylation of straight chain saturated fatty acids are good examples. Three types of initial oxidation are seen *in vivo*: α-hydroxylation, β-hydroxylation, and ω-hydroxylation (positions shown in eq 6).²⁸ These three reactions are performed by several different enzymes in various locations.



β-Hydroxylation is the most common pathway for fatty acid metabolism and is catalyzed by a number of different enzymes, each of which is specific for a particular substrate chain length, and all of which operate on fatty acid CoA esters.²⁸ α-Hydroxylation of the free fatty acids in most animal tissues takes place when the β-position of the fatty acid is blocked.³⁴ α-Hydroxylation in the brain is responsible for the formation of cerebronic acid (1-hydroxy-C₂₄) from lignoceric acid (C₂₄).³⁵ In plants, α-hydroxylation of free fatty acids is a major pathway for the breakdown of fatty acids.³⁴

Biosynthesis of steroid hormones from cholesterol²⁵ by mammalian isozymes of cytochrome P450 also show a high degree of regioselectivity. The reactions include hydroxylation at carbons 20 and 22 of cholesterol, hydroxylation at C₁₁ of either 11-deoxycorticosterone or 11-deoxycortisol, hydroxylation of C₁₇ of progesterone and subsequent side-chain cleavage generating androstenedione, and C-C bond cleavage of 20,22-dihydroxycholesterol generating pregnenolone.

Another class of P450s capable of high regioselectivities are the fatty acid ω-hydroxylases,²⁵ which hydroxylate long chain fatty acids exclusively at the terminal methyl group. ω-Hydroxylation in animals, catalyzed by a cytochrome P450,^{36,37} is more common for long chain (>C₂₀) fatty acids, but is not the major pathway for their breakdown. In plants, ω-hydroxylation of free fatty acids is more important and seems also to be catalyzed by a cytochrome P450.³⁸ Work on the site specific mutagenesis of human fatty acid ω-hydroxylase has shown that its selectivity and activity are both very

sensitive to alteration of the binding site.³⁶ It is also proving possible to provide the necessary reduction equivalents for fatty acid ω -hydroxylases electrochemically, which will be critical for pharmaceutical or industrial applications of cytochrome P450 catalysis.³⁷

The effects of halo-substitution of benzene hydroxylation by P450 show the interplay of electronic and steric control in regioselectivity. Koerts et al.³⁹ concluded that for the fluorobenzenes studied the main factors directing the regioselectivity of their aromatic hydroxylation are the nucleophilic chemical reactivity of the site to be hydroxylated and the steric influence of the substituent ortho with respect to the site of hydroxylation. The steric effects are negligible for fluoro, chloro, and cyano substituents, but become significant for bromo and iodo substitution.

Our understanding and ability to model the active site of P450 and its interactions with substrates now permits at least rational attempts at *de novo* design. The ability to engineer cytochrome P450 for specific bioremediation needs is likely to see success in the near future.⁴⁰

B. Synthetic Metalloporphyrins

1. Mechanisms of Oxidation

There are two distinct aspects of mechanisms of hydrocarbon oxidation by P450 and its analogues. The first deals with O₂ activation, a reaction that nature handles easily, but which still provides major difficulties in synthetic analogue chemistry. The second concerns the actual substrate oxidation and the reactions of highly oxidized metal intermediates with various hydrocarbons.

Our understanding of the details of the enzymatic activation of O₂ by cytochrome P450_{cam} has been significantly advanced by Sligar and coworkers,⁴⁰⁻⁴² using a combination of site-specific mutagenesis and kinetic solvent isotope effects. They were able to provide convincing evidence for a charge relay model of protonation of the bound O₂. This protonation involves the distal tyrosine and aspartic acid residues that lie near the coordinated O₂, as shown in Figure 5.

[FIGURE 5 HERE]

Isotope labeling experiments by Sligar and coworkers⁴³ suggested a two-step mechanism for the hydroxylation of camphor by the high-valent iron-oxo species of cytochrome P450_{cam}. Deuterium isotope experiments demonstrated stereochemical scrambling during the hydrogen abstraction step but no scrambling in the hydroxylation step. If the mechanism had involved a concerted oxygen insertion, deuterium scrambling would have been seen for the hydroxylation.

In general, the active species in metalloporphyrin oxidations is thought to be a high-valent metal-oxo species, usually generated by reaction of a metal(III) porphyrin complex with an oxygen atom donor (e.g., iodosylbenzene, peroxyacids, etc.). Groves and coworkers^{10,20} has proposed that hydrocarbon hydroxylation with metalloporphyrin catalysts proceeds via a radical pathway in a "rebound" mechanism. In this mechanism (Figure 6), an oxygen atom is transferred from an oxidant to the metalloporphyrin to form a high-valent metal-oxo species. Hydroxylation has generally been assumed to occur from radical abstraction of a hydrogen from the substrate by an oxy-ferryl (Fe=O), analogous to the less reactive Compound I of the hydroperoxidases, forming a metal hydroxide complex and substrate radical. The metal hydroxide complex then rapidly transfers the hydroxyl group back to the substrate. In 1998, however, some rather strong kinetic evidence was presented by Collman and coworkers that there is an agostic intermediate.⁴⁴ Other, less plausible intermediates have also been suggested.⁴⁵

[FIGURE 6 HERE]

Significant controversy remains, however, over the mechanisms of epoxidation of olefins by metalloporphyrin catalysts.⁴⁶⁻⁴⁹ Several intermediates have been proposed for the oxygen transfer from a high-valent metal-oxo species to an alkene, as shown in Figure 7. The topmost pathway, involving a concerted addition of the oxygen atom from the metalloporphyrin to the double bond, appears to be most favored. As discussed later in this Chapter (Section III.C.), shape selectivity studies have demonstrated that there are in fact multiple pathways possible in these oxidations, which explains, in part, the lack of consensus in these complex mechanistic issues.

The nature of the transition state also remains open. Groves and Nemo⁵⁰ proposed that the preferred geometry of the interaction between an alkene and the metal-oxo intermediate should be side-on, based on orbital interactions. This side-on geometry for substrate approach, however, may not be exclusive. Epoxidation still occurs with sterically bulky metalloporphyrin catalysts on substrates that are unable to approach the metal-oxo moiety in a side-on fashion.^{51,52}

[FIGURE 7 HERE]

2. Metalloporphyrin Catalyzed Oxidations

In attempting to mimic the reactivity of heme proteins, many researchers have used metalloporphyrins to catalyze a variety of hydrocarbon oxidations with various oxygen donors.^{6,50-54} Metalloporphyrin catalyzed oxidations include hydroxylation, epoxidation, N-oxidation, and cleavage of 1,2-diols. The largest bulk of reports have been with Mn^{III}, Fe^{III}, Ru^{III}, or Cr^{III} porphyrins, in that order. Mn^{III} complexes are generally preferred in terms of rates and efficiency. Mn^{III}, Ru^{III}, or Fe^{III} complexes will

catalyze both epoxidation and hydroxylation reactions; Cr^{III} complexes are competent only for epoxidation.

An enormous range of oxidants have been used as oxygen atom transfer reagents to the metalloporphyrins.⁵³ These include iodosylbenzenes, peroxyacids, hypochlorite, chlorite, hydroperoxides, N-oxides, hydrogen peroxide, monoperoxyphthalate, and potassium monopersulfate (Oxone™). Iodosylbenzene was one of the very first oxidants and remains in use because it is often mechanistically cleaner than some alternatives. Some work has also been accomplished using various reductants (especially borohydrides) with O₂ to produce substrate oxidation. Other macrocycles have been investigated to a lesser extent^{55,56} (especially for asymmetric epoxidation, as discussed later), but porphyrins, especially those with electron withdrawing substituents, appear to have a strong advantage with respect to stability. Table 2 provides the abbreviations used in this Chapter.

In order to use any catalyst for oxidation of hydrocarbons, the catalyst be oxidatively robust compared to the substrate. Unfortunately, simple metalloporphyrins are readily decomposed under oxidizing conditions. This oxidative degradation occurs readily at the *meso* ring position (the methine carbons), and in fact this is the route used for the catabolism of heme *in vivo*.⁵⁷ Both electronic and steric factors can be manipulated to improve the oxidative robustness of metalloporphyrins. The use of electron-withdrawing substituents on the porphyrin periphery (Figure 8), especially halogenated and perhalogenated phenyl porphyrins,⁵⁸⁻⁶² has proved very successful in producing robust catalysts. Steric protection of the *meso*- position of the porphyrin has also been used effectively.^{17,50,63-67} In practice, however, these are not entirely separate approaches, since nearly all of the electron-withdrawing substituents will also contribute significant steric protection to the metalloporphyrin.

[FIGURE 8 HERE]

A semi-quantitative comparison of the rates of porphyrin degradation in these systems is enlightening. In dilute solutions of manganese tetraarylporphyrins ($\approx 10 \mu\text{M}$), the half-lives of the metalloporphyrins upon addition of a large excess of oxidant are independent of oxidant concentration, but strongly dependent on steric encumbrance at the *meso* position: Mn(TPP)(OAc) has a half-life of 5 minutes, Mn(TTMPP)(OAc) of 10 minutes, and Mn(TTPPP)(OAc) of 25 hours.⁶⁶ Thus, steric protection of the periphery of metalloporphyrins can substantially enhance the oxidative robustness of the catalyst.

III. Shape Selective Oxidation of Hydrocarbons

Two general approaches have been used to create regioselective catalysts. The first involves the synthesis of homogeneous catalysts that have a superstructure designed

to recognize and bind incoming substrates, or at least to limit orientation of their access to the metal site. The second utilizes a heterogeneous environment to restrict substrate orientation or access by using either a solid heterogeneous catalyst (e.g., a microporous solid with a simple metal complex imbedded within it) or a micro-heterogeneous liquid-liquid system (e.g., a complex imbedded in a lipid bilayer).

In general, both hydrocarbon hydroxylation and alkene epoxidation have been examined for most of these approaches. By far, hydroxylation is the more demanding of the two, both from the thermodynamic differences required to induce selectivity and in the oxidative stability of the catalyst required to prevent self-degradation. It is worth noting that the presence of a large excess of easily oxidized substrate (e.g., alkene) will provide kinetic protection against oxidative destruction of the catalyst.

A. Homogeneous Catalysts

1. Hydroxylation

Selective hydroxylation presents the most troublesome challenge to catalytic oxidation. The thermodynamics of selectively replacing a C-H bond with a C-OH unit are exceedingly difficult to control for three reasons. First, the bond strength of the C-H bond places high demands on the stability of the catalyst to avoid self-oxidation. Second, the susceptibility of oxidized products to further oxidation is severe, leading ultimately to complete combustion. Third, and most relevant here, most organic substrates have multiple C-H bonds so that selectivity becomes an especially important but difficult goal. Thus there is inherently an important role for shape selective hydroxylation of hydrocarbons.

In hydroxylations, regioselectivity is essentially under thermodynamic control in the absence of other steric restraints. Radical based oxidations show little or no regioselectivity beyond that based on bond strengths. For this reason, hydroxylation selectivities are generally dominated by C-H bond strengths (Table 1). The expected rates of oxidation are therefore allylic C-H > benzylic > 3° >> 2° >> 1°, and there is no significant preference for one 2° site over another 2° site, etc.

The catalytic selectivity for hydroxylation, however, can be modified by controlling access of the incoming substrate to the active oxidant. For example, with sterically bulky catalysts, access of an alkane to the metal would be restricted to the more exposed C-H bonds, giving rise to shape selectivity. Since the most exposed C-H bonds will be the least substituted ones (e.g., 1° > 2° > 3°), the possibility for reversal of selectivities by steric means is therefore established. A second approach is to build polar, hydrogen-bonding, or other specific weak-bonding interactions into the catalyst superstructure to direct substrate orientation.

The most difficult substrate for the demonstration of regioselectivity by any catalyst must be alkyl chains, which lack any functionality or polarity with which the catalyst may differentiate one site from another. Only relatively modest differences in shape make one methylene distinct from another. Even more challenging is the selection

of terminal methyl groups. Nonetheless, the selective oxidation of alkyl chains and alkanes remains an important scientific and commercial goal, because the terminal hydroxylation of alkyl chains is an important metabolic pathway in mammals as well as in bacteria, and because alkanes could become inexpensive chemical feedstocks.

Metalloporphyrins with sterically demanding superstructures have been used to induce substantial selectivity in some hydroxylation reactions. As one would expect, such selectivity is not seen with unhindered or modestly hindered metalloporphyrins,^{50,63-66,68-72} such as complexes of TPP or TTMPP. In these cases, only very modest shape selectivity proved possible. Slight regioselectivity for hydroxylation of one secondary carbon versus another was observed, but no significant terminal hydroxylation and production of primary alcohols occurred. These subtle differences in shape selectivity were demonstrated by noting the production of 2-ols relative to 3-ols from n-alkane hydroxylation, for a large number of substituted metalloporphyrin systems, as shown in Figure 9. In this graph, if there is no discrimination between one secondary site and another, the normalized [2-ol]/[3-ol] ratio would be 1.0, as observed for unhindered metalloporphyrins. As the level of steric restraint increases, however, this ratio can become considerably greater than 1.

[FIGURE 9 HERE]

The selectivity for the most accessible secondary site is greatest for the extremely hindered, bis-pocket porphyrin, TTPPP, even for substrates as small as pentane.⁶⁶ For this porphyrin, the calculated pocket dimensions from molecular modeling (Figure 10) are 4.0Å across by 5.0Å deep (measured from the van der Waals surfaces^{64,66}). This pocket size suggests that shape selectivities should increase as the alkane chain length increases, preventing side-on entrance to the metal-oxo species, which proves to be the case.

[FIGURE 10 HERE]

Regioselectivity among primary sites of different steric environments may be exhibited in the hydroxylation of branched alkanes. 2,2-Dimethylbutane [(CH₃)₃CCH₂CH₃] is an especially interesting case, since it has both a 2° site and two quite different 1° sites. This substrate is shaped like a fist with a sore thumb, and as such is well suited as a probe for shape selectivity. The secondary alcohol is the predominant product (>90%) for catalysis by either Mn(TPP)(OAc) or Mn(TTMPP)(OAc). With the deeply pocketed Mn(TTPPP)(OAc), however, the steric inaccessibility of the 2° site is quite pronounced and 3,3-dimethylbutan-2-ol becomes only a minor product (<25%). Even more striking is the selectivity shown in favor of the most exposed methyl group (to form 3,3-dimethylbutan-1-ol) and against the hindered *tert*-butyl group methyls (to

form 2,2-dimethylbutan-1-ol). The ratio of the primary alcohols, weighted for their total number of hydrogens, increases from 0.3 to 0.89 to 34 for Mn(TPP)(OAc), Mn(TTMPP)(OAc), and Mn(TTPPP)(OAc), respectively. Thus, 2,2-dimethylbutane may enter the pocket of Mn(TTPPP)(OAc) with only one orientation to minimize the steric interaction between the bulky *tert*-butyl group and the triphenylphenyl substituents on the porphyrin's periphery. This very specific, enzyme-like, shape selection of the substrate by the catalyst gives rise to the impressive preference for hydroxylation of the sterically most accessible methyl group.

The ability to produce oxidation catalysts selective for methyl group hydroxylation remains an economically important challenge. The most important goal in this research is clearly the hydroxylation of terminal methyl groups in n-alkanes. In order to make meaningful comparisons between various alkane substrates, a primary selectivity index is defined for Figure 11 as the ratio of the concentration of primary alcohol to secondary alcohols, normalized for the respective number of hydrogens.

[FIGURE 11 HERE]

As expected, unpocketed and shallow pocketed porphyrins give nearly exclusively 2° alcohols upon hydroxylation of n-alkanes. Using Mn(TTPPP)(OAc) and various oxygen donors, Suslick and coworkers were able to direct hydroxylation to the primary carbons of alkanes.^{65,66} When Mn(TPP)(OAc) is used as the hydroxylation catalyst, the products are primarily 2° alcohols (95-99%) which would be predicted using relative C-H bond strengths. Using Mn(TTPPP)(OAc) as the catalyst increases the yield of 1° alcohols, up to 26% with *n*-heptane as the substrate. Also seen was a decrease in the percentage of ω-2 and ω-3 oxidation, indicating that these positions are less able to access the manganese-oxo center. Relatively large increases in the primary selectivity index are observed from pentane to hexane to heptane, after which much smaller increases are observed with each added methylene unit. Thus, heptane marks the size cutoff for the "side-ways" entry of n-alkanes into the pocket of this porphyrin, and alkanes of larger size are restricted in their entry to an end-on approach. Even more difficult will be the selection for primary over tertiary hydroxylation, due to the large difference in bond dissociation energies; this remains largely unsuccessful at this time, even in the most hindered systems.

2. Epoxidation

This same sort of shape selectivity can be extended to alkene epoxidation, as well. In general, there are two classes of probes for such selectivity: *intramolecular* and *intermolecular*. Intramolecular probes require the oxidation of (non-conjugated) dienes in which the double bonds are sterically and electronically inequivalent. Alternatively, intermolecular competition between two differently shaped alkenes is a more general, but perhaps less unambiguous probe from a mechanistic perspective.

A number of researchers have examined the effect of small steric restraints and electronegative substitution on the regioselectivity of some alkene epoxidations⁷³⁻⁷⁷ and the related catalyzed cyclopropanation.⁷⁸ For norbornene oxidation, the *exo* to *endo* ratio is exquisitely sensitive to steric and electronic factors. Just the addition of an *ortho*-chloro substitution (as in TDCPP) will give a tenfold decrease in the production of *exo*-epoxynorbornane.⁷³ Another intramolecular test case is epoxidation of the *cis* versus *trans* double bonds of the symmetric 1,5,9-*trans,cis,trans*-dodecatriene. The comparison of TMP complexes to TPP shows a ten to fifteen fold increase in selectivity for the *cis* epoxide.^{50,76} The facile epoxidation of *cis*-stilbene compared to the very low reactivity of the sterically demanding *trans*-stilbene, even with unhindered porphyrins is another example of the importance of steric concerns with bulky substrates.

In order to compare more highly selective catalysts, one must relax the steric demands of the substrates. To this end, a series of non-conjugated dienes of varying shapes and sizes have been developed as intramolecular probes of shape selectivity^{63,64,67} in analogy to the shape selective hydroxylation of alkanes. The same series of unpocketed, shallow pocketed and deeply pocketed porphyrins were used as catalysts for the epoxidation of these dienes. In all cases, Mn(TTPPP)(OAc) exhibits enhanced selectivity for epoxidation of the most exposed double bond of the substrate (Figure 12). Even with sterically undemanding, straight-chain dienes, Mn(TTPPP)(OAc) shows a substantial preference for epoxidation at the terminal position. As expected, this selectivity for terminal epoxidation increases as the steric bulk of the diene increases, similar to the trend discussed for the hydroxylation of n-alkanes by these same catalysts. The shape selectivity originates from the steric demands of the metalloporphyrins' superstructures. Consistent with this, the ratio of enhancement for terminal epoxidation of linear, non-conjugated dienes is very similar to that observed for hydroxylation of n-hexane versus n-octane.

[FIGURE 12 HERE]

Limonene (**7** in Figure 12) and its structural analogue 4-vinyl-1-cyclohexene (**III**) are very useful chiral starting materials for many organic syntheses.⁷⁹ With standard oxidants available for epoxidation of these molecules (such as MCPBA), ring epoxidation occurs exclusively, rather than external epoxidation. Likewise, ring epoxidation dominates with the unhindered Mn(TPP)(OAc) and the modestly hindered Mn(TTMPP)(OAc). The extremely hindered Mn(TTPPP)(OAc), however, enhances the epoxidation of the external double bond, and for the more sterically demanding limonene, external epoxide is the major product formed.⁶⁷ Even higher selectivity is observed in the epoxidation of 1-methyl-1,4-cyclohexadiene (**5** in Figure 12), where epoxidation of the sterically less-hindered double bond with Mn(TTPPP)(OAc) accounts for 95% of the product.

In a versatile and elegant synthetic approach to the creation of shape-selective catalysts, Collman and coworkers^{15,16,80,81} have used a variety of manganese(III) picnic-

basket porphyrins (Figure 13) to regioselectively epoxidize olefins. With this class of complexes, a variety of pockets can be designed and optimized for specific substrates. For this class of catalysts, however, the open face of the porphyrin must be blocked with a large axial ligand, such as 3,5-di-*tert*-butylphenoxide. The greatest selectivities (Table 3) were seen using the C₆- and *p*-xylyl picnic-basket porphyrins (C₆PBP and PXLBPB respectively). The ratios of epoxidation were greater than a thousand to one for *cis*-2-octene versus cyclooctene for Mn(PXLBPB) as the catalyst. Selectivity for a disubstituted double bond over a trisubstituted double bond was also explored using *cis*-2-octene and 2-methyl-2-pentene. For either Mn(C₆PBP) or Mn(PXLBPB), the ratio of epoxidation for these two olefins was >1000:1. Selectivity for terminal olefin epoxidation versus internal olefin epoxidation was examined using 1-octene and cyclooctene. Modest selectivities were obtained using Mn(C₆-PBP) and Mn(PXLBPB). Collman and coworkers noted that some reaction occurs with cyclooctene, possibly indicating slow oxidation at the open face of the porphyrin complex.⁸⁰

[FIGURE 13 HERE]

Moore, Suslick, and coworkers synthesized a new class of sterically hindered dendrimer-metalloporphyrins for use as shape-selective catalysts.⁸²⁻⁸⁴ A series of oxidatively robust poly(phenylester) and poly(phenylamide) dendrimers was prepared through a convergent synthesis (Figure 14). Monodendrons were appended either to the *meta*-positions of 5,10,15,20-tetrakis(3',5'-hydroxyphenyl)porphyrinatomanganese(III) chloride or to the *ortho*-positions of 5,10,15,20-tetrakis(3',6'-hydroxyphenyl)porphyrinatomanganese(III) chloride to provide extreme steric protection of the metal center (Figure 15). These complexes range in size from 4000 to 12,000 amu, so they are comparable in size to small heme proteins.

[FIGURES 14 AND 15 HERE]

These complexes have been examined as regioselective oxidation catalysts for the epoxidation of dienes and of alkene mixtures of 1-alkene and cyclooctene. While access from the top is extremely restricted in all of the dendrimer-metalloporphyrins, the *meta*-phenyl substituted complexes show a significant side opening (10 Å and 7 Å, van der Waals surface to surface, for the first and second generation dendrons, respectively). The *meta*-substitution causes the dendrons to sweep away from the metal site before branching back over it. This limits the degree of regioselectivity that can be achieved with *meta*-substitution of a tetraphenylporphyrin. Consequently, the shape selectivity observed for these dendrimer-metalloporphyrins is good, but still surpassed by the bis-pocket porphyrin, TTPPP.

In contrast, *ortho*-substitution provides an extremely hindered active site and is an extraordinary shape-selective oxidation catalyst. An amide-linked, oxidatively-robust monodendron (3,5-bis(4'-*tert*-butylphenylamido)benzoic acid) was used to esterify all eight of the *ortho*-phenyl positions of 5,10,15,20-tetrakis(2',6'-hydroxyphenyl)-porphinatomanganese(III) chloride to create a highly hindered metal center. To probe the potential this dendrimer-metalloporphyrin as a shape selective oxidation catalyst, selectivities of were determined for both intermolecular and intramolecular epoxidations. Epoxidation of 1:1 intermolecular mixture of 1-alkenes and *cis*-cyclooctene and of non-conjugated dienes were carried out with iodobenzene as the oxygen donor. The Mn^{III} dendrimer-porphyrin complex showed excellent shape selectivity relative to the unsubstituted Mn(TPP)Cl, comparable to the best previous (non-dendrimer) catalysts (Figures 16 and 17). Molecular modeling studies on the dendrimer-porphyrin delineate the steric control around the porphyrin periphery and show that substrate access to the metal is limited to a ≈ 0.5 nm gap between the dendrimer substituents (Figure 18). Thus, there is substantial steric control of substrate access to the metal site and that the limited access available is side-on to the oxo-manganese intermediate.

[FIGURES 16, 17, AND 18 HERE]

One might have been concerned that the use of a sterically restrictive superstructure to alter the regioselectivity of the catalysts would also substantially diminish their activity. Fortunately, this proves not to be the case.⁸³ Turnover numbers for the *ortho*-dendrimer-metalloporphyrin, Mn(T(2',6'-G1AP)P)Cl are typically 1 to 2 sec⁻¹, which is only modestly slower than those for the unhindered Mn(TPP)Cl, which are typically 3 to 4 sec⁻¹. While these rates are not large compared to some catalytic systems, they are of the same order as the rates of oxidation seen with cytochrome P450. Yields in terms of oxidant used are also a matter of potential concern. In all cases studied, the yields based on oxidant consumed are very good and range between 70 and 80%.⁸³

While catalytic oxidation studies probe shape selectivity in a kinetic sense, one can also examine steric pocket effects on equilibria. To this end, molecular recognition of metal-binding ligands by these dendrimer-metalloporphyrins was probed using nitrogenous bases of varying shapes and sizes.⁸⁴ The *ortho*-dendrimer Zn porphyrin has a narrow binding site sterically constrained by the dendrimer substituents and shows remarkable selectivity differences between linear and non-linear amines, with changes greater than 10⁴ in equilibrium binding constants. In contrast, the *meta*-dendrimer Zn porphyrins, which have more open binding sites, do not show selectivity and instead actually increase several-fold binding of all bases relative to Zn(TPP). Thermodynamic parameters for ligation have also been determined: the steric control of binding of bulky ligands in these systems is primarily enthalpic. The K_{eq} values of the *ortho*-substituted system were exquisitely sensitive to the shape and size of the substrates. Linear amines (4-phenylpyridine or dodecylamine) were bound a bit more strongly by the dendrimer-

porphyrins than by Zn(TPP) itself, due to attractive interactions between the ligand and the aromatic dendrons and to solvation effects. In the case of non-linear amines, however, differences in K_{eq} of 10³ to 10⁵ were observed among the dendrimer-metalloporphyrins.

Other studies have emphasized the steric demands of the substrates, rather than those of the catalysts. Large, complex substrates often have substantial differences in steric accessibility from site to site within the substrate. For a wide range of natural products, sterically unencumbered ruthenium porphyrins have been shown to be regioselective as well as stereoselective epoxidation catalysts.⁸⁵⁻⁹⁰ Marchon and Ramasseul used *trans*-dioxo(tetramesitylporphyrinato)ruthenium(VI) (Ru(TMP)(O)₂) to catalyze epoxidation of steroids. Yields of the $\Delta^{5,6}$ -epoxide ranged from 76% to 94%.⁸⁵⁻⁸⁸ Formation of the β -epoxide predominated with reported selectivities of 92% to 99%. $\Delta^{5,6}$ selectivity was reported for steroids with more than one double bond, although stereoselectivity was lost with some substrates.^{88,89} An extensive examination of the selectivity of ruthenium porphyrins in the epoxidation of dienes, especially natural product dienes, was published by Hirobe and coworkers.⁹⁰ These workers have produced an efficient catalytic system using aromatic N-oxides as the oxidant; in some cases, turnover numbers above 10⁵ were observed. High selectivities for *cis* vs. *trans* double bonds were observed. In β -acetoxy substituted dienes, a strong preference was shown for the most electron rich, trisubstituted double bond, which means that steric control is not dominant even with the tetramesitylporphyrin ruthenium complex.

3. Comparisons to Enzymatic Selectivity

Direct comparisons of the regioselectivities of various monooxygenase enzymes and the biomimetic oxidation catalysts just discussed are difficult due to the variations of one isozyme to another, to limited biochemical data on a range of chemically useful substrates, and to the weak binding of many non-natural substrates in enzyme active sites. The best comparisons are made to the ω -hydroxylases, of which there are two classes: a non-heme iron monooxygenase found in bacteria,²⁴ and specific isozymes of cytochrome P450 found, in bacteria, yeast, plants, and mammalian mitochondria.^{21,25,26} With *in vivo* substrates (*e.g.*, fatty acids and cholesterol steroids), the regioselectivities can be quite striking.⁹¹ The ratio of $\omega/(\omega-1)$ hydroxylation of capric acid by kidney cytochrome P450, for example, can be as high as 20, which represents an extreme example of kinetic control of product formation.

Although several forms of P450 have been isolated (especially from bacterial sources) that give terminal hydroxylation of n-alkanes, data are seldom given for the amounts of secondary alcohols which may also be produced. Data are available⁹¹⁻⁹⁴ for the hydroxylation of hexane and heptane by rat liver microsomal cytochrome P450. As one might expect, the regioselectivities shown for these n-alkanes are not nearly as high as those shown for fatty acids. The primary selectivity, as defined earlier, of rat liver microsomal P450 (uninduced) is 0.16 for hexane and 0.26 for heptane, as compared to 0.32 and 0.59, respectively, for Mn(TTPPP)(OAc). Upon treatment with phenobarbital,

different and less selective isozymes of cytochrome P450 are induced, with primary selectivities of 0.03 for hexane and 0.10 for heptane.

Certain isozymes of the heme protein cytochrome P450 are capable of dramatic regioselective epoxidation, as well.⁹⁵ A comparison of the selectivities for epoxidation of limonene and of 4-vinyl-1-cyclohexene can be made between the synthetic metalloporphyrins and limonene-induced rat liver microsomal P450. As the steric demands of the active site of the oxidizing system increase from uncatalyzed *meta*-chloroperoxybenzoic acid to the very bulky Mn(TTPPP)(OAc), the selectivity for external epoxidation dramatically increases, and Mn(TTPPP)(OAc) is nearly as selective as the native enzyme.

Thus, for the most successful homogeneous catalysts, regioselectivities for simple substrates are comparable to those of native cytochromes P450. Although the details of the steric interactions undoubtedly differ between the enzyme and our synthetic analogues, the total steric interaction must be quite similar in magnitude for both Mn(TTPPP)(OAc) and various isozymes of cytochrome P450. A comparison of the relative size and shape of binding sites in the enzymes to the synthetic analogues should prove interesting as more structures become available.

B. Heterogeneous and Micro-Heterogeneous Catalysts

Less work has been done with heterogeneous catalysis for shape selective oxidation, in part because such systems are inherently more difficult to characterize than the homogeneous catalysts already discussed. Nonetheless, this approach retains much promise. There are two classes of catalysts in this area: micro-heterogeneous systems that utilize micelles or lipid bilayers to achieve a steric isolation of the catalytic center, and microporous solids with interior catalytic sites (usually zeolites). Each will be considered in turn.

A number of researchers have incorporated porphyrins into micellar or bilayer structures, and there have been two reports of the use of such systems to induce shape selective oxidation. The first is an intriguing, but often overlooked, note by Shilov and coworkers.⁹⁶ These researchers used a long-tailed iron porphyrin complex (tetrakis(4'-hexadecyloxyphenyl)porphyrin, H₂(T(4-HDP)P) incorporated into Triton X-100 micelles or phospholipid vesicles to hydroxylate hexane. The preference for ω -1 hydroxylation to give 2-hexanol is good in both cases, as shown in Figure 11. Terminal hydroxylation occurs, albeit to a limited extent. The primary selectivity index is 0.04 for the micellar system and 0.10 for the vesicles, as compared to 0.31 for the bis-pocket porphyrin, Mn(TTPPP)(OAc). Even more remarkable, however, is the effect of added β -cyclodextrin to Fe(T(4-HDP)P)Cl; in this system, the [2-ol]/[3-ol] ratio is reasonably good, but the terminal hydroxylation is amazing, with a primary selectivity index of 0.47. The origin of this effect has not been explained, and the effect of substrate or oxidant also requires further examination.

Metalloporphyrins have also been incorporated into lipid bilayer vesicles for both O₂ binding and oxidation.^{97,98} Groves and coworkers have succeeded in using the system represented in Figure 19 to regioselectively epoxidize sterols and fatty acids.^{20,99,100} Electron paramagnetic resonance (EPR) experiments demonstrated that the porphyrin was oriented perpendicular to the phospholipid bilayer chains. Given a sufficiently large sterol, the selectivity for the more extended double bond can be significant. In the case of simple diene fatty acids, however, the selectivities are relatively modest. Alkanes are apparently not effective substrates. Self-poisoning of the catalyst is also a problem with these systems, since the products appear to remain in the binding site and certainly in the bilayer.

[FIGURE 19]

One interesting approach uses the orientation of a porphyrin molecule in a thermotropic nematic liquid crystal to control substrate access to the metal. The alignment of a porphyrin with mesogenic substituents was determined by time resolved EPR spectroscopy of the triplet state of the free base porphyrin. The Mn^{III} complexes of TPP and of the mesogenic porphyrin then were used as catalysts for the epoxidation of alkenes using iodobenzene as oxidant. Reaction yields and regioselectivity for elongated substrates such as *cis*-stilbene and 4-vinylbiphenyl were somewhat dependent on the alignment of the alkene and its carbon-carbon double bond relative to the director and metalloporphyrin catalyst.

Various workers have explored the use of modified zeolites as shape selective heterogeneous oxidation catalysts.^{72,102-108} These systems have potential advantages in terms of oxidative robustness, but their selectivities are in many cases less than those of the better homogeneous systems. For example, Herron and Tolman used a modified small pore zeolite, Fe(II)/Pd(II) exchanged zeolite 5A (Si/Al \approx 1.2%), to hydroxylate alkanes in the presence of H₂/O₂ mixtures.¹⁰⁴ Good shape selectivity was observed for product *extracted* from within the zeolite: [2-ol]/[3-ol] ratios were comparable to moderately hindered porphyrins (Figure 11), and the primary selectivity index for terminal hydroxylation of octane was very high. There are four considerations, however, which significantly limit the utility of this system. First, in the absence of a surface poison (such as 2,2'-bipyridine), most oxidation occurs in a *nonspecific* fashion on the surface of the zeolite, with little terminal hydroxylation in the total product distribution. The reported product analyses only examined product caught in the interior of the zeolite. Second, product formed in the interior of the zeolite is permanently trapped there, and must be extracted by *dissolution of the zeolite* in concentrated sulfuric acid. Third, the catalyst is self-poisoning; since product is entrapped, substrate cannot continue to have access to the catalytic sites (turnovers are 0.3/Fe). Finally, more than 95% of the H₂ is utilized in the formation of H₂O rather than substrate oxidation. If a larger pore zeolite host is used (such as ZSM-5), the products can be removed without zeolite dissolution, but the selectivities are reduced. In spite of these concerns,

microporous inorganic solids have tremendous potential for future industrial application to selective oxidation catalysis.

Incorporating bioinorganic complexes into solid supports has received some attention as well. The "ship-in-the-bottle" approach synthesized the metallomacrocyclic complex within the confines of a large pore zeolite, isolating and entrapping the catalytic center. Iron phthalocyanines prepared *in situ* within a zeolite have been examined as an alkane hydroxylation system.^{102,103} The number of turnovers observed were quite low because the zeolite pores become clogged with product. No terminal hydroxylation was observed. For octane with the most selective zeolite (type Y with 0.13 wt.% Fe), the ω -1 selectivity was 1.33, which may be compared to moderately hindered porphyrins. A modification of this work by Belgian workers has incorporated similar Fe(Pc) complexes inside zeolite Y and imbedded the zeolite in a silicone polymer.¹⁰² In spite of publicity and rather audacious claims, the effects on selectivity through this approach are quite modest.

Balkus et al. used a perfluorinated Ru phthalocyanine as the seed for the growth of zeolite NaX around it.¹¹⁰ Metal complex loadings were roughly 1 complex per 125 zeolite supercages. This approach has the advantage of starting with pure metal complex and apparently does not lead to blockage of the zeolite pore structure, at least at the low loadings used in this study. Fluorination of the Ru(Pc) complex dramatically improved the lifetime of the catalyst and encapsulation in the zeolite prevented bimolecular reactions to form μ -oxo dimers, which are catalytically less active. Oxidation of cyclohexane to cyclohexanone occurred at slow turnover rates of roughly 0.03 s^{-1} with no deactivation after 20,000 turnovers (corresponding to 70% conversion of cyclohexane). A roughly tenfold selectivity was seen for cyclohexane over cyclododecane hydroxylation to the ketones, which reflects steric demands of diffusion of substrate (or product) through the zeolite pores. Intramolecular selectivities have not yet been determined but will be very interesting in probing the immediate environment of the catalytic site.

Other groups have attached oxidatively robust porphyrins to silica surfaces¹¹¹ or incorporated them into layered phosphonates,^{112,113} again with very modest alteration of selectivity. Mansuy and coworkers have generated "metalloporphyrinosilicas" by co-condensation of halosilanes with trifluorosilyl-substituted iron porphyrins.¹¹⁴ The specific areas of these materials are $\approx 60 \text{ m}^2/\text{g}$. These are efficient catalysts for alkene epoxidation by PhIO or *tert*-BuOOH and alkane hydroxylation by PhIO. Relatively modest shape selectivity for alkenes was observed in some cases.

Also interesting is the work of Mansuy and coworkers on manganese porphyrins intercalated into various layered minerals.¹¹⁵ The tetracationic 5,10,15,20-methylpyridylporphyrin manganese complexes intercalated into Montmorillonite clay produce an oxidatively robust catalyst that is quite efficient for alkane hydroxylation. Interestingly, there are significant intermolecular selectivities found, for example, in competitive oxidation of adamantane versus *n*-alkanes, but very little intramolecular regioselectivity within a single alkane. This result suggests that diffusion of substrate

into the porphyrin site is controlled by the layered mineral, but that the active site near the metalloporphyrin is relatively unconstrained.

Finally, a brief mention will be made of the so-called Gif reaction,⁴⁸ which has an expanding zoo of variations, but basically uses an iron salt, zinc, and O_2 in a pyridine/acetic acid suspension to form ketones from non-activated methylene groups in hydrocarbons. The system does not generally attack either primary or tertiary carbons. Although the selectivity is quite high, it does not appear that this is a case of shape selectivity, but must represent an unusual mechanistic requirement. The reaction pathways of this reaction are under continued investigation, and they remain controversial.¹¹⁶⁻¹¹⁹ Many unusual speculations have been made concerning the mechanism of the Gif reaction,⁴⁵ but it appears most likely that a free radical mechanism involving hydroperoxyl intermediates is responsible for its unusual selectivity.¹¹⁸

C. Shape Selectivity as a Mechanistic Probe

The presence and degree of shape selectivity can be used as a mechanistic probe of various porphyrin-catalyzed oxidations. The detailed mechanisms of hydroxylation and of epoxidation are different, and the discussion will be divided accordingly.

The shape selective hydroxylation of an alkane with various oxidants in the presence of a sterically hindered metal complex can demonstrate whether the hydroxylation reaction occurs at the metal center or in the bulk solution. For example, when iodosylbenzene, pentafluoriodosylbenzene or *meta*-chloroperbenzoic acid are used as oxidants with hindered manganese porphyrins, the primary alcohol selectivities are all very similar, indicating that these three oxidants generate the same catalytically active species at the metal.⁶⁶ A high spin d^2 , Mn(V)-oxo complex is the generally accepted intermediate.^{20,120} For iodosylbenzene oxidations, it had also been suggested that the active hydroxylating agent might be a metalloporphyrin-iodosylbenzene complex.¹²¹ This hypothesis, however, is inconsistent with the constancy of the primary selectivity index observed with iodosylbenzene, pentafluoriodosylbenzene, and *meta*-chloroperoxybenzoic acid. μ -Oxo dimer species can also be ruled out as the catalytic species, because these sterically hindered complexes cannot form dimers. Thus, the active oxidant in all likelihood is the terminal oxo complex.

In contrast, while *tert*-butylhydroperoxide acts as an efficient oxidant for alkane hydroxylation, alkane regioselectivity is *independent* of the steric demands of the manganese porphyrin catalyst. Therefore, with this oxidant, hydroxylation is *not* taking place at the metal center; rather, it must be due to a free radical chain pathway initiated by the metalloporphyrin. The regioselectivity for *n*-heptane hydroxylation by this radical chain shows little primary product, and the predominant secondary product is at the ω -1 methylene position similar to radical chlorination.⁶⁶

Shape selectivity is observed for both Mn and Fe porphyrins, indicating that substrate oxidation occurs in close proximity to the metal center. Primary selectivity, however, is diminished for iron relative to manganese porphyrin complexes. The

diminution in selectivity must be caused by differences in the steric constraints present during the transition state of H-atom abstraction; in the transition state more C-H bond breaking is occurring in the Fe system than in the Mn. This conclusion is confirmed by the relative isotope effects observed for Fe ($k_H/k_D = 11.5$ for cytochrome P450 and 12.9 for Fe(TPP)Cl with iodosylbenzene¹²²) as compared to Mn ($k_H/k_D = 3.5$).⁶⁶ The difference in the transition states reflects inherent electronic differences between the two different oxometalloporphyrin intermediates.

The cost in free energy of the steric contact generated between substrate and metalloporphyrin during hydroxylation can be calculated from the relative rates of 1° vs. 2° alcohol production. For TTPPP relative to TPP with either Mn or Fe, this calculated energy is 1.6-1.7 kcal/mole for *both* metal systems during the hydroxylation of *n*-alkanes longer than pentane.

For alkene epoxidation catalyzed by metalloporphyrins, several reaction intermediates have been proposed, as discussed earlier in this Chapter (Section II.B.). As shown in Figure 7, these include long-lived metalloxetane intermediates, metal-bound radical or carbocation intermediates from electron transfer mechanisms, or direct oxygen atom transfer. In addition, radical autoxidation (mostly at allylic positions) via radical chain pathways can be initiated by metalloporphyrins. The substantial selectivity observed with Mn(TTPPP)(OAc) is essentially independent of oxidant used and is insensitive to the addition of nitrogenous bases.^{64,67} These results are consistent with initial oxygen atom transfer from the oxidant to form a monomeric $Mn^V=O$ and demonstrate that epoxidation proceed through very similar transition states for all of these systems. Interestingly, selectivity is not significantly altered by addition of ligands (such as imidazoles). Although these ligands hasten the reaction of the metalloporphyrin with the oxidant in forming the active oxidizing species,⁷⁶ surprisingly, they do not significantly alter the geometry or energetics of the transition state.

The Fe(III) complexes of these porphyrins also show shape selectivity for epoxidation, albeit less so than Mn. The transition state for epoxidation by Fe must be less sterically demanding relative to Mn, just as in the case of hydroxylation. This may mean that there is a ring open radical or carbocation intermediate, as expected from an electron transfer mechanism, or simply that there is a less compact transition state in a concerted atom transfer. For epoxidations involving iron porphyrins and peroxyacids, there is a striking solvent dependence on the regioselectivity.¹²³ Furthermore, for *conjugated* dienes, the regioselectivity is nearly independent of the steric demands of the metalloporphyrin.⁶⁷ Thus, the observed regioselectivities argue that under different conditions several different mechanisms are probably operable, which may help resolve some of the apparent literature conflicts in this area.

Steric constraints have also been used to discriminate between active sites in metalloproteins. Shteinman, for example, has discussed the differences in mechanisms between cytochrome P450 and soluble methane monooxygenase in terms their putative oxidizing intermediates.¹²⁴ He argues that a bridged intermediate bis- μ -oxo-diiron(IV) species, in which both oxygen atoms are derived from the dioxygen molecule in methane monooxygenase would have a stronger steric selectivity for substrates compared to the

putative terminal oxenoid species in P450, in keeping with the unusual selectivity observed in alkane oxidation by methane monooxygenase.

D. Regioselectivity Based On Polarity

Oxidation of polar substrates directed by the polarity of substituents built into the catalyst structure has been relatively little explored for either heterogeneous or homogeneous systems. For example, the substrate specificity observed in the previously discussed (Section III.B.) phospholipid bilayer work of Groves and coworkers is likely to originate from both polarity and shape selectivity.⁹⁹ A few examples do exist for polarity selectivity in homogeneous systems.

Ogoshi and coworkers have used a cyclodextrin sandwiched porphyrin and singlet molecular oxygen to selectively oxidize linoleic acid to the 13-hydroperoxy derivative with a very high degree of regioselectivity.¹²⁵ Oxidation with the cyclodextrin porphyrin seems to take place in the pocket. The preference for $\Delta^{12,13}$ oxidation can be explained since that double bond is furthest from the carboxylic acid end. They have also used the iron derivative of the cyclodextrin porphyrin to epoxidize non-polar alkenes in aqueous solution using iodosylbenzene as the oxygen donor.¹²⁶ Yields of epoxide range from 14% for norbornene to 55% for cyclohexene; in contrast, the yield of cyclohexene epoxide using a simple water soluble iron porphyrin as the catalyst was <2%. This result can be attributed to the affinities of the hydrophobic substrates for the non-polar pocket of the cyclodextrin. The high yield of cyclohexene oxide versus norbornene oxide may reflect the size of the cyclodextrin pocket.

Several groups have used cationic, water-soluble porphyrins as selective oxidants for the cleavage of nucleic acids. The discussion will be brief here, since substantial reviews have been published elsewhere.¹²⁷ Tetrakis(N-methylpyridinium-4-yl)porphyrinatomanganese(III) (i.e., $Mn(TMPyP)^+$) has been used with $KHSO_5$ and KO_2 to cleave supercoiled double-stranded DNA.¹²⁸⁻¹³⁰ $H_2(TMPyP)$ had been previously shown to have a high affinity for DNA due to its positive charge.¹³¹ The manner of cleavage is thought to be similar to that of bleomycin-Fe(III), although Mn(TMPyP) is not able to intercalate into DNA.¹³² Mn(TMPyP) has been shown to bind in the minor groove of A-T rich regions of DNA.¹³³ To enhance DNA binding and cleavage, Meunier and coworkers have used several cationic metalloporphyrin-ellipticine complexes as cleavage agents.¹³³ The ellipticine moiety intercalates into the DNA near the A-T region where the metalloporphyrin binds, providing a two-pronged hold on the DNA. In a similar fashion, site specific cleavage reagents based on Mn porphyrins have been developed for both DNA¹³⁴ and RNA¹³⁵ scissions.

IV. Enantioselective Oxidations

Enantioselective oxidations are not precisely within the venue of this Chapter and is examined in greater detail elsewhere in the literature.^{7, 136-139} Nonetheless, enantioselective oxidations are intimately related to issues of shape selectivity, so a brief

discussion is appropriate here. The increasing importance of enantioselective reactions for the synthesis of pharmaceuticals continues to drive the exploration of chiral epoxidation catalysts.¹⁴⁰ Several systems, based on superstructured porphyrins or salen complexes, are proving highly successful for the asymmetric epoxidation of various substrates.^{15,136-139}

Groves and coworkers pioneered metalloporphyrin catalysts with chiral pockets and succeeded with the iron(III) complex of the sterically hindered vaulted binaphthyl porphyrin (Figure 20) [5 α ,10 β ,15 α ,20 β -tetrakis[(S)-2'-(carboxymethyl)-1,1'-binaphthyl-2-carboxyamidophenyl]porphyrin (TBNAPP) to enantioselectively hydroxylate alkanes, epoxidize alkenes, and oxidize sulfides.¹⁴¹⁻¹⁴³ Hydroxylation of a variety of alkyl substituted aromatics showed enantioselectivities from 40% ee to 72% ee with product yields ranging from 19-72%. Enantioselectivities seem to be higher with lower yields. Hydroxylations using Mn(TBNAPP)Cl showed much higher yields, up to 98%, but lower stereoselectivities, 12-26% ee, and lower alcohol to ketone ratios relative to Fe(TBNAPP)Cl.¹⁴³ From mechanistic studies of stereoselectivity in hydroxylation of pure enantiomers of 1-d-ethylbenzene, Groves and Viski concluded that the hydrogen abstraction step controls the stereochemistry of the major hydroxylation product.¹⁴² Groves and coworkers have also examined the origins of chiral induction by FT-NMR T₁ relaxation techniques.¹⁴⁴ A new chiral vaulted porphyrin with (S)-binaphthyl-L-alanine straps across both faces of a porphyrin was synthesized and characterized. (R)-styrene oxide was obtained in >90% ee in the initial stages of styrene epoxidation with this vaulted porphyrin with F₅PhIO as oxidant. The transition state for olefin epoxidation with high-valent metal-oxo species was modeled by coordinating epoxides to paramagnetic copper complexes of the corresponding ligands. The epoxide enantiomer that better fit the chiral cavity of the catalyst, as revealed by T₁ relaxation measurements, was also the major product of catalytic olefin epoxidation. These results are consistent with the "lock-and-key" mechanism of asymmetric catalysis by metalloporphyrins. However, a chiral Cu salen complex showed no differentiation in terms of T₁ relaxation rates between the enantiomers of cis-beta-methylstyrene oxide in spite of its high enantioselectivity for catalytic epoxidation.¹⁴⁴

[FIGURE 20 HERE]

Mansuy et al.¹⁴⁵ has used the chloroiron(III) complex of various picket-fence and basket-handle porphyrins (Figure 20) to selectively epoxidize *para*-chlorostyrene with yields of 35-50% and enantioselectivities of 12-50% ee. O'Malley and Kodadek¹⁴⁶ has used the manganese(III) chloride complex of a chiral wall porphyrin (Figure 21), 5 α ,10 β ,15 α ,20 β -tetrakis-[(R)-1,1'-binaphth-2-yl]porphyrin (TBNP) to enantioselectively epoxidize several styrene derivatives. Enantioselectivities for these epoxidations range from 15% ee, for *trans*- β -methylstyrene, to 40% ee, for *cis*- β -methylstyrene. No epoxide yields were reported.

[FIGURE 21 HERE]

Naruta and coworkers¹⁴⁷ have used chloroiron(III) complexes of two twin-coronet porphyrins (Figure 22) as stereoselective epoxidation catalysts. Two possible isomers exist for twin-coronet porphyrins, staggered and eclipsed, which will interact differently with the prochiral substrate. The enantioselectivities of epoxidation of substituted styrenes range from 11% ee, for 4-methylstyrene, to 89% ee, for 2-nitrostyrene. Their results indicate that the twin coronet porphyrin derived from bitetralin is a more selective catalyst than the porphyrin derived from binaphthalene due to the added steric bulk of the bitetralin.

[FIGURE 22 HERE]

Konishi et al.¹⁴⁸ have used chloromanganese(III) complexes of chiral strapped porphyrins to stereoselectively epoxidize alkenes. Unlike the previously discussed chiral porphyrins, which are derivatives of TPP, the strapped porphyrins are derivatives of dihexyldeuteroporphyrin. The stereoselectivities obtained with these porphyrins range from 58% ee for indene oxide down to 8% ee for 4-chlorostyrene oxide, using 2-phenylimidazole as the base, with fair to good yields of the epoxides and modest turnover numbers.

Halterman and Jan¹⁴⁹ have prepared a D₄ symmetric porphyrin based on a chiral 5,10,15,20-dimethanoanthracenylporphyrin (Figure 23). With arene-conjugated *cis*-alkenes, good yields of epoxides were obtained with moderate enantioselectivities (41 to 76% ee). *Trans*-alkenes did not epoxidize well.

[FIGURE 23 HERE]

Collman and coworkers further developed their picnic-basket porphyrin series with chiral threitol straps^{15,150,151} (Figure 24), complete with X-ray structure of one of the derivatives. This framework is easily modified by the condensation of aldehydes or ketones with the 2,3-diol of the threitol strap, which permits optimization of the chiral pocket for specific substrates. The epoxidation of 1,2-dihydronaphthalene, for example, can be epoxidized in an 88% ee with the Mn derivative of a 1,2-diphenoxyethane strapped porphyrin. As in several other chiral oxidation systems, turnovers are relatively low, and evidence was found for significant hydroxylation of the superstructure after roughly 100 turnovers. Significant differences in enantioselectivities were observed with different oxidants: for example, iodosylbenzene gave the best selectivities frequently with >80% ee, whereas LiOCl or *tert*-BuOOH giving very low selectivities (\approx 10% ee). This may either reflect oxidation of the porphyrin superstructure, possible the

participation of a metal-bound oxidant in the epoxidation, or in the case of low ee epoxidation, oxidation from species not bound to the metal.

[FIGURE 24 HERE]

Finally for metalloporphyrin catalysts, there is one report of an unusual example of a different class of enantioselective oxidations, carbon-carbon bond cleavage by dioxygen. Ohkubo and coworkers¹⁵² have used chiral manganese porphyrins to catalyze stereoselective cleavage of the carbon-carbon double bond of racemic N-acetyltryptophan by dioxygen. Yields of the dioxygenation product are relatively low compared to the percent consumption of substrate, and yields of the other products were not given.

The use of non-porphyrinic tetra-coordinating ligand complexes, usually of salen (N,N'-bis(salicylideneamino)ethane), has had substantial success due to the high synthetic yields of the catalysts, high product yields, and extremely high enantioselectivities. The facile synthesis of salen complexes with a chiral superstructure also provides an easy means to change systematically the catalyst for each class of substrates (Figure 25).

[FIGURE 25 HERE]

The most visible work in this field has been the discoveries by Jacobsen and coworkers of highly enantioselective epoxidation by chiral manganese(III) salen complexes.^{136,137,153-159} Katsuki and coworkers have also been active in developing this class of catalysts.^{138,160,161} Chiral salen complexes are relatively easily synthesized from substituted ethylenediamines and substituted salicylaldehydes, and there are now more than 100 complexes of this sort that have been tested to various degrees. The most effective of these are derived from chiral *trans*-1,2-diaminocyclohexane. Using inexpensive oxidants (notably sodium hypochlorite solutions), these catalysts are very effective for the chiral epoxidation of conjugated *cis*-disubstituted and trisubstituted alkenes, and at low temperature, even for terminal alkenes, such as styrene itself. Enantioselectivities are often above 90% ee for otherwise non-functionalized *cis*-alkenes. Yields of epoxide generally are above 80%. This work has been extended to the synthesis of chiral *trans*-epoxides from *cis*-alkenes by the simple addition of chiral quaternary amines, but the mechanism for this is unclear at present.¹⁵⁷

The salen complexes, unfortunately, are not particularly robust, and turnover numbers are typically below 40. Oxidation of the imine groups in the salen complex is the likely source of catalyst degradation. In spite of this, Merck is currently using one of the Jacobsen catalysts for the synthesis of antihypertensive chromanol derivatives.¹⁴⁰

Insight into the general mechanism of enantioselectivity has been provided by both the groups of Katsuki^{138,161} and of Jacobsen.^{137,159} The high enantioselectivities are clearly a consequence of restricting the available approaches of the substrate molecules to the putative metal-oxo intermediate. The most enantioselective catalysts provide only one unhindered (favored) approach for the substrate to reach the metal-oxo center with the other approaches hindered by *tert*-butyl or other sterically restricting groups. Apparently, one must consider π - π interactions as well, at least in the case of enyne substrates. The stereogenic centers of the salen complexes are much closer to the metal-oxo center than those of porphyrins, which provides for a greater level of interaction with the substrate than in most chiral porphyrin catalysts. Jacobsen and coworkers have found that enantioselectivity in the (salen)Mn-catalyzed asymmetric epoxidation reaction correlates directly with the electronic properties of the ligand substituents, with complexes bearing electron-donating substituents affording highest selectivity.¹⁵⁹ Their conclusion is that enantioselectivity is tied to the position of a transition state along the reaction coordinate, which may hold general implications for the design of asymmetric catalysts, particularly those that effect reactions without substrate binding.

V. Conclusions

A variety of approaches have been developed to create oxidation catalysts that can recognize organic substrates and selectively oxidize specific sites. Sterically hindered metalloporphyrins have proved successful as shape selective catalysts for hydrocarbon hydroxylation and especially olefin epoxidation. A few catalysts (both homogeneous and heterogeneous) show remarkable enhancements for primary hydroxylation of branched and *n*-alkanes. Such selectivity is unprecedented in non-biological catalysis and often comparable to enzymatic ω -hydroxylase activity. Nonetheless, the absolute level of selectivity for *n*-alkane hydroxylation remains modest. In addition, the turnover rates and catalyst stability for hydroxylation are often relatively low (in both synthetic and enzymatic systems). Clearly, industrial application of this work remains only a future possibility. The situation is distinctly better, however, for regioselective and enantioselective epoxidation.

The presence and degree of shape selectivity is offered as conclusive proof of direct metalloporphyrin involvement during the actual hydroxylation and epoxidation of substrates with some, but not all, oxidants under conditions of homogeneous catalysis. Similar selectivity for both hydroxylation and epoxidation has been observed for several different classes of oxidants, proving metal-based oxidation via a common monomeric intermediate (probably a terminal metal-oxo complex) for these systems.

VI. Acknowledgments

The contributions from my own group reported herein have been supported generously by the National Institutes of Health (HL25934) and the Department of

Defense (DAAG55-97-1-0126). I gratefully acknowledge S. Van Deusen-Jeffries for early assistance in the preparation of this manuscript.

VII. References

- (1) *Selectivity in Catalysis*; Davis, M. E.; Suib, S. L., Eds. American Chemical Society: Washington, D.C., 1993.
- (2) *Handbook of Heterogeneous Catalysis*; Ertl, G.; Knozinger, H.; Weitkamp, J., Eds. Wiley-VCH: Weinheim, 1997
- (3) *Metal Catalyzed Oxidation of Organic Compounds*; Sheldon, R. A.; Kochi, J. A. Academic Press: New York, 1986.
- (4) *Activation and Functionalization of Alkanes*; Hill, C. L., Ed. John Wiley and Sons: New York, 1989.
- (5) *Bioinorganic Chemistry*; Bertini, I.; Gray, G. B.; Lippard, S. J.; Valentine, J. S. University Science Books: Mill Valley, CA, 1994.
- (6) *Metalloporphyrins in Catalytic Oxidations*; Sheldon, R. A., Ed. Marcel Dekker: New York, 1994.
- (7) *Catalytic Asymmetric Synthesis*; Ojima, I., Ed. VCH: New York, 1993.
- (8) Groves, J. T. *Nature*. **1997**, 389, 329.
- (9) *Comprehensive Supramolecular Chemistry*; Atwood, J. L.; Davies, J. E. D.; MacNicol, D. D.; Vögtle, F.; Eds. Pergamon: New York, 1996.
- (10) Groves, J. T.; Kruper, W. J., Jr.; Haushalter, R. C. *J. Am. Chem. Soc.* **1980**, 102, 6375.
- (11) Hill, C. L.; Schardt, B. C. *J. Am. Chem. Soc.* **1980**, 102, 6374.
- (12) *Handbook of Chemistry and Physics*; Lide, D. R., Ed. CRC Press: Boca Raton, 1991; 71th ed., pp. 9-95.
- (13) March, J. *Advanced Organic Chemistry: Reactions, Mechanisms, and Structure*, 4th ed. Wiley-Interscience: New York, 1992, pp. 826-828.
- (14) Suslick, K. S.; Reinert, T. J. *J. Chem. Ed.* **1985**, 62, 974.
- (15) Collman, J. P.; Zhang, X.; Lee, V. J.; Uffelman, E. S.; Brauman, J. I. *Science*, **1993**, 261, 1404.
- (16) Collman, J. P.; Zhang, X. In *Comprehensive Supramolecular Chemistry*; Atwood, J. L.; Davies, J. E. D.; MacNicol, D. D.; Vögtle, F., Eds.; Pergamon: New York, 1996; vol. 5, pp. 1-32.
- (17) Suslick, K. S.; van Deusen-Jeffries, S. In *Comprehensive Supramolecular Chemistry*; Atwood, J. L.; Davies, J. E. D.; MacNicol, D. D.; Vögtle, F., Eds. ; Pergamon: New York, 1996; vol. 5, pp. 141-170.
- (18) *Cytochrome P450: Structure, Mechanism and Biochemistry*; Ortiz de Montellano, P. R., Ed.; Plenum: New York, 1st ed., 1986; 2nd ed., 1995.
- (19) Mansuy, D.; Battioni, P. In *Metalloporphyrins in Catalytic Oxidations*; Sheldon, R. A., Ed.; Marcel Dekker: New York, 1994; pp. 99-132.
- (20) Groves, J. T.; Han, Y. Z. In *Cytochrome P450*, 2nd ed., Ortiz De Montellano, P., Ed. Pergamon, New York: 1995; pp. 1-45.
- (21) Sligar, S. G.; Murray, R. I. In *Cytochrome P450: Structure, Mechanism and Biochemistry*; Ortiz de Montellano, P. R., Ed.; Plenum: New York, 1986; pp. 429ff and references therein.
- (22) Matson, R. S.; Stein, R. A.; Fulco, A. J. *Biochem. Biophys. Res. Commun.* **1980**, 97, 955.
- (23) Caron, C.; Mitscher, A.; Riviere, G.; Ricard, L.; Schappacher, M.; Weiss, R. *J. Am. Chem. Soc.* **1979**, 101, 7401.
- (24) McKenna, E. J.; Coon, M. J. *J. Biol. Chem.* **1970**, 245, 3882.
- (25) Jefcoate, C. F. In *Cytochrome P450: Structure, Mechanism, and Biochemistry*; Ortiz de Montellano, P. R.; Plenum Press: New York, 1986; p. 387.
- (26) Kappeli, O. *Microbiol. Rev.* **1986**, 50, 244.
- (27) Fitzpatrick, F. A.; Murphy, R. C. *Pharmacol. Rev.* **1989**, 40, 229.
- (28) *Fatty Acid Metabolism and Its Regulation*; Numa, S., Ed.; Elsevier: Amsterdam, 1984.
- (29) Poulos, T. L.; Finzel, B. C.; Howard, A. J. *Biochemistry* **1986**, 25, 5314.
- (30) Atkins, W. H.; Sligar, S. G. *J. Am. Chem. Soc.* **1989**, 111, 2715.
- (31) Fowler, S. M.; England, P. A.; Westlake, A. C. G.; Rouch, D. R.; Nickerson, D. P.; Blunt, C. *J.C.S. Chem. Commun.* **1994**, 2761.
- (32) Ruettinger, R. T.; Fulco, A. J. *J. Biol. Chem.* **1981**, 256, 5728.
- (33) Miura, Y.; Fulco, A. J. *Biochim. Biophys. Acta* **1975**, 388, 305.
- (34) Mize, C. E.; Steinberg, D.; Avigan, J.; Falls, H. M. *Biochem. Biophys. Res. Commun.* **1966**, 25, 359.
- (35) Akanuma, H.; Kisimoto, Y. *J. Biol. Chem.* **1979**, 254, 1050.
- (36) Dierks, E. A.; Zhang, Z. P.; Johnson, E. F.; Demontellano, P. R. O. *Journal of Biological Chemistry* **1998**, 273, 23055.
- (37) Faulkner, K. M.; Shet, M. S.; Fisher, C. W.; Estabrook, R. W. *Proc. Natl. Acad. Sci. U.S.A.* **1995**, 92, 7705.
- (38) Soliday, C. M.; Kolattukudy, P. E. *Arch. Biochem. Biophys.* **1978**, 188, 338.
- (39) Koerts, J.; Verlaeds, M. C.; Soffers, A. E. M. F.; Vervoort, J.; Rietjens, I. M. C. M. *Chem. Res. Toxicol.* **1997**, 10, 279-288.
- (40) Sligar, S. G.; Kellner, D. G.; Maves, S. A. *Curr. Opinion Biotech.* **1997**, 8, 274.
- (41) Aikens, J.; Sligar, S. G. *J. Am. Chem. Soc.* **1994**, 116, 1143.
- (42) Vidakovic, M.; Sligar, S. G.; Li, H. Y.; Poulos, T. L. *Biochemistry* **1998**, 37, 9211.
- (43) Gelb, M. H.; Heimbrook, D. C.; Malkonen, P.; Sligar, S. G. *Biochemistry* **1982**, 21, 370
- (44) Collman, J. P.; Chien, A. S.; Eberspacher, T. A.; Brauman J. I. *J. Am. Chem. Soc.* **1998**, 120, 425.
- (45) Barton, D. H. R. *J. Molec. Catal. A-Chem.* **1997**, 117, 3.
- (46) Traylor, T. G.; Kim, C.; Richards, J. L.; Xu, F.; Perrin, C. L. *J. Am. Chem. Soc.* **1995**, 117, 3468.
- (47) Ostovic, D.; He, G.-X.; Bruice, T. C. In *Metalloporphyrins in Catalytic Oxidations*; Sheldon, R. A., Ed.; Marcel Dekker: New York, 1994; pp. 29-68.
- (48) Mirafzal, G. A.; Kim, T.; Liu, J.; Bauld, N. L. *J. Am. Chem. Soc.* **1992**, 114, 10968.

- (49) Ostovic, D.; Bruce, T. C. *Acc. Chem. Res.*, **1992**, *25*, 314.
- (50) Groves, J. T.; Nemo, T. E. *J. Am. Chem. Soc.* **1983**, *105*, 5786.
- (51) Traylor, T. G.; Mikszal, A. R. *J. Am. Chem. Soc.* **1989**, *111*, 7443.
- (52) He, G.-X.; Mei, H.-Y.; Bruce, T. C. *J. Am. Chem. Soc.* **1991**, *113*, 5644.
- (53) Meunier, B. *Chem. Rev.* **1992**, *92*, 1411.
- (54) Bruce, T. C. *Acct. Chem. Res.* **1991**, *24*, 243.
- (55) Srinivason, K.; Michaud, P.; Kochi, J. K. *J. Am. Chem. Soc.* **1986**, *108*, 2309.
- (56) Busch, D. H. In *Transition metals in Supramolecular Chemistry*, (NATO ASI Ser. C 448); Fabbriizzi, L.; Poggi, A., Eds.; Kluwer Academic: Dordrecht, 1994, pp. 55-80.
- (57) Rawn, J. D. *Proteins, Energy, and Metabolism*; Neil Patterson: Burlington, 1989; p. 622.
- (58) Traylor, P. S.; Dolphin, D.; Traylor, T. G. *J. Chem. Soc., Chem. Commun.* **1984**, 279.
- (59) Nappa, M. J.; Tolman, C. A. *Inorg. Chem.* **1985**, *24*, 4711.
- (60) Traylor, T. G.; Byun, Y. S.; Traylor, P. S.; Battioni, P.; Mansuy, D. *J. Am. Chem. Soc.* **1991**, *113*, 7821.
- (61) Ellis, P. E., Jr.; Lyons, J. E. *Coord. Chem. Rev.* **1990**, *105*, 181.
- (62) Hoffman, P.; Labat, G.; Robert, A.; Meunier, B. *Tetrahedron Lett.* **1991**, *31*, 1991.
- (63) Suslick, K. S. In *Activation and Functionalization of Alkanes*; Hill, C. L., Ed.; John Wiley and Sons: New York, 1989; pp. 219-241.
- (64) Suslick, K. S.; Cook, B. R. In *Inclusion Phenomena and Molecular Recognition*; Atwood, J., Ed.; Plenum: New York, 1990; pp. 209-215.
- (65) Suslick, K.; Cook, B.; Fox, M. *J. Chem. Soc., Chem. Commun.* **1985**, 580.
- (66) Cook, B. R.; Reinert, T. J.; Suslick, K. S. *J. Am. Chem. Soc.* **1986**, *108*, 7281.
- (67) Suslick, K. S.; Cook, B. R. *J. Chem. Soc., Chem. Commun.* **1987**, 200.
- (68) Mansuy, D.; Bartoli, J.-F.; Momenteau, M. *Tetrahedron Lett.* **1982**, *23*, 2781.
- (69) Khenkin, A.; Shteinman, A. *J. Chem. Soc., Chem. Commun.* **1984**, 1219.
- (70) Khenkin, A.; Koifman, O.; Semeikin, A.; Shilov, A.; Shteinman, A. *Tetrahedron Lett.* **1985**, *26*, 4247.
- (71) Traylor, T. G.; Tsuchiya, S. *Inorg. Chem.* **1987**, *26*, 1338.
- (72) Tolman, C. A.; Druliner, J. D.; Nappa, M. J.; Herron, N. In *Activation and Functionalization of Alkanes*; Hill, C. L., Ed.; John Wiley and Sons: New York, 1989; pp. 303-360.
- (73) Traylor, T. G.; Nakano, T.; Dunlap, B. E.; Traylor, P. S.; Dolphin, D. *J. Am. Chem. Soc.* **1986**, *108*, 2782.
- (74) De Carvalho, M. E.; Meunier, B. *New J. Chem.* **1986**, *10*, 223.
- (75) Lindsay Smith, J. R.; Sleath, P. R. *J. Chem. Soc., Perkin Trans. 2* **1982**, 1009.
- (76) Collman, J. P.; Brauman, J. I.; Meunier, B.; Hayashi, T.; Kodadek, T.; Raybuck, S. A. *J. Am. Chem. Soc.* **1985**, *107*, 2000.
- (77) Ahn, K.-H.; Groves, J. T. *Bull. Korean Chem. Soc.* **1994**, *15*, 957.
- (78) Wolf, J. R.; Hamaker, C. G.; Djukic, J.-P.; Kodadek, T.; Woo, L. K. *J. Am. Chem. Soc.* **1995**, *117*, 9194.
- (79) Szabo, W. A.; Lee, H. T. *Aldrichimica Acta* **1980**, *13*, 13.
- (80) Collman, J. P.; Zhang, X.; Hembre, R. T.; Brauman, J. I. *J. Am. Chem. Soc.* **1990**, *112*, 5356.
- (81) Collman, J. P.; Zhang, Z.; Lee, V.; Hembre, R. T.; Brauman, J. I. In *Homogeneous Transition Metal Catalyzed Reactions*; American Chemical Society: Washington, D.C., 1992; pp. 153-62.
- (82) Bhyrappa, P.; Young, J. K.; Moore, J. S.; Suslick, K. S. *J. Molec. Catal. A* **1996**, *113*, 109.
- (83) Bhyrappa, P.; Young, J. K.; Moore, J. S.; Suslick, K. S. *J. Am. Chem. Soc.* **1996**, *118*, 5708; and unpublished work.
- (84) Bhyrappa, P.; Vijayanthimala, G.; Suslick, K. S. *J. Am. Chem. Soc.*, **1999**, *121*, 262.
- (85) Marchon, J. C.; Ramasseul, R. *J. Chem. Soc., Chem. Commun.* **1988**, 298.
- (86) Marchon, J. C.; Ramasseul, R. *J. Mol. Catal.* **1989**, *51*, 29.
- (87) Marchon, J. C.; Ramasseul, R. *Synthesis* **1989**, 389.
- (88) Tavares, M.; Ramasseul, R.; Marchon, J. C. *Catal. Lett.* **1990**, *4*, 163.
- (89) Tavares, M.; Ramasseul, R.; Marchon, J. C.; Valleegoyet, D.; Gramain, J. C. *J. Chem. Res.-S.* **1994**, 74.
- (90) Ohtake, H.; Higuchi, T.; Hirobe, M. *Heterocycles* **1995**, *40*, 867.
- (91) Ellin, A.; Orrenius, S. *Molec. Cell Biochem.* **1975**, *8*, 69.
- (92) Frommer, U.; Ullrich, V.; Standinder, H.; Orrenius, S. *Biochim. Biophys. Acta* **1972**, *280*, 487.
- (93) Morohashi, K.; Sadano, H.; Okada, Y.; Omura, T. *J. Biochem.* **1983**, *93*, 413.
- (94) Karasevich, E. I. and Khenkin, A. M. *Biokhimiya (Moscow)* **1986**, *51*, 1454.
- (95) *Assessment of the Use of Single Cytochrome P450 Enzymes in Drug Research*; Waterman, M. R., and Hildebrand, M., Eds. Springer-Verlag: New York, 1994.
- (96) Sorokin, A. B.; Khenkin, A. M.; Marakushev, S. A.; Shilov, A. E.; Shteinman, A. A. *Dokl. Akad. Nauk. SSSR.* **1984**, *279*, 939.
- (97) Tsuchida, E.; Kaneko, M.; Nishide, H.; Hoshino, M. *J. Phys. Chem.*, **1986**, *90*, 2283.
- (98) Gosling, P. A.; Klein Gebbink, R. J. M.; Schenning, A. P. H. J.; Feiters, M. C.; Nolte, R. J. M. In *Transition metals in Supramolecular Chemistry*, (NATO ASI Ser. C 448); Fabbriizzi, L.; Poggi, A., Eds.; Kluwer Academic: Dordrecht, 1994, pp. 291-308.
- (99) Groves, J. T.; Neumann, R. *J. Am. Chem. Soc.* **1989**, *111*, 2900.
- (100) Ungashe, S. B.; Groves, J. T. *Adv. Inorg. Biochem.* **1993**, *9*, 318.
- (101) Neumann, R. *Molec. Cryst. Liq. Cryst. Sci. Tech. A* **1994**, *240*, 33-37.
- (102) Herron, N.; Stucky, G. D.; Tolman, C. A. *J. Chem. Soc., Chem. Commun.* **1986**, 1521.
- (103) Herron, N. *J. Coord. Chem.* **1988**, *19*, 25.
- (104) Tolman, C. A.; Herron, N. *J. Am. Chem. Soc.* **1987**, *109*, 2837.
- (105) Chang, C. D.; Hellring, S. D. "Shape Selective Catalytic Oxidation of Phenol," U.S. Patent 4578521, 25 March 1986.
- (106) Dessau, R. M. *J. Catal.* **1982**, *77*, 304.
- (107) Tatsumi, T.; Nakamura, M.; Negishi, S.; Tominaga, H. *J. Chem. Soc., Chem. Commun.* **1990**, 476.

- (108) Tatsumi, T.; Nakamura, M.; Yuasa, K.; Tominaga, H. *Catal. Lett.* **1991**, *10*, 259.
- (109) Parton, R. F.; Vankelecom, I. F. J.; Casselman, M. J. A.; Bezoukhanova, C. P.; Uytterhoeven, J. B.; Jacobs, P. A. *Nature* **1994**, *370*, 541.
- (110) Balkus, Jr., K. J.; Eissa, M.; Levado, R. *J. Am. Chem. Soc.* **1995**, *117*, 10753.
- (111) Gilmartin, C.; Lindsay Smith, J. R. *J. Chem. Soc., Perkin Trans. 2* **1995**, 243.
- (112) Deniaud, D.; Schollorn, B.; Mansuy, D.; Rouxel, J.; Battioni, P.; Bujoli, B. *Chem. Mater.* **1995**, *7*, 995.
- (113) Deniaud, D.; Spyroulias, G. A.; Bartoli, J. F.; Battioni, P.; Mansuy, D.; Pinel, C.; Odobel, F.; Bujoli, B. *New J. Chem.* **1998**, *22*, 901.
- (114) Battioni, P.; Cardin, E.; Louloudi, M.; Schollhorn, B.; Spyroulias, G. A.; Mansuy, D.; Traylor, T. G.; *J. Chem. Soc., Chem. Commun.* **1996**, 2037.
- (115) Barloy, L.; Lallier, J. P.; Battioni, P.; Mansuy, D.; Piffard, Y.; Tournoux, M.; Valim, J. B.; Jones, W. *New J. Chem.* **1992**, *16*, 71.
- (116) Bardin, C.; Barton-D. H. R.; Hu, B.; Rojaswahl, R.; Taylor D. K. *Tetrahedron Lett.* **1994**, *35*, 5805.
- (117) Minisci, F. Fontana, F. *Tetrahedron Lett.* **1994**, *35*, 1427.
- (118) Barton, D. H. R.; Hill, D. R. *Tetrahedron Lett.* **1994**, *35*, 1431.
- (119) Minisci, F.; Fontana, F.; Araneo, S.; Recupero, F.; Banfi, S.; Quici, S. *J. Am. Chem. Soc.* **1995**, *117*, 226.
- (120) Groves, J. T.; Stern, M. K. *J. Am. Chem. Soc.*, **1987**, *109*, 3812.
- (121) Birchall, T.; Smegal, J. A.; Hill, C. L. *Inorg. Chem.* **1984**, *23*, 1910.
- (122) Groves, J. T.; Nemo, T. E. *J. Am. Chem. Soc.* **1983**, *105*, 6243.
- (123) Watanabe, Y.; Yamaguchi, K.; Morishima, I.; Takehira, K.; Shimizu, M.; Hayakawa, T.; Orita, H. *Inorg. Chem.* **1991**, *30*, 2581.
- (124) Shteinman, A. A. *J. Biol. Inorg. Chem.* **1998**, *3*, 325-330.
- (125) Kuroda, Y.; Sera, T.; Ogoshi, H. *J. Am. Chem. Soc.* **1991**, *113*, 2793.
- (126) Kuroda, Y.; Hiroshige, T.; Ogoshi, H. *J. Chem. Soc., Chem. Commun.* **1990**, 1594.
- (127) Murakami, Y., Vol. Ed. *Comprehensive Supramolecular Chemistry; Vol. 4, Bioorganic Systems*; Atwood, J.L.; Davies, J.E.D.; MacNicol, D.D.; Vögtle, F., Eds. Pergamon: New York, 1996.
- (128) Pratviel, G.; Bernadou, J.; Ricci, M.; Meunier, B. *Biochem. Biophys. Res. Commun.* **1989**, *160*, 1212.
- (129) Fouquet, E.; Pratviel, G.; Bernardou, J.; Meunier, B. *J. Chem. Soc., Chem. Commun.* **1987**, 1169.
- (130) Raner, G.; Goodisman, J.; Drabrowiak, J. C. In *Metal-DNA Chemistry*; American Chemical Society: Washington, D. C., 1989; p. 74ff.
- (131) Praseuth, D.; Gaudemer, A.; Verlac, J.-B.; Kralic, I.; Sissoeff, I.; Guille, E. *Photochem. Photobiol.* **1986**, *44*, 717.
- (132) Ward, B.; Skorobogaty, A.; Dabrowiak, J. C. *Biochemistry* **1986**, *25*, 7827.
- (133) Ding, L.; Etemad-Moghadam, G.; Cros, S.; Auclair, C.; Meunier, B. *J. Med. Chem.* **1991**, *34*, 900.
- (134) Groves, J.T.; Marla, S.S. *J. Am. Chem. Soc.* **1995**, *117*, 9578.
- (135) Duarte, V.; Sixou, S.; Meunier, B. *J.C.S. Dalton Trans.* **1997**, 4113.
- (136) Jacobsen, E. J. In *Catalytic Asymmetric Synthesis*; Ojima, I., Ed.; VCH: New York, 1993, pp. 159-202.
- (137) Jacobsen, E.N. In *Comprehensive Organometallic Chemistry II*; Wilkinson, G.; Stone, F.G.A.; Abel, E.W.; Hegedus, L.S., Eds.; Pergamon: N.Y., 1995; vol. 12, ch. 11.1.
- (138) Katsuki, T. *Coord. Chem. Rev.* **1995**, *140*, 189.
- (139) Naruta, Y. In *Metalloporphyrins in Catalytic Oxidations*; Sheldon, R. A., Ed.; Marcel Dekker: New York, 1994; pp. 241-260.
- (140) Nugent, W.A.; RajanBabu, T.V.; Burk, M.J. *Science* **1993**, *259*, 479.
- (141) Groves, J. T.; Myers, R. S. *J. Am. Chem. Soc.* **1983**, *105*, 5791.
- (142) Groves, J. T.; Viski, P. *J. Am. Chem. Soc.* **1989**, *111*, 8537.
- (143) Groves, J. T.; Viski, P. *J. Org. Chem.* **1990**, *55*, 3628.
- (144) Groves, J.T.; Crowley, S.J.; Shalyaev, K.V. *Chirality* **1998**, *10*, 106.
- (145) Mansuy, D.; Battioni, P.; Renaud, J.-P.; Guerin, P. *J. Chem. Soc., Chem. Commun.* **1985**, 155.
- (146) O'Malley, S.; Kodadek, T. *J. Am. Chem. Soc.* **1989**, *111*, 9116.
- (147) Naruta, Y.; Tani, F.; Ishihara, N.; Maruyama, K. *J. Am. Chem. Soc.* **1991**, *113*, 6865.
- (148) Konishi, K.; Oda, K.; Nishida, K.; Aida, T.; Inoue, S. *J. Am. Chem. Soc.* **1992**, *114*, 1313.
- (149) Halterman, R. L.; Jan, S.-T. *J. Org. Chem.* **1991**, *56*, 5253.
- (150) Collman, J. P.; Lee, V. J.; Zhang, X.; Ibers, J. A.; Brauman, J. I. *J. Am. Chem. Soc.* **1993**, *115*, 3834.
- (151) Collman, J. P.; Lee, V. J.; Kellen-Yuen, C. J.; Zhang, X.; Ibers, J. A.; Brauman, J. I. *J. Am. Chem. Soc.* **1995**, *117*, 692.
- (152) Ohkubo, K.; Sagawa, T.; Kuwata, M.; Hata, T. Ishida, H. *J. Chem. Soc., Chem. Commun.* **1989**, 352.
- (153) Zhang, W.; Loebach, J. L.; Wilson, S. R.; Jacobsen, E. N. *J. Am. Chem. Soc.* **1990**, *112*, 2801.
- (154) Zhang, W.; Jacobsen, E. N. *J. Org. Chem.* **1991**, *56*, 2296.
- (155) Jacobsen, E. N.; Zhang, W.; Muci, A. R.; Ecker, J. R.; Deng, L. *J. Am. Chem. Soc.* **1991**, *113*, 7063.
- (156) Palucki, M.; Pospisil, P. J.; Zhang, W.; Jacobsen, E. N. *J. Am. Chem. Soc.* **1994**, *116*, 9333.
- (157) Chang, S.; Galvin, J. M.; Jacobsen, E. N. *J. Am. Chem. Soc.* **1994**, *116*, 6937.
- (158) Allain, E. J.; Hager, L. P.; Deng, L.; Jacobsen, E. N. *J. Am. Chem. Soc.* **1993**, *115*, 4415.
- (159) Palucki, M.; Finney, N.S.; Pospisil, P.J.; Guler, M.L.; Ishida, T.; Jacobsen E.N. *J. Am. Chem. Soc.* **1998**, *120*, 948.
- (160) Irie, R.; Noda, K.; Ito, Y.; Katsuki, T. *Tetrah. Lett.* **1991**, *32*, 1055.
- (161) Hamada, T.; Irie, R.; Katsuki, T. *Synlett* **1994**, 479.

Table 1. Selected Bond Dissociation Energies.¹²

H-C Bond	Bond Type	Bond Dissociation Energy kJ mol ⁻¹
H-C ₆ H ₅	phenyl	464
H-CH ₃	methane	438
H-C ₂ H ₅	primary	420
H-n-C ₃ H ₇	primary	417
H-CH ₂ C(CH ₃) ₃	primary	418
H-CH(CH ₃) ₂	secondary	401
H-C ₆ H ₁₁	secondary	400
H-C(CH ₃) ₃	tertiary	390
H-CH ₂ C ₆ H ₅	benzyl primary	368
H-CH(CH ₃)C ₆ H ₅	benzyl secondary	357
H-C(CH ₃) ₂ C ₆ H ₅	benzyl tertiary	353
H-CH ₂ CH=CH ₂	allyl primary	361
H-CH(CH ₃)CH=CH ₂	allyl secondary	345

Table 2. List of Abbreviations

C _n PBP	n-carbon picnic-basket porphyrin
MCPBA	<i>meta</i> -chloroperoxybenzoic acid
Pc	phthalocyanine
PXLPBP	<i>p</i> -xylyl strapped picnic-basket porphyrin
salen	N,N'-bis(salicylideneamino)ethane
T(2',6'-DHP)P	5,10,15,20-tetrakis(2',6'-dihydroxy phenyl)porphyrinate
T(2-MeP)P	5,10,15,20-tetrakis(2'-methylpyridyl)porphyrinate
T(3',5'-DHP)P	5,10,15,20-tetrakis(3',5'-dihydroxy phenyl)porphyrinate
T(4-HDP)P	5,10,15,20-tetrakis(4'-hexadecyloxyphenyl)porphyrinate
TBNAPP	5 α ,10 β ,15 α ,20 β -tetrakis[(S)-2''-(carboxymethyl)-1',1''-binaphthyl-2'-carboxyamidophenyl]porphyrinate
TBNP	5 α ,10 β ,15 α ,20 β -tetrabinaphthylporphyrinate
TDCPP	5,10,15,20-tetrakis(2',6'-dichlorophenyl)porphyrinate
TMP	5,10,15,20-tetramesitylporphyrinate, 5,10,15,20-tetrakis(2',4',6'-trimethylphenyl)porphyrinate
TMPyP	5,10,15,20-tetrakis(N-methylpyridinium-4'-yl)porphyrinate
TPP	5,10,15,20-tetraphenylporphyrinate
TPPyP	5,10,15,20-tetra-4'-pyridylporphyrinate
TTMPP	5,10,15,20-tetrakis(2',4',6'-trimethoxyphenyl)porphyrinate
TTPPP	5,10,15,20-tetrakis(2',4',6'-triphenylphenyl)porphyrinate

Table 3. Intermolecular Shape Selectivity with the Picnic-basket Porphyrins⁸⁰

catalyst	epoxide ratio			
				
Mn(TPP)(OAr)	1.2	1.1	0.03	0.9
Mn(TMP)(OAr)	14.4	0.7	0.04	2.5
Mn(C ₂ PBP)(OAr)	0.4	1.1	0.05	1.3
Mn(C ₄ PBP)(OAr)	1.0	2.1	0.4	1.8
Mn(C ₆ PBP)(OAr)	70	67	1.7	>1000
Mn(PXYLPBP)(OAr)	29	>1000	7.0	>1000
Mn(C ₈ PBP)(OAr)	12.7	1.6	0.06	21.1
Mn(C ₁₀ PBP)(OAr)	8.8	0.2	0.04	17.9

IX. Figure Captions

- Figure 1. Catalytic cycles of the hydroperoxidases.
- Figure 2. Main types of oxidations catalyzed by cytochrome P450.¹⁹
- Figure 3. Cytochrome P450 reaction cycle.
- Figure 4. Active site of cytochrome P450_{cam}.⁵
- Figure 5. Charge relay models for the activation of O₂ and formation of a oxo complex in cytochrome P450_{cam}.⁴¹
- Figure 6. Rebound mechanism of metalloporphyrin catalyzed hydroxylations.
- Figure 7. Proposed mechanisms for epoxidation with metalloporphyrins.
- Figure 8. Peripherally substituted metalloporphyrins. M(TPP): R²=R³=R⁴=R⁵=R⁶=H; M(TDCPP): R³=R⁴=R⁵=H, R²=R⁶=Cl; M(T(3',5'-DHP)P): R²=R⁴=R⁶=H, R³=R⁵=OH; M(T(2',6'-DHP)P): R³=R⁴=R⁵=H, R⁴=R⁶=OH; M(TMP): R³=R⁵=H, R²=R⁴=R⁶=CH₃; M(TTMPP): R³=R⁵=H; R²=R⁴=R⁶=OCH₃; M(TTPPP): R³=R⁵=H; R²=R⁴=R⁶=C₆H₅.
- Figure 9. Secondary vs. secondary C-H hydroxylation in pentane: ω-1 selectivity as a function of steric hindrance of the catalyst.⁶³
- Figure 10. Molecular models of sterically hindered porphyrins; for scale, heptane is also shown. The porphyrins represented are the unhindered TPP, the moderately hindered TTMPP and the deeply pocketed TTPPP. For clarity, atomic radii shown are only 0.8 of the van der Waals radii.⁶³
- Figure 11. Shape selectivity for hydroxylation of the terminal methyl of *n*-alkanes vs. chain length, normalized for relative numbers of hydrogens.⁶³
- Figure 12. Intramolecular shape selectivity for nonconjugated diene epoxidation. The less hindered double bond is highlighted in the drawing.⁶³
- Figure 13. Picnic-basket porphyrins and their intermolecular shape selectivity.¹⁵
- Figure 14. Chemical structures of monodendrons, porphyrin precursors, and sterically hindered dendrimer-porphyrins.
- Figure 15. Molecular models of dendrimer-porphyrins. A: *meta*-substituted H₂T(3',5'-G1P)P. B: *ortho*-substituted H₂T(2',6'-G1AP)P. C: *meta*-substituted second generation dendrimer-porphyrin H₂T(3',5'-G2P)P.
- Figure 16. Intramolecular selectivities (ratio of epoxidation of the least hindered to most hindered double bond) for catalytic epoxidation of various non-conjugated dienes by manganese(III) dendrimer-porphyrins, normalized to [Mn(TPP)]⁺. The most sterically accessible double bond of each diene is indicated by heavy lines. Estimated errors are ≈6% relative.
- Figure 17. Intermolecular selectivities for catalytic epoxidation of 1-alkenes relative to *cis*-cyclooctene, normalized to [Mn(TPP)]⁺. Estimated errors are ≈5% relative.
- Figure 18. Molecular models showing an enlarged side view of the binding sites of dendrimer porphyrins. A: *meta*-substituted H₂T(3',5'-G1P)P. B: *ortho*-substituted dendrimer-porphyrin H₂T(2',6'-G1AP)P. Note the open cavity of ≈10 Å versus a narrow slit of ≈5, respectively; in both cases, top access to the porphyrin is completely blocked.
- Figure 19. Idealized molecular assembly of a tetra-sterol substituted porphyrin and desmosterol as substrate in a phospholipid bilayer.⁹⁹
- Figure 20. Enantioselective superstructured metalloporphyrins: Groves' vaulted binaphthyl porphyrin¹⁴¹ (upper R group) and Mansuy's¹⁴⁵ basket-handle porphyrin (lower R group).
- Figure 21. An enantioselective superstructured metalloporphyrin: Kodadek's¹⁴⁶ chiral wall porphyrin.
- Figure 22. Enantioselective superstructured metalloporphyrins: Naruta's¹⁴⁷ twin-coronet porphyrins.
- Figure 23. Enantioselective superstructured metalloporphyrins: Collman's picnic-basket porphyrin with chiral threitol straps.¹⁵
- Figure 24. An enantioselective superstructured metalloporphyrin: a D₄ symmetric porphyrin based on a chiral 5,10,15,20-dimethanoanthracenyl porphyrin.¹⁴⁹
- Figure 25. Some enantioselective manganese(III) salen (N,N'-bis(salicylideneamino)-ethane) complexes;¹³⁶ X = H, CH₃, *tert*-Bu; Y = *tert*-Bu, C*H(Et)(C₆H₅).

Fig 1

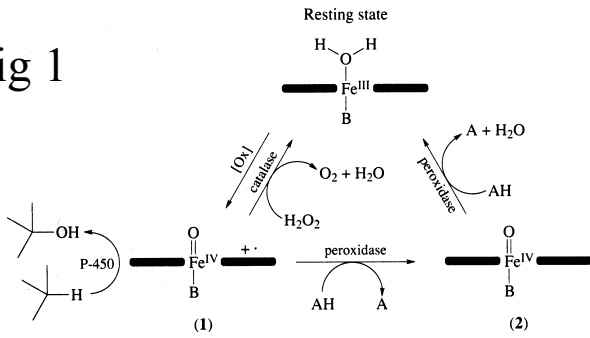


Fig 4

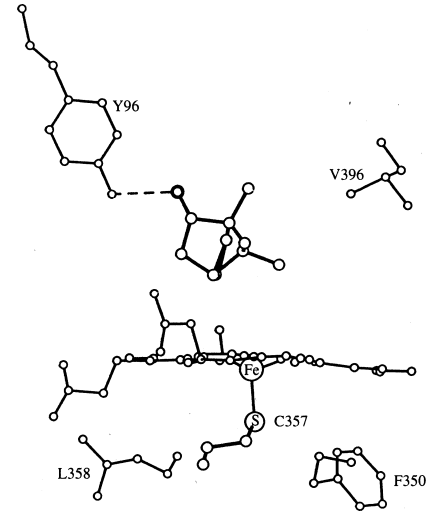


Fig 2

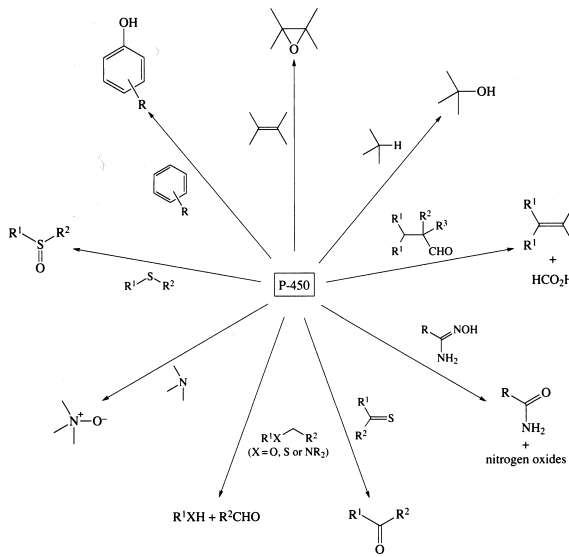


Fig 5

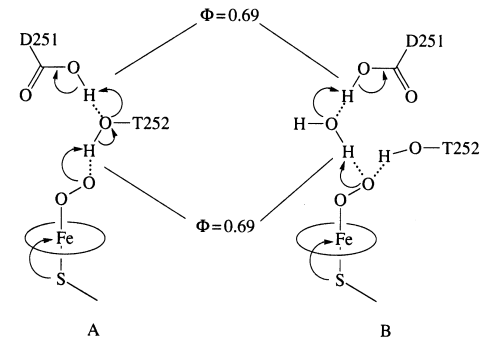


Fig 3

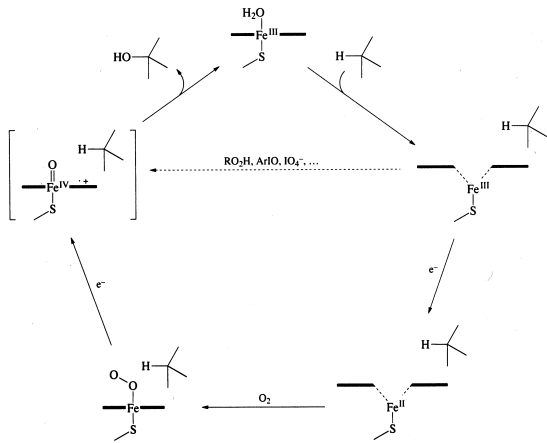


Fig 6

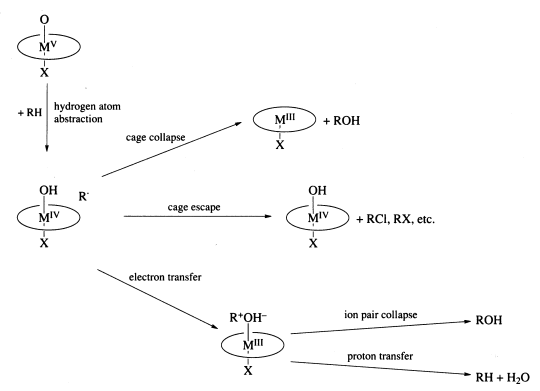


Fig 7

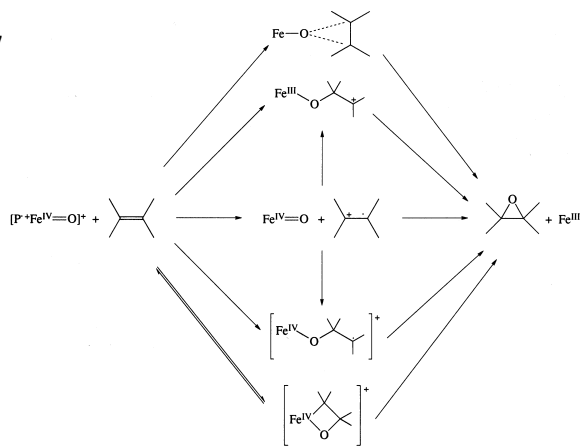


Fig 10

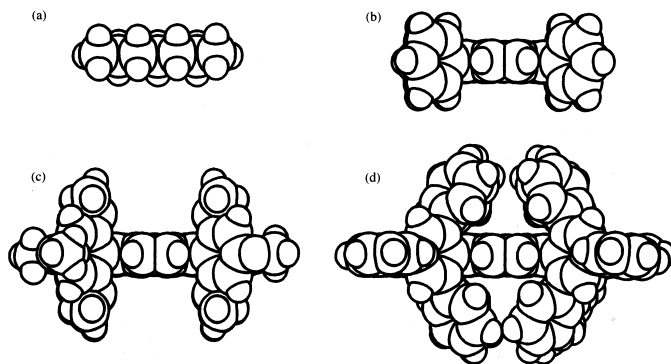


Fig 8

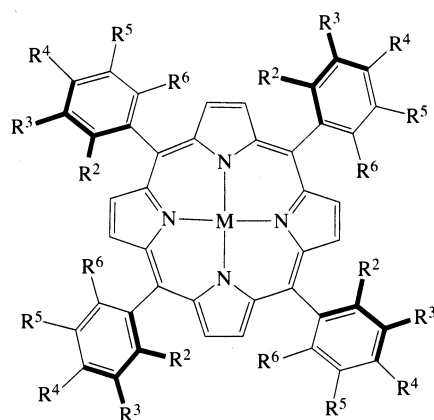


Fig 11

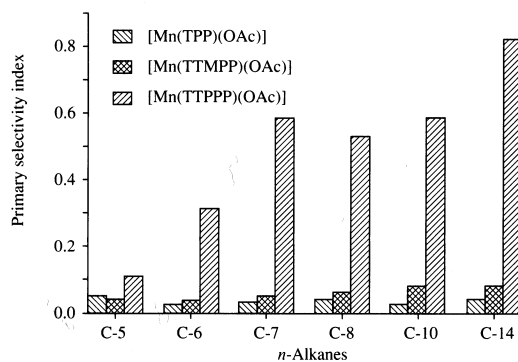


Fig 9

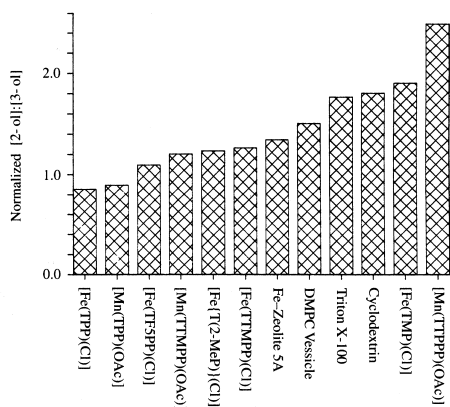


Fig 12

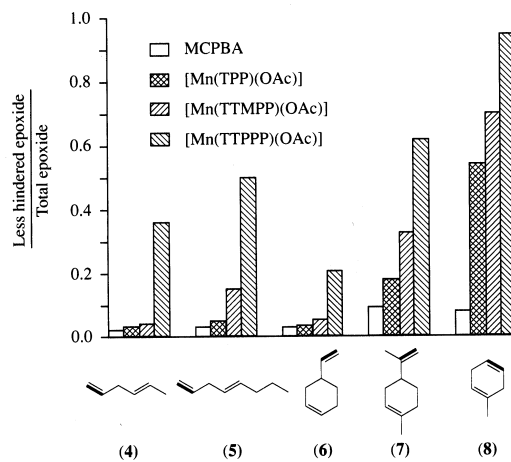


Fig 13

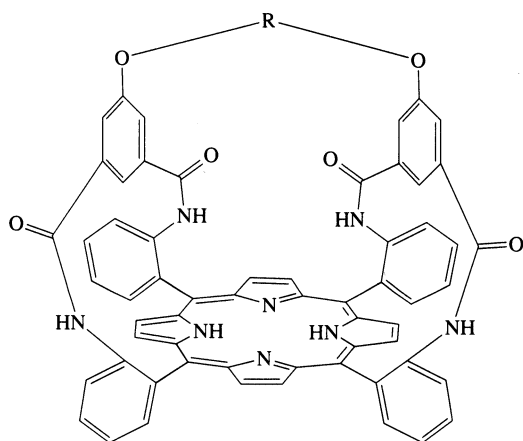
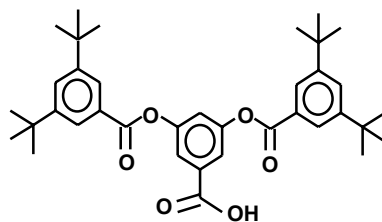
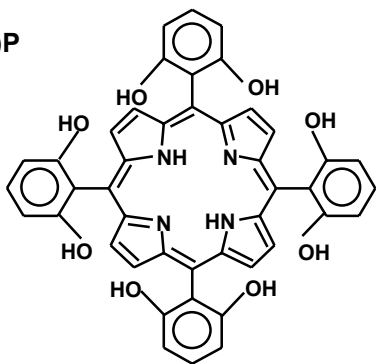
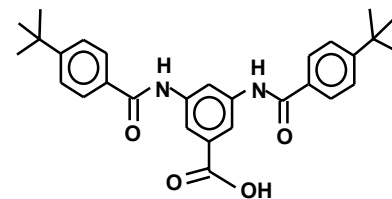


Fig 14

$H_2T(2',6'-DHP)P$

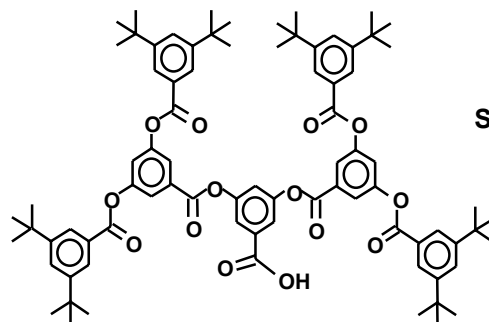
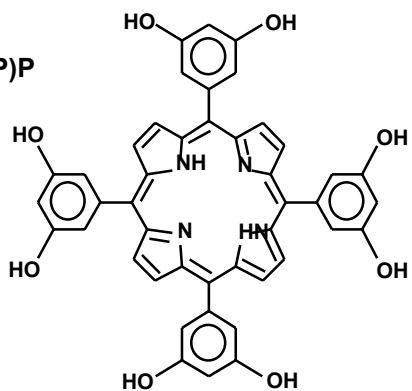


First Generation
Ester Dendrimer
(G1 acid)



First Generation
Amide Dendrimer
(G1A acid)

$H_2T(3',5'-DHP)P$



Second Generation
Ester Dendrimer
(G2 acid)

Fig 15

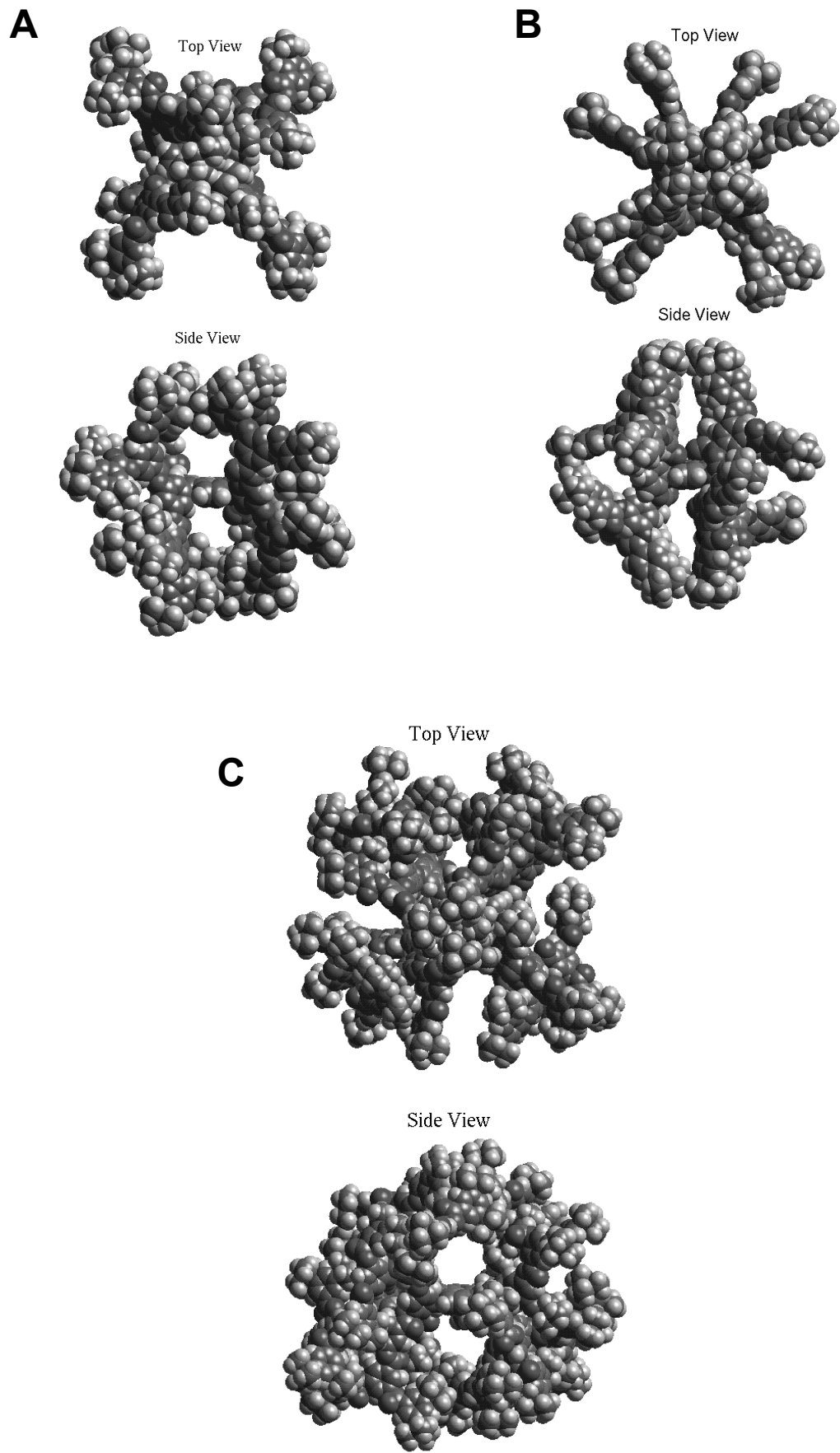


Fig 16

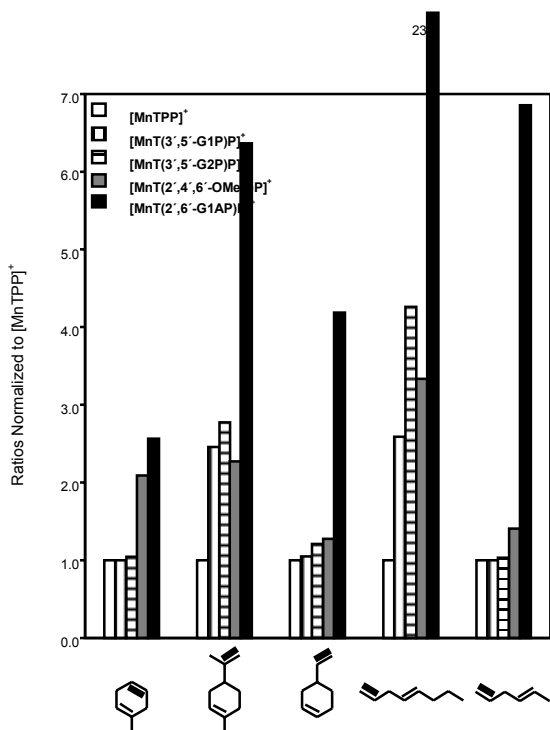


Fig 18



Fig 17

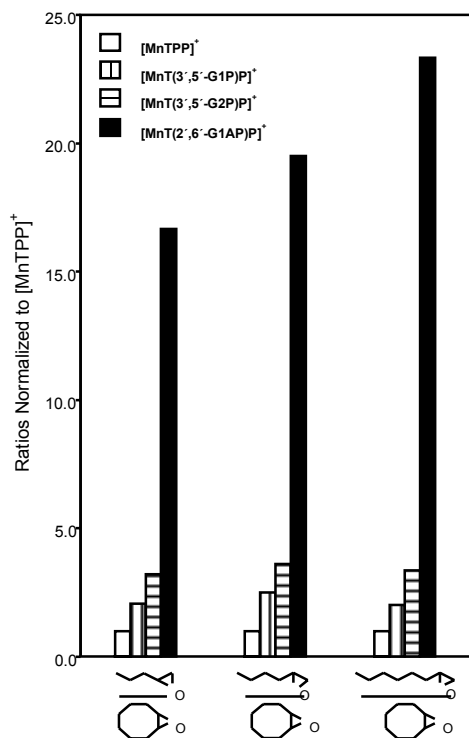


Fig 19

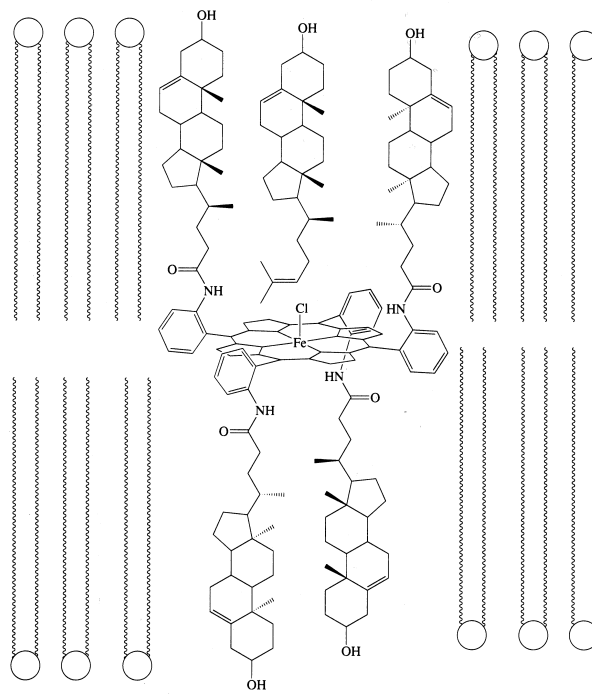


Fig 20

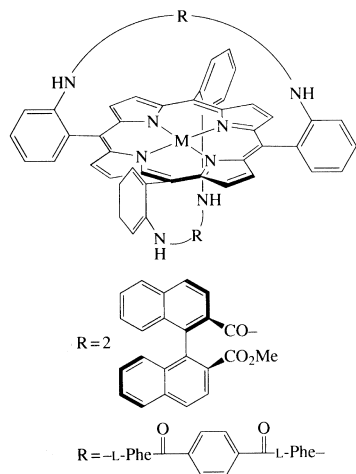


Fig 23

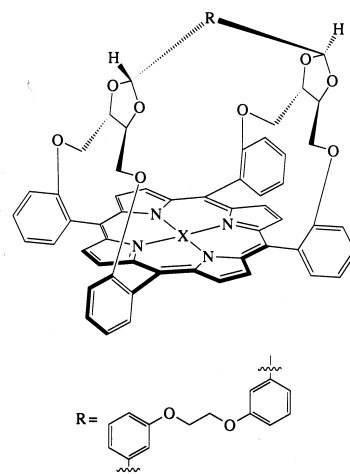


Fig 21

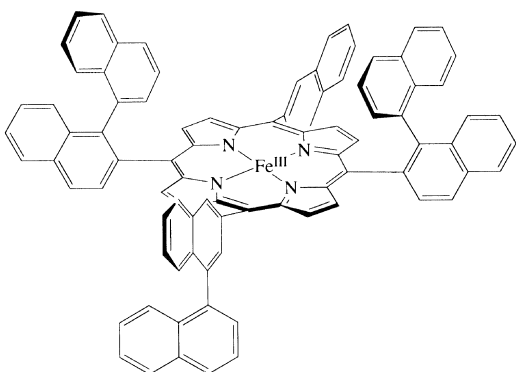


Fig 24

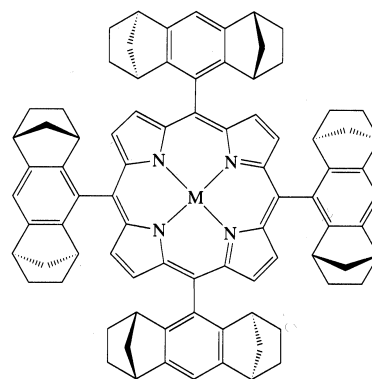


Fig 22

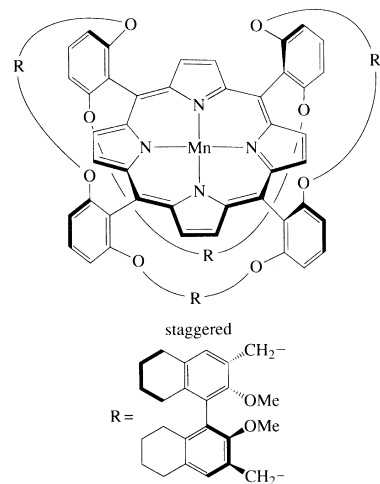
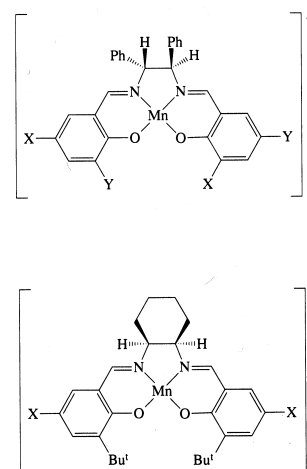


Fig 25



Applications of Porphyrins and Metalloporphyrins to Materials Chemistry

Jun-Hong Chou[†], Margaret E. Kosal[†], Hari Singh Nalwa[‡],
Neal A. Rakow[†], and Kenneth S. Suslick[†]

School of Chemical Sciences
University of Illinois at Urbana-Champaign
600 S. Goodwin Av.
Urbana, IL 61801

and

Hitachi Research Laboratory,
Hitachi Ltd.
7-1-1 Ohmika-cho,
Hitachi City, Ibaraki 319-1292
JAPAN

I. Introduction

II. Photonic Materials

- A. Mesogenic Porphyrins and Metalloporphyrins
 - 1. Octa-substituted Porphyrins
 - 2. Tetra-substituted Porphyrins
 - 3. Di-substituted Porphyrins
- B. Porphyrins and Metalloporphyrins as Nonlinear Optical Materials
 - 1. Second-Order NLO Systems
 - 2. Third-Order NLO Systems
 - 3. Optical Limiting Systems
- C. Porphyrins and Metalloporphyrins as Opto-Materials
 - 1. Artificial Photosynthetic Systems
 - 2. Porphyrins for Optoelectronics
 - 3. Synthetic Light-Harvesting Antenna

III. Porphyrinic Solids

- A. Microporous Solids
 - 1. Porous Molecular Porphyrin Structures
 - 1. Hydrogen-Bonded Network Materials
 - 2. Metal Ion Coordination Network Materials
 - 3. Porphyrin-Incorporated Zeolites
 - 4. Clays and Layered Materials Incorporating Porphyrins
 - a. Smectite Clays
 - b. Layered Double Hydroxides and Other Layered Materials
- B. Conductive Polymers and Ferroelectrics
 - 1. Conductive Porphyrin Polymers
 - a. Shish Kebab Porphyrin Polymers
 - b. Covalent, Conjugated Porphyrin Polymers
 - c. Conductive Porphyrin-Linked Polymers and Porphyrin Arrays
 - 2. Ferroelectric Porphyrin Materials

[†] University of Illinois

[‡] Hitachi

- C. Porphyrin-Based Chemical Sensors
 - 1. Gas Sensors
 - a. Oxygen
 - b. Other Gases
 - c. Porphyrin Array Vapor Sensors
 - 2. Sensors for Solution Species
 - a. Anion Detection
 - b. Cation Detection
 - c. Sensors for Organic Molecules
- IV. Conclusions
- V. Acknowledgments
- VI. References
- VII. Tables
- VIII. Figure Captions
- IX. Figures

I. Introduction

Porphyrins and related macrocycles provide an extremely versatile synthetic base for a variety of materials applications. The exploration of metalloporphyrin assemblies as building blocks for tailored materials properties has found rapid growth during the past decade¹. In this chapter, we shall review the rather diverse applications of porphyrins to materials chemistry and try to draw the common threads between these topics as possible.

Porphyrins and metalloporphyrins have found broad applications as field-responsive materials, particularly for optoelectronic applications. For example, the facile substitution of the periphery of various porphyrins has generated a series of unusual liquid crystalline materials. The porphyrin ligand serves as a platform on which one can erect desirable molecular and materials properties, including very large dipole moments, polarizabilities, and hyperpolarizabilities. The nonlinear optical properties of these materials are of special interest, in part for energy transfer with molecular control, and in part for potential applications in optical communications, data storage, and electrooptical signal processing. The stability of mono- and di-cation porphyrin π -radicals makes these systems especially interesting for photoionization processes, closely related to the so-called special-pair reaction center of photosynthesis and the photogeneration of electron transfer. As another example, various polymeric porphyrins have been examined for their unusual low-dimensional conductivity.

In contrast to their interaction with applied electric, magnetic or electromagnetic fields, porphyrins and metalloporphyrins can also interact with other chemical species. One might view such interactions as chemo-responsive rather than field-responsive. The development of chemo-responsive materials based on porphyrins, however, has seen somewhat less development. As an example of such applications, porphyrin solids are often highly porous and the intentional development of molecularly-based molecular sieves or shape-selective solid catalysts is currently under development. Porphyrins and metalloporphyrins have also been examined for a variety of sensor applications, which clearly represent an important class of chemo-responsive materials.

II. Photonic Materials

A. Mesogenic Porphyrins

Appending long alkyl chains to the periphery of a rigid tetrapyrrolic core has proved to be a general methodology for the synthesis of liquid crystalline materials. Liquid crystals possess properties of both the liquid and solid phases, possessing order over intermediate distances, but retaining many of the rheological properties of liquids. Phthalocyanine derivatives have been widely investigated as thermotropic mesogenic materials,^{2,3} whereas porphyrins and metalloporphyrins have received only cursory examination. The larger phthalocyanines tend to have high melting points; porphyrins offer a similar geometrical structure and a greater ease of functionalization, while

having a smaller inner core and therefore lower, more useable melting points. The majority of porphyrin mesogenic materials have a discotic columnar nature in which the porphyrins stack like saucers along their short axis.

1. Octa-substituted Porphyrins

The first reported porphyrin exhibiting mesophasic behavior was an octa- β -substituted *uro*-porphyrin I octa-*n*-dodecyl ester (Figure 1).⁴ The investigation was modeled on the observation that similarly-shaped flat, hexagonal molecules had previously displayed discotic liquid crystal phases. Upon heating the porphyrin compound melted directly from a crystal to an isotropic liquid. During cooling, a mesomorphic phase of 0.1°C was noted between 96.8 °C and 96.7 °C. This phase was characterized as having discotic order via microscopic texture analysis and miscibility experiments in comparison to known discotic materials.

[Figure 1]

Fox and co-workers have synthesized and investigated the physical properties of a series of octyl-ether and octyl-ester porphyrin materials. The free base and metalated derivatives of 2,3,7,8,12,13,17,18-octakis(β -*n*-alkoxy)ethylporphyrin, $H_2((OC_nH_{2n+1})OEP)$ (abbreviations given in Table 1), were examined as possible liquid crystalline porphyrin materials (Figure 1). Of the free base species examined, only the *n*-octyl porphyrin displayed a narrow five degree liquid crystalline phase (Table 2). The metalated ($M = Zn, Cu, Pd, Cd$) porphyrins demonstrated discotic mesomorphism. The lowest melting point (61 °C) was observed for an equimolar mixture of the *n*-octyl and *n*-decyl zinc octaether porphyrin materials. Appendage of a single electron donating cyano group to the 5-position of *n*-octyl octaether porphyrin ($H_2((OC_nH_{2n+1})OECNP)$) resulted in depression of the melting point and the clearing point. Substitution of an electron accepting nitro group in the same position ($H_2((OC_nH_{2n+1})OENO_2P)$) produced a depression of the clearing point without affecting the melting transition, thereby reducing the total range of liquid crystalline behavior. The authors attribute this to distortion of the planar macrocyclic ring by the large nitro group.⁵ The free base and zinc(II) derivatives of three similar octaester porphyrins ($H_2((O_2C_nH_{2n+1})OEP)$) were found to exhibit discotic columnar mesophases (Figure 2). The *n*-hexyl ester exhibited lower melting points than either the *n*-butyl or *n*-octyl species (Table 2).⁶ It was noted that in both the octa-ether and octa-ester porphyrin materials metallation contributed a stabilizing factor inducing wider mesomorphic temperature regimes.

[Table 1]

[Figure 2]

[Table 2]

The orientation of *n*-nonoxyethyl octa-substituted liquid crystalline material was explored by X-ray diffraction. The molecules were found to structurally order in columns such that the macrocyclic planes tilt at an angle of 46° to the columns (Figure 2).⁷ The intricacies of the structure was further elaborated for the *n*-decoyl derivative. The interfacial porphyrin-porphyrin distance was found to be 3.98Å, and the inter-column separation was 23.59Å (Figure 3). This structure has been suggested as a one-dimensional “molecular wire” motif for electronic conduction.⁸

[Figure 3]

Thin films of the zinc-octakis(β -decoxyethyl)porphyrin material included in indium-tin-oxide (ITO) electrodes were explored as an electrooptical data storage system. Capillary filling of the porphyrin into the ITO cell provided the physical construction of the photoconductive system. A scanning tunneling microscope (STM) was used to initiate charge trapping (“writing”) and measurement (“reading”). A storage density of ~3 gigabits per cm^2 was maintained over 2000 hours of continual subjection to charge, and greater than 60% of the current signal was still “readable” after ~1500 readings. Subsequent work demonstrated 1.5 billion “writing” and “reading” sequences of the material without substantial change in output signal (Figure 4).⁹⁻¹¹

[Figure 4]

Motivated by interest in exploring stronger intermolecular interactions than those of previously described porphyrin or phthalocyanine mesophasic materials, Doppelt and Huille reported the mesogenic behavior of sulfur-substituted azaporphyrin species (Figure 5). Mesogenic phases were not observed in the free base 2,3,7,8,12,13,17,18-octakis(octylthio)tetraazaporphyrin, whereas the Co(II/III), Ni(II), Cu(II), and Zn(II) complexes revealed a discotic hexagonal columnar liquid crystal (D_h). By optical microscopy and differential scanning calorimetry (DSC), the cobalt material was found to exhibit the largest mesophasic range between 48 and 206 °C. The copper(II) and the nickel(II) species manifested liquid crystalline behavior from 71.5 °C to 120 °C and 65 °C to 154.5 °C, respectively. The zinc(II) complex underwent a crystal to crystal phase transition at 44 °C, followed by an observed melting point at 55.5 °C and a clearing point at 125.5 °C. X-ray diffraction experiments furnished an inter-columnar distance of 23.6 Å for the Zn, Ni, and Cu materials. A slightly small inter-columnar distance of 22.8 Å was observed for the cobalt complex.¹²

[Figure 5]

2. Tetra-substituted Porphyrins

An investigation of the photophysics of 5,10,15,20-tetrakis(4-*n*-pentadecylphenyl)porphyrin, $H_2(T(4-n-C_{15}H_{31})PP)$, produced the second porphyrin liquid crystal material to be well-documented in the literature and the first to utilize a tetraphenylporphyrin core (Figure 6).¹³ Three mesogenic phases were reported; melting of the crystalline phase was observed upon heating at 27 °C, a second mesomorphic transition followed at 56 °C, onset of the third mesophase was noted at 65.5 °C and the material cleared to an isotropic liquid at 134.5 °C. A correlation between the photoconductive properties of the material as part of an electrochemical cell and the phase transitions of free base porphyrin ($H_2(T(4-n-C_{15}H_{31})PP)$) was found. Discontinuities in the photocurrent and dark-current were observed at the phase transitions (Figures 7 and 8). The third-order nonlinear susceptibilities of benzene solutions of $M(T(4-n-C_{15}H_{31})PP)$, where $M = H_2, Co, Ni, Cu, Zn$ or $V=O$, were studied using the degenerate four-wave mixing (DFWM) technique. The $\chi^{(3)}$ value for all samples was determined to be on the order of $\sim 10^{-11}$ esu calculated at 532 nm.¹⁴ Two mesomorphic phases were observed for a similar species 5,10,15,20-tetrakis(4-*n*-dodecylphenyl)porphyrin. Phase transitions were observed at 31.0 °C, 52.0 °C and 155.0 °C. This material was determined to be a discotic lamellar (D_L) liquid crystal via X-ray diffraction studies.¹⁵ Novel ferromagnetic materials were prepared by mixing two different paramagnetic $M(T(4-n-C_{12}H_{25})PP)$ materials ($M = Cu(II), V(IV), Co(II), Mo(V), Ag(II)$ or $Fe(II)$).¹⁶

[Figure 6]

[Figure 7]

[Figure 8]

The mesogenic behavior of 5,10,15,20-tetrakis(4-*n*-alkoxyphenyl)porphyrins, ($H_2(T(p-n-OC_{10}H_{21})PP)$ and $H_2(T(p-n-OC_{12}H_{25})PP)$), was explored by Kugimiya and Takemura. Two liquid crystalline phases were attributed to each the free base and cobalt(II) derivatives of $T(p-n-OC_{10}H_{21})PP$. A large temperature regime for mesomorphism was found for $Co^{II}(T(p-n-OC_{10}H_{21})PP)$. The zinc(II) complex featured three liquid crystal phases between -16 °C and 170 °C. The first two phases were not observed during repeated melting cycles of the material.¹⁷

Ohta and coworkers presented a number of porphyrins synthesized specifically in order to examine their liquid crystalline characteristics. The highly substituted 5,10,15,20-tetrakis(3,4,3'',4''-tetradecyloxy-*o*-terphenyl)porphyrins ($H_2(T(C_{12}H_{25}O)_{16}TP)$), although possessing core tetra-substituted porphyrin rings, have sixteen long alkyl chains for inducing mesogenic behavior (Figure 9). The di-substituted dodecyl ether porphyrin, $H_2(T(C_{12}H_{25}O)_{16}TP)$, displayed an extremely complicated DSC trace — at least four different mesophases were noted. By X-ray diffraction, a discotic hexagonal ordered columnar material (D_{ho}) was identified which melted at -80 °C and cleared at 39 °C. A second mesophase that cleared at 59 °C was determined to be discotic hexagonal disordered columnar (D_{hd}). Upon cooling, two other phases that could not be identified were observed. The similar di-substituted dodecyl ether copper complex, $Cu(T(C_{12}H_{25}O)_{16}TP)$, exhibited one D_{hd} mesophase that melted at -37 °C and cleared at 57 °C. The authors credit steric influences of the sixteen long alkoxy chains to the formation of a columnar assembly (versus lamellar which was observed for by Shimizu.¹⁵). When one of the alkoxy groups on

each of the eight pendant phenyl groups was replaced with a proton, $H_2(T(C_{12}H_{25}O)_8TP)$, a high-melting (202.2 °C), non-liquid crystalline material resulted.¹⁸ Di-substituted *o*-terphenyl mesogenic porphyrins materials were also studied and are reviewed subsequently.

[Figure 9]

Controlled orientation of the porphyrin macrocycle in a liquid solution for use in electron pair resonance (EPR) experiments was the motivation for the synthesis of an *ortho*-amino-tetraphenylporphyrin based liquid crystalline material. Appending biphenyl long chain alkoxy groups to the *ortho*-amino substituents generated a mesogenic material in which the porphyrin macrocyclic plane was orthogonal relative to the director *L* in a nematic phase matrix. Unaltered tetraphenylporphyrin aligns such that the macrocyclic ring is parallel to *L* (Figure 10).^{19,20}

[Figure 10]

Griesar et al. synthesized a material that had both liquid crystal and ferrimagnetic properties. A discotic mesophase was observed between 108 °C and 155 °C for $Mn^{III}(T(p-n-OC_{12}H_{25})PP)(TCNE) \cdot 2$ toluene (TCNE = tetracyanoethylene). The X-ray diffraction pattern revealed that the material possessed a hexagonal columnar lattice with a characteristic inter-columnar spacing of 30Å. The system was also found to display ferrimagnetic behavior below 25.0 K.²¹

Liquid crystalline behavior can also be induced in some hydroxy-substituted porphyrins by incorporating them as “guest” molecules in a mesogenic matrix of “clipper” host molecules (Figures 11). Two smectic phases were observed between 15 °C and 150 °C for the 5,10,15,20-tetrakis(3,5-dihydroxyphenyl)porphyrin complex. Mesomorphic behavior was not observed for 2,6-substituted-dihydroxyphenylporphyrins due to steric restrictions which prevented the “host” complex from binding the in the *ortho*-positions.²²

[Figure 11]

Patel and Suslick recently reported the synthesis and properties of a series of mesogenic porphyrins with liquid crystal phases stable over an extremely wide temperature range, which greatly increases their potential utility. In addition, they isolated novel metalloporphyrin mesogens that permitted axial ligation to the metal, including one novel phase possessing a permanent dipole moment. Hexagonal columnar discotic liquids crystals of the *n*-alkyl esters of free base 5,10,15,20-tetrakis(3,5-dicarboxyphenyl)porphyrin ($H_2(T(3,5-CO_2R)PP)$, $R = n-C_nH_{2n+1}$, $n = 10,12,14,16,18,20,22$) displayed a narrowing range of mesogenic behavior as the alkyl chain length increased (Figure 12). These porphyrins feature pocketed sites on both faces of the porphyrin macrocyclic ring due to the relative rotation of the phenyl groups (Figure 13). The presence of these protected pockets for axial ligation was utilized to construct a unique five-coordinate vanadyl derivative with dodecyloxy chains. This approach produced both a liquid crystalline range of over 246°C and a substantial dipole moment perpendicular to the porphyrin plane.²³

[Figure 12]

[Figure 13]

An early report of mesogenic behavior in a porphyrin species was originally presented by Gaspard in 1984. In an attempt to discover the minimum number of pendant long alkyl chains need to induce a liquid crystalline phase in a porphyrin system, derivatives of 5-phenalkoxy-10,15,20-tritolylporphyrin and 5,15-di(phenalkoxy)-2,3,7,8,12,13,17,18-octamethylporphyrin were explored. The free base compounds proved to not be mesogenic. This was attributed to the non-planar orientation of the tolyl and phenoxy groups relative to the porphyrin macrocyclic ring. However, mixtures of the copper(II) derivatives of 5-phenyl-*n*-dodecyloxy-10,15,20-tritolylporphyrin with one single long alkoxy chain were reported to display metastable mesophases in combination with paraffin or halogenated long alkyl chains.²⁴

3. Di-substituted Porphyrins

Due to the disc-like geometry of the porphyrin macrocycle, discotic mesophases have generally been the most common for porphyrin liquid crystalline materials. The first porphyrin liquid crystals featuring “rod-like”

calamitic mesophases were described by Bruce and coworkers using substituted 5,15-di(phenyl) zinc porphyrin complexes as the basic molecular building block.²⁵⁻²⁹ The first materials studied were derivatives of 5,15-(4-*n*-alkoxyphenyl)porphyrins ($H_2((OC_nH_{2n+1})DPP)$, $n = 8, 10, 12, 14, 16$) which feature long alkoxy chains directly attached in the *para*-phenyl position (Figure 14).²⁵ Mesogenic compounds of the *n*-octyloxy and *n*-decyloxy porphyrin systems have relatively high melting points. Liquid crystalline materials with shorter alkoxy chains ($R = R' = C_nH_{2n+1}$, $n = 8, 10$) were characterized as having smectic B phases; whereas, the less ordered smectic E or smectic E' phases were observed in the longer chain materials ($R = R' = C_nH_{2n+1}$, $n = 12, 14, 16$).²⁵

[Figure 14]

Subsequent extensions of this motif incorporated a cyclohexane ester or phenyl ester spacer between the *n*-alkoxy groups and the *meso*-phenyl group on a single or both sides of the core diphenylporphyrin (Figure 15, $R = C_6H_{10}-C_7H_{15}$, $R' = H$; or $R = C_6H_4-OC_7H_{15}$, $R' = H$; or $R = R' = C_6H_{10}-C_7H_{15}$; or $R = R' = C_6H_4-OC_7H_{15}$).²⁶ The observed mesophase transition type and temperatures as determined by polarizing microscopy and differential scanning calorimetry are delineated below (Table 3). The melting points remained high with the addition of ester groups, and the observed mesophases were of the more disordered nematic and smectic A variety. Although the melting temperatures were similar, the substitution of a second phenyl or spacer group raised the clearing temperature. In the case of di-substituted cyclohexyl spacer, the clearing temperature was increased by 31 °C; a second phenyl spacer more dramatically produced an clearing temperature elevated 113 °C compared to that observed for the mono-substituted material.²⁶

[Figure 15]

[Table 3]

In order to depress the melting points of the diphenyl porphyrin materials, synthetic modifications were employed to limit intermolecular π - π attractions between macrocyclic rings. Long lateral alkoxy chains were attached to the *ortho*-position of the phenyl ester (Figure 15) or in the *ortho*-position of the 5,15-diphenyl groups (Figures 16 and 17) as an attempt to restrict attractive electrostatic interactions. This approach proved less successful than that of Patel and Suslick. While the melting points of these materials were significantly lowered in comparison to the previously studied materials, some of the compounds no longer displayed liquid crystalline phases. The materials with lateral alkoxy substituents appended to the 5,10,15,20-phenyl ring manifested both decreased melting points and mesomorphic behavior (Figures 16 and 17). It was noted that two of the compounds with phenyl spacers (Figure 15, $R = (2',4'-OC_8H_{17})C_6H_4$, and Figure 17, $R = C_6H_4-O-C_8H_{17}$) are structural isomers – illustrating the dependence of specific orientation of the lateral alkoxy chain in affording liquid crystalline properties to otherwise similar porphyrin systems. A material with a single lateral chain substituent (Figure 16) displayed a smaller temperature range for mesophasic behavior (~20 °C) than those with two lateral chains (Figure 17). Nematic mesophases, more disordered than the smectic type, were observed for these materials. This is also attributed to the presence of the lateral chains.²⁷

[Figure 16]

[Figure 17]

Further attempts to restrict porphyrin to porphyrin interactions culminated in the synthesis of novel “donor-acceptor” and “strapped” porphyrin compounds. Instead of alkoxy chains, lateral *p*-nitrophenylsulfonyl groups were substituted on the 5,10,15,20-phenyl ring (Figure 18). The phenyl ester species ($R = C_6H_4-O-nC_7H_{15}$) displayed a high melting point and a small nematic mesomorphic range (28 °C) before decomposing. The cyclohexane ester ($R = C_6H_{10}-nC_7H_{15}$) decomposed directly from the melt. Significant distortion of the macrocyclic ring in the xylene “strapped” porphyrin complex ($R = C_6H_4-O-nC_7H_{15}$), was cited for the lack of mesogenic behavior (Figure 19).²⁸

[Figure 18]

[Figure 19]

Efforts have been directed to increasing the “rod-like” geometry of the zinc porphyrin systems by extending the linear expanse through additional phenyl ester groups (Figures 20 and 21). This approach generally resulted in

lower temperatures for the onset of the first phase transition, however, in the some cases, this was a crystalline to crystalline phase change. At high temperatures, both a smectic C and a nematic phase were observed in the 3,4-*n*-dodecyloxyphenyl compound. One system that featured eight linear phenyl ester moieties but no lateral chains dangling over the porphyrin macrocyclic ring (Figure 20. $Y = OC_{12}H_{25}$; $n = 12$, $m = 2$) manifested a columnar mesophase. A relatively low phase transition (50 °C) to a nematic phase was seen in the material with both lateral chains and eight linear phenyl ester groups (Figure 21. $Y = OC_{12}H_{25}$; $m = 2$). The material cleared to an isotropic fluid at 153°C.²⁹

[Figure 20]

[Figure 21]

Ohta and coworkers studied the liquid crystalline behavior of a series of disubstituted phenyl porphyrins. Similar to the highly substituted tetraphenyl species, 5,15-bis(3,4,3'',4''-tetra(alkoxy-*o*-terphenyl))porphyrins, $H_2(B(C_nH_{2n+1}O)_mTP)$ where $n = 12$ or 16 and $m = 4$ or 8, were prepared with as many as eight long alkoxy chains (Figure 22). A discotic, rectangular disordered columnar (D_{rd}), arrangement was observed for $H_2(B(C_{12}H_{25}O)_8TP)$. Increasing the alkyl chain length (e.g., $H_2(B(C_{16}H_{33}O)_8TP)$) produced a material that also exhibited a D_{rd} columnar mesophase, which cleared to an isotropic liquid at nearly the same temperature as the dodecyloxy compound. Substitution of one of the dodecyloxy chains on each porphyrin with a proton, generated a material with two discotic lamellar mesophases. The clearing point of this compound (228.6°C) was approximately 100° higher than that of either di-substituted compounds (136.7 °C and 132.9 °C, respectively).¹⁸

[Figure 22]

Two other di-substituted species were examined by Ohta and coworkers. The tetra alkoxy-containing 5,15-bis(3,4-didodecyloxyphenyl)porphyrin displayed a discotic lamellar mesophase with a melting pointing of 60.4 °C and clearing point of 200.7 °C (Figure 23). Four crystalline phases and one undetermined mesophase were delineated for 5,15-bis(4-didodecyloxybiphenyl)porphyrin between initial crystalline phase transitions at 40.1 °C to melting to the mesomorphic material at 430.9 °C (Figure 24). The material was observed to decompose at 450.5 °C.¹⁸

[Figure 23]

[Figure 24]

B. Porphyrins as Nonlinear Optical Materials

The synthesis and chemistry of nonlinear optical (NLO) porphyrin-based materials has been examined in some detail. Porphyrins have several desirable properties for use in optoelectronics: they have greater thermal stability (compared to typical organic chromophores); their extended π -conjugated macrocyclic ring gives large NLO effects; and subtle variation in their physical properties can be made easily through chemical modification of their periphery. Here we highlight progress in the development of NLO porphyrinic materials describing their second-, and third-order nonlinear optical properties. Due to space limitations, we provide only the most cursory introduction to the physics of nonlinear optical phenomena; several excellent references are available for further details.³⁰⁻³⁷

The optical properties of a medium are characterized by the optical susceptibility, χ . This optical susceptibility is closely related to the refractive index and the dielectric constant. In an isotropic medium at optical frequencies (ω), the relationship between the linear susceptibility, the refractive index (n), and the dielectric constant (ϵ) can be expressed as:

$$1 + 4\pi\chi(\omega) = n^2(\omega) = \epsilon(\omega) \quad (1)$$

The microscopic polarization (p) induced in an isolated molecule under the applied electric field (E) of an incident electromagnetic wave can be expressed by the following equation:

$$p = \alpha E + \beta EE + \gamma EEE \quad (2)$$

where p and E are related to the tensor quantities α , β , γ , which are referred to as the polarizability, first hyperpolarizability and second hyperpolarizability, respectively. Similarly, the macroscopic polarization induced in the bulk media can also be expanded in the external field power series:

$$P = \chi^{(1)} E + \chi^{(2)} EE + \chi^{(3)} EEE + \dots \quad (3)$$

where $\chi^{(1)}$ is the linear optical susceptibility, and $\chi^{(2)}$ and $\chi^{(3)}$ are the second and third-order nonlinear optical susceptibilities; these physical meanings similar to their microscopic counterparts α , β , and γ , respectively. The even-order tensor $\chi^{(2)}$ is zero in a centrosymmetric environment, whereas the odd-order tensor $\chi^{(3)}$ does not have any symmetry restrictions and produces a non-vanishing higher order optical susceptibility. Therefore, $\chi^{(n)}$ are (n+1) rank tensor associated with the nonlinear optical response of the medium. Both the field E and the polarization P are vectors, while the nonlinear optical coefficients are tensors. The $\chi^{(n)}$ is frequency dependent, and as a result, resonant and non-resonant parameters can differ significantly depending upon frequencies used. There are 9 elements of $\chi^{(1)}$, 27 elements of $\chi^{(2)}$, and 81 elements of $\chi^{(3)}$; the number of independent elements, however, is usually much smaller. For example, in liquids, gasses and isotropic solids, there are only three independent elements for $\chi^{(3)}$: $\chi^{(3)}_{xxxx}$, $\chi^{(3)}_{xyyx}$, and $\chi^{(3)}_{xyxy}$.

1. Second-Order NLO Systems

Suslick et al.³⁸ measured the first hyperpolarizabilities (β) of porphyrins having electron donor (amino) and acceptor (nitro) groups in the *para*-position of 5,10,15,20-substituted tetraphenylporphyrins (Figure 25) using electric field induced second harmonic generation (EFISH) technique at 1.19 μm with chloroform solutions. The dipole moment (μ) and β values were affected by the position of donor and acceptor groups. A β value of 30×10^{-30} esu and dipole moment of 7×10^{-18} esu were measured for the porphyrin having $R^1=R^2=\text{NO}_2$, $R^3=R^4=\text{NH}_2$; and the porphyrin with $R^1=\text{NO}_2$, $R^2=R^3=R^4=\text{NH}_2$ exhibited a β value of 20×10^{-30} esu and dipole moment of 5×10^{-18} esu ($1 \text{ au} = 1.48176 \times 10^{-25} \text{ esu} = 1.64877 \times 10^{-41} \text{ C}^2\text{m}^2\text{J}^{-1}$). In these cases, the amino group “pushes” electron density macrocycle while the nitro groups “pull,” increasing the hyperpolarizability substantially. The β value of a porphyrin with $R^1=R^2=R^3=\text{NO}_2$, $R^4=\text{NH}_2$ was found to be $\geq 10 \times 10^{-30}$ esu. The well-aligned charge transfer gives rise to large β values.

[Figure 25]

Since second order NLO response occurs only in a non-centrosymmetric environment, the incorporation of porphyrins into a polar (in the sense of poled or asymmetric) array is mandatory for most optoelectronic applications. The importance of the organizational structure is shown in Figure 26. Langmuir-Blodgett (LB) films are an extremely effective means of providing the necessary asymmetric environment for good NLO response. Suslick and coworkers incorporated similar “push-pull” porphyrins derivatives into Langmuir-Blodgett films in order evaluate bulk response of the material.³⁹ They found that good films could be created from these push-pull porphyrins, simply by conjugating a long chain fatty acid to the free phenylamine functionalities. The mean molecular area of these LB films depended strongly on the number of alkyl chains, as shown in the LB isotherms (Figure 27). The number of alkyl chains did not change the porphyrin orientation, but rather altered the packing density of the porphyrins.

[Figure 26]

[Figure 27]

Sen et al.^{40,41} measured β values of a series of donor-acceptor substituted fluoroarylporphyrins by using hyper-Rayleigh scattering (HRS) at 1064 nm (Table 5). The first hyperpolarizabilities are influenced by the nature and position of donor and acceptor groups. An increase in β values was observed when a β -pyrrole position of the TPP chromophores was substituted with an electron accepting nitro group. The open-shell Cu(II) (d^9) porphyrins show larger β values than closed-shell Zn(II) (d^{10}) porphyrins. The high observed β values in Zn(II) porphyrins are due to the large change in dipole moment upon excitation. The highest β values were obtained for porphyrins having N,N'-dimethylamino and nitro substituents. These porphyrins absorb at 532 nm; two-photon resonance enhancement contributes to large β values but the effect of metal d-electrons is more pronounced.

[Table 4]

Priyadarshy et al.⁴² calculated the first hyperpolarizabilities of porphyrin-bridged donor-acceptor molecules using semi-empirical INDO/SCI-SOS method. The chemical structures and calculated β values are shown

below (Table 6). The β values of 5-((4'-dimethylaminophenyl)ethynyl)-15-((4''-nitrophenyl)ethynyl)-10,20-diphenylporphyrinatozinc(II) (D-Zn(DPP)-A) (4) calculated at 830 and 1064 nm were 8152×10^{-30} and 477×10^{-30} cm^5/esu , respectively. From such calculations, it is clear that resonant enhancements of hyperpolarizabilities can be extremely important. This makes comparison between experiments difficult unless the wavelengths used are far removed from the intense porphyrin absorbance bands. The calculated $\mu\beta$ value at 1907 nm was 2548×10^{-48} cm^5/esu . The first hyperpolarizabilities are one order of magnitude larger than other porphyrin-bridged donor-acceptor molecules. The dimethylamino donor - nitro acceptor zinc species was determined to have a β value four times greater than that a similar compound lacking the nitro acceptor substituent. This indicates that extended π -conjugation length and strength of donor and acceptor groups significantly increase the β value. The β value varied slightly as a function of aryl group composition for a series of compounds with phenylamine donors and nitrophenyl or nitrophenylethynyl acceptor groups.

[Table 5]

LeCoers et al.⁴³ synthesized “push-pull” arylethynyl porphyrins and measured their β values by hyper-Rayleigh scattering (HRS) in chloroform solutions. The donor-acceptor compound (D-Zn(DPP))-A produced approximately frequency independent β values: 5142×10^{-30} esu at 830 nm and 4933×10^{-30} esu at 1064 nm. The copper analogue (D-Cu(DPP))-A exhibited frequency-dependent β values of 4374×10^{-30} esu at 830 nm and 1501×10^{-30} esu at 1064 nm. Significant shifts in molecular dipole moment were observed for the “push-pull” arylethynyl porphyrins by electroabsorption or Stark effect spectroscopy.⁴⁴ The β value of the zinc porphyrin dimer (D-Zn(DPP))-Zn(DPP))-A calculated at 1064 nm was 742×10^{-30} cm^5/esu (Figure 28). The calculated $\mu\beta$ value at 1907 nm was 3299×10^{-48} cm^5/esu . The β value of D-Zn(DPP))-Zn(DPP))-A is 1.6 times larger than that of D-Zn(DPP))-A. The larger β value is associated with two Zn(DPP) units linked together by an ethynyl bridge connecting the chromophores at their 5- and 5'-positions.

[Figure 28]

The first nickel “push-pull” 5,15-diphenylporphyrin derivatives were recently synthesized by Yeung.⁴⁵ Using an amino arylethynyl group as the donor substituent and a formyl or a dicyanoethynyl group as the acceptor group on the porphyrin, the nickel-containing species exhibited significant first hyperpolarizability. Using EFISH at 1907 nm, the first hyperpolarizabilities were determined as 124×10^{-30} esu and 66×10^{-30} esu for the formyl and dicyanoethynyl species, respectively. The larger β value for dicyanoethynyl compound is attributed to its higher relative electronic acceptor strength.

Albert et al.⁴⁶ calculated β values of “push-pull” porphyrins using semi-empirical INDO/S Hamiltonian and singles-only CI (Table 6). The calculated optimized β values and chemical structures are therein. The β value increased as the benzene ring was replaced by an electron-deficient moiety such as diazene or tetra-azine or by an electron-rich ring such as thiophene or pyrrole. The β_{vec} and $\mu\beta$ increased by a factor of two by replacing the benzene rings at the donor end by electron-donating pyrrole rings. A series of porphyrins with reduced dihedral twist of the phenyl rings were synthesized and present very large β values. Small dihedral angles were observed for the alkyne bridged (7°) and for the azo-bridged species (0.5°).

[Table 6]

A multifunctional polyimide consisting of a free base porphyrin and a NLO chromophore side chain was synthesized by Peng and associates (Figure 29).⁴⁷ This photorefractive molecular system was modeled on the charge transfer properties observed in porphyrin electron acceptors of photosynthetic processes. The polyimide exhibited a T_g of 250 °C. Absorption peaks at 510, 540 and 630 nm from the porphyrin rings and at 458 nm from the NLO-chromophore were observed. This multifunctional polyimide system is photoconductive as well as SHG active. The photoconductivity was determined to be 1.1×10^{-12} S/cm under an external field of 1500 kV/cm at 690 nm. The polymer film showed a NLO coefficient d_{33} of 110 pm/V at 1.064 μm after corona poling. Interestingly, the NLO coefficient d_{33} showed no decay at 90 and 150 °C, and the d_{33} of 80% was retained even at 170 °C after 120 hours. This porphyrin containing polyimide displayed both higher NLO coefficient as well as stability of second

harmonic generation at high temperature. Additional photorefractive effects were also observed in the two beam coupling experiment. An optical gain coefficient of 22.2 cm^{-1} under zero-field condition was noted.

[Figure 29]

Another new photorefractive polyimide (Figure 30) with a main-chain zinc porphyrin ($m=0.005$) and a NLO-chromophore side chain ($n=0.995$) was reported by Peng et al.⁴⁸ This porphyrin-containing fluorinated polyimide displayed a T_g of $228 \text{ }^\circ\text{C}$ and maintained thermal stability to $350 \text{ }^\circ\text{C}$. The photoconductivity was found to be electric field dependent. The SHG remained unchanged to $180 \text{ }^\circ\text{C}$.

[Figure 30]

Li et al.⁴⁹ looked at the SHG properties of self-assembled monolayer thin films of tetra-*para*-pyridylporphyrin ($\text{H}_2(\text{TPyP})$) and some derivatives on fused quartz and silicon surfaces. By covalently bonding the TPyP molecules to an alkyl- or phenyl- siloxy group, the centrosymmetric nature of the porphyrin is nullified. The SHG response at 532 nm was observed ($\chi_{zzz} \sim 2 \times 10^{-8} \text{ esu}$). This relatively large value was attributed to a completely delocalized π -electron system in the in the porphyrin monolayer.

2. Third-Order NLO Systems

As with phthalocyanines, the third order nonlinear optical susceptibility, $\chi^{(3)}$, of porphyrins can be manipulated by chemical substitution. The third-order NLO properties of several tetraphenylporphyrin compounds were first reported by Meloney et al.⁵⁰ The $\chi^{(3)}$ was measured by the degenerate four-wave mixing (DFWM) technique from toluene solutions of free base, zinc, and cobalt-containing TPPs. The effective $\chi^{(3)}$ values of these materials were estimated from the thermally induced refractive index changes. All porphyrin derivatives showed $\chi^{(3)}$ values on the order of 10^{-11} esu . Sakaguchi et al.⁵¹ also used DFWM for determining the $\chi^{(3)}$ values of cobalt, nickel, zinc, copper, and oxovanadium complexes of 5,10,15,20-tetrakis(4-*n*-pentadecylphenyl)porphyrins, $\text{H}_2(\text{T}(4\text{-n-C}_{15}\text{H}_{31})\text{PP})$. The measurements were made in a benzene solution with concentrations of 0.02-0.05%. The $\chi^{(3)}$ values were found to be in the range of 10^{-11} esu , however, these values are influenced by concentration. The $\text{Cu}(\text{T}(4\text{-n-C}_{15}\text{H}_{31})\text{PP})$ having a 0.05% weight dissolved in benzene showed $\chi^{(3)}$ of $1.8 \times 10^{-11} \text{ esu}$ whereas the $\text{Ni}(\text{T}(4\text{-n-C}_{15}\text{H}_{31})\text{PP})$ accorded $\chi^{(3)}$ of 10^{-10} esu at a concentration of 0.5 g/L. The $\chi^{(3)}$ values did not exhibit any significant effect of the metal atom.

Rao et al.⁵² measured $\chi^{(3)}$ values of a series of metal containing tetrabenzoporphyrin derivatives in tetrahydrofuran employing the DFWM technique at 532 nm . The chemical structures of these porphyrins and their abbreviated names are listed below (Figure 31, Table 1). These benzoporphyrins were substituted at the 5,10,15,20-positions with a variety of functional groups such as *m*-fluorophenyl, *p*-methoxyphenyl and *p*-methylphenyl. Values as high as $2.8 \times 10^{-8} \text{ esu}$ for $\chi^{(3)}$ were observed for zinc 5,10,15,20-tetrakis(*p*-dimethylaminophenyl)tetrabenzoporphyrin, $\text{H}_2(\text{TMAPTBP})$. In particular, large $\chi^{(3)}$ values were recorded for benzoporphyrins containing electron donating 5,10,15,20-phenyl groups. Guha et al.⁵³ evaluated imaginary and real parts of $\chi^{(3)}$ for the zinc tetraphenyl benzoporphyrin species [$\text{Zn}(\text{TPTBP})$] and the *p*-methoxyphenyl substituted version [$\text{Zn}(\text{TMOPTBP})$] in THF by using picosecond and nanosecond laser pulses. The imaginary parts of $\chi^{(3)}$ and γ (second hyperpolarizability) of these two porphyrins at 532 nm were found to be five to ten times larger than the real parts measured at $1.064 \text{ }\mu\text{m}$. The $\text{Zn}(\text{TMOPTBP})$ showed an imaginary $\chi^{(3)}$ of $9 \times 10^{-13} \text{ esu}$ and γ of $8.0 \times 10^{-31} \text{ esu}$ whereas a $\chi^{(3)}$ of approximately $1.8 \times 10^{-13} \text{ esu}$ and γ of $1.6 \times 10^{-31} \text{ esu}$ was observed for $\text{Zn}(\text{TPTBP})$ at a concentration of 0.46 g/L. Nonlinear refractive index values (n_2) of 7.8×10^{-10} and $9.1 \times 10^{-10} \text{ cm}^2/\text{MW}$ were estimated for $\text{Zn}(\text{TMOPTBP})$ and $\text{Zn}(\text{TPTBP})$, respectively.

[Figure 31]

Hosada et al.⁵⁴ measured $\chi^{(3)}$ of spin-coated films of free base and manganese chloride derivatives of octaethylporphyrin (OEP) and N,N',N'',N'''-tetramethyl-octaethylporphyrin(+2) bis(trifluoroacetate) [$\text{Me}_4^+(\text{OEP})^{2-}$] by third harmonic generation (THG) at $1.907 \text{ }\mu\text{m}$ to investigate the effect of increasing ring size on third-order optical nonlinearity (Figure 32). The $\chi^{(3)}$ of $\text{Me}_4^+(\text{OEP})^{2-}$, with an extended π -conjugation, was about five times

larger than that of $H_2(OEP)$, illustrating the increase in $\chi^{(3)}$ as the number of π -electrons in the conjugated ring increases. A similar effect is observed in one-dimensional π -conjugated polymers such as polyacetylenes. The $Mn(OEP)Cl$ showed slightly larger $\chi^{(3)}$ than $H_2(OEP)$ presumably due to the inclusion of a metal atom.

[Figure 32]

Norwood and Sounik⁵⁵ measured $\chi^{(3)}$ values of magnesium octaphenyltetraporphyrin ($Mg(OPTAP)$) (Figure 33) as a 5% weight incorporation in poly(methyl methacrylate) (PMMA). The thin films showed $\chi_{xxxx}^{(3)}$ and $\chi_{xyyx}^{(3)}$ values of the order of 1.17×10^{-11} and 3.03×10^{-12} esu, respectively from DFWM at 598 nm. The ratio of $\chi_{xxxx}^{(3)}$ to $\chi_{xyyx}^{(3)}$ was three, implying that the optical nonlinearity is predominantly electronic. The $Mg(OPTAP)$ showed a response time of 44 ps.

[Figure 33]

Anderson et al.⁵⁶ synthesized the soluble conjugated porphyrin polymer of 5,10,15,20-diethylzinc porphyrin ($(DEtP)_n$) using Glaser-Hay coupling (Figure 34). The real and imaginary components of $\chi^{(3)}(-\omega;0,0,\omega)$ of these polymers were calculated from the electroabsorption spectra. The $\chi^{(3)}(-\omega;0,0,\omega)$ on the order of 7.3×10^{-8} esu was obtained at the peak resonance due to resonance enhancement.

[Figure 34]

Bao and Yu⁵⁷ synthesized free base and Zn-metalloporphyrin-containing polymers (Figure 35) and measured their $\chi^{(3)}$ values by DFWM technique at 532 nm. These polymers possess photoconductive and photovoltaic properties. Notable $\chi^{(3)}$ values were obtained for the polymeric materials. The $\chi^{(3)}$ value found for $Zn(TPP)$ was twice as large as the free base porphyrin. The $\chi^{(3)}$ values were on the order of 10^{-10} esu for thin films. Polymer solutions showed $\chi^{(3)}$ values of 1×10^{-12} and 1.9×10^{-12} esu for the Zn and free base porphyrin polymer materials, respectively, which was more than two orders of magnitude smaller than those obtained for thin films. These $\chi^{(3)}$ values were enhanced due to the resonant contributions.

[Figure 35]

Kandasamy et al.[Kandasamy, 1997 #20] measured second hyperpolarizabilities of six tetraphenylporphyrin derivatives using the Z-scan technique at 784 nm. The γ value grew with increasing negative value of the Hammett constant. All porphyrins showed negative γ values both in neutral and acidic media. The γ value of porphyrins increased three to five times in an acidic medium compared to neutral. One species, $H_2(T(o-OCH_2CO_2C_2H_5)PP)$, showed γ values of -273.5×10^{-30} esu in acidic medium, about 5 times larger than in the neutral medium. The $H_2(T(o-OCH_2CO_2C_2H_5)PP)$ material also accorded a γ value 36 times larger than $H_2(TPP)$ in an acidic medium. The NLO properties of $H_2(T(o-OCH_2CO_2C_2H_5)PP)$ were significantly higher than the other materials because of the substituted electron donor groups at the *ortho* phenyl positions.

Kandasamy et al.⁵⁸ measured second hyperpolarizabilities of divalent $M(TPP)$ derivatives using the Z-scan technique at 802 nm. The γ value was enhanced by metal substitution, and it increased from the completely filled d-shell of Zn to the partially filled d-shell of Cu and Ni. The γ value of $Ni(TPP)$ was more than three times that of $Zn(TPP)$. The γ value of Sn(IV) substituted 5,10,15,20-tetrakis((4-carboethoxymethyleneoxy)phenyl) porphyrins [$Sn(TEMP)X_2$; $X=I, N_3^-, Br^-, Cl^-$ or OH^-] was determined by the same method at 802 nm in order to investigate the effect of axial ligand substitution on γ values. The γ value increased when a strongly electronegative axial ligand such as iodine was substituted. The high charge density at the core gives rise to larger γ values. The large γ value observed for the azido axial ligand porphyrin originates from its strong electron donor activity. These porphyrins produced negative γ values confirming their self-defocusing optical nonlinearity.

Kumar et al.⁵⁹ reported third-order optical nonlinearities in basket handle porphyrins (PSI) using DFWM technique at 532 nm (Figure 36). The planar $Cu(TPP)$ porphyrin showed $\chi^{(3)}(-\omega;\omega,\omega,-\omega)$ of 1.03×10^{-12} esu, while the value for the ruffled PSI molecules was found to be approximately 10^{-13} esu.

[Figure 36]

The $\chi^{(3)}$ of thin films of C_{60} and $H_2(TPP)$ composites were measured by a research team at Naval Research Laboratory using DFWM and nonlinear transmission at 590.5 nm.^{60,61} Kajzar and associates⁶² measured $\chi^{(3)}$ values in multilayer and composite C_{60} -based thin films with tetraphenylporphyrin, $H_2(TPP)$, and tetraphenylphthalocyanine, $H_2(TPN)$, using THG at 1.907 μm . Lower $\chi^{(3)}$ values were observed for both composite films and multilayered structures compared to C_{60} films.

Third order nonlinearity of solution-state and thin films of triethoxysilane-substituted $Zn(TPP)$ polymers were examined by Sinha et al.⁶³ Using DFWM, $\chi^{(3)}$ was measured in solution at 3.06×10^{-10} esu at 532 nm and 0.36×10^{-10} esu at 1064 nm, demonstrating resonance enhancement at the higher frequency. A cured polysiloxane film containing the same porphyrin provided a $\chi^{(3)}$ of 3.25×10^{-10} esu at 532 nm. The corresponding γ values were determined to be 24.49×10^{-32} and 2.81×10^{-32} esu, in solution at 532 and 1064 nm, respectively, and 60.10×10^{-32} esu for the thin film at 532 nm. Additionally, the polymer film was determined to be thermally stable in excess of 500°C by thermogravimetric analysis.

A comparison of the third-order optical nonlinearity on various metalloporphyrins results is summarized below (Table 7). The $\chi^{(3)}$ values vary as much as seven orders of magnitude depending upon chemical structures, measurement technique, wavelength, state of matter, and resonant contributions.

[Table 7]

3. Optical Limiting Systems

Optical limiting properties of fullerenes, porphyrins and phthalocyanines have attracted much attention since they have applications in passive solid-state sensors and the human eye protection from high-intensity visible light sources.^{64,65}

Although metallophthalocyanines have been studied in detail, there are few reports on optical limiting properties of porphyrins. Blau et al.⁶⁶ showed reverse saturable absorption (RSA) by cobalt and zinc TPP complexes. Fei et al.⁶⁷ reported RSA in $Fe(TPP)$. Nonlinear excited state absorption in a series of metallo-tetraphyrin compounds (Figure 37) in acetonitrile solutions using 8 ns and 23 ps optical pulses at 532 nm was noted by Shi et al.^{68,69} The tetraphyrin compounds show reverse saturable absorption at weakly fluorescent bands for nanosecond pulses, while saturable absorption occurs for highly fluorescent bands only for picosecond pulses. A six level model was presented to explain the nonlinear absorption effects. Cadmium tetraphyrin showed strong RSA and nonlinear absorption while it was very weak in the other metallo-tetraphyrin derivatives.

[Figure 37]

Su and Cooper⁷⁰ reported optical limiting properties of free base octabromo-tetraphenylporphyrin ($H_2(Br_8TPP)$) and its metal-containing derivatives (Figure 38). Nonlinear optical absorption efficiency was measured at 532 nm. The efficiency data showed a trend as $Zn(Br_8TPP) > Cd(Br_8TPP) > H_2(Br_8TPP) > Pb(Br_8TPP) > Cu(Br_8TPP) \approx Cd(Br_8TPP)$ which was related to the spin state of the central metal atom. Comparable to phthalocyanines, $Zn(Br_8TPP)$ showed the strongest nonlinear absorption efficiency observed among porphyrins.

[Figure 38]

C. Porphyrins and Metalloporphyrins as Opto-materials

In photosynthesis, the chlorophylls and pheophytins (close cousins of metalloporphyrins and porphyrins, respectively) play key roles in adsorbing light energy over a wide spectral range and converting it into the highly directional transfer of electrons.⁷¹⁻⁷⁶ It is a marvelous but highly complex process that has inspired considerable interest in the synthesis of porphyrin arrays. A biomimetic approach to the photosynthetic apparatus may also lead to applications of similar systems as opto-electronic devices. After brief overviews of artificial photosynthetic models and light harvesting antennae to set the stage, this section will focus predominantly on porphyrinic materials in applications to optoelectronics.

The remarkable efficiency of reaction center photochemistry has encouraged the design and the study of synthetic models. Most research on artificial photosynthesis has been directed toward mimicry of the natural

reaction center (RC). The center functions as a molecular-scale solar photovoltaic device that converts light energy into chemical energy that can be transported and stored for maintenance, growth, and reproduction of the organism. Green plants employ chlorophyll, a magnesium-chlorin, as the chromophore to harvest light. The trapped light energy is used to promote electrons into high-energy excited states. However, these excited states tend to decay to their ground states within nanoseconds, wasting the harvested energy as heat. Chromophores in green plants prevent this from happening by extremely rapid electron transfer. The acceptors are chlorophyll and pheophytin molecules initially, and quinones eventually. The resulting separation of negative and positive charges at the reaction center preserves a substantial fraction of the photon energy as chemical potential energy by generating a potential across the organelle membrane. At the minimum, then, an artificial reaction center requires some kind of chromophore that can absorb light and act as electron donor, an electron acceptor, and an organized superstructure that controls the electronic interaction between the donor and the acceptor. Initial work on model systems involved simple mixing of donor pigment molecules with acceptor molecules in solution. The electron transfer events were monitored by observing ion pairs that were the result of donor/acceptor collisions. Flash photolysis, nanosecond, and picosecond emission spectroscopy were used to characterize transient intermediates to better understand electron transfer kinetics.

1. Artificial Photosynthetic Systems

Achieving a long-lived charge separation after photoinduced electron transfer is the key to realizing artificial photosynthesis. This section will focus on molecules designed to maximize the lifetime of a charge-separated state. The ultimate goal here is to create a sufficiently long-lived excited state that chemical reactions can compete with the back reaction and convert the excited state free energy into a less volatile form. The first such systems, developed in the 1970s, were molecules consisting of synthetic porphyrins covalently linked to quinones. The porphyrin first excited singlet state is a strong reductant and is easily observed by flash kinetics. Simple porphyrin-quinone complexes are relatively easy to synthesize. The use of porphyrin pairs (as in the reaction center itself) is rather a more difficult challenge, however⁷⁷. Following absorption of light, the porphyrin (P) transfers an electron to the quinone (Q) resulting a charge-separated state consisting of a cationic radical $P^{\bullet+}$ and an anionic $Q^{\bullet-}$. The lifetime of $P^{\bullet+}-Q^{\bullet-}$ is usually very short because of the back-reaction. The electron rapidly returns to the porphyrin molecule, losing energy as heat, and the ground state of the molecule is restored.

Kong and Loach described the first reaction center mimic to have a covalently-bound porphyrin-quinone linkage.^{78,79} Shortly thereafter, Tabushi and coworkers designed a porphyrin-quinone molecule in which the quinone is bound to the porphyrin *via* an amide linkage.⁸⁰ These early systems outlined the basic conditions upon which future systems have dramatically improved. An extensive collection of porphyrin-quinone model compounds have been generated for the purpose of investigating long-lived charge-separated states. This overview will not be comprehensive, but instead will discuss a few illustrative examples. Interested readers are encouraged to consult an excellent review by Wasielewski on this subject.⁸¹

Substantial success has been made in using these complexes for biomimetic studies. In the 1980s, Gust and Moore have shown that the back reaction could be slowed substantially using a “triad” molecule composed of a tetraphenylporphyrin covalently linked to both a carotenoid and a quinone.⁸²⁻⁸⁶ The slowing results from the formation of the charge-separated state in which the two radical ions are separated by a neutral porphyrin (Figure 39). Carotenoporphyrin-quinone molecules possess a long-lived ion-pair lifetime on the microsecond timescale. For comparison, a typical donor-acceptor excited state lives for only several hundred picoseconds due to efficient charge recombination. Wasielewski and coworkers designed an octaethylporphyrin triad to effect a long-lived charge-separated state also based on the multistep principles found in carotenoid systems. The donor and acceptor distance was controlled by triptycene-derived quinone and amine groups. Electron transfer from N, N-dimethylaniline (D) to P^+ was competitive with charge recombination in the $D-P^+-Q^-$ state; therefore, a long-lived charge-separated state was observed. Gust and Moore incorporated the successful multistep strategy in a pentad comprised of carotenoid-diporphyrin-diquinone subunits. The pentad adopted an extended linear shape about 80Å in length. Irradiation at 650 nm produced the porphyrin first excited singlet state, which underwent a series of complex electron transfer events. The final charge-separated state $D^{\bullet+}-P^+-Q^{\bullet-}$ was long-lived and formed with a quantum yield that approach unity.

[Figure 39]

In the early 1990s, Osuka developed elaborate covalently-linked porphyrin dimers bound to a quinone electron acceptor, tethered via an aromatic hydrocarbon linkage.^{87,88} The structural and functional aspects found in reaction center chromophores were modeled using stacked porphyrins that roughly mimic special pair, at least in general structure (Figure 40). Because Osuka's system featured octa-alkylated porphyrins as the primary donor, the optically well-defined P⁺ cation intermediate absorption at 670 nm provided a suitable marker to monitor transients. The anthracene-pillared coplanar system had charge-separated state lifetimes that survived for only several hundred picoseconds. One failing of this system is the large separation between the porphyrin faces in the porphyrin pair relative to that found in photosynthetic reaction center special pair.

[Figure 40]

Osuka has also designed a system comprised of a zinc porphyrin dimer (DP), a zinc porphyrin monomer (ZnP), and a pyromellitimide (pm) in place of the quinone.⁸⁹ The pyromellitimide anion absorbs at 715 nm, which is spectrally resolved from the porphyrin absorption bands. Upon photoexcitation in THF at 532 nm, these triads give DP⁺—ZnP—pm⁻ ion pairs with lifetime of 2.4 μs in relatively low quantum yield. By replacing the intermediate Zn porphyrin with the non-metalated free base (Figure 41),⁹⁰ reasonable functional similarity to the photosynthetic reaction center was obtained. An efficient electron transfer relay, ${}^1\text{DP}^*-\text{P}-\text{pm} \rightarrow \text{DP}^+-\text{P}^--\text{pm} \rightarrow \text{DP}^+-\text{P}-\text{pm}^-$, was observed, similar to the primary electron transfer events in the reaction centers.

[Figure 41]

A spectacular example of a long-lived, charge-separated donor-acceptor triad was demonstrated by Gust and Moore.⁹¹ The Arizona researchers reported a molecular triad consisting of a diarylporphyrin (P) covalently linked to a carotenoid polyene (C) and a fullerene (C₆₀) (Figure 42). In 2-methyltetrahydrofuran solution, the triad undergoes photoinduced electron transfer to yield C—P^{•+}—C₆₀^{•-}, which evolves into C^{•+}—P—C₆₀^{•-} with an overall quantum yield of 0.14. This state decays by charge recombination to yield the carotenoid triplet state with a time constant of 170 ns. The results demonstrate that fullerenes can act as effective primary electron acceptors in multicomponent systems that generate long-lived charge-separated states. The C^{•+}—P—C₆₀^{•-} charge-separated state recombines to yield the carotenoid triplet state, rather than the molecular ground state, as in photosynthetic reaction centers.

[Figure 42]

Finally it should be mentioned that among the numerous synthetic analogs made for the photosynthetic reaction center⁸¹, nearly all utilize only a single porphyrin as the initial photoelectron donor, rather than a porphyrinic dimer as in the reaction center. The use of face-to-face bisporphyrin complexes linked to a quinone is perhaps the most sophisticated of these and provides a starting point for combination of synthetic light harvesting systems with synthetic electron donor-acceptor complexes.^{77,92}

2. Porphyrins for Optoelectronics

An ultimate goal in microelectronics is the design of electronic switches, wires, transistors, and gates made of single molecules. Approaches to this goal borrow heavily from the photosynthetic reaction center, both in their physics and in their chemistry. In principle, porphyrin arrays connected with conducting or insulating molecular wires could be converted into such molecular photo-electronic devices. In practice, however, the majority of the models have yet to function as electronic switching devices or molecular wires.

Toward that goal, Wasielewski et al. have designed a molecule (Figure 43) consisting of two porphyrin donors rigidly attached to the two-electron acceptor N N'-diphenyl-3,4,9,10-perylenebis(dicarboximide) (PBDCI), that acts as a picosecond electron switch when exposed to short pulse of light.⁹³ Excitation of the porphyrins within this molecule with subpicosecond laser pulses results in single or double reduction of the acceptor depending on the light intensity. The singly and doubly reduced electron acceptors absorb light strongly at 713 and 546 nm respectively.

[Figure 43]

More recently, the same research group reported a prototype molecular switch by utilizing photoinduced electron transfer in a donor-acceptor (D-A) system.⁹⁴ The underlying principle is that the local electric field produced by a photogenerated donor-acceptor ($D_1^+ - A_1^-$) ion pairs in the first unit can be used to control the photoinduced electron transfer reaction in a second donor-acceptor ($D_2^+ - A_2^-$) ion pair. They constructed a donor1-acceptor1-acceptor2-donor2 molecule ($D^1 - A^1 - A^2 - D^2$) (Figure 43), in which they selectively excite the second donor. Zinc 5-phenyl-10,15,20-tri(*n*-pentyl)porphyrin (D^1) and phenyldimethylpyrromethene dye (D^2) were chosen because they can be independently excited at 416 and 512 nm, respectively. The two acceptors were chosen because their ground states absorb only weakly at 416 and 512 nm and their radical anion absorption bands are well separated. Two ultrafast (150 fs) laser pulses were used to control the rate of a photoinduced electron transfer within the molecule. The results suggest that this type of molecule may lead to the realization of molecular electronic devices.

Lindsey and Wagner have investigated a variety of multi-porphyrin arrays that are connected by diarylethyne bridges for studies of artificial photosynthesis and molecular photonics. They have synthesized a "molecular photonic wire" consisting of array of metalloporphyrins 90 Å in length.⁹⁵ The difference between a molecular electronic wire and molecular photonic wire is that latter supports excited-state energy transfer rather than electron/hole transfer process. The wire consists of a boron-dipyrromethene dye as an input chromophore at one end, a linear array of three zinc porphyrins as a signal transmission element, and a free base porphyrin as an optical output element at the other end (Figure 44). Absorption of a photon by the input chromophore at one end causes the emission of a photon as the optical output at the other end. The overall yield of energy transmission from input to output is 76%.

[Figure 44]

Crossley and Burn also reported a molecular wire based on a more conjugated backbone.⁹⁶ The tetrakis(porphyrin) is about 65 Å in length and possesses a number of *tert*-butylporphyrin groups along the backbone that provide the molecule with good solubility in a number of organic solvent systems. Individual porphyrins are either directly fused or are linked by a coplanar aromatic system and are expected to be reasonably conductive. (Figure 45)

[Figure 45]

The synthesis of this extended porphyrin system involved a seven-step procedure. The final porphyrin tetramer was obtained by the condensation of porphyrin- α -dione with a bis- α -diamine. "Molecular optoelectronic gates" were also prepared by the same research group to see if the emission signal at the output chromophore in the photonic wire could be turned on/off in a controlled manner.⁹⁷ In order to achieve this goal a different metalloporphyrin was inserted into the molecular wire as a redox switch. To serve as a redox switch, this metalloporphyrin must meet four design conditions: (1) It must have a higher absorption energy, in the neutral state, so that the energy transfer does not occur between the free base and the metalloporphyrin. (2) When oxidized, the

metalloporphyrin should not fluoresce upon excitation. (3) It must have reversible redox properties. (4) It should possess the highest HOMO of all pigments in the assembly to ensure that oxidation takes place at the designated site. Mg-porphyrins seem to meet all the criteria. A schematic of the two designed gates is shown in Figure 46. The linear design has the switch attached to the end of the wire while the T-shape gate has the redox switch attached to the Zn-porphyrin. Oxidation was achieved by either chemical method or electrochemical method. In both cases the fluorescence of the free base porphyrin decreased significantly. Addition of triethylamine causes reduction of the Mg-porphyrin radical cation and recovery of the fluorescence.

[Figure 46]

Shimidsu et al. have obtained both one-dimensional and two-dimensional porphyrin polymers with oligothiophenyl molecular wires.⁹⁸⁻¹⁰¹ The electron conductivity of the 1-D polymers with conjugating oligothiophene was strongly enhanced by irradiation of light and was dependent on the light intensity. The 1-D porphyrin array with insulating wire was prepared by condensing the dichloro-P-porphyrin and the corresponding diol. The 2-D porphyrin network was synthesized by electropolymerization of the corresponding phosphorus-porphyrin with four oligothiophenyl groups at the *meso* positions. The 2-D porphyrin arrays showed similar functions as the 1-D porphyrin arrays with conjugating wires (Figure 47).

[Figure 47]

3. Synthetic Light-Harvesting Antenna

Photosynthetic microorganisms use light-harvesting antenna to trap solar energy and funnel it to the reaction centers.¹⁰²⁻¹⁰⁵ The energy conversion and migration can involve hundreds of pigments. A light-harvesting antenna should be a multicomponent assembly including chromophores that can absorb strongly in the blue and red regions of the solar spectrum and an energy-acceptor component to accept it. Synthetic porphyrins arrays are obvious candidates for the design of artificial antenna since chlorophylls are the main natural chromophores. Such exploration, however, has been limited by a lack of appropriate synthetic methodology for the preparation of large porphyrin arrays. Conventional synthetic strategies frequently involve a large number of sequential steps and extensive chromatographic purification. Consequently, the majority of the research done in this area focus on the synthesis of multi-porphyrin networks. Viable syntheses of suitable large arrays have only recently become available with the development of building-block methodologies.

In this section, we will concentrate on synthetic methods since the materials synthesized are potential light-harvesting antennas. Burrell and coworkers described the synthesis of functionalized TPPs building blocks that have been successfully used to prepare a variety of porphyrin arrays including trimers, pentamers, and nonamers (Figures 48 and 49).

[Figure 48]

[Figure 49]

In the early 1990s, Osuka et al. reported the synthesis of linear and stacked trimeric and pentameric porphyrins bridged by rigid aromatic spacers.¹⁰⁶ When the number of porphyrin rings increased, serious solubility problems occurred which prevented study of higher homologs. To circumvent this difficulty, peripheral substituents were placed on the porphyrin in hopes of increasing the solubility so that larger porphyrin arrays could be manipulated in common organic solvents. Using this strategy, they reported linear 1,4-phenylene-bridged porphyrin arrays including the dimer, trimer, pentamer, heptamer, and nonamer by acid-catalyzed condensation of formyl-substituted porphyrins with di(3-ethyl-4-methylpyrrol-2-yl)methane.¹⁰⁷ The molecular length of the nonamer is estimated upwards of 122 Å (Figure 50).

[Figure 50]

The same research group also reported the first bridgeless 5,10,15,20-linked porphyrin arrays which were synthesized by direct oxidative coupling of zinc porphyrins.¹⁰⁸ Treatment of zinc(II) 5,15-di(-3,5-di-*tert*-butylphenyl)porphyrin with AgPF₆ in acetonitrile for 5 h produced the dimer and the trimer in low yield. The

proposed mechanism is an initial one-electron oxidation of the zinc porphyrin by the Ag(I) followed by the nucleophilic attack of the neutral zinc porphyrin. The dimer and the trimer were separated by size exclusion chromatography. Reaction of the dimer under similar conditions afforded the tetramer in modest yield (Figure 51).

[Figure 51]

An extension of this work was reported for orthogonally-arranged, windmill-like porphyrin arrays, involving a 5,10,15,20-linked porphyrin dimer unit.¹⁰⁹ The synthesis involved the preparation of a symmetric, linear 1,4-phenylene-bridged porphyrin trimer. The reaction of the trimer with two equivalents of AgPF₆ produced windmill-like porphyrin hexamer and nonamer systems. (Figure 52)

[Figure 52]

Other groups are also pursuing light-harvesting porphyrin arrays. In 1993, Lindsey et al. reported a convergent strategy for the synthesis of soluble covalently-linked porphyrin arrays.^{110,111} The porphyrins are linked together via homogeneous Pd-catalyzed couplings of iodo- and ethyne-substituted tetraarylporphyrins (Figure 53). Reaction of the iodo-porphyrin and the ethyne-porphyrin in pyridine/triethylamine at 100°C for 12 h afforded a mixture of products including higher molecular weight material, the pentamer, dimer, and unreacted starting materials. Chromatography on silica gel yielded the pentamer in 50% yield. The absorption spectrum of the pentamer is similar to the monomers with a slight red-shift of the Soret band. Arrays with various metallation states are readily available. The fluorescence spectrum of the system with a central free base porphyrin and peripheral zinc porphyrins is dominated by the emission of the free base porphyrin. The yield of energy transfer from the zinc to free base porphyrin is estimated to be ~ 90%.

[Figure 53]

An excellent example of employing secondary pigment to enhance the absorption properties of the porphyrin was reported by Lindsey, Holten, Bocian, Birge and coworkers. They designed and synthesized light-harvesting arrays comprised of a central porphyrin with one, two, or eight boron-dipyrrin (BDPY) pigments (Figure 54).¹¹² In order to connect as many as eight boron-dipyrrin pigments around a central porphyrin, the *meta*-position of the 5,10,15,20-aryl rings on the porphyrin was utilized. Instead of the “porphyrin first, coupling second” approach, they decided to build the BDPY unit into the aryl aldehyde unit at the 4- or 3,5- positions using a Pd-catalyzed coupling reaction. The BDPY-incorporated aldehyde is then condensed with pyrrole to afford the desired BDPY-substituted porphyrin arrays. This strategy eliminated successive Pd-catalyzed coupling reactions and relied on the robust Lindsey porphyrin condensation. The synthetic routes of 4-(BDPY)benzaldehyde and 3,5-bis(BDPY)benzaldehyde are shown in Figure 54. Porphyrin arrays containing one, two, and eight BDPY dyes were prepared by mixed-aldehyde condensation reactions. These arrays are soluble in common organic solvents and can be easily metalated by treating the corresponding arrays with Zn(O₂CCH₃)₂ in methanol. Two important results with regard to the photophysical properties of the BDPY-porphyrin arrays are: (1) The intense blue-green absorption bands of the BDPY dyes complement the porphyrin Soret bands. (2) The energy transfer efficiency between the BDPY dyes and the central porphyrin is nearly quantitative in the arrays with one or two BDPY units, but drops (to 80–90%) in the arrays with eight BDPY units. The authors suggest that “the BDPY-porphyrin arrays are excellent candidates for inclusion in light-harvesting model system and as input elements of prototypical molecular photoic devices.”

[Figure 54]

Another popular approach in the construction of supramolecular porphyrin arrays uses metal-ligand interactions.¹¹³⁻¹²⁰ Most of this work has concentrated on 5,10,15,20-pyridylporphyrin (TpyP) and the porphyrin arrays prepared from TpyP range from dimeric molecule through polymeric networks. This synthetic strategy was adopted by Lehn and Drain for the preparation of multi-porphyrin arrays with square architecture (Figure 55).¹¹³ Their most impressive assembly is a 21-component structure consisting of nine porphyrins linked together by 12 palladium cations (Figure 56).¹²¹ It is composed of three different kinds of porphyrins: a tetrapyrrolylporphyrin

coordinated to four metal ions forms the center of the array; tripyridylporphyrins coordinated to three metal ions constitutes the sides of the array; and the dipyrindyl porphyrins form the corners. The synthesis involved placing these components in solution with the correct ratio at room temperature. The product was isolated in an amazing yield of 90%.

[Figure 55]

[Figure 56]

In an effort to prepare new biomimetic light-harvesting systems, Therien and coworkers have adopted recently developed metal-mediated cross-coupling methodologies and synthesized a new class of porphyrin arrays.¹²² The porphyrins are linked together by yne and polyynyl units (Figure 57). They believe that ethyne, oligoethyne, and multiethyne linkages between the porphyrins will produce multichromophoric systems with unusually strong excitonic and electronic coupling. The most important feature of these porphyrin arrays is that their spectroscopic data bear strong similarity to that of the purple bacterial light-harvesting complexes as well as to the light-harvesting structures in green photosynthetic bacteria.

[Figure 57]

III. Porphyrinic Solids

A. Microporous Solids

A number of researchers have explored synthetic strategies for the construction of porphyrinic solids that contain molecularly sized cavities or channels. Porphyrin macrocycles can be envisioned as flat, rigid, geometrically square building blocks approximately 1 nm wide. Out-of-plane twisting by the 5,10,15,20-substituted phenyl rings (as necessitated by steric constraints) provides a route to construct structures extending beyond the porphyrin macrocycle plane. Chemical modification of the perimeter is facile in many cases. Additionally the thermal stability makes them an attractive precursor for potential use at elevated temperatures. Furthermore, metalloporphyrins have demonstrated catalytic ability in a wide variety of reactions;^{123,124} thus, porous metalloporphyrin networks have the potential to act as shape- and size-selective catalysts.

1. Porous Molecular Porphyrin Structures

Strouse and coworkers,¹²⁵⁻¹²⁷ examined the extensive crystal structure library of free base and metalated porphyrin lattice clathrates in which the predominant intermolecular bonding interactions were of a very weak nature. In addition to H₂(TPP), their database included simple substituted porphyrins such as *o*-amino- (H₂(T(*o*-NH₂)PP)), *p*-methoxy- (H₂(T(*p*-OCH₃)PP)) and *p*-bromo- (H₂(T(*p*-Br)PP)) tetraphenylporphyrins. While the most commonly metalloporphyrin studied was the Zn(II) species, at least eleven other metalloporphyrins were examined. They realized that the large majority of these structures contained a high concentration of solvates and were in effect “porphyrin sponges.”

These TPP derivative materials were held together by van der Waals forces and found to exhibit a comparable packing modes generalized as the simple body-centered-cubic (BCC) arrangement. The driving force for clathrate formation was identified as the efficient packing of the porphyrin moieties in two dimensions. A third dimension is accessible for inclusion of guest molecules. The dominant interaction is described as “porphyrin-porphyrin interactions” between perpendicularly oriented phenyl groups on adjacent molecules. Similar packing modes were observed for over sixty-five different TPP species.¹²⁵

Channels of solvate molecules exist between chains of parallel porphyrin molecules (Figure 58). Estimates of the size of channel width were based on the *d*(002) lattice parameter essentially corresponding to half of the face to face porphyrin separation. The axial coordination sites or faces of the porphyrin macrocyclic ring line the edge of the channels. In the free base and 4-coordinate metalloporphyrin materials, the most commonly observed ratio was two guest molecules per porphyrin host molecule (Figure 59); notable exceptions were in cases of large solvate molecules (i.e. *p*-xylene, phenanthracene or naphthacenequinone) (Figure 60). Two axial ligands occupy the channels in six-coordinate metalloporphyrins; and, in the 5-coordinate materials, a single axial ligand and a single guest molecule were observed to alternately fill the voids (Figure 61). This is cited as an example of “programmability” in design of the clathrate materials. Porphyrin to guest ratios as high as 1:5 were observed for Fe^{III}(TPP)(*tert*-

$\text{MeUro}_2(\text{SbF}_6)(\text{THF})_2$ and $\text{Mn}^{\text{III}}(\text{TPP})(\text{MeOH})_2(\text{SbCl}_6)(\text{CH}_2\text{Cl}_4\text{H}_2)_2$. The latter compound was also characterized as having multiple channels (Figure 62).¹²⁶

[Figure 58]

[Figure 59]

[Figure 60]

[Figure 61]

[Figure 62]

Channel width was generally observed to be on the order of 3.4-6.6Å. Some of the smallest guest filled channels were observed in the $\text{Zn}(\text{TPP})(m\text{-fluoronitrobenzene})_2$, $\text{Zn}(\text{TPP})(2,4\text{-dinitrobenzene})_2$ and $\text{Zn}(\text{TPP})(\text{acridine})_2$ systems – all which had channel widths calculated at less than 4Å. The largest spacing for a “normal” clathrate material was observed for $\text{Ru}^{\text{II}}(\text{TPP})((\text{Ph}_2\text{P})_2\text{Me})_2(\text{CH}_2\text{Cl}_2)$.¹²⁶ Layered materials with $d(002)$ spacing of 6.8Å were observed for $\text{Rh}^{\text{III}}(\text{TPP})(\text{benzylisocyano})(\text{PF}_6)_2$ in which a single layer of guest molecules is located between a double layer of the host porphyrin species, and an even larger $d(002)$ spacing of 7.8Å was noted for a material with a double layer of host $\text{Ce}^{\text{IV}}(\text{TPP})^{+2}$ separated by another double layer of phthalocyanine molecules and SbCl_6^- anions (Figure 63).¹²⁷

[Figure 63]

Pursued applications of these clathrate “porphyrin sponges” include as materials to selectively “immobilize and isolate molecular species” and as intercalation compounds. The forces holding these solids together, however, are very weak. Consequently, upon removal of solvent, rapid structural changes to a different crystalline phase or to an amorphous material typically occur. In some cases, reintroduction of a vapor phase guest to the desolvated materials can produce a powder pattern that matched that of the crystalline clathrate materials grown in solution.¹²⁸ One specific application mentioned incorporating insect attractants as guest species into the lattice clathrate materials.¹²⁷

Goldberg and coworkers have synthesized porphyrinic solids that utilize other weak intermolecular interactions between porphyrin building blocks. The structures of inclusion compounds formed from halogen substituted tetraphenylporphyrins displayed three general motifs. The most commonly observed patterns involve halogen-halogen attractions between the halo-substituted phenyl groups and attractions between halogen atoms and β -pyrrole hydrogen atoms; these can lead to both one- and two-dimensional arrays (Figure 64). Inclusion compounds of this variety were observed for $\text{Zn}(\text{T}(p\text{-Cl})\text{PP})$ species with guests: guaiacol, nitrobenzene, DMSO, methyl salicylate,¹²⁹ methyl phenylacetate, mesitylene, ethyl benzoate and acetophenone.¹³⁰ and $\text{Zn}(\text{T}(p\text{-Br})\text{PP})$ species with guests: benzylacetate, methyl salicylate, ethyl benzoate, bromobenzene or *p*-xylene.¹³¹ The intermolecular $\text{Cl}\cdots\text{Cl}$ distance defines the width of the guest cavities. The $\text{Cl}\cdots\text{Cl}$ separation of 3.63Å reported for $\text{Zn}(\text{T}(p\text{-Cl})\text{PP})\bullet\text{C}_7\text{H}_8\text{O}_2$ (Figure 65) is typical of the 1:1 inclusion complexes; values for 1:2 inclusion compounds such as $\text{Zn}(\text{T}(p\text{-Cl})\text{PP})\bullet 2\text{C}_2\text{H}_6\text{OS}$ (3.90Å) were higher.¹²⁹ Slightly offset stacking of the porphyrin macrocycles in subsequent layers defined the depth of the cavities. The intermolecular $\text{Br}\cdots\text{Br}$ contact distances were reported as 3.837Å for a 1:2 $\text{Zn}(\text{T}(p\text{-Br})\text{PP})\bullet 2\text{C}_8\text{H}_8\text{O}_3$ (methyl salicylate) inclusion material. Thermal gravimetric analysis (TGA) was reported for $\text{Zn}(\text{T}(p\text{-Br})\text{PP})\bullet 2\text{C}_8\text{H}_8\text{O}_3$, showing a 21% weight loss for loss of solvent (theoretical 23%) at ~125°C without further loss to 350°C.¹³¹ In the case of the 1:1 $\text{Zn}(\text{T}(p\text{-Cl})\text{PP})$:nitrobenzene inclusion compound, the observed helical arrangement of the porphyrin backbone produced a polarized cavity environment (Figure 66). Guest molecules were observed to order in response.¹³⁰ The *p*-xylene clathrate of $\text{Zn}(\text{T}(p\text{-F})\text{PP})$ featured a linear chain structure similar to that noted in the chloro- and bromo-derivatives. However, the non-bonding $\text{F}\cdots\text{F}$ contact distances have increased to 4.1Å and 4.2Å, characteristic of a repulsive interaction rather than attractive force as observed in other halogenated porphyrin materials.¹²⁹

[Figure 64]

[Figure 65]

[Figure 66]

A second motif observed by Strouse and coworkers is characterized by tightly packed herringbone-like layers (Figure 67). Structures of this type were observed for $\text{Zn}(\text{T}(\text{p-Cl})\text{PP})\bullet\text{C}_7\text{H}_7\text{Cl}$ (*o*-chlorotoluene),¹²⁹ $\text{Zn}(\text{T}(\text{p-Br})\text{PP})\bullet\text{3C}_5\text{H}_5\text{N}$ and $\text{Zn}(\text{T}(\text{p-Br})\text{PP})\bullet\text{4C}_9\text{H}_{12}$ (mesitylene).¹³¹ In the *p*-bromo compounds, ligation of two pyridines to the Zn(II) ion was observed. The remaining uncoordinated guest molecules were observed to occupy voids between the porphyrin moieties.

[Figure 67]

A third motif, also observed in Strouse's TPP materials, is characterized by tightly packed corrugated layers in which the guest molecules intercalate between the layers: $\text{Zn}(\text{T}(\text{p-Br})\text{PP})\bullet\text{4C}_6\text{H}_7\text{N}$ (aniline) and $\text{Zn}(\text{T}(\text{p-Br})\text{PP})\bullet\text{2C}_8\text{H}_{11}\text{N}$ (methylbenzylamine) (Figure 68).¹³¹

[Figure 68]

2. Hydrogen-Bonded Network Materials

In an effort to synthesize more robust frameworks, hydrogen-bond interactions have been explored as basis for linking porphyrin molecules. Hydrogen bonds offer the additional advantages of directionality and selectivity.¹³² While hydrogen bonding is certainly a stronger interaction than the van der Waals interactions that hold the "porphyrin sponge" solids together, even multiple hydrogen bonds per porphyrin still provide only modest stabilization of the solids in the absence of their solvates.

Goldberg and co-workers have explored a number of substituted tetraphenylporphyrins as building blocks for porous solids. Some of the inclusion compounds of 5,10,15,20-tetra(4-hydroxy)phenyl porphyrins ($\text{H}_2(\text{T}(\text{p-OH})\text{PP})$) featured structures similar to those observed in halogenated species.¹³⁰ In a motif similar to the previously observed linear polymeric chains, the $\text{Zn}(\text{T}(\text{p-OH})\text{PP})\bullet\text{2C}_6\text{H}_6\text{O}\bullet\text{2H}_2\text{O}$ (phenol), $\text{Zn}(\text{T}(\text{p-OH})\text{PP})\bullet\text{2C}_9\text{H}_{10}\text{O}\bullet\text{H}_2\text{O}$ (benzyl acetate) and $\text{Zn}(\text{T}(\text{p-OH})\text{PP})\bullet\text{2C}_7\text{H}_6\text{O}\bullet\text{H}_2\text{O}$ (benzaldehyde) clathrate materials are characterized by dual *cis*-side OH•OH intermolecular attractions. There are no intermolecular interactions between *para*-substituted hydroxyl groups and β -pyrrole hydrogen atoms of adjacent linear chains (as observed in the halogenated materials). Instead, *para*-substituted hydroxyl groups hydrogen bond with hydroxyl groups on adjacent linear chains, forming a two-dimensional porphyrin network. A guest water molecule participates in this interchain bonding arrangement (Figure 69). In this manner, two different guest cavities are formed – voids between porphyrins in a polymeric chain and between chains in the two-dimensional array. Layers are stacked in an offset manner, therefore forming pores instead of channels in which axially coordinated ligands partially occupy the voids in successive layers.

[Figure 69]

Similar *cis*-side OH•••OH interactions are observed in the $\text{Cu}(\text{T}(\text{p-OH})\text{PP})\bullet\text{4C}_8\text{H}_8\text{O}$ (acetophenone), $\text{Zn}(\text{T}(\text{p-OH})\text{PP})\bullet\text{2C}_8\text{H}_{10}\bullet\text{4CH}_3\text{OH}$ (*o*-xylene and methanol) and $\text{Zn}(\text{T}(\text{p-OH})\text{PP})\bullet\text{5C}_7\text{H}_8\text{O}_2$ (guaiacol) materials. The linear porphyrinic chains are separated by guest molecules which hydrogen bond to the hydroxyl groups (Figure 70). In the acetophenone and *o*-xylene included materials, porphyrin macrocyclic planes of successive layers are offset preventing the formation of distinct channels. The parallel porphyrin macrocycles of successive layers are directly aligned in the guaiacol-included material generating $\sim 9\text{\AA}$ cavities. Between layers of porphyrin macrocycles is located, "sandwiched", a single parallel-orientated guest molecule (Figure 71). There is another guest guaiacol molecule situated below the area of hydrogen-bonding between porphyrin molecules.¹³⁰

[Figure 70]

[Figure 71]

For the toluene inclusion solid, $\text{Zn}(\text{T}(\text{p-OH})\text{PP})\bullet\text{3C}_7\text{H}_8$, a three-dimensional framework is observed (Figure 72). Hydrogen bonding between *trans*-orientated porphyrin hydroxyl groups and parallel chains form a geometry approximating a body-centered cubic arrangement. Porphyrins within successive layers of *trans*-hydrogen bonded chains have a interlayer separation of 6.5\AA in which a guest molecule resides. Channels perpendicular to the layers of porphyrin chains are observed. The significant translational and rotational disorder of guest species in the crystal

structure supports the presence of channels. *Trans*-OH•••OH interactions define the framework of the Zn(T(*p*-OH)PP)•2C₇H₈O•2H₂O (*p*-cresol) inclusion solid. One dimensional hydrogen-bonded chains between *trans*-hydroxyl groups on porphyrins which are stacked partly overlapping the porphyrin macrocyclic ring resulting in a layered material with intercalated guest species (Figure 73).¹³⁰

[Figure 72]

[Figure 73]

The clathrate of equimolar 5,10,15,20-tetra(4-methoxy)phenylporphyrinatozinc(II), phenol and water, Zn(T(*p*-OCH₃)PP)•C₆H₆O•H₂O, exhibits intermolecular hydrogen-bonding between methoxy substituents and axially coordinated water molecules in successive porphyrin layers (Figure 74). This arrangement generates a three-dimensional cross-linked framework in which phenol molecules occupy cavities between layers of porphyrin molecules similar to results reported for tetraphenylporphyrin inclusion solids by Strouse with *m*-xylene guest molecules.¹²⁵ A corrugated sheet-like geometry is observed in the Zn(T(*p*-CH₂OH)PP)•2C₈H₈O₂ (*o*-hydroxyacetophenone) material (Figure 75).¹³⁰

[Figure 74]

[Figure 75]

For clathrates of 5,10,15,20-tetra(4-cyano)phenyl porphyrin, H₂(T(*p*-CN)PP), four structural motifs were encountered by Goldberg et al.¹³³ The first hydrogen-bonding motif involves open two-dimensional networks in which a cyano group hydrogen bonds to β-hydrogen atoms on an adjacent porphyrin pyrrole rings in a dimeric fashion (Figure 76). The individual [-C≡N ••• H-(β-pyrrole)] interactions are described as short (3.41-3.59Å) and linear, although the two H-bond interactions of the dimer are not parallel to each other. The 1:2 inclusion compound of Cu(T(*p*-CN)PP) with chloroform produced a framework with elliptical interporphyrin cavities (6.4Å x 11Å) (Figure 77) whereas larger square-shaped cavities (10Å x 10Å) were observed for Zn(T(*p*-CN)PP) with two ethyl benzoate molecules – one axially ligated to the central Zn(II) ion and the other located within the interporphyrin void (Figure 78).

[Figure 76]

[Figure 77]

[Figure 78]

One dimensional chains utilizing similar dimeric interactions were observed for the inclusion solids Zn(T(*p*-CN)PP)•3C₇H₈O₂ (where the solvate is guaiacol) and Zn(T(*p*-CN)PP)•2.5C₇H₈O (anisole) (Figure 79). In the guaiacol-included material, a 20.06Å x 4.1Å cavity is noted. A similar structure is observed for Zn(T(*p*-NO₂)PP)•3C₁₀H₁₂O₂ (eugenol) with a large cavity of dimensions 23.34Å x 4.19Å (Figure 80). Herringbone-type interchain interaction between a single cyano substituent and a β-pyrrole hydrogen atom is characteristic of the third type of pattern observed for *para*-cyanophenyl porphyrin materials (Figure 81). Interlayer spacing of 4.3Å was observed for Zn(T(*p*-CN)PP)•CHCl₃•C₆H₆. In the Cu(II) porphyrin species, Cu(T(*p*-CN)PP)•2C₆H₅NO₂, cross-linking between adjacent chains is observed (Figure 82). The fourth bonding pattern utilizes ligand to metal coordination and is addressed subsequently.¹³³

[Figure 79]

[Figure 80]

[Figure 81]

[Figure 82]

Two clathrates of 5,10,15,20-tetra(4-carboxy)phenylporphyrin have been reported by Dasitidar et al.¹³⁴ Interpenetrating networks in the 1:1 Zn(T*p*CPP) : *sec*-phenethyl alcohol included material are formed when a porphyrin molecule hydrogen bonds to four other porphyrins via 'typical' carboxylic acid dimer aggregation. A planar two-dimensional array is formed in this manner (Figure 83). The *sec*-phenethyl alcohol is axially bound to the central zinc ion. Porphyrin macrocycles of parallel layers overlap and are interpenetrated by layers approximately

perpendicular (a dihedral angle of $\sim 70^\circ$ is reported). Observation of “a large central cavity of a rhombic shape” with dimensions $18\text{\AA} \times 16\text{\AA} \times 21\text{\AA}$ is reported. However, in reality this “cavity” is nonexistent: it is actually fully filled by two metalloporphyrins from perpendicular arrays.

[Figure 83]

Construction of $\text{Zn}(\text{TpCPP})\bullet 3\text{C}_2\text{H}_6\text{SO}$ (DMSO) porous material is based on *cis*-side interaction of carboxylic acid groups with hydrogen bonding to a bridging DMSO molecule resulting in generation of a one-dimensional polymer chain. Additional DMSO molecules bridge parallel polymeric chains creating a two-dimensional array. Each layer is intersected by an approximately perpendicular network. There are no H-bonds between perpendicular layers (Figure 84). A cavity of $6.5 \times 10\text{\AA}$ is reported, and TGA results suggests loss of solvents in two steps (axially-coordinated versus guest DMSO molecules).¹³⁴

[Figure 84]

Supramolecular networks based on hydrogen bonding between symmetrically substituted octahydroxyporphyrins were explored by Suslick and coworkers.^{135,136} Both *ortho*- and *meta*-dihydroxyphenylporphyrins (Figure 85) and their Zn(II) and Mn(III) derivatives were developed as molecular building blocks for nanoporous materials. The position of the peripheral hydroxyl groups, the choice of metalated or free base porphyrin, and the nature of the solvate dramatically influence structural features. These materials featured significant void volumes, as high as 67% calculated channel volume from x-ray crystal structures (Table 8).

[Figure 85]

[Table 8]

A one-dimensional hydrogen-bonding structure was found for $\text{H}_2(\text{T}(3',5'\text{-DHP})\text{P})\bullet 5\text{EtOAc}$ in which porphyrin macrocycles stack in a columnar fashion. These columns of porphyrins align parallel to one another, forming a porous three-dimensional network with channels of $6.5\text{\AA} \times 6.5\text{\AA}$ between them and $3.4\text{\AA} \times 3.4\text{\AA}$ running perpendicular to the columns (Figure 86). These columns are held together by weak van der Waals interactions. When benzonitrile is used as the solvent species, the structure of $\text{H}_2(\text{T}(3',5'\text{-DHP})\text{P})\bullet 7\text{C}_6\text{H}_5\text{CN}$ changes substantially to a two dimensional array of porphyrins interconnecting via hydrogen bonds generating a three-dimensional corrugated-sheet configuration. The observed variation in solid-state structure is credited to steric requirements necessitated by the larger benzonitrile guest molecules. Channels parallel to the corrugated layers with dimensions $5.5\text{\AA} \times 6.0\text{\AA}$ and another set approximately perpendicular calculated to be $4.0\text{\AA} \times 5.0\text{\AA}$ were identified (Figure 87).

[Figure 86]

[Figure 87]

Both the Zn(II) and Mn(II) derivatives of the *meta*-hydroxyl species featured three-dimensional hydrogen-bonded networks. $\text{Zn}(\text{T}(3',5'\text{-DHP})\text{P})(\text{THF})_2\bullet 2\text{THF}\bullet 3\text{CH}_2\text{Cl}_2$ has an interconnected layer motif in which the metalloporphyrins are arranged in a “slipped stack” orientation (Figure 88). In the structure of $\text{Mn}(\text{T}(3',5'\text{-DHP})\text{P})(\text{Cl})\bullet 2\text{EtOAc}$, the chloride anion bridges four hydroxyl groups from four separate porphyrins in a square planar arrangement with an average $\text{Cl}\bullet\bullet\bullet\text{O}$ distance of 3.01\AA creating a two-dimensional array (Figure 89). Hydrogen bonding between layers generates a three-dimensional network with $4.6\text{\AA} \times 3.4\text{\AA}$ wide channels (Figure 90).

[Figure 88]

[Figure 89]

[Figure 90]

When the hydroxyl substituents are simply changed from the *meta*- to the *ortho*-phenyl positions, an essentially two-dimensional layered material results. The peripheral hydroxyl groups of $\text{H}_2(\text{T}(2',6'\text{-DHP})\text{P})\bullet 4\text{EtOAc}$ induce a slight ruffling of the porphyrin macrocyclic rings and show strong directional hydrogen

bonding (Figure 91). Channels $3.0\text{\AA} \times 3.6\text{\AA}$ wide were formed by the packing of the layers (Figure 92). A similar packing motif was observed for the Zn(II) metalloporphyrin species.¹³⁵

[Figure 91]

[Figure 92]

3. Metal Ion Coordination Network Materials

In the last decade significant progress toward the rational construction of three-dimensional solids constructed from metal cations and organic molecules has been described.^{137,138} Of particular interest have been metal-organic coordination networks possessing nanoscale pores.¹³⁹ Metal-ligand interactions are often quite strong and should therefore provide a more robust framework than those based on van der Waals, hydrogen-bonds or π - π interactions.

Goldberg and coworkers have reported a number of inclusion compounds utilizing coordination of substituted tetraphenylporphyrins. Porphyrinic inclusion compounds of 5,10,15,20-tetra(4-pyridyl)porphyrin, $H_2(\text{TPyP})$, exhibited two general motifs.¹⁴⁰ Crystallization of the Zn(TPyP) complex resulted in a geometry featuring “zigzag” polymer chains in which the central Zn(II) ion is axially ligated by pyridyl substituent from an adjacent porphyrin (Figure 93). A similar arrangement was observed for inclusion compounds of aromatic solvents such as aniline (Figure 94). Only one pyridyl moiety per porphyrin building block coordinates to another porphyrin, thereby limiting ligand-metal interactions to one-dimensional polymeric chains. The guest species is located in a cavity adjacent to the pyridyl substituent *trans*- to the pyridyl axially ligating the metal center of an adjacent porphyrin in the zigzag chain.

[Figure 93]

[Figure 94]

A second motif encountered in tetrapyrrolylporphyrin systems is typified by inclusion compounds with wet methanol and water that produce three-dimensional coordination polymers. *Trans*-pyridyl substituents on a Zn(TPyP) were observed to axially ligate the metal centers of adjacent porphyrin moieties generating a polymeric chain in one dimension. Cross-linking in a second dimension occurs when the original porphyrin molecule is coordinated by two pyridyl moieties from two additional porphyrin molecules (Figure 95). The two remaining pyridyl groups participate in hydrogen-bonding with included water molecules. An intricate three dimensional framework results (Figure 96).

[Figure 95]

[Figure 96]

For inclusion solids of 5,10,15,20-tetra(4-cyano)phenylporphyrin, $H_2(\text{T(p-CN)PP})$, one of the four structural motifs encountered by Goldberg involved ligand to metal interactions.¹³³ Two-dimensional coordination networks similar to those observed for Zn(TPyP) materials were found in $Zn(\text{T(p-CN)PP}) \cdot 2C_6H_5NO_2$ (nitrobenzene), $Zn(\text{T(p-CN)PP}) \cdot CHCl_3$ (chloroform) and $Zn(\text{T(p-CN)PP}) \cdot C_7H_8O$ (anisole) materials (Figure 97). The guest species intercalate between the porphyrin layers (Figure 98).

[Figure 97]

[Figure 98]

Attempting to mimic the topology of the PtS structure, Robson and coworkers explored metal to ligand coordinative bonding as means to build more robust porphyrinic materials. They reported a structure in which Pd(TPyP) molecules are interconnected by Cd(II) centers.¹⁴¹ Each porphyrin is coordinated by two *trans* pyridyl donor porphyrin molecules and by two *cis* donor porphyrin molecules (Figure 99). The overall neutral framework $[Pd(\text{TPyP}) \cdot Cd(NO_3)_2 \cdot 8.6H_2O]$ features infinite interwoven layers of the porphyrin network.

[Figure 99]

In subsequent work, Robson and coworkers.¹⁴² reported three-dimensional network solids using the copper porphyrin complexes of 5,10,15,20-tetra-4'-pyridylporphyrin, Cu(TPyP), and 5,10,15,20-tetra-4'-cyanophenylporphyrin, Cu(TCNPP). Large extended channels (10-20Å) were observed in which tetrahedral Cu(I) ions (as opposed to the square planar Cu(II) ions bound to the center of the porphyrin ring) coordinate to pyridyl or cyano groups on the periphery of four porphyrin molecules. While the cationic frameworks were reported to occupy less than half the volume of the crystal, the void spaces were occupied by non-coordinating anions (BF₄⁻) and highly disordered solvent molecules (acetonitrile/nitrobenzene); upon removal of the anions, crystallinity was lost. In the tetrapyrindyl system, a single infinite PtS-like network was revealed (Figure 100). In contrast, in the tetracyano system, two independent, interpenetrating networks were delineated (Figure 101). The tetrahedral Cu(I) ions in the tetrapyrindyl system are located closer to the large pyridyl ring, which sterically restricts the inclusion of another independent network.

[Figure 100]

[Figure 101]

Anionic functional groups on the organic molecules circumvent the problems of a charged framework. Suslick and coworkers have explored the use of carboxylic acid-substituted porphyrins for building microporous porphyrinic solids. Tetraphenylporphyrins with carboxylate functionalities, i.e., 5,10,15,20-tetra-(4-carboxy)phenylporphyrin, H₂(TpCPP), and 5,10,15,20-tetra-(3,5-dicarboxy)phenylporphyrin, H₂(DiCarPP),¹⁴³ were selected as organic precursors. The carboxylic acids serve to solubilize of the large porphyrin molecules and, when deprotonated, to provide an anionic site for coordination of cationic metal atoms. A tightly packed and interpenetrated linear polymeric array was observed in the solid-state structure of the free base *p*-carboxylate porphyrin with Ca(II) bridging centers (Figure 102). Hydrogen-bonding between coordinated water molecules in the calcium layers was observed to stabilize the 3-dimensional structure.¹⁴⁴ Porous network material of the Co(III) and Mn(III) derivatives of *p*-carboxylate porphyrin have been characterized by X-ray crystallography and gas adsorption studies (Figures 103 and 104).¹⁴⁵ The tetrakis(di-*meta*-carboxyphenyl)porphyrin, H₂(DiCarPP), is anticipated to have a greater possibility of producing an intricate 3-dimensional structure due to the geometrical orientation of the carboxylic acid groups. In the crystal structure of the free base porphyrin, channels were observed to form in the packing of the discrete porphyrin molecules (Figure 105).¹⁴³

[Figure 102]

[Figure 103]

[Figure 104]

[Figure 105]

4. Porphyrin-Incorporated Zeolites

Zeolites are crystalline alumina-silica based open anionic framework structures with uniformly sized, rigid pores and channels. Incorporation of porphyrins into zeolites has been explored as means to biomimetic oxidation catalysts.¹⁴⁶

The initial efforts to combine porphyrins with zeolites resulted in materials in which the porphyrins were supported on the external zeolite surfaces rather than encapsulated inside the pores. The first of this type of material was reported by Bedioui and coworkers^{147,148} in which the Mn(III), Co(III) and Fe(III) metalated species of multi-charged 5,10,15,20-tetra(4-*N*-methylpyridinium)porphyrins, H₂(TMPyP), were adsorbed onto zeolite Y (faujasite) surfaces. The electrochemical behavior of these electrocatalytic surface materials was studied by cyclic voltammetry. Subsequent work extended the inorganic supports to include ZSM-5 and EMC-2 zeolites and the VPI-5 molecular sieve.¹⁴⁹ A significant positive shift of the electrochemical potential value of Mn^{III}/Mn^{II} redox pair was noted for the porphyrins adsorbed on zeolite surfaces (up to +380 mV in DMSO/H₂O). The effect of the interaction of the negatively charged zeolite surface with the metal ion is credited for this result.

Mallouk and co-workers explored the electrochemistry and photochemical evolution of hydrogen from water using a zeolite modified electrode. Methylviologen (MV²⁺) was encapsulated in platinumized zeolite L powder onto which Zn(TMPyP⁴⁺) was externally adsorbed (Figure 106).¹⁵⁰ Taking advantage of the zeolite microstructure in an attempt to construct an artificial photosynthetic system, addition of EDTA as an electron donor resulted in

production of hydrogen from aqueous solutions. Substitution of the larger tetra(trimethylamino)-4-phenylporphyrin Zn(II) derivative, inhibited evolution of hydrogen gas from a similar system. Examining the electrochemistry of adsorbed Zn(TMPyP)Cl and Zn(TMPyP)Cl on zeolite Y, a positive shift of the reduction potential by 200 mV was reported versus aqueous solution.¹⁵¹

[Figure 106]

Other zeolitic materials with adsorbed porphyrins on external surface include the immobilization of Sn(TMPyP)Cl₂ and Sn(TPyP)Cl₂ on zeolite Y for use as a solid photosensitizer material in the photodegradation of organic substrates.¹⁵² Zeolite supported Fe(T(*n*-MPy)P) (*n* = 2, 3 or 4) was explored in heterogeneous catalytic autoxidations of sulfite. It was observed that the *ortho*-methyl pyridyl substituted porphyrinic materials demonstrated approximately twice the catalytic activity of the *meta*- and *para*-substituted systems.¹⁵³ A Cu(TPP)/zeolite Y material was coated onto an electrode as part of a carbon paste to be used as an electrochemical sensor. No catalytic activity was noted when glutathione was used as a substrate for electrooxidation, cysteine was observed to block electrooxidation, and efficient activity for the electrocatalytic oxidation of hydrazine was observed. The authors cited this as an example of conferred selectivity due to the presence of the Cu(TPP)/zeolite material (Figure 107).¹⁵⁴

[Figure 107]

The first of the so-called “ship-in-bottle” porphyrin systems in which the porphyrin macrocycle is synthesized from molecular precursors inside the zeolite cavities was reported by Tatsumi and coworkers.¹⁵⁵ Refluxing pyrrole and acetaldehyde under Rothmund conditions in the presence of ion-exchanged zeolite Y led to the formation of metalated 5,10,15,20-tetramethylporphyrin, H₂(TMP) within the zeolitic pore structure. H₂(TMP) is cited as being sterically amenable to the internal zeolite pores. Diffuse reflectance UV-Vis spectroscopy was used to characterize the materials (Figure 108). Significantly increased yields of cyclohexanol and cyclohexane from the oxidative conversion of cyclohexane were reported for the ion-exchanged zeolite complexes of Mn(II) and Fe(II) complexes of TMP versus the free metalloporphyrins.

[Figure 108]

The dioxygen affinity of Co(TMP) encapsulated in zeolite Y by similar “ship-in-bottle” methodology was studied by Govind et al.¹⁵⁶ The porphyrin-free zeolite exhibits quantitatively similar absorption isotherms for both oxygen and argon. In comparison, the Co(TMP) encapsulated zeolite compound was observed to absorb eight times the amount of oxygen to argon (Figure 109).

[Figure 109]

A larger pore zeolite, MCM-41, was used for the first reported encapsulation of a tetraphenylporphyrin and the first porphyrin-ligated second row transition metal. Surface modification of the zeolite with 3-aminopropyltriethoxysilane (APTES) was necessary to achieve encapsulation of ruthenium (II) 5,10,15,20-tetra(4-chlorophenyl)porphyrin, Ru(T(p-Cl)PP)(CO)(EtOH). The encapsulated porphyrin/zeolite material was characterized by vibrational and diffuse reflectance spectroscopy and powder x-ray diffraction (Figure 110). Twenty to forty times higher product turnovers were reported for oxidative catalysis of alkene substrates by *tert*-butylhydroperoxide with the porphyrin/MCM-41 material versus free Ru(T(p-Cl)PP)(CO)(EtOH).¹⁵⁷

[Figure 110]

Kevan and coworkers synthesized, via physisorption, H₂(TPP) encapsulated within mesoporous MCM-41 hosts. Generated by photoinduced electron transfer, the long-lived H₂(TPP^{•+}) cation was characterized by electron spin resonance (ESR) and diffuse reflectance electronic spectroscopy (Figure 111). For a series of (H₂(TPP)/C_n-MCM-41, C_n = C₁₀, C₁₂, C₁₄ and C₁₆) materials, an increase in photoyield was observed to correspond with an

increase in alkyl chain length (causing increased pore size). The photoionization efficiency was observed to increase along the series AlMCM-41 < MCM-41 < TiMCM-41.¹⁵⁸

[Figure 111]

The first inverse of the “ship-in-bottle” synthesis, in which the zeolite cage is constructed around a porphyrin template, was reported by Li and Zhan.¹⁵⁹ The Fe(II) and Mn(II) derivatives of tetra(*N,N,N*-trimethylanilinium)porphyrin and H₂(TMPyP) were used as cationic templates in zeolite hydrothermal synthesis. Attempts to incorporate an anionic porphyrin species, metallo-tetra(4-sulfonatophenyl)porphyrin, were unsuccessful; and trials with neutral TPP species resulted in trace encapsulation. High activity for the catalytic oxidation of cyclohexene by *tert*-butyl hydroperoxide was reported.

Using similar methodology, encapsulation of the positively charged species 5,10,15,20-tetra(5-trimethylaminopentyl)porphyrin, H₂(TMAP), in MCM-41 was reported by Stein and coworkers (Figure 112). Free base porphyrins were metalated with Cu(II), Ni(II) or Fe(II) ions subsequent to zeolite incorporation. For comparison, H₂(TMAP) was also encapsulated by ion-exchange. It was cited by comparison of UV-Vis spectral intensities that porphyrins incorporated via ion-exchange did not remain isolated from other porphyrin species and the surrounding zeolite framework. The opposite was observed in the material encapsulated as a template during hydrothermal preparation of the zeolite. The catalytic activity of the Cu(TMAP)/MCM-41 material was explored.¹⁶⁰

[Figure 112]

5. Clays and Layered Materials Incorporating Porphyrins

Metalloporphyrins catalyze a large number of reactions including important biological oxidations.[Suslick, 1996 #4; Collman, 1993 #67; Sheldon, 1994 #69; Groves, 1997 #68] There has been increased interest in supported catalysts based on such metalloporphyrins absorbs or covalently linked to polymer systems. Organic polymers,¹⁶¹ and inorganic supports such as silica,¹⁶² and zeolites,¹⁶³⁻¹⁶⁵ have been to capture these catalysts. Layered materials that are able to intercalate neutral or ionic guests into the interlayer spaces offer unique opportunity into this research area. Through the incorporation of a guest species into a layered host, novel solids may be engineered with desirable physical and chemical properties. Many layered materials such as clays, metal dichalcogenides, metal phosphate and phosphonates have been studied as potential catalysts. The synthetic methods of these intercalated materials involved co-precipitation or ion-exchange and are straightforward.

Clays are colloidal layered hydrous aluminosilicates. There are relatively few examples of porphyrin intercalation into clays reported, mostly with either smectite clays or layered double hydroxides (LDH). Smectite clays consist of negatively charged layered aluminosilicate sheets. These sheets are separated by cations and water molecules. The layers are constructed from tetrahedral SiO₄ and octahedral AlO₆. The layer charge originates from the substitution of Al(III) by Mg(II). The clay layers are held together through weak dipole and van der Waals forces and can be easily separated by insertion of charged-balanced cations. LDHs are available as naturally occurring minerals and as synthetic materials, and consist of positively charged mixed metal hydroxide layers that are charge-balanced by interlayered anions.

a. Smectite clays

Porphyrins were first introduced into clays in 1977 by the physical absorption of porphyrin molecules into montmorillonite in aqueous solutions.¹⁶⁶ The most common examples are the binding of tetra-cationic M(TMPyP) porphyrins (M = Co(II), Mn(III), Fe(III)) into montmorillonite clays. Co(TMPyP)⁺⁴ was the first porphyrin to be intercalated into montmorillonite by ion exchange in acid solution.¹⁶⁷ The interlayer distance expanded from 27Å to 37Å upon intercalation. UV-visible studies revealed the retention of cobalt ions in the porphyrin molecules. Mansuy and coworkers have extended this approach and prepared the Mn-porphyrins intercalated materials and found it to be an efficient alkene epoxidation and alkane hydroxylation catalyst.¹⁶⁸ Additionally, the catalyst exhibited a marked shape selectivity in favor of small linear alkanes when compared to a more bulky substrates. It was also shown that the intercalated solid obtained did not release its porphyrin even after week-long extraction with CH₃CN. Recently, Carrado, and Wasserman examined the complexation chemistry of Cu(II) and Fe(III) with

TMPyP within the interlayers of smectite clays.¹⁶⁹ They demonstrated that Cu(II) porphyrins are stable within the slightly acidic clay environments and that the free base porphyrin can be metalated inside a Cu(II)-exchanged clay. Unlike the copper moieties, Fe(III) ions do not complex the free base porphyrin inside the clays.

Another method for the intercalation of metalloporphyrins into clays has been explored using porphyrins and metalloporphyrins as organic templates in the hydrothermal synthesis of layered silicates.¹⁷⁰ X-ray powder diffraction data indicated that the porphyrins are intercalated parallel between the silicate layers. Microanalysis and UV-visible diffuse reflectance spectra indicated that the porphyrins are incorporated intact.

b. Layered Double Hydroxides and Other Layered Materials

Anionic porphyrins and metalloporphyrins can be ion-exchanged into layered double hydroxide (LDH) materials (Figure 113). The first example of an LDH-porphyrin composite material was reported by Kato and coworkers in 1989.¹⁷¹ The X-ray powder diffraction pattern of the intercalated material showed the d-spacing increased to 22.4Å from 8.0Å upon intercalation. This increase in the gallery height strongly indicated that the porphyrin were arranged perpendicular to the LDH layers.

[Figure 113]

Tetra-anionic Mn^{III}(TSPP)-LDH was prepared by anion-exchange.¹⁷² The resulting LDH material contained 2.5 to 4.5% of Mn-porphyrin; even after prolong soaking in methanol and water, the metalloporphyrin was not extracted. More recently, Besse and coworkers reported the intercalation of carboxylate (H₂(TpCPP)) and sulfonate (H₂(TSPP)) porphyrins in LDH systems by coprecipitation and anionic exchange.¹⁷³ Powder X-ray diffraction data and UV-visible diffuse reflectance absorption spectra of the intercalated LDH show complete intercalation. Interlayer d-spacing increased from 18.5Å for H₂(ToCPP)-LDH to 22.9Å for H₂(pTSPP)-LDH and 22.7Å for H₂(TpCPP)-LDH. Several orientations of the porphyrin molecules between the LDH were proposed (Figure 114). The authors suggest that the interlayer arrangement is determined by both the layer charge density of the host materials and the isomeric position of the anionic groups substituted on the guest molecules.

[Figure 114]

Binding of tetracationic porphyrins on layered antimony hydrogen phosphate and zirconium hydrogen phosphate (α -ZrP) have been reported by Thompson and coworkers.¹⁷⁴ Both monolayer and bilayer guest structures have been prepared with the heme guests adopting parallel or tilted orientation relative to the host layers. The authors argue that the orientation results from maximization of electrostatic and hydrogen-bonding interactions between the host and the guest.

From the work mentioned above, it is clear that clay-intercalation of porphyrins can be done efficiently. The rapid development of materials such as larger-pore pillared clays should lead to more intense exploration of this area.

B. Conductive Polymers and Ferroelectrics

Studies in the areas of conductive polymers and ferroelectric materials constitute a relatively small subset of porphyrin materials research. Nonetheless, the versatility of porphyrins has allowed for some interesting and useful results in these areas. We will examine the variety of approaches toward the creation of porphyrin-based conductive polymers and the potential applicability of porphyrinic polymers as ferroelectric materials.

1. Conductive Porphyrin Polymers

Electrical conductivity of polymers continues to be one of the most important research areas for materials science. The conductivity of metals (typically $10^2 \sim 10^3 \Omega^{-1}\text{cm}^{-1}$ at room temperature) is generally higher than for semiconductors, but it is the temperature dependence that truly defines the difference: electrical conductivity of metallic substances increases with decreasing temperature, while that of a semiconductor decreases.¹⁷⁵ The interest in superconducting materials parallels the interest in synthetic metals. In a sense, the copper oxide high temperature superconductors (e.g., YBa₂Cu₃O_{7-x} with T_c ~ 95 K) are two dimensional coordination polymers, but we will not discuss them further here.¹⁷⁶⁻¹⁷⁸

Porphyrins constitute a versatile building block for the preparation of conductive polymers. The large π system of porphyrins and metalloporphyrins yields a HOMO and LUMO which are generally separated by only 2 eV.¹⁷⁹ This gap can be narrowed via polymerization or additional conjugation, leading to interesting conductivity possibilities. In addition to conduction through the π system, metal-metal conductivity is possible within a chain of metalloporphyrins. Because porphyrins are able to coordinate a wide range of metals, conductivity is readily tunable in these cases.

a. Shish Kebab Porphyrin Polymers

The "shish kebab" approach¹⁸⁰⁻¹⁸² yields a class of coordination polymers based on stacked macrocyclic metal complexes (Figure 115). Here, macrocyclic complexes are linked together by axial coordination of bridging ligands. Until recently, "shish kebab" polymers with bridging ligands larger than a single atom were rare. $[\text{Sn}^{\text{IV}}(\text{OEP})(\text{pimelate})]_{\infty}$ and $[\text{Zr}(\text{OEP})(\text{succinate})]_{\infty}$ were two early examples.¹⁸³ In the late seventies, Hanack et al. started to prepare a large family of such polymers employing phthalocyanines of the type $[\text{M}(\text{Pc})(\text{L-L})]_{\infty}$.¹⁸¹

[Figure 115]

Collman and coworkers have reported similar "shish-kebab" polymers of the type $[\text{M}(\text{OEP})(\text{L-L})]_{\infty}$ ($\text{M} = \text{Fe}$, Ru , Os , and $\text{L-L} = \text{pyz}$, bpy , dabco) and examined their conductivities.^{182,184,185} Many of these "shish kebab" coordination polymers can be doped with iodine, which drastically increases their conductivity (e.g., $\sigma_{300\text{K}} = 1 \times 10^{-6} \Omega^{-1}\text{cm}^{-1}$ for $[\text{Fe}^{\text{II}}(\text{Pc})(\text{pyz})]_{\infty}$; $\sigma_{300\text{K}} = 2 \times 10^{-1} \Omega^{-1}\text{cm}^{-1}$ for $[\text{Fe}^{\text{II}}(\text{Pc})(\text{pyz})\text{I}_{2.54}]_{\infty}$). The conductivity of these doped "shish kebab" polymers depends on the interaction of the metal d_{π} orbitals with the π^* level of the bridging ligand. Collman et al. found that the metal-metal communication is greater for the better π -bonding metals (e.g., $\text{Os} > \text{Ru} > \text{Fe}$) and the more π -acidic bridging ligand (e.g., $\text{pyz} > \text{bpy} \gg \text{dabco}$). The X-ray single crystal structure of the related non-macrocyclic metal complex $[\text{Co}^{\text{II}}(\text{dmgH})_2(\text{pyz})]_{\infty}$ confirmed that the polymeric "shish kebab" type structure can be formed with symmetric multi-atom bridges.¹⁸⁶

b. Covalent, Conjugated Porphyrin Polymers

Porphyrins linked with conjugated organic bridges form another subclass of conductive porphyrin materials. Work toward such polymers was done by Crossley and coworkers, who synthesized linearly conjugated porphyrin systems.¹⁷⁹ Seen in Figure 116 is their conjugated tetrakis(porphyrin) system. Preliminary spectroscopic data on this system indicated a significant decrease in the HOMO-LUMO gap (by *ca.* 0.8 eV) compared with the porphyrin monomer. In related studies, Yu et al. used the Heck coupling reaction to synthesize conjugated porphyrinic polymers.¹⁸⁷ A series of polymers (Figure 117) were generated with M_w values of 5,000 to 46,000. The polymers were soluble in a range of organic solvents and were cast as optical films onto glass slides. Their conductivities were studied, showing a steady increase in current upon photo-irradiation.

[Figure 116]

[Figure 117]

Recent studies by Jones and coworkers have produced conjugated porphyrin polymers with oligophenylenevinylene bridges.^{188,189} Using the Wittig reaction, as illustrated in Figure 118, a series of polymers were synthesized, labeled PP1 through PP3. The molecular weights, as determined by GPC, were inversely proportional to bridge length, ranging from $M_n = 6692$ (PP3) to 12230 (PP1). To increase solubility of the polymers in organic solvents, long alkoxy groups were appended to the bridges, which allowed casting of porphyrin films from toluene solution. Preliminary results showed that the non-doped polymers had conductivities of less than $10^{-12} \Omega^{-1}\text{cm}^{-1}$. Doping with nitromethane solutions of anhydrous FeCl_3 increased conductivities to approximately $10^{-6} \Omega^{-1}\text{cm}^{-1}$. The visible spectrum of the doped polymer, which showed red shifting of the absorption bands relative to the porphyrin monomer, was indicative of the narrowed HOMO-LUMO gap.

[Figure 118]

c. Conductive Porphyrin-Linked Polymers and Porphyrin Arrays

Another approach taken toward the creation of porphyrin-containing conductive polymers has been to incorporate porphyrins into the backbone of traditional conductive polymers. This approach has been studied extensively by Shimidzu and coworkers.^{190,191} As shown in Figure 119, P(TPP)(Cl)₂ can react with thienyl or oligothienyl alcohols to generate the corresponding polymer precursors. Electrochemical oxidation of the thiophene-containing precursor gives the polymer. These types of polymers have also been built two dimensionally via electrochemical polymerization of 5,10,15,20-oligothienyl substituted porphyrins. The 1-D polymers are particularly interesting in that their conductivities are enhanced by photoirradiation. The conductivities of poly-2 and poly-3 were $1.2 \times 10^{-9} \Omega^{-1}\text{cm}^{-1}$ and $5.1 \times 10^{-8} \Omega^{-1}\text{cm}^{-1}$, respectively, under dark conditions. When irradiated with photons from a 500 W Xe lamp, conductivity enhancements of greater than threefold were seen.

[Figure 119]

2. Ferroelectric Porphyrin Materials

Very little work has been done in the development of coordination polymers as molecular-based ferroelectric materials. Ferroelectrics carry a permanent, macroscopic electric dipole moment (*i.e.*, polarization) in the absence of electric field. Furthermore, the polarization of ferroelectric materials can be switched with the application of an external electric field. Ferroelectrics have unusual electro-optical, photorefractive and pyroelectric properties. They can be fabricated into electronic oscillators, high frequency filters, electroacoustic converters, pyroelectric radiant-energy receivers, and nonlinear capacitive elements. Most ferroelectrics are metal oxides.¹⁹²⁻¹⁹⁴ (such as BaTiO₃ and LiNbO₃); a few are liquid crystal materials.¹⁹⁵⁻¹⁹⁸

In a further development of the "shish-kabob" class of polymers, metalloporphyrin coordination polymers have been suggested as possible ferroelectric materials.^{180,199,200} Coordination polymers of non-planar metalloporphyrins with *non-symmetrical* bridging ligands carry an aligned dipole moment along the stacking axis (Figure 120). The dipole moment originates from the charge separation between the bowl-shaped porphyrinato core and the metal atom (Figure 121). The metal atom tends to be pulled out of the porphyrin plane by strong axial ligands. If the metalloporphyrin has two different axial ligands, the metal atom will be pulled toward one side, depending on relative ligation strength and steric demands. Various monomeric structures of metalloporphyrins.²⁰¹⁻²⁰⁴ suggest that a double-well potential can be present, as shown schematically in Figure 122. By analogy to the metal oxide compounds,²⁰⁵⁻²⁰⁷ the direction of the bulk polarization in such coordination polymers may respond to an external field.

[Figure 120]

[Figure 121]

Suslick and Chen have prepared several one-dimensional coordination polymers of metalloporphyrins with non-symmetric bridging ligands (Figure 123) as candidates for molecular ferroelectric materials.^{180,199,200} Metalloporphyrin complexes of Fe(II), Fe(III) and Sn(IV) were examined. Structures determined by single-crystal X-ray diffraction include [Fe^{II}(TPP)(pyCN)]_∞, [Fe^{III}(TPP)(pyCO₂)]_∞, and [Fe^{III}(TPP)(ImPhO)]_∞ (Figure 124). The chain alignment of the bridging ligand is disordered in [Fe^{II}(TPP)(pyCN)]_∞, antiparallel in [Fe^{III}(TPP)(pyCO₂)]_∞, but aligned and polar in [Fe^{III}(TPP)(ImPhO)]_∞. [Fe^{III}(TPP)(ImPhO)]_∞ crystallizes in a non-centrosymmetric space group, *Pna2*₁, with the normal to the metalloporphyrin ring about 20° off the c-axis. Therefore, a net dipole moment or macroscopic polarization parallel to the c-axis can be expected only from [Fe^{III}(TPP)(ImPhO)]_∞. The small size of the doming of the porphyrin in this complex, combined with the large unit cell dimensions, suggests that the spontaneous polarization of [Fe^{III}(TPP)(ImPhO)]_∞ will be much smaller than that of BaTiO₃.²⁰⁸⁻²¹⁰ The organic portion of the Fe^{III}(TPP)(ImPhO) polymer does not contribute much to the dipole moment, although it is the major component in the unit cell.

[Figure 122]

[Figure 123]

[Figure 124]

C. Porphyrin-Based Chemical Sensors

Because of their inherent stability, unique optical properties, and synthetic versatility, porphyrins and metalloporphyrins are excellent candidates for a variety of sensing materials applications. Research in this area has

focused on incorporation of synthetic porphyrins and metalloporphyrins into a variety of material matrices, such as polymers, glasses, and Langmuir-Blodgett (LB) films. Substantial work has been done in the areas of solution and gas phase sensing, and highlights of both areas will be discussed. We will also briefly examine molecular recognition and receptor studies, as developments in these areas figure to further the development of porphyrin-based sensing materials.

1. Gas Sensors

Considering the well-understood ability of heme to bind a variety of gases, such as NO, CO₂, and O₂, porphyrins would indeed seem a suitable choice for the detection of gaseous species. During the 1990s, much work has been done involving the porphyrin-based detection of a series of gases, such as oxygen, ammonia, and chlorine. In addition, recent work has entailed utilization of metalloporphyrin arrays for the detection of organic odorants, such as amines, thiols, and phosphines. Many gas sensors take advantage of analyte binding to the porphyrin metal center, which gives a detectable optical change. Other methods, such as the use of piezoelectric substrates coated with porphyrin films, have also been utilized for gas detection.

a. Oxygen

The use of metalloporphyrin-based materials for the detection of molecular oxygen is well developed. One approach that has been employed extensively involves the well known phenomenon of quenching of metalloporphyrin phosphorescence by O₂. Due to their high phosphorescence quantum yields and short triplet lifetimes, platinum and palladium porphyrins were originally suggested as probes for oxygen by Eastwood and Gouterman.²¹¹ The quenching of porphyrin phosphorescence is described by the Stern-Volmer relationship:

$$I_0/I = 1 + K_{sv}(pO_2)$$

where I_0 and I are the phosphorescence intensities in the absence and presence of the quencher, respectively, K_{sv} is the Stern-Volmer constant, and pO_2 is the partial pressure of O₂. Since $1/K_{sv}$ is equal to the pO_2 level at which the phosphorescence intensity is reduced by 50%, it is commonly reported as a characteristic for oxygen detectors. Clearly, K_{sv} will be highly dependent upon the oxygen permeability of the matrix in which the porphyrin is immobilized. Hence, much of the research in this area focuses on these matrices, such as polymers or sol-gel glasses, in addition to the synthesis of new porphyrins.

Okura and coworkers have utilized sol-gels to make optically transparent glasses containing Pt(OEP).²¹² This approach is aimed at creating chemically inert, photostable materials which can be used in a variety of environments. As shown in Figure 125, the response is rapid, with a 5 second 90% response time (t_{90}). Reversibility was demonstrated upon exposure to 100% nitrogen followed by 100% oxygen. The sensor shows nearly linear behavior of a range from 0 to 100% oxygen concentration, but no estimate of detection limit was given. One major concern with the use of porphyrins for gas sensing is photo-bleaching. In an effort to enhance porphyrin stability toward photodegradation, Wong and coworkers have used halogenated platinum porphyrins immobilized inside silicone films as materials for oxygen sensing.²¹³ The porphyrins, Pt(TDCPP), Pt(TFMPP), and Pt(Br₈TMP) (where TDCPP = 5,10,15,20-tetra(2,6-dichlorophenyl)porphyrinate, TFMPP = 5,10,15,20-tetra(3,5-bis(trifluoromethyl)phenyl)porphyrinate, and Br₈TMP = 5,10,15,20-tetramesityl-β-octabromoporphyrinate), were chosen to provide enhanced stability due to their increased oxidation potentials compared to Pt(TPP). The best performance was observed for the Pt(TFMPP) film, with a ($1/K_{sv}$) value of 3.7 torr and a response time of 14 seconds. Stability studies on the porphyrin/rubber films revealed that all of the halogenated porphyrins were indeed more stable than Pt(TPP). After 48 hours of illumination, the Pt(TPP) luminescence intensity was only 43% of its original value, while (Br₈TMP)Pt remained at 93%. Another approach towards enhanced stability is the use of porphyrin ketone complexes. For instance, Hartmann and coworkers have utilized platinum(II) and palladium(II) octaethylporphyrin ketones (Figure 126) in polystyrene matrices for oxygen sensing.²¹⁴ Films of Pt(OEPK) have been reported to be ten times more stable than their Pt(OEP) counterparts to photodegradation.²¹⁵ The palladium-based sensor gave an excellent ($1/K_{sv}$) value of 0.59 torr.

[Figure 125]

[Figure 126]

Mills and coworkers have recently employed Pt(OEP) and Pd(OEP) in a variety of different encapsulating matrices for the detection of molecular oxygen.²¹⁵ Using cellulose acetate butyrate (CAB), poly(methyl methacrylate) (PMMA), and PMMA/CAB polymer blends to encapsulate the porphyrins on glass slide supports, the

researchers studied the K_{sv} and response time variation with polymer composition. They found that amounts of tributyl phosphate (TBP) plasticizer dramatically increased both the sensitivity and response times of the film. As shown in Figure 127, both the pO_2 and the t_{90} response time decrease significantly to give minimum values at about 120 parts per hundred resin (phr) of plasticizer. The $(1/K_{sv})$ value for Pd(OEP) in CAB/plasticizer was 0.24 torr, while the 90% response time was 1.4 seconds.

[Figure 127]

Impressive response times for detection of oxygen via luminescent porphyrins have been demonstrated by Callis, Gouterman, and coworkers.²¹⁶ Using special instrumentation designed to characterize coatings for video luminescent barometry (VLB), the researchers demonstrated submillisecond response times upon exposing immobilized Pt(OEP) to ambient air at pressures ranging from 0.1 to 700 torr. This type of system has been studied in an effort to provide aerodynamicists with a method for determining surface pressures during wind-tunnel tests.²¹⁷

Reversible binding of oxygen to cobalt porphyrins forms the basis for another series of oxygen sensors. Systems involving cobalt porphyrins have employed a variety of signal transduction techniques. Work by Oblesby, Leighty, Collman et al. has utilized synthetic cobalt porphyrins for surface acoustic wave (SAW) sensing of oxygen.²¹⁸ The SAW sensor, which registers a resonance frequency decrease upon adsorption of an analyte, is coated with the porphyrin, both in the presence and absence of an imidazole or pyridine containing copolymer. Porphyrins used for the study were the cobalt(II) picket-fence porphyrin, Co(PFP),²¹⁹ and cobalt(II) picnic basket porphyrins, Co(PBP)²²⁰ (Figure 128). The sensor response to oxygen is reversible, though some hysteresis is noted, which is due to slow diffusion of O_2 out of the polymer matrix. The picnic-basket porphyrins are particularly interesting because they allow easy tailoring of the oxygen binding constant, either by changing the central metal ion or by altering the length of the bridge or "handle". This allows for sensing over a wide range of oxygen concentrations. In related studies, Pretsch and coworkers have utilized picket fence cobalt porphyrins for optical detection of oxygen.²²¹ Immobilized on poly(octylmethacrylate-*co*-1-vinylimidazole) or poly(2,2,3,3,4,4,5,5-octafluoropentylmethacrylate-*co*-1-vinylimidazole) polymer membranes, the porphyrin gives a readily detectable shift in its visible absorbance spectrum upon binding of molecular oxygen. The useful range of the sensor is 1-1000 kPa oxygen partial pressure, or 0.1-100% of atmospheric pressure. Optimum response is achieved with the fluorinated membrane, at a thickness of 20 μm , which gave a 90% response time range of 5-15 seconds.

[Figure 128]

b. Other Gases

Porphyrin-based sensors have also been used for the detection of gases such as ammonia, hydrazine, and NO. Narayanaswamy and coworkers have developed optical ammonia sensing films based upon immobilized Zn(TPP) in silicone rubber.²²² Upon ligation of the metal center, the well-known phenomena of visible and/or fluorescence spectral shifts can be used to quantify exposure to the analyte. The Zn(TPP)-silicone films gave a linear range of 0-8.5 ppm NH_3 with a detection limit of 0.7 ppm. The equilibration time upon exposure was found to be 4 minutes with good reversibility of the ligation. This approach, of course, could be expanded to other amines, as well as to other ligating vapors. Ammonia detection has also been studied by Valli and coworkers, who have explored Langmuir-Blodgett films grown from a conjugated dimer of nickel(II) octaethylporphyrin.²²³ (see Figure 129). The films were created by combining the dimer with arachidic acid, followed by deposition onto hydrophobic quartz substrates. Gold contacts were sputtered onto the film ends to allow for resistivity measurements as a function of vapor exposure. As seen in Figure 130, the sensor demonstrates a series of equilibria as the ammonia concentration is increased in a stepwise fashion, followed by a return to the original resistance value upon exposure to air. At 500 ppm of NH_3 , the response time is 200 seconds, with a recovery time of 500 seconds. The authors postulate that the decreased resistivity upon analyte exposure results from electronic holes created in the porphyrin film upon electron transfer to ammonia molecules.

[Figure 129]

[Figure 130]

Detection of nitric oxide has become particularly important in light of its regulatory role in many physiological processes. In an example of NO detection via porphyrin-based sensors, Malinski and coworkers have used microelectrode sensors consisting of layers of a polymeric porphyrin and Nafion deposited on a thermally sharpened carbon fiber.²²⁴ Tetrakis(3-methoxy-4-hydroxyphenyl)porphyrinatonicel(II) was polymerized onto the fiber electrochemically from a solution of 0.1 M NaOH containing the monomer. The resulting sensor operates based on the electrochemical oxidation of NO at the porphyrin-doped electrode. A 10 ms response time and a detection limit of 10 nM have been observed, and the sensor has been applied to NO analysis from single endothelial cells in the pulmonary artery as well as for NO quantitation in the blood.

c. Porphyrin Array Vapor Detectors

Array based sensing has emerged as a powerful approach to vapor detection. Combinations of chemically diverse sensing elements are capable of responding to a variety of analytes. Materials such as polymers, functionalized self-assembled monolayers, metal oxides, and dendrimers have been used in electronic devices via coupling with piezoelectric, SAW, and semiconductor transducers. In notable examples, Lewis and coworkers have utilized composites of carbon black and polymers for electronic sensing,²²⁵ while immobilization of fluorescent dyes in polymer matrices has allowed for optical detection of non-ligating vapors by Walt et al.²²⁶ Much of the work in this area has been driven by a desire to mimic the mammalian sense of smell, which is based upon a large (approximately 1000 members) family of receptor cells.²²⁷ More than half of the receptors respond to any given odorant exposure,²²⁸ and create a temporal response signature that is mapped in the olfactory bulb and interpreted by the brain.

While much work has been done for the detection of non-ligating organic odorants, detection of metal-ligating vapors via array based sensing has been less explored. Included in this class of analytes are noxious ligands such as amines, phosphines, and thiols, as well as more toxic substances, e.g., nerve toxins such as Tabun. Due to their synthetic versatility and excellent chemical and thermal stability, metalloporphyrins are a natural choice for the detection of such species. Natale and coworkers have utilized metalloporphyrin films in piezoelectric sensing arrays, where they have shown some success in detection of ligating vapors and determination of food quality.^{229,230} Their approach has been to coat quartz crystalline microbalances with an array of porphyrins, consisting of Ru(TPP)(CO), Rh(TPP)Cl, Mn(TPP)Cl, Co(TPP), Sn(TPP)Cl₂, Co(TpNO₂PP), Co(Tp-OCH₃PP), and Mn-octamethylcorrole. Responses to different ligating species occur upon ligand binding, which induces mass changes detectable by the microbalances. As seen in Figure 131, the array gives high sensitivities for a series of ligating vapors, though the response is limited for alcohols and sulfur-based ligands. This type of array has been applied to the evaluation of quality of several types of foods, such as fish, meats, and wine.

[Figure 131]

Suslick et al. have recently exploited the colorimetric properties of metalloporphyrin arrays for detection of various ligating vapors.²³¹ Metalloporphyrin visible spectra are known to exhibit shifts in wavelength and intensity upon binding of axial ligands. These shifts produce color changes that are often quite noticeable. The color changes are dependent upon a variety of factors, but vary in large part based upon the degree of polarizability of the analyte.^{232,233} Upon exposure to a given analyte, therefore, an array of metalloporphyrins is expected to give a unique color change signature. A series of metalated tetraphenylporphyrins was prepared and spotted onto a reverse phase silica gel plate to give the detector shown in Figure 132. Subtraction of scanned images taken before and after exposure to analytes gives the color change profiles shown in the figure. All of the vapors studied did indeed reveal a unique color change pattern. Particularly notable is the fact that ligands of similar functionality, such as pyridine/hexylamine, or n-tributylphosphine/triethylphosphite, are readily distinguishable. Analyte concentrations of less than 1 ppm can be detected by the array. Ongoing work with this system involves incorporation of functionalized metalloporphyrins, such as dendrimer-metalloporphyrins, which will be discussed later.

[Figure 132]

2. Sensors for Solution Species

Porphyrin-based materials have been widely applied toward the analysis of several types of solution species, including ions and organic analytes. Much of the research in these areas is based upon incorporation of

metalloporphyrins into electrode membranes, where ion-porphyrin interactions can be monitored potentiometrically, or where electrochemical reactions with analyte substrates can be mediated by the porphyrin. As with gas sensors, this is a research area where molecular recognition studies will allow for continued progress.

a. Anion Detection

Detection of anions in solution via potentiometric techniques has been widely studied. If lipophilic electrode membrane materials are employed, the selectivity of the detector is based upon the solubility of the anions in the membrane layer. This gives rise to the Hofmeister pattern, whereby lipophilic anions are preferentially incorporated into the membrane, in the order $\text{ClO}_4^- > \text{IO}_4^- > \text{I}^- > \text{Br}^- > \text{Cl}^- > \text{HCO}_3^-$.²³⁴ Deviation from Hofmeister selectivity can be achieved by incorporating a range of compounds, including porphyrins, metallocorrins, and phthalocyanines, into the membrane. The varying affinities that anions have for the chosen macrocycle metal center can change the ion preference of the material. Porphyrins are also utilized because their synthetic versatility allows for creation of size-selective pockets about the metal center, lending additional selectivity. For instance, Meyerhoff and coworkers have examined various synthetic manganese porphyrins by incorporating them into PVC polymer membranes.²³⁵ The porphyrins, shown in Figure 133, were chosen to give a wide range of steric access and/or hydrophobicity to the metal center anion ligation site. Table 9 lists the anion selectivity coefficients for the membranes containing these porphyrins. The tetraphenylporphyrins, (2 and 3) deviate from the Hofmeister trend due to selectivity imparted by axial binding to the manganese center. The tetrahalonaphthylporphyrins (5,6,7) are even more exclusive of perchlorate and iodate, owing to their more hindered metal centers. Porphyrins 8 and 9, meanwhile, which contain nitrogenous axial ligands, destabilize anion coordination to the metal, restoring the Hofmeister selectivity. Improved affinity for salicylate was subsequently achieved by incorporation of $\text{Sn}(\text{TPP})\text{Cl}_2$ into the electrode membranes.²³⁶

[Figure 133]

[Table 9]

Zheng and coworkers have employed a similar methodology and have demonstrated that PVC membranes doped with indium tetraphenylporphyrin show high relative sensitivity to nitrite ions.²³⁷ Manganese and indium porphyrins immobilized in silicone by Paeng et al. have been used for the potentiometric analysis of serum chloride levels.²³⁸

Studies of synthetic porphyrin-based anion receptors should form the basis for more effective sensors. Metallocene-substituted porphyrins examined by Beer and coworkers have proven successful in the solution phase binding of ions such as chloride, bromide, and nitrate.²³⁹ The cobaltocenium-substituted and ferrocene-substituted porphyrins (Figure 134) bind ions in solution, as shown by ^1H NMR and electrochemical studies. The latter measurements reveal that the porphyrin and ferrocene redox potentials vary with bound ion. Studies of the various atropisomers of the ferrocene-substituted zinc porphyrin have shown interesting isomer-dependent selectivities. For example, the $\alpha,\alpha,\alpha,\beta$ isomer shows a preference for nitrate over chloride, where the other atropisomers show a preference for spherical ions such as chloride and bromide. In related work, Sessler and coworkers have shown sapphyrins to be potentially useful receptors for anion sensing. These expanded species are more basic than their porphyrin counterparts, and hence readily form dicationic species in solution.²⁴⁰ The positively charged dication core forms a site for anion binding. A deca-alkyl sapphyrin was originally shown to bind fluoride ion, as shown by the crystal structure in Figure 135.²⁴¹ The ion is believed to be stabilized via a combination of electrostatic and hydrogen bonding interactions. In more recent studies, Sessler et al. have found that sapphyrins appended to silica gel show high affinities for phosphate and arsenate, as well as an ability to separate a wide range of anionic species when used as HPLC solid phases.²⁴² These types of materials may be applicable to more specific anion sensing applications.

[Figure 134]

[Figure 135]

b. Cation Detection

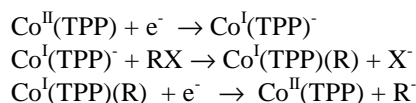
While detection of cations via porphyrin-based materials has been less explored than anion sensing, the ability of a porphyrin to coordinate different metals and the unique spectral signatures that result form the basis for metal ion detection. Use of free base porphyrins in polymer matrices has allowed for the detection of heavy metal ions by Ache et al.²⁴³ Immobilization of 5,10,15,20-tetrakis(4-N-methylpyridyl)porphyrin on Nafion membranes permitted detection of cadmium and mercury in solution with detection limits of 5×10^{-8} M and 2×10^{-7} M, respectively over a 20 minute measuring period. The method is subject to interferences from other metal ions, but the researchers were able to detect several ions simultaneously using pattern recognition techniques, such as principal component analysis. Sol-gel films doped with 5,10,15,20-tetra(p-sulfonatophenyl)porphyrin have also been used by Ache and coworkers for the fluorimetric determination of mercury in solution, with a detection limit of approximately 7×10^{-9} M.²⁴⁴

Porphyrin-doped electrodes have been employed for the electrochemical and potentiometric detection of nickel(II) in aqueous solutions. Malinski and coworkers have utilized polymeric tetrakis(3-methoxy-4-hydroxyphenyl)porphyrin, H₂(TMHPP), film electrodes for nickel determination.²⁴⁵ The films are grown by electrochemical deposition from a solution of 0.1 M NaOH containing 5×10^{-4} M Ni(TMHP). The film is then demetalated in acid solution, yielding a polymer that the authors postulate to have enhanced selectivity for nickel due to its formation from the nickel monomer. Using differential pulse voltammetry to monitor the Ni(II)/Ni(III) oxidation, a detection limit of 8×10^{-8} M was obtained for a 60 second exposure to a nickel containing solution. The calibration curve shown in Figure 136 shows linear response over a range of 10^{-7} to 2×10^{-6} M. In the presence of interferences (e.g., zinc(II), cadmium(II), or copper(II)), some reduction in signal is seen; however, no ion showed redox activity in the region of detection. Gupta and coworkers have utilized H₂(TPP) and H₂(TTP) in PVC-based membranes for the potentiometric detection of nickel(II).²⁴⁶ The sensor demonstrated linear response in the range of 5.6×10^{-6} - 1.0×10^{-1} M, with a response time of 20 seconds. The primary observed interferences were Co²⁺ and Na⁺ ions. Quantitative determination of Ni²⁺ in chocolate samples using this detector gave good agreement with values obtained from atomic absorption spectroscopy.

[Figure 136]

c. Sensors for Organic Molecules

Many current organic molecular sensors employing metalloporphyrins are based upon the ability of the porphyrin to act as a catalyst for the reduction or oxidation of organic substrates. This concept has been used by Saini and coworkers, who have recently used porphyrin-modified electrodes for the determination of organohalide species in aqueous solution.²⁴⁷ By precipitating (TPP)Co on a graphite foil working electrode, the researchers were able to induce the reduction of various organohalides, such as carbon tetrachloride, perchloroethylene, and iodobenzene. The sensor is believed to function via a porphyrin-mediated, two electron reduction pathway, shown below:



Amperometric studies, with a working potential of -500 mV, gave a detection limit of 0.75 ppm for carbon tetrachloride. The amperometric calibration curves for carbon tetrachloride and perchloroethylene are shown in Figure 137. Greatest sensitivities were seen for haloalkanes, with less sensitivity for haloalkenes or haloarenes. Interference from non-halogenated organics (e.g, ethanol, allyl alcohol, phenol) was not seen, though addition of phosphate ions gave slight decreases in response intensity. In related work, Priyantha and Weerabahu used Fe(TPP)Cl for the amperometric detection of the herbicide propanil.²⁴⁸ The porphyrin was coated on a glassy carbon working electrode, which was used for the reduction of 3,4-dichloropropionanilide, the main component of the herbicide. The resulting detector provided a detection limit of 80 μM .

[Figure 137]

As alluded to earlier in this section, studies of molecular receptors figure to provide a series of new sensors, particularly for the detection of solution phase species. Towards this end, a series of porphyrin complexes and assemblies have proven successful in assessing the selective binding of organic molecules. Design of shape selective

binding pockets and hydrogen bonding arrangements have proven especially successful using macrocyclic oligosaccharides. By using porphyrins as displaceable substrates of the binding sites, analysis of relative binding of other analytes can be easily monitored through visible spectroscopy: displacement of the porphyrin from within the macrocycle produce observable spectral shifts. For instance, morphine recognition has been probed by Sanders and coworkers via the synthesis of a porphyrin-cyclocholesterol molecular bowl, shown in Figure 138.²⁴⁹ Compared to tetrakis(3-methoxyphenyl)porphyrin, which was used as a reference compound, the bowl shows a binding constant for morphine 3.8×10^3 times higher, resulting from favorable hydrogen bonding interactions between the bowl and morphine molecule. The bowl also binds other amines such as codeine and pyridine, but with lower binding constants than for morphine. In similar fashion, a cyclodextrin-porphyrin assembly has been demonstrated to have high selectivity for pentachlorophenol (PCP) by Luong and coworkers.²⁵⁰ Shown in Figure 139, the assembly is organized via hydrogen bonds between the carboxylic acid groups of the tetracarboxy porphyrin and hydroxy groups on the cyclodextrin. PCP is well suited for the cyclodextrin-porphyrin assembly cavity, due to its proper size, sufficient hydrophobicity, and hydroxyl group, which can hydrogen bond to the pyrrole nitrogens of the porphyrin. Visible spectroscopy studies of Soret band shifting upon binding showed that of a range of chlorinated aromatic species, only PCP and 2,3,5,6-tetrachlorophenol exhibited binding.

[Figure 138]

[Figure 139]

Shinkai and coworkers have created a unique sugar sensing system based on the cooperative interactions of two boronic acid receptor moieties.²⁵¹ The first is linked to a zinc tetraphenylporphyrin, and the second to a coordinated pyridine. Binding of saccharides to the porphyrin-pyridine complex, as shown in Figure 140, produces spectral shifts. Studies in which solid sugars were extracted into dichloromethane solutions containing the receptor were conducted, and percentage of extracted sugar was determined via circular dichroism spectroscopy. Among a series of sugars, the highest affinities were seen for D and L configurations of fructose and arabinose.

[Figure 140]

Dendrimer-porphyrins are another class of molecular receptors which have been recently demonstrated to have interesting shape-selective ligand binding capabilities by Suslick et al.²⁵² Linking of first- and second-generation carboxylic acid dendrons to zinc tetrakis(3,5-dihydroxyphenyl)porphyrinate and zinc tetrakis(2,6-dihydroxyphenyl)porphyrinate produced a series of dendrimer-metalloporphyrins (Figure 141). Quantitative determination of the binding constants nitrogenous bases to the zinc were made using visible spectroscopy. The meta-substituted dendrimer-porphyrins interestingly show increased affinity for the bases relative to unhindered Zn(TPP), a phenomenon due to favorable interactions between the amines and the aromatic dendrimer structure. The ortho-substituted dendrimer-porphyrins, however, showed excellent shape-selectivity, as demonstrated by the $\log(K_{eq})$ values (Figure 142). Particularly striking for the ortho-substituted dendrimer porphyrins is the difference in binding affinity between linear and nonlinear amines, such as that between 4-phenylpyridine and quinine (K_{eq} difference $> 10^5$). This type of selectivity could potentially be exploited in sensors for ligating species in either solution or the gas phase.

[Figure 141]

[Figure 142]

IV. Conclusions

Because of their synthetic versatility and chemical robustness, porphyrins and metalloporphyrins are proving to be a very useful platform on which to tailor field-responsive and chemo-responsive materials. Diverse applications of porphyrins and metalloporphyrins to materials chemistry have been developed over the past decade, both for their optical properties and their applications as sensors.

Notably, porphyrins and metalloporphyrins have found applications as field-responsive materials, particularly for optoelectronic applications, including mesomorphic materials and optical-limiting coatings. Porphyrins show interesting second- and third-order NLO properties, due to their exceptionally large π -electron conjugation length. The primary attention has focused on third-order NLO properties and optical limiting materials. Improvements in the area of nonlinearity versus transparency trade-off should be possible via molecular engineering.

The molecular design of novel porphyrins possessing desired physical, optical and nonlinear optical properties for specific photonic applications remains a difficult, but often rational, challenge. Ingenuous designs and newly developed synthetic methodologies have also led to significant progress in the development of molecular optoelectronic porphyrinic materials. Long term stability against photodegradation remains an important problem to overcome, however, and may preclude effective devices for many molecular electronic applications.

The development of chemo-responsive materials based on porphyrins as highly porous, molecularly-based molecular sieves or shape-selective solid catalysts is currently under development. Porphyrins and metalloporphyrins have also been examined for a variety of sensor applications, which clearly represent an important emerging class of chemo-responsive materials. The unique spectral characteristics and synthetic versatility of porphyrins allow for a variety of sensing applications. In the case of oxygen detection via luminescent porphyrins, the sensing characteristics of the porphyrin are well established, and work on the immobilization matrix is the key to sensor performance. Other areas, such as array-based detection of organic vapors and detection of ionic species in solution, will depend upon continued development of well-designed receptors that exhibit high specificities.

V. Acknowledgments

The contributions from the Suslick research group reported herein have been supported generously by the National Institutes of Health (HL25934), the Department of Energy (DEFG0291ER45439), and the Department of Defense (DAAG55-97-1-0126). We gratefully acknowledge the early efforts by Drs. Chin-Ti Chen, Homer Chou, Christopher L. Hein, Philip A. Gorlin, and Bimal Patel in the development of this work.

VI. References

- 1) Suslick, K. S. *Comprehensive Supramolecular Chemistry; Bioinorganic Systems*; Elsevier: Oxford, 1996; Vol. 5.
- 2) Simon, J.; Bassoul, P. *Phthalocyanines: Properties and Applications*; Leznoff, C. C. and Lever, A. B. P., Ed.; VCH: New York, 1989; Vol. 2.
- 3) van Nostrum, C. F.; Nolte, R. J. M. *J. Chem. Soc., Chem. Commun.* **1996**, 2385.
- 4) Goodby, J. W.; Robinson, P. S.; Teo, B. K.; Cladis, P. E. *Mol. Cryst. Liq. Cryst.* **1980**, *56*, 303.
- 5) Gregg, B. A.; Fox, M. A.; Bard, A. J. *J. Amer. Chem. Soc.* **1989**, *111*, 3024.
- 6) Gregg, B. A.; Fox, M. A.; Bard, A. J. *J. Chem. Soc., Chem. Commun.* **1987**, 1134.
- 7) Schouten, P. G.; Warman, J. M.; de Haas, M. P.; Fox, M. A.; Pan, H.-L. *Nature* **1991**, *353*, 736.
- 8) Liu, C. Y.; Pan, H. L.; Tang, H.; Fox, M. A.; Bard, A. J. *J. Phys. Chem.* **1995**, *99*, 7632.
- 9) Gregg, B. A.; Fox, M. A.; Bard, A. J. *J. Phys. Chem.* **1990**, *94*, 1586.
- 10) Liu, C.-H.; Pan, H.-I.; Fox, M. A.; Bard, A. J. *Science* **1993**, *231*, 897.
- 11) Liu, C.-Y.; Pan, H. L.; Fox, M. A.; Bard, A. J. *Chem. Mater.* **1997**, *9*, 1422.
- 12) Doppelt, P.; Huille, S. *New J. Chem* **1990**, *14*, 607.
- 13) Shimizu, Y.; Ishikawa, A.; Kusabayashi, S. *Chem. Lett.* **1986**, 1041.
- 14) Sakaguchi, T.; Shimizu, Y.; Miya, M.; Fukumi, T.; Ohta, K.; Nagata, A. *Chem. Lett.* **1992**, 281.
- 15) Shimizu, Y.; Miya, M.; Nagata, A.; Ohta, K.; Matsumura, A.; Yamamoto, I.; Kusabayashi, S. *Chem. Lett.* **1991**, 25.
- 16) Shimizu, Y.; Miya, M.; Nagata, A. *Process for preparing ferromagnetic material*: European Patent #676775, 1995.
- 17) Kugimiya, S.-I.; Takemura, M. *Tetrahedron Lett.* **1990**, *31*, 3157.
- 18) Ohta, K.; Yamaguchi, N.; Yamamoto, I. *J. Mater. Chem.* **1998**, *8*, 2637.
- 19) Neumann, R.; Hugerat, M.; Michaeli, S.; Natt, A.; Bernitz, M.; Levanon, H. *Chem. Phys. Lett.* **1991**, *182*, 249.
- 20) Michaeli, S.; Hugerat, M.; Levanon, H.; Bernitz, M.; Natt, A.; Neumann, R. *J. Amer. Chem. Soc.* **1992**, *114*, 3612.
- 21) Griesar, K.; Athanassopoulou, M. A.; Bustamante, E. A. S.; Tomkowicz, Z.; Zaleski, A. J.; Haase, W. *Adv. Mater.* **1997**, *9*, 45.
- 22) van Nunen, J. L. M.; Folmer, B. F. B.; Nolte, R. J. M. *J. Amer. Chem. Soc.* **1997**, *119*, 283.
- 23) Patel, B. R.; Suslick, K. S. *J. Amer. Chem. Soc.* **1998**, *120*, 11802.
- 24) Gaspard, S.; Maillard, P.; Billard, J. *Mol. Cryst. Liq. Cryst.* **1985**, *123*, 369.
- 25) Bruce, D. W.; Dunmar, D. A.; Santa, L. S.; Wali, M. A. *J. Mater. Chem.* **1992**, *2*, 363.
- 26) Bruce, D. W.; Wali, M. A.; Wang, Q. M. *J. Chem. Soc., Chem. Commun.* **1994**, 2089.

- 27) Wang, Q. M.; Bruce, D. W. *J. Chem. Soc., Chem. Commun.* **1996**, 2505.
- 28) Wang, Q. M.; Bruce, D. W. *Tetrahedron Lett.* **1996**, 37, 7641.
- 29) Wang, Q. M.; Bruce, D. W. *Angew. Chem. Int. Ed. Engl.* **1997**, 36, 150.
- 30) Nalwa, H. S. *Nonlinear Optics of Organic Molecular and Polymeric Materials*; Nalwa, H. S. and Miyata, S., Ed.; CRC Press: Boca Raton, FL, 1997, pp 611-797.
- 31) Nalwa, H. S.; Watanabe, T.; Miyata, S. *Nonlinear Optics in Organic Molecular and Polymeric Materials*; Nalwa, H. S. and Miyata, S., Ed.; CRC Press: Boca Raton, FL, 1997, pp 89-350.
- 32) Nalwa, H. S. *Handbook of Organic Conductive Molecules and Polymers*; Nalwa, H. S., Ed.; John Wiley & Sons: Chichester, 1997, pp 261-363.
- 33) Nalwa, H. S. *Handbook of Organic Conductive Molecules and Polymers*; John Wiley & Sons: Chichester, 1997; Vol. 1-4.
- 34) Nalwa, H. S.; Shirk, J. S. *Phthalocyanines: Properties and Applications*; Leznoff, C. C. and Lever, A. B. P., Ed., 1996; Vol. 4, pp 79-118.
- 35) Nalwa, H. S. *Adv. Mater.* **1993**, 5, 341.
- 36) Nalwa, H. S. *Appl. Organometal. Chem.* **1991**, 5, 349.
- 37) Chemla, D. S.; Zyss, J. *Nonlinear Optical Properties of Organic Molecules and Crystals*; Academic Press: Orlando, 1987.
- 38) Suslick, K. S.; Chen, C. T.; Meredith, G. R.; Cheng, L. T. *J. Am. Chem. Soc.* **1992**, 114, 6928-30.
- 39) Chou, H.; Chem, C.-T.; Stork, K. F.; Bohn, P. W.; Suslick, K. S. *J. Phys. Chem.* **1994**, 98, 383.
- 40) Sen, A.; Ray, P. C.; Das, P. K.; Krishnan, V. J. *J. Phys. Chem.* **1996**, 100, 19611.
- 41) Sen, A.; Krishnan, V. *J. Chem. Soc., Faraday Trans.* **1997**, 93, 4281.
- 42) Priyadarshy, S.; Therien, M. J.; Beratan, D. N. *J. Am. Chem. Soc.* **1996**, 118, 1504.
- 43) LeCoers, S. M.; Guan, H.-W.; Dimagno, S. G.; Wang, C. H.; Therien, M. J. *J. Am. Chem. Soc.* **1996**, 118, 1497.
- 44) Karki, L.; Vance, F. W.; Hupp, J. T.; LeCoers, S. M.; Therien, M. J. *J. Am. Chem. Soc.* **1998**, 120, 2606.
- 45) Yeung, M.; Ng, A. C. H.; Drew, M. G. B.; Vorpapel, E.; Breitung, E. M.; McMahon, R. J.; Ng, D. K. P. *J. Org. Chem.* **1998**, 63, 7143.
- 46) Albert, I. D. L.; Marks, T. J.; Ratner, M. A. *Chem. Mater.* **1998**, 10, 753.
- 47) Peng, Z.; Bao, Z.; Yu, L. *J. Am. Chem. Soc.* **1994**, 116, 6003.
- 48) Peng, Z.; Gharavi, A.; Yu, L. *Polym. Preprints* **1995**, 36, 41.
- 49) Li, D.; Swanson, B.; Robinson, J. M.; Hoffbauer, M. A. *J. Am. Chem. Soc.* **1993**, 115, 6975.
- 50) Meloney, C.; Byrne, H.; Dennis, W. H.; Blau, W.; Kelly, J. M. *Chem. Phys.* **1988**, 121, 21.
- 51) Sakaguchi, T.; Shimizu, Y.; Miya, M.; Fukumi, T.; Ohta, K.; Nagata, A. *Chem. Lett.* **1992**, 281.
- 52) Rao, D. V. G. L. N.; Arando, F. J.; Roach, J. F.; Remy, D. E. *Appl. Phys. Lett.* **1991**, 58, 1241.
- 53) Guha, S.; Kang, K.; Porter, P.; Roach, J. E.; Remy, D. E.; Arando, F. J.; Rao, D. V. G. L. N. *Opt. Lett.* **1992**, 17, 264.
- 54) Hosada, M.; Wada, T.; Garito, A. F.; Sasabe, H. *Japan. J. Appl. Phys.* **1992**, 31, L249.
- 55) Norwood, R. A.; Sounik, J. R. *Appl. Phys. Lett.* **1992**, 60, 295.
- 56) Anderson, H. L.; Martin, S. J.; Dradley, D. D. C. *Angew. Chem. Int. Ed. Engl.* **1994**, 33, 655.
- 57) Bao, Z.; Yu, L. *Proc. ACS Mtg. Polym. Mater. Sci. (PMSE)* **1994**, 71, 781.
- 58) Kandasamy, K.; Shetty, S. J.; Puntambekar, P. N.; Srivastava, T. S.; Kundu, T.; Singh, B. P. *J. Porph. Phthalocyanines* **1998**, 2, (In Press).
- 59) Kumar, G. R.; Ravikanth, M.; Banerjee, S.; Sevian, A. *Opt. Comm.* **1997**, 144, 245.
- 60) Kafafi, Z. H.; Flom, S. R.; Sarkas, H. W.; Pong, R. G. S.; Merritt, C. D.; Bartoli, F. J. *SPIE Proc.* **1994**, 2284, 134.
- 61) Flom, S. R.; Pong, R. G. S.; Bartoli, F. J.; Kafafi, Z. H. *Nonlin. Opt.* **1995**, 10, 183.
- 62) Kajzar, F.; Shudo, Y. O.; Meritt, C.; Kafafi, Z. *Synth. Metals* **1998**, 94, 91.
- 63) Sinha, A.; Bihari, B.; Mandal, K.; Chen, L. *Macromolecules* **1995**, 28, 5681.
- 64) Tutt, L. W.; Kost, A. *Nature* **1992**, 356, 225.
- 65) Perry, J. W. *Nonlinear Optics of Organic Molecules and Polymers*; Nalwa, H. S., Ed.; CRC Press: Boca Raton, FL, 1997, pp 813-840.
- 66) Blau, W.; Byrne, H.; Dennis, W. M.; Kelly, J. M. *Opt. Comm.* **1985**, 56, 25.
- 67) Fei, H. S.; Han, L.; Ai, X. C.; Yin, R.; Shen, J. C. *J. Chin. Sci. Bull.* **1992**, 37, 298.
- 68) Shi, J.; Yang, M.; Wang, Y.; Zhang, L.; Li, C. *Appl. Phys. Lett.* **1994**, 64, 3083.
- 69) Shi, J.; Yang, M.; Wang, Y.; Zhang, L.; Li, C.; Wang, D.; Dong, S.; Sun, W. *Opt. Comm.* **1994**, 109, 487.

- 70) Su, W.; Cooper, T. M. *Chem. Mater.* **1998**, *10*, 1212.
- 71) Robison, G. W. *Brookhaven Symp. Biol.* **1967**, *19*, 16.
- 72) Pearlstein, R. H. *New Compr. Biochem.* **1987**, *15*, 299.
- 73) Fleming, G. R.; Martin, J.-L.; Breton, J. *Nature* **1988**, *333*, 190.
- 74) Paddock, M. L.; Rongey, S. H.; Feher, G.; Okamura, M. Y. *Proc. Natl. Acad. Sci. U.S.A.* **1989**, *86*.
- 75) Feher, G.; Allen, J. P.; Okamura, M. Y.; Rees, D. C. *Nature* **1989**, *339*, 111.
- 76) Holten, D.; Kirmarier, C. *Photosynth.* **1987**, *13*, 225.
- 77) Girolami, G. S.; Hein, C. L.; Suslick, K. S. *Angew. Chem. Intl. Ed.* **1996**, *35*, 1223-1225.
- 78) Kong, J. L.; Loach, P. A. *Frontiers Biol. Energ.* **1978**, *1*, 73-82.
- 79) Kong, J. L.; Loach, P. A. *J. Heterocyclic Chem.* **1980**, *17*, 737.
- 80) Tabushi, I.; Koga, N.; Yanagita, M. *Tetrahedron Lett.* **1979**, 257.
- 81) Wasielewski, M. R. *Chem. Rev.* **1992**, *92*, 435.
- 82) Moore, T. A.; Gust, D.; Mathis, P.; Mialocq, J. C.; Chachaty, C.; Bensasson, R. V.; Land, E. J.; Doisi, D.; Liddell, P. A.; Lehman, W. R.; Nemeth, G. A.; Moore, A. L. *Nature* **1984**, *307*, 630.
- 83) Gust, D.; Moore, T. A.; Liddell, P. A.; Nemeth, G. A.; Makings, L. R.; Moore, A. L.; Barrett, D.; Pessiki, P. J.; Bensasson, R. V.; Rougee, M.; Chachaty, C.; De Schryver, F. C.; Van der Auweraer, M.; Holzwarth, A. R.; Connolly, J. S. *J. Am. Chem. Soc.* **1987**, *109*, 846.
- 84) Gust, D.; Moore, T. A.; Moore, A. L.; Barrett, D.; Harding, L. O.; Makings, L. R.; Liddell, P. A.; De Schryver, F. C.; Van der Auweraer, M.; Bensasson, R.; Raugee, M. *J. Am. Chem. Soc.* **1988**, *110*, 321.
- 85) Gust, D.; Moore, T. A.; Moore, A. L.; Makings, L. R.; Seely, G. R.; Ma, X.; Trier, T. T.; Gao, F. *J. Am. Chem. Soc.* **1988**, *110*, 7567.
- 86) Gust, D.; Moore, T. A.; Moore, A. L.; Seely, G.; Liddell, P.; Barrett, D.; Harding, L. O.; Ma, X.; Lee, S. J.; Gao, F. *Tetrahedron* **1989**, *45*, 4867.
- 87) Osuka, A.; Nagata, T.; Maruyama, K. *Chem. Lett.* **1991**, 481.
- 88) Osuka, A.; Maruyama, K.; Magata, N.; Asahi, T.; Yamazaki, I.; Tamai, N.; Nishimura, Y. *Chem. Phys. Lett.* **1991**, *181*, 413.
- 89) Osuka, A.; Nakajima, S.; Maruyama, K.; Magata, N.; Asahi, T.; Yamazaki, I.; Y., N.; Ohno, T.; Nozaki, K. *J. Am. Chem. Soc.* **1993**, *115*, 4577.
- 90) Osuka, A.; Nakajima, S.; Okada, T.; Taniguchi, S.; Nozaki, K.; Ohno, T.; Yamazaki, I.; Nishimura, Y.; Magata, N. *Angew. Chem. Intl. Ed. Engl.* **1996**, *35*, 92.
- 91) Liddell, P. A.; Kuciauskas, D.; Sumida, J. P.; Nash, B.; Nguyen, D.; Moore, A. L.; Moore, T. A.; Gust, D. *J. Am. Chem. Soc.* **1997**, *119*, 1400.
- 92) Girolami, G. S.; Gorlin, P. A.; Suslick, K. S. *Inorg. Chem.* **1994**, *33*, 626-627.
- 93) O'Neil, M. P.; Niemczyk, M. P.; Svec, W. A.; Gosztola, D.; Gaines, G. L.; Wasielewski, M. R. *Science* **1992**, *257*, 63.
- 94) Debreczeny, M. P.; Svec, W. A.; Wasielewski, M. R. *Science* **1996**, *274*, 584.
- 95) Wagner, R.; Lindsey, J. S. *J. Am. Chem. Soc.* **1994**, *116*, 9759.
- 96) Crossley, M.; Burn, P. L. *J. Chem. Soc., Chem. Commun.* **1991**, 1569.
- 97) Wagner, R. W.; Lindsey, J. S.; Seth, J.; Palaniappan, V.; Bocian, D. F. *J. Am. Chem. Soc.* **1996**, *118*, 3996.
- 98) Segawa, H.; Nakayama, N.; Shimidzu, T. *J. Chem. Soc., Chem. Commun.* **1992**, 784.
- 99) Segawa, H.; Kunitomo, K.; Susumu, K.; Taniguchi, M.; Shimidzu, T. *J. Am. Chem. Soc.* **1994**, *116*, 11193.
- 100) Shimidzu, T. *Pure & Appl. Chem.* **1995**, *67*, 2039.
- 101) Shimidzu, T.; Jehneke, S. A. W., Kenneth J., Ed.; Am. Chem. Soc.: Washington, D.C., 1997, pp 460-474.
- 102) Mauzerall, D. C.; Greenbaum, N. L. *Biochim. Biophys. Acta* **1989**, *974*, 119.
- 103) Hunter, C. N.; Van Grondelle, R.; Olsen, J. D. *Trends Biochim. Sci.* **1989**, *14*, 72.
- 104) McDermott, G.; Prince, S. M.; Freer, A. A.; Haworthornthwaite-Lawless, A. M.; Papiz, M. Z.; Cogdell, R. J.; Isaacs, N. W. *Nature* **1995**, *374*, 517.
- 105) Karrasch, S.; Bullough, P. A.; Ghosh, R. *EMBO J.* **1995**, *14*, 631.
- 106) Nagata, T.; Osuka, A.; Maruyama, K. *J. Am. Chem. Soc.* **1990**, *112*, 3055.
- 107) Osuka, A.; Tanabe, N.; Nakajima, S.; Maruyama, K. *J. Chem. Soc., Perkin. Trans. 2* **1995**, 199.
- 108) Osuka, A.; Shimidzu, H. *Angew. Chem. Intl. Ed. Engl.* **1997**, *36*, 135.
- 109) Nakano, A.; Osuka, A.; Yamazaki, I.; Yamazaki, T.; Nishimura, Y. *Angew. Chem. Intl. Ed. Engl.* **1998**, *37*, 3023.
- 110) Prathapan, S.; Johnson, T.; Lindsey, J. *J. Am. Chem. Soc.* **1993**, *115*, 7519.

- 111) Seth, J.; Palaniappan, V.; Johnson, T.; Prathapan, S.; Lindsey, J. S.; Bocian, D. F. *J. Am. Chem. Soc.* **1994**, *116*, 10578.
- 112) Li, F.; Yang, S. I.; Ciringh, Y.; Seth, J.; Martin, C. H.; Singh, D. L.; Kim, D.; Birgh, R. R.; Bocian, D. F.; Holten, D.; Lindsey, J. S. *J. Am. Chem. Soc.* **1998**, *120*, 10001.
- 113) Drain, C. M.; Lehn, J.-M. *J. Chem. Soc., Chem. Commun.* **1994**, 2313.
Drain, C.M.; Nifiatis, F.; Vasenko, A.; Batteas, J.D. *Angew. Chem. Int. Ed.* **1998**, *37*, 2344.
- 114) Yuan, H.; Thomas, L.; Woo, L. K. *Inorg. Chem.* **1996**, *35*, 2808.
- 115) Sasaki, Y.; Imamura, T.; Kariya, N. *Inorg. Chem.* **1997**, *36*, 833.
- 116) Alessio, E.; Macchi, M.; Heath, S.; Marzilli, L. G. *J. Chem. Soc., Chem. Commun.* **1996**, 1411.
- 117) Funatsu, K.; Kimura, A.; Imamura, T.; Ichimura, A.; Sasaki, Y. *Inorg. Chem.* **1997**, *36*, 1625.
- 118) Woiaczynski, J.; Latos-Grazynski, K. *Inorg. Chem.* **1996**, *35*, 4812.
- 119) Chernook, A. V.; Rempel, U.; von Broczyskowski, C.; Shulga, A. M.; Zenkevich, E. I. *Chem. Phys. Lett.* **1996**, *254*, 229.
- 120) Abrahams, B. F.; Hoskins, B. F.; Michail, D. M.; Robson, R. *Nature* **1994**, *369*, 727.
- 121) Dagani, D. *Chem & Eng. News* **1998**, 35.
- 122) Lin, V. S.; DiMagno, S. G.; Therien, M. J. *Science* **1994**, *264*, 1105.
- 123) Suslick, K. S.; Van Deusen-Jeffries, S. *Biomimetic Shape-Selective Oxidations*; Suslick, K. S., Ed.; Elsevier Science, Ltd.: Oxford, 1996; Vol. 5, pp 733-756.
- 124) Meunier, B. *Metalloporphyrins Catalyzed Oxidations*; Monanari, F. and Casella, L., Ed.; Kluwer Academic Publishers: Boston, 1994, pp 1-47.
- 125) Byrn, M. P.; Curtis, C. J.; Khan, S. I.; Sawin, P. A.; Tsurumi, R.; Strouse, C. E. *J. Amer. Chem. Soc.* **1990**, *112*, 1865.
- 126) Byrn, M. P.; Curtis, C. J.; Goldberg, I.; Hsiou, Y.; Khan, S. I.; Sawin, P. A.; Tendick, S. K.; Strouse, C. E. *J. Amer. Chem. Soc.* **1991**, *113*, 6549.
- 127) Byrn, M. P.; Curtis, C. J.; Hsiou, Y.; Khan, S. I.; Sawin, P. A.; Tendick, S. K.; Terzis, A.; Strouse, C. E. *J. Amer. Chem. Soc.* **1993**, *115*, 9480.
- 128) Byrn, M. P.; Curtis, C. J.; Goldberg, I.; Huang, T.; Hsiou, Y.; Khan, S. I.; Sawin, P. A.; Tendick, S. K.; Terzis, A.; Strouse, C. E. *Mol. Cryst. Liq. Cryst.* **1992**, *211*, 135.
- 129) Krupitsky, H.; Stein, Z.; Goldberg, I. *J. Incl. Phenom. Mol. Recog. Chem.* **1995**, *20*, 211.
- 130) Goldberg, I.; Krupitsky, H.; Stein, Z.; Hsiou, Y.; Strouse, C. E. *Supramol. Chem.* **1995**, *4*, 203.
- 131) Dastidar, P.; Krupitsky, H.; Stein, Z.; Goldberg, I. *J. Incl. Phenom. Mol. Recog. Chem.* **1996**, *24*, 241.
- 132) Philip, D.; Stoddart, J. F. *Angew. Chem., Int. Ed. Engl.* **1996**, *35*, 1154.
- 133) Kumar, R. K.; Balasubramanian, S.; Goldberg, I. *Inorg. Chem.* **1998**, *37*, 541.
- 134) Dastidar, P.; Stein, Z.; Goldberg, I.; Strouse, C. E. *Supramol. Chem.* **1996**, *7*, 257.
- 135) Bhyrappa, P.; Wilson, S. R.; Suslick, K. S. *J. Amer. Chem. Soc.* **1997**, *119*, 8492.
- 136) Bhyrappa, P.; Suslick, K. S. *Supramolec. Chem.* **1998**, *9*, 169-174.
- 137) Robson, R. *Infinite Frameworks*; MacNicol, D. D., Toda, F. and Bishop, R., Ed.; Pergamon: New York, 1996; Vol. 6, pp 733-759.
- 138) Bowes, C. L.; Ozin, G. A. *Adv. Mater.* **1996**, *8*, 13-28.
- 139) Yaghi, O. M.; Li, H.; Davis, C.; Richardson, D.; Groy, T. L. *Acc. Chem. Res.* **1998**, *1998*, 474.
- 140) Krupitsky, H.; Stein, Z.; Goldberg, I. *J. Incl. Phenom. Mol. Recog. Chem.* **1994**, *18*, 177.
- 141) Abrahams, B. F.; Hoskins, B. F.; Robsin, R. *J. Amer. Chem. Soc.* **1991**, *113*, 3606.
- 142) Abrahams, B. F.; Hoskins, B. F.; Michall, D. M.; Robson, R. *Nature* **1994**, *369*, 727.
- 143) Patel, B. *Porphyrin Liquid Crystals*; University of Illinois at Urbana-Champaign: Urbana, 1996.
- 144) Kosal, M. E.; Suslick, K. S. *unpublished results* .
- 145) Chou, J. H.; Kosal, M. E.; Suslick, K. S. *unpublished results* .
- 146) Bedioui, F. *Coord. Chem. Rev.* **1995**, *144*, 39.
- 147) de Vismes, B.; Bedioui, F.; Devynck, J.; Bied-Charreton, C. *J. Electroanal. Chem.* **1985**, *187*, 197.
- 148) de Vismes, B.; Bedioui, F.; Devynck, J.; Bied-Charreton, C.; Perree-Fauvet, M. *New J. Chem.* **1986**, *10*, 81.
- 149) Gaillon, L.; Bedioui, F.; Devynck, J. *J. Mater. Chem.* **1994**, *4*, 1215.
- 150) Li, Z.; Wang, C. M.; Persaud, L.; Mallouk, T. E. *J. Phys. Chem.* **1988**, *92*, 2592.
- 151) Persad, L.; Bard, A. J.; Canpion, A.; Fox, M. A.; Mallouk, T. E.; Webber, S. E.; White, J. M. *J. Amer. Chem. Soc.* **1987**, *109*, 7309.
- 152) Le Guern, F.; Bied-Charreton, C.; Faure, J. *Bull. Soc. Chim. Fr.* **1993**, *130*, 753.

- 153) Chen, S.-M. *J. Mol. Cat. A* **1996**, *112*, 277.
- 154) Guerra, S. V.; Xavier, C. R.; Nakagaki, S.; Kubota, L. T. *Electroanal.* **1998**, *10*, 462.
- 155) Nakamura, M.; Tatsumi, T.; Tominaga, H. *Bull. Chem. Soc. Jpn.* **1990**, *63*, 3334.
- 156) Li, G. Q.; Govind, R. *Inorg. Chim. Acta.* **1994**, *217*, 135.
- 157) Liu, C.-J.; Li, S.-G.; Pang, W. Q.; Che, C. M. *Chem. Commun.* **1997**, 65.
- 158) Sung-Suh, H. M.; Luan, Z.; Kevan, L. *J. Phys. Chem.* **1997**, *101*, 10455.
- 159) Zhan, B.-Z.; Li, X. Y. *Chem. Comm.* **1998**, 349.
- 160) Holland, B. T.; Walkup, C.; Stein, A. *J. Phys. Chem. B* **1998**, *102*, 4301.
- 161) Anson, F. C.; Ni, C.; Saveant, J. *J. Am. Chem. Soc.* **1985**, *107*, 3442.
- 162) Battioni, P.; Lallier, J. P.; Barloy, L.; Mansuy, D. *J. Chem. Soc., Chem. Commun.* **1989**, 1149.
- 163) Persaud, L.; Bard, A. J.; Campion, A.; Fox, M. A.; Mallouk, T. E.; Webber, S. E.; White, J. M. *J. Am. Chem. Soc.* **1987**, *109*, 7309.
- 164) Li, Z.; Wang, C. M.; Persaud, L.; Mallouk, T. E. *J. Phys. Chem.* **1988**, *92*, 2592.
- 165) DeVismes, B.; Bedioui, F.; Devynck, J.; Bied-Charreton, C.; Peree-Fauvet, M. *Nouv. J. Chim.* **1986**, *10*, 81.
- 166) Kosiur, D. R. *Clays Clay Minerals* **1977**, 365.
- 167) Kameyama, H.; Suzuki, H.; Amano, A. *Chem. Lett.* **1988**, 1117.
- 168) Barloy, L.; Battioni, P.; Mansuy, D. *J. Chem. Soc., Chem. Commun.* **1990**, 1365.
- 169) Carrado, K. A.; Wasserman, S. R. *Chem. Mater.* **1996**, *8*, 219.
- 170) Carrado, K. A.; Thiyagarajan, P.; Winans, R. E.; Botto, R. E. *Inorg. Chem.* **1991**, *30*, 794.
- 171) Park, I. Y.; Kuroda, K.; Kato, C. *Chem. Lett.* **1989**, 2057.
- 172) Barloy, L.; Lallier, J. P.; Battioni, P.; Mansuy, D.; Piffard, Y.; Tournoux, M.; Vali, J. B.; Jones, W. *New J. Chem.* **1992**, *16*, 71.
- 173) Bonnet, S.; Forano, C.; De Roy, A.; Besse, J. P. *Chem. Mater.* **1996**, *8*, 1962.
- 174) Kim, R. M.; Pillion, J. E.; Burwell, D. A.; Groves, J. T.; Thompson, M. E. *Inorg. Chem.* **1993**, *32*, 4509.
- 175) Borg, R. J.; Dienes, G. J. *The Physical Chemistry of Solids*; Academic Press: New York, 1992.
- 176) Beno, M. A.; Soderholm, D. W.; Capone II, D. W.; Hinks, D. G.; Jorgensen, J. D.; Segre, C. U.; Zhang, K. *Appl. Phys. Lett.* **1987**, *51*, 57.
- 177) Sleight, A. W. *Science* **1987**, *242*, 1519.
- 178) Steinflink, H.; Sinnea, J. S.; Sui, T. Z.; Hsu, H. M.; Goodenough, J. B. *J. Am. Chem. Soc.* **1987**, *109*, 3348.
- 179) Crossley, M. J.; Burn, P. L. *J. Chem. Soc., Chem. Commun.* **1991**, 1569-1571.
- 180) Chen, C.-T.; Suslick, K. S. *Coord. Chem. Rev.* **1993**, *128*, 293-322.
- 181) Hanack, M.; Deger, S.; Lange, A. *Coord. Chem. Rev.* **1988**, 83.
- 182) Collman, J. P.; McDevitt, J. T.; Yee, G. T.; Leidner, C. R.; McCullough, L. G.; Little, W. A.; Torrance, J. B. *Proc. Natl. Acad. Sci. U.S.A.* **1986**, *83*, 4581.
- 183) Buchler, J. W.; Smith, K. M., Ed.; Elsevier: Amsterdam, 1976.
- 184) Collman, J. P.; McDevitt, J. T.; Yee, G. T.; Zisk, M. B.; Torrance, J. B.; Little, W. A. *Synth. Met.* **1986**, *15*, 129.
- 185) Collman, J. P.; McDevitt, J. T.; Leidner, C. R.; Yee, G. T.; Torrance, J. B.; Little, W. A. *J. Am. Chem. Soc.* **1987**, *109*, 4606.
- 186) Kubel, F.; Strahle, J. A. *Naturforsch. Teil B* **1981**, *36*, 441.
- 187) Bao, Z.; Chen, Y.; Yu, L. *Macromolecules* **1994**, *27*, 4629-4631.
- 188) Jiang, B.; Szu-Wei, Y.; Jones Jr., W. E. *Chem. Mater.* **1997**, *9*, 2031-2034.
- 189) Jiang, B.; Yang, S. W.; Bailey, S. L.; Hermans, L. G.; Niver, R. A.; Bolcar, M. A.; Jones, J., W. E. *Coord. Chem. Rev.* **1998**, *171*, 365-386.
- 190) Segawa, H.; Nakayama, N.; Shimidzu, T. *J. Chem. Soc., Chem. Commun.* **1992**, 784-786.
- 191) Segawa, H.; Kunimoto, K.; Susumu, K.; Taniguchi, M.; Shimidzu, T. *J. Am. Chem. Soc.* **1994**, *116*, 11193-11194.
- 192) Burfoot, J. C. *Ferroelectrics*; Van Nostrand: London, 1967.
- 193) Mitsui, T.; Tatsuzaki, I.; Nakamura, E. *An Introduction to the Physics of Ferroelectrics*; Gordon and Breach: New York, 1976.
- 194) West, A. R. *Solid State Chemistry and its Applications*; Wiley: New York, 1984.
- 195) Goodby, J. W.; Leslie, T. M. *Mol. Cryst. Liq. Cryst.* **1984**, *110*, 175.
- 196) Walba, D. M.; Slater, S. C.; Thurmes, W. N.; Clark, N. A.; Handschy, M. A.; Supon, F. *J. Am. Chem. Soc.* **1986**, *108*, 5210.

- 197) Wahl, J.; Matuszczyk, T.; Lagerwall, S. T. *Mol. Cryst. Liq. Cryst.* **1987**, *146*, 143.
- 198) Walba, D. M.; Razavi, H. A.; Clark, N. A.; Parmar, D. S. *J. Am. Chem. Soc.* **1988**, *110*, 5686.
- 199) Suslick, K. S.; Chen, C.-T. *Polym. Mater. Sci. Eng.* **1990**, *63*, 272.
- 200) Chen, C.-T. *Porphyrins and Metalloporphyrins as Field Responsive Materials*; University of Illinois at Urbana-Champaign: Urbana, IL, 1992.
- 201) Adams, K.; Rasmussen, P. G.; Scheidt, W. R.; Hatono, K. *Inorg. Chem.* **1979**, *18*, 1892.
- 202) Scheidt, W. R.; Lee, Y. A.; Geiger, D. K.; Taylor, K.; Hatono, K. *J. Am. Chem. Soc.* **1982**, *104*, 3367.
- 203) Collman, J. P.; Brauman, J. I.; Rose, E.; Suslick, K. S. *Proc. Natl. Acad. Sci. U.S.A.* **1978**, *57*, 1052.
- 204) Woolery, G. M.; Walter, A.; Suslick, K. S.; Powers, J.; Spiro, T. G. *J. Am. Chem. Soc.* **1985**, *107*, 2370.
- 205) Caspari, M. E.; Merz, W. J. *Phys. Rev.* **1950**, *80*, 1082.
- 206) Blinov, L. M.; Kirichenko, N. A. *Sov. Phys. Solid State* **1970**, *12*, 1246.
- 207) Frauenheim, T.; Hamann, C.; Muller, M. *Phys. Status Solidi A* **1984**, *86*, 736.
- 208) Kaenzig, W. *Helv. Phys. Acta* **1951**, *24*, 175.
- 209) Frazer, B. C.; Danner, H. R.; Pepinsk, R. *Phys. Rev.* **1955**, *100*, 745.
- 210) Wells, A. F. *Structural Inorganic Chemistry*; Clarendon Press: Oxford, 1984.
- 211) Eastwood, D.; Gouterman, M. *J. Mol. Spec.* **1970**, *35*, 359.
- 212) Lee, S.; Okura, I. *Analyst* **1997**, *122*, 81-84.
- 213) Weekey, W.; Kwok-Yin, W.; Xiang-Ming, L.; Yiu-Bong, L.; Chi-Shing, C.; Chan, K. *J. Mater. Chem.* **1993**, *3*, 1031-1035.
- 214) Hartmann, P.; Wolfgang, T. *Anal. Chem.* **1996**, *68*, 2615-2620.
- 215) Mills, A.; Lepre, A. *Anal. Chem.* **1997**, *69*, 4653-4659.
- 216) Baron, A. E.; Danielson, J. D. S.; Gouterman, M.; Wan, J. R.; Callis, J. B. *Rev. Sci. Instrum.* **1993**, *64*, 3394-3402.
- 217) Kavandi, J.; Callis, J.; Gouterman, M.; Khalil, G.; Wright, D.; Green, E.; Burns, D.; McLachlan, B. *Rev. Sci. Instrum.* **1990**, *61*, 3340-3347.
- 218) Oglesby, D. M.; Upchurch, B. T.; Leighty, B. D.; Collman, J. P.; Zhang, X.; Herrmann, P. C. *Anal. Chem.* **1994**, *66*, 2745-2751.
- 219) Collman, J. P.; Gagne, R. R.; Reed, C. A.; Halbert, T. R.; Lang, G.; Robinson, W. T. *J. Am. Chem. Soc.* **1975**, *97*, 1427-1439.
- 220) Collman, J. P.; Brauman, J. I.; Fitzgerald, J. P.; Hampton, P. D.; Naruta, Y.; Sparapany, J. W.; Ibers, J. A. *J. Am. Chem. Soc.* **1988**, *110*, 3477-3486.
- 221) Roosli, S.; Presch, E.; Morf, W. E.; Tsuchida, E.; Nishide, H. *Anal. Chim. Acta* **1997**, *338*, 119-125.
- 222) Vaughan, A. A.; Baron, M. G.; Narayanaswamy, R. *Analytical Communications* **1996**, *33*, 393-396.
- 223) Arnold, D. P.; Manno, D.; Micocci, G.; Serra, A.; Tepore, A.; Valli, L. *Langmuir* **1997**, *13*, 5951-5956.
- 224) Malinski, T.; Taha, Z. *Nature* **1992**, *358*, 676-678.
- 225) Lonergan, M. C.; Severin, E. J.; Doleman, B. J.; Beaver, S. A.; Grubbs, R. H.; Lewis, N. S. *Chem. Mater.* **1996**, *8*, 2298-2312.
- 226) Dickinson, T. A.; White, J.; Kauer, J. S.; Walt, D. R. *Nature* **1996**, *382*, 697-700.
- 227) Axel, R. *Scientific American* **1995**, 154-159.
- 228) Kauer, J. S. *Trends Neurosci.* **1991**, *14*, 79-85.
- 229) Natale, C. D.; Macagnano, A.; Davide, F.; D'Amico, A.; Paolesse, R.; Boschi, T.; Faccio, M.; Ferri, G. *Sensors and Actuators B* **1997**, *44*, 521-526.
- 230) Natale, C. D.; Macagnano, A.; Repole, G.; Saggio, G.; D'Amico, A.; Paolesse, R.; Boschi, T. *Materials Science and Engineering C* **1998**, *5*, 209-215.
- 231) Rakow, N.; Suslick, K. S. *Unpublished Results* **1998**.
- 232) Gouterman, M.; Schwarz, F. P.; Smith, P. D. *The Journal of Chemical Physics* **1973**, *59*, 676-690.
- 233) Nappa, M.; Valentine, J. S. *J. Am. Chem. Soc.* **1978**, *100*, 5075-5080.
- 234) Hofmeister, F. *Arch. Exp. Pathol. Parmakol.* **1888**, *24*, 247-260.
- 235) Chaniotakis, N. A.; Chasser, A. M.; Meyerhoff, M. E. *Anal. Chem.* **1988**, *60*, 185-188.
- 236) Chaniotakis, N. A.; Park, S. B.; Meyerhoff, M. E. *Anal. Chem.* **1989**, *61*, 566-570.
- 237) Gao, D.; Li, J.; Ru-Qin, Y.; Zheng, G. *Anal. Chem.* **1994**, *66*, 2245-2249.
- 238) Yoon, I. J.; Shin, J. H.; Paeng, I. R.; Nam, H.; Cha, G. S.; Paeng, K. *Anal. Chim. Acta* **1998**, *367*, 175-181.
- 239) Beer, P. D.; Drew, M. G. B.; Heseck, D.; Jagessar, R. *J. Chem. Soc. Chem. Comm.* **1995**, 1187-1189.
- 240) Kral, V.; Furuta, H.; Shreder, K.; Lynch, V.; Sessler, J. L. *J. Am. Chem. Soc.* **1996**, *118*, 1595-1607.

- 241) Sessler, J. L.; Cyr, M. J.; Lynch, V.; McGhee, E.; Ibers, J. A. *J. Am. Chem. Soc.* **1990**, *112*, 2810-2813.
- 242) Sessler, J. L.; Kral, V.; Genge, J. W.; Thomas, R. E.; Iverson, B. L. *Anal. Chem.* **1998**, *70*, 2516-2522.
- 243) Morales-Bahnik, A.; Czolk, R.; Reichert, J.; Ache, H. J. *Sensors and Actuators B* **1993**, *13-14*, 424-426.
- 244) Plaschke, M.; Czolk, R.; Ache, H. J. *Anal. Chim. Acta* **1995**, *304*, 107-113.
- 245) Malinski, T.; Ciszewski, A.; Fish, J. R.; Czuchajowski, L. *Anal. Chem.* **1990**, *62*, 909-914.
- 246) Gupta, V. K.; Ajay, K. J.; Singh, L. P.; Khurana, U. *Anal. Chim. Acta* **1997**, *355*, 33-41.
- 247) Dobson, D. J.; Saini, S. *Anal. Chem.* **1997**, *69*, 3532-3538.
- 248) Priyantha, N.; Weerabahu, D. *Anal. Chim. Acta* **1996**, *320*, 263-268.
- 249) Bonar-Law, R. P.; Mackay, L. G.; Sanders, J. K. M. *J. Chem. Soc. Chem. Comm.* **1993**, 456-458.
- 250) Zhao, S.; Luong, J. H. T. *J. Chem. Soc., Chem. Comm.* **1995**, 663-664.
- 251) Takeuchi, M.; Kijima, H.; Hamachi, I.; Shinkai, S. *Bull. Chem. Soc. Jpn.* **1997**, *70*, 699-705.
- 252) Bhyrappa, P.; Vaijayanthimala, G.; Suslick, K. S. *Accepted as Communication to the Editor, J. Am. Chem. Soc.* **1999**.
- 253) Kandasamy, K.; Shetty, S. J.; Puntambekar, P. N.; Srivastava, T. S. K., T.; Singh, B. P. *J. Chem. Soc., Chem. Commun.* **1997**, 1159.

Table 1. Abbreviations

(DEtyP) _n	5,10,15,20-diethylnylporphyrin polymer
(O ₂ C _n H _{2n+1})OEP	2,3,7,8,12,13,17,18-octakis(β- <i>n</i> -alkylester)ethylporphyrinate
(OC _n H _{2n+1})DPP	5,15-bis(4- <i>n</i> -alkoxyphenyl)porphyrinate
(OC _n H _{2n+1})OECNP	2,3,7,8,12,13,17,18-octakis(β- <i>n</i> -alkoxy)ethyl-5-cyanoporphyrinate
(OC _n H _{2n+1})OENO ₂ P	2,3,7,8,12,13,17,18-octakis(β- <i>n</i> -alkoxy)ethyl-5-nitroporphyrinate
(OC _n H _{2n+1})OEP	2,3,7,8,12,13,17,18-octakis(β- <i>n</i> -alkoxy)ethylporphyrinate
(C _n H _{2n+1})Cy) ₂ DPP	5,15-bis(4'- <i>n</i> -alkylcyclohexyl-4-esterphenyl)porphyrinate
(C _n H _{2n+1})Cy)OHPP	5-(4'- <i>n</i> -alkylcyclohexyl-4-esterphenyl)-15-(4-hydroxyphenyl)porphyrinate
((OC _n H _{2n+1}) ₂ Ph) ₂ DPP	5,15-bis(2',4'- <i>n</i> -alkoxyphenyl-4-esterphenyl)porphyrinate
((OC _n H _{2n+1}) ₃ Ph) ₂ DPP	5,15-bis(2',4',6'- <i>n</i> -alkoxyphenyl-4-esterphenyl)porphyrinate
((OC _n H _{2n+1})Ph) ₂ DPP	5,15-bis(4'- <i>n</i> -alkoxyphenyl-4-esterphenyl)porphyrinate
((OC _n H _{2n+1})Ph)OHPP	5-(4'- <i>n</i> -alkoxyphenyl-4-esterphenyl)-15-(4-hydroxyphenyl)porphyrinate
APTES	3-aminopropyltriethoxysilane
B(C _n H _{2n+1} O) _m TP	5,15-bis(3,4,3'',4''-tetra-alkoxy- <i>o</i> -terphenyl)porphyrinate
BDPY	boron-dipyrin
Bpy	Bipyridine
Br ₈ TPP	2,3,7,8,12,13,17,18-octabromo-5,10,15,20-tetraphenylporphyrinate
D-(DPP)-A	[5-((4'-(dimethylamino)-phenyl)ethynyl)-15((4''-nitrophenyl)ethynyl)-10,20-diphenylporphyrinate
D-A	donor-acceptor pair
dabco	1,4-Diazabicyclooctane
DEtyP	5,10,15,20-diethylnylporphyrinate
DFWM	degenerate four-wave mixing
dmg	Dimethylglyoximate
DMTBP	5,10,15,20-tetrakis((dimethyl)tetrabenzo)porphyrinate
DP	diporphyrinate
DPP	5,20-diphenylporphyrinate
DSC	differential scanning calorimetry
EFISH	electric field induced second harmonic generation
EPR	electron pair resonance
G1A	3,5-di(4'- <i>tert</i> -butylphenylamido)benzoyl
G1	3,5-bis(3',5'-di(<i>tert</i> -butyl)phenylester)benzoyl
G2	3,5-bis(3',5'-bis(3'',5''-di(<i>tert</i> -butyl)phenylester)phenylester)benzoyl
GPC	Gel Permeation Chromatography

HRS	hyper-Rayleigh scattering
ITO	indium-tin-oxide
(Me ₄ OEP) ⁺²	N,N',N'',N'''-tetramethyl-octaethylporphyrin(+2)
MV ²⁺	methylviologen
NLO	nonlinear optical
OEP	2,3,7,8,12,13,17,18-octaethylporphyrinate
OEPK	2,3,7,8,12,13,17,17-octaethyl-18-oxo-porphyrinate ketone
OPTAP	2,3,7,8,12,13,17,18-octaphenyltetrazaporphyrinate
PBDCI	N,N'-diphenyl-3,4,9,10-perylenebis(dicarboximide)
Pc	phthalocyaninato
pim	dianion of pimelic acid
pm	pyromellitimide
PMMA	poly(methyl methacrylate)
PSI	5,15,10,20-bis{2,2'-[3,3'-(<i>p</i> -phenylene)-dimethoxy]diphenyl}porphyrinate
pyz	pyrazine
RSA	reverse saturable absorption
SHG	second harmonic generator
STM	scanning tunneling microscope
suc	dianion of succinic acid
T(2',6'-G1A)P	5,10,15,20-tetrakis(2',6'-octa-G1A-phenyl)porphyrinate
T(2',6'-DHP)P	5,10,15,20-octakis(2,6-hydroxyphenyl)porphyrinate
T(3,5-CO ₂ H)PP	5,10,15,20-tetrakis(3,5-dicarboxyphenyl)porphyrinate
T(3,5-CO ₂ R)PP	5,10,15,20-tetrakis(3,5-dicarboxyalkylphenyl)porphyrinate
T(3',5'-DHP)P	5,10,15,20-octakis(3,5-hydroxyphenyl)porphyrinate
T(3',5'-G1P)P	5,10,15,20-tetrakis(2',6'-octa-G1-phenyl)porphyrinate
T(3',5'-G2P)P	5,10,15,20-tetrakis(2',6'-octa-G2-phenyl)porphyrinate
T(4- <i>n</i> -C ₁₂ H ₂₅)PP	5,10,15,20-tetrakis(4- <i>n</i> -dodecylphenyl)porphyrinate
T(4- <i>n</i> -C ₁₅ H ₃₁)PP	5,10,15,20-tetrakis(4- <i>n</i> -pentadecylphenyl)porphyrinate
T(4- <i>n</i> -C ₁₅ H ₃₁)PP	5,10,15,20-tetrakis(4- <i>n</i> -pentadecylphenyl)porphyrinate
T(C ₁₂ H ₂₅ O) ₁₆ TP	5,10,15,20-tetrakis(3,4,3'',4''-tetradodecyloxy- <i>o</i> -terphenyl)porphyrinate
T(<i>o</i> -NH ₂)PP	5,10,15,20-tetrakis(2-aminophenyl)porphyrinate
T(<i>o</i> -OCH ₂ CO ₂ C ₂ H ₅)PP	5,10,15,20-tetrakis(2-OCH ₂ CO ₂ C ₂ H ₅ phenyl)porphyrinate
T(<i>p</i> -Br)PP	5,10,15,20-tetrakis(4-bromophenyl)porphyrinate
T(<i>p</i> -Cl)PP	5,10,15,20-tetrakis(4-chlorophenyl)porphyrinate
T(<i>p</i> -CN)PP	5,10,15,20-tetra(4-cyanophenyl)porphyrinate

T(<i>p</i> -CO ₂ H)PP	5,10,15,20-tetra(4-carboxy)phenylporphyrinate
T(<i>p</i> -F)PP	5,10,15,20-tetrakis(4-fluorophenyl)porphyrinate
T(<i>p</i> -NO ₂)PP	5,10,15,20-tetrakis(4-nitrophenyl)porphyrinate
T(<i>p-n</i> -OC ₁₀ H ₂₁)PP	5,10,15,20-tetrakis(4- <i>n</i> -decyloxyphenol)porphyrinate
T(<i>p-n</i> -OC ₁₂ H ₂₅)PP	5,10,15,20-tetrakis(4- <i>n</i> -dodecyloxyphenol)porphyrinate
T(<i>p</i> -OCH ₃)PP	5,10,15,20-tetrakis(4-methoxyphenyl)porphyrinate
T(<i>p</i> -OH)PP	5,10,15,20-tetra(4-hydroxyphenyl)porphyrinate
TCEMPP	5,10,15,20-tetrakis((4-carboethoxymethyleneoxy)phenyl)porphyrinate
TCNE	tetracyanoethylene
TFPTBP	5,10,15,20-tetrakis(3-fluorophenyl)tetrabenzoporphyrinate
TFTBP	2, 3, 4, 5-tetrakis(fluoro)tetrabenzoporphyrinate
T _g	glass transition temperature
THF	tetrahydrofuran
THG	third harmonic generation
TMAP	5,10,15,20-tetra(5-trimethylaminopentyl)porphyrinate
TMAPTBP	5,10,15,20-tetrakis(4-dimethylaminophenyl)tetrabenzoporphyrinate
TMOPTBP	5,10,15,20-tetrakis(4-dimethoxyphenyl)tetrabenzoporphyrinate
TMP	5,10,15,20-tetramethylporphyrinate
TMPTBP	5,10,15,20-tetrakis(<i>p</i> -methylphenyl)tetrabenzoporphyrinate
TMPyP	5,10,15,20-tetrakis(4- <i>N</i> -methylpyridinium)porphyrinate
TMTBP	5,10,15,20-(tetramethyl)tetrabenzoporphyrinate
TPN	5,10,15,20-tetraphenylnaphthacene
TPP	5,10,15,20-tetraphenylporphyrinate
TPTBP	5,10,15,20-(tetraphenyl)tetrabenzoporphyrinate
TPyP	5,10,15,20-tetra- <i>para</i> -pyridylporphyrinate

Table 2. Mesomorphism of the octa-substituted porphyrins.

compound	transition*	T/ °C	reference
H ₂ ((OC ₄ H ₉)OEP)	K- I	154	5
Zn((OC ₄ H ₉)OEP)	K-D D-I	159 164	5
H ₂ ((OC ₆ H ₁₃)OEP)	K-D	111	5
Zn((OC ₆ H ₁₃)OEP)	K-D D-I	114 181	5
H ₂ ((OC ₈ H ₁₇)OEP)	K-D D-I	84 89	5
Zn((OC ₈ H ₁₇)OEP)	K-D D-I	107 162	5
Cu((OC ₈ H ₁₇)OEP)	K-D D-I	84 132	5
Pd((OC ₈ H ₁₇)OEP)	K-D D-I	89 123	5
Cd((OC ₈ H ₁₇)OEP)	K-D D-I	103 136	5
Zn((OC ₁₀ H ₂₁)OEP)	K-D D-I	86 142	5
Zn((OC ₈ H ₁₇)OECNP)	K-D D-I	61 147	5
Zn((OC ₈ H ₁₇)OENO ₂ P)	K-D D-I	85 140	5
Zn((OC ₈ H ₁₇)OEP) / Zn((OC ₁₀ H ₂₁)OEP) (1:1)	K-D D-I	93 118	5
H ₂ ((O ₂ C ₄ H ₉)OEP)	K-D D-I	178 222	6
Zn((O ₂ C ₄ H ₉)OEP)	K-D D-I	184 273	6
H ₂ ((O ₂ C ₆ H ₁₃)OEP)	K-D D-D' D'-I	59 132 220	6
Zn((O ₂ C ₆ H ₁₃)OEP)	K-D D-D' D'-I	61 136 232	6
H ₂ ((O ₂ C ₈ H ₁₇)OEP)	K-D D-D' D'-I	96 99 166	6
Zn((O ₂ C ₈ H ₁₇)OEP)	K-D D-D' D'-I	91 101 208	6

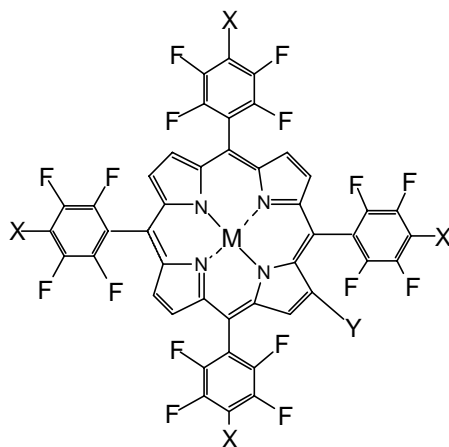
* Abbreviations: K = Crystalline phase, D = discotic columnar phase, I = isotropic fluid.

Table 3. Mesomorphism of the di-substituted zinc porphyrins.

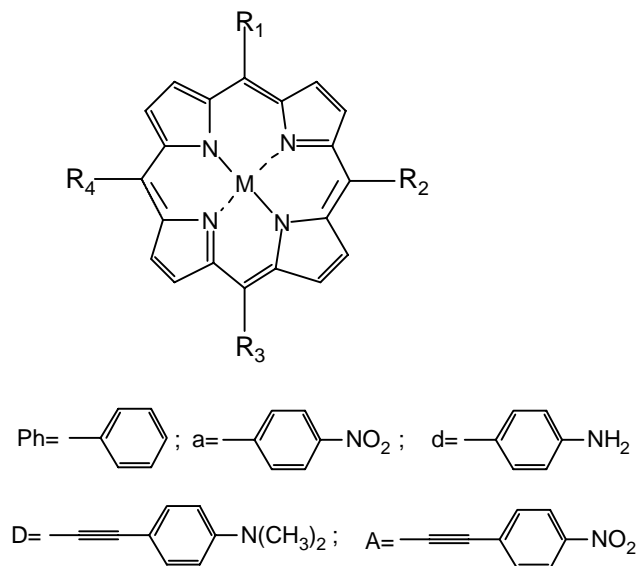
compound	transition*	T/ °C	reference
Zn((OC ₈ H ₁₇)DPP)	K-K'	233	25
	K'-S _b	243	
	S _b -I	270	
Zn((OC ₁₀ H ₂₁)DPP)	K-K'	181	25
	K'-S _b	235	
	S _b -I	249	
Zn((OC ₁₂ H ₂₅)DPP)	K-S _e '	140	25
	S _e '-S _e	207	
	S _e -S _b	224	
	S _b -I	234	
Zn((OC ₁₄ H ₂₉)DPP)	K-S _e '	144	25
	S _e '-S _e	176	
	S _e -S _b	181	
	S _b -I	213	
Zn((OC ₁₆ H ₃₁)DPP)	K-S _e '	156	25
	S _e '-S _e	162	
	S _e -S _b	181	
	S _b -I	200	
Zn((C ₇ H ₁₅)Cy)OHPP)	K-N	330	26
	N-I	353	
Zn(((OC ₇ H ₁₅)Ph)OHPP)	K-N	298	26
	N-I	320	
Zn((C ₇ H ₁₅)Cy) ₂ DPP)	K-S _a	330	26
	S _a -I	384	
Zn(((OC ₇ H ₁₅)Ph) ₂ DPP)	K-N	309	26
	N-I	433	
Zn(((OC ₈ H ₁₇) ₂ Ph) ₂ DPP)	K-I	177	27
Zn(((OC ₁₄ H ₂₉) ₂ Ph) ₂ DPP)	K-K'	37	27
	K'-I	143	
Zn(((OC ₈ H ₁₇) ₃ Ph) ₂ DPP)	K-K'	126	27
	K'-I	130	
Zn(((OC ₇ H ₁₅)Ph) ₂ DPP) with single ortho-OC ₈ H ₁₇ chain on 5-phenyl group	K-N	212	27
	N-I	244	
Zn(((C ₇ H ₁₅)Cy) ₂ DPP) with two ortho-OC ₈ H ₁₇ chains on 5,15-phenyl groups	K _{αα} -K _{αβ}	129	27
	(K _{αα} +K _{αβ})-I	178	
Zn(((OC ₇ H ₁₅)Ph) ₂ DPP) with two ortho-OC ₈ H ₁₇ chains on 5,15-phenyl groups	K _{αβ} -N	141	27
	N-I	177	
	K _{αα} -I	192	
Zn(((OC ₈ H ₁₇)Ph) ₂ DPP) with two ortho-OC ₈ H ₁₇ chains on 5,15-phenyl groups	K _{αβ} -N	122	27
	N-I	160	
	K _{αα} -I	176	
Zn(((OC ₇ H ₁₅)Ph) ₂ DPP) with two ortho-OSO ₂ -p-C ₆ H ₅ NO ₂ chains on 5,15-phenyl groups	K-N	310	28
	N-T _d	338	
Zn(((C ₇ H ₁₅)Cy) ₂ DPP) with two ortho-OSO ₂ -p-C ₆ H ₅ NO ₂ chains on 5,15-phenyl groups	K-T _d	323	28

Zn(((OC ₇ H ₁₅)Ph) ₂ DPP) with ortho-xylyl "strap" between 5,15-phenyl groups	K-K' K'-I	213 317	28
Zn(((OC ₁₀ H ₂₁) ₂ Ph) ₂ DPP)	K-I	251	29
Zn(((OC ₁₂ H ₂₅) ₂ Ph) ₂ DPP) with an additional phenyl ester spacer	K-K' K'-S _c S _c -N N-I	138 276 287 321	29
Zn(((OC ₁₂ H ₂₅) ₃ Ph) ₂ DPP) with two additional phenyl ester spacers	K-K' K-D D-I	107 188 288	29
Zn(((OC ₁₂ H ₂₅) ₂ Ph) ₂ DPP) with additional phenyl ester spacer and with two <i>o</i> -OC ₈ H ₁₇ chains on 5,15-phenyl groups	K-N N-I	133 169	29
Zn(((OC ₁₂ H ₂₅) ₃ Ph) ₂ DPP) with two additional phenyl ester spacers and with two <i>o</i> -OC ₈ H ₁₇ chains on 5,15-phenyl groups	K-N N-I	50 153	29

* Abbreviations: K = Crystalline phase, D = columnar phase, S_B = smectic B phase, S_E = smectic E phase, S_C = smectic C phase, S_A = smectic A phase, N = nematic phase, I = isotropic fluid, T_d = thermal decomposition.; αα and αβ refer to isomers of porphyrin.

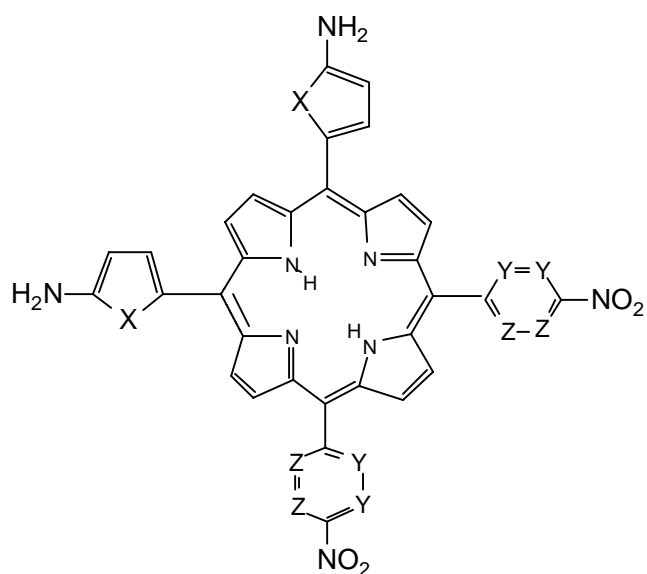
Table 4. Structure and first hyperpolarizability of Sen's β -pyrrole substituted "push-pull" fluoroarylporphyrins.^{40,41}

X	Y	M	β_{HRS} (10^{-30} esu)
F	H	2H	1.90 (Calc. 1.20)
N(CH ₃) ₂	H	2H	7.20 (Calc. 3.20)
F	NO ₂	2H	10.1 (Calc. 4.60)
N(CH ₃) ₂	NO ₂	2H	54.0 (Calc. 32.0)
F	H	Zn	2.80
N(CH ₃) ₂	H	Zn	11.2
F	NO ₂	Zn	11.8
N(CH ₃) ₂	NO ₂	Zn	92.0
F	H	Cu	3.90
N(CH ₃) ₂	H	Cu	19.2
F	NO ₂	Cu	19.6
N(CH ₃) ₂	NO ₂	Cu	118

Table 5. INDO/SCI-SOS calculated β values at 1064 nm for porphyrin-bridged donor-acceptor molecules.⁴²

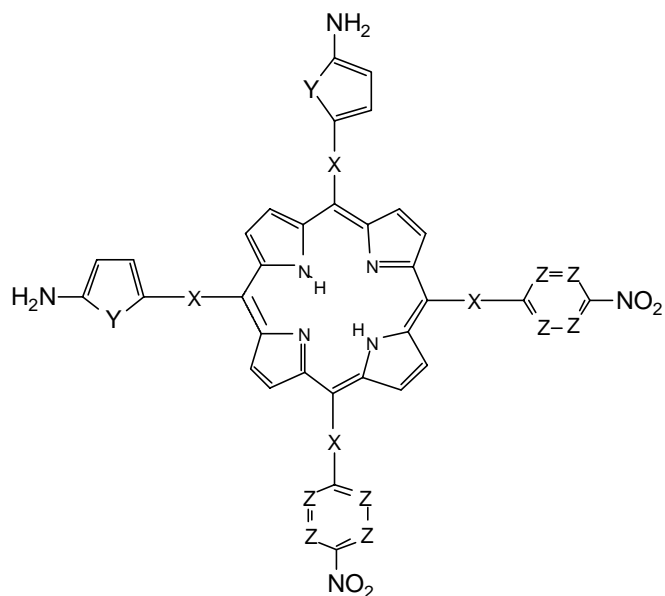
No.	Porphyrins	R ¹	R ²	R ³	R ⁴	M	β (10 ⁻³⁰ esu)
1	Zn(DPP)	Ph	H	Ph	H	Zn	-
2	D-Zn(DPP)	Ph	D	Ph	H	Zn	106.7
3	Zn(DPP)-A	Ph	H	Ph	A	Zn	147.5
4	D-Zn(DPP)-A	Ph	D	Ph	A	Zn	477.3
5	d-H ₂ (DPP)-A	Ph	d	Ph	a	H ₂	50.9
6	d ₂ -H ₂ (P)-a ₂	d	d	a	a	H ₂	95.3
7	d ₃ -H ₂ (P)-a	d	d	d	a	H ₂	53.6
8	d-H ₂ (P)-a ₃	d	a	a	a	H ₂	65.2

Table 6. INDO/S Hamiltonian and singles-only CI calculated β values for pyrrole substituted triphenyl porphyrins.⁴⁶



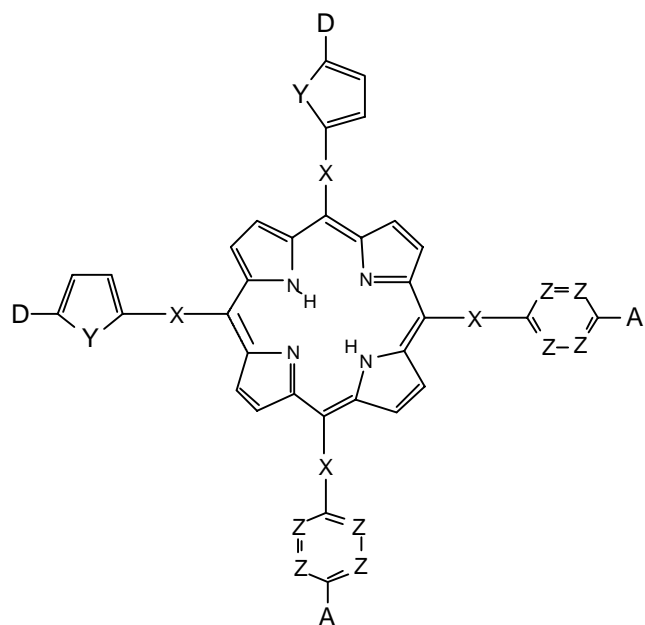
No.	X	Y	Z	$\beta_x (10^{-30} \text{ esu})$	$\mu\beta_x (10^{-48} \text{ esu})$
1a	CH=CH	N	CH	64.02	687.76
1b	CH=CH	N	N	78.98	1349.74
1c	O	CH	CH	75.55	908.32
1d	O	N	CH	87.68	942.84
1e	O	N	N	85.02	1222.98
1f	S	CH	CH	46.42	838.73
1g	S	N	CH	59.44	1042.33
1h	S	N	N	69.35	1352.37
1i	NH	CH	CH	80.43	839.91
1j	NH	N	CH	89.19	742.33
1k	NH	N	N	93.14	1071.33

Table 6 (cont.)



No.	X	Y	Z	$\beta_x (10^{-30} \text{ esu})$	$\mu\beta_x (10^{-48} \text{ esu})$
2a	C=C	CH=CH	CH	146.75	2633.8
2b	N=N	CH=CH	CH	193.96	5454.7
2c	N=N	NH	N	245.49	5892.8

Table 6 cont.



No.	D	A	X	Y	Z	$\beta_x (10^{-30} \text{ esu})^*$	$\mu\beta_x (10^{-48} \text{ esu})$
3a	NH ₂	NO ₂	C=C	CH=CH	CH	157.22	2492.4
3b	NH ₂	NO ₂	N=N	CH=CH	CH	218.76	4625.4
3c	NH ₂	NO ₂	N=N	NH	N	345.75	3616.78
3d	NO ₂	NH ₂	C=C	CH=CH	CH	98.86	2390.65
3e	NO ₂	NH ₂	N=N	CH=CH	CH	352.69	6435.4
3f	NO ₂	NH ₂	N=N	NH	N	305.22	8897.73

Table 7. Third-order nonlinear optical susceptibility data of metalloporphyrins compounds measured by different techniques.³⁰

Porphyrin	γ (10^{-30} esu)	$\chi^{(3)}$ (10^{-12} esu)	Wave-length (μm)	Measure-ment Technique	Reference
H ₂ (TPP)	-	28.6	0.532	DFWM	50
	-10.2	-	0.802	Z-Scan	58
Zn(TPP)		14.3	0.532	DFWM	50
	-16.6	-	0.802	Z-Scan	58
Co(TPP)		7.16	0.532	DFWM	50
H ₂ (TC ₁₃ PP)		40.0	0.532	DFWM	51
Co(T(4-n-C15H31)PP)		56.0	0.532	DFWM	51
Ni(T(4-n-C15H31)PP)		69.0	0.532	DFWM	51
Cu(T(4-n-C15H31)PP)		50.0	0.32	DFWM	51
Zn(T(4-n-C15H31)PP)		15.0	0.532	DFWM	51
V(T(4-n-C15H31)PP)(O)		32.0	0.532	DFWM	51
Zn(TMAPTBP)	10	28000	0.532	DFWM	52
Zn(TMTBP)	3.3	15000	0.532	DFWM	52
Zn(TFPTBP)	3.8	13000	0.532	DFWM	52
Zn(TMOPTBP)	4.8	14000	0.532	DFWM	52
	0.0010	0.078	1.064	OKE	53
Zn(TMPTBP)	4.0	12000	0.532	DFWM	52
Mg(OMTBP)	1.6	8000	0.532	DFWM	52
Zn(TPTBP)	0.90	3000	0.532	DFWM	52
	0.0018	0.091	1.064	OKE	53
Zn(TFTBP)	0.70	2000	0.532	DFWM	52
H ₂ (TBP)	0.50	3000	0.532	DFWM	52

H ₂ OEP	0.00049	1.9	1.907	THG	54
Mn(OEP)Cl	0.0006	2.6	1.907	THG	54
Me ₄ (OEP) ⁺²	0.0024	10	1.907	THG	54
Mg(OPTAP)	-	11.7	0.598	DFWM	55
Porphyrin Polymer		73000	-	-	56
H ₂ DEtyP monomer		0.6	0.532	DFWM	57
Zn(DEtyP) monomer		1.2	0.532	DFWM	57
(H ₂ (DEtyP)) _n polymer		510	0.532	DFWM	57
(Zn(DEtyP)) _n polymer		128	0.532	DFWM	57
(TPP)-1	-8.5	-	0.784	Z-Scan	253
(TPP)-2	-48.2	-	0.784	Z-Scan	253
(TPP)-3	-6.5	-	0.784	Z-Scan	253
(TPP)-4	-6.7	-	0.784	Z-Scan	253
(TPP)-5	-6.3	-	0.784	Z-Scan	253
(TPP)-6	-6.2	-	0.784	Z-Scan	253
Cu(TPP)	-26.7	-	0.802	Z-Scan	58
Ni(TPP)	-52.8	-	0.802	Z-Scan	58
Sn(TCEMPP)I ₂	-109.7	-	0.802	Z-Scan	58
Sn(TCEMPP)(N ₃) ₂	-9.7	-	0.802	Z-Scan	58
Sn(TCEMPP)Br ₂	-7.5	-	0.802	Z-Scan	58
Sn(TCEMPP)Cl ₂	-4.7	-	0.802	Z-Scan	58
Sn(TCEMPP)(OH) ₂	-3.9	-	0.802	Z-Scan	58
Cu(PSI)	-	0.88	0.532	DFWM	59
Cu(PSIBr ₈)	-	0.50	0.532	DFWM	59
Cu(PSIBr ₉)	-	0.47	0.532	DFWM	59

Cu(PSIBr ₁₂)	-	0.40	0.532	DFWM	59
Cu(MSICl ₈)	-	0.35	0.532	DFWM	59
Cu(TPP)	-	1.03	0.532	DFWM	59
C ₆₀ :(TPP) (film)	5720		0.590	DFWM	60
C ₆₀ :(TPP) (multilayer)		7.74	1.907	THG	62
C ₆₀ :(TPP) (composite)		11.5	1.907	THG	62

Table 8. Channel Volumes for Various Porphyrin Complexes.¹³⁵

Porphyrin Complex	Z	Unit Cell Volume (Å ³)	Porphyrin Volume/unit cell ^a (Å ³)	Solvate Volume/unit cell ^a (Å ³)	Void Volume/unit cell ^a (Å ³)	Total Channel Volume/unit cell ^b (Å ³)
H ₂ (TPP)	1	801.9	590.8	0	211	211 [26.3%]
H ₂ (T(3',5'-DHP)P) • 5 EtOAc	1	1581	620.8	412.5	547.7	960.2 [60.7%]
H ₂ (T(2',6'-DHP)P) • 4 EtOAc	2	2770.9	1233.0	660	877.9	1537.9 [55.5%]
H ₂ (T(3',5'-DHP)P) • 7 C ₆ H ₅ CN	2	3811	1241.6	1547	1022	2569.4 [67.4%]
Zn(T(2',6'-DHP)P)(EtOAc) ₂ • 2 EtOAc	1	1387.2	804.1	168	415.2	583.2 [42.0%]
Zn(T(3',5'-DHP)P)(THF) ₂ • 3 CH ₂ Cl ₂ • 2 THF	1	1597.6	755.8	326.9	514.8	841.7 [52.7%]
Mn(T(3',5'-DHP)P)(THF) ₂ • Cl ⁻ • 2 THF • 5 C ₆ H ₅ CH ₃	2	4289	1612.2	1355	1321.8	2676.7 [62.4%]

^aPorphyrin and solvate van der Waals volumes were calculated from Quanta for each unit cell. Void volume is defined as the unit cell volume minus the sum of the porphyrin volume and the solvate volume. For the metalloporphyrins, the volumes of the coordinated ligands were counted as part of the porphyrin volume.

^bTotal channel volume is defined as the sum of void and solvate volume, in Å³. Values in brackets refer to the percentage of total channel volume in the unit cell.

Table 9: Logarithm of Anion Selectivity Coefficients for Mn(III) Porphyrin Based Membranes

Anion	Por 1	Por 2	Por 3	Por 4	Por 5	Por 6	Por 7	Por 8	Por 9
Cl ⁻	0.0	0.0	0.0	0.0	0.0	0.0	0.0	0.0	0.0
Br ⁻	0.6	0.3	0.5	0.2	0.2	0.4	0.3	0.4	0.6
I ⁻	2.8	1.5	1.5	1.5	1.6	1.5	1.7	2.1	2.5
Sal	2.7	2.1	2.4	3.2	2.0	2.4	2.4	2.4	2.3
SCN ⁻	3.0	1.3	1.6	2.5	3.5	3.0	3.2	2.0	2.0
IO ₄ ⁻	4.0	1.8	2.1	1.7	0.6	1.5	1.0	3.0	2.6
ClO ₄ ⁻	4.6	1.5	1.7	1.5	0.4	1.2	0.8	3.5	3.3

VIII. Figure Captions

- Figure 1.** Structure of *uro*-porphyrin I octa-*n*-dodecyl ester ($R = \text{CH}_2\text{CO}_2\text{C}_{12}\text{H}_{25}$, $M = \text{H}_2$) and other octylether and octylester porphyrins ($R = \text{CH}_2\text{OC}_n\text{H}_{2n+1}$, $n = 4, 6, 8, 10$ or $R = \text{CH}_2\text{O}_2\text{C}_n\text{H}_{2n+1}$, $n = 4, 6, 8$; $M = \text{H}_2, \text{Zn}, \text{Cu}, \text{Pd}, \text{Cd}$).
- Figure 2.** Schematic representation of the tilted columnar stacking.⁷
- Figure 3.** Schematic representation of the columnar arrangement of discotic zinc *n*-decyl ether octa-substituted porphyrin stacks.⁸
- Figure 4.** Readout current pulses with the same writing conditions: (a) initial readout and (b) after 1.5 billion write/erase cycles.¹¹
- Figure 5.** Structure of sulfur-substituted azaporphyrin.
- Figure 6.** Structure of *n*-pentadecylphenyl porphyrin.
- Figure 7.** Temperature dependence of the dark-current under 4000 V/cm.¹³
- Figure 8.** Temperature dependence of the photocurrent at 620 nm under 4000 V/cm.¹³
- Figure 9.** Structure of substituted 5,10,15,20-tetrakis(3,4,3'',4''-tetradecyloxy-*o*-terphenyl)porphyrins ($R^1 = R^2 = n\text{-C}_{12}\text{H}_{25}\text{O}$; $M = \text{H}_2$ or Cu ; or $R^1 = n\text{-C}_{12}\text{H}_{25}\text{O}$, $R^2 = \text{H}$; $M = \text{H}_2$).
- Figure 10.** Orientation of $\text{H}_2(\text{TPP})$ and Neumann's mesogenic *o*-amino-substituted tetraphenylporphyrin in nematic liquid crystal phase.²⁰
- Figure 11.** Structure of Nolte's mesomorphic inducing "clipper" molecule.²² and schematic representation of a tetra-substituted porphyrin guest being held by the "clipper" molecule.²²
- Figure 12.** Histogram of DSC results for T(3,5-COOR)PP materials: black = solid phase, white = mesophase, gray = isotropic.
- Figure 13.** Structure of 3,5-di-carboxyphenyl porphyrin.
- Figure 14.** Structure of ether-substituted di-phenyl porphyrins ($R = \text{C}_n\text{H}_{2n+1}$, $n = 8, 10, 12, 14, 16$)^{25,26}
- Figure 15.** Structure of ester substituted diphenyl porphyrins ($R = \text{CO-C}_6\text{H}_{10}\text{-OC}_7\text{H}_{15}$, $R' = \text{H}$; or $R = \text{CO-C}_6\text{H}_4\text{-OC}_7\text{H}_{15}$, $R' = \text{H}$; or $R = R' = \text{CO-C}_6\text{H}_{10}\text{-OC}_7\text{H}_{15}$; or $R = R' = \text{CO-C}_6\text{H}_4\text{-OC}_7\text{H}_{15}$; or $R = R' = (2',4'\text{-OC}_8\text{H}_{16})\text{C}_6\text{H}_4$ or $R = R' = (2',4'\text{-OC}_{14}\text{H}_{29})\text{C}_6\text{H}_4$ or $R = R' = (2',4',6'\text{-OC}_8\text{H}_{16})\text{C}_6\text{H}_4$).
- Figure 16.** Structure of ester substituted di-phenyl porphyrin with single lateral chain.
- Figure 17.** Structure of ester substituted di-phenyl porphyrins with two lateral chains ($R = \text{C}_6\text{H}_{10}\text{-}n\text{-C}_7\text{H}_{15}$; or $R = \text{C}_6\text{H}_4\text{-O-}n\text{-C}_m\text{H}_{2m+1}$, $m = 7,8$).
- Figure 18.** Structure of *o*-(*p*-nitrophenylsulfonyl)oxy substituted Zn^{II} di-phenyl porphyrin ($R = \text{C}_6\text{H}_4\text{-O-}n\text{C}_7\text{H}_{15}$ or $R = \text{C}_6\text{H}_{10}\text{-}n\text{C}_7\text{H}_{15}$). Wang, 1996 #104]
- Figure 19.** Structure of "strapped" Zn^{II} di-phenyl porphyrin ($R = \text{-C}_6\text{H}_4\text{-O-}n\text{C}_7\text{H}_{15}$).²⁸
- Figure 20.** Structure of catenane substituted di-phenyl porphyrin systems ($Y = \text{H}$; $n = 10, m = 0$; or $Y = \text{H}$; $n = 12, m = 1$; $Y = \text{OC}_{12}\text{H}_{25}$; $n = 12, m = 2$).²⁹
- Figure 21.** Structure of catenane substituted di-phenyl porphyrin systems with lateral chains ($Y = \text{H}$; $m = 1$; or $Y = \text{OC}_{12}\text{H}_{25}$; $m = 2$)²⁹
- Figure 22.** Structure of 5,15-bis(3,4,3'',4''-tetradecyloxy-*o*-terphenyl)porphyrin derivatives ($R^1 = R^2 = \text{C}_{12}\text{H}_{25}\text{O}$; or $R^1 = R^2 = \text{C}_{16}\text{H}_{33}\text{O}$; or $R^1 = \text{C}_{12}\text{H}_{25}\text{O}$, $R^2 = \text{H}$).
- Figure 23.** Structure of 5,15-bis(3,4-didodecyloxyphenyl)porphyrin.
- Figure 24.** Structure of 5,15-bis(4-didodecyloxybiphenyl)porphyrin.
- Figure 25.** Structure of Suslick's donor-acceptor "push-pull" tetraphenylporphyrin, $R = \text{NO}_2$ or NH_2 .
- Figure 26.** Effects of environment on second-order NLO behavior.
- Figure 27.** Langmuir-Blodgett isotherms or amphiphilic derivatives of push-pull porphyrins.
- Figure 28.** Structure of LeCoer's zinc porphyrin dimer.
- Figure 29.** Structure of Peng's porphyrin polyimide.
- Figure 30.** Structure of Peng's zinc porphyrin polyimide system with pendant organic NLO chromophore.
- Figure 31.** Structure of Rao's tetrabenzoporphyrin derivatives $\text{Zn}(\text{TMAPTBP})$: $M = \text{Zn}$, $X = \text{H}$, $R = p\text{-C}_6\text{H}_4\text{-N}(\text{CH}_3)_2$; $\text{Zn}(\text{TMTBP})$: $M = \text{Zn}$, $X = \text{H}$, $R = \text{CH}_3$; $\text{Zn}(\text{TFPTBP})$: $M = \text{Zn}$, $X = \text{H}$, $R = m\text{-FC}_6\text{H}_4$; $\text{Zn}(\text{TMOPTBP})$: $M = \text{Zn}$, $X = \text{H}$, $R = p\text{-CH}_3\text{O-C}_6\text{H}_4$; $\text{Zn}(\text{TMPTBP})$: $M = \text{Zn}$, $X = \text{H}$, $R = p\text{-}$

$\text{CH}_3\text{C}_6\text{H}_4$; Mg(DMTBP): M = Mg, X = 8-H and 8- CH_3 , R = H; Zn(TPTBP): M = Zn, X = H. R = C_6H_5 ; Zn(TFTBP): M = Zn, X = F, R = H; TBP: M = H_2 , X = R = H).

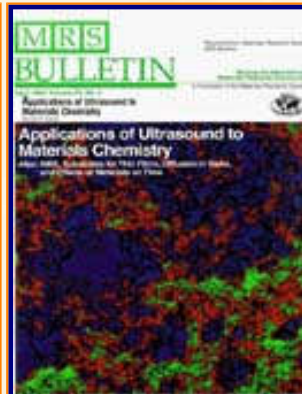
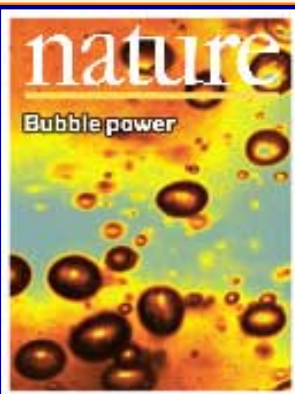
- Figure 32.** Structure of Hosoda's extended porphyrinic ring system.
- Figure 33.** Structure of Norwood's magnesium octaphenyltetrazaporphyrin.
- Figure 34.** Structure of Anderson's 5,10,15,20-diethynylporphyrinatozinc polymer.
- Figure 35.** Structure of Bao's porphyrin monomer and polymer.
- Figure 36.** Structure of Kumar's basket handle porphyrins (Cu(PSI): $\text{R}^1\text{-R}^8 = \text{H}$; X = H; Cu(PSIBr₉): $\text{R}^1 = \text{Br}$, $\text{R}^2 - \text{R}^8 = \text{H}$, X = Br; Cu(PSI₁₂): $\text{R}^1 = \text{R}^2 = \text{R}^5 = \text{R}^6 = \text{Br}$, $\text{R}^3 = \text{R}^4 = \text{R}^7 = \text{R}^8 = \text{H}$, X = Br).
- Figure 37.** Structure of Shi's metallotexaphyrin compounds (M = Cd, R = H, Cl, CH_3 ; M = Sn, R = H, M = Gd, R = CO_2Na).
- Figure 38.** Structure of Su's β -octabromo(TPP)s (M = H_2 , Co, Cu, Pb, Cd, Zn).
- Figure 39.** Gust and Moore's triad (top) and pentad (bottom) and Wasielewski's triad (middle).
- Figure 40.** Osuka's stacked porphyrin model for special pair.
- Figure 41.** Osuka's triads, diporphyrin—porphyrin—pyromellitimide.
- Figure 42.** Molecular triad of diarylporphyrin(P)-carotenoid polyene (C)-fullerene (C_{60}).
- Figure 43.** Structure of PDBCI.
- Figure 44.** Structure of $\text{D}_1\text{-A}_1\text{-A}_2\text{-D}_2$.
- Figure 45.** Molecular wires prepared by (A) Crossley and Burn. (B) Wagner and Lindsey.
- Figure 46.** Molecular gates (A) linear. (B) T-shape.
- Figure 47.** Porphyrin Assemblies. (A) Porphyrin monomer with two oligothiophene. (B) 1-D porphyrin arrays connected with molecular conjugated wires and (C) insulating wires. (D) 2-D porphyrin arrays connected with molecular conjugated wires.
- Figure 48.** Porphyrin Assemblies. (A) Functionalized M(TPP) as building block. (B) Porphyrin trimer. (C) Porphyrin pentamer.
- Figure 49.** Porphyrin Assemblies. (A) Functionalized M(TPP) bridged-dimer as building block. (B) Porphyrin pentamer. (C) porphyrin monomer.
- Figure 50.** 1,4-Phenylene-bridged linear porphyrin arrays. (A) dimer. (B) trimer to nonamer.
- Figure 51.** 5,10,15,20-Linked porphyrin arrays.
- Figure 52.** Windmill-like porphyrin arrays.
- Figure 53.** Convergent strategy for the synthesis of porphyrin pentamer.
- Figure 54.** The synthetic routes of 4-(BDPY)benzaldehyde, 3,5-bis(BDPY)benzaldehyde, and mixed-aldehyde condensation reactions for PDPY-substituted porphyrin arrays.
- Figure 55.** Self-assembly of square multi-porphyrin arrays.
- Figure 56.** A 21-component multi-porphyrin array. Drain, C.M.; Nifiatis, F.; Vasenko, A.; Batteas, J.D. *Angew. Chem. Int. Ed.* **1998**, *37*, 2344.
- Figure 57.** Porphyrin arrays linked by yne and polyene units.
- Figure 58.** Porphyrin and guest packing in a typical porphyrin sponge.¹²⁷
- Figure 59.** Examples of typical porphyrin sponges with 1:2 porphyrin:guest ratio.¹²⁶
- Figure 60.** Porphyrin sponges with large guest molecules.¹²⁶
- Figure 61.** Basic packing motif for porphyrin clathrates in 6-, 5-, and 4-coordinate TPP complexes.¹²⁶
- Figure 62.** Examples of materials with high porphyrin:guest ratios.¹²⁷
- Figure 63.** Examples of layered clathrate materials.¹⁴⁰
- Figure 64.** Schematic of interporphyrin interactions in *p*-chloro- and *p*-bromo-substituted TPPs.¹³¹
- Figure 65.** Layered structure in $\text{Zn}(\text{T}(\text{p-Cl})\text{PP})\bullet\text{C}_7\text{H}_8\text{O}_2$ in which arrows indicate guest filled-channels (top); illustration of channels in the same material (bottom)¹²⁹
- Figure 66.** Helical packing in $\text{Zn}(\text{T}(\text{p-Cl})\text{PP})\bullet\text{C}_6\text{H}_2\text{NO}_2$ ¹³⁰
- Figure 67.** Herring-bone packing arrangement of $\text{Zn}(\text{T}(\text{p-Cl})\text{PP})\bullet\text{C}_7\text{H}_7\text{Cl}$.¹²⁹
- Figure 68.** Corrugated layer arrangement in $\text{Zn}(\text{T}(\text{p-Br})\text{PP})\bullet\text{C}_6\text{H}_7\text{N}$.¹³¹
- Figure 69.** Hydrogen-bonding network in $\text{Zn}(\text{T}(\text{p-OH})\text{PP})\bullet\text{C}_7\text{H}_6\text{O}\bullet\text{H}_2\text{O}$.¹³⁰
- Figure 70.** Layered structure in $\text{Cu}(\text{T}(\text{p-OH})\text{PP})\bullet\text{C}_8\text{H}_8\text{O}$ (top); illustration of guest-filled channels in the same material (bottom)¹³⁰

- Figure 71.** Illustration of “sandwich” packing of guest molecule in $\text{Zn}(\text{T}(p\text{-OH})\text{PP}) \bullet 5\text{C}_7\text{H}_8\text{O}_2$ ¹³⁰
- Figure 72.** Packing arrangement observed in $\text{Zn}(\text{T}(p\text{-OH})\text{PP}) \bullet 3\text{C}_7\text{H}_8$ and xylene species (average guest position represented by a hexamethylbenzene above)¹³⁰
- Figure 73.** Crystal packing in $\text{Zn}(\text{T}(p\text{-OH})\text{PP}) \bullet 2\text{C}_7\text{H}_8\text{O} \bullet 2\text{H}_2\text{O}$ ¹³⁰
- Figure 74.** Layered structure in $\text{Zn}(\text{T}(p\text{-OCH}_3)\text{PP}) \bullet \text{C}_6\text{H}_6\text{O} \bullet \text{H}_2\text{O}$ (top); illustration of channels in the same material (bottom).¹³⁰
- Figure 75.** The crystal structure of $\text{Zn}(\text{T}(p\text{-CH}_2\text{OH})\text{PP}) \bullet 2\text{C}_8\text{H}_8\text{O}_2$ showing (a) guest-filled channels and (b) corrugated layer structure.¹³⁰
- Figure 76.** Hydrogen-bond dimer between $-\text{CN}$ group and β -pyrrole hydrogen.¹³³
- Figure 77.** Crystal packing showing interporphyrin bonding and oval-shaped cavities in $\text{Cu}(\text{T}(p\text{-CN})\text{PP}) \bullet \text{CHCl}_3$ ¹³³
- Figure 78.** Crystal packing showing interporphyrin bonding and square-shaped cavities in $\text{Zn}(\text{T}(p\text{-CN})\text{PP}) \bullet \text{C}_7\text{H}_8\text{O}$.¹³³
- Figure 79.** Crystal packing showing offset stacking and expanded layer arrangement in $\text{Zn}(\text{T}(p\text{-CN})\text{PP}) \bullet 2.5\text{C}_9\text{H}_{10}\text{O}_2$ ¹³³
- Figure 80.** Crystal packing showing interporphyrin hydrogen-bonding in $\text{Zn}(\text{T}(p\text{-NO}_2)\text{PP}) \bullet 3\text{C}_{10}\text{H}_{12}\text{O}_2$ (solvent molecules omitted for clarity)¹³³
- Figure 81.** Crystal packing observed in $\text{Zn}(\text{T}(p\text{-CN})\text{PP}) \bullet \text{CHCl}_3 \bullet \text{C}_6\text{H}_6$ ¹³³
- Figure 82.** Crystal packing observed in $\text{Cu}(\text{T}(p\text{-CN})\text{PP}) \bullet 2\text{C}_6\text{H}_5\text{NO}_2$ ¹³³
- Figure 83.** Interporphyrin bonding, layered structure and cavities in $\text{Zn}(\text{TpCPP}) \bullet \text{C}_8\text{H}_{10}\text{O}$.¹³⁴
- Figure 84.** Interporphyrin bonding and interpenetrating networks in $\text{Zn}(\text{TpCPP}) \bullet 3\text{C}_2\text{H}_6\text{SO}$.¹³⁴
- Figure 85.** 5,10,15,20-Tetrakis(2',6'-dihydroxyphenyl)porphyrin, $\text{H}_2(\text{T}(2',6'\text{-DHP})\text{P})$, and 5,10,15,20-Tetrakis(3',5'-dihydroxyphenyl)porphyrin, $\text{H}_2(\text{T}(3',5'\text{-DHP})\text{P})$.
- Figure 86.** Molecular packing diagrams of $\text{H}_2(\text{T}(3',5'\text{-DHP})\text{P}) \bullet 5\text{EtOAc}$ showing (a) channels between porphyrins columns; (b) channels perpendicular to the columns.¹³⁵
- Figure 87.** Molecular packing diagrams of $\text{H}_2(\text{T}(3',5'\text{-DHP})\text{P}) \bullet 7\text{C}_6\text{H}_5\text{CN}$: (a) showing channels formed by one-dimensional corrugated sheets (light and dark shading); (b) showing approximately perpendicular channels.¹³⁵
- Figure 88.** (a) Two-dimensional layer from the crystal structure of $\text{Zn}(\text{T}(3',5'\text{-DHP})\text{P})(\text{THF})_2 \bullet 2\text{THF} \bullet 3\text{CH}_2\text{Cl}_2$. (b) Molecular packing diagram showing interconnected layers. Porphyrins in dark and light shades indicate two different layers. Hydrogen-bonding interactions are shown with dotted lines. Non-coordinated solvates are omitted for clarity.¹³⁵
- Figure 89.** Molecular packing diagram of $\text{Mn}(\text{T}(3',5'\text{-DHP})\text{P})(\text{THF})_2 \bullet \text{Cl} \bullet 2\text{THF} \bullet 5\text{C}_6\text{H}_5\text{CH}_3$ showing two-dimensional sheets of porphyrin linked by unusual square-planar Cl^- anions hydrogen bonding to four metalloporphyrins. Spheres indicate bridging chloride ions. Solvate molecules and coordinated THF ligands omitted for clarity.¹³⁵
- Figure 90.** Space-filled diagram showing channels in $\text{Mn}(\text{T}(3',5'\text{-DHP})\text{P})(\text{THF})_2 \bullet \text{Cl} \bullet 2\text{THF} \bullet 5\text{C}_6\text{H}_5\text{CH}_3$. Solvate molecules and coordinated THF ligands omitted for clarity.¹³⁵
- Figure 91.** Molecular packing diagram of $\text{H}_2(\text{T}(2',6'\text{-DHP})\text{P}) \bullet 4\text{EtOAc}$ showing two-dimensional layered structure. Hydrogen-bonding interactions between the hydroxyl groups are shown with dotted lines. Solvent molecules are omitted for clarity.¹³⁵
- Figure 92.** Molecular packing diagram of $\text{H}_2(\text{T}(2',6'\text{-DHP})\text{P}) \bullet 4\text{EtOAc}$ showing channels between the porphyrin layers. Solvent molecules are omitted for clarity.¹³⁵
- Figure 93.** Crystal packing in $\text{Zn}(\text{TPyP})$ coordination polymers.¹⁴⁰
- Figure 94.** Zigzag packing in $\text{Zn}(\text{TPyP}) \bullet \text{C}_6\text{H}_7\text{N}$.¹⁴⁰
- Figure 95.** Three-dimensional interporphyrin bonding observed in $\text{Zn}(\text{TPyP}) \bullet 3\text{H}_2\text{O}$.¹⁴⁰

- Figure 96.** Crystal structure of $\text{Zn}(\text{TPyP})\bullet\text{CH}_3\text{OH}\bullet 2\text{H}_2\text{O}$. The marked hexagons indicate hydrogen-bonding interactions between six water molecules and pyridyl groups of porphyrins in adjacent unit cells.¹⁴⁰
- Figure 97.** Interporphyrin coordination in $\text{Zn}(\text{T}(\text{p-CN})\text{PP})\bullet 2\text{C}_6\text{H}_5\text{NO}_2$ to form two-dimensional network. Guest molecules removed for clarity.¹³³
- Figure 98.** Crystal structure of $\text{Zn}(\text{T}(\text{p-CN})\text{PP})\bullet 2\text{C}_6\text{H}_5\text{NO}_2$ showing arrangement of guest molecules.¹³³
- Figure 99.** Schematic illustration of three-dimensional porphyrin network in $\text{Pd}(\text{TPyP})\bullet\text{Cd}(\text{NO}_3)_2\bullet 8.6\text{H}_2\text{O}$ in which porphyrins are represented as squares and cadmium ions as circles. Solvent molecules are omitted for clarity.¹⁴¹
- Figure 100.** Packing arrangement in $[\text{Cu}(\text{TPyP})\bullet\text{Cu}]_n^{n+}$ framework. Larger circles represent copper ions. Solvent and non-coordinating anions omitted for clarity.¹⁴²
- Figure 101.** (a) Packing arrangement in $[\text{Cu}(\text{TCNPP})\bullet\text{Cu}]_n^{n+}$ framework. Separate frameworks are indicated by light and dark shading. Large circles represent copper ions. (b) Schematic representation of extended framework. Cu(II) ions in center of porphyrin macrocycle represented by small circles. Cu(I) ions coordinating between porphyrin molecules indicated by large circles. Solvate and non-coordinating anions omitted for clarity.¹⁴²
- Figure 102.** Parallel polymeric porphyrin bands showing coordinate bonding between tetrabidentate porphyrin carboxylate and calcium ions both as space filling and schematic models (top). In this schematic model, intersection of cylinders represents center of porphyrin macrocycle and corners represent calcium ions. Extended three-dimensional structure showing interpenetration of porphyrin bands (bottom). Guest pyridine molecules and coordinated water molecules have been omitted for clarity.¹⁴⁴
- Figure 103.** Crystal packing in cobalt coordinative network of Co(III) derivative of $\text{H}_2(\text{TpCPP})$.¹⁴⁵
- Figure 104.** Crystal packing in Mn(II) coordinative network of Mn(III) derivative of $\text{H}_2(\text{TpCPP})$.¹⁴⁵
- Figure 105.** Crystal packing in $\text{H}_2(\text{DiCarPP})$ molecular species showing channels between porphyrin columns. Solvent molecules omitted for clarity.¹⁴³
- Figure 106.** (Top) Schematic of zeolite L main channel and (bottom) idealized $\text{Zn}(\text{TMPyP}^{4+})$ methylviologen (MV^{2+})_n complex.¹⁵¹
- Figure 107.** Cyclic voltammograms obtained for Cu(TPP)/zeolite Y modified carbon paste electrode in absence (A), presence of $1.0 \times 10^{-5} \text{ mol L}^{-1}$ hydrazine (B) and $1.0 \times 10^{-3} \text{ mol L}^{-1}$ cysteine (C). Supporting electrolyte of $0.5 \text{ mol L}^{-1} \text{ NaClO}_4$ at pH 7 and a scan rate of 20 mV s^{-1} .¹⁵⁷
- Figure 108.** Diffuse reflectance spectra of zeolite Y with (top) encapsulated Mn(TMP) showing porphyrin Soret band and (bottom) Mn(II) ions.¹⁵⁵
- Figure 109.** Comparison of dioxygen and argon absorption isotherms of Co(TMP)/zeolite Y material at 25°C .¹⁵⁶
- Figure 110.** XRD patterns of (a) $\text{Ru}(\text{T}(\text{p-Cl})\text{PP})(\text{CO})(\text{EtOH})$, (b) a physical mixture of $\text{Ru}(\text{T}(\text{p-Cl})\text{PP})(\text{CO})(\text{EtOH})$ and APTES surfaced modified MCM-41 in a mass ratio of 8:92, (c) 8.3 mass % APTES surface modified Ru/M-41 and (d) MCM-41 and APTES surface modified MCM-41.¹⁵⁷
- Figure 111.** EPR spectra of photoinduced $\text{H}_2(\text{TPP}^{\bullet+})$ in TiMCM-41, MCM-41 and AIMCM-41 after 30 minutes irradiation with $\lambda > 350 \text{ nm}$ at room temperature.¹⁵⁸
- Figure 112.** Structure of $\text{M}(\text{TMAP})$ species.¹⁶⁰
- Figure 113.** Postulated arrangement of the intercalated $\text{H}_2(\text{TSPP})$ inside the LDH.
- Figure 114.** Schematic representation of the $(\text{TpCPP})^{4+}$ (a) and $(\text{ToCPP})^{4+}$ (b) oriented in the interlayers of LDH.
- Figure 115.** Various “shish kebab” one-dimensional coordination polymers.
- Figure 116.** A linearly conjugated porphyrin tetramer.
- Figure 117.** Synthesis of a porphyrin polymer via the Heck reaction.
- Figure 118.** Synthesis of conjugated porphyrin polymers via the Wittig reaction.
- Figure 119.** Synthesis of one-dimensional porphyrin-oligothiophene polymers.

- Figure 120.** Schematic representation of a ferroelectric coordination polymer and dipole moment switching in response to an external field.
- Figure 121.** The dipole moment of metalloporphyrins.
- Figure 122.** The double-well potential of the position of the metal atom relative to the porphyrin core.
- Figure 123.** Three classes of the non-symmetrical bridging ligands.
- Figure 124.** Three alignments of bridging ligands in metalloporphyrin polymers and ORTEP plots of the packing diagrams.
- Figure 125.** Response of Pt(OEP)-doped sol-gel glass on switching between (a) 100% Nitrogen and (b) 100% oxygen.
- Figure 126.** A metalloporphyrin ketone, M(OEPK), R = C₂H₅.
- Figure 127.** Variation of (a) pO₂ and (b) t₉₀ with TBP plasticizer content.
- Figure 128.** Collman's "picnic basket" porphyrins.
- Figure 129.** Structure of a conjugated Ni(OEP) dimer.
- Figure 130.** Langmuir-Blodgett Film Sensor Response at varying NH₃ concentrations.
- Figure 131.** Response of porphyrin array towards 14 chemical species.
- Figure 132.** Black and white projection of color change fingerprints for a series of ligating vapors. In color, the differences among analytes are considerably more distinct.
- Figure 133.** Structures of quaternary ammonium and manganese metalloporphyrin species used for membrane preparation.
- Figure 134.** Metallocene containing porphyrins for anion recognition.
- Figure 135.** Molecular structure of deca-alkyl sapphyrin binding fluoride ion.
- Figure 136.** Response of TMHPP film based nickel sensor at varying concentration.
- Figure 137.** Response of Co(TPP)/graphite electrode to carbon tetrachloride (CT) and perchloroethylene (PCE).
- Figure 138.** A Porphyrin-cyclochole Bowl.
- Figure 139.** Cyclodextrin-porphyrin assembly for recognition of pentachlorophenol.
- Figure 140.** Binding of saccharides to a boronic-acid containing receptor.
- Figure 141.** Molecular models showing a side view of the binding sites of dendrimer porphyrins. Upper: *meta*-substituted H₂(T(3',5'-G1P)P). Lower: *ortho*-substituted dendrimer-porphyrin H₂(T(2',6'-G1AP)P). Note the open cavity of ≈10Å versus a narrow slit of ≈5, respectively; in both cases, top access to the porphyrin is completely blocked.
- Figure 142.** Binding of axial ligands to dendrimer porphyrins; log(K_{eq}) values for a series of nitrogenous bases with various shapes.

The Suslick Research Group



[Overview](#)

[Outline of
Research Projects](#)

[Introduction to
Sonochemistry](#)

[Exec. Summary:
Sonochemistry](#)

[Exec. Summary:
Porphyrin Research](#)

[Exec. Summary: Smell-
Seeing](#)

[Complete
Publication List](#)

[Abbreviated Curriculum
Vitae](#)

[Academic
Genealogy](#)

[Press
Clippings](#)

FIGURES

**"Applications of Porphyrins and Metalloporphyrins to Materials Chemistry" by Chou, J.-H.; Kosal, M. E.; Nalwa, H.S.; Rakow, N.A.; Suslick, K. S.
in *The Porphyrin Handbook*
Kadish, K.; Smith, K.; Guillard, R., ed.; Academic Press:
New York, 2000; vol. 6, ch. 41, pp. 43-131.**

[For the article text \(without figures\), in PDF format, click here.](#)

1.

[Current Research
Funding](#)

[Excerpts from
Funded Research](#)

[Inventory of
Group Equipment](#)

[Information
for Visiting](#)

[Current Research Group
Members](#)

[Group
Meetings](#)

[Group
Chores](#)

[Past Research
Group Members](#)

[Group
Photogallery](#)

[Web Resources](#)

[Laboratory Safety
Resources](#)

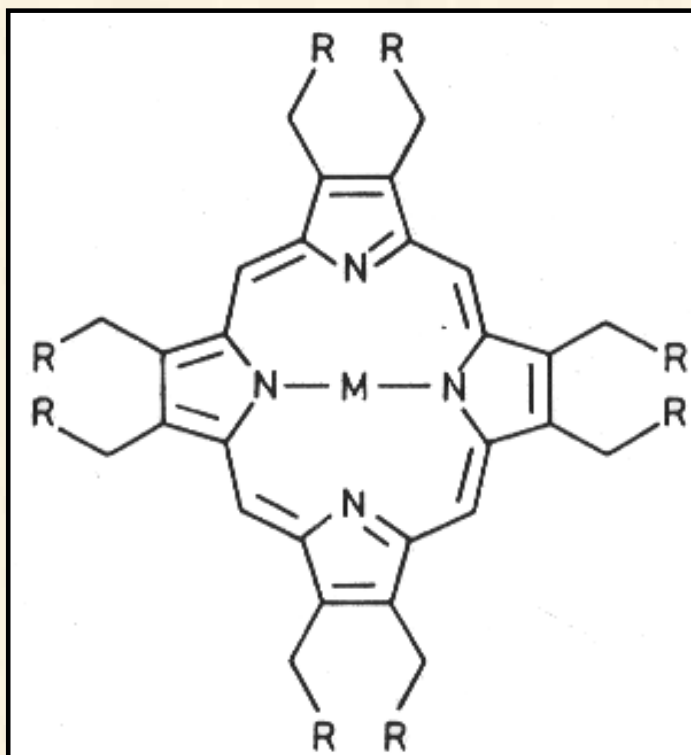
[Art and Science:
Journal Covers](#)

[Sculpture &
Masks](#)

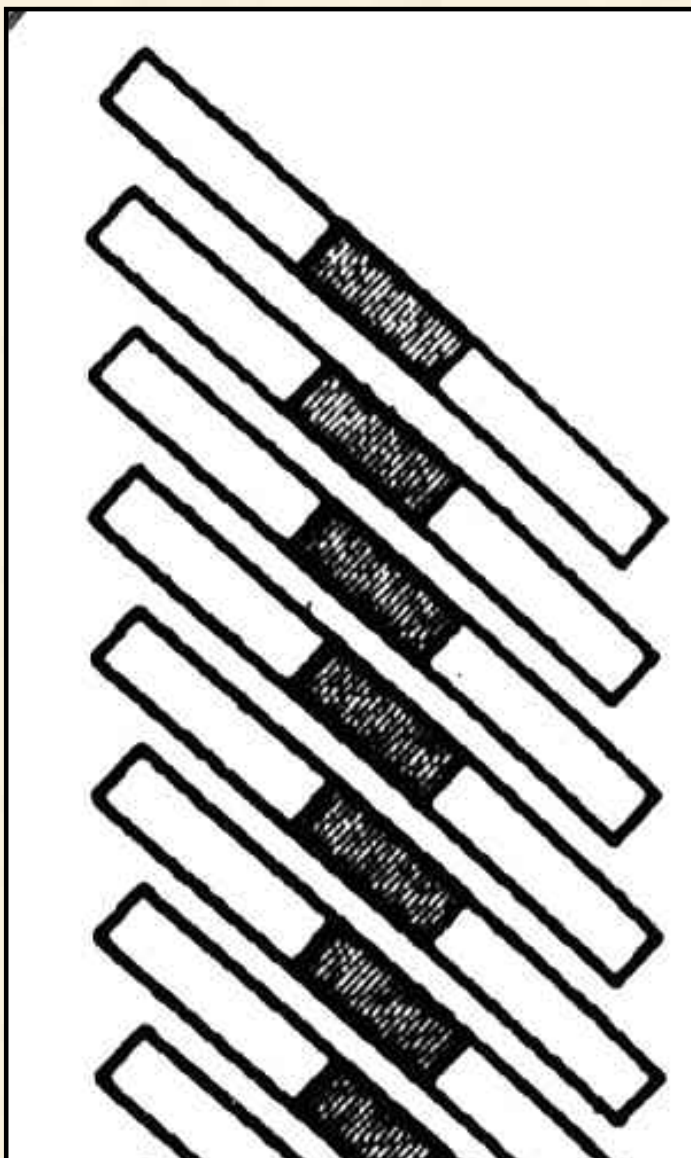
[A Chemist
Meets Hollywood](#)

[Chymistes: The Distillers
of Waters](#)

[A Chemist
In Court](#)



2.



Humor and
Wisdom

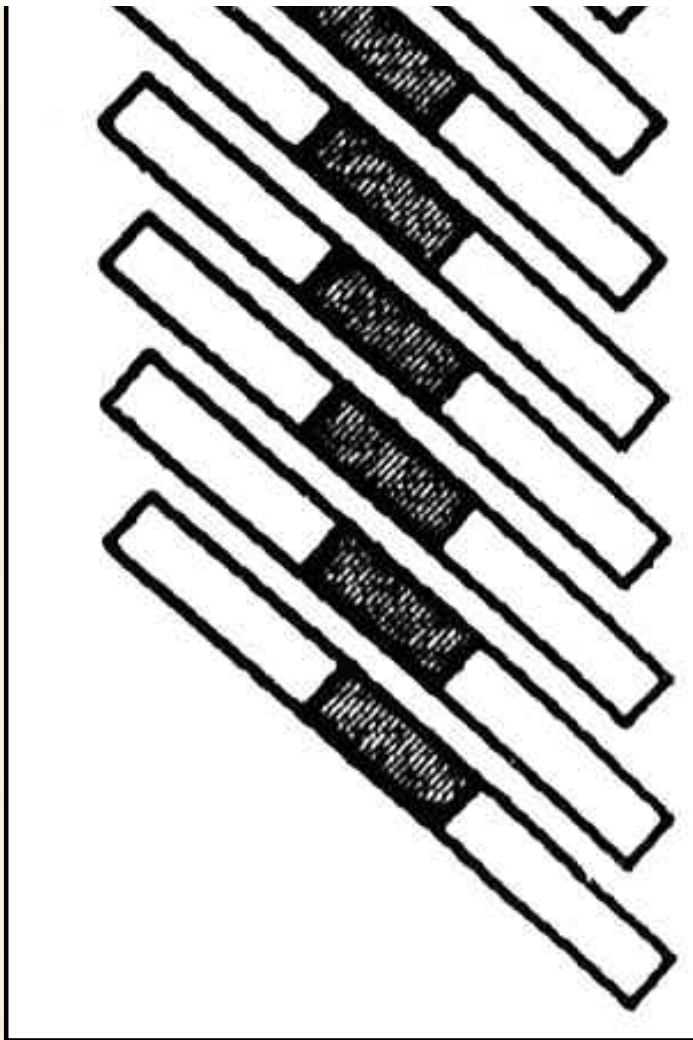
Laws of the Universe

Cartoons of Humor and
Wisdom

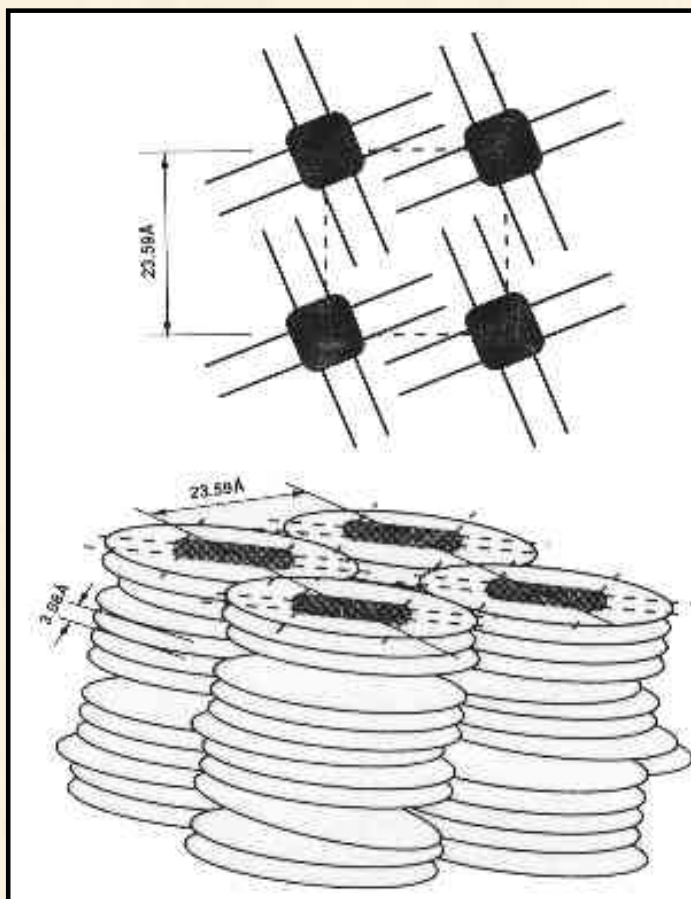


Chem 115: Chemistry of
Everyday Phenomena

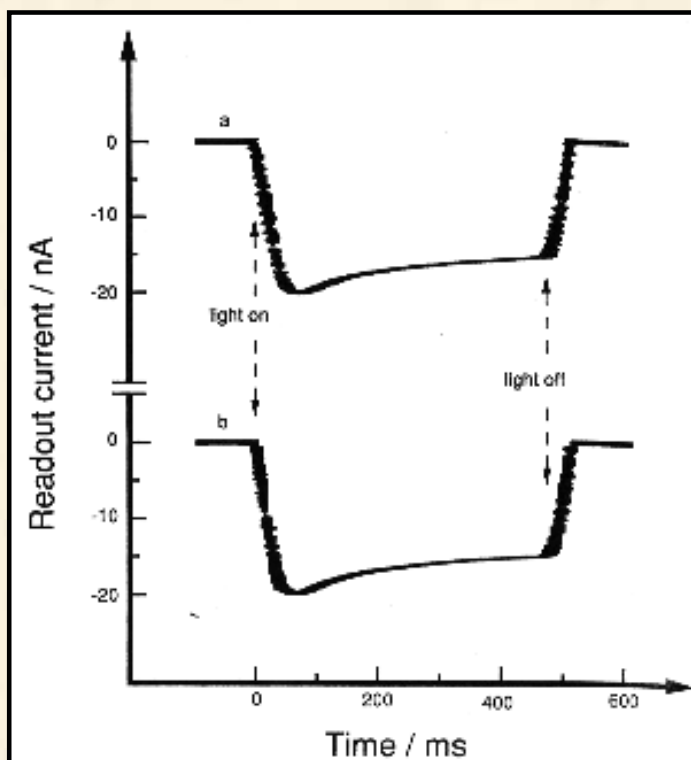
Chem 315: Inorganic
Chemistry



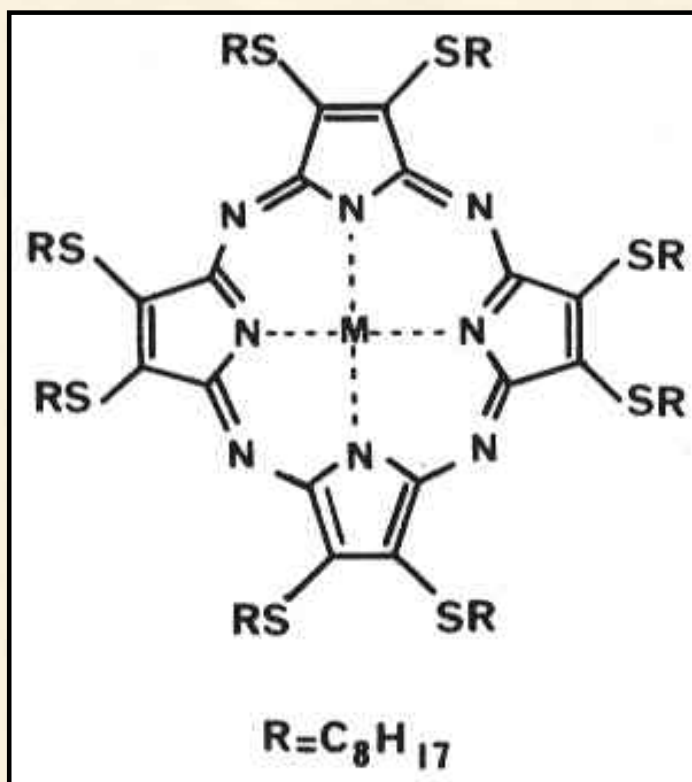
3.



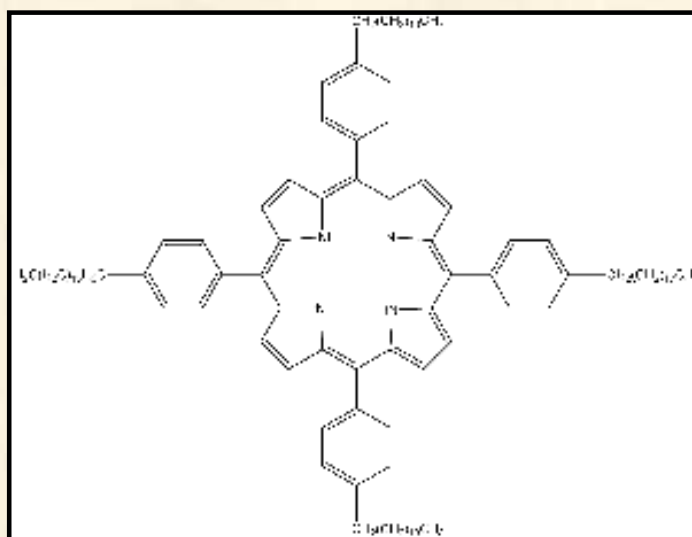
4.



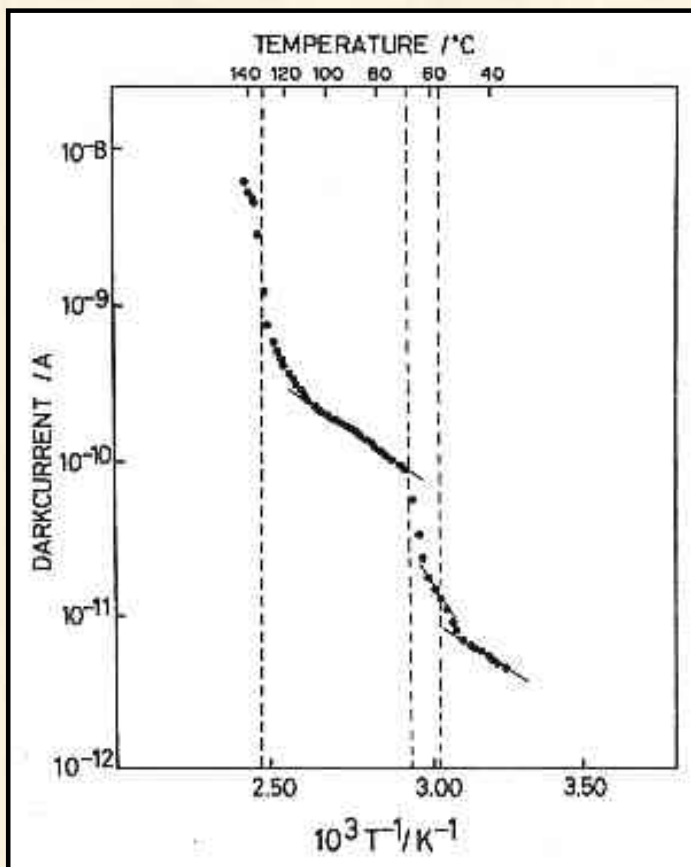
5.



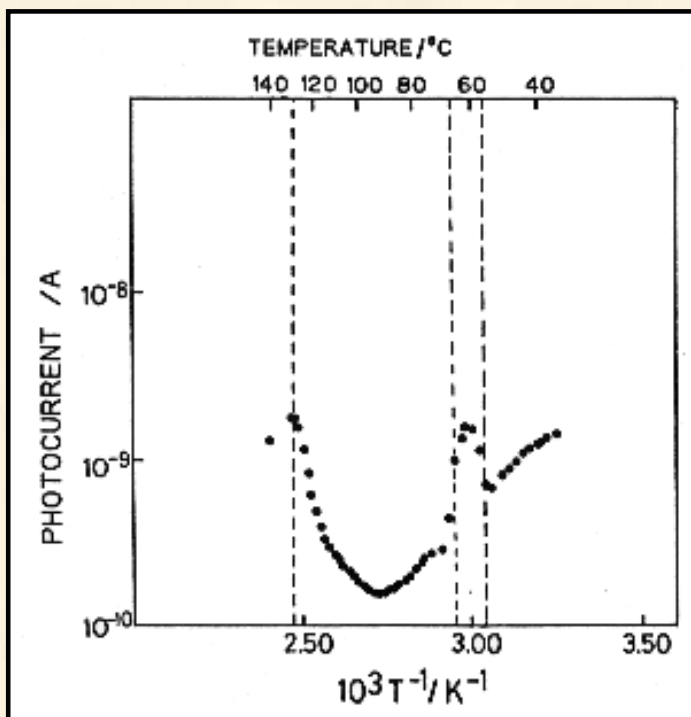
6.



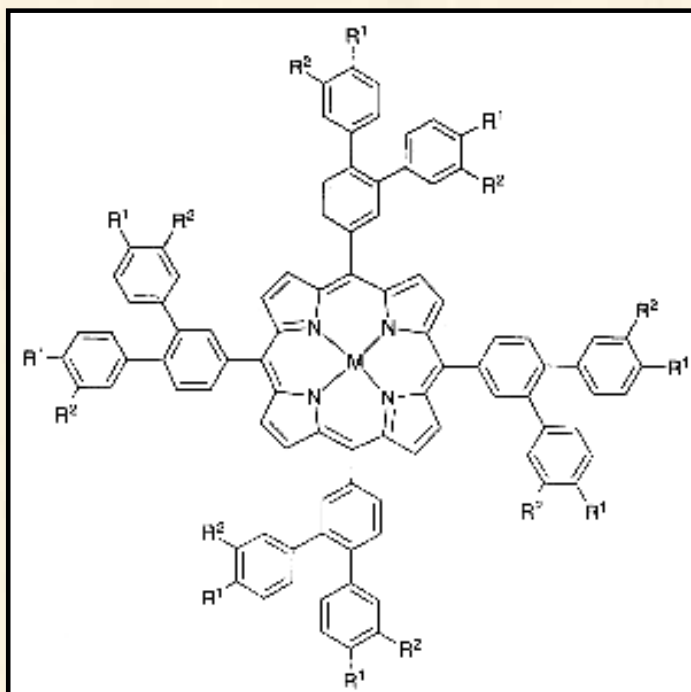
7.



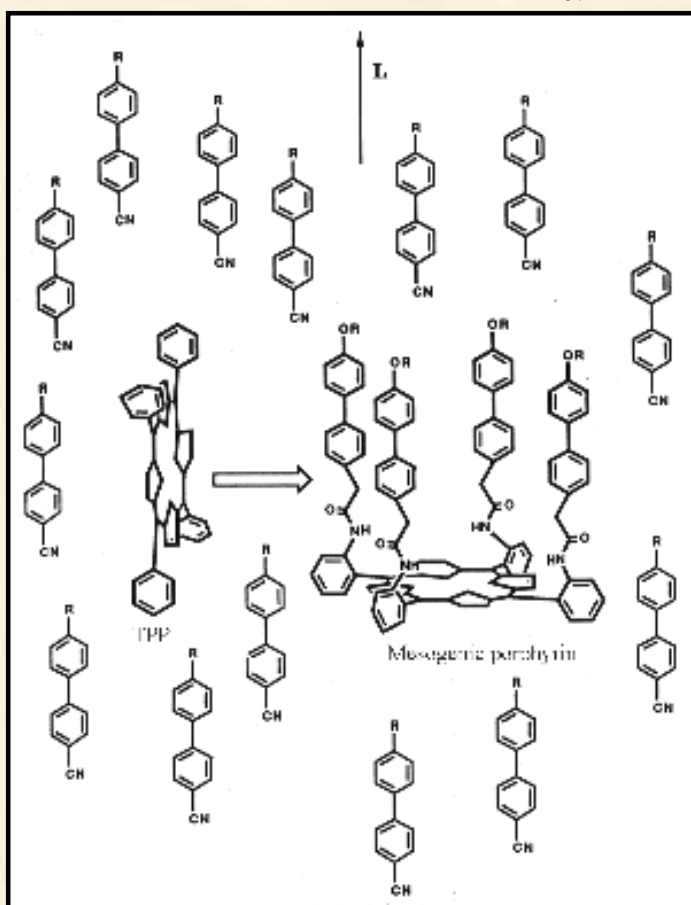
8.



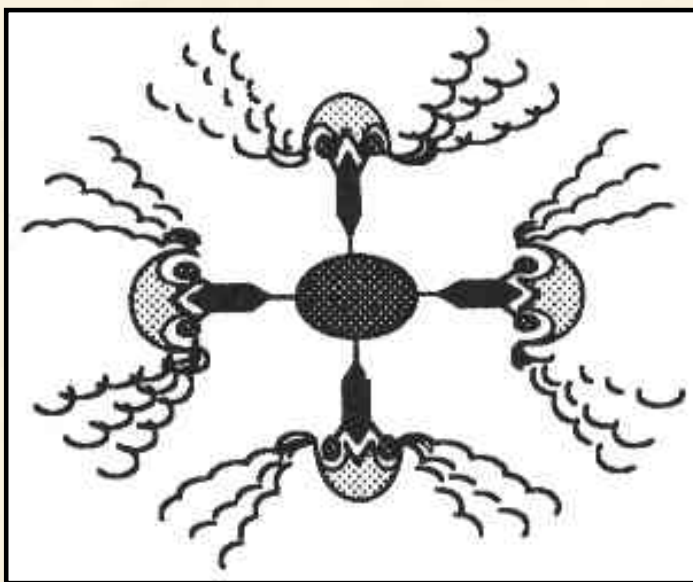
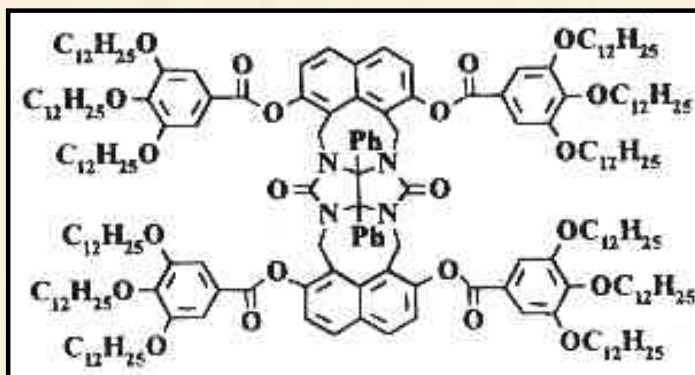
9.



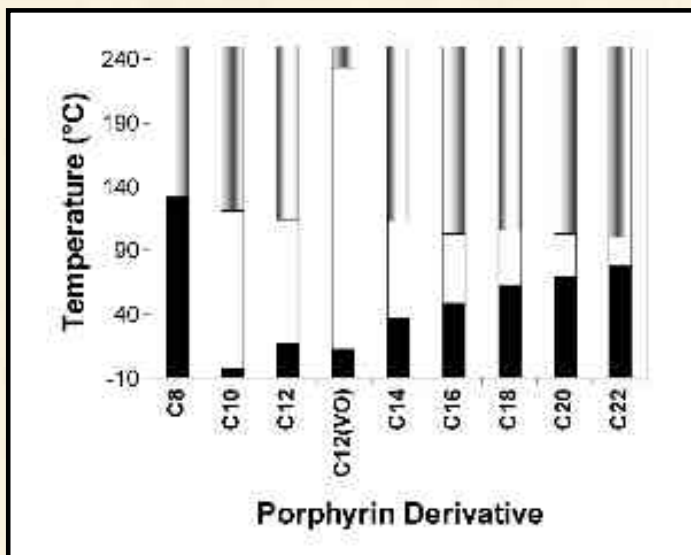
10.

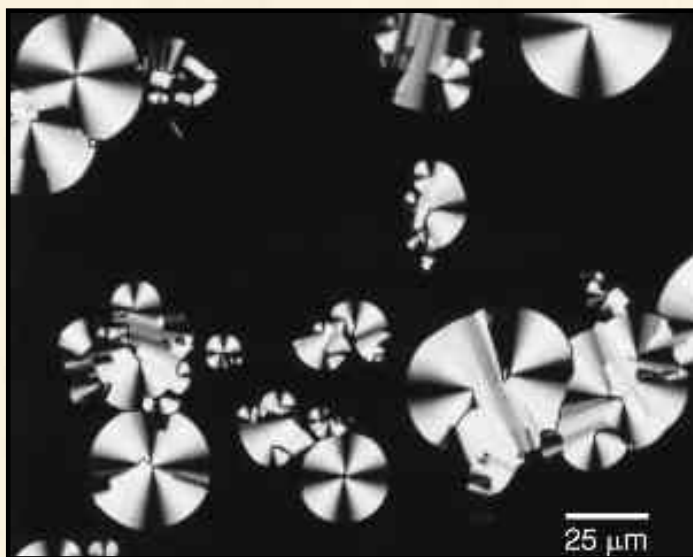


11.

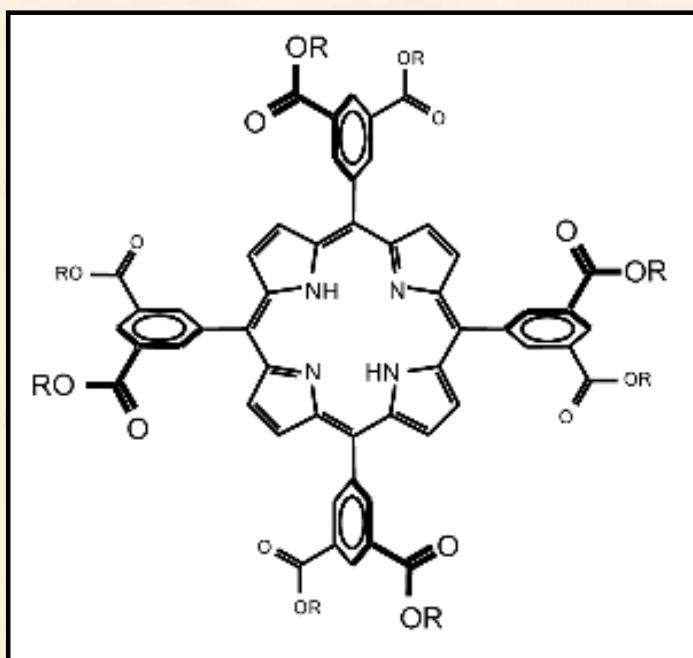


12.

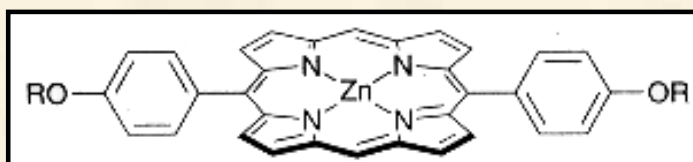




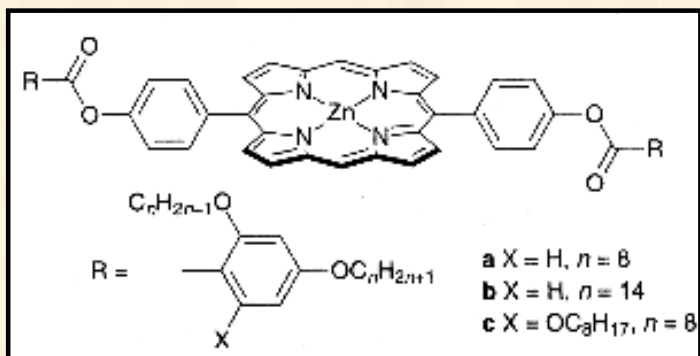
13.



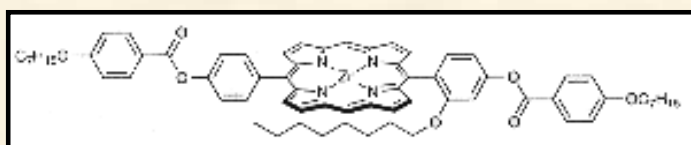
14.



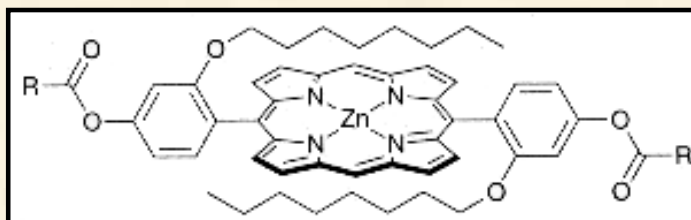
15.



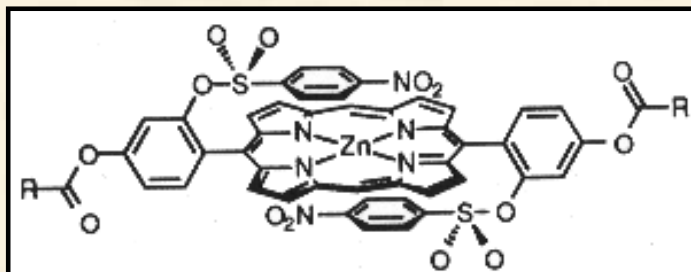
16.



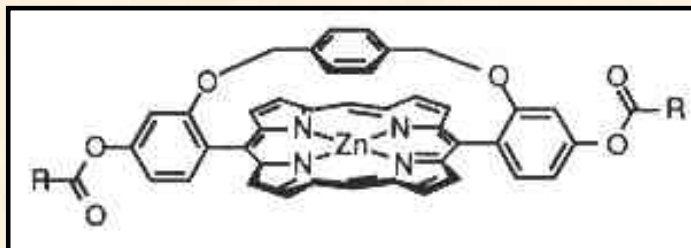
17.



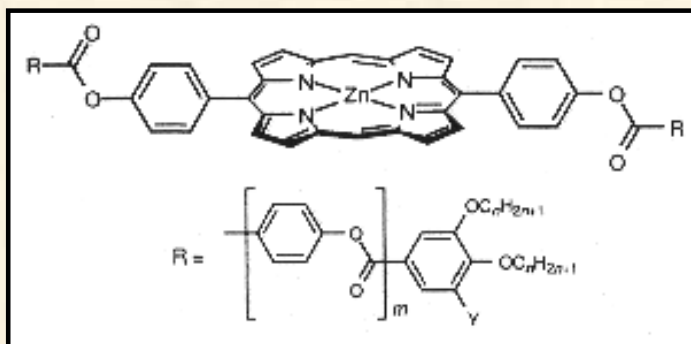
18.



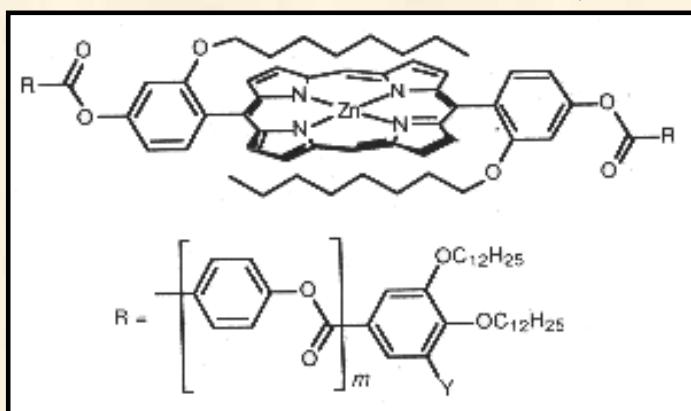
19.



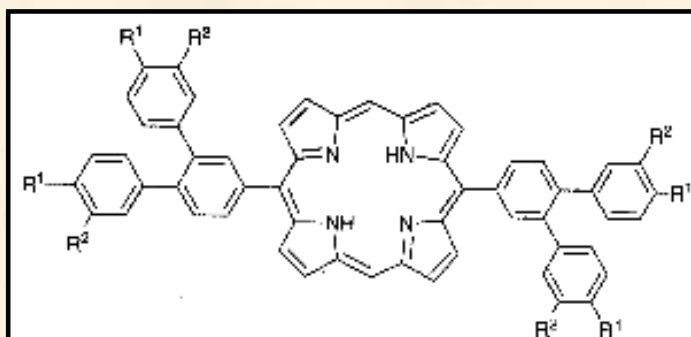
20.



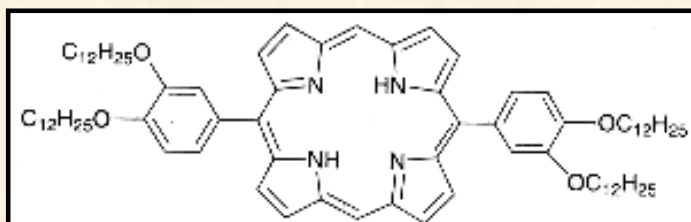
21.



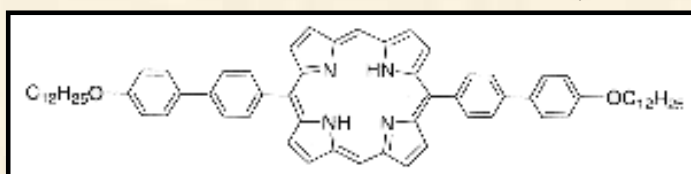
22.



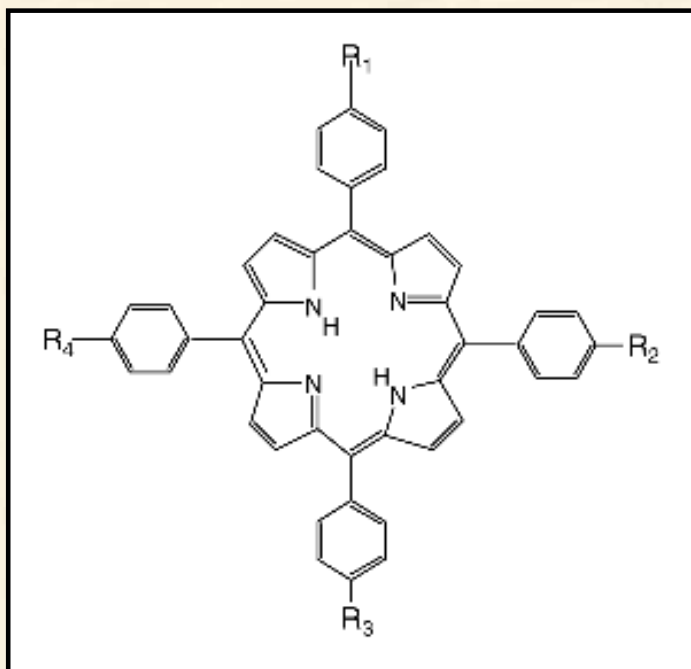
23.



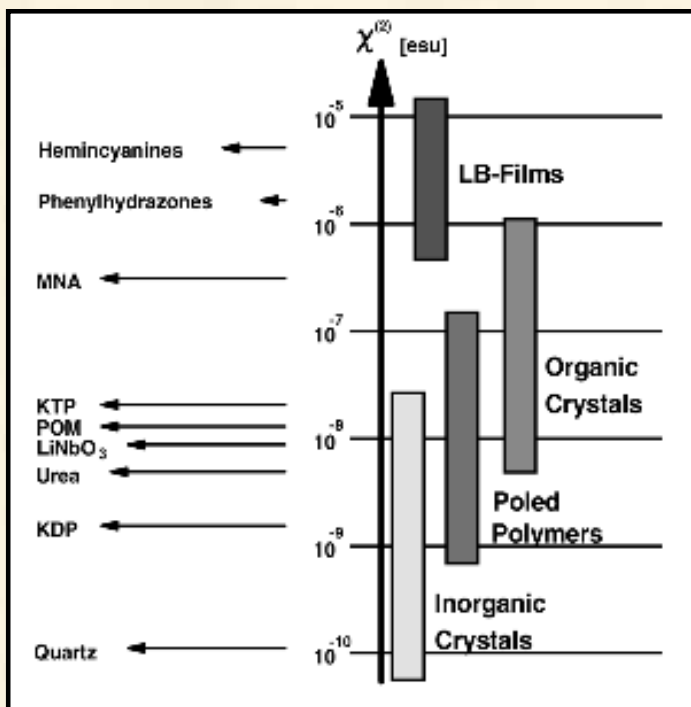
24.



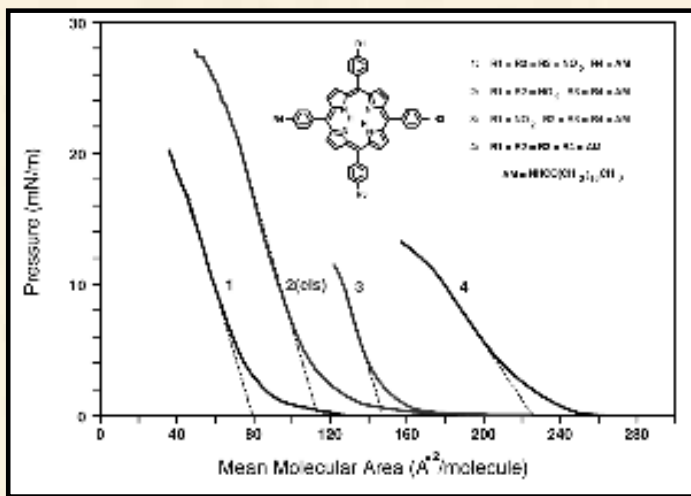
25.



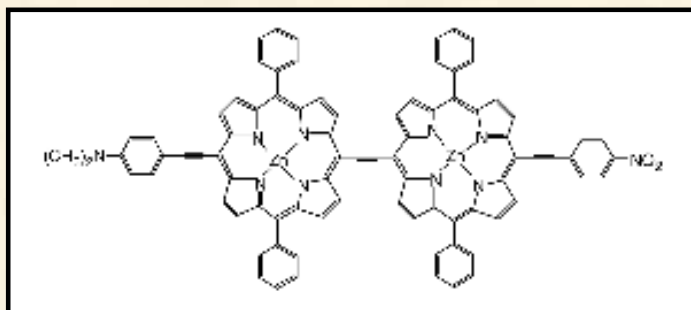
26.



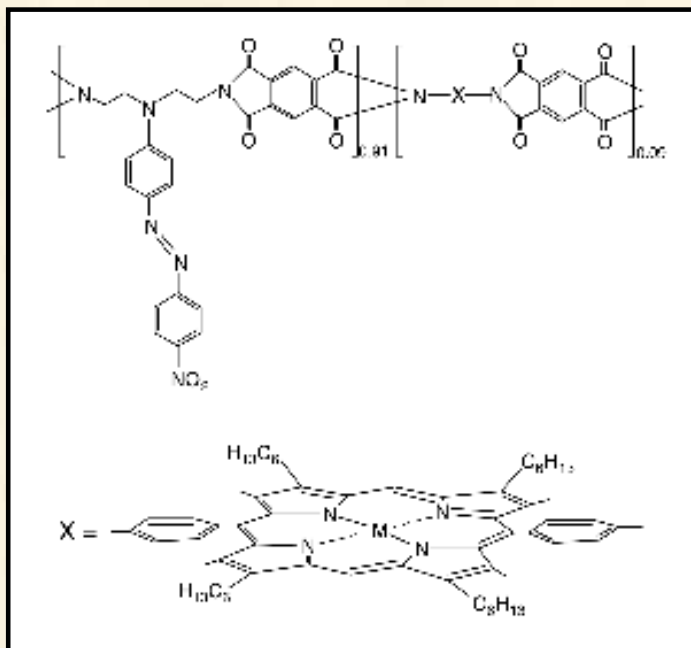
27.



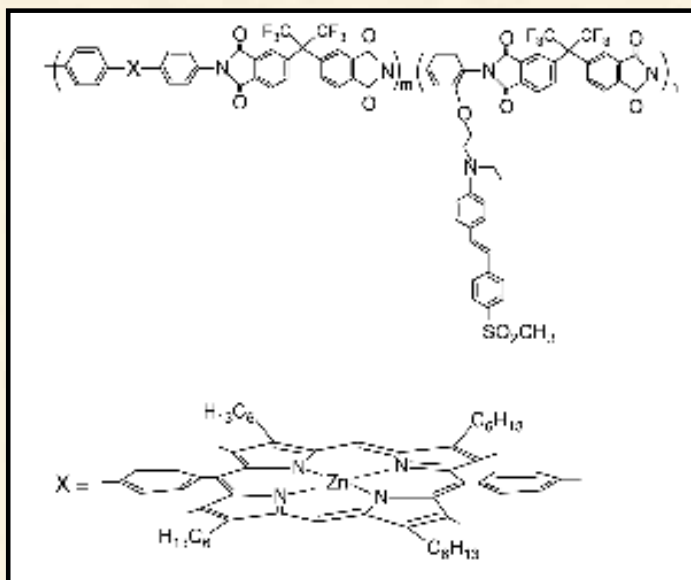
28.



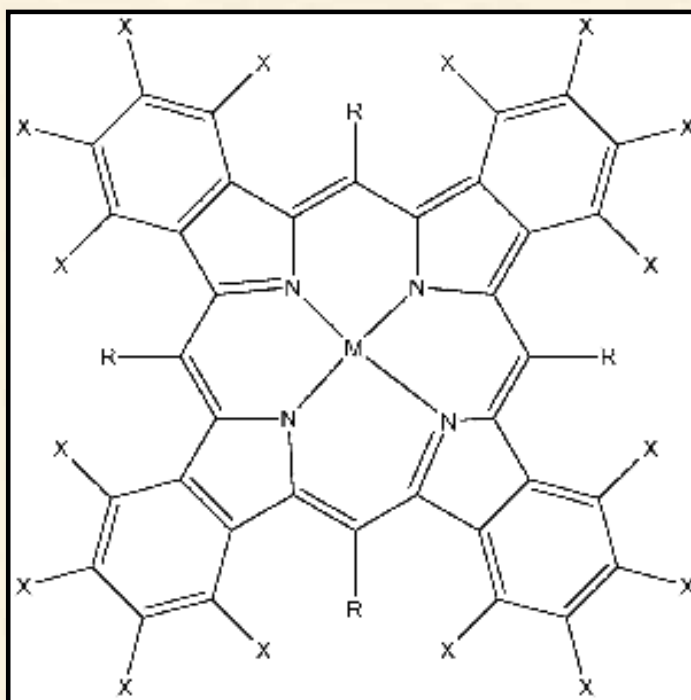
29.



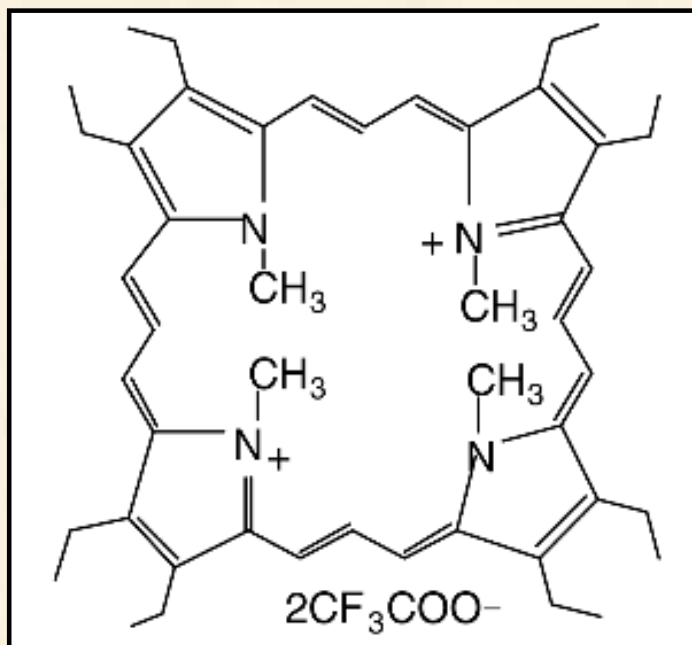
30.



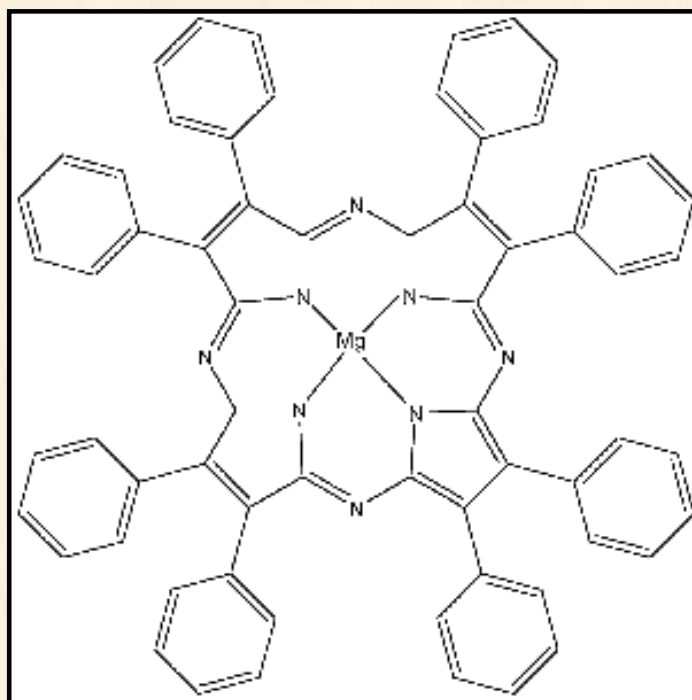
31.



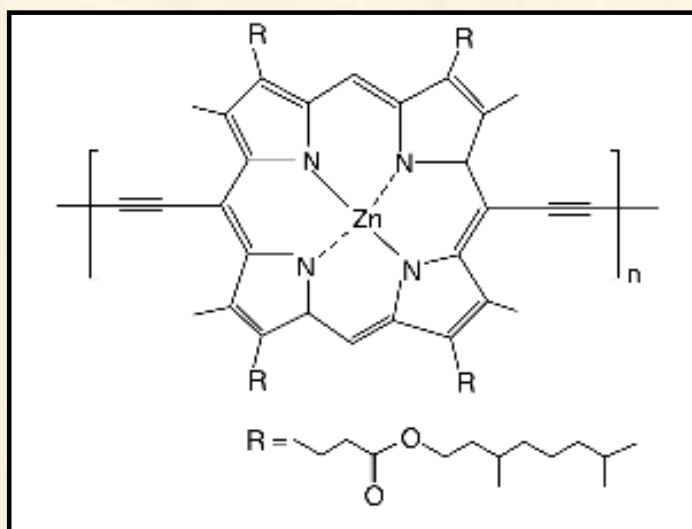
32.



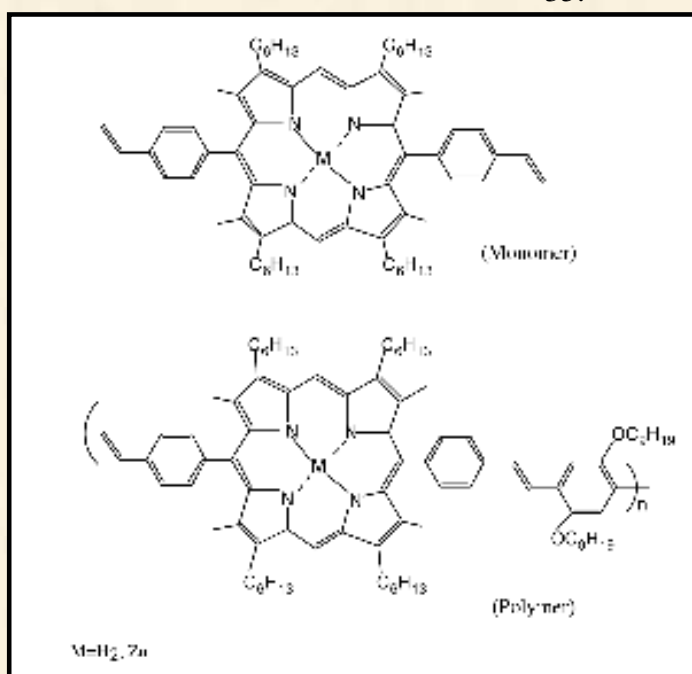
33.



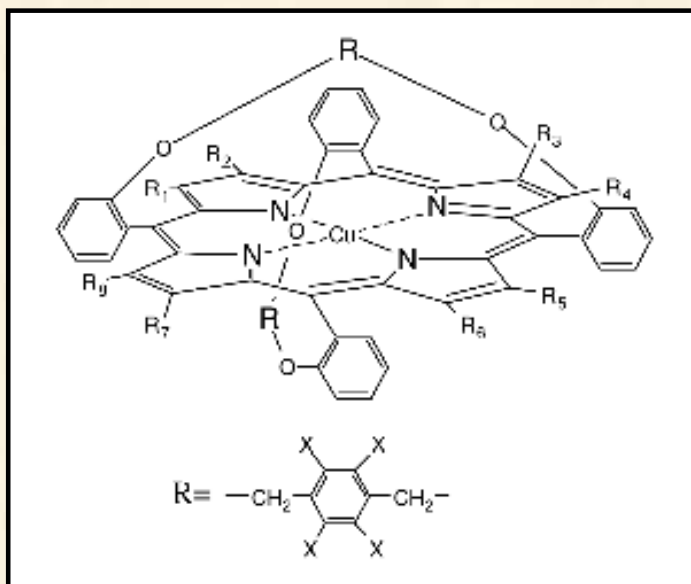
34.



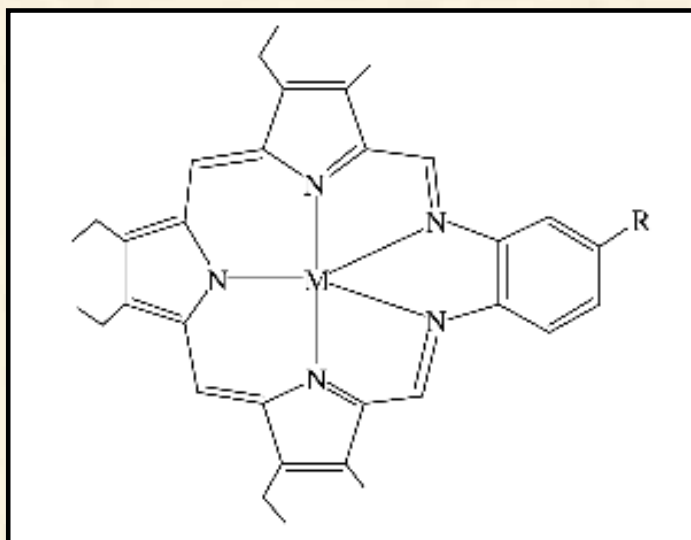
35.



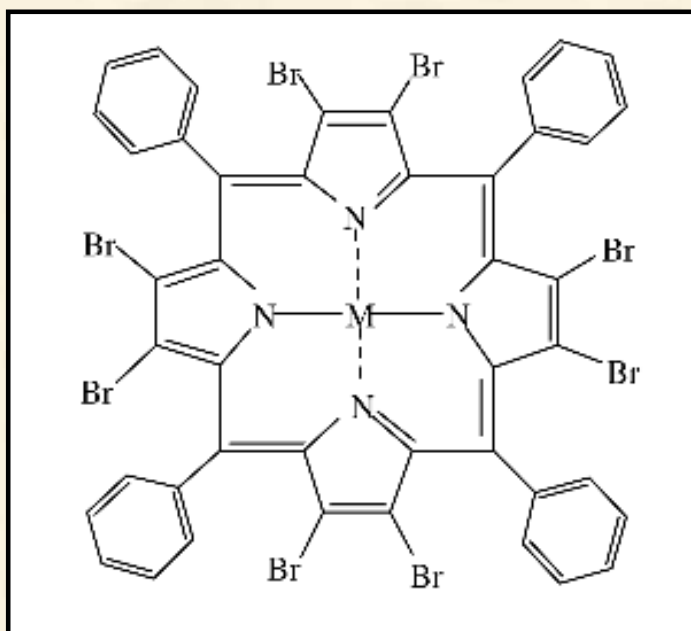
36.



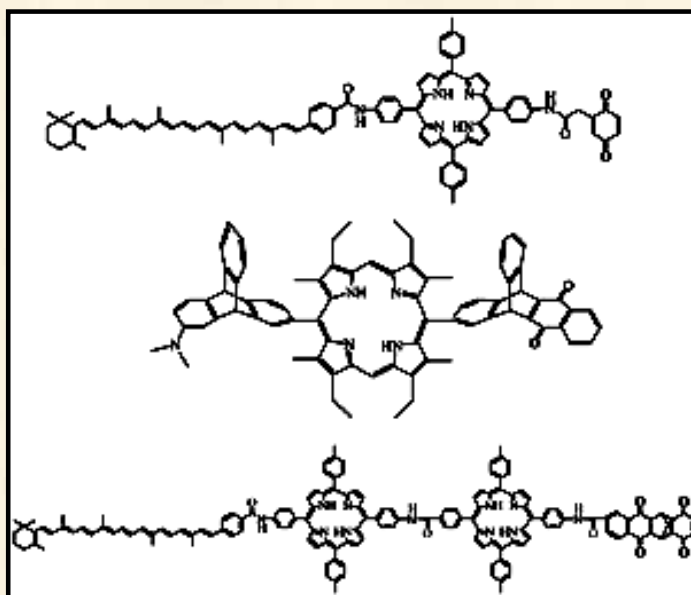
37.



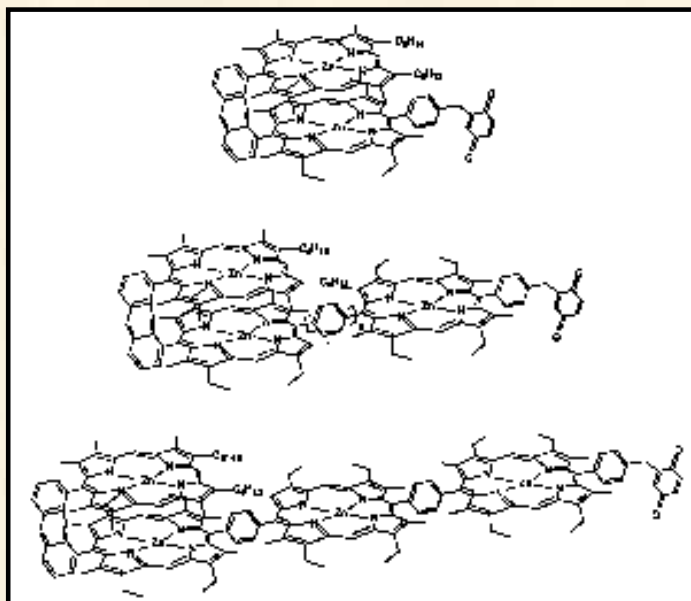
38.



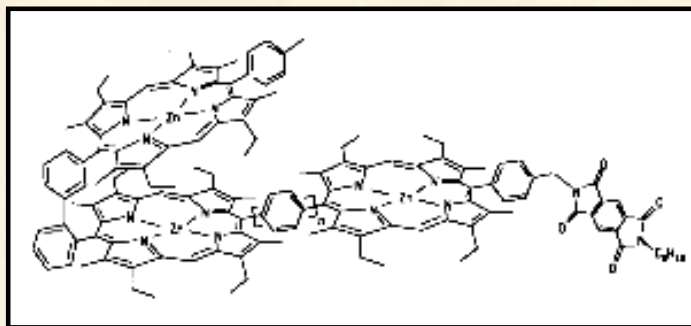
39.



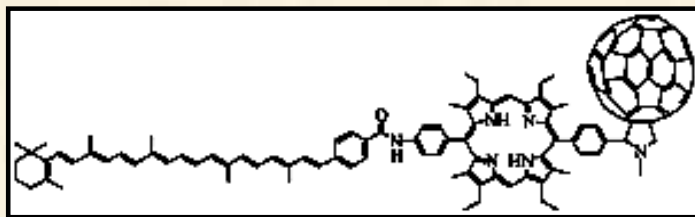
40.



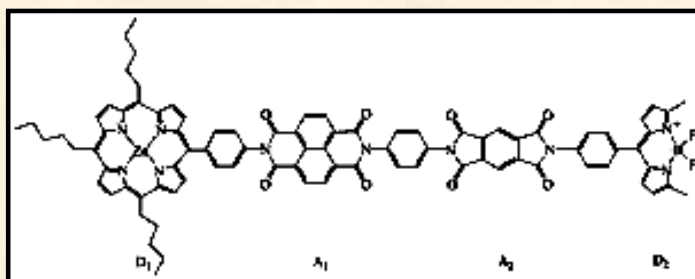
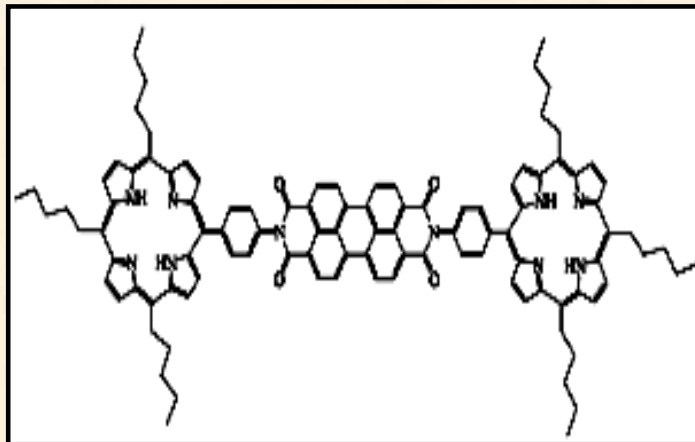
41.



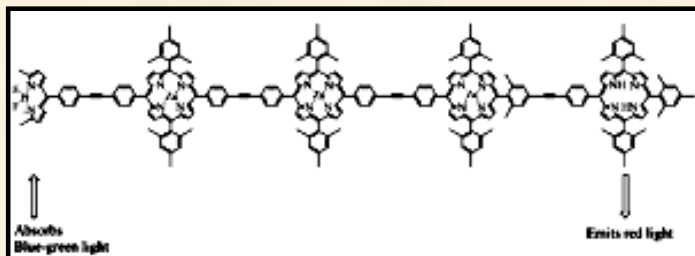
42.



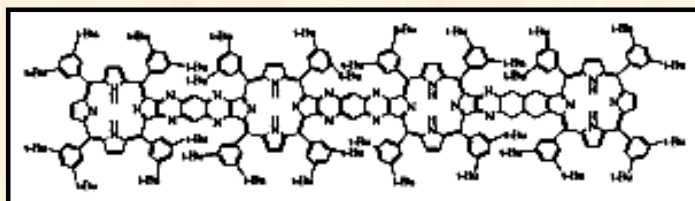
43.



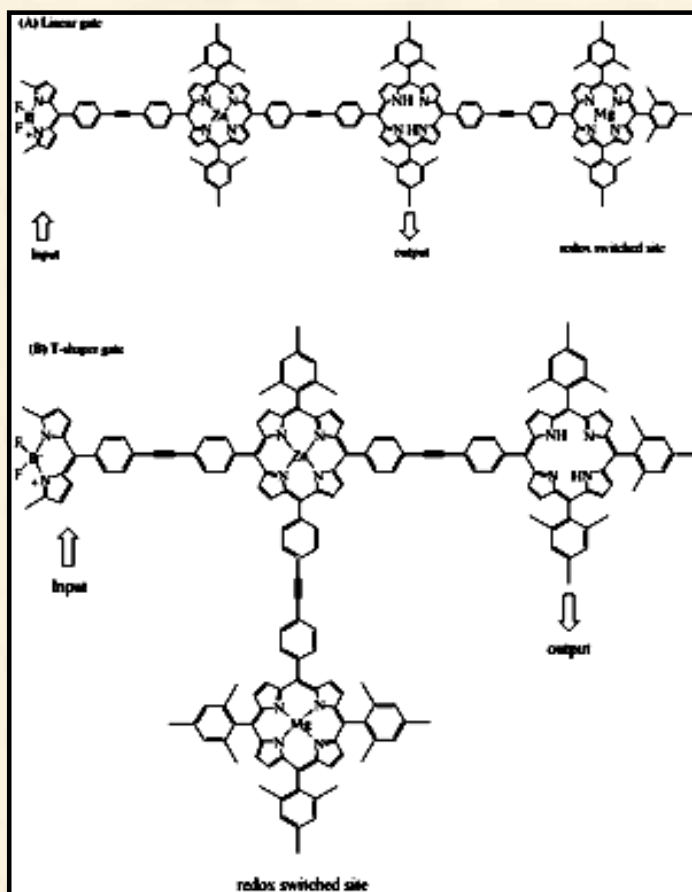
44.



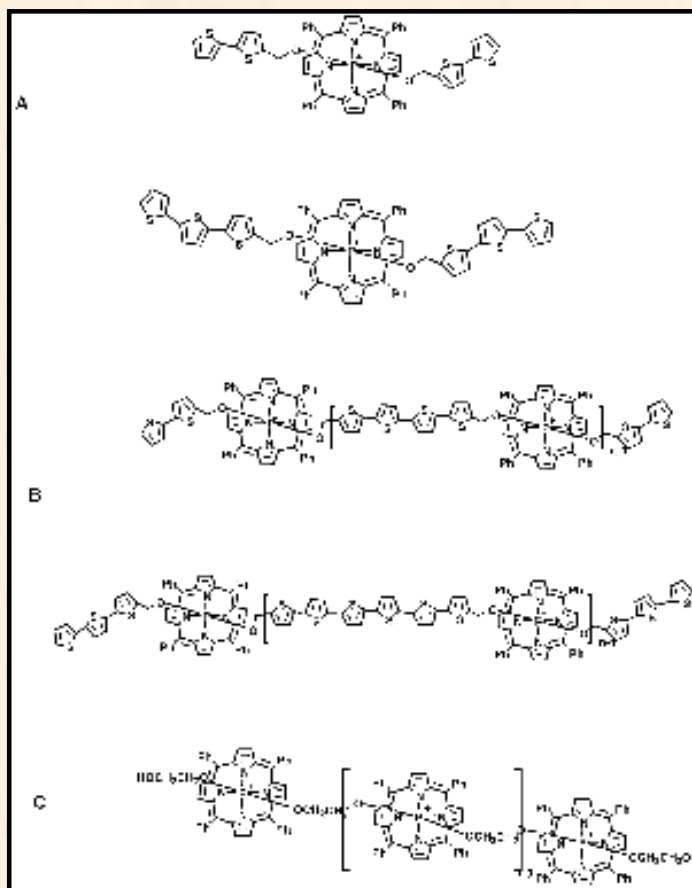
45.

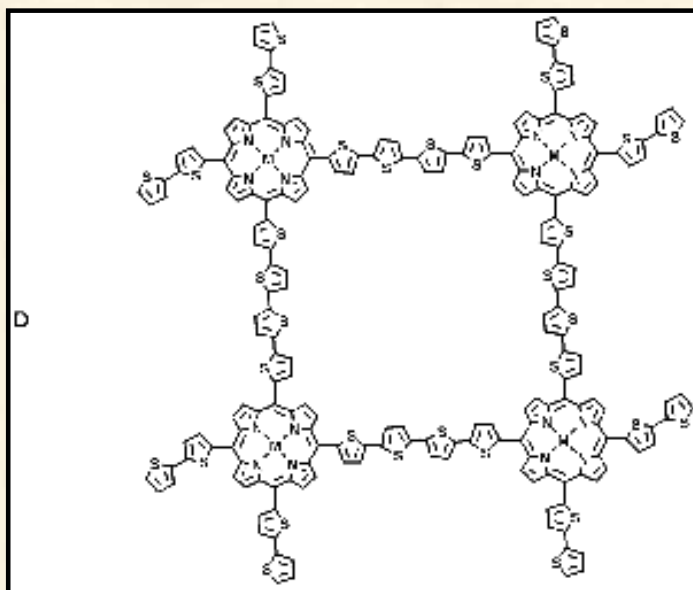


46.

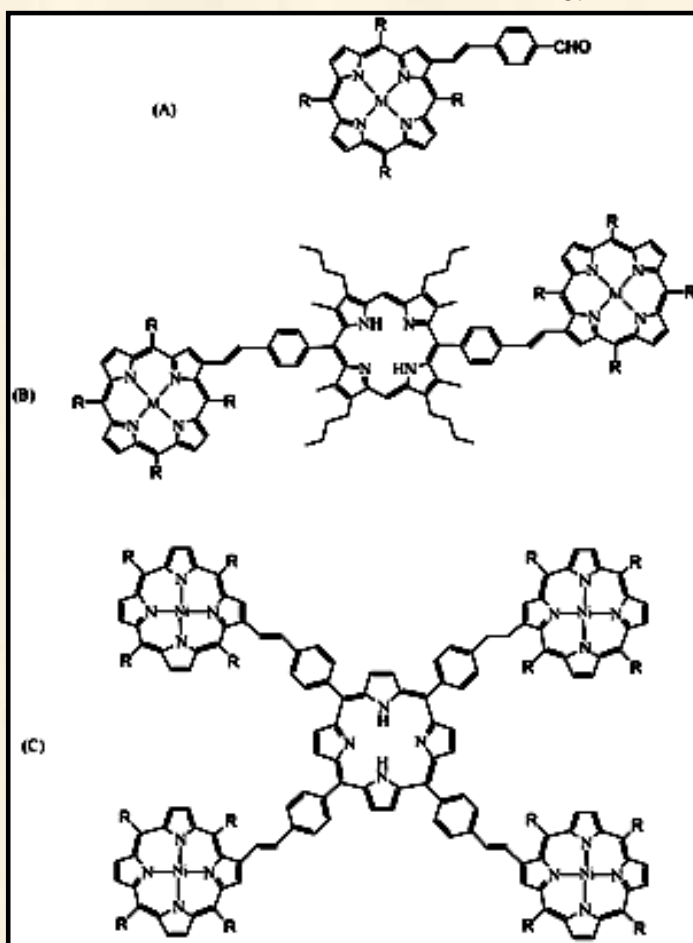


47.

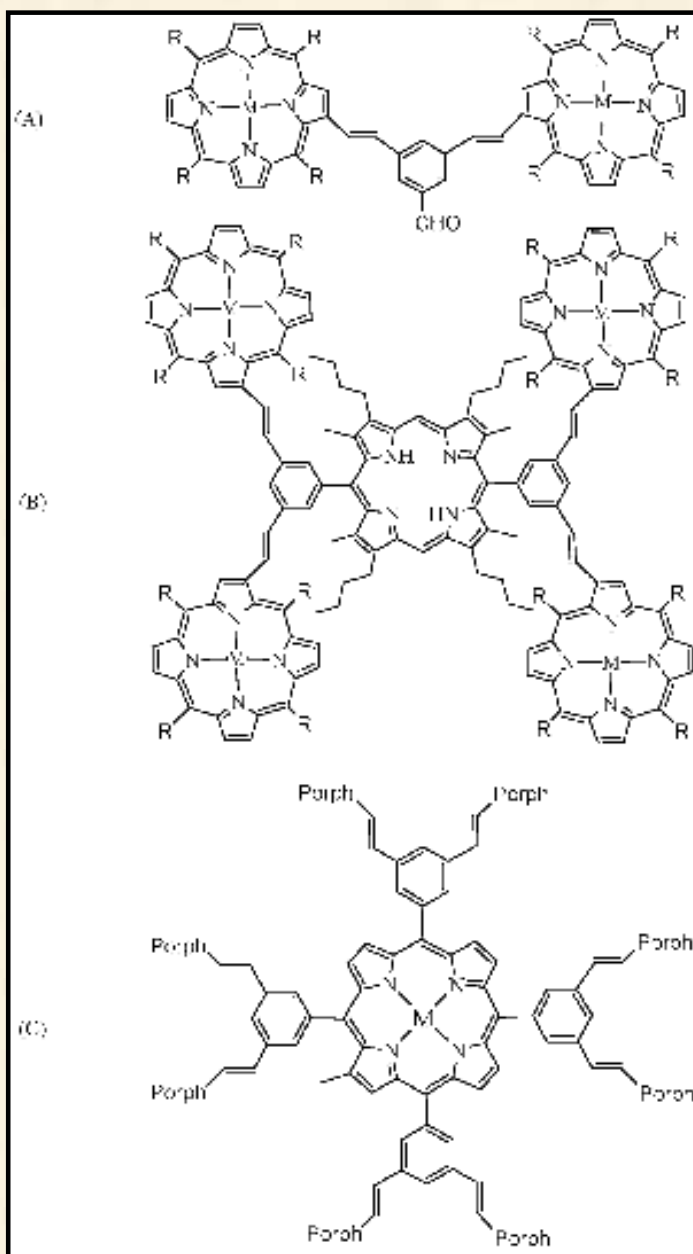




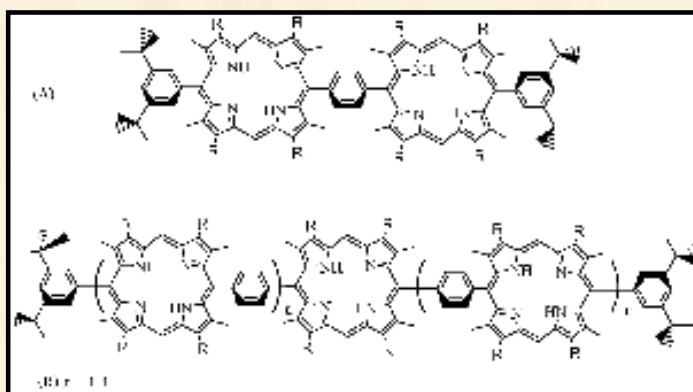
48.



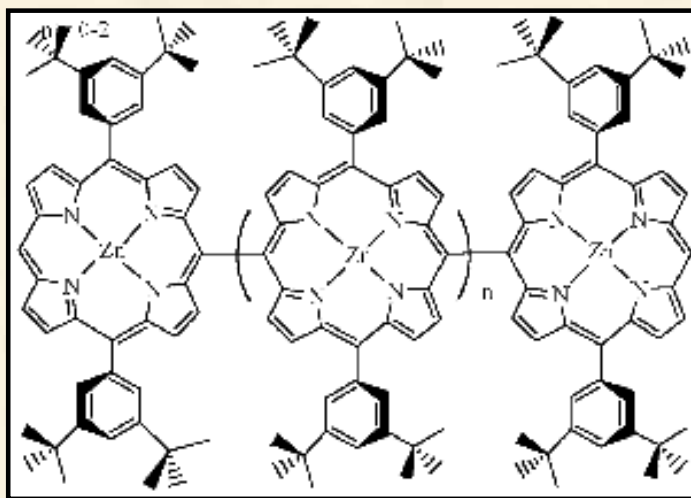
49.



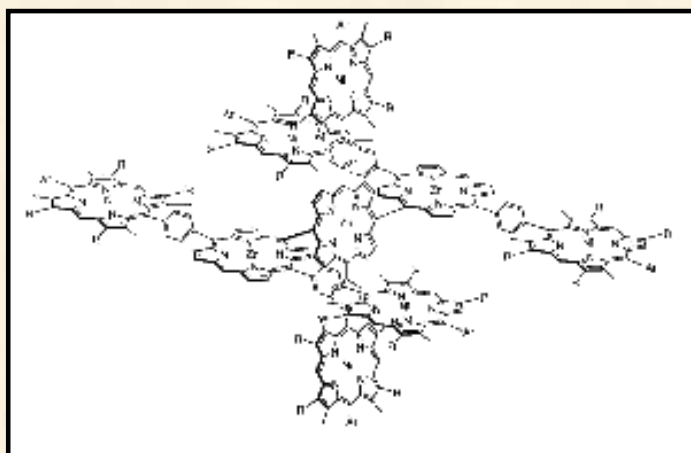
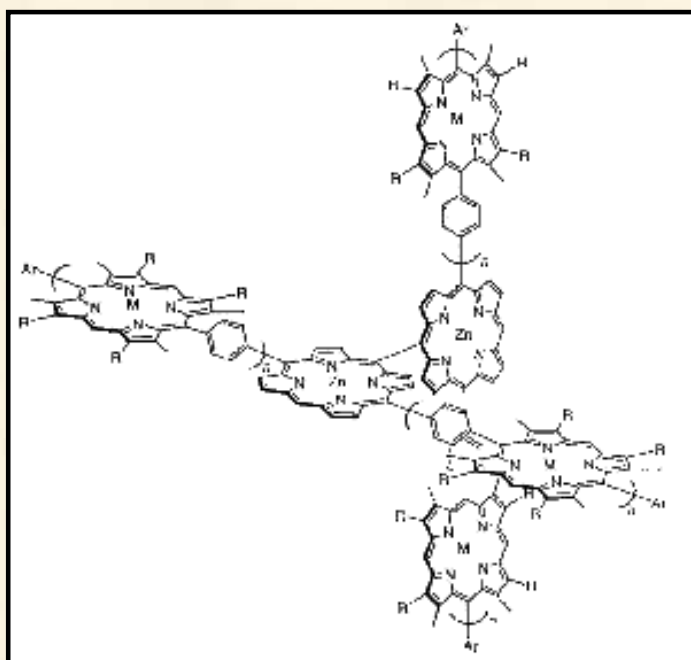
50.



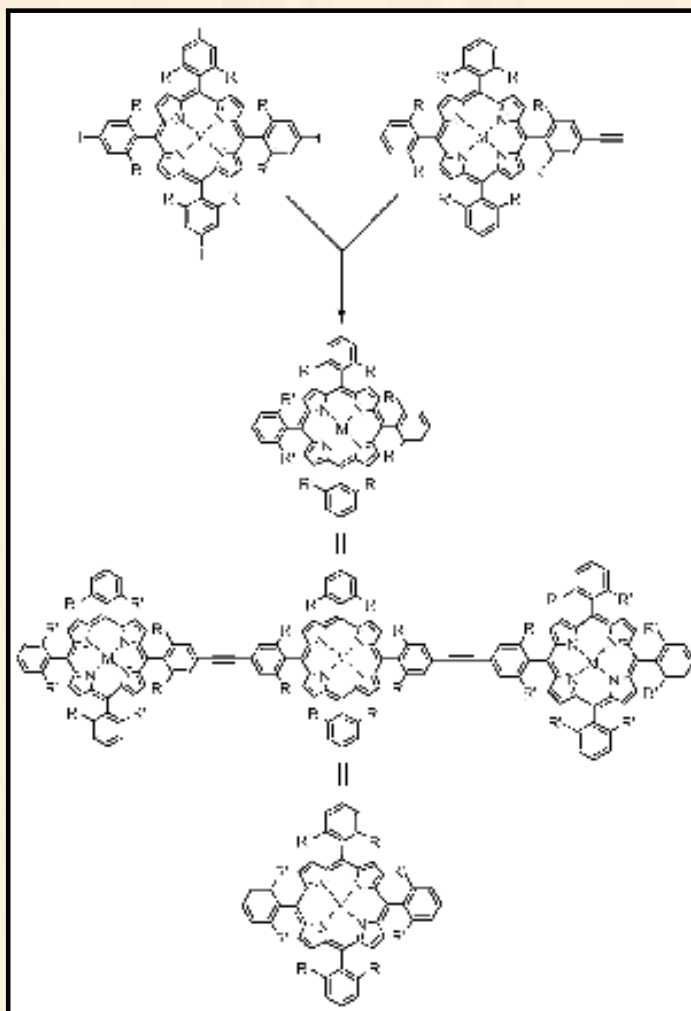
51.



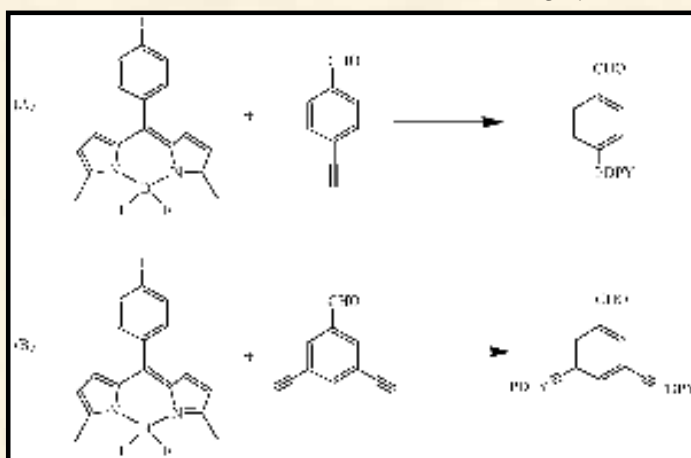
52.

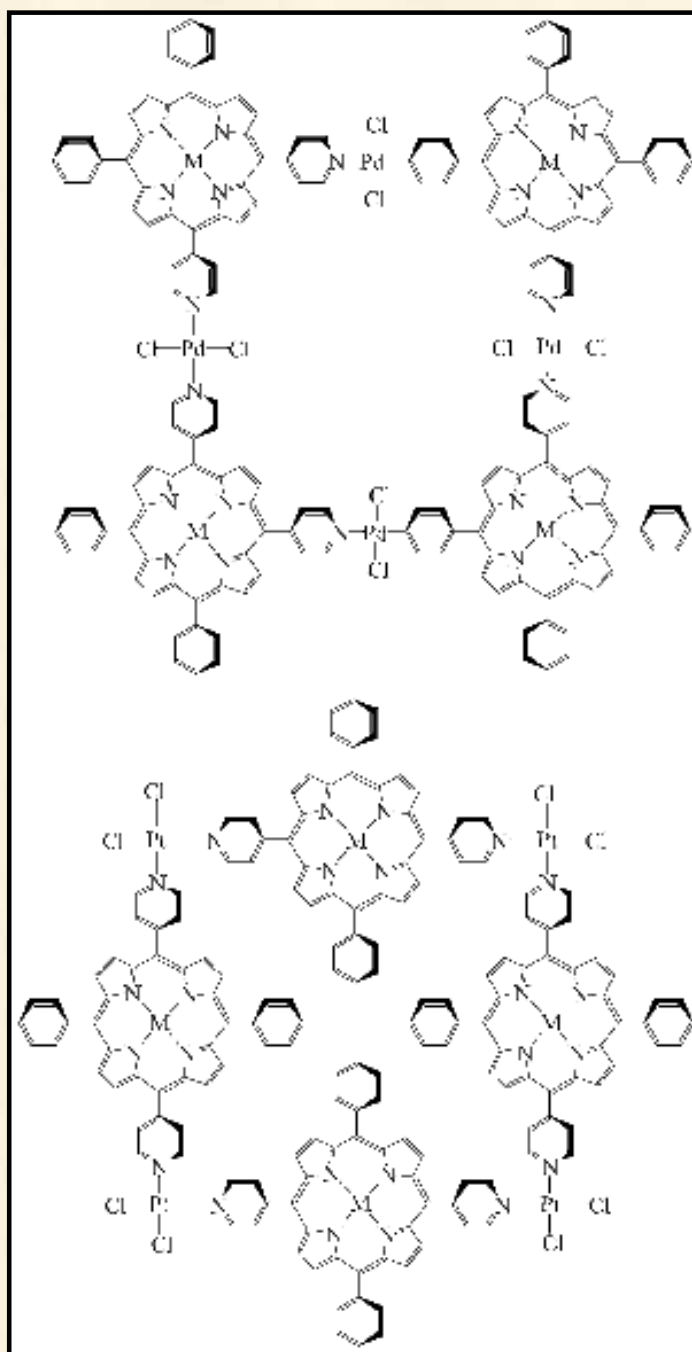


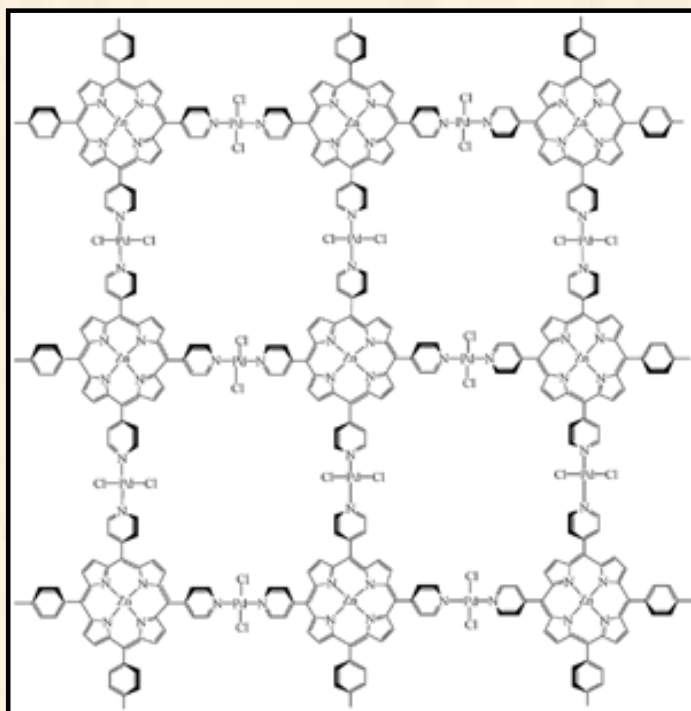
53.



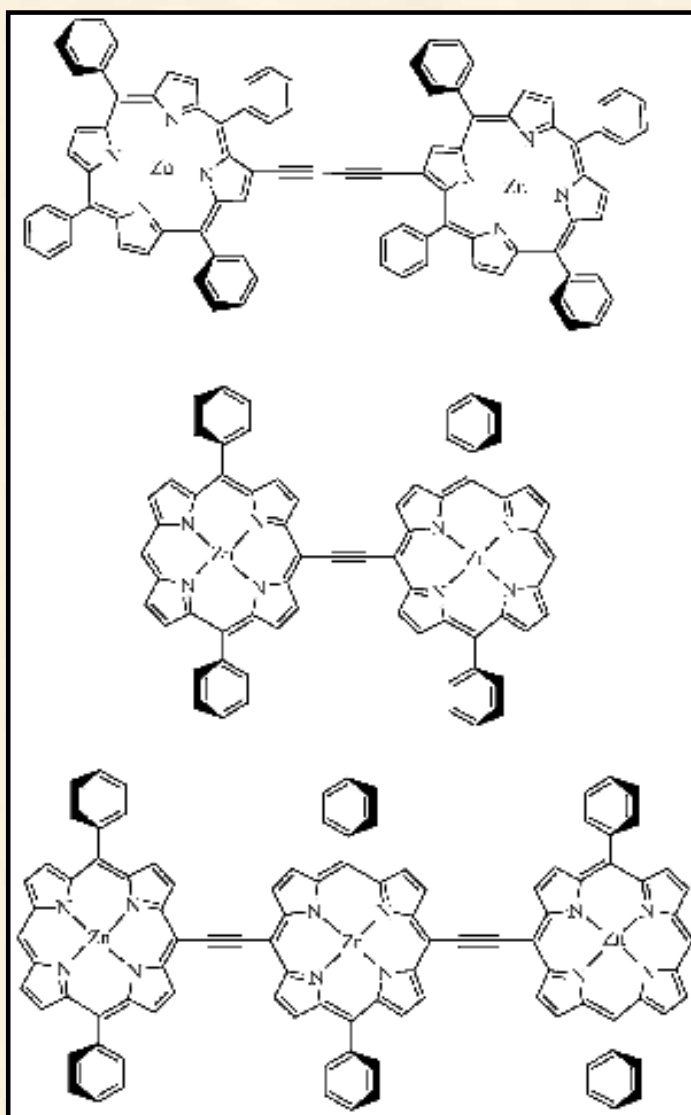
54.



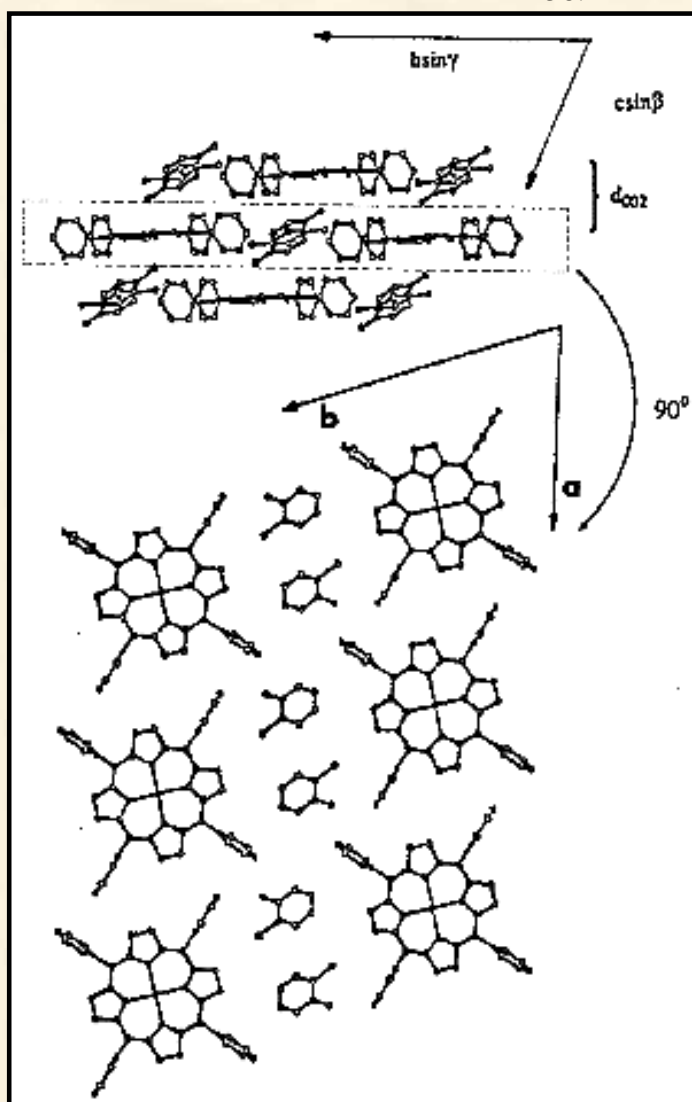




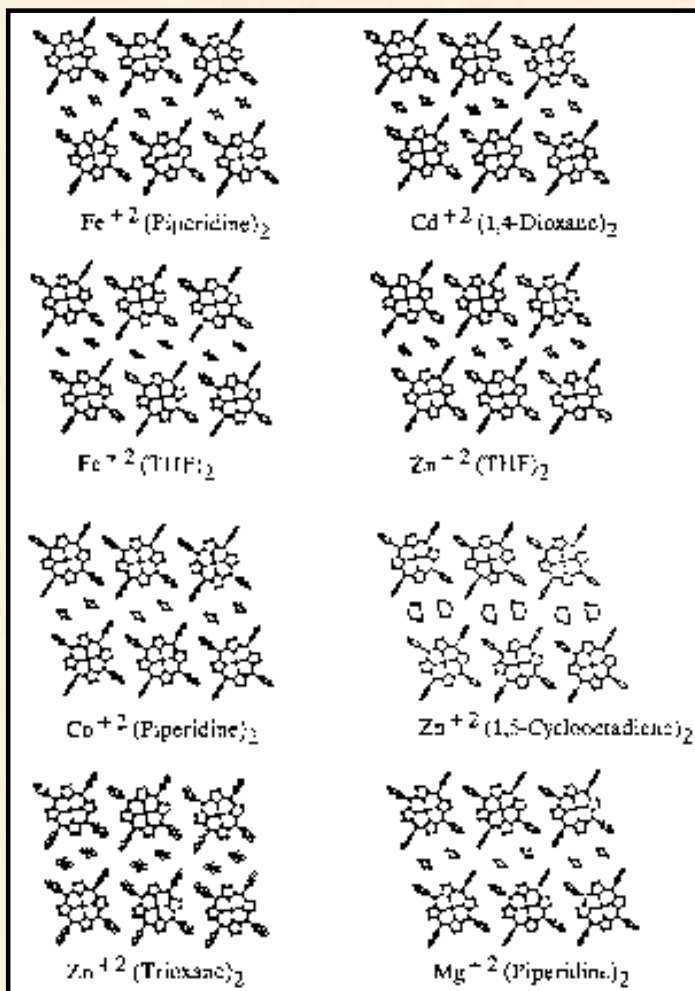
57.



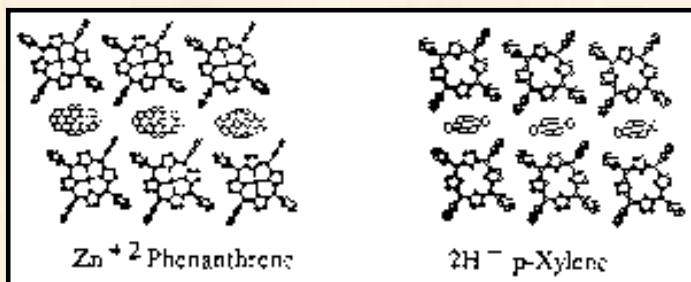
58.



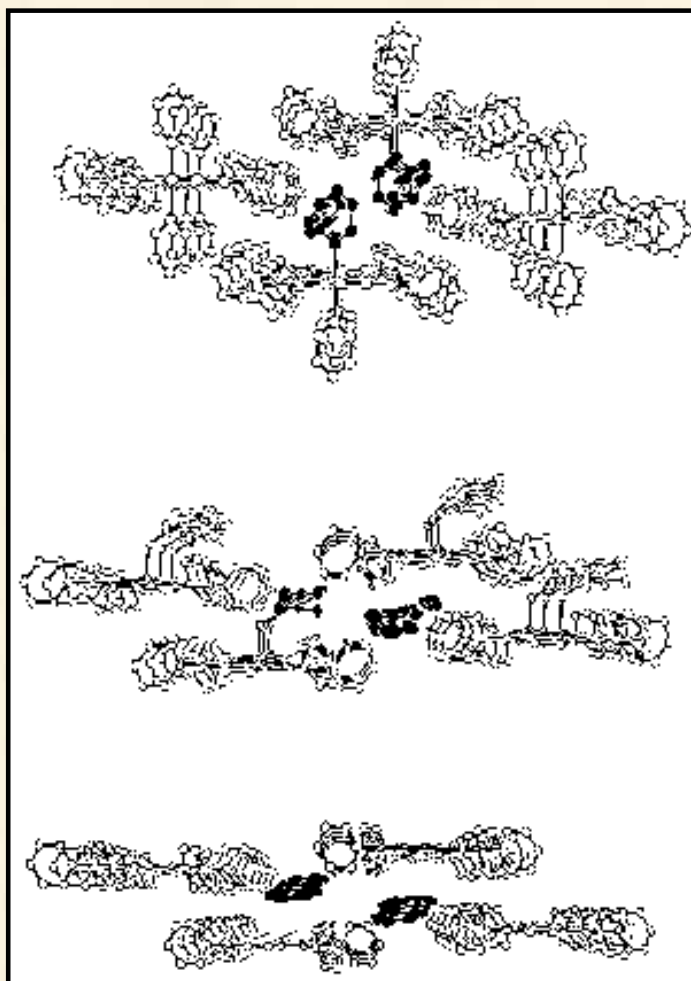
59.



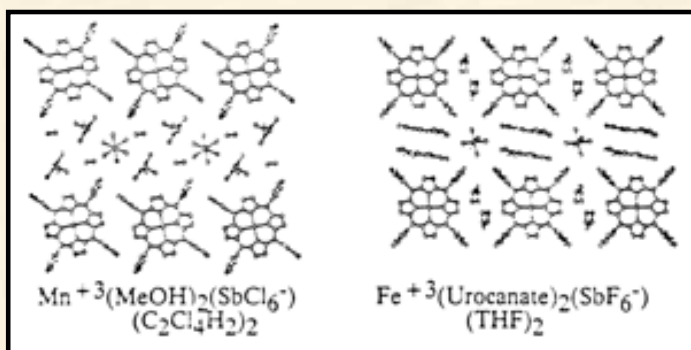
60.



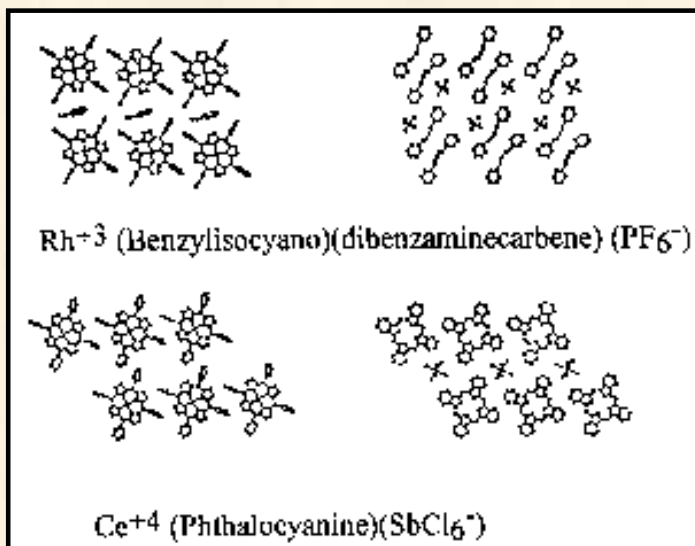
61.



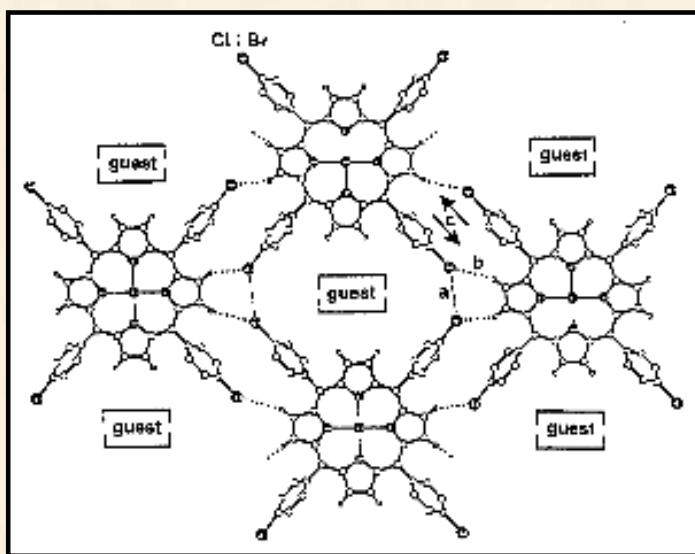
62.



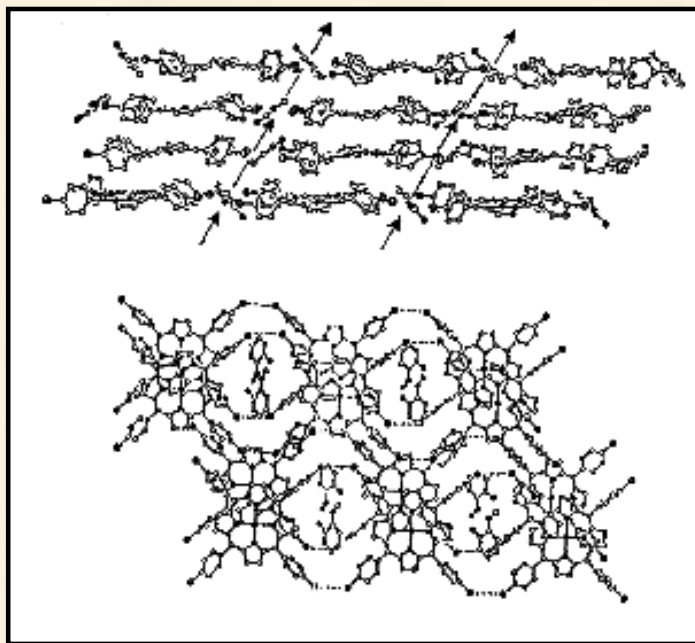
63.



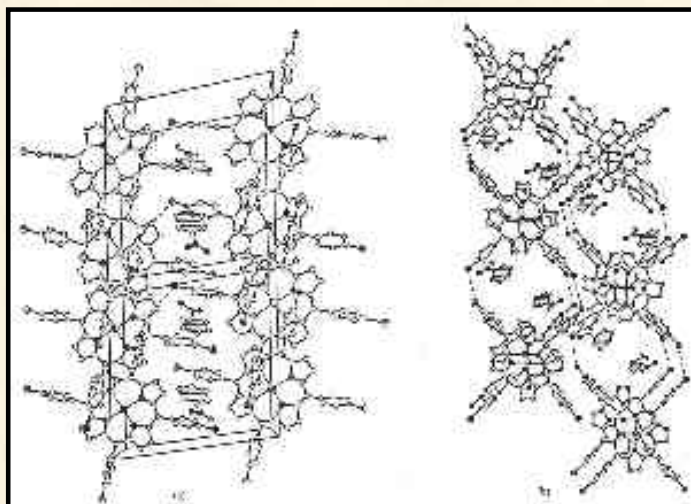
64.



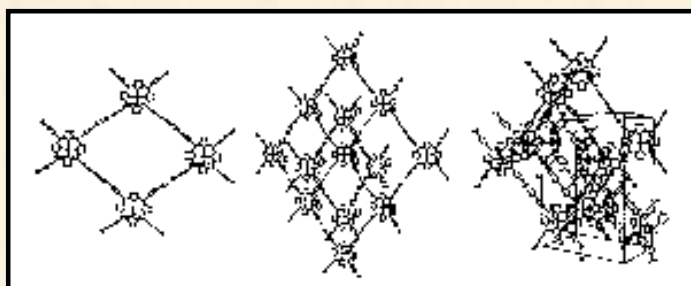
65.



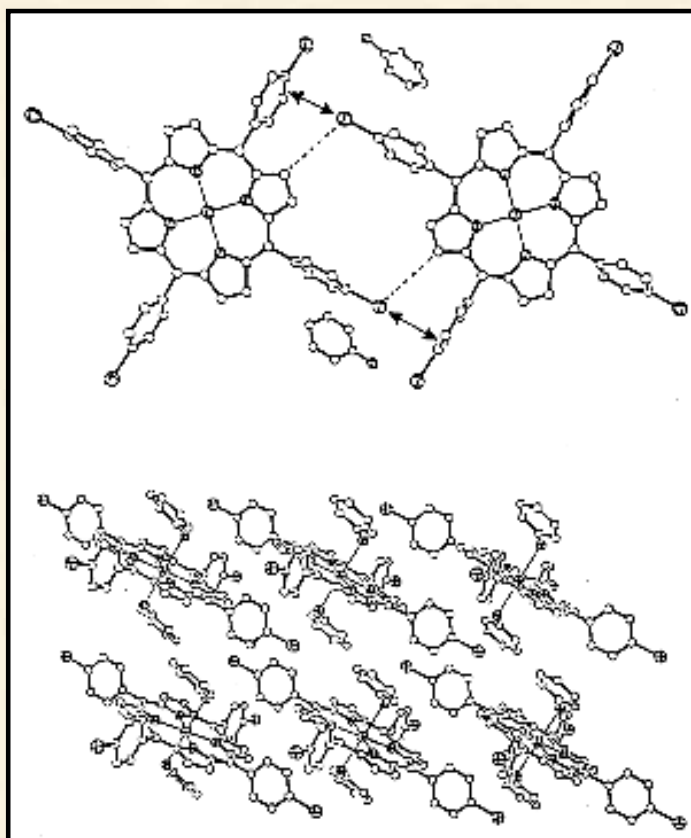
66.

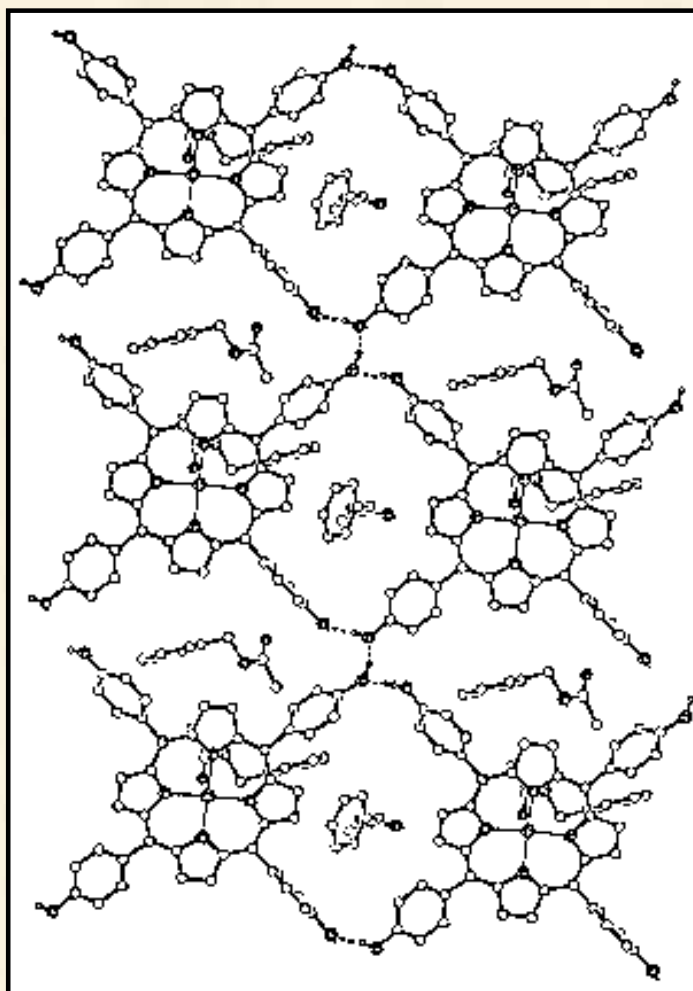


67.

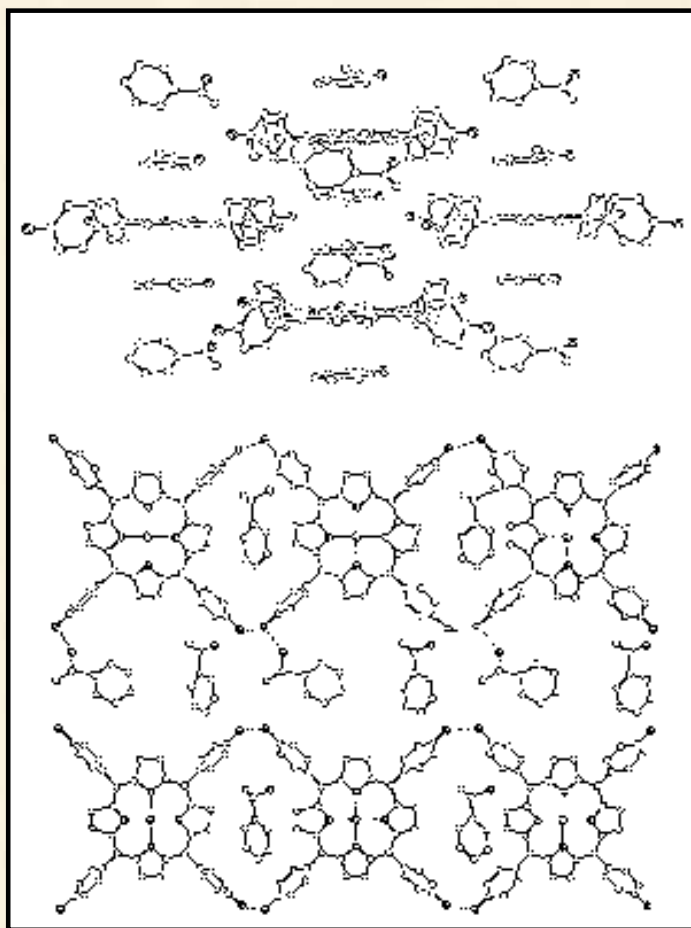


68.

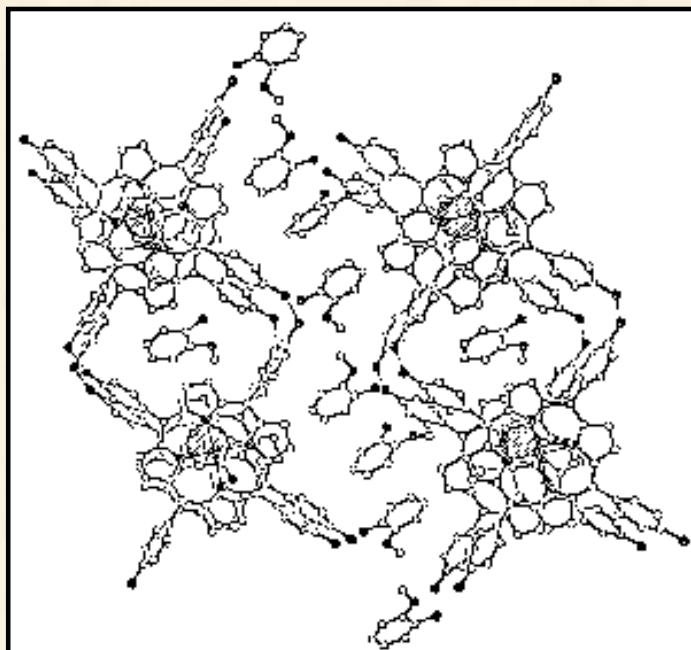




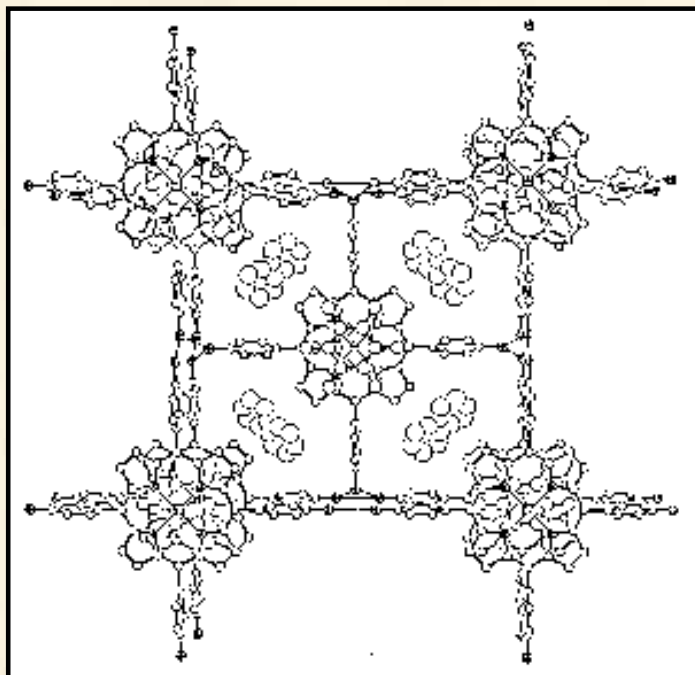
70.



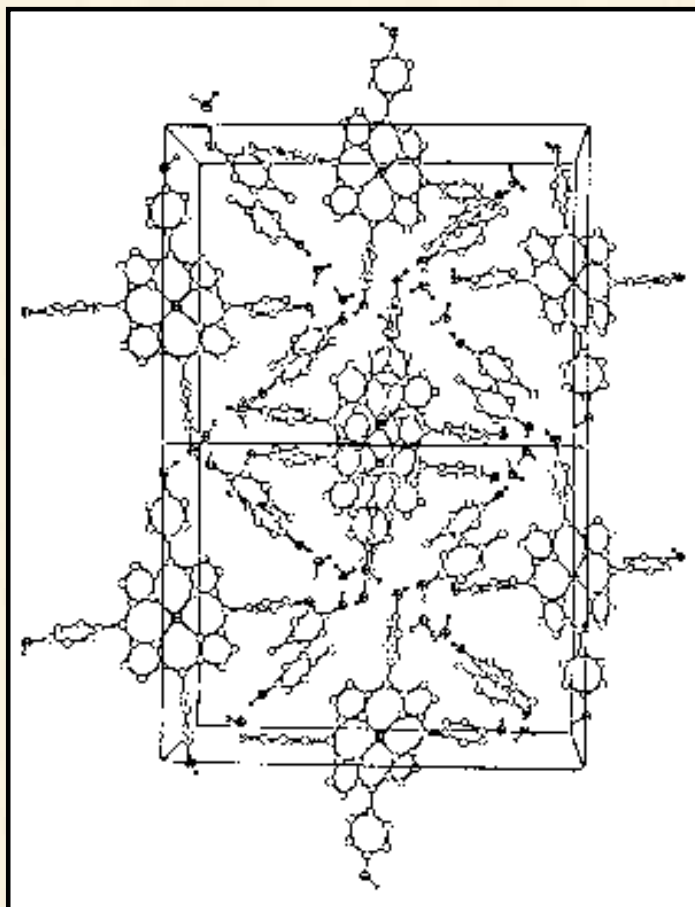
71.



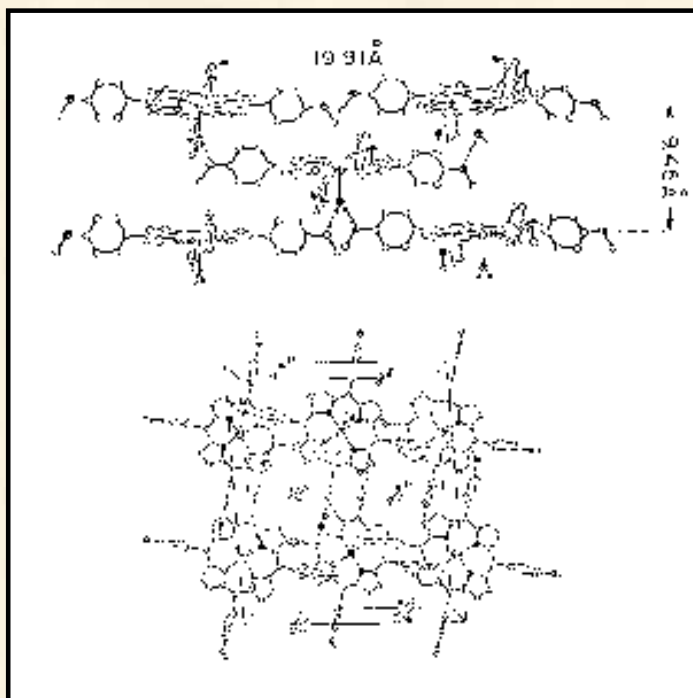
72.



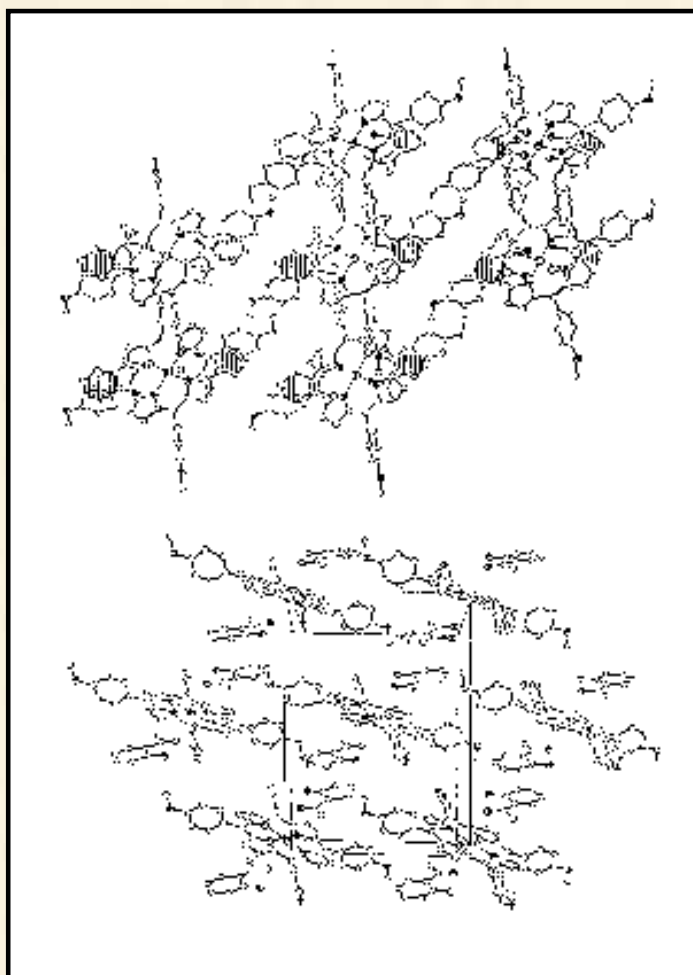
73.



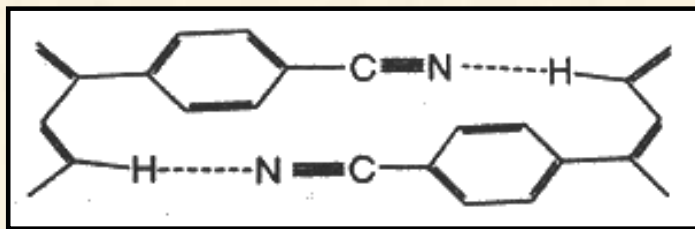
74.



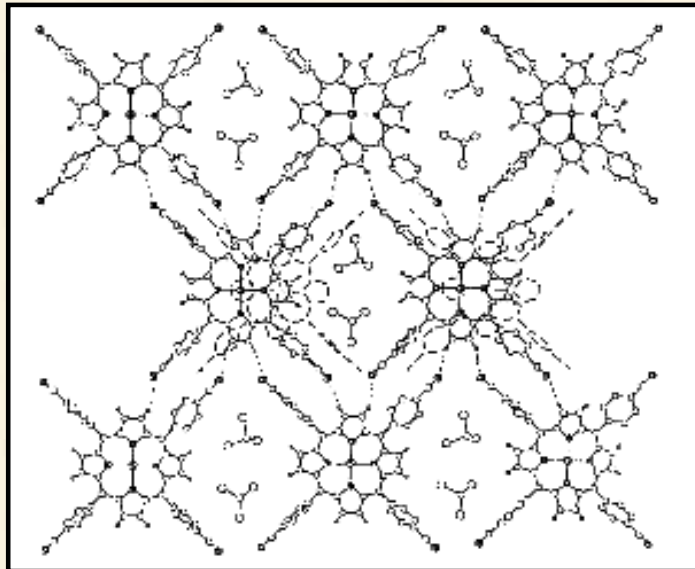
75.



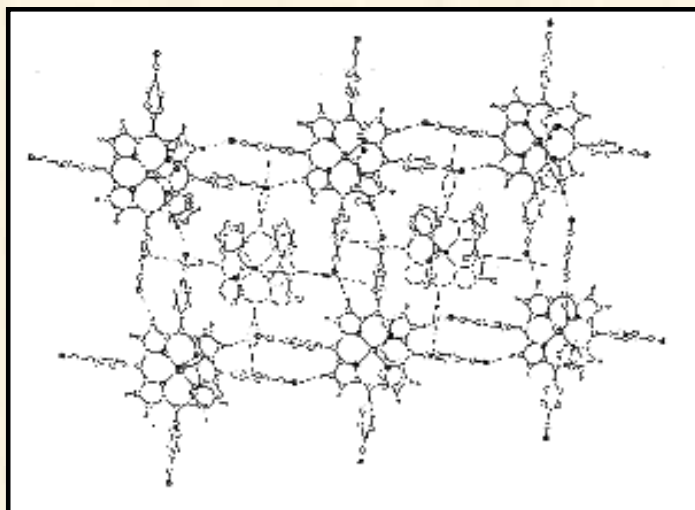
76.



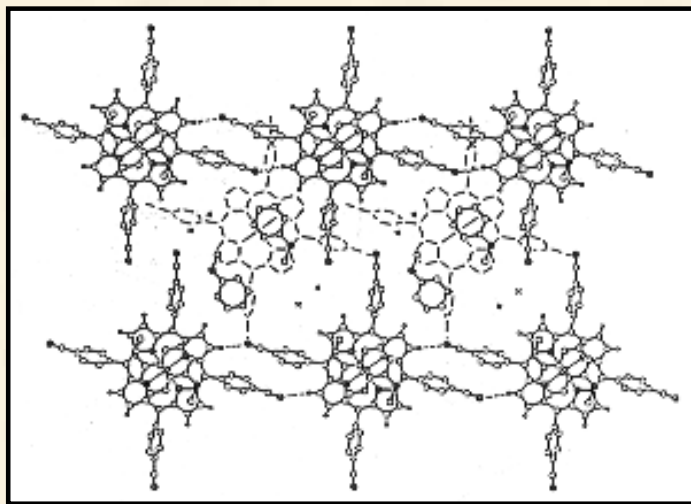
77.



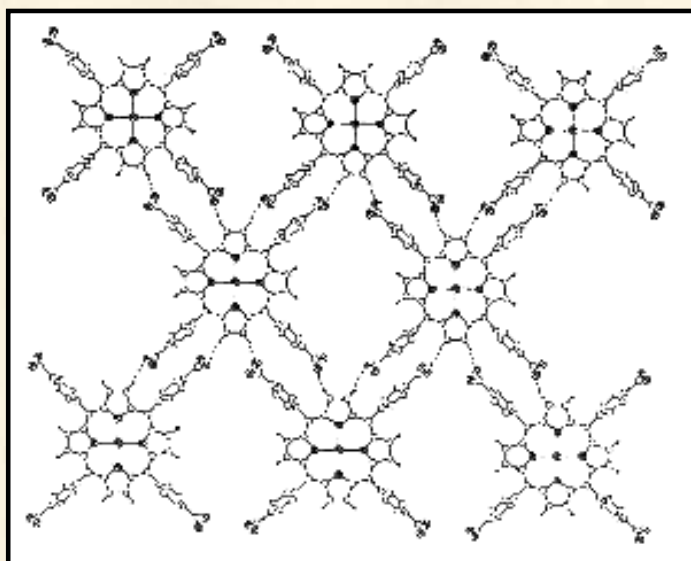
78.



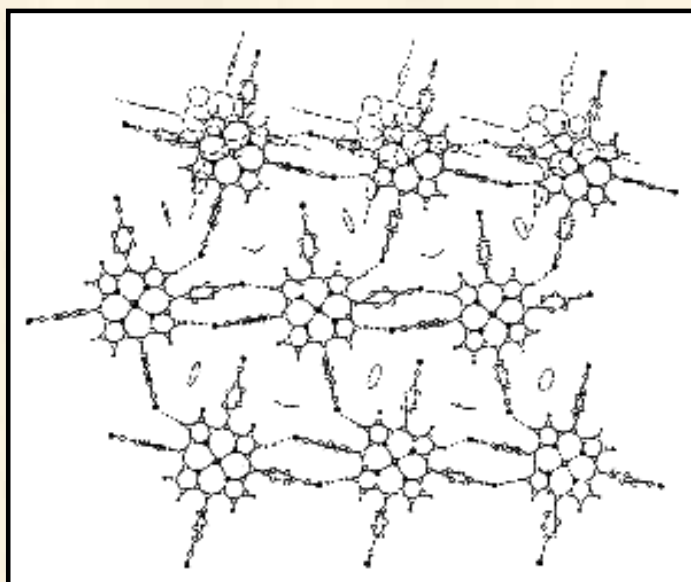
79.



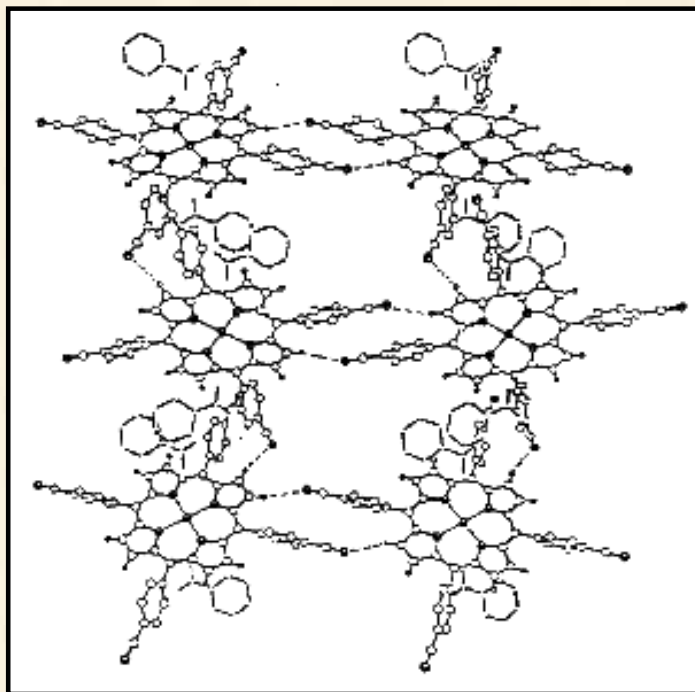
80.



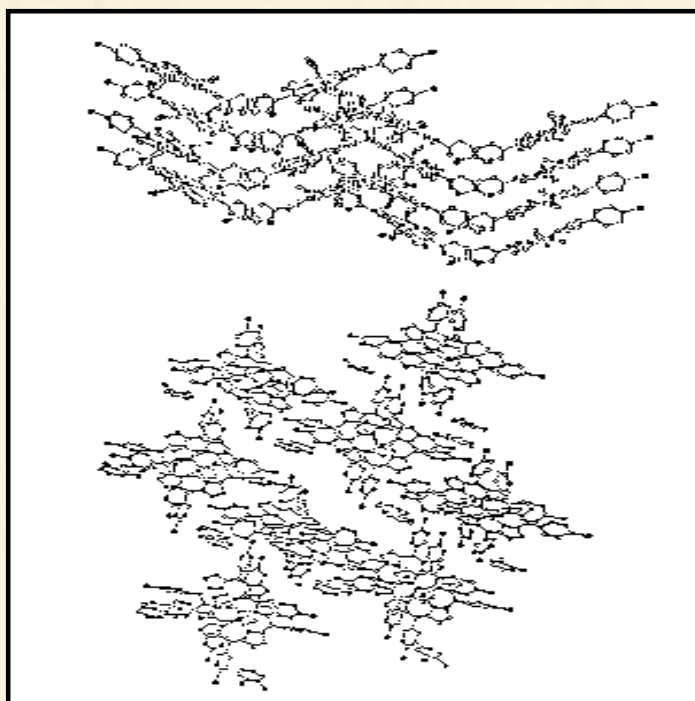
81.



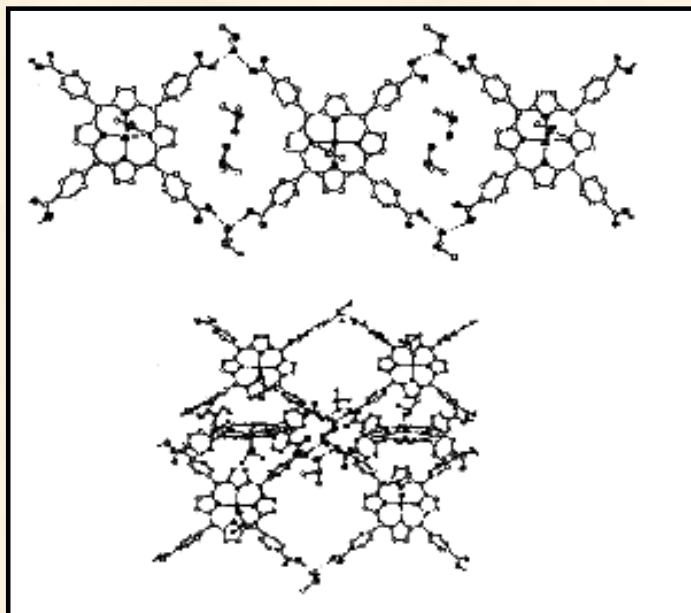
82.



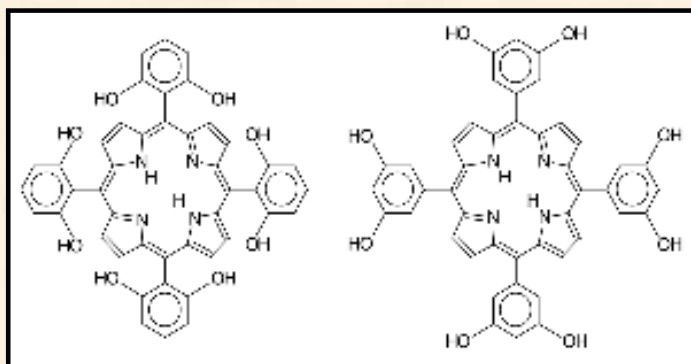
83.



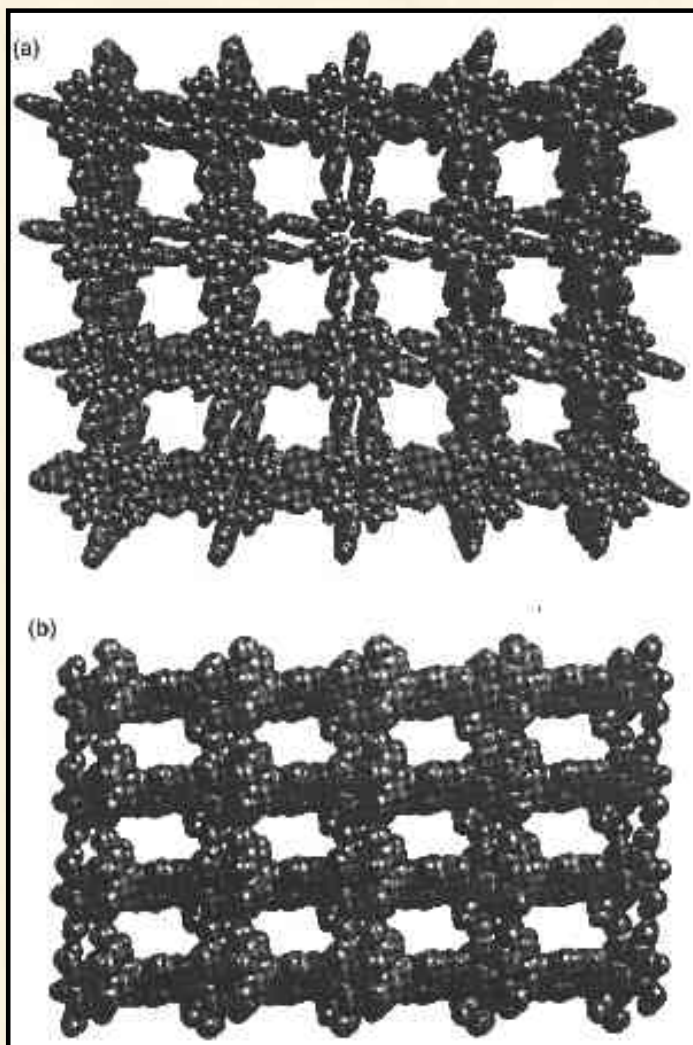
84.



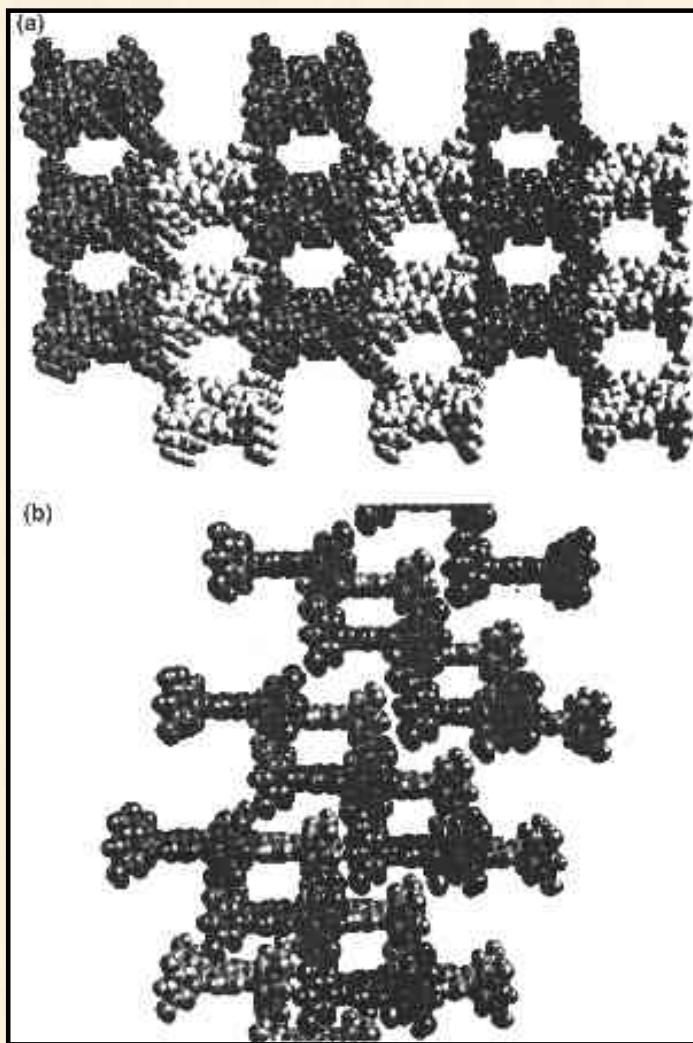
85.

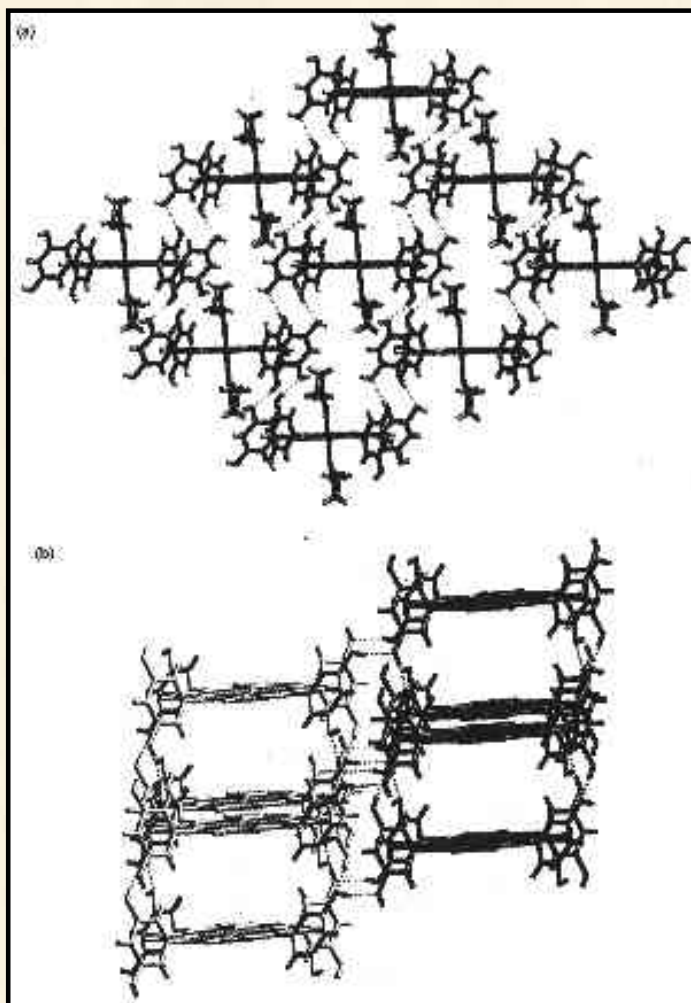


86.

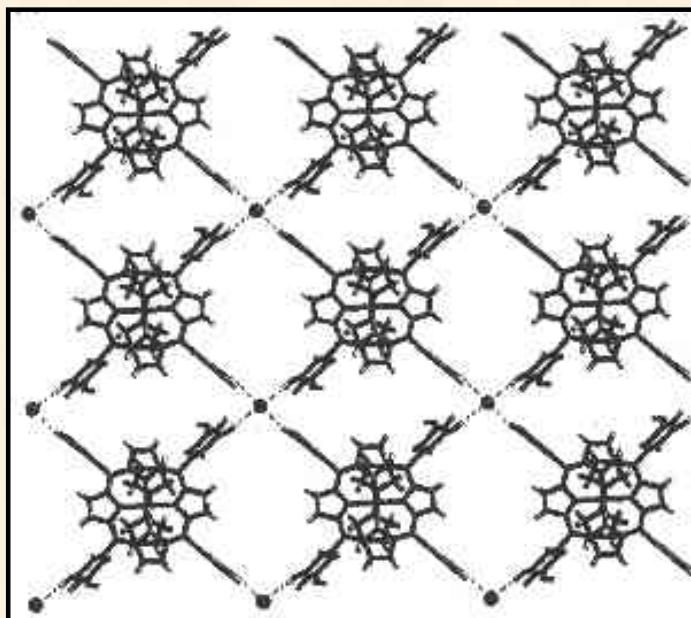


87.

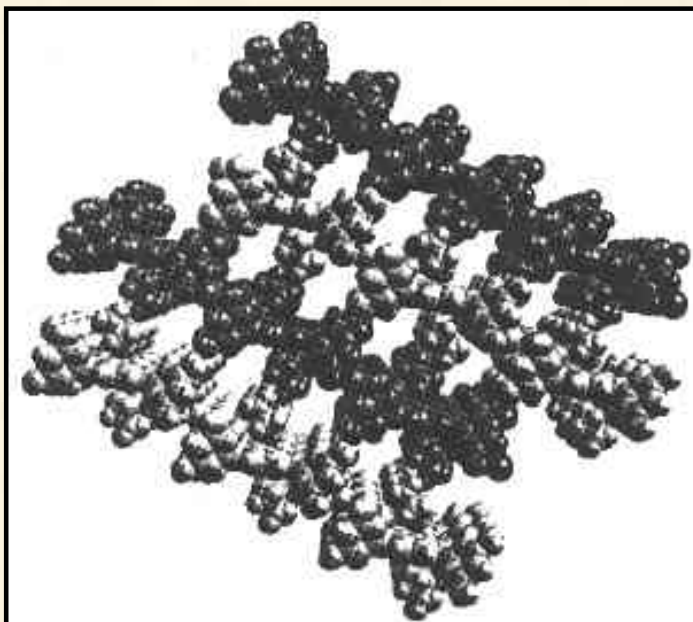




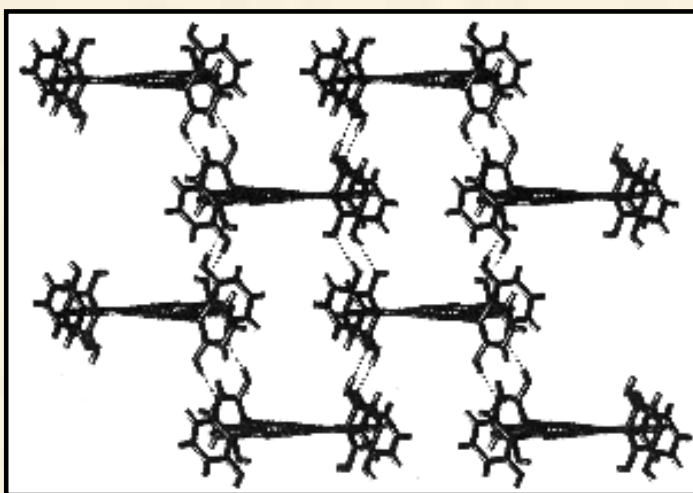
89.



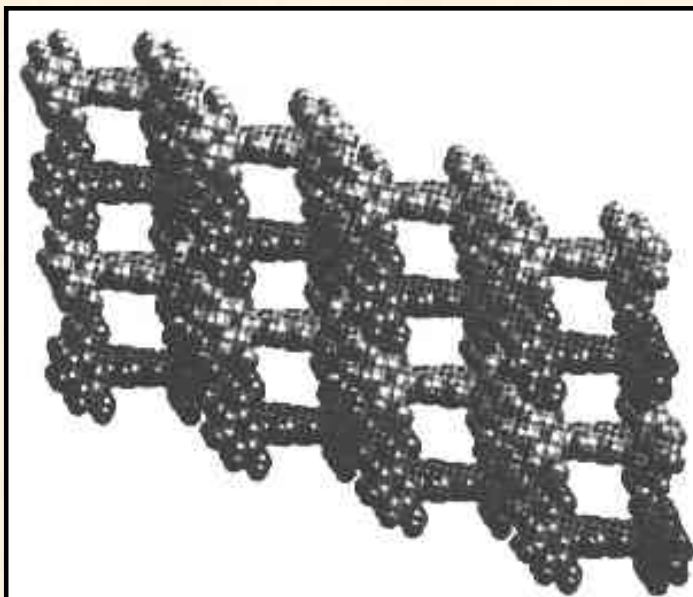
90.

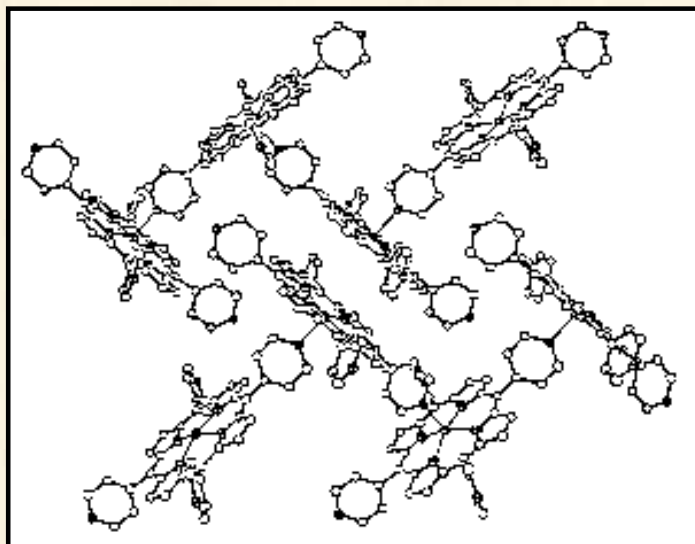


91.

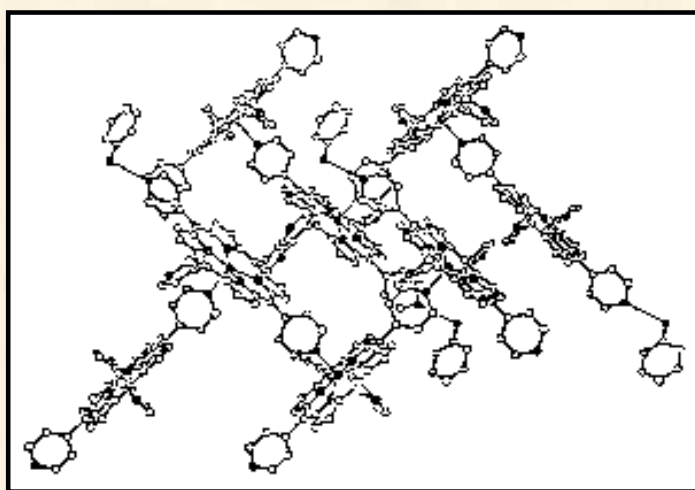


92.

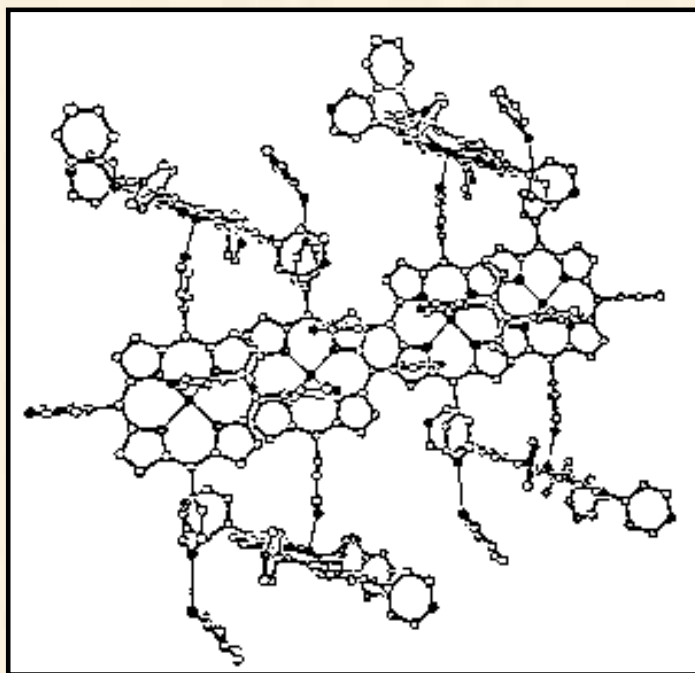


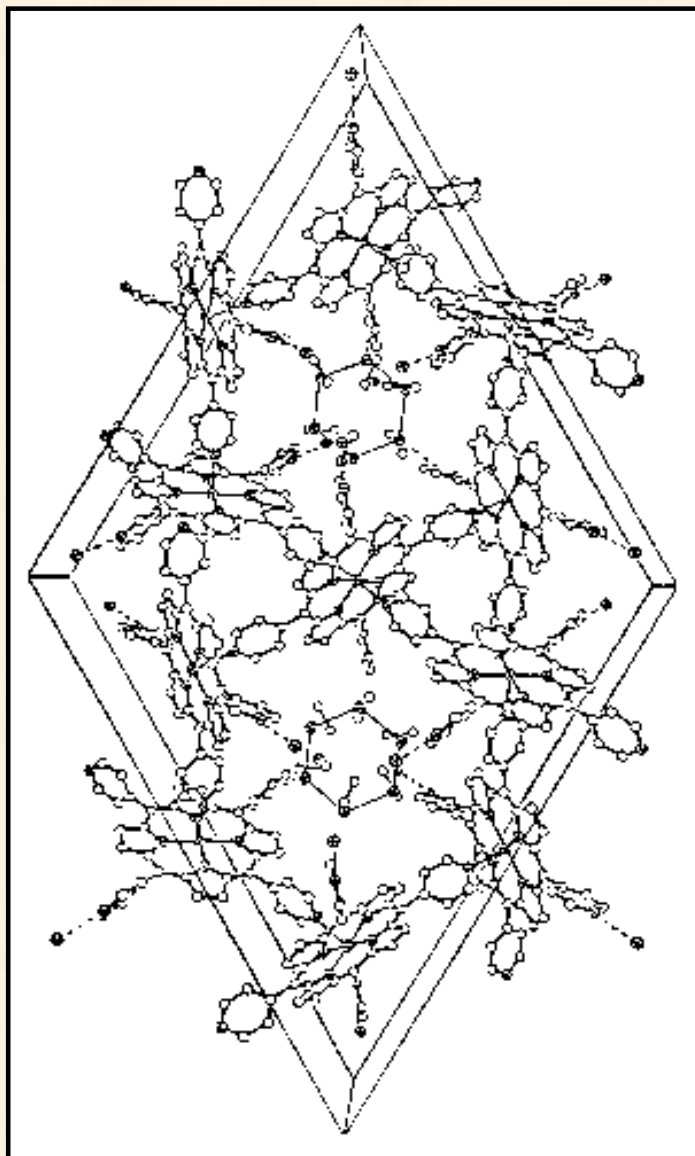


94.

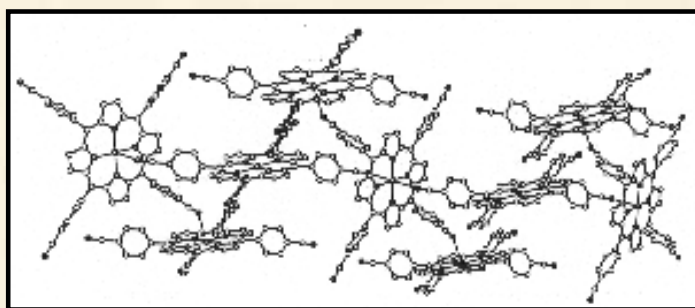


95.

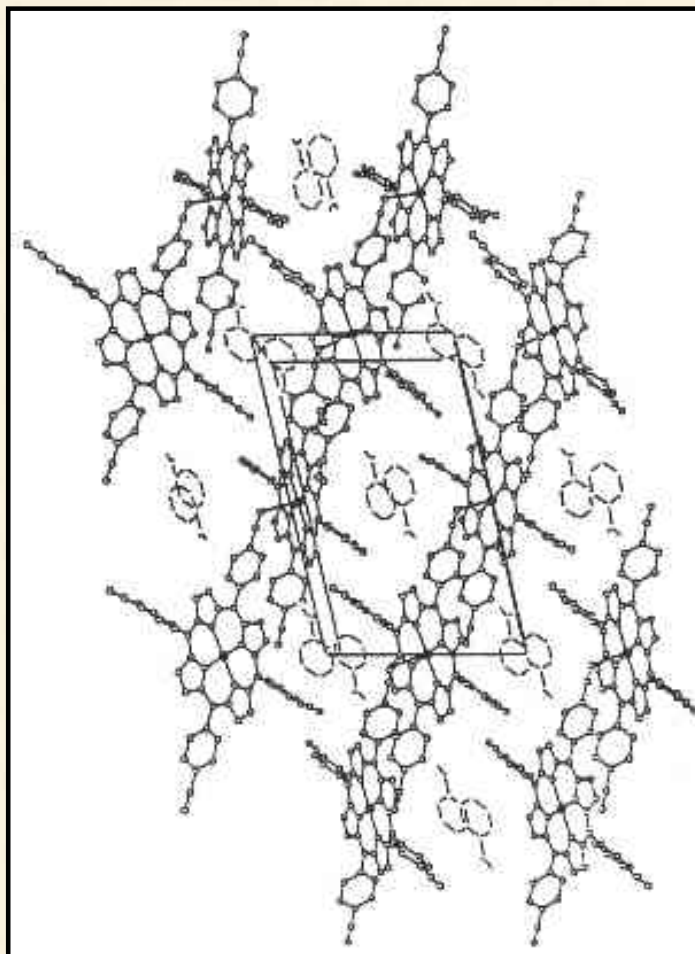




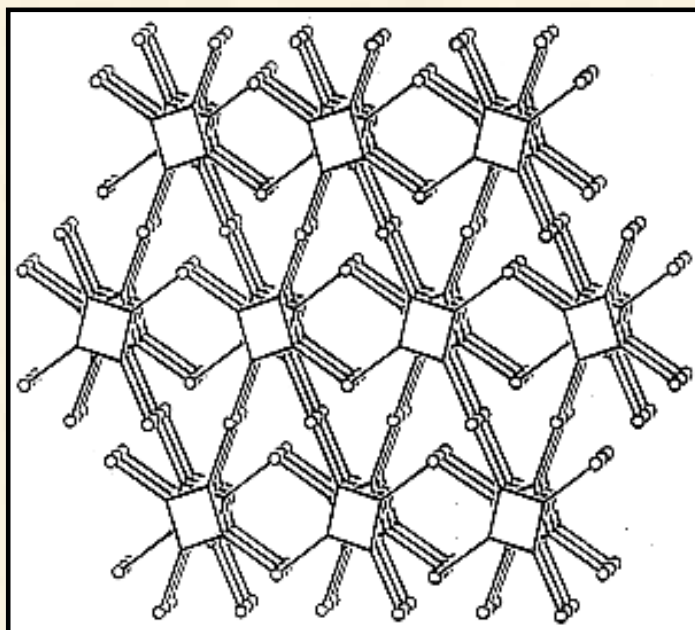
97.



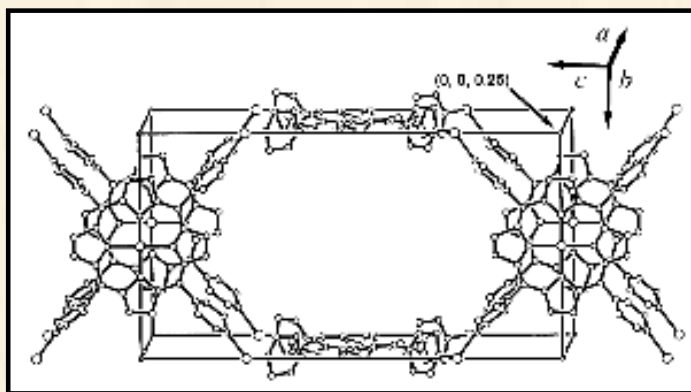
98.



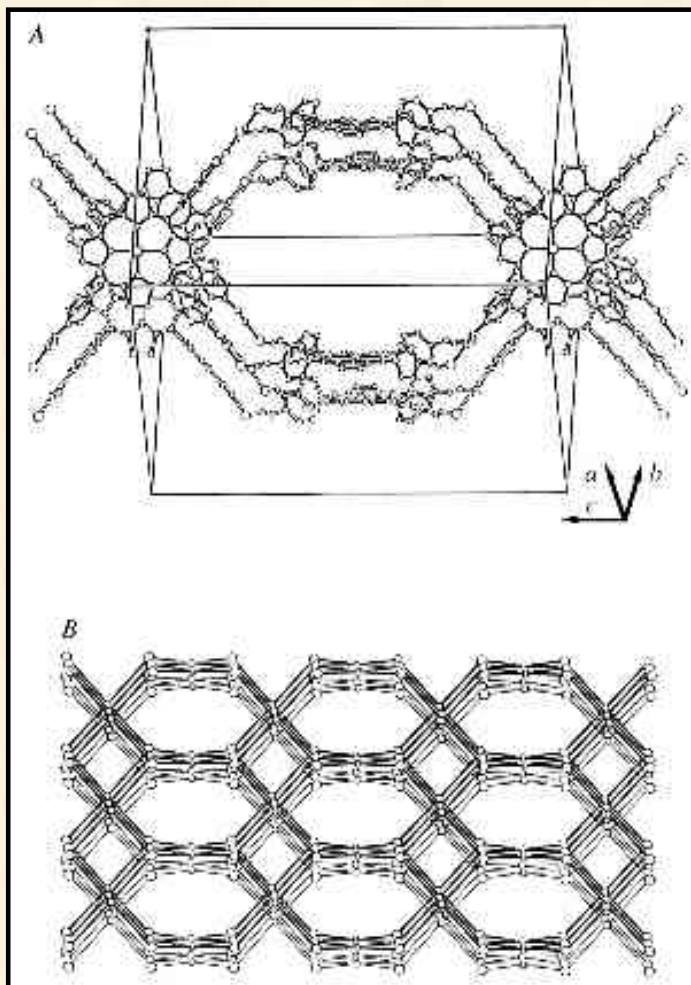
99.



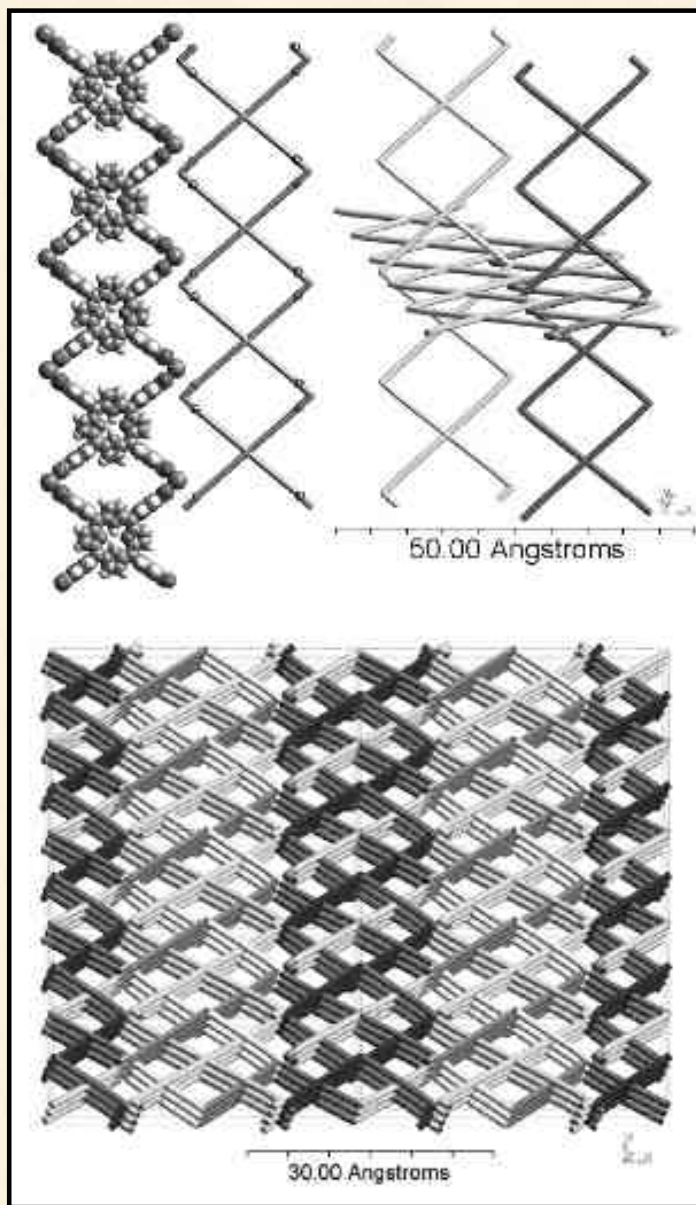
100.



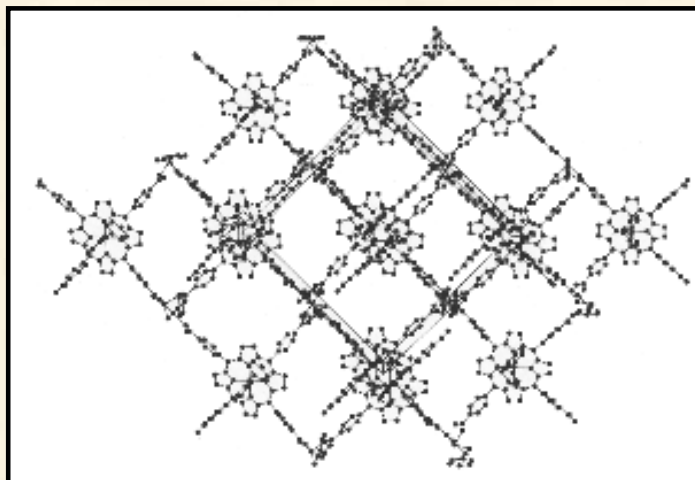
101.



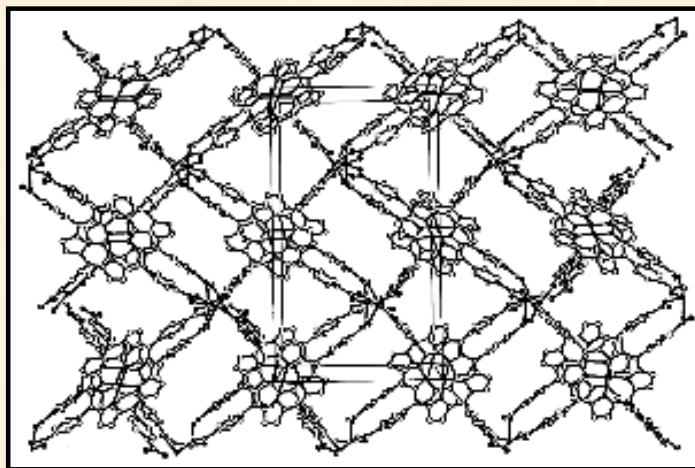
102.



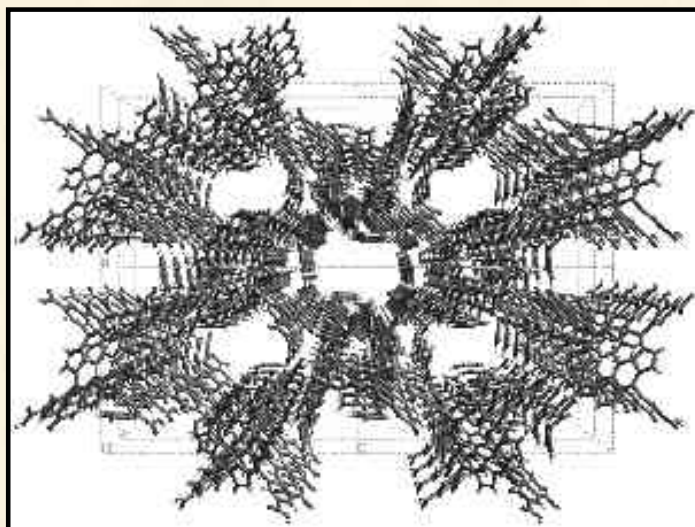
103.



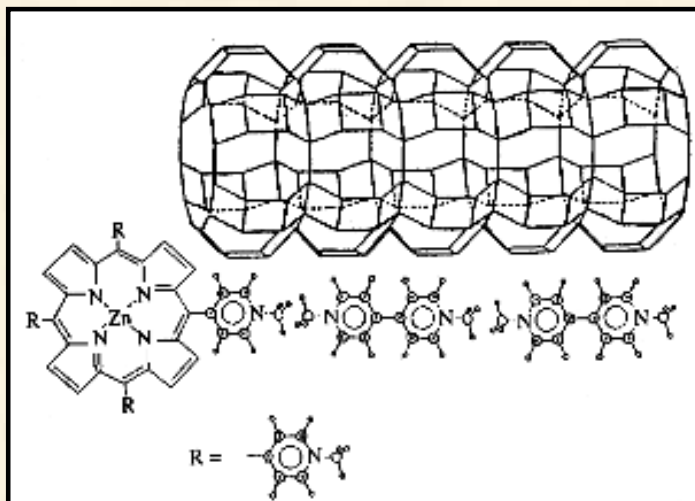
104.



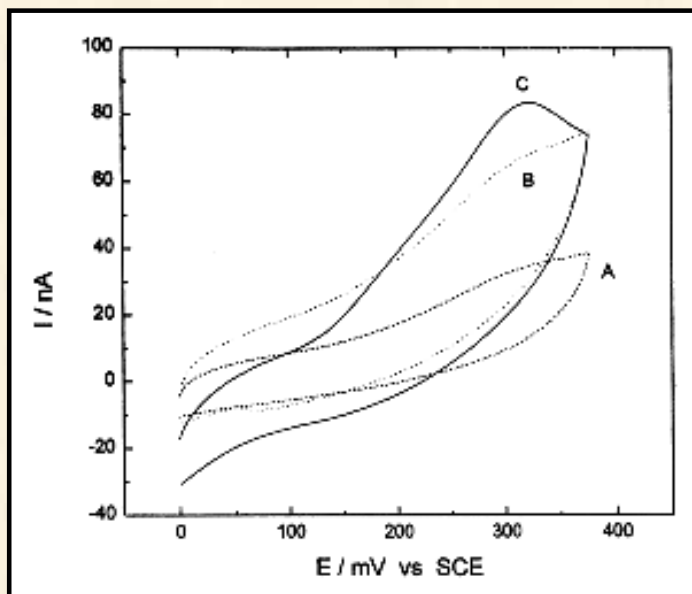
105.



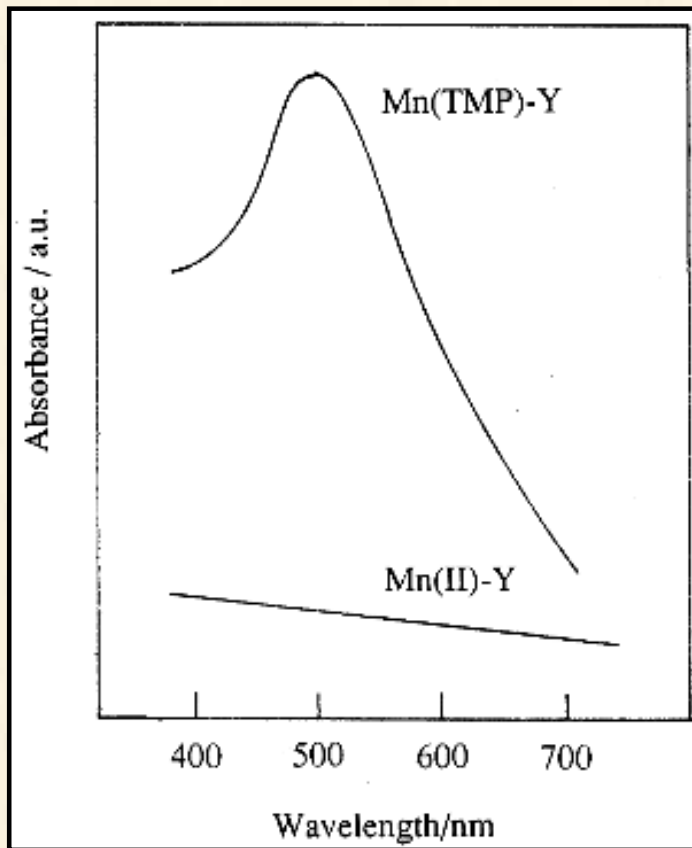
106.



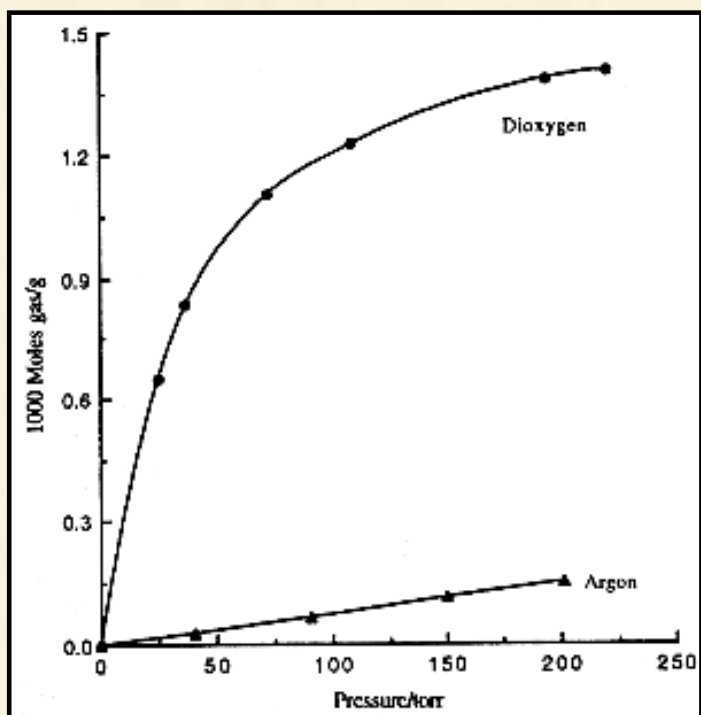
107.



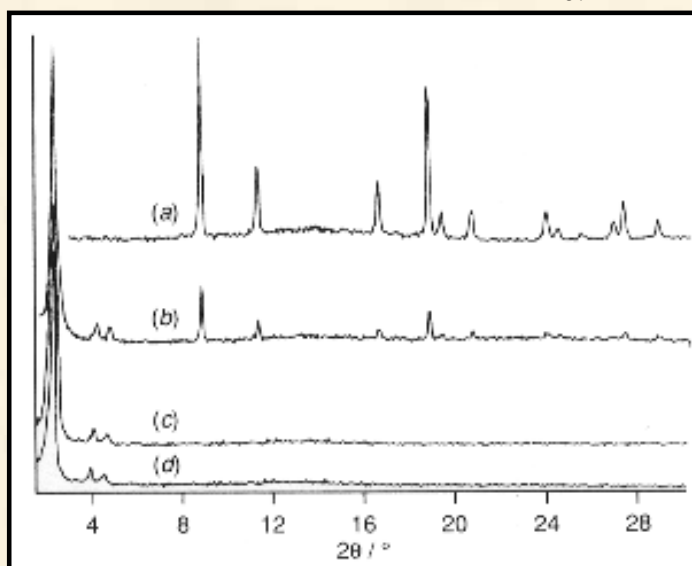
108.



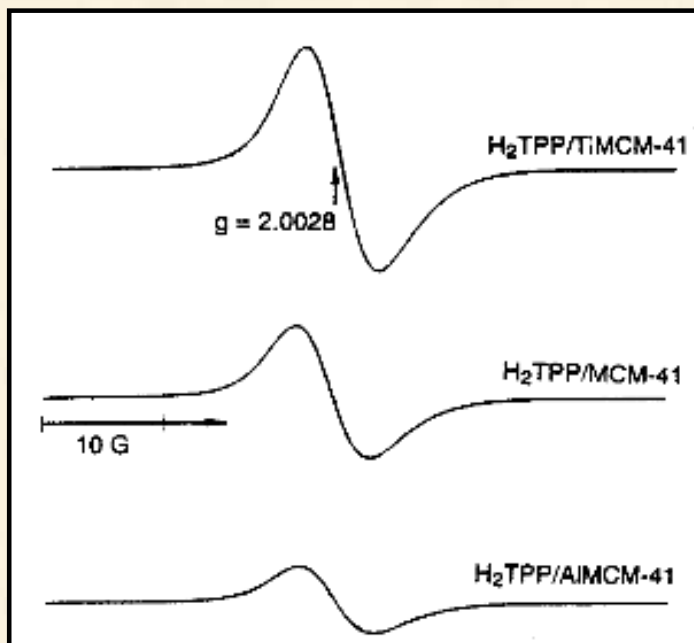
109.



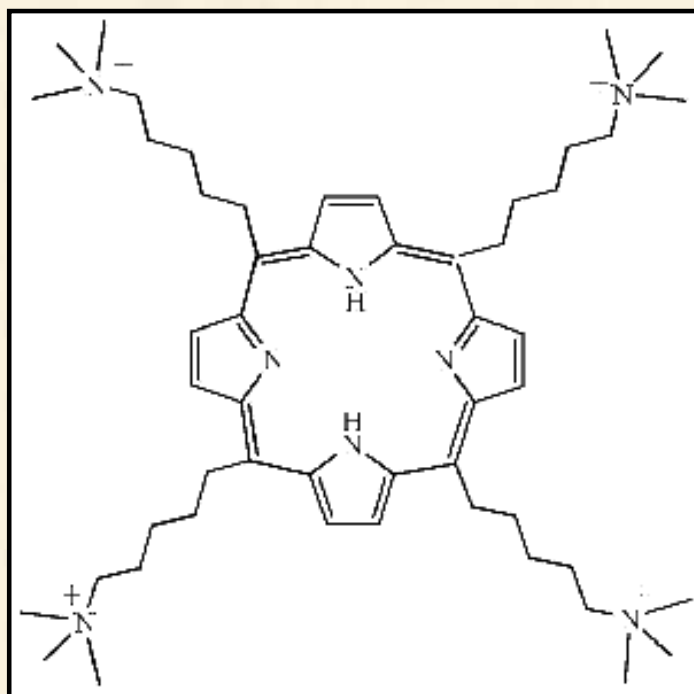
110.



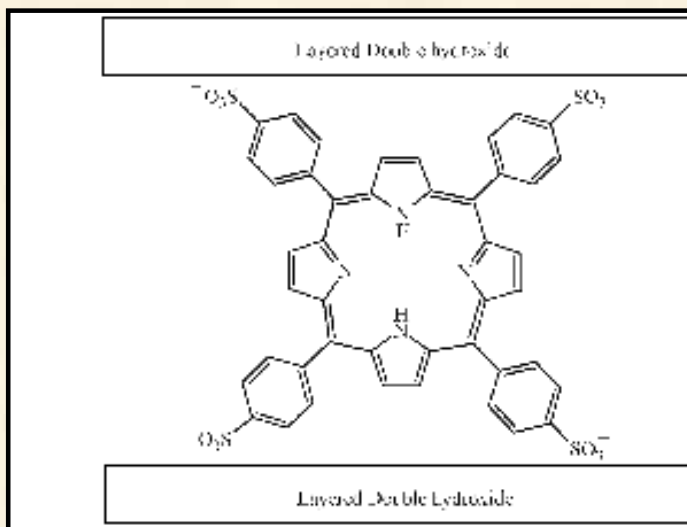
111.



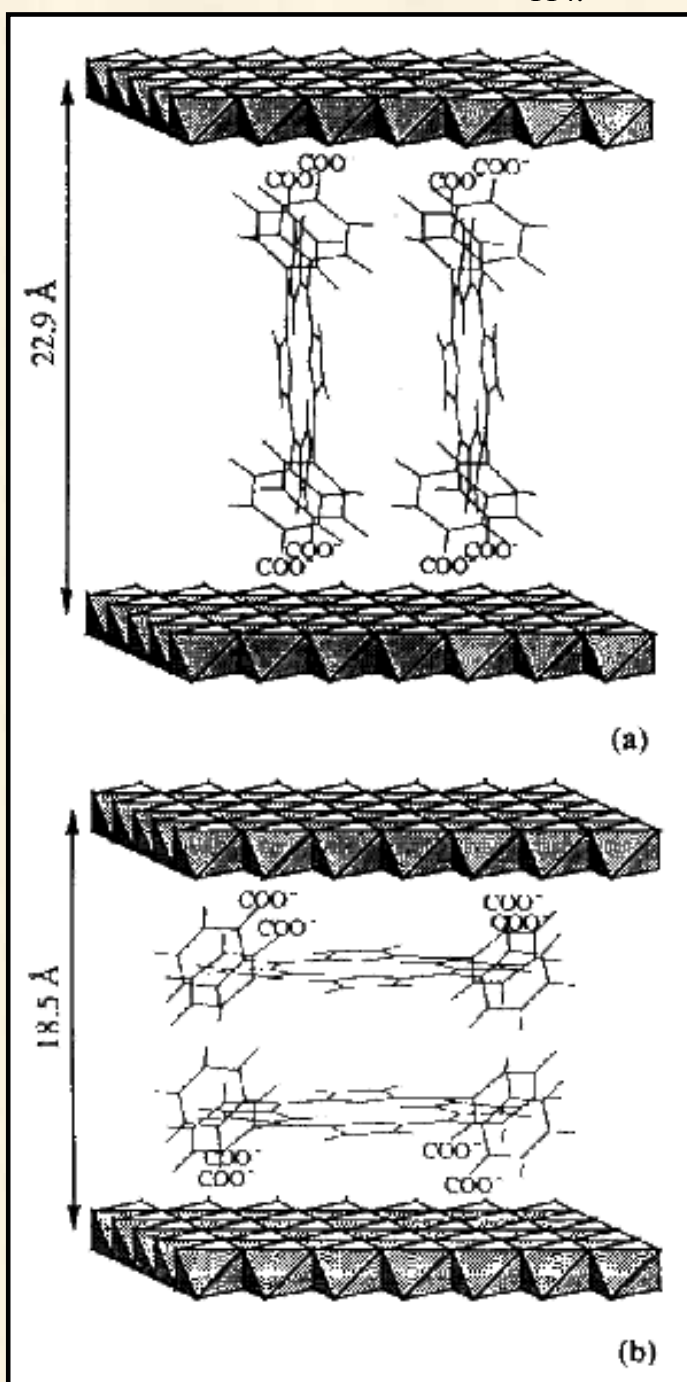
112.



113.

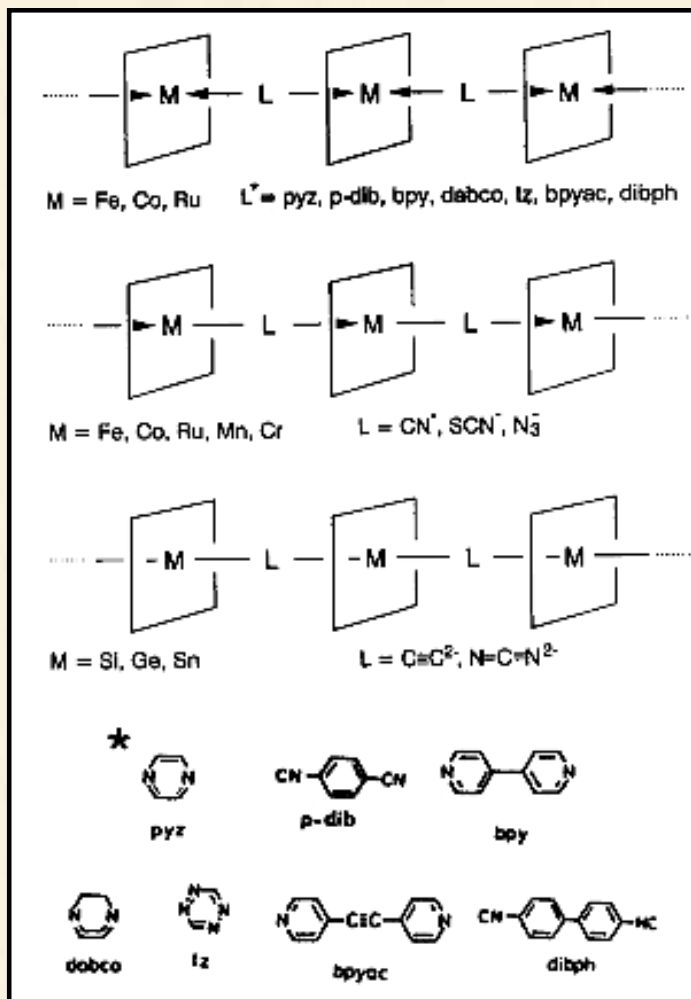


114.

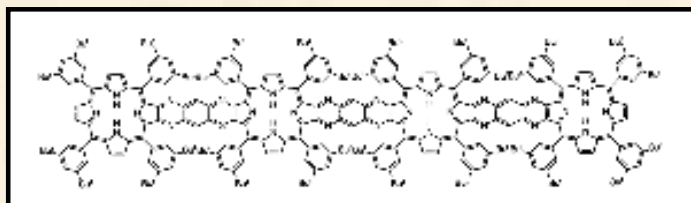


(b)

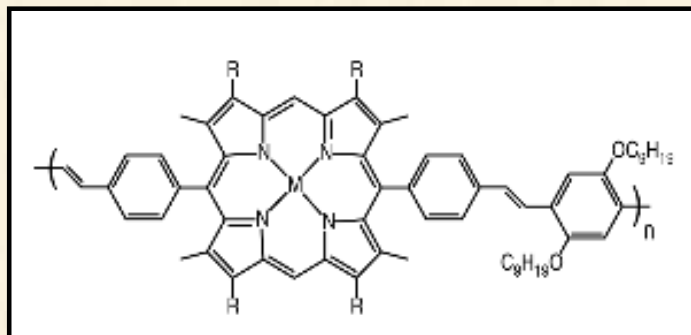
115.



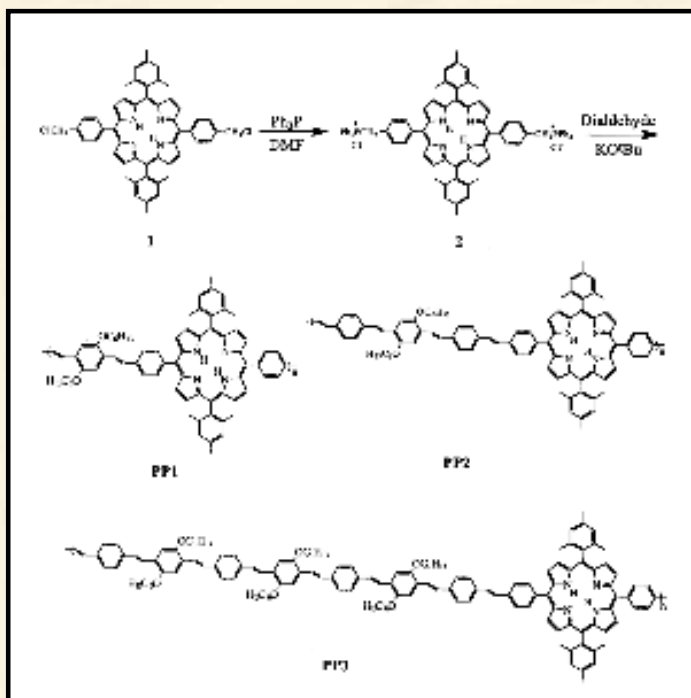
116.



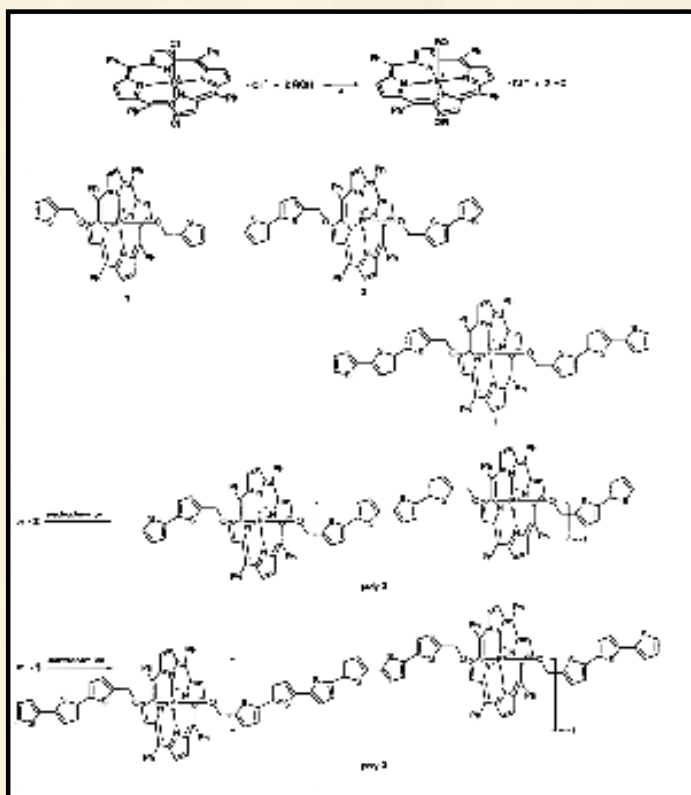
117.



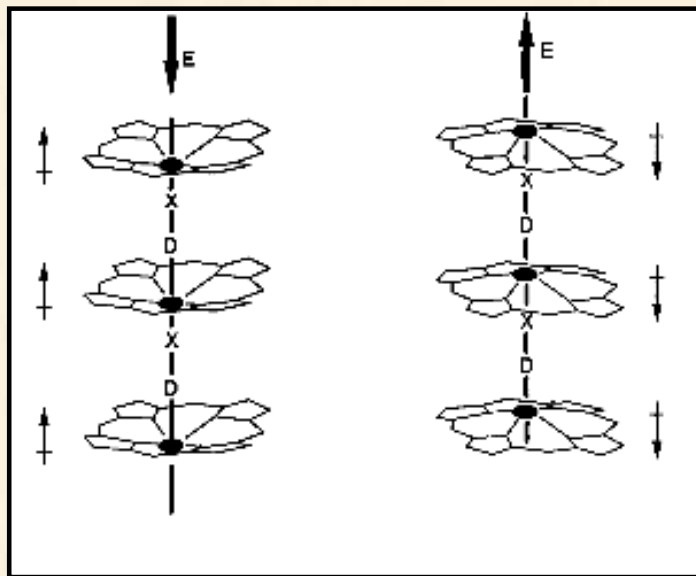
118.



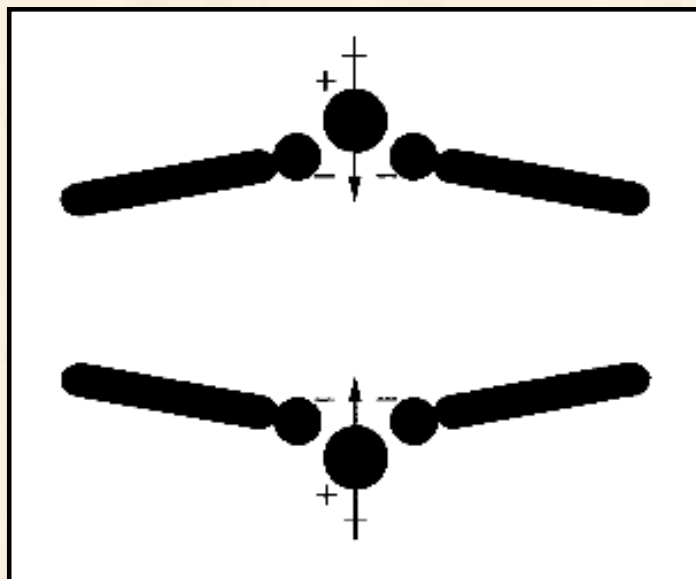
119.



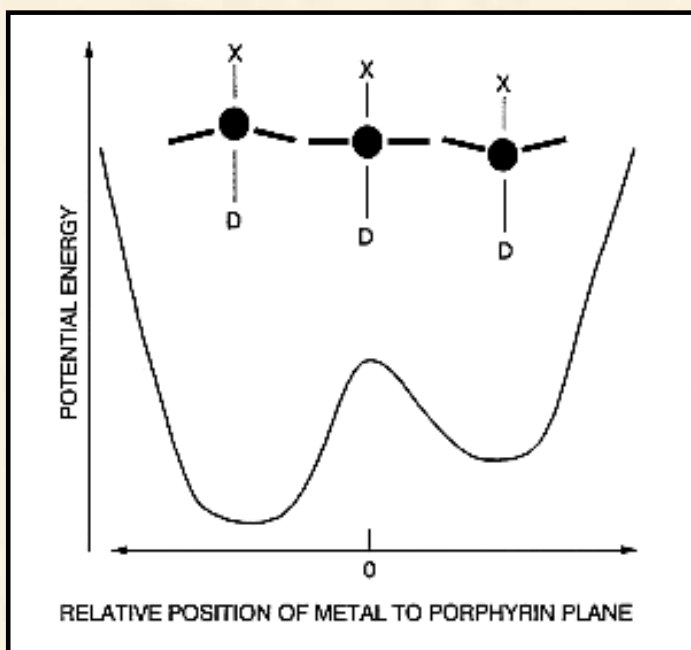
120.



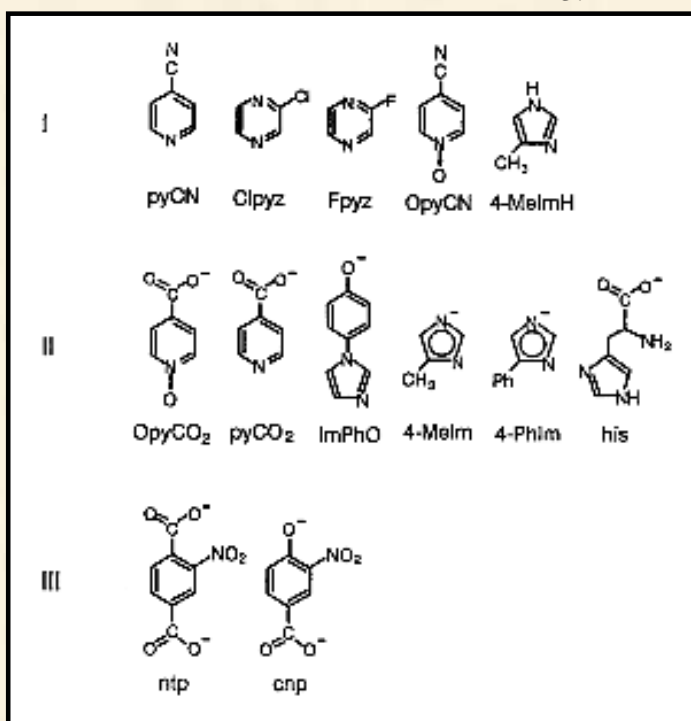
121.



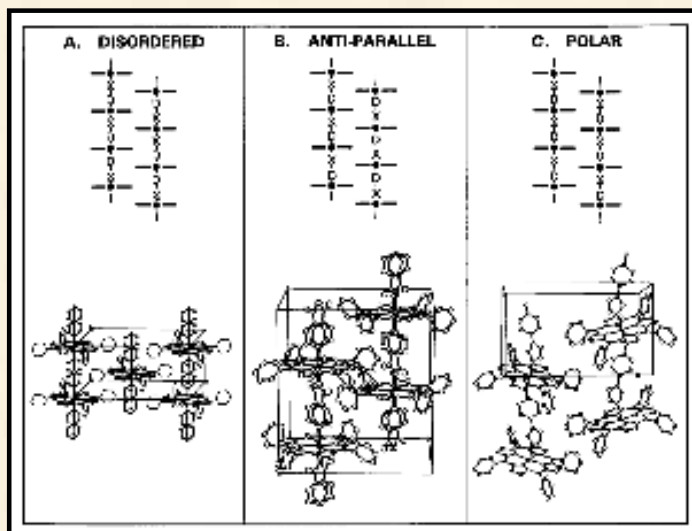
122.



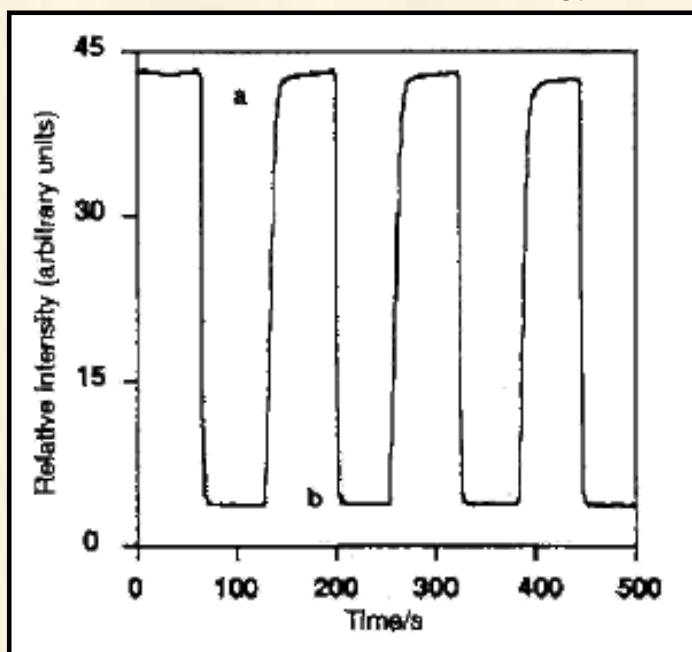
123.



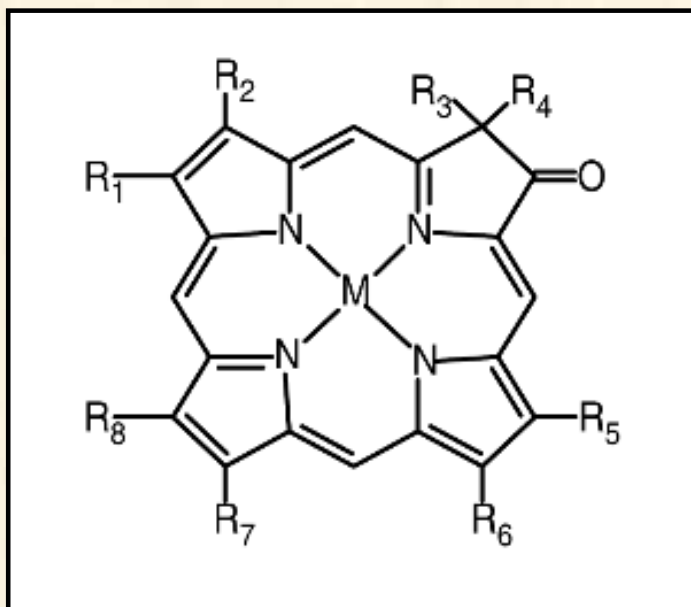
124.



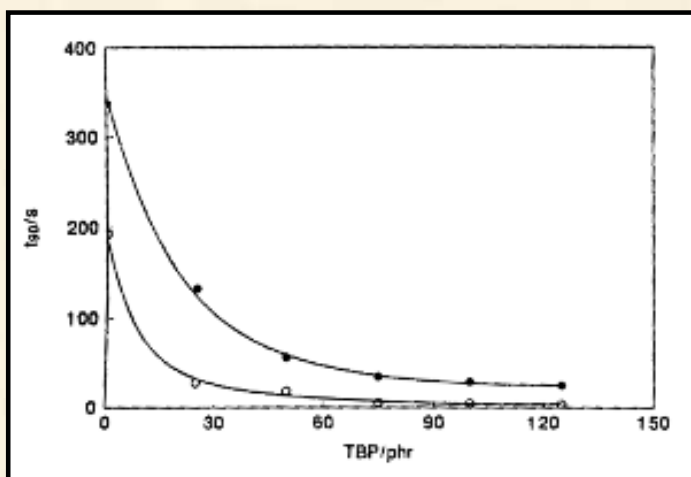
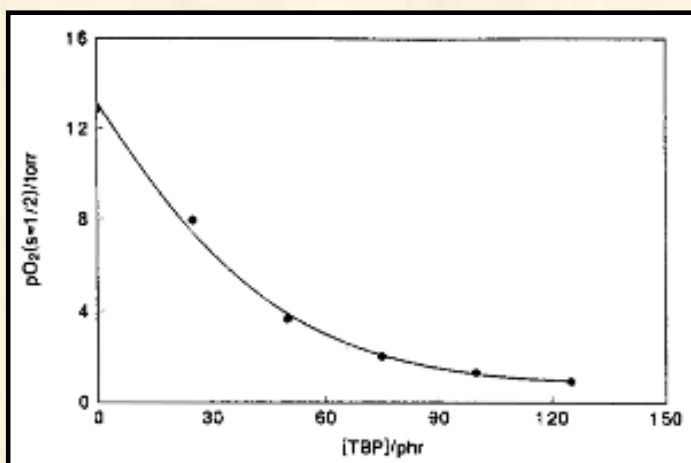
125.



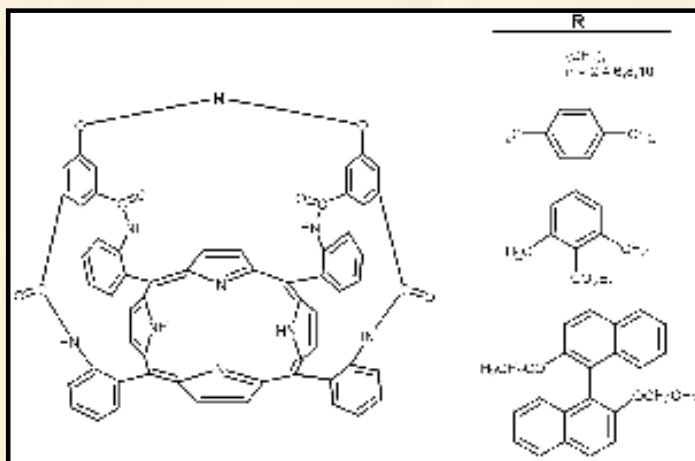
126.



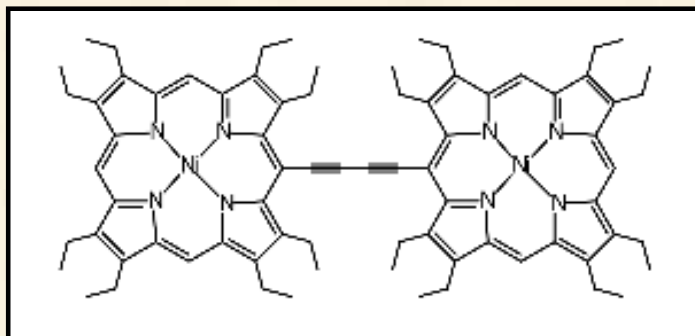
127.



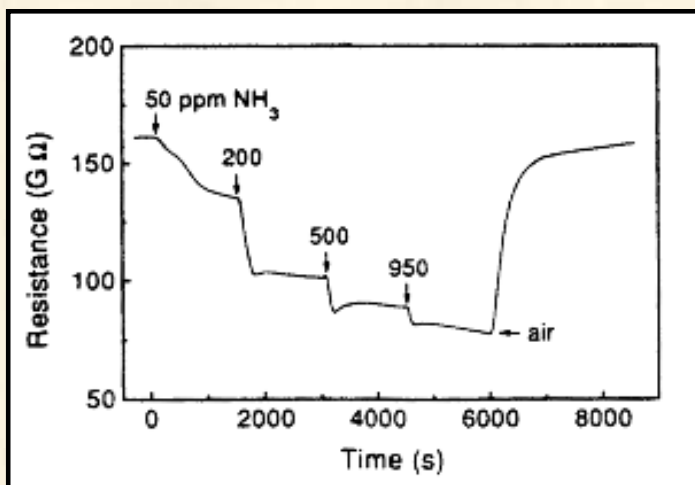
128.



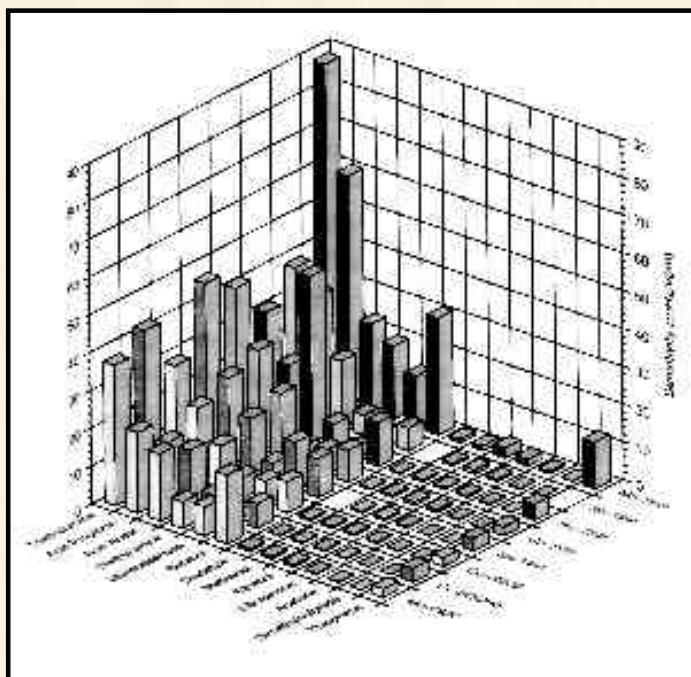
129.



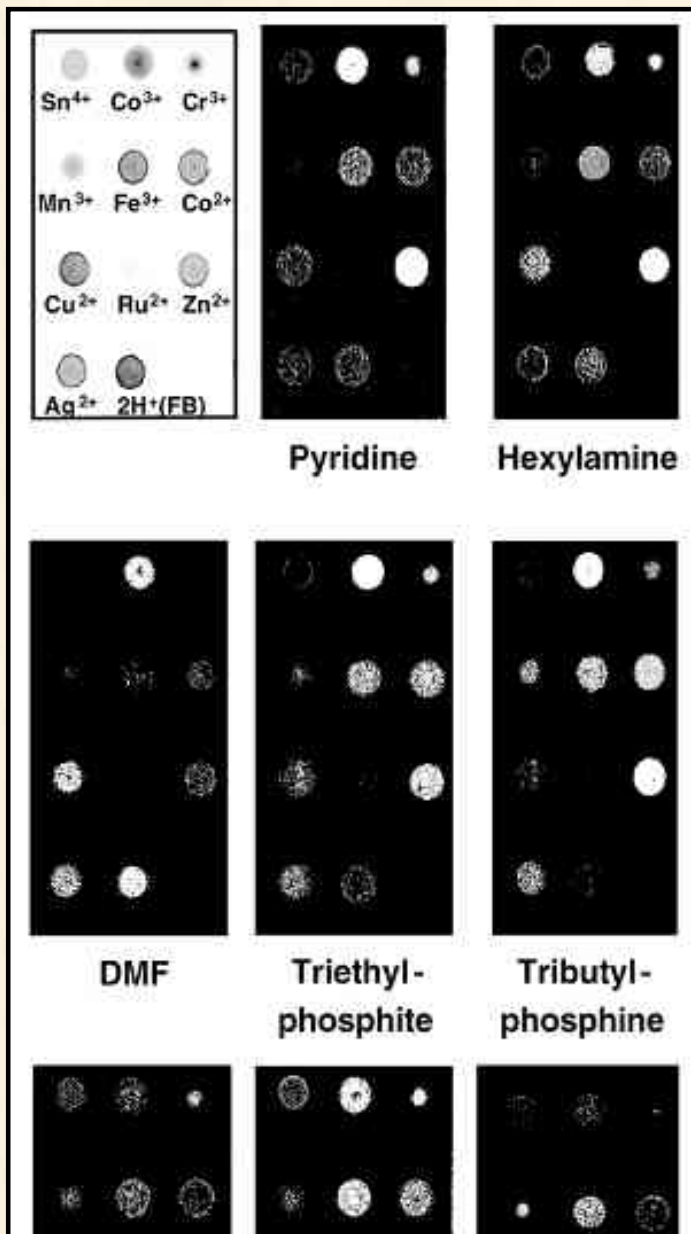
130.

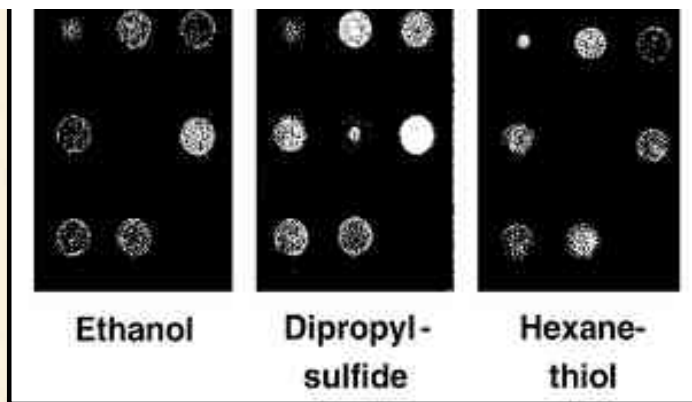


131.

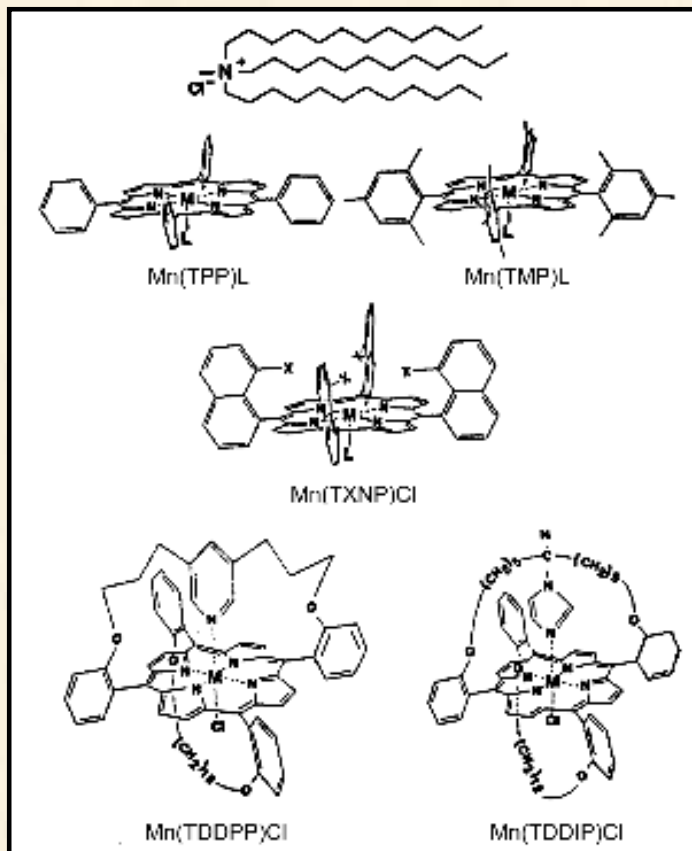


132.

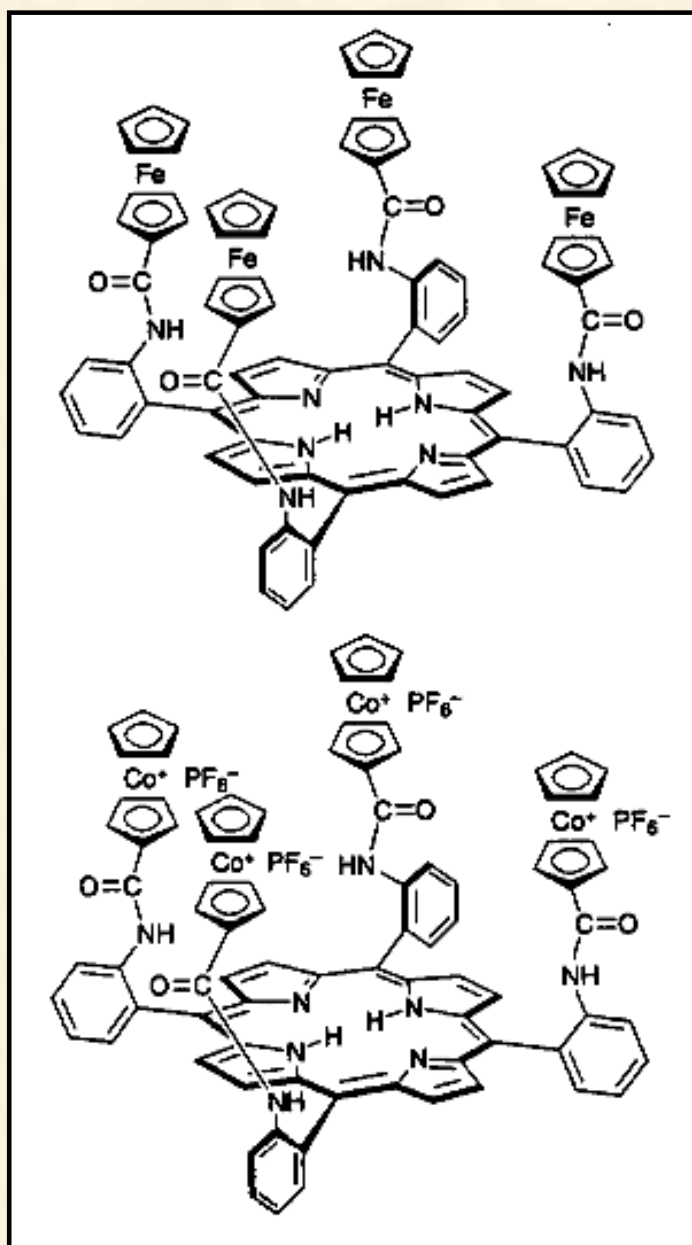




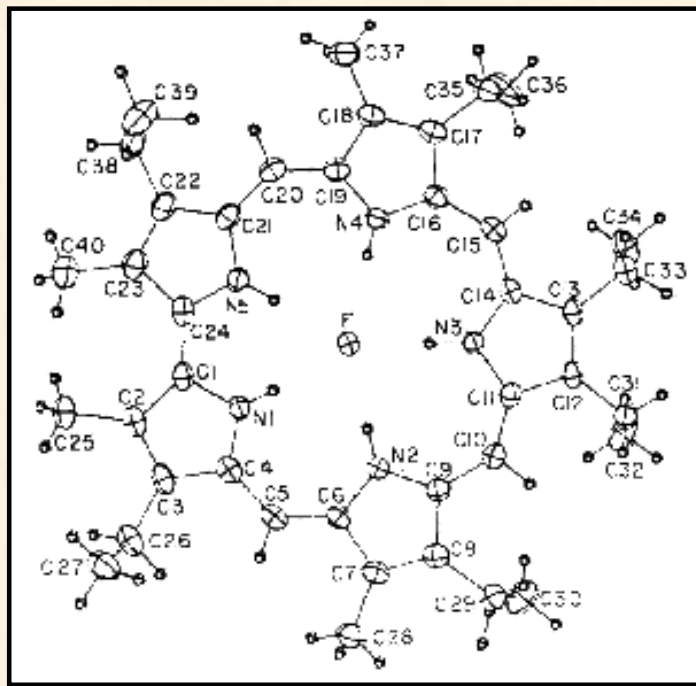
133.



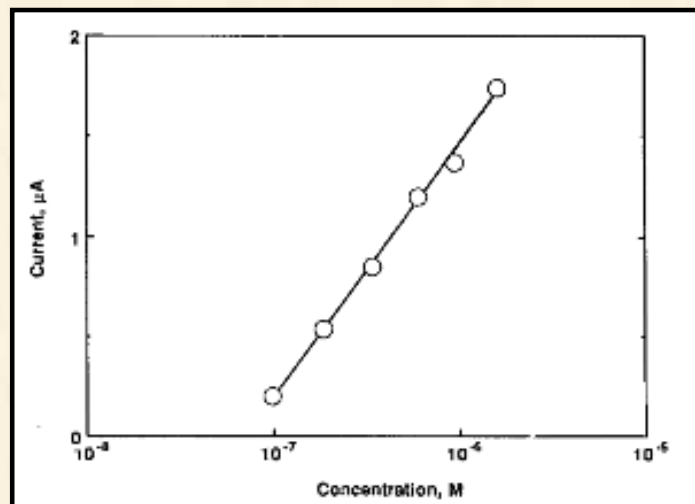
134.



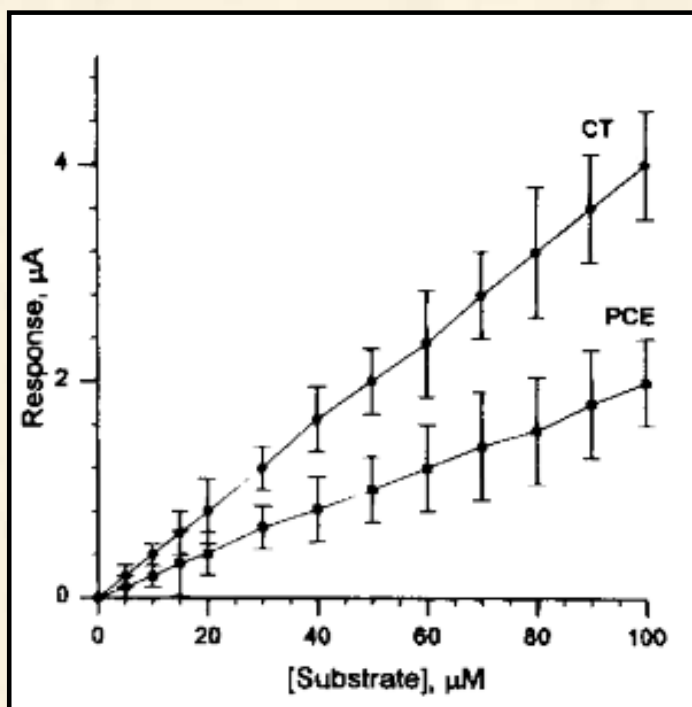
135.



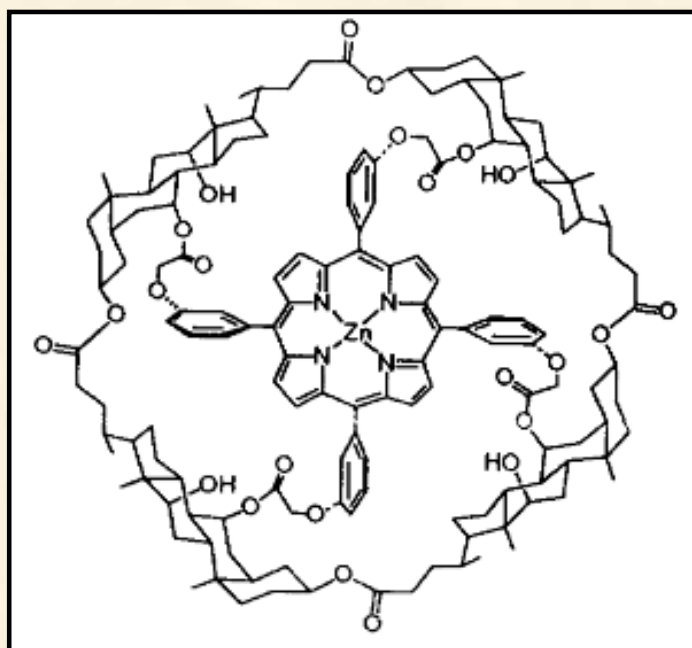
136.



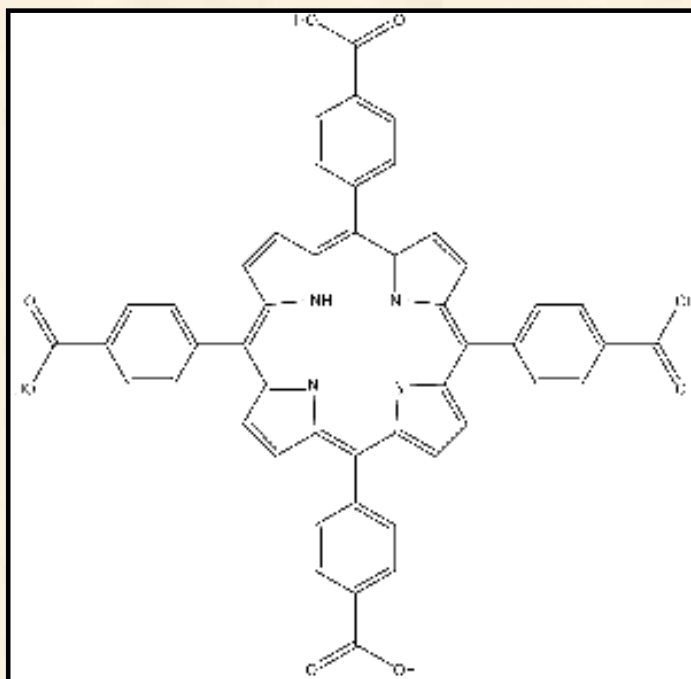
137.



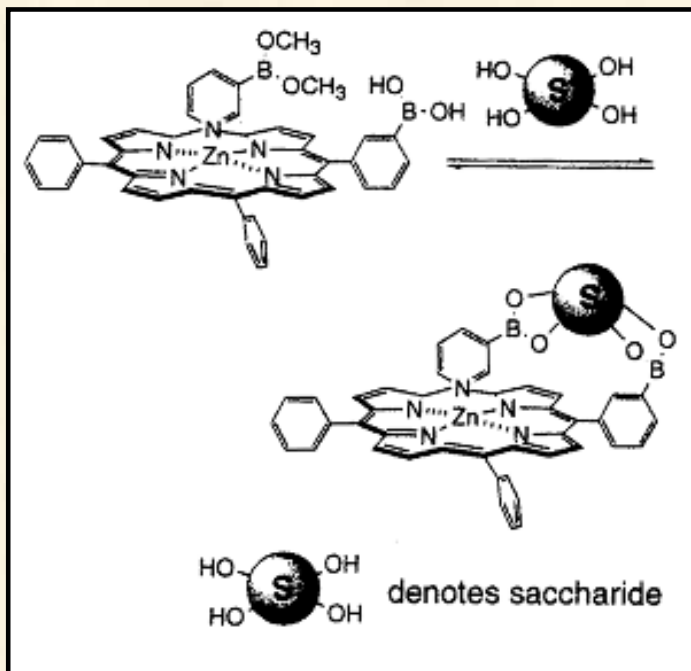
138.



139.



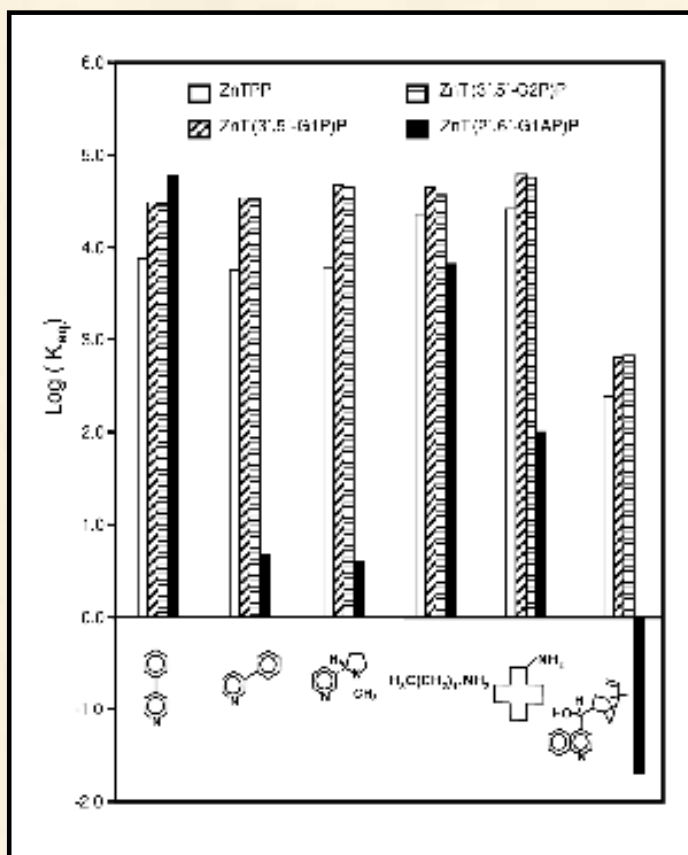
140.



141.



142.



SUSLICK GROUP WEBSITE:

THE SCIENCE	THE GROUP	THE MAÎTRE D'	LAGNIAPPE: A LITTLE EXTRA
Overview	Current Group Members	CV: Abbreviated, Full	Art and Science
Outline of Projects	Group Meetings	Suslick Group Brochure	Chymistes: The Distillers of Waters
Synopsis: Sonochemistry	Group Responsibilities	Complete Publication List	A Chemist Meets Hollywood
Metalloporph.			

<u>Executive Summary: Smell-Seeing</u>	<u>Web Based Resources</u>	<u>Academic Genealogy</u>	<u>A Chemist In Court</u>
<u>Introduction to Sonochemistry</u>	<u>Safety Resources</u>	<u>Press Clippings</u>	<u>Words of Humor and Wisdom</u>
<u>Proposal Excerpts</u>	<u>Group Equipment</u>	<u>How To Give A Seminar</u>	<u>Laws of the Universe</u>
<u>Funding</u>	<u>Past Group Members</u>	<u>Ch315 Inorganic Chemistry</u>	<u>Cartoons of Humor and Wisdom</u>
<u>Information for Visitors</u>	<u>Group Photogallery</u>	<u>Construction of the CLS Lab</u>	<u>Sculpture & Masks</u>

©2003, K.S. Suslick; all rights reserved.

Comments and suggestions: ksuslick@uiuc.edu

Sonoluminescence and Sonochemistry

Kenneth S. Suslick

Department of Chemistry, University of Illinois at Urbana-Champaign

600 S. Mathews Av., Urbana, IL 61801

- I. Introduction to Cavitation
- II. Sonoluminescence
- III. Sonochemistry
- IV. Summary
- V. Bibliography
- VI. Tables and Figures

Glossary

Cavitation The formation, growth, and collapse of gas and vapor filled bubbles in a liquid. Irradiation of liquids with sound or ultrasound can create acoustic cavitation; turbulent flow of liquids can create hydrodynamic cavitation.

Heterogeneous Sonochemistry The use of high intensity sound or ultrasound to alter chemical reactions in a two phase system, usually a liquid and a solid.

Homogeneous Sonochemistry The use of high intensity sound or ultrasound to alter chemical reactions in a single liquid.

Multi-Bubble Sonoluminescence (MBSL) Emission of light from a cloud of cavitating bubbles formed during ultrasonic irradiation of a liquid.

Single-Bubble Sonoluminescence (SBSL) Emission of light from a single cavitating bubble in a liquid, usually water.

Sonochemistry The use of high intensity sound or ultrasound to alter chemical reactions.

Sonoluminescence Emission of light during ultrasonic irradiation of liquids.

Surprisingly, when liquids are exposed to intense ultrasound, high-energy chemical reactions occur, often with accompanied by the emission of light. Acoustic cavitation is responsible for both sonochemistry and sonoluminescence. Bubble collapse in liquids results in an enormous concentration of energy from the conversion of the kinetic energy of liquid motion into heating of the contents of the bubble. The high local temperatures and pressures, combined with extraordinarily rapid cooling, provide a unique means for driving chemical reactions under extreme conditions. There are three classes of sonochemical reactions: so-called homogeneous sonochemistry of liquids, heterogeneous sonochemistry of liquid-liquid or liquid-solid systems, and sonocatalysis (which overlaps the first two). Sonoluminescence may generally be considered a special case of homogeneous sonochemistry. In some cases, ultrasonic irradiation can increase reactivity by nearly a million-fold. A diverse set of applications of ultrasound to enhance chemical reactivity has been explored, with important applications in mixed phase synthesis, materials chemistry, and biomedical uses. For example, the sonochemical decomposition of volatile organometallic precursors in low-volatility solvents produces nanostructured materials in various forms with high catalytic activities. Nanostructured metals, alloys, carbides and sulfides, nanometer colloids, and nanostructured supported-catalysts can all be prepared by this general route. Another important application of sonochemistry to materials chemistry has been the preparation of biomaterials, most notably protein microspheres. Especially for liquid-solid reactions, the rate enhancements that ultrasound can provide have proved extremely useful for the synthesis of organic and organometallic compounds. Because cavitation can only occur in liquids, chemical reactions are not generally seen in the ultrasonic irradiation of solids or solid-gas systems.

I. Introduction to Cavitation

When a liquid is irradiated with high intensity sound or ultrasound, acoustic cavitation (the formation, growth, and implosive collapse of bubbles in liquids irradiated with sound) generally occurs. This is the phenomena responsible for sonochemistry and sonoluminescence. During cavitation, the collapse of bubbles produces intense local heating and high pressures, with very short lifetimes. In clouds of cavitating bubbles, these hot-spots have equivalent temperatures of roughly 5000 K, pressures of about 1000 atmospheres, and heating and cooling rates above 10^{10} K/s. In single bubble cavitation, conditions may be even more extreme. Cavitation, then, can create extreme physical and chemical conditions in otherwise cold liquids.

If liquids containing solids are irradiated with ultrasound, related phenomena can occur. Near an extended solid surface, cavity collapse becomes non-spherical, which drives high-speed jets of liquid into the solid surface. These jets and associated shock waves can cause substantial surface damage and expose fresh, highly heated surfaces. In addition, high velocity inter-particle collisions will occur during ultrasonic irradiation of liquid-powder suspensions through cavitation and the shockwaves it creates in such slurries. The resultant collisions are capable of inducing dramatic changes in surface morphology, composition, and reactivity.

A. Acoustic Cavitation

Ultrasound spans the frequencies of roughly 15 kHz to 1 GHz. With typical sound velocities in liquids of ≈ 1500 m/s, acoustic wavelengths range from roughly 10 to 10^{-4} cm. These are not molecular dimensions. Consequently, the chemical effects of ultrasound do not arise from a direct interaction with molecular species: no direct coupling of the acoustic field on a molecular level is responsible for sonochemistry or sonoluminescence. Instead, sonochemistry and sonoluminescence derive principally from acoustic cavitation, which serves as an effective means of concentrating the diffuse energy of sound. Compression of a gas generates heat. When the compression of bubbles occurs during cavitation, it is more rapid than thermal transport and consequently generates a short-lived, localized hot-spot. There is a general consensus that this hot-spot is the source of homogeneous sonochemistry. In 1917, Rayleigh's mathematical model for the collapse of cavities in incompressible liquids predicted enormous local temperatures and pressures. Ten years later, Richards and Loomis reported the first chemical and biological effects of ultrasound.

If a moderately intense acoustic field (greater than ≈ 0.5 MPa) is applied to a liquid, the liquid can fail during the expansion (i.e., tensile or negative pressure) portion of the sound field; weak sites within the liquid (e.g., preexisting gas pockets, called "cavitation nuclei") are caused to rapidly grow, thereby producing vapor and gas-filled cavities (i.e., bubbles). These bubbles continue to grow during the negative pressure portion of the sound field, until the sound field pressure turns positive. The resulting inertial implosion of the bubbles (now mostly filled with vapor and thus unable to provide stiffness) can be extremely violent, leading to an enormous concentration of energy within the small residual volume of the collapsed bubble (Fig. 1). This violent cavitation event has been termed "transient cavitation." A normal consequence of this unstable growth and subsequent collapse is that the cavitation bubble

itself is destroyed. Gas-filled remnants from the collapse, however, may serve as nucleation sites for subsequent cycles.

For the generally accepted hot-spot theory, the potential energy of the bubble increases as it expands to maximum size, and this energy is then spatially and temporally concentrated into a heated gas core as the bubble implodes. The oscillations of a gas bubble driven by an acoustic field are generally described by "Rayleigh-Plesset" equation; one form of which, called the Gilmore equation, can be expressed a second-order nonlinear differential equation given as

$$R\left(1-\frac{U}{C}\right)\frac{d^2R}{dt^2}+\frac{3}{2}\left(1-\frac{U}{3C}\right)\left(\frac{dR}{dt}\right)^2-\left(1+\frac{U}{C}\right)H-\frac{R}{C}\left(1-\frac{U}{C}\right)\frac{dH}{dt}=0. \quad \text{eqn. 1}$$

The radius and velocity of the bubble wall are given by R and U respectively. The values for H, the enthalpy at the bubble wall, and C, the local sound speed, may be expressed as follows, using the Tait equation of state for the liquid.

$$H = \frac{n}{n-1} \frac{A^{1/n}}{\rho_o} \left[(P(R)+B)^{n-1/n} - (P_\infty(t)+B)^{n-1/n} \right] \quad \text{eqn. 2}$$

and
$$C = [c_o^2 + (n-1)H] \quad \text{eqn. 3}$$

The linear speed of sound in the liquid is c_o . A, B, and n are constants which should be set to the appropriate values (for water these values are A=3001 atm., B=A-1, and n=7). The term $P_\infty(t)$ is the pressure far from the bubble, and includes the ambient pressure plus an appropriate acoustic forcing function. The pressure at the bubble wall (assuming an ideal gas obeying the polytropic law) is given by

$$P(R) = \left(P_o + \frac{2\sigma}{R} \right) \left(\frac{R_o}{R} \right)^{3\gamma} - \frac{2\sigma}{R} - \frac{4\mu U}{R} \quad \text{eqn. 4}$$

where the initial radius of the bubble at time zero is R_o . The ambient pressure of the liquid is P_o , the surface tension σ , the shear viscosity μ , and the polytropic exponent γ .

The validity of the Gilmore equation to compute the behavior of a single, isolated cavitating bubble has been experimentally confirmed. For example, using a light scattering technique, various researchers have obtained measurements of the radius-time curve for single cavitating bubbles (Fig. 2), simultaneous with optical emission

from sonoluminescence (see below). The single-bubble sonoluminescent emission is seen as the sharp spike, appearing at the final stages of bubble collapse. Note that these emissions occur at the point of minimum bubble size, and that the general shape of the theoretical radius-time curve is reproduced.

B. Two-Site Model of Sonochemical Reactivity

Unfortunately, the complex environment that is present in a cavitation field, in which hundreds or thousands of cavitation bubbles interact during their transient cavitation behavior, precludes conventional measurement of the conditions generated during bubble collapse. Chemical reactions themselves, however, can be used to probe reaction conditions. The effective temperature realized by the collapse of clouds of cavitating bubbles can be determined by the use of competing unimolecular reactions whose rate dependencies on temperature have already been measured. This technique of "comparative-rate chemical thermometry" was used by Suslick, Hammerton, and Cline to first determine the effective temperature reached during cavity collapse. The sonochemical ligand substitutions of volatile metal carbonyls were used as these comparative rate probes. These kinetic studies revealed that there were in fact *two* sonochemical reaction sites: the first (and dominant site) is the bubble's interior gas-phase while the second is an *initially* liquid phase. The latter corresponds either to heating of a shell of liquid around the collapsing bubble or to droplets of liquid ejected into the hot-spot by surface wave distortions of the collapsing bubble, as shown schematically in Fig. 3.

In addition, for both sites an effective local temperatures was determined by combining the relative sonochemical reaction rates with the known temperature behavior of these reactions. The effective temperature of these hot-spots was measured at ≈ 5200 K in the gas-phase reaction zone and ≈ 1900 K in the initially liquid zone. Of course, the comparative rate data represent only a composite temperature: during the collapse, the temperature has a highly dynamic profile, as well as a spatial temperature gradient. This two-site model has been confirmed with other reactions and alternative measurements of local temperatures by multi-bubble sonoluminescence are consistent, as discussed later.

C. Microjet Formation during Cavitation at Liquid-Solid Interfaces

Very different phenomena occur for cavitation near extended liquid-solid interfaces. There are two mechanisms for the effects of cavitation near surfaces: microjet impact and shockwave damage. Whenever a cavitation bubble is

produced near a boundary, the asymmetry of the liquid particle motion during cavity collapse induces a deformation in the cavity. The potential energy of the expanded bubble is converted into kinetic energy of a liquid jet that extends through the bubble's interior and penetrates the opposite bubble wall. Because most of the available energy is transferred to the accelerating jet, rather than the bubble wall itself, this jet can reach velocities of hundreds of meters per second. Because of the induced asymmetry, the jet often impacts the local boundary and can deposit enormous energy densities at the site of impact, especially for larger bubbles (i.e., lower frequency). Fig. 4 shows a photograph of a jet developed in a collapsing cavity. The second mechanism of cavitation-induced surface damage invokes shockwaves created by cavity collapse in the liquid. The impingement of microjets and shockwaves on the surface creates the localized erosion responsible for ultrasonic cleaning and many of the sonochemical effects on heterogeneous reactions. The erosion of metals by cavitation generates newly exposed, highly heated surfaces. Such energy concentration can result in severe damage to the boundary surface; this is less true at higher (MHz) frequencies, simply because the cavitation bubbles are much smaller. This explains the increasing interest in high frequency ultrasonic cleaning for microelectronics (which has been given unfortunate marketing nom-de-guerre of "megasonics").

In order to induce substantial distortions during bubble collapse, the solid surface must be several times larger than the resonance bubble size: at ≈ 20 kHz, jet formation becomes important if the solid particles are larger than ≈ 200 μm . For smaller particles, the shockwaves created by homogeneous cavitation can create high velocity interparticle collisions, as discussed later

II. Sonoluminescence

A. Types of Sonoluminescence

Ultrasonic irradiation of liquids can also produce light, termed "sonoluminescence," as first observed from water in 1934 by Frenzel and Schultes. As with sonochemistry, sonoluminescence derives from acoustic cavitation. There are two classes of sonoluminescence: multiple-bubble sonoluminescence (MBSL) and single-bubble sonoluminescence (SBSL). Since cavitation is a nucleated process and liquids generally contain large numbers of particulates that serve as nuclei, the "cavitation field" generated by a propagating or standing acoustic wave typically consists of very large numbers of interacting bubbles, distributed over an extended region of the liquid. Such cavitation can be sufficiently intense to produce MBSL.

For rather specialized but easily obtainable conditions, it is now established that a single, stable gas bubble can be forced into such large amplitude pulsations that it produces sonoluminescence emissions on each (and every) acoustic cycle. This phenomenon is called single-bubble sonoluminescence (SBSL). Under the appropriate conditions, the acoustic force on a bubble can be used to balance against its buoyancy, holding the bubble stable in the liquid by acoustic levitation. This permits examination of the dynamic characteristics of a single cavitating bubble in considerable detail, from both a theoretical and an experimental perspective. Such a bubble is quite small, compared to an acoustic wavelength (e.g., at 20 kHz, the maximum bubble size before collapse is $\sim 50 \mu\text{m}$ and at minimum during collapse $< 1 \mu\text{m}$).

B. Multiple-Bubble Sonoluminescence

The sonoluminescence of aqueous solutions has been studied extensively over the past thirty years. The spectrum of MBSL in water consists of a peak at 310 nm and a broad continuum throughout the visible region. An intensive study of aqueous MBSL was conducted by Verrall and Sehgal and later by Didenko. The emission at 310 nm is from excited-state OH^\bullet , but the continuum is difficult to interpret. MBSL from aqueous and alcohol solutions of many metal salts have been reported and are characterized by emission from metal atom excited states.

Flint and Suslick reported the first MBSL spectra of organic liquids. With various hydrocarbons, the observed emission is from excited states of C_2 ($d^3\Pi_g - a^3\Pi_u$, the Swan lines), the same emission seen in flames. Furthermore, the ultrasonic irradiation of alkanes in the presence of N_2 (or NH_3 or amines) gives emission from CN excited states, but not from N_2 excited states. Emission from N_2 excited states would have been expected if the MBSL originated from microdischarge, whereas CN emission is typically observed from thermal sources. When oxygen is present, emission from excited states of CO_2 , CH^\bullet , and OH^\bullet is observed, again similar to flame emission.

Ultrasonic irradiation of volatile organometallics (such as $\text{Fe}(\text{CO})_5$ or $\text{Cr}(\text{CO})_6$) in a low volatility organic liquid produces intense sonoluminescence that corresponds to the known atomic emission lines of the metals, again analogous to flame emission. Hot spot temperatures are sufficient not only to dissociate all the CO ligands from the metal complex, but also to produce excited state metal atoms. Fig. 5 shows a typical MBSL spectrum from a metal carbonyl solution ($\text{Cr}(\text{CO})_6$ in this example). Note the intense line emission from the metal atom excited states as well as bands from excited states of the diatomics, C_2 and CH . This metal atom emission provides a useful spectroscopic thermometer, as described below.

For both aqueous and non-aqueous liquids, the emission spectra from MBSL suggests that the principal source of light emission is from chemical reactions involving high-energy species formed during cavitation by bubble collapse. MBSL is principally a form of chemiluminescence, just as flame emission is.

C. Single-Bubble Sonoluminescence

At the time of this writing, SBSL remains under active investigation with unsettled controversies. Theoretical interpretations of the experimental findings continue to be refined. It is not yet possible to provide a definitive mechanism for the light emission process, although the most favored model involves compressional heating (though probably without a convergent shockwave) of the bubble contents, similar to MBSL. The spectra of MBSL and SBSL, however, show some dramatic differences. While MBSL is generally dominated by atomic and molecular emission lines, SBSL is an essentially featureless emission that increases with decreasing wavelength. For example, an aqueous solution of NaCl shows evidence of excited states of both OH^\bullet and Na in the MBSL spectrum; however, the SBSL spectrum of an identical solution shows no evidence of either of these peaks. Nevertheless, the commonality of cause (acoustic cavitation) and effect (light emission) suggests some association in the underlying physics of sonoluminescence for both MBSL and SBSL.

Fig. 6 illustrates a typical experimental setup for generating SBSL. A piezoelectric, mounted to a water-filled acoustic levitation cell, is driven to set up a standing wave within the water. The drive frequency depends on the size and geometry of the levitation cell (which can be spherical, cylindrical, or even rectangular). The water is typically degassed to about 10% of saturation. A bubble is introduced by injecting air through a syringe into the water. The large bubbles rise to the surface, while the small bubbles are attracted to pressure antinodes. The final size of the remaining bubble at the antinode depends on gas diffusion steady state conditions and instabilities present: if the bubble is too small, gas will transport into the bubble; if the bubble is too large, small microbubbles will be ejected from the main bubble. In this manner, the final bubble comes into a diffusive steady state. Once the bubble is positioned at the pressure antinode, the drive pressure amplitude is increased until sonoluminescence is observed.

The radial motion of the bubble was illustrated in Fig. 2. During the main collapse of the bubble, the interior heats up and at the final stages of collapse, light is emitted. With SBSL, the light emission process may occur each and every acoustic cycle, with a synchronicity better than 1 part per billion; for instance, in a 20 kHz sound field (with a period of 50 μs), the light emission can have a jitter of less than 50 picoseconds.

One intriguing aspect of SBSL is the extremely short duration of the sonoluminescence flash. The measured pulse duration of the light flash has been shown to be below 200 ps, and possibly less than 50 ps in some cases. Due to the low levels of light output from a sonoluminescent bubble, one can not simply use picosecond-response photodiodes. More sophisticated experiments are required. In this case, time-correlated single photon counting is used to measure the pulse duration. Since the experiment measures the time difference between two photons occurring during the same flash, this measurement produces an autocorrelation of the pulse. Due to the complex and transient nature of cavitation fields, one can not employ such averaging techniques to MBSL. The most recent studies of MBSL have shown that for aqueous systems involving air and noble gases, the pulse width is also extremely short, less than 1 ns.

The most plausible explanation for the differences between MBSL and SBSL is simply the degree of compression and the extent of consequent local heating. In SBSL, the bubble collapse is much more spherical than is likely in the complex acoustics of a bubble cloud. As a consequence, the effective temperature reached in single bubble cavitation is probably sufficiently high to induce significant ionization and plasma formation. Under these circumstances, SBSL will be dominated by featureless bremsstrahlung emission, rather than bands from atomic or molecular emission as in MBSL.

In keeping with this hypothesis, Suslick and coworkers recently found a series of polar aprotic liquids that can support very strong SBSL, and for the first time, observed line emission from molecular excited states during SBSL. This provides a spectroscopic bridge between SBSL and MBSL and gives direct proof of the existence of chemical reactions and the formation of molecular excited states during single bubble cavitation. In these liquids, both stationary and moving single bubbles could be created. As the sphericity of bubble collapse increases (from MBSL to moving bubble SBSL to stationary bubble SBSL), the efficacy of compression increases, the effective temperatures within the bubble increase, and the emission changes from spectra dominated by excited state molecular emission to featureless (Bremsstrahlung-like) spectra (Fig. 7).

Another major difference between SBSL and MBSL may lie in the contents of the cavitating bubbles. For MBSL, it is generally accepted that a particular bubble in the cavitation field only lasts for a few acoustic cycles before being destroyed, and therefore its contents represent the equilibrium vapor pressures of the solution and its dissolved gases. In contrast, in SBSL, a single bubble can remain stable, emitting light for hours. For air bubbles in water, it is now generally assumed that nitrogen and oxygen molecules dissociate because of the high temperatures, forming NO_x compounds that dissolve in the surrounding water, leaving behind only the non-reactive argon inside

the bubble. Thus, even though argon represents only a small fraction of the air concentration dissolved in water, the SBSL bubble acts as a chemical reaction chamber that rectifies argon over thousands of acoustic cycles, until the bubble contents are mostly rarefied argon.

D. Spectroscopic Probes of Cavitation Conditions

Determination of the temperatures reached in cavitating bubbles has remained a difficult experimental problem. As a spectroscopic probe of the cavitation event, MBSL provides a solution. High resolution MBSL spectra from silicone oil under Ar have been reported and analyzed. The observed emission comes from excited states of diatomic carbon (C_2) and has been modeled with synthetic spectra as a function of rotational and vibrational temperatures. From comparison of synthetic to observed spectra, the effective cavitation temperature is 5050 ± 150 K. The excellence of the match between the observed MBSL and the synthetic spectra provides definitive proof that the sonoluminescence event is a thermal, chemiluminescence process. The agreement between this spectroscopic determination of the cavitation temperature and that made by comparative rate thermometry of sonochemical reactions is surprisingly close.

A second spectroscopic thermometer comes from the relative intensities of atomic emission lines in the sonoluminescence spectra of excited state metal atoms produced by sonolysis of volatile Fe, Cr, and Mo carbonyls. Sufficient spectral information about emissivities of many metal atom excited states are available to readily calculate emission spectra as a function of temperature. Because of this, the emission spectra of metal atoms are extensively used by astronomers to monitor the surface temperature of stars. From comparison of calculated spectra and the observed MBSL spectra from metal carbonyls, another measurement of the cavitation temperature can be obtained. The effective emission temperature during cavitation under argon at 20 kHz is 4900 ± 250 K, as shown in the example given in Fig. 8. Again, agreement with prior comparative rate thermometry and the MBSL emission temperature of C_2^* excited states is excellent.

One may also be able to control the temperature within the cavitation bubble simply by changing the bubble contents. Upon addition of gaseous hydrocarbons (methane, ethylene, or propane), the observed emission temperatures from Cr atom excited states systematically decrease: just 3% propane in Ar, for example, reduces the measured emission temperature to 2500 K. As polyatomic molecules are added to the bubble contents, the polytropic ratio of the gas in the bubble decreases, and so too does the expected temperature from adiabatic

compression. The presence of the polyatomic gas simply provides vibrational and rotational modes that will divert much of the kinetic energy of collapse away from a direct temperature increase. The effects of the addition of polyatomic gases on the observed cavitation emission temperature can be quantitatively modeled by simple adiabatic compression of a bubble during cavitation collapse. This simple model predicts pressures on the order of 10^3 Bar, which is quantitatively consistent with the linewidth broadening and small peak wavelength shifts observed in the metal atom emission. The lifetime of the hot spot is less well determined. Certainly it is under a microsecond and may be considerably less, given the 200 ps emission lifetimes seen in SBSL. The cooling rates, even at μ s lifetimes, are enormous: above 10^{10} K/s.

The interpretation of the spectroscopy of SBSL in water is much less clear. At this writing, SBSL has been observed primarily in aqueous fluids, and the spectra obtained are surprisingly featureless. Some very interesting effects are observed when the gas contents of the bubble are changed. Furthermore, the spectra show practically no evidence of OH emissions, and when He and Ar bubbles are considered, continue to increase in intensity even into the deep ultraviolet. These spectra are reminiscent of black body or bremsstrahlung emission with temperatures in excess of 10^4 K. Several other alternative explanations for SBSL have been presented, and there exists considerable theoretical activity in this particular aspect of SBSL.

II. Sonochemistry

In a fundamental sense, chemistry is the interaction of energy and matter. Chemical reactions require energy in one form or another to proceed: chemistry stops as the temperature approaches absolute zero. One has only limited control, however, over the nature of this interaction. In large part, the properties of a specific energy source determines the course of a chemical reaction. Ultrasonic irradiation differs from traditional energy sources (such as heat, light, or ionizing radiation) in duration, pressure, and energy per molecule. The immense local temperatures and pressures and the extraordinary heating and cooling rates generated by cavitation bubble collapse mean that ultrasound provides an unusual mechanism for generating high energy chemistry. Like photochemistry, very large amounts of energy are introduced in a short period of time, but it is thermal, not electronic, excitation. As in flash pyrolysis, high thermal temperatures are reached, but the duration is very much shorter (by $>10^4$) and the temperatures are even higher (by five- to ten-fold). Similar to shock-tube chemistry or multiphoton infrared laser

photolysis, cavitation heating is very short lived, but occurs within condensed phases. Furthermore, sonochemistry has a high-pressure component, which suggests that one might be able to produce on a microscopic scale the same macroscopic conditions of high temperature-pressure "bomb" reactions or explosive shockwave synthesis in solids. Fig. 9 presents an interesting comparison of the parameters that control chemical reactivity (time, pressure, and energy) for various forms of chemistry.

The same limitations apply to the control of sonochemical reactions as in any thermal process: the Boltzmann energy distribution means that the energy per individual molecule will vary widely. One does have easy control, however, over the intensity of heating generated by acoustic cavitation using various physical parameters. The origin of these influences is easily understood in terms of the hot-spot mechanism of sonochemistry. The most important parameters are thermal conductivity of dissolved gases (which can effect the degree of adiabaticity), polyatomic content inside the bubble (which reduces compressional heating), and acoustic pressure. As acoustic pressure is increased, there is a threshold value for nucleation and bubble growth and hence sonochemistry, followed by an increase in sonochemical rates due to increased numbers of effectively cavitating bubbles. At sufficiently high intensities, the cavitation of the liquid near the radiating surface becomes so intense as to produce a shroud of bubbles, diminishing penetration of sound into the liquid and decreasing sonochemical rates. In contrast, frequency appears to be less important, at least within the range where cavitation can occur (a few hertz to a few megahertz), although there have been few detailed studies of its role.

Homogeneous sonochemistry typically is not a very energy efficient process, whereas heterogeneous sonochemistry is several orders of magnitude better. Since ultrasound can be produced with nearly perfect efficiency from electric power, the primary energy inefficiency is due to the small fraction of the acoustic power actually involved in the cavitation events. This might be significantly improved, however, if a more efficient means of coupling the sound field to generate cavitation can be found.

A. Experimental Design

A variety of devices have been used for ultrasonic irradiation of solutions. There are three general designs in use presently: the ultrasonic cleaning bath, the direct immersion ultrasonic horn, and flow reactors. The originating source of the ultrasound is generally a piezoelectric material, usually a lead zirconate titanate ceramic (PZT), which is subjected to a high AC voltage with an ultrasonic frequency (typically 15 to 50 kHz). For industrial use, the more robust magnetostrictive metal alloys (usually of Ni) can be used as the core of a solenoid generating an alternating

magnetic field with an ultrasonic frequency. The vibrating source is attached to the wall of a cleaning bath, to an amplifying horn, or to the outer surfaces of a flow-through tube or diaphragm.

The ultrasonic cleaning bath is clearly the most accessible source of laboratory ultrasound and has been used successfully for a variety of liquid-solid heterogeneous sonochemical studies. The low intensity available in these devices ($\approx 1 \text{ W/cm}^2$), however, means that even in the case of heterogeneous sonochemistry, an ultrasonic cleaning bath must be viewed as an apparatus of limited capability. The most intense and reliable source of ultrasound generally used in the chemical laboratory is the direct immersion ultrasonic horn (50 to 500 W/cm^2), as shown in Fig. 10, which can be used for work under either inert or reactive atmospheres or at moderate pressures (< 10 atmospheres). These devices are available from several manufacturers at modest cost. Commercially available flow-through reaction chambers that will attach to these horns allow the processing of multi-liter volumes. The acoustic intensities are easily and reproducibly variable; the acoustic frequency is well controlled, albeit fixed (typically at 20 kHz). Since power levels are quite high, counter-cooling of the reaction solution is essential to provide temperature control. Large-scale ultrasonic generation in flow-trough configurations is a well-established technology. Liquid processing rates of 200 L/min are routinely accessible from a variety of modular, in-line designs with acoustic power of $\approx 20 \text{ kW}$ per unit. The industrial uses of these units include 1) degassing of liquids, 2) dispersion of solids into liquids, 3) emulsification of immiscible liquids and 4) large-scale cell disruption.

B. Homogeneous Sonochemistry: Bond Breaking and Radical Formation

The chemical effect of ultrasound on aqueous solutions have been studied for many years. The primary products are H_2 and H_2O_2 ; there is strong evidence for various high-energy intermediates, including HO_2 , H^\bullet , OH^\bullet , and perhaps $e^-_{(\text{aq})}$. The work of Riesz and collaborators used electron paramagnetic resonance with chemical spin-traps to demonstrate definitively the generation of H^\bullet and OH^\bullet during ultrasonic irradiation, even with clinical sources of ultrasound. The extensive work in Henglein's laboratory involving aqueous sonochemistry of dissolved gases has established clear analogies to combustion processes. As one would expect, the sonolysis of water, which produces both strong reductants and oxidants, is capable of causing secondary oxidation and reduction reactions, as often observed. Most recently there has been strong interest shown in the use of ultrasound for remediation of low levels of organic contamination of water. The OH^\bullet radicals produced from the sonolysis of water are able to attack essentially all organic compounds (including halocarbons, pesticides, and nitroaromatics) and through a series of

reactions oxidize them fully. The desirability of sonolysis for such remediation lies in its low maintenance requirements and the low energy efficiency of alternative methods (e.g., ozonolysis, UV photolysis).

In contrast, the ultrasonic irradiation of organic liquids has been less studied. Suslick and coworkers established that virtually all organic liquids will generate free radicals upon ultrasonic irradiation, as long as the total vapor pressure is low enough to allow effective bubble collapse. The sonolysis of simple hydrocarbons (for example, n-alkanes) creates the same kinds of products associated with very high temperature pyrolysis. Most of these products (H_2 , CH_4 , and the smaller 1-alkenes) derive from a well-understood radical chain mechanism.

The sonochemistry of solutes dissolved in organic liquids also remains largely unexplored. The sonochemistry of metal carbonyl compounds is an exception. Detailed studies of these systems led to important mechanistic understandings of the nature of sonochemistry. A variety of unusual reactivity patterns have been observed during ultrasonic irradiation, including multiple ligand dissociation, novel metal cluster formation, and the initiation of homogeneous catalysis at low ambient temperature.

C. Applications of Sonochemistry to Materials Synthesis and Catalysis

Of special interest is the recent development of sonochemistry as a synthetic tool for the creation of unusual inorganic materials. As one example, the recent discovery of a simple sonochemical synthesis of amorphous iron helped settle the longstanding controversy over its magnetic properties. More generally, ultrasound has proved extremely useful in the synthesis of a wide range of nanostructured materials, including high surface area transition metals, alloys, carbides, oxides and colloids. Sonochemical decomposition of volatile organometallic precursors in high boiling solvents produces nanostructured materials in various forms with high catalytic activities. Nanometer colloids, nanoporous high surface area aggregates, and nanostructured oxide supported catalysts can all be prepared by this general route, as shown schematically in Fig. 11. There remains much to explore in the sonochemical synthesis of inorganic materials, and this technique has only begun to be exploited.

Heterogeneous catalysis is extremely important in the chemical and petroleum industries, and the applications of ultrasound to catalysis have been reviewed recently. The effects of ultrasound on catalysis can occur in three distinct stages: (i) during the formation of supported catalysts, (ii) activation of pre-formed catalysts, or (iii) enhancement of catalytic behavior during a catalytic reaction. In the cases of modest rate increases, it appears likely that the cause is increased effective surface area; this is especially important in the case of catalysts supported on

brittle solids. More impressive accelerations, however, have included hydrogenations and hydrosilations by Ni powder, Raney Ni, and Pd or Pt on carbon. For example, the hydrogenation of alkenes by Ni powder is enormously enhanced ($>10^5$ -fold) by ultrasonic irradiation. As discussed in the next section, this dramatic increase in catalytic activity is due to the formation of uncontaminated metal surfaces from interparticle collisions caused by cavitation-induced shockwaves.

Heterogeneous catalysts often require rare and expensive metals. The use of ultrasound offers some hope of activating less reactive, but also less costly, metals. As one example, ultrasonic irradiation of solutions of $\text{Mo}(\text{CO})_6$ produces aggregates of nanometer-sized clusters of face centered cubic molybdenum carbide. The material was extremely porous with a high surface area and consisted of aggregates of ≈ 2 nm sized particles. The catalytic properties showed the molybdenum carbide generated by ultrasound is an active and highly selective dehydrogenation catalyst comparable to commercial ultrafine platinum powder.

The sonochemical synthesis of nanostructured molybdenum sulfide provides another example of the utility of sonochemistry to the production of active catalysts. MoS_2 is best known as a standard automotive lubricant; its lubricant properties are due to its layered structure. Planes of molybdenum atoms are sandwiched on both faces by planes of sulfur atoms tightly bonded to the Mo. Interactions between the sulfur planes are weak, thus producing lubrication properties similar to graphite. Of greater interest here, however, MoS_2 is also the predominant hydrodesulfurization catalyst heavily used by the petroleum industry to remove sulfur from fossil fuels before combustion. Sonochemistry provides an unusual morphology of MoS_2 by the irradiation of solutions of molybdenum hexacarbonyl, as shown in Fig. 12. Conventional MoS_2 shows a plate-like morphology typical for such layered materials. The sonochemical MoS_2 exists as a porous agglomeration of clusters of spherical particles with an average diameter of 15 nm. Despite the morphological difference between the sonochemical and conventional MoS_2 , TEM images of both sulfides show lattice fringes with interlayer spacings of 0.62 ± 0.01 nm. The sonochemically prepared MoS_2 , however, shows much greater edge and defect content, as the layers must bend, break or otherwise distort to form the outer surface of the 15 nm particle size. It is well established that the activity of MoS_2 is localized at the edges and not on the flat basal planes. Given the inherently higher edge concentrations in nanostructured materials, the catalytic properties of sonochemically prepared shows substantially increased activity for hydrodesulfurization, comparable to those observed with RuS_2 , one of the best prior catalysts.

Sonochemistry is also proving to have important applications with polymeric materials. Substantial work has been accomplished in the sonochemical initiation of polymerization and in the modification of polymers after

synthesis. The use of sonolysis to create radicals which function as radical initiators has been well explored. Similarly the use of sonochemically prepared radicals and other reactive species to modify the surface properties of polymers is being developed, particularly by G. Price. Other effects of ultrasound on long chain polymers tend to be mechanical cleavage, which produces relatively uniform size distributions of shorter chain lengths.

Another important application has been the sonochemical preparation of biomaterials, most notably protein microspheres. Using high intensity ultrasound and simple protein solutions, a remarkably easy method to make both air-filled microbubbles and nonaqueous liquid-filled microcapsules has been developed. As shown in Fig. 13, These protein microspheres have a wide range of biomedical applications, including their use as echo contrast agents for sonography, magnetic resonance imaging contrast enhancement, drug delivery, among others, and have generated a substantial patent estate. The microspheres are stable for months, and being slightly smaller than erythrocytes, can be intravenously injected to pass unimpeded through the circulatory system. The mechanism responsible for microsphere formation is a combination of *two* acoustic phenomena: emulsification and cavitation. Ultrasonic emulsification creates the microscopic dispersion of the protein solution necessary to form the proteinaceous microspheres. The long life of these microspheres comes from a sonochemical cross-linking of the protein shell. Protein cysteine residues are oxidized during microsphere formation by sonochemically produced superoxide.

D. Heterogeneous Sonochemistry: Reactions of Solids with Liquids

The use of ultrasound to accelerate chemical reactions in heterogeneous systems has become increasingly widespread. The physical phenomena that are responsible include the creation of emulsions at liquid-liquid interfaces, the generation of cavitation erosion and cleaning at liquid-solid interfaces, the production of shock wave damage and deformation of solid surfaces, the enhancement in surface area from fragmentation of friable solids, and the improvement of mass transport from turbulent mixing and acoustic streaming.

. Suslick and coworkers have found that the turbulent flow and shockwaves produced by intense ultrasound can drive metal particles together at sufficiently high speeds to induce effective melting in direct collisions (Fig. 14) and the abrasion of surface crystallites in glancing impacts (Fig. 15). A series of transition metal powders were used to probe the maximum temperatures and speeds reached during interparticle collisions. Using the irradiation of Cr, Mo, and W powders in decane at 20 kHz and 50 W/cm², agglomeration and essentially a localized melting occurs for the first two metals, but not the third. On the basis of the melting points of these metals, the effective transient

temperature reached at the point of impact during interparticle collisions is roughly 3000°C (which is unrelated to the temperature inside the hot-spot of a collapsing bubble). From the volume of the melted region of impact, the amount of energy generated during collision was determined. From this, a lower estimate of the velocity of impact is roughly one half the speed of sound, in agreement with expected particle velocities from cavitation-induced shockwaves in the liquid.

To enhance the reactivity of reactive metals as stoichiometric reagents, ultrasonic irradiation has become an especially routine synthetic technique for many heterogeneous organic and organometallic reactions particularly those involving reactive metals, such as Mg, Li or Zn. This development originated from the early work of Renaud and the more recent breakthroughs of Luche and others. Examples are shown in equations 5 through 7, where R represents an organic functional group and))) represents ultrasonic irradiation. The effects are quite general and apply to reactive inorganic salts and to main group reagents as well. Less work has been done with unreactive metals (e.g., V, Nb, Mo, W), but results here are promising as well. Rate enhancements of more than tenfold are common, yields are often substantially improved, and byproducts avoided.



The mechanism of the sonochemical rate enhancements in both stoichiometric and catalytic reactions of metals is associated with dramatic changes in morphology of both large extended surfaces and of powders. As discussed earlier, these changes originate from microjet impact on large surfaces and high-velocity interparticle collisions in slurries. Surface composition studies by Auger electron spectroscopy and sputtered neutral mass spectrometry reveal that ultrasonic irradiation effectively removes surface oxide and other contaminating coatings. The removal of such passivating coatings can dramatically improve reaction rates. The reactivity of clean metal surfaces also appears to be responsible for the greater tendency for heterogeneous sonochemical reactions to involve single electron transfer rather than acid-base chemistry.

Applications of ultrasound to electrochemistry have also seen substantial recent progress. Beneficial effects of ultrasound on electroplating and on organic synthetic applications of organic electrochemistry have been known for quite some time. More recent studies have focused on the underlying physical theory of enhanced mass transport near electrode surfaces. Another important application for sonoelectrochemistry has been developed by J. Reisse and coworkers for the electroreductive synthesis of sub-micrometer powders of transition metals.

III. Summary

The phenomenon of acoustic cavitation results in an enormous concentration of energy. The enormous local temperatures and pressures so created result in both sonochemistry and sonoluminescence, which provide a unique means for fundamental studies of chemistry and physics under extreme conditions. The chemical consequences of acoustic cavitation are far reaching, both in homogeneous liquids and in mixed-phase systems. In the latter, cavitation can have dramatic effects on the reactivities of both extended solid surfaces and on fine powder slurries through microjet and shock wave impact (on large surfaces) and interparticle collisions (with powders). The applications of sonochemistry are diverse and still emerging, especially in the areas of mixed phase synthesis, materials chemistry, and biomedical products.

Bibliography

Cheeke, J. D. N. (1997) *Can. J. Phys.* **75**, 77-96.

Crum, L. A. (1994) *Physics Today*, **47**, 22,.

Crum, L. A., Mason, T. J., Reisse, J., Suslick, K. S., eds. (1999) *Sonochemistry and Sonoluminescence*.

Kluwer Publishers: Dordrecht, Netherlands, NATO ASI Series C, v. 524.

Leighton, T.G. *The Acoustic Bubble* Academic Press: London, 1994.

Luche, J.-L., Bianchi, C. *Synthetic Organic Chemistry* (1998). Kluwer Publishers: Dordrecht, Netherlands.

Mason, T. J. ed. *Advances in Sonochemistry*, vols. 1-5. JAI Press: New York, 1990, 1991, 1993, 1996, 1999.

Putterman, S. J., Weninger, K.R. (2000) Sonoluminescence: How bubbles turn sound into light. *Annual Review of Fluid Mechanics*. **32**, 445-476.

Suslick, K. S., Crum, L. A. (1997) "Sonochemistry and Sonoluminescence" in *Encyclopedia of Acoustics*.

Crocker, M. J., ed., Wiley-Interscience: New York, vol. 1, ch. 26, pp. 271-282.

Suslick, K. S. (1997) "Sonocatalysis" in *Handbook of Heterogeneous Catalysis*. Ertl, G., Knozinger, H., Weitkamp, J., eds., Wiley-VCH: Weinheim, vol. 3, ch. 8.6, pp. 1350-1357.

Suslick, K. S. (1998) "Sonochemistry" in *Kirk-Othmer Encyclopedia of Chemical Technology*, 4th Ed.

J. Wiley & Sons: New York, vol. 26, 517-541.

Suslick, K. S., Didenko, Y., Fang, M. M., Hyeon, T., Kolbeck, K. J., McNamara III, W. B.,

Mdleleni, M. M., Wong, M. (1999) "Acoustic Cavitation and Its Chemical Consequences"

Phil. Trans. Roy. Soc. London A, **357**, 335-353.

Suslick, K. S., Price, G. (1999) "Applications of Ultrasound to Materials Chemistry" *Annu. Rev. Mat. Sci.* **29**, 295-326.

Figure Legends

Fig. 1. Transient acoustic cavitation: the origin of sonochemistry and sonoluminescence.

Fig. 2. Radius-time curves for single cavitating bubbles. A laser is used as a light source to scatter light off the bubble. The scattered light is collected with a lens and focused onto a photomultiplier tube (PMT). The intensity of the scattered light gives the bubble radius, using Mie scattering theory. The collected scattered light is fit to the Gilmore equation, in this case for $R_0 = 5.25 \mu\text{m}$, $P_a = 1.40 \text{ atm}$, and $R_{\text{max}} = 35 \mu\text{m}$, $f = 33.8 \text{ kHz}$. Reproduced with permission.

Fig. 3. Two-site models of the sonochemical reactions sites. Reproduced with permission.

Fig. 4. Photograph of liquid jet produced during collapse of a cavitation bubble near a solid surface. The width of the bubble is about 1 mm. Reproduced with permission.

Fig. 5. Typical MBSL spectrum from a metal carbonyl solution in silicone oil.

Fig. 6. A single-bubble sonoluminescence apparatus. A piezoelectric transducer (PZT), mounted to a water-filled levitation cell, is driven by a frequency generator/power amplifier combination. The frequency generator drives the PZT at the appropriate frequency to generate a standing acoustic wave profile within the levitation cell. For experiments to measure the pulse duration from single-bubble sonoluminescence, a time-correlated single photon counting method works so long as the bubble remains stable and light emission occurs in a synchronous fashion.

Fig. 7. Moving, single bubble sonoluminescence spectra of adiponitrile. Acoustic pressure increases from bottom to top from 1.7 B to 1.9 B. The excited state CN comes from the liquid vapor rather than from the nitrogen gas initially present inside the bubble. Reproduced with permission.

Fig. 8. . Sonoluminescence of excited state Fe atoms produced during sonolysis of $\text{Fe}(\text{CO})_5$ dissolved in silicone oil under Ar compared to the calculated spectrum. The emission temperature observed from MBSL from excited state Fe, Cr, and Mo atoms is 4900 ± 250 K. Reproduced with permission.

Fig. 9. Chemistry: the interaction of energy and matter. Reproduced with permission.

Fig. 10. A typical sonochemical apparatus with direct immersion ultrasonic horn. Ultrasound can be easily introduced into a chemical reaction with good control of temperature and ambient atmosphere. The usual piezoelectric ceramic is PZT, a lead zirconate titanate ceramic.

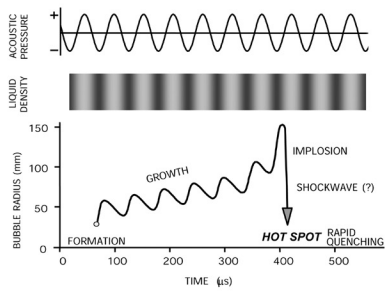
Fig. 11. Sonochemical synthesis of various forms of nanostructured materials. Reproduced with permission.

Fig. 12. Morphology of conventional and sonochemically prepared MoS_2 . Reproduced with permission.

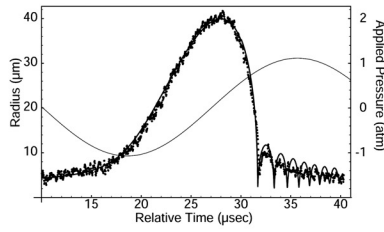
Fig. 13. Scanning electron micrograph of sonochemically prepared protein microspheres made from hemoglobin. Reproduced with permission.

Fig. 14. Scanning electron micrograph of 5 μm diameter Zn powder after ultrasonic irradiation of a slurry. Neck formation from localized melting is caused by high-velocity interparticle collisions. Similar micrographs and elemental composition maps (by Auger electron spectroscopy) of mixed metal collisions have also been made. Reproduced with permission.

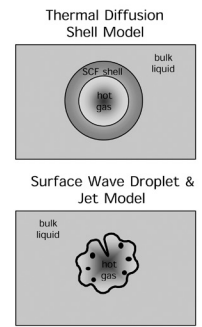
Fig. 15. The effect of ultrasonic irradiation on the surface morphology and particle size of Ni powder. Initial particle diameters before ultrasound were ≈ 160 μm ; after ultrasound, ≈ 80 μm . High-velocity interparticle collisions caused by ultrasonic irradiation of slurries are responsible for the smoothing and removal of passivating oxide coating. Reproduced with permission.



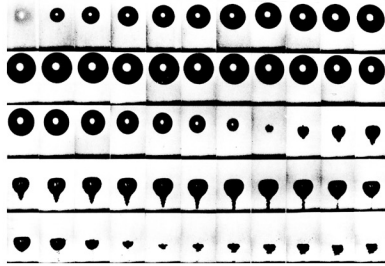
suslick.fig01.eps



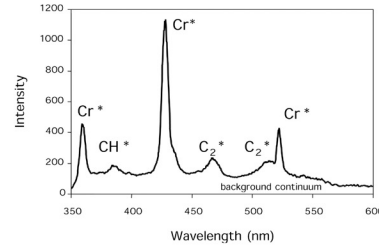
suslick.fig02.eps



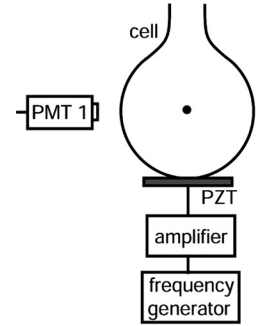
suslick.fig03.eps



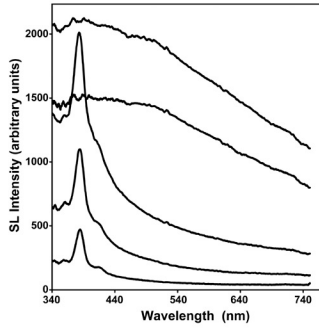
suslick.fig04.tif



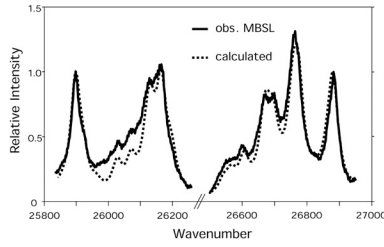
suslick.fig05.eps



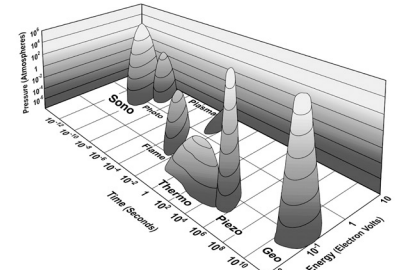
suslick.fig06.eps



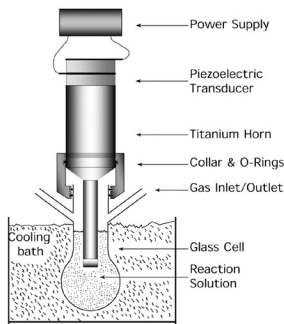
suslick.fig07.eps



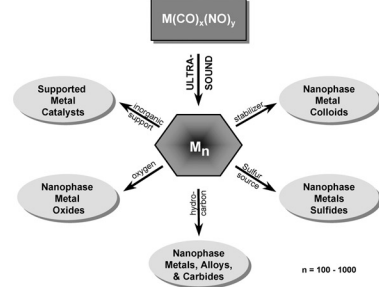
suslick.fig08.eps



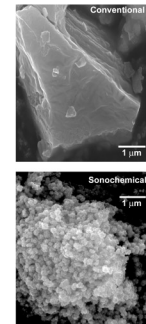
suslick.fig09.tif



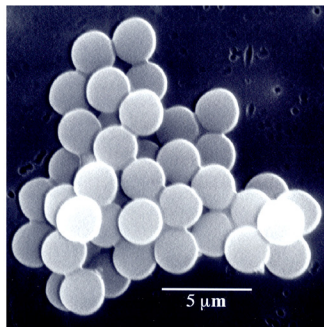
suslick.fig10.tif



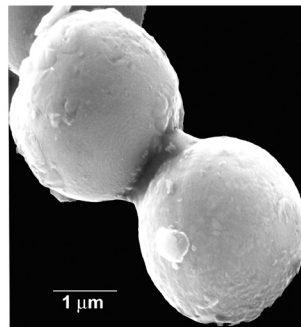
suslick.fig11.eps



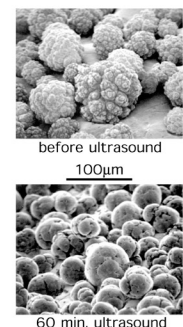
suslick.fig12.tif



suslick.fig13.tif

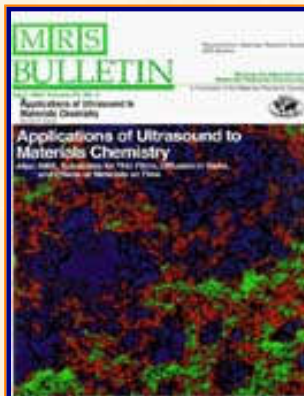


suslick.fig14.tif



suslick.fig15.jpg

The Suslick Research Group



PRESS CLIPPINGS OF THE SUSLICK RESEARCH GROUP

"Publicity is good.
Good publicity is better."
-- P.T. Barnum

Highlighted articles below are either in HTML or downloadable in PDF format.
To get the free Adobe PDF reader, click on this text.

Caution: Some pdf files are as large as 1 MB.

- **Wang, J.; Luthey-Schulten, Z.; Suslick, K. S. "Is the Olfactory Receptor A Metalloprotein?" *Proc. Natl. Acad. Sci. U.S.A.*, 2003, 100, 3035-3039.**

Chemical & Engineering News, Mar. 3, 2003.

"The Right Snuff," *St. Louis Post-Dispatch*, (Front Page!) Feb. 25, 2003.

Champaign News Gazette, p. 2, Mar. 2, 2003.

"Heavy Metals Play Crucial Role in the Ability to Smell" *Orlando Sentinel*, Mar. 2, 2003.

"Metals Attract Strong, Bad Odors" *Baltimore Sun*, Mar. 3, 2003.

"Raising A Stink" *San Diego Union Tribune*, Mar. 12, 2003.

"Metals Ions May Play Big Role In How We Sense Smells" *Science Daily*, Mar. 3, 2003.

[Overview](#)

[Outline of
Research Projects](#)

[Introduction to
Sonochemistry](#)

[Exec. Summary:
Sonochemistry](#)

[Exec. Summary:
Porphyrin Research](#)

[Exec. Summary: Smell-
Seeing](#)

[Complete
Publication List](#)

[Abbreviated Curriculum
Vitae](#)

[Academic
Genealogy](#)

[Press
Clippings](#)

[Current Research Funding](#)

[Excerpts from Funded Research](#)

[Inventory of Group Equipment](#)

[Information for Visiting](#)

[Current Research Group Members](#)

[Group Meetings](#)

[Group Chores](#)

[Past Research Group Members](#)

[Group Photogallery](#)

[Web Resources](#)

[Laboratory Safety Resources](#)

[Art and Science: Journal Covers](#)

[Sculpture & Masks](#)

[A Chemist Meets Hollywood](#)

[Chymistes: The Distillers of Waters](#)

[A Chemist In Court](#)

["The Nose of the Matter" *Food Navigator*, Mar. 2, 2003.](#)

["The Right Snuff," *STL Today* Feb. 24, 2003.](#)

["Dead Nose," *Die Zeit Wissen* Mar. 1, 2003. /b>](#)

- **"Chemistry Highlights of 2002," *Chemical & Engineering News***

["Chemical & Engineering News," Chemistry Highlights of 2002: Physical Chemistry" Dec. 16, 2002.](#)

["Chemical & Engineering News," Chemistry Highlights of 2002: Supramolecular Chemistry" Dec. 16, 2002.](#)

- **National Science Foundation**

[National Science Foundation Summary of 2004 Budget Request to Congress \(see p. 4\)](#)

[National Science Foundation: Highlights from 2002](#)

- **Rosenblatt, M.M.; Huffman, D.L.; Wang, X. Remmer, H.A.; Suslick, K. S. "Cyclic and Hairpin Peptide Complexes of Heme" *J. Am. Chem. Soc.* 2002, 12412394.**

["Chemists Create Synthetic Cytochrome" *Science Daily*, 08 Oct. 2002.](#)

- **Kosal, M. E.; Chou, J.-H.; Wilson, S. R.; Suslick, K. S. "A Functional Zeolite Analogue Assembled From Metalloporphyrins" *Nature Materials*, 2002, 1, 118-121.**

[Humor and
Wisdom](#)

[Laws of the Universe](#)

[Cartoons of Humor and
Wisdom](#)

[Chem 115: Chemistry of
Everyday Phenomena](#)

[Chem 315: Inorganic
Chemistry](#)

["Molecular Separations: New artificial sieve traps molecules" *Science News*,
05 Oct 2002](#)

["Ein Sieb zum Wasserfangen" *Wissenschaft* 25 Sept 2002.](#)

- **Didenko, Y.; Suslick, K. S. "The Energy Efficiency of Formation of Photons, Radicals, and Ions During Single Bubble Cavitation" *Nature* 2002, 418, 394-397.**

[News & Views Commentary,"Inside a Microreactor",*Nature* 2002, 418, 382-383.](#)

["Sonoluminescence: Bubble Power" *Nature* 2002, 418.](#)

["Single Bubble Microreactors" *Chemical & Engineering News*, July 29, 2002.](#)

["Chemistry Casts Doubt on Bubble Reactions" *Science*, News of the Week;
July 29, 2002.](#)

["Fusion Experiment Disappoints" *BBC News*, 25 July 2002.](#)

["Bubble bursts for bench-top nuclear fusion" *New Scientist*, 24 July 2002.](#)

["Researchers Probe Chemistry of Bubbles" *Photonics Technology*, Sept. 2002.](#)

["UI Report Casts Doubt on Bubble Fusion" *Chicago Tribune*, 25 July 2002](#)

["Bubble Fusion More Difficult to Produce" *UPI*, July 24, 2002.](#)

["Bubble bursts for 'sono-fusion'" *Physics Web*, July 24, 2002.](#)

["New Bubble Reaction Findings Make Fusion Claims Unlikely" *Scientific
American*, July 25, 2002.](#)

["Violent chemistry saps sonobubble energy" *Science News*, August 24, 2002.](#)

["Scientists measure energy dissipation in a single cavitating bubble" *Inside
Illinois*, August 2002.](#)

["Chemistry Casts Doubt on Bubble Fusion" *Daily InSCIght*, July 24, 2002](#)

- **Zimmerman, S. C.; Wendland, M. S.; Rakow, N. A.; Zharov, I.; Suslick, K. S. "Synthetic Hosts by Monomolecular Imprinting Inside Dendrimers"**

[Nature 2002, 418, 399-403.](#)

[News & Views Commentary, "Much Binding in the Lab", Nature 2002, 418, 375-376.](#)

["Building a Better Binding Site" Chemical & Engineering News, July 29, 2002.](#)

["Creating a Good Impression," News & Views Commentary, Nature Biotechnology 2002, 20\(9\), 884-885](#)

["UI researchers sculpt molecules" News Gazette, July 28, 2002.](#)

["Mimicking the Best of Nature's Binders" Science News, July 27, 2002.](#)

[Faculty of 1000 Commentary](#)

- **Rakow, N. A.; Suslick, K. S. "A Colorimetric Sensor Array for Odour Visualization" [Nature, 2000, 406, 710-714.](#)**

[News & Views Commentary, 17 Aug 00,](#)

["Picture the Smell", Nature 2000, 406, 682-683](#)

[CBS Evening News \(WCIA, Champaign, IL\), 8/16/00;
3 min. video clip in RealPlayer format \(3.7 MB\).](#)

[To download the free RealPlayer Basic viewer, click here.](#)

[CNBC, 8/17/00:](#)

["What's That Smell? Get a Good Look."](#)

[ABC News in Science 21/08/00:](#)

["Artificial nose sees smell"](#)

[CBC News \(Canadian Broadcasting Corp.\), 8/21/00:](#)

["Fake nose actually smells"](#)

[Chemical & Engineering News, 08/21/00:](#)

["NEWS OF THE WEEK - A 'Nose' That Shows Scents In Color"](#)

[Business Week, 09/04/00:](#)

["Developments To Watch"](#)

[New Scientist, 08/17/00:](#)

["Sniffing out fakes"](#)

[The News-Gazette, 8/17/00, p. 1 \(!\):](#)

["UI scientists say smells are really quite a sight to see."](#)

[Chicago Tribune, 8/17/00, sect. 1, p. 5:](#)

["U. OF I. Researcher Provides Whiff of Brand-New Technology"](#)

[Reuters/Yahoo News; 8/17/00:](#)

["Artificial Nose 'Sees'" Smells](#)

[Inside Illinois, 8/17/00:](#)

["Artificial Nose Knows"](#)

[NewsDay, 9/19/00:](#)

["The Artificial Sniffer" p. C8-C9.](#)

[The Scientist 14\[17\]:19, Sep. 4, 2000:](#)

["Does The Nose Always Know?"](#)

[Nature Science Update, 8/17/00:](#)

["Seeing scents."](#)

[Discovery.com, 8/16/00:](#)

["Paper Nose Detects Toxics."](#)

[Chemistry and Industry, 08/21/2000](#)

["Artificial nose sniffs out colour of odours."](#)

[Photonics Spectra, Nov. 2000](#)

["Color-Changing Array Identifies Odors"](#)

[Biophotonics International, Nov. 2000](#)

["What the nose knows can also be seen"](#)

[Environmental Health Perspectives \(NIH\), March, 2001](#)

["Smelling in Color: A Rainbow of Possibilities"](#)

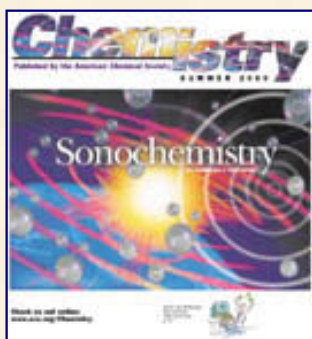
[Scientific American, March 2001](#)

["Plenty to Sniff At"](#)

- **Didenko, Y.; McNamara III, W. B.; Suslick, K. S. "Molecular Emission from Single Bubble Sonoluminescence" *Nature*, 2000, 406, 877-879.**

[Physics Web, October 18, 2000](#)

- **"Sonochemistry"** [Chemistry, Summer 2000, pp. 3, 17-22.](#)



Chemistry is a free quarterly magazine published by the American Chemical Society and distributed to its more than 160,000 members and student affiliates.

- **McNamara III, W. B.; Didenko, Y.; Suslick, K. S. "Sonoluminescence Temperatures During Multibubble Cavitation"** [Nature, 1999, 401, 772-775.](#)

"Taking a Collapsing Bubble's Temperature"

[C & E News, 25 Oct 99](#)

"Bubbling to Extreme Temperatures"

[Science News, 25 Oct 99](#)

"Bubbling Hot!"

[Nature, 21 Oct 99](#)

"Bubbling to Extremes" Science News 29 Oct 99

"Chemists Shed Light on Bubbly Furnaces"

[Chemistry, Spring 2000](#)

- **Bhyrappa, P.; Vijayanthimala, G.; Suslick, K. S. "Shape-Selective Ligation to Dendrimer-Metalloporphyrins,"** [J. Am. Chem. Soc., 1999, 121, 262-263.](#)

"On the scent"

[New Scientist, 16 Jan 99](#)

- **Collman, J. P.; Brauman, J. I.; Halbert, T. R.; Suslick, K. S. "Nature of Oxygen and Carbon Monoxide Binding to Metalloporphyrins and Heme Proteins," *Proc. Natl. Acad. Sci., U.S.A.* 1976, 73, 3333-3337.**

"A Mechanism Essential to Life: Scientists pursue consensus and closure on mechanism of binding of CO and O₂ to myoglobin and hemoglobin." Chemical & Engineering News, December 6, 1999, p. 31-33

- **Suslick, K. S.; Mdeleleni, M. M.; Ries, J. T. "Chemistry Induced by Hydrodynamic Cavitation" *J. Am. Chem. Soc.*, 1997, 119, 9303-9304.**

"Scientists have a blast learning how to break chemical bonds" Dallas Morning News, 13 Oct 97

- **Suslick, K. S. "Sonoluminescence, Camera, Action!" *Engineering & Science (California Institute of Technology)* 1997 40 (#2), 4-5.**

Suslick, K. S. "Set for a 'Chain Reaction'" Hollywood, Suslick Research Group Chemistry University of Illinois*Inside Illinois* 1997, 16 (#17), 5.

**"Illinois chemist snagged briefly by movie industry"
C&E News, 7 Apr 97**

**"Sonoluminescence, camera, action!"
Engineering & Science, Apr 97**

- **Suslick, K. S.; Fang, M.; Hyeon, T. "Sonochemical Synthesis of Iron Colloids" *J. Am. Chem. Soc.*, 1996, 118, 11960-11961.**

"Sonochemistry"

Aviation Weekly & Space Technology, 17 Mar 97

"Bubbly synthesis yields iron nanocolloids"

C&E News, 13 Jan 97

- **Hyeon, T.; Fang, M.; Suslick, K. S. "Nanostructured Molybdenum Carbide: Sonochemical Synthesis and Catalytic Properties," *J. Am. Chem. Soc.*, 1996, 118, 5492-5493.**

"Mysterious blue light of minute bubbles finding practical uses"

New York Times, 31 Dec 96

"Shattering sounds"

Economist, 29 May 96

- **Girolami, G. S.; Hein, C. L.; Suslick, K. S. "Bis(porphyrin) Sandwich Complex with an Appended Quinone," *Angew. Chem. Intl. Ed.* 1996, 35, 1223-1225.**

"Plants point the way to renewable energy"

New Scientist, 8 Jun 96

Some Older Press Clippings:

"Ultrasonic cleaning cuts waste, energy use"

C&E News, 3 Jul 95

"Waves of excitement"

London Financial Times, 27 May 95

"Bubbles hotter than the sun"

New Scientist, 29 Apr 95

"Nanostructured catalysts prepared"

C&E News, 24 Apr 95

"Booster bubbles for artificial blood"

Business Week, 23 Jan 95

"Small sphere lead to big ideas"

Science, 20 Jan 95, vol. 267, p. 327,

"Microspheres play role in medical, sensor, energy, space technologies" C&E News, 19 Dec 1994, p. 33

"New shot at fusion by pumping sound waves into tiny bubbles"

New York Times, 20 Dec 94

"A shot in the arm for synthetic blood"

New Scientist, 17 Dec 94

"Flashes of insight"

Dallas Morning News, 21 Nov 94

"Nobel Laureate Signature Award for Graduate Education in Chemistry"

C&E News, 11 Oct 1993

"Ultrasound proves to be a versatile tool for chemists."

C&E News, 7 Oct 1991, p. 18-21

"Light Comes from Ultrasound"

Physics Today, Oct. 1991, p. 17-18

"Chemistry: Putting good vibrations to work"

Washington Post, 7 Oct 91

"Sonic Boom"

Economist, 5 Oct 91

"Ultrasonic boom"

Dallas Morning News, 4 Jun 90

"Sound is shaped into dazzling tool with many uses"

New York Times, 9 Feb 88

"Sonoluminescence seen in nonaqueous liquids"

C&E News, 25 Jan 1988

"Snap, crackle, pop"

Economist, 19 May 84

SUSLICK GROUP WEBSITE:

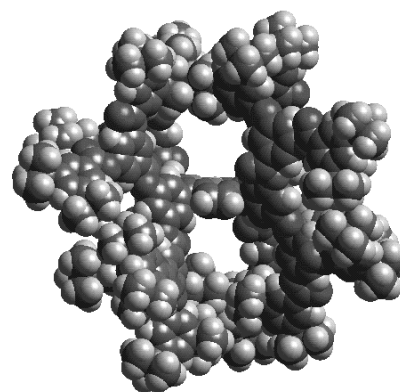
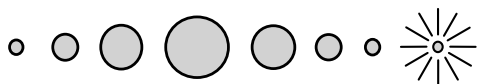
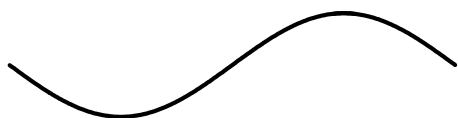
THE SCIENCE	THE GROUP	THE MAÎTRE D'	LAGNIAPPE: A LITTLE EXTRA
<u>Overview</u>	<u>Current Group Members</u>	<u>CV: Abbreviated, Full</u>	<u>Art and Science</u>
<u>Outline of Projects</u>	<u>Group Meetings</u>	<u>Suslick Group Brochure</u>	<u>Chymistes: The Distillers of Waters</u>
<u>Synopses: Sonochemistry</u> <u>Metalloporph.</u>	<u>Group Responsibilities</u>	<u>Complete Publication List</u>	<u>A Chemist Meets Hollywood</u>
<u>Executive Summary: Smell-Seeing</u>	<u>Web Based Resources</u>	<u>Academic Genealogy</u>	<u>A Chemist In Court</u>
<u>Introduction to Sonochemistry</u>	<u>Safety Resources</u>	<u>Press Clippings</u>	<u>Words of Humor and Wisdom</u>
<u>Proposal Excerpts</u>	<u>Group Equipment</u>	<u>How To Give A Seminar</u>	<u>Laws of the Universe</u>

<u>Funding</u>	<u>Past Group Members</u>	<u>Ch315 Inorganic Chemistry</u>	<u>Cartoons of Humor and Wisdom</u>
<u>Information for Visitors</u>	<u>Group Photogallery</u>	<u>Construction of the CLS Lab</u>	<u>Sculpture & Masks</u>

©2003, K.S. Suslick; all rights reserved.

Comments and suggestions: ksuslick@uiuc.edu

RESEARCH IN THE SUSLICK GROUP



Introduction	p. 1
Outline of Research Projects	2
Selected Recent Publications	3
Current Research Group Members	4
Research Funding	5
Executive Summaries of Research.....	6
Abbreviated Curriculum Vitae	10
Major Equipment Inventory	12
Past Research Group Members	14

Cover Page Figure Captions:

The figure on the left shows the growth and collapse of a transient cavitation bubble during the final acoustic cycle. The implosive collapse of the bubble generates enormous local heating and high pressures, but for only a very short time. This phenomenon is responsible both for sonochemical reactions, including the dramatic enhancements in liquid-solid sonochemical reactions (including Grignards and lithiations), and for sonoluminescence, the emission of light during ultrasonic irradiation of liquids.

The figure on the right is a side view of a bis-pocketed dendrimer porphyrin. The protecting pockets on both faces of the macrocycle prevent bimolecular oxidation of Fe(II) complexes and provides steric constraints of the pocket for molecular recognition of incoming substrates and for shape selective catalytic oxidation of alkanes and alkenes, in analogy to cytochrome P-450. This project involves the use of dendrimers in the design of catalytic systems capable of molecular recognition and shape selectivity.

Current versions of this information and *more information* are available on the Web at
<http://www.scs.uiuc.edu/suslick>

Contact information:

Kenneth S. Suslick
School of Chemical Sciences
University of Illinois at Urbana-Champaign
A422 Chemical & Life Sciences Laboratory
600 S. Mathews Avenue
Urbana, Illinois 61801

Office: (217) 333-2794
Lab: (217) 333-1532
Fax: (217) 333-2685
Email: ksuslick@uiuc.edu

INTRODUCTION

The multi-disciplinary nature of our research projects involves individuals with interests not only in inorganic, but also in bio-organic, materials, and physical chemistry. Our two major research areas are the chemical effects of ultrasound and the bioinorganic and materials chemistry of metalloporphyrins and heme proteins. As part of this diversity, we often collaborate with other researchers both at UIUC and at other universities across the world. Several of the students in this group are joint members in other research groups in the School of Chemical Sciences.

We have been exploring a broad range of both mechanistic and synthetic applications of ultrasound. The origin of "sonochemistry" is acoustic cavitation: the formation, expansion, and implosive collapse of bubbles in liquids irradiated with ultrasound. The compression within such bubbles generates intense local heating and high local pressures. We have recently been able to measure these conditions spectroscopically from light emission during cavitation: ≈ 5000 K at 1000 atm., but lifetimes less than a microsecond. The chemistry generated by these hot-spots is different than either ordinary thermal or photochemical processes, and sonochemistry represents a fundamentally unique interaction of energy and matter.

Much of our work in this area has dealt with organometallic and catalytic sonochemistry. Examples include multiple ligand substitution and clusterification, homogeneous catalysis, intercalation into layered inorganic solids, and activation of heterogeneous catalysis. In some cases, we have been able to enhance reaction rates by as much as a million-fold! We recently discovered a simple process for the sonochemical synthesis of amorphous metals, unusual materials without the long-range order of ordinary metals or crystalline materials. In these studies, we make heavy use of sophisticated surface analysis techniques to characterize the effects of ultrasound on solids.

The second research area in the group is metalloporphyrin chemistry. In order to gain new insights into the structure and function of metalloproteins, we are involved in the design, synthesis, and physical characterization of small (or at least smallish!) molecules that look like and behave like enzyme active sites. Our principal focus is on heme

proteins including myoglobin and hemoglobin (O_2 binding), peroxidase and catalase (peroxide detoxification), and cytochrome P-450 (oxidative metabolism, including drugs and carcinogens).

Metalloporphyrins provide a versatile synthetic base on which to design desired properties: i.e., molecular engineering. To probe the origins of molecular recognition, we have used sterically hindered, "bis-pocket" porphyrins to *reverse* the normal reactivity of hydrocarbons. In this work with synthetic metalloporphyrins and with dendrimer-porphyrins, we are developing superstructured macrocycles as shape, size, and polarity selective oxidation catalysts and as selective molecular sensors. We are also exploring the binding of totally synthetic polypeptides to metalloporphyrins. Our goal here is the generation of rationally designed artificial heme proteins, the ultimate interface between inorganic and biological chemistry.

We have also recently discovered a new and simple approach to detection of odorants using the colorimetric response from a library of immobilized vapor-sensing metalloporphyrins and other chemoresponsive dyes. We call this technique "smell-seeing". This technology is presently being successfully commercialized by a start-up company, ChemSensing, Inc.

Other porphyrin projects are more materials and biomaterials oriented. For example, we are developing the use of porphyrins as nanoporous catalytic materials. The latter involves the use of poly-functionalized metalloporphyrins as building blocks for the *molecular* assembly of molecular sieves.

In a project that bridges between our two research areas, we have recently discovered a sonochemical preparation of proteinaceous microspheres for drug delivery and blood substitutes. Ultrasonic irradiation of various proteins (e.g., serum albumin and Hb) creates micron-sized spheres that can be either gas-filled or non-aqueous liquid-filled. We have had substantial success in recent development of proteinaceous microspheres as blood substitutes for O_2 transport, as contrast agents for magnetic resonance imaging, and as spin-label probes for *in vivo* O_2 and temperature profiling.

OUTLINE OF CURRENT RESEARCH PROJECTS

I. Porphyrins, Metalloporphyrins, and Bio-In/Organic Chemistry of Heme Proteins

Molecular Recognition: Oxidation Catalysis and Molecular Sensors

Molecular Recognition, Shape and Polarity Selectivity with Super-Structured Porphyrins
Dendrimer Porphyrins, Oxygen Atom Transfers; Cytochrome P450 Intermediates
Artificial Olfaction: "Smell-Seeing" and Selective Molecular Sensors

Porphyritic Materials Chemistry

Network Solids; Hydrogen Bonded Porphyritic Networks, Coordination Polymers
Nanoporous Solids, Shape Selective Heterogeneous Catalysts, Non-fullerene Nanotubes

Totally Synthetic Heme Proteins: Peptides as Ligands

Oligopeptide Binding to Metalloporphyrins; Olfactory Receptors

II. The Chemical Effects of Ultrasound

Physical and Mechanistic Sonochemistry and Sonoluminescence

Mechanisms of Sonochemistry, Surface-Surface Reactivity
Spectroscopic Probes of Cavitation Conditions, Multi-Bubble and Single-Bubble Cavitation

Synthetic, Materials, and Catalytic Applications of Sonochemistry

Organometallic Sonochemistry; Heterogeneous and Organic Sonochemistry
Liquid-Solid Reactions; Interparticle Mechanochemistry
Heterogeneous Catalysis; Nanostructured and Amorphous Metals, Carbides, Sulfides

Biomedical Applications of Sonochemistry

Protein Microspheres and Microencapsulation; Drug Delivery Systems
Medical Imaging Contrast Agents (OCT, MRI, sonographic, x-ray)

RECENT PUBLICATIONS

Professor Suslick has edited four books and published more than 230 scientific papers; below is a sampling of these, available as reprints in PDF format at his website: www.scs.uiuc.edu/suslick/ Along with his journal publications, he takes some pride in his popularizations of sonochemistry and in his contributions to art in science. The former include invited feature articles in *Scientific American* (1989), the British equivalent *New Scientist* (1990 & 1996), *Science* (1990), the *Encyclopaedia Britannica Yearbook of Science and the Future* (1993), and numerous technical encyclopedias. The latter include numerous journal covers: two *Science* (23 Mar. 1990 and 20 Sept. 1991), *Nature* (25 Jul 2002), *Bulletin of the Materials Research Society* (April, 1995), and *Supramolecular Chemistry* (Sept., 1999).

The Chemical Effects of Ultrasound

1. Suslick, K. S.; Choe, S. B.; Cichowlas, A. A.; Grinstaff, M. W. "Sonochemical Synthesis of Amorphous Iron," *Nature* **1991**, 353, 414-416.
2. Suslick, K. S.; Fang, M.; Hyeon, T. "Sonochemical Synthesis of Iron Colloids" *J. Am. Chem. Soc.*, **1996**, 118, 11960-11961.
3. Mdleleni, M. M.; Hyeon, T.; Suslick, K. S. "Sonochemical Synthesis of Nanostructured Molybdenum Sulfide" *J. Am. Chem. Soc.*, **1998**, 120, 6189-6190.
4. Suslick, K. S.; Didenko, Y.; Fang, M. M.; Hyeon, T.; Kolbeck, K. J.; McNamara, W. B. III; Mdleleni, M. M.; Wong, M. "Acoustic Cavitation and Its Chemical Consequences," *Phil. Trans. Roy. Soc. A*, **1999**, 357, 335-353.
5. McNamara III, W. B.; Didenko, Y.; Suslick, K. S. "Sonoluminescence Temperatures During Multibubble Cavitation," *Nature*, **1999**, 401, 772-775.
6. Dantsin, G.; Suslick, K.S. "Sonochemical Preparation of a Nanostructured Bifunctional Catalyst" *J. Am. Chem. Soc.* **2000**, 122, 5214-5215.
7. Dhas, N.A.; Ekhtiarzadeh, A.; Suslick, K.S. "Sonochemical Preparation of Supported Hydrodesulfurization Catalysts" *J. Am. Chem. Soc.*, **2001**, 123, 8310-8316.
8. Didenko, Y.; Suslick, K. S. "Photons, Radicals, and Ions from a Single Bubble: An Energy Inventory During Cavitation" *Nature* **2002**, 418, 394-397.

Metalloporphyrins and Bio-Inorganic Chemistry

1. Bhyrappa, P.; Wilson, S. R.; Suslick, K. S. "Hydrogen Bonded Porphyrinic Solids: Surpramolecular Networks of Octahydroxy Porphyrins," *J. Am. Chem. Soc.*, **1997**, 119, 8492-8502.
2. Huffman, D. L.; Rosenblatt, M. M.; Suslick, K. S. "Synthetic Heme-Peptide Complexes," *J. Am. Chem. Soc.*, **1998**, 120, 6183-6184.
3. Patel, B. R.; Suslick, K. S. "Discotic Liquid Crystals from a Bis-Pocketed Porphyrin" *J. Am. Chem. Soc.*, **1998**, 120, 11802-11803.
4. Bhyrappa, P.; Vaijayanthimala, G.; Suslick, K. S. "Shape-Selective Ligation to Dendrimer-Metalloporphyrins," *J. Am. Chem. Soc.*, **1999**, 121, 262-263.
5. Rakow, N. A.; Suslick, K. S. "A Colorimetric Sensor Array for Odour Visualization" *Nature* **2000**, 406, 710-714.
6. Zimmerman, S. C.; Wendland, M. S.; Rakow, N. A.; Zharov, I.; Suslick, K. S. "Synthetic Hosts by Monomolecular Imprinting Inside Dendrimers" *Nature* **2002**, 418, 399-403.
7. Kosal, M. E.; Chou, J.-H.; Wilson, S. R.; Suslick, K. S. "A Functional Zeolite Analogue Assembled From Metalloporphyrins" *Nature Materials*, **2002**, 1, 118-121
8. Wang, J.; Luthey-Schulten, Z.; Suslick, K. S. "Is the Olfactory Receptor A Metalloprotein?" *Proc. Natl. Acad. Sci. U.S.A.*, **2003**, 100, 3035-3039.

Some Introductory Reviews

1. Suslick, K. S. "The Chemical Effects of Ultrasound," *Scientific American*, **1989** (2), 260, 80-86.
2. Suslick, K. S. "The Chemistry of Ultrasound," in *Encyclopaedia Britannica Yearbook of Science and the Future 1994*, Britannica: Chicago; 1994; pp. 138-155.
3. Suslick, K. S.; Van Deusen-Jeffries, S. "Shape Selective Biomimetic Oxidation Catalysis" *Comprehensive Supramolecular Chemistry*, vol. 5; Lehn, J. M., ed. Elsevier Publishers: Oxford, 1996; pp. 141-170.
4. K.S. Suslick "Sonochemistry," *Kirk-Othmer Encyclopedia of Chem. Tech*; 4th Ed. Wiley: 1998, vol. 26, 517-541.
5. Suslick, K.S.; Price, G. "Applications of Ultrasound to Materials Chem.," *Annu. Rev. Matl. Sci.*, **1999**, 29, 295-326.
6. Chou, J.-H.; Kosal, M. E.; Nalwa, H.S.; Rakow, N.A.; Suslick, K. S. "Applications of Porphyrins and Metalloporphyrins to Materials Chemistry" in *The Porphyrin Handbook*, Acad. Press: 2000; vol. 6, ch. 41, pp. 43-131.

CURRENT RESEARCH GROUP MEMBERS, 8/02

Porphyrin Projects

Jie Bai

B.S., Beijing University, 2002.

Ming Fang

B.S., Jilin Univ., 2001

Dennis Smithenry

B.S., University of Illinois, 1999.

Jennifer Ponder-Wilson

B.S., Ball State University, 2000.

Chen Zhang

B.S., Beijing University, 2001.

Microsphere Projects

Farah Jean-Jacques

B.S., State Univ. New York, Stony Brook, 2000.

Elizabeth Dibbern

B.S., Univ. of Nebraska, 2002.

Sonochemistry Projects

Yury Didenko

B.S., M.S., Moscow State University, 1970-75.
Ph.D., Moscow State University, 1985.
Head of Laboratory, Pacific Oceanological Inst.,
Vladivostok, Russia.
Research Associate, Univ. of Illinois.

David Flannigan

B.S., Univ. of Minnesota, 2001

Steve Hopkins

B.S., Washington & Lee University, 2000.

Dongkyu Lee

Professor, Chemical Engineering, Chungbuk
National University (Korea).

James D. Oxley

B.S., Texas Christian University, 1998.
Ph.D., UIUC, 2003; "Environmental Applications
of Ultrasound."

Annabeth Ryder

B.S., Indiana Univ., 2002.

Sara Skrabalak

B.A., Washington Univ., 2002.

Tanya Prozorov

M.S., Bar-Ilan University, 1998.

Won Hyuk Suh

M.S. Seoul National Univ., 2002.

Group Executive Manager

Ronald Shen

B.S., Pharmaceutical Chemistry, Beijing Medical Univ.
M.S., Medicinal Chemistry, Univ. Toledo, 1996.
Research Associate, ChemRx Advanced Technologies.

RESEARCH FUNDING

Major Research Funding, Current:

- 2003 – 06 NSF; "Chemical Effects of High Intensity Ultrasound" \$562,500 / 3 yrs.
2001 - 04 NIH; "Heme Proteins, Microspheres, & Their Synthetic Analogs" \$1,365,000 / 4 yrs.
1999 - 04 DARPA; "Chemical Control of Single Bubble Cavitation" \$637,121 / 4 yrs.
1990 - xx DOE; UIUC Materials Res. Lab; "Field Responsive Porphyrinic Materials" \$100,000 / yr.

Major Research Funding, Recent Past:

- 2000 – 03 NSF; "Chemical Effects of High Intensity Ultrasound" \$480,000 / 3 yrs.
2000 - 01 PG Research Foundation; "Ultrasonic Gas Dispersion and Dissolution" \$72,538 / yr.
1997 - 02 DOD; "Dendritic Materials Systems MURI" \$500,000 / 5 yrs (KSS portion).
1997 - 00 NIH; "Heme Proteins, Microspheres, & Their Synthetic Analogs" \$924,944 / 4 yrs.
1994 - 99 NSF; "Chemical Effects of Ultrasound" \$738,673 / 4 yrs.
1996 - 99 DOE; "Cavitation Hydrothermal Oxidation" \$478,027 / 3 yrs.
1995 - 99 VivoRx Pharmaceuticals, Inc.; "Biomedical Applications of Protein Microspheres" \$60,000 / yr.
1995 - 98 University of Illinois Foundation, UIUC University Scholar; \$36,000 / 3 yrs.
1996 DOE; "Sonoluminescence", subcontract from Lawrence Livermore Natl. Lab; \$10,000.
1995 - 97 UIUC Critical Research Initiative; "Non-Natural Self-Organizing Molecules" \$120,000 / 2 yrs.
1992 - 96 NIH; "Heme Proteins and Their Synthetic Analogs" \$782,447 / 4 yrs.
1989 - 96 NSF; UIUC Materials Res. Lab; "Effects of Ultrasound on Heterog. Catalysis" \$386,000 / 5 yrs.
1992 - 95 NSF; "Visualization in Teaching Chemistry" with S. S. Zumdahl, \$368,505 / 3 yrs.

EXECUTIVE SUMMARIES OF RESEARCH

The Chemical and Physical Effects of Ultrasound

Our research group has pioneered the exploration of sonochemistry, most recently as a tool in materials chemistry. Our research has developed new approaches to the synthesis of amorphous and nanostructured materials, has shown great promise for the activation of heterogeneous catalysts, and has created a whole new class of medically important biomaterials.

Background — Ultrasonic irradiation of liquids causes high energy chemical reactions to occur [1]. The origin of sonochemistry is acoustic cavitation: the formation, growth, and implosive collapse of bubbles in liquids irradiated with high intensity sound. The collapse of bubbles caused by cavitation produces intense local heating and high pressures, with very short lifetimes.

Accomplishments — In order to understand the origins of sonochemistry, we found it essential to understand better the nature of cavitation and the conditions created during bubble collapse. To this end, we developed sonoluminescence as a spectroscopic probe of the cavitation hot spot [1, 2, 3]. In clouds of cavitating bubbles, these hot-spots [2,3] have equivalent temperatures of roughly 5000 K, pressures of about 1000 atmospheres, and heating and cooling rates above 10^{10} K/s. Thus, cavitation can create extraordinary physical and chemical conditions in otherwise cold liquids. Fig. 1 places sonochemistry in relationship to other forms of chemistry.

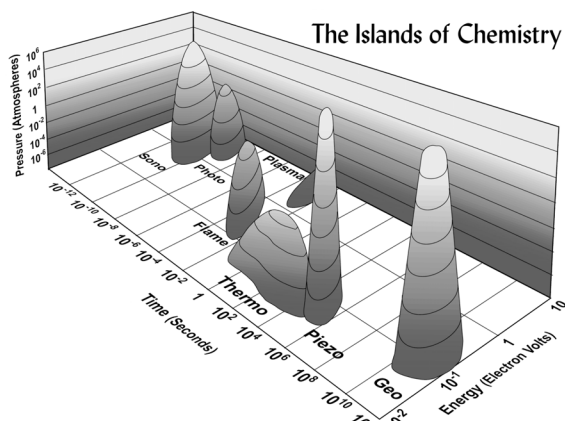


Fig. 1. Chemistry: the interaction of energy and matter.

Ultrasound has proved extremely useful in the synthesis of a wide range of nanostructured materials, including high surface area transition metals, alloys, carbides, oxides and colloids [4]. Sonochemical decomposition of volatile organometallic precursors in high boiling solvents

produces nanostructured materials in various forms with high catalytic activities. Nanometer colloids, nanoporous high surface area aggregates, and nanostructured oxide supported catalysts can all be prepared by this general route. As one example, our discovery of a simple sonochemical synthesis of amorphous iron helped settle the longstanding controversy over its magnetic properties. Another example, shown in Fig. 2, provides an easy route to nanostructured heterogeneous catalysts with extremely high activities [4, 5].

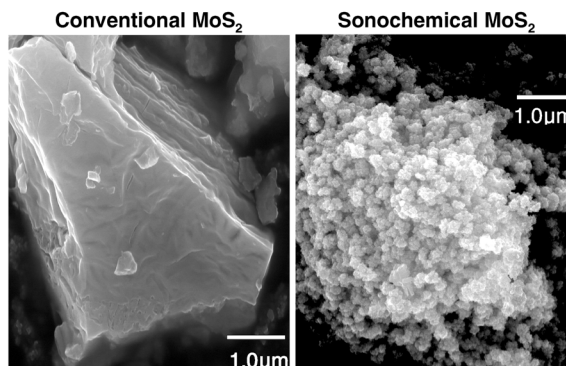


Fig. 2. Scanning electron micrographs of MoS₂, the predominant industrial hydrodesulfurization catalyst [5].

Another important application has been the sonochemical preparation of biomaterials, most notably protein microspheres [6]. Using high intensity ultrasound and simple protein solutions, a remarkably easy method to make both air-filled microbubbles and nonaqueous liquid-filled microcapsules has been developed. Figure 3 shows an electron micrograph of sonochemically prepared microspheres. These microspheres are stable for months, and being slightly smaller than erythrocytes, can be intravenously injected to pass unimpeded through the circulatory system. These protein microspheres, have a wide range of biomedical applications, including their use as echo contrast agents for sonography, magnetic resonance imaging contrast enhancement, drug delivery, among others.

EXECUTIVE SUMMARIES OF RESEARCH

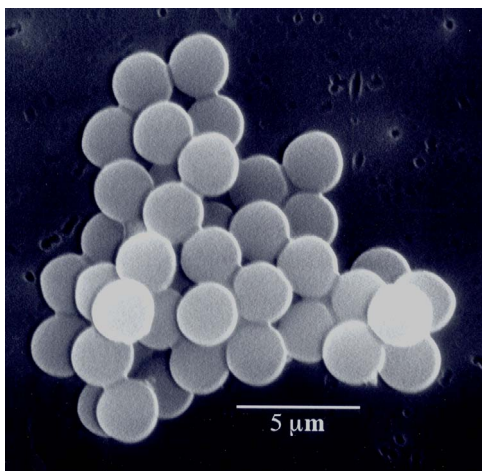


Fig. 3. Scanning electron micrograph of sonochemically synthesized hemoglobin microspheres.

When liquids that contain solids are irradiated with ultrasound, related phenomena can occur [1, 7]. When cavitation occurs near an extended solid surface, cavity collapse is non-spherical and drives high-speed jets of liquid into the surface. These jets and associated shock waves can cause substantial surface damage and expose fresh, highly heated surfaces.

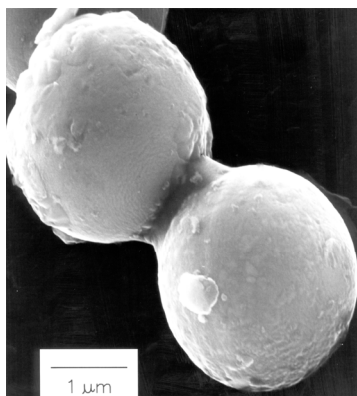


Fig. 4. Scanning electron micrograph of 5 μm diameter Zn powder. Neck formation from localized melting is caused by high-velocity interparticle collisions.

Ultrasonic irradiation of liquid-powder suspensions produces another effect: high velocity inter-particle collisions [7]. Cavitation and the shockwaves it creates in a slurry can accelerate solid particles to high velocities (Fig. 4). The resultant collisions are capable of inducing dramatic changes in surface morphology, composition, and reactivity. Heterogeneous catalysts often require rare and expensive metals. The use of ultrasound offers some hope of activating less reactive, but also less costly,

metals. For example, the effects of ultrasound on Ni powder is shown in Fig. 5, with the chemical consequence of enormously increasing the catalytic rates of hydrogenation by Ni powder ($>10^5$ -fold) [8].

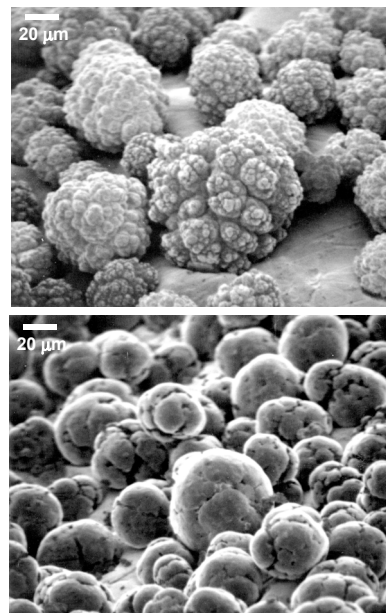


Fig. 5. The effect of ultrasonic irradiation on the surface morphology and particle size of Ni powder. High-velocity interparticle collisions caused by ultrasonic irradiation of slurries are responsible for the smoothing and removal of passivating oxide coating.

[1] K.S. Suslick et al. "Acoustic Cavitation and Its Chemical Consequences," *Phil. Trans. Roy. Soc. A*, **1999**, 357, 335-353.

[2] McNamara III, W. B.; Didenko, Y.; Suslick, K. S. "Sonoluminescence Temperatures During Multibubble Cavitation" *Nature*, **1999**, 401, 772-775.

[3] Didenko, Y.; Suslick, K. S. "Photons, Radicals, and Ions from a Single Bubble: An Energy Inventory During Cavitation" *Nature* **2002**, 418, 394-397

[4] Suslick, K. S.; Price, G. "Applications of Ultrasound to Materials Chemistry" *Annu. Rev. Matl. Sci.*, **1999**, 29, 295-326.

[6] Mdleleni, M. M.; Hyeon, T.; Suslick, K. S. "Sonochemical Synthesis of Nanostructured Molybdenum Sulfide" *J. Am. Chem. Soc.*, **1998**, 120, 6189-6190.

[6] K.S. Suslick, M.W. Grinstaff, *J. Am. Chem. Soc.* 112, 7807 (1990)

[7] S.J. Doktycz, K.S. Suslick *Science*, 247, 1067 (1990).

[8] K.S. Suslick in *Handbook of Heterogeneous Catalysis*; Ertl, G.; Knozinger, H.; Weitkamp, J.; eds.; Wiley-VCH: Weinheim, 1997; vol. 3, ch. 8.6.

EXECUTIVE SUMMARIES OF RESEARCH

Porphyrin and Metalloporphyrin Chemistry

Our research team been at the leading edge of research on synthetic metalloporphyrins for applications as synthetic analogs of heme proteins, shape selective oxidations, and diverse materials chemistry applications including nanoporous network solids, non-linear optical materials, and selective sensors.

Background — Porphyrins (which comes from the Greek for “purple”) are based on 16-atom rings containing four nitrogen atoms (Fig. 1); they are of perfect size to bind nearly all metal ions. Heme proteins (which contain iron porphyrins) are ubiquitous in nature and serve many roles, including O₂ storage and transport (myoglobin and hemoglobin), electron transport (cytochromes b and c), and O₂ activation and utilization (cytochrome P450 and cytochrome oxidase).

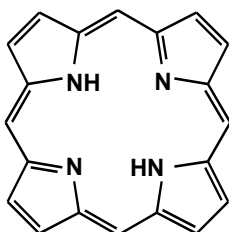


Fig. 1. Porphine, the simplest porphyrin.

In order to gain new insights into the structure and function of metalloproteins, we are involved in the design, synthesis, and physical characterization of complex molecules that look and behave like heme protein active sites. Here we are concerned with issues of oxidation chemistry, catalysis, and molecular recognition [1].

Metalloporphyrins and related macrocycles also provide an extremely versatile synthetic base on which to design physical and chemical properties. Another goal of our research effort has been the exploration of metalloporphyrin assemblies as field responsive materials, particularly for photo-responsive applications. Porphyrins can be molecularly engineered to provide erect desirable molecular and materials properties, including very large dipole moments, polarizabilities, and hyperpolarizabilities. The non-linear optical properties of these materials are of special interest. These molecules can be built for energy transfer with molecular control, giving them potential applications in optical communications, data storage, and electrooptical signal processing [2].

Accomplishments — To probe the origins of molecular recognition, we have used sterically hindered, "bis-pocket" porphyrins to *reverse* the normal reactivity of hydrocarbons, enabling us to oxidize selectively primary C-H bonds or the least substituted double bonds. In this work with synthetic metalloporphyrins and with dendrimer-porphyrins, we have synthesized superstructured macrocycles as shape, size, and polarity selective oxidation catalysts for both hydroxylation and epoxidation [1, 3].

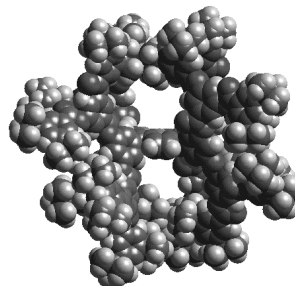


Fig. 2. A bis-pocketed dendrimer porphyrin. The protecting pockets on both sides of the porphyrin provides for molecular recognition of incoming substrates and for shape selective catalytic oxidation of alkanes and alkenes.

In other work, we are interested in the interaction of metalloporphyrins with peptides [4, 5]. For example, we have designed synthetic heme-peptide complexes by the coordination of amphiphilic peptides to heme and have been examined to determine the influence of the peptide on the properties of the heme and vice versa. The presence of hydrophobic residues flanking a coordinated histidine dramatically increases peptide binding to the heme by a factor of nearly 6000 relative to histidine. Hydrophobic interactions between the porphyrin face and the non-polar side chains of the amino acid residues make a major contribution to the stability of the heme-peptide complexes. Circular dichroism spectra demonstrate that heme binding induces substantial helix formation, presumably to maximize the hydrophobic stabilization. The complexes with the most hydrophobic peptides are the most difficult to reduce, as expected from relative ligand binding to Fe^{II} vs. Fe^{III}.

EXECUTIVE SUMMARIES OF RESEARCH

Other projects are more materials and biomaterials oriented. For example, we are developing the use of porphyrins as non-linear optical materials and as nanoporous catalytic materials.

Metalloporphyrins also are a versatile base for molecular engineering of desired properties. As one example, we have recently created a new class of bis-pocketed discotic liquid crystals of metalloporphyrins to create nanostructured assemblies of photoresponsive materials [6]. We are currently expanding this approach to generate cross-linked non-fullerene nanotubes for applications to catalysis and separations. Other projects involve the solid-state design of nanoporous porphyrinic solids, using hydrogen bonding or metal coordination network polymers to provide a catalytically active, shape-selective solid.

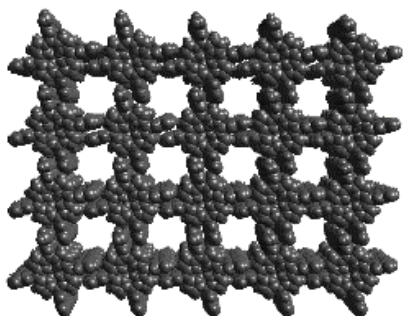


Fig. 3. A porphyrin nanoporous solid. Eight hydrogen bonds per porphyrin produce a columnar stacking in this molecular packing diagram of the x-ray structure of tetrakis(3,5-dihydroxyphenyl)porphyrin.

We are also developing new nanoporous network solids of highly functionalized porphyrins to provide controlled porphyrin orientation in the solid state and to produce molecularly-designed molecular sieves [7, 8]. We intend to explore the use of these solids as heterogeneous shape-selective oxidation catalysts. An example of one such structure is shown above. Other work has involved molecular imprinting of porphyrins into crosslinkable dendrimers, producing a synthetic analog of antibody-antigen systems [9]

We have also recently discovered a new and simple approach to detection of odorants using the colorimetric response from a library of immobilized vapor-sensing metalloporphyrins [10]. We call this technique “smell-seeing”. We can visually identify a wide range of ligating vapors (including alcohols, amines, ethers,

phosphines, phosphites, and thiols) and even weakly ligating vapors (arenes, halocarbons, and ketones). Unique color fingerprints can be obtained below 10 ppb for many biogenic odorants.

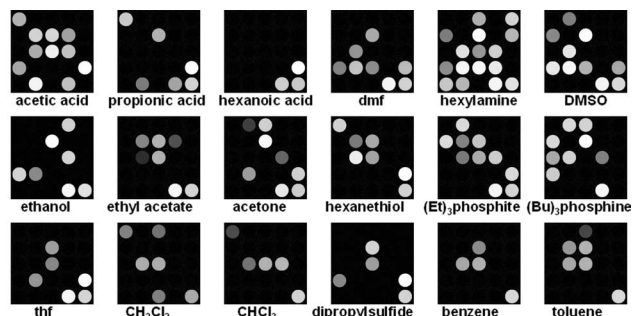


Fig. 4. The color changes from our “smell-seeing” array of metalloporphyrins are unique for each analyte. Sensitivities are generally better than the human nose.

- [1] Suslick, K. S.; van Duesen-Jeffries, S. "Shape Selective Oxidation Catalysis" *Comprehensive Supramolecular Chemistry*, vol. 5; ed. Suslick, K.S.; Elsevier Publishers: Oxford, 1996, pp. 141-170.
- [2] Chou, J.-H.; Kosal, M. E.; Nalwa, H.S.; Rakow, N.A.; Suslick, K. S. in *The Porphyrin Handbook*, Kadish, K.; Smith, K.; Guillard, R., ed.; Academic Press: New York, 2000; vol. 6, ch. 41, pp. 43-131.
- [3] Bhyrappa, P.; Vijayanthimala, G.; Suslick, K. S. "Shape-Selective Ligation to Dendrimer-Metalloporphyrins" *J. Am. Chem. Soc.* **1999**, *121*, 262-263.
- [4] Huffman, D. L.; Rosenblatt, M. M.; Suslick, K. S. "Synthetic Heme-Peptide Complexes," *J. Am. Chem. Soc.*, **1998**, *120*, 6183-6184.
- [5] Rosenblatt, M.M.; Huffman, D.L.; Wang, X. Remmer, H.A.; Suslick, K. S. "Cyclic and Hairpin Peptide Complexes of Heme" *J. Am. Chem. Soc.*, **2002**, *124*, in press.
- [6] Patel, B. R.; Suslick, K. S. "Discotic Liquid Crystals from a Bis-Pocketed Porphyrin," *J. Am. Chem. Soc.*, **1998**, *120*, 11802-11803.
- [7] Bhyrappa, P.; Wilson, S. R.; Suslick, K. S. "Hydrogen Bonded Porphyrinic Solids," *J. Am. Chem. Soc.*, **1997**, *119*, 8492-8502.
- [8] Kosal, M. E.; Chou, J.-H.; Wilson, S. R.; Suslick, K. S. "A Functional Zeolite Analogue Assembled From Metalloporphyrins" *Nature Materials*, **2002**, *1*, in press.
- [9] Zimmerman, S. C.; Wendland, M. S.; Rakow, N. A.; Zharov, I.; Suslick, K. S. "Synthetic Hosts by Monomolecular Imprinting Inside Dendrimers" *Nature* **2002**, *418*, 399-403.
- [10] Rakow, N. A.; Suslick, K. S. "A Colorimetric Sensor Array for Odour Visualization" *Nature* **2000**, *406*, 710-714.

ABBREVIATED CURRICULUM VITAE

KENNETH S. SUSLICK

Education:

- 1978 Ph. D., Stanford University, *Synthetic Analogs of Myoglobin and Hemoglobin*.
1974 B. S., California Institute of Technology (with Honors).

Research and Professional Positions:

- 1997 – *William H. & Janet Lycan* Professor of Chemistry, University of Illinois at Urbana-Champaign.
2001 – Founder and Chief Technical Officer, ChemSensing, Inc., Northbrook, IL.
1988 – Professor of Chemistry, University of Illinois at Urbana-Champaign.
1993 – Professor of Materials Science and Engineering, University of Illinois at Urbana-Champaign.
1993 – 98 Member, Board of Directors; Ney Ultrasonics Inc.; Bloomfield, Connecticut.
1994 – 98 Member, Scientific Advisory Board, VivoRx Inc.; Santa Monica, California.
1995 – 97 *Alumni Research Scholar* Professor of Chemistry, University of Illinois at Urbana-Champaign.
1989 – 92 Professor, Beckman Institute for Advanced Science and Technology.
1986 Visiting Fellow, Balliol College and Inorganic Chemistry Laboratory, Oxford University.
1984 – 88 Associate Professor, University of Illinois at Urbana-Champaign.
1978 – 84 Assistant Professor, University of Illinois at Urbana-Champaign.
1974 – 78 Research and Teaching Assistant, Stanford University.
1974 – 75 Chemist, Lawrence Livermore Laboratory, Laser Isotope Separation.
1971 – 74 Research and Teaching Assistant, California Institute of Technology.
1972 AEC Research Trainee, Lawrence Berkeley Laboratory.

Selected Honors and Awards:

- 2004 American Chemical Society Senior Cope Scholar Award
2003 J.T. Donald Lecturer, McGill University, Montreal.
2001 Wolfgang Göpel Award, 8th Intl. Symp. on Olfaction & Electronic Noses (ISOEN-8).
2000 1st Place, Illinois Technology Center Inventorship Competition.
1997 University of Melbourne Special Public Lectureship.
1997 W. Heinlen Hall Lectureship, Bowling Green State University.
1994 American Chemical Society Nobel Laureate Signature Award for Graduate Education.
1994 Materials Research Society Medal for Exceptional Recent Achievements in Materials Research.
1992 – Fellow, American Association for the Advancement of Science.
1994 – Fellow, Acoustical Society of America.
1994 Robert A. Welch Foundation Lecturer.
1994 Senior University Scholar, University of Illinois.
1992 – 94 NSF Special Creativity Extension Award.
1993 Excellence in Teaching Award, UIUC School of Chemical Sciences.
1991 – 92 Beckman Associate, UIUC Center for Advanced Study.
1985 – 90 NIH Research Career Development Award.
1985 – 87 Alfred P. Sloan Foundation Research Fellow.
1985 Excellence in Teaching Award, UIUC School of Chemical Sciences.
1979 – 80 DuPont Young Faculty Fellow.
1974 – 78 Silver Medal and Fellow, Royal Society for the Arts, Manufactures, and Commerce (London).
1974 – 78 Hertz Foundation Predoctoral Fellowship.
1973 American Chemical Society Undergraduate Award in Analytical Chemistry.

Personal Data:

b., Chicago, September 16, 1952. Spouse: Adele Mazurek, m. 1975. Son: Benjamin, b. 1992.
Hobbies: Bronze sculpting, folk and Celtic music, ethnographic art

ABBREVIATED CURRICULUM VITAE

Some Recent Special Lectures:

2003

J.T. Donald Lecturer, McGill University, Montreal.
Five College Lecturer (Amherst, Mount Holyoke, Smith, Hampshire and U. Mass. Amherst).

2002

Invited Lecturer, International Symposium on Innovative Materials Processing (IMP2002), Miyagi, Japan.
Invited Lecturer, 16th International Symposium on Nonlinear Acoustics (ISNA-16), Moscow.
Invited Speaker, 9th Intl. Symp. on Olfaction & Electronic Noses (ISOEN-2002), Rome.
Invited Speaker, R.G. Bergman Symposium, University of California, Berkeley.
Invited Speaker, 2nd International Congress on Porphyrins and Phthalocyanines, Kyoto.
Invited Speaker, Chicago Technology Forum 2002.

2001

Plenary Lecturer, EURODEUR-AIRODEUR Conference, Paris.
Invited Speaker, 8th Intl. Symp. on Olfaction & Electronic Noses (ISOEN-8), Washington, D.C.
Plenary Lecturer, 17th Intl. Congress on Acoustics, Rome.
Plenary Lecturer, World Congress on Ultrasonics/IEEE Intl. Ultrasonics Symposium, Atlanta, GA.

2000

Keynote Speaker, Ultrasonics Industry Association Meeting, Columbus.
Invited Speaker and Symposium Organizer, Pacifichem 2000, Honolulu.
Invited Speaker and Symposium Organizer, 1st International Congress on Porphyrins and Phthalocyanines, Dijon.
Invited Speaker, 7th Meeting of the European Sonochemistry Society, Biarritz.
Invited Speaker, Chemistry under Extreme Conditions Symp., ACS Natl. Meeting, Washington, D.C.

1999

Pittsburgh Conference Lectureship, Duquesne University, Pittsburgh.
Invited Speaker, "Unusual Techniques in Inorganic Chemistry," 82nd Canadian Soc. for Chemistry Conf., Toronto.
Invited Speaker, 15th International Symposium on Nonlinear Acoustics, Göttingen.

1998

Director's Colloquium Speaker, Los Alamos National Laboratory.
Invited Speaker, Gordon Research Conference, Chemistry and Biology of Tetrapyrroles.
Invited Lecturer, 6th Meeting of the European Sonochemistry Society, Rostock.
Invited Speaker, Sonochemistry & Sonoluminescence Symposium, Acoustic Soc. Amer. Meeting, Seattle.

Current Major Research Funding:

2000 – 04 NIH 5R01-HL25934 "Heme Proteins, Microspheres, and Their Synthetic Analogs" \$353,992 / yr.
1999 – 03 DARPA; "Chemical Control of Single Bubble Cavitation" \$637,121 / 3.5 yrs.
1999 – 03 NSF; "Chemical Effects of Ultrasound," \$480,000 / 3 yrs.
1997 – 02 DOD; Army MURI, "Dendrimeric Materials," Multi-PI proposal; K.S.S. portion: \$100,000 / yr.
2000 – 02 PG Research Foundation "Ultrasonic Gas Dispersion and Dissolution" \$52,933.
1990 – DOE; UIUC Materials Res. Lab, "Field Responsive Porphyrinic Materials," \$100,000 / yr.

Student and Postdoctoral Associates, Past and Present:

13 Ph.D. Graduate Students presently in group (08/03).
4 Postdoctoral Research Associates presently in group (08/03).
36 Ph.D. Graduate Students supervised and theses completed.
23 Past Postdoctoral Research Associates.
4 M.S. Graduate Students supervised and theses completed.
15 Undergraduate Research Assistants supervised.

MAJOR EQUIPMENT IN THE SUSLICK GROUP

Laboratory Space:

Contiguous labs and offices in the Chemical and Life Sciences Laboratory (dedicated April, 1997):
588 ft² office space;
3500 ft² laboratory space;
17 fume hoods;
224 linear feet of bench space.

Spectroscopic and Photochemical Instrumentation:

Perkin-Elmer 1650 FTIR Spectrometer.
Hitachi 3300 Double Monochromator UV-vis Spectrophotometer with Constant Temperature Cell Housing
Hitachi Diffuse Reflectance Integrating Sphere.
HP 8452A Diode Array UV-vis Spectrophotometer with Constant Temperature Sample Holder.
Matrix Isolation Rig with Leybold-Heraeus Closed Cycle 8K Refrigerator.
Electrochemical Analysis Apparatus, Bioanalytical Systems CV51W.
2 Photochemistry rigs, 300 W Eimac compact Xe arcs with quartz optics and filters.
1 Photochemistry rig, 500 W compact Xe arc.

Chromatographic Equipment:

Hewlett-Packard 6890/5973 Gas Chromatograph / Mass Spectrometer.
Hewlett-Packard 5734A Gas Chromatograph with Dual FID/TCD.
Varian 3770 Capillary Gas Chromatograph with 50m Columns, FID.
Waters 600E Multisolvent HPLC with Waters 996 Diode Array Detector.
Spectrophysics Ternary HPLC with ISCO Spectrophotometric Detector and Fraction Collector.
Chromatotron Centrifugal Preparative Thin Layer Chromatograph.
4 Reporting Integrators (HP 3380A; HP 3394A; Shimadzu CR3A).

Heterogeneous Catalysis Microreactor:

Flow Microreactor for Gas-Solid Heterogeneous Catalysis, interfaced to
Hewlett-Packard 5734A Gas Chromatograph with Dual FID/TCD, with
MKS Mass Flow Controllers,
Digital Baratron Manometer,
High Vacuum Line, Turbomolecular Pump and Penning Gauge, and
Quadrupole Mass Spectrometer Residual Gas Analyzer, Spectra #245-320.

Ultrasonic Equipment:

4 Heat-Systems Ultrasonics 300 to 600W Immersion Ultrasonic Horns
and Power Supplies with High Pressure Cells and Inert Atmosphere Cells.
4 Sonics and Materials 500 - 600W, 20 kHz Immersion Ultrasonic Horns and Power Supplies.
Sonics and Materials 40 kHz Immersion Ultrasonic Horn and Power Supply.
Power Amplifier, AR 700A1, 700 W, 10 kHz-1MHz.
Power Amplifier, ENI AP400B, 400W, 10 kHz-2MHz
2 Function Generators, HP 8904A
Power Piezoceramic Transducers, 20 - 800 kHz.
Magnetostrictive Transducer, 4 kW, manufactured by Russian Academy of Sciences.
Calibrated Hydrophone, Bruel&Kjaer 8103
Measuring Amplifier, Bruel&Kjaer 2525
Needle Hydrophone, Dapco Ind.
Dual Trace Oscilloscope, Hewlett-Packard 33120.
2 Digitizing Oscilloscopes, HP 54111D and 54112D, 100 MHz

MAJOR EQUIPMENT IN THE SUSLICK GROUP

Sonoluminescence Equipment:

Sonoluminescence Rigs:

Princeton Instruments Optical Multichannel Analyzer with CCD Array Detector.
0.5 m Acton Research 505F with 3 grating turret and 0.2 m Thermal-Jarrell Ash Monochromators.
CCD Optical Spectrometer, Jobin Yvon-Spex TR190/CCD3000 system.
Gas Mixing/Mass Flow Controllers, 4-channel readout/power supply, MKS Model 247.

Image station for measurement of bubble dynamics.

Infivar video imaging system (Infinity Photo-optical Company)
Long distance video microscope main body with doubler tube (Infivar KV/CFV-4).
Fiber optic illumination system, 150 W illuminator PL-800.
CCD monochrome camera Sony XC-77 with video capture card/PC interface.

Inert Atmosphere Equipment:

Vacuum Atmospheres Double Length Inert Atmosphere Chamber with O₂ Monitor & MO-40 Dritrain
Vacuum Atmospheres Single Length Inert Atmosphere Chamber with O₂ Monitor, MO-20 Dritrain,
interfaced with internal sonicator and cooling.
12 Dual Argon-Vacuum Manifolds with Airless Glassware.
20 Two-Stage Vacuum Pumps
High Vacuum Line, Diffusion Pump and Penning Gauge.

Particle Sizing and Microscopy Instrumentation:

Optical/Fluorescence Microscope, Zeiss Axioskop with polarization analyzer and fluorescence optics.
Optical Microscope, Inverted Configuration, Olympus CK2 with video imaging system.
Particle Counter and Sizer, Coulter Multisizer IIE, with computer interface.
Particle Sifter, ATM Sonic Sifter with Sieves.

Computers and Graphics Equipment:

4 PC Pentium 450 MHz Microcomputers.
3 PC Pentium 350 MHz Microcomputers.
17 PC Pentium 400 MHz Microcomputers (one per desk).
5 PC Pentium 133 MHz Microcomputers.
3 CD-RW CD Writers.
Silicon Graphics Indigo² Extreme graphics workstation,
R4400 processor, with 8.5 GB Hard Drives, 256 MB RAM, 19" 24-bit color monitor, DAT Tape
Drive, CD-R, Molecular Simulations software suite for molecular modeling.
3 Hewlett-Packard Desk-Jet Color Printers.
6 Hewlett-Packard LaserJet printers.
3 high resolution color scanners.
1 Minolta 7000i Automatic 35 mm Camera with multiple lens.
1 Kodak DC-215 Digital Camera.

Other Laboratory Equipment:

12 Dual Argon-Vacuum Manifolds with Airless Glassware.
20 Two-Stage Vacuum Pumps
High Vacuum Line, Diffusion Pump and Penning Gauge.
6 Refrigerated Constant Temperature Baths; Braun, Fisher.
NANOpure Water Purification System, Bioresearch Grade D4751.
Fisher Marathon 13K Centrifuge.
Vacuum Lyophilizer, 12 Port.
3 Buchi Rotary Evaporators, and 7 Solvent Stills.
4 Mettler Analytical and Sartorius Analytical Top-loading Balances.
5 Laboratory Refrigerators and 1 Laboratory Storage Freezer.
4 Large Laboratory Ovens, including 2 temperature programmable ovens.

PAST RESEARCH GROUP MEMBERS

Chemical Effects of Ultrasound

Oleg Abramov

Professor, Russian Academy of Sciences;
Director of Research, Institute for Inorganic and
General Chemistry.
Visiting Professor, UIUC, 1994.

B.S., University of Scranton, 1997.

Ph.D., UIUC, "Sonochemically Generated
Materials", 2001.

Research Scientist, Bettis National Laboratories.

Dominick J. Casadonte, Jr.

B.Sc., Case Western Reserve Univ., 1980.
Ph.D., Purdue Univ., 1984 (D. McMillin).
Postdoctoral Associate, UIUC, 1984-1986.
Associate Professor, Texas Tech Univ.

Mingming Fang

B.S., M.S., Beijing Univ., 1987-1990.

Ph.D., UIUC, "Catalytic and Magnetic Properties
of Nanostructured Materials Generated by
Ultrasound," 1995.

Staff Scientist, Cabot Corp.

Seok-Burm Choe

B.Sc., Seoul National Univ., Korea.
Ph.D., Kansas State Univ. (K. Klabunde).
Postdoctoral Associate, UIUC, 1987-8.
Professor, Kei-Mgung Univ., Taegu, Korea.

Edward B. Flint

B.Sc., Kenyon College, 1983.

Ph.D., UIUC, "Sonoluminescence," 1989.

Postdoctoral Associate, Professor H. Suhr,
Tubingen, Germany.

Associate Professor, Bradley Univ.

Andrzej A. Cichowlas

Postdoctoral Associate, UIUC, 1991-1994.
Research Scientist, Polish Academy of Sciences.

Mark W. Grinstaff

A.B., Occidental College, 1987.

Ph.D., UIUC, "The Sonochemical Synthesis of
Inorganic and Biological Materials," 1992.

T. S. Piper Thesis Research Prize, UIUC, 1991.

NIH Postdoctoral Fellow, Caltech.

ACS Nobel Laureate Signature Awardee, 1994.

Asst. Prof., Department of Chemistry, Duke Univ.

Gennady Dantsin

B.S., State U. of New York, Binghamton, 1996.
Ph.D., UIUC, "Ultrasound Mediated Synthesis of
Catalytic and Polymeric Materials", 2001.
Research Scientist, Air Products Corp.

Chanchal K. Ghosh

B.Sc., M.S., Univ. of Dhaka, Bangladesh, 1975.

Ph.D., Univ. of Alberta, 1989.

Staff Scientist, Fabric & Hard Surface

Technology, Procter and Gamble Company.

Arul Dhas

B.S., Madurai Kamaraj University, 1988.
Ph.D., Indian Inst. of Science, Bangalore, 1994.
Postdoc. Assoc., Bar-Ilan U., Israel, 1995-1998.
Postdoc., UIUC, 1999-2001.
Research Scientist, Advanced Materials.

Lev Grundel

Ph.D., M.S., Moscow Univ., 1983

Postdoctoral Associate, UIUC, 1991.

Staff Scientist, Great Lakes Analytical, Chicago.

Steven J. Doktycz

B.Sc., UIC, 1984.

Ph.D., UIUC, "Effects of Ultrasound on Solid-
Liquid Reactions," 1989.

T. S. Piper Thesis Research Prize, UIUC, 1989.

Staff Scientist, Dow Chemical Co.

Chief Financial Officer, ANGUS (Dow Corp.).

David A. Hammerton

B.Sc., Southern Connecticut State College, 1981.

Ph.D., UIUC, "The Sonochemical Hot Spot"
1987.

Staff Scientist, Rohm and Haas, Inc.

Technical Manager, UCB Chemicals.

Theodore Dolter

B.Sc., St. Louis Univ.

M.S., Univ. of Illinois.

Science Teacher, Rosary High School, St. Louis.

Arash Ekhtiarzadeh

PAST RESEARCH GROUP MEMBERS

Taeghwan Hyeon

B.S., M.S., Seoul National Univ., 1991.
Ph.D., UIUC, "Nanostructured Catalytic and
Magnetic Materials: Sonochemical Synthesis
and Characterization", 1996.
T. S. Piper Thesis Research Prize, UIUC, 1996.
P.D. Res. Assoc. Northwestern Univ., 1996-97.
Assistant Professor, Seoul Natl. Univ., Korea.

Robert E. Johnson

B.Sc., Univ. of Wisconsin-Milwaukee, 1977.
Ph.D., Univ. of Wisconsin-Madison, 1981 (L.
Dahl).
Postdoctoral Associate, UIUC, 1983-84.
Staff Scientist, HOECHST Celanese Inc.

Kathleen A. (Kemper) House

B.Sc., M.S., Illinois State Univ., 1989.
Ph.D., UIUC, "Sonoluminescence As a Probe of
Cavitation", 1994.
Asst. Professor, Illinois Wesleyan Univ.

Keith S. Kostecka

B.Sc., Illinois Benedictine College, 1982.
M.S., UIUC, 1985.
D.Ed., UIUC at Chicago, 1990.
Associate Professor, Columbia College, Chicago.

Kenneth Kolbeck

B.S., Univ. of New Mexico, 1991.
Ph.D., UIUC, 1999; M.D., UIUC, 2000.
Radiology Resident, College of Medicine,
Dartmouth.

Gregory Kufner

B.S., Illinois Wesleyan, 1995.
Ph.D., UIUC, "Surface Modification of Protein
Microspheres" 2000.
Staff Scientist, Abbott Pharmaceuticals.

William B. McNamara, III

B.S., Univ. of California, Santa Barbara, 1992.
Ph.D., UIUC, "Multi- and Single Bubble
Sonoluminescence," 2002.
Staff Scientist, ChemSensing, Inc.

Millan M. Mdleleni

B.Sc., Univ. of Fort Hare (S. Africa), 1987.
Ph.D., UCSB, 1995.
Postdoctoral Associate, UIUC, 1995-98.
Staff Scientist, Sasol Industries, S.A.

Christian Petrier

Ph.D., Univ. of Grenoble, 1982

Postdoctoral Associate, UIUC, 1988-89
Professor, ESIGEC/Universite de Savoie, France.

Paul F. Schubert

B.Sc., Univ. of Arkansas, 1978.
Ph.D., UIUC, "Sonochemistry of Some Metal
Carbonyl Complexes," 1982.
Group Leader, Catalytica Res. and Development.
Vice-President for Research and Development,
Syntroleum Corp.

Gregory Szewczyk

B.A., Northwestern Univ., 1995.
Ph.D., UIUC, "Disulfide Crosslinking in Protein
Microspheres" 2000.
Staff Scientist, Colgate-Palmolive Corp.

Hau H. Wang

B.Sc., National Tsing Hua Univ., Taiwan, 1975.
Ph.D., Univ. of Minnesota, 1981, (L. Pignolet).
Postdoctoral Associate, UIUC, 1981-83.
Staff Scientist, Argonne National Laboratory.

Mike Wong

B.S., Univ. of Tulsa, 1991.
Ph.D., UIUC, "Sonochemically Produced
Proteinaceous Microspheres," 1996.
Staff Scientist, Colgate-Palmolive, N.J.

PAST RESEARCH GROUP MEMBERS

Bioinorganic Chemistry

- Francis V. Acholla
B.Sc., Univ. of Nairobi, Kenya.
Ph.D., Univ. of Kansas, 1985 (K. B. Mertes).
Postdoctoral Associate, UIUC, 1985-86.
Asst. Professor, Univ. of Nairobi, 1985-91.
Senior Research Chemist, Rohm & Haas.
B.S., National Cheng Kung Univ., Taiwan, 1982.
Ph.D., Michigan State Univ., 1995.
Staff Scientist, Merck Pharmaceuticals.
- Mark D. Ball
B.S., Purdue Univ., 1982.
Ph.D., Iowa State Univ., 1987 (J. A. Olson).
Postdoctoral Associate, UIUC, 1988-90.
Associate Professor, Rose-Hulman Inst. Tech.
- David Benson
B. A., Goshen College, 1990.
Ph.D., UIUC, "New Intermediates of Cytochrome P450" 1997. (with Steve Sligar)
Postdoctoral Associate, Duke Univ.
Asst. Prof., Wayne State Univ.
- Puttaiah Bhyrappa
B.S., M.S., Bangalore Univ., 1986
Ph.D., Indian Inst. of Science, Bangalore, 1991.
Postdoctoral Associate, UIUC, 1994-97.
Assistant Professor, Indian Institute of Technology, Madras.
- Mala Bhyrappa
B.S., M.S., Bangalore Univ., 1991
Ph.D., Indian Inst. of Science, Bangalore, 1996.
Postdoctoral Associate, UIUC, 1997.
- Chin-Ti Chen
B.S., Tamkang Univ., Taiwan, 1978.
M.S., National Taiwan Univ., 1982.
Ph.D., UIUC, "Porphyrins and Metalloporphyrins as Field Responsive Materials," 1992.
Postdoctoral Associate, S. Marder, Caltech.
Research Faculty, Institute of Chemistry, Academia Sinica, Taiwan.
- Homer Chou
B.S. Univ. of Chicago, 1989.
Ph.D., UIUC, "Porphyrins as Second Order Nonlinear Optical Materials," 1995.
T. S. Piper Thesis Research Prize, UIUC, 1995.
Postdoc. Res. Fellow, Northwestern U., 1995-97.
Staff Scientist, Cabot Corporation.
- Richard Jun-Hong Chou
B.S., Hope College, 1981.
Ph.D., UIUC, "Shape Selective Oxidation of Hydrocarbons," 1986.
Staff Scientist, Exxon Corporate Res. & Engin.
- Bruce R. Cook
B.S., Hope College, 1981.
Ph.D., UIUC, "Shape Selective Oxidation of Hydrocarbons," 1986.
Staff Scientist, Exxon Corporate Res. & Engin.
- Daniel R. English
B.S., Ohio State Univ., 1979.
Ph.D., UIUC, "Synth. Fe Porphyrins as Models for Heme Proteins", 1984.
Unit Director, Eastman Kodak Company.
- Mary M. Fox
B.S., Indiana Univ.-Evansville, 1978.
Ph.D., UIUC, "A Bis-Pocket Porphyrin," 1983.
Staff Scientist, Procter & Gamble Corp.
- Philip Gorlin (Joint with Greg Girolami)
B.S., Univ. of Texas at Austin, 1989.
Ph.D., UIUC, "Metalloporphyrin Sandwich Complexes," 1994.
Staff Scientist, Colgate Palmolive Corp.
- Christopher L. Hein
B.S., Univ. of Colorado at Boulder, 1992.
Ph.D., UIUC, "Photosynthetic Reaction Center Analogs", 1997 (with Greg Girolami)
Staff Scientist, G. E. Plastics Corp.
- David Huffman
B.S., M.S., Illinois State Univ., 1988.
Ph.D., UIUC, "Oligopeptide-Heme Complexes," 1993.
NIH Postdoctoral Fellow, T. O'Halloran, Northwestern Univ.
Asst. Prof., Univ. Western Michigan.
- Vijay K. Joshi
B.Sc., Punjab Univ., 1969.
M.Sc., Univ. of Jodhpur, 1971.
Ph.D., SUNY Buffalo, 1987 (J. H. Wang).
Postdoctoral Associate, UIUC, 1987-8.
Staff Scientist, Reheis Chemical Co.
- Warren A. Kaplan
B.S., Brandeis Univ., 1984.

PAST RESEARCH GROUP MEMBERS

- Ph.D., UIUC, "Ligand Binding to Ni Porphyrins and F430," 1989.
Staff Scientist, Shell Corporate Research.
Research Chemist, Stepan Company.
- Michael G. Kinnaird
B.S., Guilford College, 1979. Ph.D., Univ. of North Carolina, 1983 (D. Whitten).
Postdoctoral Associate, Univ. of Kyoto, 1984 (I. Tabushi).
Postdoctoral Associate, UIUC, 1984-86.
Staff Scientist, BASF Chemical Co.
- Stanley N. Milam
B.S., Univ. of Texas at Austin, 1984.
Ph.D., UIUC "Actinide Porphyrin Chemistry," (with G. Girolami), 1989
Staff Scientist, Shell Chemical Co.
- Margaret Kosal
B.S., University of Southern California, 1995.
Ph.D., UIUC, "Porphyrin Network Materials", 2001.
Staff Scientist, Monterey Institute.
- Shirley Nakagaki
Sabbatical Associate, 2003.
Prof., Federal University of Paraná, Brazil.
- Saad N. Nemeah
B.S., Univ. of Applied Chemistry, Syria, 1976.
Ph.D., Univ. of California, Santa Barbara, 1984 (W. Kaska).
Postdoctoral Associate, UIUC, 1984-5.
Staff Scientist, Englehardt Chemical Co.
- Bimal Patel
A.B., Occidental College, 1990.
Ph.D., UIUC, "Porphyrin Liquid Crystals," 1996.
Staff Scientist, G.E. Plastics Corp.
- Alicia Paterno
B.S., Ithaca College, 1996.
Ph.D., UIUC, "Supramolecular Porphyrin Assemblies", 2001.
Visiting Asst. Prof., Duquesne University
- Jennifer Beck Ralph
B.S., Ph.D., Univ. of Queensland, Australia, 1983, 1987.
Postdoctoral Associate, UIUC, 1987-9 (joint with S. G. Sligar).
Research Scientist, Australian National Univ.
- Neal Rakow
B.S., Colorado School of Mines, 1996.
Ph.D., UIUC, "Metalloporphyrin Based Colorimetric Nose: 'Smell-Seeing,'" 2001.
T. S. Piper Thesis Research Prize, UIUC, 2001.
Research Scientist, 3M Corporate R&D Center.
- Thomas J. Reinert
B.S., Iowa State Univ., 1979.
Ph.D., UIUC, "Mechanistic Probes of Heme Proteins" 1987.
Professor, Linfield College, Oregon.
- Michael Rosenblatt
B.S., Towson State Univ., 1992.
Ph.D., UIUC, "Mb Microspheres and Metalloporphyrin-Peptide Complexes" 2000.
Postdoctoral Associate, Univ. of Pennsylvania (W. DeGrado)
- Avijit Sen
B.S., Jadavpur University, Calcutta, 1989.
Ph.D., Indian Inst. of Science, Bangalore, 1998.
Postdoctoral Associate, UIUC, 1998-2001.
Staff Scientist, ChemSensing, Inc.
- Cynthia A. Smith
B.Sc., Kenyon College, 1978.
M.S., UIUC, 1981.
Regulatory Officer, ICI Specialty Chemicals.
- Shawne Van Deusen-Jeffries
A.B., Occidental College, 1987.
M.S., UIUC, 1991.
Research Scientist, Eli Lilly.
Chemist, AMTX Products, XEROX Inc.

PAST RESEARCH GROUP MEMBERS

Jiangyun Wang

B.S., Univ. Science & Tech. of China, 1998.
Ph.D., UIUC, 2003, "De Novo Heme Protein
Design"

Randall A. Watson

B.Sc., Indiana State Univ., 1986.
Ph.D., UIUC, "Photochemistry of Metallo-
porphyrins" 1990.
Staff Scientist, Procter and Gamble Company.

Christopher Ziegler

A.B., Bowdoin College, 1992.
NSF Predoctoral Fellow, 1993-1996.
Ph.D., UIUC, "Ligand Studies of Group 8 Triad
Metalloporphyrins," 1997.
Postdoctoral Associate, MIT, Steve Lippard.
Assistant Professor, Univ. of Akron.

PAST RESEARCH GROUP MEMBERS

Undergraduate Research Assistants

Jocelyn Bautista

B.Sc., UIUC, "Photochemistry of Manganese, Iron, and Chromium Porphyrin Oxoanion Complexes by Matrix Isolation" 1991.
M.D., Washington Univ., St. Louis, 1995.
Resident Doctor, Yale New Haven Hospital.

Ann Burkybile

B.Sc., UIUC, "Synthesis and Characterization of Discotic Macrocyclic Liquid Crystals," 1995.
Graduate Student in Biochemistry, UIUC Fellow.

James Corbett

B.Sc., UIUC, 1982.
Ph.D., Univ. of California, Berkeley, 1987.

Jennifer Cormack

Undergraduate Res. Asst., UIUC, Summer 1993.
B.Sc., California Institute of Technology, 1995.
M.D., UCSF, 2000.

Peter Dorhout

B.Sc., UIUC, 1985.
Ph.D., Univ. of Wisconsin at Madison, 1989.
Postdoctoral Fellow, Iowa State Univ., 1989-91.
Associate Professor, Colorado State Univ.

Joann Eisenhart

B.Sc., UIUC, "Synthesis and Characterization of a "Bis-Pocket" Porphyrin, 1981.
Ph.D., Univ. of Wisconsin at Madison, 1986.
Quality Consultant, Rohm & Haas Company.

Julie Katzenberger

B.Sc., UIUC, "The Synthesis of 5, 10, 15, 20-Tetrakis-(2, 4, 6-Triphenylphenyl) Porphyrin and the Effect of Hydrogen Bonding on FeTPP(1, 2-Me₂ Im)(CO), 1984.
M.S., Colorado State Univ., 1995.

Melissa Lucarelli

B.Sc., UIUC, 1993.
M.D., Univ. of Wisconsin.
Family Practice Resident, St. Mary's Hospital, Milwaukee.

Eugene Mueller

B.Sc., UIUC, "Linkage of Bisporphyrin Complexes to Generate an Eight Coordinate, Chiral Molecule," 1987.
Ph.D., Harvard Univ.
Associate Professor, Univ. of Delaware.

Kristin Musgrave

B.Sc., UIUC, "Special Pair Models: Bisporphyrin-Sandwich Quinone Complexes," 1995.
Graduate Student, Stanford University.

Shannon Nebolsky

B.Sc., UIUC, "A Novel Synthesis of 5, 10, 15, 20-Tetrakis-(2, 4, 6-Triphenylphenyl) Porphyrin: The "Bis-Pocket Porphyrin" 1987
Ph.D., Northwestern Univ., 1995.
J.D., Northwestern Univ., 1996.
Technical Associate, Welsh & Katz, Ltd.

Jennifer Plaszczynski

B.Sc., UIUC, "Polymeric Microspheres," 1994.
Graduate Student in Pharmacy, UIC.

Dimitrii Rassokhin

B.Sc., Moscow Lomonosov State Univ., Dept. of Chemistry, 1983-88.
Non-matriculated Student, UIUC, 1995.
Ph.D., Moscow Lomonosov State Univ., 1996.

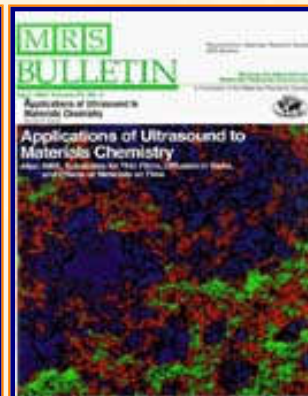
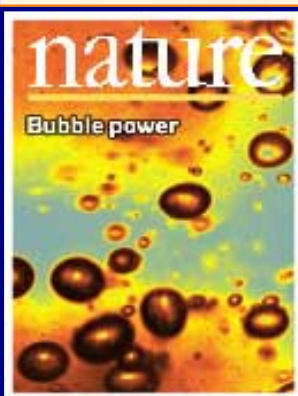
Nicole Stewart

B.Sc., UIUC, 2003

Anita Yu

B.Sc., UIUC, "The Synthesis, Characterization and Photochemistry of Oxo(5, 10, 15, 20-Tetraphenylporphyrinato)Chromium (IV), 1989.
Ph.D., Univ. of Wisconsin at Madison, 1986.
Assistant Professor, Department of Chemistry, Univ. of Wisconsin, Eau Claire.

The Suslick Research Group



[Overview](#)

[Outline of
Research Projects](#)

[Introduction to
Sonochemistry](#)

[Exec. Summary:
Sonochemistry](#)

[Exec. Summary:
Porphyrin Research](#)

[Exec. Summary: Smell-
Seeing](#)

[Complete
Publication List](#)

[Abbreviated Curriculum
Vitae](#)

[Academic
Genealogy](#)

[Press
Clippings](#)

PUBLICATION LIST:

[Books](#)

[Major Reviews](#)

[Popularizations](#)

[Patents](#)

[Journal Articles](#)

(chronological for each publication type)

**To download the full article in PDF format,
click on the highlighted references below**

[To get the free Adobe PDF reader, click on this text.](#)

[For a PDF file of Professor Suslick's
complete Curriculum Vitae, click on this text.](#)

Books:

1. Suslick, K. S., ed. *High Energy Processes in Organometallic Chemistry*, ACS Symposium Series #333: Washington, DC, 1987.
2. Suslick, K. S., ed. *Ultrasound: Its Chemical, Physical, and Biological Effects*; VCH Publishers: New York, 1988.
3. Suslick, K. S., ed. *Comprehensive Supramolecular Chemistry, vol. 5, Bioinorganic Systems*; Elsevier Publishers: Oxford, 1996.
4. Crum, L. A.; Mason, T. J.; Reisse, J.; Suslick, K. S., eds. *Sonochemistry and Sonoluminescence*, Kluwer Publishers: Dordrecht, Netherlands, 1999; NATO ASI Series C, v. 524.

[Current Research
Funding](#)

[Excerpts from
Funded Research](#)

[Inventory of
Group Equipment](#)

[Information
for Visiting](#)

[Current Research Group
Members](#)

[Group
Meetings](#)

[Group
Chores](#)

[Past Research
Group Members](#)

[Group
Photogallery](#)

[Web Resources](#)

[Laboratory Safety
Resources](#)

[Art and Science:
Journal Covers](#)

[Sculpture &
Masks](#)

[A Chemist
Meets Hollywood](#)

[Chymistes: The Distillers
of Waters](#)

[A Chemist
In Court](#)

Major Reviews:

- Collman, J. P.; Halbert, T. R.; Suslick, K. S. "O₂ Binding by Metalloporphyrins," in *Metal Ion Activation of Dioxygen*; Spiro, T. G., ed.; Prentice-Hall: New York, 1980; pp. 1-72.
- Suslick, K. S.; Reinert, T. J. "Synthetic Analogs of O₂ Binding Heme Proteins," *J. Chem. Ed. "State of the Art: Bioinorganic Chemistry" issue*, **1985**, *62*, 974-982.
- Suslick, K. S. "Organometallic Sonochemistry," *Adv. Organomet. Chem.* **1986**, *25*, 73-119.
- Suslick, K. S. "Synthetic Applications of Ultrasound," *Modern Synthetic Methods* **1986**, *4*, 1-60.
- Suslick, K. S. "Homogeneous Sonochemistry" in *Ultrasound: Its Chemical, Physical and Biological Effects*; Suslick, K. S., ed.; VCH Publishers: New York, 1988; pp. 123-164.
- Suslick, K. S. "Shape Selective Hydrocarbon Oxidation" in *Activation and Functionalization of Alkanes*; Hill, C. L., ed.; Wiley & Sons: New York, 1989; pp. 219-241.
- Suslick, K. S.; Cook, B. R. "Shape Selective Oxidation as a Mechanistic Probe," in *Inclusion Phenomena and Molecular Recognition*; Atwood, J. L., ed.; Plenum Press: London, 1990; pp. 209-215.
- Suslick, K. S.; Doktycz, S. J. "The Effects of Ultrasound on Solids" in *Advances in Sonochemistry*; Mason, T. J., Ed.; JAI Press: New York, 1990; vol.1, pp 197-230.
- Suslick, K. S. "Sonochemistry," [*Science*, **1990**, *247*, 1439-45.](#)
- Suslick, K. S.; Watson, R. A. "The Photochemistry of Chromium, Manganese, and Iron Porphyrin Complexes," [*New J. Chem.* **1992**, *16*, 633-642.](#)
- Suslick, K. S.; Grinstaff, M. W. "Proteinaceous Microspheres," *Macromolecular Assemblies*; Stroeve, P.; Balazs, A. C., eds.; Am. Chem. Soc.: Washington, D.C., 1992; pp. 218-226.
- Suslick, K. S. "Ultrasound: Applications to Materials Chemistry," in *Encyclopedia of Materials Science and Engineering*; Cahn, R. W., ed.; Pergamon Press: Oxford, 1993; 3rd Suppl., pp. 2093-2098.
- Chen, C.-T.; Suslick, K. S. "One-Dimensional Coordination Polymers," *Coord. Chem. Rev.*, **1993**, *128*, 293-322.
- Suslick, K. S. "Sonochemistry of Transition Metal Compounds," in *Encyclopedia of Inorganic Chemistry*; King, R. B., ed.; J. Wiley & Sons: New York, 1994; vol. 7, pp. 3890-3905.
- Suslick, K. S. "Applications of Ultrasound to Heterogeneous Catalysis," *Advances in Catalyst Preparation*; Catalytica Studies Division; 1995.
- Suslick, K. S. "Applications of Ultrasound to Materials Chemistry," [*MRS Bulletin* **1995**, *20*, 29-34.](#)
- Suslick, K. S.; Van Deusen-Jeffries, S. "Shape Selective Biomimetic Oxidation Catalysis" *Comprehensive Supramolecular Chemistry*, vol. 5; Lehn, J. M., ed. Elsevier Publishers: Oxford, 1996; pp. 141-170.
- Suslick, K. S.; Crum, L. A. "Sonochemistry and Sonoluminescence," in

[Humor and
Wisdom](#)

[Laws of the Universe](#)

[Cartoons of Humor and
Wisdom](#)

[Chem 115: Chemistry of
Everyday Phenomena](#)

[Chem 315: Inorganic
Chemistry](#)

- Encyclopedia of Acoustics*; Crocker, M. J., ed.; Wiley-Interscience: New York, 1997; vol. 1, ch. 26, pp. 271-282.
23. Suslick, K. S. "Sonocatalysis," in [Handbook of Heterogeneous Catalysis](#); Ertl, G.; Knozinger, H.; Weitkamp, J.; eds.; Wiley-VCH: Weinheim, 1997; vol. 3, ch. 8.6, pp. 1350-1357.
 24. Suslick, K. S. "Sonoluminescence and Sonochemistry," *IEEE Ultrasonics Symp. Proc.* **1997**, v. 1, pp. 523-534.
 25. Suslick, K. S.; Crum, L. A. "Sonochemistry and Sonoluminescence," in *Handbook of Acoustics*; Crocker, M. J., ed.; Wiley-Interscience: New York, 1998; pp. 243-253.
 26. Suslick, K. S.; Didenko, Y.; Fang, M. M.; Hyeon, T.; Kolbeck, K. J.; McNamara, W. B. III; Mdeleleni, M. M.; Wong, M. "Acoustic Cavitation and Its Chemical Consequences" *Phil. Trans. Roy. Soc. A*, **1999**, *357*, 335-353.
 27. Suslick, K. S.; Matula, T. J. "Acoustic Cavitation, Sonochemistry, and Sonoluminescence," in *Encyclopedia of Electrical and Electronics Engineering*; Webster, J. G., ed.; Wiley-Interscience: New York, 1998.
 28. Chou, J.-H.; Kosal, M. E.; Nalwa, H.S.; Rakow, N.A.; Suslick, K. S. "[Applications of Porphyrins and Metalloporphyrins to Materials Chemistry](#)" in *The Porphyrin Handbook*, Kadish, K.; Smith, K.; Guillard, R., ed.; Academic Press: New York, 2000; vol. 6, ch. 41, pp. 43-131.
([This PDF file is without figures; for figures in html format, click here](#))
 29. Suslick, K. S. "[Shape Selective Oxidation by Metalloporphyrins](#)," in *The Porphyrin Handbook*, Kadish, K.; Smith, K.; Guillard, R., ed.; Academic Press: New York, 2000; vol. 4, ch. 28, pp. 41-63.
 30. Suslick, K. S.; Price, G. "Applications of Ultrasound to Materials Chemistry" *Annu. Rev. Matl. Sci.*, **1999**, *29*, 295-326.
 31. Suslick, K. S. "Sonochemistry: A Physical Perspective" in *Nonlinear Acoustics at the Turn of the Millennium*, Lauterborn, W.; Kurz, T., eds. Amer. Inst. Physics: Melville, NY, 2000, pp. 95-104.

Popularizations:

32. Suslick, K. S. "Sonochemistry and Sonocatalysis," in *1988 McGraw-Hill Yearbook of Science and Technology*, McGraw-Hill: New York, 1987, pp 430-433.
33. Suslick, K. S. "The Chemical Effects of Ultrasound," [Scientific American](#) **1989 (2)** *260*, 80-86. (color figures, but reduced in size; large file, 1MB)
34. Suslick, K. S. "Sounding Out New Chemistry," *New Scientist* **1990**, *1702*, 50-53.
35. Suslick, K. S. "Cavitation" and "Sonochemistry," in *McGraw-Hill Encyclopedia of Science and Technology*, McGraw-Hill: New York; 7th Ed., 1992, pp. 320, pp. 683-685; 8th Ed., 1997, pp. 744-747.
36. Suslick, K. S. "Sonochemistry," in *McGraw-Hill Encyclopedia of Chemistry*; McGraw-Hill: New York, 2nd Ed., 1992, pp. 1021-1023.
37. Suslick, K. S. "The Chemistry of Ultrasound," in [Encyclopaedia Britannica Yearbook of Science and the Future 1994](#),

[Britannica: Chicago; 1994; pp. 138-155.](#)

38. Crum, L. A.; Suslick, K. S. "Bubbles Hotter than the Sun," *New Scientist* **1995**, *146* (#1975), 36-40.
39. Suslick, K. S. "Set for a 'Chain Reaction'" [Hollywood, Suslick Research Group Chemistry University of Illinois](#) *Inside Illinois* **1997**, *16* (#17), 5.
40. Suslick, K. S. "Sonoluminescence, Camera, Action!" [Engineering & Science \(California Institute of Technology\)](#) **1997** *40* (#2), 4-5.
41. Suslick, K. S. "Sonochemistry," in *1999 McGraw-Hill Yearbook of Science and Technology*; McGraw-Hill: New York, 1998.
42. Suslick, K. S. "Sonochemistry," in [Kirk-Othmer Encyclopedia of Chemical Technology](#), 4th Ed., J. Wiley & Sons: New York, 1998, vol. 26, 517-541.
43. Suslick, K. S. "Sonochemistry," in *McGraw-Hill Encyclopedia of Science and Technology*; McGraw-Hill: New York; 9th Ed., 1999.
44. Suslick, K. S. "UI Chemist Meets the Federal District Court" [Inside Illinois](#) **1999**, *18* (#19), 7.
45. Suslick, K. S. "[Sonochemistry and Sonoluminescence](#)" in *Encyclopedia of Physical Science and Technology*, 3rd ed. Academic Press: San Diego, 2001, vol. 17, pp. 363-376.

Patents:

46. Suslick, K. S. "Isotope Separation by Photochromatography," [U.S. Patent 4,010,100; March 1, 1977.](#)
47. Desai, N. P.; Soon-Shiong, P.; Sandford, P. A.; Grinstaff, M. W.; Suslick, K. S. "Magnetic Resonance Imaging with Fluorocarbons Encapsulated in a Cross-linked Polymeric Shell," [U. S. Patent 5,362,478; Nov. 8, 1994.](#)
48. Desai, N. P.; Soon-Shiong, P.; Sandford, P. A.; Grinstaff, M. W.; Suslick, K. S. "Methods for *In Vivo* Delivery of Substantially Water Insoluble Pharmacologically Active Agents and Compositions Useful Therefor," [U. S. Patent 5,439,686; Aug. 8, 1995.](#)
49. Grinstaff, M. W.; Soon-Shiong, P.; Wong, M.; Sandford, P. A.; Suslick, K. S.; Desai, N. P. "Composition Useful for *In Vivo* Delivery of Biologics and Methods Employing Same," [U. S. Patent 5,498,421; Mar. 12, 1996.](#)
50. Grinstaff, M. W.; Desai, N. P.; Suslick, K. S.; Soon-Shiong, P.; Sandford, P. A.; Merideth, N. R. "Method for the Preparation of Fluorocarbon-Containing Polymeric Shells for Medical Imaging," [U. S. Patent 5,505,932; Apr. 9, 1996.](#)
51. Grinstaff, M. W.; Desai, N. P.; Suslick, K. S.; Soon-Shiong, P.; Sandford, P. A.; Merideth, N. R. "Non-Fluorinated Polymeric Shells for Medical Imaging," [U. S. Patent 5,508,021; Apr. 16, 1996.](#)
52. Grinstaff, M. W.; Desai, N. P.; Suslick, K. S.; Soon-Shiong, P.; Sandford, P. A.; Merideth, N. R. "Polymeric Shells for Medical Imaging Prepared from Synthetic Polymers, and Methods for the Use Thereof" [U. S. Patent 5,512,268; Apr. 30, 1996.](#)
53. Desai, N. P.; Soon-Shiong, P.; Sandford, P. A.; Grinstaff, M. W.; Suslick, K. S.; "Methods for *In Vivo* Delivery of Substantially Water Insoluble

- Pharmacologically Active Agents and Compositions for the Use Thereof" [U. S. Patent 5,560,933; Oct. 1, 1996.](#)
54. Grinstaff, M. W.; Soon-Shiong, P.; Wong, M.; Sandford, P. A.; Suslick, K. S.; Desai, N. P. "Methods for the Preparation of Blood Substitutes for *In Vivo* Delivery," [U. S. Patent 5,635,207; June 3, 1997.](#)
 55. Grinstaff, M. W.; Soon-Shiong, P.; Wong, M.; Sandford, P. A.; Suslick, K. S.; Desai, N. P. "Methods For The Preparation Of Nucleic Acids For *In Vivo* Delivery" [U. S. Patent 5,639,473; June 17, 1997.](#)
 56. Grinstaff, M. W.; Soon-Shiong, P.; Wong, M.; Sandford, P. A.; Suslick, K. S.; Desai, N. P. "Methods For *In Vivo* Delivery Of Nutraceuticals And Compositions Useful Therefor" [U. S. Patent 5,650,156; July 22, 1997.](#)
 57. Grinstaff, M. W.; Soon-Shiong, P.; Wong, M.; Sandford, P. A.; Suslick, K. S.; Desai, N. P. "Methods for the Preparation of Pharmaceutically Active Agents for *In Vivo* Delivery," [U. S. Patent 5,665,382; Sept. 9, 1997.](#)
 58. Grinstaff, M. W.; Soon-Shiong, P.; Wong, M.; Sandford, P. A.; Suslick, K. S.; Desai, N. P. "Methods for the Preparation of Immunostimulating Agents for *In Vivo* Delivery," [U. S. Patent 5,665,383; Sept. 9, 1997.](#)
 59. Suslick, K. S.; Rakow, N. A. "Colorimetric Artificial Nose Having an Array of Dyes and Method for Artificial Olfaction" [U.S. Patent 6,368,558; April 9, 2002.](#)
 60. Suslick, K. S.; Rakow, N. A.; Sen, A. "Colorimetric Artificial Nose Having an Array of Dyes and Method for Artificial Olfaction: Shape Selective Sensors" [U.S. Patent 6,495,102 B1; Dec. 17, 2002.](#)

Journal Articles:

61. Collman, J. P.; Brauman, J. I.; Suslick, K. S. "Oxygen Binding to Iron Porphyrins," [J. Am. Chem. Soc. 1975, 97, 7185-7186.](#)
62. Collman, J. P.; Brauman, J. I.; Halbert, T. R.; Suslick, K. S. "Nature of Oxygen and Carbon Monoxide Binding to Metalloporphyrins and Heme Proteins," [Proc. Natl. Acad. Sci., U.S.A. 1976, 73, 3333-3337.](#)
63. Collman, J. P.; Suslick, K. S. "Models for Cooperative Oxygen Binding in Hemoglobin," [Pure and Applied Chemistry 1978, 50, 951-961.](#)
64. Collman, J. P.; Brauman, J. I.; Doxsee, K. M.; Halbert, T. R.; Hayes, S. E.; Suslick, K. S. "Oxygen Binding to Cobalt Porphyrins," [J. Am. Chem. Soc. 1978, 100, 2761-2766.](#)
65. Collman, J. P.; Brauman, J. I.; Doxsee, K. M.; Halbert, T. R.; Suslick, K. S. "Model Compounds for the 'T' State of Hemoglobin," [Proc. Natl. Acad. Sci., U.S.A. 1978, 75, 564-568.](#)
66. Collman, J. P.; Brauman, J. I.; Rose, E.; Suslick, K. S. "Cooperativity in Oxygen Binding to Iron Porphyrins," [Proc. Natl. Acad. Sci., U.S.A. 1978, 75, 1052-1055.](#)
67. Jameson, G. B.; Molinaro, F. S.; Ibers, J. A.; Collman, J. P.; Brauman, J. I.; Rose, E.; Suslick, K. S. "Structural Changes Upon Oxygenation of an Fe(II) (porphyrinato)(imidazole) Complex," [J. Am. Chem. Soc. 1978, 100, 6769-](#)

[6770.](#)

68. 70. Jameson, G. B.; Molinaro, F. S.; Ibers, J. A.; Collman, J. P.; Brauman, J. I.; Rose, E.; Suslick, K. S. "Models for the Active Site of Oxygen Binding Hemoproteins. Dioxygen Binding Properties and the Structures of (2-Methylimidazole)-meso-tetra(o-pivalamidophenyl)porphyrinatoiron(II)-Ethanol and Its Dioxygen Adduct." *J. Am. Chem. Soc.* **1980**, *102*, 3224-3237.
69. Walters, M. A.; Spiro, T. G.; Collman, J. P.; Suslick, K. S. "Resonance Raman of O₂ Bound to Fe(II)(porphyrinato)(hindered-imidazole) Complexes," *J. Am. Chem. Soc.* **1980**, *102*, 6857-6858.
70. Suslick, K. S.; Schubert, P. F.; Goodale, J. W. "Sonochemistry and Sonocatalysis of Iron Carbonyls," *J. Am. Chem. Soc.* **1981**, *103*, 7342-7344.
71. Suslick, K. S.; Schubert, P. F.; Goodale, J. W. "Chemical Dosimetry of Ultrasonic Cavitation," *IEEE Ultrason. Symp. Proc.* **1981**, *2*, 612-616.
72. Suslick, K. S.; Fox, M. M. "A Bis-Pocket Porphyrin," *J. Am. Chem. Soc.* **1983**, *105*, 3507-3510.
73. Suslick, K. S.; Goodale, J. W.; Wang, H. H.; Schubert, P. F. "Sonochemistry and Sonocatalysis of Metal Carbonyls," *J. Am. Chem. Soc.* **1983**, *105*, 5781-5785.
74. Suslick, K. S.; Schubert, P. F. "Sonochemistry of Mn₂(CO)₁₀ and Re₂(CO)₁₀," *J. Am. Chem. Soc.* **1983**, *105*, 6042-6044.
75. Suslick, K. S.; Schubert, P. F.; Wang, H. H.; Goodale, J. W. "Organometallic Sonochemistry and Sonocatalysis," in *Inorganic Chemistry: Toward the 21st Century*; Chisholm, M. A., ed.; American Chemical Society: Washington, D.C., **1983**; p. 550.
76. English, D. R.; Hendrickson, D. N.; Suslick, K. S. "Mössbauer Spectra of Oxidized Iron Porphyrin Dimers," *Inorg. Chem.* **1983**, *22*, 367-368.
77. Suslick, K. S.; Gawienowski, J. W.; Schubert, P. F.; Wang, H. H. "Alkane Sonochemistry," *J. Phys. Chem.* **1983**, *87*, 2299-2301.
78. Suslick, K. S.; Fox, M. M.; Cook, B. R.; English, D. R. "New Synthetic Analogs of Heme Proteins," *Inorg. Chem. Acta* **1983**, *79(B7)*, 109-110.
79. Suslick, K. S.; Gawienowski, J. W.; Schubert, P. F.; Wang, H. H. "Sonochemistry in Non-aqueous Liquids," *Ultrasonics* **1984**, *22*, 33-36.
80. Bocian, D. F.; Finsden, E. W.; Hoffman, J. A.; Schick, G. A.; English, D. R.; Hendrickson, D. N.; Suslick, K. S. "Interaction of Dioxygen and Binuclear Nitride-Bridged Iron Porphyrins," *Inorg. Chem.* **1984**, *23*, 800-807.
81. Suslick, K. S.; English, D. R.; Hendrickson, D. N.; Spiro, T. G.; Crisanti, M. "Resonance Raman Spectra of High Oxidation State Iron Porphyrin Dimers," *Inorg. Chem.* **1984**, *23*, 3897-3901.
82. Suslick, K. S.; Fox, M. M.; Reinert, T. J. "Influence on CO and O₂ Binding by Fe(II) Porphyrinates," *J. Am. Chem. Soc.* **1984**, *106*, 4522-4525.
83. Finke, R. G.; Droege, M. W.; Cook, J. C.; Suslick, K. S. "Fast Atom Bombardment Mass Spectroscopy (FABMS) of Polyoxoanions," *J. Am. Chem. Soc.* **1984**, *106*, 5750-5751.
84. Suslick, K. S.; Johnson, R. E. "Sonochemical Activation of Transition Metals," *J. Am. Chem. Soc.* **1984**, *106*, 6856-6858.

85. English, D. R.; Hendrickson, D. N.; Suslick, K. S.; Eigenbrot, Jr., C. W.; Scheidt, W. R. "A Low-Spin Five-Coordinate Ferric Porphyrin Complex: [5,10,15,20-tetra(4-methoxyphenyl)- porphyrinato](hydrosulfido)iron(III)," [*J. Am. Chem. Soc.* **1984**, *106*, 7258-7259.](#)
86. Suslick, K. S.; Cook, B. R.; Fox, M. M. "Shape Selective Hydroxylation of Hydrocarbons," [*J. Chem. Soc., Chem. Commun.* **1985**, 580-582.](#)
87. Woolery, G.; Walter, M. A.; Suslick, K. S.; Powers, J.; Spiro, T. G. "EXAFS Evidence for Elongated Fe-O₂ Bond Lengths in O₂ Adducts of "Picket-Fence" Hemes: Implications of Hb Cooperativity," [*J. Am. Chem. Soc.* **1985**, *107*, 2370-2372.](#)
88. Suslick, K. S.; Cline, Jr., R. E.; Hammerton, D. A. "Determination of Local Temperatures Caused by Acoustic Cavitation," *IEEE Ultrasonics Symp. Proc.* **1985**, *4*, 1116-1121
89. Suslick, K. S.; Hammerton, D. A. "The Site and Nature of Sonochemical Reactions," *Ultrasonics Intl.* **1985**, 231-236.
90. Suslick, K. S. "A Non-Coercive, Menu-Driven Grading System," *J. Chem. Ed.* **1985**, *61*, 408-409.
91. English, D. R.; Hendrickson, D. N.; Suslick, K. S. "(FeTPP)₂N²⁺: an Fe(IV)-Porphyrin π -Radical Cation," [*Inorg. Chem.* **1985**, *24*, 121-122.](#)
92. Suslick, K. S.; Hammerton, D. A. "The Site of Sonochemical Reactions," *IEEE Trans. Ultrasonics, Ferroelec., Freq. Contr.* **1986**, *33*, 143-147.
93. Finke, R. G.; Droege, M. W.; Cook, J. C.; Suslick, K. S. "Fast Atom Bombardment Mass Spectrometry (FABMS) of Large Clusters," [*Inorg. Chem.* **1986**, *25*, 241-243.](#)
94. Suslick, K. S.; Cline, Jr., R. E.; Hammerton, D. A. "The Sonochemical Hot Spot," [*J. Am. Chem. Soc.* **1986**, *108*, 5641-5642.](#)
95. Cook, B. R.; Reinert, T. J.; Suslick, K. S. "Shape Selective Alkane Hydroxylation by Metalloporphyrin Catalysts," [*J. Am. Chem. Soc.* **1986**, *108*, 7281-7286.](#)
96. Suslick, K. S.; Casadonte, D. J.; Green, M. L. H.; Thompson, M. E. "Effects of High Intensity Ultrasound on Inorganic Solids" *Ultrasonics* **1987**, *25*, 56-59.
97. Suslick, K. S.; Cook, B. R. "Regioselective Epoxidations of Dienes with Manganese(III) Porphyrin Catalysts" [*J. Chem. Soc., Chem. Comm.* **1987**, 200-202.](#)
98. Hendrickson, D. N.; Kinnaird, M. G.; Suslick, K. S. "Photochemistry of (5,10,15,20-Tetraphenyl- porphyrinato)iron(III) Halide Complexes, Fe(TPP)(X)" [*J. Am. Chem. Soc.* **1987**, *109*, 1243-1244.](#)
99. Suslick, K. S.; Acholla, F. V.; Cook, B. R. "Photocatalytic Oxidation of Hydrocarbons by (5,10,15,20-Tetraphenylporphyrinato)manganese(III) Perchlorate and Periodate" [*J. Am. Chem. Soc.* **1987**, *109*, 2818-2819.](#)
100. Suslick, K. S.; Casadonte, D. J. "Heterogeneous Sonocatalysis with Nickel Powder" [*J. Am. Chem. Soc.* **1987**, *109*, 3459-3461.](#)
101. Girolami, G. S.; Milam, S. N.; Suslick, K. S. "Synthesis and Characterization of Actinide Mono- and Bis(porphyrin) Complexes" [*Inorg. Chem.* **1987**, *26*, 343-344.](#)
102. Suslick, K. S.; Flint, E. B.; Jensen, J. A. "A Kinetics FT-IR Experiment for

- the Undergraduate Laboratory," *J. Chem. Ed.* **1987**, *64*, 547-549.
103. Chatakondur, K.; Green, M. L. H.; Thompson, M. E.; Suslick, K. S. "The Enhancement of Intercalation Reactions by Ultrasound" *J. Chem. Soc., Chem. Comm.* **1987**, 900-901.
 104. Suslick, K. S. "The Sonochemistry of Organometallic Compounds" in *High Energy Processes in Organometallic Chemistry*, Suslick, K. S., ed.; ACS Symp. Series #333: Washington, D.C., 1987; pp. 191-208.
 105. Suslick, K. S.; Acholla, F. V.; Cook, B. R.; Kinnaird, M. G. "Photochemistry of Fe(III) and Mn(III) Porphyrins," *Recl. Trav. Chim.* **1987**, *106*, 329.
 106. Suslick, K. S. "Porphyrins: Excited States and Dynamics,' bk. rev." *J. Med. Chem.* **1987**, *30*, 1702.
 107. Suslick, K. S.; Flint, E. B. "A Versatile Sonochemical Reaction Vessel," in *Experimental Organometallic Chemistry: A Practicum in Synthesis and Characterization*; Wayda, A. and Darensbourg, M.Y., eds.; ACS Symposium Series: Washington, D.C.; 1987, p. 195.
 108. Suslick, K. S.; Flint, E. B. "Sonoluminescence of Non-Aqueous Liquids," *Nature* **1987**, *330*, 553-555.
 109. Girolami, G. S.; Milam, S. N.; Suslick, K. S. "Actinide Bis(porphyrinate) π -Radical Cations and Dications, including X-ray Crystal Structure of [(TPP)₂Th][SbCl₆]" *J. Am. Chem. Soc.* **1988**, *110*, 2011-2012.
 110. Suslick, K. S. "The Production of High Energy Species by Turbulent Flow," *Nature* **1988**, *334*, 375.
 111. Suslick, K. S.; Casadonte, D. J.; Doktycz, S. J. "The Effects of Ultrasound on Nickel and Copper Powders," *Solid State Ionics.* **1989**, *32/33*, 444-452.
 112. Suslick, K. S. "Chemistry and Biochemistry of N-substituted Porphyrins' bk. rev." *Med. Chem.* **1989**, *32*, 1410.
 113. Suslick, K. S.; Doktycz, S. J. "Ultrasonic Irradiation of Copper Powder," *Chem. Materials* **1989**, *1(1)*, 6-8.
 114. Suslick, K. S.; Doktycz, S. J. "The Sonochemistry of Zinc," *J. Am. Chem. Soc.* **1989**, *111*, 2342-2344.
 115. Flint, E. B. ; Suslick, K. S. "Sonoluminescence from Nonaqueous Liquids: Emissions from Small Molecules" *J. Am. Chem. Soc.* **1989**, *111*, 6987-6992.
 116. Kaplan, W. A.; Scott, R. A.; Suslick, K. S. "Probing Macrocyclic Flexibility: Ligand Binding to Zn and Ni Tetraphenylhydroporphyrins" *J. Am. Chem. Soc.* **1990**, *112*, 1283-1285.
 117. Doktycz, S. J.; Suslick, K. S. "Interparticle Collisions Driven by Ultrasound," *Science*, **1990**, *247* 1067-1069.
 118. Suslick, K. S.; Doktycz, S. J.; Flint, E. B. "On The Origins of Sonochemistry and Sonoluminescence," *Ultrasonics* **1990**, *28*, 280-290.
 119. Suslick, K. S.; Watson, R. A. "Photochemical Oxygen Atom Transfer by Metalloporphyrins," *Proc. Symp. O₂ Activation in Catalysis; Prepr. Am. Chem. Soc. Div. Pet. Chem.* **1990**, *35*, 169.
 120. Bilsel, O.; Rodriguez, J.; Holten, D.; Girolami, G. S.; Milam, S. N.; Suslick, K. S. "A New Low-Energy Fluorescent Excited State in Strongly-Coupled Porphyrin Dimers" *J. Am. Chem. Soc.* **1990**, *112*, 4075-4077.
 121. Davies, M. D.; Qin, L.; Beck, J. L.; Suslick, K. S.; Koga, H.; Horiuchi, T.; Sligar, S. G. "Putidaredoxin Reduction of Cytochrome P-450_{cam}:"

- Dependence of Electron Transfer on the Identity of Putidaredoxin's C-terminal Amino Acid" *J. Am. Chem. Soc.* **1990**, *112*, 7396-7398.
122. Suslick, K. S.; Grinstaff, M. W. "Protein Microencapsulation of Nonaqueous Liquids" *J. Am. Chem. Soc.* **1990**, *112*, 7807-7809.
123. Suslick, K. S.; Chen, C.-T. "Polymeric Metalloporphyrins for Field Responsive Materials," *Polym. Mater. Sci. Eng.* **1990**, *63*, 272-278.
124. Suslick, K. S.; Casadonte, D. J.; Choe, S. B.; Cichowlas, A. A.; Dokytcz, S. J.; Ghosh, C. K.; Grinstaff, M.W. "Heterogeneous Sonochemistry and Sonocatalysis," *Materials Research Society Proceedings: Synthesis and Properties of New Catalysts* **1990**, EA-24, 209-212.
125. Suslick, K. S.; Flint, E. B. "Sonoluminescence of Alkali Metal Salts," *J. Phys. Chem.* **1991**, *95*, 1484-1488.
126. Kaplan, W. A.; Suslick, K. S.; Scott, R. A. "Core Size and Flexibility of Metallohydroporphyrin Macrocycles. Implications for F₄₃₀ Coordination Chemistry," *J. Am. Chem. Soc.* **1991**, *113*, 9824-9827.
127. Suslick, K. S.; Watson, R. A.; Wilson, S. R. "The Structures and Photochemistry of Metalloporphyrin Sulfate Complexes," *Inorg. Chem.* **1991**, *30*, 2311-2317.
128. Cho, S. I.; Girolami, G. S.; Gorlin, P.; Kim, H.-J.; Kim, K.; Lee, W. S.; Suslick, K.S. "Synthesis and Structure of Transition Metal Bis(porphyrinato) Complexes. Characterization of Zr(TPP)₂ and Zr(OEP)₂" *Inorg. Chem.* **1991**, *30*, 2652-56.
129. Grinstaff, M.W; Suslick, K.S. "Nonaqueous Liquid Filled Microcapsules" *Polym. Prepr.* **1991**, *32*, 255-256.
130. Suslick, K. S.; Watson, R. A. "Photochemical Nitrate and Nitrite Reduction by Mn and Fe Porphyrins," *Inorg. Chem.* **1991**, *30*, 912-919.
131. Suslick, K. S.; Bautista, J. F.; Watson, R. A. "Metalloporphyrin Photochemistry with Matrix Isolation," *J. Am. Chem. Soc.* **1991**, *113*, 6111-6114.
132. Suslick, K. S.; Grinstaff, M. W. "Proteinaceous Microbubbles: Synthesis of an Echo Contrast Agent," *Proc. Natl. Acad. Sci. USA* **1991**, *88*, 7708-7710.
133. Flint, E. B.; Suslick, K. S. "The Temperature of Cavitation," *Science* **1991**, *253*, 1397-1399.
134. Suslick, K. S.; Choe, S. B.; Cichowlas, A. A.; Grinstaff, M. W. "Sonochemical Synthesis of Amorphous Iron," *Nature* **1991**, *353*, 414-416.
135. Jeffries, J. B.; Copeland, R. A.; Flint, E. B.; Suslick, K. S. "Thermal Equilibration During Cavitation," *Science* **1992**, *256*, 248.
136. Grinstaff, M. W.; Cichowlas, A. A.; Choe, S. B.; Suslick, K. S. "Effect of Cavitation Conditions on Amorphous Metal Synthesis," *Ultrasonics* **1992**, *30*, 168-172.
137. Suslick, K. S.; Chen, C.-T.; Meredith, G. R.; Cheng, L.-T. "Push-Pull Porphyrins as Non-Linear Optical Materials," *J. Am. Chem. Soc.* **1992**, *114*, 6928-6930.
138. Bilsel, O.; Rodriguez, J.; Milam, S. N.; Gorlin, P. A.; Girolami, G. S.; Suslick, K. S.; Holten, D. "Electronic States and Optical Properties of Porphyrin in van der Waals Contact: Th(IV) Sandwich Complexes," *J. Am. Chem. Soc.* **1992**, *114*, 6528-6538.

139. Becker, L.; Bada, J. L.; Kemper, K.; Suslick, K. S. "Sonoluminescence Spectrum of Seawater" *Marine Chem.* **1992**, *40*, 315-320.
140. Girolami, G. S.; Riehl, M. E.; Suslick, K. S.; Wilson, S. R. "A Rare Example of a Monomeric Aryllithium Complex. X-ray Structure of (2,4,6-Triphenylphenyl)lithium Bis(diethyl ether)" *Organomet.* **1992**, *11*, 3907-3910.
141. Tuncay, A.; Dustman, J. A.; Fisher, G.; Tuncay, C. I.; Suslick, K. S. "Ultrasound Promoted Hypervalent Iodine Reactions: α -Tosyloxylation of Ketones," *Tetrahedron Lett.* **1992**, *33*, 7647-7650.
142. Suslick, K. S.; Flint, E. B.; Grinstaff, M. W.; Kemper, K. A. "Sonoluminescence from Metal Carbonyls," *J. Phys. Chem.* **1993**, *97*, 3098-3099.
143. Bilsel, O.; Milam, S. N.; Girolami, G. S.; Suslick, K. S.; Holten, D. "Ultrafast Electronic Deactivation and Vibrational Dynamics of Photoexcited Uranium (IV) Porphyrin Sandwich Complexes," *J. Phys. Chem.* **1993**, *97*, 7216-7221.
144. Grinstaff, M. W.; Salamon, M. B.; Suslick, K. S. "Magnetic Properties of Amorphous Iron," *Phys. Rev. B* **1993**, *48*, 269-273.
145. Bellissent, R.; Galli, G.; Grinstaff, M. W.; Migliardo, P.; Suslick, K. S. "Neutron Diffraction by Amorphous Iron Powder," *Phys. Rev. B* **1993**, *48*, 15797-15800.
146. Suslick, K. S.; Kemper, K. A. "The Effect of Fluorocarbon Gases on Sonoluminescence: A Failure of the Electrical Hypothesis," *Ultrasonics* **1993**, *31*, 463-465.
147. Suslick, K. S. "The Chemical Effects of Ultrasound," *Proc. 1st Intl. EPRI/NSF Symp. Advanced Oxidation*; EPRI: Palo Alto, 1993, vol. 2, pp 6-27.
148. Webb, A. G.; Wong, M.; Wilmes, L. J.; Kolbeck, K. J.; Magin, R. L.; Suslick, K. S. "⁵⁹Co Functional Agents for Localized In-Vivo Temperature Measurements," *Proc. 12th Annual Mtg. Soc. Magnetic Resonance in Medicine*; New York, 1993; p. 245.
149. Wilmes, L. J.; Webb, A. G.; Kolbeck, K. J.; Wong, M.; Magin, R. L.; Suslick, K. S. "Microencapsulation of Perfluorocarbons as a Magnetic Resonance Imaging Agent," *Proc. 12th Annual Mtg. Soc. Magnetic Resonance in Medicine*; New York, 1993, pp 756-757.
150. Suslick, K. S.; Kemper, K. A.; Flint, E. B. "Spectrally Resolved Sonoluminescence as a Probe of Cavitation," *IEEE Ultrasonics Symp. Proc.* **1993**, 777-784.
151. Chou, H.; Chen, C.-T.; Stork, K. F.; Bohn, P. W.; Suslick, K. S. "Langmuir-Blodgett Films of Amphiphilic Push-Pull Porphyrins," *J. Phys. Chem.* **1994**, *98*, 383-385.
152. Desai, N. P.; Soon-Shiong, P.; Grinstaff, M. W.; Yao, Z.; Sandford, P. A.; Suslick, K. S. "Controlled and Targeted Drug Delivery with Biocompatible Protein Shell Microspheres," *Proc. Soc. Biomaterial*, **1994**, *20*, 112.
153. Suslick, K. S.; Grinstaff, M. W.; Kolbeck, K. J.; Wong, M. "Characterization of Sonochemically Prepared Proteinaceous Microcapsules," *Ultrasonics Sonochemistry* **1994**, *1*, S65-S68.
154. Girolami, G. S.; Gorlin, P. A.; Suslick, K. S. "Electronically Asymmetric Bis (porphyrin) Sandwich Complexes," *Inorg. Chem.* **1994**, *33*, 626-627.
155. Grinstaff, M. W.; Kolbeck, K. A.; Magin, R. L.; Suslick, K. S.; Webb, A.; Wilmes, L. J.; Wong, M.; Desai, N. P.; Sandford, P. A.; Soon-Shiong, P.

- "Fluorocarbon Filled Protein Microspheres as Contrast Agents for MRI," *Proc. Soc. Biomaterial*, **1994**, *20*, 113.
156. Suslick, K. S.; Kemper, K.A. "Pressure Measurements During Acoustic Cavitation by Sonoluminescence" *Bubble Dynamics and Interface Phenomena*; Blake J.R.; Thomas, N.; eds. Kluwer Publishers: Dordrecht, Netherlands, 1994; pp 311-320.
157. Suslick, K. S.; Hyeon, T.; Fang, M.; Cichowlas, A. A. "Sonochemical Synthesis and Catalytic Properties of Nanostructured Molybdenum Carbide," *Molecularly Designed Nanostructured Materials*, MRS Symp. Proc., v. 351. Gonsalves, K.E.; Chow, G.M.; Xiao, T.O.; Cammarata, R.C., eds. Materials Research Society: Pittsburgh, 1994; pp 201-206.
158. Suslick, K. S.; Fang, M.; Hyeon, T.; Cichowlas, A. A. "Nanostructured Fe-Co Catalysts Generated by Ultrasound," *Molecularly Designed Nanostructured Materials*, MRS Symp. Proc., vol. 351. Gonsalves, K. E.; Chow, G. M.; Xiao, T. O.; Cammarata, R. C., Eds. Materials Research Society: Pittsburgh, 1994; pp 443-448.
159. Suslick, K.S. "The Mechanochemical Effects of Ultrasound" *Proc. First Intl. Conf. Mechanochemistry: InCoMe '93*, Ko-ice, Slovakia; Cambridge Interscience: Cambridge, 1994; vol.1, pp 43-49.
160. Liu, K. J.; Grinstaff, M. W.; Jiang, J.; Suslick, K. S.; Swartz, H. M.; Wang, W. "In Vivo Measurement of Oxygen Concentration Using Sonochemically Synthesized Microspheres," *Biophys. J.* **1994**, *67*, 896-901.
161. Milam, S. N.; Gorlin, P. A.; Girolami, G. S.; Suslick, K. S.; Wilson, S. R. "Bis (porphyrin)actinide Complexes and their Radical Cations and Dications," *J. Coord. Chem.* (T. L. Brown Retirement Issue) **1994**, *32*, 173-212.
162. Hill, J. R.; Dlott, D. D.; Fayer, M. D.; Peterson, K. A.; Rella, C. W.; Rosenblatt, M. M.; Suslick, K. S.; Ziegler, C. J. "Vibrational Relaxation of Carbon Monoxide in Model Heme Compounds: 6-Coordinate Metalloporphyrins (M=Fe, Ru, Os)" *Chem. Phys. Lett.*, **1995**, *244*, 218-223.
163. Matula, T. J.; Roy, R. A.; Mourad, P. D.; McNamara III, W. B.; Suslick, K. S. "Comparison of Multi-Bubble and Single-Bubble Sonoluminescence Spectra," *Phys. Rev. Lett.*, **1995**, *75*, 2602-2605.
164. Webb, A. G.; Wong, M.; Niesman, M.; Kolbeck, K. J.; Wilmes, L. J.; Magin, R. L.; Suslick, K. S. "In-Vivo NMR Thermometry with Liposomes Containing ⁵⁹Co Complexes," *Int. J. Hyperthermia* **1995**, *11*, 821-827.
165. Bellissent, R.; Galli, G.; Hyeon, T.; Magazu, S.; Majolino, D.; Migliardo, P.; Suslick, K. S. "Structural Properties of Amorphous Bulk Fe, Co, and Fe-Co Binary Alloys," *Phys. Scripta* **1995**, *T57*, 79-83.
166. Fang, M.; Hyeon, T.; Cichowlas, A. A.; Suslick, K. S. "Sonochemical Preparation of Nanostructured Catalysts," *Am. Chem. Soc. Div. Petrol. Chem. Preprints*, **1995**, 67-71.
167. Hyeon, T.; Fang, M.; Cichowlas, A. A.; Suslick, K. S. "Catalytic Activity of Nanophase Metals Prepared Sonochemically," *Am. Chem. Soc. Div. Fuel Chem. Preprints*, **1995**, *40*, 365-9.
168. Wong, M.; Suslick, K. S. "Sonochemically Produced Hemoglobin Microbubbles," *Hollow and Solid Spheres and Microspheres*; *MRS Symp. Proc. v. 372*; Wilcox, D. L; Berg, M.; Bernat, T.; Kellerman, D.; Corchran, J. K., eds. *Matl. Res. Soc.: Pittsburgh, 1995*; pp 89-94.
169. Hyeon, T.; Fang, M.; Cichowlas, A. A.; Suslick, K. S. "Sonochemical

- Synthesis of Nanostructured Catalysts" [Matl. Sci. Eng. A, 1995, 204, 186-192.](#)
170. Suslick, K. S.; Hyeon, T.; Fang, M.; Ries, J. T.; Cichowlas, A. A. "Sonochemical Synthesis of Nanophase Metals, Alloys, and Carbides," *Materials Science Forum* (Transtec Publ., N.Y.), **1996**, 225-227, 903-912.
 171. Girolami, G. S.; Hein, C. L.; Suslick, K. S. "Bis(porphyrin) Sandwich Complex with an Appended Quinone," [Angew. Chem. Intl. Ed. 1996, 35, 1223-1225.](#)
 172. Bhyrappa, P.; Young, J. K.; Moore, J. S.; Suslick, K. S. "Shape-Selective Epoxidation of Alkenes by Metalloporphyrin-Dendrimers," [J. Molec. Catalysis, 1996 \(special issue on biomimetic oxidation\), A113, 109-116.](#)
 173. Ziegler, C. J.; Suslick, K. S. "The Photochemistry of Metalloporphyrin Carbene Complexes," [J. Am. Chem. Soc., 1996, 118, 5306-5307.](#)
 174. Hyeon, T.; Fang, M.; Suslick, K. S. "Nanostructured Molybdenum Carbide: Sonochemical Synthesis and Catalytic Properties," [J. Am. Chem. Soc., 1996, 118, 5492-5493.](#)
 175. Eckburg, J. J.; Chato, J. C.; Liu, K. J.; Grinstaff, M. W.; Swartz, H. M.; Suslick, K. S.; Auteri, F. P. "Biological Temperature Measurements using Electron Paramagnetic Resonance Spectroscopy," [J. Biomech. Eng. 1996, 118, 193-200.](#)
 176. Webb, A. G.; Wong, M.; Kolbeck, K. J.; Magin, R. L.; Wilmes, L. J.; Suslick, K. S. "Sonochemically Produced Fluorocarbon Microspheres: A New Class of MRI Contrast Agents," [J. Mag. Res. Imaging, 1996, 6, 675-683.](#)
 177. Suslick, K. S.; Hyeon, T.; Fang, M.; Cichowlas, A. A. "Sonochemical Preparation of Nanostructured Catalysts," *Advanced Catalysts and Nanostructured Materials*; Moser, W. R., ed. Academic Press: New York, 1996, pp. 197-211.
 178. Suslick, K. S.; Hyeon, T.; Fang, M. "Nanostructured Materials Generated by High Intensity Ultrasound," [Chem. Materials 1996, 8, 2172-2179 \(special issue on nanostructured materials\).](#)
 179. Bernstein, L. S.; Zakin, M. R.; Flint, E. B.; Suslick, K. S. "Cavitation Thermometry using Molecular and Continuum Sonoluminescence," [J. Phys. Chem. 1996, 100, 6612-6619.](#)
 180. Bellissent, R.; Galli, G.; Hyeon, T.; Migliardo, P.; Parette, P.; Suslick, K. S. "Magnetic And Structural Properties Of Amorphous Transition Metals And Alloys," [J. Noncryst. Solids, 1996, 205-207, 656-659.](#)
 181. Bhyrappa, P.; Young, J. K.; Moore, J. S.; Suslick, K. S. "Dendrimer-Metalloporphyrins: Synthesis and Characterization," [J. Am. Chem. Soc., 1996, 118, 5708-5711.](#)
 182. Dlott, D. D.; Fayer, M. D.; Hill, J. R.; Rella, C. W.; Suslick, K. S.; Ziegler, C. J. "Vibrational Relaxation in Metalloporphyrin CO Complexes" [J. Am. Chem. Soc., 1996, 118, 7853-7854.](#)
 183. Ziegler, C. J.; Suslick, K. S. "Photochemical Activation of Metalloporphyrin Carbene Complexes," [J. Organomet. Chem. 1996, 528, 83-90.](#)
 184. Hill, J. R.; Ziegler, C. J.; Suslick, K. S.; Dlott, D. D.; Rella, C. W.; Fayer, M. D. "Tuning the Vibrational Relaxation of CO Bound to Heme and Metalloporphyrin Complexes" [J. Phys. Chem., 1996, 100, 18023-18032.](#)

185. Suslick, K. S.; Fang, M.; Hyeon, T. "Sonochemical Synthesis of Iron Colloids" *J. Am. Chem. Soc.*, **1996**, *118*, 11960-11961.
186. Benson, D. E.; Suslick, K. S.; Sligar, S. G. "Reduced Oxy Intermediate Observed in D251N Cytochrome P450cam," *Biochem.*, **1997**, *36*, 5104-5107.
187. Peterson, K. A.; Boxer, S. G.; Decatur, S.; Dlott, D. D.; Fayer, M. D.; Hill, J. R.; Rella, C. W.; Rosenblatt, M. M.; Suslick, K. S.; Ziegler, C. J. "Vibrational Relaxation of CO in Myoglobin Mutants and Model Heme Compounds" *Proc. 7th Intl. Conf. Time Resolved Vibr. Spectrosc.*, 1997, 173-177.
188. Bhyrappa, P.; Wilson, S. R.; Suslick, K. S. "Hydrogen Bonded Porphyrinic Solids: Supramolecular Networks of Octahydroxy Porphyrins," *J. Am. Chem. Soc.*, **1997**, *119*, 8492-8502.
189. Suslick, K. S.; Mdleleni, M. M.; Ries, J. T. "Chemistry Induced by Hydrodynamic Cavitation" *J. Am. Chem. Soc.*, **1997**, *119*, 9303-9304.
190. Bhyrappa, P.; Suslick, K. S. "Supramolecular Networks of Octahydroxy Porphyrins," *Supramolec. Chem.*, **1998**, *9*, 169-174.
191. Suslick, K. S. "Sonochemical preparation of protein microspheres" *Proc. 16th Intl. Conf. Acoustics* (Ac. Soc. Am., Seattle: 1998), pp. 1533-35.
192. Suslick, K. S.; Didenko, Y. T.; McNamara III, W. B. "Conditions during Multi-Bubble Sonoluminescence" *Proc. 16th Intl. Conf. Acoustics* (Ac. Soc. Am., Seattle: 1998), pp. 2577-79.
193. Bhyrappa, P.; Suslick, K. S. "Synthesis and Crystal Structure of 5,10,15,20-Tetrakis(3,5-dinitrophenyl)porphyrin," *J. Porph. Phthalocyn.*, **1998**, *2*, 391-396. (special V. Krishnan retirement issue)
194. Long, G. J.; Hautot, D.; Pankhurst, Q. A.; Vandormael, D.; Grandjean, F.; Gaspard, J. P.; Briois V.; Hyeon. T.; Suslick, K. S. "Mössbauer-effect and X-Ray Absorption Spectral Study of Sonochemically Prepared Amorphous Iron" *Phys. Rev., B*, **1998**, *57*, 10716-10722.
195. Huffman, D. L.; Rosenblatt, M. M.; Suslick, K. S. "Synthetic Heme-Peptide Complexes," *J. Am. Chem. Soc.*, **1998**, *120*, 6183-6184.
196. Mdleleni, M. M.; Hyeon, T.; Suslick, K. S. "Sonochemical Synthesis of Nanostructured Molybdenum Sulfide" *J. Am. Chem. Soc.*, **1998**, *120*, 6189-6190.
197. Patel, B. R.; Suslick, K. S. "Discotic Liquid Crystals from a Bis-Pocketed Porphyrin" *J. Am. Chem. Soc.*, **1998**, *120*, 11802-11803.
198. Bhyrappa, P.; Vijayanthimala, G.; Suslick, K. S. "Shape-Selective Ligation to Dendrimer-Metalloporphyrins," *J. Am. Chem. Soc.*, **1999**, *121*, 262-263.
199. Salzmann, R.; Ziegler, C. J.; Godhout, N.; McMahan, M.; Suslick, K. S.; Oldfield, E. "CO Complexes of Fe(II), Ru(II), and Os(II) 5,10,15,20-Tetraphenylporphyrinates: A comparative Investigation by X-ray, Solid-State NMR and Density Functional Theory" *J. Am. Chem. Soc.*, **1998**, *120*, 11323-11334.
200. Tuncay, A.; Anaclerio, B. M.; Zolodz, M.; Suslick, K. S. "New One-Pot Method for the Synthesis of Alkynyl Sulfonate Esters Using Ultrasound," *Tetrahedron Lett.* **1999**, 599-602.
201. Suslick, K. S.; McNamara III, W. B.; Didenko, Y. "Hot Spot Conditions During Multi-Bubble Cavitation" in *Sonochemistry and Sonoluminescence*,

- [Crum, L. A.; Mason, T. J.; Reisse, J.; Suslick, K. S., eds. Kluwer Publishers: Dordrecht, Netherlands, 1999, pp. 191-204.](#)
202. Suslick, K. S.; Fang, M. M.; Hyeon, T.; Mdeleeni, M. M. "Applications of Sonochemistry to Materials Synthesis" in [Sonochemistry and Sonoluminescence, Crum, L. A.; Mason, T. J.; Reisse, J.; Suslick, K. S., eds. Kluwer Publishers: Dordrecht, Netherlands, 1999, pp. 291-320.](#)
203. Didenko, Y. T.; McNamara III, W. B.; Suslick, K. S. "Hot Spot Conditions During Cavitation in Water," [J. Am. Chem. Soc., 1999, 121, 5817-5818.](#)
204. Li, S.; Lee, J.S.; Hyeon, T.; Suslick, K. S. "Catalytic Hydrodenitrogenation of Indole over Molybdenum Nitride and Carbides with Different Structures" [Applied Catal. A, 1999, 184, 1-9.](#)
205. McNamara III, W. B.; Didenko, Y.; Suslick, K. S. "Sonoluminescence Temperatures During Multibubble Cavitation" [Nature, 1999, 401, 772-775.](#)
206. Didenko, Y.; McNamara III, W. B.; Suslick, K. S. "The Temperature of Multi-Bubble Sonoluminescence in Water," [J. Phys. Chem. A, 1999, , 103, 10783-10788.](#)
207. McNamara III, W. B.; Didenko, Y.; Suslick, K. S. "Effect of Noble Gases on Sonoluminescence Temperatures During Multibubble Cavitation" [Phys. Rev. Lett., 2000, 84, 777-780.](#)
208. Suslick, K. S.; McNamara III, W. B.; Didenko, Y. "Conditions During Multibubble Cavitation" " in *Nonlinear Acoustics at the Turn of the Millennium*, Lauterborn, W.; Kurz, T., eds. Amer. Inst. Physics: Melville, NY, 2000, pp. 463-466
209. Kosal, M. E.; Suslick, K. S. "Microporous Porphyrin and Metalloporphyrin Materials," [J. Sol. St. Chem., 2000, 152, 87-98 \(invited review\).](#)
210. Brunner, R.; Kosal, M. E.; Suslick, K. S.; Lamche, R.; Marti, O.; White, J.O. "Near-Field Scanning Optical Microscopy of Zinc-Porphyrin Crystals," [Ultramicroscopy, 2000, 84, 149-157.](#)
211. Suslick, K. S.; Rakow, N. A.; Kosal, M. E.; Chou, J.-H. "[The Materials Chemistry of Porphyrins and Metalloporphyrins,](#)" [J. Porph. Phthal., 2000, 4, 407-413](#) (invited review).
212. Dantsin, G.; Suslick, K.S. "Sonochemical Preparation of a Nanostructured Bifunctional Catalyst" [J. Am. Chem. Soc., 2000, 122, 5214-5215.](#)
213. McNamara III, W. B.; Didenko, Y.; Suslick, K. S. "The Nature of the Continuum in Multi-Bubble Sonoluminescence" [J. Am. Chem. Soc., 2000, 122, 8563-8564.](#)
214. Ashokkumar, M.; Crum, L. A.; Frensley, C. A.; Grieser, F.; Matula, T. J.; McNamara III, W. B.; Suslick, K. S. "Effect of Solutes on Single-Bubble Sonoluminescence in Water" [J. Phys. Chem. A, 2000, 104, 8462-8465.](#)
215. Huffman, D. L.; Suslick, K. S. "Hydrophobic Interactions in Metalloporphyrin-Peptide Complexes" [Inorg. Chem. 2000, 39, 5418-5419.](#)
216. Sen, A; Suslick, K. S. "Shape-Selective Discrimination of Small Organic Molecules" [J. Am. Chem. Soc., 2000, 122, 11565-11566.](#)
217. Rakow, N. A.; Suslick, K. S. "A Colorimetric Sensor Array for Odour Visualization" [Nature, 2000, 406, 710-714.](#)
218. Didenko, Y.; McNamara III, W. B.; Suslick, K. S. "Molecular Emission from Single Bubble Sonoluminescence" [Nature, 2000, 407, 877-879.](#)
219. Petrier C.; Suslick, K. S. "Ultrasound-Enhanced Reactivity Of Calcium In The Reduction Of Aromatic Hydrocarbons" [Ultrasonics Sonochemistry 2000, 7, 53-61.](#)
220. Suslick, K. S.; Rakow, N. A. "[A Colorimetric Nose: 'Smell-Seeing'](#)" *Artificial Chemical Sensing: Olfaction and the Electronic Nose*, Stetter, J.R.; Pensrose, W.

- R., eds. *Electrochem. Soc.*: Pennington, NJ, 2001, pp. 8-14.
221. Suslick, K.S.; Kosal, M.E.; Rakow, N. A.; Sen, A. "'Smell-Seeing:' A New Approach to Artificial Olfaction" *Proc. EURODEUR*, Paris, 2001, pp. PA2SL 14-15.
222. Suslick, K. S.; Didenko, Y.; McNamara III, W. B.; "Single Bubble Sonoluminescence from Non-Aqueous Liquids" *Proc. 17th Intl. Congr. Acoustics*, Rome, 2001,
223. Suslick, K. S. "The Chemical Consequences of Cavitation" *Proc. 17th Intl. Congr. Acoustics*, Rome, 2001, pp. PA2SL 2-5.
224. Dhas, N. A.; Ekhtiarzadeh, A.; Suslick, K. S. "Sonochemical Preparation of Supported Hydrodesulfurization Catalysts" *J. Am. Chem. Soc.* **2001**, *123*, 8310.
225. Drain, C. M.; Hupp, J. T.; Suslick, K. S.; Wasielewski, M. R.; Chen, X. "A Perspective on New Porphyrin-Based Functional Materials and Devices" *J. Porph. Phthal.*, **2002**, *6*, 243-259.
226. Margaret E. Kosal, Jun-Hong Chou Suslick, K. S.; "A Calcium-Bridged Porphyrin Coordination Network" *J. Porph. Phthal.*, **2002**, *6*, 377-381.
227. Suslick, K. S.; Didenko, Y. T. "The Chemical Consequences of Single-Bubble Cavitation" *Nonlinear Acoustics at the Beginning of the 21st Century*, Rudenko, O. V.; Sapozhnikov, O.A., ed. Moscow State Univ. Press: Moscow, 2002; vol. 2, pp. 1063-1069.
228. Didenko, Y.; Suslick, K. S. "The Energy Efficiency of Formation of Photons, Radicals, and Ions During Single Bubble Cavitation" *Nature* **2002**, *418*, 394-397.
229. Zimmerman, S. C.; Wendland, M. S.; Rakow, N. A.; Zharov, I.; Suslick, K. S. "Synthetic Hosts by Monomolecular Imprinting Inside Dendrimers" *Nature* **2002**, *418*, 399-403.
230. Rosenblatt, M.M.; Huffman, D.L.; Wang, X. Remmer, H.A.; Suslick, K. S. "Cyclic and Hairpin Peptide Complexes of Heme" *J. Am. Chem. Soc.* **2002**, *124* 12394.
231. Kosal, M. E.; Chou, J.-H.; Wilson, S. R.; Suslick, K. S. "A Functional Zeolite Analogue Assembled From Metalloporphyrins" *Nature Materials*, **2002**, *1*, 118-121.
232. Wang, J.; Luthey-Schulten, Z.; Suslick, K. S. "Is the Olfactory Receptor A Metalloprotein?" *Proc. Natl. Acad. Sci. U.S.A.*, **2003**, *100*, 3035-3039.
233. Suslick, K.S.; Rakow, N.A.; Kosal, M.E.; McNamara III, W.B.; Sen, A. "Chemosensing: A Colorimetric Array Detector" *Proc. ISOEN 02* (ed. A. D'Amico and C. DiNatale; IEEE: Baltimore, 2003) pp. 46-52.
234. McNamara III, W. B.; Didenko, Y.; Suslick, K. S. "Pressure during Acoustic Cavitation" *J. Phys. Chem.* **2003**, *107*, 7303-7306 (*Henglein Festschrift*).
235. Lee, T. M.; Oldenburg, A. L.; Sitafalwalla, S.; Marks, D. L.; Luo, W.; Toublan, F. J.-J.; Suslick, K. S.; Boppart, S. A. "Engineered Microsphere Contrast Agents for Optical Coherence Tomography" *Optics Lett.* **2003**, *28*, 1546-1548.
236. Oxley, J. D.; Prozorov, T.; Suslick, K. S. "Sonochemistry and Sonoluminescence of Room-Temperature Ionic Liquids" *J. Am. Chem. Soc.*, **2003**, *125*, 11138-11139.
237. Rosenblatt, M.M.; Wang, J.; Suslick, K. S. "De Novo Designed Cyclic-Peptide Heme Complexes" *Proc. Natl. Acad. Sci. U.S.A.*, **2003**, *100*, 13140-13145.
238. Prozorov, T.; Prozorov, R.; Snezhko, A.; Suslick, K. S. "Sonochemical Modification of the Superconducting Properties of MgB₂" *Appl. Phys. Lett.* **2003**, *83*, 2019-2021
239. Zimmerman, S. C.; Zharov, I.; Wendland, M. S.; Rakow, N. A.; Suslick, K.S. "Molecular Imprinting Inside Dendrimers" *J. Am. Chem. Soc.* **2003**, *125*, 13504 - 13518.

[Books](#)
[Major Reviews](#)
[Popularizations](#)
[Patents](#)
[Journal Articles](#)

SUSLICK GROUP WEBSITE:

THE SCIENCE	THE GROUP	THE MAÎTRE D'	LAGNIAPPE: A LITTLE EXTRA
Overview	Current Group Members	CV: Abbreviated, Full	Art and Science
Outline of Projects	Group Meetings	Suslick Group Brochure	Chymistes: The Distillers of Waters
Synopsis: Sonochemistry	Group Responsibilities	Complete Publication List	A Chemist Meets Hollywood
Metalloporph.			
Executive Summary: Smell-Seeing	Web Based Resources	Academic Genealogy	A Chemist In Court
Introduction to Sonochemistry	Safety Resources	Press Clippings	Words of Humor and Wisdom
Proposal Excerpts	Group Equipment	How To Give A Seminar	Laws of the Universe

<u>Funding</u>	<u>Past Group Members</u>	<u>Ch315 Inorganic Chemistry</u>	<u>Cartoons of Humor and Wisdom</u>
<u>Information for Visitors</u>	<u>Group Photogallery</u>	<u>Construction of the CLS Lab</u>	<u>Sculpture & Masks</u>

©2003, K.S. Suslick; all rights reserved.

Comments and suggestions: ksuslick@uiuc.edu

KENNETH S. SUSLICK

*School of Chemical Sciences
University of Illinois at Urbana-Champaign
Chemical & Life Sciences Laboratory
600 S. Mathews Av.
Urbana, Illinois 61801*

*Office: (217) 333-2794
Lab: (217) 333-1532
Fax: (217) 333-2685
Email: ksuslick@uiuc.edu
Web: www.scs.uiuc.edu/suslick*

Education:

- 1978 Ph. D., Stanford University, *Synthetic Analogs of Myoglobin and Hemoglobin*.
1974 B. S., California Institute of Technology (with Honors).

Research and Professional Positions:

- 1997 – *William H. & Janet Lycan* Professor of Chemistry, University of Illinois at Urbana-Champaign.
2001 – Founder and Member of Board of Directors; ChemSensing, Inc., Northbrook, IL.
1988 – Professor of Chemistry, University of Illinois at Urbana-Champaign.
1993 – Professor of Materials Science and Engineering, University of Illinois at Urbana-Champaign.
1993 – 98 Member, Board of Directors; Ney Ultrasonics Inc.; Bloomfield, Connecticut.
1994 – 98 Member, Scientific Advisory Board; VivoRx Inc.; Santa Monica, California.
1995 – 97 *Alumni Research Scholar* Professor of Chemistry, University of Illinois at Urbana-Champaign.
1989 – 92 Professor, Beckman Institute for Advanced Science and Technology.
1986 Visiting Fellow, Balliol College and Inorganic Chemistry Laboratory, Oxford University.
1984 – 88 Associate Professor, University of Illinois at Urbana-Champaign.
1978 – 84 Assistant Professor, University of Illinois at Urbana-Champaign.
1974 – 78 Research and Teaching Assistant, Stanford University.
1974 – 75 Chemist, Lawrence Livermore Laboratory, O-Group, Physics Division; Laser Isotope Separation.
1971 – 74 Research and Teaching Assistant, California Institute of Technology.
1972 AEC Research Trainee, Lawrence Berkeley Laboratory.

Honors and Awards:

- 2004 American Chemical Society Senior Cope Scholar Award
2003 J.T. Donald Lecturer, McGill University, Montreal.
2001 Wolfgang Göpel Award, 8th Intl. Symp. on Olfaction & Electronic Noses.
2000 1st Place, Illinois Technology Center Inventorship Competition.
1997 University of Melbourne Special Public Lectureship.
1997 W. Heinlen Hall Lectureship, Bowling Green State University.
1994 American Chemical Society Nobel Laureate Signature Award for Graduate Education.
1994 Materials Research Society Medal for Exceptional Recent Achievements in Materials Research.
1992 – Fellow, American Association for the Advancement of Science.
1994 – Fellow, Acoustical Society of America.
1994 Robert A. Welch Foundation Lecturer.
1994 Senior University Scholar, University of Illinois.
1992 – 94 NSF Special Creativity Extension Award.
1993 Excellence in Teaching Award, UIUC School of Chemical Sciences.
1991 – 92 Beckman Associate, UIUC Center for Advanced Study.
1985 – 90 NIH Research Career Development Award.
1985 – 87 Alfred P. Sloan Foundation Research Fellow.
1985 Excellence in Teaching Award, UIUC School of Chemical Sciences.
1979 – 80 DuPont Young Faculty Fellow.
1974 – 78 Silver Medal and Fellow, Royal Society for the Arts, Manufactures, and Commerce (London).
1974 – 78 Hertz Foundation Predoctoral Fellowship.
1973 American Chemical Society Undergraduate Award in Analytical Chemistry.
-
-

Recent Special Lectures:

2003

J.T. Donald Lecturer, McGill University, Montreal.
Five College Lecturer (Amherst, Mount Holyoke, Smith, Hampshire and U. Mass. Amherst).
Invited Speaker, Gordon Conference on Chemical Sensors.
Invited Speaker, Symposium on Sonoluminescence, Acoustic Society of America Mtg., Nashville.
Frontiers of Chemistry Lecturer, Wayne State University.

2002

Invited Lecturer, 16th International Symposium on Nonlinear Acoustics (ISNA-16), Moscow.
Invited Speaker, 9th Intl. Symp. on Olfaction & Electronic Noses (ISOEN-2002), Rome.
Plenary Lecturer, Catalyst Club of Chicago.
Invited Speaker, Symposium Honoring J. I. Brauman, Stanford University.
Invited Speaker, Symposium Honoring R. G. Bergman, University of California, Berkeley.
Invited Speaker, Chicago Technology Forum 2002.

2001

Plenary Lecturer, EURODEUR-AIRODEUR Conference, Paris.
Invited Speaker, 8th Intl. Symp. on Olfaction & Electronic Noses, Washington, D.C.
Plenary Lecturer, 17th Intl. Congress on Acoustics, Rome.
Plenary Lecturer, World Congress on Ultrasonics/IEEE Intl. Ultrasonics Symposium, Atlanta, GA.

2000

Keynote Speaker, Ultrasonics Industry Association Meeting, Columbus.
Invited Speaker and Symposium Organizer, Pacificchem 2000, Honolulu.
Invited Speaker and Symposium Organizer, 1st International Congress on Porphyrins and Phthalocyanines, Dijon.
Invited Speaker, 7th Meeting of the European Sonochemistry Society, Biarritz.
Invited Speaker, Chemistry under Extreme Conditions Symp., ACS Natl. Meeting, Washington, D.C.

1999

Pittsburgh Conference Lectureship, Duquesne University, Pittsburgh.
Invited Speaker, "Unusual Techniques in Inorganic Chemistry," 82nd Canadian Soc. for Chemistry Conf., Toronto.
Invited Speaker, 15th International Symposium on Nonlinear Acoustics, Göttingen.

1998

Director's Colloquium Speaker, Los Alamos National Laboratory.
Invited Speaker, Gordon Research Conference, Chemistry and Biology of Tetrapyrroles.
Invited Speaker, DARPA Workshop on Sonoluminescence, Arlington.
Invited Lecturer, 6th Meeting of the European Sonochemistry Society, Rostock.
Invited Speaker, Sonochemistry & Sonoluminescence Symposium, Acoustic Soc. Amer. Mtg., Seattle.

1997

Plenary Lecturer, COST Intl. Meeting on Chemistry Under Extreme Conditions, Santorini, Greece.
Instructor, NATO Advanced Study Institute on Sonochemistry and Sonoluminescence, Leavenworth, WA.
Plenary Lecturer, IEEE International Ultrasonics Symposium, Toronto.
University Special Public Lecturer, University of Melbourne.
Invited Speaker, 8th International Conference on Bioinorganic Chemistry, Yokohama.
Invited Speaker, Symposium on Mesogenic Materials, 213rd ACS National Meeting, Las Vegas.
Invited Speaker, Symposium on Sonoluminescence, James Franck Institute, University of Chicago.
W. Heinlen Hall Lectureship, Bowling Green State University.
Chemical & Life Sciences Laboratory Dedication Speaker, University of Illinois.
Invited Speaker, Science Innovation Symposium, AAAS National Meeting, Seattle.

1996

Invited Speaker, 3rd NSF Workshop on Materials Chemistry, Philadelphia.
Colloquium Lecturer, James Franck Institute, University of Chicago.
Invited Speaker, Acoustical Society of America Meeting, Honolulu.
Plenary Lecturer, 5th Meeting of the European Sonochemistry Society, Cambridge.
Invited Speaker, 4th Intl. Conf. Molecular Reaction Dynamics in Condensed Matter, Newport Beach.
Invited Speaker, Symposium on Novel Materials Preparation, Am. Phys. Soc. Mtg., St. Louis.
Invited Speaker, Symposium on Hybrid Materials, 211th ACS National Meeting, New Orleans.

Industrial Consulting Positions with Confidentiality Agreements:

Current

Teltech Resource Network, Minneapolis; 1985 – .
ChemSensing, Inc., Northbrook; 2001 –
Dispersed Systems, Oceanside, CA.

2002

Dispersed Systems, Oceanside, CA.
PDVSA, Caracas, Venezuela.

2001

PG Research Foundation, 1999 – 2001.
UOP Corp. Research, Chicago.
Aramco (Saudi Arabian Oil Co.), Dhahran.
Eveready Corp., Cincinnati.

2000

Exxon ERDL, Baton Rouge.
Vitroseal, Inc., Evanston, IL.

1999

VivoRx Pharmaceuticals, Santa Monica.; 1991 – 99.
Exxon ERDL, Baton Rouge.
CQ Inc., Homer City, PA.

1998

Exxon ERDL, Baton Rouge.
Abbot Pharmaceuticals, North Chicago.
MacroSonix Corp., Richmond, VA.

1997

Ney Ultrasonics, Bloomfield, CT.
U.S. Army Construction Eng. Res. Lab.
Storz Instrument Co., St. Louis.

1996

Storz Instrument Co., St. Louis.
National Starch and Chemical Corp., Plainfield, NJ.
Exxon Corporate Research, Annandale, NJ.
Ney Ultrasonics, Bloomfield, CT.
U.S. Army Construction Eng. Res. Lab.

1995

Kimberly-Clark Corp., Neenah, WI.
3M Corporate Research, Minneapolis.
Ney Ultrasonics, Bloomfield, CT.

1994

Exxon ERDL, Baton Rouge.
Dow-Elanco, Indianapolis.
Ney Ultrasonics, Bloomfield, CT.

1993

Foster-Wheeler Corporation, Livingston, NJ.
Exxon ERDL, Baton Rouge.
Orentreich Institute, Cold Spring On Hudson, NY.
duPont Imaging, Glasgow.
Gas Research Institute / Alfred Univ.; 1992-93.
Catalytica Associates, Mountain View, CA; '91-93.

1992

Exxon ERDL, Baton Rouge.
Dean Technology, Hanover, Connecticut; 1990-92.
3M Corporate Research, Minneapolis.

1991

Exxon Corporate Research, Annandale, NJ.
Hoechst-Celanese, Providence.
Chem Systems, Houston.
duPont-Merck Pharmaceuticals, Bellirica, NY.
BP Chemicals, London.

1990

Hoechst-Celanese, Corpus Christi.
Exxon Chemical Co., Linden, NJ.
Union Carbide Corporation, Bound Brook, NJ.
duPont Chemicals Corporation, Wilmington, DE.
Molecular Biosystems, Inc., San Diego; 1987-90.

1989

Dow Chemicals, Midland and Freeport.
Institute for Gas Technology, Chicago; 1987-89.

1988

Vulcan Chemicals, Wichita.
Exxon ERDL, Baton Rouge.
Sun Oil Research & Dev. Lab., Marcus Hook, NJ.
AMOCO Chemicals, Naperville, Illinois; 1987-88.

1976 – 1987

Eli Lilly Co., Indianapolis, 1987.
Mobil Research & Development, Paulsboro, 1987.
M & T Chemicals, New Jersey; 1986-87.
Ciba-Geigy Ltd., Basel, Switzerland; 1986.
Imperial Chemicals Industry, Runcorn, UK; 1986.
Shell Chemicals, Amsterdam; 1986.
Exxon Corporate Research, Annandale, NJ; 1984-86.
Digital Engineering, Thunder Bay, Canada; 1982.
Harper and Row, Hughey's *Inorg. Chem.*; 1981-82.
Catalytica Associates, Mountain View, CA; 1978.
Lawrence Livermore Natl. Laboratory; 1975-76.

Expert Witness and Other Legal Consulting:

1998 – 1999

Mentor v. MDA, Lysonix, Mysonix;
U.S. District Court (Central District of California);
Court Appointed (Rule 706) Expert Witness.

Mentor v. MDA, Lysonix, Mysonix;
Quinn, Emmanuel, Urquhart, Oliver, & Hedges, LLP
Plaintiff Expert Witness.

1996 – 1997

Alcon Laboratories v. Storz Instruments Co.;
Finnegan, Henderson, Farabow, Garrett (DC)
Defense Expert Witness.

1990 – 1991

Keller v. Feinstein; Virginia State Courts;
Thompson & McMullan (Richmond, VA);
Plaintiff Expert Witness.

Other Invited Lectures and Presentations

2003

224th ACS Meeting, New Orleans
Northwestern University
University of California, Irvine

2002

University of Notre Dame
University of Akron
University of Delaware
Pfizer Pharmaceuticals, Groton, CT
223rd ACS Natl. Mtg., Boston
3M Technology Center, Minneapolis
Abbot Pharmaceuticals, North Chicago
Colgate Corporate Research, Piscataway, NJ
Avery-Dennison, Cincinnati
Argonne National Laboratory, Argonne, IL

2001

University of Michigan
Massachusetts Institute of Technology
Motorola Adv. Tech. Center, Schaumburg, IL
Federal Bureau of Investigation, Washington, D.C.
Colgate-Palmolive Co., Piscataway, NJ
Procter & Gamble Corp., Cincinnati, OH
University of Illinois at Urbana-Champaign, MATSE
Mayo Clinic, Biomed. Eng., Rochester, MN
221st ACS Natl. Mtg., San Diego

2000

University of California, Santa Barbara
PacifiChem 2000, Honolulu
Illinois Technology Center, Savoy
220th ACS Natl. Mtg., Washington, D.C.
219th ACS Natl. Mtg., San Francisco
University of Wisconsin, Madison
DARPA Symposium on Meta-Materials

1999

218th ACS Natl. Mtg., New Orleans
217th ACS Natl. Mtg., Anaheim
University of New Orleans, Adv. Matl. Res. Inst
University of Missouri, St. Louis
MURI Conference, Aberdeen Proving Grounds, MD
University of Colorado
Colorado State University
University of Wyoming

1998

9th Midwest Organic Solid State Chemistry Symposium
216th ACS Natl. Mtg., Boston
Ball State University
DOE EMSP Symposium, Chicago
DOA Dendrimer MURI Symposium, Natick

1997

Indiana University, Bloomington
Indiana University-Purdue University at Indianapolis
ACS Chicago Section Meeting, Plenary Lecturer
Saturday Outreach, Dept. Physics, UIUC
213th ACS Natl. Mtg., Las Vegas
University of Minnesota
Great Lakes Regional ACS Meeting, Chicago

1996

University of Northern Iowa
Lawrence Livermore Natl. Labs
Stanford University
TAM, UIUC
Regional ACS Mtg., ISU
Inorg Awards Sym, 212th ACS Natl Mtg, San Francisco

1995

PacifiChem '95, Honolulu.
210th ACS Natl. Mtg., Chicago.
Materials Research Society Meeting, Boston.

Keynote Speaker, Ultrasonics Industry Association
Technical Meeting, Columbus.
Ultrasonics in Biophy. Bioeng. Symp., Allerton Park.
ISMANAM-95, Quebec.
209th ACS Natl. Mtg., Anaheim.
University of Pennsylvania
Iowa State University, Ames
Grinnell College, Grinnell, Iowa
Kimberley-Clark Corporate Research
Central States Microscopy Soc. Meeting
Ohio State University, Columbus

1994

Naval Research Laboratory, Washington, DC
Society for Biomaterials, Boston
North Carolina State University, Raleigh
Free University of Brussels, Belgium
University of California, Berkeley
Concordia University, Montreal
IEEE Eng. Med. Biol. Mtg., San Diego
Stanford Colloid Symposium, Stanford
Moderator, Ultrasonics in Biophysics and
Bioengineering Symp., Allerton Park
Soc. Magn. Reson. Medicine, San Francisco
Materials Research Soc. Spring Mtg., S.F.
207th ACS National Meeting, San Diego
Dow-Elanco, Indianapolis

1993

Invited Speaker, 1st NSF Workshop on
Materials Chemistry, Albuquerque.
IEEE Ultrasonics '93 Symposium, Baltimore.
Invited Speaker, 6th ICBIC, San Diego.
Keynote Speaker, Ultrasonics Industry Association
Technical Meeting, Columbus.
Plenary Lecturer, 1st International Conference on
Mechanochemistry, Kosice, Slovakia.
Invited Speaker, 3rd Eur. Sonochemistry Soc, Portugal.
Invited Speaker, NSF/EPRI Symposium on Advanced
Oxidation Technologies, San Francisco.
Michigan State University, East Lansing
Washington University, St. Louis
DOE Program Review, Washington, D.C.
IUTAM Symposium, Birmingham, U.K.
Duke University
DuPont Imaging and Medical, Glasgow
Orentreich Institute, New York
205th ACS National Meeting, Denver

1992

Invited Speaker, Gordon Res. Conf., Organomet. Chem.
Invited Speaker, Symp. on Cluster, Surfaces, & Solids,
204th ACS National Mtg., Washington, D.C.
Invited Speaker, Adv. Catal. Tech. Symp., Catalytica.
Colloquium Speaker, Center for Adv. Study, UIUC.

Invited Speaker, Symp. Reactions in Organized Media,
203rd ACS Natl. Mtg, San Francisco.
Northwestern University.
University of California, Santa Barbara
Princeton University
AAAS National Meeting, Chicago
DOE UIUC Corrosion Center Symposium
3rd Rocky Mountain Conf. Analytical Chem.
American Society of Mechanical Engineers,
Winter Natl. Meeting, Boulder

1991

Invited Speaker, Frontiers of Science Workshop on
Catalysis, Exxon Corporate Research Lab
Plenary Lecturer, 1st Meeting of the European
Sonochemistry Society, Lago Gardo, Italy
Colloquium Speaker, Department of Chemistry,
University of Chicago
Invited Speaker, Ultrasonics Industry Association Mtg.
Invited Speaker, Symp. on Macromolecular Assemblies,
202nd ACS National Meeting, Atlanta.
Colloquium Speaker, Department of Chemistry,
University of Illinois at Urbana-Champaign.
Invited Speaker, Acoustical Soc. Am. Mtg., Baltimore.
Materials Research Society, Fall Meeting
Eastern Illinois University
Materials Research Society National Meeting
Colloquium Lecturer, Dept. Chem., UIUC
American Physical Society National Meeting
DePauw University
BP Chemicals, London
Hoechst Celanese, Providence
Stanford University
University of California, Berkeley
University of Oregon
Lexington ACS Section

1990

Materials Research Society, Boston
NCPA, U. Miss., Oxford, MS.
199th ACS National Meeting, Boston
Union Carbide, Bound Brook
University of Delaware
University of New Mexico
Central New Mexico ACS Section
University of Illinois, Biophysics
Argonne National Laboratory
Nazerene-Olivetti University, Kankakee
duPont & Co., Wilmington
Hoechst-Celanese, Corpus Christi
Carleton University, Ottawa

1989

Plenary Lecturer, New York Catalysis Society, N.Y.
Academy of Sciences, New York
Pacific Basin Societies Mtg., Honolulu
Beckman Institute for Advanced Science and
Technology, University of Illinois
Invited Speaker and Convener, 4th International
Conf. on Bioinorganic Chemistry, Oxford
Plenary Lecturer, International Symposium on
Photochemistry, Ferrara, Italy
Gas Research Institute, Chicago
University of Maryland, College Park
NSF, Washington, D.C.
External Site Visit, Mat. Res. Lab., UIUC
Storz Instrument Co., St. Louis
University of Maryland
Dow Chemicals, Midland
Los Alamos National Laboratory
Sandia Laboratory, Albuquerque
Dow Chemicals, Freeport
Illinois State University
Case Western Reserve University
North Carolina State University

1988

Plenary Lecturer, 5th Intl. Symp. on Inclusion &
Molecular Recognition, Orange Beach
Porphyrin Symposium, 196th ACS National Meeting,
Los Angeles
Plenary Lecturer, Philadelphia Catalysis Club
Tribology Symp., 3rd Chemical Congress of
North America, Toronto
University of New Orleans
Exxon Engineering R. & D., Baton Rouge
Wichita State University
Vulcan Chemicals, Wichita
11th Intl. Symp. on the Reactivity of Solids,
Princeton, New Jersey
Beckman Institute External Review
Committee Meeting
Sun Oil R. & D., Marcus Hook, PA
AMOCO Chemicals, Naperville, IL
Purdue University

1987

Plenary Lecturer, EUCHEM Symposium on Unusual
Methodologies in Organic Synth., France
Invited Speaker, NATO Workshop on Selective
Activation of C-H & C-C Bonds, France
Invited Speaker, NSF Workshop on Organometallic
Chemistry, Asilomar
Molecular Biosystems, San Diego
Mobil R. & D., Paulsboro, NJ
Rensselaer Polytechnic University

State University of New York at Albany
General Electric Corp. Research, Schenectady
194th ACS National Meeting, New Orleans
Eli Lilly Co., Indianapolis
M & T Chemicals, New Jersey
University of Paris V (Rene Descartes)
Biennial Inorganic Chem. Symp., Harvard University
3rd International Conference on Bioinorganic
Chemistry, Netherlands
Institute for Gas Technology, Chicago
University of Pittsburgh
University of Ill., Dept. of Matl. Sciences
Johns Hopkins University
Moderator, Ultrasonics in Biophysics and
Bioengineering Symp., Allerton Park

1986

Sonochemistry Symposium, Royal Society of
Chemistry Annual Congress, Warwick
Plenary Lecturer, 4th International Seminar on
Modern Synthetic Methods, Assoc. of Swiss Chemists
Symp. on New Synthetic Approaches, Oxford Univ.
Symposium on High Energy Processes in
Organometallic Chem., 192nd Natl. ACS
Carnegie-Mellon University
M & T Chemicals, New Jersey
Imperial Chemicals, Runcorn, England
University of Edinburgh
University of Stirling, Scotland
Technical University of Darmstadt
Ciba-Geigy, Basel, Switzerland
Shell Chemicals, Amsterdam
Procter & Gamble, Cincinnati
University of Southampton
University of Liverpool
Cambridge University
University of Bristol
University of Nottingham
191st ACS National Meeting, New York
University of Illinois

1985

Symposium on Anionic Organometallics, 190th National
ACS Meeting, Chicago
Discussion Leader, Biennial Inorganic Chemical Symp.
Toronto
State-of-the-Art Symposium on Bioinorganic
Chemistry, 189th National ACS Meeting
Excited States of Porphyrins Symp., Little Rock
IEEE National Meeting, San Francisco
Exxon Corporate Research, Annandale
Ultrasonics Intl. 85 Conference, London

1984

University of North Carolina, Chapel Hill
University of South Carolina, Charleston
Exxon Corporate Research, Annandale
Amoco Chemicals, Naperville
Intl. Congress of Pacific Basin Chem. Soc.
N.Y. Catalysis Society, N.Y. Acad. Sciences
23rd ICC, Vancouver
Southeast Regional ACS Meeting
Henkel Corporation, Minneapolis
University of Minnesota, Minneapolis
Midwest Regional ACS Meeting, Kalamazoo
Chemplex Corporation, Rolling Meadows
187th ACS National Meeting, St. Louis
University of Iowa, Iowa City
Engelhard Chemicals, Summit

1983

University of Illinois at Urbana-Champaign
Northwestern University, Evanston
University of California, Riverside
University of California, Santa Barbara
University of California, Irvine
University of California, Los Angeles
University of Southern California, L. A.
California Institute of Technology, Pasadena
University of California, Davis
Stanford University, Stanford
University of California, Berkeley
University of Oregon, Eugene
University of Wisconsin, Madison
186th ACS Natl. Meeting, Washington, D.C.
Eastman Kodak, Kingsport, Tenn.
Intl. Conference Bioinorg. Chem., Florence
University of Chicago
Celanese Corporate Research, Summit, NJ.
Ohio State University
Princeton University
DuPont Central Research, Wilmington, DE
Massachusetts Institute of Technology
Harvard University
Marquette University
185th ACS National Meeting, Seattle

1982

Shell Development, Westhallow
3rd Intl. Symp. on Homogen. Catal., Milan
Gordon Research Conf., Inorganic Chemistry
Gordon Research Conf., Organometallics
DIC Biennial Symposium, Indiana University
184th ACS National Meeting, Kansas City
University of Illinois, Chicago Circle

1981

Standard Oil of Ohio, Cleveland
28th IUPAC Congress, Vancouver
Ball State University
IEEE Ultrasonics Symposium, Chicago
17th Midwest Regional ACS Meeting
181st ACS National Meeting, Atlanta

1980 - 1977

Gordon Research Conf., Inorganic Chemistry, 1980.
California Institute of Technology, 1979.
Harvard University, 1978.
Bell Laboratories, Murray Hill, 1978.
IBM, Yorktown and San Jose, 1978.
University of California, Berkeley, 1978.
University of California, Los Angeles, 1978.
Stanford University, 1978.
Exxon Corporate Research, Linden, NJ, 1977.
University of Illinois at Urbana-Champaign, 1977.
Pacific Conf. on Chemistry and Spectroscopy, 1977.

Editorships:

- 1997 – 98 Co-editor, *Sonochemistry and Sonoluminescence*, Kluwer Academic Publishers.
1996 – Editorial Board, *Ultrasonics Sonochemistry*, Elsevier Science Publishers.
1996 – Founding Editorial Board, *Journal of Porphyrins and Phthalocyanines*, Wiley Publishers.
1993 – 1996 Founding Editorial Board, *Intl. J. of Mechanochemistry & Mech. Alloying*, Cambridge Interscience.
1993 – 1996 Founding Editorial Board, *Advanced Oxidation Technologies*, AOT Press.
1993 – 96 Volume Editor, *Comprehensive Supramolecular Chemistry*, Elsevier/Pergamon Press.
1993 – 96 Founding Editor, *Ultrasonics Sonochemistry*, Elsevier Science Publishers.
1992 – 96 Editorial Board, *Ultrasonics*, Elsevier Science Publishers.
1991 – 94 Editorial Board, *Research on Chemical Intermediates*, Elsevier Science Publishers.
1990 Guest Editor, Special Issue on Sonochemistry, *Ultrasonics*, Butterworth Publishing.
1985 – 87 Editor, *Ultrasound: Its Chemical, Physical, and Biological Effects*, 1st ed.; VCH Publishers.
1986 – 87 Editor, *High Energy Processes in Organometallic Chemistry*, ACS Books.

Other Recent Professional Activities:

- 2003 NASA proposal evaluation panel, Scientific Projects in Microgravity.
2000 Organizer, Sonochemistry Symposium, Pacifichem 2000 International Congress, Honolulu.
1997 – 00 Chairman, MRS Medal Awards Subcommittee, Materials Research Society.
1996 – 00 Awards Committee, Materials Research Society.
1998 Sonochemistry & Sonoluminescence Symposium Co-organizer, Joint ASA/EAA Intl. Meeting, Berlin.
1998 Sonochemistry Symposium Co-organizer, Acoustic Society of America Meeting, Seattle.
1996 – International Scientific Committee, European Society of Sonochemistry.
1997 NSF Career Award Selection Committee.
1996 – 97 Co-Organizer, NATO Advanced Study Institute on Sonochemistry and Sonoluminescence.
1993 – North American Board Member, International Mechanochemistry Association, IUPAC.
1990 – Hertz Foundation Graduate Fellowship Interviewer.
1993 – 95 Organizer, Chemical Effects of Ultrasound Symp., Pacifichem '95 Intl. Congress, Honolulu.
1989 – 93 Organizer, Eli Lilly Lectureship on Molecular Recognition; Beckman Institute.
1991 Co-Organizer, Cavitation Symposium, Natl. Meeting, Acoustical Society of America, Baltimore.
1989 Organizer, Molecular Recognition Symposium, 4th Intl. Conf. on Bioinorganic Chemistry.
1989 Co-Organizer, Dow Molecular Recognition Symposium, Beckman Institute.
1988 – 89 Organizer, Sonochemistry Symposium, Pacifichem '89 International Congress, Honolulu.
1987 – 89 Chairman, ACS Local Section, Campaign-Urbana.

Professional Society Memberships:

- Acoustical Society of America (*Fellow*)
Alpha Chi Sigma (Professional Chemistry Fraternity)
American Association for the Advancement of Science (*Fellow*)
American Chemical Society
European Sonochemistry Society (Charter Member)
International Mechanochemical Association (IUPAC chartered)
Materials Research Society
Royal Society for the Arts, Manufactures, and Commerce, 1974–82 (*Fellow*)

Personal Data:

b., Chicago, September 16, 1952. Spouse: Adele Mazurek, m. 1975. Son: Benjamin, b. 1992.

Major Research Funding (past ten years):

2003 – 06 NSF; "Chemical Effects of High Intensity Ultrasound" \$562,500 / 3 yrs.
2000 – 04 NIH 5R01-HL25934 "Heme Proteins, Microspheres, and Their Synthetic Analogs" \$1,365,000 / 4 yrs.
1999 – 04 DARPA; "Chemical Control of Single Bubble Cavitation" \$637,121 / 3.5 yrs.
1999 – 03 NSF; "Chemical Effects of Ultrasound," \$480,000 / 3 yrs.
1990 – xx DOE; UIUC Materials Res. Lab, "Field Responsive Porphyrinic Materials," \$100,000 / yr.
1997 – 02 DOD; Army MURI, "Dendrimeric Materials," Multi-PI proposal; K.S.S. portion: \$100,000 / yr.
2000 – 02 PG Research Foundation "Ultrasonic Gas Dispersion and Dissolution" \$52,933.
1997 – 00 NIH; "Heme Proteins, Protein Microspheres, and Their Synthetic Analogs," \$924,944 / 4 yrs.
1995 – 99 VivoRx Pharmaceuticals, Inc., "Biomedical Applications of Protein Microspheres," \$150,000.
1994 – 99 NSF; "Chemical Effects of Ultrasound," \$738,673 / 5 yrs.
1996 – 99 DOE; "Cavitation Hydrothermal Oxidation," \$478,027 / 3 yrs.
1992 – 97 NIH; "Heme Proteins and Their Synthetic Analogs," \$782,447 / 4 yrs.
1996 DOE; "Sonoluminescence", subcontract from Lawrence Livermore Natl. Lab, \$10,000.
1995 – 97 UIUC Critical Research Initiative, "Non-Natural Self-Organizing Molecules," \$120,000 / 2 yrs.
1989 – 96 NSF; UIUC Materials Res. Lab, "Effects of Ultrasound on Heterogeneous Catalysis," \$386,000 / 5 yrs.
1992 – 95 NSF; "Visualization in Teaching Chemistry," with S. S. Zumdahl, \$368,505 / 3 yrs.
1992 – 94 NSF; Special Creativity Extension; "Chemical Effects of Ultrasound," \$260,000 / 2 yrs.
1992 – 94 ACS-PRF; type AC; "Porphyrin Assemblies," \$40,000 / 2 yrs.
1993 Exxon Research & Engineering Corp., "Coal Depolymerization New Leads Program," \$15,000.
1992 VivoRx, Inc.; "Proteinaceous Microspheres"; \$5,000.
1989 - 94 Eli Lilly & Co.; UIUC Molecular Recognition Lectureship, \$25,000 total costs.
1987 - 92 NIH; "Synthetic Analogs of Heme Proteins," \$795,000/5 yrs.
1990 - 92 NSF; "Chemical Effects of High Intensity Ultrasound," \$301,000/3 yrs.

Student and Postdoctoral Associates, Past and Present:

13 Ph.D. Graduate Students presently in group (08/03).
4 Postdoctoral Research Associates presently in group (08/03).
36 Ph.D. Graduate Students supervised and theses completed.
23 Past Postdoctoral Research Associates.
4 M.S. Graduate Students supervised and theses completed.
15 Undergraduate Research Assistants supervised.

Teaching Responsibilities:

Chem 101 General Chemistry; 1980.
Chem 109 Advanced Placement General Chemistry Laboratory, 1999.
Chem 115 Chemistry of Everyday Phenomena; 1990, 1991, 1992, 1993, 1997, 1998.
Chem 315 Inorganic Chemistry; 1982, 1991, 1994, 1995, 1999, 2000.
Chem 319 Instrumental Characterization of Chemical Systems Laboratory, 2000.
Chem 383 Dynamics, Structure and Physical Methods Laboratory; 1982, 1983, 1984, 1994.
Chem 405 Inorganic Graduate Seminar; 1978, 1979, 1980, 1985, 1996, 1997, 1998, 1999.
Chem 406 Physical Methods in Inorganic Chemistry; 1978, 1980, 1982, 1984.
Chem 566 Graduate Level Materials Chemistry
Chem 407 Special Topics in Inorganic Chemistry: Bioinorganic Chem.; 1979, 1982, 1987, 1989, 1993, 2003.
Chem 407 Special Topics in Inorganic Chemistry: Biological Electron Transfer; 1984.
Chem 407 Materials Synthesis; 1996, 2004.

Committee and Administrative Duties:

University of Illinois at Urbana-Champaign, Search Committee for MacArthur Chaired Professorships, 2003.
University of Illinois at Urbana-Champaign, Search Committee for Director of Materials Research Laboratory, 1999.
University of Illinois at Urbana-Champaign, Center for Microscopy and Imaging Advisory Committee, 1997 – 2000.
University of Illinois at Urbana-Champaign, Chair, Evaluation Committee of Director of the Environmental Council, 1998-99
University of Illinois at Urbana-Champaign Task Force on the Environment, 1993.
University of Illinois at Urbana-Champaign, Senator (elected post), 1986 – 1987.

College of Liberal Arts and Sciences, Search Committee for Director of the School of Chemical Sciences, 1999.
College of Liberal Arts and Sciences, Chair, Administrative Evaluation of Director of School of Life Sciences, 1993–94.
College of Liberal Arts and Sciences, Council on General Education (elected post), 1982 – 84.
College of Liberal Arts and Science, Ad Hoc B.A./B.S. Curriculum Committee, 1985 – 86.

College of Engineering, Materials Research Laboratory Director Search Committee, 1998–1999
College of Engineering, Materials Research Laboratory Council, 1997 – .

Beckman Institute for Advanced Science and Technology, Program Advisory Committee, 1989 – 91.
Beckman Institute for Advanced Science and Technology, Molecular Recognition Group Leader, 1988 – 91.

School of Chemical Sciences, Brochure Co-Editor, 1980 – 81; 1984 – 85.
School of Chemical Sciences, New Building Committee, 1993 – 95.
School of Chemical Sciences, Safety, 1979 – 80.
School of Chemical Sciences, Service Facilities, 1988 – 89; 2001 – 03.
School of Chemical Sciences, Supplies and Stockrooms, 1983 – 86; chairman, 1986 – 92.
School of Chemical Sciences, Teaching Evaluation and Awards, 1982 – 87.

Department of Chemistry, Building and Space Allocation, 1981 – 82, 1993.
Department of Chemistry, Budget and Operations, Core Laboratories, 1984 – 88.
Department of Chemistry, Budget and Operations, Inorganic Chemistry, 1989 – 92, 1996 – 1997.
Department of Chemistry, Courses and Curriculum, 1987 – 90.
Department of Chemistry, Department Colloquium Chairman, 1987 – 89.
Department of Chemistry, Department Reorganization Committee, 1997.
Department of Chemistry, Executive Advisory Committee, 1994 – 95, 2002 – 04.
Department of Chemistry, General Chemistry, 1981 – 82.
Department of Chemistry, Graduate Student Advising, 1980 – 85.
Department of Chemistry, Graduate Student Fellowships, 1986 – 87.
Department of Chemistry, Graduate Student Recruitment and Appointments, 1978 – 81, 1996 – 99; chair, 2000 – 01.
Department of Chemistry, Inorganic Seminar Chairman, 1978 – 81, 1996 – 99.
Department of Chemistry, Staff Committee, 1996 – 03.

Publications List:

(chronological by publication type)

Books:

1. Suslick, K. S., ed. *High Energy Processes in Organometallic Chemistry*; Am. Chem. Soc.: Washington, DC, 1987; Symposium Series #333.
2. Suslick, K. S., ed. *Ultrasound: Its Chemical, Physical, and Biological Effects*; VCH Publishers: New York, 1988.
3. Suslick, K. S., ed. *Comprehensive Supramolecular Chemistry*, vol. 5, *Bioinorganic Systems*; Elsevier Publishers: Oxford, 1996.
4. Crum, L. A.; Mason, T. J.; Reisse, J.; Suslick, K. S., eds. *Sonochemistry and Sonoluminescence*, Kluwer Publishers: Dordrecht, Netherlands, 1999; NATO ASI Series C, v. 524.

Major Reviews:

5. Collman, J. P.; Halbert, T. R.; Suslick, K. S. "O₂ Binding by Metalloporphyrins" in *Metal Ion Activation of Dioxygen*; Spiro, T. G., ed.; Prentice-Hall: New York, 1980; pp. 1-72.
6. Suslick, K. S. "Organometallic Sonochemistry" *Adv. Organomet. Chem.* **1986**, *25*, 73-119.
7. Suslick, K. S. "Synthetic Applications of Ultrasound" *Modern Synthetic Methods* **1986**, *4*, 1-60.
8. Suslick, K. S. "Homogeneous Sonochemistry" in *Ultrasound: Its Chemical, Physical and Biological Effects*; Suslick, K. S., ed.; VCH Publishers: New York, 1988; pp. 123-164.
9. Suslick, K. S. "Shape Selective Hydrocarbon Oxidation" in *Activation and Functionalization of Alkanes*; Hill, C. L., ed.; Wiley & Sons: New York, 1989; pp. 219-241.
10. Suslick, K. S.; Cook, B. R. "Shape Selective Oxidation as a Mechanistic Probe" in *Inclusion Phenomena and Molecular Recognition*; Atwood, J. L., ed.; Plenum Press: London, 1990; pp. 209-215.
11. Suslick, K. S.; Doktycz, S. J. "The Effects of Ultrasound on Solids" in *Advances in Sonochemistry*; Mason, T. J., Ed.; JAI Press: New York, 1990; vol.1, pp 197-230.
12. Suslick, K. S. "Sonochemistry" *Science* **1990**, *247*, 1439-1445.
13. Suslick, K. S.; Grinstaff, M. W. "Proteinaceous Microspheres" *Macromolecular Assemblies*; Stroeve, P.; Balazs, A. C., eds.; Am. Chem. Soc.: Washington, D.C., 1992; pp. 218-226.
14. Suslick, K. S. "Ultrasound: Applications to Materials Chemistry" in *Encyclopedia of Materials Science and Engineering*; Cahn, R. W., ed.; Pergamon Press: Oxford, 1993; 3rd Suppl., pp. 2093-2098.

Major Reviews (continued):

15. Chen, C.-T.; Suslick, K. S. "One-Dimensional Coordination Polymers" *Coord. Chem. Rev.*, **1993**, *128*, 293-322.
16. Suslick, K. S. "Sonochemistry of Transition Metal Compounds" in *Encyclopedia of Inorganic Chemistry*; King, R. B., ed.; J. Wiley & Sons: New York, 1994; vol. 7, pp. 3890-3905.
17. Suslick, K. S. "Applications of Ultrasound to Heterogeneous Catalysis" *Advances in Catalyst Preparation*; Catalytica Studies Division; 1995.
18. Suslick, K. S. "Applications of Ultrasound to Materials Chemistry" *MRS Bulletin* **1995**, *20*, 29-34.
19. Suslick, K. S.; Van Deusen-Jeffries, S. "Shape Selective Biomimetic Oxidation Catalysis" *Comprehensive Supramolecular Chemistry*, vol. 5; Lehn, J. M., ed. Elsevier Publishers: Oxford, 1996; pp. 141-170.
20. Suslick, K. S.; Crum, L. A. "Sonochemistry and Sonoluminescence" in *Encyclopedia of Acoustics*; Crocker, M. J., ed.; Wiley-Interscience: New York, 1997; vol. 1, ch. 26, pp. 271-282.
21. Suslick, K. S. "Sonocatalysis" in *Handbook of Heterogeneous Catalysis*; Ertl, G.; Knozinger, H.; Weitkamp, J.; eds.; Wiley-VCH: Weinheim, 1997; vol. 3, ch. 8.6, pp. 1350-1357.
22. Suslick, K. S. "Sonoluminescence and Sonochemistry" *IEEE Ultrasonics Symp. Proc.* **1997**, vol. 1, pp. 523-534.
23. Suslick, K. S.; Matula, T. J. "Acoustic Cavitation, Sonochemistry, and Sonoluminescence" in *Wiley Encyclopedia of Electrical & Electronics Engineering*; Webster, J.G., ed.; Wiley-Interscience: New York, 1999, vol. 22, pp. 646-657.
24. Suslick, K. S.; Crum, L. A. "Sonochemistry and Sonoluminescence" in *Handbook of Acoustics*; Crocker, M. J., ed.; Wiley-Interscience: New York, 1998; pp. 243-253.
25. Suslick, K. S. "Sonochemistry" in *Kirk-Othmer Encyclopedia of Chemical Technology*; 4th Ed. J. Wiley & Sons: New York, 1998, vol. 26, 517-541.
26. Suslick, K. S.; Didenko, Y.; Fang, M. M.; Hyeon, T.; Kolbeck, K. J.; McNamara III, W. B.; Mdleleni, M. M.; Wong, M. "Acoustic Cavitation and Its Chemical Consequences" *Phil. Trans. Roy. Soc. London A* **1999**, *357*, 335-353.
27. Suslick, K. S.; Price, G. "Applications of Ultrasound to Materials Chemistry" *Annu. Rev. Matl. Sci.*, **1999**, *29*, 295-326.
28. Chou, J.-H.; Kosal, M. E.; Nalwa, H.S.; Rakow, N.A.; Suslick, K. S. "Applications of Porphyrins and Metalloporphyrins to Materials Chemistry" in *The Porphyrin Handbook*, Kadish, K.; Smith, K.; Guillard, R., eds.; Academic Press: New York, 2000; vol. 6, ch. 41, pp. 43-131.
29. Suslick, K. S. "Shape Selective Oxidation by Metalloporphyrins" in *The Porphyrin Handbook*, Kadish, K.; Smith, K.; Guillard, R., ed.; Academic Press: New York, 2000; vol. 4, ch. 28, pp. 41-63.
30. Suslick, K. S. "Sonochemistry: A Physical Perspective" in *Nonlinear Acoustics at the Turn of the Millennium*, Lauterborn, W.; Kurz, T., eds. Amer. Inst. Physics: Melville, NY, 2000, pp. 95-104.
31. Kosal, M. E.; Suslick, K. S. "Microporous Porphyrin and Metalloporphyrin Materials" *J. Sol. St. Chem.* **2000**, *152*, 87-98 (invited review).
32. Suslick, K. S. "Sonochemistry" in *Comprehensive Coordination Chemistry 2*; Elsevier Science: New York, 2003.

Popularizations:

33. Suslick, K. S.; Reinert, T. J. "Synthetic Analogs of O₂ Binding Heme Proteins" *J. Chem. Ed. "State of the Art: Bioinorganic Chemistry"* issue, **1985**, *62*, 974-982.
34. Suslick, K. S. "Sonochemistry and Sonocatalysis" in *1988 McGraw-Hill Yearbook of Science and Technology*; McGraw-Hill: New York, 1987, pp 430-433.
35. Suslick, K. S. "The Chemical Effects of Ultrasound" *Scientific American* **1989** (**2**) *260*, 80-86.
36. Suslick, K. S. "Sounding Out New Chemistry" *New Scientist* **1990**, *1702*, 50-53.
37. Suslick, K. S. "Cavitation" and "Sonochemistry" in *McGraw-Hill Encyclopedia of Science and Technology*; McGraw-Hill: New York; 7th Ed., 1992, pp. 320, pp. 683-685; 8th Ed., 1997, pp. 744-747.
38. Suslick, K. S. "Sonochemistry" in *McGraw-Hill Encyclopedia of Chemistry*; 2nd Ed. McGraw-Hill: New York, 1992, pp. 1021-1023.
39. Suslick, K. S. "The Chemistry of Ultrasound" in *Yearbook of Science & the Future 1994*; Encyclopaedia Britannica: Chicago, 1994; pp 138-155.
40. Crum, L. A.; Suslick, K. S. "Bubbles Hotter than the Sun" *New Scientist* **1995**, *146* (#1975), 36-40.
41. Suslick, K. S. "Set for a 'Chain Reaction'" *Inside Illinois* **1997**, *16* (#17), 5.
42. Suslick, K. S. "Sonoluminescence, Camera, Action!" *Engineering & Science (California Institute of Technology)* **1997** *40* (#2), 4-5.
43. Suslick, K. S. "Sonochemistry" in *1999 McGraw-Hill Yearbook of Science and Technology*; McGraw-Hill: New York, 1998, pp. 342-344.
44. Suslick, K. S. "Sonochemistry" in *Kirk-Othmer Concise Encyclopedia of Chemical Technology*; 4th Ed. J. Wiley & Sons: New York, 1999, pp. 1867-1868.
45. Suslick, K. S. "Sonochemistry" in *McGraw-Hill Concise Encyclopedia of Science and Technology*; 9th Ed. McGraw-Hill: New York; 1999, 342-344.
46. Suslick, K. S. "UI Chemist Meets the Federal District Court" *Inside Illinois* **1999**, *18* (#19), 7.
47. Suslick, K. S. "Sonochemistry and Sonoluminescence" in *Encyclopedia of Physical Science and Technology*, 3rd ed. Academic Press: San Diego, 2001, vol. 17, pp. 363-376.

Patents:

48. Suslick, K. S. "Isotope Separation by Photochromatography" *U.S. Patent 4,010,100*; March 1, 1977.
49. Desai, N. P.; Soon-Shiong, P.; Sandford, P. A.; Grinstaff, M. W.; Suslick, K. S. "Magnetic Resonance Imaging with Fluorocarbons Encapsulated in a Cross-linked Polymeric Shell" *U. S. Patent 5,362,478*; Nov. 8, 1994.
50. Desai, N. P.; Soon-Shiong, P.; Sandford, P. A.; Grinstaff, M. W.; Suslick, K. S.; "Methods for *In Vivo* Delivery of Substantially Water Insoluble Pharmacologically Active Agents and Compositions Useful Therefor" *U. S. Patent 5,439,686*; Aug. 8, 1995.
51. Grinstaff, M. W.; Soon-Shiong, P.; Wong, M.; Sandford, P. A.; Suslick, K. S.; Desai, N. P. "Composition Useful for *In Vivo* Delivery of Biologics and Methods Employing Same" *U. S. Patent 5,498,421*; Mar. 12, 1996.
52. Grinstaff, M. W.; Desai, N. P.; Suslick, K. S.; Soon-Shiong, P.; Sandford, P. A.; Merideth, N. R. "Method for the Preparation of Fluorocarbon-Containing Polymeric Shells for Medical Imaging" *U. S. Patent 5,505,932*; Apr. 9, 1996.
53. Grinstaff, M. W.; Desai, N. P.; Suslick, K. S.; Soon-Shiong, P.; Sandford, P. A.; Merideth, N. R. "Non-Fluorinated Polymeric Shells for Medical Imaging" *U. S. Patent 5,508,021*; Apr. 16, 1996.
54. Grinstaff, M. W.; Desai, N. P.; Suslick, K. S.; Soon-Shiong, P.; Sandford, P. A.; Merideth, N. R. "Polymeric Shells for Medical Imaging Prepared from Synthetic Polymers, and Methods for the Use Thereof" *U. S. Patent 5,512,268*; Apr. 30, 1996.
55. Desai, N. P.; Soon-Shiong, P.; Sandford, P. A.; Grinstaff, M. W.; Suslick, K. S.; "Methods for *In Vivo* Delivery of Substantially Water Insoluble Pharmacologically Active Agents and Compositions for the Use Thereof" *U. S. Patent 5,560,933*; Oct. 1, 1996.
56. Grinstaff, M. W.; Soon-Shiong, P.; Wong, M.; Sandford, P. A.; Suslick, K. S.; Desai, N. P. "Methods for the Preparation of Blood Substitutes for *In Vivo* Delivery" *U. S. Patent 5,635,207*; June 3, 1997.
57. Grinstaff, M. W.; Soon-Shiong, P.; Wong, M.; Sandford, P. A.; Suslick, K. S.; Desai, N. P. "Methods For The Preparation Of Nucleic Acids For *In Vivo* Delivery" *U. S. Patent 5,639,473*; June 17, 1997.
58. Grinstaff, M. W.; Soon-Shiong, P.; Wong, M.; Sandford, P. A.; Suslick, K. S.; Desai, N. P. "Methods For *In Vivo* Delivery Of Nutraceuticals And Compositions Useful Therefor" *U. S. Patent 5,650,156*; July 22, 1997.
59. Grinstaff, M. W.; Soon-Shiong, P.; Wong, M.; Sandford, P. A.; Suslick, K. S.; Desai, N. P. "Methods for the Preparation of Pharmaceutically Active Agents for *In Vivo* Delivery" *U. S. Patent 5,665,382*; Sept. 9, 1997.
60. Grinstaff, M. W.; Soon-Shiong, P.; Wong, M.; Sandford, P. A.; Suslick, K. S.; Desai, N. P. "Methods for the Preparation of Immunostimulating Agents for *In Vivo* Delivery" *U. S. Patent 5,665,383*; Sept. 9, 1997.
61. Suslick, K. S.; Rakow, N. A. "Colorimetric Artificial Nose Having an Array of Dyes and Method for Artificial Olfaction" *U.S. Patent 6,368,558*; April 9, 2002.
62. Suslick, K. S.; Rakow, N. A.; Sen, A. "Colorimetric Artificial Nose Having an Array of Dyes and Method for Artificial Olfaction: Shape Selective Sensors" *U.S. Patent 6,495,102 B1*; Dec. 17, 2002.

Journal Publications:

63. Collman, J. P.; Brauman, J. I.; Suslick, K. S. "Oxygen Binding to Iron Porphyrins" *J. Am. Chem. Soc.* **1975**, *97*, 7185-7186.
64. Collman, J. P.; Brauman, J. I.; Halbert, T. R.; Suslick, K. S. "Nature of Oxygen and Carbon Monoxide Binding to Metalloporphyrins and Heme Proteins" *Proc. Natl. Acad. Sci., U.S.A.* **1976**, *73*, 3333-3337.
65. Collman, J. P.; Suslick, K. S. "Models for Cooperative Oxygen Binding in Hemoglobin" *Pure and Applied Chemistry* **1978**, *50*, 951-961.
66. Collman, J. P.; Brauman, J. I.; Doxsee, K. M.; Halbert, T. R.; Hayes, S. E.; Suslick, K. S. "Oxygen Binding to Cobalt Porphyrins" *J. Am. Chem. Soc.* **1978**, *100*, 2761-2766.
67. Collman, J. P.; Brauman, J. I.; Doxsee, K. M.; Halbert, T. R.; Suslick, K. S. "Model Compounds for the 'T' State of Hemoglobin" *Proc. Natl. Acad. Sci., U.S.A.* **1978**, *75*, 564-568.
68. Collman, J. P.; Brauman, J. I.; Rose, E.; Suslick, K. S. "Cooperativity in Oxygen Binding to Iron Porphyrins" *Proc. Natl. Acad. Sci., U.S.A.* **1978**, *75*, 1052-1055.
69. Jameson, G. B.; Molinaro, F. S.; Ibers, J. A.; Collman, J. P.; Brauman, J. I.; Rose, E.; Suslick, K. S. "Structural Changes Upon Oxygenation of an Fe(II)(porphyrinato)(imidazole) Complex" *J. Am. Chem. Soc.* **1978**, *100*, 6769-6770.
70. Jameson, G. B.; Molinaro, F. S.; Ibers, J. A.; Collman, J. P.; Brauman, J. I.; Rose, E.; Suslick, K. S. "Models for the Active Site of Oxygen Binding Hemoproteins. Dioxygen Binding Properties and the Structures of (2-Methylimidazole)-meso-tetra($\alpha,\alpha,\alpha,\alpha$ -o-pivalamidophenyl)porphyrinatoiron(II)—Ethanol and Its Dioxygen Adduct." *J. Am. Chem. Soc.* **1980**, *102*, 3224-3237.
71. Walters, M. A.; Spiro, T. G.; Collman, J. P.; Suslick, K. S. "Resonance Raman of O₂ Bound to Fe(II)(porphyrinato)(hindered-imidazole) Complexes" *J. Am. Chem. Soc.* **1980**, *102*, 6857-6858.
72. Suslick, K. S.; Schubert, P. F.; Goodale, J. W. "Sonochemistry and Sonocatalysis of Iron Carbonyls" *J. Am. Chem. Soc.* **1981**, *103*, 7342-7344.
73. Suslick, K. S.; Schubert, P. F.; Goodale, J. W. "Chemical Dosimetry of Ultrasonic Cavitation" *IEEE Ultrason. Symp. Proc.* **1981**, *2*, 612-616.
74. Suslick, K. S.; Fox, M. M. "A Bis-Pocket Porphyrin" *J. Am. Chem. Soc.* **1983**, *105*, 3507-3510.
75. Suslick, K. S.; Goodale, J. W.; Wang, H. H.; Schubert, P. F. "Sonochemistry and Sonocatalysis of Metal Carbonyls" *J. Am. Chem. Soc.* **1983**, *105*, 5781-5785.
76. Suslick, K. S.; Schubert, P. F. "Sonochemistry of Mn₂(CO)₁₀ and Re₂(CO)₁₀" *J. Am. Chem. Soc.* **1983**, *105*, 6042-6044.
77. Suslick, K. S.; Schubert, P. F.; Wang, H. H.; Goodale, J. W. "Organometallic Sonochemistry and Sonocatalysis" in *Inorganic Chemistry: Toward the 21st Century*; Chisholm, M.A., ed.; Am. Chem. Soc.: Washington, D.C., 1983; p.550.
78. English, D. R.; Hendrickson, D. N.; Suslick, K. S. "High Oxidation State Iron Porphyrin Dimers" *Inorg. Chem.* **1983**, *22*, 367-368.
79. Suslick, K. S.; Gawienowski, J. W.; Schubert, P. F.; Wang, H. H. "Alkane Sonochemistry" *J. Phys. Chem.* **1983**, *87*, 2299-2301.
80. Suslick, K. S.; Fox, M. M.; Cook, B. R.; English, D. R. "New Synthetic Analogs of Heme Proteins" *Inorg. Chem. Acta* **1983**, *79(B7)*, 109-110.

-
-
81. Suslick, K. S.; Gawienowski, J. W.; Schubert, P. F.; Wang, H. H. "Sonochemistry in Non-aqueous Liquids" *Ultrasonics* **1984**, *22*, 33-36.
 82. Bocian, D. F.; Findsen, E. W.; Hoffman, J. A.; Schick, G. A.; English, D. R.; Hendrickson, D. N.; Suslick, K. S. "Interaction of Dioxygen and Binuclear Nitride-Bridged Iron Porphyrins" *Inorg. Chem.* **1984**, *23*, 800-807.
 83. Suslick, K. S.; English, D. R.; Hendrickson, D. N.; Spiro, T. G.; Crisanti, M. "Resonance Raman Spectra of High Oxidation State Iron Porphyrin Dimers" *Inorg. Chem.* **1984**, *23*, 3897-3901.
 84. Suslick, K. S.; Fox, M. M.; Reinert, T. J. "Influence on CO and O₂ Binding by Fe(II) Porphyrinates" *J. Am. Chem. Soc.* **1984**, *106*, 4522-4525.
 85. Finke, R. G.; Droege, M. W.; Cook, J. C.; Suslick, K. S. "Fast Atom Bombardment Mass Spectroscopy of Polyoxoanions" *J. Am. Chem. Soc.* **1984**, *106*, 5750-5751.
 86. Suslick, K. S.; Johnson, R. E. "Sonochemical Activation of Transition Metals" *J. Am. Chem. Soc.* **1984**, *106*, 6856-6858.
 87. English, D. R.; Hendrickson, D. N.; Suslick, K. S.; Eigenbrot, Jr., C. W.; Scheidt, W. R. "A Low-Spin Five-Coordinate Ferric Porphyrin Complex: [5,10,15,20-tetra(4-methoxyphenyl)porphyrinato](hydrosulfido)iron(III)" *J. Am. Chem. Soc.* **1984**, *106*, 7528-7529.
 88. Suslick, K. S.; Cook, B. R.; Fox, M. M. "Shape Selective Hydroxylation of Hydrocarbons" *J. Chem. Soc. Chem. Commun.* **1985**, 580-582.
 89. Woolery, G.; Walter, M. A.; Suslick, K. S.; Powers, J.; Spiro, T. G. "EXAFS Evidence for Elongated Fe-O₂ Bond Lengths in O₂ Adducts of "Picket-Fence" Hemes: Implications of Hb Cooperativity" *J. Am. Chem. Soc.* **1985**, *107*, 2370-2372.
 90. Suslick, K. S.; Cline, Jr., R. E.; Hammerton, D. A. "Determination of Local Temperatures Caused by Acoustic Cavitation" *IEEE Ultrasonics Symp. Proc.* **1985**, *4*, 1116-1121
 91. Suslick, K. S.; Hammerton, D. A. "The Site and Nature of Sonochemical Reactions" *Ultrasonics Intl.* **1985**, 231-236.
 92. Suslick, K. S. "A Non-Coercive, Menu-Driven Grading System" *J. Chem. Ed.* **1985**, *61*, 408-409.
 93. English, D. R.; Hendrickson, D. N.; Suslick, K. S. "(FeTPP)₂N²⁺: an Fe(IV)-Porphyrin π -Radical Cation" *Inorg. Chem.* **1985**, *24*, 121-122.
 94. Suslick, K. S.; Hammerton, D. A. "The Site of Sonochemical Reactions" *IEEE Trans. Ultrasonics, Ferroelec., Freq. Contr.* **1986**, *33*, 143-147.
 95. Finke, R. G.; Droege, M. W.; Cook, J. C.; Suslick, K. S. "Fast Atom Bombardment Mass Spectrometry (FABMS) of Large Clusters" *Inorg. Chem.* **1986**, *25*, 241-243.
 96. Suslick, K. S.; Cline, Jr., R. E.; Hammerton, D. A. "The Sonochemical Hot Spot" *J. Am. Chem. Soc.* **1986**, *108*, 5641-5642.
 97. Cook, B. R.; Reinert, T. J.; Suslick, K. S. "Shape Selective Alkane Hydroxylation by Metalloporphyrin Catalysts" *J. Am. Chem. Soc.* **1986**, *108*, 7281-7286.
 98. Suslick, K. S.; Casadonte, D. J.; Green, M. L. H.; Thompson, M. E. "Effects of High Intensity Ultrasound on Inorganic Solids" *Ultrasonics* **1987**, *25*, 56-59.
-
-

-
-
99. Suslick, K. S.; Cook, B. R. "Regioselective Epoxidations of Dienes with Manganese(III) Porphyrin Catalysts" *J. Chem. Soc. Chem. Comm.* **1987**, 200-202.
 100. Hendrickson, D. N.; Kinnaird, M. G.; Suslick, K. S. "Photochemistry of (5,10,15,20-Tetraphenylporphyrinato)iron(III) Halide Complexes, Fe(TPP)(X)" *J. Am. Chem. Soc.* **1987**, *109*, 1243-1244.
 101. Suslick, K. S.; Acholla, F. V.; Cook, B. R. "Photocatalytic Oxidation of Hydrocarbons by (5,10,15,20-Tetraphenylporphyrinato)manganese(III) Perchlorate and Periodate" *J. Am. Chem. Soc.* **1987**, *109*, 2818-2819.
 102. Suslick, K. S.; Casadonte, D. J. "Heterogeneous Sonocatalysis with Nickel Powder" *J. Am. Chem. Soc.* **1987**, *109*, 3459-3461.
 103. Girolami, G. S.; Milam, S. N.; Suslick, K. S. "Synthesis and Characterization of Actinide Mono- and Bis(porphyrin) Complexes" *Inorg. Chem.* **1987**, *26*, 343-344.
 104. Suslick, K. S.; Flint, E. B.; Jensen, J. A. "A Kinetics FT-IR Experiment for the Undergraduate Laboratory" *J. Chem. Ed.* **1987**, *64*, 547-549.
 105. Chatakondur, K.; Green, M. L. H.; Thompson, M. E.; Suslick, K. S. "The Enhancement of Intercalation Reactions by Ultrasound" *J. Chem. Soc. Chem. Comm.* **1987**, 900-901.
 106. Suslick, K. S. "The Sonochemistry of Organometallic Compounds" in *High Energy Processes in Organometallic Chemistry*; Suslick, K. S., ed.; ACS Symp. Series #333: Washington, D.C., 1987; pp. 191-208.
 107. Suslick, K. S.; Acholla, F. V.; Cook, B. R.; Kinnaird, M. G. "Photochemistry of Fe(III) and Mn(III) Porphyrins" *Recl. Trav. Chim.* **1987**, *106*, 329.
 108. Suslick, K. S. "'Porphyrins: Excited States and Dynamics,' bk. rev." *J. Med. Chem.* **1987**, *30*, 1702.
 109. Suslick, K. S.; Flint, E. B. "A Versatile Sonochemical Reaction Vessel" in *Experimental Organometallic Chemistry: A Practicum in Synthesis and Characterization*; Wayda, A. and Darenbourg, M.Y., eds.; ACS Symposium Series: Washington, D.C.; 1987, p. 195.
 110. Suslick, K. S.; Flint, E. B. "Sonoluminescence of Non-Aqueous Liquids" *Nature* **1987**, *330*, 553-555.
 111. Girolami, G. S.; Milam, S. N.; Suslick, K. S. "Actinide Bis(porphyrinate) π -Radical Cations and Dications, including X-ray Crystal Structure of [(TPP)₂Th][SbCl₆]" *J. Am. Chem. Soc.* **1988**, *110*, 2011-2012.
 112. Suslick, K. S. "The Production of High Energy Species by Turbulent Flow" *Nature* **1988**, *334*, 375.
 113. Suslick, K. S.; Casadonte, D. J.; Doktycz, S. J. "The Effects of Ultrasound on Nickel and Copper Powders" *Solid State Ionics* **1989**, *32/33*, 444-452.
 114. Suslick, K. S. "'Chemistry and Biochemistry of N-substituted Porphyrins' bk. rev." *Med. Chem.* **1989**, *32*, 1410.
 115. Suslick, K. S.; Doktycz, S. J. "Ultrasonic Irradiation of Copper Powder" *Chem. Materials* **1989**, *1(1)*, 6-8.
 116. Suslick, K. S.; Doktycz, S. J. "The Sonochemistry of Zinc" *J. Am. Chem. Soc.* **1989**, *111*, 2342-2344.
 117. Flint, E. B.; Suslick, K. S. "Sonoluminescence from Nonaqueous Liquids: Emissions from Small Molecules" *J. Am. Chem. Soc.* **1989**, *111*, 6987-6992.
-
-

-
-
118. Kaplan, W. A.; Scott, R. A.; Suslick, K. S. "Probing Macrocyclic Flexibility: Ligand Binding to Zn and Ni Tetraphenylhydroporphyrins" *J. Am. Chem. Soc.* **1990**, *112*, 1283-1285.
 119. Suslick, K.S.; Dokytcz, S.J. "Inter-Particle Collisions Driven by Ultrasound" *Science* **1990**, *247*, 1067-1069.
 120. Suslick, K. S.; Dokytcz, S. J.; Flint, E. B. "On The Origins of Sonochemistry and Sonoluminescence" *Ultrasonics* **1990**, *28*, 280-290.
 121. Suslick, K. S.; Watson, R. A. "Photochemical Oxygen Atom Transfer by Metalloporphyrins" *Proc. Symp. O₂ Activation in Catalysis; Prepr. Am. Chem. Soc. Div. Pet. Chem.* **1990**, *35*, 169.
 122. Davies, M. D.; Qin, L.; Beck, J. L.; Suslick, K. S.; Koga, H.; Horiuchi, T.; Sligar, S. G. "Putidaredoxin Reduction of Cytochrome P-450_{cam}: Dependence of Electron Transfer on the Identity of Putidaredoxin's C-terminal Amino Acid" *J. Am. Chem. Soc.* **1990**, *112*, 7396-7398.
 123. Suslick, K. S.; Grinstaff, M. W. "Protein Microencapsulation of Nonaqueous Liquids" *J. Am. Chem. Soc.* **1990**, *112*, 7807-7809.
 124. Bilsel, O.; Rodriguez, J.; Holten, D.; Girolami, G. S.; Milam, S. N.; Suslick, K. S. "A New Low-Energy Fluorescent Excited State in Strongly-Coupled Porphyrin Dimers" *J. Am. Chem. Soc.* **1990**, *112*, 4075-4077.
 125. Suslick, K. S.; Chen, C.-T. "Polymeric Metalloporphyrins for Field Responsive Materials" *Polym. Mater. Sci. Eng.* **1990**, *63*, 272-278.
 126. Suslick, K. S.; Casadonte, D. J.; Choe, S. B.; Cichowlas, A. A.; Dokytcz, S. J.; Ghosh, C. K.; Grinstaff, M.W. "Heterogeneous Sonochemistry and Sonocatalysis" *Materials Research Society Proceedings: Synthesis and Properties of New Catalysts* **1990**, EA-24, 209-212.
 127. Suslick, K. S.; Flint, E. B. "Sonoluminescence of Alkali Metal Salts" *J. Phys. Chem.* **1991**, *95*, 1484-1488.
 128. Kaplan, W. A.; Suslick, K. S.; Scott, R. A. "Core Size and Flexibility of Metallohydroporphyrin Macrocycles. Implications for F₄₃₀ Coordination Chemistry" *J. Am. Chem. Soc.* **1991**, *113*, 9824-9827.
 129. Suslick, K. S.; Watson, R. A.; Wilson, S. R. "The Structures and Photochemistry of Metalloporphyrin Sulfate Complexes" *Inorg. Chem.* **1991**, *30*, 2311-2317.
 130. Kim, K.; Lee, W. S.; Kim, H.-J.; Cho, S. I.; Girolami, G. S.; Gorlin, P.; Suslick, K. S. "Synthesis and Structure of Transition Metal Bis(porphyrinato) Complexes. Characterization of Zr(TPP)₂ and Zr(OEP)₂" *Inorg. Chem.* **1991**, *30*, 2652-2656.
 131. Grinstaff, M.W; Suslick, K.S. "Nonaqueous Liquid Filled Microcapsules" *Polym. Prepr.* **1991**, *32*, 255-256.
 132. Suslick, K. S.; Watson, R. A. "Photochemical Nitrate and Nitrite Reduction by Mn and Fe Porphyrins" *Inorg. Chem.* **1991**, *30*, 912-919.
 133. Suslick, K. S.; Bautista, J. F.; Watson, R. A. "Metalloporphyrin Photochemistry with Matrix Isolation" *J. Am. Chem. Soc.* **1991**, *113*, 6111-6114.
 134. Grinstaff, M. W.; Suslick, K. S. "Proteinaceous Microbubbles: Synthesis of an Echo Contrast Agent" *Proc. Natl. Acad. Sci. USA* **1991**, *88*, 7708-7710.
 135. Flint, E. B.; Suslick, K. S. "The Temperature of Cavitation" *Science* **1991**, *253*, 1397-1399.
-
-

-
-
136. Suslick, K. S.; Choe, S. B.; Cichowlas, A. A.; Grinstaff, M. W. "Sonochemical Synthesis of Amorphous Iron" *Nature* **1991**, 353, 414-416.
 137. Suslick, K. S.; Watson, R. A. "The Photochemistry of Chromium, Manganese, and Iron Porphyrin Complexes" *New J. Chem.* **1992**, 16, 633-642.
 138. Jeffries, J. B.; Copeland, R. A.; Flint, E. B.; Suslick, K. S. "Thermal Equilibration During Cavitation" *Science* **1992**, 256, 248.
 139. Grinstaff, M. W.; Cichowlas, A. A.; Choe, S. B.; Suslick, K. S. "Effect of Cavitation Conditions on Amorphous Metal Synthesis" *Ultrasonics* **1992**, 30, 168-172.
 140. Suslick, K. S.; Chen, C.-T.; Meredith, G. R.; Cheng, L.-T. "Push-Pull Porphyrins as Non-Linear Optical Materials" *J. Am. Chem. Soc.* **1992**, 114, 6928-6930.
 141. Bilsel, O.; Rodriguez, J.; Milam, S. N.; Gorlin, P. A.; Girolami, G. S.; Suslick, K. S.; Holten, D. "Electronic States and Optical Properties of Porphyrin in van der Waals Contact: Th(IV) Sandwich Complexes" *J. Am. Chem. Soc.* **1992**, 114, 6528-6538.
 142. Becker, L.; Bada, J. L.; Kemper, K.; Suslick, K. S. "Sonoluminescence Spectrum of Seawater" *Marine Chem.* **1992**, 40, 315-320.
 143. Girolami, G. S.; Riehl, M. E.; Suslick, K. S.; Wilson, S. R. "A Rare Example of a Monomeric Aryllithium Complex. X-ray Structure of (2,4,6-Triphenylphenyl)lithium Bis(diethyl ether)" *Organomet.* **1992**, 11, 3907-3910.
 144. Tuncay, A.; Dustman, J. A.; Fisher, G.; Tuncay, C. I.; Suslick, K. S. "Ultrasound Promoted Hypervalent Iodine Reactions: α -Tosyloxylation of Ketones" *Tetrahedron Lett.* **1992**, 33, 7647-7650.
 145. Suslick, K. S.; Flint, E. B.; Grinstaff, M. W.; Kemper, K. A. "Sonoluminescence from Metal Carbonyls" *J. Phys. Chem.* **1993**, 97, 3098-3099.
 146. Bilsel, O.; Milam, S. N.; Girolami, G. S.; Suslick, K. S.; Holten, D. "Ultrafast Electronic Deactivation and Vibrational Dynamics of Photoexcited Uranium(IV) Porphyrin Sandwich Complexes" *J. Phys. Chem.* **1993**, 97, 7216-7221.
 147. Grinstaff, M. W.; Salamon, M. B.; Suslick, K. S. "Magnetic Properties of Amorphous Iron" *Phys. Rev. B* **1993**, 48, 269-273.
 148. Bellissent, R.; Galli, G.; Grinstaff, M. W.; Migliardo, P.; Suslick, K. S. "Neutron Diffraction by Amorphous Iron Powder" *Phys. Rev. B* **1993**, 48, 15797-15800.
 149. Suslick, K. S.; Kemper, K. A. "The Effect of Fluorocarbon Gases on Sonoluminescence: A Failure of the Electrical Hypothesis" *Ultrasonics* **1993**, 31, 463-465.
 150. Suslick, K. S. "The Chemical Effects of Ultrasound" *Proc. 1st Intl. EPRI/NSF Symp. Advanced Oxidation*; EPRI: Palo Alto, 1993, vol. 2, pp 6-27.
 151. Webb, A. G.; Wong, M.; Wilmes, L. J.; Kolbeck, K. J.; Magin, R. L.; Suslick, K. S. "⁵⁹Co Functional Agents for Localized In-Vivo Temperature Measurements" *Proc. 12th Annual Mtg. Soc. Magnetic Resonance in Medicine*; New York, 1993; p. 245.
 152. Wilmes, L. J.; Webb, A. G.; Kolbeck, K. J.; Wong, M.; Magin, R. L.; Suslick, K. S. "Microencapsulation of Perfluorocarbons as a Magnetic Resonance Imaging Agent" *Proc. 12th Annual Mtg. Soc. Magnetic Resonance in Medicine*; New York, 1993, pp 756-757.

-
-
153. Suslick, K. S.; Kemper, K. A.; Flint, E. B. "Spectrally Resolved Sonoluminescence as a Probe of Cavitation" *IEEE Ultrasonics Symp. Proc.* **1993**, 777-784.
154. Chou, H.; Chen, C.-T.; Stork, K. F.; Bohn, P. W.; Suslick, K. S. "Langmuir-Blodgett Films of Amphiphilic Push-Pull Porphyrins" *J. Phys. Chem.* **1994**, *98*, 383-385.
155. Desai, N. P.; Soon-Shiong, P.; Grinstaff, M. W.; Yao, Z.; Sandford, P. A.; Suslick, K. S. "Controlled and Targeted Drug Delivery with Biocompatible Protein Shell Microspheres" *Proc. Soc. Biomaterial*, **1994**, *20*, 112.
156. Suslick, K. S.; Grinstaff, M. W.; Kolbeck, K. J.; Wong, M. "Characterization of Sonochemically Prepared Proteinaceous Microcapsules" *Ultrasonics Sonochemistry* **1994**, *1*, S65-S68.
157. Girolami, G. S.; Gorlin, P. A.; Suslick, K. S. "Electronically Asymmetric Bis(porphyrin) Sandwich Complexes" *Inorg. Chem.* **1994**, *33*, 626-627.
158. Grinstaff, M. W.; Kolbeck, K. A.; Magin, R. L.; Suslick, K. S.; Webb, A.; Wilmes, L. J.; Wong, M.; Desai, N. P.; Sandford, P. A.; Soon-Shiong, P. "Fluorocarbon Filled Protein Microspheres as Contrast Agents for MRI" *Proc. Soc. Biomaterial* **1994**, *20*, 113.
159. Suslick, K. S.; Kemper, K. A. "Pressure Measurements During Acoustic Cavitation by Sonoluminescence" *Bubble Dynamics and Interface Phenomena*; Blake J.R.; Thomas, N.; eds. Kluwer Publ.; Dordrecht, 1994; pp 311-320.
160. Suslick, K. S.; Hyeon, T.; Fang, M.; Cichowlas, A. A. "Sonochemical Synthesis and Catalytic Properties of Nanostructured Molybdenum Carbide" *Molecularly Designed Nanostructured Materials*, MRS Symp. Proc., v. 351. Gonsalves, K.E.; Chow, G.M.; Xiao, T.O.; Cammarata, R.C., eds. Materials Res. Soc.: Pittsburgh, 1994; pp 201-206.
161. Suslick, K. S.; Fang, M.; Hyeon, T.; Cichowlas, A. A. "Nanostructured Fe-Co Catalysts Generated by Ultrasound" *Molecularly Designed Nanostructured Materials*, MRS Symp. Proc., vol. 351. Gonsalves, K. E.; Chow, G. M.; Xiao, T. O.; Cammarata, R. C., Eds. Materials Res. Soc.: Pittsburgh, 1994; pp 443-448.
162. Suslick, K.S. "The Mechanochemical Effects of Ultrasound" *Proc. First Intl. Conf. Mechanochemistry: InCoMe '93*, Košice, Slovakia; Cambridge Interscience: Cambridge, 1994; vol.1, pp 43-49.
163. Liu, K. J.; Grinstaff, M. W.; Jiang, J.; Suslick, K. S.; Swartz, H. M.; Wang, W. "In Vivo Measurement of Oxygen Concentration Using Sonochemically Synthesized Microspheres" *Biophys. J.* **1994**, *67*, 896-901.
164. Milam, S. N.; Gorlin, P. A.; Girolami, G. S.; Suslick, K. S.; Wilson, S. R. "Bis(porphyrin)actinide Complexes and their Radical Cations and Dications" *J. Coord. Chem.* **1994**, *32*, 173-212. (T. L. Brown Retirement Issue)
165. Hill, J. R.; Dlott, D. D.; Fayer, M. D.; Peterson, K. A.; Rella, C. W.; Rosenblatt, M. M.; Suslick, K. S.; Ziegler, C. J. "Vibrational Relaxation of CO in Model Heme Compounds: 6-Coordinate Metalloporphyrins (M=Fe, Ru, Os)" *Chem. Phys. Lett.*, **1995**, *244*, 218-223.
166. Matula, T. J.; Roy, R. A.; Mourad, P. D.; McNamara III, W. B.; Suslick, K. S. "Comparison of Multi-Bubble and Single-Bubble Sonoluminescence Spectra" *Phys. Rev. Lett.*, **1995**, *75*, 2602-2605.
167. Webb, A. G.; Wong, M.; Niesman, M.; Kolbeck, K. J.; Wilmes, L. J.; Magin, R. L.; Suslick, K. S. "In-Vivo NMR Thermometry with Liposomes Containing ⁵⁹Co Complexes" *Int. J. Hyperthermia* **1995**, *11*, 821-827.
168. Bellissent, R.; Galli, G.; Hyeon, T.; Magazu, S.; Majolino, D.; Migliardo, P.; Suslick, K. S. "Structural Properties of Amorphous Bulk Fe, Co, and Fe-Co Binary Alloys" *Phys. Scripta* **1995**, *T57*, 79-83.
169. Fang, M.; Hyeon, T.; Cichowlas, A. A.; Suslick, K. S. "Sonochemical Preparation of Nanostructured Catalysts" *Am. Chem. Soc. Div. Petrol. Chem. Preprints* **1995**, 67-71.
-
-

-
-
170. Hyeon, T.; Fang, M.; Cichowlas, A. A.; Suslick, K. S. "Catalytic Activity of Nanophase Metals Prepared Sonochemically" *Am. Chem. Soc. Div. Fuel Chem. Preprints* **1995**, *40*, 365-9.
 171. Wong, M.; Suslick, K. S. "Sonochemically Produced Hemoglobin Microbubbles" *Hollow and Solid Spheres and Microspheres*; MRS Symp. Proc. v. 372; Wilcox, D. L.; Berg, M.; Bernat, T.; Kellerman, D.; Corchran, J. K., eds. Matl. Res. Soc.: Pittsburgh, 1995; pp 89-94.
 172. Hyeon, T.; Fang, M.; Cichowlas, A. A.; Suslick, K. S. "Sonochemical Synthesis of Nanostructured Catalysts" *Matl. Sci. Eng. A*, **1995**, *204*, 186-192.
 173. Suslick, K. S.; Hyeon, T.; Fang, M.; Ries, J. T.; Cichowlas, A. A. "Sonochemical Synthesis of Nanophase Metals, Alloys, and Carbides" *Materials Science Forum* (Transtec Publ., N.Y.), **1996**, *225-227*, 903-912 (1996).
 174. Girolami, G. S.; Hein, C. L.; Suslick, K. S. "Bis(porphyrin) Sandwich Complex with an Appended Quinone" *Angew. Chem. Intl. Ed.* **1996**, *35*, 1223-1225.
 175. Bhyrappa, P.; Young, J. K.; Moore, J. S.; Suslick, K. S. "Shape-Selective Epoxidation of Alkenes by Metalloporphyrin-Dendrimers" *J. Molec. Catalysis* **1996**, *A113*, 109-116. (special issue on biomimetic oxidation)
 176. Ziegler, C. J.; Suslick, K. S. "The Photochemistry of Metalloporphyrin Carbene Complexes" *J. Am. Chem. Soc.* **1996**, *118*, 5306-5307.
 177. Hyeon, T.; Fang, M.; Suslick, K. S. "Nanostructured Molybdenum Carbide: Sonochemical Synthesis and Catalytic Properties" *J. Am. Chem. Soc.* **1996**, *118*, 5492-5493.
 178. Eckburg, J. J.; Chato, J. C.; Liu, K. J.; Grinstaff, M. W.; Swartz, H. M.; Suslick, K. S.; Auteri, F. P. "Biological Temperature Measurements using Electron Paramagnetic Resonance Spectroscopy" *J. Biomech. Eng.* **1996**, *118*, 193-200.
 179. Webb, A. G.; Wong, M.; Kolbeck, K. J.; Magin, R. L.; Wilmes, L. J.; Suslick, K. S. "Sonochemically Produced Fluorocarbon Microspheres: A New Class of MRI Contrast Agents" *J. Mag. Res. Imaging*, **1996**, *6*, 675-683.
 180. Suslick, K. S.; Hyeon, T.; Fang, M.; Cichowlas, A. A. "Sonochemical Preparation of Nanostructured Catalysts" *Advanced Catalysts and Nanostructured Materials*; Moser, W. R., ed. Academic Press: New York, 1996, pp. 197-211.
 181. Suslick, K. S.; Hyeon, T.; Fang, M. "Nanostructured Materials Generated by High Intensity Ultrasound" *Chem. Materials* **1996**, *8*, 2172-2179 (special issue on nanostructured materials).
 182. Bernstein, L. S.; Zakin, M. R.; Flint, E. B.; Suslick, K. S. "Cavitation Thermometry using Molecular and Continuum Sonoluminescence" *J. Phys. Chem.* **1996**, *100*, 6612-6619.
 183. Bellissent, R.; Galli, G.; Hyeon, T.; Migliardo, P.; Parette, P.; Suslick, K. S. "Magnetic And Structural Properties Of Amorphous Transition Metals And Alloys" *J. Noncryst. Solids* **1996**, *205-207*, 656-659.
 184. Bhyrappa, P.; Young, J.K.; Moore, J.S.; Suslick, K.S. "Dendrimer-Metalloporphyrins: Synthesis and Catalysis" *J. Am. Chem. Soc.* **1996**, *118*, 5708-5711.
 185. Dlott, D. D.; Fayer, M. D.; Hill, J. R.; Rella, C. W.; Suslick, K. S.; Ziegler, C. J. "Vibrational Relaxation in Metalloporphyrin CO Complexes" *J. Am. Chem. Soc.* **1996**, *118*, 7853-7854.
 186. Ziegler, C. J.; Suslick, K. S. "Photochemical Activation of Metalloporphyrin Carbene Complexes" *J. Organomet. Chem.* **1996**, *528*, 83-90.
 187. Hill, J. R.; Ziegler, C. J.; Suslick, K. S.; Dlott, D. D.; Rella, C. W.; Fayer, M. D. "Tuning the Vibrational Relaxation of CO Bound to Heme and Metalloporphyrin Complexes" *J. Phys. Chem.* **1996**, *100*, 18023-18032.
-
-

-
-
188. Suslick, K. S.; Fang, M.; Hyeon, T. "Sonochemical Synthesis of Iron Colloids" *J. Am. Chem. Soc.* **1996**, *118*, 11960-11961.
189. Benson, D. E.; Suslick, K. S.; Sligar, S. G. "Reduced Oxy Intermediate Observed in D251N Cytochrome P450_{cam}" *Biochem.* **1997**, *36*, 5104-5107.
190. Peterson, K. A.; Boxer, S. G.; Decatur, S.; Dlott, D. D.; Fayer, M. D.; Hill, J. R.; Rella, C. W.; Rosenblatt, M. M.; Suslick, K. S.; Ziegler, C. J. "Vibrational Relaxation of CO in Myoglobin Mutants and Model Heme Compounds" *Proc. 7th Intl. Conf. Time Resolved Vibr. Spectrosc.*, 1997, 173-177.
191. Bhyrappa, P.; Wilson, S. R.; Suslick, K. S. "Hydrogen Bonded Porphyrinic Solids: Supramolecular Networks of Octahydroxy Porphyrins" *J. Am. Chem. Soc.* **1997**, *119*, 8492-8502.
192. Suslick, K. S.; Mdleleni, M. M.; Ries, J. T. "Chemistry Induced by Hydrodynamic Cavitation" *J. Am. Chem. Soc.* **1997**, *119*, 9303-9304.
193. Bhyrappa, P.; Suslick, K. S. "Surpramolecular Networks of Octahydroxy Porphyrins" *Supramolec. Chem.* **1998**, *9*, 169-174.
194. Suslick, K. S. "Sonochemical preparation of protein microspheres" *Proc. 16th Intl. Conf. Acoustics* Acoust. Soc. Am.: Seattle, 1998, pp. 1533-35.
195. Suslick, K. S.; Didenko, Y. T.; McNamara III, W. B. "Conditions during Multi-Bubble Sonoluminescence" *Proc. 16th Intl. Conf. Acoustics* Acoust. Soc. Am.: Seattle, 1998, pp. 2577-79.
196. Bhyrappa, P.; Suslick, K. S. "Synthesis and Crystal Structure of 5,10,15,20-Tetrakis(3,5-dinitrophenyl)porphyrin" *J. Porph. Phthalocyn.* **1998**, *2*, 391-396. (V. Krishnan retirement issue)
197. Long, G. J.; Hautot, D.; Pankhurst, Q. A.; Vandormael, D.; Grandjean, F.; Gaspard, J. P.; Briois V.; Hyeon, T.; Suslick, K. S. "Mössbauer-effect and X-Ray Absorption Spectral Study of Sonochemically Prepared Amorphous Iron" *Phys. Rev. B* **1998**, *57*, 10716-10722.
198. Huffman, D. L.; Rosenblatt, M. M.; Suslick, K. S. "Synthetic Heme-Peptide Complexes" *J. Am. Chem. Soc.* **1998**, *120*, 6183-6184.
199. Mdleleni, M. M.; Hyeon, T.; Suslick, K. S. "Sonochemical Synthesis of Nanostructured Molybdenum Sulfide" *J. Am. Chem. Soc.* **1998**, *120*, 6189-6190.
200. Salzmann, R.; Ziegler, C. J.; Godhout, N.; McMahan, M.; Suslick, K. S.; Oldfield, E. "CO Complexes of Fe(II), Ru(II), and Os(II) 5,10,15,20-Tetraphenylporphyrinates: A comparative Investigation by X-ray, Solid-State NMR and Density Functional Theory" *J. Am. Chem. Soc.* **1998**, *120*, 11323-11334.
201. Patel, B. R.; Suslick, K. S. "Discotic Liquid Crystals from a Bis-Pocketed Porphyrin" *J. Am. Chem. Soc.* **1998**, *120*, 11802-11803.
202. Suslick, K. S.; McNamara III, W. B.; Didenko, Y. "Hot Spot Conditions During Multi-Bubble Cavitation" in *Sonochemistry and Sonoluminescence*, Crum, L. A.; Mason, T. J.; Reisse, J.; Suslick, K. S., eds. Kluwer Publishers: Dordrecht, Netherlands, 1999, pp. 191-204.
203. Suslick, K. S.; Fang, M. M.; Hyeon, T.; Mdleleni, M. M. "Applications of Sonochemistry to Materials Synthesis" in *Sonochemistry and Sonoluminescence*, Crum, L. A.; Mason, T. J.; Reisse, J.; Suslick, K. S., eds. Kluwer Publishers: Dordrecht, Netherlands, 1999, pp. 291-320.
204. Bhyrappa, P.; Vijayanthimala, G.; Suslick, K. S. "Shape-Selective Ligation to Dendrimer-Metalloporphyrins" *J. Am. Chem. Soc.* **1999**, *121*, 262-263.
-
-

-
-
205. Tuncay, A.; Anaclerio, B. M.; Zolodz, M.; Suslick, K. S. "New One-Pot Method for the Synthesis of Alkynyl Sulfonate Esters Using Ultrasound" *Tetrahedron Lett.* **1999**, *40*, 599-602.
 206. McNamara III, W. B.; Didenko, Y.; Suslick, K. S. "Hot Spot Conditions During Cavitation in Water" *J. Am. Chem. Soc.* **1999**, *121*, 5817-5818.
 207. Li, S.; Lee, J.S.; Hyeon, T.; Suslick, K. S. "Catalytic Hydrodenitrogenation of Indole over Molybdenum Nitride and Carbides with Different Structures" *Applied Catal. A* **1999**, *184*, 1-9.
 208. Didenko, Y.; McNamara III, W. B.; Suslick, K. S. "The Temperature of Multi-Bubble Sonoluminescence in Water" *J. Phys. Chem. A* **1999**, *103*, 10783-10788.
 209. McNamara III, W. B.; Didenko, Y.; Suslick, K. S. "Sonoluminescence Temperatures During Multibubble Cavitation" *Nature* **1999**, *401*, 772-775.
 210. Suslick, K. S.; McNamara III, W. B.; Didenko, Y. "Conditions During Multibubble Cavitation" in *Nonlinear Acoustics at the Turn of the Millennium*, Lauterborn, W.; Kurz, T., eds. Amer. Inst. Physics: Melville, NY, 2000, pp. 463-466.
 211. Suslick, K. S.; Rakow, N. A.; Kosal, M. E.; Chou, J.-H. "The Materials Chemistry of Porphyrins and Metalloporphyrins" *J. Porph. Phthal.* **2000**, *4*, 407-413. (invited review).
 212. Petrier C.; **Suslick**, K. S. "Ultrasound-Enhanced Reactivity Of Calcium In The Reduction Of Aromatic Hydrocarbons" *Ultrasonics Sonochemistry* **2000**, *7*, 53-61.
 213. McNamara III, W. B.; Didenko, Y.; Suslick, K. S. "Effect of Noble Gases on Sonoluminescence Temperatures During Multibubble Cavitation" *Phys. Rev. Lett.* **2000**, *84*, 777-780.
 214. Huffman, D. L.; Suslick, K. S. "Hydrophobic Interactions in Metalloporphyrin-Peptide Complexes" *Inorg. Chem.* **2000**, *39*, 5418-5419.
 215. Brunner, R.; Kosal, M. E. Suslick, K. S.; Lamche, R.; Marti, O.; White, J. O. "Near-field Scanning Optical Microscopy of Zinc-Porphyrin Crystals" *Ultramicroscopy* **2000**, *84*, 149-157.
 216. Dantsin, G.; Suslick, K. S. "Sonochemical Preparation of a Nanostructured Bifunctional Catalyst" *J. Am. Chem. Soc.* **2000**, *122*, 5214-5215.
 217. McNamara III, W. B.; Didenko, Y.; Suslick, K. S. "The Nature of the Continuum in Multi-Bubble Sonoluminescence" *J. Am. Chem. Soc.* **2000**, *122*, 8563-8564.
 218. Ashokkumar, M.; Crum, L. A.; Frenley, C. A.; Grieser, F.; Matula, T. J.; McNamara III, W. B.; Suslick, K. S. "Effect of Solutes on Single-Bubble Sonoluminescence in Water" *J. Phys. Chem. A* **2000**, *104*, 8462-8465.
 219. Sen, A.; Suslick, K. S. "Shape-Selective Discrimination of Small Organic Molecules" *J. Am. Chem. Soc.* **2000**, *122*, 11565-11566.
 220. Rakow, N. A.; Suslick, K. S. "A Colorimetric Sensor Array for Odor Visualization" *Nature* **2000**, *406*, 710-714.
 221. Didenko, Y.; McNamara III, W. B.; Suslick, K. S. "Molecular Emission from Single Bubble Sonoluminescence" *Nature* **2000**, *407*, 877-879.
 222. Suslick, K. S.; Rakow, N. A. "A Colorimetric Nose: 'Smell-Seeing'" *Artificial Chemical Sensing: Olfaction and the Electronic Nose*, Stetter, J.R.; Pensrose, W.R., eds. Electrochem. Soc.: Pennington, NJ, 2001, pp. 8-14.
 223. Suslick, K. S. "The Chemical Consequences of Cavitation" *Proc. 17th Intl. Congr. Acoustics* (ICA: Rome, 2001), pp. PA2SL 2-5.
-
-

-
-
224. Suslick, K. S.; Didenko, Y.; McNamara III, W. B.; "Single Bubble Sonoluminescence from Non-Aqueous Liquids"
Proc. 17th Intl. Congr. Acoustics (ICA: Rome, 2001), pp. PA2SL 14-15.
225. Suslick, K. S.; Kosal, M. E.; Rakow, N. A.; Sen, A. "Smell-Seeing: A New Approach to Artificial Olfaction"
Proc. EURODEUR-AIRODEUR, Paris, 2001, pp. 1-4.
226. Dhas, N.A.; Ekhtiarzadeh, A.; Suslick, K.S. "Sonochemical Preparation of Supported Hydrodesulfurization Catalysts"
J. Am. Chem. Soc., **2001**, *123*, 8310-8316.
227. Drain, C. M.; Hupp, J. T.; Suslick, K. S.; Wasielewski, M. R.; Chen, X. "A Perspective on New Porphyrin-Based Functional Materials and Devices" *J. Porph. Phthal.*, **2002**, *6*, 243-259.
228. Rosenblatt, M.M.; Huffman, D.L.; Wang, X. Remmer, H.A.; Suslick, K. S. "Cyclic and Hairpin Peptide Complexes of Heme" *J. Am. Chem. Soc.*, **2002**, *124*, 12394-12395.
229. Kosal, M. E.; Chou, J. H.; Suslick, K. S.; "A Calcium-Bridged Porphyrin Coordination Network"
J. Porph. Phthal., **2002**, *6*, 377-381.
230. Suslick, K. S.; Didenko, Y. T. "The Chemical Consequences of Single-Bubble Cavitation"
Nonlinear Acoustics at the Beginning of the 21st Century, Rudenko, O.V.; Sapozhnikov, O.A., ed.
Moscow State Univ. Press: Moscow, 2002; vol. 2, pp. 1063-1069.
231. Kosal, M. E.; Chou, J.-H.; Wilson, S. R.; Suslick, K. S. "A Functional Zeolite Analogue Assembled From Metalloporphyrins" *Nature Materials*, **2002**, *1*, 118-121.
232. Didenko, Y.; Suslick, K. S. "The Energy Efficiency of Formation of Photons, Radicals, and Ions During Single Bubble Cavitation" *Nature* **2002**, *418*, 394-397.
233. Zimmerman, S. C.; Wendland, M. S.; Rakow, N. A.; Zharov, I.; Suslick, K. S. "Synthetic Hosts by Monomolecular Imprinting Inside Dendrimers" *Nature* **2002**, *418*, 399-403.
234. Wang, J.; Luthey-Schulten, Z.; Suslick, K. S. "Is the Olfactory Receptor A Metalloprotein?"
Proc. Natl. Acad. Sci. U.S.A., **2003**, *100*, 3035-3039.
235. Suslick, K.S.; Rakow, N.A.; Kosal, M.E.; McNamara III, W.B.; Sen, A. "Chemsensing: A Colorimetric Array Detector"
Proc. ISOEN 02 (ed. A. D'Amico and C. DiNatale; IEEE: Baltimore, 2003), pp. 46-52.
236. Rosenblatt, M.M.; Wang, J.; Suslick, K. S. "De Novo Designed Cyclic-Peptide Heme Complexes"
Proc. Natl. Acad. Sci. U.S.A., **2003**, *101*, in press.
237. McNamara III, W. B.; Didenko, Y.; Suslick, K. S. "Pressure during Acoustic Cavitation"
J. Phys. Chem. B **2003**, *107*, 7303-7306 (Henglein Festschrift).
238. Lee, T. M.; Oldenburg, A. L.; Sitafalwalla, S.; Marks, D. L.; Luo, W.; Toublan, F. J.-J.; Suslick, K. S.; Boppart, S. A. "Engineered Microsphere Contrast Agents for Optical Coherence Tomography" *Optics Lett.* **2003**, *28*, 1546-1548.
239. Oxley, J. D.; Mdleleni, M. M.; Suslick, K. S. "Hydrodehalogenation with Sonochemically Prepared Mo₂C and W₂C"
Catalyst Today, **2003**, in press.
240. Oxley, J. D.; Prozorov, T.; Suslick, K. S. "Sonochemistry and Sonoluminescence of Room-Temperature Ionic Liquids"
J. Am. Chem. Soc., **2003**, *125*, 11138-11139.
241. Prozorov, T.; Prozorov, R.; Snezhko, A.; Suslick, K. S. "Sonochemical Modification of the Superconducting Properties of MgB₂" *Appl. Phys. Lett.* **2003**, *83*, 2019-2021.
-
-

KENNETH S. SUSLICK

*School of Chemical Sciences
University of Illinois at Urbana-Champaign
Chemical & Life Sciences Laboratory
600 S. Mathews Av.
Urbana, Illinois 61801*

*Office: (217) 333-2794
Lab: (217) 333-1532
Fax: (217) 333-2685
Email: ksuslick@uiuc.edu
Web: www.scs.uiuc.edu/suslick*

Education:

- 1978 Ph. D., Stanford University, *Synthetic Analogs of Myoglobin and Hemoglobin*.
1974 B. S., California Institute of Technology (with Honors).

Research and Professional Positions:

- 1997 – *William H. & Janet Lycan* Professor of Chemistry, University of Illinois at Urbana-Champaign.
2001 – Founder, Member of Board of Directors; ChemSensing, Inc., Northbrook, IL.
1988 – Professor of Chemistry, University of Illinois at Urbana-Champaign.
1993 – Professor of Materials Science and Engineering, University of Illinois at Urbana-Champaign.
1993 – 98 Member, Board of Directors; Ney Ultrasonics Inc.; Bloomfield, Connecticut.
1994 – 98 Member, Scientific Advisory Board, VivoRx Inc.; Santa Monica, California.
1995 – 97 *Alumni Research Scholar* Professor of Chemistry, University of Illinois at Urbana-Champaign.
1989 – 92 Professor, Beckman Institute for Advanced Science and Technology.
1986 Visiting Fellow, Balliol College and Inorganic Chemistry Laboratory, Oxford University.
1984 – 88 Associate Professor, University of Illinois at Urbana-Champaign.
1978 – 84 Assistant Professor, University of Illinois at Urbana-Champaign.
1974 – 78 Research and Teaching Assistant, Stanford University.
1974 – 75 Chemist, Lawrence Livermore Laboratory, Laser Isotope Separation.
1971 – 74 Research and Teaching Assistant, California Institute of Technology.
1972 AEC Research Trainee, Lawrence Berkeley Laboratory.

Selected Honors and Awards:

- 2004 American Chemical Society Senior Cope Scholar Award
2003 J.T. Donald Lecturer, McGill University, Montreal.
2001 Wolfgang Göpel Award, 8th Intl. Symp. on Olfaction & Electronic Noses (ISOEN-8).
2000 1st Place, Illinois Technology Center Inventorship Competition.
1997 University of Melbourne Special Public Lectureship.
1997 W. Heinlen Hall Lectureship, Bowling Green State University.
1994 American Chemical Society Nobel Laureate Signature Award for Graduate Education.
1994 Materials Research Society Medal for Exceptional Recent Achievements in Materials Research.
1992 – Fellow, American Association for the Advancement of Science.
1994 – Fellow, Acoustical Society of America.
1994 Robert A. Welch Foundation Lecturer.
1994 Senior University Scholar, University of Illinois.
1992 – 94 NSF Special Creativity Extension Award.
1993 Excellence in Teaching Award, UIUC School of Chemical Sciences.
1991 – 92 Beckman Associate, UIUC Center for Advanced Study.
1985 – 90 NIH Research Career Development Award.
1985 – 87 Alfred P. Sloan Foundation Research Fellow.
1985 Excellence in Teaching Award, UIUC School of Chemical Sciences.
1979 – 80 DuPont Young Faculty Fellow.
1974 – 78 Silver Medal and Fellow, Royal Society for the Arts, Manufactures, and Commerce (London).
1974 – 78 Hertz Foundation Predoctoral Fellowship.
1973 American Chemical Society Undergraduate Award in Analytical Chemistry.

Some Recent Special Lectures:

2003

J.T. Donald Lecturer, McGill University, Montreal.
Five College Lecturer (Amherst, Mount Holyoke, Smith, Hampshire and U. Mass. Amherst).

2002

Invited Lecturer, 16th International Symposium on Nonlinear Acoustics (ISNA-16), Moscow.
Invited Speaker, 9th Intl. Symp. on Olfaction & Electronic Noses (ISOEN-2002), Rome.
Plenary Lecturer, Catalyst Club of Chicago.
Invited Speaker, Symposium Honoring J. I. Brauman, Stanford University.
Invited Speaker, Symposium Honoring R. G. Bergman, University of California, Berkeley.
Invited Speaker, Chicago Technology Forum 2002.

2001

Plenary Lecturer, EURODEUR-AIRODEUR Conference, Paris.
Invited Speaker, 8th Intl. Symp. on Olfaction & Electronic Noses (ISOEN-8), Washington, D.C.
Plenary Lecturer, 17th Intl. Congress on Acoustics, Rome.
Plenary Lecturer, World Congress on Ultrasonics/IEEE Intl. Ultrasonics Symposium, Atlanta, GA.

2000

Keynote Speaker, Ultrasonics Industry Association Meeting, Columbus.
Invited Speaker and Symposium Organizer, Pacifichem 2000, Honolulu.
Invited Speaker and Symposium Organizer, 1st International Congress on Porphyrins and Phthalocyanines, Dijon.
Invited Speaker, 7th Meeting of the European Sonochemistry Society, Biarritz.
Invited Speaker, Chemistry under Extreme Conditions Symp., ACS Natl. Meeting, Washington, D.C.

1999

Pittsburgh Conference Lectureship, Duquesne University, Pittsburgh.
Invited Speaker, "Unusual Techniques in Inorganic Chemistry," 82nd Canadian Soc. for Chemistry Conf., Toronto.
Invited Speaker, 15th International Symposium on Nonlinear Acoustics, Göttingen.

1998

Director's Colloquium Speaker, Los Alamos National Laboratory.
Invited Speaker, Gordon Research Conference, Chemistry and Biology of Tetrapyrroles.
Invited Lecturer, 6th Meeting of the European Sonochemistry Society, Rostock.
Invited Speaker, Sonochemistry & Sonoluminescence Symposium, Acoustic Soc. Amer. Meeting, Seattle.

Current Major Research Funding:

2003 – 06 NSF; "Chemical Effects of High Intensity Ultrasound" \$562,500 / 3 yrs.
2000 – 04 NIH 5R01-HL25934 "Heme Proteins, Microspheres, and Their Synthetic Analogs" \$1,365,000 / 4 yrs.
1999 – 04 DARPA; "Chemical Control of Single Bubble Cavitation" \$637,121 / 3.5 yrs.
1990 – DOE; UIUC Materials Res. Lab, "Field Responsive Porphyrinic Materials," \$100,000 / yr.

Student and Postdoctoral Associates, Past and Present:

13 Ph.D. Graduate Students presently in group (08/03).
4 Postdoctoral Research Associates presently in group (08/03).
36 Ph.D. Graduate Students supervised and theses completed.
23 Past Postdoctoral Research Associates.
4 M.S. Graduate Students supervised and theses completed.
15 Undergraduate Research Assistants supervised.

Personal Data:

b., Chicago, September 16, 1952. Spouse: Adele Mazurek, m. 1975. Son: Benjamin, b. 1992.

Selected Publications List (out of >230):

Books:

- Suslick, K. S., ed. *High Energy Processes in Organometallic Chemistry*; ACS: Washington, DC, 1987; Symp. Ser. #333.
- Suslick, K. S., ed. *Ultrasound: Its Chemical, Physical, and Biological Effects*; VCH Publishers: New York, 1988.
- Suslick, K. S., ed. *Comprehensive Supramolecular Chemistry, vol. 5, Bioinorganic Systems*; Elsevier: Oxford, 1996.
- Crum, L. A.; Mason, T. J.; Reisse, J.; Suslick, K. S., eds. *Sonochemistry and Sonoluminescence*, Kluwer Publishers: Dordrecht, Netherlands, 1999; NATO ASI Series C, v. 524.

Selected Reviews and Popularizations:

- Suslick, K. S. "The Chemical Effects of Ultrasound" *Scientific American* **1989** (2) 260, 80-86.
- Suslick, K. S. "Sonochemistry" *Science* **1990**, 247, 1439-1445.
- Suslick, K. S. "The Chemistry of Ultrasound" in *Yearbook of Science & the Future 1994*; Encyclopaedia Britannica: Chicago, 1994; pp 138-155.
- Suslick, K. S. "Applications of Ultrasound to Materials Chemistry" *MRS Bulletin* **1995**, 20, 29-34.
- Suslick, K. S.; Van Deusen-Jeffries, S. "Shape Selective Biomimetic Oxidation Catalysis" *Comprehensive Supramolecular Chemistry*, vol. 5; Lehn, J. M., ed. Elsevier Publishers: Oxford, 1996; pp. 141-170.
- Suslick, K. S.; Crum, L. A. "Sonochemistry and Sonoluminescence" in *Handbook of Acoustics*; Crocker, M. J., ed.; Wiley-Interscience: New York, 1998; pp. 243-253.
- Suslick, K. S. "Sonochemistry" in *Kirk-Othmer Encyclopedia of Chemical Technology*; 4th Ed. J. Wiley & Sons: New York, 1998, vol. 26, 517-541.
- Suslick, K. S.; Price, G. "Applications of Ultrasound to Materials Chemistry" *Annu. Rev. Matl. Sci.*, **1999**, 29, 295-326.
- Chou, J.H.; Kosal, M.E.; Nalwa, H.S.; Rakow, N.A.; Suslick, K.S. "Applications of Porphyrins and Metalloporphyrins to Materials Chemistry" in *The Porphyrin Handbook*, Kadish, K.; Smith, K.; Guillard, R., eds.; Acad. Press: NY, 2000; vol. 6, pp. 43-131.
- Suslick, K. S. "Sonochemistry and Sonoluminescence" in *Encyclopedia of Physical Science and Technology*, 3rd ed. Academic Press: San Diego, 2001, vol. 17, pp. 363-376.
- Suslick, K. S. "Sonochemistry" in *Comprehensive Coordination Chemistry 2*; Elsevier Science: New York, 2003.

Selected Recent Patents (out of 16):

- Grinstaff, M. W.; Soon-Shiong, P.; Wong, M.; Sandford, P. A.; Suslick, K. S.; Desai, N. P. "Composition Useful for *In Vivo* Delivery of Biologics and Methods Employing Same" *U. S. Patent 5,498,421*; Mar. 12, 1996.
- Grinstaff, M. W.; Desai, N. P.; Suslick, K. S.; Soon-Shiong, P.; Sandford, P. A.; Merideth, N. R. "Polymeric Shells for Medical Imaging Prepared from Synthetic Polymers, and Methods for the Use Thereof" *U. S. Patent 5,512,268*; Apr. 30, 1996.
- Desai, N. P.; Soon-Shiong, P.; Sandford, P. A.; Grinstaff, M. W.; Suslick, K. S.; "Methods for *In Vivo* Delivery of Substantially Water Insoluble Pharmacologically Active Agents and Compositions" *U. S. Patent 5,560,933*; Oct. 1, 1996.
- Grinstaff, M. W.; Soon-Shiong, P.; Wong, M.; Sandford, P. A.; Suslick, K. S.; Desai, N. P. "Methods for the Preparation of Blood Substitutes for *In Vivo* Delivery" *U. S. Patent 5,635,207*; June 3, 1997.
- Grinstaff, M. W.; Soon-Shiong, P.; Wong, M.; Sandford, P. A.; Suslick, K. S.; Desai, N. P. "Methods For *In Vivo* Delivery Of Nutraceuticals And Compositions Useful Therefor" *U. S. Patent 5,650,156*; July 22, 1997.
- Grinstaff, M. W.; Soon-Shiong, P.; Wong, M.; Sandford, P. A.; Suslick, K. S.; Desai, N. P. "Methods for the Preparation of Immunostimulating Agents for *In Vivo* Delivery" *U. S. Patent 5,665,383*; Sept. 9, 1997.
- Suslick, K. S.; Rakow, N. A. "Colorimetric Artificial Nose Having an Array of Dyes and Method for Artificial Olfaction" *U.S. Patent 6,368,558*; April 9, 2002; *U.S. Patent 6,495,102*; Dec. 17, 2002.

Selected Recent Journal Publications:

- Huffman, D. L.; Rosenblatt, M. M.; Suslick, K. S. "Synthetic Heme-Peptide Complexes" *J. Am. Chem. Soc.* **1998**, *120*, 6183-6184.
- Mdleleni, M. M.; Hyeon, T.; Suslick, K. S. "Sonochemical Synthesis of Nanostructured Molybdenum Sulfide" *J. Am. Chem. Soc.* **1998**, *120*, 6189-6190.
- Bhyrappa, P.; Vaijayanthimala, G.; Suslick, K. S. "Shape-Selective Ligation to Dendrimer-Metalloporphyrins" *J. Am. Chem. Soc.* **1999**, *121*, 262-263.
- McNamara III, W. B.; Didenko, Y.; Suslick, K. S. "Hot Spot Conditions During Cavitation in Water" *J. Am. Chem. Soc.* **1999**, *121*, 5817-5818.
- McNamara III, W. B.; Didenko, Y.; Suslick, K. S. "Sonoluminescence Temperatures During Multibubble Cavitation" *Nature* **1999**, *401*, 772-775.
- McNamara III, W.B.; Didenko, Y.; Suslick, K.S. "Effect of Noble Gases on Sonoluminescence Temperatures During Cavitation" *Phys. Rev. Lett.* **2000**, *84*, 777-780.
- Dantsin, G.; Suslick, K. S. "Sonochemical Preparation of a Nanostructured Bifunctional Catalyst" *J. Am. Chem. Soc.* **2000**, *122*, 5214-5215.
- McNamara III, W. B.; Didenko, Y.; Suslick, K. S. "The Nature of the Continuum in Multi-Bubble Sonoluminescence" *J. Am. Chem. Soc.* **2000**, *122*, 8563-8564.
- Sen, A.; Suslick, K. S. "Shape-Selective Discrimination of Small Organic Molecules" *J. Am. Chem. Soc.* **2000**, *122*, 11565- 66.
- Rakow, N. A.; Suslick, K. S. "A Colorimetric Sensor Array for Odor Visualization" *Nature* **2000**, *406*, 710-714.
- Didenko, Y.; McNamara III, W. B.; Suslick, K. S. "Molecular Emission from Single Bubble Sonoluminescence" *Nature* **2000**, *407*, 877-879.
- Rosenblatt, M.M.; Huffman, D.L.; Wang, X. Remmer, H.A.; Suslick, K. S. "Cyclic and Hairpin Peptide Complexes of Heme" *J. Am. Chem. Soc.*, **2002**, *124*, 12394-12395.
- Dhas, N.A.; Ekhtiarzadeh, A.; Suslick, K.S. "Sonochemical Preparation of Supported Hydrodesulfurization Catalysts" *J. Am. Chem. Soc.*, **2001**, *123*, 8310-8316.
- Kosal, M. E.; Chou, J.-H.; Wilson, S. R.; Suslick, K. S. "A Functional Zeolite Analogue Assembled From Metalloporphyrins" *Nature Materials*, **2002**, *1*, 118-121.
- Didenko, Y.; Suslick, K. S. "Photons, Radicals, and Ions from a Single Bubble: An Energy Inventory During Cavitation" *Nature* **2002**, *419*, 394-397.
- Zimmerman, S. C.; Wendland, M. S.; Rakow, N. A.; Zharov, I.; Suslick, K. S. "Synthetic Hosts by Monomolecular Imprinting Inside Dendrimers" *Nature* **2002**, *418*, 399-403.
- Wang, J.; Luthey-Schulten, Z.; Suslick, K. S. "Is the Olfactory Receptor A Metalloprotein?" *Proc. Natl. Acad. Sci. U.S.A.*, **2003**, *100*, 3035-3039.
- Suslick, K.S.; Rakow, N.A.; Kosal, M.E.; McNamara III, W.B.; Sen, A. "Chemsensing: A Colorimetric Array Detector" *Proc. ISOEN 02* (ed. A. D'Amico and C. DiNatale; IEEE: Baltimore, 2003), pp. 46-52.
- Rosenblatt, M.M.; Wang, J.; Suslick, K. S. "De Novo Designed Cyclic-Peptide Heme Complexes" *Proc. Natl. Acad. Sci. U.S.A.*, **2003**, *101*, in press.
- McNamara III, W. B.; Didenko, Y.; Suslick, K. S. "Pressure during Acoustic Cavitation" *J. Phys. Chem. B* **2003**, *107*, 7303-7306 (Henglein Festschrift).
- Lee, T. M.; Oldenburg, A. L.; Sitafalwalla, S.; Marks, D. L.; Luo, W.; Toublan, F. J.-J.; Suslick, K. S.; Boppart, S. A. "Engineered Microsphere Contrast Agents for Optical Coherence Tomography" *Optics Lett.* **2003**, *28*, 1546-1548.
- Oxley, J. D.; Prozorov, T.; Suslick, K. S. "Sonochemistry and Sonoluminescence of Room-Temperature Ionic Liquids" *J. Am. Chem. Soc.*, **2003**, *125*, 11138-11139.
- Prozorov, T.; Prozorov, R.; Snezhko, A.; Suslick, K. S. "Sonochemical Modification of the Superconducting Properties of MgB₂" *Appl. Phys. Lett.* **2003**, *83*, 2019-2021.

The Suslick Research Group



[Overview](#)

[Outline of
Research Projects](#)

[Introduction to
Sonochemistry](#)

[Exec. Summary:
Sonochemistry](#)

[Exec. Summary:
Porphyrin Research](#)

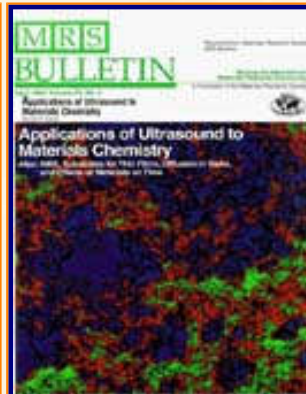
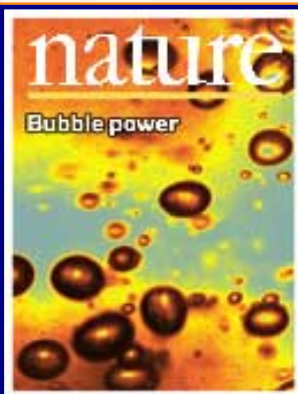
[Exec. Summary: Smell-
Seeing](#)

[Complete
Publication List](#)

[Abbreviated Curriculum
Vitae](#)

[Academic
Genealogy](#)

[Press
Clippings](#)



COVER ART

[Cover Art by Ken Suslick](#)

[Bronze Sculpture by Ken Suslick](#)

[Masks from the Collection of Ken Suslick](#)

[The Pouring of Bronze](#)

[SCIENCE:
March 1990](#)



[Current Research
Funding](#)

[Excerpts from
Funded Research](#)

[Inventory of
Group Equipment](#)

[Information
for Visiting](#)

[Current Research Group
Members](#)

[Group
Meetings](#)

[Group
Chores](#)

[Past Research
Group Members](#)

[Group
Photogallery](#)

[Web Resources](#)

[Laboratory Safety
Resources](#)

[Art and Science:
Journal Covers](#)

[Sculpture &
Masks](#)

[A Chemist
Meets Hollywood](#)

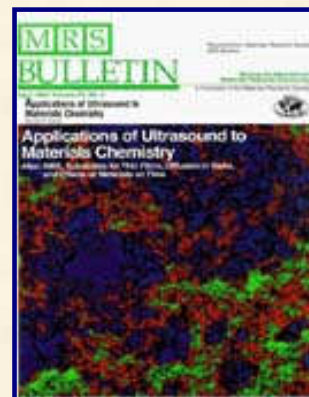
[Chymistes: The Distillers
of Waters](#)

[A Chemist
In Court](#)

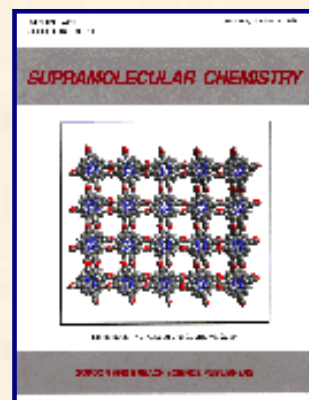
SCIENCE:
September 1991



MRS BULLETIN:
April 1995



SUPRAMOLECULAR CHEMISTRY:
September 1998



NATURE:
25 July 2002



[Humor and
Wisdom](#)

[Laws of the Universe](#)

[Cartoons of Humor and
Wisdom](#)

[Chem 115: Chemistry of
Everyday Phenomena](#)

[Chem 315: Inorganic
Chemistry](#)

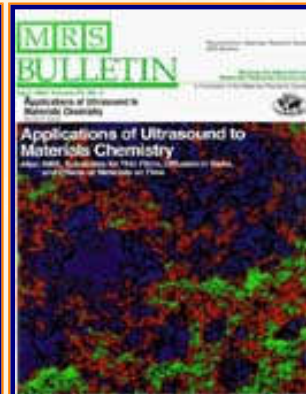
SUSLICK GROUP WEBSITE:

THE SCIENCE	THE GROUP	THE MAÎTRE D'	LAGNIAPPE: A LITTLE EXTRA
Overview	Current Group Members	CV: Abbreviated, Full	Art and Science
Outline of Projects	Group Meetings	Suslick Group Brochure	Chymistes: The Distillers of Waters
Synopsis: Sonochemistry	Group Responsibilities	Complete Publication List	A Chemist Meets Hollywood
Metalloporph.			
Executive Summary: Smell-Seeing	Web Based Resources	Academic Genealogy	A Chemist In Court
Introduction to Sonochemistry	Safety Resources	Press Clippings	Words of Humor and Wisdom
Proposal Excerpts	Group Equipment	How To Give A Seminar	Laws of the Universe
Funding	Past Group Members	Ch315 Inorganic Chemistry	Cartoons of Humor and Wisdom
Information for Visitors	Group Photogallery	Construction of the CLS Lab	Sculpture & Masks

©2003, K.S. Suslick; all rights reserved.

Comments and suggestions: ksuslick@uiuc.edu

The Suslick Research Group



SUSLICK GROUP MEETINGS

MONDAY MORNINGS: 9:00 am, A414 CLSL, *except as otherwise noted.*

New students are always welcome to attend.

[For the schedule of meetings in pdf format, click here.](#)

[Overview](#)

[Outline of
Research Projects](#)

[Introduction to
Sonochemistry](#)

[Exec. Summary:
Sonochemistry](#)

[Exec. Summary:
Porphyrin Research](#)

[Exec. Summary: Smell-
Seeing](#)

[Complete
Publication List](#)

[Abbreviated Curriculum
Vitae](#)

[Academic
Genealogy](#)

[Press
Clippings](#)

SMALL GROUP MEETINGS are informal gatherings to discuss research results, problems and ideas. Be prepared: know what you wish to discuss and have the appropriate spectra, etc., available at the meeting. *Be succinct:* conciseness is always appreciated.

LITERATURE TALKS should use 3-4 papers from a single author or on a single topic, taken from good journals over the past 2 years. A brief handout for all group members (currently 15) should be prepared in advance; this should contain a list of the chosen papers, a 1 page summary of the important points of the chosen papers, a xerox of the abstract of each full paper, and a xerox of each short communication. Bring a complete copy of each of the full papers to the meeting.

INDIVIDUAL MEETINGS will be for candid evaluation of progress and goals. *At the time of the meeting*, please have a typed, one-page, *three-holed* summary. Two copies are needed: one for you and one for me. My copy is filed for future reference at the *next* individual meeting. This summary should include: **1)** your accomplishments since the last individual meeting; **2)** a separate paragraph of your goals for the next 2 months; and **3)** an attached copy of critical spectra.

RESEARCH TALKS should be 30-40 minutes long, semi-formal (slides if you've got them; overheads otherwise), with a brief *handout* of important data, spectra, and conclusions. The day after your research presentation, please post your presentation on the group server and give me a copy of the file as a CD-ROM, after any corrections have been made.

SUSLICK GROUP WEBSITE:[Current Research Funding](#)[Excerpts from Funded Research](#)[Inventory of Group Equipment](#)[Information for Visiting](#)[Current Research Group Members](#)[Group Meetings](#)[Group Chores](#)[Past Research Group Members](#)[Group Photogallery](#)[Web Resources](#)[Laboratory Safety Resources](#)[Art and Science: Journal Covers](#)[Sculpture & Masks](#)[A Chemist Meets Hollywood](#)[Chymistes: The Distillers of Waters](#)[A Chemist In Court](#)

THE SCIENCE	THE GROUP	THE MAÎTRE D'	LAGNIAPPE: A LITTLE EXTRA
Overview	Current Group Members	CV: Abbreviated, Full	Art and Science
Outline of Projects	Group Meetings	Suslick Group Brochure	Chymistes: The Distillers of Waters
Synopses: Sonochemistry	Group Responsibilities	Complete Publication List	A Chemist Meets Hollywood
Metalloporph.			
Executive Summary: Smell-Seeing	Web Based Resources	Academic Genealogy	A Chemist In Court
Introduction to Sonochemistry	Safety Resources	Press Clippings	Words of Humor and Wisdom
Proposal Excerpts	Group Equipment	How To Give A Seminar	Laws of the Universe
Funding	Past Group Members	Ch315 Inorganic Chemistry	Cartoons of Humor and Wisdom
Information for Visitors	Group Photogallery	Construction of the CLS Lab	Sculpture & Masks

©2003, K.S. Suslick; all rights reserved.

Comments and suggestions: ksuslick@uiuc.edu

[Humor and
Wisdom](#)

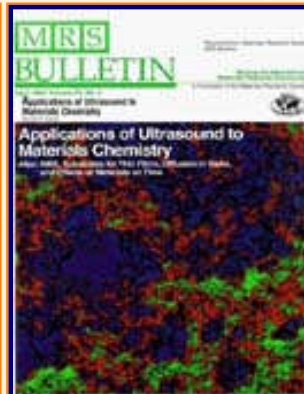
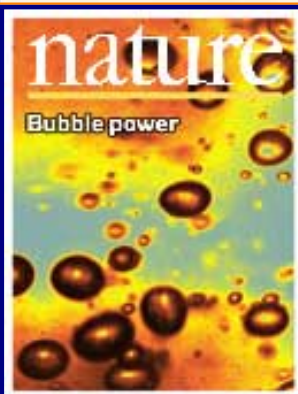
[Laws of the Universe](#)

[Cartoons of Humor and
Wisdom](#)

[Chem 115: Chemistry of
Everyday Phenomena](#)

[Chem 315: Inorganic
Chemistry](#)

The Suslick Research Group



Chymistes: The Distillers of Waters

On the Occasion of the Dedication
of the Chemical and Life Sciences Laboratory,
April 25, 1997

Kenneth S. Suslick

[Overview](#)

[Outline of
Research Projects](#)

[Introduction to
Sonochemistry](#)

[Exec. Summary:
Sonochemistry](#)

[Exec. Summary:
Porphyrin Research](#)

[Exec. Summary: Smell-
Seeing](#)

[Complete
Publication List](#)

[Abbreviated Curriculum
Vitae](#)

[Academic
Genealogy](#)

[Press
Clippings](#)

Last spring, Steve Sligar asked me to present an after-dinner speech to the visiting alumni, as part of the dedication ceremonies for our new *Chemical & Life Sciences Laboratory*. In one of those moments of a sense of duty (that we all have and mostly come to regret later!), I agreed.

It was made clear to me that this was not to be a standard research presentation. Rather, I was to provide an overview for an audience with diverse background (remember there were a lot of biologists and University administrators in the audience, too). I took this as a challenge, in some ways much like my course Chem 115, "The Chemistry of Everyday Phenomena." The talk went well enough that Steve requested an encore in the form of an article for the SCS Newsletter.

This presentation was a fancy slide show---well, actually there weren't any slides---it came straight off my laptop and onto the screen via an SVGA LCD projector, complete with full color, animation, and dissolves. Very high tech, and to my amazement, it actually all worked. I can't really reproduce it all on paper, but I can best reprise the talk primarily with its images. So, I've edited down the slides and provided brief commentary as needed.

[Current Research
Funding](#)

[Excerpts from
Funded Research](#)

[Inventory of
Group Equipment](#)

[Information
for Visiting](#)

[Current Research Group
Members](#)

[Group
Meetings](#)

[Group
Chores](#)

[Past Research
Group Members](#)

[Group
Photogallery](#)

[Web Resources](#)

[Laboratory Safety
Resources](#)

[Art and Science:
Journal Covers](#)

[Sculpture &
Masks](#)

[A Chemist
Meets Hollywood](#)

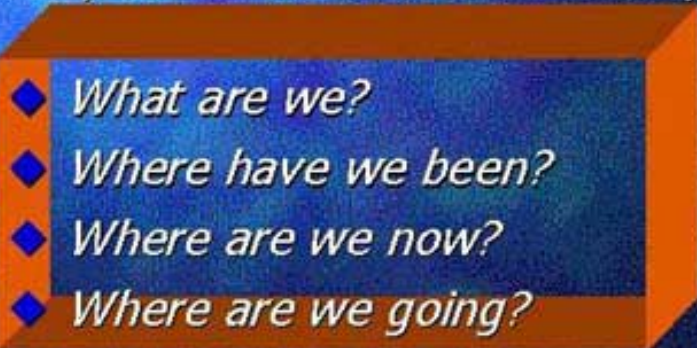
[Chymistes: The Distillers
of Waters](#)

[A Chemist
In Court](#)

Chymistes: The Distillers of Waters

Kenneth S. Suslick

School of Chemical Sciences
University of Illinois at Urbana-Champaign

- 
- ◆ *What are we?*
 - ◆ *Where have we been?*
 - ◆ *Where are we now?*
 - ◆ *Where are we going?*

I made the theme of the talk four simple questions, posed in the figure above.

Bon Mots

- ◆ Bulleyn, *Book of Simples*, 1562:
"Chymistes, The Distillers of Waters"
- ◆ Francis Bacon, *Sylva*, 1626:
"The industry of the Chymists,
discerning by their separations, the Oily,
Crude, Pure, Impure, Fine, and Gross..."
- ◆ Alexander Pope, *Essays on Man*, 1732:
"The starving Chymist in his golden
views Supremely blest..."

[Humor and
Wisdom](#)

[Laws of the Universe](#)

[Cartoons of Humor and
Wisdom](#)

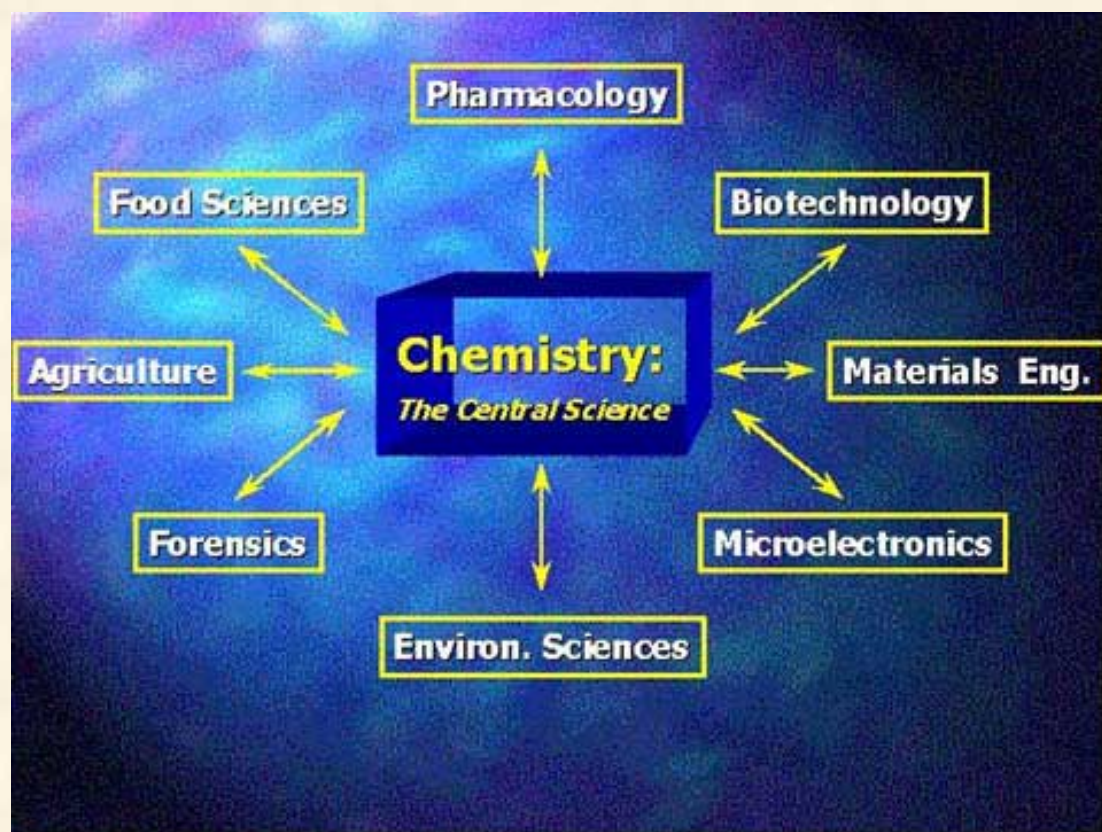
[Chem 115: Chemistry of
Everyday Phenomena](#)

[Chem 315: Inorganic
Chemistry](#)

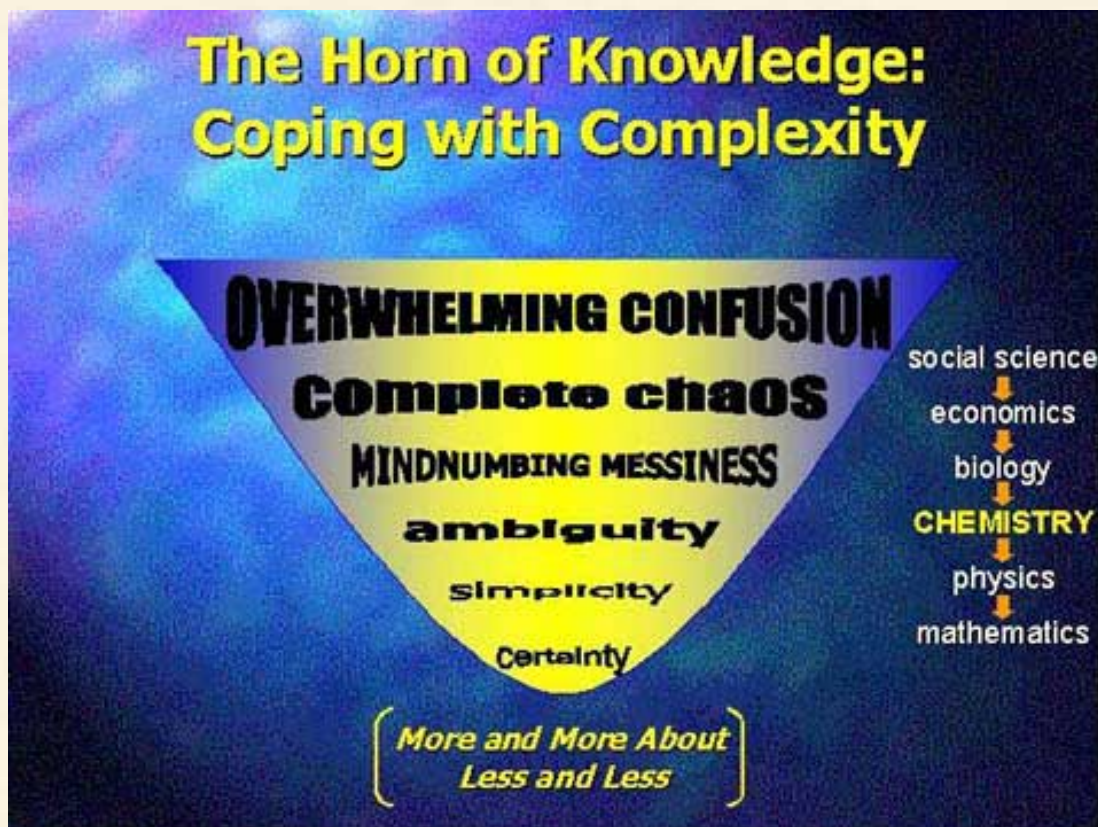
To answer the first of my four questions (***What are we?***), the first thing I did was to go online and look up "chemist" in the Oxford English Dictionary (<http://www.uiuc.edu/cgi-bin/oed>).

This immediately gave me my title, which is the first written reference to "chemist" in English. Back then, "simples" were the miracle drugs of the time (i. e., vegetable or herbal remedies distilled from alcohol extracts), and "waters" were any liquid, especially the intoxicating sort! Bulleyn, by the way, was a cousin to Anne Bulleyn, one of the Queens of England during Henry VIII's reign; he also wrote the 1564 best seller, *Dialog Against the Pestilence: A Cordial Ointment against the Pestilence*, which provided recipes for liqueurs.

From Bacon's quotation, it is clear that much of what we do hasn't truly changed over the past 400 years. My real favorite, however, is from Alexander Pope, who clearly was referring to our non-industrial brethren!

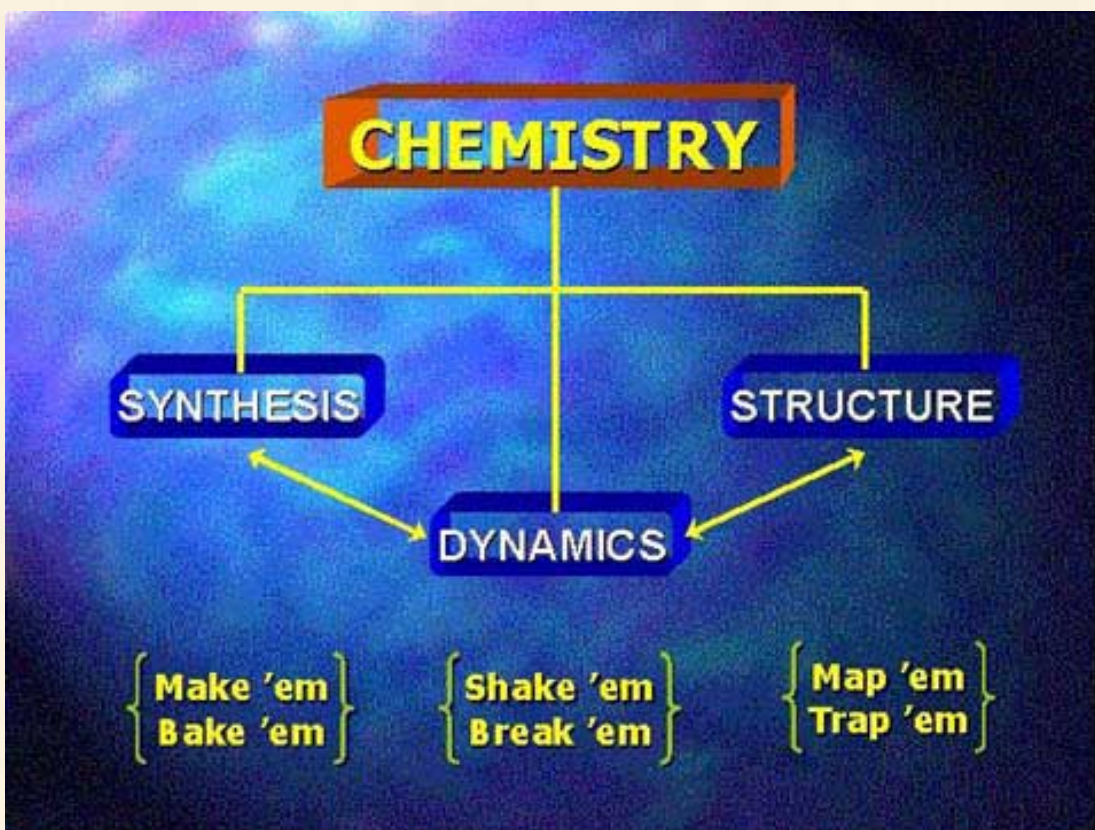


Ted Brown has had for many years one of the best selling general chemistry textbooks: "Chemistry: The Central Science". The truth of this sobriquet is self-evident and even truer now than with Ted's first edition of 25 years ago. All physical sciences and technologies are fundamentally rooted in chemistry. It is no surprise therefore that Ted should have been the first Director of the Beckman Institute for Advanced Science and Technology, nor that Jiri Jonas, also a chemist, should be the second.

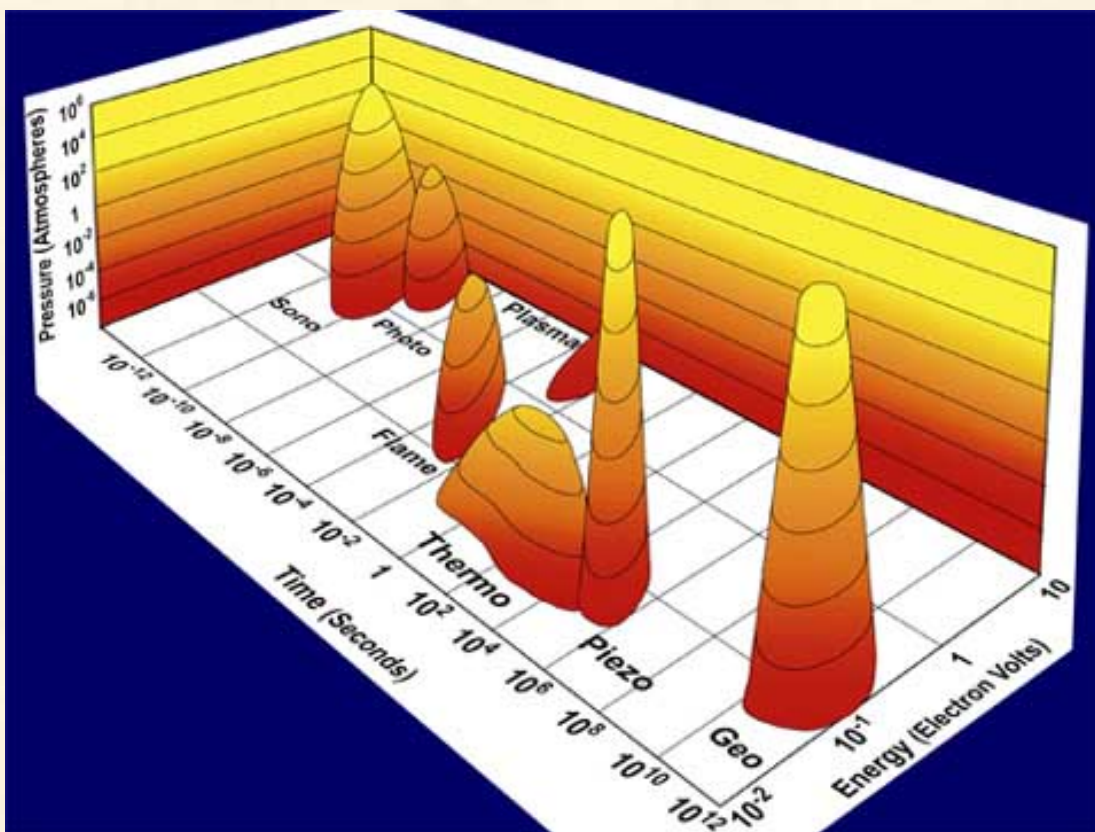


Chemistry is central not only with respect to providing a foundation for other sciences and technologies, but also in its place in what I refer to as the "Horn of Knowledge." In many ways, this slide expresses a very real tragedy of human existence: the frustration of never being able to know all of everything. There are really two parts to this dilemma, however: the problem of information overload and the problem of variables versus determinables. Fundamentally, these two problems represent kinetic versus thermodynamic control!

Larry Smarr, Director of the NCSA (née National Center for Supercomputing Applications, now the National Computational Science Alliance), has referred to the kinetics part of this problem as trying to drink from a fire hydrant. I fear, however, that it is the second problem, the thermodynamics, which really represents the inherent complexity of different fields, is even more limiting. Chemistry is central in this scheme of things, as well. The number of variables with which chemists must cope is not quite at the level of mind-numbing messiness, but it is also well above the pristine simplicity that many hope to strive for. Well, after all, chemistry is just the physics of interesting systems!



George Hammond, when at Caltech, tried to renormalize chemistry and the undergraduate curriculum around 1970. This had significant influence in the laboratory curriculum here as well. As an undergrad, I enrolled in Hammond's course on "Chemical Education," which may well have been the only "Education Course" ever taught at Caltech! Rather than the parochial divisionalization of chemistry based on historical precedent, Hammond saw the underlying conceptual links among the subdisciplines. George has no responsibility for the bracketed rap lyrics, for which I alone take the blame.



I am particularly proud of this figure, which does what every freshman thought we could do: here is all of chemistry on a single slide. Fundamentally, chemistry is the interaction of energy and matter. The parameters that control that interaction are the time of the interaction, the amount of energy in the interaction, and the pressure or density at which the interaction occurs. Together these describe a three-dimensional space in which different kinds of chemistry can be placed. The figure shows the heavily populated island of thermal chemistry at medium pressure, time, and energy. Chemistry under geological conditions, at high pressures and long-time scales, is shown as the spike on the far right. The island of sonochemistry is in the back corner, near shock and photochemistry. All of these are related because they are all forms of interacting energy and matter. Each, however, has its own specific characteristics because each occupies a different region of this three-dimensional space.

Chemistry at UIUC: Where have we been?



Out of Time

by Piet Hein

My old clock used to tell the time
and subdivide diurnity;
but now it's lost both hands and chime
and only tells eternity.

Having defined what chemists are and what chemistry is, the talk then moved on to "Where have we been."

Areas of Chemistry: 1900

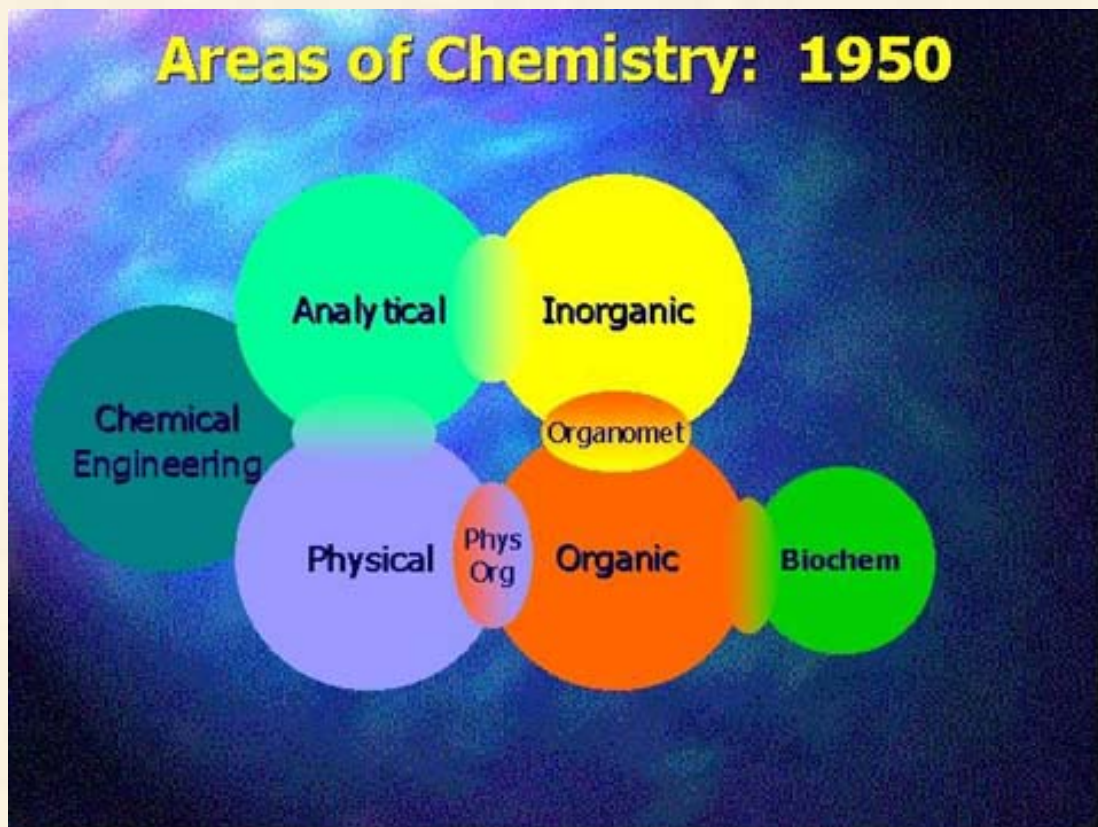
Analytical

Inorganic

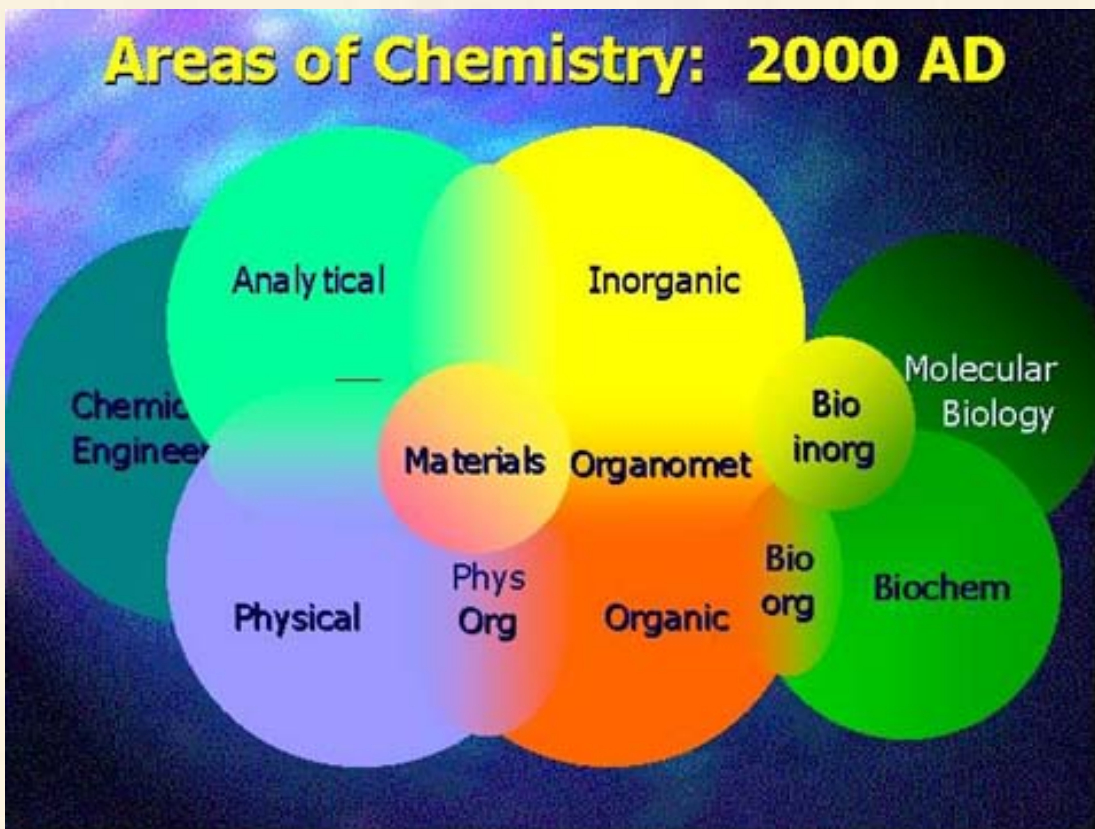
Physical

Organic

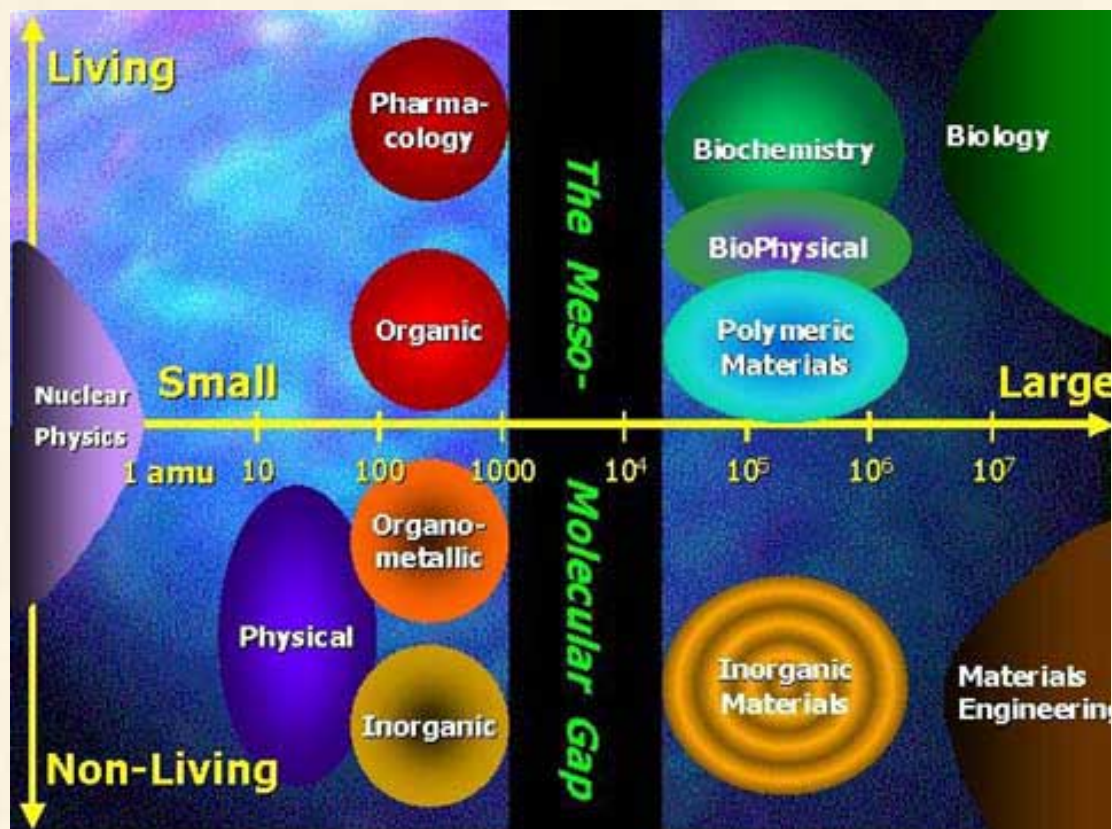
The traditional divisions of chemistry predate this century. While they are certainly present even in contemporary research, their biggest role lies in the subdivision of undergraduate teaching. Universities in the U.S. have never been quite as divided as the European schools, where it is not uncommon, even today, to find completely separate departments with completely separate faculty and facilities, and even with nearly completely separate undergraduate curricula.



By the middle of this century, the blurring of fields was well underway. Separate departments of Chemical Engineering and Biochemistry were being established everywhere, including UIUC, and newer research areas that spanned the traditional divisions became some of the most active areas of research.



At this point in time, we can't even represent the molecular sciences in two dimensions, in spite of this cartoon. This is only a projection of a multi-dimensional space where all of the subdisciplines overlap with each other. Even Chemical Engineering and Biochemistry, which once were nearly antipodal, have substantial common interests and methodologies. The politics of internal resources, of course, is a whole other issue!



I have another way of portraying the various fields of science: a plot of molecular weight against some measure of living/non-living. One aspect of this leaps out at me, and that is what I've called the "Meso-Molecular Gap". Between small molecules and macromolecules, there lies a region of relatively unexplored chemistry that deals with things that mass between roughly 1000 and 10,000 amu. Supramolecular chemistry falls in this space, but so does much synthetic peptide work and also inorganic clusters and nanophase materials. Only recently have tools been developed for both synthesis and characterization of molecules in this region. Needless to say, this gap is being rapidly closed and quite actively so at the University of Illinois.

Chemistry at UIUC: Early Days

YEAR EVENTS

1868	Illinois Industrial University opens: March 11, 1868. Chemistry in basement of University Hall; 2 faculty. A.P.S. Stuart (Harvard), 1st Chem. Chair; salary: \$2000. Total prop. budget, \$30,000; actual, \$5000!
1888	Dept. of Applied Chemistry opens; 3 faculty. Harker Hall.
1891	S. W. Parr, Chair of Applied Chemistry.
1896	Harker fire – lightning: water tank smashes thru 4 floors.
1902	New Laboratory (Noyes Lab) opened: 15 Faculty.
1903	1st Ph.D. from UI: W.H. Dehn, in Chemistry.
1907	W. A. Noyes, Head of Combined Chemistry Department.
1916	New Wing of Noyes Lab completed. Roger Adams arrives as Asst. Prof. 62 Faculty; about 20 Ph.D. students.

There is a wonderful discussion of the early days of chemistry at the University of Illinois in a brochure prepared for our Centennial in 1967. Articles by Parr and Fuson were included (and I'll try to put them on the Web sometime). I don't know what \$5000 in 1868 would be worth in current dollars, but I'll wager it isn't what we now spend on Xeroxing in a year! It is impressive that by 1916, the year that Roger Adams arrived as an Assistant Professor, we had 62 faculty in all areas of chemical sciences (there are 78 now) and occupied what was at the time the largest university chemistry laboratory in the world.



University Hall , 1868-1888



Harker Hall, 1888-1902

**Noyes Lab,
1902/1916 - ...**



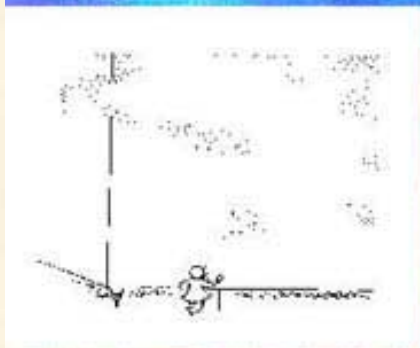
As we dedicate the newest chemical laboratory, it seemed appropriate to look back at the labs that started it all. Chemistry started out in the basement of University Hall, the founding building of the University. Appropriately enough, the site of University Hall is now occupied by the Beckman Institute for Advanced Science and Technology. A separate Department of Applied Chemistry was added and labs opened in the Harker Hall, which proved to be too small, too quickly. Besides that, after the lightning strike started the fire that burned through the beams that supported the water tank that smashed through four floors, that finished Harker as a laboratory! It has been recently "renovated" as the home of the University Foundation; you sure can't tell it was ever a dirty old lab. Noyes, of course, has changed very little (either on the outside or on the inside). If you look closely at the photo, however, you may note that the new wing of Noyes (completed 1916) is missing from this postcard (which is dated Feb. 7, 1907). The postcard is from a Freshman to his parents; on the front of the card, he wrote "Oh yes! I got through chemistry!"; it's good to see that some challenges never change.

Chemistry at UIUC: 20th Century

Year	Buildings	Some UI Discoveries & Achievements
1900	Harker	Calorimetry
1910	Noyes (old)	Founding of Chem. Abs. Polymer Synthesis
1920	Noyes (new)	Aerosol Spray Can
1930	Chem Annex	Pt Hydrogenation Catalyst Last Vitamins & Amino Acid
1940		Peptide Hormones
1950	East Chem	1st Artificial Sweetener
1960	EC Addition	Modern Coordination Chem. High Pressure Spectroscopy
1970	(EC \Rightarrow RAL)	Electron Transfer Theory
1980		NMR for Chemical Analysis
1990		
2000	CLSL	<i>TO BE DETERMINED BY POSTERITY.</i>

This is my own list of the most important chemical discoveries to come out of the UIUC this century. If I've left out your favorite, please accept my apologies. Better yet, send me your suggestions and I'll add them. You'll notice that I stopped the countdown at t-minus 20 years. It isn't that we haven't made progress in that time, it's just that I'd prefer to keep what few friends I have!

Chemistry at UIUC: Where are we now?



Atomyriades

by Piet Hein

Nature, it seems, is the popular name for milliards and milliards and milliards of particles playing their infinite game of billiards and billiards and billiards.

"The past is prologue." Enough of where we've been, now where are we?

Chemistry at UIUC: NOW

Faculty

SCS Total	78	19 in CLSL
Chemistry	52	
Biochemistry	15	
Chem Eng.	11	

Graduate Students

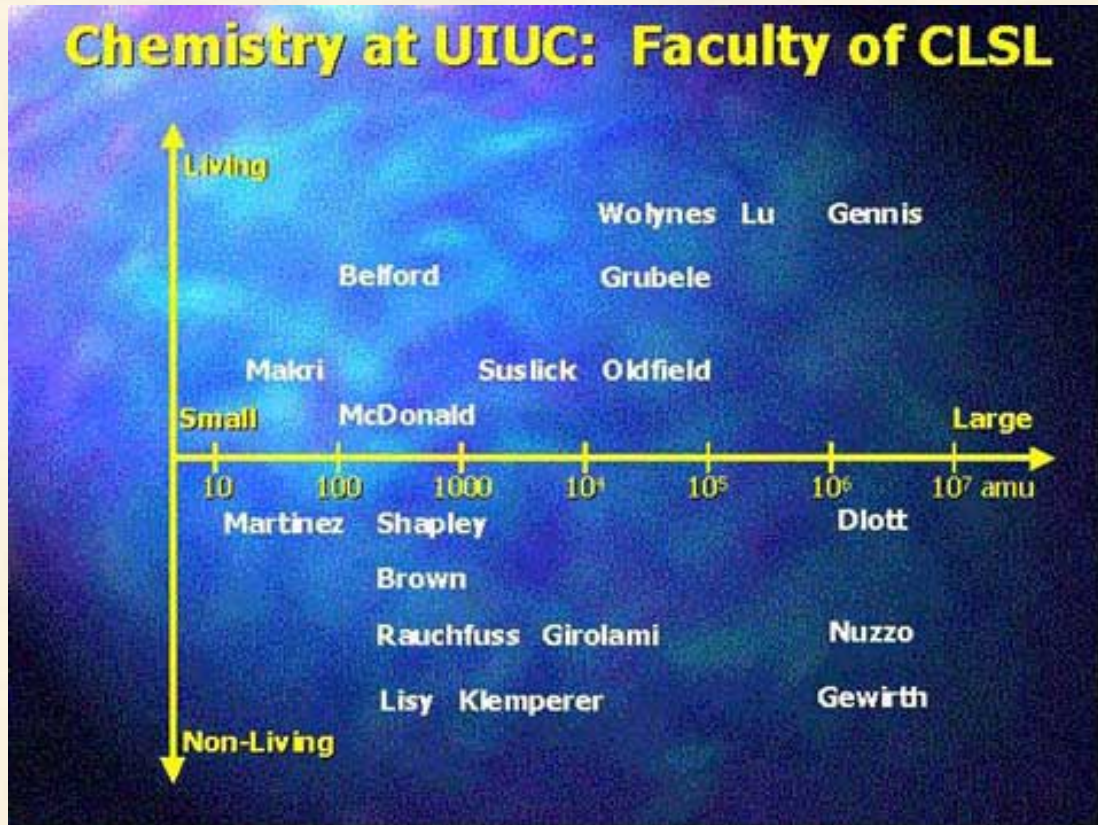
SCS Total	461	120 in CLSL
Chemistry	300	
Biochemistry	95	
Chem Eng.	66	

Undergrad Students

SCS Total	1,052
Chemistry	385
Biochemistry	244
Chem Eng.	423

Total Full Time Faculty	2,660	(2.9% SCS)
Total Stud. Population	36,164	(2.9% SCS)

The School of Chemical Sciences is 3% of the University in numbers, but probably a whole lot more in prestige (and funding, and clout).



At the risk of annoying my colleagues, I've attempted to map the research interests of the SCS faculty in the Chemical and Life Sciences Laboratory onto my chemical plane of size versus livingness. This isn't completely successful, partly do to my own ignorance and partly because many faculty have multiple interests in very different parts of this plane. Regardless, I think that it is pretty neat the way that the space is nearly filled.

Chemistry at UIUC: Where are we going?

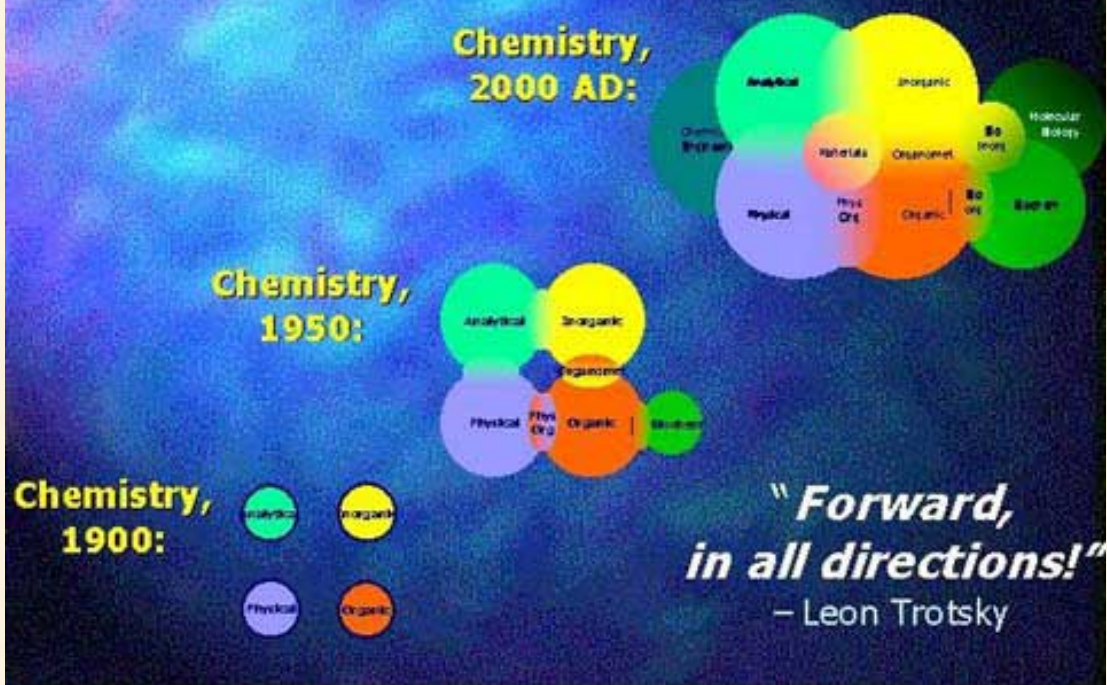


I'd Like –
by Piet Hein

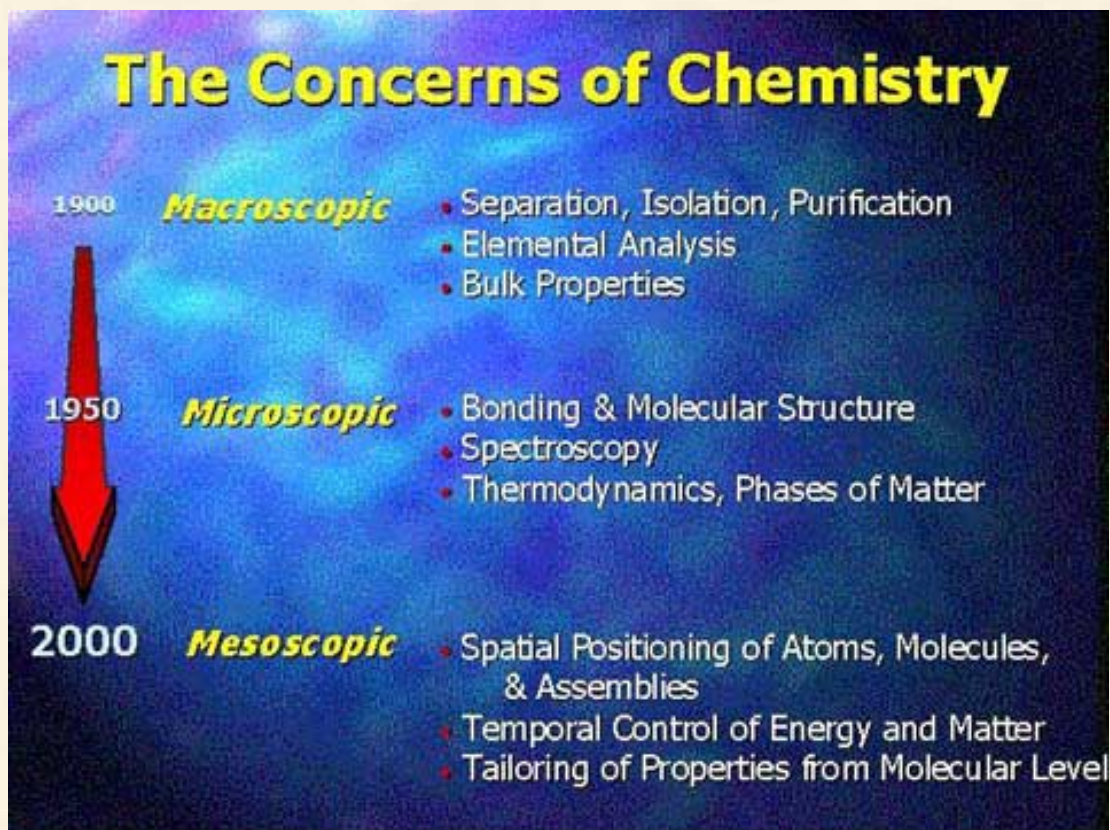
I'd like to know
what this whole show
is all about,
before it's out.

Where do we go from here?

Chemistry at UIUC: The Future

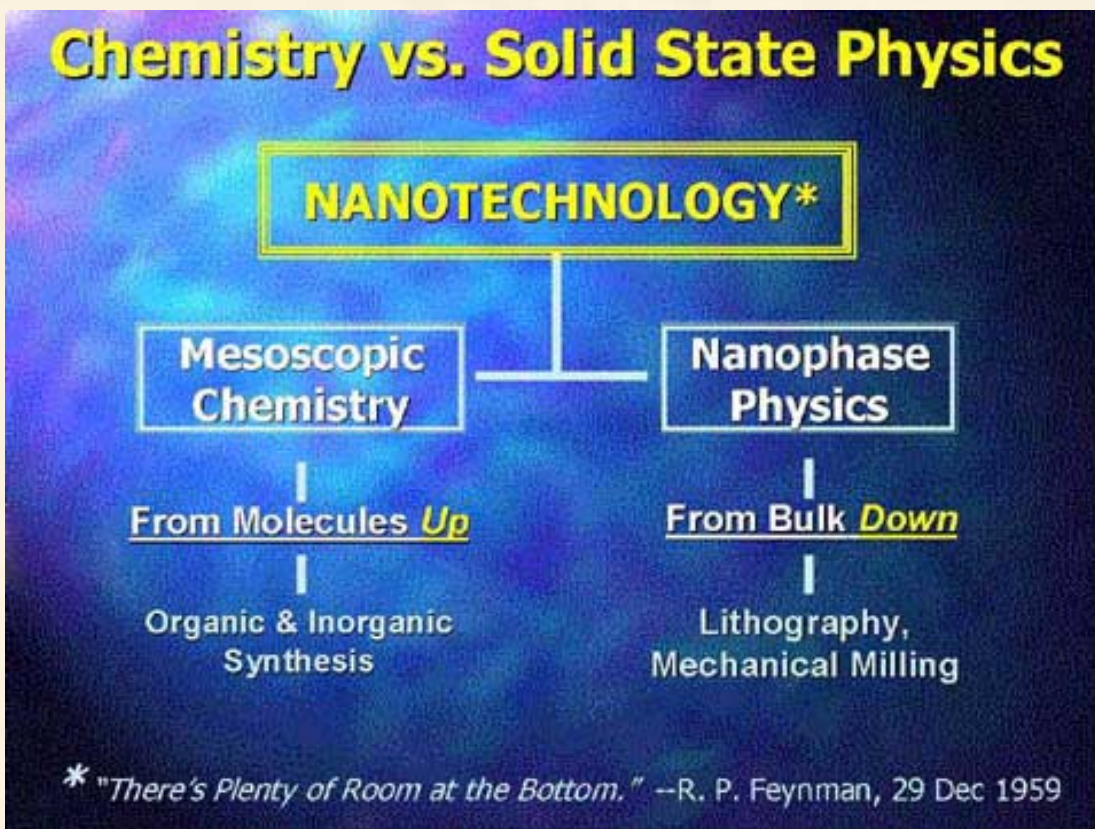


I offer Trotsky's motto.



At the turn of the century, only macroscopic properties of chemical and materials could be measured. By mid-century, chemists could probe things at the molecular and atomic level, but the middle ground remained inaccessible. I believe that the developments of the next half-century will be primarily in the "mesoscopic" regime: that is, the control of individual atoms and molecules on scale of the macroscopic. The kind of control over molecular and material properties that will develop from this would seem like magic to our predecessors (and maybe even to us!).

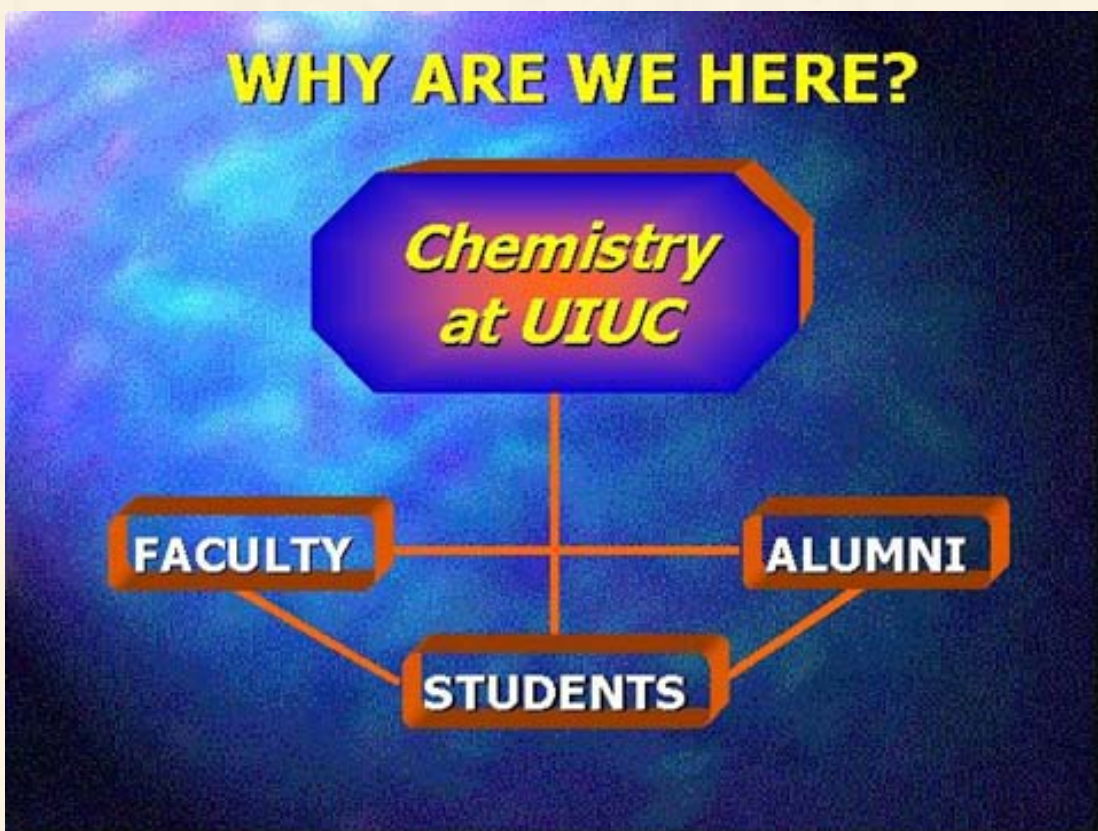
Chemistry vs. Solid State Physics



The patron saint of this new domain was Richard Feynman; his prescience (nice word that) in 1959 envisioning the nanoscale control of materials and machines remains impressive. The complete text can be found at [a Xerox Corp. webpage](#). There is a big difference, however, in the ways that chemists view this regime compared to physicists or engineers. We build from the bottom up, whereas they do it from the top down. It is the difference between bronze casting and marble carving; few artists can do both well, but both methods can produce masterpieces.



Here we are now. Please come and visit our new labs when you have the chance. We are proud of them and love to show them off!



To answer the last question of my talk, I ended with a Nasrudin story. The Mulla Nasrudin is the wise-fool of Sufiism and there are hundreds of stories about him that are used to teach the important lessons of life (Idries Shah has collected some of the best). This particular one, I used for the opening of my own Ph.D. thesis.

Walking one evening along a deserted road, Mulla Nasrudin saw in the distance a troop of horsemen coming towards him. His imagination started to work; he saw himself captured, beaten, and sold as a slave or impressed into the army. Nasrudin bolted, and dove into a ditch at the side of the road where he lay on his stomach, quivering with his hands covering. Puzzled at his strange behavior, the men, friends of Nasrudin, after all, stopped and asked, "What are you doing down there? Can we help?" "Just because you can ask a question, does not mean that there is a straightforward answer," said Nasrudin, who now realized what had happened. "It all depends on your point of view. If you must know, however: I am here because of you, and you are here because of me."

SUSLICK GROUP WEBSITE:

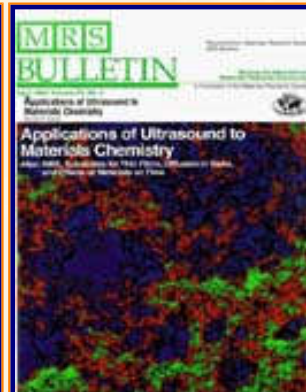
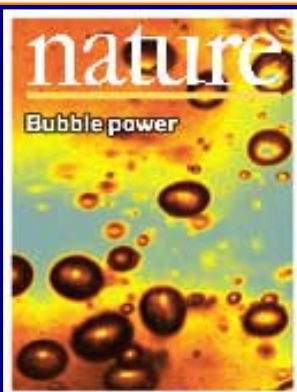
THE SCIENCE	THE GROUP	THE MAÎTRE D'	LAGNIAPPE: A LITTLE EXTRA
<u>Overview</u>	<u>Current Group Members</u>	<u>CV: Abbreviated, Full</u>	<u>Art and Science</u>
<u>Outline of Projects</u>	<u>Group Meetings</u>	<u>Suslick Group Brochure</u>	<u>Chymistes: The Distillers of Waters</u>
<u>Synopses: Sonochemistry</u>	<u>Group Responsibilities</u>	<u>Complete Publication List</u>	<u>A Chemist Meets Hollywood</u>
<u>Metalloporph.</u>			

<u>Executive Summary: Smell-Seeing</u>	<u>Web Based Resources</u>	<u>Academic Genealogy</u>	<u>A Chemist In Court</u>
<u>Introduction to Sonochemistry</u>	<u>Safety Resources</u>	<u>Press Clippings</u>	<u>Words of Humor and Wisdom</u>
<u>Proposal Excerpts</u>	<u>Group Equipment</u>	<u>How To Give A Seminar</u>	<u>Laws of the Universe</u>
<u>Funding</u>	<u>Past Group Members</u>	<u>Ch315 Inorganic Chemistry</u>	<u>Cartoons of Humor and Wisdom</u>
<u>Information for Visitors</u>	<u>Group Photogallery</u>	<u>Construction of the CLS Lab</u>	<u>Sculpture & Masks</u>

©2003, K.S. Suslick; all rights reserved.

Comments and suggestions: ksuslick@uiuc.edu

The Suslick Research Group



SUSLICK GROUP RESPONSIBILITIES

September, 2002

CHORE	RATING	PERSON
Accounting	(* , 1)	Hribar
Catalyst Rig & GC (HP)	(* , 1)	Dantsin
Centrifuges	(* , 1)	Rakow
Chromatotron	(* , 1)	Rakow
Clean-up, Commons Room (A424)	(* , 1)	Hribar
Clean-up, Catalyst Lab (A427)	(* , 1)	Prozorov
Clean-up, Instrument Lab (A441)	(* , 1)	Didenko



[Overview](#)

[Outline of
Research Projects](#)

[Introduction to
Sonochemistry](#)

[Exec. Summary:
Sonochemistry](#)

[Exec. Summary:
Porphyrin Research](#)

[Exec. Summary: Smell-
Seeing](#)

[Complete
Publication List](#)

[Abbreviated Curriculum
Vitae](#)

[Academic
Genealogy](#)

[Press
Clippings](#)

[Current Research Funding](#)

[Excerpts from Funded Research](#)

[Inventory of Group Equipment](#)

[Information for Visiting](#)

[Current Research Group Members](#)

[Group Meetings](#)

[Group Chores](#)

[Past Research Group Members](#)

[Group Photogallery](#)

[Web Resources](#)

[Laboratory Safety Resources](#)

[Art and Science: Journal Covers](#)

[Sculpture & Masks](#)

[A Chemist Meets Hollywood](#)

[Chymistes: The Distillers of Waters](#)

[A Chemist In Court](#)

Electrochem Rig & IBM UV-vis	(* , 1)	Paterno
Electrophoresis	(* , 1)	Wang
FTIR	(* , 1)	Kosal
GC (Varian)	(* , 1)	Kosal
GC-MS (HP)	(* , 1)	Dantsin
Glove Box, Single + Pumps	(** , 2)	Dhas & Dantsin
Glove Box, Double + Pumps	(** , 2)	Kosal & Sen
HPLC	(** , 1)	Paterno
Librarian, Catalog Files	(* , 1)	Hribar
Microscopes & Video	(* , 1)	Wang
N₂ House Line	(* , 1)	Dhas
NMR	(** , 1)	Kosal
Particle Counter	(* , 1)	Lawrence
PC's	(*** , 3)	Ektiarzadeh, Oxley, Lawrence

[Humor and
Wisdom](#)

[Laws of the Universe](#)

[Cartoons of Humor and
Wisdom](#)

[Chem 115: Chemistry of
Everyday Phenomena](#)

[Chem 315: Inorganic
Chemistry](#)

pH Meters & Water Purification	(* , 1)	Wang
Recycling & Broken Glassware	(** , 1)	Hribar
Refrigerators	(** , 1)	Dhas
Safety	(* , 1)	Didenko
Silicon Graphics	(** , 1)	Ektiarzadeh
Sonoluminescence Rig & Computer	(* , 2)	Didenko & McNamara
Stills	(** , 1)	Sen
UV-vis	(* , 1)	Rakow
Vac Ovens	(* , 1)	Oxley
Waste Disposal	(** , 3)	Wang, McNamara, Prozorov
Web Site Master	(* , 1)	Ektiarzadeh

DESCRIPTIONS

Rating: (*,1): Number of astericks indicates nastiness; numeral is number of people assigned to the chore.

Accounting: Circulate monthly stockroom charges within 72 hours among all group; members and insure corrections are made by the Business Office.

Catalyst Rig: Routine maintenance. IMPORTANT: Change pump oil on the First Monday of every month. Date Pump Label each time.

Centrifuges: Cleaning, routine maintenance.

Chromatotron: Training other users, updated how-to-use brochure, routine maintenance.

Clean-up: Pick up common areas each Monday. For A424, clear out food refrigerator as needed.

Electrochem. Rig: Routine Maintenance as needed. Protect the electrodes!

Electrophoresis: Routine maintenance including purchase of necessary stockpile of gels and supplies.

FTIR: Monthly Realignment on the First Monday of every month. IMPORTANT: CHANGE DESSICANT JAN. 1, APR 1, JUL 1, and OCT 1.

GC: Routine maintenance including change of septa each Monday when GC's are in moderate use. Pick up of GC area each Monday.

Glove Box & Pumps: Regeneration as needed; IMPORTANT: Change antechamber pump oil after regeneration. Instruct new users. Every Monday, police the box and its area and keep litter free. IMPORTANT: Change both pump's oil on the First Monday of every month.

HPLC: Training other users, updated how-to-use brochure, routine maintenance.

Librarian Maintain Catalog files; supervision of undergraduate xerox person.

Microscope: Routine Maintenance as needed.

N₂ Line Arrange for replacement of liquid N₂ tank for house N₂ as needed.

NMR: Instruction and Check out others on MSL NMR's.

Particle Counter: Routine Maintenance as needed.

pH Meters & Water Purifier Routine maintenance; order replacement parts as needed. Protect the electrodes!

Recycling: Haul away cans, recyclable paper. Salvage broken glassware with Glass shop help.

Refrigerators Check all refrigerators for un-stopped and unlabelled containers EACH Monday.

Safety: Inspections and Plenipotentiary Rights to order procedural changes in matters of lab safety.

Silicon Graphics: System Updates, group handouts, user training.

Sonoluminescence Rig: Maintenance of detector and 286 PC.

Stills: Maintenance, cleaning, and refilling of stills, as needed in timely fashion.

UV-vis: Routing maintenance. Pick up UV-vis area each Monday.

Vacuum Oven & Routing maintenance. IMPORTANT: change pump oil on the First Monday of every month

High Vac Line: (Date Pump Label each time).

Waste Disposal: Organize liquid and solid waste disposal carry-outs as needed.

SUSLICK GROUP WEBSITE:

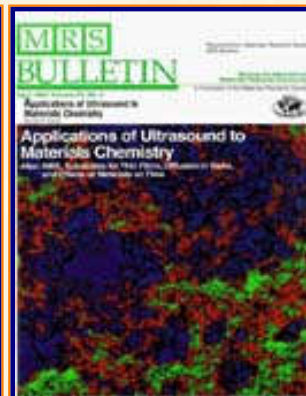
THE SCIENCE	THE GROUP	THE MAÎTRE D'	LAGNIAPPE: A LITTLE EXTRA
<u>Overview</u>	<u>Current Group Members</u>	<u>CV: Abbreviated, Full</u>	<u>Art and Science</u>
<u>Outline of Projects</u>	<u>Group Meetings</u>	<u>Suslick Group Brochure</u>	<u>Chymistes: The Distillers of Waters</u>
<u>Synopses: Sonochemistry</u>	<u>Group Responsibilities</u>	<u>Complete Publication List</u>	<u>A Chemist Meets Hollywood</u>
<u>Metalloporph.</u>			
<u>Executive Summary: Smell-Seeing</u>	<u>Web Based Resources</u>	<u>Academic Genealogy</u>	<u>A Chemist In Court</u>
<u>Introduction to Sonochemistry</u>	<u>Safety Resources</u>	<u>Press Clippings</u>	<u>Words of Humor and Wisdom</u>

<u>Proposal Excerpts</u>	<u>Group Equipment</u>	<u>How To Give A Seminar</u>	<u>Laws of the Universe</u>
<u>Funding</u>	<u>Past Group Members</u>	<u>Ch315 Inorganic Chemistry</u>	<u>Cartoons of Humor and Wisdom</u>
<u>Information for Visitors</u>	<u>Group Photogallery</u>	<u>Construction of the CLS Lab</u>	<u>Sculpture & Masks</u>

©2003, K.S. Suslick; all rights reserved.

Comments and suggestions: ksuslick@uiuc.edu

The Suslick Research Group



SOUND, LIGHTS, CAMERA, ACTION!

Kenneth S. Suslick

University of Illinois at Urbana-Champaign

(edited version from

Suslick, K. S. "Sonoluminescence, Camera, Action!"

*Engineering & Science (California Institute of Tech.) 1997 40 (#2), 4-5;
and from Inside Illinois, 3/20/97)*

It's not nominated for an "Oscar"(and no one is saying it should be), but last fall's movie "Chain Reaction" has its own links to ultrasound. Ken Suslick, William H. & Janet Lycan Professor of Chemistry, University of Illinois at Urbana-Champaign, recounts what happened when Hollywood came calling.

Some of you may have seen a movie last fall called "Chain Reaction". If so, you have my condolences. Nonetheless, it isn't too often that a chemist finds himself involved with Hollywood, much less gets money for his school off a bad movie.



[Overview](#)

[Outline of
Research Projects](#)

[Introduction to
Sonochemistry](#)

[Exec. Summary:
Sonochemistry](#)

[Exec. Summary:
Porphyrin Research](#)

[Exec. Summary: Smell-
Seeing](#)

[Complete
Publication List](#)

[Abbreviated Curriculum
Vitae](#)

[Academic
Genealogy](#)

[Press
Clippings](#)

[Current Research
Funding](#)

[Excerpts from
Funded Research](#)

[Inventory of
Group Equipment](#)

[Information
for Visiting](#)

[Current Research Group
Members](#)

[Group
Meetings](#)

[Group
Chores](#)

[Past Research
Group Members](#)

[Group
Photogallery](#)

[Web Resources](#)

[Laboratory Safety
Resources](#)

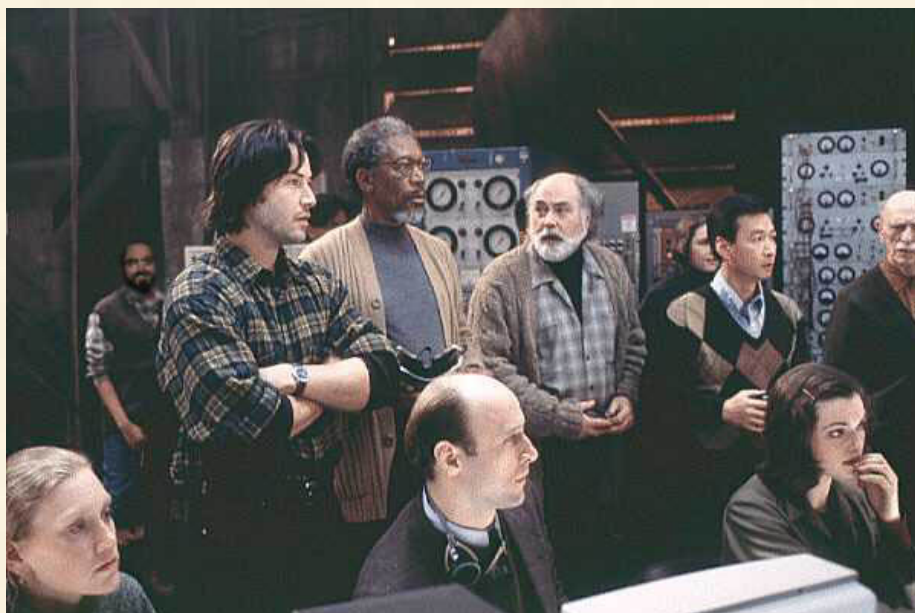
[Art and Science:
Journal Covers](#)

[Sculpture &
Masks](#)

[A Chemist
Meets Hollywood](#)

[Chymistes: The Distillers
of Waters](#)

[A Chemist
In Court](#)



(Note the lurker in the background.)

A pleasant fall day in 1994, I receive a message from my secretary that from someone claiming to be a Hollywood director. "Yeah, right!" I remember thinking as I dial the number. It turns out the caller, Gene Serdena, is the set director of a 20th Century Fox movie tentatively titled "Dead Drop"!

The movie is about a Nobel laureate professor and his graduate student who discover the use of sonoluminescence to produce unlimited quantities of hydrogen (the ultimate clean fuel) from water, catalytically. (Minor technical errors — such as violations of the Laws of Thermodynamics — are obviously no problem for Hollywood.) The professor is killed when the bad guys try to steal the discovery and the intrepid graduate student runs through chase scene after chase scene to expose the evildoers. This is no surprise since the director is Andrew ("The Fugitive") Davis. Serdena tells me that the student hero will be played by Keanu Reeves, the love interest by Nicole Kidman, and the prof would probably be Alan Arkin (or maybe--*I kid you not*--Marlon Brando). Now, by the time the movie actually gets going, Kidman has been traded for a new starlet and Brando has been downsized to Morgan Freeman.

Humor and
Wisdom

Laws of the Universe

Cartoons of Humor and
Wisdom

Chem 115: Chemistry of
Everyday Phenomena

Chem 315: Inorganic
Chemistry



*Let's see, now. Shockwave velocity ~1000 mph.
Motorcycle velocity ~100 mph.*

Hmmm... Good thing Keanu has the scriptwriter on his side!

Gene called me because of my work on sonoluminescence and other chemical effects of high intensity ultrasound. He wants to visit our labs to see what a chemistry lab *actually* looks like. So Gene and his assistant drive in from Chicago for a visit. With video and still cameras, they shoot *everything* that didn't move. It was fun showing him around and trying to explain why things were set up the way they were. They even give disposable cameras to my graduate students and myself to see how we live. Cinema vérité, at least for the set design!

A week later, Gene calls and wants to rent equipment from the lab for the set. I explain to him that we do actually use this stuff and that it's very expensive equipment. He sounds disappointed, and then it hits me — he doesn't want equipment that works, only that *looks* like it works. And I know about this cavernous storage area in the basement of Roger Adams Lab that is full of old equipment — stuff too good to throw away at the time it was hauled down there, but of no use now. Things like ancient Infracord spectrophotometers, several dozen old black and white monitors, pre-war lathes (not sure which war), and so on. I suggest that maybe they'd like to see the "scientific equipment" in our storage area. His assistant returns to Champaign and with flashlights in hand we go spelunking into the depths of RAL. She photographs everything (again) and goes away.

When Gene calls next, about 48 hours later, I can practically hear him salivating over the phone. This room full of useless equipment turns out to be just the sort of place a set director dreams about (apparently set directors have very weird dreams). The question is, how do we sell this detritus of dead equipment to them? It turns out the university cannot sell equipment — no matter how useless —

without rampant rivers of red tape. We can, however, declare old stuff surplus once it is of no further use, and simply take it off the books. Whether the junk then goes into a dumpster or into a truck, makes no difference.



Will the real sonochemist, please stand up!

So, with help from our business office manager, I arrange for a donation of \$10,000 from 20th Century Fox to the school. I didn't even ask a finder's fee. They then send down a crew of four humongous guys and a moving van to match and spend a full day hauling away junk that we've been wondering how to get rid of for years!

Two years later the movie comes out, now called "Chain Reaction." On opening day last fall, we shut down our lab, and I take the whole crew out to the first matinee. I bought the tickets, but my students had to get their own popcorn. Afterwards, we agreed the best part of the film was the labs, which were only slightly hokey. In fact, that was just about the only good thing in the entire movie. Even Siskel and Ebert gave it thumbs down. Fortunately, the UI's School of Chemical Sciences is not listed in the credits, so our anonymity remains preserved for posterity (until now!).

SUSLICK GROUP WEBSITE:

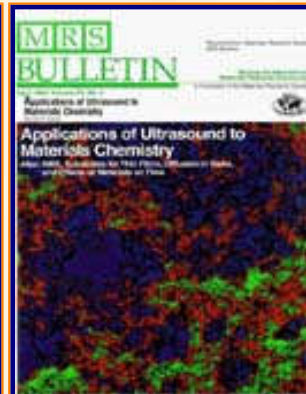
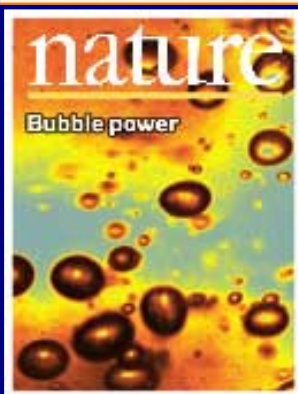
THE SCIENCE	THE GROUP	THE MAÎTRE D'	LAGNIAPPE: A LITTLE EXTRA
Overview	Current Group Members	CV: Abbreviated, Full	Art and Science

<u>Outline of Projects</u>	<u>Group Meetings</u>	<u>Suslick Group Brochure</u>	<u>Chymistes: The Distillers of Waters</u>
<u>Synopses: Sonochemistry</u>	<u>Group Responsibilities</u>	<u>Complete Publication List</u>	<u>A Chemist Meets Hollywood</u>
<u>Metalloporph.</u>			
<u>Executive Summary: Smell-Seeing</u>	<u>Web Based Resources</u>	<u>Academic Genealogy</u>	<u>A Chemist In Court</u>
<u>Introduction to Sonochemistry</u>	<u>Safety Resources</u>	<u>Press Clippings</u>	<u>Words of Humor and Wisdom</u>
<u>Proposal Excerpts</u>	<u>Group Equipment</u>	<u>How To Give A Seminar</u>	<u>Laws of the Universe</u>
<u>Funding</u>	<u>Past Group Members</u>	<u>Ch315 Inorganic Chemistry</u>	<u>Cartoons of Humor and Wisdom</u>
<u>Information for Visitors</u>	<u>Group Photogallery</u>	<u>Construction of the CLS Lab</u>	<u>Sculpture & Masks</u>

©2003, K.S. Suslick; all rights reserved.

Comments and suggestions: ksuslick@uiuc.edu

The Suslick Research Group



[Overview](#)

[Outline of
Research Projects](#)

[Introduction to
Sonochemistry](#)

[Exec. Summary:
Sonochemistry](#)

[Exec. Summary:
Porphyrin Research](#)

[Exec. Summary: Smell-
Seeing](#)

[Complete
Publication List](#)

[Abbreviated Curriculum
Vitae](#)

[Academic
Genealogy](#)

[Press
Clippings](#)

WEB BASED RESOURCES

[School of Chemical Sciences Library](#)

[Journals](#)

[Databases](#)

[On-Line Chemistry Applications](#)

[Manuscript templates](#)

[SCS VOICE NMR Information](#)

[Other Science Links](#)

Online Journals:

- [Available On-line Journals](#)
- [ACS Journals](#)
- [AIP Journals](#)
- [Annual Reviews](#)
- [Angew. Chem.](#)
- [Chemistry and Biology](#)
- [Chem. -Eur. J.](#)
- [J. Am. Chem. Soc.](#)
- [Journal of Biological Chemistry](#)
- [J. Org. Chem.](#)
- [Macromolecules](#)
- [Nature](#)
- [Org. Lett.](#)
- [PNAS](#)
- [Science](#)
- [Wiley Interscience](#)

[Current Research
Funding](#)

[Excerpts from
Funded Research](#)

[Inventory of
Group Equipment](#)

[Information
for Visiting](#)

[Current Research Group
Members](#)

[Group
Meetings](#)

[Group
Chores](#)

[Past Research
Group Members](#)

[Group
Photogallery](#)

[Web Resources](#)

[Laboratory Safety
Resources](#)

[Art and Science:
Journal Covers](#)

[Sculpture &
Masks](#)

[A Chemist
Meets Hollywood](#)

[Chymistes: The Distillers
of Waters](#)

[A Chemist
In Court](#)

Databases:

- [Abbott Laboratories](#)
- [ChemACX](#) (chemical compounds)
- [Directory of Graduate Research](#)
- [OVID](#)
- [Symbios Inc.:](#) This website offers a searchable database featuring the complete job listings of nearly 500 companies within the Biotechnology (both human and agricultural), Pharmaceutical, Medical Device and Instrumentation Industries. The positions offered cover the full spectrum from Entry Level to Senior Management.
- [U.S. Patent and Trademark Office](#),
- [Intellectual Property Network \(IBM\)](#)
- [Web of Science](#) (citations)
- [Web Virtual Library](#) (chemistry sites and services)
- [Science Citation Index](#)
- [Medline](#)
- [Protein Data Bank](#)
- [Nucleic Acid Database](#)
- [National Center for Biotechnology Information](#)

Online Applications:

- [MacroModel](#) online manual set

Manuscript and Abstract Templates:

- [ACS abstract](#)
- [ACS POLY preprint](#)
- [JACS COMM ED:](#) For PC Microsoft Word, see [Ken Mac Word](#)

HTML Resources:

- [HTML Goodies](#)
- [HYPE's Color Specifier for Netscape v.3](#)
- [The Banner Generator](#)
- [GIFWorld](#)
- [shareware.com](#)

[Humor and
Wisdom](#)

[Laws of the Universe](#)

[Cartoons of Humor and
Wisdom](#)

[Chem 115: Chemistry of
Everyday Phenomena](#)

[Chem 315: Inorganic
Chemistry](#)

- [UNIX reference desk](#)
- [File Transfer Protocols](#)

SCS NMR Information:

- [VOICE NMR Facility](#)
- [VOICE NMR Schedule](#)

Other Science Links

- [Biochemistry Online](#)
- [Pedro's Biomolecular Research Tools](#)
- [WWW Virtual Library : Biosciences](#)
- [WWW Virtual Library : Chemistry](#)
- [Nanothinc](#)
- [Molecular Probes](#)
- [MIT Virtual Reference Collection](#)
- [Fundamental Physical Constants](#)
- [Dictionary of Units, Measures, and Conversions](#)
- [Chemical Acronyms Database](#)

SUSLICK GROUP WEBSITE:

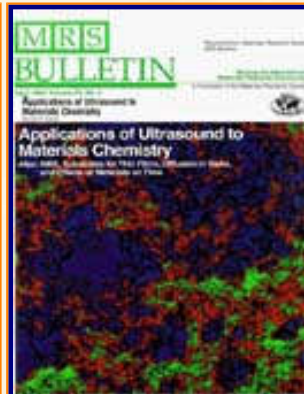
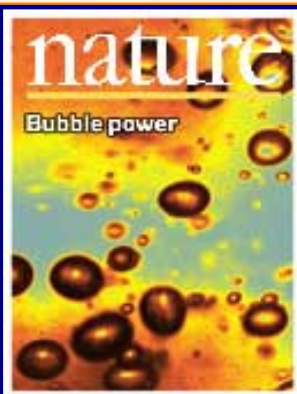
THE SCIENCE	THE GROUP	THE MAÎTRE D'	LAGNIAPPE: A LITTLE EXTRA
Overview	Current Group Members	CV: Abbreviated, Full	Art and Science
Outline of Projects	Group Meetings	Suslick Group Brochure	Chymistes: The Distillers of Waters

<u>Synopses: Sonochemistry</u>	<u>Group Responsibilities</u>	<u>Complete Publication List</u>	<u>A Chemist Meets Hollywood</u>
<u>Metalloporph.</u>			
<u>Executive Summary: Smell-Seeing</u>	<u>Web Based Resources</u>	<u>Academic Genealogy</u>	<u>A Chemist In Court</u>
<u>Introduction to Sonochemistry</u>	<u>Safety Resources</u>	<u>Press Clippings</u>	<u>Words of Humor and Wisdom</u>
<u>Proposal Excerpts</u>	<u>Group Equipment</u>	<u>How To Give A Seminar</u>	<u>Laws of the Universe</u>
<u>Funding</u>	<u>Past Group Members</u>	<u>Ch315 Inorganic Chemistry</u>	<u>Cartoons of Humor and Wisdom</u>
<u>Information for Visitors</u>	<u>Group Photogallery</u>	<u>Construction of the CLS Lab</u>	<u>Sculpture & Masks</u>

©2003, K.S. Suslick; all rights reserved.

Comments and suggestions: ksuslick@uiuc.edu

The Suslick Research Group



[Overview](#)

[Outline of
Research Projects](#)

[Introduction to
Sonochemistry](#)

[Exec. Summary:
Sonochemistry](#)

[Exec. Summary:
Porphyrin Research](#)

[Exec. Summary: Smell-
Seeing](#)

[Complete
Publication List](#)

[Abbreviated Curriculum
Vitae](#)

[Academic
Genealogy](#)

[Press
Clippings](#)

ACADEMIC GENEALOGY

To view the genealogical charts, you will need to view a PDF file.

To get the free Adobe PDF reader, click on this text.

Academic Genealogy of Ken Suslick

To see the full Mainz/Girolami Chemical Genealogy Database, click here.

For a PDF file of Professor Suslick's
complete Curriculum Vitae, click on this text.

Suslick Family Genealogy

SUSLICK GROUP WEBSITE:[Current Research Funding](#)[Excerpts from Funded Research](#)[Inventory of Group Equipment](#)[Information for Visiting](#)[Current Research Group Members](#)[Group Meetings](#)[Group Chores](#)[Past Research Group Members](#)[Group Photogallery](#)[Web Resources](#)[Laboratory Safety Resources](#)[Art and Science: Journal Covers](#)[Sculpture & Masks](#)[A Chemist Meets Hollywood](#)[Chymistes: The Distillers of Waters](#)[A Chemist In Court](#)

THE SCIENCE	THE GROUP	THE MAÎTRE D'	LAGNIAPPE: A LITTLE EXTRA
Overview	Current Group Members	CV: Abbreviated, Full	Art and Science
Outline of Projects	Group Meetings	Suslick Group Brochure	Chymistes: The Distillers of Waters
Synopses: Sonochemistry	Group Responsibilities	Complete Publication List	A Chemist Meets Hollywood
Metalloporph.			
Executive Summary: Smell-Seeing	Web Based Resources	Academic Genealogy	A Chemist In Court
Introduction to Sonochemistry	Safety Resources	Press Clippings	Words of Humor and Wisdom
Proposal Excerpts	Group Equipment	How To Give A Seminar	Laws of the Universe
Funding	Past Group Members	Ch315 Inorganic Chemistry	Cartoons of Humor and Wisdom
Information for Visitors	Group Photogallery	Construction of the CLS Lab	Sculpture & Masks

©2003, K.S. Suslick; all rights reserved.

Comments and suggestions: ksuslick@uiuc.edu

[Humor and
Wisdom](#)

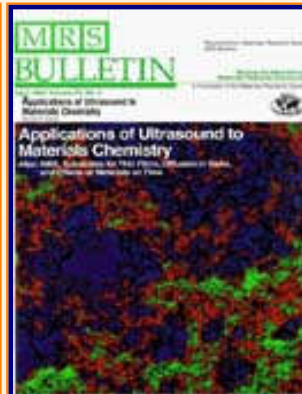
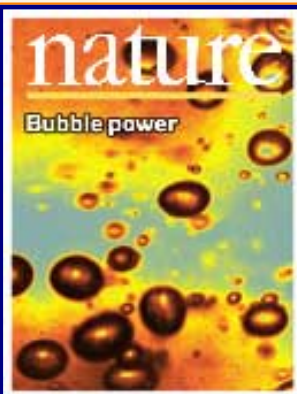
[Laws of the Universe](#)

[Cartoons of Humor and
Wisdom](#)

[Chem 115: Chemistry of
Everyday Phenomena](#)

[Chem 315: Inorganic
Chemistry](#)

The Suslick Research Group



A CHEMIST IN COURT

Kenneth S. Suslick

*The events are real.
Only the names have been removed
to protect the guilty.*

Feb. 3, 1999



In early December, I was approached by both the Plaintiff and Defense attorneys of two major medical ultrasonic equipment manufacturers. They wanted to find out if I was available to act as a Court-appointed independent expert witness (invoking the seldom-used Federal Court "Rule 706" — which sounds like a great title for a detective novel). While I've served as an expert witness before, I'd never been a Rule 706 expert before.

As an expert witness for either the defendant or the plaintiff, the job is like being a hired gun in an old western. As a court-appointed expert, however, it's a lot more like being a deputy sheriff. My role was to act as a technical arbitrator between conflicting expert witness testimony in the interpretation of a patent.

The dispute was over the scientific interpretation of a patent owned by the plaintiff that claimed the invention of "ultrasound-assisted liposuction." The procedure involves inserting a long titanium metal tube about the diameter of a McDonald's straw into rich people's fatty tissues and vibrating the tube 20,000 times a second, back and forth three thousandths of an inch. This liquefies the fat inside

[Overview](#)

[Outline of
Research Projects](#)

[Introduction to
Sonochemistry](#)

[Exec. Summary:
Sonochemistry](#)

[Exec. Summary:
Porphyrin Research](#)

[Exec. Summary: Smell-
Seeing](#)

[Complete
Publication List](#)

[Abbreviated Curriculum
Vitae](#)

[Academic
Genealogy](#)

[Press
Clippings](#)

[Current Research
Funding](#)

[Excerpts from
Funded Research](#)

[Inventory of
Group Equipment](#)

[Information
for Visiting](#)

[Current Research Group
Members](#)

[Group
Meetings](#)

[Group
Chores](#)

[Past Research
Group Members](#)

[Group
Photogallery](#)

[Web Resources](#)

[Laboratory Safety
Resources](#)

[Art and Science:
Journal Covers](#)

[Sculpture &
Masks](#)

[A Chemist
Meets Hollywood](#)

[Chymistes: The Distillers
of Waters](#)

[A Chemist
In Court](#)

the body, and it's then sucked out with a vacuum pump. Surgeons can remove 25 pounds of fat at a time this way, and yes, it is just as completely gross as you probably think!

The trial was set to go to court in the second week of January, so the Court needed a pretty rapid response from me. As described by the lawyers for both sides, my charge from the Court was to write a report based on two fifteen page summaries from both sides, followed a few days later by five page rebuttals from both sides. Seemed simple enough, and I thought I'd have the time over the winter break. What they didn't tell me, but I learned a week later, was that each side would *also* send me 1000 pages of "supporting material" to go with their 15 page briefs and 5 page rebuttals. Who'd have thought there was so much to read about fat-sucking? So, 60 hours of reading and writing later, that is how I spent the holidays (reasonably well-paid by the hour, admittedly).

I filed my report, and two days later, on Dec. 31, the lawyers came out to take my deposition. Since these guys wanted to try and get out of Champaign for New Year's Eve (can't imagine why...), we started early and took only the most minimal of breaks. Even so, the deposition went on for ten long hours (both sides got to cross-exam me, of course, since I wasn't supposed to be a hired gun for either side). The Defendant's attorney was particularly aggressive, since my report had been strongly in favor of the Plaintiff's point of view. They never did get out of town that night — serves 'em right!

For the trial, I flew out to L.A. about half-way through the Plaintiff's case, only to discover that the Judge had ruled my testimony should be presented in the rebuttals rather than in the direct testimony. This judge is the archetypal Hollywood version of the old curmudgeon judge: completely cynical of attorneys' motives, irascible and bullying. At one point, four lawyers were standing up, all arguing a motion in front of the Court, when the Judge slaps his forehead with his palm, turns to the jury and says vehemently, "Do you see what I have to put up with every day?! In my last trial, I lost seven pounds because of things like this!" Fun to watch.

So, I go back home (no complaints from me — I'm getting paid by the hour, portal to portal). A week later, the Plaintiff lawyer calls me and asks me to come out again. Now it turns out that the Defense and conceded the major point of the case to which I was the Rule 706 Expert. The Judge rules that I can still be called as an expert witness by either side, in the rebuttal. He will not allow me to be identified as the Court-appointed witness, however, for fear of unduly weighting my testimony, but with the following caveat:

[The Court]:

Suslick, okay. I have made a ruling and I'm going to stay with it to a point and that ruling is that the witness is not The Court's witness, and that he will be identified as the witness of the Plaintiff. However, there are limits to what I perceive as just, here; and that is, if the Defendant embarks upon an impeachment about your witness, then I don't believe that it's appropriate to leave it your witness. I will take

[Humor and
Wisdom](#)

[Laws of the Universe](#)

[Cartoons of Humor and
Wisdom](#)

[Chem 115: Chemistry of
Everyday Phenomena](#)

[Chem 315: Inorganic
Chemistry](#)

the next step and say that he was a joint witness, and one side decided to select him to testify.

So, I will listen to you, as the Defense, but what I am telling you is, my preliminary ruling is: you start mucking around with impeaching that witness, and you're looking at a real fast ball right at your head from the Plaintiff. The fast ball is going to be: both of you selected him, and one of you got a good answer; and so, the Plaintiff used him.

I think that's the fair way to play this out. And I think that I am able to craft this kind of response under the law.

If there is any input from the Defense, I'll certainly listen to you.

[Defense Attorney]:

I understand your ruling, your honor; and I don't intend to impeach Dr. Suslick, at all. In fact, I like his testimony.

So, here I am in L.A. again a week later, during the rebuttal witnesses, and the Plaintiffs are trying to get the Judge to change his mind and inform the jury of my original status as court-appointed. He won't.

During the rebuttal phase of the trial, the Plaintiff's expert witnesses are doing a bang-up job dismantling the Defendants' earlier expert witnesses testimony. The Plaintiff's lawyers decide that the case is going well enough that they don't want to call me as a witness after all. As an independent expert, I was about in 80% agreement with them, but they were worried about what the Defense would do with the other 20%. They very politely ask me to go back home yet again. I depart, stage rear.

The next day in court, the Plaintiffs announce that they won't be calling me as a witness after all. The Defense attorney then gets very upset and, in front of the jury, starts attacking the Plaintiff's lawyers' motives for their decision, stating that my evidence was important to their Defense — odd, since the Defense had been trying to block my testimony all along! The Judge gets pissed off at this and announces to the jury that I was originally appointed by the court at the mutual selection of both sides. With this revelation, the Plaintiffs now do want to put me on the stand, but alas, I'm already on a plane somewhere over Nebraska. There are advantages to being paid like a taxi driver.

The Plaintiffs rest. The Defense rests. After a week's worth of travel and court time, but *absolutely no* time on the stand, I'm already resting.

This was a week ago, the jury is still out, so I don't know the verdict yet.

P.S. The Plaintiff won; justice is served. 2/5/99

This piece appeared in *Inside Illinois* 1999, 18 (#19), 7.

SUSLICK GROUP WEBSITE:

THE SCIENCE	THE GROUP	THE MAÎTRE D'	LAGNIAPPE: A LITTLE EXTRA
<u>Overview</u>	<u>Current Group Members</u>	<u>CV: Abbreviated, Full</u>	<u>Art and Science</u>
<u>Outline of Projects</u>	<u>Group Meetings</u>	<u>Suslick Group Brochure</u>	<u>Chymistes: The Distillers of Waters</u>
<u>Synopses: Sonochemistry</u>	<u>Group Responsibilities</u>	<u>Complete Publication List</u>	<u>A Chemist Meets Hollywood</u>
<u>Metalloporph.</u>			
<u>Executive Summary: Smell-Seeing</u>	<u>Web Based Resources</u>	<u>Academic Genealogy</u>	<u>A Chemist In Court</u>
<u>Introduction to Sonochemistry</u>	<u>Safety Resources</u>	<u>Press Clippings</u>	<u>Words of Humor and Wisdom</u>
<u>Proposal Excerpts</u>	<u>Group Equipment</u>	<u>How To Give A Seminar</u>	<u>Laws of the Universe</u>
<u>Funding</u>	<u>Past Group Members</u>	<u>Ch315 Inorganic Chemistry</u>	<u>Cartoons of Humor and Wisdom</u>

[Information
for Visitors](#)

[Group
Photogallery](#)

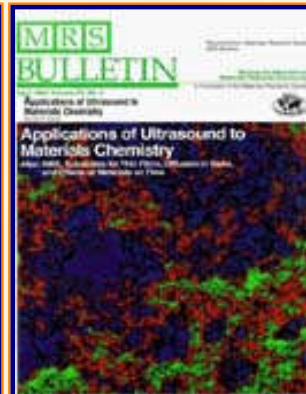
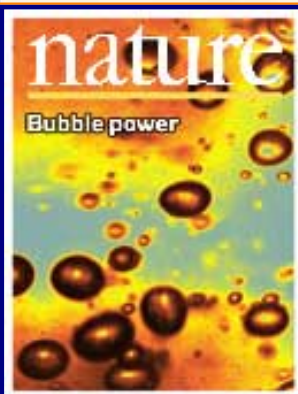
[Construction of the
CLS Lab](#)

[Sculpture
&
Masks](#)

©2003, K.S. Suslick; all rights reserved.

Comments and suggestions: ksuslick@uiuc.edu

The Suslick Research Group



[Overview](#)

[Outline of
Research Projects](#)

[Introduction to
Sonochemistry](#)

[Exec. Summary:
Sonochemistry](#)

[Exec. Summary:
Porphyrin Research](#)

[Exec. Summary: Smell-
Seeing](#)

[Complete
Publication List](#)

[Abbreviated Curriculum
Vitae](#)

[Academic
Genealogy](#)

[Press
Clippings](#)

SAFETY

[UIUC DEHS Home](#)

[UIUC Division of Environmental and Health Safety](#)

- [Biological Safety](#)
- [Chemical Safety](#)
- [Environmental Compliance](#)
- [Occupational Safety & Health](#)
- [Quality Assurance](#)
- [Radiation Safety](#)

[School of Chemical Sciences Safety Resources](#)

SUSLICK GROUP SAFETY RULES

1. No Bench shall have more than 10 solvent bottles and 10 chemical solids bottles stored on it or above it.
2. ALL Chemicals purchased in the stockroom or by special order **MUST BE DATED AND INITIALED** by the person who bought them.
3. All ethers (including THF) must be used or disposed of within six months of being opened. Older bottles may contain explosive peroxides (which must be removed prior to disposal by adding CuI). Test paper for peroxides is available in the stockroom.
4. Solvents used infrequently must be stored in the group liquid storage cabinets as labeled. After using such a bottle, return it to the joint storage area!

[Current Research Funding](#)

[Excerpts from Funded Research](#)

[Inventory of Group Equipment](#)

[Information for Visiting](#)

[Current Research Group Members](#)

[Group Meetings](#)

[Group Chores](#)

[Past Research Group Members](#)

[Group Photogallery](#)

[Web Resources](#)

[Laboratory Safety Resources](#)

[Art and Science: Journal Covers](#)

[Sculpture & Masks](#)

[A Chemist Meets Hollywood](#)

[Chymistes: The Distillers of Waters](#)

[A Chemist In Court](#)

5. Never return any liquid to the bottle after removing it from the bottle. The preferred means of removing liquids is to pour into a beaker or flask. Only clean unused disposable pipets may be used for small amounts of solvent removal directly from the bottle. When in doubt use a new pipet.

Remember Schaupenauer's Law of Entropy: if you add a tablespoon of wine to a barrel of sewage, you have a barrel of sewage; if you add a tablespoon of sewage to a barrel of wine, you have a barrel of sewage.

6. Known carcinogens, especially volatile ones, such as benzene and CCl_4 , must be used **ONLY** in the hoods with gloves. These bottles **MUST** be used and stored only in the hoods! They are never to be opened on desk tops. Extreme care should be made in handling these materials for running spectra, etc. In general, think about using hexane, toluene, acetone, acetonitrile, dichloromethane, or THF instead.

7. Waste Solvent containers cannot be left open. Do not leave the funnel in an open container, even in the hood.

8. **ALWAYS, ALWAYS WEAR SAFETY GLASSES** when in the laboratories. **NO EXCEPTIONS.**

9. **NO EATING OR DRINKING IN THE LABS** (and this includes your desk)! Sorry, no exceptions. **USE THE COMMONS ROOM FOR MEALS AND SNACKS.**

10. Backup your data and hard-drives regularly. Keep a copy at home. The thesis you save may be your own!

SUSLICK GROUP WEBSITE:

THE SCIENCE	THE GROUP	THE MAÎTRE D'	LAGNIAPPE: A LITTLE EXTRA
Overview	Current Group Members	CV: Abbreviated, Full	Art and Science

[Humor and
Wisdom](#)

[Laws of the Universe](#)

[Cartoons of Humor and
Wisdom](#)

[Chem 115: Chemistry of
Everyday Phenomena](#)

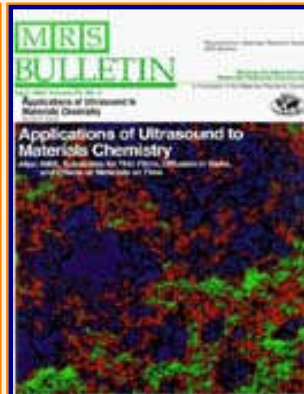
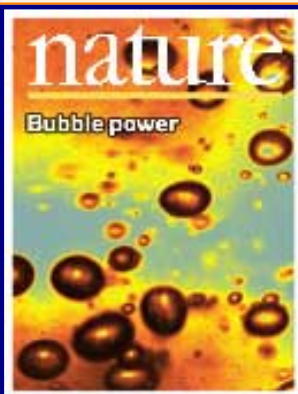
[Chem 315: Inorganic
Chemistry](#)

Outline of Projects	Group Meetings	Suslick Group Brochure	Chymistes: The Distillers of Waters
Synopsis: Sonochemistry	Group Responsibilities	Complete Publication List	A Chemist Meets Hollywood
Metalloporph.			
Executive Summary: Smell-Seeing	Web Based Resources	Academic Genealogy	A Chemist In Court
Introduction to Sonochemistry	Safety Resources	Press Clippings	Words of Humor and Wisdom
Proposal Excerpts	Group Equipment	How To Give A Seminar	Laws of the Universe
Funding	Past Group Members	Ch315 Inorganic Chemistry	Cartoons of Humor and Wisdom
Information for Visitors	Group Photogallery	Construction of the CLS Lab	Sculpture & Masks

©2003, K.S. Suslick; all rights reserved.

Comments and suggestions: ksuslick@uiuc.edu

The Suslick Research Group



WORDS OF HUMOR AND WISDOM

Humor is the great thing, the saving thing. The minute it crops up, all our irritations and resentments slip away and a sunny spirit takes their place. —Mark Twain.

Time spent laughing is time spent with the gods. —Japanese proverb

When a thing has been said, and said well, have no scruple. Take it and copy it. — Anatole France

[Overview](#)

[Outline of
Research Projects](#)

[Introduction to
Sonochemistry](#)

[Exec. Summary:
Sonochemistry](#)

[Exec. Summary:
Porphyrin Research](#)

[Exec. Summary: Smell-
Seeing](#)

[Complete
Publication List](#)

[Abbreviated Curriculum
Vitae](#)

[Academic
Genealogy](#)

[Press
Clippings](#)

[C'est moi.](#)

[The Mulla Nasrudin](#)

[Piet Hein's Grooms](#)

[Aphorisms: Wisdom in Absurdity](#)

[Aphorisms: Thinking](#)

[Aphorisms: Learning and Teaching](#)

[Aphorisms: Science and Knowledge](#)

[Aphorisms: Chemistry](#)

[Aphorisms: Society](#)

[Aphorisms: Life, the Future, and its Alternatives](#)

[Current Research
Funding](#)

[Excerpts from
Funded Research](#)

[Inventory of
Group Equipment](#)

[Information
for Visiting](#)

[Current Research Group
Members](#)

[Group
Meetings](#)

[Group
Chores](#)

[Past Research
Group Members](#)

[Group
Photogallery](#)

[Web Resources](#)

[Laboratory Safety
Resources](#)

[Art and Science:
Journal Covers](#)

[Sculpture &
Masks](#)

[A Chemist
Meets Hollywood](#)

[Chymistes: The Distillers
of Waters](#)

[A Chemist
In Court](#)

C'est moi.

Stories that make us laugh are good.
Stories that teach us are good.
Stories that make us laugh and teach us are best. —KSS

Knowledge comes by the truckload,
but wisdom arrives one mouthful at a time. —KSS

Suslick's Scheme of Priorities:
If it isn't worth doing,
it isn't worth doing right.

Suslick's Law of Threes:
It always takes three times to do anything right.
The first time you either overshoot or undershoot;
the second time you either over-compensate or under-compensate;
it's not until the third time that you have a chance to get it right.

Suslick's First Law of Maps:
All countries are the same size—one map page.

The plural of 'anecdote' is not 'data'. —KSS

Science is fundamentally a neurotic behavior. The 'well-adjusted', by definition, do not wish to understand or change the world; they simply accept it. Only the neurotic wants to know why and how. Only the neurotic wants change. —KSS

Never be intimidated by your own ignorance. All of us are mostly ignorant of what is known and infinitely ignorant of everything that isn't! —KSS

Ego is a house cat. It's nice to stroke, but watch out for the claws; it needs feeding often, and heaven help you if it gets out the front door. —KSS

Ties are what administrators use to cut off the flow of blood to their brains. —KSS

Student Leader: a thug with big friends.

[Humor and
Wisdom](#)

[Laws of the Universe](#)

[Cartoons of Humor and
Wisdom](#)

[Chem 115: Chemistry of
Everyday Phenomena](#)

[Chem 315: Inorganic
Chemistry](#)

Political Leader: a thug with rich friends.
World Leader: a thug with an army. —KSS

Cynicism is the first refuge of the romantic. —KSS

To settle a violent dispute, two men went to the Rabbi. The wizened old scholar listened with care to the first man's tale and said, "You're right."

But the second man leaped up, crying "Rabbi, it wasn't like that at all. It was this way...." After this version, the Rabbi turned to the second man and said, "*You're* right."

A spectator, bewildered by all these goings-on, called out, "Rabbi, first you say one is right and then the other. But they both can't be right!"

And the Rabbi winked at the bystander and whispered, "*You're right, too!*"

—*In memory of Alvin Suslick, M.D.*

Other Pages:

[**DIE GOTTERDAMMERBLASE:
A Cycle of Cavitation Limericks**](#)

[**THE POKEMON COOKBOOK**](#)

The Mulla Nasrudin

The Mulla Nasrudin is the wise-fool of Sufiism and there are hundreds of stories about him that are used to teach the important lessons of life (Idries Shah has collected some of the best). This particular one, I

used for the opening of my own Ph.D. thesis.



Walking one evening along a deserted road, Mulla Nasrudin saw in the distance a troop of horsemen coming towards him. His imagination started to work; he saw himself captured, beaten, and sold as a slave or impressed into the army. Nasrudin bolted, and dove into a ditch at the side of the road where he lay on his stomach, quivering with his hands covering.

Puzzled at his strange behavior, the men, friends of Nasrudin, after all, stopped and asked, "What are you doing down there? Can we help?"

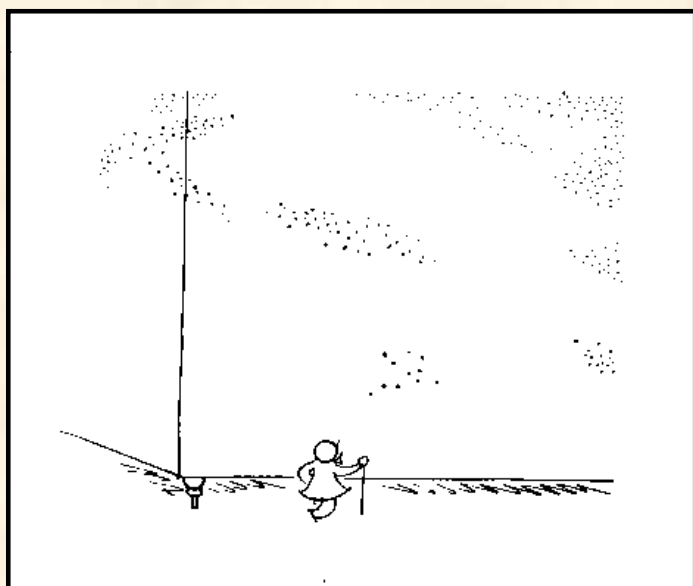
"Just because you can ask a question, does not mean that there is a straightforward answer," said Nasrudin, who now realized what had happened. "It all depends on your point of view. If you must know, however: I am here because of you, and you are here because of me."

Nasrudin was often quite absentminded. One night before going to bed, he lit a match to see if he'd blown the candle out.

Another time, Nasrudin left a note on the door of his shop saying that he would return in an hour. When he returned, he saw the note and sat down to wait.

Piet Hein's *Grooks*

Grooks are short, often humorous, poems that are meant to teach some piece of wisdom. Piet Hein (Danish mathematician and architect) invented them during World War II, when Denmark was occupied by Germany. The short poems usually had a hidden meaning that was just below the sensitivities of the authorities. The name of these poems, as well as the signature used, "Kumbel", were picked simply because nothing else could be associated with them.



Atomyriades

Nature, it seems is the popular name for milliards and milliards and milliards of particles playing their infinite game of billiards and billiards and billiards.

('billion' is an obsolete Britishism for thousand million)

Similarity

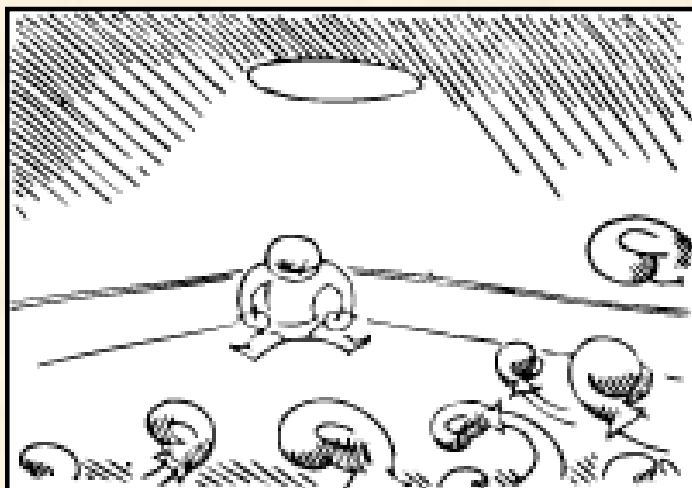
Commutative Law

No cow's like a horse,
and no horse like a cow.
That's one similarity, anyhow.

The Paradox of Life

Philosophical grook.

A bit beyond perception's reach
I sometimes believe I see
that Life is two locked boxes, each
containing the other's key.



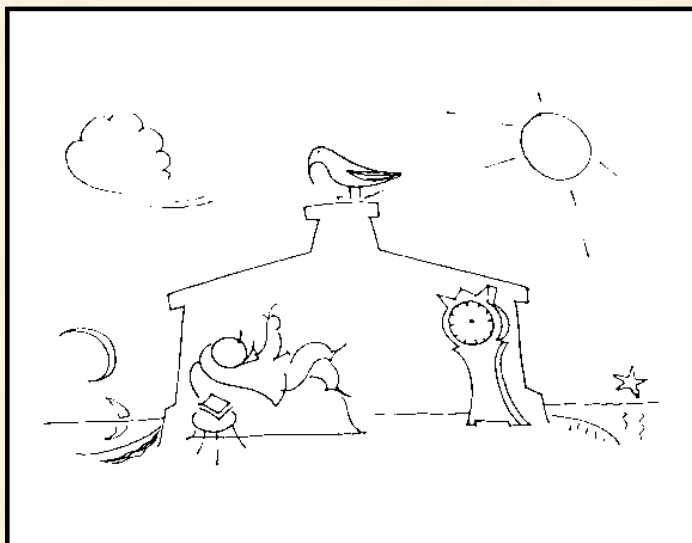
Problems

Problems worthy
of attack
prove their worth
by hitting back.

Nothing is Indispensable

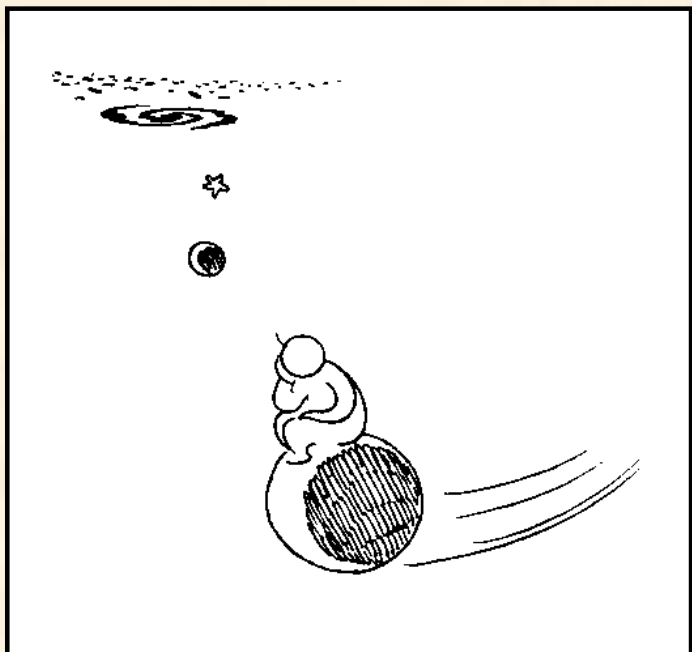
Grook to warn the universe against megalomania

The universe may
be as great as they say.
But it wouldn't be missed
if it didn't exist.



Out of Time

My old clock used to tell the time
and subdivide diurnity;
but now its lost both hands and chime
and only tells eternity.



I'd Like—

I'd like to know
what this whole show
is all about
before it's out.

Wisdom and Aphorism

Wisdom in Absurdity

First things first, but not necessarily in that order. —Joe Palmer

If you come to a fork in the road, take it. —Yogi Berra

Whenever I think of the past, it brings back so many memories... —Steven Wright

I was trying to daydream, but my mind kept wandering. —Steven Wright

Mr. Dryer believes in a sense of humor and to facilitate this, he does not sleep. —Joel S. Dryer

There was only one catch and that was Catch22, which specified that a concern for one's safety in the face of dangers that were real and immediate was the process of a rational mind. Orr was crazy and could be grounded. All he had to do was ask, and as soon as he did, he would no longer be crazy and would have to fly more missions. Orr would be crazy to fly more missions and sane if he didn't, but if he was sane he had to fly them. If he flew them he was crazy and didn't have to; but if he didn't want to he was sane and had to. —Joseph Heller, *Catch22*

Vegetarians taste better. —bumper-sticker

If a Vegetarian eats only vegetables, what does a Humanitarian eat?
— anon.

If coconut oil comes from coconuts, and corn oil comes from corn, where does baby oil come from? — anon.

He was carefully treading in his own footsteps. —KSS

Outside of a dog, a book is man's best friend. Inside of a dog, it's too dark to read. —Groucho Marx

Time flies like an arrow. Fruit flies like a banana. —Groucho Marx

Anything free is worth what you paid for it. —Gary O'Brien

Everyone is entitled to my opinion. —Gary O'Brien

I used to think I was indecisive, but now I'm not so sure. —anon.

Right now I'm having amnesia and deja vu at the same time. I think I've forgotten this before. —Steven Wright

How much deeper would oceans be if sponges didn't live in them?
—George Carlin

What's another word for Thesaurus? —Steven Wright

What if there were no hypothetical questions? —Gary O'Brien

No sense in being pessimistic, it probably wouldn't work anyway. —Gary O'Brien

What is the Hokey Pokey really all about? —Joe Palmer

You better cut the pizza in four pieces because I'm not hungry enough to eat six. —Yogi Berra

I have an answering machine in my car. It says, "I'm home now. But leave a message and I'll call when I'm out" —Steven Wright

I got an answering machine for my phone...now, when I'm not home and somebody calls me up...they hear a recording of a busy signal. —Steven Wright

I played a blank tape on full volume. The mime who lived next door complained. —Steven Wright

I almost had a psychic girlfriend, but she left me before we met. —anon.

Whatever can be said can be said clearly. —L. Wittgenstein (ironic for this maxim to come from the author of *Tractatus Logico-Philosophicus*)

Thinking

Never Ask Why

My dad was a great raconteur. He would tell this story about his training as a psychiatrist:

An elder, very German psychiatrist would play act as a patient and my father would interview him. The "patient" would describe some behavior or anxiety, and my father was supposed to probe gently, saying such things as "And this bothers you?" or "Interesting..." or "And does this suggest anything to you?"

After one particularly peculiar description by the "patient", my father asked, "And why do you do this?"

At this point, the elder psychiatrist stood up, looked down over his thick, round glasses, and screamed, "Vhy? Vhy? Becuss I'm crazy, zat's vhy!"

Never ask a crazy person why. — KSS

Bodily exercise, when compulsory, does no harm to the body; but knowledge which is acquired under compulsion obtains no hold on the mind. — Plato, *The Republic. Book VII.*

Most people would rather die than think; in fact, they do so.
—Bertrand Russell

The whole problem with the world is that fools and fanatics are always so certain of themselves, and wiser people so full of doubts. —Bertrand Russell

By all means let's be open-minded,
but not so open-minded that our brains fall out. —R. Dawkins,
Science, Delusion & the Appetite for Wonder

I used to think that the brain was the most wonderful organ in my body. Then I remembered who was telling me this. —Emo Philips

Learning and Teaching

We don't raise children by lowest common denominator.
—Nell Minow

Don't let school interfere with your education. —Mark Twain

Everybody is ignorant, only on different subjects. —Will Rogers

I was gratified to be able to answer promptly. I said I didn't know.
—Mark Twain

If you think education is expensive, try ignorance. —Andy McIntyre

The beginning is the most important part of the work. —Plato, *The Republic. Book II.*

The less you know, the more you think you know, because you don't know you don't know. —Ray Stevens

A person who knows not and knows not that he knows not is a fool,
shun him.

A person who knows not and knows that he knows not is a child,
teach him.

A person who knows and knows not that he knows is asleep,
wake him.

A person who knows and knows that he knows is wise,
follow him.

—Ancient Babylonian Aphorism

He who asks is a fool for five minutes, but he who does not ask
remains a fool forever. —Chinese proverb

If you are planning for a year, sow rice; if you are planning for a
decade, plant trees; if you are planning for a lifetime, educate
people. —Chinese proverb

A little knowledge is a dangerous thing. So is a lot. —Albert Einstein
(1879-1955) U. S. physicist, born in Germany.

The pure and simple truth is rarely pure and never simple. —Oscar Wilde

Never tell people how to do things. Tell them what to do and they will surprise you with their ingenuity. —General George S. Patton

What did you ask at school today? —Richard Feynman

Gil Haight, Professor Emeritus of the University of Illinois, used to tell a story about Albert Einstein:

Gil was a graduate student at Princeton when Einstein was there, and they shared an interest in classical music. Einstein, in fact, was a gifted amateur violinist.

At a special concert presented by Yehudi Menuhin, Gil was seated just in front of Einstein. As the first piece began, Einstein was nodding his head with his eyes half shut and very softly humming to the music. Midway through the first piece, Einstein quietly said, "Ooooh, I can do zat!"

A bit later, he crooned excitedly, "Yes, yes, I can do zat, too!"

Finally, after a particularly difficult passage, Einstein shook his head slowly, sighed, and said softly and sadly, "Och, I could never do zat!"
—KSS

Science and Knowledge

Never be intimidated by your own ignorance. All of us are mostly ignorant of what is known and infinitely ignorant of everything that isn't! —KSS

Though we travel the world over to find the beautiful, we must carry it with us or we find it not. —Ralph Waldo Emerson

I am enough of an artist to draw freely upon my imagination. Imagination is more important than knowledge. Knowledge is limited. Imagination encircles the world. —Albert Einstein

Never mistake knowledge for wisdom. One helps you make a living;

the other helps you make a life. —Sandra Carey

Man will occasionally stumble over the truth, but most of the time he will pick himself up and continue on. —Winston Churchill

For every complex problem, there is a solution that is simple, neat, and wrong. —H. L. Mencken (1880-1956)

Seek simplicity and distrust it. —Alfred North Whitehead

If all you have is a hammer, everything looks like a nail. —Unknown

It is a capital mistake to theorize before one has data. Insensibly one begins to twist facts to suit theories instead of theories to suit facts.
—Sherlock Holmes, the fictional creation of Arthur Conan Doyle (1859-1930) British physician and novelist.

The reasonable man adapts himself to the world; the unreasonable one persists in trying to adapt the world to himself. Therefore all progress depends on the unreasonable man. —George Bernard Shaw

Science is fundamentally a neurotic behavior. The 'well-adjusted', by definition, do not wish to understand or change the world; they simply accept it. Only the neurotic wants to know why and how. Only the neurotic wants change. —KSS

Science is facts; just as houses are made of stone, so is science made of facts; but a pile of stones is not a house, and a collection of facts is not necessarily science. —Jules Henri Poincaré (1854-1912) French mathematician.

Science is not formal logic—it needs the free play of the mind in as great a degree as any other creative art. It is true that this is a gift which can hardly be taught, but its growth can be encouraged in those who already possess it. —Max Born (1882-1970) German Physicist. Nobel Prize, 1954.

[Science is] a great game. It is inspiring and refreshing. The playing field is the universe itself. —Isidor Isaac Rabi (1898-1988) U. S. physicist. Nobel prize 1944.

The most incomprehensible thing about our universe is that it can be comprehended. —Albert Einstein (1879-1955) U. S. physicist, born in Germany.

Reality is that which, when you stop believing in it, doesn't go away. —Philip K. Dick

Now, my own suspicion is that the universe is not only queerer than we suppose, but queerer than we can suppose. I have read and heard many attempts at a systematic account of it, from materialism and theosophy to the Christian system or that of Kant, and I have always felt that they were much too simple. I suspect that there are more things in heaven and earth that are dreamed of, or can be dreamed of, in any philosophy. That is the reason why I have no philosophy myself, and must be my excuse for dreaming. —John Burden Sanderson Haldane (1892-1964) English geneticist. *Possible Worlds and other Essays* (1927)

I believe there is no philosophical high-road in science, with epistemological signposts. No, we are in a jungle and find our way by trial and error, building our road behind us as we proceed. —Max Born (1882-1970) German Physicist. Nobel Prize, 1954.

The chess-board is the world; the pieces are the phenomena of the universe; the rules of the game are what we call the laws of Nature. The player on the other side is hidden from us. We know that his play is always fair, and patient. But also we know, to our cost, that he never overlooks a mistake, or makes the smallest allowance for ignorance. —Thomas Henry Huxley (1825-95) English biologist.

Necessity, who is the mother of invention. —Plato, *The Republic. Book II.*

There ain't no rules around here! We're trying to accomplish

something! —Thomas Alva Edison (1847-1931) U. S. inventor.

The plural of `anecdote' is not `data'. —K. S. Suslick

Get your facts first, and then you can distort them as much as you please. —Mark Twain

To argue from the general absence of evidence that there is no evidence for one's opponent's point of view is to write with an economy of truth. —A.B. Lovins, W.C. Patterson *Nature* **254**, 280 (1975).

Never make a calculation until you know the answer: make an estimate before every calculation, try a simple physical argument ... before every derivation, guess the answer to every puzzle. Courage: no one else needs to know what the guess is. Therefore make it quickly, by instinct. A right guess reinforces this instinct. A wrong guess brings the refreshment of surprise. In either case, life ... is more fun! —Wheeler, John A. and Edwin F. Taylor. *Spacetime Physics*, Freeman, 1966. Page 60.

If an experiment requires statistical analysis to establish a result, then one should do a better experiment. —Ernest Rutherford (1st Baron Rutherford of Nelson) (1871- 1937) English physicist, born in New Zealand. Nobel prize for chemistry 1908.

No effect that requires more than 10 percent accuracy in measurement is worth investigating. —Walther Nernst (1864-1941) German physicist, chemist. Nobel prize, 1920.

Ever wonder what the speed of lightning would be if it didn't zig-zag?
—George Carlin.

If any student comes to me and says he wants to be useful to mankind and go into research to alleviate human suffering, I advise him to go into charity instead. Research wants real egotists who seek their own pleasure and satisfaction, but find it in solving the puzzles of nature.
—Albert Szent-Györgi (1893-1986) U. S. biochemist.

The problem with this seminar is that the ratio of hype to results is too high, and I have nothing against large numbers. —KSS, January 28, 1997

All of physics is either impossible or trivial. It is impossible until you understand it, and then it becomes trivial. —Ernest Rutherford (1st Baron Rutherford of Nelson) (1871- 1937) English physicist, born in New Zealand. Nobel prize for chemistry 1908.

A man must have a certain amount of intelligent ignorance to get anywhere. —Charles Franklin Kettering (1876-1958) U. S. engineer and inventor.

You can observe a lot by watching. —Yogi Berra

If you can't imitate him, don't copy him. —Yogi Berra

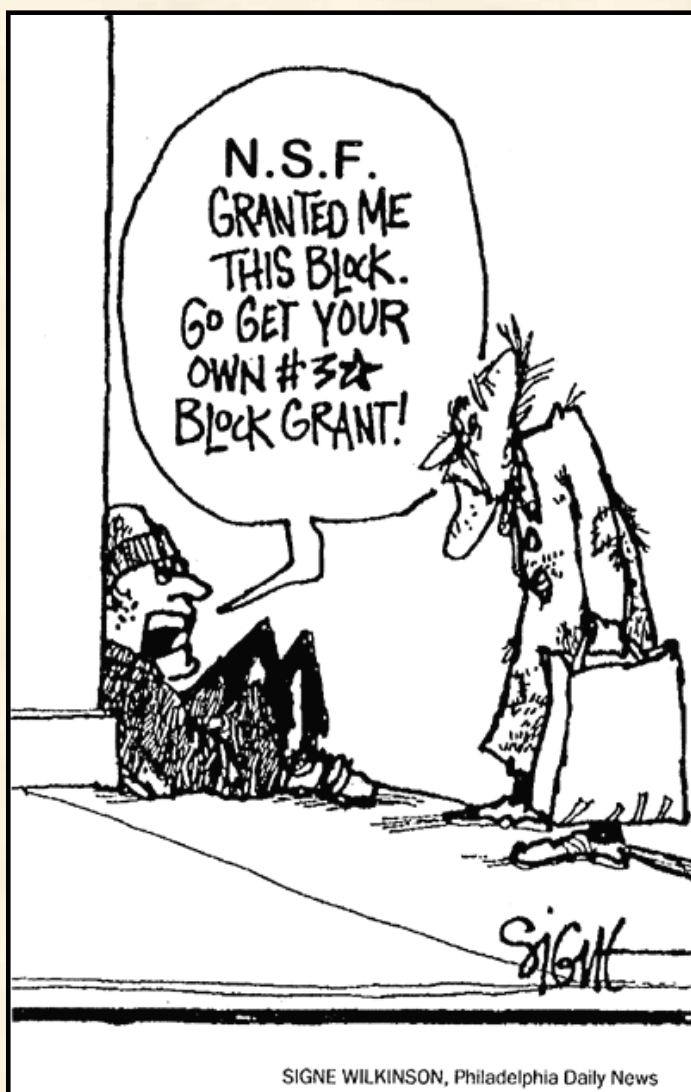
If at first you don't succeed, then sky diving definitely isn't for you.
—anon.

Basic research is what I am doing when I don't know what I am doing.
—Werner Von Braun (1912-1977) German rocket engineer, in U. S. after 1945.

Every honest researcher I know admits he's just a professional amateur. He's doing whatever he's doing for the first time. That makes him an amateur. He has sense enough to know that he's going to have a lot of trouble, so that makes him a professional. —Charles Franklin Kettering (1876-1958) U. S. engineer and inventor.

Big whirls have little whirls,
That feed on their velocity;
And little whirls have lesser whirls,
And so on to viscosity.

—Lewis Fry Richardson (1881-) English physicist, psychologist.
Summarizing his classic paper, *The Supply of Energy From and To Atmospheric Eddies* (1920).



Chemistry

If you're not part of the solution, you're part of the precipitate. —Steven Wright

You can't change thermodynamics by encouragement. —S. Lippard, January 28, 1997

I bought some powdered water, but I don't know what to add. —Steven Wright

Organic chemistry just now is enough to drive one mad. It gives me the impression of a primeval tropical forest full of the most remarkable things: a monstrous and boundless thicket with no way of escape, and into which one may well dread to enter. —1835, Friedrich Wohler (1800-1882), first to make an 'organic' compound (urea) from 'inorganic' precursors.

To say that a man is made up of certain chemical elements is a satisfactory description only for those who intend to use him as a fertilizer. —Hermann Joseph Muller (1890-1967) U. S. geneticist. Nobel prize for medicine 1946.

Organic chemistry is the chemistry of carbon compounds. Biochemistry is the study of carbon compounds that crawl. —Mike Adams

One day a man walked in and said "If I melt dry ice, can I swim without getting wet?" —Steven Wright

How do you tell when you're out of invisible ink? —anon.

It doesn't matter what temperature the room is; it's always room-temperature. —Steven Wright

Society

No one ever went broke underestimating the taste of the American public. —H. L. Mencken (1880-1956)

There's no system foolproof enough to defeat a sufficiently great fool. —Edward Teller, quoted in "Nuclear Reactions", by Joel Davis in *Omni*, May 1988, p. 46.

In this world of sin and sorrow there is always something to be thankful for. As for me, I rejoice that I am not a Republican. —H. L. Mencken (1880-1956)



The current state of our two-party system. —KSS

All happy families are alike; each unhappy family is unhappy in its own way. —Leo Tolstoy; opening line of Anna Karenina.

Why should I care about posterity?
What's posterity ever done for me?
—Groucho Marx

The trouble with being punctual is that
nobody's there to appreciate it.
—Franklin P. Jones

The early bird gets the worm, but the second mouse gets the
cheese. —anon.

Not to the swift, the race.

Not to the strong, the fight. —Henry Van Dyke

The race may not always be to the swift,
nor the battle to the strong,
but that's the way to bet. —Daymon Runyon

Those who live by the sword will be shot by those who don't. —Gary Hamel

The conquistador is inclined to put a swift sword to the natives;
the capitalist finds it more profitable to work them slowly to death.
—Michael Parenti

Student Leader: a thug with big friends.
Political Leader: a thug with rich friends.
World Leader: a thug with an army. —KSS

A thing is not necessarily true because a man dies for it. —Oscar Wilde (Oscar Fingal O'Flahertie Wills) (1854-1900) Irish writer.

When Change threatens to rule,
then the rules suddenly change.
— Michael Parenti's 2nd Law of Politics

Annual income 20 £, annual expenditure 19 £, 19 shillings:
result happiness.
Annual income 20 £, annual expenditure 20 £, 1 shilling:
result misery.
—Charles Dickens

To succeed in the world it is not enough to be stupid, you must also be well-mannered. —Voltaire

Hard work pays off in the future. Laziness pays off now. —anon.

We should distrust any enterprise that requires new clothes.
—Henry David Thoreau

Ties are what administrators use to cut off the flow of blood to their brains. —KSS

You may have heard that a dean is to faculty as a hydrant is to a dog.
—Alfred Kahn

Expecting the world to treat you fairly because you are a good person is a little like expecting the bull not to attack you because you are a vegetarian. —Dennis Wholey

If it's true that we are here to help others, then what *exactly* are the others here for? — George Carlin

We all know that there are people who do not love their fellow man, and I hate people like that! —Tom Lehrer

Everyone has a photographic memory. Some just don't have film. —anon.

Do not do unto others as you would they should do unto you. Their tastes may not be the same. —George Bernard Shaw, *Man and Superman*

If there's anything more important than my ego around, I want it caught and shot now. —Zaphod via Douglas Adams.

Ego is a house cat. It's nice to stroke, but watch out for the claws; it needs feeding often, and heaven help you if it gets out the front door. —KSS

The right to swing my fist ends where the other man's nose begins. —Oliver Wendell Holmes

I assume full responsibility for my actions, except for the ones that are someone else's fault. —Steve Sanderson

This is an exact replication of National Public Radio (NPR) interview between a female broadcaster and US Army General Weinwald who was about to sponsor a Boy Scout Troop visiting his military installation.

FEMALE INTERVIEWER: "So, General Weinwald, what things are you going to teach these young boys when they visit your base?"

GENERAL WEINWALD: "We're going to teach them climbing, canoeing, archery, and shooting."

FEMALE INTERVIEWER: "Shooting! That's a bit irresponsible, isn't it?"

GENERAL WEINWALD: "I don't see why, they'll be properly supervised on the rifle range."

FEMALE INTERVIEWER: "Don't you admit that this is a terribly dangerous activity to be teaching children?"

GENERAL WEINWALD: "Don't see how... we will be teaching them proper rifle discipline before they even touch a firearm."

FEMALE INTERVIEWER: "But you are equipping them to become violent killers."

GENERAL WEINWALD: "Well, you're equipped to be a prostitute, but you're not one, are you?"

The radio went silent and the interview ended.

Friends help you move. Real friends help you move bodies. —anon.

Man is the only animal that blushes. Or needs to. —Mark Twain

When choosing between two evils I always like to try the one I've never tried before. —Mae West

The avalanche has started, it is too late for the pebbles to vote. —
Vorlon Ambassador Kosh Naranek, *Babylon 5: Believers*; J. Michael Straczynski.

I was walking across a bridge one day, and I saw a man standing on the edge, about to jump off. So I ran over and said "Stop! Don't do it!"
"Why shouldn't I?" he said.

I said, "Well, there's so much to live for!"

He said, "Like what?"

I said, "Well...are you religious or atheist?"

He said, "Religious."

I said, "Me too! Are you Christian or Buddhist?"

He said, "Christian."

I said, "Me too! Are you Catholic or Protestant?"

He said, "Protestant."

I said, "Me too! Are you Episcopalian or Baptist?"

He said, "Baptist!"

I said, "Wow! Me too! Are you Baptist Church of God or Baptist Church of the Lord?"

He said, "Baptist Church of God!"

I said, "Me too! Are you original Baptist Church of God, or are you Reformed Baptist Church of God?"

He said, "Reformed Baptist Church of God!"

I said, "Me too! Are you Reformed Baptist Church of God, reformation of 1879, or Reformed Baptist Church of God, reformation of 1915?"

He said, "Reformed Baptist Church of God, reformation of 1915!"

I said, "Die, heretic scum!!", and pushed him off.

—Emo Philips

Do not speak unless your words improve upon the silence. —Quaker Proverb

Life, the Future, and its Alternative

There was a young lady, quite bright,
Whose speed was far faster than light.
She left one day
In a relative way,
And returned home the previous night! —Anon

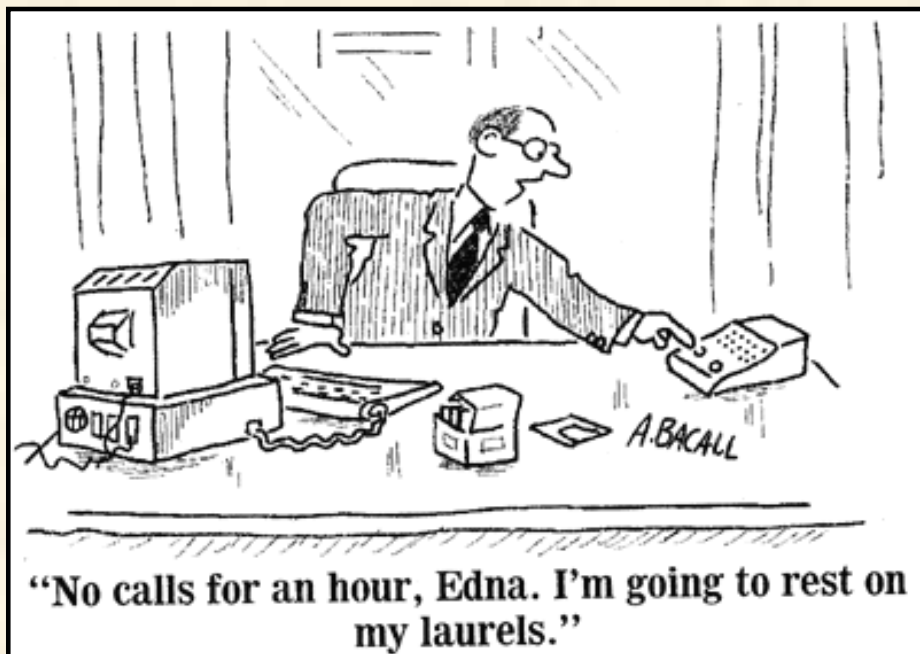
For years I wanted to be older, and now I am. —Margaret Atwood

Everybody wants to get old, but nobody wants to be old. —Goethe

It's a sobering thought that by the time Mozart was my age, he'd been dead for five years. —Tom Lehrer

In dog years, I'm dead. —Joe Palmer

The aging process has you firmly in its grasp if you never get the urge to throw a snowball. —Doug Larson



Roses smell sweetest just before the petals fall off. —Gary Hamel

I don't want to achieve immortality through my work;
I want to achieve it through not dying. —Woody Allen

If you don't go to other men's funerals, they won't go to yours. —Clarence Day

I'm so pessimistic that I think of perfect health as a pre-cancerous condition. —Joe Palmer

What happens if you get scared half to death twice? —anon.

I'm not afraid to die. I just don't want to be there when it happens. —Woody Allen

It is impossible to experience one's own death objectively and still

carry a tune. —Woody Allen

You should emulate your heroes, but don't carry it too far. Especially if they are dead. — anon.

Time is a great teacher, but unfortunately it kills all its pupils. —Hector Berlioz

Soon we'll be out amid the cold world's strife.
 Soon we'll be sliding down the razor blade of life.
 So let's give a toast, as each of us recalls,
 to ivy-covered professors in ivy-covered halls.
 —Tom Lehrer

The future ain't what it used to be. —Yogi Berra

SUSLICK GROUP WEBSITE:

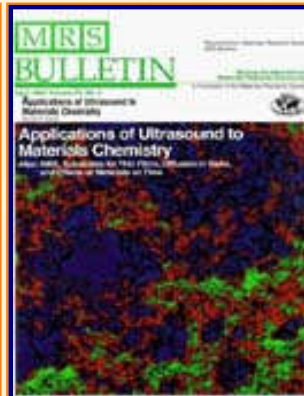
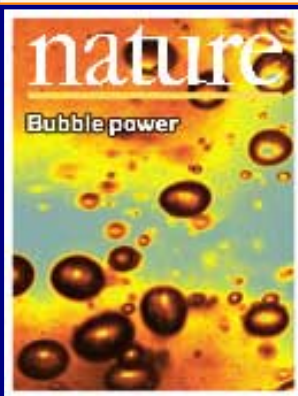
THE SCIENCE	THE GROUP	THE MAÎTRE D'	LAGNIAPPE: A LITTLE EXTRA
<u>Overview</u>	<u>Current Group Members</u>	<u>CV: Abbreviated, Full</u>	<u>Art and Science</u>
<u>Outline of Projects</u>	<u>Group Meetings</u>	<u>Suslick Group Brochure</u>	<u>Chymistes: The Distillers of Waters</u>
<u>Synopses: Sonochemistry</u>	<u>Group Responsibilities</u>	<u>Complete Publication List</u>	<u>A Chemist Meets Hollywood</u>
<u>Metalloporph.</u>			
<u>Executive Summary: Smell-Seeing</u>	<u>Web Based Resources</u>	<u>Academic Genealogy</u>	<u>A Chemist In Court</u>

<u>Introduction to Sonochemistry</u>	<u>Safety Resources</u>	<u>Press Clippings</u>	<u>Words of Humor and Wisdom</u>
<u>Proposal Excerpts</u>	<u>Group Equipment</u>	<u>How To Give A Seminar</u>	<u>Laws of the Universe</u>
<u>Funding</u>	<u>Past Group Members</u>	<u>Ch315 Inorganic Chemistry</u>	<u>Cartoons of Humor and Wisdom</u>
<u>Information for Visitors</u>	<u>Group Photogallery</u>	<u>Construction of the CLS Lab</u>	<u>Sculpture & Masks</u>

©2003, K.S. Suslick; all rights reserved.

Comments and suggestions: ksuslick@uiuc.edu

The Suslick Research Group



THE CHEMICAL EFFECTS OF HIGH INTENSITY ULTRASOUND

EXCERPTS FROM FUNDED RESEARCH PROPOSALS:

[The Chemical Effects of High Intensity Ultrasound](#)

[Heme Proteins, Microspheres, and their Synthetic Analogs](#)

[Metalloporphyrins as Field Responsive Materials](#)

[Dendrimer-Porphyrins as Sensor Materials](#)

[Smell-Seeing and Molecular Recognition](#)

The following is taken from our NSF Grant, 2000-2003, \$480,000 / 3 yrs.

PROJECT SUMMARY:

The chemical effects of ultrasound do not come from a direct interaction with molecular species. Instead, sonochemistry arises from acoustic cavitation: the formation, growth, and implosive collapse of bubbles in a liquid. Cavitation produces intense local heating (~5000 K), high pressures (~1000 atm), and enormous heating and cooling rates ($>10^{10}$ K/sec). Acoustic cavitation provides a unique interaction of energy and matter. A three-dimensional visualization of the comparison between sonochemistry and other forms of chemistry is shown below.

[Overview](#)

[Outline of
Research Projects](#)

[Introduction to
Sonochemistry](#)

[Exec. Summary:
Sonochemistry](#)

[Exec. Summary:
Porphyrin Research](#)

[Exec. Summary: Smell-
Seeing](#)

[Complete
Publication List](#)

[Abbreviated Curriculum
Vitae](#)

[Academic
Genealogy](#)

[Press
Clippings](#)

[Current Research Funding](#)

[Excerpts from Funded Research](#)

[Inventory of Group Equipment](#)

[Information for Visiting](#)

[Current Research Group Members](#)

[Group Meetings](#)

[Group Chores](#)

[Past Research Group Members](#)

[Group Photogallery](#)

[Web Resources](#)

[Laboratory Safety Resources](#)

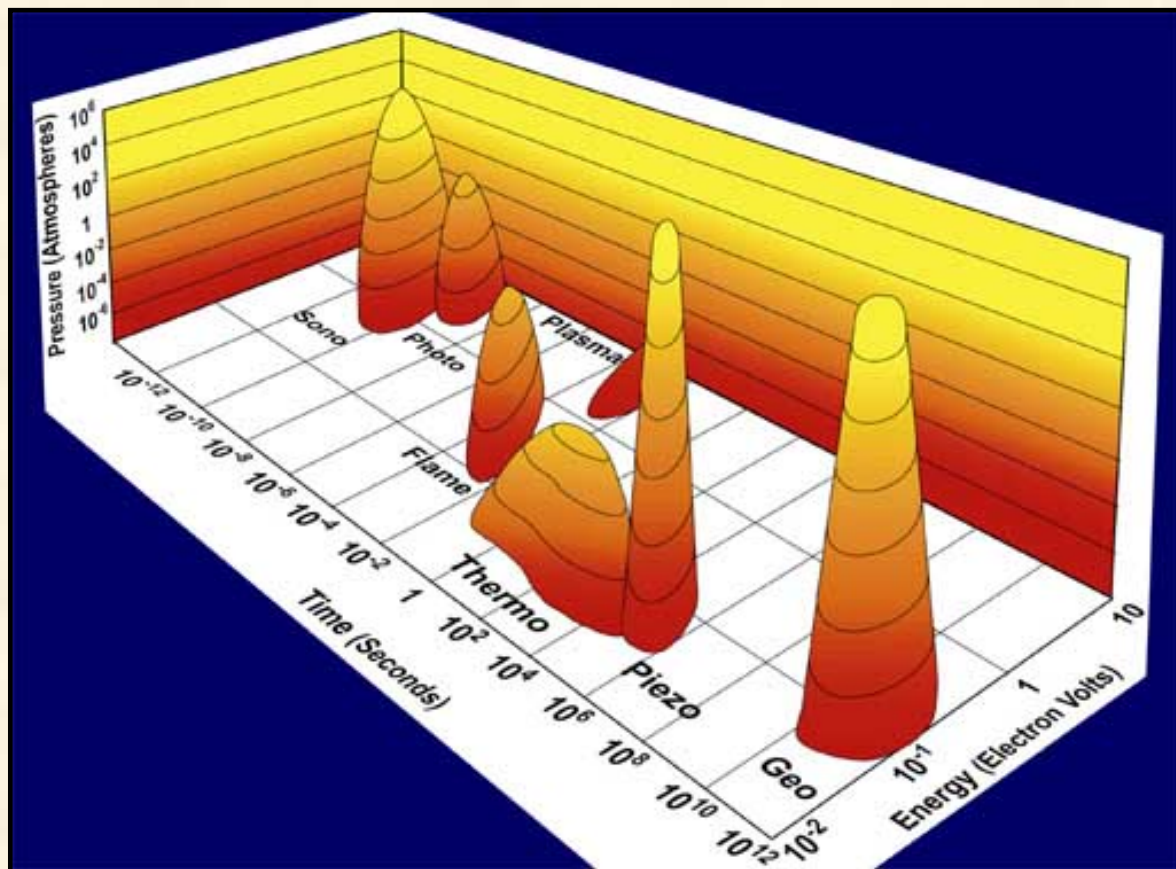
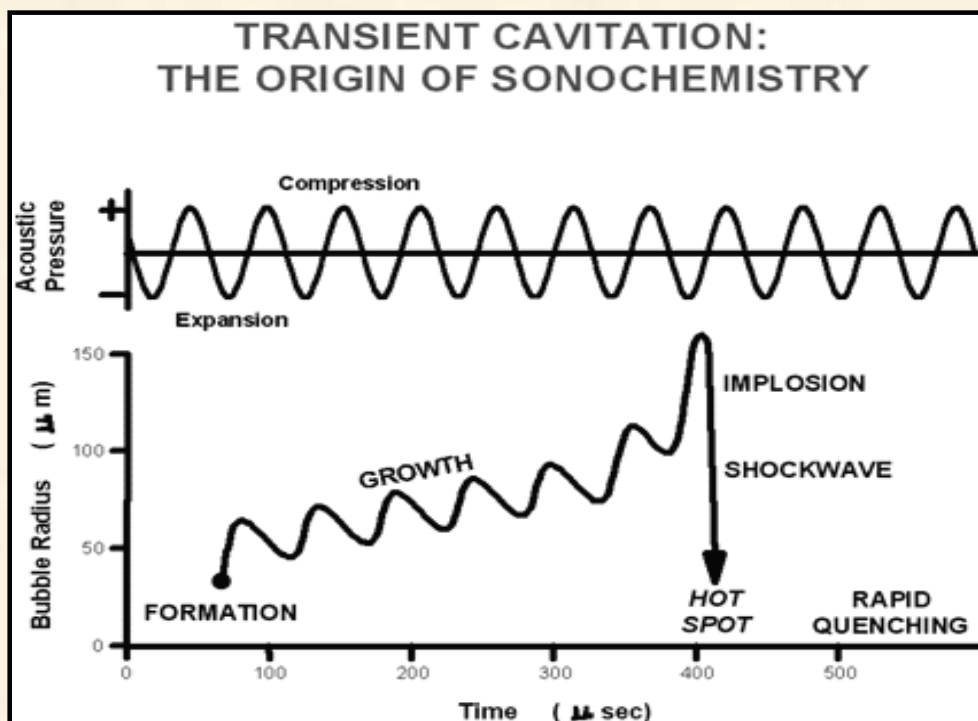
[Art and Science: Journal Covers](#)

[Sculpture & Masks](#)

[A Chemist Meets Hollywood](#)

[Chymistes: The Distillers of Waters](#)

[A Chemist In Court](#)



The field of sonochemistry has undergone a renaissance during the past decade. As our understanding of the nature of the chemical effects of ultrasound has grown, so too has the impact of sonochemistry on the chemical community and on a wide range of the physical sciences. Sonochemistry also has substantial strategic research significance to our industrial economy. Ultrasound already has major industrial applications, and the U.S. controls the world market in the production of ultrasonic equipment. Commercial generators of high-intensity ultrasound for large scale liquid processing is available off the

[Humor and
Wisdom](#)

[Laws of the Universe](#)

[Cartoons of Humor and
Wisdom](#)

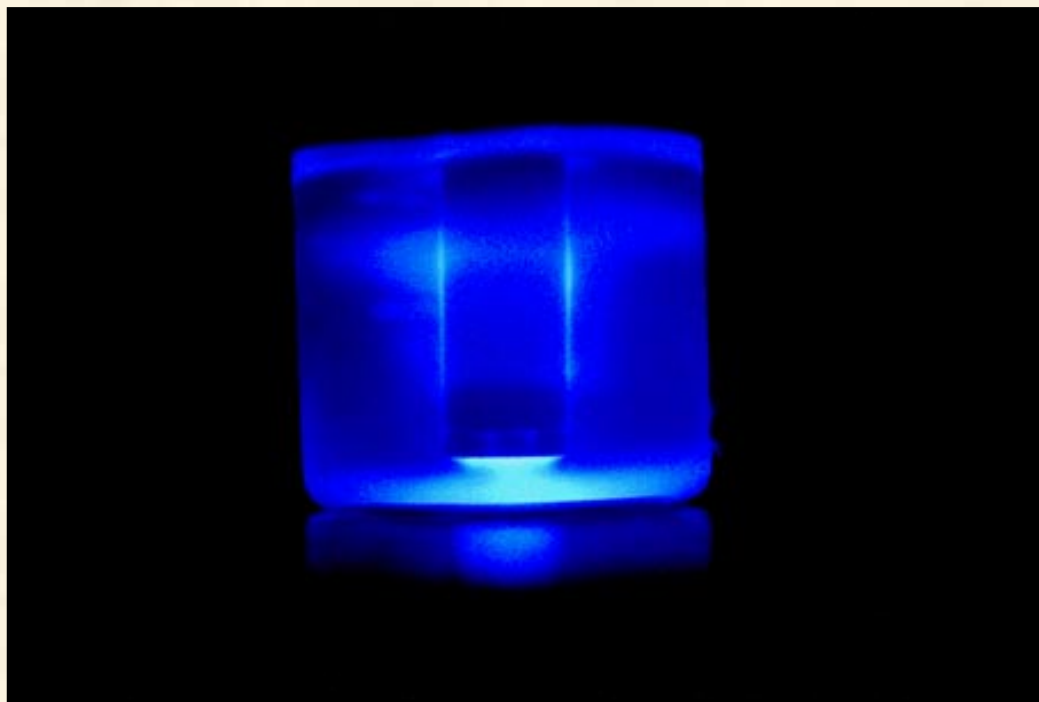
[Chem 115: Chemistry of
Everyday Phenomena](#)

[Chem 315: Inorganic
Chemistry](#)

shelf at quite modest costs. Ultrasonic cleaning now dominates both general purpose industrial and microelectronics applications, due to increasing restrictions on the use of halocarbon and other organic solvents. In addition, high intensity ultrasound has a large industrial base for welding, cutting, emulsification, solvent degassing, powder dispersion, cell disruption, and atomization. Thus, the development of sonochemistry and its applications will advance a global market in which the U.S. has a significant advantage.

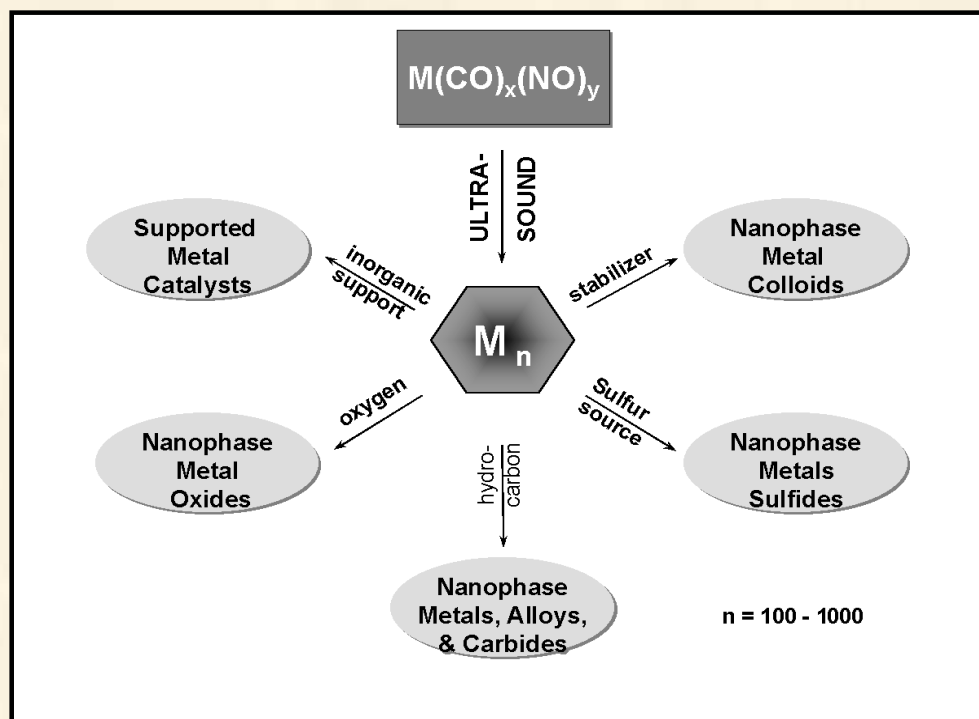
The previous grant period was enormously productive, resulting in 47 publications (published or in press). These papers fell relatively evenly into five categories: (1) Cavitation Phenomena and Sonoluminescence, (2) Inorganic Materials Chemistry, (3) Applications to Heterogeneous Catalysis, (4) Biomaterials, and (5) Popularizations.

During the current grant period, experimental measurements of the conditions created during acoustic cavitation were successful. The effective temperatures during cavitation were probed using sonoluminescence spectra. It proved possible for the first time to experimentally measure the temperatures during cavitation. In this fashion, systematic control of the metal atom emission temperatures was demonstrated from 5000 K down to 2000 K.



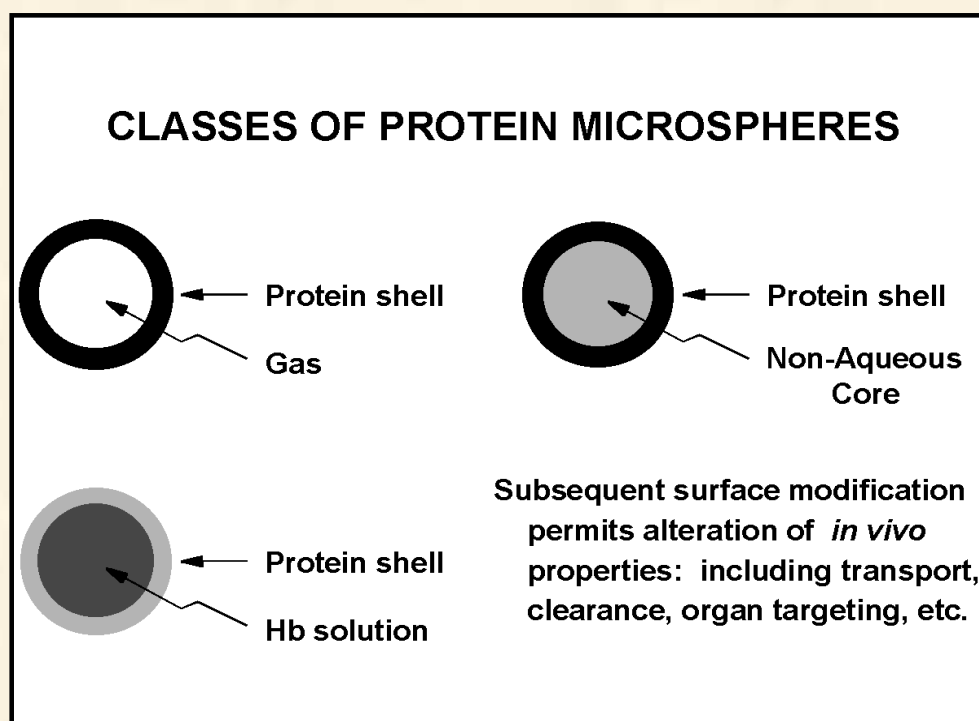
Multi-bubble sonoluminescence

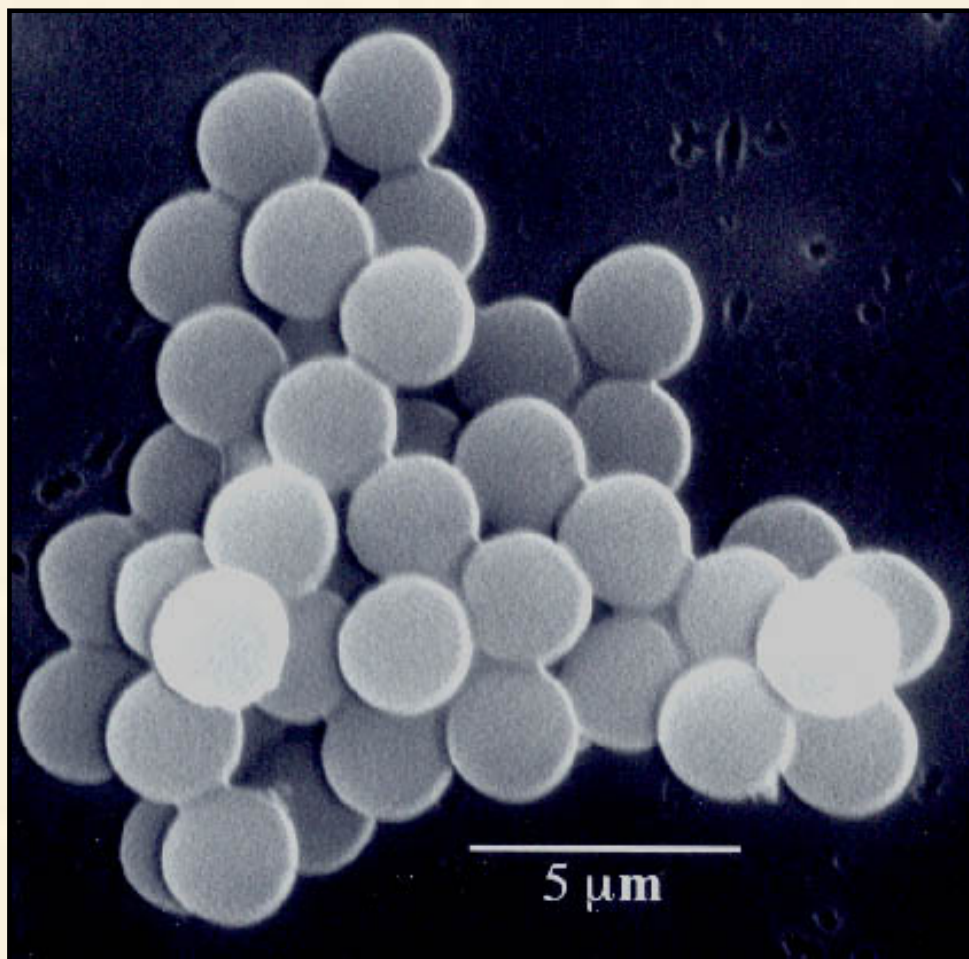
In other work, the sonochemical decomposition of volatile organometallic precursors was shown to produce nanostructured materials in various forms with high catalytic activities. This has proved extremely useful in the synthesis of a wide range of nanostructured inorganic materials, including high surface area transition metals, alloys, carbides, oxides, and sulfides, as well as colloids of nm clusters.



Applications of Sonochemistry to Materials Synthesis

Another important application has been the sonochemical preparation of biomaterials, most notably protein microspheres. Using high intensity ultrasound and simple protein solutions, a remarkably easy method to make both air-filled microbubbles and liquid-filled microcapsules was developed. This sonochemical method of microencapsulation uses high intensity ultrasound both to induce emulsification and to create oxidative crosslinking of protein cysteines. These microspheres are stable for months, and being slightly smaller than erythrocytes, can be intravenously injected. These protein microspheres have a wide range of biomedical applications, including uses for *in vivo* thermography, *in vivo* oximetry, MRI contrast agents, and drug delivery.





Sonochemical Preparation of Protein Microspheres

The overall goal in this research is to develop a fundamental understanding of the nature and applications of ultrasound in chemical reactivity. The specific objectives in this proposed work fall into three areas: 1) mechanistic and spectroscopic probes of the cavitation event, 2) novel inorganic materials synthesis and the sonochemical preparation of heterogeneous catalysts, and 3) biomaterials synthesis. In order to gain further understanding of the conditions present during cavitation, sonoluminescence will continue to be developed as a spectroscopic probe of the conditions created during bubble collapse. The use of ultrasound for the synthesis of novel inorganic materials will continue to focus on nanostructured and amorphous metals, alloys, carbides, oxides, and sulfides and their applications as heterogeneous catalysts for a variety of industrially important reactions. Finally, the development of the sonochemical synthesis of biomedical microstructures, especially proteinaceous microspheres, will be expanded. Biomedical applications of sonochemically prepared proteinaceous microspheres will be further developed, including their use as MRI agents. The functional properties of proteinaceous microspheres made from proteins with enzymatic activity will be delineated.

[Next project](#)

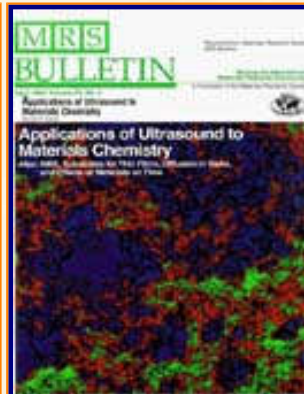
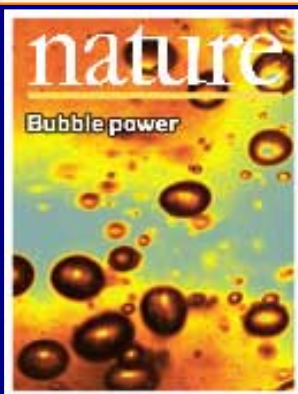
SUSLICK GROUP WEBSITE:

THE SCIENCE	THE GROUP	THE MAÎTRE D'	LAGNIAPPE: A LITTLE EXTRA
<u>Overview</u>	<u>Current Group Members</u>	<u>CV: Abbreviated, Full</u>	<u>Art and Science</u>
<u>Outline of Projects</u>	<u>Group Meetings</u>	<u>Suslick Group Brochure</u>	<u>Chymistes: The Distillers of Waters</u>
<u>Synopses: Sonochemistry</u> <u>Metalloporph.</u>	<u>Group Responsibilities</u>	<u>Complete Publication List</u>	<u>A Chemist Meets Hollywood</u>
<u>Executive Summary: Smell-Seeing</u>	<u>Web Based Resources</u>	<u>Academic Genealogy</u>	<u>A Chemist In Court</u>
<u>Introduction to Sonochemistry</u>	<u>Safety Resources</u>	<u>Press Clippings</u>	<u>Words of Humor and Wisdom</u>
<u>Proposal Excerpts</u>	<u>Group Equipment</u>	<u>How To Give A Seminar</u>	<u>Laws of the Universe</u>
<u>Funding</u>	<u>Past Group Members</u>	<u>Ch315 Inorganic Chemistry</u>	<u>Cartoons of Humor and Wisdom</u>
<u>Information for Visitors</u>	<u>Group Photogallery</u>	<u>Construction of the CLS Lab</u>	<u>Sculpture & Masks</u>

©2003, K.S. Suslick; all rights reserved.

Comments and suggestions: ksuslick@uiuc.edu

The Suslick Research Group



INVENTORY OF GROUP EQUIPMENT

Laboratory Space:

Contiguous labs and offices in the Chemical and Life Sciences Laboratory (dedicated April, 1997):

588 ft² office space;
3300 ft² laboratory space;
17 fume hoods;
224 linear feet of bench space.

Spectroscopic Instrumentation:

Perkin-Elmer 1650 FTIR Spectrometer.

Hitachi 3300 Double Monochromator UV-vis Spectrophotometer with Constant Temperature Cell Housing and Diffuse Reflectance Integrating Sphere.

IBM 9430 Double Monochromator UV-vis Spectrophotometer with Constant Temperature Sample Holder.

HP 8452A Diode Array UV-vis Spectrophotometer with Constant Temperature Sample Holder.

Matrix Isolation Rig with Leybold-Heraeus Closed Cycle 8K Refrigerator.

2 Photochemistry rigs, 300 W Eimac compact Xe arcs with quartz optics and filters.

1 Photochemistry rig, 500 W compact Xe arc.

[Overview](#)

[Outline of
Research Projects](#)

[Introduction to
Sonochemistry](#)

[Exec. Summary:
Sonochemistry](#)

[Exec. Summary:
Porphyrin Research](#)

[Exec. Summary: Smell-
Seeing](#)

[Complete
Publication List](#)

[Abbreviated Curriculum
Vitae](#)

[Academic
Genealogy](#)

[Press
Clippings](#)

[Current Research Funding](#)

[Excerpts from Funded Research](#)

[Inventory of Group Equipment](#)

[Information for Visiting](#)

[Current Research Group Members](#)

[Group Meetings](#)

[Group Chores](#)

[Past Research Group Members](#)

[Group Photogallery](#)

[Web Resources](#)

[Laboratory Safety Resources](#)

[Art and Science: Journal Covers](#)

[Sculpture & Masks](#)

[A Chemist Meets Hollywood](#)

[Chymistes: The Distillers of Waters](#)

[A Chemist In Court](#)

Chromatographic Equipment:

Hewlett-Packard 6890/5973 Gas Chromatograph / Mass Spectrometer.

Hewlett-Packard 5734A Gas Chromatograph with Dual FID/TCD.

Varian 3770 Capillary Gas Chromatograph with 50m Columns, FID.

Waters 600E Multisolvant HPLC with Waters 996 Diode Array Detector.

Spectrophysics Ternary HPLC with ISCO Spectrophotometric Detector and Fraction Collector.

Chromatotron Centrifugal Preparative Thin Layer Chromatograph.

4 Reporting Integrators (HP 3380A; HP 3394A; Shimadzu CR3A).

Ultrasonic and Related Equipment:

4 Heat-Systems Ultrasonics 300 to 600W Immersion Ultrasonic Horns and Power Supplies with High Pressure Cells and Inert Atmosphere Cells.

4 Sonics and Materials 500 - 600W, 20 kHz Immersion Ultrasonic Horns and Power Supplies.

Sonics and Materials 40 kHz Immersion Ultrasonic Horn and Power Supply.

Power Amplifier, AR 700A1, 700 W, 10 kHz-1MHz.

Hewlett-Packard 33120 Function Generator and Dual Trace Oscilloscope.

Power Piezoceramic Transducers, 500 kHz.

Branson 2 kW Ultrasonic Welder, with Pneumatic Actuator.

Magnetostrictive Transducer, 4 kW, manufactured by Russian Academy of Sciences.

Sonoluminescence Rig:

Princeton Optical Multichannel Analyzer with Intensified Diode Array Detector.

0.5 m Acton Research 505F and 0.2 m Thermal-Jarrell Ash Monochromators.

[Humor and
Wisdom](#)

[Laws of the Universe](#)

[Cartoons of Humor and
Wisdom](#)

[Chem 115: Chemistry of
Everyday Phenomena](#)

[Chem 315: Inorganic
Chemistry](#)

6 Braun Refrigerated Constant Temperature Baths.

Other Major Instrumentation:

Vacuum Atmospheres Double Length Inert Atmosphere Chamber with O₂ Monitor.

Vacuum Atmospheres Single Length Inert Atmosphere Chamber with O₂ Monitor, interfaced with internal sonicator and cooling.

Electrochemical Analysis Apparatus, Bioanalytical Systems CV51W.

Flow Microreactor for Gas-Solid Heterogeneous Catalysis with

MKS Mass Flow Controllers and Digital Baratron Manometer,

High Vacuum Line, Turbomolecular Pump and Penning Gauge, and

Quadrupole Mass Spectrometer Residual Gas Analyzer, Spectra #245-320.

Optical Microscope, Inverted Configuration, Olympus CK2 with video imaging system.

Particle Counter and Sizer, Elzone 180XY, with computer interface.

Particle Counter and Sizer, Coulter Multisizer IIE, with computer interface.

Particle Sifter, ATM Sonic Sifter with Sieves.

Computers and Graphics Equipment:

15 PC Pentium 200 MHz MMX Micron Microcomputers (one per desk).

3 PC PentiumII 400 MHz Dell Microcomputer Graphics Workstations with CD-RW.

3 PC Pentium 133 MHz Microcomputers.

6 PC 80486/66DX2 66MHz Microcomputers for Data Analysis and Spectrometer Interface.

Silicon Graphics Indigo² Extreme supermicrocomputer graphics workstation,

R4400 processor, with 8.5 GB Hard Drives, 64 MB RAM, 19" 24-bit color monitor, DAT Tape

Drive, 2x CD-ROM Player, Molecular Simulations software suite for molecular modeling.

1 Tektronics Phaser 550 Color Laser Printer.

2 Hewlett-Packard Desk-Jet 660C Color Printers.

2 Hewlett-Packard ColorPro Plotters.

5 Hewlett-Packard LaserJet II, III, and IV laser printers.

1 Hewlett-Packard Scan Jet 3c high resolution color scanner.

4 Ink Jet printers.

1 Minolta 7000i Automatic 35 mm Camera with multiple lens.

Other Laboratory Equipment:

12 Dual Argon-Vacuum Manifolds with Airless Glassware.

20 Two-Stage Vacuum Pumps

High Vacuum Line, Diffusion Pump and Penning Gauge.

NANOpure Water Purification System, Bioresearch Grade D4751.

Fisher Marathon 13K Centrifuge.

Vacuum Lyophilizer, 12 Port.

3 Buchi Rotary Evaporators.

7 Solvent Stills.

4 Mettler Analytical and Sartorius Analytical Top-loading Balances.

5 Laboratory Refrigerators.

1 Laboratory Storage Freezer.

4 Large Laboratory Ovens

2 Liquid N₂ Storage Dewars, 30 L, with Withdrawal Device.

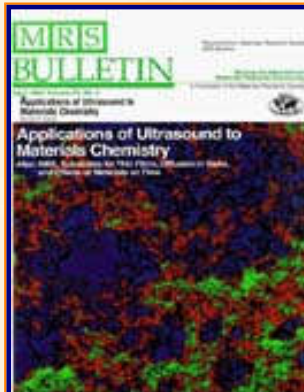
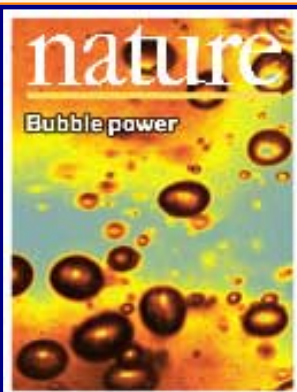
SUSLICK GROUP WEBSITE:

THE SCIENCE	THE GROUP	THE MAÎTRE D'	LAGNIAPPE: A LITTLE EXTRA
<u>Overview</u>	<u>Current Group Members</u>	<u>CV: Abbreviated, Full</u>	<u>Art and Science</u>
<u>Outline of Projects</u>	<u>Group Meetings</u>	<u>Suslick Group Brochure</u>	<u>Chymistes: The Distillers of Waters</u>
<u>Synopses: Sonochemistry</u>	<u>Group Responsibilities</u>	<u>Complete Publication List</u>	<u>A Chemist Meets Hollywood</u>
<u>Metalloporph.</u>			
<u>Executive Summary: Smell-Seeing</u>	<u>Web Based Resources</u>	<u>Academic Genealogy</u>	<u>A Chemist In Court</u>
<u>Introduction to Sonochemistry</u>	<u>Safety Resources</u>	<u>Press Clippings</u>	<u>Words of Humor and Wisdom</u>
<u>Proposal Excerpts</u>	<u>Group Equipment</u>	<u>How To Give A Seminar</u>	<u>Laws of the Universe</u>
<u>Funding</u>	<u>Past Group Members</u>	<u>Ch315 Inorganic Chemistry</u>	<u>Cartoons of Humor and Wisdom</u>
<u>Information for Visitors</u>	<u>Group Photogallery</u>	<u>Construction of the CLS Lab</u>	<u>Sculpture & Masks</u>

©2003, K.S. Suslick; all rights reserved.

Comments and suggestions: ksuslick@uiuc.edu

The Suslick Research Group



SEMINAR ON SEMINARS: HOW TO GIVE A TALK

My group prides itself on the excellence of our presentations. Here are some of our secrets.

[To download a pdf file of this "Seminar on Seminars", click here.](#)

[Overview](#)

[Outline of
Research Projects](#)

[Introduction to
Sonochemistry](#)

[Exec. Summary:
Sonochemistry](#)

[Exec. Summary:
Porphyrin Research](#)

[Exec. Summary: Smell-
Seeing](#)

[Complete
Publication List](#)

[Abbreviated Curriculum
Vitae](#)

[Academic
Genealogy](#)

[Press
Clippings](#)

Seminar on Seminars

Professor Kenneth S. Suslick

**School of Chemical Sciences
University of Illinois at Urbana-Champaign**

- **Planning & Organization**
- **Slide Format**
- **Slide Content**
- **The Presentation**

[Current Research
Funding](#)

[Excerpts from
Funded Research](#)

[Inventory of
Group Equipment](#)

[Information
for Visiting](#)

[Current Research Group
Members](#)

[Group
Meetings](#)

[Group
Chores](#)

[Past Research
Group Members](#)

[Group
Photogallery](#)

[Web Resources](#)

[Laboratory Safety
Resources](#)

[Art and Science:
Journal Covers](#)

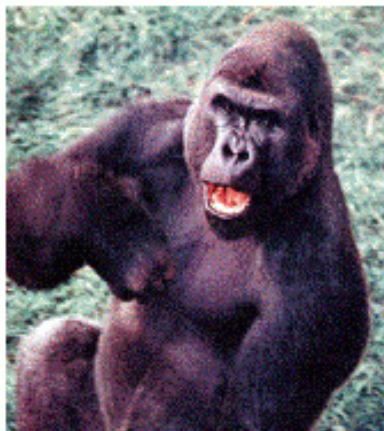
[Sculpture &
Masks](#)

[A Chemist
Meets Hollywood](#)

[Chymistes: The Distillers
of Waters](#)

[A Chemist
In Court](#)

Caveats



- **Do as I say, not as I do.**
This presentation, of necessity, is word-heavy and graphics-light.
- **De gustibus non disputandum est.**
(*There is no arguing about tastes.*)
These are my opinions.
I could be wrong, but I'm not.
- **Snepscheut's Law:** In theory, there is no difference between theory and practice. But in practice, there is.
- **Monk's Commentary:**
You'll thank me later.

Planning & Organization



[Humor and
Wisdom](#)

[Laws of the Universe](#)

[Cartoons of Humor and
Wisdom](#)

[Chem 115: Chemistry of
Everyday Phenomena](#)

[Chem 315: Inorganic
Chemistry](#)



Planning the Talk

- What is **THE** point of your seminar?
It's unlikely you'll be able to make more than 1.
- Why will your audience be interested?
Always keep the audience in mind.
- Where will the talk be held?
What will impact your visual aids?
Big room vs. small room, ambient light level ...



The Audience

- **AGAIN:** Always keep the audience in mind.
- Gear your talk at the right level.
Better to aim just a little low than too high.
- Be kind to the old fogies.
Eyesight declines significantly beyond 40.
Use big text, high contrast.
Rapid changes in light intensity are painful.



Planning the Organization of the Talk

- You are telling a story.
Tell it so they understand.
- Graphics & figures first, then words.
Easier to organize your talk.
- Verbal comprehension is limited:
Tell them what you are going to tell them,
then tell them,
then tell them what you told them.



Outlining the Plan

- YOU need a detailed outline of the talk,
BUT your audience needs only a broad outline.
- Number of sub-divisions **MUST** be ≥ 2 and ≤ 5 .
- Think about the logic of the flow.
- Slides for explicit division of sections are OK.



Title and Introduction

- **Short titles are best:**
It's a title, **NOT** an abstract!
- **1st slide: give the title, your name & brief outline.**
- **2nd slide: set the background —**
Why should we care about this topic?



How Many Slides?

- **It depends on your slides or overheads!**
Use low content slides and lots of them.
- **Present only ONE main idea per slide.**
- **Most people plan on ~2 min/slide,**
but it depends on the slides:

Can be as little as 1 min/slide for images.



KIS: Keep It Simple!

- A talk is **NOT** a full research paper.
- Your job is to convince and inform, **NOT** to archive.
- Present enough data to establish the point, **NOT** all the data possibly available.
- Simplify graphics when possible.



Slide Format





Type of Slides

- **Text Only:** usually bulleted or numbered.
- **Conceptual (cartoon):** use judiciously, be credible.
- **Graphs:** x-y and bar **strongly** preferred.
- **Tables:** usually better as graph,
large tables (> 9 numbers) **NEVER** work.
- **Images:** micrographs, ORTEPS, spectra, etc.
mid-quality jpg or png at <200 dpi is enough.



General Format

- Landscape format is standard.
- Use page effectively:
Fill the page, but **don't overfill**.
- Consider carefully your blank space.
Use it to improve visibility and
to separate topics, ideas, etc.
- **The natural tendency is to cram things too close together**
so that they'll fit in the space rather than to edit the text to the bare minimum needed;
most people tend to be much too wordy and detailed, and to go on and on and on and on,
when what they should do is just shut up!



General Format

- I like 1.2 line spacing with 0.8 after paragraph.
- Manually break lines yourself (shift-enter).
DON'T let Microsoft control line breaks!
- Turn **OFF** WordWrap in Text Box.
- Avoid all Microsoft Design Templates!
Keep logos (if any) simple and relevant.



Titles should be 36 pt. Arial Bold Maybe 32 pt., but be consistent.

- **Avoid serif fonts:** use Arial, Helvetica, Swiss...
- **Major Divisions:** Arial, ~28 pt., bold.
Minor Divisions: Arial, ~24 pt., bold usually best.
Avoid text below 20 pt., generally, especially un-bolded. e.g., 16 pt.
- Leave extra line spacing between divisions.
- **CAPS ARE HARD TO READ FAST:** avoid them.
- **Spell-Check** your work!!
- Be consistent with punctuation at line ends.



Color

- **Color should be used judiciously!**
Use vivid, **readable** colors with limited shades.
Design artists are partial to pastels: I'm not.
- Use of **color** is very desirable for graphs, etc.
- Avoid **overusing color for MOST** text.
Most effective when used **for emphasis.**



Microsoft Overkill

- ❖ **Avoid over-use of bullets:**
 - ☹ **Use Solid and simple bullets.**
 - Ⓢ Use on major level only! Indent sets the gap.
 - 💧 **DON'T** get cute.
- ♥ **Don't distract your audience from your content.**
- ✓ **Avoid 'clip-art', especially the stupid Microsoft stuff.**





Direct Computer Projection

- Now the default (even in Moscow!), but check.
- Bring your own computer (if you can).
NEVER change from PC to Mac or vice versa.
- Avoid distracting backgrounds.
Clear, unshaded backgrounds usually best.
- Be careful with big images (use jpg or png not tiff)
- **DON'T overuse animation.**
- **DON'T get cute.**



Suslick's Rule of Fist

- ***You're always too close to the computer monitor.***
This makes for a strong tendency to over-stuff slides.
Much better to have less per slide and more slides.
 - Get far enough away from the screen^{*}
so that, with your arm fully extended,
your fist blocks the whole slide.
 - Slides legible at that distance
will be visible even at back of the hall.
- ^{*}or make the magnification small enough: ~33%

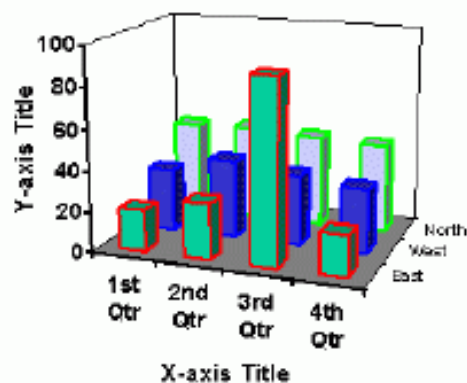
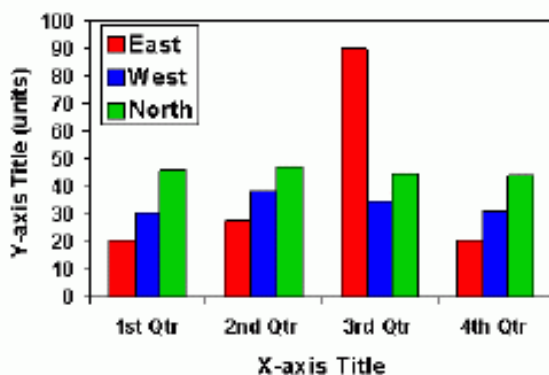


Keywords

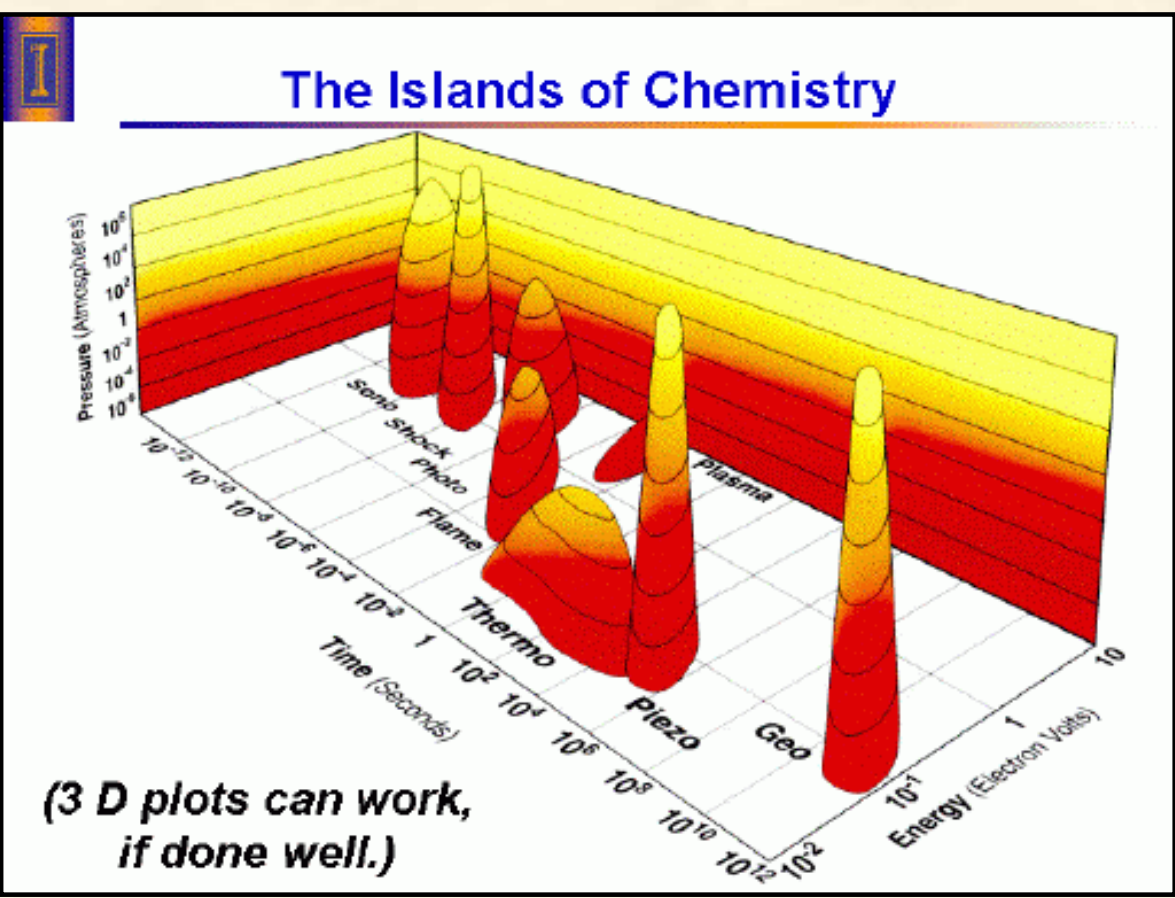
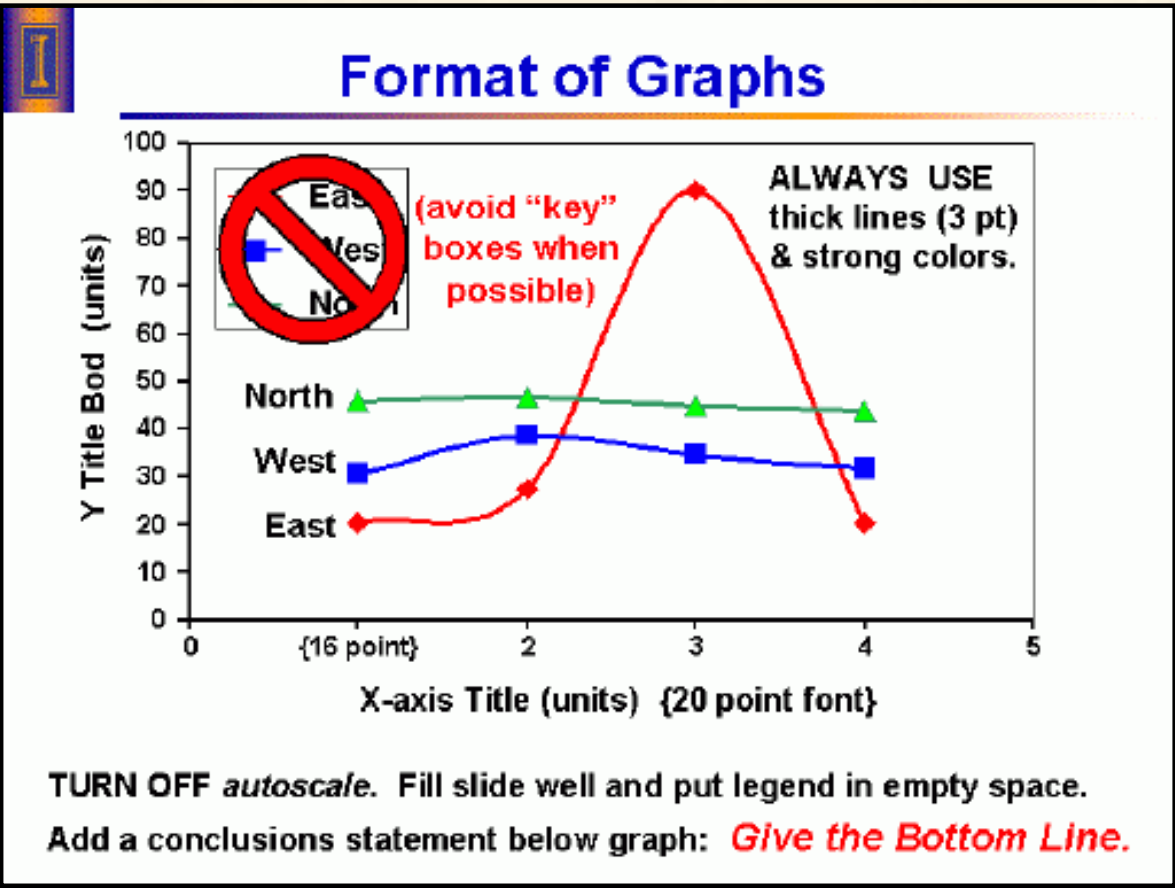
- Use minimal number of words in slides.
- **DON'T** type long, complete sentences.
Avoid “read along with the bouncing ball...”
- Use keywords, shortened text.
- Make it easy to read: One idea per line.
- Don't break idea or phrase at end of the line.



Type of Graphs and Tables



- **ALWAYS** label axes! **ALWAYS** show units!
- **KEEP IT SIMPLE:** 3-D graphs usually *don't* work well.
Avoid novel graph forms.
- **USE STRONG COLORS.**
Avoid complex hatch markings.



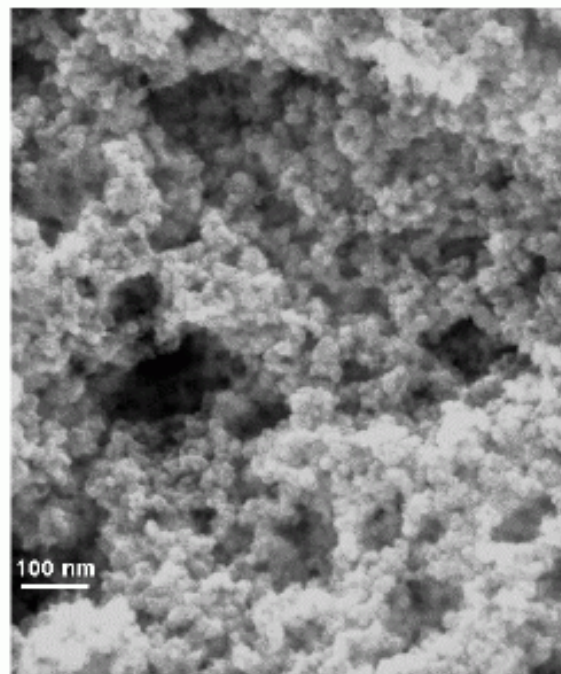


Micrographs Can Project Well.

- Give information with image:

Sonication of $\text{Fe}(\text{CO})_5$
in $\text{C}_{18}\text{H}_{34}$, under Ar,
25°C, 20 KHz, 80 W

- **ALWAYS** provide size scale.
- For projected image,
medium quality jpeg or png
at 200 dpi
(unless original is very small).



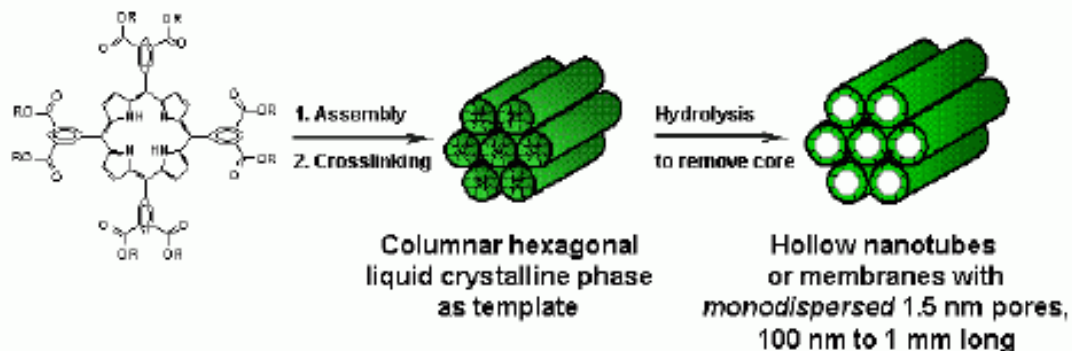
Slide Content





Conceptual (Cartoon) Slides

Non-Fullerene Nano-Tubes



Be careful to back up cartoons with **real** data.



Spectra & Raw Data

- **Spectroscopic data can provide credibility.**
Spectra must be well labeled (remember units!).
Label important assignments. Highlight with color.
Provide chemical structure with spectrum.
BE SURE your spectrum means what you say it does!
- **ORTEPs vs. computer models.**
Designate x-ray structures vs. computer models as such
Give the chemical structure or formula.
- **Don't overdo it.**
Too many spectra will obscure the big issues.



Jargon & Abbreviations

- **Avoid jargon – you'll lose your audience.**
- **Use rational abbreviations, sparingly.**
Watch out for TLA's (*three letter acronyms*).
- **If there are lots of abbreviations, use a separate slide for them.**
Consider using a second (overhead) projector or even a separate handout.



Equations

- **Keep them simple.**
Remember your goal is to convince, not 'prove'.
Proofs belong in the written work, not a presentation.
Only show the important equations, limit the details.
- **Define all symbols.**
Keep your audience's ignorance foremost in mind!
- **Make the equations big enough.**
Sub- and superscripts are often too small.



References

- If you use someone else's data or figure, you **MUST** provide the citation.*
- It's always nice to point your audience to lead references, *especially* if they are yours.
- Don't cluster references on a single slide. Give them one or two per slide when relevant, so the audience can jot them down.

*16 point at the bottom of the slide is OK, 18 point or 20 point is better.



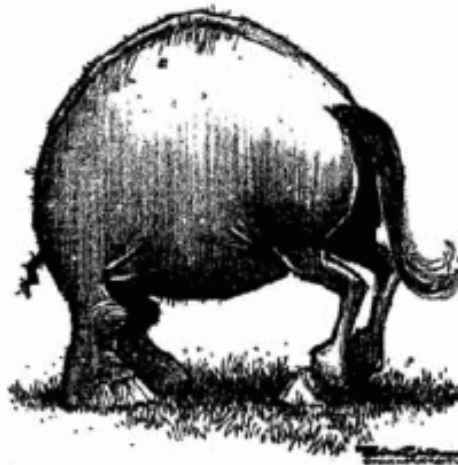
Humor

- Be very, very careful.
Many scientists are badly humor impaired.
(A defect *not* covered by the American Disabilities Act.)
- Visual humor often best,
especially for an international audience.
- Rank has its privileges:
The more senior you are,
the more you can get away with.
(*i.e., the boss's jokes always get more laughs.*)

I

Humoresque

Cover your ass: always be politically correct.
(Well, almost always.)



Current State of Our Two-Party System

I

Humor

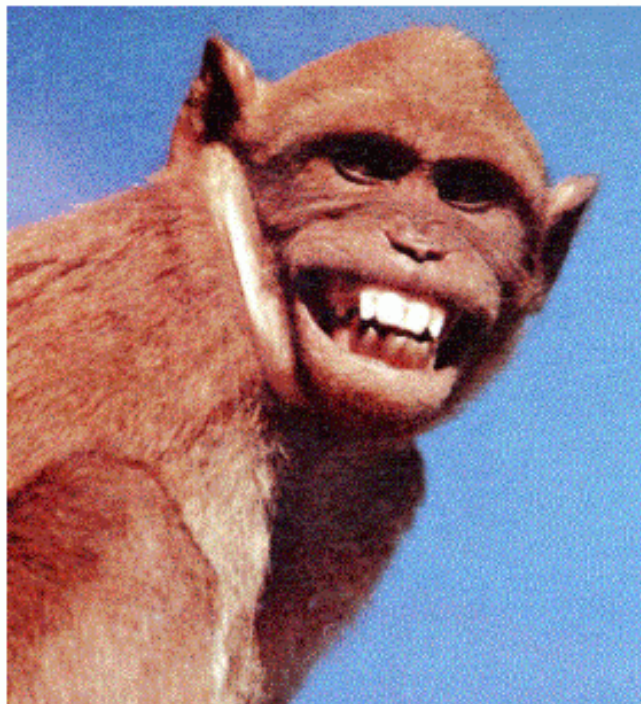
DILBERT by Scott Adams



Make sure it's appropriate for the occasion.



The Presentation



How Long?

- Practice talks are always **s l o w e r** than real presentations: adrenaline rush!
- **DON'T** go more than 50 min.
(After 55 min., your audience stops listening and starts wondering if they can catch their bus and if their bladders will hold out.)
- At meetings, **KEEP** to the schedule!
Don't worry if your audience leaves — worry when they start coming at you!



Practice Talks

- “Be prepared.” It’s hard to practice too much.
- Your goal is to communicate naturally. Stream of consciousness **doesn’t work**. A written script **won’t work**, either – too boring.
- Get some friends to hear the talk, **AFTER** you’ve already practiced a little bit.
- Listen to their feedback. Don’t be defensive. If they’re confused, so will your real audience.
- Watch out for “um”, “O.K.”, “you know”, and other distracting habits.



Pointers for Pointers

- Bring your own laser pointer.
- Always carry an extra set of batteries. Tygon tube connector prevents shorts.
- Green is great. Red ok if 640 nm, NOT 670 nm.
- **DON’T** keep the laser on all the time. Push the button **ONLY** sparingly!
- **DON’T** get the shakes. Use two hands if needed.



The Room

- Know your room in advance.
- Figure out the best lighting **BEFORE** the talk!
- Think about where to stand.
Don't block out screen from audience.
Best to be in the open, away from podium.
- With transparencies, point at the screen,
NOT the overhead! Audience looks where you do.



The Presentation

- Slow down!
- Modulate the voice: don't drone in **MONOTONE**.
- Keep eye contact with all of audience.
- **Don't try to impress, try to INFORM.**
An informed audience will BE impressed.
Audiences can smell bullshit or condescension.
- Relax and be modestly confident. Remember:
You know more than they do about your talk.
- Show enthusiasm – it's contagious!



The Conclusions Slide

- **Verbal comprehension is limited:**
The **Conclusions Slide** should tell them what you told them.
- **Present only the TAKE-HOME messages:**
i.e., what should they remember in 1 month.
- **Keywords, NOT long sentences.**



Q and A



- “Don’t be nervous, don’t be frightened, don’t be scared: be prepared.” — T. Lehrer.
- **Don’t be defensive!**
- **If you don’t understand a question, just say so, and ask for rephrasing.**
- “I was gratified to be able to answer promptly. I said I didn’t know.” — Mark Twain



Acknowledgments and Ending

- Note American spelling of “acknowledgments”.
- Make it brief and to the point.
- Best closing line:

“And finally, I’d like to thank you for your very kind attention.”

(Then, **shut up and wait** for the applause!)

SUSLICK GROUP WEBSITE:

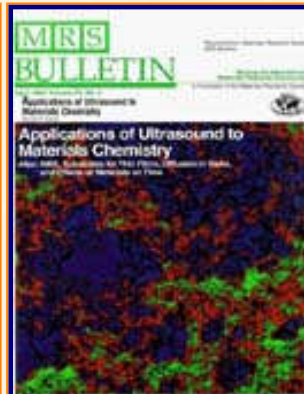
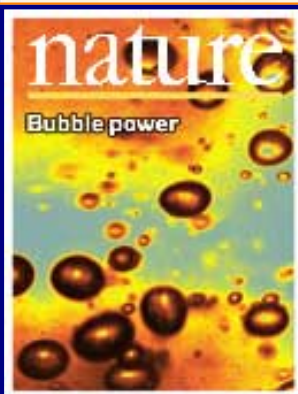
THE SCIENCE	THE GROUP	THE MAÎTRE D'	LAGNIAPPE: A LITTLE EXTRA
Overview	Current Group Members	CV: Abbreviated, Full	Art and Science
Outline of Projects	Group Meetings	Suslick Group Brochure	Chymistes: The Distillers of Waters
Synopsis: Sonochemistry	Group Responsibilities	Complete Publication List	A Chemist Meets Hollywood
Metalloporph.			

<u>Executive Summary: Smell-Seeing</u>	<u>Web Based Resources</u>	<u>Academic Genealogy</u>	<u>A Chemist In Court</u>
<u>Introduction to Sonochemistry</u>	<u>Safety Resources</u>	<u>Press Clippings</u>	<u>Words of Humor and Wisdom</u>
<u>Proposal Excerpts</u>	<u>Group Equipment</u>	<u>How To Give A Seminar</u>	<u>Laws of the Universe</u>
<u>Funding</u>	<u>Past Group Members</u>	<u>Ch315 Inorganic Chemistry</u>	<u>Cartoons of Humor and Wisdom</u>
<u>Information for Visitors</u>	<u>Group Photogallery</u>	<u>Construction of the CLS Lab</u>	<u>Sculpture & Masks</u>

©2003, K.S. Suslick; all rights reserved.

Comments and suggestions: ksuslick@uiuc.edu

The Suslick Research Group



[Overview](#)

[Outline of
Research Projects](#)

[Introduction to
Sonochemistry](#)

[Exec. Summary:
Sonochemistry](#)

[Exec. Summary:
Porphyrin Research](#)

[Exec. Summary: Smell-
Seeing](#)

[Complete
Publication List](#)

[Abbreviated Curriculum
Vitae](#)

[Academic
Genealogy](#)

[Press
Clippings](#)

LAWS OF THE UNIVERSE

Murphy's Seven Original Laws:

1. In any field of scientific endeavor, anything that can go wrong, will go wrong.
2. Left to themselves, things always go from bad to worse.
3. If there is a possibility of several things going wrong, the one that will go wrong, is the one that will do the most damage.
4. Nature always sides with the hidden flaw.
5. Mother Nature is a bitch.
6. If everything seems to be going well, you obviously overlooked something.

Levy's Seven Laws of the Disillusionment of the True Liberal

—Marion J. Levy, Jr.

1. Large numbers of things are determined, and therefore not subject to change.
2. Anticipated events never live up to expectations.
3. That segment of the community with which one has the greatest sympathy as a liberal inevitably turns out to be one of the most narrow

[Current Research
Funding](#)

[Excerpts from
Funded Research](#)

[Inventory of
Group Equipment](#)

[Information
for Visiting](#)

[Current Research Group
Members](#)

[Group
Meetings](#)

[Group
Chores](#)

[Past Research
Group Members](#)

[Group
Photogallery](#)

[Web Resources](#)

[Laboratory Safety
Resources](#)

[Art and Science:
Journal Covers](#)

[Sculpture &
Masks](#)

[A Chemist
Meets Hollywood](#)

[Chymistes: The Distillers
of Waters](#)

[A Chemist
In Court](#)

mindful and bigoted segments of the community.

(M. S. Kelly, Jr.'s reformulation: *Last guys don't finish nice.*)

4. Always pray that your opposition be wicked. In wickedness there is a strong strain toward rationality. Therefore, there is always the possibility, in theory, of handling the wicked by outthinking them. Corollary one: good intentions randomize behavior.

5. In unanimity, there is cowardice and uncritical thinking.

6. To have a sense of humor is to be a tragic figure.

7. To know thyself is the ultimate form of aggression.

Aigner's Axiom:

No matter how well you perform your job, a superior will seek to modify the results.

The Airplane Law:

When the plane you are on is late, the plane you want to transfer to is on time.

Baruch's Observation:

If all you have is a hammer, everything looks like a nail.

Bedfellow's Rule:

The one who snores will always fall asleep first.

Berra's Second Law:

Anyone who is popular is bound to be disliked.

Blair's Observation:

The best laid plans of mice and men are usually about equal.

Bucy's Law:

Nothing is ever accomplished by a reasonable man.

[Humor and
Wisdom](#)

[Laws of the Universe](#)

[Cartoons of Humor and
Wisdom](#)

[Chem 115: Chemistry of
Everyday Phenomena](#)

[Chem 315: Inorganic
Chemistry](#)

The Bureaucracy Principle:
Only a bureaucracy can fight a bureaucracy.

Cole's Law:
thinly sliced cabbage.

Dedera's Law of Probabilities:
In a three-story building served by one elevator, nine times out of ten the elevator car will be on a floor where you are not.

Etorre's Observation:
The other line always moves faster.

First Law of Aviation:
Takeoff is optional, landing is compulsory.

First Law of Debate:
Never argue with a fool -- people might not know the difference.

First Law of Socio-Genetics:
Celibacy is not hereditary.

First Law of Travel:
It always takes longer to get there than to get back.

Glasner's Law:
If it says "one size fits all," it doesn't fit anyone.

Goldenstern's Rules:
1. Always hire a rich attorney.
2. Never buy from a rich salesman.

Gourd's Axiom:
A meeting is a event at which the minutes are kept and the hours are lost.

Gualtieri's law of Inertia:

Where there's a will, there's a won't.

Harris Lamnet:

All the good ones are taken.

Helga's Rule:

Say no, then negotiate.

Heller's Law:

The first myth of management is that it exists.

Hershiser's Second Rule:

The label "NEW" and/or "IMPROVED" means the price went up.

Oliver Herford's Rule of Publishing

A manuscript is something submitted in haste and returned at leisure.

Hockett's Fundamental Principle of Mathematicizing:

If you know exactly how to, you don't have to!

Howden's Law:

You remember to mail a letter only when you're nowhere near a mailbox.

Howe's Law:

Everyone has a scheme that will not work.

Munder's Corollary to Howe's Law:

Everyone who does not work has a scheme that does.

Imbesi's Law of the Conservation of Filth:

In order for something to become clean, something else must become dirty.

Freeman's Extension:

... but you can get everything dirty without getting anything clean.

Jacquin's Postulate on Democratic Government:

No mans life, liberty, or property are safe while the legislature is in session.

Las Vegas Law:

Never be on a loser because you think his luck is bound to change.

Law of Probable Dispersal:

Whatever hits the fan will not be evenly distributed.

Lieberman's Law:

Everybody lies, but it doesn't matter since nobody listens.

Lynch's Law:

When the going gets tough, everyone leaves.

McDonald's Corollary to Murphy's Law's:

In any given set of circumstances, the proper course of action is determined by subsequent events.

Meadow's Maxim:

You can't push on a rope.

Meyer's Law:

In a social situation, that which is most difficult to do is usually the right thing to do.

Mitchell's law of Committees:

A simple problem can be made insoluble if enough meetings are hold to discuss it.

Mollison's Bureaucracy Hypothesis:

If any idea can survive a bureaucratic review and be implemented, it

wasn't worth doing.

Mr. Cole's Axiom:

The sum of the intelligence on the planet is constant; the population is growing.

Nagler's Comment of the Origin of Murphy's Law:

Murphy's Law was not propounded by Murphy, but by another man of the same name.

Ninety Rules of Project Schedules:

The first ninety percent of the take takes ten percent of the time, and the last ten percent takes the other ninety percent.

Olivier's Law:

Experience is something you don't get until just after you need it.

Pfeifer's Principle:

Never make a decision you can get someone else to make.

Pudder's Law:

Anything that begins well, ends badly. Anything that begins badly ends worse.

The Queue Principle:

The longer you wait in line, the greater the likelihood that you are standing in the wrong line.

Ringwald's Law of Household Geometry:

Any horizontal surface is soon piled up.

The Roman Rule:

The one who says it cannot be done should never interrupt the one who is doing.

Rule of the Great:

When people you greatly admire appear to be thinking deep

thoughts, they are probably thinking about lunch.

Schopenhauer's Law of Entropy:

If you put a spoonful of wine in a barrel full of sewage, you get sewage. If you put a spoonful of sewage in a barrel full of wine, you get sewage.

Shapiro's Explanation:

The grass is always greener on the other side - but that's because they use more manure.

Simon's Law of Destiny:

Glory may be fleeting, but obscurity if forever.

Skoff's Law:

A child will not spill on a dirty floor.

Smith's Law:

No real problem has a solution.

Sociology's Iron Law of Oligarchy:

In every organized activity, no matter the sphere, a small number will become the oligarchical leaders and the others will follow.

Stewart's Law of Retroaction:

It is easier to get forgiveness than permission.

Suslick's First Law of Maps:

All countries are the same size—one map page.

(Many Europeans do not realize the sense of scale of the U.S. For example, a visiting French postdoc a few years ago was bitterly disappointed to discover that he couldn't just drive from Illinois over to Colorado to go skiing for the weekend.)

Suslick's First Law of Infant Gravity:

You can't fall off the floor.

Suslick's Second Law of Infant Gravity:

It takes an infant 6 months to learn this.

Suslick's Law of Threes:

It always takes three times to do anything right.

The first time you either overshoot or undershoot;
the second time you either over-compensate or under-compensate;
it's not until the third time that you have a chance to get it right.

Suslick's Scheme of Priorities:

If it isn't worth doing,
it isn't worth doing right.

Swipple's Rule of Order:

He who shouts loudest has the floor.

Thal's Law:

For every vision, there is an equal and opposite revision.

Trischmann's Paradox:

A pipe gives a wise man time to think and a fool something to stick in his mouth.

Vile's Law of Value:

The more an item costs, the farther you have to send it for repairs.

Westheimer's Rule:

To estimate the time it takes to do a task: estimate the time you think it should take, multiply by 2, and change the unit of measure to the next highest unit. Thus we allocate 2 days for a one-hour task.

Wethern's Law of Suspended Judgment:

Assumption is the mother of all screw-ups.

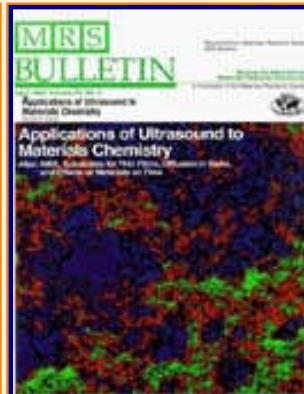
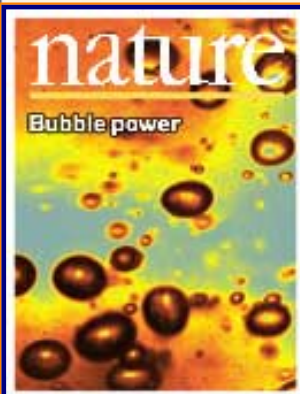
SUSLICK GROUP WEBSITE:

THE SCIENCE	THE GROUP	THE MAÎTRE D'	LAGNIAPPE: A LITTLE EXTRA
<u>Overview</u>	<u>Current Group Members</u>	<u>CV: Abbreviated, Full</u>	<u>Art and Science</u>
<u>Outline of Projects</u>	<u>Group Meetings</u>	<u>Suslick Group Brochure</u>	<u>Chymistes: The Distillers of Waters</u>
<u>Synopses: Sonochemistry</u>	<u>Group Responsibilities</u>	<u>Complete Publication List</u>	<u>A Chemist Meets Hollywood</u>
<u>Metalloporph.</u>			
<u>Executive Summary: Smell-Seeing</u>	<u>Web Based Resources</u>	<u>Academic Genealogy</u>	<u>A Chemist In Court</u>
<u>Introduction to Sonochemistry</u>	<u>Safety Resources</u>	<u>Press Clippings</u>	<u>Words of Humor and Wisdom</u>
<u>Proposal Excerpts</u>	<u>Group Equipment</u>	<u>How To Give A Seminar</u>	<u>Laws of the Universe</u>
<u>Funding</u>	<u>Past Group Members</u>	<u>Ch315 Inorganic Chemistry</u>	<u>Cartoons of Humor and Wisdom</u>
<u>Information for Visitors</u>	<u>Group Photogallery</u>	<u>Construction of the CLS Lab</u>	<u>Sculpture & Masks</u>

©2003, K.S. Suslick; all rights reserved.

Comments and suggestions: ksuslick@uiuc.edu

The Suslick Research Group



[Overview](#)

[Outline of
Research Projects](#)

[Introduction to
Sonochemistry](#)

[Exec. Summary:
Sonochemistry](#)

[Exec. Summary:
Porphyrin Research](#)

[Exec. Summary: Smell-
Seeing](#)

[Complete
Publication List](#)

[Abbreviated Curriculum
Vitae](#)

[Academic
Genealogy](#)

[Press
Clippings](#)

RESEARCH FUNDING

Major Research Funding, Current:

2003 - 06 NSF;
"Chemical Effects of High Intensity Ultrasound"
\$562,500 / 3 yrs.

2001 - 04 NIH;
"Heme Proteins, Microspheres, & Their Synthetic Analogs"
\$1,365,000 / 4 yrs.

1999 - 04 DARPA;
"Chemical Control of Single Bubble Cavitation"
\$637,121 / 4 yrs.

1990 - xx DOE; UIUC Materials Res. Lab;
"Field Responsive Porphyrinic Materials"
\$100,000 / yr.

2000 - 03 NSF;
"Chemical Effects of Ultrasound"
\$480,000 / 3 yrs.

Major Research Funding, Recent Past:

1997 - 02 DOD;
"Dendritic Materials Systems MURI"
\$500,000 / 5 yrs (KSS portion).

1997 - 01 NIH;
"Heme Proteins, Microspheres, & Their Synthetic Analogs"
\$924,944 / 4 yrs.

[Current Research Funding](#)

[Excerpts from Funded Research](#)

[Inventory of Group Equipment](#)

[Information for Visiting](#)

[Current Research Group Members](#)

[Group Meetings](#)

[Group Chores](#)

[Past Research Group Members](#)

[Group Photogallery](#)

[Web Resources](#)

[Laboratory Safety Resources](#)

[Art and Science: Journal Covers](#)

[Sculpture & Masks](#)

[A Chemist Meets Hollywood](#)

[Chymistes: The Distillers of Waters](#)

[A Chemist In Court](#)

1994 - 99 NSF;
"Chemical Effects of Ultrasound"
\$738,673 / 4 yrs.

1996 - 99 DOE;
"Cavitation Hydrothermal Oxidation"
\$478,027 / 3 yrs.

1995 - 99 VivoRx Pharmaceuticals, Inc.;
"Biomedical Applications of Protein Microspheres"
\$60,000 / yr.

1995 - 98 University of Illinois Foundation,
UIUC University Scholar;
\$36,000 / 3 yrs.

1996 DOE;
"Sonoluminescence", subcontract from Lawrence Livermore Natl. Lab
\$10,000.

1995 - 97 UIUC Critical Research Initiative;
"Non-Natural Self-Organizing Molecules"
\$120,000 / 2 yrs.

1992 - 96 NIH;
"Heme Proteins and Their Synthetic Analogs"
\$782,447 / 4 yrs.

1989 - 96 NSF; UIUC Materials Res. Lab;
"Effects of Ultrasound on Heterog. Catalysis"
\$386,000 / 5 yrs.

SUSLICK GROUP WEBSITE:

THE SCIENCE	THE GROUP	THE MAÎTRE D'	LAGNIAPPE: A LITTLE EXTRA
Overview	Current Group Members	CV: Abbreviated, Full	Art and Science

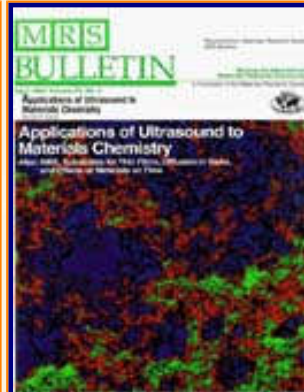
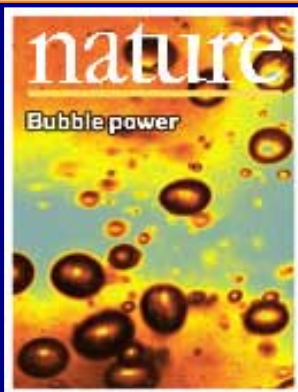
[Humor and Wisdom](#)[Laws of the Universe](#)[Cartoons of Humor and Wisdom](#)[Chem 115: Chemistry of Everyday Phenomena](#)[Chem 315: Inorganic Chemistry](#)

<u>Outline of Projects</u>	<u>Group Meetings</u>	<u>Suslick Group Brochure</u>	<u>Chymistes: The Distillers of Waters</u>
<u>Synopses: Sonochemistry</u>	<u>Group Responsibilities</u>	<u>Complete Publication List</u>	<u>A Chemist Meets Hollywood</u>
<u>Metalloporph.</u>			
<u>Executive Summary: Smell-Seeing</u>	<u>Web Based Resources</u>	<u>Academic Genealogy</u>	<u>A Chemist In Court</u>
<u>Introduction to Sonochemistry</u>	<u>Safety Resources</u>	<u>Press Clippings</u>	<u>Words of Humor and Wisdom</u>
<u>Proposal Excerpts</u>	<u>Group Equipment</u>	<u>How To Give A Seminar</u>	<u>Laws of the Universe</u>
<u>Funding</u>	<u>Past Group Members</u>	<u>Ch315 Inorganic Chemistry</u>	<u>Cartoons of Humor and Wisdom</u>
<u>Information for Visitors</u>	<u>Group Photogallery</u>	<u>Construction of the CLS Lab</u>	<u>Sculpture & Masks</u>

©2003, K.S. Suslick; all rights reserved.

Comments and suggestions: ksuslick@uiuc.edu

The Suslick Research Group



[Overview](#)

[Outline of
Research Projects](#)

[Introduction to
Sonochemistry](#)

[Exec. Summary:
Sonochemistry](#)

[Exec. Summary:
Porphyrin Research](#)

[Exec. Summary: Smell-
Seeing](#)

[Complete
Publication List](#)

[Abbreviated Curriculum
Vitae](#)

[Academic
Genealogy](#)

[Press
Clippings](#)

PAST GROUP MEMBERS

[Message to Past Group Members](#)

[Past Group Members, listed year by year.](#)

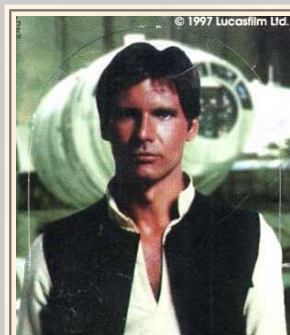
[Table of Past Group Members, printer friendly](#)

[Chemical Effects of Ultrasound](#)

[Bioinorganic Chemistry of Heme Proteins](#)

[Undergraduate Research Assistants](#)

Chemical Effects of Ultrasound:



Oleg Abramov

Professor, Russian Academy of Sciences;
Director of Research, Institute for Inorganic and General
Chemistry.
Visiting Professor, UIUC, 1994.

[Current Research
Funding](#)

[Excerpts from
Funded Research](#)

[Inventory of
Group Equipment](#)

[Information
for Visiting](#)

[Current Research Group
Members](#)

[Group
Meetings](#)

[Group
Chores](#)

[Past Research
Group Members](#)

[Group
Photogallery](#)

[Web Resources](#)

[Laboratory Safety
Resources](#)

[Art and Science:
Journal Covers](#)

[Sculpture &
Masks](#)

[A Chemist
Meets Hollywood](#)

[Chymistes: The Distillers
of Waters](#)

[A Chemist
In Court](#)



Dominick J. Casadonte, Jr.

B.Sc., Case Western Reserve University, 1980.
Ph.D., Purdue University, 1984 (D. McMillin).
Postdoctoral Associate, UIUC, 1984-1986.
Associate Professor, Texas Tech University.



Seok-Burm Choe

B.Sc., Seoul National University, Korea.
Ph.D., Kansas State University (K. Klabunde).
Postdoctoral Associate, UIUC, 1987-8.
Associate Professor, Kei-Mgung University, Taegu, Korea.



Richard Jun-Hong Chou

B.S., National Cheng Kung University, Taiwan, 1982.
Ph.D., Michigan State University, 1995.
Staff Scientist, Merck Pharmaceuticals



Andrzej A. Cichowlas

Postdoctoral Associate, UIUC, 1991-1994.
Research Scientist, Polish Academy of Sciences, Warsaw.



Gennady Dantsin

B.S., State Univ. of New York, Binghamton, 1996. Ph.D.,
UIUC, 2001.
Staff Scientist, Air Products, NJ

[Humor and
Wisdom](#)

[Laws of the Universe](#)

[Cartoons of Humor and
Wisdom](#)

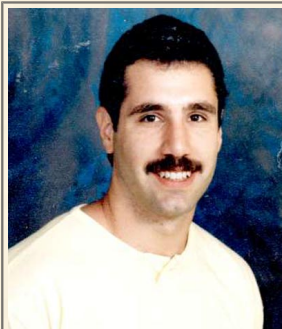
[Chem 115: Chemistry of
Everyday Phenomena](#)

[Chem 315: Inorganic
Chemistry](#)



Arul Dhas

B.S., Madurai Kamaraj University, 1988.
Ph.D., Indian Institute of Science, Bangalore, 1994.
Postdoctoral Associate, Bar-Illan University, Israel, 1995-1998.
Postdoctoral Associate, UIUC, 1998-2001.
Staff Scientist, Novellus Systems, San Jose, CA



Steven J. Doktycz

B.Sc., UIC, 1984.
Ph.D., UIUC, "Effects of Ultrasound on Solid-Liquid
Reactions," 1989.
T. S. Piper Thesis Research Prize, UIUC, 1989.
Staff Scientist, Dow Chemical Co.
Chief Financial Officer, ANGUS (Dow subsidiary), 1999 - .



Theodore Dolter

B.Sc., St. Louis University.
M.S., University of Illinois.
Assistant Professor, Southwestern Illinois College tdolter@icon-
stl.net



Arash Ekhtiarzadeh

B.S., University of Scranton, 1997. Ph.D., UIUC, 2001.
Staff Scientist, Bettis National Laboratory, Pittsburgh



Mingming Fang

B.S., M.S., Beijing University, 1987-1990.
Ph.D., UIUC, "Catalytic and Magnetic Properties of
Nanostructured Materials Generated by Ultrasound," 1995.
Postdoctoral Research Fellow, Pennsylvania State University.
Staff Scientist, Cabot Corp.



Edward B. Flint

B.Sc., Kenyon College, 1983.
Ph.D., UIUC, "Sonoluminescence," 1989.
Postdoctoral Associate, Professor H. Suhr, Tubingen, Germany.
Associate Professor, Bradley University.



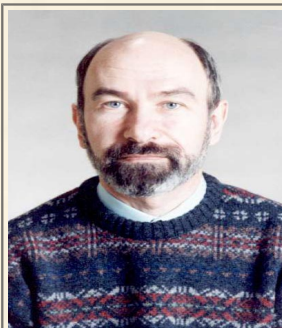
Chanchal K. Ghosh

B.Sc., M.S., University of Dhaka, Bangladesh, 1975.
Ph.D., University of Alberta, 1989.
Staff Scientist, Fabric & Hard Surface Technology, Procter and Gamble Company.



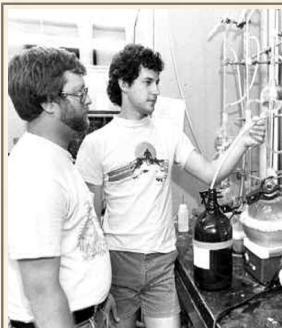
Mark W. Grinstaff

A.B., Occidental College, 1987.
Ph.D., UIUC, "The Sonochemical Synthesis of Inorganic and Biological Materials," 1992.
T. S. Piper Thesis Research Prize, UIUC, 1991.
NIH Postdoctoral Fellow, H. G. Gray, California Institute of Technology.
ACS Nobel Laureate Signature Awardee, 1994.
Asst. Prof., Department of Chemistry, Duke University.



Lev Grundel

Ph.D., M.S., Moscow University, 1983
Postdoctoral Associate, UIUC, 1991.
Staff Scientist, Great Lakes Analytical, Chicago.



David A. Hammerton

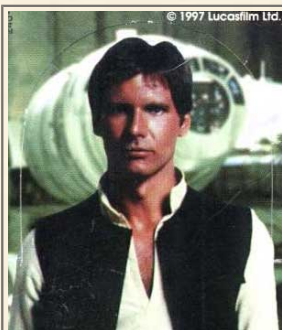
B.Sc., Southern Connecticut State College, 1981.
Ph.D., UIUC, "The Sonochemical Hot Spot," 1987.
Staff Scientist, Rohm and Haas, Inc.
Technical Manager, UCB Chemicals.



Kathleen A. (Kemper) House B.Sc., M.S., Illinois State University, 1989. Ph.D., UIUC, "Sonoluminescence As a Probe of Cavitation", 1994. Asst. Professor, Illinois Wesleyan University.



Taeghwan Hyeon
B.S., M.S., Seoul National University, 1991.
Ph.D., UIUC, "Nanostructured Catalytic and Magnetic Materials: Sonochemical Synthesis and Characterization", 1996.
T. S. Piper Thesis Research Prize, UIUC, 1996.
Postdoctoral Research Associate, Northwestern University (W. Sachler), 1996-97.
Assistant Professor, Seoul National University, Korea.



Robert E. Johnson
B.Sc., University of Wisconsin-Milwaukee, 1977.
Ph.D., University of Wisconsin-Madison, 1981 (L. Dahl).
Postdoctoral Associate, UIUC, 1983-84.
Staff Scientist, HOECHST Celanese Inc.



Kenneth Kolbeck
B.S., University of New Mexico, 1991.
Ph.D., "Biomedical Applications of Protein Microspheres", University of Illinois, 1999.
M.D., University of Illinois, 2000.
Radiology Resident, Dartmouth Medical School, 2000- .

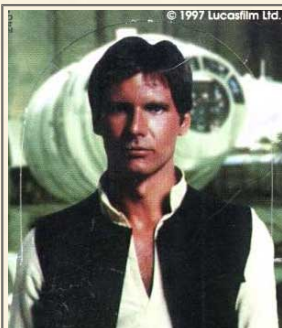


Gregory Kufner
B.S., Illinois Wesleyan, 1995.
Ph.D., "Production and Surface Modification of Protein Microspheres," University of Illinois, 2000.
Staff Scientist, Abott Pharmaceuticals.



Keith S. Kostecka

B.Sc., Illinois Benedictine College, 1982. M.S., UIUC, 1985.
D.Ed., UIUC at Chicago, 1990.
Associate Professor, Columbia College, Chicago.



Millan M. Mdleleni

B.Sc., University of Fort Hare (S. Africa), 1987.
Ph.D., Univ. of California at Santa Barbara, 1995.
Postdoctoral Associate, Univ. of Illinois, 1995-98.
Staff Scientist, Sasol Industries, S.A.



Christian Petrier

Ph.D., Laboratoire de Photochimie U.S.M., Grenoble, 1982
Postdoctoral Associate, UIUC, 1988-89
Professor, ESIGEC/Universite de Savoie, France.



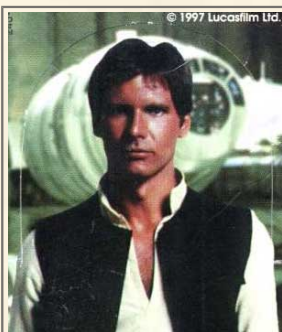
Paul F. Schubert

B.Sc., University of Arkansas, 1978.
Ph.D., UIUC, "Sonochemistry of Some Metal Carbonyl
Complexes," 1982. First Group Thesis!
Vice-President of Research & Development Syntroleum Corp.,
Tulsa



Gregory Szewczyk

B.A., Northwestern University, 1995.
Ph.D., "Disulfide Crosslinking in Protein Microspheres",
University of Illinois, 2000.
Staff Scientist, Colgate-Palmolive, N.J.



Hau H. Wang

B.Sc., National Tsing Hua University, Taiwan, 1975.
Ph.D., University of Minnesota, 1981, (L. Pignolet).
Postdoctoral Associate, UIUC, 1981-83.
Staff Scientist, Argonne National Laboratory.



Mike Wong

B.S., University of Tulsa, 1991.
Ph.D., Univ. of Illinois, "Sonochemically Produced
Proteinaceous Microspheres," 1996.
Senior Staff Scientist, Colgate-Palmolive, N.J.

Bioinorganic Chemistry of Heme Proteins:



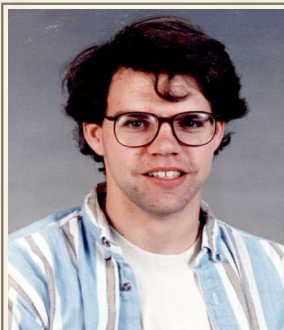
Francis V. Acholla

B.Sc., University of Nairobi, Kenya.
Ph.D., University of Kansas, 1985 (K. B. Mertes).
Postdoctoral Associate, UIUC, 1985-86.
Assistant Professor, University of Nairobi, 1985-91.
Senior Research Chemist, Rohm & Haas.



Mark D. Ball

B.S., Purdue University, 1982.
Ph.D., Iowa State University, 1987 (J. A. Olson).
Postdoctoral Associate, UIUC, 1988-90.
Associate Professor of Chemistry and Biomedical Engineering,
Rose-Hulman Institute of Technology.



David Benson

B. A., Goshen College, 1990.
Ph.D., UIUC, "New Intermediates of Cytochrome P450" 1997.
(with Steve Sligar)
Postdoctoral Associate, Duke University.



Puttaiah Bhyrappa

B.S., M.S., Bangalore University, 1986
Ph.D., Indian Institute of Science, Bangalore, 1991.
Postdoctoral Associate, Univ. So. Cal., , 1991-93.
Postdoctoral Associate, Univ. of Illinois, 1994-97.
Assistant Professor, Indian Institute of Technology, Madras.



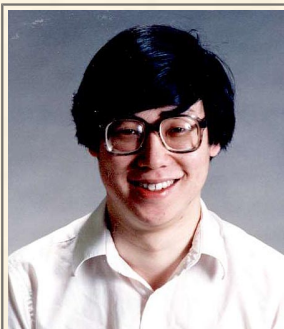
Mala Bhyrappa

B.S., M.S., Bangalore University, 1991
Ph.D., Indian Institute of Science, Bangalore, 1996.
Postdoctoral Associate, Univ. of Illinois, 1997.



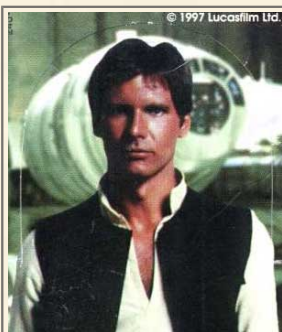
Chin-Ti Chen

B.S., Tamkang University, Taiwan, 1978.
M.S., National Taiwan University, 1982.
Ph.D., UIUC, "Porphyrins and Metalloporphyrins as Field Responsive Materials," 1992.
Postdoctoral Associate, S. Marder, California Institute of Technology.
Research Faculty, Institute of Chemistry, Academia Sinica, Taiwan.



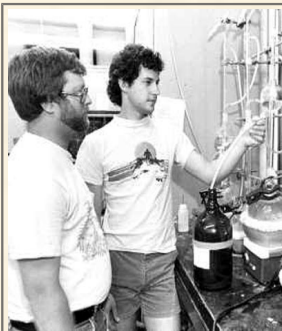
Homer Chou

B.S. University of Chicago, 1989.
Ph.D., UIUC, "Porphyrins as Second Order Nonlinear Optical Materials," 1995.
T. S. Piper Thesis Research Prize, UIUC, 1995.
Postdoctoral Research Fellow, Northwestern University.
Staff Scientist, Cabot Corp., Aurora



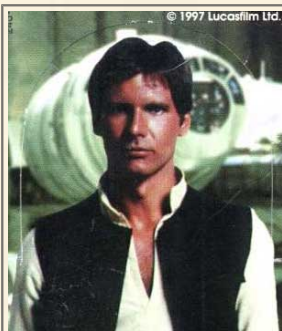
Bruce R. Cook

B.S., Hope College, 1981.
Ph.D., UIUC, "Shape Selective Oxidation of Hydrocarbons,"
1986.
Staff Scientist, Exxon Research and Engineering.



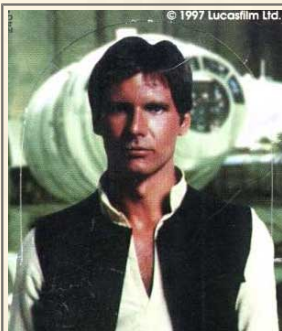
Daniel R. English

B.S., Ohio State University, 1979.
Ph.D., UIUC, "Synth. Fe Porphyrins as Models for Heme
Proteins" (w/ D. N. Hendrickson), 1984.
Unit Director, Eastman Kodak Company.



Mary M. Fox

B.S., Indiana University-Evansville, 1978.
Ph.D., UIUC, "A Bis-Pocket Porphyrin," 1983.
Staff Scientist, Procter & Gamble Corp.



Philip Gorlin

B.S., University of Texas at Austin, 1989.
Ph.D., UIUC, "Metalloporphyrin Sandwich Complexes," 1994.
(with Greg Girolami)
Staff Scientist, Colgate Palmolive



Christopher L. Hein

B.S., University of Colorado at Boulder, 1992.
Ph.D., UIUC, "Photosynthetic Reaction Center Analogs", 1997
(with Greg Girolami)
Staff Scientist, General Electric Corp.



David Huffman

B.S., M.S., Illinois State University, 1988.
Ph.D., UIUC, "Oligopeptide-Heme Complexes," 1993.
NIH Postdoctoral Fellow, T. O'Halloran, Northwestern University, 1993-1997.
Staff Academic Professional, Northwestern University, 1997-



Vijay K. Joshi

B.Sc., Punjab University, 1969. M.Sc., University of Jodhpur, 1971.
Ph.D. and Postdoctoral Associate, SUNY Buffalo, 1987 (J. H. Wang).
Postdoctoral Associate, UIUC, 1987-8.
Staff Scientist, Reheis Chemical Co.



Warren A. Kaplan

B.S., Brandeis University, 1984.
Ph.D., UIUC, "Ligand Binding to Ni Porphyrins and F430," 1989.
Staff Scientist, Shell Corporate Research.
Research Chemist, Stepan Company.



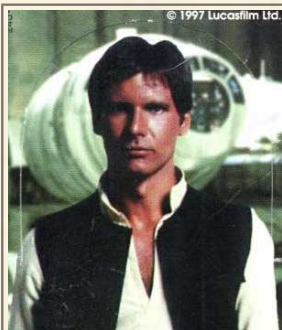
Michael G. Kinnaird

B.S., Guilford College, 1979. Ph.D., University of North Carolina, 1983 (D. Whitten).
Postdoctoral Associate, University of Kyoto, 1984 (I. Tabushi).
Postdoctoral Associate, UIUC, 1984-86.
Staff Scientist, BASF Chemical Co.



Stanley N. Milam

B.S., University of Texas at Austin, 1984.
Ph.D., UIUC "Actinide Porphyrin Chemistry," (with G. Girolami) 1989
Staff Scientist, Shell Chemical Co.



Saad N. Neme

B.S., University of Applied Chemistry, Syria, 1976.
Ph.D., University of California, Santa Barbara, 1984 (W. Kaska).
Postdoctoral Associate, UIUC, 1984-5.
Staff Scientist, Millennium Inorganic Chemicals, Baltimore.



Bimal R. Patel

A.B., Occidental College, 1990.
Ph.D., UIUC, "Porphyrin Liquid Crystals," 1996.
Staff Scientist, General Electric Corp., Evansville.



Alicia Paterno

B.S., Ithaca College, 1996.
Ph.D., UIUC, 2001.
Postdoctoral Research Associate, University of Pittsburgh

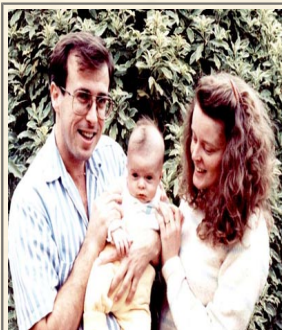


Neil Rakow

B.S., Colorado School of Mines, 1996.
Ph.D., UIUC, 2001.
Staff Scientist, 3M, Minneapolis.

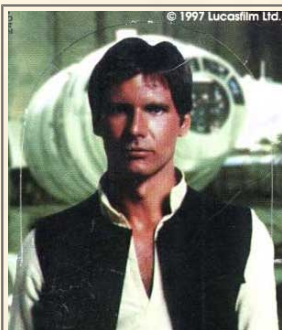
nrakow@s.scs.uiuc.edu

217-333-1532



Jennifer Beck Ralph

B.S., Ph.D., University of Queensland, Australia, 1983, 1987.
Postdoctoral Associate, UIUC, 1987-9 (joint with S. G. Sligar).
Research Scientist, Australian National University.



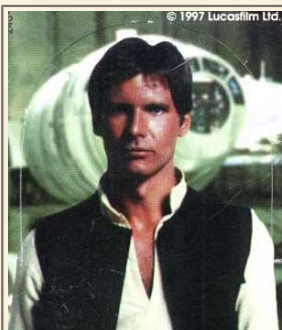
Thomas J. Reinert

B.S., Iowa State University, 1979.
Ph.D., UIUC, "Mechanistic Probes of Heme Proteins" 1987.
Professor, Linfield College, Oregon.



Michael Rosenblatt

B.S., Towson State University, 1992. Ph.D., UIUC, "Synthetic Heme Peptide Complexes", 2000. Postdoctoral Associate, U. Penn., W. DeGrado, 2000- .



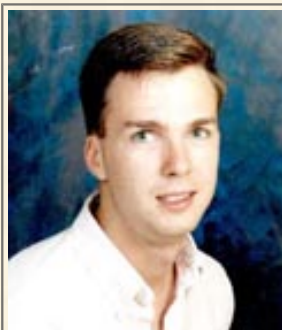
Cynthia A. Smith

B.Sc., Kenyon College, 1978.
M.S., UIUC, 1981.
Regulatory Consultant, Lorton, VA.



Shawne Van Deusen-Jeffries

A.B., Occidental College, 1987.
M.S., UIUC, 1991.
Research Scientist, Eli Lilly.
Chemist, AMTX Products, Division of XEROX Inc.



Randall A. Watson

B.Sc., Indiana State University, 1986.
Ph.D., UIUC, "Photochemistry of Metalloporphyrins" 1990.
Section Head, Beijing Technical Center, Procter and Gamble Company.



Christopher Ziegler

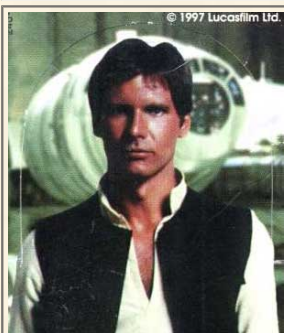
A.B., Bowdoin College, 1992.
NSF Predoctoral Fellow, 1993-1996.
Ph.D., UIUC, "Ligand Studies of Group 8 Triad
Metalloporphyrins," 1997.
Postdoctoral Associate, MIT, Steve Lippard.

Undergraduate Research Assistants:



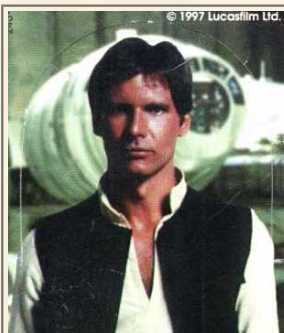
Jocelyn Bautista

B.Sc., UIUC, "Photochemistry of Manganese, Iron, and
Chromium Porphyrin Oxoanion Complexes by Matrix Isolation"
1991.
M.D., Washington University, St. Louis, 1995.
Resident Doctor, Yale New Haven Hospital.



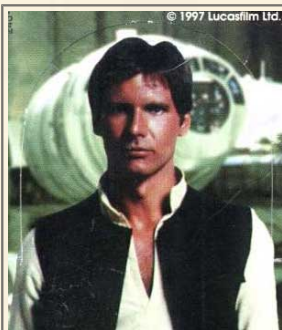
Ann Burkybile

B.Sc., UIUC, "Synthesis and Characterization of Discotic
Macrocyclic Liquid Crystals," 1995.
Graduate Student in Biochemistry, UIUC Fellow.



James Corbett

B.Sc., UIUC, 1982.
Ph.D., University of California, Berkeley, 1987.



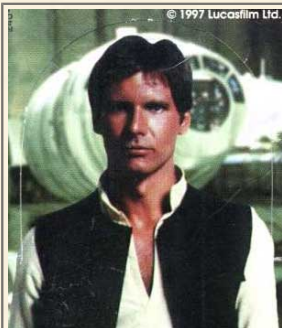
Jennifer Cormack

Undergraduate Research Assistant, UIUC, Summer 1993.
B.Sc., California Institute of Technology, 1995.



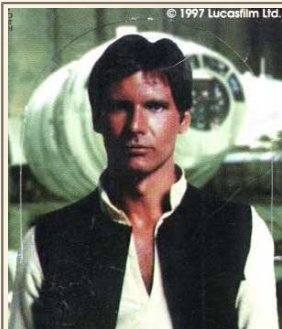
Peter Dorhout

B.Sc., UIUC, 1985.
Ph.D., University of Wisconsin at Madison, 1989.
Postdoctoral Fellow, Iowa State University, 1989-91.
Associate Professor, Colorado State University.



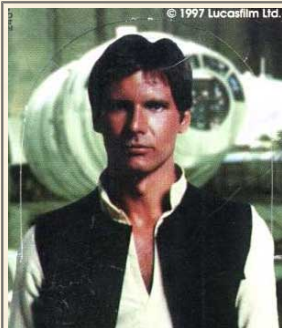
Joann Eisenhart

B.Sc., UIUC, "Synthesis and Characterization of a "Bis-Pocket"
Porphyrin, 1981.
Ph.D., University of Wisconsin at Madison, 1986.
Quality Consultant, Rohm & Haas Company.



Julie Katzenberger

B.Sc., University of Illinois, "The Synthesis of 5, 10, 15, 20-
Tetrakis- (2, 4, 6-Triphenylphenyl) Porphyrin and the Effect of
Hydrogen Bonding on FeTPP(1, 2-Me₂ Im) (Co), 1984.
M.S., Colorado State University, 1995.
Technical Librarian, Colorado State University.



Melissa Lucarelli

B.Sc., UIUC.
M.D., University of Wisconsin.
Family Practice Resident, St. Mary's Hospital, Milwaukee.



Eugene Mueller

B.Sc., UIUC, "Linkage of Bisporphyrin Complexes to Generate an Eight Coordinate, Chiral Molecule," 1987.

Ph.D., Harvard University.

Assistant Professor, University of Delaware.



Kristin Musgrave

B.Sc., UIUC, "Special Pair Models: Bisporphyrin-Sandwich Quinone Complexes," 1995.

Graduate Student, Stanford University.



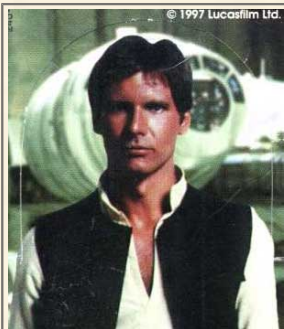
Shannon Nebolsky

B.Sc., UIUC, "A Novel Synthesis of 5, 10, 15, 20-Tetrakis- (2, 4, 6-Triphenylphenyl) Porphyrin: The "Bis-Pocket Porphyrin" 1987.

Ph.D., Northwestern University, 1995.

J.D., Northwestern University, 1996.

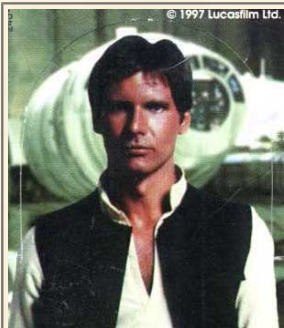
Patent Attorney, Welsh & Katz, Ltd., Chicago.



Jennifer Plaszczynski

B.Sc., UIUC, "Polymeric Microspheres," 1994.

Graduate Student in Pharmacy, UIC.



Dimitrii Rassokhin

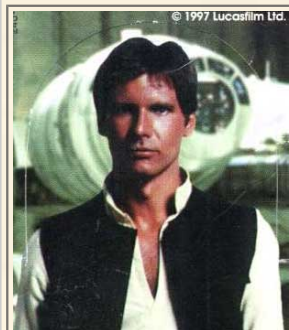
B.Sc., Moscow Lomonosov State University, Dept. of Chemistry, 1983-88.

Non-matriculated Student, UIUC, 1995.

Ph.D., Moscow Lomonosov State University, 1996.



Nicole Stewart
B.S., UIUC, 2002.



Anita Yu
B.Sc., UIUC, "The Synthesis, Characterization and Photochemistry of Oxo(5, 10, 15, 20-Tetraphenylporphyrinato) Chromium (IV), 1989.
Ph.D., University of Wisconsin at Madison, 1986.
Assistant Professor, Department of Chemistry, University of Wisconsin, Eau Claire.

SUSLICK GROUP WEBSITE:

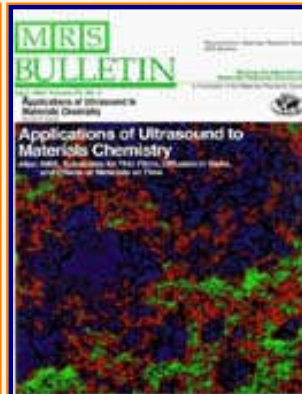
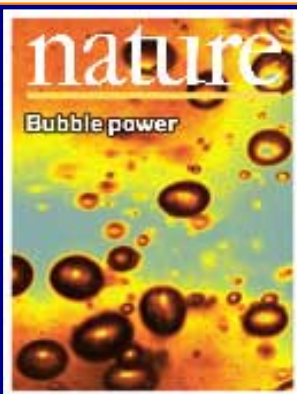
THE SCIENCE	THE GROUP	THE MAÎTRE D'	LAGNIAPPE: A LITTLE EXTRA
<u>Overview</u>	<u>Current Group Members</u>	<u>CV: Abbreviated, Full</u>	<u>Art and Science</u>
<u>Outline of Projects</u>	<u>Group Meetings</u>	<u>Suslick Group Brochure</u>	<u>Chymistes: The Distillers of Waters</u>
<u>Synopses: Sonochemistry</u>	<u>Group Responsibilities</u>	<u>Complete Publication List</u>	<u>A Chemist Meets Hollywood</u>
<u>Metalloporph.</u>			
<u>Executive Summary: Smell-Seeing</u>	<u>Web Based Resources</u>	<u>Academic Genealogy</u>	<u>A Chemist In Court</u>

<u>Introduction to Sonochemistry</u>	<u>Safety Resources</u>	<u>Press Clippings</u>	<u>Words of Humor and Wisdom</u>
<u>Proposal Excerpts</u>	<u>Group Equipment</u>	<u>How To Give A Seminar</u>	<u>Laws of the Universe</u>
<u>Funding</u>	<u>Past Group Members</u>	<u>Ch315 Inorganic Chemistry</u>	<u>Cartoons of Humor and Wisdom</u>
<u>Information for Visitors</u>	<u>Group Photogallery</u>	<u>Construction of the CLS Lab</u>	<u>Sculpture & Masks</u>

©2003, K.S. Suslick; all rights reserved.

Comments and suggestions: ksuslick@uiuc.edu

The Suslick Research Group



CARTOONS OF HUMOR AND WISDOM

SONOCHEMICAL CARTOONS

THE ACADEMIC BESTIARY

OTHER CARTOONS

SOME FAVORITE DILBERT CARTOONS



[Overview](#)

[Outline of
Research Projects](#)

[Introduction to
Sonochemistry](#)

[Exec. Summary:
Sonochemistry](#)

[Exec. Summary:
Porphyrin Research](#)

[Exec. Summary: Smell-
Seeing](#)

[Complete
Publication List](#)

[Abbreviated Curriculum
Vitae](#)

[Academic
Genealogy](#)

[Press
Clippings](#)



SONOCHEMICAL CARTOONS

[Current Research
Funding](#)

[Excerpts from
Funded Research](#)

[Inventory of
Group Equipment](#)

[Information
for Visiting](#)

[Current Research Group
Members](#)

[Group
Meetings](#)

[Group
Chores](#)

[Past Research
Group Members](#)

[Group
Photogallery](#)

[Web Resources](#)

[Laboratory Safety
Resources](#)

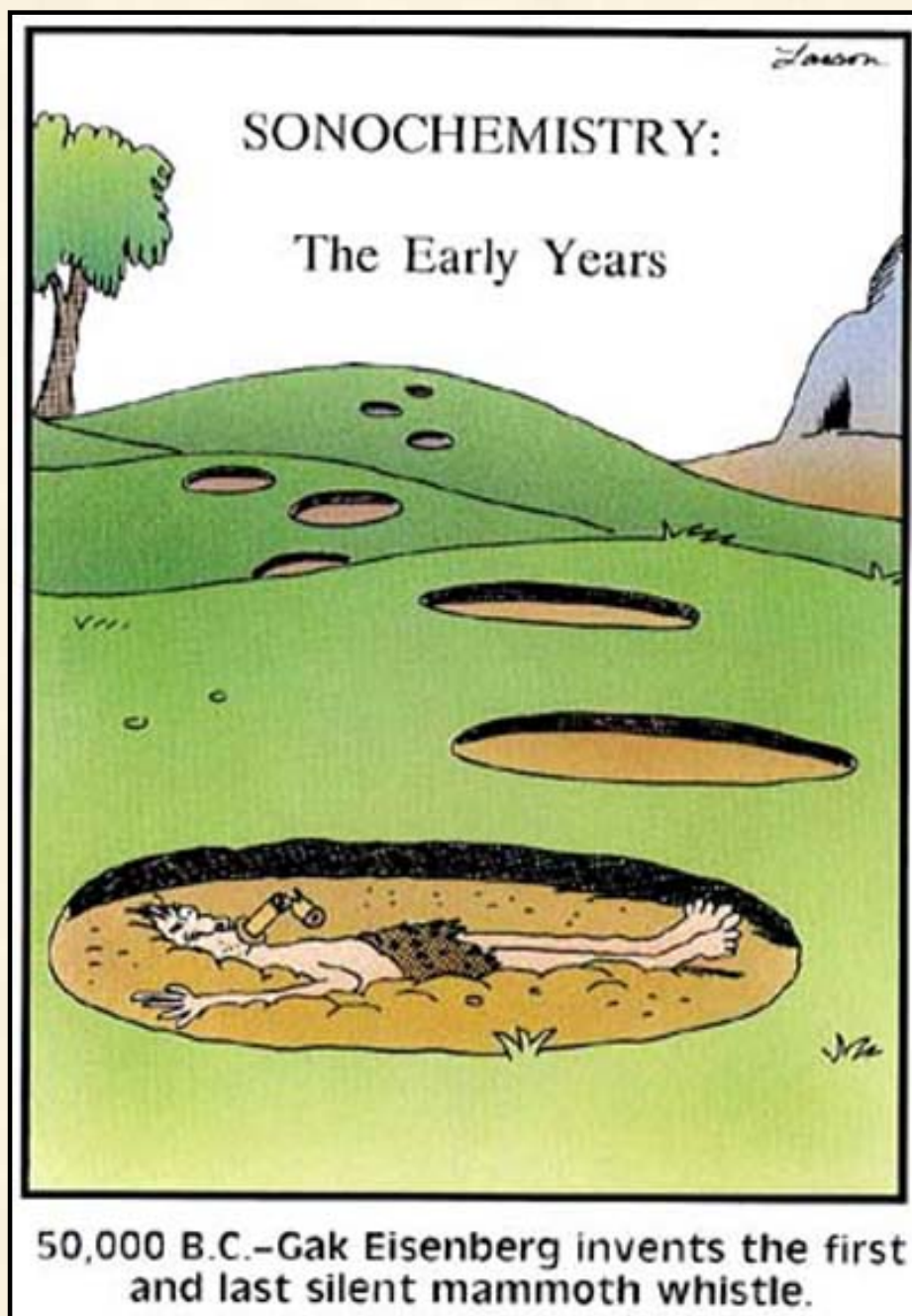
[Art and Science:
Journal Covers](#)

[Sculpture &
Masks](#)

[A Chemist
Meets Hollywood](#)

[Chymistes: The Distillers
of Waters](#)

[A Chemist
In Court](#)



Humor and
Wisdom

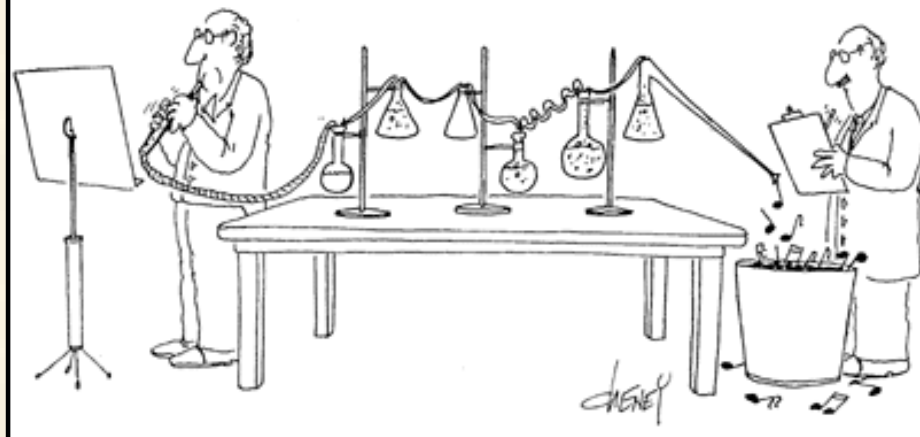
Laws of the Universe

Cartoons of Humor and
Wisdom

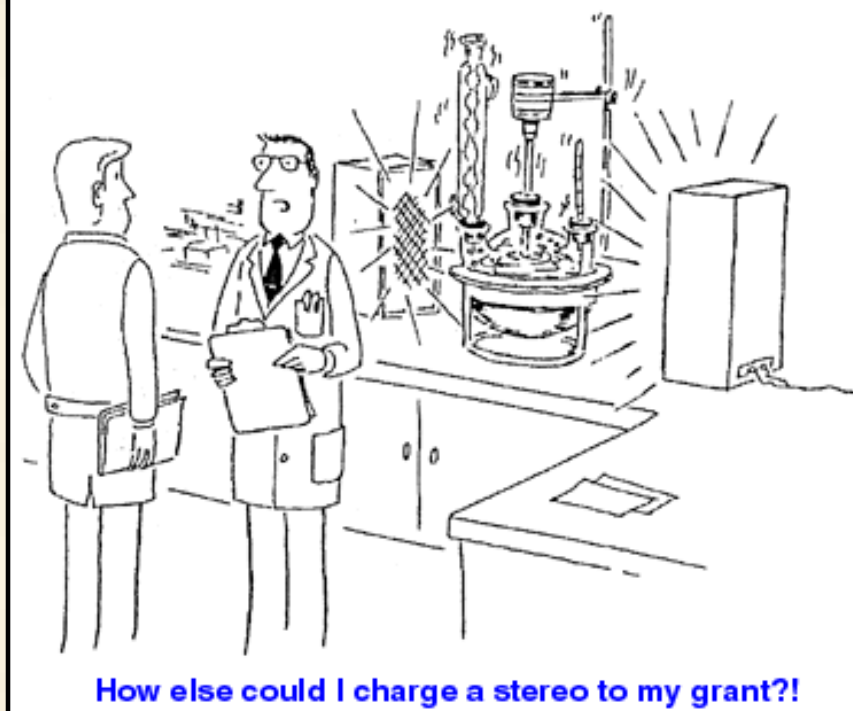
Chem 115: Chemistry of
Everyday Phenomena

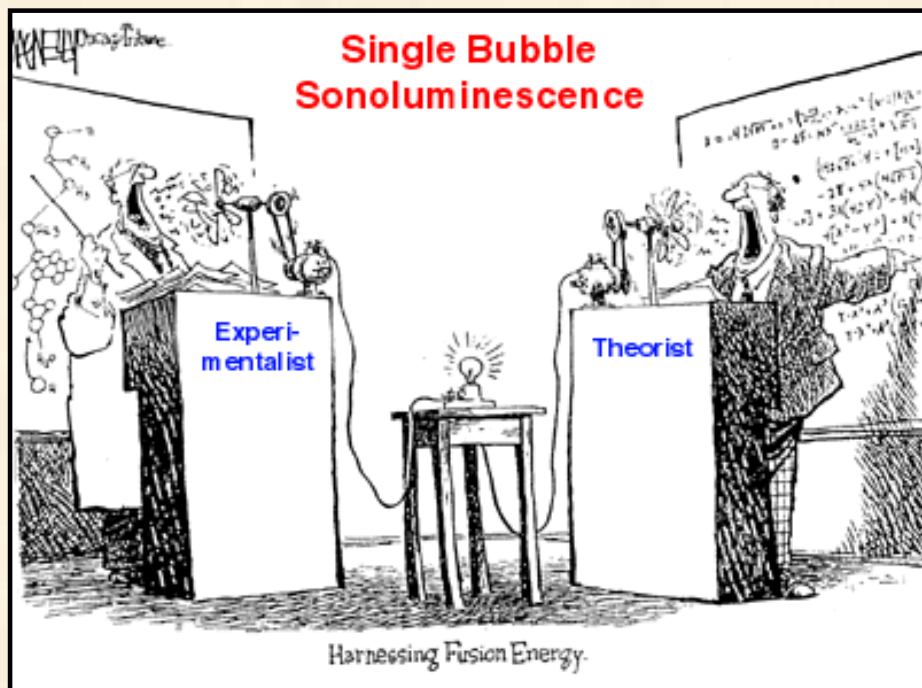
Chem 315: Inorganic
Chemistry

Sonochemistry: The Baroque Period



Sonochemistry: The Heavy Metal Era





THE ACADEMIC BESTIARY
by Richard Armour
illustrated by Paul Darrow

The ACADEMIC BESTIARY

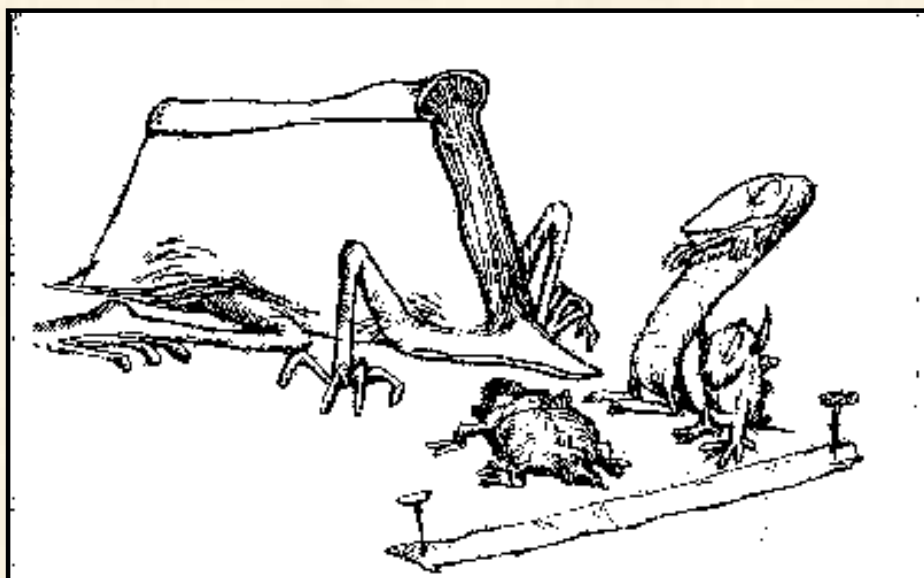
by Richard Armour

Illustrated by Paul Darrow



William Morrow & Company, Inc., New York, 1974

Title Page

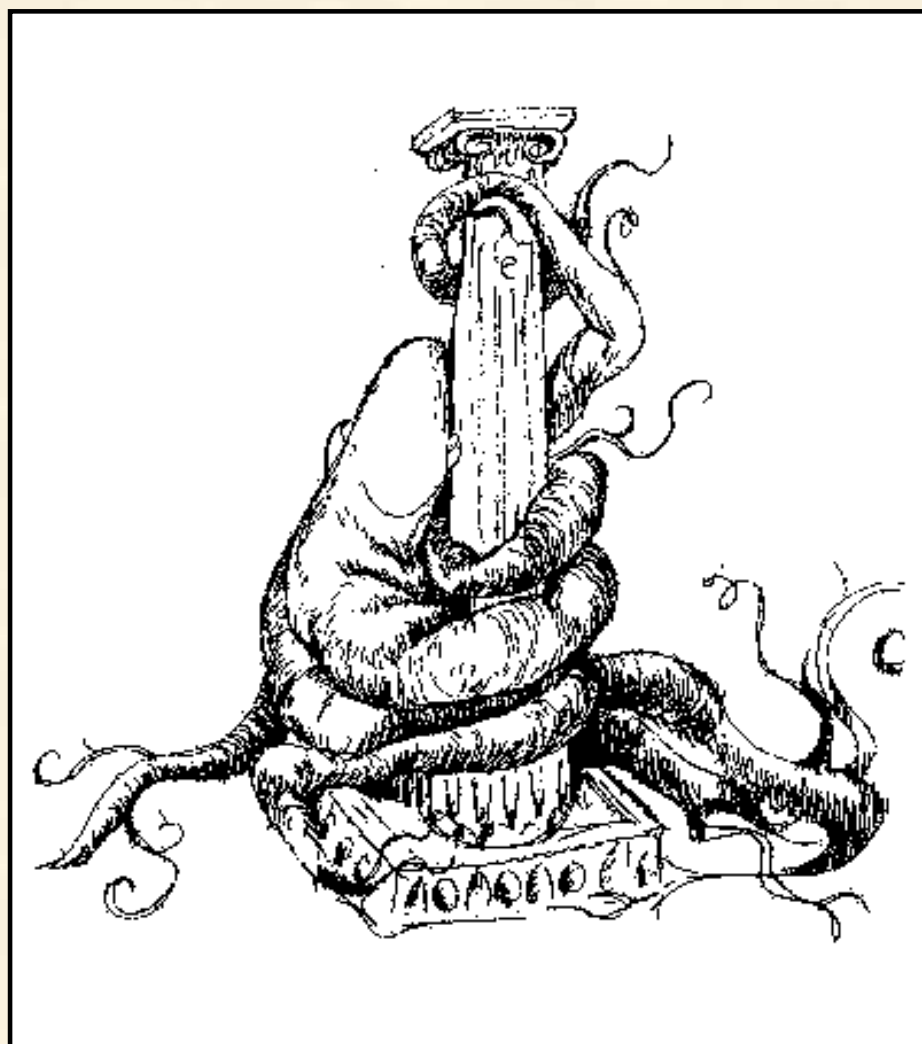


The Thesis

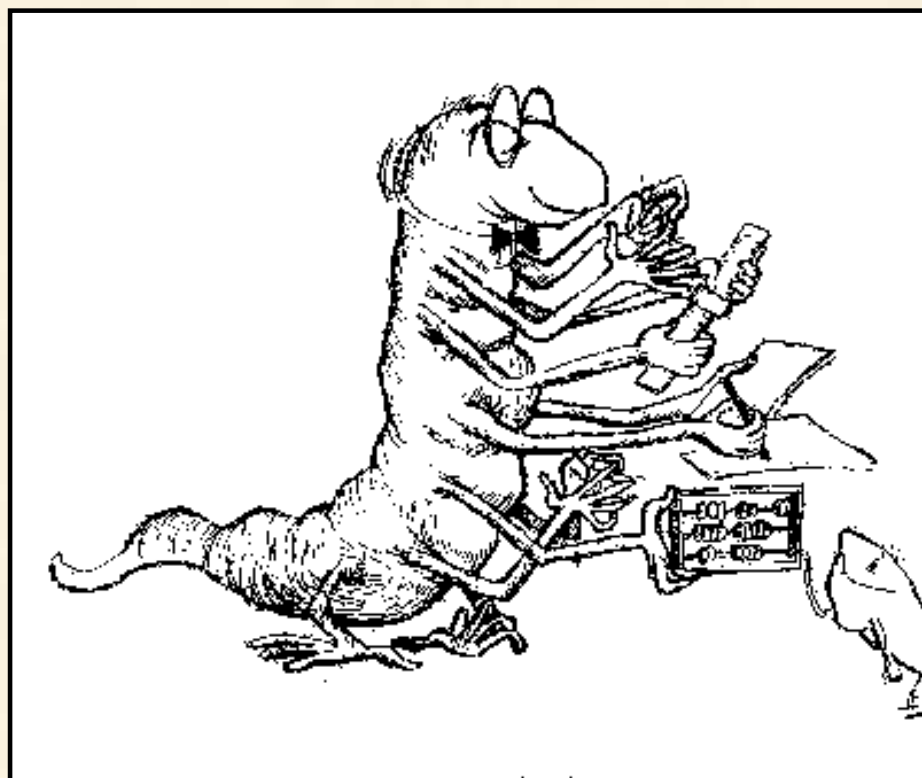




The Assistant Professor



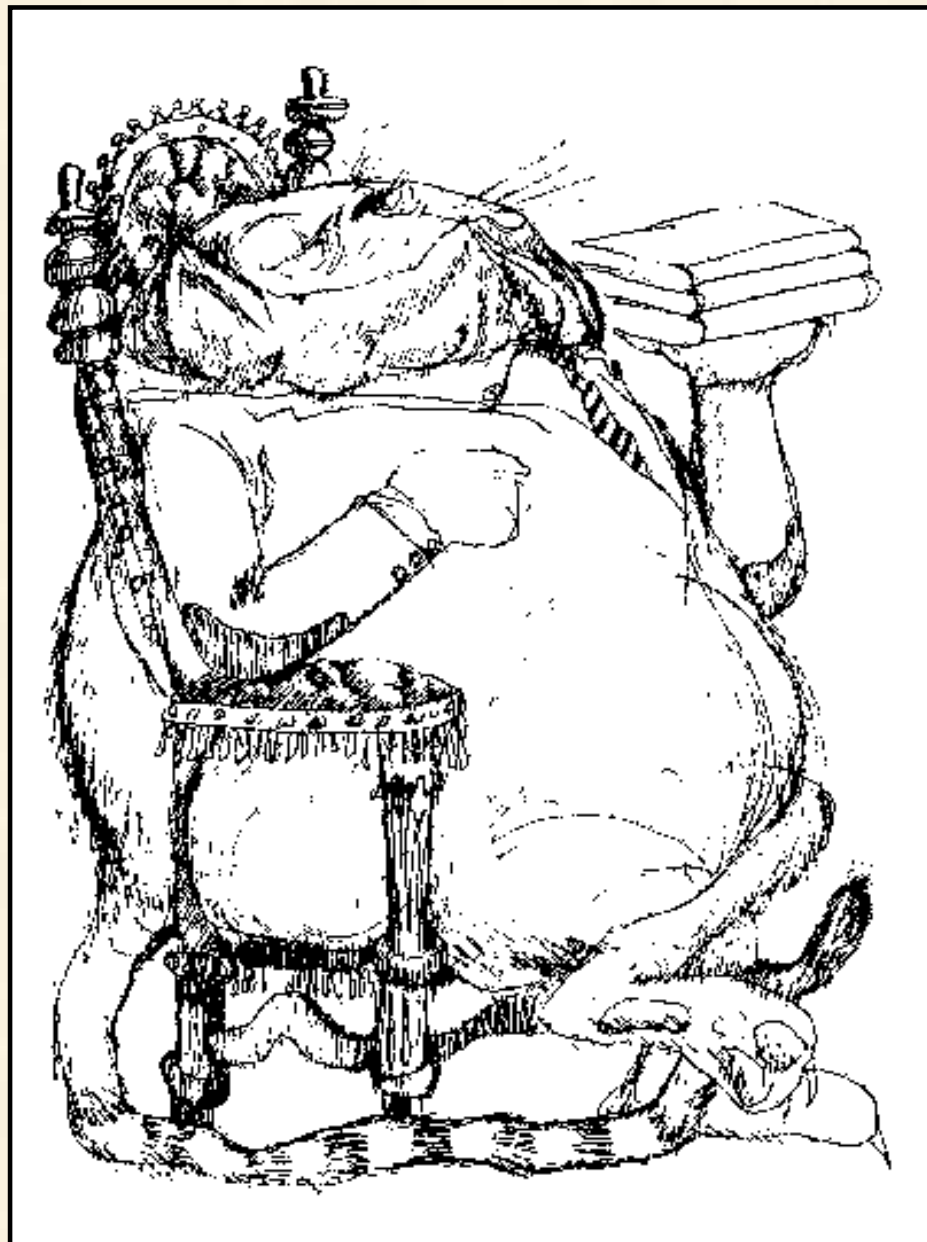
Tenure



The Science Professor

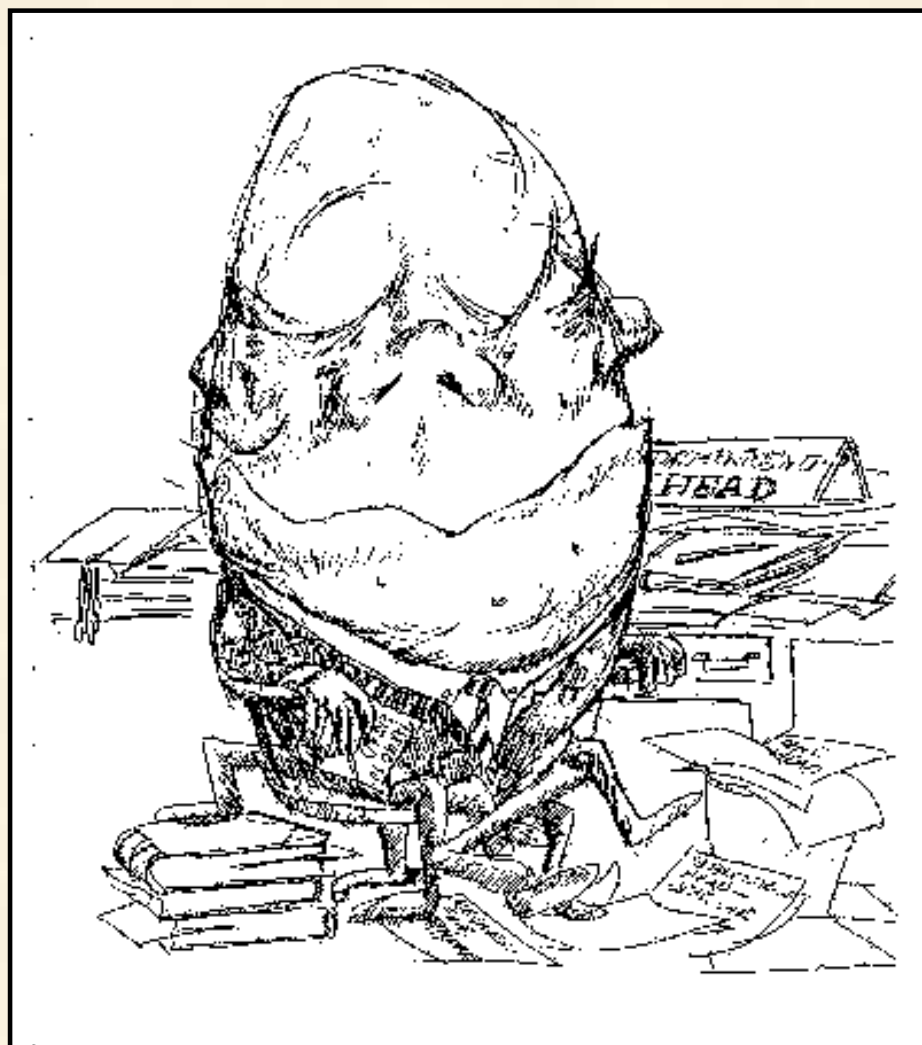


The Professor of Philosophy



The Full Professor

(I've always wondered, "Full of what?" --KSS)



The Head



The Emeritus Professor



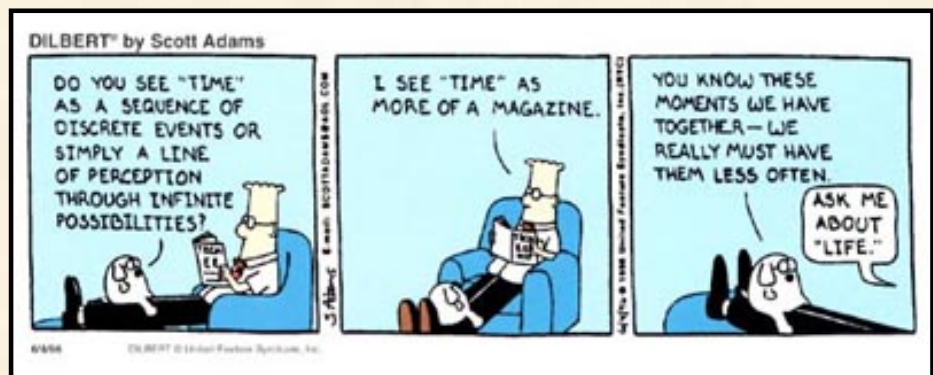
The Rule

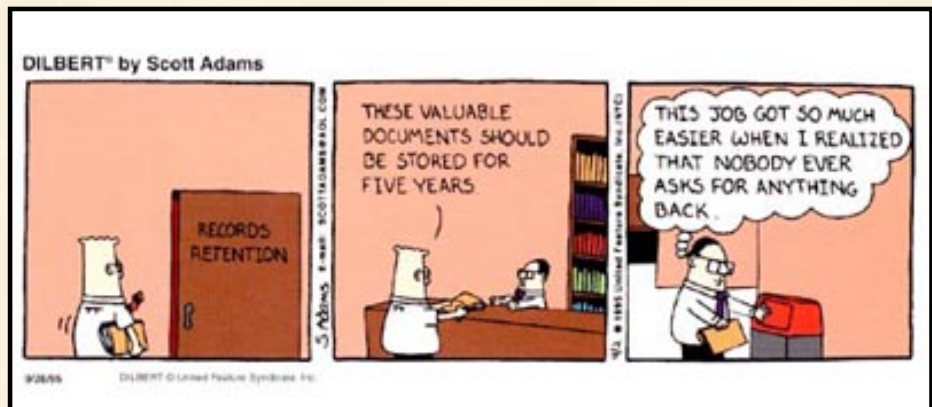
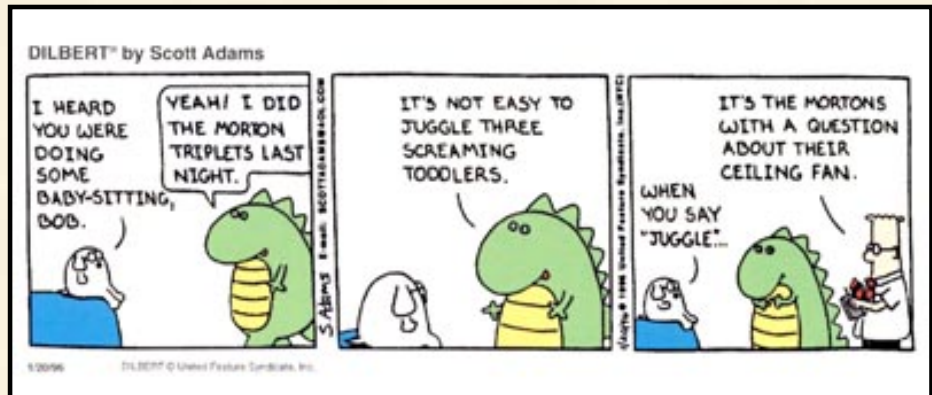
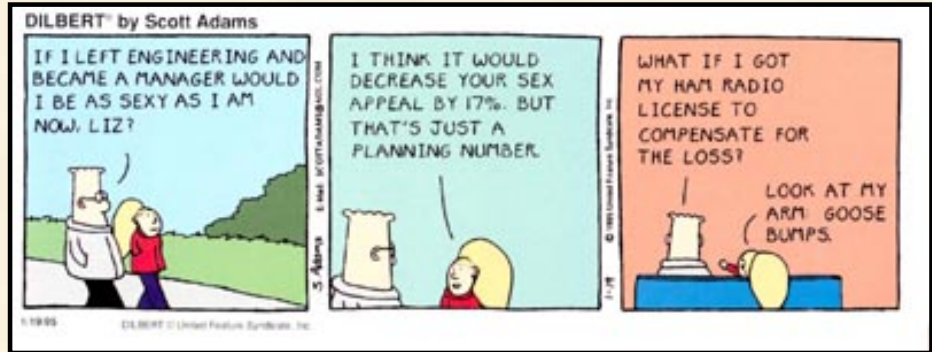
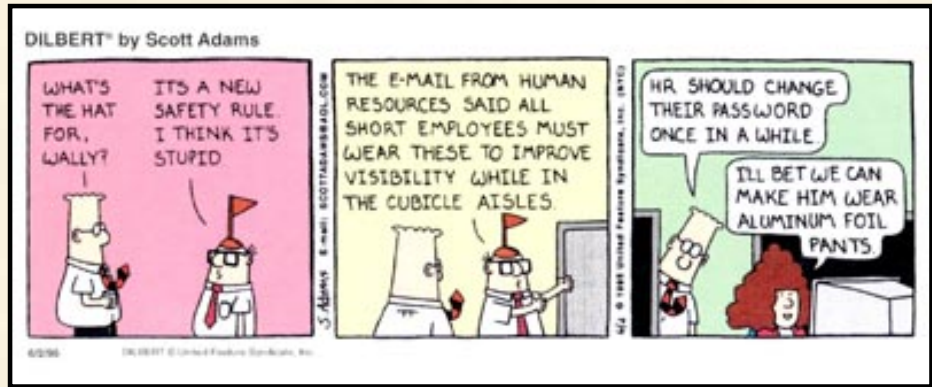
OTHER CARTOONS

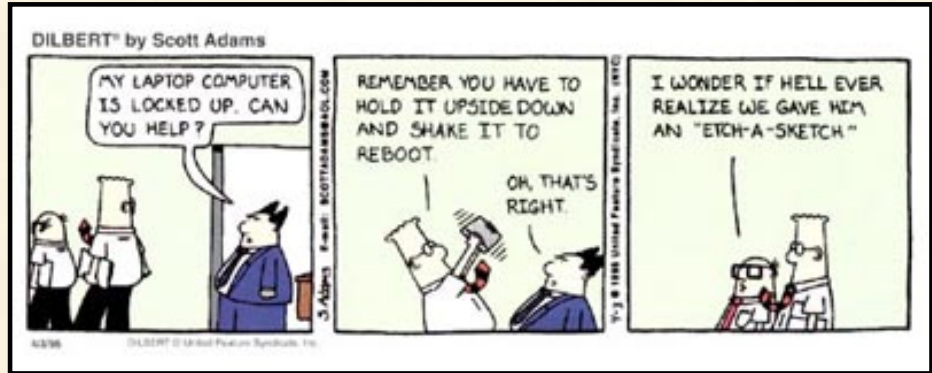


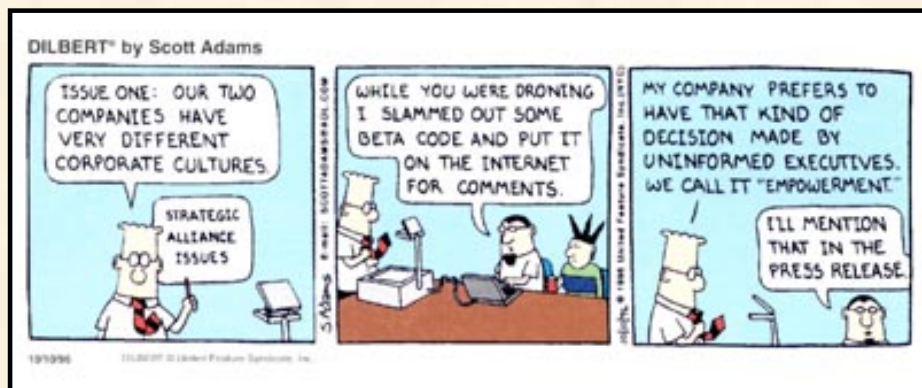
"A little knowledge is a dangerous thing.
But, then, so is a lot." --A. Einstein

SOME OF MY FAVORITE DILBERT CARTOONS









SUSLICK GROUP WEBSITE:

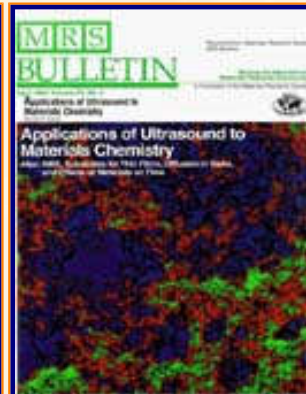
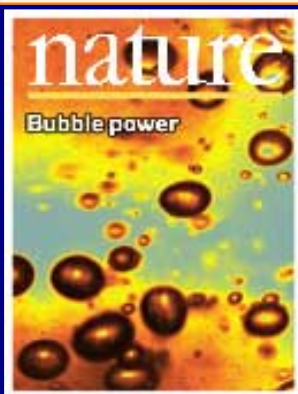
THE SCIENCE	THE GROUP	THE MAÎTRE D'	LAGNIAPPE: A LITTLE EXTRA
<u>Overview</u>	<u>Current Group Members</u>	<u>CV: Abbreviated, Full</u>	<u>Art and Science</u>
<u>Outline of Projects</u>	<u>Group Meetings</u>	<u>Suslick Group Brochure</u>	<u>Chymistes: The Distillers of Waters</u>
<u>Synopses: Sonochemistry</u> <u>Metalloporph.</u>	<u>Group Responsibilities</u>	<u>Complete Publication List</u>	<u>A Chemist Meets Hollywood</u>
<u>Executive Summary: Smell-Seeing</u>	<u>Web Based Resources</u>	<u>Academic Genealogy</u>	<u>A Chemist In Court</u>
<u>Introduction to Sonochemistry</u>	<u>Safety Resources</u>	<u>Press Clippings</u>	<u>Words of Humor and Wisdom</u>
<u>Proposal Excerpts</u>	<u>Group Equipment</u>	<u>How To Give A Seminar</u>	<u>Laws of the Universe</u>

<u>Funding</u>	<u>Past Group Members</u>	<u>Ch315 Inorganic Chemistry</u>	<u>Cartoons of Humor and Wisdom</u>
<u>Information for Visitors</u>	<u>Group Photogallery</u>	<u>Construction of the CLS Lab</u>	<u>Sculpture & Masks</u>

©2003, K.S. Suslick; all rights reserved.

Comments and suggestions: ksuslick@uiuc.edu

The Suslick Research Group



HOW TO GET HERE

The University of Illinois [Homepage](#) has [directions](#), [maps](#) (which don't yet have our new lab marked!), and [lots of information](#) about Champaign-Urbana.

[Overview](#)

[Outline of Research Projects](#)

[Introduction to Sonochemistry](#)

[Exec. Summary: Sonochemistry](#)

[Exec. Summary: Porphyrin Research](#)

[Exec. Summary: Smell- Seeing](#)

[Complete Publication List](#)

[Abbreviated Curriculum Vitae](#)

[Academic Genealogy](#)

[Press Clippings](#)

We have a very modern airport, code letters CMI, named [Willard Airport](#), that is serviced by American Airlines, Trans World Airlines, Northwest Airlines, and US Air. The airport is about 4 miles south of campus. All planes are met by A-1 Limo vans, which will pick up and deliver door-to-door, and there are the usual rental car agencies as well.

Our research group is located on the 4th Floor of the new Chemical and Life Sciences Laboratory, 601 S. Goodwin Ave.; Urbana, IL 61801. We're right across the street from the Krannert Center for Performing Arts

[Current Research Funding](#)

[Excerpts from Funded Research](#)

[Inventory of Group Equipment](#)

[Information for Visiting](#)

[Current Research Group Members](#)

[Group Meetings](#)

[Group Chores](#)

[Past Research Group Members](#)

[Group Photogallery](#)

[Web Resources](#)

[Laboratory Safety Resources](#)

[Art and Science: Journal Covers](#)

[Sculpture & Masks](#)

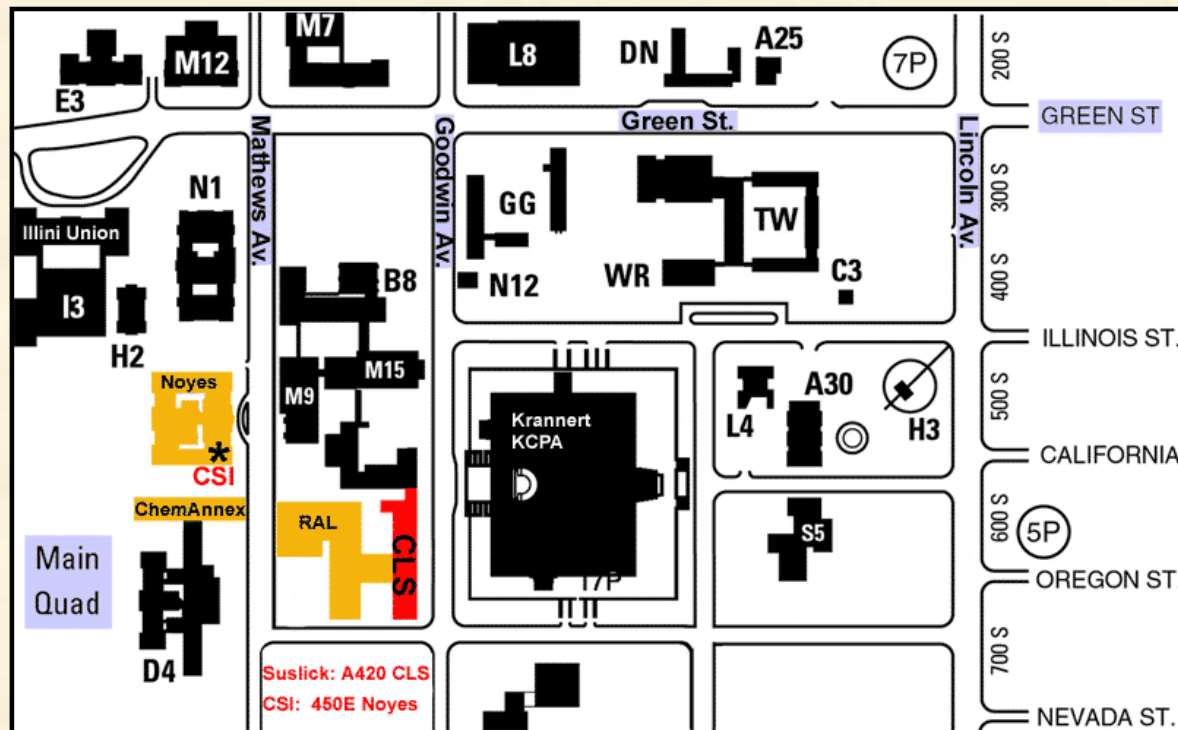
[A Chemist Meets Hollywood](#)

[Chymistes: The Distillers of Waters](#)

[A Chemist In Court](#)



The Chemical and Life Sciences Laboratory.
Cost: 63 M\$. Dedication: April 25, 1997.



CLS (Chemical and Life Science Lab) is shown in red.

[For a map of the full campus in PDF format, click here.](#)

1. From Chicago:

[Humor and
Wisdom](#)

[Laws of the Universe](#)

[Cartoons of Humor and
Wisdom](#)

[Chem 115: Chemistry of
Everyday Phenomena](#)

[Chem 315: Inorganic
Chemistry](#)

Use I-57S (From O'Hare take I-294S Tri State Tollway, look for signs for I-57S)

When you reach Urbana-Champaign, take I-74E to Lincoln Ave (about 2 miles)

Take Lincoln Ave. South to Green St. Green St. is a light about 1.6 miles down Lincoln. It is the sixth light. The traffic lights go in this sequence: Killarney, Bradley, Fairview, University, Springfield, Green.

Turn Right on Green St. Go to the next light, Goodwin Ave.. Turn Left on Goodwin.

We are on the right about 1 block down, 601 S. Goodwin, Chemical and Life Sciences Building, across the street from the Performing Arts Center.

There are two parts to the building. You want the south part (Building A) which runs parallel to Goodwin.

2. From St. Louis:

You reach Urbana-Champaign on I-72 going East

I-72 turns into University Ave.

Continue on University Ave. for about 4 miles. As you near the University, you will see the numbered streets, First, Second, Sixth Street, then Wright Street (a light with a big gas station). A bit after Wright street you will see a Hampton Inn and a Perkins. That is the sign you have reached Goodwin. Turn right on Goodwin. Continue past the stop sign, two lights (the 2nd light is Green St.) Then 1 block on your right is our building.

3. From Indianapolis (airport)

The airport exits onto I-465. Take I-465N about 5 miles to I-74W

It is about 115 miles on I-74W to Champaign-Urbana

The first Champaign-Urbana exit is University Ave. Take the University Ave. exit going toward town (West)

About 1 mile on University, you will come to a stoplight with diagonal RR tracks. That is Lincoln Ave. Continue a bit past Lincoln (across the RR tracks) to Goodwin and turn left. Goodwin is where the Perkins is located. Continue past the stop sign and 2 stop lights and we are 1 more block on the right.

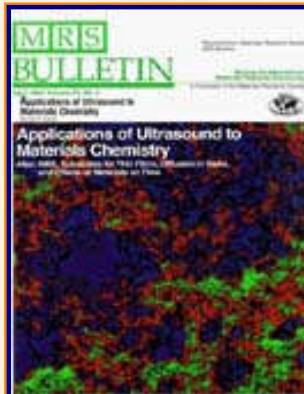
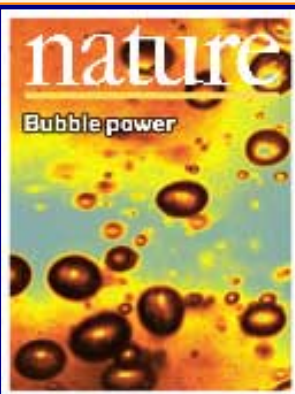
SUSLICK GROUP WEBSITE:

THE SCIENCE	THE GROUP	THE MAÎTRE D'	LAGNIAPPE: A LITTLE EXTRA
<u>Overview</u>	<u>Current Group Members</u>	<u>CV: Abbreviated, Full</u>	<u>Art and Science</u>
<u>Outline of Projects</u>	<u>Group Meetings</u>	<u>Suslick Group Brochure</u>	<u>Chymistes: The Distillers of Waters</u>
<u>Synopses: Sonochemistry</u>	<u>Group Responsibilities</u>	<u>Complete Publication List</u>	<u>A Chemist Meets Hollywood</u>
<u>Metalloporph.</u>			
<u>Executive Summary: Smell-Seeing</u>	<u>Web Based Resources</u>	<u>Academic Genealogy</u>	<u>A Chemist In Court</u>
<u>Introduction to Sonochemistry</u>	<u>Safety Resources</u>	<u>Press Clippings</u>	<u>Words of Humor and Wisdom</u>
<u>Proposal Excerpts</u>	<u>Group Equipment</u>	<u>How To Give A Seminar</u>	<u>Laws of the Universe</u>
<u>Funding</u>	<u>Past Group Members</u>	<u>Ch315 Inorganic Chemistry</u>	<u>Cartoons of Humor and Wisdom</u>
<u>Information for Visitors</u>	<u>Group Photogallery</u>	<u>Construction of the CLS Lab</u>	<u>Sculpture & Masks</u>

©2003, K.S. Suslick; all rights reserved.

Comments and suggestions: ksuslick@uiuc.edu

The Suslick Research Group



[Overview](#)

[Outline of
Research Projects](#)

[Introduction to
Sonochemistry](#)

[Exec. Summary:
Sonochemistry](#)

[Exec. Summary:
Porphyrin Research](#)

[Exec. Summary: Smell-
Seeing](#)

[Complete
Publication List](#)

[Abbreviated Curriculum
Vitae](#)

[Academic
Genealogy](#)

[Press
Clippings](#)

GROUP PHOTOGALLERY Past and Present

Always very much under construction!

Additions from past or present group members are most welcome! Email them to Ken as jpg attachments at ksuslick@uiuc.edu or send photos and we'll scan and carefully return them.

[Also, please update us on your current whereabouts by clicking on this form. Thanks!](#)

*"Long ago, it must be. I have a photograph.
Preserve your memories, they're all that's left you..."
--Paul Simon*

[Recent Group Events](#)

[Formal Group Shots](#)

[Group Members, A through F](#)

[Current Research Funding](#)

[Excerpts from Funded Research](#)

[Inventory of Group Equipment](#)

[Information for Visiting](#)

[Current Research Group Members](#)

[Group Meetings](#)

[Group Chores](#)

[Past Research Group Members](#)

[Group Photogallery](#)

[Web Resources](#)

[Laboratory Safety Resources](#)

[Art and Science: Journal Covers](#)

[Sculpture & Masks](#)

[A Chemist Meets Hollywood](#)

[Chymistes: The Distillers of Waters](#)

[A Chemist In Court](#)

Group Members, G through M

Group Members, N through Z

Shots of Ken

Construction of the Chemical and Life Sciences Laboratory

The MOVE

SUSLICK GROUP WEBSITE:

THE SCIENCE	THE GROUP	THE MAÎTRE D'	LAGNIAPPE: A LITTLE EXTRA
Overview	Current Group Members	CV: Abbreviated, Full	Art and Science
Outline of Projects	Group Meetings	Suslick Group Brochure	Chymistes: The Distillers of Waters
Synopsis: Sonochemistry	Group Responsibilities	Complete Publication List	A Chemist Meets Hollywood
Metalloporph.			
Executive Summary: Smell-Seeing	Web Based Resources	Academic Genealogy	A Chemist In Court

[Humor and
Wisdom](#)

[Laws of the Universe](#)

[Cartoons of Humor and
Wisdom](#)

[Chem 115: Chemistry of
Everyday Phenomena](#)

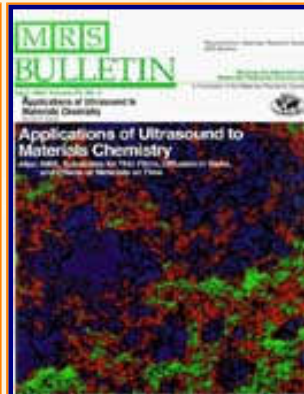
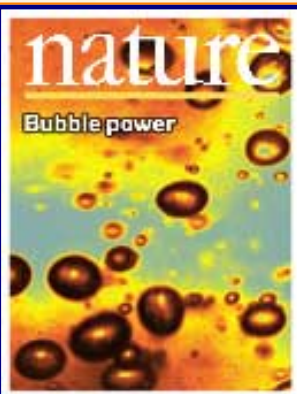
[Chem 315: Inorganic
Chemistry](#)

<u>Introduction to Sonochemistry</u>	<u>Safety Resources</u>	<u>Press Clippings</u>	<u>Words of Humor and Wisdom</u>
<u>Proposal Excerpts</u>	<u>Group Equipment</u>	<u>How To Give A Seminar</u>	<u>Laws of the Universe</u>
<u>Funding</u>	<u>Past Group Members</u>	<u>Ch315 Inorganic Chemistry</u>	<u>Cartoons of Humor and Wisdom</u>
<u>Information for Visitors</u>	<u>Group Photogallery</u>	<u>Construction of the CLS Lab</u>	<u>Sculpture & Masks</u>

©2003, K.S. Suslick; all rights reserved.

Comments and suggestions: ksuslick@uiuc.edu

The Suslick Research Group



[Overview](#)

[Outline of
Research Projects](#)

[Introduction to
Sonochemistry](#)

[Exec. Summary:
Sonochemistry](#)

[Exec. Summary:
Porphyrin Research](#)

[Exec. Summary: Smell-
Seeing](#)

[Complete
Publication List](#)

[Abbreviated Curriculum
Vitae](#)

[Academic
Genealogy](#)

[Press
Clippings](#)

Construction of the Chemical and Life Sciences Laboratory: 1993-1997

Photographs courtesy of
James A. Gray,
Supervisor of SCS Graphic Design



June, 1992

[Current Research
Funding](#)

[Excerpts from
Funded Research](#)

[Inventory of
Group Equipment](#)

[Information
for Visiting](#)

[Current Research Group
Members](#)

[Group
Meetings](#)

[Group
Chores](#)

[Past Research
Group Members](#)

[Group
Photogallery](#)

[Web Resources](#)

[Laboratory Safety
Resources](#)

[Art and Science:
Journal Covers](#)

[Sculpture &
Masks](#)

[A Chemist
Meets Hollywood](#)

[Chymistes: The Distillers
of Waters](#)

[A Chemist
In Court](#)



June,1993



June,1993

Humor and
Wisdom

Laws of the Universe

Cartoons of Humor and
Wisdom

Chem 115: Chemistry of
Everyday Phenomena

Chem 315: Inorganic
Chemistry



July,1993



July,1993



October,1993



October,1993



November,1993



November,1993



February, 1994





April,1994



April,1994



June,1994



June,1994



June,1994



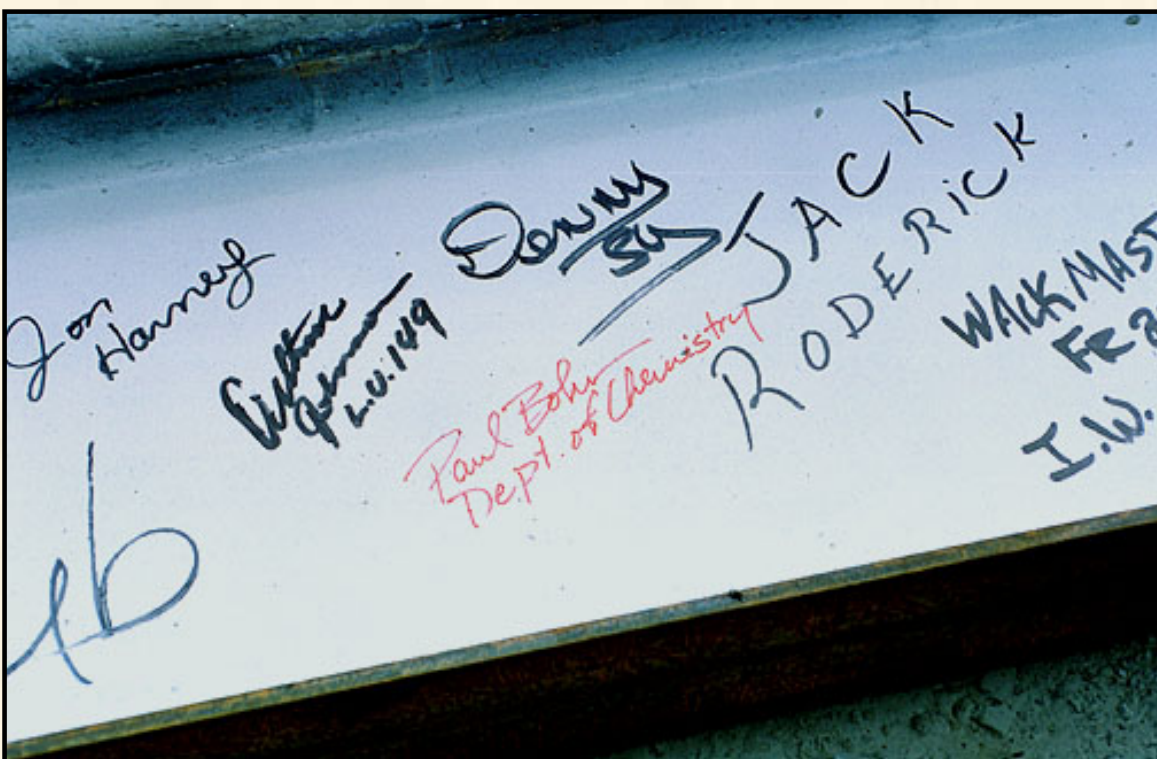
June,1994



July,1994



August, 1994



August, 1994



August, 1994



August, 1994



November,1994



November,1994



November, 1994



February, 1995



February, 1995



April, 1995



April,1995



May,1996



 The MOVE



Dedication of CLSL: April 25, 1997.

SUSLICK GROUP WEBSITE:

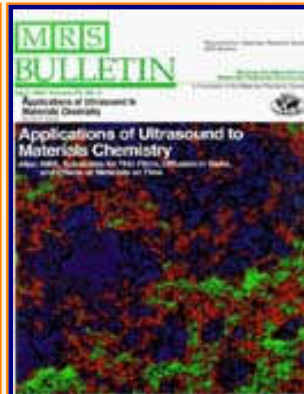
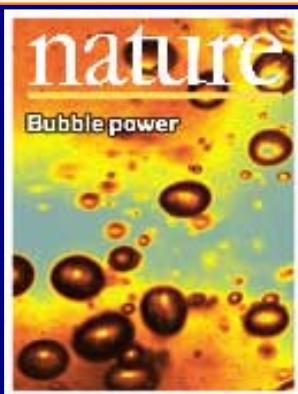
THE SCIENCE	THE GROUP	THE MAÎTRE D'	LAGNIAPPE: A LITTLE EXTRA
<u>Overview</u>	<u>Current Group Members</u>	<u>CV: Abbreviated, Full</u>	<u>Art and Science</u>
<u>Outline of Projects</u>	<u>Group Meetings</u>	<u>Suslick Group Brochure</u>	<u>Chymistes: The Distillers of Waters</u>
<u>Synopses: Sonochemistry</u>	<u>Group Responsibilities</u>	<u>Complete Publication List</u>	<u>A Chemist Meets Hollywood</u>
<u>Metalloporph.</u>			

<u>Executive Summary: Smell-Seeing</u>	<u>Web Based Resources</u>	<u>Academic Genealogy</u>	<u>A Chemist In Court</u>
<u>Introduction to Sonochemistry</u>	<u>Safety Resources</u>	<u>Press Clippings</u>	<u>Words of Humor and Wisdom</u>
<u>Proposal Excerpts</u>	<u>Group Equipment</u>	<u>How To Give A Seminar</u>	<u>Laws of the Universe</u>
<u>Funding</u>	<u>Past Group Members</u>	<u>Ch315 Inorganic Chemistry</u>	<u>Cartoons of Humor and Wisdom</u>
<u>Information for Visitors</u>	<u>Group Photogallery</u>	<u>Construction of the CLS Lab</u>	<u>Sculpture & Masks</u>

©2003, K.S. Suslick; all rights reserved.

Comments and suggestions: ksuslick@uiuc.edu

The Suslick Research Group



[Overview](#)

[Outline of
Research Projects](#)

[Introduction to
Sonochemistry](#)

[Exec. Summary:
Sonochemistry](#)

[Exec. Summary:
Porphyrin Research](#)

[Exec. Summary: Smell-
Seeing](#)

[Complete
Publication List](#)

[Abbreviated Curriculum
Vitae](#)

[Academic
Genealogy](#)

[Press
Clippings](#)

BRONZE SCULPTURE BY KEN SUSLICK

[Cover Art by Ken Suslick](#)

[Bronze Sculpture by Ken Suslick](#)

[Masks from the Collection of Ken Suslick](#)

[The Pouring of Bronze](#)

Immediately at birth, we recognize and respond to faces.
This is why masks are universal.

[Current Research
Funding](#)

[Excerpts from
Funded Research](#)

[Inventory of
Group Equipment](#)

[Information
for Visiting](#)

[Current Research Group
Members](#)

[Group
Meetings](#)

[Group
Chores](#)

[Past Research
Group Members](#)

[Group
Photogallery](#)

[Web Resources](#)

[Laboratory Safety
Resources](#)

[Art and Science:
Journal Covers](#)

[Sculpture &
Masks](#)

[A Chemist
Meets Hollywood](#)

[Chymistes: The Distillers
of Waters](#)

[A Chemist
In Court](#)



[Humor and
Wisdom](#)

[Laws of the Universe](#)

[Cartoons of Humor and
Wisdom](#)

[Chem 115: Chemistry of
Everyday Phenomena](#)

[Chem 315: Inorganic
Chemistry](#)



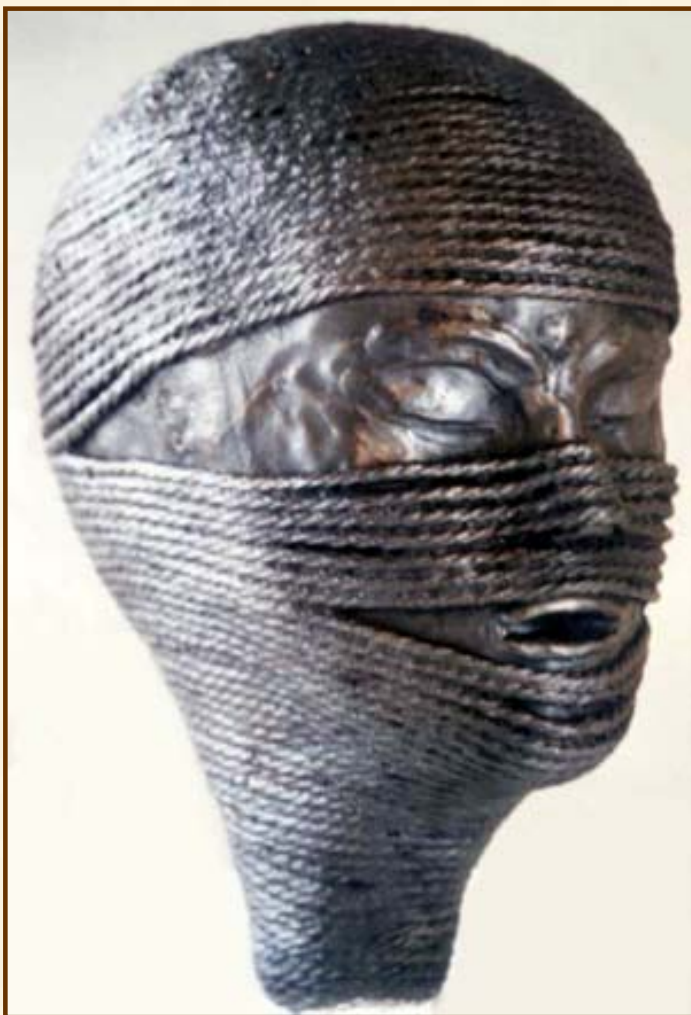






















SUSLICK GROUP WEBSITE:

THE SCIENCE	THE GROUP	THE MAÎTRE D'	LAGNIAPPE: A LITTLE EXTRA
<u>Overview</u>	<u>Current Group Members</u>	<u>CV: Abbreviated, Full</u>	<u>Art and Science</u>
<u>Outline of Projects</u>	<u>Group Meetings</u>	<u>Suslick Group Brochure</u>	<u>Chymistes: The Distillers of Waters</u>

<u>Synopses: Sonochemistry</u>	<u>Group Responsibilities</u>	<u>Complete Publication List</u>	<u>A Chemist Meets Hollywood</u>
<u>Metalloporph.</u>			
<u>Executive Summary: Smell-Seeing</u>	<u>Web Based Resources</u>	<u>Academic Genealogy</u>	<u>A Chemist In Court</u>
<u>Introduction to Sonochemistry</u>	<u>Safety Resources</u>	<u>Press Clippings</u>	<u>Words of Humor and Wisdom</u>
<u>Proposal Excerpts</u>	<u>Group Equipment</u>	<u>How To Give A Seminar</u>	<u>Laws of the Universe</u>
<u>Funding</u>	<u>Past Group Members</u>	<u>Ch315 Inorganic Chemistry</u>	<u>Cartoons of Humor and Wisdom</u>
<u>Information for Visitors</u>	<u>Group Photogallery</u>	<u>Construction of the CLS Lab</u>	<u>Sculpture & Masks</u>

©2003, K.S. Suslick; all rights reserved.

Comments and suggestions: ksuslick@uiuc.edu